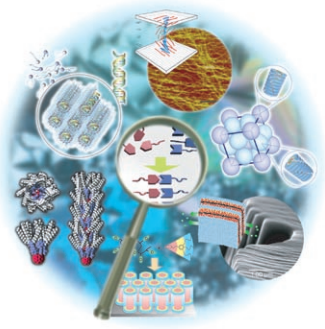
Cover Picture

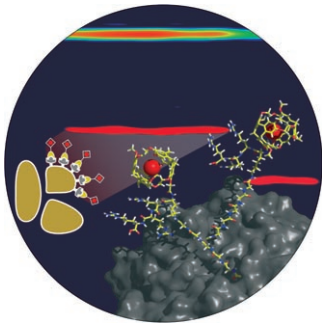


Nazario Martín,* Margarita Altable, Salvatore Filippone, Angel Martín-Domenech, Luis Echegoyen,* and Claudia M. Cardona

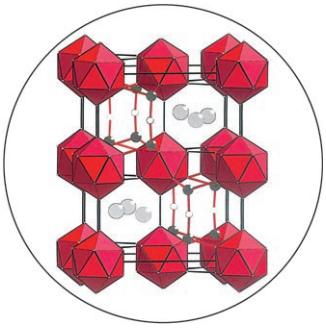
Retro-cycloaddition of easily prepared pyrrolidinofullerenes affords quantitatively pristine fullerenes, and thus can be used as a new protection-deprotection protocol in the chemistry of fullerenes, as shown in the cover picture. In their Communication on page 110 ff., N. Martín, L. Echegoyen, and co-workers report on this promising finding, which has already allowed the selective isolation of the I_h constitutional isomer of $Sc_3N@C_{80}$.



Liquid Crystals
In their Review on page 38 ff., T. Kato et al. explain the design of new liquid crystals through supramolecular approaches. Ordering principles and potential application are described.



Imaging Agents
The use of hyperpolarized xenon for the NMR detection of immobilized avidin analyte with high sensitivity is described in the Communication by C. Hilty et al. on page 70 ff.



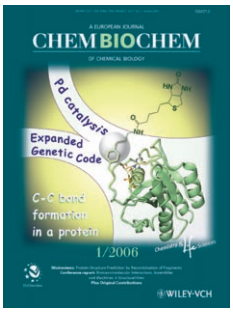
Boride Carbides
The structures of $Li_2B_{12}C_2$ and $LiB_{13}C_2$ are shown by H. Hillebrecht and N. Vojteer in their Communication on page 165 ff. to consist of a 3D framework of B_{12} icosahedra and C_2 and CBC units, respectively, with Li cations in the voids.

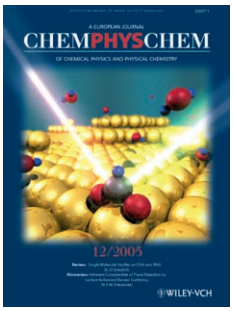
All Good Things Come in Threes...

DOI: 10.1002/anie.200504178

...and this saying is particularly apt for the new projects that will come to fruition in 2006 with the help of *Angewandte Chemie*. This help comes from three sources, the Gesellschaft Deutscher Chemiker (GDCh, the German Chemical Society), to which *Angewandte Chemie* belongs, the publishers Wiley-VCH, who publish the journal, and the editorial team that produces it.

The year begins with the inaugural issue of *ChemMedChem*. The Societá Chimica Italiana (SCI) will close its journal *Il Farmaco* at the end of 2005 and, in 2006 will launch *ChemMedChem*, in conjunction with the GDCh and the other European chemical societies that co-own *Chemistry—A European Journal*, and the publishers Wiley-VCH. The new journal offers a first class forum for scientific articles at the interface between biology, chemistry, and medicine, as further confirmed by its subtitle "Chemistry Enabling Drug Discovery". The Editorial Board is headed by Professor Rainer Metternich (Schering, Berlin) who is also on the Editorial Board of *Angewandte Chemie*, and Professor Giorgio Tarzia (Università degli Studi di Urbino, Italy), the former Editor of *Il Farmaco*. You can learn more about *ChemMedChem* in the Editorial in the first issue, in the Notice to Authors, and of course by reading the first articles which are already available online in EarlyView, see www.chemmedchem.org. All good things come in threes: *ChemBioChem*, *ChemPhysChem*, and now *ChemMedChem*.







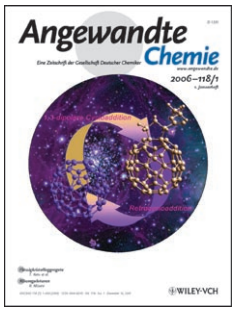
Following the example of *Chemistry—A European Journal*, its Asian counterpart, *Chemistry—An Asian Journal,* will be launched in 2006. Chemical societies from China, India, Japan, and Korean have agreed, together with Wiley-VCH, and with the support of the GDCh to found the "Asian Journal" as a sister journal to the "European Journal", and once again *Angewandte Chemie* is the godfather. The chairman of the Editorial Board of *Chemistry—An Asian Journal* is Professor Ryoji Noyori, President of RIKEN in Japan and one of the winners of the Nobel Prize in chemistry in 2001; R. Noyori is also a member of the International Advisory Board of *Angewandte Chemie*. The new journal will, like *Chemistry—A European Journal*, publish original full papers as well as Focus Reviews, which are short review articles on current, important topics. The journal will be guided by an Asian Editorial Board and produced by an editorial team based in Weinheim, which will work closely with the teams of *Angewandte Chemie* and *Chemistry—A European Journal*. An International Advisory Board will ensure that *Chemistry—An Asian Journal* also packs the necessary international punch.



Ryoji Noyori, Chairman of the Editorial Board of *Chemistry—An Asian Journal.*

Japan has been an important scientific country for decades and recently the rapid growth of science in other Asian countries has been impossible to miss. Thus, it is only natural that top scientific journals should not only come out of America and Europe but also out of Asia. *Chemistry—An Asian Journal* is the beginning and with *Chemistry—A European Journal* and *Angewandte Chemie* we have another group of good things that come in threes. The European chemical societies that co-own the "European Journal", and in particular the GDCh, welcome and support these developments that contribute greatly to international scientific exchange. From the beginning of 2006, authors can submit manuscripts to *Chemistry—An Asian Journal* (www.chemasianj.org); soon after, readers will be able to see the first articles online in the EarlyView mode of Wiley InterScience, and the publication of the first issue is planned for the middle of the year.







In the first year, both *Chemistry—An Asian Journal* and *ChemMedChem* will be free

© 2006 Wiley-VCH Verlag GmbH & Co. KGaA, Weinheim

of charge to all institutional subscribers of *Angewandte Chemie*; in addition, other institutions can opt for full electronic access to these journals. This guarantees the highest possible visibility for all articles published in these new journals and will allow institutions to monitor the usage of these journals.

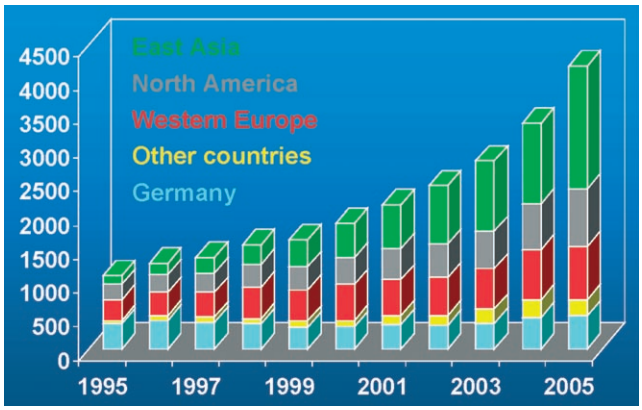


Figure 1. Distribution of Communications submitted between 1995 and 2005 by geographic region.

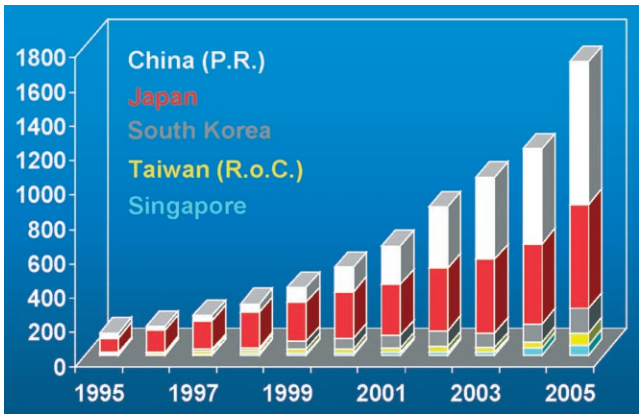


Figure 2. Country of origin of Communications submitted from East Asia between 1995 and 2005. All countries from which more than 50 Communications were received in 2005 are included.

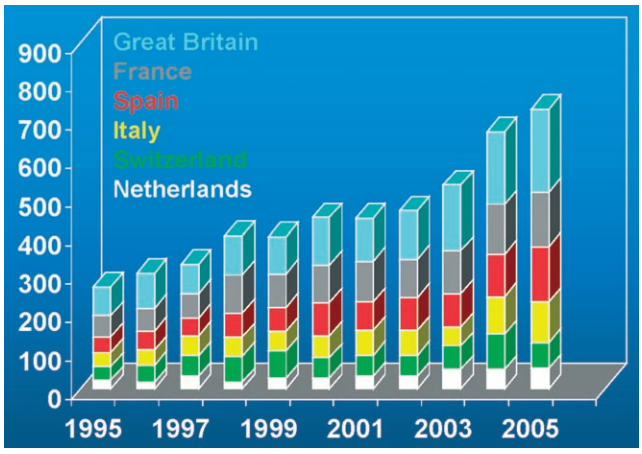


Figure 3. Country of origin of Communications submitted from Western Europe between 1995 and 2005. All countries from which more than 50 Communications were received in 2005 are included. The number of submissions from Germany can be found in Figure 1.

With so many new things to report it is important not to forget our review of 2005, a year which saw approximately 4200 Communications submitted to *Angewandte Chemie*, which is about 25% more than in the previous year (see Table 1 and Figures 1–3). The percentage growth in submissions from all the Asian countries is significant, the largest growth in numbers of manuscripts received was from China (Figure 2); similarly, each year more manuscripts come from Western Europe, although the growth is more moderate (Figure 3). Also the number of manuscripts sent from Germany has increased noticeably in the last few years (Table 1 and Figure 1). The editorial team has risen to this challenge and published 1304 Communications in 2005 (+22% compared to 1072 in 2004); the rejection rate increased from 66% to 68%, with around 15% of manuscripts being rejected directly by the editors.

The very large increase in manuscript submissions to *Angewandte Chemie* (in the last five years it has almost doubled!) and other journals with high Impact Factors will continue so long scientists are "evaluated" by criteria that make heavy use of these numbers. There is a lot of justified concern about this development. The misuse of these figures on the one hand (see my Editorial in issue 35/2005) and the temptation to influence these figures unfairly on the other hand are an indication that the Impact Factor should be seen more critical than ever.

There were also technological improvements in 2005 from which readers and authors will benefit. In Wiley InterScience "Forward Linking" was

Table 1: Country of origin of Communications submitted in the last five years (percentage in parentheses). Manuscripts with multinational authors are assigned to the country of the submitting author.

Country	2003	2004	2005[a]
China (P.R.)	477 (17)	570 (17)	830 (20)
USA	506 (18)	612 (18)	749 (18)
Japan	429 (15)	464 (14)	606 (15)
Germany	383 (14)	458 (14)	488 (12)
Great Britain	171 (6)	190 (6)	216 (5)
South Korea	83 (3)	104 (3)	144 (4)
Spain	87 (3)	110 (3)	144 (4)
France	110 (4)	128 (4)	140 (3)
India	89 (3)	115 (3)	116 (3)
Italy	50 (2)	98 (3)	106 (3)
Canada	52 (2)	64 (2)	97 (2)
Taiwan (R.C.)	31 (1)	42 (1)	70 (2)
Switzerland	61 (2)	92 (3)	67 (2)
Singapore	14 (1)	41 (1)	58 (1)
Netherlands	50 (2)	50 (1)	53 (1)
Israel	28 (1)	35 (1)	41 (1)
Sweden	16 (1)	25 (0.7)	32 (1)
Poland	9 (0.3)	10 (0.3)	18 (0.4)
Russia	12 (0.4)	16 (0.4)	13 (0.3)
Other	123 (4)	140 (4)	174 (4)
Total	2781 (+ 15.0 %)	3364 (+20.9%)	4162 (+ 23.7%)

[a] The data for 2005 are extrapolated from the data for the first 10 months of the year.

© 2006 Wiley-VCH Verlag GmbH & Co. KGaA, Weinheim

Changes to the Editorial and International Advisory Boards of *Angewandte Chemie* in 2006:

Editorial Board

Departing members

Reinhart Ahlrichs, Karlsruhe, Germany
Fred-Robert Heiker, Wuppertal, Germany
Peter Raddatz, Darmstadt, Germany

New members

Michael Dröscher, Düsseldorf, Germany
Walter Thiel, Mülheim an der Ruhr, Germany
Otto Wolfbeis, Regensburg, Germany

International Advisory Board

Departing members

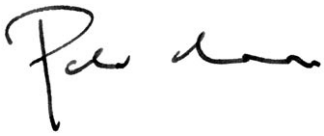
Daniel Bellus, Basel, Switzerland
Thomas R. Cech, Boulder, USA
Robert J. P. Corriu, Montpellier, France
Meir Lahav, Rehovot, Israel
Colin Raston, Perth, Australia
Bernard Raveau, Caen, France

New members

Lia Addadi, Rehovot, Israel
Chun-Li Bai, Beijing, P.R. China
Scott Biller, Cambridge, USA
Andrew Holmes, Melbourne, Australia
Yuan-Tseh Lee, Taipei, Taiwan
Shengming Ma, Shanghai, P.R. China
Bernard Meunier, Toulouse, France
Chad Mirkin, Evanston, USA
Klaus Müller, Basel, Switzerland
Eiichi Nakamura, Tokyo, Japan
Luis Oro, Zaragoza, Spain

introduced. The traditional "Reference Linking" courtesy of CrossRef has for some time enabled readers to jump easily to the cited literature, and now, with the aid of Forward Linking, the reader can jump to later articles in which the earlier article has been cited. This gem can be found in Wiley InterScience under "Citation Tracking", after clicking on "References" or "Abstracts". For authors, the editorial team recently released a manuscript template with which it is possible to see how the article could look in an issue.

It is important to remember that regardless of the technological advances it is people who determine the quality of a journal. The technology of scientific publishing has changed completely in the 25 years that I have worked for *Angewandte Chemie*; the role of the Editor has not: read and listen, and these corner stones of an editor's job can not be accelerated through technology. Naturally, a decisive factor is what you get to read and who you get to listen to. In these matters the members of the Editorial and International Advisory Boards play a most important role. At the end of 2005, the terms of office of several of our trusted advisors on these boards came to an end (see box), I would like to express my personal thanks to these scientists and also convey the gratitude of the editorial team, the publishers, and the GDCh. The scientists who are joining these boards are also listed in the box, and they are introduced more fully in the News on page 22. With advisors such as those who are leaving, those who are remaining, and those who are new, one need have no fear for the future.



Peter Gölitz

PS: The complete International Edition of *Angewandte Chemie*, from the very first issue in 1962, has been available electronically for around two years. Now the German Edition, from issue 1 of 1887 is being made available electronically as a "Society Backfile" together with all the volumes of "Berichte" and "Annalen" and with the first three years of *Chemistry—A European Journal* (see below). In particular the early years of the traditional and, at the time, world-leading German chemistry journals are a treasure trove, and making them available electronically is a great service. And even for the oldest issues CrossRef and Forward Linking are possible!

Study the past if you would define the future. — Confucius

CHEMISTRY SOCIETIES:
Annalen, Angewandte, Berichte and more
BACKFILE COLLECTION

- Nearly 900,000 pages, spanning two centuries of chemistry research
- Coverage back to Volume I, Issue 1
- Fully searchable articles with HTML headers and references
- One-time purchase

© 2006 Wiley-VCH Verlag GmbH & Co. KGaA, Weinheim

VIP The following Communications have been judged by at least two referees to be "very important papers" and will be published online at www.angewandte.org soon:

*J. Deschamp, O. Chuzel, J. Hannedouche, O. Riant**
Highly Diastereo- and Enantioselective Copper-Catalyzed Tandem Conjugated Reduction/Aldol Reaction to Ketones

J. W. Bode, R. M. Fox, K. D. Baucom*
Chemoselective Amide Ligations by Decarboxylative Condensations of *N*-Alkylhydroxylamines and α-Keto Acids

A. Oleksi, A. G. Blanco, R. Boer, I. Usón, J. Aymamí, A. Rodger, M. J. Hannon, M. Coll**
Molecular Recognition of a Three-Way DNA Junction by a Metallosupramolecular Helicate

J. E. Banham, C. R. Timmel, R. J. M. Abbott, S. M. Lea, G. Jeschke**
A New Tool for Characterization of Weak Protein–Protein Interactions: Evidence from DEER for the Trimerization of a von Willebrand Factor A Domain in Solution

B. H. Lipshutz, B. A. Frieman, A. E. Tomaso, Jr.*
Copper-in-Charcoal (Cu/C): Heterogeneous, Copper-Catalyzed Asymmetric Hydrosilylations

J. T. Shaw, J. M. Mitchell*
A Structurally Diverse Library of Polycyclic Lactams Resulting from the Systematic Placement of Proximal Functional Groups

News

New Members of the Editorial Board and the International Advisory Board ____ 22

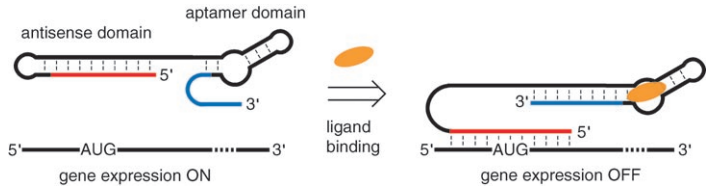
Obituary

Richard E. Smalley (1943–2005) Fullerenes *H. Kroto* ____ 26

Books

Valency and Bonding F. Weinhold, C. Landis *reviewed by P. Pyykkö* ____ 28

Highlights



A flexible platform for control of gene expression is represented by rationally designed antiswitches. These *trans*-acting riboregulators consist of an antisense domain and an aptamer domain. They are responsive to small ligands, modular, and fully tunable to target any gene of interest (see picture).

Gene Expression

R. Micura* ____ 30–31

Programmable Ligand-Controlled Riboregulators

Essays

How does one find out whether an interesting water aggregate observed in an organic crystal structure is novel? The first place to look is in the Cambridge Structural Database (CSD). The data are there, but analysis is difficult and it is not routinely done. The result? Many of the water chains, rings, sheets, and clusters reported as novel in the recent literature are actually redundant with published structures in the CSD.

Structure Elucidation

M. Mascal,* L. Infantes,* J. Chisholm* ____ 32–36

Water Oligomers in Crystal Hydrates—What's News and What Isn't?

© 2006 Wiley-VCH Verlag GmbH & Co. KGaA, Weinheim

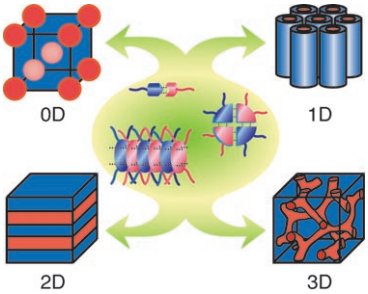
Contents

Reviews

Supramolecular Chemistry

T. Kato,* N. Mizoshita, K. Kishimoto ——— **38 – 68**

Functional Liquid-Crystalline Assemblies: Self-Organized Soft Materials



Order is power: New dynamically functional liquid crystals are formed through supramolecular self-assembly and nanosegregation. These materials exhibit anisotropic and/or enhanced properties, such as electron, ion, or molecular transport, sensory, catalytic, optical, and bioactivity.

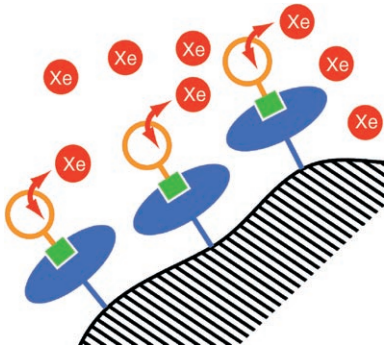
Communications

Imaging Agents

C. Hilty,* T. J. Lowery, D. E. Wemmer, A. Pines ——— **70 – 73**

Spectrally Resolved Magnetic Resonance Imaging of a Xenon Biosensor

Going hyper: A continuous flow of water saturated with hyperpolarized xenon through a glass tube assembly containing a xenon biosensor attached through its biotin tag to immobilized avidin–agarose beads (see picture) packed in between two frits results in distinct NMR signals that allow detection of the immobilized avidin analyte with high sensitivity.

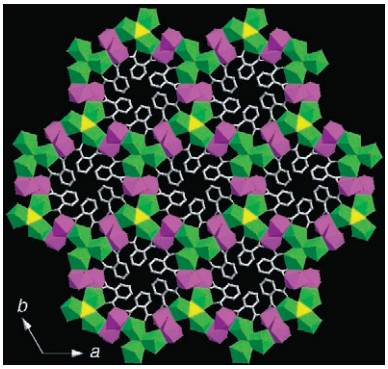


Hydrothermal Synthesis

J.-W. Cheng, J. Zhang, S.-T. Zheng, M.-B. Zhang, G.-Y. Yang* ——— **73 – 77**

Lanthanide–Transition-Metal Sandwich Framework Comprising $\{Cu_3\}$ Cluster Pillars and Layered Networks of $\{Er_{36}\}$ Wheels

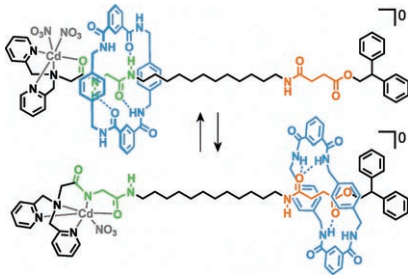
Synergistic coordination between isonicotinate (ina) and 1,2-benzenedicarboxylate (bdc) ligands under hydrothermal conditions results in the formation of two new coordination polymers, $[Er_7(\mu_3\text{-}O)(\mu_3\text{-}OH)_6(bdc)_3](ina)_9[Cu_3X_4]$ (X = Cl, Br). Wheel-shaped $[Er_{36}(\mu_3\text{-}OH)_{30}(\mu_3\text{-}O)_6(bdc)_6]^{54+}$ ions form a 2D network (see picture), which is further pillared by $[Cu_3X_4(ina)_6]^{4-}$ to give a 3D framework.



For the USA and Canada:
ANGEWANDTE CHEMIE International Edition (ISSN 1433-7851) is published weekly by Wiley-VCH PO Box 191161, D 69451 Weinheim, Germany. Air freight and mailing in the USA by Publications Expediting Inc. 200 Meacham Ave., Elmont, NY 11003. Periodicals postage paid at Jamaica NY 11431. US POSTMASTER: send address changes to *Angewandte Chemie*, Wiley-VCH, 111 River Street, Hoboken, NJ 07030. Annual subscription price for institutions: US$ 5685/5168 (valid for print and electronic / print or electronic delivery); for individuals who are personal members of a national chemical society prices are available on request. Postage and handling charges included. All prices are subject to local VAT/sales tax.

© 2006 Wiley-VCH Verlag GmbH & Co. KGaA, Weinheim

Shuttle service: Progressive binding of a transition-metal ion to a peptide station (highlighted in green in the picture) displaces the macrocycle (blue) to an alternative station (orange) in a hydrogen-bonded molecular shuttle.

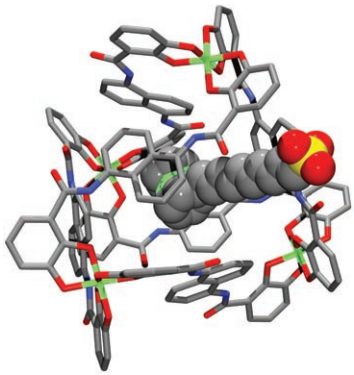


Rotaxanes

D. S. Marlin, D. González Cabrera, D. A. Leigh,* A. M. Z. Slawin —— 77 – 83

Complexation-Induced Translational Isomerism: Shuttling through Stepwise Competitive Binding

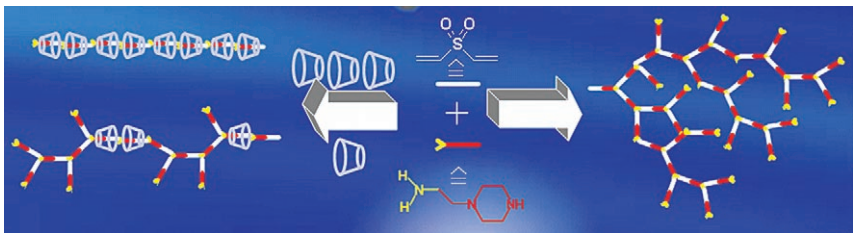
A protruding tail: A guest composed of a cationic sandwich complex, an alkyl chain, and a sulfonate anionic group is partially incorporated within a host $[Ga_4L_6]^{12-}$ cluster (see scheme). The cationic head group is quickly incorporated into the cavity of the host, while the sulfonate unit at the other end of the chain is not, as the alkyl sulfonate tail protrudes through an opening in a triangular face of the tetrahedral cluster.



Host–Guest Systems

B. E. F. Tiedemann, K. N. Raymond* —— 83 – 86

Dangling Arms: A Tetrahedral Supramolecular Host with Partially Encapsulated Guests



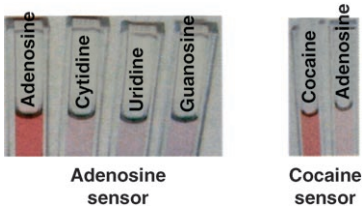
Polymer Architectures

L. Chen, X. Zhu,* D. Yan,* Y. Chen, Q. Chen, Y. Yao —— 87 – 90

Controlling Polymer Architecture through Host–Guest Interactions

A supramolecular method to control polymer architectures (see picture) is demonstrated with the synthesis of a series of poly(sulfone–amine) samples with various degrees of branching merely by changing the amount of host (β-cyclodextrin) present. Further modification of the polymer chains allows the preparation of condensation polymers with peculiar topological structures, functionalities, and properties.

Apt to change color: DNA aptamers have been used to assemble DNA-functionalized gold nanoparticles to produce highly sensitive and selective colorimetric sensors with an instantaneous color response on addition of a substrate. The general method has been shown for adenosine and cocaine (see picture), but should be applicable to any aptamer of choice.



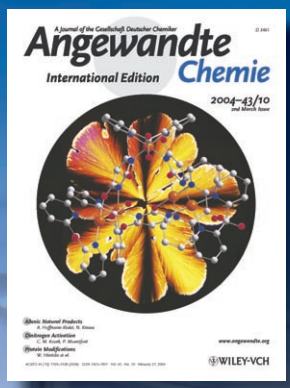
Biosensors

J. Liu, Y. Lu* —— 90 – 94

Fast Colorimetric Sensing of Adenosine and Cocaine Based on a General Sensor Design Involving Aptamers and Nanoparticles

© 2006 Wiley-VCH Verlag GmbH & Co. KGaA, Weinheim

The best in chemistry – for more than hundred years



A Journal of the Gesellschaft Deutscher Chemiker

Angewandte
International Edition **Chemie**

www.angewandte.org

1888: ***The beginning of a success story***

Constant Innovations

1962: *First issue of the International Edition*
1976: *Graphical abstracts*
1979: *Cover pictures*
1988: *Centenary of Angewandte*
1989: *Routine use of color*
1991: *New section: Highlights*
1992: *Computerized editorial tracking system*
1995: *Internet service for readers*
1998: *Regular press service; full-text online*
2000: *New section: Essays; EarlyView: Communications available online ahead of the printed version*
2001: *New section: Microreviews*
2002: *Online submission of manuscripts*
2003: *Weekly publication; new section: News; new layout*
2004: *Backfiles (1962-1997); ManuscriptXpress: Online system for authors and referees*



Angewandte's advisors...

K.C. Nicolaou
The Scripps Research Institute and University of California San Diego (La Jolla, USA)

» ***Angewandte Chemie*** *has been highly influential in shaping the art of publishing chemical innovations and I feel privileged to be part of its Advisory Board. Eliciting admiration and respect from both readers and authors alike, its editorial staff should be commended for creating a new and exciting image of this most admired journal.* «

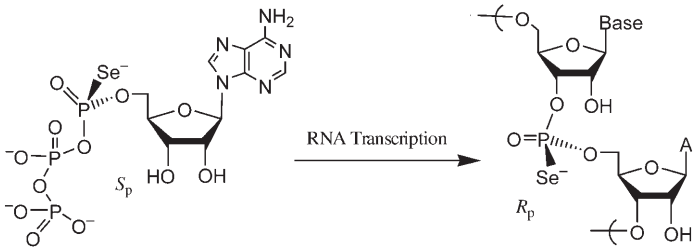
Angewandte Chemie International Edition *is a journal of the German Chemical Society (GDCh)*

GDCh

WILEY InterScience® DISCOVER SOMETHING GREAT

WILEY-VCH

95203123_gu

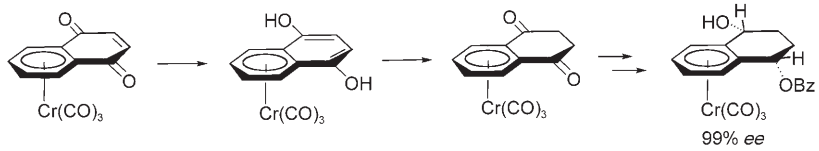


Seleno-Modified RNA

N. Carrasco, J. Caton-Williams, G. Brandt, S. Wang, Z. Huang* ——— 94 – 97

Efficient Enzymatic Synthesis of Phosphoroselenoate RNA by Using Adenosine 5′-(α-*P*-Seleno)triphosphate

Se the way to RNA: Adenosine 5′-(α-*P*-seleno)triphosphate (ATPαSe) has been synthesized and efficiently and diastereoselectively incorporated into RNA through enzymatic synthesis (see scheme). The digestion of the phosphoroselenoate RNA with phosphodiesterase is slower than that of the nonmodified RNA. This enzymatic synthesis can be generally applied in the preparation of multimilligram quantities of selenium-derivatized RNAs for X-ray crystallography.



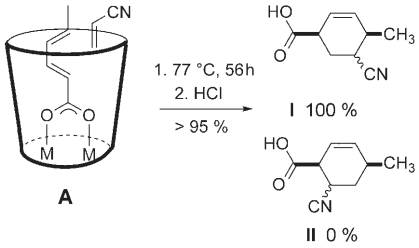
Tautomerism

E. P. Kündig,* A. Enríquez García, T. Lomberget, G. Bernardinelli ——— 98 – 101

Rediscovery, Isolation, and Asymmetric Reduction of 1,2,3,4-Tetrahydronaphthalene-1,4-dione and Studies of Its [Cr(CO)3] Complex

For 25 years it has been known that 1,4-dihydroxynaphthalene and tetrahydronaphthalene-1,4-dione coexist as stable tautomers; however, the dione has now emerged as an interesting starting material for synthesis. Its efficient isolation is reported, and the corresponding [Cr(CO)3] complexes of the two tautomers are prepared, thus leading to efficient desymmetrization using chiral diamine acyl-transfer catalysts (see scheme).

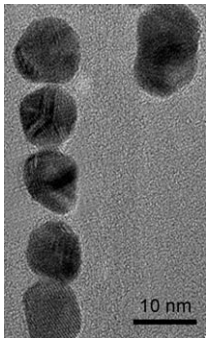
The regioselectivity of the Diels–Alder reaction between ω-substituted dienoates and unsymmetrical dienophiles can be strictly controlled by "calixarene-like" metal complexes of type **A** (see scheme). The reaction of the dienoate coligand in **A** with acrylonitrile leads to the exclusive formation of the regioisomer adduct **I**, which is in striking contrast to the low regioselectivity of the background reaction.



Synthetic Methods

S. Käss, T. Gregor, B. Kersting* ——— 101 – 104

Diels–Alder Reactivity of Binuclear Complexes with Calixarene-like Structures



A simple and facile method has been developed that allows water-soluble hybrid materials of Au nanoparticles and hole-doped single-walled carbon nanotubes (SWNTs) to be prepared. Uniformly arranged Au nanoparticles (see TEM image) were obtained by the addition of metal salts to surfactant-suspended SWNTs in water using the solution-phase dispersion technique.

Nanostructures

D. S. Kim, T. Lee, K. E. Geckeler* ——— 104 – 107

Hole-Doped Single-Walled Carbon Nanotubes: Ornamenting with Gold Nanoparticles in Water

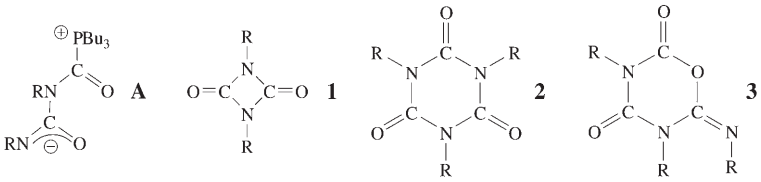
© 2006 Wiley-VCH Verlag GmbH & Co. KGaA, Weinheim

Contents

Reaction Mechanisms

Z. Pusztai, G. Vlád, A. Bodor, I. T. Horváth,* H. J. Laas, R. Halpaap, F. U. Richter* _____ **107 – 110**

In Situ NMR Spectroscopic Observation of a Catalytic Intermediate in Phosphine-Catalyzed Cyclo-Oligomerization of Isocyanates

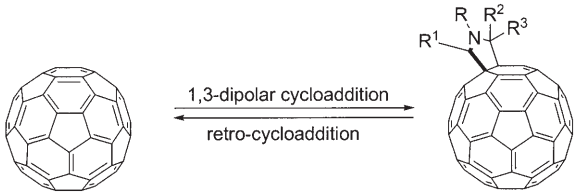


Caught in action: A mechanistic understanding of the tri-*n*-butylphosphine-catalyzed cyclo-oligomerization of alkyl isocyanates (RNCO, R = *n*Bu, *n*Hex) to products **1**–**3** has been developed at the molecular level. One of the key catalytic intermediates **A** was structurally characterized by in situ NMR spectroscopic analysis.

Fullerene Chemistry

N. Martín,* M. Altable, S. Filippone, A. Martín-Domenech, L. Echegoyen,* C. M. Cardona _____ **110 – 114**

Retro-Cycloaddition Reaction of Pyrrolidinofullerenes

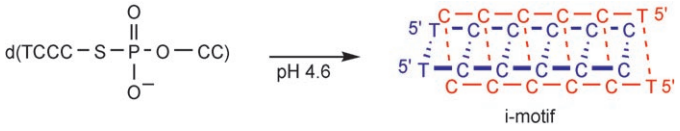


All things retro: Pyrrolidinofullerenes undergo a retro-cycloaddition reaction to afford the corresponding fullerene (C_{60}, C_{70}, or an endohedral C_{80} metallofullerene; see scheme) in quantitative yield upon treatment with an excess of a dipolarophile (maleic anhydride or *N*-phenylmaleimide) in *o*-dichlorobenzene. The reaction works efficiently with higher fullerenes and has allowed the isolation of one of the constitutional isomers of $Sc_3N@C_{80}$.

DNA Structures

J. A. Brazier, J. Fisher,* R. Cosstick* _____ **114 – 117**

Stabilization of the DNA I-Motif Structure by Incorporation of 3′-*S*-Phosphorothiolate Linkages

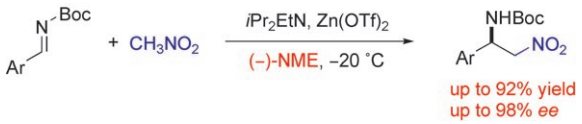


A stable i: The i-motif is a unique, four-stranded DNA structure associated with cytosine-rich sequences at the ends of human chromosomes. This is the first report of an i-motif stabilized by a deoxycytidine analogue and demonstrates the importance of the sugar conformation in the i-motif structure.

Aza-Henry Reaction

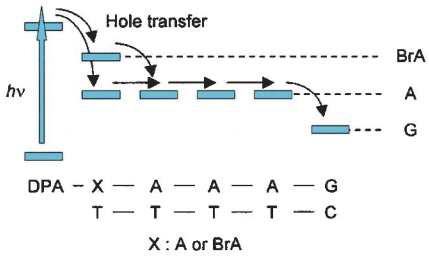
C. Palomo,* M. Oiarbide, R. Halder, A. Laso, R. López _____ **117 – 120**

Enantioselective Aza-Henry Reactions Assisted by Zn^{II} and *N*-Methylephedrine



Hooray aza-Henry! A combination of zinc triflate, an amine base, and (−)-*N*-methylephedrine (NME), which can be easily recovered and reused, leads to high enantioselectivities in the aza-Henry reaction of *N*-Boc-protected aldimines and nitromethane (see scheme; Boc = *tert*-butyloxycarbonyl).

© 2006 Wiley-VCH Verlag GmbH & Co. KGaA, Weinheim

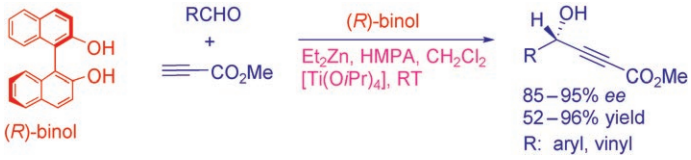


Base jumping: A long-lived charge-separated state has been generated in high yield for DNA modified with a diphenylacetylene derivative (DPA) through an adenine(A)-base-hopping mechanism (see diagram). Modulation of the redox properties of the photosensitizer and bridge bases (e.g., by employing a brominated adenine (BrA)) can improve the yield of the charge-separated state.

DNA Devices

T. Takada, K. Kawai, M. Fujitsuka, T. Majima* ——— **120 – 122**

High-Yield Generation of a Long-Lived Charge-Separated State in Diphenylacetylene-Modified DNA

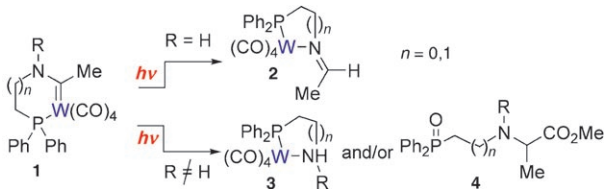


Alkynoates are added to aromatic and α,β-unsaturated aldehydes in the synthesis of the title compounds in optically active form. This highly enantioselective and useful method is carried out under mild reaction conditions and employs the readily available chiral 1,1′-bi-2-naphthol (binol) ligand and the metal reagents Et_2Zn and $[Ti(OiPr)_4]$ (see scheme; HMPA = hexamethylphosphoramide).

Asymmetric Synthesis

G. Gao, Q. Wang, X.-Q. Yu,* R.-G. Xie, L. Pu* ——— **122 – 125**

Highly Enantioselective Synthesis of γ-Hydroxy-α,β-acetylenic Esters by Asymmetric Alkyne Addition to Aldehydes

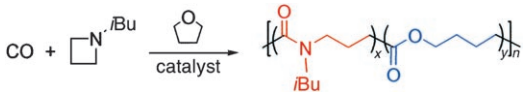


The light fantastic: Tungsten(0) Fischer carbene complexes, previously considered to be photo-inert, produce, by adequately choosing the ligands, three classes of photoproducts (see scheme). Thus, irradiation of tetracarbonyltungsten(0) carbene complexes **1** leads to *syn*-metalated imines **2**, amino complexes **3**, and α-amino esters **4**. Reasonable reaction pathways are proposed for all these processes.

Carbene Complex Chemistry

I. Fernández, M. A. Sierra,* M. Gómez-Gallego, M. J. Mancheño, F. P. Cossío* ——— **125 – 128**

The Photochemical Reactivity of the "Photo-Inert" Tungsten (Fischer) Carbene Complexes



A living polymerization: Poly(amide-*co*-ester)s with either gradient or segmental ester distribution are formed by the cobalt-catalyzed polymerization of azetidine in THF in the absence or presence of LiI, respectively. Periodic addition of azetidine results in copolymers with multiple amide blocks separated by ester segments (see picture). The polymers undergo a two-stage chemical degradation.

Polymerization

G. Liu, L. Jia* ——— **129 – 131**

Cobalt-Catalyzed Carbonylative Copolymerization of *N*-Alkylazetidines and Tetrahydrofuran

© 2006 Wiley-VCH Verlag GmbH & Co. KGaA, Weinheim

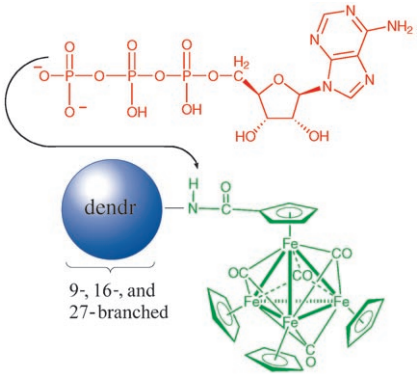
Contents

Dendrimers

J. R. Aranzaes, C. Belin, D. Astruc* ——— 132 – 136

Assembly of Dendrimers with Redox-Active [{CpFe(μ_3-CO)}$_4$] Clusters at the Periphery and Their Application to Oxo-Anion and Adenosine-5′-Triphosphate Sensing

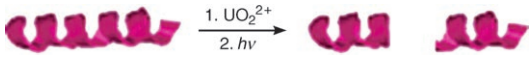
9, 16, or 27 [CpFe(μ_3-CO)]$_4$ clusters contain the title assemblies (see picture). The one-electron oxidation $Fe_4 \rightarrow Fe_4^+$ of all Fe_4 units appears as a single reversible cyclic voltammetry wave and was used in solution and with dendrimer-modified electrodes for oxo-anion recognition. ATP^{2-} is selectively recognized and better than $H_2PO_4^-$. The larger the dendrimer, the easier is the re-use of the modified electrode sensor.



Protein Photocleavage

M. R. Duff, Jr., C. V. Kumar* — 137 – 139

Site-Selective Photocleavage of Proteins by Uranyl Ions



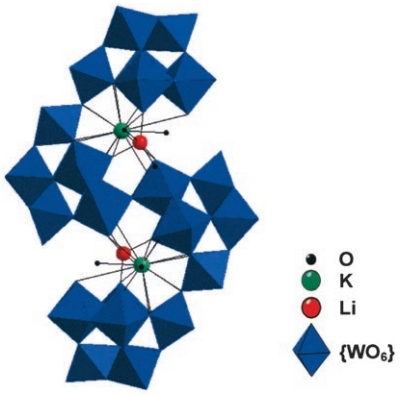
Footprints of a metal: The uranyl ion (UO_2^{2+}) binds to selected proteins, at specific sites, with high affinities. This property was exploited to photocleave proteins at the UO_2^{2+}-binding site. Quenching studies show that free UO_2^{2+} is not responsible for the cleavage. This is the first report of protein photocleavage with high selectivity by the uranyl ion, upon excitation with visible light.

Polyoxometalates

N. Leclerc-Laronze, M. Haouas, J. Marrot, F. Taulelle, G. Hervé* ——— 139 – 142

Step-by-Step Assembly of Trivacant Tungstosilicates: Synthesis and Characterization of Tetrameric Anions

Tungstosilicate building blocks: Two dimeric anions, α-[{$K(H_2O)_2$}-$Si_2W_{18}O_{66}$]$^{15-}$, obtained by self-association of the monomeric species $[SiW_9O_{34}]^{10-}$ upon acidification, can be connected directly (see picture). However, in the presence of silicic acid the anions are linked through an electrophilic $[Si_4O_4]^{8+}$ ring.

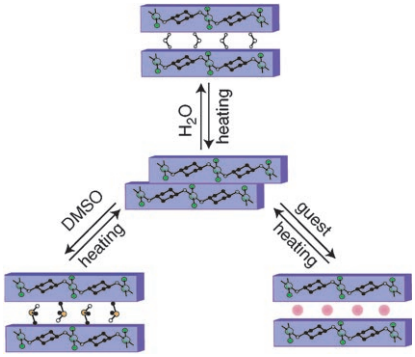


Host–Guest Systems

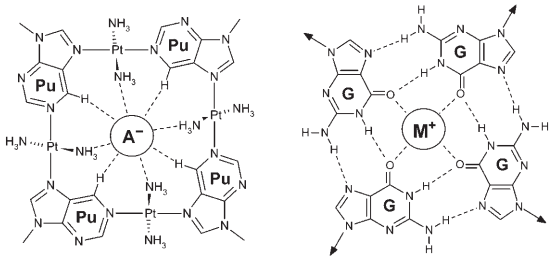
D. Braga,* M. Curzi, A. Johansson, M. Polito, K. Rubini, F. Grepioni* ——— 142 – 146

Simple and Quantitative Mechanochemical Preparation of a Porous Crystalline Material Based on a 1D Coordination Network for Uptake of Small Molecules

Kneading them in: A versatile porous material based on the 1D coordination network [$CuCl_2$(dace)]$_\infty$ (dace = *trans*-1,4-diaminocyclohexane) can be inexpensively prepared by a mechanochemical reaction followed by mild thermal treatment. The system is able to reversibly absorb molecules from solution or by simple kneading, while guest desorption from the product invariably leads back to the unsolvated form.



© 2006 Wiley-VCH Verlag GmbH & Co. KGaA, Weinheim

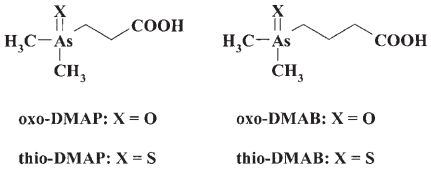


Variations on nature: Coordinative metal–ligand bonds instead of cyclic hydrogen bonds, an anion (sulfate) in the center rather than a cation, and an overall positive charge instead of a negative one are the major differences between the artificial platinum–purine quartet **2** (left) and the naturally occurring guanine quartet G_4 (right).

Nucleobase–Metal Complexes

M. Roitzsch, B. Lippert* ——— **147 – 150**

Inverting the Charges of Natural Nucleobase Quartets: A Planar Platinum–Purine Quartet with Pronounced Sulfate Affinity

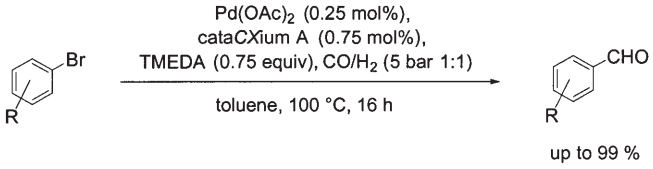


Is fish a healthy food? Arsenolipids present in cod liver are metabolized by humans to arsenic-containing fatty acids. Four of these metabolites were identified in human urine after consumption of cod liver and characterized by mass spectrometry and chromatography.

Arsenic Metabolites

E. Schmeisser, A. Rumpler, M. Kollroser, G. Rechberger, W. Goessler, K. A. Francesconi* ——— **150 – 154**

Arsenic Fatty Acids Are Human Urinary Metabolites of Arsenolipids Present in Cod Liver



The key to the general and efficient palladium-catalyzed formylation of aryl and heteroaryl bromides is the use of the di-1-adamantyl-*n*-butylphosphane (cataCXium A) as ligand. Low pressure of the synthesis gas and appropriate choice of the base are also important for high yields (up to 99%) of a broad range of (hetero)aromatic aldehydes at unprecedented low catalyst concentrations (see scheme; TMEDA = *N*,*N*,*N*′,*N*′-tetramethylethylenediamine).

Reductive Carbonylation VIP

S. Klaus, H. Neumann, A. Zapf, D. Strübing, S. Hübner, J. Almena,* T. Riermeier, P. Groß, M. Sarich, W.-R. Krahnert, K. Rossen, M. Beller* ——— **154 – 158**

A General and Efficient Method for the Formylation of Aryl and Heteroaryl Bromides



The conversion of electron-rich aryl bromides into the corresponding Grignard compounds proceeds within 2 h at 25 °C in the presence of 0.55 equivalents of the new reagent $sBu_2Mg{\cdot}LiCl$. The high reactivity of magnesiates is rationalized by quantum chemical model calculations, and selected examples illustrate the benefits of aryl magnesium compounds for organic syntheses.

Grignard Reagents

A. Krasovskiy, B. F. Straub,* P. Knochel* ——— **159 – 162**

Highly Efficient Reagents for Br/Mg Exchange

© 2006 Wiley-VCH Verlag GmbH & Co. KGaA, Weinheim

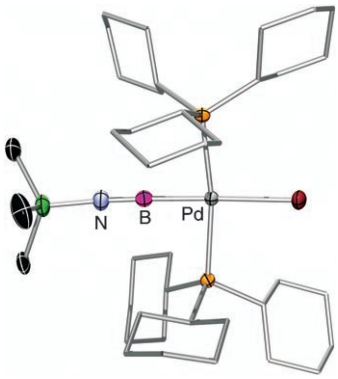
Contents

Iminoboryl Complexes

H. Braunschweig,* K. Radacki, D. Rais, K. Uttinger ——— **162 – 165**

Synthesis and Characterization of Palladium and Platinum Iminoboryl Complexes

A terminal condition: The palladium and platinum complexes *trans*-[$(Cy_3P)_2M(B{\equiv}NSiMe_3)(Br)$] feature an unprecedented terminally bound iminoboryl ligand. The compounds are synthesized upon facile elimination of Me_3SiBr at room temperature from the postulated intermediates *trans*-[$(Cy_3P)_2M(Br)\{B(Br)N(SiMe_3)_2\}$], which are obtained by oxidative addition of the B–Br bond in $(Me_3Si)_2NBBr_2$ to $[M(PCy_3)_2]$ (M = Pd, Pt). Cy = cyclohexyl.

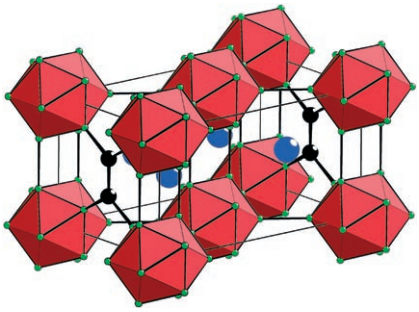


Boride Carbides

N. Vojteer, H. Hillebrecht* ——— **165 – 168**

$Li_2B_{12}C_2$ and $LiB_{13}C_2$: Colorless Boron-Rich Boride Carbides of Lithium

Wade was right: $Li_2B_{12}C_2$ and $LiB_{13}C_2$, the first boron-rich boride carbides of lithium, are (nearly) colorless and stoichiometrically composed. Their crystal structures are characterized by B_{12} icosahedra and C_2 and CBC units, respectively, forming a three-dimensional framework with Li cations in the voids. The charge distribution can be described by Wade's rules: $(Li^+)_2B_{12}^{2-}C_2$ and $(Li^+)B_{12}^{2-}(CBC^+)$. The synthesis succeeded in molten metals at high temperatures.



The issues for December 2005 appeared online on the following dates
Issue 45: November 16 · Issue 46: November 22 · Issue 47: December 2 · Issue 48: December 8

Sources

Product and Company Directory

You can start the entry for your company in "Sources" in any issue of *Angewandte Chemie*.

If you would like more information, please do not hesitate to contact us.

Wiley-VCH Verlag – Advertising Department
Tel.: 0 62 01 - 60 65 65
Fax: 0 62 01 - 60 65 50
E-Mail: MSchulz@wiley-vch.de

Service

Notice to Authors ——— *20 – 21*

Keywords ——— *170*

Authors ——— *171*

Preview ——— *173*

© 2006 Wiley-VCH Verlag GmbH & Co. KGaA, Weinheim

Corrigendum

The following article should be cited for its contribution to the preparation of organometallic polymer gels using ligand-anchored polyoxometalates: S. Favette, B. Hasenknopf, J. Vaissermann, P. Gouzerh, C. Roux, *Chem. Commun.* **2003**, 2664–2665. The authors apologize for the oversight.

Molecular and Polymeric Hybrids Based on Covalently Linked Polyoxometalates and Transition-Metal Complexes

J. Kang, B. Xu, Z. Peng,* X. Zhu, Y. Wei, D. R. Powell _____ **6902–6905**

Angew. Chem. Int. Ed. **2005**, *44*

DOI 10.1002/anie.200501924

I want to be recognised.

The 2005 AstraZeneca Research Awards in Organic Chemistry

AstraZeneca is one of the world's leading pharmaceutical companies, with a powerful range of products focused on important areas of healthcare. We are committed to maintaining a flow of innovation to research new products that meet patient needs worldwide.

As a major science-based company, we believe in encouraging and rewarding scientific excellence. We are therefore pleased to announce the 2005 AstraZeneca Research Awards in Organic Chemistry. The awards were established in 1990 to recognise the achievements of outstanding young chemists in academia. The award is made each year to two European scientists under 40 years of age who have made significant contributions to the field of Organic Chemistry. In 2005, each winner will receive £12,500 to further their research activities, as well as ongoing studentship support.

A selection panel, consisting of a senior UK academic and researchers from AstraZeneca discovery and development, have chosen the following winners for 2005:

Dr Veronique Gouverneur (University of Oxford) for her innovative research into efficient methodologies towards the synthesis of fluorinated compounds and the development of catalytic antibodies and their application towards the synthesis of key chiral intermediates.

Professor Adam Nelson (University of Leeds) for his imaginative research in the synthesis of complex molecules, in particular two-dimensional approaches for the synthesis of chiral late-stage natural product precursors by desymmetrisation.

The awards will be presented on Tuesday 29th November at AstraZeneca Charnwood. For further information visit our website at www.astrazeneca.co.uk



AstraZeneca
life inspiring ideas

© 2006 Wiley-VCH Verlag GmbH & Co. KGaA, Weinheim



New Members of the Editorial Board...

The Members of the Editorial Board of *Angewandte Chemie* are selected by the GDCh (German Chemical Society) to advise the journal's editorial team on the content and organization of the journal. The members, who represent universities, research establishments (Max Planck Society; MPG), and industry, meet once annually at the editorial board meeting. The term of office is usually four years, although reappointment is possible.

Physical Chemistry: Michael Dröscher



M. Dröscher

Since 2002, M. Dröscher has been Senior Vice-President of Corporate Innovation Management at Degussa AG in Düsseldorf. His career started at the University of Mainz (Germany), where he obtained his PhD in physical chemistry under the guidance of G. Wegner in 1975. He subsequently spent a year at IBM in San José (USA) as a postdoctoral fellow. He completed his habilitation in macromolecular chemistry in 1981 at the University of Freiburg, where he worked among other things on segmented polyetheresters. In 1982 he moved into industry (Hüls AG, Marl), where he was involved in the development of technical plastics. In 1988 he was appointed Honorary Professor at the University of Münster. From 1990 to 1992 he was director of the pilot plant in Herne, before taking over as head of the department of plastics and the environment. In 1996 he was appointed Spokesman of the Screening Committee, whose task was the identification of new business ventures for Hüls AG. These project ideas led, at the end of 1997, to the creation of CREAVIS Technologies and Innovations, which was directed by Dröscher until 2002. The German Bunsen Society for Physical Chemistry (Deutsche Bunsengesellschaft für Physikalische Chemie) has elected Dröscher as its chairman for 2005/06.

Theoretical Chemistry: Walter Thiel

W. Thiel and co-workers at the Max Planck Institute (MPI) for Coal Research in Mülheim deal with theoretical chemistry, using ab initio, density functional, semiempirical, and combined quantum/molecular mechanical methods. These methods are applied to investigate enzymatic reactions, the structure and reactivity of small molecules, and catalytic reactions of transition-metal compounds. Recently, Thiel reported in *ChemPhysChem* on unusual temperature effects in propene polymerization using stereorigid zirconocene catalysts.[1]



W. Thiel

Thiel received his PhD in 1973 under the guidance of A. Schweig at the University of Marburg (Germany). He then carried out postdoctoral research with M. J. S. Dewar at the University of Texas in Austin (USA). He returned to Marburg, where in 1981 he completed his habilitation. In 1983 he joined the University of Wuppertal, and in 1992 he moved to the University of Zürich. Since 1999, he is director at the MPI in Mülheim.

Analytical Chemistry: Otto S. Wolfbeis

O. Wolfbeis completed his PhD under the supervision of H. Junek at the University of Graz (Austria) in 1972 and subsequently carried out postdoctoral work with E. A. Koerner von Gustorf at the Max Planck Institute for Radiochemistry in Mülheim and then E. Lippert at the Technical University of Berlin. He then joined the University of Graz, and in 1990 he founded the Institute of Optical Sensors in Graz. In 1995 he accepted a chair of analytical and interface chemistry at the University of Regensburg (Germany). The research interests of his group are focused on chemical and biochemical sensors and laser fluorescence spectroscopy, including the development of probes and stains, as well as enzyme, protein, and gene assays. Wolfbeis and co-workers recently reported on chameleon labels for staining and quantifying proteins in *Angewandte Chemie*.[2]



O. S. Wolfbeis

... and the International Advisory Board

Since 1995, an international advisory board supports the work of the editorial team. To an extent, the members of the advisory board act as ambassadors for *Angewandte Chemie* and their reputations help increase the confidence of its readers and authors.

Biochemistry: Lia Addadi

L. Addadi studied organic chemistry at the Università degli Studi di Padova (Italy) and obtained her PhD in 1979 from the Weizmann Institute in Rehovot (Israel) under the guidance of M. Lahav. She then worked as a postdoctoral researcher in the group of J. R. Knowles at Harvard University (USA) before returning in 1988 to the Weizmann Institute as a professor. The research interests of her group lie in bio-



L. Addadi

WILEY InterScience DISCOVER SOMETHING GREAT
© 2006 Wiley-VCH Verlag GmbH & Co. KGaA, Weinheim

mineralization and the interactions of cells, proteins, and antibodies with crystals. Addadi serves as a member of the advisory board for *ChemBioChem*, and recently discussed therein the concept of the spatial and temporal sequence of events during cell adhesion, and reported on a new family of proteins rich in aspartic acid from the prismatic shell matrix of the bivalve *Atrina rigida*.[3]

Novel Materials: Chun-Li Bai

C.-L. Bai obtained his PhD in 1985 from the Institute of Chemistry of the Chinese Academy of Sciences in Beijing. After a postdoctoral stay at the California Institute of Technology in Pasadena (USA), he returned to China in 1987. During 1991–92, he was a visiting professor in Japan at the University of Tohoku in Sendai. Bai is interested in the development of new scanning probe microscopes for surface analysis. He recently reported in *Angewandte Chemie* on the mass production and high photocatalytic activity of ZnS nanoporous nanoparticles, and in *ChemPhysChem* on the effect of polarity on co-adsorbed molecular nanostructures of substituted phthalocyanine and thiol molecules.[4] Bai is Executive Vice-President of the Chinese Academy of Sciences and President of the Chinese Chemical Society.



C.-L. Bai

Medicinal Chemistry: Scott Biller



S. Biller

S. Biller is Head of Global Discovery Chemistry at the Novartis Institutes for Biomedical Research and is responsible for projects in combinatorial, medicinal, and computational chemistry across the Novartis sites in Basel, Cambridge (MA), Vienna, and Horsham (UK). He carried out undergraduate research with K. B. Sharpless (Massachusetts Institute of Technology, USA), completed his PhD in 1982 with D. Evans at the California Institute of Technology, and then worked as a postdoctoral fellow with G. Stork at Columbia University in New York (1982–83). During his career he has held many key positions in the field of drug development, including Vice-President of Pharmaceutical Candidate Optimization at Bristol–Myers Squibb (BMS), Head of Discovery Chemistry at BMS, and Executive Director of Metabolic Diseases Chemistry.

Organic Chemistry: Andrew B. Holmes

A. B. Holmes studied chemistry at the University of Melbourne (Australia) and completed his PhD on heteroannulenes in 1971 under the guidance of F. Sondheimer at University College in London. He made the transition to natural products synthesis during his postdoctoral stay with A. Eschenmoser at the ETH Zürich. In 1972 he joined the University of Cambridge (UK) as a lecturer. In 1994 he was appointed Director of the Melville Laboratory for Polymer Synthesis and was later promoted to professor in 1998. In 2004 Holmes moved to Imperial College London before returning to the University of Melbourne. His research interests range from the chemistry of natural products to the development of conjugated polymers for diodes, transistors, and solar cells. He recently reported on blue-light-emitting polyfluorene copolymers with twisted biphenyl moities.[5] In 2000 Holmes was elected as a Fellow of the Royal Society. He is a member of the editorial boards for *Macromolecular Chemistry and Physics* and *Macromolecular Rapid Communications*, among others.



A. B. Holmes

Physical Chemistry: Yuan-Tseh Lee

Y.-T. Lee studied chemistry in Taiwan. In 1965 he completed his PhD under the guidance of B. Mahan at the University of California in Berkeley (USA), where he continued postdoctoral research before joining D. R. Herschbach at Harvard University in 1967. He then joined the University of Chicago as assistant professor and was promoted to full professor five years later. In 1974 he moved back to Berkeley as professor of chemistry and principal investigator at the Lawrence Berkeley Laboratory of the University of California. In 1994 he was appointed President of the Academia Sinica in Taipeh (Taiwan). His research concerns the dynamics of chemical elementary processes, the topic for which he was jointly awarded the Nobel Prize for Chemistry, with D. R. Herschbach and J. C. Polanyi, in 1986.[6] His group are interested in the use of crossed molecular beams and laser techniques to study general reactions. Lee serves, amongst others, as a member of the editorial board for *ChemPhysChem*.



Y.-T. Lee

Organic Chemistry: Shengming Ma

S. Ma received his Masters degree (1988) and his PhD (1990) from the Shanghai Institute of Organic Chemistry (SIOC) of the Chinese Academy of Sciences under the guidance of X. Lu. He left his position as assistant professor there in 1992 to carry out postdoctoral research with L. M. Venanzi at the ETH Zürich and then with E. Negishi at Purdue University (West Lafayette, IN, USA). In 1997 he returned to the SIOC as professor, and since 2003 he is professor at the Zhejiang University in Hangzhou. Ma is deputy editor-in-chief of the *Chinese Journal of Chemistry*. In 2005, his group published two communica-



S. Ma

© 2006 Wiley-VCH Verlag GmbH & Co. KGaA, Weinheim

tions in *Angewandte Chemie* on catalytic allene chemistry and a minireview on the 1,4-migration of rhodium and palladium in catalytic organometallic reactions.[7]

Bioinorganic Chemistry: Bernard Meunier



B. Meunier

B. Meunier studied organometallic chemistry with R. Corriu and H. Felkin. He has worked for the CNRS (Centre National de la Recherche Scientifique) since 1973, first at the Institute for the Chemistry of Natural Products in Gif-sur-Yvette near Paris, then from 1979 at the Laboratory of Coordination Chemistry in Toulouse, where he has been associate director since 2003. He has also taught at the École Polytechnique in Paris since 1993. Meunier has been a member of the French Academy of Sciences since 1999, and since 2004 he is President of the CNRS. The research activities of his group are focused on biomimetic catalysis, oxidation reactions, and bioinorganic and medicinal chemistry. In 2005, he reported in *ChemBioChem* on the use of short duplexes for the analysis of sequence-dependent cleavage of DNA by a chemical nuclease.[8a] In a review in *Advanced Synthesis & Catalysis*, he presented a survey of biomimetic catalysts for the oxidative activation of drugs.[8b] Meunier is a member of the editorial boards of the *European Journal of Inorganic Chemistry* and *ChemBioChem*.

Nanotechnology: Chad Mirkin



C. Mirkin

C. Mirkin obtained his PhD under the guidance of G. L. Geoffroy at Pennsylvania State University (USA) in 1989, and then worked with M. Wrighton at the Massachusetts Institute of Technology. His main focus there was synthetic organometallic chemistry. In 1991 he joined the Northwestern University at Evanston (Chicago) as assistant professor. Presently he holds several chairs there and is also Director of the Institute for Nanotechnology. His interests lie in the development of methods to control the architecture of molecules and materials on the nanometer scale and the application of such components in chemical and biological analytics, lithography, catalysis, and optics. Mirkin is a chairman of the editorial board of *Small*. In *Angewandte Chemie* he reviewed the development of dip-pen nanolithography, while more recently in *Small* he reported on parallel dip-pen nanolithography on the centimeter scale with less than 100 nm resolution.[9]

Bioorganic Chemistry: Klaus Müller

K. Müller completed his PhD in 1970 under the guidance of A. Eschenmoser at the ETH Zürich and then carried out postdoctoral research with G. L. Closs at the University of Chicago, where he studied reactions of radical ions using NMR spectroscopy.



K. Müller

During 1971–74, he was a visiting lecturer of theoretical and physical organic chemistry at Harvard University. He then returned to the ETH Zürich and completed his habilitation in 1977 on the relationship between the structure, properties, and reactivity of strained heterocycles. In the early 1980s, his focus turned toward molecular recognition and exploration of biomacromolecular structures. In 1982, Müller joined Hoffmann La Roche AG (Basel) and set up a group for the molecular modeling and structure determination of biomacromolecules. He is presently Head of Science and Technology Relations and a member of the board of the Roche Research Foundation. Since 1990, he is professor at the University of Basel. He is a member of the editorial boards of *Chemistry – A European Journal* and *ChemBioChem*, for which he was the guest editor of a special issue on "Fluorine in the Life Sciences" (5/2004). He co-authored a review on the orthogonal multipolar interactions in chemical and biological structures, which recently appeared in *Angewandte Chemie*.[10]

Organic Chemistry: Eiichi Nakamura

E. Nakamura obtained his PhD in 1978 from the Tokyo Institute of Technology under the guidance of I. Kuwajima. After a postdoctoral stay in the group of G. Stork at Columbia University (New York), he returned in 1980 as assistant professor to the Tokyo Institute of Technology, where he was later appointed full professor (1993). Since 1995, he is affiliated to the University of Tokyo. In 2001 Nakamura received the Silver Nagoya Medal. In 2000 he founded the Tateshina Conference on Organic Chemistry, which now takes place on a regular basis. During 2005 his research group published three communications in *Angewandte Chemie* reporting on the ultrarapid synthesis of ^{15}O-labeled 2-deoxy-D-glucose, the mechanism of remote conjugate additions of a lithium organocuprate to polyconjugated carbonyl compounds, and the synthesis of chiral α-fluoroketones.[11]



E. Nakamura

Organometallic Chemistry: Luis Oro

The research group of L. Oro at the University of Zaragoza focuses on organometallic chemistry (particularly with the transition metals rhodium, iridium, ruthenium, and osmium) and catalysis (hydrations, hydrosilylations, C–H activation). Oro is a foreign member of the French Academy of Sciences, President of the Real Sociedad Española de Química 2001–



L. Oro

© 2006 Wiley-VCH Verlag GmbH & Co. KGaA, Weinheim

2005, member of the advisory board of the *European Journal of Inorganic Chemistry* and joint editor of a multivolume handbook on metal clusters.[12a].

Oro obtained his PhD in 1970 at the University of Zaragoza. Following postdoctoral work with J. Lewis at the University of Cambridge, he accepted successive positions at the Universities of Zaragoza, Madrid (Complutense), and Santander. In 1982 he returned to the University of Zaragoza as professor of inorganic chemistry. His research group recently reported on oxygen activation and the formation of a doubly oxygen-bridged dirhodium complex in *Angewandte Chemie*.[12b]

[1] V. R. Jensen, M. Graf, W. Thiel, *ChemPhysChem* **2005**, *6*, 1929.

[2] B. K. Wetzl, S. M. Yarmoluk, D. B. Craig, O. S. Wolfbeis, *Angew. Chem.* **2004**, *116*, 5515; *Angew. Chem. Int. Ed.* **2004**, *43*, 5400.

[3] a) M. Cohen, D. Joester, B. Geiger, L. Addadi, *ChemBioChem* **2004**, *5*, 1393; b) B.-A. Gotliv, N. Kessler, J. L. Sumerel, D. E. Morse, N. Tuross, L. Addadi, S. Weiner, *ChemBioChem* **2005**, *6*, 304.

[4] a) J.-S. Hu, L.-L. Ren, Y.-G. Guo, H.-P. Liang, A.-M. Cao, L.-J. Wan, C.-L. Bai, *Angew. Chem.* **2005**, *117*, 1295; *Angew. Chem. Int. Ed.* **2005**, *44*, 1269, b) Z.-Y. Yang, S.-B. Lei, L.-H. Gan, L.-J. Wan, C. Wang, C.-L. Bai, *ChemPhysChem* **2005**, *6*, 65.

[5] S.-F. Lim, R. H. Friend, I. D. Rees, J. Li, Y. Ma, K. Robinson, A. B. Holmes, E. Hennebicq, D. Beljonne, F. Cacialli, *Adv. Funct. Mater.* **2005**, *15*, 981.

[6] Y.-T. Lee, *Angew. Chem.* **1987**, *99*, 967; *Angew. Chem. Int. Ed. Engl.* **1987**, *26*, 939.

[7] a) R. Qian, H. Guo, Y. Liao, Y. Guo, S. Ma, *Angew. Chem.* **2005**, *117*, 4849; *Angew. Chem. Int. Ed.* **2005**, *44*, 4771; b) S. Ma, P. Lu, L. Lu, H. Hou, J. Wei, Q. He, Z. Gu, X. Jiang, X. Jin, *Angew. Chem.* **2005**, *117*, 5409; *Angew. Chem. Int. Ed.* **2005**, *44*, 5275; c) S. Ma, Z. Gu, *Angew. Chem.* **2005**, *117*, 7680; *Angew. Chem. Int. Ed.* **2005**, *44*, 7512.

[8] a) S. Mourgues, A. Kupan, G. Pratviel, B. Meunier, *ChemBioChem* **2005**, *6*, 2326; b) J. Bernadou, B. Meunier, *Adv. Synth. Catal.* **2004**, *346*, 171.

[9] a) D. S. Ginger, H. Zhang, C. A. Mirkin, *Angew. Chem.* **2004**, *116*, 30; *Angew. Chem. Int. Ed.* **2004**, *43*, 30; b) K. Salaita, S. W. Lee, X. Wang, L. Huang, T. M. Dellinger, C. Liu, C. A. Mirkin, *Small* **2005**, *1*, 940.

[10] R. Paulini, K. Müller, F. Diederich, *Angew. Chem.* **2005**, *117*, 1820; *Angew. Chem. Int. Ed.* **2005**, *44*, 1788.

[11] a) H. Yorimitsu, Y. Murakami, H. Takamatsu, S. Nishimura, E. Nakamura, *Angew. Chem.* **2005**, *117*, 2768; *Angew. Chem. Int. Ed.* **2005**, *44*, 2708; b) N. Yoshikai, T. Yamashita, E. Nakamura, *Angew. Chem.* **2005**, *117*, 4799; *Angew. Chem. Int. Ed.* **2005**, *44*, 4721; c) M. Nakamura, A. Hajra, K. Endo, E. Nakamura, *Angew. Chem.* **2005**, *117*, 7414; *Angew. Chem. Int. Ed.* **2005**, *44*, 7248.

[12] a) *Metal Clusters in Chemistry*, (Eds.: P. Braunstein, L. A. Oro, P. R. Raithby), Wiley-VCH, Weinheim, **1999**; b) C. Tejel, M. A. Ciriano, E. Sola, M. Pilar del Río, G. Ríos-Moreno, F. J. Lahoz, L. A. Oro, *Angew. Chem.* **2005**, *117*, 3331; *Angew. Chem. Int. Ed.* **2005**, *44*, 3267.

DOI: 10.1002/anie.200504113

© 2006 Wiley-VCH Verlag GmbH & Co. KGaA, Weinheim

Richard E. Smalley: Fullerenes

Richard Errett Smalley, known to everyone as Rick, died in Houston at the age of 62 from leukemia, a disease he had battled courageously for some eight years. Together, Rick, Robert Curl, and I were awarded the Nobel Prize for Chemistry in 1996 for the discovery of C_{60} buckminsterfullerene, the third form of the element carbon.[1]



In April 1984, I visited Rice University at the invitation of my friend and fellow spectroscopist Bob Curl, who gave me a paper that Rick's group had just completed. The paper described a study of a fascinating molecule containing carbon and silicon (CCSi), and the triangular structure they had obtained fitted in neatly with our related studies at Sussex. Curl encouraged me to visit Rick's laboratory.

When I arrived there I was confronted by a dynamic and ebullient character, who enthusiastically clambered over his newest creation—a very big machine some 12 ft high which he lovingly called "Ap2". Rick liked to say *"We do things big in Texas"*. He proudly explained that his "laser vaporization cluster beam machine" could vaporize metals and other refractory materials to produce aggregates of tens of atoms stuck together in clusters. I called them "wadges", a colloquial English term which he took to (Rick liked offbeat terms like these, particularly if he coined them himself).

This really was a major technical breakthrough in materials science as up till then it had only been possible to study isolated metal atoms and occasionally dimers. Rick had now developed a way to make much bigger aggregates and study such major problems as, at what size such aggregates would start to exhibit bulk material behavior. The answer to this question is a key to understanding how one might make, for example, smaller and smaller computers.

As Rick described to me how his laser could vaporize metals, I started to wonder if he would consider a somewhat mundane little problem that had been on my mind for a few years. This was to vaporize graphite to see if ideas that I had developed about the atmospheres that surround carbon stars were right. That evening I asked Bob to work on Rick and try to get him to agree to this problem, which was really only of importance to me. I also added, as bait, the possibility that we might also solve the so-called "diffuse interstellar lines" problem, which was, and still is, a major puzzle after some 60 years.

In September 1985, we carried out the experiment and to our amazement discovered that a cage molecule consisting of sixty carbon atoms, with the same pattern as a soccer ball and now affectionately called the "buckyball", formed spontaneously. Rick was the sort of scientist who was really only interested in tackling the really *big* problems, and his genius lay in his ability not only to work out how they might be solved but to build the complex and often *large* state-of-the-art apparatus needed.

He had the rare gift of being able to get such systems to work. I remember watching him working with a colleague as the two of them pooled their considerable expertise in a synergistic and highly competitive struggle to solve a particularly complicated technical problem. I and others admired the fact that he knew every intricate detail of the problems that he was trying to solve and the apparatus he designed. He seemed to thrive on competition and even to love it.

Rick was a proud scientist; proud of what he had achieved and particularly proud of any students in his group who had green fingers similar to those he had himself. The ability to get a difficult experiment to work successfully was for Rick the supreme quality he admired. It would be fair to say that he had very strong opinions on the merits of other scientists, and few measured up to his, in my opinion somewhat restricted, subjective definition.

There were very few whom he considered worthy rivals. This may have been one reason for the fact that several papers, which were written just after our discovery, clutched at straws to try to prove wrong our contention that we had discovered the third form of carbon. I once jested after a particularly hostile paper appeared that I did not need any of his enemies as I already had enough of my own. These were difficult times (1985–1990), and both he and I were determined to prove that our contention was based on, what Rick liked to call, compelling evidence. We were able to do that; he together with Bob and his group in Texas, and I with my group in the UK, as well as together.[1]

Rick completed his PhD with Donald Levy at Chicago, and his breakthrough there was arguably as important as the development later of the cluster beam system. This system was to use an ingenious nozzle that had been developed by Wharton to effectively cool molecules down to very low temperatures so that their study by the recently developed laser fluorescence technique was facilitated. This was the launch pad for his stellar research career and I suspect his aim to tackle only *big* problems—indeed ones that he may have thought only he was capable of solving.

After the breakthrough in the isolation of C_{60} in 1990 and the discovery of its long tall cousins, the nanotubes, Rick, with typical single-mindedness, ended all his previous research programs and devoted himself to the task of realizing what he saw as the revolutionary potential of these minute tubes, which theoretically could be infinitely long but only a nanometer (100 million times smaller than a soccer ball) in diameter. It is fair to say that noone has made more important technical advances in this area than Rick, but it is also fair to say that there is still a very long way to go before the really revolutionary advances that he sought are likely to be achieved.

About two years after the Nobel Prize was awarded, Rick was diagnosed with leukemia. He fought this disease with the same steely resilience and determination he used to fight any other problem. Like many highly opinionated people who have been very successful and have strong characters, he was not always that easy to get on with. With his flamboyantly uncompromising and inspiring presentation style, he became the most visible champion of nanotechnology and its promise

WILEY InterScience DISCOVER SOMETHING GREAT
© 2006 Wiley-VCH Verlag GmbH & Co. KGaA, Weinheim

to lead to revolutionary sustainable technologies. He backed his strong opinions—in particular, in his well-publicized battles with Eric Drexler, the writer of a best-selling book on nanotechnology—with sound science and lucid argument and became an influential science advisor to the US Government.

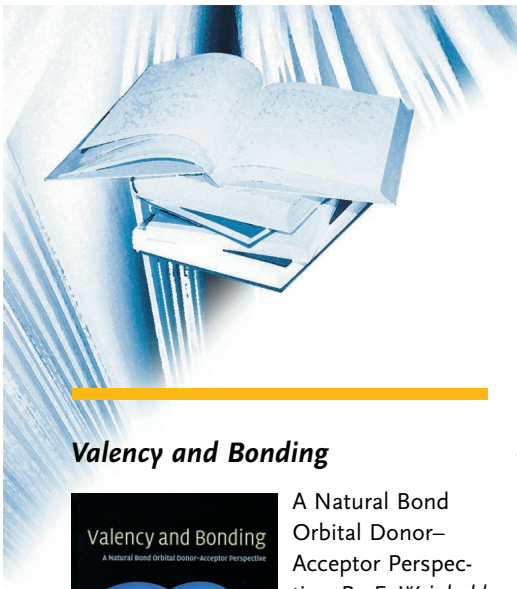
Rick has two sons, Chad by his first wife and Preston by his third. He married his fourth wife shortly before he died. The impact of Rick on my life has been immense, always exciting, always exhilarating, and always turbulent. If the efforts that Rick has initiated to realize his dream of sustainable technologies and massive energy efficiencies through nanotechnology are successful, then his influence on the future will be truly immense.

Harold Kroto
The Florida State University

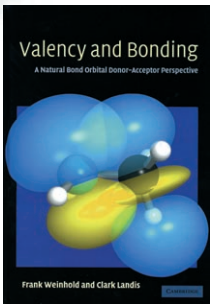
[1] a) R. E. Smalley, *Angew. Chem.* **1997**, *109*, 1667; *Angew. Chem. Int. Ed. Engl.* **1997**, *36*, 1594; b) R. F. Curl, *Angew. Chem.* **1997**, *109*, 1637; *Angew. Chem. Int. Ed. Engl.* **1997**, *36*, 1566; c) H. Kroto, *Angew. Chem.* **1997**, *109*, 1649; *Angew. Chem. Int. Ed. Engl.* **1997**, *36*, 1578.

DOI: 10.1002/anie.200504094

© 2006 Wiley-VCH Verlag GmbH & Co. KGaA, Weinheim



Valency and Bonding



A Natural Bond Orbital Donor–Acceptor Perspective. By *F. Weinhold* and *C. Landis*. Cambridge University Press, Cambridge 2005. 749 pp., hardcover £ 60.00.—ISBN 0-521-83128-4

The quantum-mechanical laws underlying chemistry are well known, and their applications to computational methods, software, and quantitative calculations are undergoing steady development. On the other hand, the step of reading out the chemistry from the final results still leaves room for personal selection, emphasis, and style. The first author is perhaps best known for his NBO (natural bond orbital) analysis, and the second one is an inorganic chemist. One opens the book with interest, to meet chemistry as interpreted by Weinhold and Landis.

Chapter 1 introduces the quantum-mechanical concepts, including natural orbitals. The Lewis pairs are identified with the NBOs that have the largest occupations. The first example in Chapter 2 is diatomic LiF, followed by its clusters and a brief discussion about electrostatic terms. The bending of heavier alkaline earth dihalides is discussed. Kaupp's review on the topic (*Angew. Chem. Int. Ed.* **2001**, *40*, 3534–3565) might have been quoted here. A new explanation in terms of π-type donor–acceptor interactions is added. Diatomic fluorides of the 3d metals are considered as models for ionic bonding to transition elements. The long Chapter 3 deals with bonding to s/p-block elements. After discussing neutral diatomics, the chapter treats conjugated and aromatic systems, hyperconjugation, and hypo- and hypervalent bonding. The bonding in H_2 is described in donor–acceptor terms. (The fact that dialkali-metal cations are longer but more strongly bonded than the neutral molecules [p. 100] was noticed by Roach and Baybutt [*Chem. Phys. Lett.* **1970**, *7*, 7] for Na_2 and K_2, but not for NaK.) Conjugation and aromaticity, hyperconjugation, hypervalency, and its counterpart hypovalency are discussed. Chapter 4 discusses the bonding in d-block elements. Some topics are the Lewis-like structures, hybridization and molecular shape, coordinative bonding, agostic interactions, and vertical trends in transition-metal bonding, including relativistic effects. Here the conclusions for Zr/Hf and Mo/W on page 551 might be checked by other methods. Dihydrogen complexes are discussed, including the *trans* effect. Chapter 5, on supramolecular bonding, covers London's theory for two partners, an NBO picture of hydrogen bonding, including dihydrogen (H···H) bonding, charge-transfer complexes, and transition-state complexes. Species, author, and subject indexes are provided.

The observations are often interesting: the traditional 2s2p hybridizations and Bent's rules come under discussion. A quantitative way to derive "natural electronegativities" from population analysis is presented. An intriguing suggestion is made (p. 480) that $TiCl_4$ could have some multiple-bonding character coming from Cl 3p π donation to the Ti 3d π orbitals. (For analogous suggestions concerning UF_6, see M. Straka et al., *Theor. Chem. Acc.* **2003**, *109*, 332.) A system of van der Waals radii, based on a given repulsion against a helium atom, is given on page 40 for the elements 1–18. These radii are useful and systematic, but naturally more compact than the alternative ones, related to the van der Waals energy minima. Interpretative aspects such as the special position of the compact, nodeless, 1s, 2p, 3d (and 4f) shells, and the general importance of nodal surfaces in increasing kinetic energy (p. 716), are mentioned.

The work also has its limitations. Most calculations in the book are based on a single model, B3LYP/6-311++G or its pseudopotential triple-zeta counterpart for heavy elements. This DFT model can be doubtful for systems with strong multiconfiguration character, such as many dimeric metal–metal bonded molecules. For van der Waals contributions, it would be entirely wrong in a supramolecular treatment. Personal terminology and symbols are used in some cases, such as "nu" bonds and "omega" bonds for *n*-electron *m*-center bonding, or the hooks for certain bonds. The statement that for a p^4 electron configuration, such as the oxygen atom ground state, the $1S^0$ state corresponds to a p sigma hole (p. 179) is wrong.

It is not always clear whether one is reading an elementary textbook, an advanced textbook, a learned treatise with careful references, or a 749-page unrefereed original article. All modes occur, and must be identified by the reader. For textbook use, the numerous examples are helpful and deserve mention. Many useful references are given, starting with Lewis, but not including all of the latest inorganic quantum chemistry. For instance, the works of Eisenstein, Frenking, and Kaupp are not quoted at length.

Bond angles are discussed carefully, but bond lengths are often not even given. The contact with modern experimental reality is sometimes completely missing. For instance, in the chapter on rare-gas chemistry, the existence and nature of the first argon compound HArF is not mentioned, while several model systems are discussed for argon. Similarly, the experimental observations on XeH_2 could have been included. Again, the metal hydrides ZrH_4, HfH_4, and WH_6 are discussed here as theoretical models without noticing that they all now exist in matrix spectroscopy. The species $[PtH_4]^{2-}$ discussed on pages 566–572 occurs as alkali salts (W. Bronger, *Angew. Chem.* **1991**, *103*, 776).

Many eyebrows will undoubtedly be raised by the authors' clearly strong convictions that both Main Group $(n-1)$d orbital contributions and transition-metal *n*p orbital contributions to bonding are negligible, and that the 18-electron rule for the latter should therefore be replaced by a 12-electron rule.

WILEY InterScience DISCOVER SOMETHING GREAT
© 2006 Wiley-VCH Verlag GmbH & Co. KGaA, Weinheim

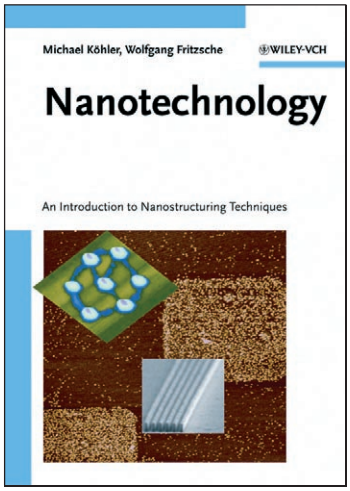
The future will show how intimately these conclusions depend on the particular systems, calculational methods, and population analysis methods that are used. The critical remarks by Maseras and Morokuma (*Chem. Phys. Lett.* **1992**, *195*, 500) on natural population analysis are not quoted. It is admitted on page 449 that the system W plus CO reacts all the way to the 18e species $W(CO)_6$.

The objections or complements to this work could easily become a book of the same size, which does not mean that the book is bad, rather the opposite. It presents its chosen view coherently, as indicated in the subtitle, based on the authors' experience, and will stimulate further work by others. Purchase recommended. Do not miss it.

Pekka Pyykkö
Department of Chemistry
University of Helsinki (Finland)

DOI: 10.1002/anie.200585341

Comprehensive Coverage of Nanotechnology



2004. XII, 272 pages, 143 figures, 9 tables. Hardcover.
ISBN 3-527-30750-8
€ 119.- /£ 85.- /US$ 160.-

MICHAEL KÖHLER and WOLFGANG FRITZSCHE

Nanotechnology
An Introduction to Nanostructuring Techniques

Nanotechnology - the generation, modification and utilization of objects with tiniest dimensions - enjoys great success due to its purposeful combination of physical, mechanical and molecular techniques.

Written for both scientists and engineers, this book offers fascinating insight into nanotechnology, starting out with the fundamentals of microtechnology and chemistry necessary for understanding the shaping of nanoscale structures, then illustrating the fabrication of nanostructures from different materials through a variety of examples and finally presenting methods for characterization of the generated structures to the reader.

"...comprehensive coverage of all underlying principles..."
Chemistry & Industry

23600511_kn

Register now for the free
WILEY-VCH Newsletter!
www.wiley-vch.de/home/pas

WILEY-VCH • P.O. Box 10 11 61 • D-69451 Weinheim, Germany
Fax: +49 (0) 62 01 - 60 61 84
e-mail: service@wiley-vch.de • http://www.wiley-vch.de

WILEY-VCH

© 2006 Wiley-VCH Verlag GmbH & Co. KGaA, Weinheim

Gene Expression

DOI: 10.1002/anie.200502700

Programmable Ligand-Controlled Riboregulators**

*Ronald Micura**

Keywords:
antisense reagents · aptamers · gene expression · riboregulators · RNA

A complex issue for all living organisms is gene expression, with hundreds of genes to be coordinated simultaneously. To handle this challenge, nature has ingeniously created a great diversity of different tools and mechanisms for control and regulation. In this context, the importance of noncoding RNA (ncRNA) has become well recognized in recent years.[1] ncRNAs include *cis*- as well as *trans*-acting RNA elements. Representatives of the first class are riboswitches, sequences in the 5′-untranslated regions (5′-UTRs) of mRNA with structural-recognition elements for specific metabolites. Binding of these small molecules leads to alternative structures that can modulate translation initiation or transcription termination.[2] Riboswitches have also been identified to exhibit ribozyme activity, resulting in cleavage of mRNA and downregulation of the corresponding gene.[3] The class of *trans*-acting ncRNA elements includes microRNAs (miRNAs), which interact with complementary sequences in mRNA and the genome,[4] small interfering RNAs (siRNAs), which function through the RNA interference (RNAi) pathway,[5] and not least, small ribozymes[6] and antisense RNAs.[7]

The prevalence of RNA-based regulators across diverse organisms from prokaryotes to humans has also stimulated scientists to engineer artificial riboregulator systems. Already in 1998, it was demonstrated that the insertion of a small-molecule aptamer (previously selected in vitro) into the 5′-UTR of a mRNA allowed its translation to be repressed by ligand addition in mammalian cells.[8] More recently, in *E. coli*, a combined *cis*/*trans* system was developed in which the *cis*-acting RNA elements inhibit translation, but interaction of the *trans*-activating RNAs with the *cis*-acting elements reinitiates translation.[9] Furthermore, a *cis*-acting ribozyme-based gene-regulation system that responds to the presence of exogenous small molecules has also been reported.[10]

A highly promising new development in the area of engineered riboregulators are so-called antiswitches, introduced by Bayer and Smolke in the single-cell eukaryote *Saccharomyces cerevisiae*.[11] An antiswitch is *trans*-acting and can, in principle, be designed to regulate the expression of any target transcript and to respond to any ligand. It consists of an aptamer domain that specifically recognizes the effector molecule (ligand) and an antisense domain (Figure 1). Importantly, effector binding induces a conformational change in the antisense domain, which is then able to interact with the target mRNA and consequently modulate its translation.

Bayer and Smolke distinguish two types of ligand-responsive riboregulators—an "off antiswitch" and an "on antiswitch". In the absence of ligand, the "off antiswitch" RNA sequesters the antisense sequence partition in an intramolecular manner within a double-stranded region and it is therefore not available for base pairing with a target mRNA. Once specific binding of the ligand occurs at the aptamer domain, the allosterically induced conformational rearrangement presents the antisense sequence as a single strand and thus allows intermolecular base pairing with the target mRNA. Consequently, the target gene is downregulated.

In contrast, the "on antiswitch" is designed with a free single-stranded antisense sequence to bind a target mRNA in the absence of the effector molecule. Upon effector binding at the aptamer domain, the "on antiswitch" undergoes a structural rearrangement that causes the antisense sequence to form an intramolecular stem loop, rendering the antiswitch RNA inactive. Thus, the target gene is upregulated.

The antiswitch concept has been demonstrated with the well-characterized theophylline aptamer[12] and a 15-nucleotide antisense sequence, which undergoes base pairing with the region around the start codon of a target mRNA that encodes the green fluorescent protein (GFP). The antiswitch RNA to be expressed in *S. cerevisiae* was cloned between two hammerhead ribozymes known for efficient self-cleavage in vivo, thus guaranteeing the creation of RNAs with defined 5′ and 3′ ends. A plasmid containing a yeast-enhanced GFP was used to transform the same cells.

Strikingly, these engineered riboregulators provide sharp transitions between gene-expression states over small changes in effector concentration. This binary on/off switch behavior most likely originates from competition between the aptamer and the antisense sequences for base pairing with the same internal sequence of the antiswitch.

The great flexibility of the novel riboregulator framework was further substantiated by additional antiswitch variants. Strategically introduced point mutations direct the switching thresh-

[*] Prof. Dr. R. Micura
Center for Molecular Biosciences CMBI
Institute of Organic Chemistry
University of Innsbruck
Innrain 52a, 6020 Innsbruck (Austria)
Fax: (+43) 512-507-2892
E-mail: ronald.micura@uibk.ac.at

[**] The author acknowledges the Austrian Science Fund (FWF) for generous funding and Claudia Höbartner for critical reading of the manuscript.

InterScience
© 2006 Wiley-VCH Verlag GmbH & Co. KGaA, Weinheim

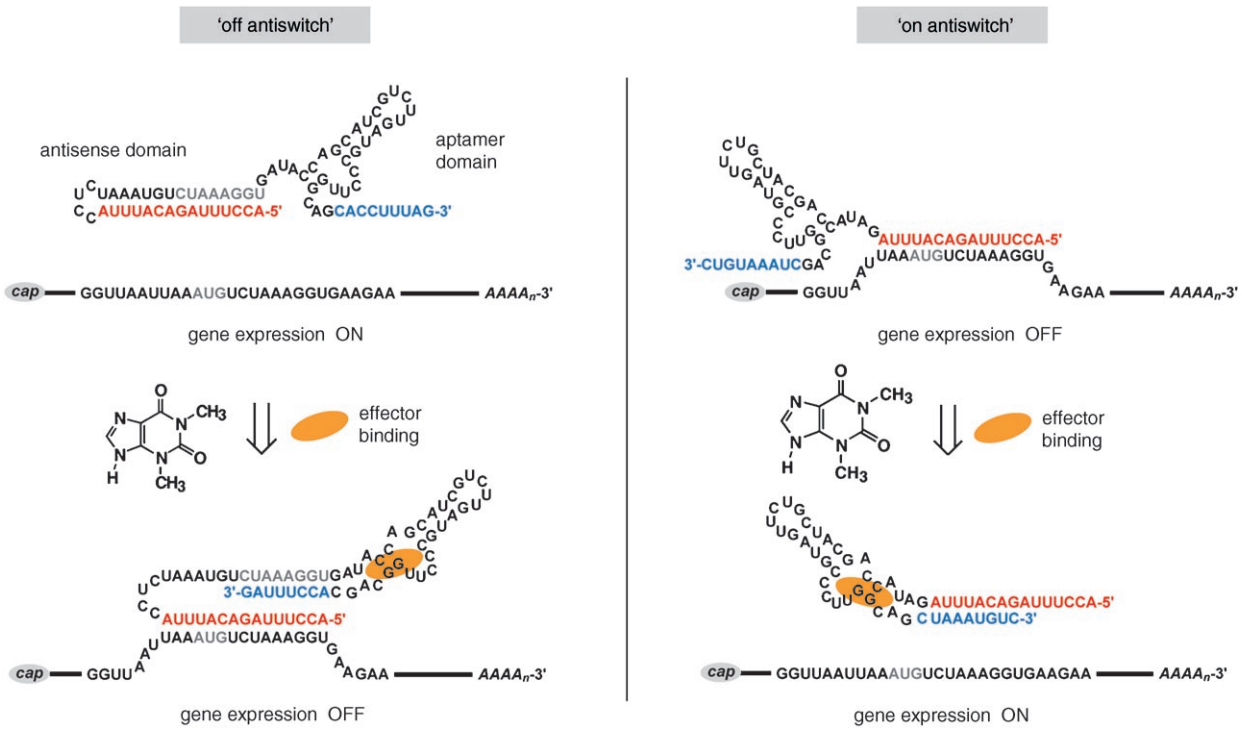


Figure 1. Programmable ligand-controlled riboregulators of eukaryotic gene expression. The so called antiswitches are *trans*-acting ncRNAs that consist of an antisense domain and an aptamer domain. For the "off antiswitch" (left), the antisense sequence (red) is sequestered in a stem loop. In the presence of ligand (theophylline; orange), an allosteric conformational change is induced, and the antisense sequence is liberated and can interact with the target mRNA at the 5′-end, thus suppressing gene expression. For the "on antiswitch" (right), the antisense sequence is free to bind to its target mRNA and gene expression is repressed. Upon ligand binding, the antiswitch is released from the target mRNA and gene expression is permitted.

olds as a function of effector concentration. Moreover, Bayer and Smolke replaced the aptamer domain for theophylline with that for tetracycline and demonstrated a similar behavior with a different effector. In addition, they also showed that two antiswitches with different aptamer domains and different antisense domains in the same cell responded independently to different ligands, each regulating a different mRNA target.

The novel antiswitches represent a highly flexible rational concept that enables both positive and negative regulation of potentially any target gene in a diverse range of organisms. The consideration of particularly tiny aptamer domains might have an additional impact on the design of antiswitches. For instance, Anderson and Mecozzi recently reduced the original theophylline aptamer to a 13-nucleotide RNA and found that the high affinity and specificity were retained.[13] A combination of these tiny aptamers and corresponding antisense domains would result in antiswitch riboregulators of a size comparable to that of siRNAs, with a potentially expanded scope of regulative applications in gene networks.

Published online: September 20, 2005

[1] A. Hüttenhofer, P. Schattner, N. Polacek, *Trends Genet.* **2005**, *21*, 289–297.
[2] M. Mandal, R. R. Breaker, *Nat. Rev. Mol. Cell Biol.* **2004**, *5*, 451–463.
[3] a) W. Winkler, A. Nahvi, A. Roth, J. A. Collins, R. R. Breaker, *Nature* **2004**, *428*, 281–285; b) R. Micura, *Angew. Chem.* **2004**, *116*, 4797–4799; *Angew. Chem. Int. Ed.* **2004**, *43*, 4692–4694.
[4] D. P. Bartel, *Cell* **2004**, *116*, 281–297.
[5] "RNA Interference": D. R. Engelke, J. J. Rossi, *Methods Enzymol.* **2004**, *392*.
[6] D. M. Lilley, *Trends Biochem. Sci.* **2003**, *28*, 495–501.
[7] L. Good, *Cell. Mol. Life Sci.* **2003**, *60*, 823–824.
[8] a) G. Werstuck, M. R. Green, *Science* **1998**, *282*, 296–298; b) Y. Tor, *Angew. Chem.* **1999**, *111*, 1681–1685; *Angew. Chem. Int. Ed.* **1999**, *38*, 1579–1582.
[9] F. J. Isaacs, D. J. Dwyer, C. Ding, D. D. Pervouchine, C. R. Cantor, J. J. Collins, *Nat. Biotechnol.* **2004**, *22*, 841–847.
[10] L. Yen, J. Svendsen, J.-S. Lee, J. T. Gray, M. Magnier, T. Baba, R. J. D'Amato, R. C. Mulligan, *Nature* **2004**, *431*, 471–476.
[11] T. S. Bayer, C. D. Smolke, *Nat. Biotechnol.* **2005**, *23*, 337–343.
[12] D. J. Patel, A. K. Suri, *Rev. Mol. Biotechnol.* **2000**, *74*, 39–60.
[13] P. C. Anderson, S. Mecozzi, *J. Am. Chem. Soc.* **2005**, *127*, 5290–5291.

© 2006 Wiley-VCH Verlag GmbH & Co. KGaA, Weinheim

Structure Elucidation

DOI: 10.1002/anie.200501839

Water Oligomers in Crystal Hydrates—What's News and What Isn't?

Mark Mascal, Lourdes Infantes,* and James Chisholm**

Keywords:
hydrates · hydrogen bonding · self-assembly · solid-state structures · water chemistry

A surge of publications dealing with the structure of water in crystal hydrates of organic compounds and coordination complexes has appeared recently. Each is apparently reporting something new; chains, rings, sheets, networks of water molecules in arrangements which may shed light on the chemistry of the world's most important molecule. About 3000 years before the above mentioned publications appeared, it was written: *What has been will be again, what has been done will be done again; and there is nothing new under the sun.*[1] Do these words convict us?

[*] Professor M. Mascal
Department of Chemistry
University of California, Davis
Davis, CA 95616 (USA)
Fax: (+1) 530-752-8995
E-mail: mascal@chem.ucdavis.edu
Dr. L. Infantes
Cambridge Crystallographic Data Centre
12 Union Rd
Cambridge, CB21EZ (UK)
and
Instituto de Química-Física "Rocasolano", CSIC
Serrano 119, 28006 Madrid (Spain)
Fax:(+34) 15-642-431
E-mail: xlourdes@iqfr.csic.es
Dr. J. Chisholm
Cambridge Crystallographic Data Centre
12 Union Road
Cambridge, CB21EZ (UK)
Fax: (+44) 223 336033
E-mail: chisholm@ccdc.cam.ac.uk

Supporting information for this article is available on the WWW under http://www.angewandte.org or from the author.

In the latest version of the Cambridge Structural Database (CSD)[2] there are over 37000 crystal structures with 3D coordinates which include at least one molecule of water per unit cell. The question becomes this: how can the novelty of any experimentally observed water oligomer be substantiated without first consulting the CSD? The data (crystal coordinates, cell parameters, and space groups for generating symmetry operations) are freely available. However, the exploration of these data for the characterization of water motifs is a substantial undertaking.

Fortunately, much work in this direction has already been done. Using a manageable subset of crystal hydrates in the CSD, it has been possible to classify a number of common aggregation states adopted by hydrogen-bonded water molecules in organic solid-state structures.[3,4] The classification system, whose nomenclature will be referred to later, is summarized here:

D (*discrete chains*): discrete groups of acyclicly connected water molecules. The symbol is D*n*, where *n* is the number of water molecules in the longest chain.

R (*discrete rings*): discrete cyclic motifs isolated within the unit cell. The symbol is R*n*, where *n* is the number of water molecules that form the ring.

C (*infinite chains* in one dimension involving no rings): the symbol is C*n*, where *n* is the number of water molecules that are traversed to reach the unit cell repeat atom.

T (*infinite tapes* in one dimension involving rings): this group describes tapes where rings are involved in one-dimensional propagation. The symbol T*n*(*q*)*m*(*r*)… gives the number of the atoms *n*, *m*, … in each ring starting with the smallest ring, followed by *q*, *r*, … in parentheses representing the number of water molecules shared between the adjacent rings. When there are acyclic links between the rings an extra qualifier A*k* is added, where *k* is the number of acyclic water molecules in the link, T*n*(*q*)A*k*.

L (*infinite layers* in two dimensions): the symbol is L*m*(*r*)*n*(*s*)*p*(*t*)… for rings of size *m*, *n*, *p*, … that share water molecules with *r*, *s*, *t*, … adjacent rings.

U (*unclassified structures*): complex networks which may be factored into combinations of R, C, T, and/or L motifs. A qualifier *n* indicates the number of dimensions.

We chose at random 17 recent publications which report extraordinary or even unprecedented assemblies of water molecules and compared these structures against those already in the CSD.[5] The results of this study, along with brief excerpts from the original publications, are given below.

InterScience
© 2006 Wiley-VCH Verlag GmbH & Co. KGaA, Weinheim

1) "Formation of Extended Tapes of Cyclic Water Hexamers in an Organic Molecular Crystal Host" (R. Custelcean et al.[6a]): *Herein we describe the formation of cyclic water hexamers with an icelike chair conformation and their self-assembly into unprecedented one-dimensional tapes with spectroscopic features similar to those of liquid water, along the channels of an organic molecular host.*

   Crystal: 2,4-dimethyl-5-aminobenzo[*b*]-1,8-naphthyridine·2.5 H_2O, CSD refcode QIPPUA.

   Comment: The aggregate is T4(2)6(2). We note 24 examples of this motif.[7]

2) "Characterization of a Planar Cyclic Form of Water Hexamer in an Organic Supramolecular Complex: An Unusual Self-Assembly of Bimesityl-3,3′-Dicarboxylic Acid" (J. N. Moorthy et al.[6b]): *Herein, we report the first X-ray structural characterization of the high-energy cyclic form of the water hexamer trapped in an organic supramolecular complex with the bimesityl dicarboxylic acid.*

   Crystal: 1,1′-bimesityl-3,3′-dicarboxylic acid monohydrate, CSD refcode OGOFAR.

   Comment: The aggregate is planar R6. We note 206 examples of the R6 motif,[8] of which 17 are planar.[9]

3) "Structure of a Self-Assembled Chain of Water Molecules in a Crystal Host" (S. Pal et al.[6c]): *Herein, we report the structure of a highly ordered infinite chain of water molecules found in a crystal host at room temperature. It is shown that the chain consists of cyclic water tetramers linked by two bridging water molecules. We believe that the water structure demonstrated herein brings to light yet another novel mode of the cooperative association of water molecules … We believe that this motif of association of the water molecules has not even been speculated previously.*

   Crystal: 1,4,7,10-tetraazacyclododecane trihydrate, CSD refcode VUCGEF01.

   Comment: The aggregate is T4(1). We note 28 examples of this motif.[10]

4) "Structures and Solid-State Dynamics of One-Dimensional Water Chains Stabilized by Imidazole Channels" (L. E. Cheruzel et al.[6d]): *Curiously, little is known of the structural constraints required in stabilizing 1D water chains … Curiously, there have been no comprehensive studies of water dynamics in systems containing infinite water-chain structures. This fact may be due in part to the limited number of well characterized continuous water chain structures involving small molecules.*

   Crystals: 4,4′-Methylenebis(2-ethyl-5-methylimidazole) dihydrate, CSD refcode BEHBOG; 1-methyl-4-imidazolecarboxaldehyde monohydrate, CSD refcode BEHBIA.

   Comment: The aggregates are C2 and C4, respectively. We note 246 examples of the former[11] and 452 of the latter,[12] as subsets of the 1048 infinite chain motifs (C) in the CSD.

5) "Formation of Two-Dimensional Supramolecular Icelike Layer Containing $(H_2O)_{12}$ Rings" (B.-Q. Ma et al.[6e]): *The unique 2D ice layer has a great similarity with ice I_h and features a novel $(H_2O)_{12}$ ring.*

   Crystals: *trans*-bis(4-pyridyl)ethylene dioxide dihydrate, CSD refcodes ITEWEJ and ITEWEJ01; *trans*-bis(4-pyridyl)ethylene dioxide pentahydrate, CSD refcodes ITEWOT and ITEWOT01.

   Comment: The aggregates are C4 and L12(6), respectively. We note 452 examples of the former[12] and 15 examples of the latter.[13] L12(6) layers exist in 3 different topologies, and there are 8 other structures which present the same topology as in ITEWOT.

6) "Novel Water Clusters in the Crystalline State: Structures of a Symmetrical, Cyclic Hexamer and an 'Opened-Cube' Octamer" (R. J. Doedens et al.[6f]): *We have now found a new type of octameric cluster in crystalline $[V(phen)_2SO_4]2O(H_2O)_4$ (phen = 1,10-phenanthroline) … Among crystallographically characterized six-membered clusters, ours is the first example to display the full symmetry and the hydrogen atom disorder of the hexagonal building block of ice.*

   Crystals: (μ_2-Oxo)bis(bis(1,10-phenanthroline)sulfatovanadium) octahydrate, CSD refcode YIPXUQ; $Ni_3V_{18}O_{42}(H_2O)_{12}(SO_4)]\cdot 24\,H_2O$, no CSD refcode.

   Comment: The aggregate is formally a U0 cluster composed of an R6 ring with two bridging water molecules describing a tricyclo[3.1.1.1^{2,4}]octyl motif. We note 6 examples of this motif.[14] A chairlike R6 aggregate is also reported in the same publication. Of the 206 examples of the R6 motif,[8] 163 are in the chair conformation.[15]

7) "Characterization of a Well Resolved Supramolecular Ice-like $(H_2O)_{10}$ Cluster in the Solid State" (L. J. Barbour et al.[6g])

8) "An intermolecular $(H_2O)_{10}$ cluster in a solid-state supramolecular complex" (L. J. Barbour et al.[6h]): *Here we report the preparation and crystal structure of a self-assembled, three-dimensional supramolecular complex that is stabilized by an intricate array of non-covalent interactions involving contributions from solvent water clusters, most notably a water decamer ($(H_2O)_{10}$) with an ice-like molecular arrangement.*

   Crystals: tetrakis(μ_2-benzene-1,3-bis(*N*-4-pyridylmethyl)carbamoyl)tetraaquadicobalt(II) tetranitrate dodecahydrate, CSD refcode DOQQAB; tetrakis(μ_2-benzene-1,3-bis(*N*-4-pyridylmethyl)carbamoyl)tetraaquadicopper(II) tetranitrate dodecahydrate, CSD refcode NUGROW.

   Comment: Publications 7 and 8 are considered together because the crystals are essentially isostructural. The

 © 2006 Wiley-VCH Verlag GmbH & Co. KGaA, Weinheim

search parameters we use[5] would have led to this aggregate being classified as R8, of which we note 43 examples.[16] Since we are interested in modeling the behavior of "free" H_2O and its analogy to water as a solvent, our searches have been restricted to solvate water molecules which participate only in hydrogen bonding and are not coordinatively bonded to a metal complex. The aggregate as described in the above two publications would formally be a U0 cluster composed of an R8 ring plus two metal-complexed water molecules in an adamantanoid motif. In our search of free water molecules, we note only one other H_2O decamer in such an arrangement.[17]

9) "Coexistence of Water Dimer and Hexamer Clusters in 3D Metal–Organic Framework Structures of Ce^{III} and Pr^{III} with Pyridine-2,6-dicarboxylic Acid" (S. K. Ghosh et al.[6i]): *Herein, we describe the presence of both cyclic chairlike hexamer and dimer water clusters in metal–organic frameworks constructed from Ce^{III} or Pr^{III} and pyridine-2,6-dicarboxylic acid. This is one of the rare examples where two different types of water clusters coexist in the same host lattice.*

Crystals: *catena*-((μ_2-pyridine-2,6-dicarboxylato)diaqua-(6-carboxypyridine-2-carboxylato)praseodymium tetrahydrate), CSD refcode ARUKIH; *catena*-((μ_2-pyridine-2,6-dicarboxylato-*N*,*O*,*O*′,*O*″)-(6-carboxypyridine-2-carboxylato-*N*,*O*,*O*')diaquacerium(III) tetrahydrate), CSD refcode LOYBAC01.

Comment: The authors describe their mixed motifs as R6 plus D2. Our search parameters[5] lead to the classification D6, since metal-coordinated water molecules are included in the aggregate which are rejected in our searches. In any case, we note 163 examples of chairlike R6 aggregates,[15] 4657 D2 motifs,[18] and 281 D6 motifs.[19] We also note that the coexistence of two different types of water clusters in the same lattice is a common observation. Among those analyzed in this work, no less than 189 refcodes include two or more different water motifs in the same crystal structure.

10) "Synthesis and Crystallographic Characterization of an Octameric Water Complex, $(H_2O)_8$" (W. B. Blanton et al.[6j]): *However, until the present work, crystallographic observation and analysis of a water octamer has not been possible.*

Crystal: bis(2,6-diacetamidopyridine)cobalt(II)-(1,2-bis-(2-oxy-2-methylpropanamido)-4,5-dimethoxybenzene)-cobalt(III) octahydrate, CSD refcode CIGGAA.

Comment: The aggregate is formally a U0 cluster composed of an R6 ring with two bridging water molecules describing a cube motif. We note 9 examples of this motif,[20] as well as another 5 in which the $(H_2O)_8$ cube is part of a larger water aggregate.[21]

11) "A Well-Resolved Ice-like $(H_2O)_8$ Cluster in an Organic Supramolecular Complex" (J. L. Atwood et al.[6k]): *In this context, we now report the observation of an ice-like, cyclic $(H_2O)_8$ cluster in the solid-state structure of an organic supramolecular complex … Figure 2 shows that the puckered arrangement of the water cluster can be superimposed remarkably well on a subset of the continuous lattice of ice Ic.*

Crystal: 4,6,10,12,16,18,22,24-Octahydroxy-2,8,14,20-tetramethylcalix(4)arene acetone solvate hexahydrate, CSD refcode OCIDIN.

Comment: The aggregate is R8. We note 43 examples of this motif,[16] 4 of which can be superimposed over the H_2O octamer of the ice I_c crystal structure. The refcodes for these 4 structures, along with the rms deviation (Å) from the I_c motif, are: OCIDIN, 0.134; DOQQAB, 0.192; NUGROW, 0.284; and LIJQOK, 0.623. Note that the best match occurs in the structure under consideration here (OCIDIN) followed by the structures in publications 7 and 8 (DOQQAB and NUGROW), by the same principle author (Atwood), which also dealt with submotifs of ice I_c.

12) "Characterization of Supramolecular $(H_2O)_{18}$ Water Morphology and Water–Methanol $(H_2O)_{15}(CH_3OH)_3$ Clusters in a Novel Phosphorus Functionalized Trimeric Amino Acid Host" (K. Raghuraman et al.[6l]): *We, herein, report the experimental evidence for the existence of a 2D cyclic supramolecular $(H_2O)_{18}$ morphology within the layers of … with structural features similar to those of liquid water … Indeed, such a large supramolecular 2D cyclic structure for water has not been observed before either in liquid water or in other low dimensional ice.*

Crystal: tris(L-alanylmethyl)phosphane tetrahydrate, CSD refcode EHULAU.

Comment: The aggregate is L18(6). We note 6 examples of this motif.[22]

13) "Two-Dimensional Water and Ice Layers: Neutron Diffraction Studies at 278, 263, and 20 K" (C. Janiak et al.[6m]): *The structure of 2D ice layers features novel rings of eight water molecules or folded-chain segments at temperatures below the freezing point. At very low temperature an unprecedented net of condensed irregular rings of 12 water molecules (plus a dangling D_2O) is observed. Both ice layers are different from hitherto known 2D ice phases which mostly consist of hexagonal honeycomb lattices.*

Crystal: bis(hydrogentris(1,2,4-triazolyl)borate)nickel(II)-hexakis(deuterium oxide) clathrate at 278, 263, and 20 K, CSD refcodes YOBSAJ02, YOBSAJ04, and YOBSAJ03, respectively.

Comment: The crystal undergoes phase transitions between the three temperatures at which data were collected. The higher-temperature motifs suffer from substantial disorder and are unremarkable. The low-temperature structure determination gives an L12(6) aggregate. We note 15 examples of this motif.[13] As noted above (publication 5), L12(6) layers exist in 3 different topologies, and there are 3 other structures which present the same topology as in YOBSAJ03.

 © 2006 Wiley-VCH Verlag GmbH & Co. KGaA, Weinheim

14) "A Cyclic Supramolecular $(H_2O)_4$ Cluster in an Unusual Fe_3 Complex that Aggregates to $\{Fe_3\}_n$ with a Zig-zag Chainlike Structure" (S. Supriya et al.[6n]): *The most striking feature of the present system is that the iron-coordinated water … and three other crystal water molecules … together form a cyclic hydrogen-bonded water tetramer.*

Crystal: (μ_3-oxo)hexakis(μ_2-acetato)aquabis(2-pyridone-*O*)triiron(III) perchlorate tetrahydrate, CSD refcode HACFIB.

Comment: The aggregate is D4. Inclusion of the metal-coordinated water gives R4. Either way, we note 796 examples of the former[23] and 102 of the latter motif.[24]

15) "Cyclic Water Hexamers and Decamers in a Porous Lanthanide–Organic Framework: Correlation Between Some Physical Properties and Crystal Structure" (A. Michaelides et al.[6o]): *In this work, we describe the unique architecture of the 2D polymeric water network, enclathrated in the channels of this material. This network is composed of hexamers with both boat and chair conformations and of cyclic decamers with boat–chair–boat (BCB) conformation, appearing for the first time.*

Crystal: *catena*-(bis(μ_4-fumarato)(μ_2-fumarato)tetraaquadierbium(III) octahydrate, CSD refcode PIZPIX01.

Comment: The aggregate is T6(2). Inclusion of the metal-coordinated water gives L6(6)6(7)10(8). We note 31 examples of T6(2),[25] but no examples of independent water molecules in an L6(6)6(7)10(8) arrangement. Additionally, we note 6 other cyclic decamers (free R10 rings or 10-membered rings comprising part of a larger water arrangement) with the BCB conformation.[26]

16) "Ice-like $(H_2O)_{12}$ and $(H_2O)_{14}$ Clusters in the Crystal Structures of Alkali Metal–Ethyl Viologen Hexacyanometallates" (M. Y. Antipin et al.[6p]): *In this work, the crystal structure of the lithium ethyl viologen hexacyanoferrate … containing a cluster of 14 water molecules was studied. The results were compared with previous data on isostructural compounds … in which $(H_2O)_{12}$ structural units were detected.*

Crystal: tris(diethylviologen)bis(tetraaqualithium)bis(hexacyanoferrate(II)) icosahydrate, CSD refcode IDOZAC.

Comment: The aggregate is formally a U1 cluster composed of 6- and 4-membered H_2O rings. We note 3 examples of this motif.[27]

17) "The Crystal and Molecular Structure of one of the Possible Conformers of 'the Smallest Piece of Ice'—A Solid-State Isolation of a Hydrogen Bonded Water Hexamer Trapped Within Channels of a Crystal of a Dirhodium Molecule" (I. Bernal et al.[6q]): *Reexamination of our study of $[Rh_2(HNOCCH_3)_4(2H_2O)]\cdot 3H_2O$ … showed it to be interesting … because it contains a hexameric cluster of waters trapped in Rh Rh lattice cavities. It may well provide an interesting model for the 'smallest piece of ice'.*

Crystal: tetrakis(μ_2-acetamidato-*O*,*N*)diaquadirhodium, CSD refcode DOKJAO.

Comment: The aggregate is distorted twist-boat R6. We note 206 examples of the R6 motif,[8] of which 11 can be described as twist-boat.[28]

First, we note that in publications 3, 5, and 9 reference [3] is actually cited, and yet, motifs which had already been described in reference [3] are still reported as novel. With the exception of publications 7, 8, 11, 14, 16, and 17, all of the above-cited publications make mistaken claims to novelty of one sort or another. Publications 14, 16, and 17, while still reporting structures redundant with those in the CSD, make no unsupportable claims. This leaves publications 7, 8, and 11, which describe unique or nearly unique hydrate structures, given the current extent to which the CSD has been analyzed (see below).

Next, it must also be noted that even in this Essay and in the studies described in references [3,4] only subsets of the hydrates in the CSD were examined; interrogation of every published hydrate structure would undoubtedly bring to light further examples of the described motifs as well as some new, even more complex ones. Beyond this, there is the Inorganic Crystal Structure Database (ICSD).[29] Of the 82676 crystal structures in the latest release of that database, at least 7395 are hydrates, the aggregation states of which, to our knowledge, have yet to be explored. And finally, what about the protein data bank (PDB)?[30] Despite the lower resolution of the crystal structures and the common disorder of solvent molecules, classification of the hydration structure of functional biomolecules could produce relevant insights into the behavior of water in the biosphere. Cursory examination of one of these structures (egg white lysozyme, PDB ID 193L) revealed a number of familiar motifs (D2, D3, D4, D6, D8, R6).

With the above in mind, due care should be exercised by authors reporting novel water aggregates and, equally, due discretion by reviewers of such work. The problem is not so much one of intentional publication of misinformation as it is the relative difficulty in establishing what is already known. One reason for this is that the systematic analysis of hydration structures in the CSD is not practical using the current CSD search engine CONQUEST, so dedicated programs must be written to undertake such work.[31] Furthermore, searching the primary literature for known water motifs is complicated by the fact that, for many of the refcodes cited in this study, the hydration structure, however interesting, may not have even been commented on. Nonetheless, the data are available, and these issues do not simply discharge authors of the responsibility to support claims to novelty and to cite relevant literature.

Finally, the preambles of many of the above publications suggest that the

 © 2006 Wiley-VCH Verlag GmbH & Co. KGaA, Weinheim

findings provide a better understanding of water in biological systems and in its bulk liquid and solid phases. Perhaps every hydrate is unique in its arrangement of water about the unit cell, although, as we have seen, a number of characteristic motifs occur more or less frequently. How does the arrangement of water molecules around any particular organic molecule or metal complex specifically progress our understanding of physical or biological processes mediated by water? The answer may be that few single results are likely to substantially advance this knowledge, but collectively these structures allow us to examine the "freezing" of water in thousands of containers of molecular dimensions. All of this ultimately leads to the question of whether manuscripts whose primary focus is on well-described aggregation states of hydrates should be published, given the emphasis on originality in the modern chemical literature. The answer must be yes, in that they contribute in some way to the overall description of the behavior of water. However, in the absence of any extraordinary function or other point of interest in the crystal structure, the form these publications should take, or the medium of publication, is a matter of debate.[32]

Published online: November 24, 2005

[1] *Old Testament, Eccl. 1:9*.

[2] F. H. Allen, *Acta Crystallogr. Sect. B* **2002**, *58*, 380 – 388.

[3] L. Infantes, S. Motherwell, *CrystEngComm* **2002**, *4*, 454 – 461.

[4] L. Infantes, J. Chisholm, S. Motherwell, *CrystEngComm* **2003**, *5*, 480 – 486.

[5] The current study was restricted to organic crystal structures with no errors, R factor < 0.1, and having at least one water–water contact with an O···O distance less than the sum of the van der Waals radii plus 0.2 Å ($d = 3.024$ Å) in CSD version 5.25 (November 2003) plus two updates (January and April 2004). Only those structures where the H_2O molecule was defined as having a coordination number of 2 ("T2") were included in the search (10926 hits). The methods used are described in references [3] and [4].

[6] a) R. Custelcean, C. Afloroaei, M. Vlassa, M. Polverejan, *Angew. Chem.* **2000**, *112*, 3224 – 3226; *Angew. Chem. Int. Ed.* **2000**, *39*, 3094 – 3096; b) J. N. Moorthy, R. Natarajan, P. Venugopalan, *Angew. Chem.* **2002**, *114*, 3567 – 3570; *Angew. Chem. Int. Ed.* **2002**, *41*, 3417 – 3420; c) S. Pal, N. B. Sankaran, A. Samanta, *Angew. Chem.* **2003**, *115*, 1783 – 1785; *Angew. Chem. Int. Ed.* **2003**, *42*, 1741 – 1743; d) L. E. Cheruzel, M. S. Pometun, M. R. Cecil, M. S. Mashuta, R. J. Wittebort, R. M. Buchanan, *Angew. Chem.* **2003**, *115*, 5610 – 5613; *Angew. Chem. Int. Ed.* **2003**, *42*, 5452 – 5455; e) B.-Q. Ma, H.-L. Sun, S. Gao, *Angew. Chem.* **2004**, *116*, 1398 – 1400; *Angew. Chem. Int. Ed.* **2004**, *43*, 1374 – 1376; f) R. J. Doedens, E. Yohannes, M. I. Khan, *Chem. Commun.* **2002**, 62 – 63; g) L. J. Barbour, G. W. Orr, J. L. Atwood, *Chem. Commun.* **2000**, 859 – 860; h) L. J. Barbour, G. W. Orr, J. L. Atwood, *Nature* **1998**, *393*, 671 – 673; i) S. K. Ghosh, P. K. Bharadwaj, *Inorg. Chem.* **2003**, *42*, 8250 – 8254; j) W. B. Blanton, S. W. Gordon-Wylie, G. R. Clark, K. D. Jordan, J. T. Wood, U. Geiser, T. J. Collins, *J. Am. Chem. Soc.* **1999**, *121*, 3551 – 3552; k) J. L. Atwood, L. J. Barbour, T. J. Ness, C. L. Raston, P. L. Raston, *J. Am. Chem. Soc.* **2001**, *123*, 7192 – 7193; l) K. Raghuraman, K. K. Katti, L. J. Barbour, N. Pillarsetty, C. L. Barnes, K. V. Katti, *J. Am. Chem. Soc.* **2003**, *125*, 6955 – 6961; m) C. Janiak, T. G. Scharmann, *J. Am. Chem. Soc.* **2002**, *124*, 14010 – 14011; n) S. Supriya, S. Manikumari, P. Raghavaiah, S. K. Das, *New J. Chem.* **2003**, *27*, 218 – 220; o) A. Michaelides, S. Skoulika, E. G. Bakalbassis, J. Mrozinski, *Cryst. Growth Des.* **2003**, *3*, 487 – 492; p) M. Y. Antipin, A. B. Ilyukhin, V. Y. Kotov, *Mendeleev Commun.* **2001**, 1 – 2; q) I. Bernal, J. L. Bear, *J. Chem. Crystallogr.* **2002**, *32*, 485 – 488.

[7] CSD refcode file 1.gcd (Supporting Information).

[8] CSD refcode file 2.gcd (Supporting Information).

[9] CSD refcode file 3.gcd (Supporting Information).

[10] CSD refcode file 4.gcd (Supporting Information).

[11] CSD refcode file 5.gcd (Supporting Information).

[12] CSD refcode file 6.gcd (Supporting Information).

[13] CSD refcode file 7.gcd (Supporting Information).

[14] CSD refcode file 8.gcd (Supporting Information).

[15] CSD refcode file 9.gcd (Supporting Information).

[16] CSD refcode file 10.gcd (Supporting Information).

[17] CSD refcode file 11.gcd (Supporting Information).

[18] CSD refcode file 12.gcd (Supporting Information).

[19] CSD refcode file 13.gcd (Supporting Information).

[20] CSD refcode file 14.gcd (Supporting Information).

[21] CSD refcode file 15.gcd (Supporting Information).

[22] CSD refcode file 16.gcd (Supporting Information).

[23] CSD refcode file 17.gcd (Supporting Information).

[24] CSD refcode file 18.gcd (Supporting Information).

[25] CSD refcode file 19.gcd (Supporting Information).

[26] CSD refcode file 20.gcd (Supporting Information).

[27] CSD refcode file 21.gcd (Supporting Information).

[28] CSD refcode file 22.gcd (Supporting Information).

[29] ICSD © FIZ Karlsruhe.

[30] H. M. Berman, J. Westbrook, Z. Feng, G. Gilliland, T. N. Bhat, H. Weissig, I. N. Shindyalov, P. E. Bourne, *Nucleic Acids Res.* **2000**, *28*, 235 – 242.

[31] The studies described in references [3] and [4] made use of a modified version of the CSD program RPLUTO (RPLUTO, A Program for Crystal Structure Visualisation, Cambridge Crystallographic Data Centre, Cambridge, **2002**). After generating intermolecular contacts defined by the chosen cutoff distance, visual examination of the resulting H_2O networks led to the present classification of the structures. Algorithms which enhance 3-D search capabilities of CSD software (see J. A. Chisholm, S. Motherwell, *J. Appl. Crystallogr.* **2004**, *37*, 331 – 334) will be implemented in due course.

[32] As a postscript, no part of this work should be construed as a slight of the numerous studies which attempt to theoretically model the chemistry of water, nor of the in-depth physical studies of water in various phases, on surfaces, or under extreme conditions (e.g., supercritical), which are delivering prodigious insights and advancing original research in their respective fields.

 © 2006 Wiley-VCH Verlag GmbH & Co. KGaA, Weinheim

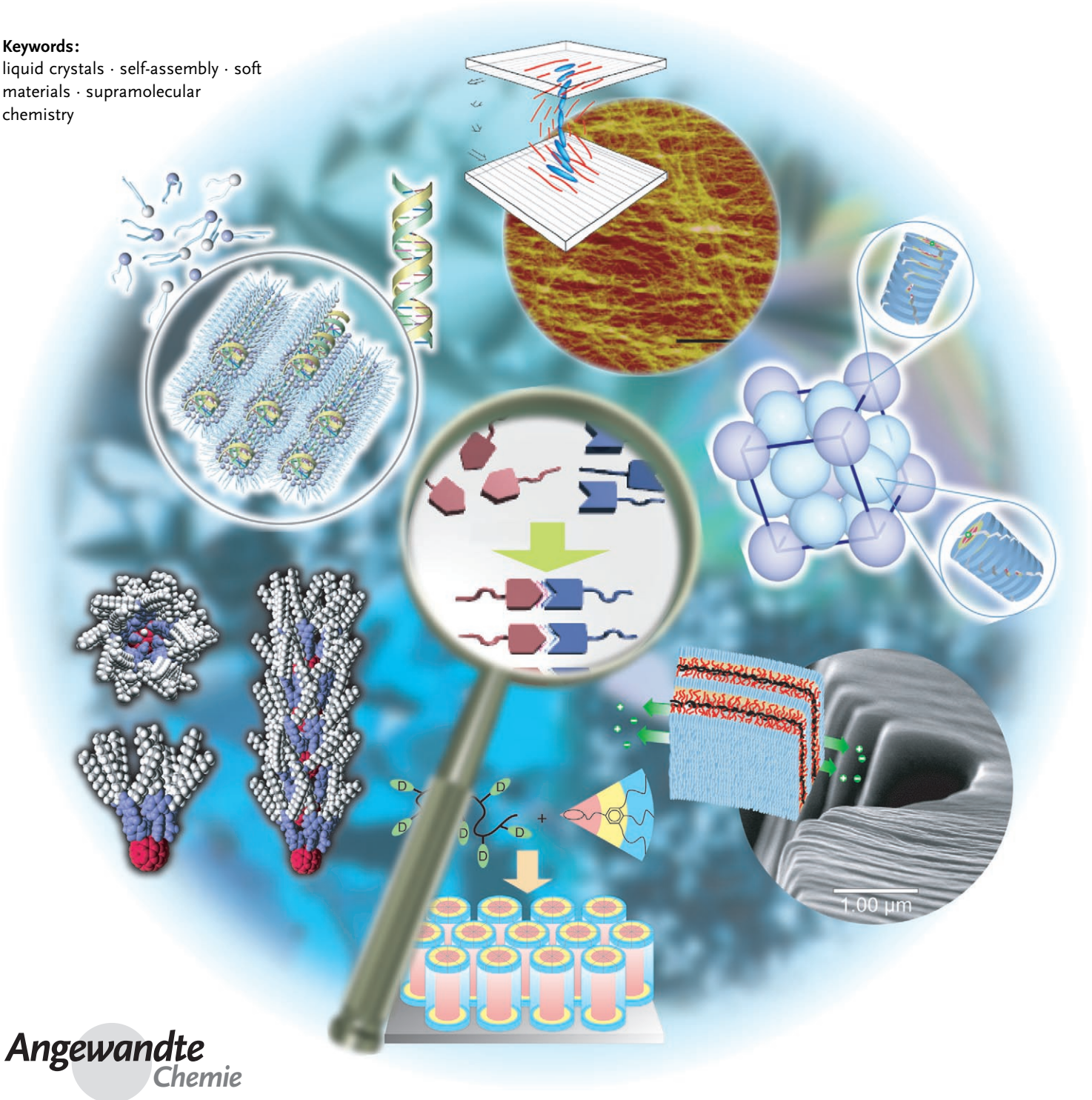
Supramolecular Chemistry

DOI: 10.1002/anie.200501384

Functional Liquid-Crystalline Assemblies: Self-Organized Soft Materials

Takashi Kato, Norihiro Mizoshita, and Kenji Kishimoto*

Keywords:
liquid crystals · self-assembly · soft materials · supramolecular chemistry



© 2006 Wiley-VCH Verlag GmbH & Co. KGaA, Weinheim

In the 21st century, soft materials will become more important as functional materials because of their dynamic nature. Although soft materials are not as highly durable as hard materials, such as metals, ceramics, and engineering plastics, they can respond well to stimuli and the environment. The introduction of order into soft materials induces new dynamic functions. Liquid crystals are ordered soft materials consisting of self-organized molecules and can potentially be used as new functional materials for electron, ion, or molecular transporting, sensory, catalytic, optical, and bio-active materials. For this functionalization, unconventional materials design is required. Herein, we describe new approaches to the functionalization of liquid crystals and show how the design of liquid crystals formed by supramolecular assembly and nano-segregation leads to the formation of a variety of new self-organized functional materials.

From the Contents

1. Introduction 39
2. New Design of Liquid-Crystalline Assemblies 41
3. Function of Liquid-Crystalline Assemblies 53
4. Liquid-Crystal Composites 59
5. Summary and Outlook 62

1. Introduction

Liquid crystals are "soft materials" that form mobile and ordered states.[1–7] Ordered self-assembled molecules can induce enhanced functions.[6] Liquid crystals are widely used in information-display technology and the anisotropic fluid states of rigid polymers are used for processing of high-strength fibers.[1a,8] In these cases, the nematic phase, which is the simplest of the liquid-crystalline phases, has been used. However, liquid-crystalline materials can self-organize into various nanostructured phases, such as layered, columnar, micellar, and bicontinuous cubic. These structures are formed by segregation of immiscible parts in molecules on the nanometer scale.[5,9–12] These ordered soft materials should have great potential in a wide variety of fields of advanced technologies.[4,5,8,13] Liquid crystals can be used as dynamically functional materials for information and mass transport, sensing, catalysis, templates, and stimuli responsiveness as well as electro-optical displays. Liquid crystals (LCs) should also be useful in bio-related fields because the self-organized structures of lyotropic liquid crystals are compatible with those in living systems.[14–17] More complex structures of these phases have been reported. One example is lyotropic lamellar complexes of DNA and cationic lipids, which have potential for gene therapy.[16]

To increase the functional capabilities of LCs, a new design of molecules and self-assembled structures from the nano to the macro scale is important.[5,18] The concept of supramolecular chemistry[19] has broadened our horizon in the design of LCs, and since 1989, supramolecular liquid-crystalline phases with well-defined structures have been formed by exploiting intermolecular hydrogen bonding (Figure 1).[7,20–30] In the conventional design of liquid-crystal molecules, "covalent" bonding had been used to "synthesize" mesogenic molecular structures.[1] In the conventional covalent approaches in the preparation of materials for information display, specific intermolecular interactions, such as hydrogen bonds, were not recognized as being very important because it was thought that the molecular interaction sites may disturb the performance and durability of such display materials. The supramolecular approach gives us another tool to build liquid-crystal "molecules", which are more dynamic.[7,20–34] These new liquid-crystal assemblies can be built by using specific molecular interactions, such as hydrogen bonds, ionic bonds, and charge-transfer interactions.[20–35] Hydrogen bonding has also been used for the preparation of a wide variety of self-assembled systems.[36–39] These noncovalent approaches have increased the possibility of introducing chemical processes, such as molecular recognition and molecular self-assembly, into the materials. These approaches have been recognized as playing a key role in the development of new dynamically functional materials.[5,40–46]

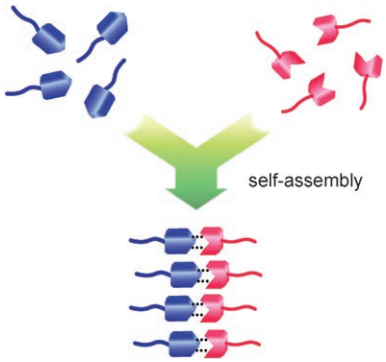


Figure 1. Supramolecular assembly of liquid-crystal complexes through specific noncovalent interactions.

For the preparation of functional self-assembled materials, control of phase-segregated structures from the nanometer to centimeter scale is also essential (Figure 2).[5,9,11,47–50] The determining factor for the function is the control of nano-

[*] Prof. T. Kato, Dr. N. Mizoshita, Dr. K. Kishimoto
Department of Chemistry and Biotechnology
School of Engineering
The University of Tokyo
Hongo, Bunkyo-ku, Tokyo 113-8656 (Japan)
Fax: (+81) 3-5841-8661
E-mail: kato@chiral.t.u-tokyo.ac.jp

© 2006 Wiley-VCH Verlag GmbH & Co. KGaA, Weinheim

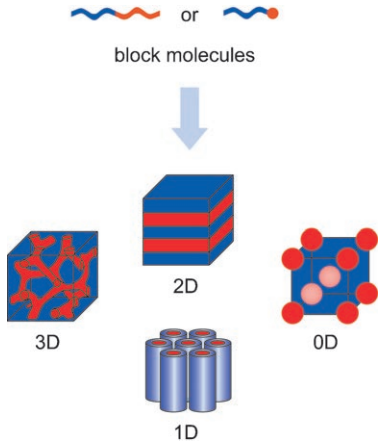


Figure 2. Liquid-crystalline phase-segregated structures of block molecules.

segregation at the molecular scale in the thermodynamically stable single phase. This segregation is completely different from macrophase separation which forms thermodynamically different phases. The nano-segregation behavior of amphiphilic molecules for lyotropic liquid crystals has long been known to induce mesomorphism.[14,15] A simpler nano-segregation of the aliphatic and aromatic parts has been used for the induction of thermotropic smectic phases. However, the potential of phase segregation for the development of functional thermotropic liquid crystals has only recently been recognized.[5,9,10] This trend has been aided by the great progress in the field of pure block copolymers.[48,49] A variety of phase-segregated structures in soft states can be built easily by self-assembly of liquid-crystal molecules that are designed to have block structures. The control of their nanoscale segregated liquid-crystal structures yields new complex nanostructures and introduces new functions, such as anisotropic mass and charge conduction.[5,51,52]

In addition to the approaches described above, a great deal of progress has also been made in the design of new molecular shapes for liquid-crystal molecules.[3,53] Although rod- and disk-shaped molecules have been standard for liquid crystals, recently many new and exotic shapes of mesogenic molecules have been prepared (Figure 3, see also Section 2.3).

We believe that the successful combination of specific intermolecular interactions, nano-segregation behavior, and the molecular shape of liquid crystals will lead to the development of a new generation of functional liquid-crystalline assemblies that form thermodynamically stable single phases.

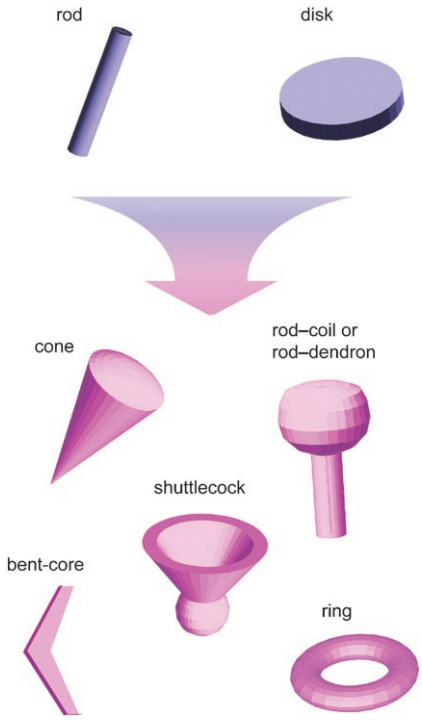


Figure 3. Molecular shapes of liquid-crystal molecules: the chronological development from conventional rods and disks to unconventional structures

Another approach to functional liquid crystals is the fabrication of liquid-crystal composite materials consisting of separated liquid-crystal and solid-state phases, which exhibit independent phase-transition behavior.[54–56] Conventional liquid-crystal composites, such as polymer-dispersed liquid crystals, are prepared by dispersing droplets of liquid crystals in the polymer.[54] Recently, self-assembly processes have been introduced into the design of liquid-crystalline composites. For example, liquid-crystalline physical gels are new composites consisting of liquid crystals and self-assembled solid fibers.[57,58] As a result of the formation of controlled phase-separated structures at the submicro- and micrometer level these gels show high performance in various functions.

Herein, we focus on functional liquid-crystalline assemblies developed by new materials design. In Section 2 we show how we design new liquid-crystalline assemblies for further



Takashi Kato received his PhD at the University of Tokyo in 1988. After postdoctoral research at Cornell University with Professor Jean M. J. Fréchet on supramolecular hydrogen-bonded liquid crystals, he joined the University of Tokyo where he is now a full professor. He received the Chemical Society of Japan Award for Young Chemists (1993), the Sakurada Memorial Award (1993), the IBM Japan Science Prize (2003), and the Japan Society for the Promotion of Science Prize (2004). He has published 220 articles in journals and books.



Norihiro Mizoshita was born in 1975. He worked on liquid-crystalline physical gels with Professor Takashi Kato at the University of Tokyo and received his PhD in 2003. Currently he is a JSPS Research Fellow at Nagoya University under the supervision of Professor Takahiro Seki. His present research interests focus on the self-assembly of functional organic molecules.

 © 2006 Wiley-VCH Verlag GmbH & Co. KGaA, Weinheim

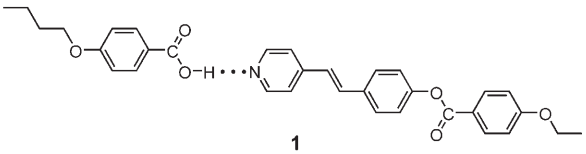
functionalization. We describe three important factors: 1) specific intermolecular interactions, 2) nano-segregation, and 3) the shape of the liquid-crystal molecules. In Section 3 we show how the design of the materials described in Section 2 allows their use for functions, such as conductivity, ion transport, optics, and catalysis. In Section 4, new approaches to self-assembled liquid-crystalline composites, which have phase-separated structures, are described.

2. New Design of Liquid-Crystalline Assemblies

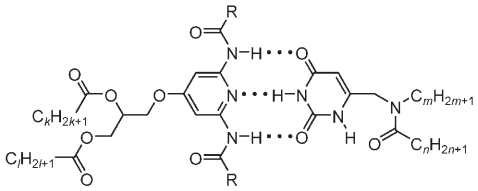
2.1. Specific Molecular Interactions for Supramolecular Assembly

2.1.1. Overview and Historical Background

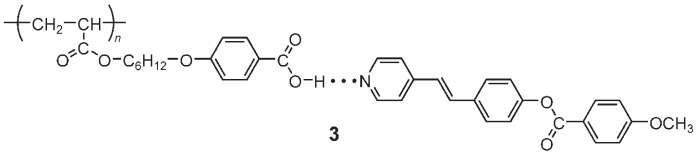
Specific intermolecular interactions play major roles in the supramolecular assembly of liquid crystals. In this Section we highlight hydrogen bonding, which drives the supramolecular self-assembly of liquid crystals and induces dynamic functions to the assemblies.[7,24,28] In nature, functional biomolecules, such as nucleic acids, sugars, proteins, and peptides, have hydrogen-donor and acceptor moieties, which serve for self-assembly and molecular recognition.[59] For synthetic liquid crystals, hydrogen-bonded materials such as benzoic acids have been known since the early 20th century.[60,61] However, hydrogen-bonded materials had not been recognized to be useful for advanced technologies until supramolecular approaches involving hydrogen bonding were introduced into the design of liquid crystals in 1989. Kato and Fréchet,[20,21] and Lehn et al.[22] reported that complementary intermolecular hydrogen bonding between different molecules leads to the formation of the well-defined structures of mesogenic complexes. The first examples of supramolecular liquid crystals were complex **1** (with one hydrogen bond) that exhibits smectic and nematic phases,[20] and complex **2** (with three hydrogen bonds) that shows a columnar phase.[22] Mesogens with rigid rod structures are simply obtained by the self-assembly of complementary molecular components. This concept was extended for the preparation of side-chain and main-chain liquid-crystal polymers **3**[21] and **4**,[23] which introduce the field of supramolecular polymers.[42,62,63]



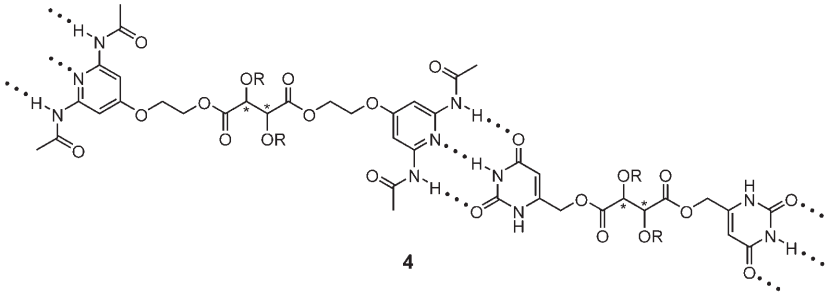
1



2



3



4

The molecular organization of liquid crystals through hydrogen bonds is classified as shown in Figure 4.[7,24,28] There are mainly two types: closed structure (Figure 4 A,B) and open structure (Figure 4 C,D). Mesogenic complexes with closed and well-defined hydrogen-bonded structures are defined as supramolecular liquid crystals in the original sense. They are obtained through the complexation of different molecular components (Figure 4 A). In addition, recently, "unconventional" complexes with elaborate closed structures consisting of identical molecules have also been referred to as supramolecular liquid crystals (Figure 4 B), whereas simpler, classical, liquid crystal benzoic acid dimers are not supramolecular liquid crystals. This supramolecular association of liquid crystals has been theoretically treated by Tanaka and co-workers.[64,65] The second type of hydrogen-bonded liquid crystals has open (non-closed) structures, such as ribbons and layers (Figure 4 C,D).[7,24,28] They are generated by the formation of sucessive hydrogen bonds, or a network of hydrogen bonds. All of these structures are obtained by self-assembly processes in which a variety of molecules spontaneously self-organize into complex and ordered structures under mild conditions.



Kenji Kishimoto started his research works on liquid-crystalline materials under the supervision of Prof. Kato at the University of Tokyo in 1999 and received his PhD in 2005. He was a JSPS Research Fellow in 2004–2005. Currently he is a research associate at the University of Tokyo. His research highlights the development and structural control of anisotropically ion-conductive polymer materials.

© 2006 Wiley-VCH Verlag GmbH & Co. KGaA, Weinheim

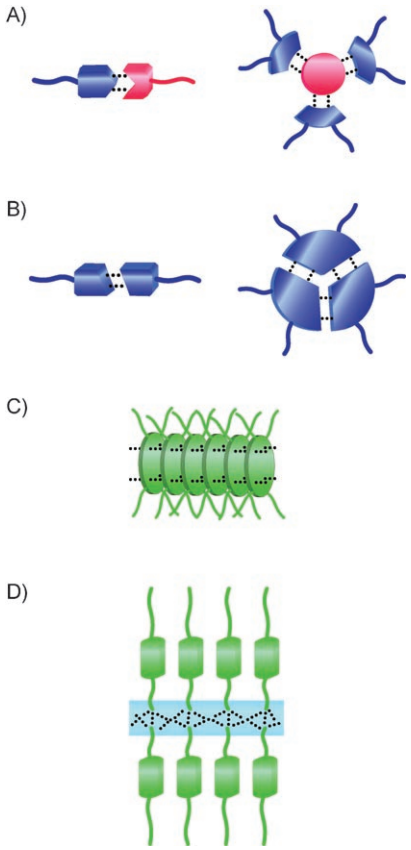


Figure 4. Hydrogen-bond formation in and between liquid-crystal molecules: supramolecular rod and disk complexes of A) different molecules; B) identical molecules; C) one-dimensional association through the formation of hydrogen-bonded chains between identical components; D) molecular association to give liquid crystals by the formation of layers linked by hydrogen-bonds.

2.1.2. *Specific Features of Supramolecular Liquid Crystals*

One of the specific features of supramolecular liquid crystals is their dynamic structures.[31] This property can be used for the design of functional systems. For example, stable, noncovalently bonded liquid-crystalline networks can be obtained from multifunctional non-mesogenic molecular components. A nematic state is induced by the complexation of compounds **5** and **6** (Figure 5).[32] In the nematic state, hydrogen bonding should be dynamic to enhance the mobile liquid-crystalline states. Moreover, these liquid-crystalline networks consisting of multifunctional hydrogen-bonding components show reversible mesomorphic–isotropic phase transitions as a result of the thermal formation and breaking (ON/OFF switching) of the hydrogen bonds. The use of such reversible cross-linking can be extended to prepare dynamic materials, such as stimuli-responsive materials.

In addition to the ON/OFF switching, the hydrogen-bonding pattern can be changed between two different arrangements "State A" (ON) to "State B" (ON) by stimuli and environment:[33,66,67] A folic acid

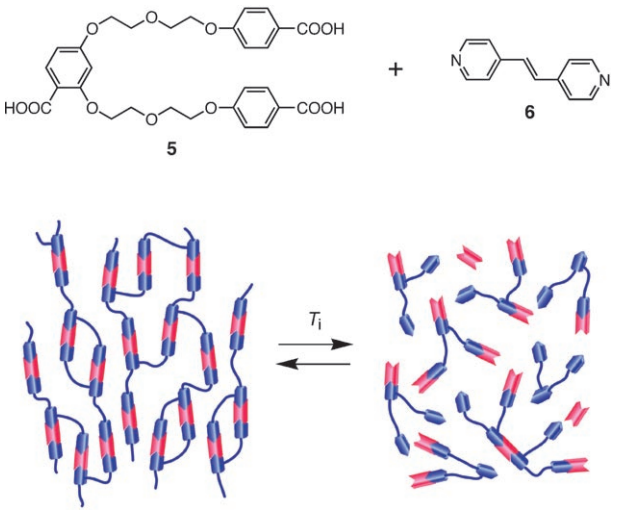
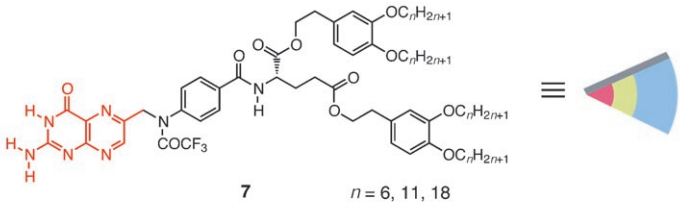


Figure 5. Supramolecular main-chain liquid-crystalline networks of **5** and **6**: at T_i a reversible phase transition occurs between nematic and isotropic phases as a result of the association and dissociation of hydrogen bonds.

derivative (**7**) having an undecyl chain has a thermotropic smectic A phase from −13 to 235 °C, whereas in the presence of a sodium salt or a lipophilic solvent, it shows a columnar phase (Figure 6). This phase change is caused by the change



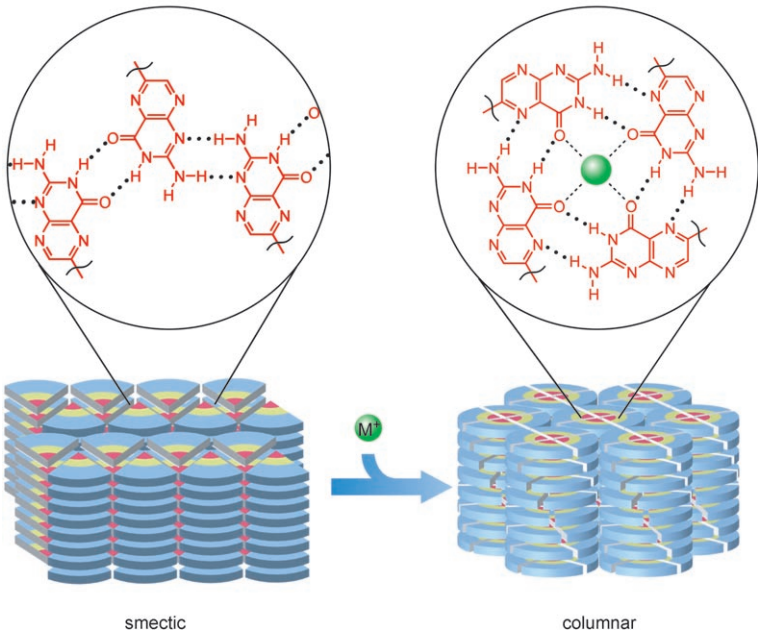
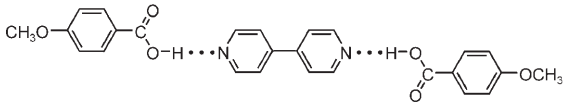


Figure 6. Structural changes of supramolecular liquid crystals based on folic acid derivatives **7**: The presence of an ion induces a change in the hydrogen-bonding pattern, as a result the ribbon structure changes to a disk structure.

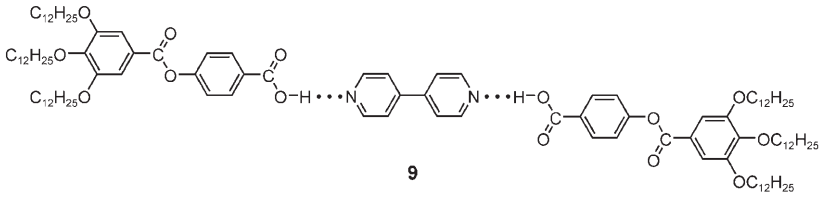
 © 2006 Wiley-VCH Verlag GmbH & Co. KGaA, Weinheim

from the ribbon-like hydrogen-bonded pattern (State A) to the disk-like pattern (State B).

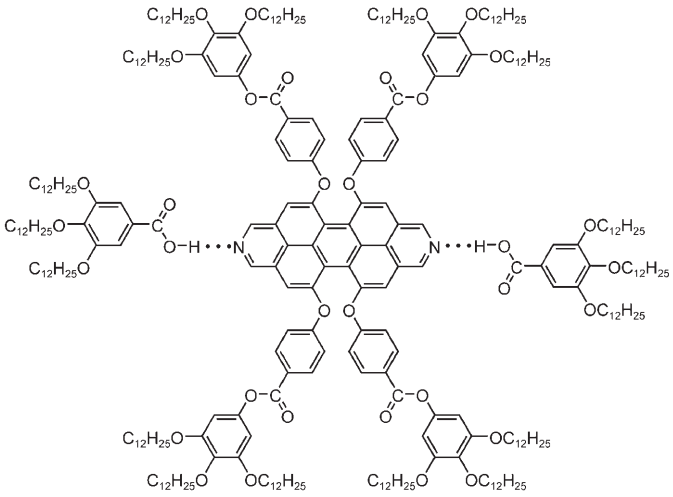
Another advantage of supramolecular liquid crystals is that complex structures are built from several different kinds of molecular components by simple assembly processes. A variety of mesogens can be formed by the combination of a small number of components. For example, a liquid-crystalline phase is induced by the 2:1 complexation of non-mesomorphic components, 4-methoxybenzoic acid and 4,4′-bipyridine.[68,69] In this case, nematic mesogen **8** is obtained by simple assembly of two independent components. A nematic phase is seen for **8** from 153 to 163 °C. When the methoxybenzoic acid is replaced by a trialkyl-substituted molecule, the resulting complex **9** shows a columnar phase up to 98 °C.[70] The materials can also be functionalized by the incorporation of a dye as a hydrogen-bond-proton acceptor: Fluorescence is observed for the complex **10**,[71] and the properties of this material may be tuned by changing hydrogen-donor components. A variety of mesogenic complexes, such as cones and bananas, have been obtained by connecting two different components through specific hydrogen bonding.[72,73]



8

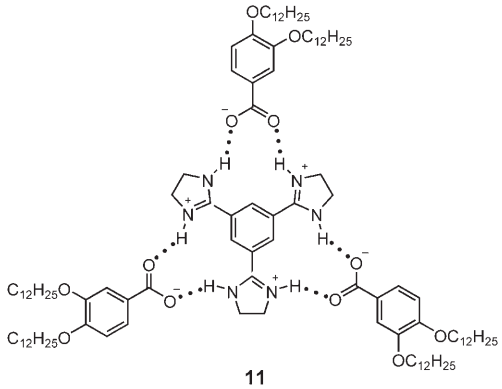


9

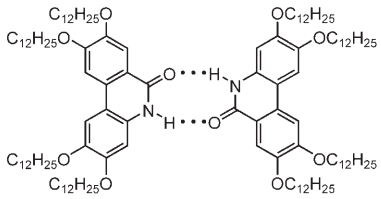


10

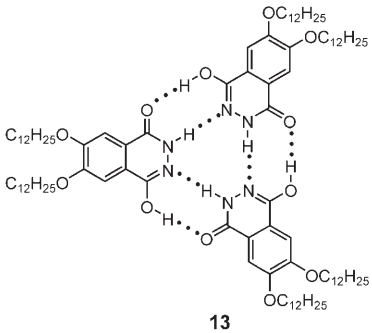
Not only rod-like mesogenic complexes but also disk-like mesogenic complexes with well-defined structures have been prepared by using various hydrogen-bonding patterns. The disk-like supramolecular, hydrogen-bonded, 3:1 complex **11** has a thermotropic columnar phase between 72 and 240 °C.[74] Disk-like dimer **12**,[75] trimer **13**[76], and tetramer **14** (Figure 7)[34] are also formed by the association of hydrogen-bonded molecules. Complexes **12** and **13** have thermally stable columnar phases up to around 200 °C as a result of stable hydrogen-bonding formation and π–π stacking. The disk tetramer (**14**) of a folic acid derivative incorporating oligo(glutamic acid) moieties has thermotropic columnar and micellar cubic (*Pm3n*) phases, and folic acid (**15**) itself was found to show lyotropic liquid-crystalline phases in water in the presence of sodium chloride (Figure 8).[34,77–79] In the presence of sodium salts, **14** forms supramolecular chiral structures in the columnar and cubic phases (Figure 7). The interactions between the hydrogen-bonded disks and the ions may fix the supramolecular chiral



11



12



13

© 2006 Wiley-VCH Verlag GmbH & Co. KGaA, Weinheim

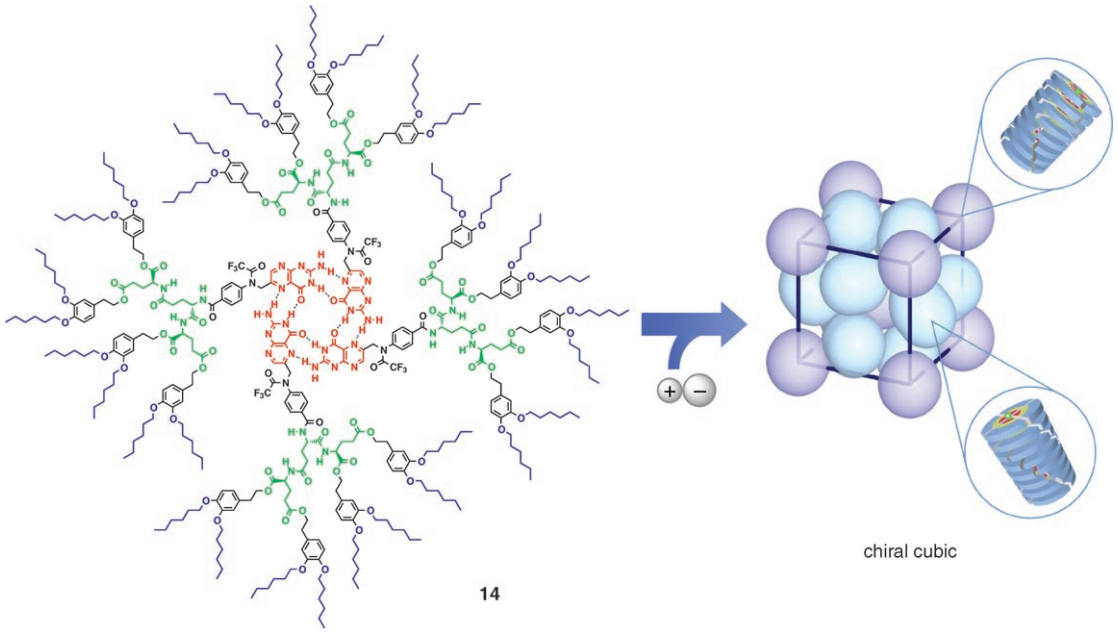


Figure 7. Supramolecular chiral cubic phases formed by the self-assembly of hydrogen-bonded chiral disk-like complex **14** and an ion.

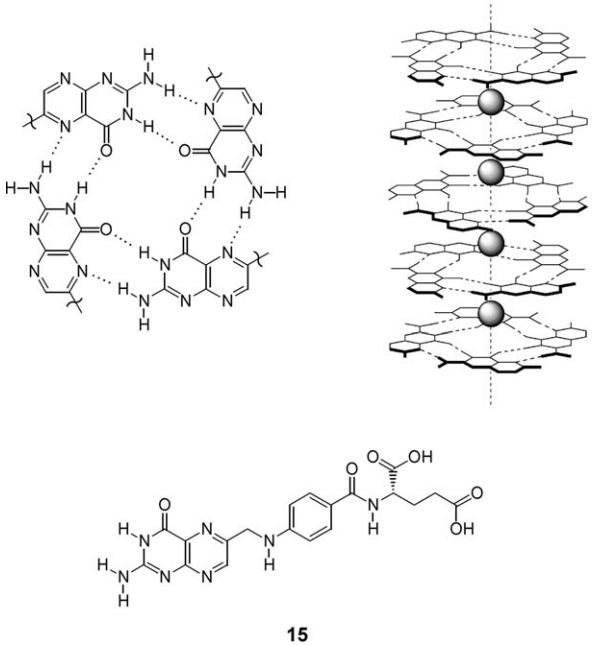


Figure 8. Formation of a disk-like hydrogen-bonded complex of folic acid **15** in aqueous solution. Stacking of the disks gives a columnar structure (spheres represent sodium ions).

structures in the columnar phase.[79–81] Moreover, supramolecular chiral micellar cubic phases have been found to form by segmentation of the chiral columns.

In addition to hydrogen bonding, ionic interactions,[82,83] charge-transfer interactions,[84–89] and halogen bridges[90] also direct liquid-crystalline molecular assemblies. Charge-transfer interactions have been used for the enhancement of columnar and smectic phases. For example, the addition of 2,4,7-trinitrofluorenone (TNF) to triphenylene derivatives induces liquid-crystalline phases.[84–86,88,89] The formation of halogen bridges was found to induce complexation of iodopentafluorobenzene and 4-alkoxystilbazole to give liquid-crystalline phases.[90]

2.1.3. *Supramolecular Liquid-Crystal Polymers*

The concept of supramolecular materials design was extended to the design of polymeric materials. Polymers with mesogenic side chains are prepared by the association of functionalized polymers and small molecules through specific intermolecular interactions (Figure 9).[7,21,24,26,28,91] Polymers with supramolecular side chains can be categorized into three types (Figure 9A–C); Type A has mesogens hydrogen-bonded to the polymer side chains, which are connected to the covalently bonded backbones. The benzoic acid/pyridine mesogenic complexes of **16** are formed through the formation of the single hydrogen bonds in the side chains.[92,93] This type of structure has been the most studied side-chain supramolecular polymer.[26,94–98] They exhibit thermally stable smectic phases. Doubly hydrogen-bonded side-chain mesogens **17** show columnar liquid-crystalline phases.[26,99,100] The details on these side-chain polymers are described in previous reviews.[26,94] The use of hydrogen bonding for the complexation in the polymer side chains has been extended to the design of a variety of non-mesomorphic polymeric systems in solution and bulk states.[43,44,101]

Supramolecular structures shown in Figure 9B are "grafted" polymers. Polymeric complexes **18**[102] and **19**[103,104] are obtained by complexation of end-functionalized mesogenic molecules and backbone-functionalized polymers, such as poly(vinylpyridine) and poly(acrylic acid).[105–108] Simple alkylphenols, which are not mesogenic, also form liquid-crystal polymer complexes **20**.[109] These supramolecular

 © 2006 Wiley-VCH Verlag GmbH & Co. KGaA, Weinheim

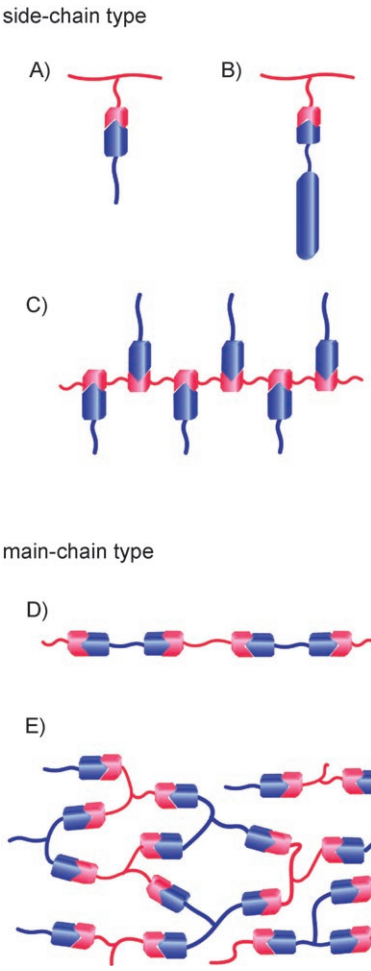


Figure 9. Supramolecular polymers: A–C) side-chains with hydrogen-bonded mesogens and D,E) main-chains containing mesogens.

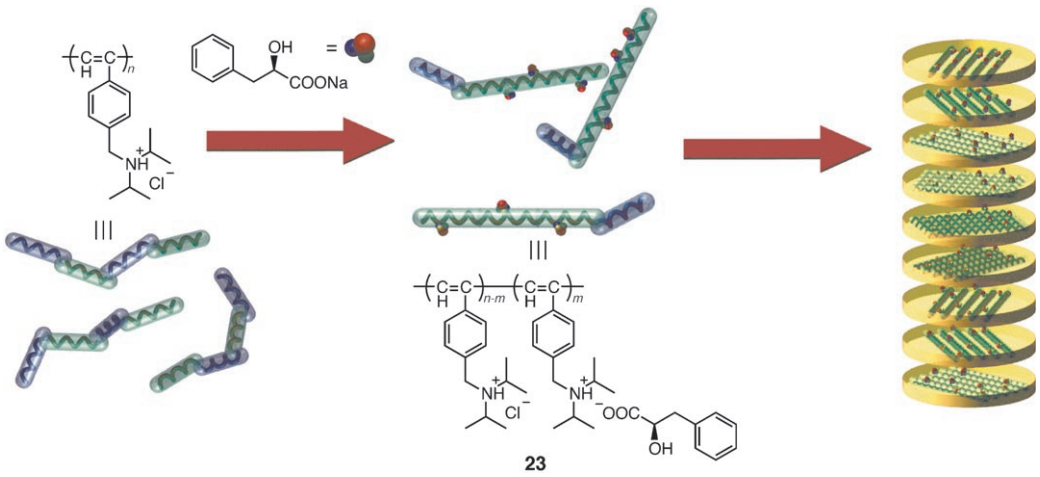
grafted polymers self-organize into hierarchical ordered structures.[47,110–115] They have been applied to the preparation of photofunctional, optical, and conductive materials (see also Section 3).[110,115]

Ionic interactions can also be used for the preparation of supramolecular side-chain structures.[82,116,117] In polymer **21** the disk-like molecules are linked to the side chain of a poly(amino acid) through the interaction between amine and carboxylic acid groups.[116] The interactions of amino groups with sulfonic moieties can also be used to connect polymer backbones and mesogenic groups.[82] Polymeric complex **22** has a smectic A phase, which tends to show a homeotropic alignment on interaction with glass surfaces.

The ionic interaction between the hydrochloride of a polymer having a *N*,*N*-diisopropylaminomethyl moiety and a small amount of chiral carboxylate leads to the formation of a helical polymer with a one-handed conformation. Cholesteric phases are induced when these supramolecular polymer complexes, such as **23**, are formed in concentrated aqueous solution (Figure 10).[118]

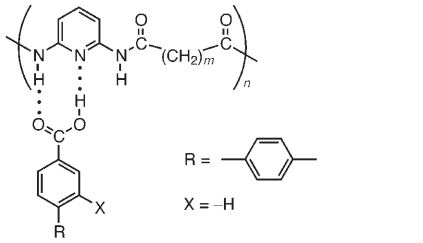
The incorporation of a hydrogen-bonding unit, 2,6-diaminopyridine moiety, into a polyamide backbone enables the polymer to recognize molecules such as benzoic acids through hydrogen-bond formation (Figure 9C).[119,120] This process leads to the formation of supramolecular liquid-crystal polyamide **24**.[119] The smectic phase displayed by **24** is

© 2006 Wiley-VCH Verlag GmbH & Co. KGaA, Weinheim

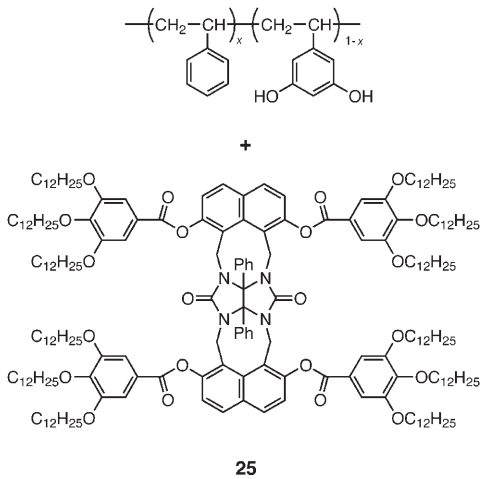


23

Figure 10. The induction of macromolecular helicity, chiral amplification, in dilute solution, and the cholesteric liquid-crystalline state for the resulting supramolecular ionic polymers.[118]



24



25

highly thermally stable up to 350 °C. Supramolecular polyurethanes have been obtained with hydrogen bonded groups in their side chains.[121]

Host–guest interactions have yielded a new type of material with supramolecular side chains.[122] Liquid-crystalline phases are observed in inclusion complexes, such as **25**, of hydroxy-functionalized polystyrenes and a clip molecule. Hydrogen bonding between the hydroxy groups of the polymer and the carbonyl moieties of the urea groups of the clip molecule plays a determining role in the formation of the host–guest complexes.

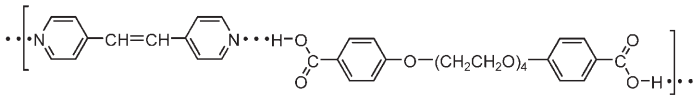
Main-chain supramolecular liquid-crystal polymers **4**,[23] **26**,[123] and **27**[124] with linear structures are prepared by the complexation of bifunctional components through the formation of hydrogen bonds (Figure 9D, see also Section 2.1.1). Griffin et al. exploited hydrogen bonding between carboxylic acid and pyridine units for the preparation of linear polymeric complexes.[123] For example, complex **26** shows smectic and nematic phases. Lyotropic rigid-rod supramolecular polymer **27** was prepared through triple hydrogen bonding between bifunctional molecules.

Hydrogen bonding host–guest type interactions in the main chain have been used for the fabrication novel linear supramolecular polymers (Figure 11).[125,126] Compound **28** forms polymeric complexes and exhibits lyotropic liquid-crystalline behavior in the presence of chloroform and *o*-dichlorobenzene. In this case, these solvents also act as guests for the complexation.

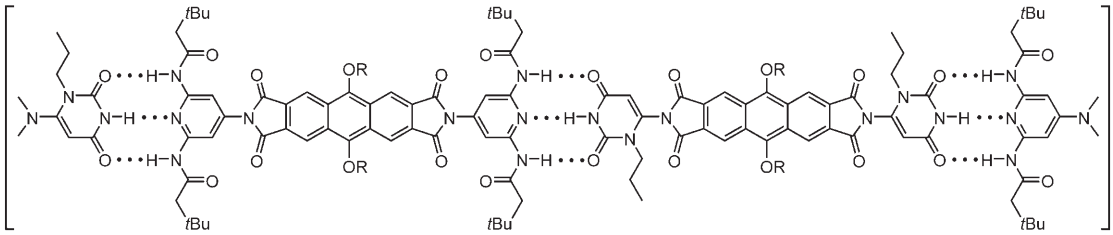
Networks of main-chain supramolecular liquid-crystal polymers exhibiting nematic, smectic, and cholesteric phases have been prepared by complexation of multifunctional components (Figure 9E).[32,127,128] For example, smectic phases are formed by trifunctional hydrogen-bond donor **29** and acceptor **30**. As is shown in Section 2.1.2, the polymer complexes undergo reversible structural changes as a result of the dynamic nature of the hydrogen bonding. Cholesteric structures of the chiral supramolecular network formed from **5** and **31** are preserved in the glass state at room temperature. Non-mesomorphic complexes are obtained for a dicarboxylic acid and a tetrapyridyl compound.[129]

Fluorescent supramolecular liquid-crystal polymers have been prepared from the nucleobase-terminated monomers **32** and **33** (Figure 12), these monomers also contain a bis(phenylethynyl)benzene moiety.[130] The mixtures of these two hydrogen-bonding molecules have liquid-crystalline phases from 125 to 154 °C. These supramolecular polymers can be

 © 2006 Wiley-VCH Verlag GmbH & Co. KGaA, Weinheim



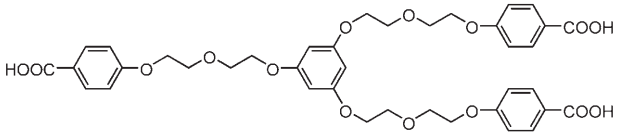
26



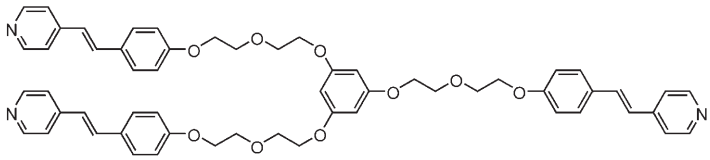
27

processed to oriented fibers exhibiting fluorescence. A merocyanine dye has also been incorporated into supramolecular liquid-crystal polymers which form a columnar mesophase.[131]

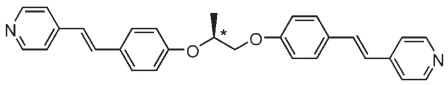
The early approaches to the fabrication of supramolecular liquid-crystal polymers have initiated the field of non-liquid-crystal supramolecular polymers (Figure 13 A).[42,63,132] Meijer and co-workers reported that a quadruple hydrogen bond is useful for the construction of stable supramolecular polymers because of its high association constant.[42,133–135] Monomer **34** possessing two ureidopyrimidone units forms stable and elongated polymer complexes (Figure 13 A).[133] In solution, these hydrogen-bonded polymer complexes show viscoelastic properties, which are similar to those of normal covalently bonded polymers. Network complexes are also obtained from compounds containing three ureidopyrimidone units.[134]



29



30



31

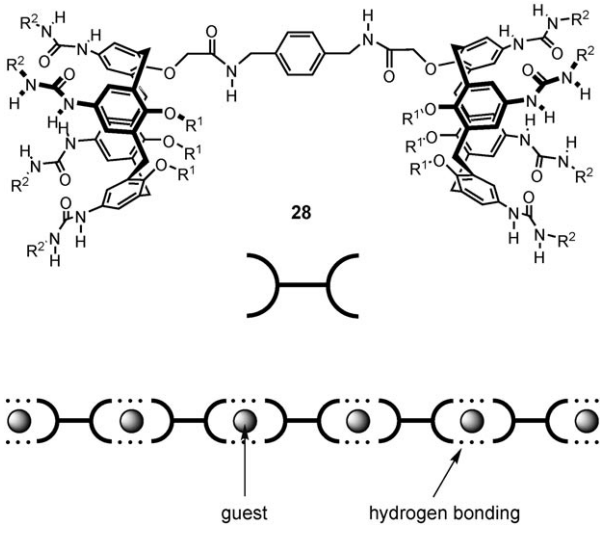


Figure 11. Self-assembly of main-chain host–guest polymer **28**.

Long and co-workers extended the use of the quadruple hydrogen bond to end-functionalized polystyrene, polyisoprene, and their block copolymers (Figure 13 B).[136,137] They reported rheological and phase-segregation behavior of associated polymers **35**. The complementary intermolecular hydrogen bonding is also introduced into the polystyrene block by anionic polymerization and the capping technique.[138]

Self-assembled solid fibers are obtained through the complexation of carboxylic acid functionalized and pyridine functionalized monomers.[139] The complexation of ammonium salts with molecules that contain two dibenzo crown ether

 © 2006 Wiley-VCH Verlag GmbH & Co. KGaA, Weinheim

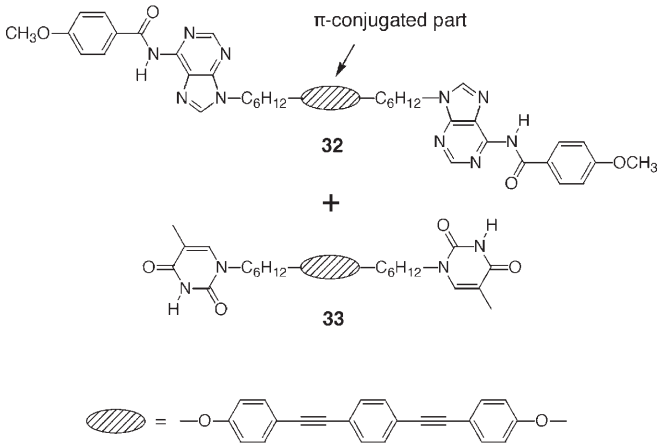


Figure 12. Complementary nucleobase derivatives **32** and **33** form fluorescent supramolecular liquid-crystal polymers.

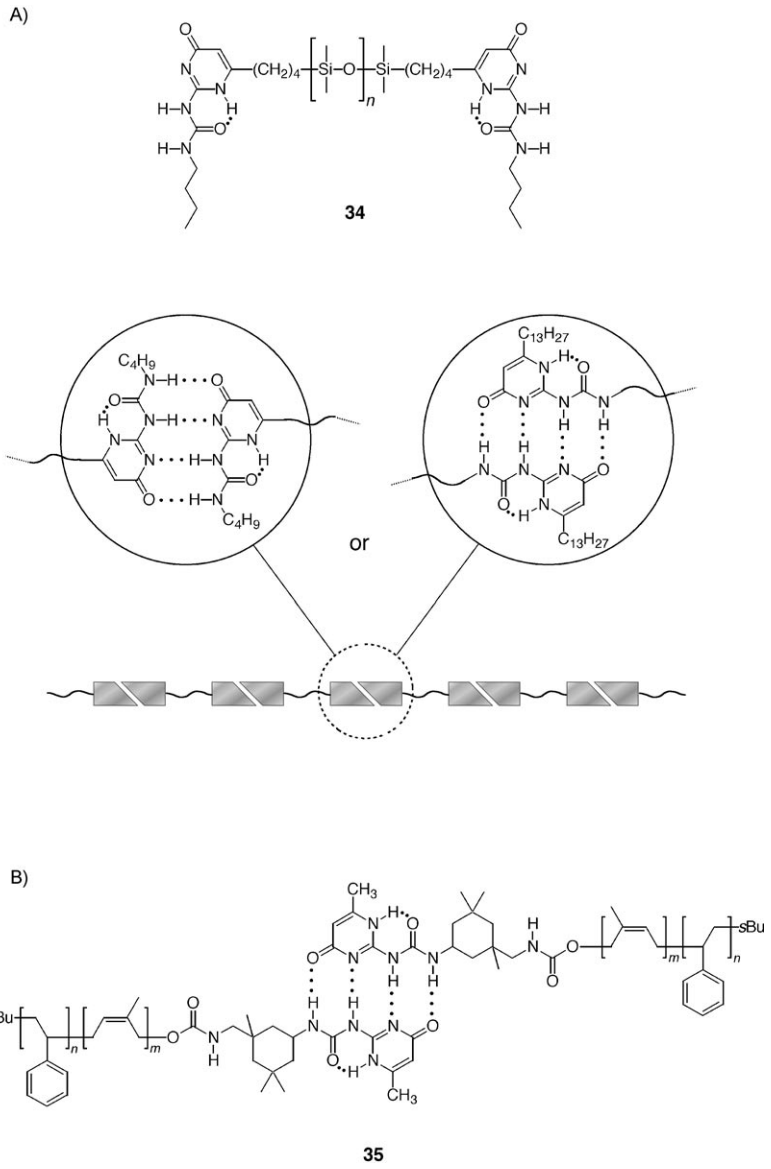
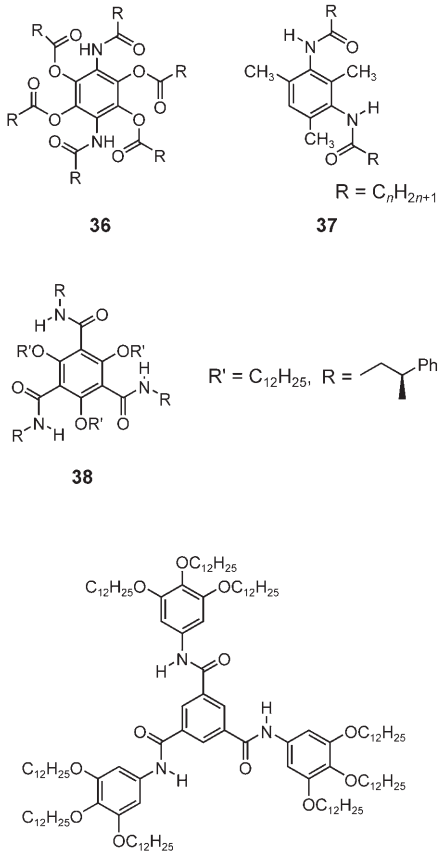


Figure 13. Self-assembly of supramolecular non-mesogenic main-chain polymers formed through quadruple hydrogen bonding: A) linear polymer **34**; B) block copolymer **35**.

units, results in the formation of supramolecular polymers through dipole–ion interactions.[140,141]

2.1.4. One-Dimensional Open-Type Assembly

A non-closed (open) type of hydrogen bonding such as that found with a one-dimensional (1D) array of aromatic amide groups leads to the formation of the liquid-crystalline aromatic stacks (Figure 4C).[7,24,142–150] This self-assembly behavior of aromatic amides, which induces liquid-crystalline phases, was found by Matsunaga and co-workers in the late 1980s.[142–144] For example, compounds **36** and **37** exhibit



columnar liquid-crystalline phases.[142,143] The introduction of amide groups into substituted benzene compounds induces or stabilizes their thermotropic liquid-crystalline phases through the formation of 1D hydrogen bonding. Nuckolls and co-workers prepared several benzene triamide compounds containing chiral moiet-

 © 2006 Wiley-VCH Verlag GmbH & Co. KGaA, Weinheim

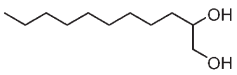
ies.[145,146] Pure compound **38** forms a thermotropic columnar mesophase and in solution states helical stacking is induced.[145,146] Larger disk-like amide molecules have been prepared, such as compound **39** which has a liquid-crystalline phase from −4 to 178 °C.[147] Amide linkages also induce and stabilize the hexagonal columnar phase of the bis(amide) compound **40**.[148,149]

Hydrogen bonds between amide linkages have long been known to serve as structure-forming interactions in proteins[59] and in synthetic polyamides, such as nylon and kevlar.[59,151,152] However, the 1D molecular organization by amide linkages still offers new features for the design of self-assembled materials not only for liquid crystals but also for functional materials in solution and solid states.[142–144,147,153–159] For example, amide hydrogen-bonding patterns are also used for the design of gelators, which form 1D fiber aggregates in solvents.[155–158] In addition, the hydrogen bonds between the urea linkages can also drive 1D self-assembly.[147,153–155]

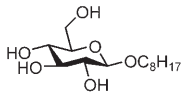
2.1.5. Two- or Three-Dimensional Open Assemblies

Another representative example of open type of hydrogen bonding is hydrogen-bonded networks (Figure 4D) of hydroxy groups. A variety of liquid-crystal compounds that contain hydroxy groups have been prepared. Details on the liquid-crystal polyhydroxy compounds were given in previous reviews.[7,160] Early examples are glycolipids[7,160–163] and dihydroxy aliphatic molecules.[164] Compounds **41**[164] and **42**[162,163] form thermotropic smectic phases. Such behavior is induced by two processes: 1) the formation of hydrogen bonds between hydroxy groups, and 2) the nano-segregation of hydrogen-bonded 2D sheets and lipophilic sections. The formation of liquid-crystalline assemblies by such segregation processes is discussed in Section 2.2.

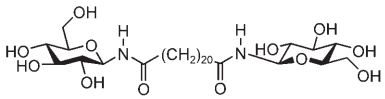
Bolaamphiphiles, in which two hydrophilic groups are connected to both extremities of a hydrophobic spacer, stabilize membrane structures.[165,166] They show more thermally stable thermotropic liquid-crystalline behavior than normal amphiphiles. Compound **43** has a mesophase from 228 to 240 °C,[166] and a smectic phase between 69 and 110 °C is observed for compound **42**. Compound **44** was synthesized as a model of a membrane component of Archaebacteria.[167] It forms a columnar liquid-crystalline phase from 65 to 115 °C. In the columnar liquid-crystal structure of **44**, it is believed that the aliphatic chains are located on the exterior and the sugar units are in the inside of the columns.



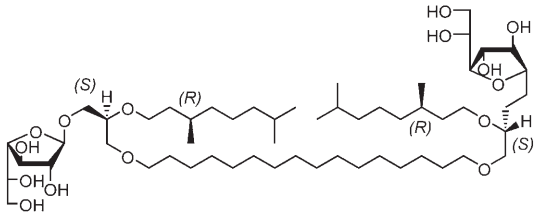
41



42



43



44

2.2. Nano-Segregation

The nano-segregation of the incompatible sections of amphiphilic or block molecules is, in addition to the anisotropic shape of molecules, a key driving force of liquid-crystal formation. Lyotropic liquid crystals of amphiphilic molecules are typical examples of nano-segregation in liquid crystals.[14,15] In these materials, the hydrophobic and hydrophilic parts of the molecules segregate at the nanometer scale in the presence of water, leading to liquid-crystalline order. For thermotropic liquid crystals, it is well known that aromatic rod-like compounds having longer aliphatic chains tend to form smectic (layered) liquid-crystalline phases.[1] In this case, segregation of aromatic and aliphatic moieties on the nanometer length scale drives layered-structure formation. Recently, new-materials design, using microphase-segregation of block polymers[48,168,169] and small molecules[10,170,171] has attracted much attention because elaborate three-dimensional (3D) nanostructures with dimensions of between tens and hundreds of nanometers are easily obtained by self-organization. The morphology of the segregation at the nanometer scale[9] is relevant to the micro-segregation behavior of block polymers.

Some representative examples of thermotropic nano-segregated liquid crystals that have been systematically studied are the hydroxy-functionalized alkanes and sugars with long alkyl chains described in Section 2.1.5. More complex structures have been systematically studied by Tschierske and co-workers.[172–174] They have studied the segregation behavior of liquid crystals on the nanometer scale by tuning the balance of the shape and volume of two incompatible parts. Compounds **45**–**47** are amphiphilic mesogenic molecules having diol moieties. These molecules show

© 2006 Wiley-VCH Verlag GmbH & Co. KGaA, Weinheim

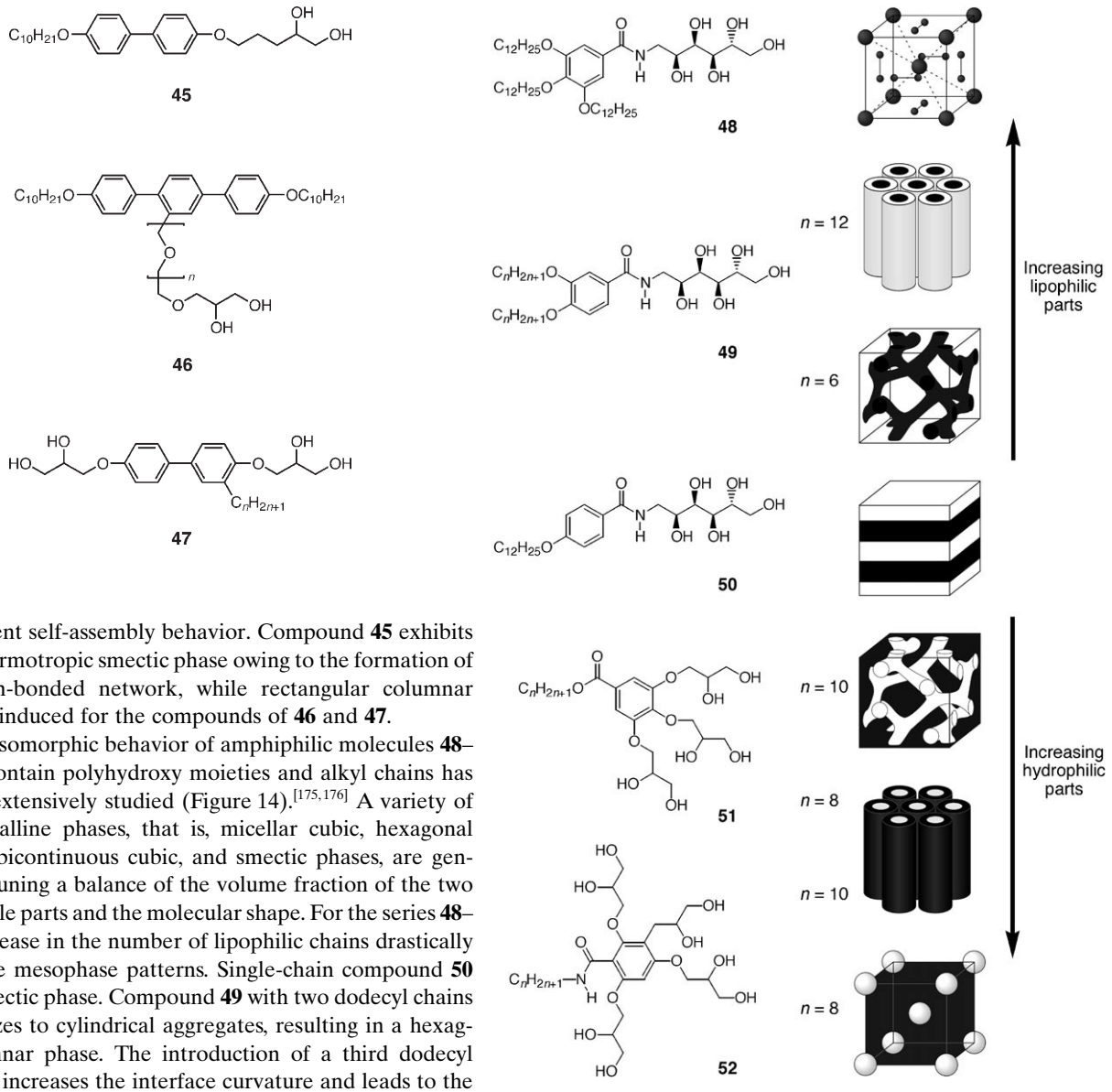


Figure 14. Dependence of mesophase morphology on the molecular structure of the polyhydroxy amphiphiles **48**–**52**.

very different self-assembly behavior. Compound **45** exhibits a stable thermotropic smectic phase owing to the formation of a hydrogen-bonded network, while rectangular columnar phases are induced for the compounds of **46** and **47**.

The mesomorphic behavior of amphiphilic molecules **48**–**52** which contain polyhydroxy moieties and alkyl chains has also been extensively studied (Figure 14).[175,176] A variety of liquid-crystalline phases, that is, micellar cubic, hexagonal columnar, bicontinuous cubic, and smectic phases, are generated by tuning a balance of the volume fraction of the two incompatible parts and the molecular shape. For the series **48**–**50**, the increase in the number of lipophilic chains drastically changes the mesophase patterns. Single-chain compound **50** forms a smectic phase. Compound **49** with two dodecyl chains self-organizes to cylindrical aggregates, resulting in a hexagonal columnar phase. The introduction of a third dodecyl chain in **48** increases the interface curvature and leads to the formation of globular aggregates arranged in a cubic lattice. In contrast, when the number of the dihydroxy groups increases for compounds **51** and **52**, columnar and cubic structures are formed which have the hydrophobic alkyl chains in the inner parts. The formation of intermolecular hydrogen-bonding networks between hydroxy groups as well as nano-segregation of hydrophilic and hydrophobic parts are the driving forces for such self-organization.

Polyphilic block molecules **53** consist of a rigid biphenyl unit, terminal polar 1,2-diol units, and a lateral semiperfluorinated chain. The incompatibility of these blocks induces a wide variety of liquid-crystalline phases (Figure 15). Columnar and lamellar phases with complex nano-segregated structures are formed by the increasing the length of the lateral semiperfluorinated chain.[177] The polyphilic block molecules with C_6 to C_{14} lateral chains form a series of columnar phases, where the nonpolar lateral chains cause the nano-segregation into columns (Figure 15B–D). The chain length influences the diameter and shape of the columns, and the lattice type of the columnar phases. Further elongation of the lateral chain induces the formation of novel mesophases with layered structures (Figure 15E). In the layered mesophases, the aromatic cores are arranged parallel to the layer planes. A sequence of subtypes described as laminated nematic and smectic phases are observed for the layered mesophases which result from the orientational and positional ordering of the biphenyl segments.

Nano-segregation of rod–coil block molecules also shows interesting self-organization behavior. Stupp and co-workers synthesized mini-triblock copolymer **54**.[10] It exhibits a thermotropic liquid-crystalline phase from 130 to 262 °C. Self-organization of molecule **54** by a crystallization process leads to the formation of supramolecular mushroom-shaped nanostructures. Lee and co-workers synthesized coil–rod–coil and rod–coil molecules consisting of aromatic rigid parts and poly(propylene oxide) coils.[178–180] The length of the coil part significantly affects the ordered structures of molecules. Coil–

 © 2006 Wiley-VCH Verlag GmbH & Co. KGaA, Weinheim

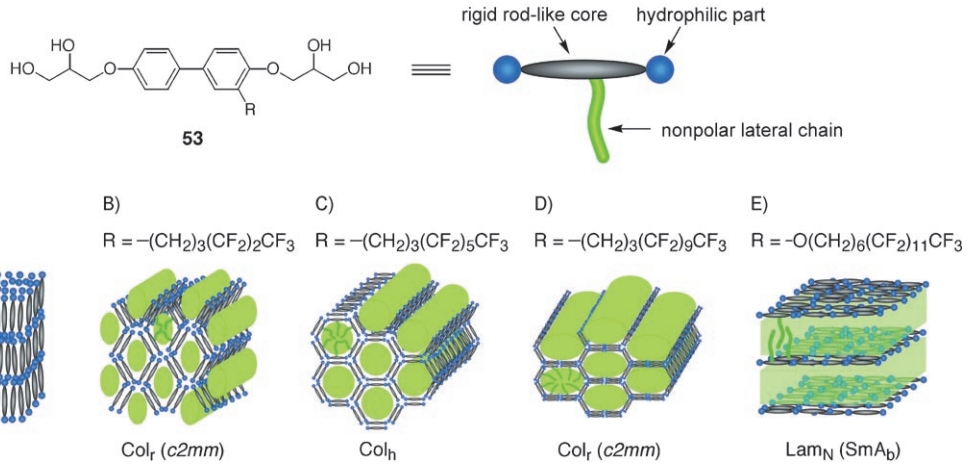
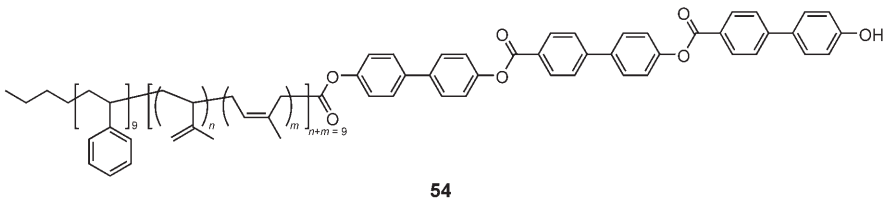


Figure 15. Liquid-crystalline phases formed from rigid bolaamphiphiles **53** containing nonpolar lateral chains; smectic A (SmA), rectangular columnar (Col_r), hexagonal columnar (Col_h), laminated nematic (Lam_N), biaxial smectic A (SmA_b).



rod–coil molecule **55** exhibits a hexagonal columnar phase from 92 to 153 °C (Figure 16). The inner core of the column consists of parallel arranged rigid rods, while the outer part

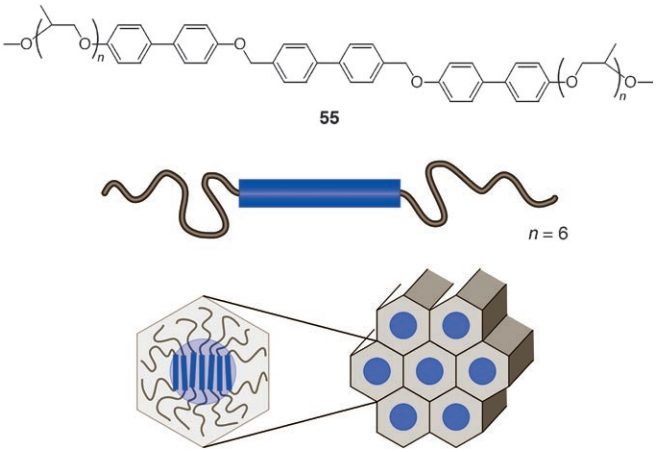


Figure 16. Self-assembly of coil–rod–coil molecule **55** into the hexagonal columnar phase.

consists of flexible coils filling the intercolumnar matrix. A rigid wedge-shaped building block with a poly(ethylene oxide) (PEO) coil part has been reported to show a variety of liquid-crystalline assembled structures.[181] Liquid-crystal rod–coil molecules based on polyisoprene were prepared by living free-radical polymerization of its monomer by using a rod block molecule as a macroinitiator.[182] A new class of micro-segregated liquid crystals, the inorganic–organic hybrids, have been developed for ordering quantum dots (Figure 17).[183] The genetically engineered M13 bacteriophage with monodisperse size and shape exhibits liquid-crystalline structures in solution states. The M13 bacteriophage which shows specific binding to ZnS crystal surfaces is selected through screening of phage display libraries. The phage is cloned and amplified to liquid-crystalline concentrations. The suspension of the complex consisting of the phage and nanocrystals of ZnS

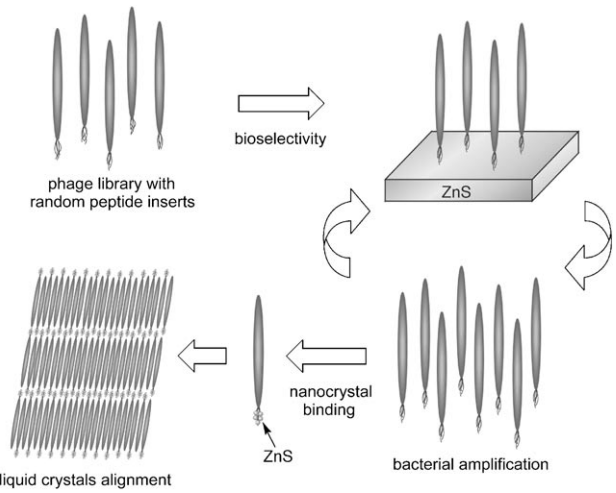


Figure 17. Generating nanocrystal alignment by the phage-display method.

forms lyotropic lamellar phases. The quantum dots are anisotropically arranged through the liquid-crystal ordering of the phage. This approach using bioselectivity is also applicable to the alignment of gold nanoparticles and organic small molecules.[184]

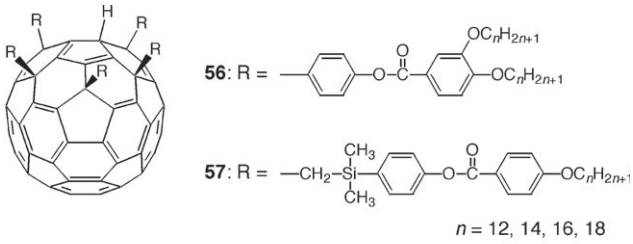
© 2006 Wiley-VCH Verlag GmbH & Co. KGaA, Weinheim

2.3. New Shapes of Molecules

The shape of the molecules is one of the most fundamental factors in the design of liquid crystals because molecular shape basically determines the molecular packing and order. Rods and disks are basic structures of thermotropic liquid-crystal molecules. The relationships between the shapes of these conventional molecules and their liquid-crystalline properties have been widely studied.[1] Recently, intensive studies have focused on unconventional shapes of liquid-crystal molecules, such as bananas (bent-core),[185–187] polycatenars,[188] and dendrons.[189–191] Metal coordination is also an important tool for the construction of new mesogenic structures, such as metallomesogens and supramolecular polymers.[192–194] However, we do not describe these materials herein because several reviews have already summarized these fields.[186,188,192,193] In this Section, several unconventional molecular shapes and their self-assembly behavior are described: cones,[195–197] shuttlecocks,[198,199] dendrimers/dendrons,[189–191,200–202] rod-dendrons,[203] and rings[204] (Figure 3). New functional supramolecular materials can be obtained based on these unconventional materials because their block molecular structures allow them to form ordered, hierarchical, and nano-segregated assemblies.

Shape-driven self-assembly can yield polar arrays of liquid crystals.[205] One approach is to prepare a "rigid" unconventional shape to drive self-assembly. Cone structures have been employed to stack the molecules one-dimensionally.[195–197] The "nano-shuttlecock" molecules **56** with conical cavities have thermotropic hexagonal columnar phases up to approximately 140 °C (Figure 18).[198] The attachment of five aromatic groups to one pentagon of a C_{60} fullerene molecule yields conical molecules that stack into columnar assemblies. Lyotropic nematic columnar and hexagonal columnar phases are also found when dodecane is used as the solvent. To make a larger cavity that has a larger loading capacity, a cup-shaped cavity is created on a fullerene with the aid of a silicon connection.[199] The larger cavity of **57** can comfortably accommodate the second fullerene molecule, which leads to the induction of thermally more stable columnar phases. The columnar–isotropic phase-transition temperature is around 180 °C.

Over the past 20 years, the chemistry of dendrimers and dendrons has been a rapidly growing area in polymer chemistry and materials science.[206] Some liquid-crystal dendrimers and dendrons have been developed as the first representatives of a new class of self-assembled materials.[189–191,200–202,207] There are two types of liquid-crystal dendrimers: In the first type, the self-assembled structure of the dendrimers or dendrons themselves act as supramolecular mesogens. Percec and co-workers synthesized a large number of liquid-crystal dendrons and dendrimers.[208–210] They reported that cone-shaped dendron **58** forms a spherical supramolecular dendrimer exhibiting micellar cubic *Pm*3*n* phases, while a columnar phase is seen for flat semicircular-shaped dendron **59** (Figure 19). A complex liquid-crystalline phase was found for the self-assembled dendrimers. It has a tetragonal three-dimensional unit cell containing 30 globular supramolecular dendrimers.[210] Wiesner and co-workers have



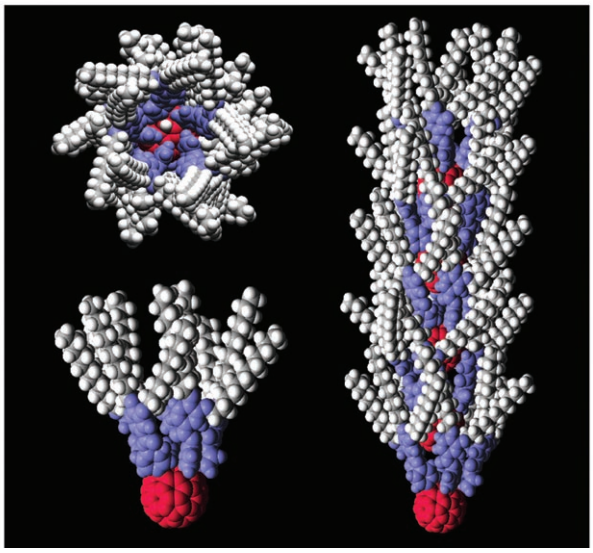


Figure 18. "Nano-shuttlecock" molecules **56** and **57** with a fullerene apex. Illustration of the stacking of **56**.[198]

shown that amphiphilic liquid-crystal dendrimers form a variety of phase structures.[211,212]

The second type of dendrimer has conventional rod mesogens that drive liquid-crystalline order; carbosilanes,[191] poly(propylene imine),[200] poly(amidoamine),[201] and polyesters[189] have been used as their backbones. Functional molecules, such as fullerenes, have been incorporated in the center of dendrimers.[189] The second type of dendrimers have been reviewed already.[213] Such molecular design has been extended to "Janus" molecules (Figure 20).[214,215] Compound **60** is obtained by connecting two units, one unit has three cyanobiphenyl moieties and the other three chiral phenyl benzoate groups. These mesogens have different characters as shown in Figure 20. Janus molecule **60** shows a chiral smectic C phase from −3 to 34 °C and a cholesteric phase between 34 and 61 °C. Stupp and co-workers prepared liquid crystals by connecting the linear aromatic rod part and dendrons.[203] Molecule **61** self-assembles to form a cubic phase up to 114 °C.

A columnar phase can be exhibited by ring-shaped molecule **62**, which is a new type of discotic molecule.[204] It shows a columnar phase on cooling from 130 to 103 °C. The tubular assemblies of **62** can accommodate small quantities of silver triflate in the columns without destroying the liquid-crystalline order, which indicates potential use as new ion-channel materials.

© 2006 Wiley-VCH Verlag GmbH & Co. KGaA, Weinheim

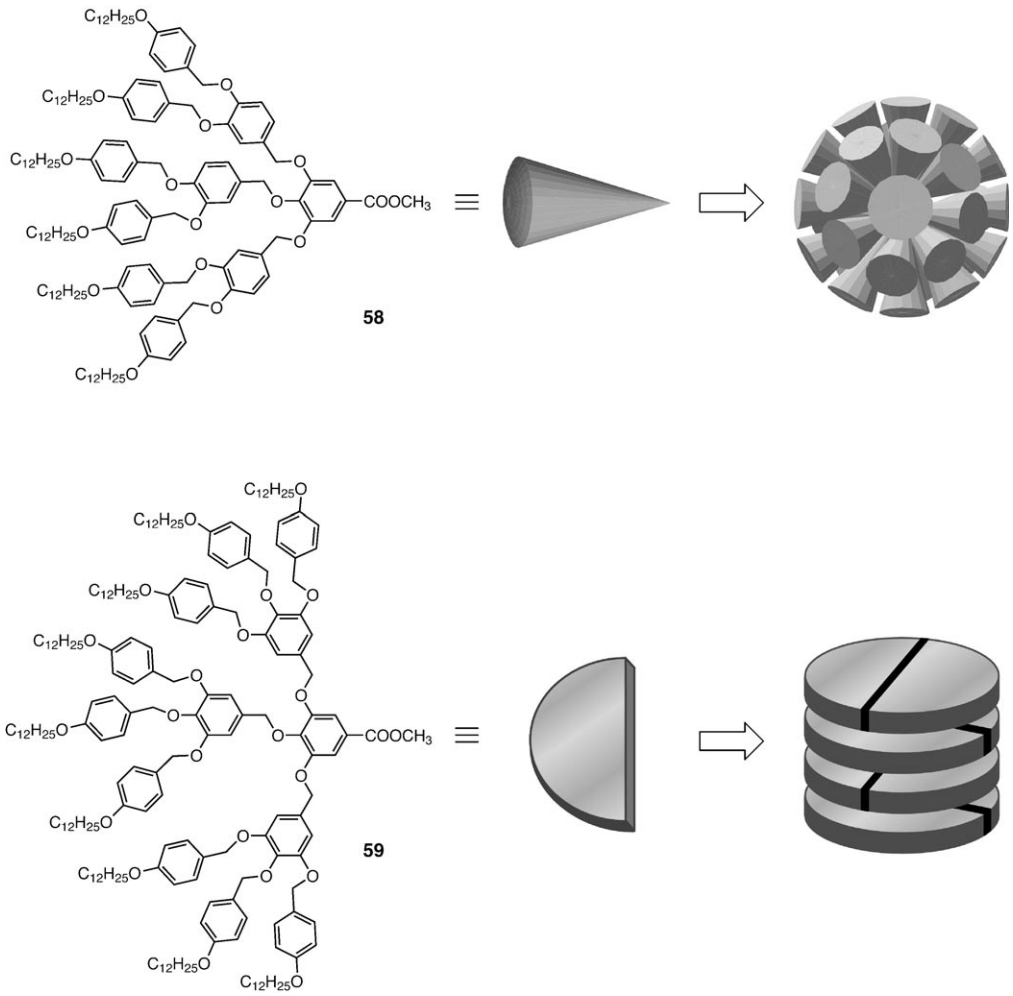


Figure 19. Self-assembly of cone and semicircular monodendrons **58** and **59**.

2.4. New Design for Functional Liquid Crystals

The properly designed combination of supramolecular approaches, nano-segregation, and unconventional shape produces a new class of liquid-crystalline materials. It should also be noted that chirality, which is not focused on in this review, is also an important factor in the functional liquid-crystal design.[34,77,78,216–219] The introduction of asymmetrical structure, that is, of chirality, has yielded interesting electro-optical properties such as ferroelectricity[216] and selective reflection.[220] The interface is also important for liquid crystals. Interactions of liquid crystals and polymers at interfaces are applied to the fabrication of twisted nematic electro-optical displays.[1,8] Oriented liquid-crystalline states in the long-range order induced by the interactions at interfaces can enhance properties. Moreover, molecular recognition,[221] photochromism,[222,223] and dynamic behavior at the interface[224,225] may lead to the induction of the dynamic function of liquid crystals. The balanced combination of these factors may open a new avenue for functional self-organized soft materials. In the next Section, approaches to functional liquid crystals by combining some design factors will be described.

3. Function of Liquid-Crystalline Assemblies

The design of liquid-crystalline assemblies for specific functions is described in this Section. The advantage of liquid crystals as functional materials is that their self-organized structures offer dynamic and mobile states. The molecular order in these states can be switched by external stimuli, such as thermal treatment and electric fields. Moreover, the formation of oriented large monodomains of liquid crystals is much more easily achieved than with other organic materials, such as single crystals and polymers. We will show how supramolecular assembly of several cooperating molecules and control of phase-segregated structures from the nanometer to centimeter length scale are important for the induction of highly functional materials.[5,9,10]

3.1. Electronics and Ionics

One promising approach to the preparation of functional liquid crystals is to form anisotropic electron-, ion-, or proton-conducting materials by using nano-segregation. The key to

 © 2006 Wiley-VCH Verlag GmbH & Co. KGaA, Weinheim

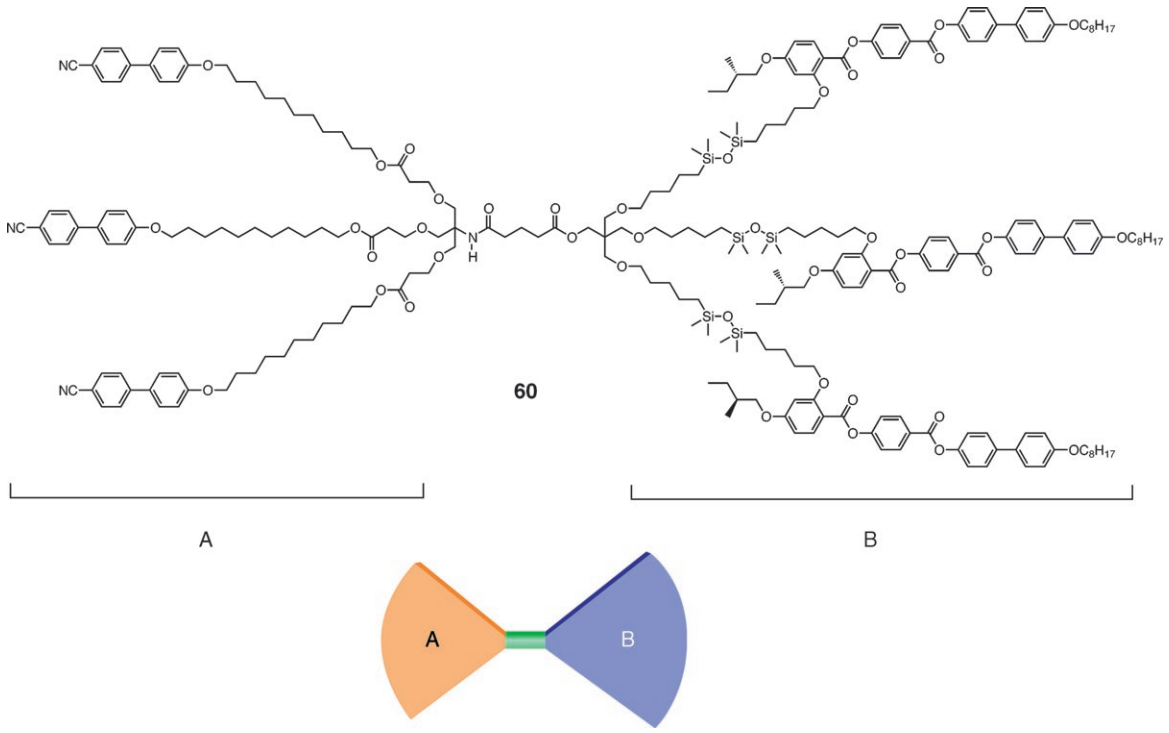
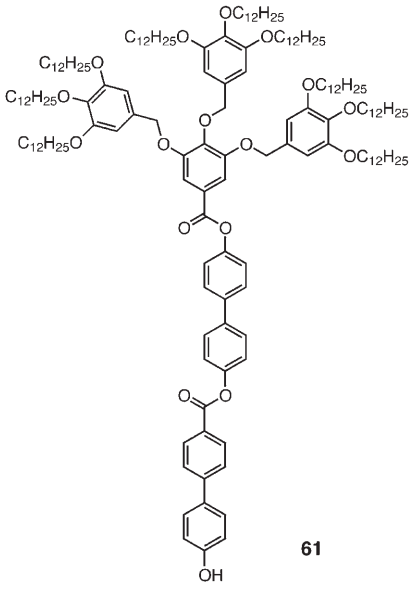
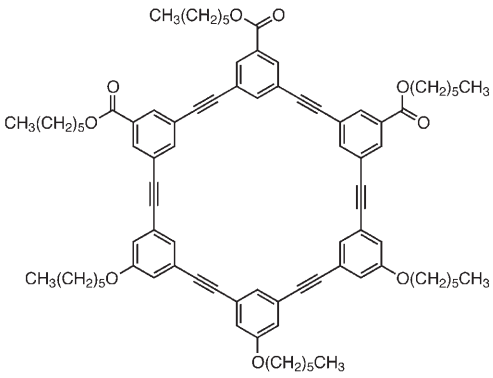


Figure 20. "Janus" liquid crystal **60** which contains two different hemispherical units. Molecule segment A is achiral and the terminally appended mesogens prefer smectic phases whereas segment B contains laterally appended chiral mesogens that adopt nematic phases.



61



62

the success is in controlling the macroscale orientation of the conducting nanostructures.[226–228]

3.1.1. 1D Conduction

Use of columnar assemblies for 1D electron or hole conduction has attracted much attention.[51,52,229] One method is to stack π-conjugated disk-like molecules such as triphenylene, hexabenzocoronene, and phthalocyanine derivatives in liquid-crystalline columnar structures.[230–237]

The introduction of a 1D array of hydrogen bonds parallel to the columnar axis of discotic aromatic liquid crystals enhances their conductivity by decreasing the π–π distance.[238]

Electron donor–acceptor (EDA) interactions and nano-segregation are employed together for the self-organization of conductive liquid-crystalline materials. The charge carrier mobilities of the complexes are facilitated by liquid-crystalline assemblies of dendrons and the formation of nano-segregated structures (Figure 21).[239] Several types of donor or acceptor moieties are attached at the apex of fluorinated dendrons. These types of dendrons form 1D columnar liquid-crystalline phases, where the functional head groups are located in the center of the columns, this arrangement is assisted by the nano-segregation of the fluorine side chains and aromatic groups. When amorphous polymers containing compatible functional groups (donor or acceptor moieties) are self-assembled with these dendrons, the polymers also reside in the center of the columns through the formation of EDA complexes. The charge carrier mobilities of these EDA complexes are enhanced by two to five orders of magnitude

 © 2006 Wiley-VCH Verlag GmbH & Co. KGaA, Weinheim

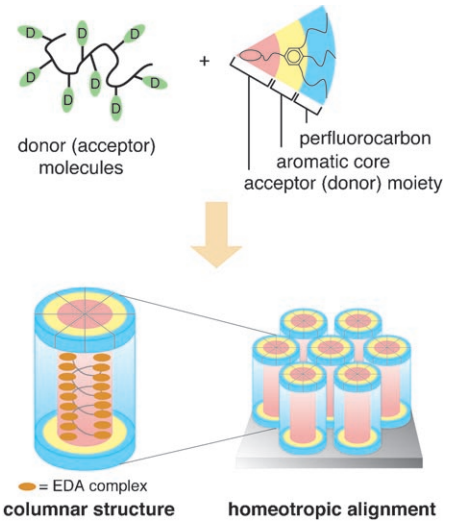


Figure 21. 1D structure of supramolecular liquid-crystalline materials with charge-transfer capability.

over those of the related EDA complexes in the amorphous states.

The assembly of polymerizable ionic amphiphiles **63** and the water-soluble precursors **64** of conducting polymers into columnar structures leads to electro-active films.[240] An aqueous solution of an amphiphilic monomer and poly(*p*-xylylenedimethylsulfonium chloride), a precursor of poly(*p*-phenylenevinylene) (PPV), forms lyotropic inverted hexagonal phases (Figure 22). Hexagonal ordered PPV nanowires are obtained by heat treatment of the precursors after photopolymerization of the amphiphiles. The photophysical properties of PPV are enhanced in these nano-segregated structures.[241]

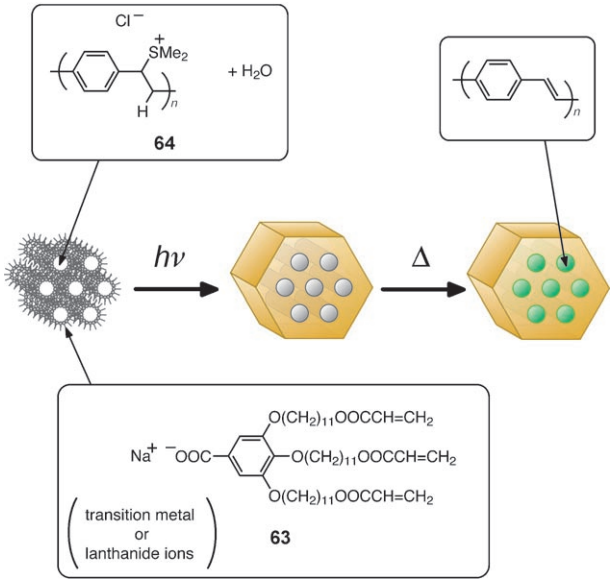
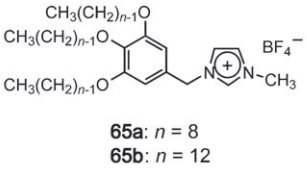


Figure 22. Formation of ordered PPV in a hexagonal polymer matrix.

Supramolecular liquid-crystalline structures based on polyaniline (PANI) have been prepared.[242] Highly ordered camphor sulfonic acid doped PANI is formed in which 4-hexylresorcinol is hydrogen-bonded to the complex. The cylindrical ordered doped PANI shows high electrical conductivity of 0.5–1.0 $S\,cm^{-1}$ while the conductivity of disordered doped PANI is approximately 5.0×10^{-3} $S\,cm^{-1}$. This increase in the electrical conductivity is probably due to the confinement of the PANI chains within the supramolecular cylinders which are obtained by the addition of 4-hexylresorcinol.

1D ion conduction has been achieved in columnar ionic liquids (Figure 23).[227] Ionic liquids have great potential as electrochemical devices, reaction solvents, and in catalysis.[243–245] However, they have been used as isotropic liquids in almost all cases. If anisotropic structures are induced into ionic liquids, their properties can be enhanced. We have prepared new ionic liquid crystals **65** consisting of two incompatible parts, the ionic imidazolium salt and the hydrophobic alkyl moieties. The self-assembly and phase segregation at the nanometer scale of these materials leads to the formation of columnar liquid-crystalline structures having inner ion-conducting paths.[227] These columnar phases are stable over a wide temperature range which includes room temperature. Higher ionic conductivities and higher anisotropy of ion conduction are observed for macroscopically oriented materials of **65** that are obtained by mechanical shearing between gold electrodes (Figure 23). In contrast, the polydomain columnar materials obtained without shearing do not show anisotropic ion conduction. This is the first example of 1D ion conduction in organic materials, which has been confirmed by anisotropic measurements of ionic conductivities. In earlier studies, ionic liquid-crystal complexes that



65a: $n = 8$
65b: $n = 12$

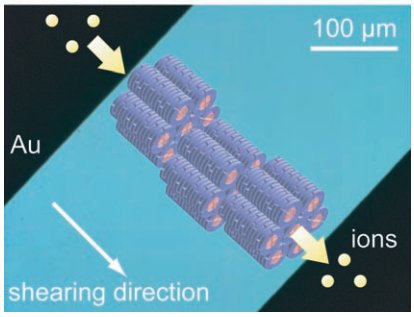
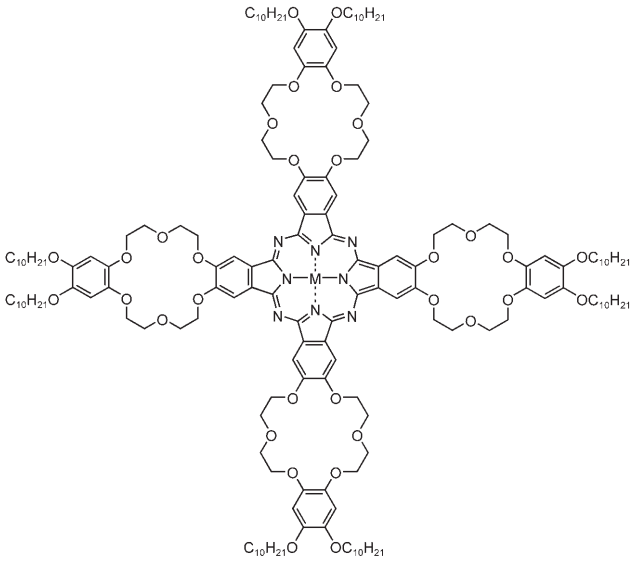


Figure 23. The oriented 1D ion-conductive ionic liquid crystals **65a** and **65b**. The columnar ionic liquid crystals are homogeneously aligned on the substrates.

© 2006 Wiley-VCH Verlag GmbH & Co. KGaA, Weinheim

were stabilized by ion–dipole interactions were prepared from metal salts and crown ethers,[237,246–248] aza crown ethers,[249] and poly(ethylene oxide)s (PEOs).[250] However, anisotropic 1D ionic conductivities were not measured for these materials. The ionic conductivities of these materials should be low because liquid-crystalline structures were not macroscopically oriented and no long-range ion-conducting paths were formed.

The combination of ion channels and electron wires has been obtained by using phthalocyanines modified with crown ether moieties.[237,246] Compounds **66** form supramolecular cables in the hexagonal columnar phases. Nanosegregation is a key for preparing desired self-assembled structures: in this case there is a central electron wire of stacked phthalocyanine cores surrounded by four ion



66a: M = 2H
66b: M = Si(OH)$_2$

channels formed from the crown ethers and jacketed by the insulating hydrocarbons.

Anisotropic proton conduction has been achieved for block copolymers **67** which have supramolecular side-chains.[11,251,252] The complexes of polystyrene-*block*-poly(4-vinyl pyridine) (PS-*b*-PVP), toluene sulfonic acid, and 3-pentadecylphenol form hierarchical phase-segregated structures (Figure 24). Lamellar structures are formed because of microphase segregation between the covalently connected PS block and PVP block. In the PVP block, the additional lamellar nanostructures are obtained as a result of stabilizing hydrogen-bonding between the phenol and PVP. The larger scale lamellar structures can be aligned to a monodomain by shear flow. In these oriented hierarchical structures, proton conductivity is different in three macroscopic directions.

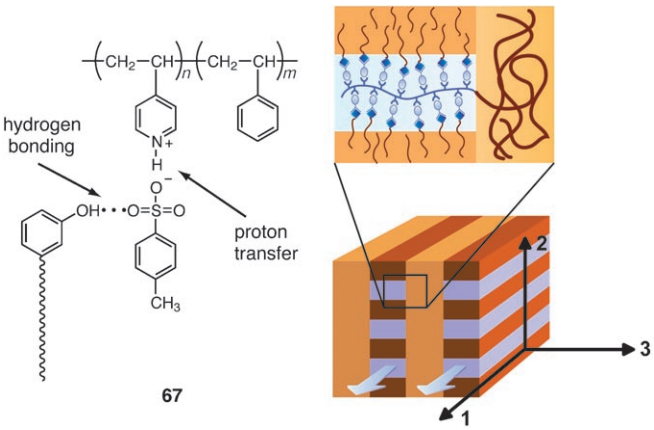
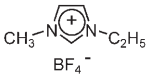


Figure 24. The oriented block copolymer **67** which has supramolecular side chains allows tridirectionally anisotropic proton conduction.

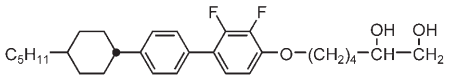
3.1.2. 2D Conduction

Two-dimensional (2D) organization of electro-active π-conjugated molecules with various molecular weights leads to the preparation of 2D conductive and photoconductive materials.[253–255] The complexes of polyaniline and aromatic phosphonic acid have been shown to form lyotropic lamellar structures because of nano-segregation.[256]

We have demonstrated two-dimensional ionic conductivities for nanostructured layered materials which include a PEO-containing polymer,[226] and an imidazolyl-containing material.[228,257–260] In particular, anisotropic measurements of both directions parallel and perpendicular to the layers have been achieved for liquid-crystalline ionic liquids.[228] We have shown that the 2D organization of ionic liquids results from the self-assembly of conventional ionic liquid **68** and hydroxy-terminated liquid-crystal molecule **69**. The interactions between hydroxy groups and ionic liquids stabilize the



68



69

layered nanostructures. The ionic conductivities parallel to the smectic layer are higher than those perpendicular to the layers. For example, the value of in-plane ionic conductivity is 5.7×10^{-4} S cm^{-1} at 50 °C and perpendicular to the plane it is 84-times less.

Oriented phase-segregated nanostructures can be preserved by in situ photopolymerization of a PEO-containing monomer.[226] The complexes formed between lithium salts and polymerizable block liquid-crystal molecules, which have

 © 2006 Wiley-VCH Verlag GmbH & Co. KGaA, Weinheim

a PEO moiety, show smectic phases. UV irradiation of the homeotropically aligned complexes in the smectic A phase results in the formation of free-standing films. This polymer complex (**70**/$LiOSO_2CF_3$) has macroscopically oriented, layered nanostructures (Figure 25). In the oriented films, an ionic conductivity of 1.5×10^{-6} S cm^{-1} parallel to the layers is

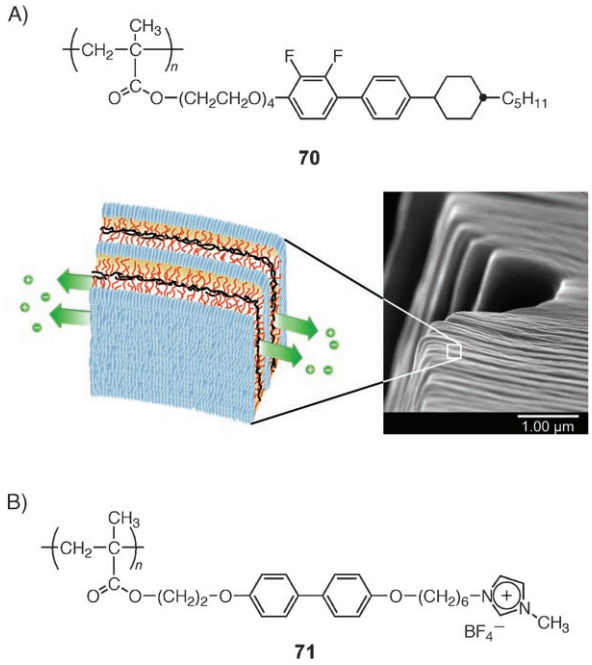
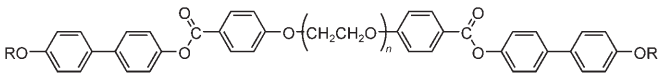


Figure 25. A) Nanostructures of anisotropic ion-conductive films of liquid crystal complex **70**/$LiOSO_2CF_3$.[226] B) Side-chain type liquid-crystal polymer **71** containing an ionic moiety.

obtained at 35 °C, which is approximately 5000-times higher than that perpendicular to the layers. Macroscopically oriented films are also prepared for side-chain liquid-crystal polymer **71** which contains an ionic moiety at the extremity of the side chain.[257] In this case, the ion-active moieties are directly attached to the side chain of the mesogenic polymers so that a 2D anisotropic ion conduction can be detected in the smectic nanostructures.

Self-assembled layered structures of block rod–coil–rod molecules containing PEO moieties (**72a**) have also been used to develop anisotropic ion-conductive materials.[261–266]

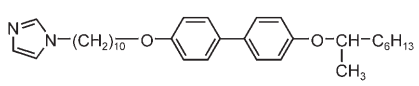


72a: R = $(CH_2)_7CH_3$
72b: R = $CH_2CH_2(CF_2)_5CF_3$

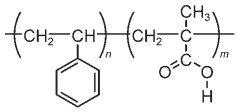
Such nano-segregation of smectic materials was facilitated by the introduction of perfluoroalkyl chains into the rod moieties (**72b**).[267] In these cases the three components (the perfluorocarbons, aromatic mesogens, and PEO moieties) formed triply layered nanostructures leading to higher ion conduction.

3.2. Optics and Ferroelectrics

Liquid-crystalline structures can also be applied to photonic materials.[268] Thomas and co-workers have prepared temperature-tunable photonic materials which have a band gap in the visible region.[110] They made hydrogen-bonded supramolecular complexes[102] from an imidazolyl-terminated mesogen (**73**) and a polystyrene-*block*-poly(methacrylic acid) (**74**). These complexes have one-dimensional periodic lamellar structures. A cast film of a complex composed of 0.60:1 molar ratio of the mesogen/polymer has a photonic band gap around the region of green light (560 nm) for normal incidence. On heating, the reflective color of the sample gradually shifts to orange (600 nm) because a change in the refractive index of the hydrogen-bonded layers occurs with the change (decease) in order. These supramolecular materials also act as a polarizing filter when the refractive index of polystyrene is matched with that of the extraordinary components of the hydrogen-bonded layers.[110]

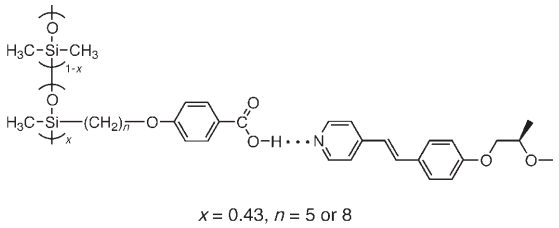


73



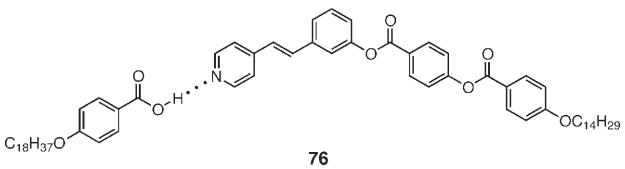
74

Ferroelectricity can occur in supramolecular liquid crystals that have chiral smectic C phases.[96,269] Electro-optical responses are observed for mixtures of stilbazoles and benzoic acid derivatives, in which one of the components is optically active. For example, supramolecular complex **75** exhibits ferroelectric smectic phases.[96] Recently, banana-shaped supramolecular liquid crystal **76** has been prepared.[73] Owing to the softness and flexibility of the mesogens, appropriate design might improve the electro-optical proper-



$x = 0.43$, $n = 5$ or 8

75



76

© 2006 Wiley-VCH Verlag GmbH & Co. KGaA, Weinheim

ties of these supramolecular materials. The effects of lateral hydrogen bonding have been examined for a chiral ferroelectric fluorenol compound.[270] The chiral smectic C phase displayed by the fluorenol is stabilized by intermolecular hydrogen bonding between the hydroxy group and the ester carbonyl group.

A quasi-ferroelectric material has been attained by monodomain formation of structurally simple amphiphilic liquid crystals (Figure 26). Second harmonic generation

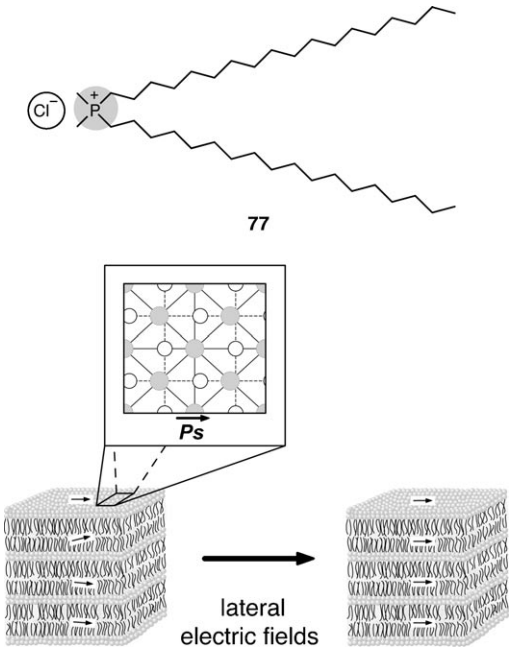


Figure 26. A quasi-ferroelectric material formed from a simple amphiphilic liquid crystal **77**.

(SHG) has been observed for amphiphile **77** in the smectic A phase. This molecule has a phosphonium chloride head group and forms layered structures as a result of nanosegregation.[271] Theoretical calculations and X-ray measurements indicate that the non-centrosymmetric atomic arrangement of ions ($[PH_4\text{-}Cl^-\text{-}PH_4]^+$; Figure 26) plays a key role for the induction of spontaneous polarization in the in-plane direction of the films leading to SHG. This simple amphiphile shows great potential for optoelectronic devices because of its easy processability and SHG-tunability.

3.3. Biological Functions

Self-organization processes leading to the formation of supramolecular liquid-crystalline structures are seen in biological systems. Some biomolecules have been known to form lyotropic liquid-crystalline states. Safinya and co-workers have reported supramolecular formation of lyotropic liquid-crystalline phases for the complexes of cationic liposomes and DNA.[16,272] Although the enhancement of transfection efficiencies by using cationic liposome with DNA was known,[273] the mechanism was not. Safinya and co-workers have revealed that ionic interactions between DNA and cationic liposomes direct the self-assembly of lyotropic liquid-crystalline lamellar or inverted hexagonal structures. In these cases, DNA forms 2D in-plane ordered structures intercalated between the lipid-membrane layers or located in the center of the hexagonal lattice (Figure 27). Understanding these supramolecular structures will lead to the development of novel synthetic gene carriers.[16,273]

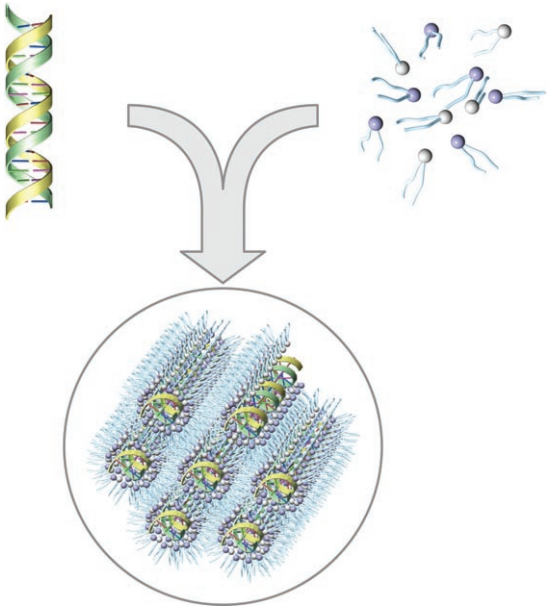


Figure 27. Supramolecular inverted hexagonal columnar structure formed by the complex of DNA and cationic liposomes.

Hydrogels of lyotropic lamellar phases have been prepared by the addition of block molecules which act as a cross-linker between the layers.[274,275] These hydrogels show potential as new types of supramolecular bioactive materials for drug-delivery or tissue-healing applications.

3.4. Catalysis and Templates for Synthesis

Ordered nanostructured liquid-crystalline materials can be used for the preparation of heterogeneous catalysts such as inorganic zeolites or mesoporous sieves. Organic liquid-crystalline materials themselves had not been used as catalysts until Gin and co-workers reported catalytic amphiphilic liquid crystals.[276–280] They showed that cross-linked, lyotropic liquid-crystalline (LLC) assemblies function effectively as catalytic platforms (Figure 28). In these systems, the reactive head groups of amphiphilic molecules are concentrated at the center of the cylinder in the lyotropic inverted hexagonal phase (H_{II}). The cross-linked H_{II} phases of these LLCs can be used as highly reactive or selective catalysts. For example, the nanostructured resin **78**, obtained by copolymerization of amphiphilic monomers carrying the SO_3H group and COOH group, acts as a Brønsted acid catalyst for the highly selective esterification of benzyl alcohol and 1-hexanoic acid (Figure 28).[280] These organic nanostructured

 © 2006 Wiley-VCH Verlag GmbH & Co. KGaA, Weinheim

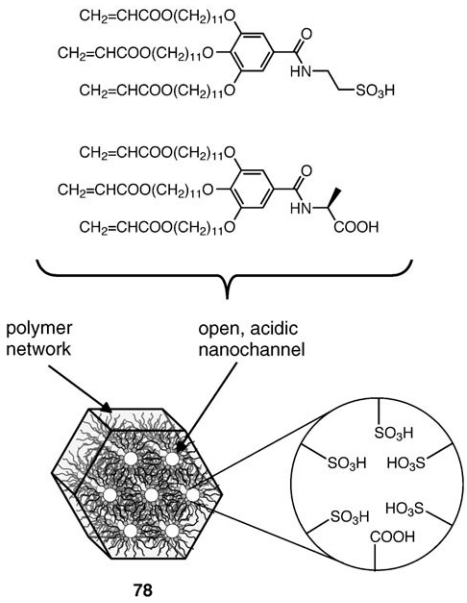


Figure 28. Nanostructured resin **78** functions as a heterogeneous catalyst.

LLCs have potential for other applications because their active sites are size- and pH-tunable.

Kim and co-workers have shown a new process for the synthesis of organic nanoporous materials by using supramolecular liquid-crystalline templates.[281] In the 3:1 complex **79**, polymerizable benzoic acid derivatives form double hydrogen bonds to a benzotri(imidazole) core thus generating a supramolecular hexagonal liquid-crystalline phase (Figure 29). Removal of the cores after photopolymerization leads to the formation of ordered channels based on the hexagonal structure. This nanoporous polymer shows a relatively high N_2 gas permeability and recognition of the original core. Such nanoporous organic materials have potential in separation, catalysis, and synthesis of nanocomposites.

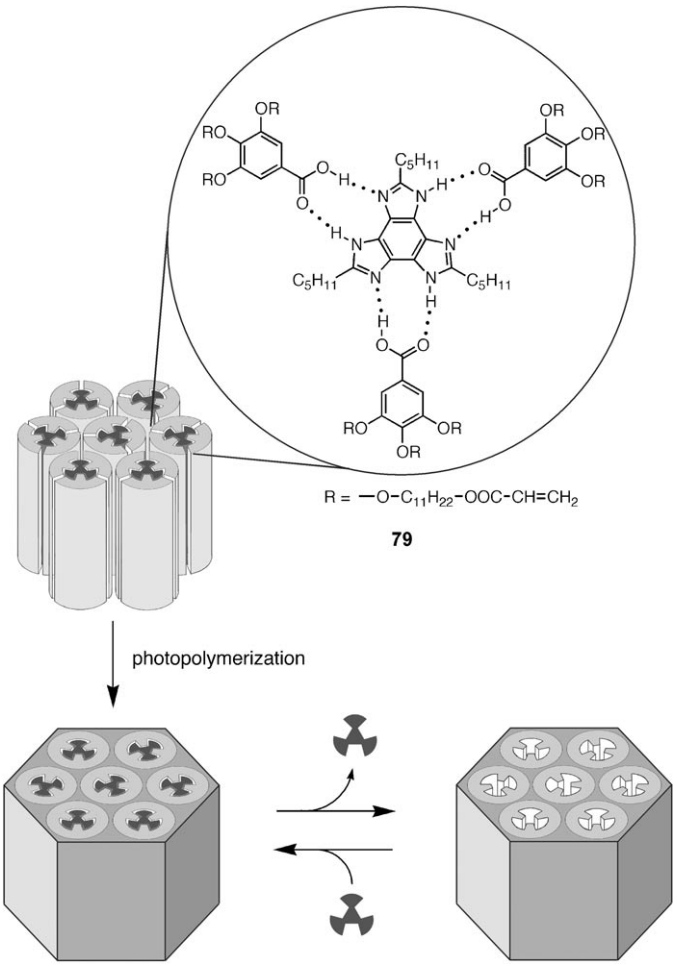


Figure 29. Organic nanoporous materials can be obtained by using supramolecular liquid-crystalline templates.

The combination of self-assembled fibers or nanoparticles and liquid-crystalline ordered states yields materials with new structures and functions. Herein we focus on the liquid-crystal composites obtained by self-assembly processes.

4. Liquid-Crystal Composites

Liquid-crystal composites are prepared by mixing two incompatible materials: liquid crystals and solids showing phase-separated structures.[54,282–284] These liquid-crystal composites differ from the liquid crystals described in the preceding section in which nano-segregation occurs in a single liquid-crystalline phase. For liquid-crystal composites, the liquid-crystal and solid components show individual transitions. Two types of liquid-crystal composites have been developed: 1) composites consisting of liquid crystals and covalently bonded polymers in the solid state.[285–290] For example, polymer-dispersed liquid crystals (PDLCs), which have been widely examined as electro-optical materials.[54,285–290] 2) Composites consisting of liquid crystals and self-assembled solid materials made of low-molecular-weight organic compounds[24,57] or nanoparticles.[291,292] This is a relatively new type of self-organized anisotropic soft solid.

4.1. Liquid Crystals with Self-Assembled Fibers

4.1.1. Structures of Liquid-Crystalline Physical Gels

Liquid-crystalline physical gels are composites consisting of liquid crystals and a small amount of self-assembled fibers.[24,58] The fibrous materials are simply formed in the liquid crystals by self-assembly of low-molecular-weight compounds **80**–**84**, a process which is driven by hydrogen-bonding or π–π interactions.[57,293,294] These materials are soft solids maintaining liquid-crystalline properties. Such gels show thermoreversible sol–gel transitions which arise from the association and dissociation of intermolecular interactions between the gelators.[24,58,295–297]

For the liquid-crystalline physical gels, two transitions occur independently: 1) liquid-crystalline gel–normal gel transitions induced by phase transition of liquid crystals, and 2) sol–gel transitions induced by association and dissociation of the gelator. The two types of phase transitions are

 © 2006 Wiley-VCH Verlag GmbH & Co. KGaA, Weinheim

observed when these have different transition temperatures. The phase-separated structures of the gels can be tuned by the choice of transition behavior of the gels (Figure 30).[24,298–301]

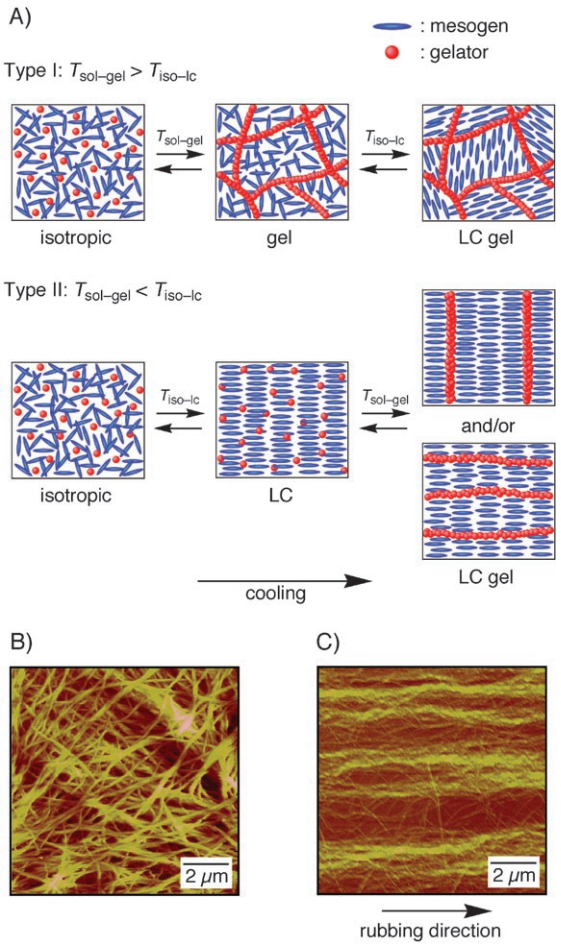
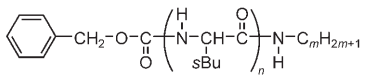


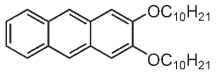
Figure 30. A) Two types of structural changes of liquid-crystalline physical gels. $T_{sol-gel}$: sol–gel transition temperature. T_{iso-lc}: isotropic–anisotropic transition temperature. B) AFM image of fibrous aggregates formed in an isotropic phase through Type I phase behavior. C) AFM image of oriented fibers formed in a homogeneously oriented nematic phase through Type II phase behavior.

When the fibrous assembly of a gelator occurs at a temperature higher than the isotropic–anisotropic transition temperature of a liquid-crystal component (Figure 30A, Type I), a randomly dispersed fiber network is formed in the isotropic medium (Figure 30B). In contrast, association of a gelator in a liquid-crystalline phase induces the formation of an oriented self-assembled fiber network, resulting in an oriented liquid-crystalline gel (Figure 30A, Type II). In this case, the liquid crystal serves as a template. The morphologies of the fibers, such as thickness and growing directions in liquid crystals, are greatly dependent on the combination of the gelators and the liquid crystals. Hydrogen-bonded fibers of **81** develop along the layer structure of a smectic A phase, that is, in the direction perpendicular to the liquid crystal alignment.[298] Similar oriented structures are observed for the 1D molecular stacking of non-hydrogen-bonded anthracene derivative **82** in homogeneously aligned cyanobiphenyl liquid crystals.[299]

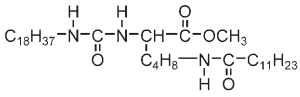
Gelators



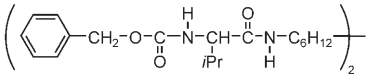
80: $n = 3$, $m = 12$
81: $n = 1$, $m = 18$



82

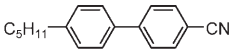


83

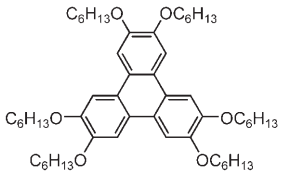


84

Mesogens



85



86

Fibrous assembly parallel to liquid-crystal alignment is seen for the nematic mixtures containing **83** (Figure 30C).[300,301]

4.1.2. *Electro-Optical Properties of Liquid-Crystalline Physical Gels*

Some electro-optical properties are enhanced by the physical gelation of liquid crystals. For the gels of Type I, light scattering electro-optical materials have been prepared by adding small amounts of nanometer-scale self-assembled fibers (0.2–3.0 wt.%) to liquid crystals.[5,302,303] Liquid-crystalline polydomains are effectively formed by random dispersion of self-assembled fibers of gelators in nematic liquid crystals. These structures induce light-scattering turbid states, which can be switched to transparent states by the application of electric fields (Figure 31). Amino acid derivative **80** has been reported to be suitable for light-scattering materials.[302] The compound forms hydrogen-bonded fibers with a diameter of approximately 30 nm in room-temperature nematic liquid crystals. The driving voltages and response times can be tuned by changing the amounts of the fibrous additives. Compared

 © 2006 Wiley-VCH Verlag GmbH & Co. KGaA, Weinheim

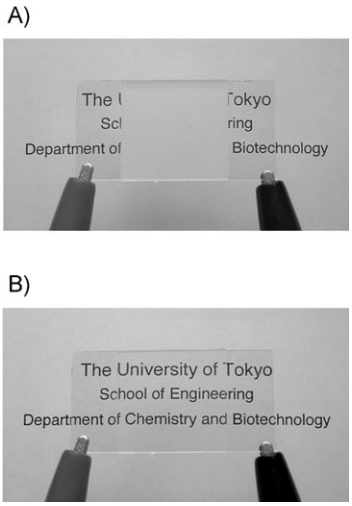


Figure 31. Photographs of a liquid-crystal cell incorporating a nematic gel consisting of **80** and **85**: A) light-scattering state (0 V); B) light-transmission state (70 V). Cell thickness is 16 μm.

to an analogous compound (**81**), the fibers of **80**, which has a greater number of amino acid moieties, are finer and thermally more stable.

For the gels of Type II, electro-optical functions of oriented nematic physical gels have been reported for the mixtures containing **83**.[300,301] When the anisotropic self-assembly of the nematic composites (Figure 30C) occurs in twisted nematic cells, the oriented self-assembled fibers grow along the twisted alignment of the liquid crystals (Figure 32).

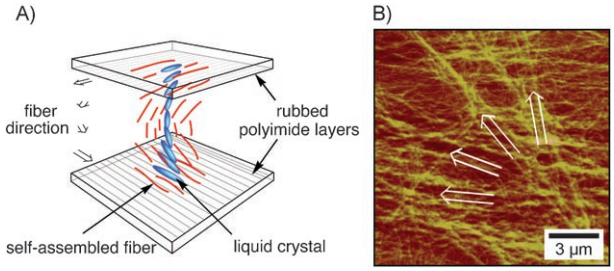


Figure 32. A) Schematic illustration of a twisted nematic cell containing oriented nanofiber networks; B) AFM image of the oriented fibrous aggregates of **83** formed in a twisted nematic cell.

These nematic gels with oriented structures show fast and high-contrast electro-optical responses.[300] The gels of Type II can be applied for light-scattering electro-optical materials in reverse mode. The nematic physical gels which form homeotropically oriented structures are transparent in electric field off-states and turbid in on-states.[301] The effects of self-assembled fibers on the electro-optical behavior of oriented ferroelectric smectic composites have been examined.[304–306] The formation of self-assembled fibers in ferroelectric liquid crystals is effective for the tuning of driving voltages and hysteresis of electro-optical responses.

4.1.3. Electro- and Photo-Function of Liquid-Crystalline Physical Gels

Liquid-crystal triphenylene derivatives can function as anisotropic photoconductors. The physical gelation of a discotic triphenylene liquid crystal has enhanced its photoconductivities.[307] When the hydrogen-bonded fibers consisting of gelator **84** are introduced into triphenylene compound **86**, the mixture exhibits a discotic liquid-crystalline gel state on cooling from 97 to 57 °C. The anisotropic gels show a hole mobility of $1.2 \times 10^{-3}\ cm^2\,V^{-1}\,s^{-1}$, which is nearly three-times higher than that of the discotic liquid crystal alone ($4.5 \times 10^{-4}\ cm^2\,V^{-1}\,s^{-1}$). The enhancement of photoconductivities can be attributed to the suppression of molecular movement in the fibrous network.

The incorporation of azobenzene moieties into the gelator leads to the preparation of the photoresponsive liquid-crystalline gels.[308] Rewritable information recording has been achieved for the photo-responsive anisotropic gels. These photoresponsive gels consist of nematic liquid crystal **85** and a chiral diamide compound with two azobenzene moieties.[308] They show reversible structural changes between two gel states: nematic and cholesteric gels, both of which are stable at room temperature. The combination of *trans–cis* photoisomerization and thermal sol–gel transition results in the formation of the two different anisotropic gel states, which can coexist after irradiation through a template (photopatterning). This process can be used for information recording. Photoinduced reorganization of liquid-crystalline physical gels containing a gelator with an azobenzene moiety can be applied to the formation of electrically switchable diffraction gratings.[56,309] For a discotic liquid-crystalline gel containing the azobenzene gelator, the size of liquid-crystalline domains can be tuned photochemically.[310]

4.2. Liquid Crystals with Nanoparticles and Micelles

Organic and inorganic nanoparticles have been incorporated into low-molecular-weight liquid crystals to develop switchable electro-optical materials.[291,292] The molecular orientation and defect formation is affected by the existence of nanoparticles.[311,312] Nanoparticles dispersed in nematic liquid crystals assemble into a network of ordered interconnected aggregates, resulting in anisotropic soft solid materials.[311,312] Homogeneous dispersion of the nanoparticle aggregates effectively induces the formation of liquid-crystalline polydomains.[311–314] These nanoparticle-filled nematics can be used as light-scattering electro-optical materials.[311–314] Electro-optical responses have also been examined for nematic composites containing submicrometer-sized polymer particles.[315] The addition of nanoparticles to ferroelectric smectic liquid crystals has been reported to provide a novel gray-scale imaging technique.[316]

The use of nanoparticles with unique surface properties leads to the preparation of functional liquid-crystal systems (Figure 33). For nematic liquid crystals filled with silica particles, bistable scattering effects which can be addressed by electric stimuli and laser irradiation have been

 © 2006 Wiley-VCH Verlag GmbH & Co. KGaA, Weinheim

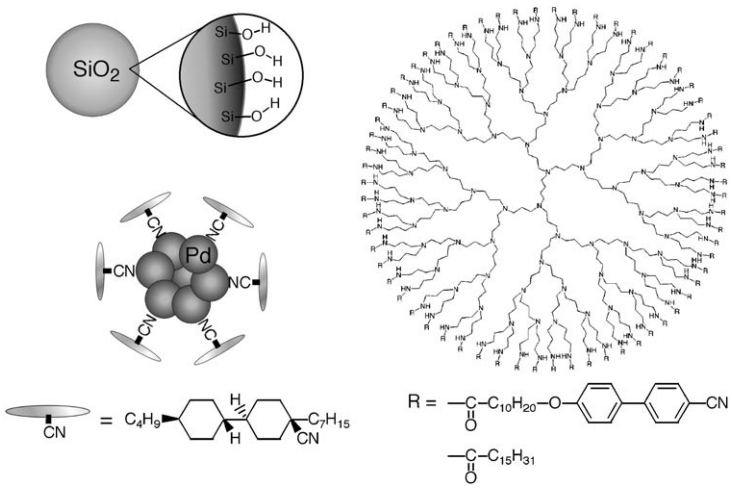


Figure 33. Modified nanoparticles can be incorporated into liquid crystals.

observed.[291] In this material, aggregates of primary silica particles form agglomerates through the hydrogen bonding of hydroxy groups. A new approach based on dendrimers dispersed in liquid crystals gave a light-scattering electro-optical switch.[317,318] The electro-optical behavior strongly depends on the terminal groups of dendrimers. The absence of hysteresis and low driving voltages have been reported for these dendrimer-filled nematics. Palladium nanoparticles modified with mesogenic molecules have been complexed with nematic liquid crystals.[319]

Optically isotropic nematic phases are formed by the dispersion of inverse micelles in nematic liquid crystals.[320] Nanometer-scale droplets of the micelles disturb the long-range nematic order, but local nematic order is maintained. The transparent nematic materials may exhibit unique optical and mechanical properties.

5. Summary and Outlook

To build highly functional soft materials using liquid crystals, polymers, and gels, it is important to design molecules with appropriate chemical structures and to control the process of their self-organization. At present, the precise control of hierarchical self-organization on a multi-length scale from nanometers to centimeters has not yet been achieved. However, new strategies to control the order of functional molecules in soft materials are being developed rapidly. Liquid crystals are promising soft materials with dynamic functions because they form ordered and dynamic structures that are unique for molecular materials. A new family of unconventional liquid crystals has been designed and prepared. They form complex self-organized structures and widen the number of potential applications of this class of materials.

We believe that supramolecular assembly through specific molecular interactions and phase-segregation at various length scales are the keys for further structural control of the materials. In addition, the control of molecular shape is also an important factor. The combination of these factors determines the formation of micellar, bicontinuous, layered, and columnar or more complexed structures. Herein, we have described unconventional liquid-crystalline materials, which show great potential as highly functional materials. We have not mentioned some new families of liquid-crystalline materials, such as banana-shaped liquid crystals and metallomesogens, because several excellent reviews have already been published on these themes.[186,192,193] Moreover, the recent development of a conventional family of liquid crystals containing rod- and disk-shaped molecules has not been mentioned. For example, hexabenzocoronenes[235] have attracted much attention within the field of discotic conductive liquid-crystalline materials. The design of these materials is also closely related to the materials design described herein.

We mainly focused on thermotropic liquid crystals. Lyotropic liquid crystals have not been described extensively because most functional materials for advanced technologies are used in the bulk state and the design of new lyotropic materials is limited. However, functional lyotropic liquid crystals are relevant to biological membranes and they can be applied in the field of biomaterials. Moreover, lyotropic liquid crystals can form more complex structures than thermotropic liquid crystals because their phase behavior depends on two parameters: temperature and concentration. This structure formation opens a wide range of possibilities for new soft materials design.

A new generation of functional liquid crystals that lies between thermotropic and lyotropic liquid crystals is emerging. For example, the mixture of ionic liquids and hydroxy-functionalized mesogenic molecules has been developed for anisotropic ion-conducting materials.[228a,259b] If ionic liquids are taken as functional molecules, the mixtures can be classified as thermotropic liquid crystals. If we take ionic liquids as (functional) solvents, the materials can be classified as lyotropic liquid crystals.[228a,259b,321] Therefore, some new mesomorphic materials will be beyond the conventional classification of liquid crystals.

Another important aspect for the functionalization of liquid crystals is composite formation. The composites prepared from liquid crystals and solid objects, such as fibers, particles, and networks, are new self-organized hybrid materials.[322,323] It should also be pointed out that the interfaces between liquid crystals and solids are important for functionalization because the order and orientation of liquid-crystal molecules are sometimes governed by interface interactions. Moreover, liquid crystals can be used as sensors at interfaces as a result of the orientation of the liquid crystals is easily altered by changes in the surface structure. More complex structures and hierarchical structural control will be demanded for new functional materials. For the successful self-organization processes of liquid crystals and other soft materials, the structures of molecules must be designed and synthesized carefully. The chemists' ability to design mesogens and orchestrate self-assembly promises new liquid crystals with precise chemical function.

We would like to thank the Ministry of Education, Culture, Sports, Science and Technology (MEXT; Grant-in-Aid for The

 © 2006 Wiley-VCH Verlag GmbH & Co. KGaA, Weinheim

21st Century COE Program for Frontiers in Fundamental Chemistry and Grant-in-Aid for Scientific Research on Priority Areas of "Dynamic Control of Strongly Correlated Soft Materials" (No. 413/13031009)) and the Japan Society of the Promotion of Science (JSPS; Grant-in-Aid for Creative Scientific Research of "Invention of Conjugated Electronic Structures and Novel Functions" (No. 16GS0209) and Grant-in-Aid for Scientific Research (B)) for financial support. We also acknowledge and are grateful to the dedication of the students and postdoctoral fellows, and assistant professors listed in the references cited. We also wish to thank professors J. M. J. Fréchet, H. Ohno, K. Hanabusa, Y. Shimizu, E. Nakamura, E. Yashima, and S. Ujiie for fruitful collaborations. We express our gratitude to Dr. T. Nishimura and Mr. T. Kagata for producing some of the Figures.

Received: April 21, 2005

[1] a) *Handbook of Liquid Crystals* (Eds.: D. Demus, J. W. Goodby, G. W. Gray, H.-W. Spiess, V. Vill), Wiley-VCH, Weinheim, **1998**; b) *Thermotropic Liquid Crystals* (Ed.: G. W. Gray), Wiley, Chichester, **1987**.
[2] P. G. de Gennes, *The Physics of Liquid Crystals*, 2nd ed., Oxford University Press, New York, **1993**.
[3] Special issue on Molecular Topology in Liquid Crystals: *J. Mater. Chem.* **2001**, *11*, 2631 – 2886.
[4] *Curr. Opin. Solid State Mater. Sci.* **2002**, *6*, 513 – 587 (Section of Liquid Crystals).
[5] T. Kato, *Science* **2002**, *295*, 2414 – 2418.
[6] a) Special issue on Supramolecular Chemistry and Self-Assembly: *Science* **2002**, *295*, 2395 – 2421; b) I. W. Hamley, *Angew. Chem.* **2003**, *115*, 1730 – 1752; *Angew. Chem. Int. Ed.* **2003**, *42*, 1692 – 1712.
[7] T. Kato, *Struct. Bonding (Berlin)* **2000**, *96*, 95 – 146.
[8] J. van Haaren, D. J. Broer, *Chem. Ind.* **1998**, 1017 – 1021.
[9] a) C. Tschierske, *J. Mater. Chem.* **2001**, *11*, 2647 – 2671; b) C. Tschierske, *Annu. Rep. Prog. Chem. Sect. C* **2001**, *97*, 191 – 267.
[10] S. I. Stupp, V. LeBonheur, K. Walker, L. S. Li, K. E. Huggins, M. Keser, A. Amstutz, *Science* **1997**, *276*, 384 – 389.
[11] O. Ikkala, G. ten Brinke, *Chem. Commun.* **2004**, 2131 – 2137.
[12] G. H. Mehl, *Angew. Chem.* **2005**, *117*, 678 – 679; *Angew. Chem. Int. Ed.* **2005**, *44*, 672 – 673.
[13] J. W. Goodby, G. H. Mehl, I. M. Saez, R. P. Tuffin, G. Mackenzie, R. Auzély-Velty, T. Benvegnu, D. Plusquellec, *Chem. Commun.* **1998**, 2057 – 2070.
[14] C. Fairhurst, S. Fuller, J. Gray, M. C. Holmes, G. J. T. Tiddy in *Handbook of Liquid Crystals, Vol. 3* (Eds.: D. Demus, J. W. Goodby, G. W. Gray, H.-W. Spiess, V. Vill), Wiley-VCH, Weinheim, **1998**, pp. 341 – 392.
[15] a) A. Skoulios, D. Guillon, *Mol. Cryst. Liq. Cryst.* **1988**, *165*, 317 – 332; b) Y. Hendrikx, A. M. Levelut, *Mol. Cryst. Liq. Cryst.* **1988**, *165*, 233 – 265.
[16] a) J. O. Rädler, I. Koltover, T. Salditt, C. R. Safinya, *Science* **1997**, *275*, 810 – 814; b) I. Koltover, T. Salditt, J. O. Rädler, C. R. Safinya, *Science* **1998**, *281*, 78 – 81.
[17] a) I. G. Denisov, Y. V. Grinkova, A. A. Lazarides, S. G. Sligar, *J. Am. Chem. Soc.* **2004**, *126*, 3477 – 3487; b) H. Ringsdorf, B. Schlarb, J. Venzmer, *Angew. Chem.* **1988**, *100*, 117 – 162; *Angew. Chem. Int. Ed. Engl.* **1988**, *27*, 113 – 158; c) T. Kunitake, *Angew. Chem.* **1992**, *104*, 692 – 710; *Angew. Chem. Int. Ed. Engl.* **1992**, *31*, 709 – 726.
[18] M. Muthukumar, C. K. Ober, E. L. Thomas, *Science* **1997**, *277*, 1225 – 1232.
[19] J.-M. Lehn, *Supramolecular Chemistry: Concepts and Perspectives*, VCH, Weinheim, **1995**.
[20] T. Kato, J. M. J. Fréchet, *J. Am. Chem. Soc.* **1989**, *111*, 8533 – 8534.
[21] a) T. Kato, J. M. J. Fréchet, *Macromolecules* **1989**, *22*, 3818 – 3819; b) Erratum: T. Kato, J. M. J. Fréchet, *Macromolecules* **1990**, *23*, 360.
[22] M.-J. Brienne, J. Gabard, J.-M. Lehn, I. Stibor, *J. Chem. Soc. Chem. Commun.* **1989**, 1868 – 1870.
[23] C. Fouquey, J.-M. Lehn, A.-M. Levelut, *Adv. Mater.* **1990**, *2*, 254 – 257.
[24] T. Kato, N. Mizoshita, K. Kanie, *Macromol. Rapid Commun.* **2001**, *22*, 797 – 814.
[25] C. M. Paleos, D. Tsiourvas, *Angew. Chem.* **1995**, *107*, 1839 – 1855; *Angew. Chem. Int. Ed. Engl.* **1995**, *34*, 1696 – 1711.
[26] T. Kato, J. M. J. Fréchet, *Macromol. Symp.* **1995**, *98*, 311 – 326.
[27] J.-M. Lehn, *Makromol. Chem. Macromol. Symp.* **1993**, *69*, 1 – 17.
[28] a) T. Kato in *Handbook of Liquid Crystals, Vol. 2B* (Eds.: D. Demus, J. W. Goodby, G. W. Gray, H.-W. Spiess, V. Vill), Wiley-VCH, Weinheim, **1998**, pp. 969 – 979; b) T. Kato in *Supramolecular Polymers, Second Edition* (Ed.: A. Ciferri), Taylor & Francis, London, **2005**, pp. 131 – 152.
[29] U. Beginn, *Prog. Polym. Sci.* **2003**, *28*, 1049 – 1105.
[30] N. Zimmerman, J. S. Moore, S. C. Zimmerman, *Chem. Ind.* **1998**, 604 – 610.
[31] T. Kato, H. Kihara, U. Kumar, T. Uryu, J. M. J. Fréchet, *Angew. Chem.* **1994**, *106*, 1728 – 1730; *Angew. Chem. Int. Ed. Engl.* **1994**, *33*, 1644 – 1645.
[32] H. Kihara, T. Kato, T. Uryu, J. M. J. Fréchet, *Chem. Mater.* **1996**, *8*, 961 – 968.
[33] K. Kanie, M. Nishii, T. Yasuda, T. Taki, S. Ujiie, T. Kato, *J. Mater. Chem.* **2001**, *11*, 2875 – 2886.
[34] T. Kato, T. Matsuoka, M. Nishii, Y. Kamikawa, K. Kanie, T. Nishimura, E. Yashima, S. Ujiie, *Angew. Chem.* **2004**, *116*, 2003 – 2006; *Angew. Chem. Int. Ed.* **2004**, *43*, 1969 – 1972.
[35] C. T. Imrie, *Trends Polym. Sci.* **1995**, *3*, 22 – 29.
[36] J. C. MacDonald, G. M. Whitesides, *Chem. Rev.* **1994**, *94*, 2383 – 2420.
[37] S. C. Zimmerman, P. S. Corbin, *Struct. Bonding (Berlin)* **2000**, *96*, 63 – 94.
[38] J.-M. Lehn, *Science* **2002**, *295*, 2400 – 2403.
[39] L. J. Prins, D. N. Reinhoudt, P. Timmerman, *Angew. Chem.* **2001**, *113*, 2446 – 2492; *Angew. Chem. Int. Ed.* **2001**, *40*, 2382 – 2426.
[40] T. Kato, N. Mizoshita, *Curr. Opin. Solid State Mater. Sci.* **2002**, *6*, 579 – 587.
[41] *Supramolecular Polymers* (Ed.: A. Ciferri), Dekker, New York, **2000**.
[42] L. Brunsveld, B. J. B. Folmer, E. W. Meijer, R. P. Sijbesma, *Chem. Rev.* **2001**, *101*, 4071 – 4097.
[43] L. P. Stubbs, M. Weck, *Chem. Eur. J.* **2003**, *9*, 992 – 999.
[44] J. M. Pollino, K. P. Nair, L. P. Stubbs, J. Adams, M. Weck, *Tetrahedron* **2004**, *60*, 7205 – 7215.
[45] E. A. Archer, H. Gong, M. J. Krische, *Tetrahedron* **2001**, *57*, 1139 – 1159.
[46] K. Chino, M. Ashiura, *Macromolecules* **2001**, *34*, 9201 – 9204.
[47] J. Ruokolainen, R. Mäkinen, M. Torkkeli, T. Mäkelä, R. Serimaa, G. ten Brinke, O. Ikkala, *Science* **1998**, *280*, 557 – 560.
[48] T. Hashimoto, *Bull. Chem. Soc. Jpn.* **2005**, *78*, 1 – 39.
[49] V. Abetz in *Supramolecular Polymers* (Ed.: A. Ciferri), Dekker, New York, **2000**, pp. 215 – 262.
[50] M. Lee, B.-K. Cho, W.-C. Zin, *Chem. Rev.* **2001**, *101*, 3869 – 3892.
[51] M. O'Neill, S. M. Kelly, *Adv. Mater.* **2003**, *15*, 1135 – 1146.

© 2006 Wiley-VCH Verlag GmbH & Co. KGaA, Weinheim

[52] N. Boden, B. Movaghar in *Handbook of Liquid Crystals, Vol. 2B* (Eds.: D. Demus, J. W. Goodby, G. W. Gray, H.-W. Spiess, V. Vill), Wiley-VCH, Weinheim, **1998**, pp. 781 – 798.
[53] J. W. Goodby, *Curr. Opin. Solid State Mater. Sci.* **1999**, *4*, 361 – 368.
[54] *Liquid Crystals in Complex Geometries Formed by Polymer and Porous Networks* (Eds.: G. P. Crawford, S. Žumer), Taylor & Francis, London, **1996**.
[55] Special issue on Polymers in Display Applications: *Macromol. Symp.* **2000**, *154*, 1 – 251.
[56] Y. Zhao, *Pure Appl. Chem.* **2004**, *76*, 1499 – 1508.
[57] a) T. Kato, T. Kutsuna, K. Hanabusa, M. Ukon, *Adv. Mater.* **1998**, *10*, 606 – 608; b) N. Mizoshita, K. Hanabusa, T. Kato, *Adv. Mater.* **1999**, *11*, 392 – 394.
[58] T. Kato, N. Mizoshita, M. Moriyama, T. Kitamura, *Top. Curr. Chem.* **2005**, *256*, 219 – 236.
[59] G. A. Jeffrey, *An Introduction to Hydrogen Bonding*, Oxford University Press, New York, **1997**.
[60] A. C. de Kock, *Z. Phys. Chem.* **1904**, *48*, 129 – 176.
[61] C. Weygand, R. Z. Gabler, *Z. Phys. Chem.* **1940**, *B46*, 270 – 275.
[62] *Supramolecular Polymers, Second Edition* (Ed.: A. Ciferri), Taylor & Francis, London, **2005**.
[63] L. Brunsveld, B. J. B. Folmer, E. W. Meijer, *MRS Bull.* **2000**, *25(4)*, 49 – 53.
[64] M. Shoji, F. Tanaka, *Macromolecules* **2002**, *35*, 7460 – 7472.
[65] F. Tanaka, *Polym. J.* **2002**, *34*, 479 – 509.
[66] K. Kanie, T. Yasuda, S. Ujiie, T. Kato, *Chem. Commun.* **2000**, 1899 – 1900.
[67] K. Kanie, T. Yasuda, M. Nishii, S. Ujiie, T. Kato, *Chem. Lett.* **2001**, 480 – 481.
[68] T. Kato, J. M. J. Fréchet, P. G. Wilson, T. Saito, T. Uryu, A. Fujishima, C. Jin, F. Kaneuchi, *Chem. Mater.* **1993**, *5*, 1094 – 1100.
[69] T. Kato, P. G. Wilson, A. Fujishima, J. M. J. Fréchet, *Chem. Lett.* **1990**, 2003 – 2006.
[70] H. Bernhardt, H. Kresse, W. Weissflog, *Mol. Cryst. Liq. Cryst.* **1997**, *301*, 25 – 30.
[71] A. Sautter, C. Thalacker, F. Würthner, *Angew. Chem.* **2001**, *113*, 4557 – 4560; *Angew. Chem. Int. Ed.* **2001**, *40*, 4425 – 4428.
[72] K. N. Koh, K. Araki, T. Komori, S. Shinkai, *Tetrahedron Lett.* **1995**, *36*, 5191 – 5194.
[73] N. Gimeno, M. B. Ros, J. L. Serrano, M. R. de la Fuente, *Angew. Chem.* **2004**, *116*, 5347 – 5350; *Angew. Chem. Int. Ed.* **2004**, *43*, 5235 – 5238.
[74] A. Kraft, A. Reichert, R. Kleppinger, *Chem. Commun.* **2000**, 1015 – 1016.
[75] R. Kleppinger, C. P. Lillya, C. Yang, *Angew. Chem.* **1995**, *107*, 1762 – 1764; *Angew. Chem. Int. Ed. Engl.* **1995**, *34*, 1637 – 1638.
[76] M. Suárez, J.-M. Lehn, S. C. Zimmerman, A. Skoulios, B. Heinrich, *J. Am. Chem. Soc.* **1998**, *120*, 9526 – 9532.
[77] Y. Kamikawa, M. Nishii, T. Kato, *Chem. Eur. J.* **2004**, *10*, 5942 – 5951.
[78] Y. Kamikawa, M. Nishii, T. Kato, *Mol. Cryst. Liq. Cryst.* **2005**, *435*, 755 – 765.
[79] F. Ciuchi, G. Di Nicola, H. Franz, G. Gottarelli, P. Mariani, M. G. P. Bossi, G. P. Spada, *J. Am. Chem. Soc.* **1994**, *116*, 7064 – 7071.
[80] T. Giorgi, S. Lena, P. Mariani, M. A. Cremonini, S. Masiero, S. Pieraccini, J. P. Rabe, P. Samori, G. P. Spada, G. Gottarelli, *J. Am. Chem. Soc.* **2003**, *125*, 14741 – 14749.
[81] G. Gottarelli, G. P. Spada, *Chem. Rec.* **2004**, *4*, 39 – 49.
[82] S. Ujiie, K. Iimura, *Macromolecules* **1992**, *25*, 3174 – 3178.
[83] C. G. Bazuin, D. Guillon, A. Skoulios, J. F. Nicoud, *Liq. Cryst.* **1986**, *1*, 181 – 188.
[84] H. Ringsdorf, R. Wüstefeld, E. Zerta, M. Ebert, J. H. Wendorff, *Angew. Chem.* **1989**, *101*, 934 – 938; *Angew. Chem. Int. Ed. Engl.* **1989**, *28*, 914 – 918.
[85] M. M. Green, H. Ringsdorf, J. Wagner, R. Wüstefeld, *Angew. Chem.* **1990**, *102*, 1525 – 1528; *Angew. Chem. Int. Ed. Engl.* **1990**, *29*, 1478 – 1481.
[86] J. W. Park, C. S. Bak, M. M. Labes, *J. Am. Chem. Soc.* **1975**, *97*, 4398 – 4400.
[87] Y. Matsunaga, N. Kamiyama, Y. Nakayasu, *Mol. Cryst. Liq. Cryst.* **1987**, *147*, 85 – 97.
[88] H. Bengs, M. Ebert, O. Karthaus, B. Kohne, K. Praefcke, H. Ringsdorf, J. H. Wendorff, R. Wüstefeld, *Adv. Mater.* **1990**, *2*, 141 – 144.
[89] K. Praefcke, D. Singer, B. Kohne, M. Ebert, A. Liebmann, J. H. Wendorff, *Liq. Cryst.* **1991**, *10*, 147 – 159.
[90] H. L. Nguyen, P. N. Horton, M. B. Hursthouse, A. C. Legon, D. W. Bruce, *J. Am. Chem. Soc.* **2004**, *126*, 16 – 17.
[91] a) C.-Y. Chao, X. Li, C. K. Ober, *Pure Appl. Chem.* **2004**, *76*, 1337 – 1343; b) J. M. Pollino, M. Weck, *Chem. Soc. Rev.* **2005**, *34*, 193 – 207.
[92] T. Kato, H. Kihara, T. Uryu, A. Fujishima, J. M. J. Fréchet, *Macromolecules* **1992**, *25*, 6836 – 6841.
[93] T. Kato, H. Kihara, S. Ujiie, T. Uryu, J. M. J. Fréchet, *Macromolecules* **1996**, *29*, 8734 – 8739.
[94] T. Kato, J. M. J. Fréchet in *Polymeric Materials Encyclopedia* (Ed.: J. C. Salamone), CRC, Boca Raton, **1996**, pp. 8158 – 8161.
[95] U. Kumar, T. Kato, J. M. J. Fréchet, *J. Am. Chem. Soc.* **1992**, *114*, 6630 – 6639.
[96] U. Kumar, J. M. J. Fréchet, T. Kato, S. Ujiie, K. Iimura, *Angew. Chem.* **1992**, *104*, 1545 – 1547; *Angew. Chem. Int. Ed. Engl.* **1992**, *31*, 1531 – 1533.
[97] U. Kumar, J. M. J. Fréchet, *Adv. Mater.* **1992**, *4*, 665 – 667.
[98] K. Araki, T. Kato, U. Kumar, J. M. J. Fréchet, *Macromol. Rapid Commun.* **1995**, *16*, 733 – 739.
[99] T. Kato, M. Nakano, T. Moteki, T. Uryu, S. Ujiie, *Macromolecules* **1995**, *28*, 8875 – 8876.
[100] T. Kato, M. Ogasawara, S. Ujiie, *Kobunshi Ronbunshu* **1999**, *56*, 410 – 413.
[101] F. Ilhan, M. Gray, V. M. Rotello, *Macromolecules* **2001**, *34*, 2597 – 2601.
[102] T. Kawakami, T. Kato, *Macromolecules* **1998**, *31*, 4475 – 4479.
[103] C. G. Bazuin, F. A. Brandys, *Chem. Mater.* **1992**, *4*, 970 – 972.
[104] C. G. Bazuin, F. A. Brandys, T. M. Eve, M. Plante, *Macromol. Symp.* **1994**, *84*, 183 – 196.
[105] F. A. Brandys, C. G. Bazuin, *Chem. Mater.* **1996**, *8*, 83 – 92.
[106] T. Kato, N. Hirota, A. Fujishima, J. M. J. Fréchet, *J. Polym. Sci. Part A* **1996**, *34*, 57 – 62.
[107] D. Stewart, C. T. Imrie, *J. Mater. Chem.* **1995**, *5*, 223 – 228.
[108] K. I. Alder, D. Stewart, C. T. Imrie, *J. Mater. Chem.* **1995**, *5*, 2225 – 2228.
[109] J. Ruokolainen, J. Tanner, O. Ikkala, G. ten Brinke, E. L. Thomas, *Macromolecules* **1998**, *31*, 3532 – 3536.
[110] C. Osuji, C.-Y. Chao, I. Bita, C. K. Ober, E. L. Thomas, *Adv. Funct. Mater.* **2002**, *12*, 753 – 758.
[111] C.-Y. Chao, X. Li, C. K. Ober, C. Osuji, E. L. Thomas, *Adv. Funct. Mater.* **2004**, *14*, 364 – 370.
[112] M. C. Luyten, G. O. R. Alberda van Ekenstein, J. Wildeman, G. ten Brinke, J. Ruokolainen, O. Ikkala, M. Torkkeli, R. Serimaa, *Macromolecules* **1998**, *31*, 9160 – 9165.
[113] M. C. Luyten, G. O. R. Alberda van Ekenstein, G. ten Brinke, J. Ruokolainen, O. Ikkala, M. Torkkeli, R. Serimaa, *Macromolecules* **1999**, *32*, 4404 – 4410.
[114] O. Ikkala, G. ten Brinke, *Mater. Res. Soc. Symp. Proc.* **2003**, *775*, 213 – 223.
[115] G. ten Brinke, O. Ikkala, *Chem. Rec.* **2004**, *4*, 219 – 230.
[116] A. F. Thünemann, S. Kubowicz, C. Burger, M. D. Watson, N. Tchebotareva, K. Müllen, *J. Am. Chem. Soc.* **2003**, *125*, 352 – 356.
[117] C. G. Bazuin, A. Tork, *Macromolecules* **1995**, *28*, 8877 – 8880.

 © 2006 Wiley-VCH Verlag GmbH & Co. KGaA, Weinheim

[118] K. Maeda, Y. Takeyama, K. Sakajiri, E. Yashima, *J. Am. Chem. Soc.* **2004**, *126*, 16284 – 16285.
[119] T. Kato, Y. Kubota, T. Uryu, S. Ujiie, *Angew. Chem.* **1997**, *109*, 1687 – 1689; *Angew. Chem. Int. Ed. Engl.* **1997**, *36*, 1617 – 1618.
[120] O. Ihata, H. Yokota, K. Kanie, S. Ujiie, T. Kato, *Liq. Cryst.* **2000**, *27*, 69 – 74.
[121] G. Ambrožič, M. Žigon, *Macromol. Rapid Commun.* **2000**, *21*, 53 – 56.
[122] J. L. M. van Nunen, B. F. B. Folmer, R. J. M. Nolte, *J. Am. Chem. Soc.* **1997**, *119*, 283 – 291.
[123] C. Alexander, C. P. Jariwala, C. M. Lee, A. C. Griffin, *Macromol. Symp.* **1994**, *77*, 283 – 294.
[124] M. Kotera, J.-M. Lehn, J.-P. Vigneron, *J. Chem. Soc. Chem. Commun.* **1994**, 197 – 199.
[125] R. K. Castellano, C. Nuckolls, S. H. Eichhorn, M. R. Wood, A. J. Lovinger, J. Rebek, Jr., *Angew. Chem.* **1999**, *111*, 2764 – 2768; *Angew. Chem. Int. Ed.* **1999**, *38*, 2603 – 2606.
[126] R. K. Castellano, R. Clark, S. L. Craig, C. Nuckolls, J. Rebek, Jr., *Proc. Natl. Acad. Sci. USA* **2000**, *97*, 12418 – 12421.
[127] H. Kihara, T. Kato, T. Uryu, J. M. J. Fréchet, *Liq. Cryst.* **1998**, *24*, 413 – 418.
[128] H. Kihara, T. Kato, T. Uryu, *Trans. Mater. Res. Soc. Jpn.* **1996**, *20*, 327 – 330.
[129] C. B. St. Pourcain, A. C. Griffin, *Macromolecules* **1995**, *28*, 4116 – 4121.
[130] S. Sivakova, S. J. Rowan, *Chem. Commun.* **2003**, 2428 – 2429.
[131] F. Würthner, S. Yao, B. Heise, C. Tschierske, *Chem. Commun.* **2001**, 2260 – 2261.
[132] C. Schmuck, W. Wienand, *Angew. Chem.* **2001**, *113*, 4493 – 4499; *Angew. Chem. Int. Ed.* **2001**, *40*, 4363 – 4369.
[133] R. P. Sijbesma, F. H. Beijer, L. Brunsveld, B. J. B. Folmer, J. H. K. K. Hirschberg, R. F. M. Lange, J. K. L. Lowe, E. W. Meijer, *Science* **1997**, *278*, 1601 – 1604.
[134] R. F. M. Lange, M. van Gurp, E. W. Meijer, *J. Polym. Sci. Part A* **1999**, *37*, 3657 – 3670.
[135] S. H. M. Söntjens, R. P. Sijbesma, M. H. P. van Genderen, E. W. Meijer, *Macromolecules* **2001**, *34*, 3815 – 3818.
[136] K. Yamauchi, J. R. Lizotte, D. M. Hercules, M. J. Vergne, T. E. Long, *J. Am. Chem. Soc.* **2002**, *124*, 8599 – 8604.
[137] K. Yamauchi, J. R. Lizotte, T. E. Long, *Macromolecules* **2003**, *36*, 1083 – 1088.
[138] K. Yamauchi, J. R. Lizotte, T. E. Long, *Macromolecules* **2002**, *35*, 8745 – 8750.
[139] K. Aoki, M. Nakagawa, K. Ichimura, *J. Am. Chem. Soc.* **2000**, *122*, 10997 – 11004.
[140] H. W. Gibson, N. Yamaguchi, J. W. Jones, *J. Am. Chem. Soc.* **2003**, *125*, 3522 – 3533.
[141] a) N. Yamaguchi, H. W. Gibson, *Angew. Chem.* **1999**, *111*, 195 – 199; *Angew. Chem. Int. Ed.* **1999**, *38*, 143 – 147; b) H. W. Gibson, Z. Ge, F. Huang, J. W. Jones, H. Lefebvre, M. J. Vergne, D. M. Hercules, *Macromolecules* **2005**, *38*, 2626 – 2637.
[142] Y. Kobayashi, Y. Matsunaga, *Bull. Chem. Soc. Jpn.* **1987**, *60*, 3515 – 3518.
[143] Y. Harada, Y. Matsunaga, N. Miyajima, S. Sakamoto, *J. Mater. Chem.* **1995**, *5*, 2305 – 2308.
[144] Y. Matsunaga, N. Miyajima, Y. Nakayasu, S. Sakai, M. Yonenaga, *Bull. Chem. Soc. Jpn.* **1988**, *61*, 207 – 210.
[145] M. L. Bushey, A. Hwang, P. W. Stephens, C. Nuckolls, *J. Am. Chem. Soc.* **2001**, *123*, 8157 – 8158.
[146] M. L. Bushey, A. Hwang, P. W. Stephens, C. Nuckolls, *Angew. Chem.* **2002**, *114*, 2952 – 2955; *Angew. Chem. Int. Ed.* **2002**, *41*, 2828 – 2831.
[147] J. J. van Gorp, J. A. J. M. Vekemans, E. W. Meijer, *J. Am. Chem. Soc.* **2002**, *124*, 14759 – 14769.
[148] G. Ungar, D. Abramic, V. Percec, J. A. Heck, *Liq. Cryst.* **1996**, *21*, 73 – 86.
[149] V. Percec, C.-H. Ahn, T. K. Bera, G. Ungar, D. J. P. Yeardley, *Chem. Eur. J.* **1999**, *5*, 1070 – 1083.
[150] a) G. Pickaert, L. Douce, R. Ziessel, D. Guillon, *Chem. Commun.* **2002**, 1584 – 1585; b) T. Kajitani, S. Kohmoto, M. Yamamoto, K. Kishikawa, *J. Mater. Chem.* **2004**, *14*, 3449 – 3456.
[151] M. G. Northolt, J. J. van Aartsen, *J. Polym. Sci. Polym. Lett. Ed.* **1973**, *11*, 333 – 337.
[152] M. G. Northolt, *Eur. Polym. J.* **1974**, *10*, 799 – 804.
[153] K. Hanabusa, K. Shimura, K. Hirose, M. Kimura, H. Shirai, *Chem. Lett.* **1996**, 885 – 886.
[154] J. J. Kane, R.-F. Liao, J. W. Lauher, F. W. Fowler, *J. Am. Chem. Soc.* **1995**, *117*, 12003 – 12004.
[155] K. Yabuuchi, E. Marfo-Owusu, T. Kato, *Org. Biomol. Chem.* **2003**, *1*, 3464 – 3469.
[156] K. Hanabusa, M. Yamada, M. Kimura, H. Shirai, *Angew. Chem.* **1996**, *108*, 2086 – 2088; *Angew. Chem. Int. Ed. Engl.* **1996**, *35*, 1949 – 1951.
[157] K. Hanabusa, A. Kawakami, M. Kimura, H. Shirai, *Chem. Lett.* **1997**, 191 – 192.
[158] K. Hanabusa, K. Hiratsuka, M. Kimura, H. Shirai, *Chem. Mater.* **1999**, *11*, 649 – 655.
[159] K. Hanabusa, H. Nakayama, M. Kimura, H. Shirai, *Chem. Lett.* **2000**, 1070 – 1071.
[160] a) C. Tschierske, *Prog. Polym. Sci.* **1996**, *21*, 775 – 852; b) C. Tschierske, *J. Mater. Chem.* **1998**, *8*, 1485 – 1508.
[161] G. A. Jeffrey, *Acc. Chem. Res.* **1986**, *19*, 168 – 173.
[162] G. A. Jeffrey, *Mol. Cryst. Liq. Cryst.* **1984**, *110*, 221 – 237.
[163] J. W. Goodby, *Mol. Cryst. Liq. Cryst.* **1984**, *110*, 205 – 219.
[164] C. Tschierske, H. Zaschke, *J. Chem. Soc. Chem. Commun.* **1990**, 1013 – 1014.
[165] a) T. Shimizu, *Polym. J.* **2003**, *35*, 1 – 22; b) T. Shimizu, *Macromol. Rapid Commun.* **2002**, *23*, 311 – 331.
[166] M. Masuda, V. Vill, T. Shimizu, *J. Am. Chem. Soc.* **2000**, *122*, 12327 – 12333.
[167] R. Auzély-Velty, T. Benvegnu, D. Plusquellec, G. Mackenzie, J. A. Haley, J. W. Goodby, *Angew. Chem.* **1998**, *110*, 2665 – 2668; *Angew. Chem. Int. Ed.* **1998**, *37*, 2511 – 2515.
[168] V. Abetz, T. Goldacker, *Macromol. Rapid Commun.* **2000**, *21*, 16 – 34.
[169] V. Abetz in *Supramolecular Polymers*, *Second Edition* (Ed.: A. Ciferri), Taylor & Francis, London, **2005**, pp. 351 – 391.
[170] M. U. Pralle, C. M. Whitaker, P. V. Braun, S. I. Stupp, *Macromolecules* **2000**, *33*, 3550 – 3556.
[171] B. W. Messmore, J. F. Hulvat, E. D. Sone, S. I. Stupp, *J. Am. Chem. Soc.* **2004**, *126*, 14452 – 14458.
[172] D. Joachimi, C. Tschierske, H. Müller, J. H. Wendorff, L. Schneider, R. Kleppinger, *Angew. Chem.* **1993**, *105*, 1205 – 1207; *Angew. Chem. Int. Ed. Engl.* **1993**, *32*, 1165 – 1167.
[173] F. Hildebrandt, J. A. Schröter, C. Tschierske, R. Festag, M. Wittenberg, J. H. Wendorff, *Adv. Mater.* **1997**, *9*, 564 – 567.
[174] M. Kölbel, T. Beyersdorff, X. H. Cheng, C. Tschierske, J. Kain, S. Diele, *J. Am. Chem. Soc.* **2001**, *123*, 6809 – 6818.
[175] P. Fuchs, C. Tschierske, K. Raith, K. Das, S. Diele, *Angew. Chem.* **2002**, *114*, 650 – 653; *Angew. Chem. Int. Ed.* **2002**, *41*, 628 – 631.
[176] X. Cheng, M. K. Das, S. Diele, C. Tschierske, *Langmuir* **2002**, *18*, 6521 – 6529.
[177] X. Cheng, M. Prehm, M. K. Das, J. Kain, U. Baumeister, S. Diele, D. Leine, A. Blume, C. Tschierske, *J. Am. Chem. Soc.* **2003**, *125*, 10977 – 10996.
[178] M. Lee, B.-K. Cho, Y.-G. Jang, W.-C. Zin, *J. Am. Chem. Soc.* **2000**, *122*, 7449 – 7455.
[179] M. Lee, B.-K. Cho, K. J. Ihn, W.-K. Lee, N.-K. Oh, W.-C. Zin, *J. Am. Chem. Soc.* **2001**, *123*, 4647 – 4648.
[180] N.-K. Oh, W.-C. Zin, J.-H. Im, J.-H. Ryu, M. Lee, *Chem. Commun.* **2004**, 1092 – 1093.

© 2006 Wiley-VCH Verlag GmbH & Co. KGaA, Weinheim

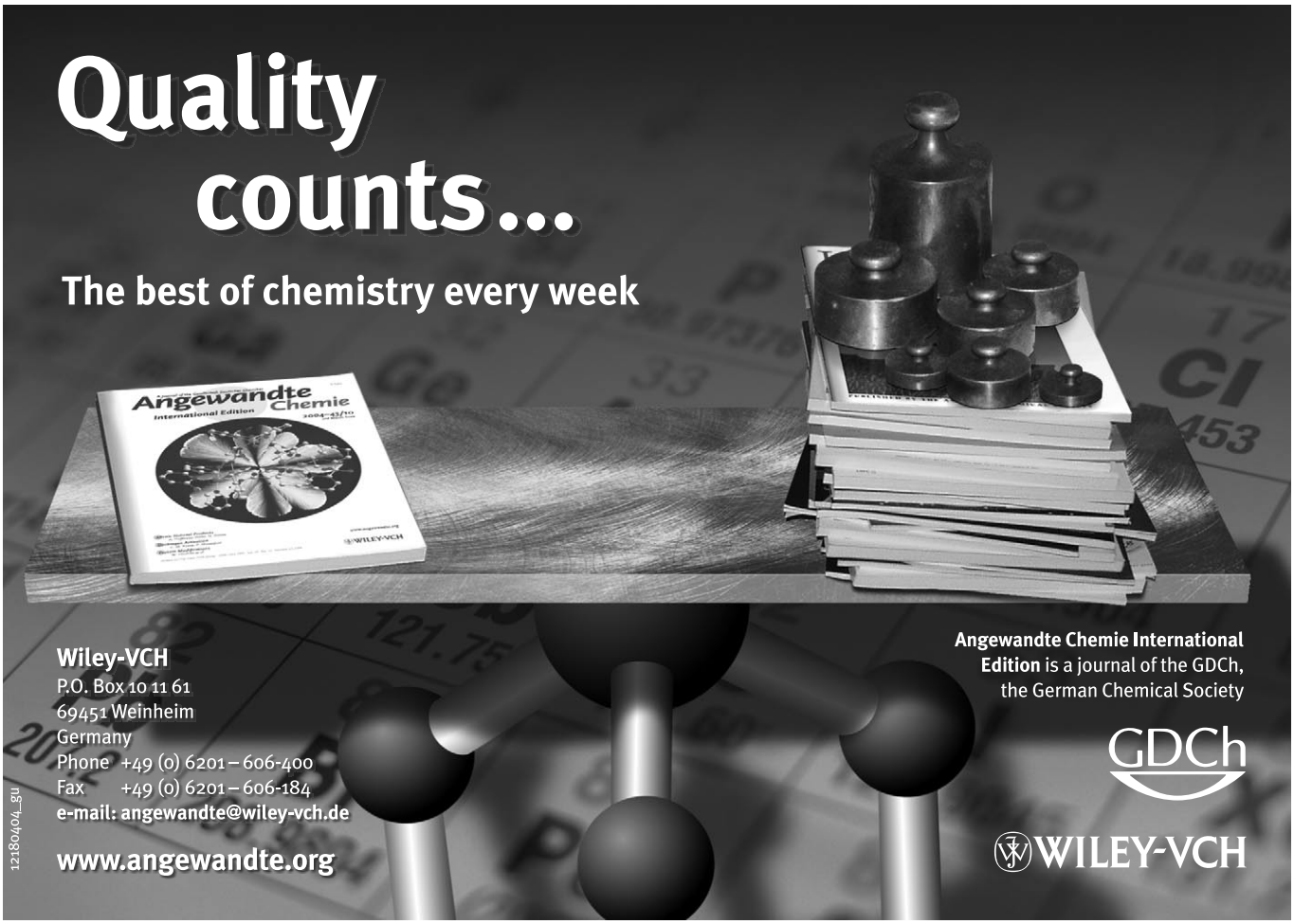
[181] J.-K. Kim, M.-K. Hong, J.-H. Ahn, M. Lee, *Angew. Chem.* **2005**, *117*, 332 – 336; *Angew. Chem. Int. Ed.* **2005**, *44*, 328 – 332.
[182] P. Gopalan, X. Li, M. Li, C. K. Ober, C. P. Gonzales, C. J. Hawker, *J. Polym. Sci. Part A* **2003**, *41*, 3640 – 3656.
[183] S.-W. Lee, C. Mao, C. E. Flynn, A. M. Belcher, *Science* **2002**, *296*, 892 – 895.
[184] S.-W. Lee, S. K. Lee, A. M. Belcher, *Adv. Mater.* **2003**, *15*, 689 – 692.
[185] T. Niori, T. Sekine, J. Watanabe, T. Furukawa, H. Takezoe, *J. Mater. Chem.* **1996**, *6*, 1231 – 1233.
[186] G. Pelzl, S. Diele, W. Weissflog, *Adv. Mater.* **1999**, *11*, 707 – 724.
[187] D. M. Walba, E. Körblova, R. Shao, J. E. Maclennan, D. R. Link, M. A. Glaser, N. A. Clark, *Science* **2000**, *288*, 2181 – 2184.
[188] H.-T. Nguyen, C. Destrade, J. Malthête in *Handbook of Liquid Crystals, Vol. 2B* (Eds.: D. Demus, J. W. Goodby, G. W. Gray, H.-W. Spiess, V. Vill), Wiley-VCH, Weinheim, **1998**, pp. 865 – 886.
[189] B. Dardel, D. Guillon, B. Heinrich, R. Deschenaux, *J. Mater. Chem.* **2001**, *11*, 2814 – 2831.
[190] V. Percec, M. N. Holerca, S. Uchida, W.-D. Cho, G. Ungar, Y. Lee, D. J. P. Yeardley, *Chem. Eur. J.* **2002**, *8*, 1106 – 1117.
[191] I. M. Saez, J. W. Goodby, R. M. Richardson, *Chem. Eur. J.* **2001**, *7*, 2758 – 2764.
[192] *Metallomesogens: Synthesis, Properties and Applications* (Ed.: J. L. Serrano), Wiley-VCH, Weinheim, **1996**.
[193] D. W. Bruce in *Inorganic Materials* (Eds.: D. W. Bruce, D. O'Hare), Wiley, Chichester, **1996**, pp. 429 – 522.
[194] D. Fazio, C. Mongin, B. Donnio, Y. Galerne, D. Guillon, D. W. Bruce, *J. Mater. Chem.* **2001**, *11*, 2852 – 2863.
[195] B. Xu, T. M. Swager, *J. Am. Chem. Soc.* **1993**, *115*, 1159 – 1160.
[196] T. Komori, S. Shinkai, *Chem. Lett.* **1993**, 1455 – 1458.
[197] J. Malthête, A. Collet, *Nouv. J. Chim.* **1985**, *9*, 151 – 153.
[198] M. Sawamura, K. Kawai, Y. Matsuo, K. Kanie, T. Kato, E. Nakamura, *Nature* **2002**, *419*, 702 – 705.
[199] Y. Matsuo, A. Muramatsu, R. Hamasaki, N. Mizoshita, T. Kato, E. Nakamura, *J. Am. Chem. Soc.* **2004**, *126*, 432 – 433.
[200] M. W. P. L. Baars, S. H. M. Söntjens, H. M. Fischer, H. W. I. Peerlings, E. W. Meijer, *Chem. Eur. J.* **1998**, *4*, 2456 – 2466.
[201] B. Donnio, J. Barberá, R. Giménez, D. Guillon, M. Marcos, J. L. Serrano, *Macromolecules* **2002**, *35*, 370 – 381.
[202] D. Guillon, J.-F. Nierengarten, J.-L. Gallani, J.-F. Exker, Y. Rio, M. del Pilar Carreon, B. Dardel, R. Deschenaux, *Macromol. Symp.* **2003**, *192*, 63 – 73.
[203] S. Lecommandoux, H.-A. Klok, M. Sayar, S. I. Stupp, *J. Polym. Sci. Part A* **2003**, *41*, 3501 – 3518.
[204] O. Y. Mindyuk, M. R. Stetzer, P. A. Heiney, J. C. Nelson, J. S. Moore, *Adv. Mater.* **1998**, *10*, 1363 – 1366.
[205] C. Zannoni, *J. Mater. Chem.* **2001**, *11*, 2637 – 2646.
[206] D. A. Tomalia, J. M. J. Fréchet, *J. Polym. Sci. Part A* **2002**, *40*, 2719 – 2728.
[207] I. M. Saez, J. W. Goodby, *J. Mater. Chem.* **2005**, *15*, 26 – 40.
[208] V. Percec, W.-D. Cho, G. Ungar, *J. Am. Chem. Soc.* **2000**, *122*, 10273 – 10281.
[209] V. Percec, W.-D. Cho, P. E. Mosier, G. Ungar, D. J. P. Yeardley, *J. Am. Chem. Soc.* **1998**, *120*, 11061 – 11070.
[210] G. Ungar, Y. Liu, X. Zeng, V. Percec, W.-D. Cho, *Science* **2003**, *299*, 1208 – 1211.
[211] B.-K. Cho, A. Jain, S. M. Gruner, U. Wiesner, *Science* **2004**, *305*, 1598 – 1601.
[212] B.-K. Cho, A. Jain, J. Nieberle, S. Mahajan, U. Wiesner, S. M. Gruner, S. Türk, H. J. Räder, *Macromolecules* **2004**, *37*, 4227 – 4234.
[213] D. Guillon, R. Deschenaux, *Curr. Opin. Solid State Mater. Sci.* **2002**, *6*, 515 – 525.
[214] I. M. Saez, J. W. Goodby, *Chem. Eur. J.* **2003**, *9*, 4869 – 4877.
[215] I. M. Saez, J. W. Goodby, *Chem. Commun.* **2003**, 1726 – 1727.
[216] a) J. W. Goodby, R. Blinc, N. A. Clark, S. T. Lagerwall, M. A. Osipov, S. A. Pikin, T. Sakurai, K. Yoshino, B. Zeks, *Ferroelectric Liquid Crystals: Principles, Properties and Applications*, Gordon & Breach, Philadelphia, **1991**; b) S. T. Lagerwall, *Ferroelectric and Antiferroelectric Liquid Crystals*, Wiley-VCH, Weinheim, **1999**.
[217] V. Percec, A. E. Dulcey, V. S. K. Balagurusamy, Y. Miura, J. Smidrkal, M. Peterca, S. Nummelin, U. Edlund, S. D. Hudson, P. A. Heiney, H. Duan, S. N. Magonov, S. A. Vinogradov, *Nature* **2004**, *430*, 764 – 768.
[218] M. M. Green, S. Zanella, H. Gu, T. Sato, G. Gottarelli, S. K. Jha, G. P. Spada, A. M. Schoevaars, B. Feringa, A. Teramoto, *J. Am. Chem. Soc.* **1998**, *120*, 9810 – 9817.
[219] a) K. Nozaki, Y. Kawashima, T. Oda, T. Hiyama, K. Kanie, T. Kato, *Macromolecules* **2002**, *35*, 1140 – 1142; b) Y. Kawashima, K. Nozaki, T. Hiyama, M. Yoshio, K. Kanie, T. Kato, *J. Polym. Sci. Part A* **2003**, *41*, 3556 – 3563.
[220] a) H. Coles in *Handbook of Liquid Crystals*, Vol. *2A* (Eds.: D. Demus, J. W. Goodby, G. W. Gray, H.-W. Spiess, V. Vill), Wiley-VCH, Weinheim, **1998**, pp. 335 – 409; b) N. Tamaoki, *Adv. Mater.* **2001**, *13*, 1135 – 1147; c) D. J. Broer, J. Lub, G. N. Mol, *Nature* **1995**, *378*, 467 – 469.
[221] R. R. Shah, N. L. Abbott, *Science* **2001**, *293*, 1296 – 1299.
[222] K. Ichimura, *Chem. Rev.* **2000**, *100*, 1847 – 1873.
[223] T. Seki, *Polym. J.* **2004**, *36*, 435 – 454.
[224] Y.-Y. Luk, K.-L. Yang, K. Cadwell, N. L. Abbott, *Surf. Sci.* **2004**, *570*, 43 – 56.
[225] M. L. Tingey, Y.-Y. Luk, N. L. Abbott, *Adv. Mater.* **2002**, *14*, 1224 – 1227.
[226] K. Kishimoto, M. Yoshio, T. Mukai, M. Yoshizawa, H. Ohno, T. Kato, *J. Am. Chem. Soc.* **2003**, *125*, 3196 – 3197.
[227] M. Yoshio, T. Mukai, H. Ohno, T. Kato, *J. Am. Chem. Soc.* **2004**, *126*, 994 – 995.
[228] a) M. Yoshio, T. Mukai, K. Kanie, M. Yoshizawa, H. Ohno, T. Kato, *Adv. Mater.* **2002**, *14*, 351 – 354; b) M. Yoshio, T. Kato, T. Mukai, M. Yoshizawa, H. Ohno, *Mol. Cryst. Liq. Cryst.* **2004**, *413*, 2235 – 2244.
[229] R. J. Bushby, O. R. Lozman, *Curr. Opin. Solid State Mater. Sci.* **2002**, *6*, 569 – 578.
[230] N. Boden, R. J. Bushby, J. Clements, *J. Chem. Phys.* **1993**, *98*, 5920 – 5931.
[231] D. Adam, P. Schuhmacher, J. Simmerer, L. Häussling, K. Siemensmeyer, K. H. Etzbach, H. Ringsdorf, D. Haarer, *Nature* **1994**, *371*, 141 – 143.
[232] A. M. van de Craats, J. M. Warman, K. Müllen, Y. Geerts, J. D. Brand, *Adv. Mater.* **1998**, *10*, 36 – 38.
[233] A. M. van de Craats, J. M. Warman, A. Fechtenkötter, J. D. Brand, M. A. Harbison, K. Müllen, *Adv. Mater.* **1999**, *11*, 1469 – 1472.
[234] C. Liu, A. Fechtenkötter, M. D. Watson, K. Müllen, A. J. Band, *Chem. Mater.* **2003**, *15*, 124 – 130.
[235] C. D. Simpson, J. Wu, M. D. Watson, K. Müllen, *J. Mater. Chem.* **2004**, *14*, 494 – 504.
[236] C. Piechoki, J. Simon, A. Skoulios, D. Guillon, P. Weber, *J. Am. Chem. Soc.* **1982**, *104*, 5245 – 5247.
[237] C. F. van Nostrum, R. J. M. Nolte, *Chem. Commun.* **1996**, 2385 – 2392.
[238] R. I. Gearba, M. Lehmann, J. Levin, D. A. Ivanov, M. H. J. Koch, J. Barberá, M. G. Debije, J. Piris, Y. H. Geerts, *Adv. Mater.* **2003**, *15*, 1614 – 1618.
[239] V. Percec, M. Glodde, T. K. Bera, Y. Miura, I. Shiyanovskaya, K. D. Singer, V. S. K. Balagurusamy, P. A. Heiney, I. Schnell, A. Rapp, H.-W. Spiess, S. D. Hudson, H. Duan, *Nature* **2002**, *419*, 384 – 387.
[240] R. C. Smith, W. M. Fischer, D. L. Gin, *J. Am. Chem. Soc.* **1997**, *119*, 4092 – 4093.

 © 2006 Wiley-VCH Verlag GmbH & Co. KGaA, Weinheim

[241] D. Gin, R. Smith, H. Deng, G. Leising, *Synth. Met.* **1999**, *101*, 52 – 55.
[242] H. Kosonen, J. Ruokolainen, M. Knaapila, M. Torkkeli, K. Jokela, R. Serimaa, G. ten Brinke, W. Bras, A. P. Monkman, O. Ikkala, *Macromolecules* **2000**, *33*, 8671 – 8675.
[243] a) *Ionic Liquids: The Front and Future of Materials Development* (Ed.: H. Ohno), CMC, Tokyo, **2003**; b) *Electrochemical Aspects of Ionic Liquids* (Ed.: H. Ohno), Wiley, Hoboken, NJ, **2005**.
[244] *Ionic Liquids in Synthesis* (Eds.: P. Wasserscheid, T. Welton), Wiley-VCH, Weinheim, **2002**.
[245] J. G. Huddleston, A. E. Visser, W. M. Reichert, H. D. Willauer, G. A. Broker, R. D. Rogers, *Green Chem.* **2001**, *3*, 156 – 164.
[246] C. F. van Nostrum, S. J. Picken, A.-J. Schouten, R. J. M. Nolte, *J. Am. Chem. Soc.* **1995**, *117*, 9957 – 9965.
[247] V. Percec, G. Johansson, J. Heck, G. Ungar, S. V. Batty, *J. Chem. Soc. Perkin Trans. 1* **1993**, 1411 – 1420.
[248] U. Beginn, G. Zipp, A. Mourran, P. Walther, M. Möller, *Adv. Mater.* **2000**, *12*, 513 – 516.
[249] J.-M. Lehn, J. Malthête, A.-M. Levelut, *J. Chem. Soc. Chem. Commun.* **1985**, 1794 – 1796.
[250] a) V. Percec, J. A. Heck, D. Tomazos, G. Ungar, *J. Chem. Soc. Perkin Trans. 2* **1993**, 2381 – 2388; b) L. Brunsveld, J. A. J. M. Vekemans, H. M. Janssen, E. W. Meijer, *Mol. Cryst. Liq. Cryst.* **1999**, *331*, 449 – 456.
[251] J. Ruokolainen, R. Mäkinen, M. Torkkeli, T. Mäkelä, R. Serimaa, G. ten Brinke, O. Ikkala, *Science* **1998**, *280*, 557 – 560.
[252] R. Mäki-Ontto, K. de Moel, E. Polushkin, G. Alberda van Ekenstein, G. ten Brinke, O. Ikkala, *Adv. Mater.* **2002**, *14*, 357 – 361.
[253] a) M. Funahashi, J. Hanna, *Appl. Phys. Lett.* **2000**, *76*, 2574 – 2576; b) R. Azumi, G. Götz, P. Bäuerle, *Synth. Met.* **1999**, *101*, 544 – 545; c) P. Liu, H. Nakano, Y. Shirota, *Liq. Cryst.* **2001**, *28*, 581 – 589; d) H. Zhang, S. Shiino, A. Kanazawa, O. Tsutsumi, T. Shiono, T. Ikeda, Y. Nagase, *Synth. Met.* **2002**, *126*, 11 – 18.
[254] I. McCulloch, W. Zhang, M. Heeney, C. Bailey, M. Giles, D. Graham, M. Shkunov, D. Sparrowe, S. Tierney, *J. Mater. Chem.* **2003**, *13*, 2436 – 2444.
[255] H. Kuroda, H. Goto, K. Akagi, A. Kawaguchi, *Macromolecules* **2002**, *35*, 1307 – 1313.
[256] S. R. Hammond, W.-J. Zhou, D. L. Gin, *Liq. Cryst.* **2002**, *29*, 1151 – 1159.
[257] K. Hoshino, M. Yoshio, T. Mukai, K. Kishimoto, H. Ohno, T. Kato, *J. Polym. Sci. Part A* **2003**, *41*, 3486 – 3492.
[258] T. Mukai, M. Yoshio, T. Kato, H. Ohno, *Chem. Lett.* **2004**, *33*, 1630 – 1631.
[259] a) T. Mukai, M. Yoshio, T. Kato, M. Yoshizawa, H. Ohno, *Chem. Commun.* **2005**, 1333 – 1335; b) M. Yoshio, T. Mukai, K. Kanie, M. Yoshizawa, H. Ohno, T. Kato, *Chem. Lett.* **2002**, 320 – 321.
[260] T. Mukai, M. Yoshio, T. Kato, H. Ohno, *Chem. Lett.* **2005**, *34*, 442 – 443.
[261] T. Ohtake, M. Ogasawara, K. Ito-Akita, N. Nishina, S. Ujiie, H. Ohno, T. Kato, *Chem. Mater.* **2000**, *12*, 782 – 789.
[262] T. Ohtake, Y. Takamitsu, K. Ito-Akita, K. Kanie, M. Yoshizawa, T. Mukai, H. Ohno, T. Kato, *Macromolecules* **2000**, *33*, 8109 – 8111.
[263] T. Ohtake, K. Ito, N. Nishina, H. Kihara, H. Ohno, T. Kato, *Polym. J.* **1999**, *31*, 1155 – 1158.
[264] T. Ohtake, K. Kanie, M. Yoshizawa, T. Mukai, K. Ito-Akita, H. Ohno, T. Kato, *Mol. Cryst. Liq. Cryst.* **2001**, *364*, 589 – 596.
[265] M. Yoshizawa, T. Mukai, T. Ohtake, K. Kanie, T. Kato, H. Ohno, *Solid State Ionics* **2002**, *154–155*, 779 – 787.
[266] K. Ito-Akita, N. Nishina, Y. Asai, H. Ohno, T. Ohtake, Y. Takamitsu, T. Kato, *Polym. Adv. Technol.* **2000**, *11*, 529 – 533.
[267] K. Hoshino, K. Kanie, T. Ohtake, T. Mukai, M. Yoshizawa, S. Ujiie, H. Ohno, T. Kato, *Macromol. Chem. Phys.* **2002**, *203*, 1547 – 1555.
[268] a) K. Yoshino, Y. Shimoda, Y. Kawagishi, K. Nakayama, M. Ozaki, *Appl. Phys. Lett.* **1999**, *75*, 932 – 934; b) M. Ozaki, Y. Shimoda, M. Kasano, K. Yoshino, *Adv. Mater.* **2002**, *14*, 514 – 518; c) N. Y. Ha, Y. K. Woo, B. Park, H. Takezoe, J. W. Wu, *Adv. Mater.* **2004**, *16*, 1725 – 1729.
[269] a) T. Kato, H. Kihara, T. Uryu, S. Ujiie, K. Iimura, J. M. J. Fréchet, U. Kumar, *Ferroelectrics* **1993**, *148*, 161 – 167; b) H. Kihara, T. Kato, T. Uryu, S. Ujiie, U. Kumar, J. M. J. Fréchet, D. W. Bruce, D. J. Price, *Liq. Cryst.* **1996**, *21*, 25 – 30.
[270] J. A. McCubbin, X. Tong, R. Wang, Y. Zhao, V. Snieckus, R. P. Lemieux, *J. Am. Chem. Soc.* **2004**, *126*, 1161 – 1167.
[271] a) A. Kanazawa, O. Tsutsumi, T. Ikeda, Y. Nagase, *J. Am. Chem. Soc.* **1997**, *119*, 7670 – 7675; b) A. Kanazawa, T. Ikeda, J. Abe, *J. Am. Chem. Soc.* **2001**, *123*, 1748 – 1754; c) A. Kanazawa, T. Ikeda, *Coord. Chem. Rev.* **2000**, *198*, 117 – 131.
[272] C. R. Safinya, *Curr. Opin. Struct. Biol.* **2001**, *11*, 440 – 448.
[273] N. Zhu, D. Liggitt, Y. Liu, R. Debs, *Science* **1993**, *261*, 209 – 211.
[274] N. L. Slack, M. Schellhorn, T. Eiselt, M. A. Chibbaro, U. Schulze, H. E. Warriner, P. Davidson, H.-W. Schmidt, C. R. Safinya, *Macromolecules* **1998**, *31*, 8503 – 8508.
[275] H. E. Warriner, S. H. J. Idziak, N. L. Slack, P. Davidson, C. R. Safinya, *Science* **1996**, *271*, 969 – 973.
[276] S. A. Miller, E. Kim, D. H. Gray, D. L. Gin, *Angew. Chem.* **1999**, *111*, 3205 – 3210; *Angew. Chem. Int. Ed.* **1999**, *38*, 3021 – 3026.
[277] W. Gu, W.-J. Zhou, D. L. Gin, *Chem. Mater.* **2001**, *13*, 1949 – 1951.
[278] D. L. Gin, W. Gu, *Adv. Mater.* **2001**, *13*, 1407 – 1410.
[279] W. Zhou, W. Gu, Y. Xu, C. S. Pecinovsky, D. L. Gin, *Langmuir* **2003**, *19*, 6346 – 6348.
[280] Y. Xu, W. Gu, D. L. Gin, *J. Am. Chem. Soc.* **2004**, *126*, 1616 – 1617.
[281] H.-K. Lee, H. Lee, Y. H. Ko, Y. J. Chang, N.-K. Oh, W.-C. Zin, K. Kim, *Angew. Chem.* **2001**, *113*, 2741 – 2743; *Angew. Chem. Int. Ed.* **2001**, *40*, 2669 – 2671.
[282] I. Dierking, *Adv. Mater.* **2000**, *12*, 167 – 181.
[283] R. A. M. Hikmet, *Adv. Mater.* **1992**, *4*, 679 – 683.
[284] R. A. M. Hikmet, J. Lub, *Prog. Polym. Sci.* **1996**, *21*, 1165 – 1209.
[285] H. G. Craighead, J. Cheng, S. Hackwood, *Appl. Phys. Lett.* **1982**, *40*, 22 – 24.
[286] P. S. Drzaic, *J. Appl. Phys.* **1986**, *60*, 2142 – 2148.
[287] J. W. Doane, N. A. Vaz, B.-G. Wu, S. Žumer, *Appl. Phys. Lett.* **1986**, *48*, 269 – 271.
[288] C. V. Rajaram, S. D. Hudson, L.-C. Chien, *Chem. Mater.* **1996**, *8*, 2451 – 2460.
[289] T. Kajiyama, A. Miyamoto, H. Kikuchi, Y. Morimura, *Chem. Lett.* **1989**, 813 – 816.
[290] F. P. Nicoletta, G. De Filpo, J. Lanzo, G. Chidichimo, *Appl. Phys. Lett.* **1999**, *74*, 3945 – 3947.
[291] M. Kreuzer, T. Tschudi, W. H. de Jeu, R. Eidenschink, *Appl. Phys. Lett.* **1993**, *62*, 1712 – 1714.
[292] M. van Boxtel, D. Broer, C. Bastiaansen, M. Baars, R. Janssen, *Macromol. Symp.* **2000**, *154*, 25 – 35.
[293] a) T. Kato, G. Kondo, K. Hanabusa, *Chem. Lett.* **1998**, 193 – 194; b) K. Yabuuchi, A. E. Rowan, R. J. M. Nolte, T. Kato, *Chem. Mater.* **2000**, *12*, 193 – 194.
[294] T. Kato, T. Kutsuna, K. Hanabusa, *Mol. Cryst. Liq. Cryst.* **1999**, *332*, 2887 – 2892.
[295] D. J. Abdallah, R. G. Weiss, *Adv. Mater.* **2000**, *12*, 1237 – 1247.
[296] J. H. van Esch, B. L. Feringa, *Angew. Chem.* **2000**, *112*, 2351 – 2354; *Angew. Chem. Int. Ed.* **2000**, *39*, 2263 – 2266.

© 2006 Wiley-VCH Verlag GmbH & Co. KGaA, Weinheim

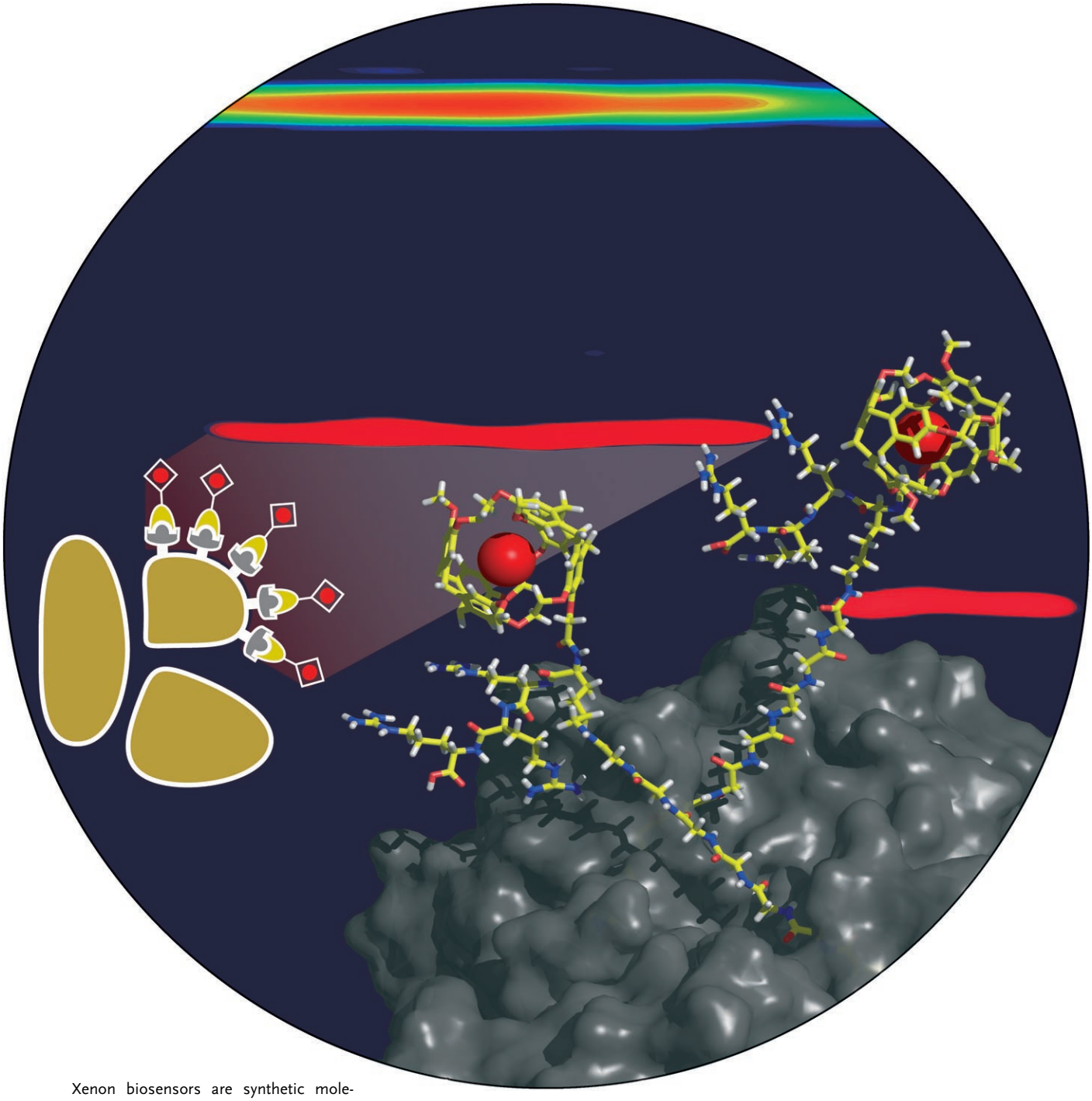
[297] K. J. C. van Bommel, A. Friggeri, S. Shinkai, *Angew. Chem.* **2003**, *115*, 1010 – 1030; *Angew. Chem. Int. Ed.* **2003**, *42*, 980 – 999.
[298] N. Mizoshita, T. Kutsuna, K. Hanabusa, T. Kato, *Chem. Commun.* **1999**, 781 – 782.
[299] T. Kato, T. Kutsuna, K. Yabuuchi, N. Mizoshita, *Langmuir* **2002**, *18*, 7086 – 7088.
[300] a) N. Mizoshita, K. Hanabusa, T. Kato, *Adv. Funct. Mater.* **2003**, *13*, 313 – 317; b) P. Cirkel, T. Kato, N. Mizoshita, H. Jagt, K. Hanabusa, *Liq. Cryst.* **2004**, *31*, 1649 – 1653.
[301] Y. Suzuki, N. Mizoshita, K. Hanabusa, T. Kato, *J. Mater. Chem.* **2003**, *13*, 2870 – 2874.
[302] a) N. Mizoshita, Y. Suzuki, K. Kishimoto, K. Hanabusa, T. Kato, *J. Mater. Chem.* **2002**, *12*, 2197 – 2201; b) N. Mizoshita, Y. Suzuki, K. Kishimoto, T. Kato, K. Hanabusa, *Mol. Cryst. Liq. Cryst.* **2004**, *409*, 175 – 181.
[303] R. H. C. Janssen, V. Stümpflen, D. J. Broer, C. W. M. Bastiaansen, T. A. Tervoort, P. Smith, *J. Appl. Phys.* **2000**, *88*, 161 – 167.
[304] C. Tolksdorf, R. Zentel, *Adv. Mater.* **2001**, *13*, 1307 – 1310.
[305] J. Prigann, C. Tolksdorf, H. Skupin, R. Zentel, F. Kremer, *Macromolecules* **2002**, *35*, 4150 – 4154.
[306] Y. Zhao, L. Guan, *Liq. Cryst.* **2003**, *30*, 81 – 86.
[307] N. Mizoshita, H. Monobe, M. Inoue, M. Ukon, T. Watanabe, Y. Shimizu, K. Hanabusa, T. Kato, *Chem. Commun.* **2002**, 428 – 429.
[308] M. Moriyama, N. Mizoshita, T. Yokota, K. Kishimoto, T. Kato, *Adv. Mater.* **2003**, *15*, 1335 – 1338.
[309] Y. Zhao, X. Tong, *Adv. Mater.* **2003**, *15*, 1431 – 1435.
[310] a) M. Moriyama, N. Mizoshita, T. Kato, *Polym. J.* **2004**, *36*, 661 – 664; b) M. Moriyama, N. Mizoshita, T. Kato, *Proc. SPIE-Int. Soc. Opt. Eng.* **2004**, *5518*, 160 – 169.
[311] S. P. Meeker, W. C. K. Poon, J. Crain, E. M. Terentjev, *Phys. Rev. E* **2000**, *61*, R6083 – R6086.
[312] M. Zapotocky, L. Ramos, P. Poulin, T. C. Lubensky, D. A. Weitz, *Science* **1999**, *283*, 209 – 212.
[313] M. C. W. van Boxtel, R. H. C. Janssen, D. J. Broer, H. T. A. Wilderbeek, C. W. M. Bastiaansen, *Adv. Mater.* **2000**, *12*, 753 – 757.
[314] M. C. W. van Boxtel, M. Wübbenhorst, J. van Turnhout, C. W. M. Bastiaansen, D. J. Broer, *Liq. Cryst.* **2003**, *30*, 235 – 249.
[315] M. C. W. van Boxtel, R. H. C. Janssen, C. W. M. Bastiaansen, D. J. Broer, *J. Appl. Phys.* **2001**, *89*, 838 – 842.
[316] A. Yasuda, H. Takanishi, K. Nito, E. Matsui, *Jpn. J. Appl. Phys.* **1997**, *36*, 228 – 231.
[317] M. W. P. L. Baars, M. C. W. van Boxtel, C. W. M. Bastiaansen, D. J. Broer, S. H. M. Söntjens, E. W. Meijer, *Adv. Mater.* **2000**, *12*, 715 – 719.
[318] M. C. W. van Boxtel, M. Wübbenhorst, J. van Turnhout, C. W. M. Bastiaansen, D. J. Broer, *Liq. Cryst.* **2004**, *31*, 1207 – 1218.
[319] H. Yoshikawa, K. Maeda, Y. Shiraishi, J. Xu, H. Shiraki, N. Toshima, S. Kobayashi, *Jpn. J. Appl. Phys.* **2002**, *41*, L1315 – L1317.
[320] J. Yamamoto, H. Tanaka, *Nature* **2001**, *409*, 321 – 325.
[321] J. Motoyanagi, T. Fukushima, T. Aida, *Chem. Commun.* **2005**, 101 – 103.
[322] N. Mizoshita, Y. Suzuki, K. Hanabusa, T. Kato, *Adv. Mater.* **2005**, *17*, 692 – 696.
[323] T. Kitamura, S. Nakaso, N. Mizoshita, Y. Tochigi, T. Shimomura, M. Moriyama, K. Ito, T. Kato, *J. Am. Chem. Soc.* **2005**, *127*, 14769 – 14775.



 © 2006 Wiley-VCH Verlag GmbH & Co. KGaA, Weinheim

Communications

DOI: 10.1002/anie.200502693



Xenon biosensors are synthetic molecules that contain tethered analyte-binding and xenon-binding moieties. When associated with the analyte, they provide unique NMR signals, with sensitivity greatly enhanced by hyperpolarization of the xenon. For further details of the use of xenon biosensors for targeted biomedical imaging, see the Communication by C. Hilty et al. on the following pages.

WILEY InterScience® DISCOVER SOMETHING GREAT

© 2006 Wiley-VCH Verlag GmbH & Co. KGaA, Weinheim

Imaging Agents

DOI: 10.1002/anie.200502693

Spectrally Resolved Magnetic Resonance Imaging of a Xenon Biosensor**

Christian Hilty, Thomas J. Lowery, David E. Wemmer, and Alexander Pines*

Nuclear magnetic resonance is the method of choice for applications as widespread as chemical analysis and medical diagnostics because of its ability to non-invasively record images, as well as elucidate molecular structure. Its detection threshold is, however, limited by the small polarization of nuclear spins in even the highest available magnetic fields. This limitation can, under certain circumstances, be alleviated by using hyperpolarized substances.[1] Xenon biosensors make use of the sensitivity gain obtained with hyperpolarized xenon to provide the capability for magnetic resonance detection of a specific low-concentration target.[2–4] Such biosensors consist of a cryptophane cage[5] which binds one xenon atom, and is connected through a linker to a targeting moiety such as a ligand or antibody (Figure 1). Recent work has shown the possibility of using the xenon biosensor to detect small amounts of a substance in a heterogeneous environment by NMR spectroscopy.[6] Here, we demonstrate that magnetic resonance (MR) provides the capability of obtaining spectrally and spatially resolved images of the distribution of the immobilized biosensor, thus opening up the possibility of using the xenon biosensor for targeted imaging.

A continuous flow of water saturated with hyperpolarized xenon was supplied by a specifically designed apparatus (Figure 2) to immobilized avidin–agarose beads (ca. 250 μL hydrated volume) packed in a glass tube assembly between two frits (Figure 3 a). The xenon biosensor was attached to the agarose beads through the affinity of its biotin tag to immobilized avidin (binding affinity: $10^{15}\,\text{M}^{-1}$). It was estimated from biochemical characterization that a biosensor concentration of 82 μM was thus achieved in the resin. The biosensor construct used is shown in Figure 1, with its xenon-binding cryptophane cage to the right and its biotin tag at the bottom.

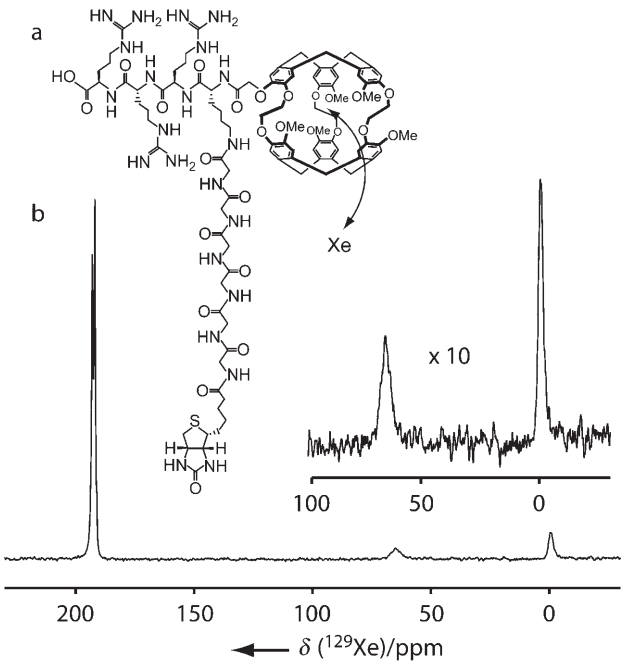


Figure 1. a) Chemical structure of the functionalized xenon biosensor.[2,6] b) NMR spectrum of the xenon biosensor bound to avidin-containing agarose beads.

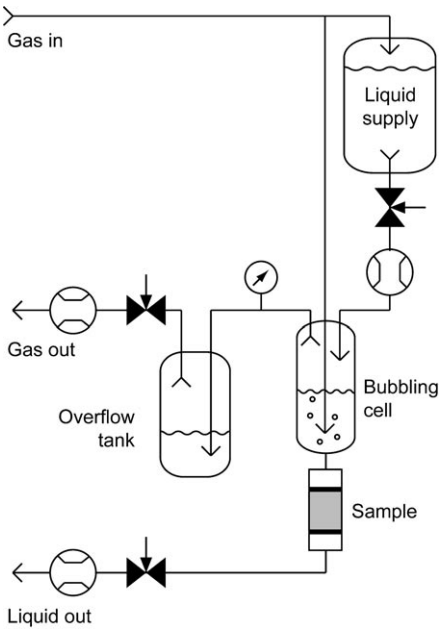


Figure 2. Instrumentation for MR imaging with xenon-saturated liquids.

[*] Dr. C. Hilty, Prof. A. Pines
Lawrence Berkeley National Laboratory
Materials Sciences Division
and
University of California Berkeley
Department of Chemistry
Berkeley CA 94720 (USA)
Fax: (+1) 510-486-5744
E-mail: hilty@berkeley.edu
T. J. Lowery, Prof. D. E. Wemmer
Lawrence Berkeley National Laboratory
Physical Biosciences Division
and
University of California Berkeley
Department of Chemistry
Berkeley CA 94720 (USA)

[**] This work was supported by the Director, Office of Science, Office of Basic Energy Sciences, Materials Sciences and Engineering Division, of the US Department of Energy under Contract No. DE-AC03-76SF00098. C.H. acknowledges support from the Schweizerischer Nationalfonds through a postdoctoral fellowship. T.L. acknowledges support from the University of California Biotechnology Research and Education Program for a training grant.

© 2006 Wiley-VCH Verlag GmbH & Co. KGaA, Weinheim

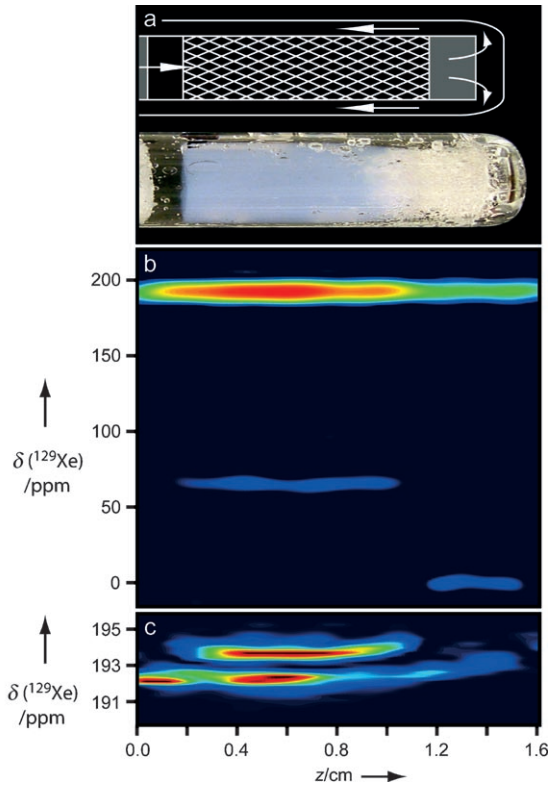


Figure 3. a) Sketch and photograph of the agarose bead sample used for the imaging experiments. The direction of liquid flow (indicated by arrows) is from left to right, through the column of beads (hatched), out the frit (shaded gray), and around the outside of the inner concentric tube. b) Spectrally resolved MR image of the immobilized xenon biosensor. The image dimension (horizontal) is shown to scale with the photograph in (a). The image was taken over 135 minutes, using a field of view along the *z*-dimension of 2 cm and a resolution of 1.2 mm. c) Image of the solution peak in (b), processed to show splitting between the xenon in the bead and xenon in water.

The signal at $\delta = 65.4$ ppm with a linewidth of 300 Hz in the ^{129}Xe NMR spectrum of this sample (Figure 1) corresponds to xenon in the biosensor. The downfield signals at $\delta =$ 193.6 and 192.5 ppm are from dissolved xenon in the agarose beads and water, respectively,[6] and the signal at $\delta = 0$ ppm is from xenon gas. The xenon resonance from the immobilized biosensor is broadened relative to that of the solution-free biosensor (ca. 20 Hz),[2,7] presumably because of motional hindrance of the cage.

A spectrally resolved image of the biosensor distribution in this sample was acquired using phase-encoded MR imaging (Figure 3). Figure 3a shows a photograph of the sample with flowing xenon-saturated water for comparison. Drawn to scale with this photograph is the xenon image that has spatial resolution along the z axis (Figure 3b). It is readily apparent that different regions of the sample give rise to the signals with different chemical shift. The image intensity at the chemical shift of the dissolved xenon ($\delta \approx 193$ ppm) extends over the entire sample space, while the signal at the chemical shift of xenon in the biosensor ($\delta = 65.4$ ppm) occurs only in the actual volume of the beads. To the right of the image, a short section of xenon gas ($\delta = 0$ ppm) is visible, which corresponds to the region in the sample where gas bubbles appear in the photograph (Figure 3a). This gas release is due to a pressure gradient over the column of beads. The spectral dimension in Figure 3b is processed with a sine bell window in which only the first part of the free induction decay (FID) is selected, where the signal corresponding to the biosensor is present. As a consequence, the signal of dissolved xenon is not resolved into its water and bead components in this image. The splitting of this signal becomes readily observable when an exponential window function that extends over the entire FID is applied (Figure 3c). Here, the extent of the bead volume can be deduced from the signal at $\delta = 193.6$ ppm, which closely corresponds to the size of the biosensor signal. The slight change in chemical shift of the solution signals between $z = 1$ to $z = 1.4$ cm may be attributable to susceptibility differences between the agarose beads, gas bubbles, and the lower frit.

These experiments show that MR imaging of a selectively targeted xenon biosensor can be accomplished with good sensitivity. The use of hyperpolarized xenon enables the distribution of a micromolar range concentration of avidin to be imaged in this heterogeneous sample. In comparison, direct detection of bead-bound avidin by ^{1}H NMR spectroscopy would be very difficult or impossible because of the low concentration, broad linewidth, and spectral crowding.

Imaging at the lower NMR coil filling factors required for most in situ samples will demand significant improvements in sensitivity. An increase in the signal by more than a factor of 10 could easily be gained by using a xenon polarizer optimized for continuous flow applications[8] to give a polarization of about 50% instead of 3%. An increase of another factor of 15 could be gained by using a biosensor that does not suffer broadening of the xenon line when immobilized. Further sensitivity could be gained by designing sensor constructs that contain more than one xenon binding cage per analyte, and by the use of isotopically enriched xenon. These improvements would boost the sensitivity of xenon biosensor imaging by a factor of at least 1000. Such an increase extrapolates to a detection threshold of about 100 nM in a small NMR coil optimized for the biosensor-bound sample volume, or to a detection limit of about 100 μM in a sample of the present size in an overall volume of several liters.[9]

From these results, the potential usefulness of a xenon biosensor construct that is targeted to markers on cell surfaces may be extrapolated. In vivo imaging with free hyperpolarized xenon has already been demonstrated.[10,11] In combination with specific targeting, for example, to tumor cells, this could lead to a new tool for medical applications such as the diagnosis of cancer. The xenon biosensor would offer advantages over other methods for the detection of low target concentrations in opaque tissue. In contrast to using hyperpolarized small molecules,[12] the biosensor could be injected well in advance to the introduction of hyperpolarized xenon and acquisition of the signal, thus allowing adequate time for target binding without compromising xenon polarization. As seen in Figure 3b, xenon in the biosensor is easily distinguished from bulk xenon through its different chemical shift. A xenon biosensor image is, therefore, an image with near-zero background, and should afford much higher

 © 2006 Wiley-VCH Verlag GmbH & Co. KGaA, Weinheim

detection fidelity than a contrast agent such as gadolinium that merely modulates the proton signal already present in the entire volume.[13] The large chemical shift bandwidth of cage-encapsulated xenon makes the use of the xenon biosensor suitable for multiple analysis, where a number of different biosensors with unique xenon chemical shifts bind to different targets.[2,4] Our results here indicate that the possibility of multiple biomolecular analysis can be extended to imaging to allow for multiple, target-selective images to be acquired simultaneously (Figure 3), which would greatly enhance the specificity and fidelity of diagnosis.

Experimental Section

An apparatus was designed to provide a continuous stream of liquid saturated with hyperpolarized xenon. Water flowed from the liquid supply (1000 mL) to the bubbling cell (5 mL), where it was saturated with hyperpolarized xenon (4.4 mM atm^{-1};[1,6] Amersham Health, Durham, NC), then through the sample to the "liquid out" port. The hyperpolarized xenon gas mixture (1% Xe at natural isotope abundance, polarized to ca. 3%, mixed with 10% N_2, 89% He; Airgas, Radnor, PA) was supplied at a pressure of 6 atm to the "gas in" port, and flowed through the bubbling cell to the "gas out" port. The gas also pressurized the liquid supply, so that gravity was sufficient for liquid to flow to the bubbling cell. Both the liquid refill and the sample flow rates were controlled with needle valves and measured with rotameters. To ensure that the bubbling cell did not empty during an experiment, the refill rate was set 50% higher than the flow rate through the sample. The excess water exited the bubbling cell together with the gas and was collected in the overflow tank. The bubbling intensity was controlled by the gas flow rate (0.7 standard liters per minute), which was adjusted at the "gas out" port. The system pressure was monitored at the inlet to the overflow tank.

For the present experiments, the sample of immobilized-avidin, 6% cross-linked, agarose beads (Pierce Biotechnology), with the xenon biosensor was designed to fit within the coil of a 10-mm NMR probe (Varian, Palo Alto, CA), which had a sensitive region of 1.8 cm along the z-axis. The probe was inserted together with a gradient coil assembly into a vertical bore superconducting NMR magnet (7 T). The sample was efficiently perfused by xenon-saturated water, which was refreshed completely every 6 s when using a liquid flow rate of 10 mL min^{-1}. The bubbling cell was located immediately above the sample.

Spectrally resolved MR images were acquired using phase encoding for spatial dimensions and chemical shift resolved acquisition.[14] The pulse sequence was thus $p_{90}-\tau_{grad}-p_{180}-\tau_{acq}$. $p_{90} = 14$ μs and $p_{180} = 28$ μs stand for rf pulses with the indicated flip angle; phase-encoding gradients were applied over $\tau_{grad} = 200$ μs; and the spectral dimension was acquired as an echo over $\tau_{acq} = 100$ ms. The phases of the 90° pulse and the receiver were cycled as $\{x, -x\}$. A delay of 6 s between transients was used.

Received: August 1, 2005
Published online: November 28, 2005

Keywords: biosensors · cage compounds · imaging agents · magnetic resonance imaging · xenon

[1] M. G. Mortuza, S. Anala, G. E. Pavlovskaya, T. J. Dieken, T. Meersmann, *J. Chem. Phys.* **2003**, *118*, 1581 – 1584.
[2] M. M. Spence, E. J. Ruiz, S. M. Rubin, T. J. Lowery, N. Winssinger, P. G. Schultz, D. E. Wemmer, A. Pines, *J. Am. Chem. Soc.* **2004**, *126*, 15287 – 15294.
[3] T. J. Lowery, S. M. Rubin, E. J. Ruiz, M. M. Spence, N. Winssinger, P. G. Schultz, A. Pines, D. E. Wemmer, *Magn. Reson. Imaging* **2003**, *21*, 1235 – 1239.
[4] M. M. Spence, S. M. Rubin, I. E. Dimitrov, E. J. Ruiz, D. E. Wemmer, A. Pines, S. Q. Yao, F. Tian, P. G. Schultz, *Proc. Natl. Acad. Sci. USA* **2001**, *98*, 10654 – 10657.
[5] A. Collet, *Tetrahedron* **1987**, *43*, 5725 – 5759.
[6] S. I. Han, S. Garcia, T. J. Lowery, E. J. Ruiz, J. A. Seeley, L. Chavez, D. S. King, D. E. Wemmer, A. Pines, *Anal. Chem.* **2005**, *77*, 4008 – 4012.
[7] T. J. Lowery, S. Garcia, L. Chavez, E. J. Ruiz, T. Wu, T. Brotin, J.-P. Dutasta, D. S. King, P. G. Schultz, A. Pines, D. E. Wemmer, *ChemBioChem* **2005**, in press.
[8] K. Knagge, J. Prange, D. Raftery, *Chem. Phys. Lett.* **2004**, *397*, 11 – 16.
[9] D. I. Hoult, *Prog. Nucl. Magn. Reson. Spectrosc.* **1978**, *12*, 41 – 77.
[10] M. S. Albert, G. D. Cates, B. Driehuys, W. Happer, B. Saam, C. S. Springer, A. Wishnia, *Nature* **1994**, *370*, 199 – 201.
[11] B. M. Goodson, Y. Q. Song, R. E. Taylor, V. D. Schepkin, K. M. Brennan, G. C. Chingas, T. F. Budinger, G. Navon, A. Pines, *Proc. Natl. Acad. Sci. USA* **1997**, *94*, 14725 – 14729.
[12] K. Golman, J. H. Ardenaer-Larsen, J. S. Petersson, S. Mansson, I. Leunbach, *Proc. Natl. Acad. Sci. USA* **2003**, *100*, 10435 – 10439.
[13] M. L. Wood, P. A. Hardy, *Magn. Reson. Imaging* **1993**, *3*, 149 – 156.
[14] P. T. Callaghan, *Principles of Nuclear Magnetic Resonance Microscopy*, Oxford University Press, New York, **1991**.

 © 2006 Wiley-VCH Verlag GmbH & Co. KGaA, Weinheim

Hydrothermal Synthesis

DOI: 10.1002/anie.200502917

Lanthanide–Transition-Metal Sandwich Framework Comprising $\{Cu_3\}$ Cluster Pillars and Layered Networks of $\{Er_{36}\}$ Wheels**

*Jian-Wen Cheng, Jie Zhang, Shou-Tian Zheng, Man-Bo Zhang, and Guo-Yu Yang**

The design and synthesis of wheel clusters still continues to attract intense interest not only because of their fascinating physical properties but also because of the architectural

[*] J.-W. Cheng, Prof. Dr. J. Zhang, S.-T. Zheng, M.-B. Zhang, Prof. Dr. G.-Y. Yang
State Key Laboratory of Structural Chemistry
and Graduate School of the Fujian Institute
of Research on the Structure of Matter
Chinese Academy of Sciences
Fuzhou, Fujian 350002 (P.R. China)
Fax: (+86) 591-8371-0051
E-mail: ygy@fjirsm.ac.cn

[**] This work was supported by the NNSF of China (Nos. 20271050/20473093), the Talents Program of Chinese Academy of Sciences, and the NSF of Fujian Province (Nos. E0510030/E0210029).

Supporting information for this article is available on the WWW under http://www.angewandte.org or from the author.

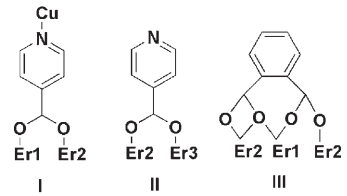
© 2006 Wiley-VCH Verlag GmbH & Co. KGaA, Weinheim
InterScience

beauty of their structures.[1–9] So far, most of the work in this area has focused on the assembly of transition-metal (TM) wheels, thus many high-nuclearity TM wheels have been obtained.[2–8] However, the analogous chemistry of lanthanides is still underdeveloped.[9] As lanthanide ions have variable and high coordination numbers as well as poor stereochemical preferences,[10] the construction of high-nuclearity lanthanide wheels is more difficult than the construction of their TM analogues. In comparison with a number of TM wheels such as $[Mo_{176}]$,[2a] $[Mn_{84}]$,[3a] $[Ni_{24}]$,[4a] $[Fe_{18}]$,[5a] $[Cr_{10}]$,[6a] $[Co_{12}]$,[7a] $[Cu_{10}]$,[8a] $[Ti_8]$,[11a] and $[V_8]$,[11b] only a few lanthanide wheels such as $[Ln_8]$,[9a,b] $[Ln_{10}]$,[9c,d] $[Ln_{12}]$,[9e,f] and $[Ln_{15}]$ have been made.[9e–g]

In general, ligands in the periphery of metal ions play an important role in forming and stabilizing metal wheels or clusters.[3–9,11,12] Recently, we reported a new class of 3D framework that contained $[Ln_{14}(\mu_6\text{-}O)(\mu_3\text{-}OH)_{20}]^{20+}$, $\{Ln_{14}\}$, cores. These compounds were synthesized by choosing isonicotinic acid (Hina) as a bridging ligand to link the $\{Ln_{14}\}$ cores with two types of Cu center.[12] If a second ligand were to be introduced, the cooperativity of both ligands may lead to a new open framework that contains lanthanide clusters different from the $\{Ln_{14}\}$ core, which would be helpful in understanding the formation mechanism of the open framework. In our search for new open frameworks constructed from lanthanide clusters, we have introduced a second ligand, 1,2-benzenedicarboxylic acid (H_2bdc).

We chose H_2bdc as the second ligand based on the following considerations: 1) it has versatile coordination modes;[13] 2) the chelating coordination of bdc may stabilize new lanthanide cluster formed in the crystallization process. Herein, we report two novel coordination polymers, $[Er_7(\mu_3\text{-}O)(\mu_3\text{-}OH)_6(bdc)_3](ina)_9[Cu_3X_4]$ (X = Cl or Br, denoted FJ-2a (**1**) and FJ-2b (**2**), respectively), in which the wheel-shaped building blocks of $[Er_{36}(\mu_3\text{-}OH)_{30}(\mu_3\text{-}O)_6(bdc)_6]^{54+}$, $\{Er_{36}\}$, with an 18 ring is currently the largest lanthanide wheel. **1** and **2** are the first sandwich frameworks based on the links by ina ligands of layered inorganic–organic hybrid polymers, built from nanosized $\{Er_{36}\}$ clusters, and TM clusters. To date, only three TM wheel-cluster polymers constructed from wheel-shaped building blocks are reported, one is a chainlike polymer linked by $\{Mo_{144}\}$ wheels,[2b] the other two are layered polymers linked by $\{Mo_{154}\}$[2c] and $\{Mo_{152}\}$[2d] wheels respectively; no systematic investigation of wheel cluster polymers, in which the metal wheels are linked to each other or linked with metal ions or clusters by organic ligands, has been carried out.

Brown hexagonal crystals of **1** and **2** were made by hydrothermal treatment of Er_2O_3, Hina, H_2bdc, and CuX_2 in water in the presence of $HClO_4$ (pH 2). X-ray crystal-structure analyses reveal that **1** and **2** are isostructural and crystallize in the high-symmetry rhombohedral space group, $R\bar{3}$.[14] Therefore, only the structure of **1** is described in detail. The asymmetric unit of **1** contains three unique Er^{3+}, one Cu^{2+}, and two Cl^- ions, and one bdc and three ina moieties with two coordination modes (see Scheme 1 and the Supporting Information). Er1 and Er2 are eight-coordinate and have bicapped trigonal prism coordination environments: three μ_3-OH groups, one μ_3-O, and two carboxylate oxygen atoms



Scheme 1. Coordination modes of the ina (I, II) and bdc (III) moieties in **1**.

(O_{COO}) from two bridging ina ligands (mode I), and two O_{COO} atoms from one bdc ligand for Er1 (see Supporting Information); two μ_3-OH groups, three O_{COO} atoms from three bridging ina ligands, and three O_{COO} atoms from two bdc ligands for Er2 (see Supporting Information). Six-coordinate Er3 has trigonal-prism coordination geometry: three μ_3-OH groups, and three O_{COO} atoms from three terminal ina ligands with mode II coordination (see Supporting Information). The Er–O bond lengths vary from 2.247(6) to 2.472(7) Å.

The Er^{3+} ions are linked by hydroxo and oxo bridges to give two types of small cluster cores: cubic $[Er_4(\mu_3\text{-}O)(\mu_3\text{-}OH)_3]^{7+}$, $\{Er_4\}$, core that contains three Er1 and one Er3 atoms and dimeric $[Er_2(\mu_3\text{-}OH)_2]^{4+}$, $\{Er_2\}$, core that contains two Er2 atoms (Figure 1a and Supporting Information). Different from the cubane $[Ln_4(\mu_3\text{-}OH)_4]^{8+}$, $[Ln_4]$, which contains four μ_3-OH groups, the $\{Er_4\}$ core in **1** consists of three μ_3-OH groups and one μ_3-O atom, which is rare in known $[Ln_4]$ cores.[9e–g,15] The $\{Er_4\}$ cores link alternately the $\{Er_2\}$ cores to form a nanosized $\{Er_{36}\}$ wheel with 18 ring (Figure 1b, Supporting Information). Remarkably, six bdc ligands are trapped in the inner of the 18 ring and bond to adjacent Er1 and Er2 atoms by four O_{COO} atoms. Although the bdc ligand has more than fifteen coordination modes,[13,16] it adopts a single μ_5-bdc mode found only in **1**; the number of coordination modes of ina is also reduced from four in $[Ln_{14}]$[12] to two in **1**, which indicates the high cooperativity between the ina and bdc ligands in the formation of **1**; the unique μ_5-bdc mode plays a key role in forming and stabilizing the $\{Er_{36}\}$ wheel (Figure 1b). It differs from ND-1, in which the 1,2-diaminocyclohexane templates stabilize the 24 ring through hydrogen bonding (see Supporting Information).[17]

Compared with TM wheels, which are formed by TM ions and organic ligands,[3–8] Ln wheels comprise not only organic ligands but also sharing Ln ions.[9] In $[Ln_8]$/$[Ln_{10}]$ wheels,[9a–d] the Ln ions are linked by OC_2H_4OMe ligands to form an 8/10 ring in which the center is empty. In $[Ln_{12}]$/$[Ln_{15}]$ wheels,[9e–g] four/five $\{Ln_4\}$ cores share Ln vertices to form a 4/5 ring around 1 or 2 halide ions in their central cavity. Notably, the construction mode of the wheel-shaped $\{Er_{36}\}$ cluster in **1** is significantly different from above discrete TM or Ln wheels.[3–9] The $\{Er_{36}\}$ wheel is made up of strictly alternating $\{Er_4\}$ and $\{Er_2\}$ cores that share μ_3-OH groups (Figure 1a, Supporting Information); the bdc ligands trapped in the 18 ring further stabilize the $\{Er_{36}\}$ wheel (Figure 1b). Additionally, bdc ligands are grouped into threes to form triangles that are stacked along the *ab*-plane in a staggered fashion and thus appear as hexagons with an empty center in a 2D projection (Figure 1b). Each $\{Er_{36}\}$ cluster is linked to surrounding clusters by sharing -Er1-OH-$\{Er2\}_2$-OH-Er1-

 © 2006 Wiley-VCH Verlag GmbH & Co. KGaA, Weinheim

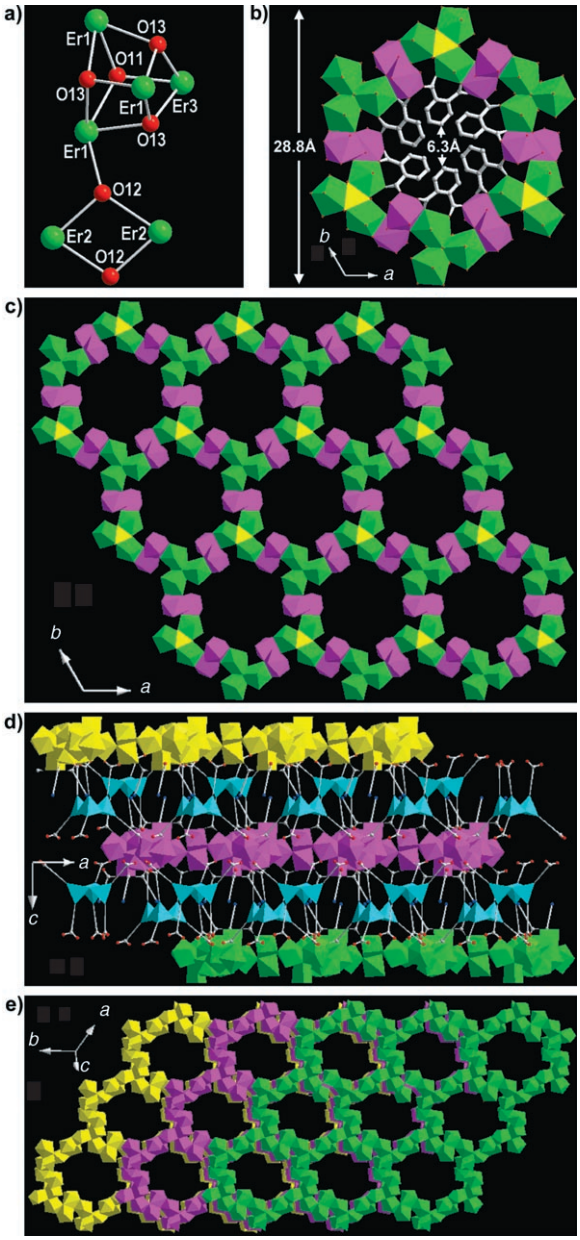


Figure 1. a) The linkage of $\{Er_4\}$ and $\{Er_2\}$ cores through μ_3-OH in **1**. b) View of the $\{Er_{36}\}$ wheel showing the bdc ligands near the walls of the 18 ring. The hollow center of the 18 ring has a diameter of about 6.3 Å. Polyhedra centered by Er1 (green), Er2 (purple), and Er3 (yellow). c) View of giant wheel clusters linked to form layered cluster network with 18 ring by an Er1-OH-$\{Er2\}_2$-OH-Er1 bridge. The bdc ligands are omitted for clarity; color scheme as in (b). d) View of sandwich framework based on linkages of 2D cluster layers and $\{Cu_3Cl_4\}$ cluster pillars by ina ligands. Three adjacent layers of $\{Er_{36}\}$ wheels are represented in green, purple, and yellow, $\{Cu_3Cl_4\}$ in cyan; white lines stand for pyridine rings of ina ligands; bdc ligands are omitted for clarity. e) View of the channels in **1** along the [211] direction. Color scheme as in (d); $\{Cu_3Cl_4\}$ cores, ina and bdc ligands are omitted for clarity.

bridges (see Supporting Information), thus forming a highly-ordered layered cluster network with hexagonal, honeycomb arrays (Figure 1c and Supporting Information). The layered hybrid networks are stacked in parallel with -ABCABC- alternations along the *c* axis, each layer is shifted by $(-\boldsymbol{a} + \boldsymbol{b} + \boldsymbol{c})/3$ with respect to the next one (Figure 1d, Supporting Information). The distance between adjacent layers is 8.3 Å.

In **1**, the five-coordinate Cu center has a nearly square-pyramidal coordination environment made up of one μ_3-Cl, two μ_2-Cl, and two N atoms from two bridging ina moieties (see Supporting Information). Three Cu ions are bridged by three μ_2-Cl and one μ_3-Cl atoms to form a $\{Cu_3Cl_4\}$ trimeric cluster (Cu···Cu 4.578(3) Å; μ_2-Cl–Cu 2.378(3)/2.712(4) Å; μ_3-Cl–Cu 2.707(2) Å, which is slightly longer than the μ_3-Cl–Cu bond length (2.576 Å) in a $[Cu_3Cl]$ cluster containing a Cl^- ligand in trigonal planar coordination mode, N–Cu 1.940(10)/1.967(9) Å.[18] Each $\{Cu_3Cl_4\}$ core caps the $\{Er_{36}\}$ cluster by three ina ligands that contain N1/O1/O2 atoms and link the $\{Er_4\}$ core of the adjacent staggered lanthanide cluster layers by another three ina ligands comprising N3/O5/O6 atoms (see Supporting Information). Thus, the $\{Cu_3Cl_4\}$ core links six ina ligands to form a new cluster $\{Cu_3Cl_4(ina)_6\}$ pillared between adjacent lanthanide cluster layers (Figure 1d and Supporting Information). While each $\{Er_{36}\}$ cluster links eight $\{Cu_3Cl_4\}$ cores through ina ligands (Supporting Information): two $\{Cu_3Cl_4\}$ cores cap two sides of the $\{Er_{36}\}$ cluster; six $\{Cu_3Cl_4\}$ cores link six $\{Er_4\}$ cores on two sides of the $\{Er_{36}\}$ cluster. The $\{Cu_3Cl_4\}$ cores at two sides of the $\{Er_{36}\}$ cluster have reverse orientation and are stacked along the *c* axis in a staggered fashion and thus appear as small and large hexagons on a 2D projection (see Supporting Information).

The linkages between 2D hybrid cluster polymers and $\{Cu_3Cl_4\}$ clusters by ina ligands give rise to an unprecedented 3D sandwich framework (Figure 1d and Supporting Information) with channels along the [211], [1$\bar{1}\bar{1}$], [12$\bar{1}$], [$\bar{2}2\bar{1}$], [42$\bar{1}$], [45$\bar{1}$], [241], [15$\bar{1}$], [1$\bar{4}\bar{1}$], [541], and [511] directions (Figure 1e and Supporting Information). As many as 54 ina ligands bond to the $\{Er_{36}\}$ cluster: 36 ina ligands (mode I) bridge and link the $\{Er_{36}\}$ cluster with the $\{Cu_3Cl_4\}$ core through O_{COO} and N atoms; eighteen ina ligands (mode II) are terminal and only bond to six Er3 atoms of the $\{Er_{36}\}$ cluster through O_{COO} atoms, the N atoms are free and are directed into the center of the channels (Figure 1d and Supporting Information). Thus, the structure is of strictly alternating lanthanide cluster hybrid layers and the $\{Cu_3Cl_4\}$ cores bridged by ina ligands of mode I coordination to form a 3D framework, in which the $\{Cu_3Cl_4\}$ cores located between adjacent layers have opposite orientations along the *c* axis (Figure 1d). It is also understood that the lanthanide cluster hybrid layers are pillared by the clusters of $\{Cu_3Cl_4(ina)_6\}$ to form a 3D sandwich framework.

The DC magnetic susceptibility of **1** was measured in the temperature range of 2–300 K under an applied magnetic field of 0.5 T. The μ_{eff} value per molecule is 24.4 μ_B at room temperature, which is less than the calculated value of 25.5 μ_B for seven Er^{3+} and three Cu^{2+} ions without magnetic interaction, and thus it suggests a possible presence of antiferromagnetic couplings between the metal ions (Er···Er and/or Cu···Cu). As the temperature is lowered, **1** shows a continuous decrease in the value of μ_{eff}, which reaches 15.4 μ_B at 2 K. This behavior may be attributed to the crystal-field splitting of the Er^{3+} ion and the contribution of overall antiferromagnetic interactions.[19] No magnetic ordering and

 © 2006 Wiley-VCH Verlag GmbH & Co. KGaA, Weinheim

frequency dependence was observed above 2 K from the variable-temperature AC magnetic susceptibility measurements (see Supporting Information).

In summary, we have made two novel 3D lanthanide–TM coordination polymers, each with a sandwich framework, under hydrothermal conditions from ina and bdc ligands. The unique μ_5-bdc coordination in the structure plays a key role in forming and stabilizing the $\{Er_{36}\}$ cluster. The linkages between the layered $\{Er_{36}\}$ cluster networks and the $\{Cu_3\}$ clusters through ina ligands result in two unusual lanthanide–TM open frameworks with multidirectional channels. To the best of our knowledge, this is the first time that such sandwich frameworks, made of nanosized $\{Er_{36}\}$ cluster polymeric layers and TM cluster pillars have been obtained. The unique cooperativity between the ina and the bdc ligands in the growth of **1** and **2** suggests that "synergistic coordination" as a useful synthetic strategy has potential application in the design and synthesis of molecular materials.

Experimental Section

1 and **2**: A mixture of Er_2O_3 (0.5 mmol, 0.191 g), Hina (2 mmol, 0.246 g), H_2bdc (1.0 mmol, 0.168 g), CuX_2 ($CuCl_2{\cdot}2H_2O$, 0.2 mmol, 0.034 g; $CuBr_2$, 0.2 mmol, 0.045 g), H_2O (10 mL), and $HClO_4$ (0.385 mmol) (pH 2) was sealed in a 30 mL Teflon-lined bomb at 170 °C for 7 days then slowly cooled to room temperature. Brown prismatic crystals of **1** and **2** were recovered by filtration, washed by distilled water, and air-dried (Yield: 25 % and 21 % based on $CuCl_2{\cdot}2H_2O$ and $CuBr_2$ for **1** and **2**, respectively). The positions of the diffraction peaks of the experimental and simulated XRD patterns corresponded well, thus indicating phase purity of the as-synthesized samples of **1** and **2** (see Supporting Information). Elemental analysis calcd (%) for $C_{78}H_{54}Cl_4Cu_3Er_7N_9O_{37}$ (**1**): C 29.16, H 1.70, N 3.92; found: C 29.21, H 2.21, N 3.65; for $C_{78}H_{54}Br_4Cu_3Er_7N_9O_{37}$ (**2**): C 27.63, H 1.61, N 3.72; found: C 28.17, H 2.08, N 3.69. EDAX gives the Cu/Cl/Er ratio in **1** as 3:3.8:6.8 (calcd Cu/Cl/Er = 3:4:7) and the Cu/Br/Er ratio in **2** as 3:4.1:7.2 (calcd Cu/Br/Er = 3:4:7). These results are in agreement with the formulas of **1** and **2** found from the single-crystal analysis. Thermogravimetric analysis indicated that **1** was stable in air up to 200 °C. Between 200 and 600 °C, weight loss corresponding to loss of ina and bdc ligands was observed.

Received: August 16, 2005
Published online: November 28, 2005

Keywords: bridging ligands · cluster compounds · copper · hydrothermal synthesis · lanthanides

[1] a) K. L. Taft, C. D. Delfs, G. C. Apaefthymiou, S. Foner, D. Gatteschi, S. J. Lippard, *J. Am. Chem. Soc.* **1994**, *116*, 823; b) L. J. De Jongh, A. R. Miedema, *Adv. Phys.* **1974**, *23*, 1; c) C. J. O'Connor, *Prog. Inorg. Chem.* **1982**, *29*, 203.

[2] a) A. Müller, E. Krichemeyer, H. Bögge, M. Schmidtmann, C. Beugholt, P. Kögerler, C. Lu, *Angew. Chem.* **1998**, *110*, 1278; *Angew. Chem. Int. Ed.* **1998**, *37*, 1220; b) A. Müller, E. Krichemeyer, H. Bögge, M. Schmidtmann, F. Peters, C. Carsten, J. Meyer, *Angew. Chem.* **1997**, *109*, 500; *Angew. Chem. Int. Ed. Engl.* **1997**, *36*, 484; c) A. Müller, S. K. Das, H. Bögge, C. Beugholt, M. Schmidtmann, *Chem. Commun.* **1999**, 1035; d) A. Müller, E. Krichemeyer, H. Bögge, M. Schmidtmann, C. Beugholt, S. K. Das, F. Peters, *Chem. Eur. J.* **1999**, *5*, 1496, and references therein.

[3] a) A. J. Tasiopoulos, A. Vinslava, W. Wernsdorfer, K. A. Abboud, G. Christou, *Angew. Chem.* **2004**, *116*, 2169; *Angew. Chem. Int. Ed.* **2004**, *43*, 2117, and references therein; b) M. Murugesu, J. Raftery, W. Wernsdorfer, G. Christou, E. K. Brechin, *Inorg. Chem.* **2004**, *43*, 4203, and references therein.

[4] a) A. L. Dearden, S. Parsons, R. E. P. Winpenny, *Angew. Chem.* **2001**, *113*, 155; *Angew. Chem. Int. Ed.* **2001**, *40*, 151, and references therein; b) C. Cadiou, M. Murrie, C. Paulsen, V. Villar, W. Wernsdorfer, R. E. P. Winpenny, *Chem. Commun.* **2001**, 2666.

[5] a) S. P. Watton, R. Fuhrmann, L. E. Pence, A. Caneschi, A. Cornia, G. L. Abbati, S. J. Lippard, *Angew. Chem.* **1997**, *109*, 2917; *Angew. Chem. Int. Ed. Engl.* **1997**, *36*, 2774, and references therein; b) O. L. Sydora, P. T. Woleczanski, E. B. Lobkovsky, *Angew. Chem.* **2003**, *115*, 2789; *Angew. Chem. Int. Ed.* **2003**, *42*, 2685, and references therein; c) L. F. Jones, A. Batsanov, E. K. Brechin, D. Collison, M. Helliwell, T. Mallah, E. J. L. McInnes, S. Piligkos, *Angew. Chem.* **2002**, *114*, 4494; *Angew. Chem. Int. Ed.* **2002**, *41*, 4318, and references therein.

[6] E. J. L. McInnes, C. Anson, A. K. Powell, A. J. Thomson, S. Poussereau, R. Sessoli, *Chem. Commun.* **2001**, 89, and references therein.

[7] E. K. Brechin, O. Cador, A. Caneschi, C. Cadiou, S. G. Harris, S. Parsons, M. Vonci, R. E. P. Winpenny, *Chem. Commun.* **2002**, 1860, and references therein.

[8] a) C.-H. Chang, K.-C. Hwang, C.-S. Liu, Y. Chi, A. J. Carty, L. Scoles, S.-M. Peng, G.-H. Lee, J. Reedijk, *Angew. Chem.* **2001**, *113*, 4787; *Angew. Chem. Int. Ed.* **2001**, *40*, 4651; b) G. A. Ardizzoia, M. A. Angaroni, G. L. Monica, F. Cariati, S. Cenini, M. Moret, N. Masciocchi, *Inorg. Chem.* **1991**, *30*, 4347.

[9] a) J. Xu, K. N. Raymond, *Angew. Chem.* **2000**, *112*, 2857; *Angew. Chem. Int. Ed.* **2000**, *39*, 2745, and references therein; b) T. Kajiwara, H. Wu, T. Ito, N. Iki, S. Miyano, *Angew. Chem.* **2004**, *116*, 1868; *Angew. Chem. Int. Ed.* **2004**, *43*,1832; c) L. G. Westin, M. Kritikos, A. Caneschi, *Chem. Commun.* **2003**, 1012; d) O. Poncelet, L. G. Hubert-Pfalzgraf, J.-C. Daran, R. Astier, *J. Chem. Soc. Chem. Commun.* **1989**, 1846; e) R. Wang, H. D. Selby, H. Liu, M. D. Carducci, T. Jin, Z. Zheng, J. W. Anthis, R. J. Staples, *Inorg. Chem.* **2002**, *41*, 278; f) Z. Zheng, *Chem. Commun.* **2001**, 2521; g) R. Wang, Z. Zheng, T. Jin, R. J. Staples, *Angew. Chem.* **1999**, *111*, 1929; *Angew. Chem. Int. Ed.* **1999**, *38*, 1813; h) R. Anwander, *Angew. Chem.* **1998**, *110*, 619; *Angew. Chem. Int. Ed.* **1998**, *37*, 599.

[10] a) F. Renaud, C. Piguet, G. Bernardinelli, J.-C. G. Bünzli, G. Hopfgartner, *J. Am. Chem. Soc.* **1999**, *121*, 9326; b) M. R. Bürgstein, M. T. Gamer, P. W. Roesky, *J. Am. Chem. Soc.* **2004**, *126*, 5213.

[11] a) H. Barrow, D. A. Brown, N. W. Alcock, H. J. Clase, M. G. H. Wallbridge, *J. Chem. Soc. Chem. Commun.* **1995**, 1231; b) H. Kumagai, S. Kitagawa, *Chem. Lett.* **1996**, 471.

[12] M.-B. Zhang, J. Zhang, S.-T Zheng, G.-Y. Yang, *Angew. Chem.* **2005**, *117*, 1409; *Angew. Chem. Int. Ed.* **2005**, *44*, 1385, and references therein.

[13] Y. Wan, L. Jin, K. Wang, L. Zhang, X. Zheng, S. Lu, *New J. Chem.* **2002**, *26*, 1590.

[14] Crystal data for **1**: $C_{78}H_{54}Cl_4Cu_3Er_7N_9O_{37}$, $M_r = 3212.54$, rhombohedral, $R\bar{3}$, $a = 18.2829(18)$, $c = 47.823(8)$ Å, $V = 13844(3)$ Å^3, $Z = 6$, $\rho = 2.312$ g cm^{-3}, $\mu = 7.171$ mm^{-1}, $F(000) = 9072$, GOF = 1.153. A total of 35759 reflections were collected and 7047 are unique ($R_{int} = 0.0717$). $R1/wR2 = 0.0587/0.1457$ for 6808 reflections ($I > 2\sigma(I)$) and 408 parameters. **2**: $C_{78}H_{54}Br_4Cu_3Er_7N_9O_{37}$, $M_r = 3390.38$, rhombohedral, $R\bar{3}$, $a = 18.3057(2)$, $c = 48.1567(3)$ Å, $V = 13975.3(2)$ Å^3, $Z = 6$, $\rho = 2.417$ g cm^{-3}, $\mu = 8.705$ mm^{-1}, $F(000) = 9504$, GOF = 1.038. A total of 36111 reflections were collected and 7121 are unique ($R_{int} = 0.0922$).

 © 2006 Wiley-VCH Verlag GmbH & Co. KGaA, Weinheim

$R1/wR2 = 0.0401/0.1044$ for 415 parameters and 6184 reflections ($I > 2\sigma(I)$). The intensity data were collected on a Mercury CCD diffractometer with graphite-monochromated $Mo_{K\alpha}$ radiation ($\lambda = 0.71073$ Å) at room temperature. All absorption corrections were performed by using the multiscan program. The structure were solved by direct methods and refined by full-matrix least squares on F^2 with the SHELXTL-97 program.[20] All non-hydrogen atoms, except N2, disordered C11/C11′ and C12/C12′ in **1** and **2**, were refined anisotropically. CCDC-279324 (**1**) and -279325 (**2**) contain the supplementary crystallographic data for this paper. These data can be obtained free of charge from The Cambridge Crystallographic Data Centre via www.ccdc.cam.ac.uk/data_request/cif.

[15] a) B. Ma, D. Zhang, S. Gao, T. Jin, C. Yan, G. Xu, *Angew. Chem.* **2000**, *112*, 3790; *Angew. Chem. Int. Ed.* **2000**, *39*, 3644; b) R. Wang, H. Liu, M. D. Carducci, T. Jin, C. Zheng, Z. Zheng, *Inorg. Chem.* **2001**, *40*, 2743.

[16] a) C. Canada-Vilalta, M. Pink, G. Christou, *Dalton Trans.* **2003**, 1121, and references therein; b) Y.-S. Song, B. Yang, *Inorg. Chim. Acta* **2005**, *358*, 191.

[17] G.-Y. Yang, S. C. Sevov, *J. Am. Chem. Soc.* **1999**, *121*, 8389.

[18] G. Seeber, P. Kogerler, B. M. Kariukj, L. Cronin, *Chem. Commun.* **2004**, 1580.

[19] a) J.-P. Costes, J. M. Clemente-Juan, F. Dahan, F. Nicodème, M. Verelst, *Angew. Chem.* **2002**, *114*, 333; *Angew. Chem. Int. Ed.* **2002**, *41*, 323; b) G. Xu, Z. Wang, Z. He, Z. Lu, C. Liao, C. Yan, *Inorg. Chem.* **2002**, *41*, 6802.

[20] G. M. Sheldrick, SHELXTL-97, Program for the Solution of Crystal Structures, University of Göttingen, Germany, **1997**.

 © 2006 Wiley-VCH Verlag GmbH & Co. KGaA, Weinheim

Rotaxanes

DOI: 10.1002/anie.200501761

Complexation-Induced Translational Isomerism: Shuttling through Stepwise Competitive Binding**

Dana S. Marlin, Diego González Cabrera, David A. Leigh, and Alexandra M. Z. Slawin*

Although many carefully designed rotaxane-forming reactions have been developed in recent years,[1] new strategies[2] for switching the position of the macrocycle on the thread in response to an external trigger[3,4]—a key requirement for developing mechanical molecular devices based on such architectures[4]—remain rare. Competitive substrate binding is often used to bring about conformational changes that elicit function in biological "machines"[5] and has been successfully utilized in artificial host–guest systems,[6] chemical sensing,[7] and molecular Boolean logic operations.[8] However, as the macrocycle–thread interactions in a rotaxane are normally chosen so as to maximize the efficiency of the template mechanism, it is difficult to find competitive binders that can effectively disrupt these threaded and inherently self-organized complementary networks.[9,10] One elegant solution[11] to this problem is to utilize the preferred binding geometries of different metal d-orbital configurations (e.g. tetrahedral Cu^{I} →five-coordinate Cu^{II} or Zn^{II}) in transition-metal-based molecular shuttles.[12,13] Here we report an alternative solution, which does not involve a change in metal ion or oxidation state but uses the binding of a transition metal to move a macrocycle in a hydrogen-bonded molecular shuttle. Coordination of Cu^{II} or Cd^{II} ions to a bis(2-picolyl)amino (BPA)-derivatized glycine "station", followed by deprotonation of the adjacent amide group progressively wraps up the peptide station which leads to displacement of the macrocycle to an intrinsically weaker hydrogen-bonding site. In the case of Cu^{II}, the change in binding mode perturbs sensitive transitions within the d orbitals and the change in position of the shuttle is consequently accompanied by a color change.

The new shuttling strategy evolved out of the chance observation of an unusual controlled stepwise binding sequence of Cu^{II} ions to a multidentate ligand. Whilst attempting to develop methodology for the attachment of paramagnetic metal ions to macrocycles in rotaxanes, we prepared ligand H**1**,[14,15] which features a glycine residue substituted with two picoline units at its N terminus. Addition of $CuCl_2{\cdot}2H_2O$ to H**1** in CH_3CN led to the formation of H**1**$CuCl_2$, light blue crystals of which separated from the saturated liquors and gave the X-ray crystal structure shown in Figure 1a.[16] Cooling the solution of H**1**$CuCl_2$ to −20 °C in the presence of an additional half-equivalent of $CuCl_2{\cdot}2H_2O$ resulted in the deposition of large emerald-green crystals[17] of [H**1**$CuCl]_2[CuCl_4]$ on the walls of the flask which yielded the crystal structure shown in Figure 1b. Addition of one equivalent of NaH to solutions of either H**1**$CuCl_2$ or [H**1**-$(CuCl)]_2[CuCl_4]$ in *N*,*N*-dimethylformamide led to a third type of BPA–Cu^{II} complex as lime-green crystals of **1**CuCl (Figure 1c). The binding of the Cu^{II} ion—from the initial tridentate chelation of $CuCl_2$ to the BPA moiety in H**1**$CuCl_2$, to loss of a Cl^- ligand and coordination to the carbonyl oxygen of the amide group in $[H\mathbf{1}CuCl]^+$, and finally exchange of the carbonyl group for the nitrogen atom upon deprotonation of the amide group in **1**CuCl—results in progressive wrapping of the peptide unit around the metal (Figure 1).[18] We reasoned that integration of this stepwise changing coordination motif into a macrocycle-binding site in a peptide-based molecular shuttle might permit the complexation-controlled translocation of the macrocycle from one station to another.

To study the chemistry of the BPA-modified peptide station in a simple model system, we first prepared thread H_2**2**

[*] Dr. D. S. Marlin, D. González Cabrera, Prof. D. A. Leigh
School of Chemistry
University of Edinburgh
The King's Buildings
West Mains Road, Edinburgh EH93JJ (UK)
Fax: (+44) 131-667-9085
E-mail: david.leigh@ed.ac.uk
Prof. A. M. Z. Slawin
School of Chemistry
University of St. Andrews
Purdie Building, St. Andrews, Fife KY169ST (UK)

[**] This work was supported by the European Union Future and Emerging Technology Program Hy3M and the EPSRC. D.S.M. is a Marie Curie Fellow.

Supporting information for this article is available on the WWW under http://www.angewandte.org or from the author.

 © 2006 Wiley-VCH Verlag GmbH & Co. KGaA, Weinheim

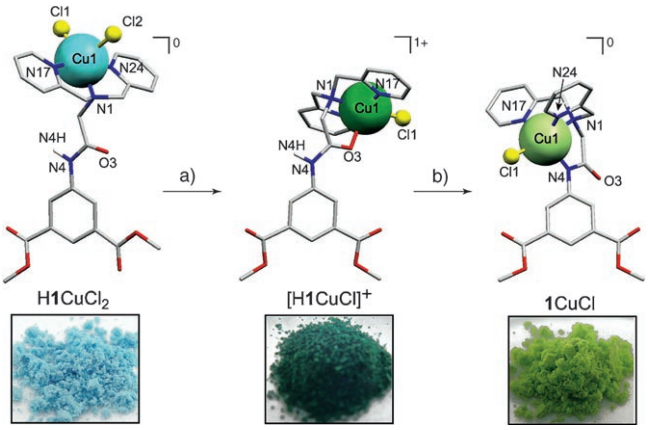
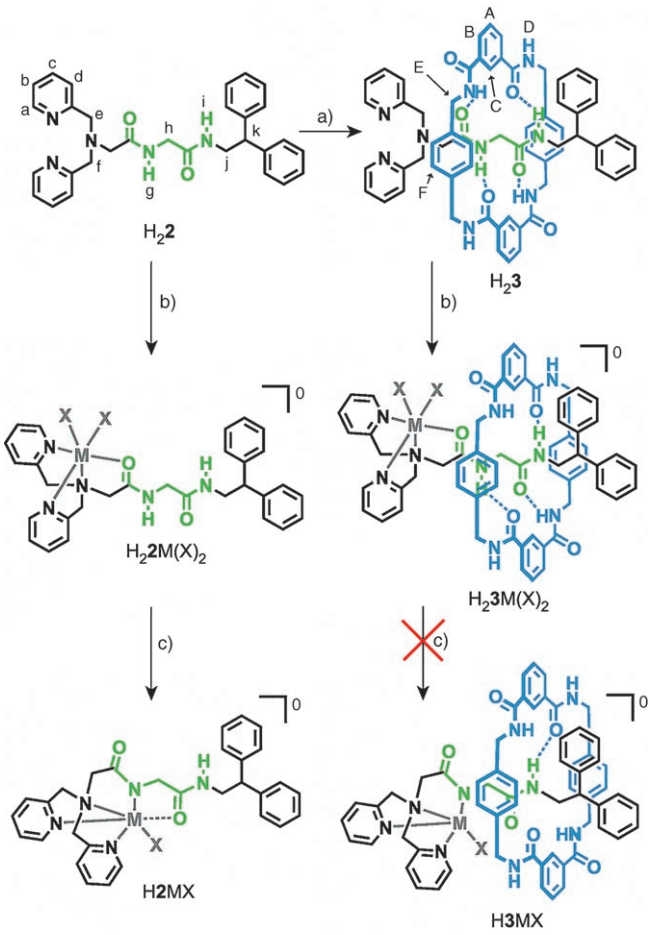


Figure 1. X-ray crystal structures[16] of H**1**$CuCl_2$ (initial), [H**1**CuCl]$^+$ (upon cooling[17]), and **1**CuCl (after addition of NaH) showing the change in binding mode of Cu^{II} to the multidentate ligand. C gray, Cl yellow, N blue, O red; all hydrogen atoms except the amide proton have been omitted for clarity. Reagents and conditions a) 0.5 equiv $CuCl_2 \cdot 2H_2O$, −20 °C, 100%; b) NaH or phosphazene P_1-*t*Bu base, 91%. The insets show photographs of the corresponding powdered, crystalline solids (from the left): H**1**$CuCl_2$, [H**1**CuCl]$_2$[$CuCl_4$], and **1**CuCl. Selected bond lengths [Å]: a) Cu1–N1 2.080, Cu1–N17 2.018, Cu1–N24 1.995, Cu1–Cl1 2.240, Cu1–Cl2 2.569; b) Cu1–N1 2.036, Cu1–N17 1.972, Cu1–N24 2.015, Cu1–Cl1 2.231, Cu1–O3 2.373; c) Cu1–N1 2.031, Cu1–N17 2.099, Cu1–N24 2.124, Cu1–Cl1 2.250, Cu1–N4 2.055.



Scheme 1. Synthesis of [2]rotaxane H_2**3** from the BPA-glycylglycine thread H_2**2**, and their respective complexes with $CuCl_2$ and $Cd(NO_3)_2$ (≡MX_2). Reagents and conditions: a) *p*-xylylene diamine, isophthaloyl chloride, Et_3N, $CHCl_3$, 44%; b) $CuCl_2 \cdot 2H_2O$ or $Cd(NO_3)_2 \cdot 4H_2O$, 90% (H_2**2**$CuCl_2$), 90% (H_2**3**$CuCl_2$), 85% (H_2**2**$Cd(NO_3)_2$), 92% (H_2**3**$Cd(NO_3)_2$); c) NaH or phosphazene P_1-*t*Bu base, 77% (H**2**CuCl), 82% (H**2**$CdNO_3$). The coordination bond indicated by a dashed line in H**2**MX is only observed in the cadmium complex.

and rotaxane H_2**3** (Scheme 1). Formation of H_2**3** proceeded in 44% yield from H_2**2** (Scheme 1, a) which suggests that the affinity of the benzylic amide macrocycle for the BPA-glycylglycine station should be similar to that of other peptide-based stations, namely, intermediate between a strongly binding preorganized fumaramide group and a more weakly binding succinic amide ester moiety.[9a] The X-ray crystal structure of rotaxane H_2**3** shows that both carbonyl groups and both amide protons in the thread are involved in intercomponent hydrogen bonding to the macrocycle in the solid state (Figure 2b).[19]

The chelation geometries adopted by the BPA-glycylglycine station were studied by binding H_2**2** and H_2**3** to Cu^{II} as well as Cd^{II}, a diamagnetic metal that generally adopts ligand-coordination geometries that are similar to those of Cu^{II} with nitrogen-containing ligands, and attempted subsequent deprotonation of one of the amide groups (Scheme 1).[20] The X-ray crystal structures of several of the resulting complexes are shown in Figure 2, and the ^{1}H NMR spectra ([D_6]acetone,[21] 298 K) of the free ligands H_2**2** and H_2**3** and their complexes with $Cd(NO_3)_2$ are shown in Figure 3. The changes in the signals for the BPA protons (H_{a-f}) upon complexation of cadmium ions and the shielding of the protons of the peptide (H_h, H_j, and H_k) by the macrocycle in the rotaxanes compared to those of the thread confirm that the structures in solution are closely related to those in the solid state.

First, addition of $CuCl_2 \cdot 2H_2O$ or $Cd(NO_3)_2 \cdot 4H_2O$ to both the thread and rotaxane smoothly generated complexes of the type H_2**2**MX_2 and H_2**3**MX_2, respectively (M = Cu, Cd; Scheme 1, b). The solid-state structure of H_2**3**$Cd(NO_3)_2$ (Figure 2d) shows a coordination geometry which is similar to that of the intermediate [H**1**CuCl]$^+$ complex (Figure 1b), that is, featuring metal coordination to the carboxamide carbonyl oxygen.

Second, addition of one equivalent of a suitable base[22] (Scheme 1, c) to the thread intermediate complexes H_2**2**$CuCl_2$ and H_2**2**$Cd(NO_3)_2$ yielded H**2**CuCl and H**2**$CdNO_3$, respectively. The X-ray crystal structure of H**2**CuCl (Figure 2a) displays a Cu^{II} coordination sphere that is similar to that of **1**CuCl (Figure 1c) as well as an additional (albeit long at 3.188 Å) directional hydrogen bond between the proton (N7H) of the second amide group and the formal nitrogen anion (N4) of the coordinating carboxamido functionality. The X-ray crystal structure of H**2**$CdNO_3$ (Figure 2c) is closely related, but with the metal ion additionally coordinated to the carbonyl oxygen of the second carboxamide group. The binding of Cd^{II} (or Cu^{II}) ion to the BPA-glycine carbonyl oxygen presumably lowers the pK_a value of the adjacent NH proton in complexes of the type H_2**1**MX_2 and H_2**2**MX_2 which

 © 2006 Wiley-VCH Verlag GmbH & Co. KGaA, Weinheim

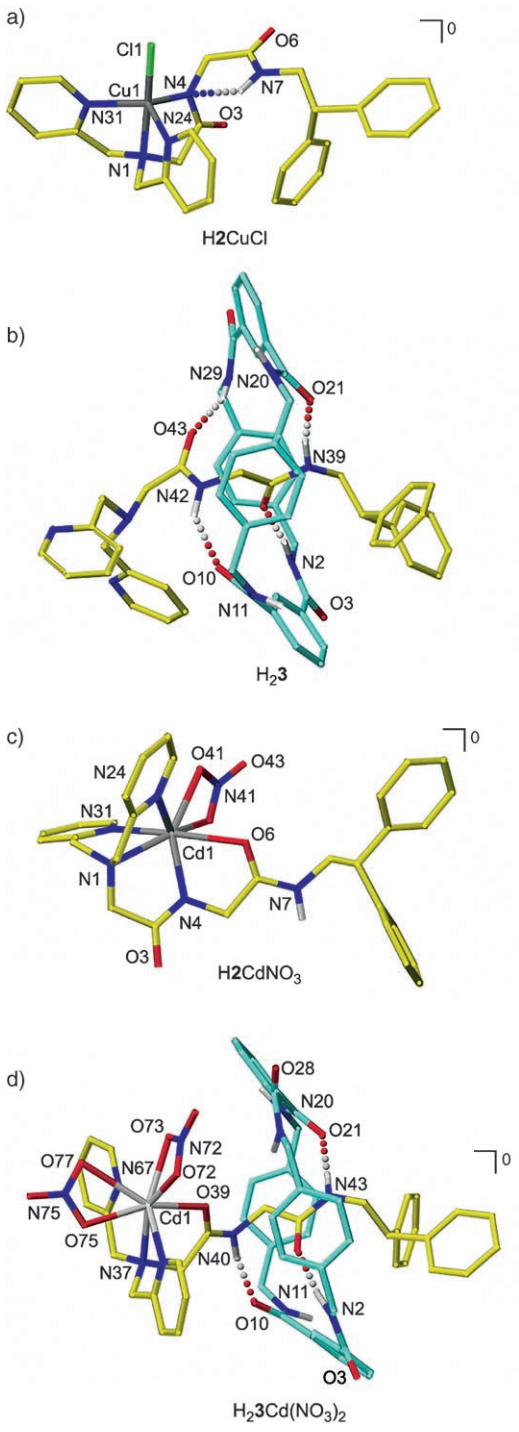


Figure 2. X-ray crystal structures[16] of a) H**2**CuCl, b) H_2**3**, c) H**2**$CdNO_3$, and d) H_2**3**$Cd(NO_3)_2$. C (thread) yellow, C (macrocycle) blue, metal atoms Cu^{II} and Cd^{II} gray; all hydrogen atoms except for the amide protons have been omitted for clarity. Selected bond lengths [Å]: a) Cu1–N1 2.052, Cu1–N4 1.968, Cu1–N24 2.176, Cu1–N31 2.079, Cu1–Cl1 2.238, N7H–N4 3.188; b) N2H–O40 1.877, N42H–O10 2.201, N39H–O21 1.944, N29H–O43 1.961; c) Cd1–N1 2.443, Cd1–N4 2.205, Cd1–O6 2.476, Cd1–N24 2.304, Cd1–N31 2.416, Cd1–O41 2.407, Cd1–O42 2.509; d) Cd1–N37 2.443, Cd1–N60 2.364, Cd1–N67 2.323, Cd1–O39 2.331, Cd1–O72 2.335, Cd1–O73 2.463, Cd1–O77 2.794, Cd1–O75 2.400, N43H–O21 1.863, N40H–O10 1.861, N2H–O42 2.017.

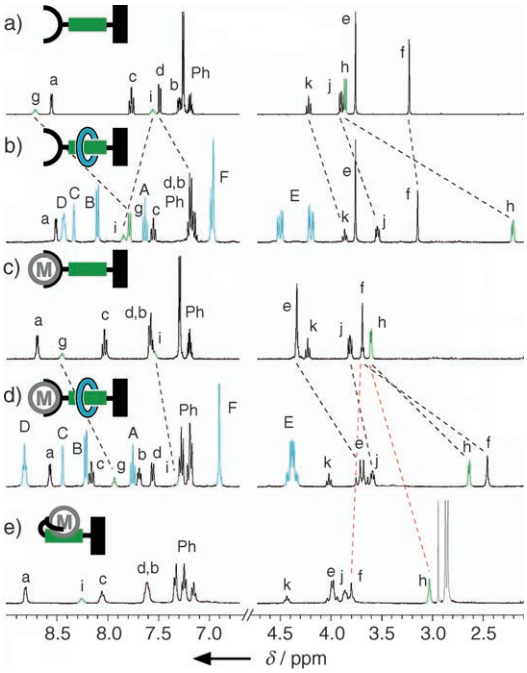


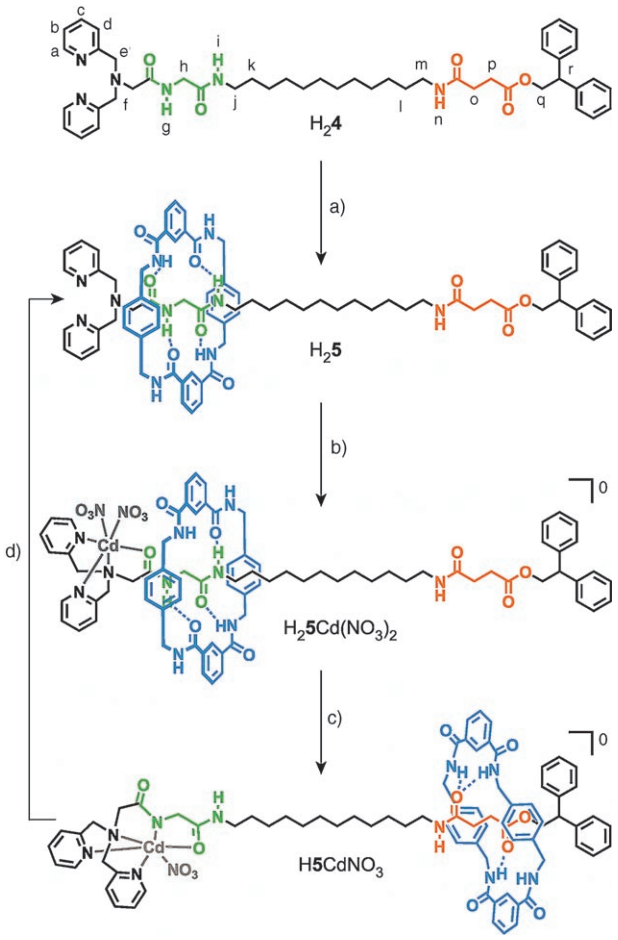
Figure 3. Partial ^{1}H NMR spectra (400 MHz, [D_6]acetone, 298 K) of a) H_2**2**, b) H_2**3**, c) H_2**2**$Cd(NO_3)_2$, d) H_2**3**$Cd(NO_3)_2$, and e) H**2**$CdNO_3$. Resonances colored and labeled as shown in Scheme 1. Peaks shown in light gray in part (e) originate from the phosphazene P_1-*t*Bu base.

allows *selective* deprotonation at this site.[23] However, neither of the metal coordination geometries shown in Figure 2 a or c would leave room on the peptide unit for a benzylic amide macrocycle to occupy, or sufficient hydrogen-bonding partners for it to bind to, in a rotaxane or molecular shuttle. Indeed, treatment of H_2**3**$CuCl_2$ or H_2**3**$Cd(NO_3)_2$ with strong bases[22] led to complicated reaction mixtures and significant degradation of the rotaxane structures, seemingly as a consequence of the macrocycle sterically preventing deprotonation of the coordination-activated carboxamide or adoption of the wrapped-up metal–ligand coordination architecture.

The model compounds confirm the generic basis of the stepwise binding chemistry and provide ^{1}H NMR spectroscopic fingerprints (Figure 3) of the various coordination modes, both with and without the macrocycle occupying the station. These spectra could be used to determine the position of the macrocycle in a more elaborate molecular shuttle, in particularly distinguishing between whether Cd^{II} is bound to a carbonyl oxygen or a carboxamido nitrogen atom and whether the macrocycle still occupies the BPA-glycylglycine station.

Accordingly, we prepared the two-station thread H_2**4** and rotaxane H_2**5** which feature BPA-derivatized glycylglycine (green) and succinic amide ester (orange) stations for the macrocycle (Scheme 2). The rationale behind the design was that although the ring would be expected to predominantly occupy the BPA-glycylglycine binding site in H_2**5**$Cd(NO_3)_2$, the ring would still spend some time away from the peptide station on the weaker binding succinic amide ester moiety. Whilst it is on the succinic amide ester station, the ring should

 © 2006 Wiley-VCH Verlag GmbH & Co. KGaA, Weinheim



Scheme 2. Conversion of thread H_2**4** to rotaxane H_2**5**, and the reversible complexation of rotaxane H_2**5** with $Cd(NO_3)_2 \cdot 4H_2O$. Reagents and conditions: a) *p*-xylylene diamine, isophthaloyl chloride, Et_3N, $CHCl_3$, 22%; b) $Cd(NO_3)_2 \cdot 4H_2O$; c) phosphazene P_1-*t*Bu base; d) NaCN, NH_4Cl. Yields for conversions b–d were quantitative by ^{1}H NMR spectroscopic analysis.

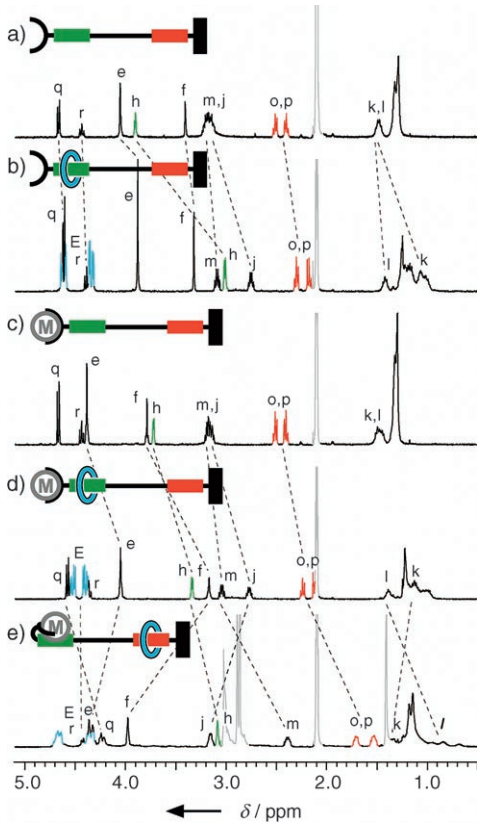


Figure 4. Partial ^{1}H NMR spectra (400 MHz, [D_6]acetone, 298 K) of a) H_2**4**, b) H_2**5**, c) H_2**4**$Cd(NO_3)_2$, d) H_2**5**$Cd(NO_3)_2$, and e) H**5**$CdNO_3$. Resonances colored and labeled as shown in Scheme 2. Peaks shown in light gray originate from residual nondeuterated solvent and, in part (e), the phosphazene P_1-*t*Bu base.

not sterically hinder the coordination-activated peptide (as it does so effectively in H_2**3**$Cd(NO_3)_2$, Scheme 1), so this minor translational isomer can then be selectively deprotonated at the carboxamide adjacent to the BPA unit. In accord with Le Chatelier's principle, H**5**$CdNO_3$ is formed. If the cadmium ion wraps itself up in the deprotonated glycylglycine residue in the manner seen with the model systems, this will switch off the peptide station and result in the macrocycle of H**5**$CdNO_3$ predominately occupying the succinic amide ester station (Scheme 2).

Pleasingly, the ^{1}H NMR spectra of the rotaxanes and threads (shown in Figure 4) were fully consistent with the predicted behavior. The relative shielding of the peptide protons in the ^{1}H NMR spectrum of H_2**5** compared to H_2**4** (Figure 4a and b, respectively) confirms that the occupancy of the macrocycle is approximately 90:10 in favor of the glycylglycine station in [D_6]acetone at 298 K.[21] Addition of one equivalent of $Cd(NO_3)_2 \cdot 4H_2O$ to H_2**4** and H_2**5** to form H_2**4**$Cd(NO_3)_2$ and H_2**5**$Cd(NO_3)_2$, respectively (Scheme 2, b), resulted in little change (except for the BPA protons) in the ^{1}H NMR spectra in [D_6]acetone at room temperature (compare Figures 4c and d with Figures 4a and b, respectively), indicating that the preferred position of the macrocycle remains unchanged despite chelation of the terminal peptide carbonyl group to a metal — the shifts experienced by the protons around the metal-binding region, for example, H_f and H_h, are similar to those in H_2**3**$Cd(NO_3)_2$ (Figure 3d). However, subsequent deprotonation of the amide proton H_g of H_2**5**$Cd(NO_3)_2$ with one equivalent of phosphazene base P_1-*t*Bu[22] (Scheme 2, c) causes major changes (Figure 4e). The upfield shifts of H_m, H_o, and H_p ($\delta = 3.2$, 2.5, and 2.4 ppm in H_2**4**$Cd(NO_3)_2$ (Figure 4c) to $\delta = 2.4$, 1.7, and 1.5 ppm, respectively) are clear evidence for the translocation of the macrocycle to the succinic amide ester station (marked in orange). Similarly, the downfield shift of H_f ($\delta = 3.2$ ppm in H_2**5**$Cd(NO_3)_2$ (Figure 4d) to $\delta = 4.0$ ppm) and the restoration of H_j to its position at $\delta = 3.2$ ppm in the thread (Figure 4c) show that the peptide station (marked in green) is no longer occupied by the benzylic amide macrocycle. The small upfield movement in H_h is consistent with the shift brought about by coordination of the deprotonated amide group to the metal, as seen with H**2**$CdNO_3$ (Figure 3e).

The transition-metal-binding-induced translocation of the macrocycle in the hydrogen-bonded shuttle is fully reversible (Scheme 2, d). Removal of the Cd^{II} ion from H**5**$CdNO_3$ with

 © 2006 Wiley-VCH Verlag GmbH & Co. KGaA, Weinheim

excess CN^- and reprotonation of the amide nitrogen atom with NH_4Cl quantitatively regenerates H_2**5**.

Finally, indirect evidence for a similar shuttling mechanism using Cu^{II} binding is provided by the change in absorption of weak (likely d–d) transitions in the low-energy region of the UV/Vis spectrum of H_2**5**$CuCl_2$ upon addition of P_1-*t*Bu (Figure 5). The color change that occurs

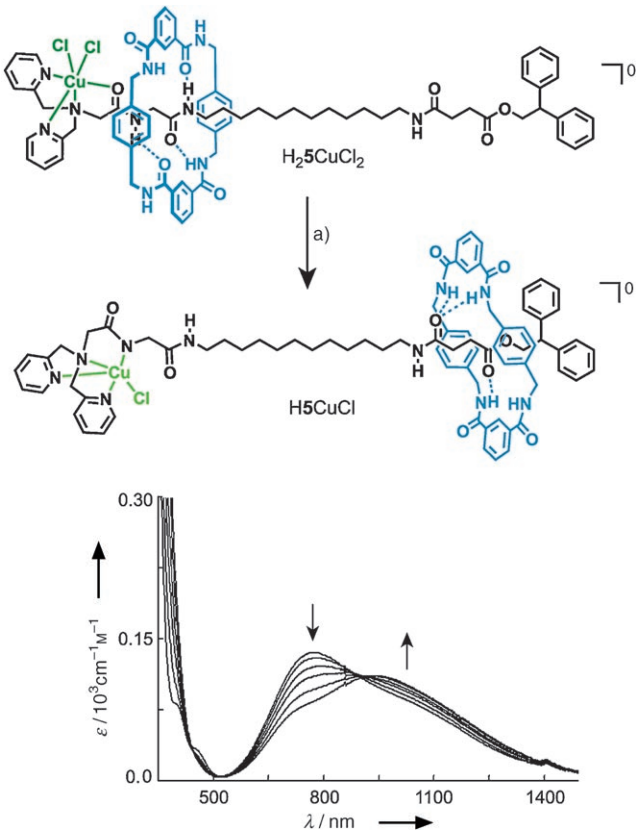


Figure 5. Change in absorption spectrum for H_2**5**$CuCl_2$ upon addition of a) phosphazene P_1-*t*Bu base (up to 1 equivalent).

during a single-spot-to-single-spot transformation, as revealed by thin layer chromatographic analysis, is almost indistinguishable to that observed during the conversion of [H**1**CuCl]$^+$ to **1**CuCl (Figure 1). As the base-promoted transformation (H_2**3**$CuCl_2$→H**3**CuCl) does *not* occur for the short rotaxane (Scheme 1, c), yet *does* take place for H_2**5**$CuCl_2$→H**5**CuCl (Figure 5), it seems reasonable to conclude that the color change is accompanied by the same change in the position of macrocycle that occurs in the cadmium-coordinated molecular shuttle (Scheme 2, c).

In conclusion, we have described a mechanism through which a large amplitude mechanical movement can be induced within a hydrogen-bonded molecular shuttle by the stepwise competitive binding of transition-metal ions. The peptide station is progressively wrapped up by the metal which disrupts hydrogen-bonding interactions between the station and macrocycle and causes displacement of the macrocycle to a second station. The control over shuttling while the metal is bound to the thread provides two well-defined states in which the macrocycle is held either close to or distant from a single metal atom. This feature could be used to construct rotaxanes that display the intriguing property of being able to switch the distance between two metal centers, which are not connected by chemical bonds, by an externally triggered mechanical motion.

Received: May 21, 2005
Revised: June 21, 2005
Published online: November 28, 2005

Keywords: coordination modes · molecular devices · noncovalent interactions · rotaxanes · transition metals

[1] For some recent examples of new rotaxane syntheses, see: a) K. M. Wollyung, K. T. Xu, M. Cochran, A. M. Kasko, W. L. Mattice, C. Wesdemiotis, C. Pugh, *Macromolecules* **2005**, *38*, 2574–2586; b) N. Kihara, S. Motoda, T. Yokozawa, T. Takata, *Org. Lett.* **2005**, *7*, 1199–1202; c) H. P. Kwan, T. M. Swager, *J. Am. Chem. Soc.* **2005**, *127*, 5902–5909; d) M. Miyauchi, T. Hoshino, H. Yamaguchi, S. Kamitori, A. Harada, *J. Am. Chem. Soc.* **2005**, *127*, 2034–2035; e) B. A. Blight, K. A. Van Noortwyk, J. A. Wisner, M. C. Jennings, *Angew. Chem.* **2005**, *117*, 1523–1528; *Angew. Chem. Int. Ed.* **2005**, *44*, 1499–1504; f) D. J. Hoffart, S. J. Loeb, *Angew. Chem.* **2005**, *117*, 923–926; *Angew. Chem. Int. Ed.* **2005**, *44*, 901–904; g) I. Yoon, M. Narita, T. Shimizu, M. Asakawa, *J. Am. Chem. Soc.* **2004**, *126*, 16740–16741; h) Y. Furusho, T. Matsuyama, T. Takata, T. Moriuchi, T. Hirao, *Tetrahedron Lett.* **2004**, *45*, 9593–9697; i) N. Kihara, M. Hashimoto, T. Takata, *Org. Lett.* **2004**, *6*, 1693–1696; j) M. J. Gunter, S. M. Farquhar, K. M. Mullen, *New J. Chem.* **2004**, *28*, 1443–1449; k) W. C. Hung, K. S. Liao, Y. H. Liu, S. M. Peng, S. H. Chiu, *Org. Lett.* **2004**, *6*, 4183–4186; l) K. Hiratani, M. Kaneyama, Y. Nagawa, E. Koyama, M. Kanesato, *J. Am. Chem. Soc.* **2004**, *126*, 13568–13569; m) K. J. Chang, Y. J. An, H. Uh, K. S. Jeong, *J. Org. Chem.* **2004**, *69*, 6556–6563; n) W. Abraham, L. Grubert, U. W. Grummt, K. Buck, *Chem. Eur. J.* **2004**, *10*, 3562–3568; o) H. Georges, S. J. Loeb, J. Tiburcio, J. A. Wisner, *Org. Biomol. Chem.* **2004**, *2*, 2751–2756; p) A. Orita, J. Okano, Y. Tawa, L. S. Jiang, J. Otera, *Angew. Chem.* **2004**, *116*, 3810–3814; *Angew. Chem. Int. Ed.* **2004**, *43*, 3724–3728; q) P. Ballester, M. Capo, A. Costa, P. M. Deya, A. Frontera, R. Gomila, *Molecules* **2004**, *9*, 278–286; r) Y. Furusho, T. Oku, G. A. Rajkumar, T. Takata, *Chem. Lett.* **2004**, *33*, 52–53; s) D. Tuncel, J. H. G. Steinke, *Macromolecules* **2004**, *37*, 288–302; t) J. Terao, A. Tang, J. J. Michels, A. Krivokapic, H. L. Anderson, *Chem. Commun.* **2004**, 56–57; u) J. D. Badjic, V. Balzani, A. Credi, S. Silvi, J. F. Stoddart, *Science* **2004**, *303*, 1845–1849; v) J. S. Hannam, S. M. Lacy, D. A. Leigh, C. G. Saiz, A. M. Z. Slawin, S. G. Stitchell, *Angew. Chem.* **2004**, *116*, 3322–3326; *Angew. Chem. Int. Ed.* **2004**, *43*, 3260–3264.

[2] a) D. A. Leigh, E. M. Pérez, *Chem. Commun.* **2004**, 2262–2263; b) B. W. Laursen, S. Nygaard, J. O. Jeppesen, J. F. Stoddart, *Org. Lett.* **2004**, *6*, 4167–4170.

[3] R. A. Bissell, E. Córdova, A. E. Kaifer, J. F. Stoddart, *Nature* **1994**, *369*, 133–137.

[4] a) *Molecular Catenanes, Rotaxanes, and Knots: A Journey Through the World of Molecular Topology* (Eds.: J.-P. Sauvage, C. Dietrich-Buchecker), Wiley-VCH, Weinheim, **1999**; b) V. Balzani, A. Credi, F. M. Raymo, J. F. Stoddart, *Angew. Chem.* **2000**, *112*, 3484–3530; *Angew. Chem. Int. Ed.* **2000**, *39*, 3348–3391; c) V. Balzani, M. Venturi, A. Credi, *Molecular Devices and*

 © 2006 Wiley-VCH Verlag GmbH & Co. KGaA, Weinheim

Machines—A Journey into the Nanoworld, Wiley-VCH, Weinheim, **2003**; d) A. H. Flood, R. J. A. Ramirez, W.-Q. Deng, R. P. Muller, W. A. Goddard, J. F. Stoddart, *Aust. J. Chem.* **2004**, *57*, 301 – 322; e) "Synthetic Molecular Machines": E. R. Kay, D. A. Leigh, *Functional Artificial Receptors* (Eds.: T. Schrader, A. D. Hamilton), Wiley-VCH, Weinheim, **2005**, pp. 333 – 406.

[5] For example, see: A. Saghatelian, K. M. Guckian, D. A. Thayer, M. R. Ghadiri, *J. Am. Chem. Soc.* **2003**, *125*, 344 – 345.

[6] For example, see: a) A. Credi, M. Montalti, V. Balzani, S. J. Langford, F. M. Raymo, J. F. Stoddart, *New J. Chem.* **1998**, *22*, 1061 – 1065; b) M. Asakawa, S. Iqbal, J. F. Stoddart, N. D. Tinker, *Angew. Chem.* **1996**, *108*, 1054 – 1056; *Angew. Chem. Int. Ed. Engl.* **1996**, *35*, 976 – 978.

[7] For example, see: L. A. Cabell, E. V. Anslyn, *Tetrahedron Lett.* **1999**, *40*, 7753 – 7756.

[8] For example, see: R. Ballardini, V. Balzani, A. Credi, M. T. Gandolfi, S. J. Langford, S. Menzer, L. Prodi, J. F. Stoddart, M. Venturi, D. J. Williams, *Angew. Chem.* **1996**, *108*, 1056 – 1059; *Angew. Chem. Int. Ed. Engl.* **1996**, *35*, 978 – 981.

[9] Intercomponent noncovalent interactions are inherently strengthened by preorganization within a rotaxane architecture (see: D. A. Leigh, P. J. Lusby, A. M. Z Slawin, D. B. Walker, *Angew. Chem.* **2005**, *117*, 4633 – 4640; *Angew. Chem. Int. Ed.* **2005**, *44*, 4557 – 4564). For example, the benzylic amide macrocycle in fumaramide-based molecular shuttles remains held in place[9a] by four macrocycle–thread amide–amide hydrogen bonds ($\beta_{amide} = 8.3$[9b]) even in neat [D$_6$]DMSO ($\beta_{DMSO} = 8.9$[9b]). a) A. Altieri, G. Bottari, F. Dehez, D. A. Leigh, J. K. Y. Wong, F. Zerbetto, *Angew. Chem.* **2003**, *115*, 2398 – 2402; *Angew. Chem. Int. Ed.* **2003**, *42*, 2296 – 2300; b) C. A. Hunter, *Angew. Chem.* **2004**, *116*, 5424 – 5439; *Angew. Chem. Int. Ed.* **2004**, *43*, 5310 – 5324.

[10] S. A. Vignon, T. Jarrosson, T. Iijima, H.-R. Tseng, J. K. M. Sanders, J. F. Stoddart, *J. Am. Chem. Soc.* **2004**, *126*, 9884 – 9885.

[11] a) D. J. Cárdenas, A. Livoreil, J.-P. Sauvage, *J. Am. Chem. Soc.* **1996**, *118*, 11980 – 11981; b) A. Livoreil, J.-P. Sauvage, N. Armaroli, V. Balzani, L. Flamigni, B. Ventura, *J. Am. Chem. Soc.* **1997**, *119*, 12114 – 12124; c) J.-P. Collin, P. Gaviña, J.-P. Sauvage, *New J. Chem.* **1997**, *21*, 525 – 528; d) N. Armaroli, V. Balzani, J.-P. Collin, P. Gaviña, J.-P. Sauvage, B. Ventura, *J. Am. Chem. Soc.* **1999**, *121*, 4397 – 4408; e) L. Raehm, J.-M. Kern, J.-P. Sauvage, *Chem. Eur. J.* **1999**, *5*, 3310 – 3317; f) M. C. Jiménez, C. Dietrich-Buchecker, J.-P. Sauvage, *Angew. Chem.* **2000**, *112*, 3422 – 3425; *Angew. Chem. Int. Ed.* **2000**, *39*, 3284 – 3287; g) M. C. Jiménez-Molero, C. Dietrich-Buchecker, J.-P. Sauvage, *Chem. Eur. J.* **2002**, *8*, 1456 – 1466; h) M. C. Jiménez-Molero, C. Dietrich-Buchecker, J.-P. Sauvage, *Chem. Commun.* **2003**, 1613 – 1616; i) I. Poleschak, J. -M, Kern, J.-P. Sauvage, *Chem. Commun.* **2004**, 474 – 476; j) P. Mobian, J.-M. Kern, J.-P. Sauvage, *Angew. Chem.* **2004**, *116*, 2446 – 2449; *Angew. Chem. Int. Ed.* **2004**, *43*, 2392 – 2395; k) J.-P. Sauvage, *Chem. Commun.* **2005**, 1507 – 1510.

[12] For recent reviews on the synthesis of interlocked molecules using transition-metal templates, see: a) T. J. Hubin, D. H. Busch, *Coord. Chem. Rev.* **2000**, *200–202*, 5 – 52; b) J.-P. Collin, C. Dietrich-Buchecker, P. Gaviña, M. C. Jiménez-Molero, J.-P. Sauvage, *Acc. Chem. Res.* **2001**, *34*, 477 – 487; c) M. J. Blanco, J. C. Chambron, M. C. Jiménez, J.-P. Sauvage, *Top. Stereochem.* **2003**, *23*, 125 – 173; d) S. J. Cantrill, K. S. Chichak, A. J. Peters, J. F. Stoddart, *Acc. Chem. Res.* **2005**, *38*, 1 – 9; see also: e) A. C. Try, M. M. Harding, D. G. Hamilton, J. K. M. Sanders, *Chem. Commun.* **1998**, 723 – 724; f) M. E. Padilla-Tosta, O. D. Fox, M. G. B. Drew, P. D. Beer, *Angew. Chem.* **2001**, *113*, 4365 – 4369; *Angew. Chem. Int. Ed.* **2001**, *40*, 4235 – 4239; g) D. A. Leigh, P. J. Lusby, S. J. Teat, A. J. Wilson, J. K. Y. Wong, *Angew. Chem.* **2001**, *113*, 1586 – 1591; *Angew. Chem. Int. Ed.* **2001**, *40*, 1538 – 1543; h) C. P. McArdle, S. Van, M. C. Jennings, R. J. Puddephatt, *J. Am. Chem. Soc.* **2002**, *124*, 3959 – 3965; i) L. Hogg, D. A. Leigh, P. J. Lusby, A. Morelli, S. Parsons, J. K. Y. Wong, *Angew. Chem.* **2004**, *116*, 1238 – 1241; *Angew. Chem. Int. Ed.* **2004**, *43*, 1218 – 1221; j) W. W. H. Wong, J. Cookson, E. A. L. Evans, E. J. L. McInnes, J. Wolowska, J. P. Maher, P. Bishop, P. D. Beer, *Chem. Commun.* **2005**, 2214 – 2216.

[13] For reviews on the synthesis of interlocked structures using transition-metal connectors, see: a) M. Fujita, *Acc. Chem. Res.* **1999**, *32*, 53 – 61; b) K. Kim, *Chem. Soc. Rev.* **2002**, *31*, 96 – 107; c) S. R. Batten, R. Robson, *Angew. Chem.* **1998**, *110*, 1558 – 1595; *Angew. Chem. Int. Ed.* **1998**, *37*, 1460 – 1494; d) A. J. Blake, N. R. Champness, P. Hubberstey, W.-S. Li, M. A. Withersby, M. Schröder, *Coord. Chem. Rev.* **1999**, *183*, 117 – 138; e) S. J. Loeb, *Chem. Commun.* **2005**, 1511 – 1518.

[14] a) D. D. Cox, S. J. Benkovic, L. M. Bloom, F. C. Bradley, M. J. Nelson, L. Que, Jr., D. E. Wallick, *J. Am. Chem. Soc.* **1988**, *110*, 2026 – 2032; Complexes of this type of ligand have previously only been reported in a single tetradentate form; see: b) S. Ito, T. Okuno, H. Matsushima, T. Tokli, Y. Nishida, *J. Chem. Soc. Dalton Trans.* **1996**, 4479 – 4484; c) T. Okuno, S. Ohba, Y. Nishida, *Polyhedron* **1997**, *16*, 3765 – 3774; d) T. Kobayashi, T. Okuno, M. Kunita, S. Ohba, Y. Nishida, *Polyhedron* **1998**, *17*, 1553 – 1559; e) N. Niklas, O. Walter, R. Alsfasser, *Eur. J. Inorg. Chem.* **2000**, 1723 – 1731; f) N. Niklas, S. Wolf, G. Liehr, C. E. Anson, A. K. Powell, R. Alsfasser, *Inorg. Chim. Acta* **2001**, *314*, 126 – 132; g) C. Incarvito, A. L. Rheingold, A. L. Gavrilova, C. Jin Qin, B. Bosnich, *Inorg. Chem.* **2001**, *40*, 4101 – 4108; h) N. Niklas, F. Hampel, O. Walter, G. Liehr, R. Alsfasser, *Eur. J. Inorg. Chem.* **2002**, 1839 – 1847; i) A. L. Gavrilova, C. Jin Qin, R. D. Sommer, A. L. Rheingold, B. Bosnich, *J. Am. Chem. Soc.* **2002**, *124*, 1714 – 1722; j) N. Niklas, O. Walter, F. Hampel, R. Alsfasser, *J. Chem. Soc. Dalton Trans.* **2002**, 3367 – 3373.

[15] H**1** = 5-[2-(bis(pyridin-2-ylmethyl)amino)acetyl)amino]isophthalic acid dimethyl ester; H$_2$**2** = 2-(bis(pyridin-2-ylmethyl)amino)-*N*-[(2,2-diphenyl-ethylcarbamoyl)methyl]acetamide; H$_2$**3** = ([2](1,7,14,20-tetraaza-2,6,15,19-tetraoxo-3,5,9,12,16,18,22,25-tetrabenzocyclohexacosane)-(2-(bis(pyridin-2-ylmethyl)amino)-*N*-[(2,2-diphenylethylcarbamoyl)methyl]acetamide) rotaxane; H$_2$**4** = 2,2-diphenylethyl 4-(12-(2-(2-(bis(pyridine-2-ylmethyl)amino)acetamido)acetamido)dodecylamino-4-oxobutanoate; H$_2$**5** = ([2](1,7,14,20-tetraaza-2,6,15,19-tetraoxo-3,5,9,12,16,18,22,25-tetrabenzocyclohexacosane)-(2,2-diphenylethyl 4-(12-(2-(2-(bis(pyridine-2-ylmethyl)amino)acetamido)acetamido)dodecylamino-4-oxobutanoate) rotaxane.

[16] X-ray crystal structural data for H**1**CuCl$_2$, [H**1**CuCl]$_2$[CuCl$_4$], H$_2$**3**, H**2**CdNO$_3$, and H$_2$**3**Cd(NO$_3$)$_2$ were collected at 93 K using a Rigaku Saturn (MM007 high-flux RA/Mo$_{K\alpha}$ radiation, confocal optic), while those for **1**CuCl and H**2**CuCl were collected at 93 K using a Mercury (MM007 high-flux RA/Mo$_{K\alpha}$ radiation, confocal optic). All data collections employed narrow frames (0.3–1.0°) to obtain at least a full hemisphere of data. Intensities were corrected for Lorentz polarization and absorption effects (multiple equivalent reflections). Structures were solved by direct methods, non-hydrogen atoms were refined anisotropically, with C–H protons refined in riding geometries (SHELXTL) against F^2. In most cases, amide protons were refined isotropically subject to a distant constraint. The protons on solvate molecules were not allowed for in the refinement. Data for H**1**CuCl$_2$·0.5 CH$_3$CN·0.055 H$_2$O: $C_{25}H_{25.61}Cl_2CuN_{4.5}O_{5.06}$, M = 604.44, crystal size $0.1 \times 0.05 \times 0.01$ mm^3, trigonal, $P\bar{3}$, a = 40.804(2), c = 8.4772(4) Å, Z = 18, ρ_{calcd} = 1.478 Mg m^{-3}; μ = 1.044 mm^{-1}, 91570 collected, 14360 unique (R_{int} = 0.0825), R = 0.1258 for 12778 observed data [$F_o > 4\sigma(Fo)$], S = 1.189 for 1037 parameters. Residual electron density extremes were 1.500 and −1.250 e Å^{-3}. Data for [H**1**CuCl]$_2$[CuCl$_4$]·0.5 H$_2$O: $C_{48}H_{49}Cl_6Cu_3N_8O_{10.5}$, M = 1309.27, crystal size $0.1 \times 0.05 \times 0.03$ mm^3, monoclinic, $P2(1)/n$, a = 8.1667(16), b = 30.257(5), c = 23.377(4) Å, Z = 4, ρ_{calcd} = 1.506 Mg m^{-3}; μ = 1.433 mm^{-1},

 © 2006 Wiley-VCH Verlag GmbH & Co. KGaA, Weinheim

51258 collected, 11852 unique ($R_{int}=0.0484$), $R=0.1234$ for 9492 observed data [$F_o>4\sigma(F_o)$], $S=1.540$ for 691 parameters. Residual electron density extremes were 2.381 and −1.117 e Å^{-3}. Data for **1**CuCl: $C_{24}H_{23}ClCuN_4O_5$, $M=546.45$, crystal size 0.2 × 0.1 × 0.1 mm^3, monoclinic, $C2/c$, $a=14.026(3)$, $b=11.390(3)$, $c=30.259(6)$ Å, $Z=8$, $\rho_{calcd}=1.513$ Mg m^{-3}; $\mu=1.065$ mm^{-1}, 9975 collected, 3728 unique ($R_{int}=0.0644$), $R=0.0456$ for 3104 observed data [$F_o>4\sigma(F_o)$], $S=1.024$ for 329 parameters. Residual electron density extremes were 0.472 and −0.383 e Å^{-3}. Data for H**2**CuCl: $C_{30}H_{30}ClCuN_5O_2$, $M=591.58$, crystal size 0.2 × 0.1 × 0.1 mm^3, monoclinic, $P2(1)/n$, $a=16.089(3)$, $b=9.9833(18)$, $c=16.968(3)$ Å, $Z=4$, $\rho_{calcd}=1.446$ Mg m^{-3}; $\mu=0.940$ mm^{-1}, 15979 collected, 4822 unique ($R_{int}=0.0333$), $R=0.0486$ for 4460 observed data [$F_o>4\sigma(F_o)$], $S=1.053$ for 357 parameters. Residual electron density extremes were 2.384 and −0.553 e Å^{-3}. Data for H_2**3**: $C_{68}H_{71}N_9O_8$, $M=1142.34$, crystal size 0.2 × 0.1 × 0.05 mm^3, monoclinic, $P2(1)/c$, $a=13.0505(10)$, $b=19.1256(14)$, $c=25.970(2)$ Å, $Z=4$, $\rho_{calcd}=1.183$ Mg m^{-3}; $\mu=0.079$ mm^{-1}, 45077 collected, 11321 unique ($R_{int}=0.1105$), $R=0.1789$ for 10284 observed data [$F_o>4\sigma(F_o)$], $S=1.190$ for 793 parameters. Residual electron density extremes were 1.387 and −0.435 e Å^{-3}. Data for H**2**$CdNO_3$: $C_{30}H_{30}CdN_6O_5$, $M=667.00$, crystal size 0.15 × 0.15 × 0.05 mm^3, monoclinic, $P2(1)/c$, $a=9.8549(14)$, $b=17.620(3)$, $c=16.444(3)$ Å, $Z=4$, $\rho_{calcd}=1.553$ Mg m^{-3}; $\mu=0.817$ mm^{-1}, 20308 collected, 4953 unique ($R_{int}=0.0301$), $R=0.0285$ for 4357 observed data [$F_o>4\sigma(F_o)$], $S=1.085$ for 384 parameters. Residual electron density extremes were 0.872 and −0.334 e Å^{-3}. Data for H_2**3**$Cd(NO_3)_2$: $C_{62}H_{59}CdN_{11}O_{12}$, $M=1262.6$, crystal size 0.1 × 0.1 × 0.03 mm^3, monoclinic, $C2/c$, $a=28.252(13)$, $b=10.588(5)$, $c=42.457(19)$ Å, $Z=8$, $\rho_{calcd}=1.439$ Mg m^{-3}; $\mu=0.426$ mm^{-1}, 27366 collected, 9652 unique ($R_{int}=0.0925$), $R=0.0814$ for 5850 observed data [$F_o>4\sigma(F_o)$], $S=1.076$ for 857 parameters. Residual electron density extremes were 0.976 and −0.640 e Å^{-3}. CCDC 269894–269900 contain the supplementary crystallographic data for this paper. These data can be obtained free of charge from The Cambridge Crystallographic Data Centre via www.ccdc.cam.ac.uk/data_request/cif.

[17] Some of the emerald-green color of [H**1**CuCl]$_2$[$CuCl_4$] can be attributed to the $[CuCl_4]^{2-}$ counterion.

[18] Wrapped up metal–peptide complexes are widely seen in biological contexts, for example, with copper and various tripeptide ligands; see: a) H. Sigel, R. B. Martin, *Chem. Rev.* **1982**, *82*, 385 – 426; b) P. Deschamps, P. P. Kulkarni, M. Gautam-Basak, B. Sarkar, *Coord. Chem. Rev.* **2005**, *249*, 895 – 909. However, the use of a designed auxiliary ligand attached to the peptide that facilitates stepwise control over the binding modes is, to the best of our knowledge, unknown.

[19] Several different hydrogen-bonding motifs are in equilibrium in solution. G. W. H. Wurpel, A. M. Brouwer, I. H. M. van Stokkum, A. Farran, D. A. Leigh, *J. Am. Chem. Soc.* **2001**, *123*, 11327 – 11328.

[20] Cd^{II} exhibits a strong binding affinity and kinetic stability for BPA-type ligands [for example, see: N. Niklas, F. Hampel, G. Liehr, A. Zahl, R. Alsfasser, *Chem. Eur. J.* **2001**, *7*, 5135 – 5141], and its stable diamagnetic ground state allows the characterization of complexes by ^{1}H NMR spectroscopy.

[21] The molecular shuttle rotaxane and thread cadmium complexes were insufficiently soluble in $CDCl_3$ or CD_2Cl_2 for ^{1}H NMR spectroscopic studies so [D_6]acetone was used throughout.

[22] For the metal complexes of the short thread, H_2**2**, either NaH or Schwesinger's phosphazene P_1-*t*Bu base (*N*′-*tert*-butyl-*N*,*N*,*N*′,*N*′,*N*″,*N*″-hexamethylphosphorimidic triamide) [R. Schwesinger, C. Hasenfratz, H. Schlemper, L. Walz, E.-M. Peters, K. Peters, H. G. von Schnering, *Angew. Chem.* **1993**, *105*, 1420 – 1422; *Angew. Chem. Int. Ed. Engl.* **1993**, *32*, 1361 – 1363] could be used to deprotonate BPA at its terminal amide group. However, for H_2**4** and H_2**5**, which contain an ester linkage, only P_1-*t*Bu proved suitable.

[23] Without this discrimination, the more-complicated molecular shuttle system containing multiple amide groups would not be able to function.

 © 2006 Wiley-VCH Verlag GmbH & Co. KGaA, Weinheim

Host–Guest Systems

DOI: 10.1002/anie.200502209

Dangling Arms: A Tetrahedral Supramolecular Host with Partially Encapsulated Guests**

*Bryan E. F. Tiedemann and Kenneth N. Raymond**

Supramolecular chemistry takes advantage of self-assembly to prepare large, discrete structures from relatively simple subunits. Using metal–ligand interactions, π stacking, and/or hydrogen bonds to link the various subunits together, many elegant examples of supramolecular assemblies have been synthesized which have been the subject of some excellent review articles.[1–5] Some examples of the utilization of host–guest properties of such clusters to modify guest reactivity include work done by Fujita,[6,7] Reek,[8–10] and Rebek.[11–14] The rational design and properties of self-assembling tetrahedral M_4L_6 supramolecular clusters ($M = Al^{III}$, Fe^{III}, Ga^{III}, Ti^{IV}; H_4L = 1,5-bis(2,3-dihydroxybenzamido)naphthalene) have been described by Raymond and co-workers, with structural features illustrated in Figure 1.[15–19] These chiral assemblies can encapsulate a variety of lipophilic monocationic molecules as guests within the 350–500-$Å^3$ cavity.[20–22] While encapsulated, guests can undergo reactions—both stoichiometric and catalytic—with significant rate enhancement and improved product selectivity in some cases.[23–25] The catalytic cycle proposed to explain these results requires the substrate to enter the host and react inside the cluster and then the product to exit. For polymer formation, the product must continually exit the host while the cluster remains intact. Can this be achieved using the M_4L_6 assembly?

[*] B. E. F. Tiedemann, Prof. Dr. K. N. Raymond
Department of Chemistry
University of California
Berkeley, CA 94720-1460 (USA)
Fax: (+1) 510-486-5283
E-mail: raymond@socrates.berkeley.edu

[**] This research is supported by NSF grant CHE-0317011. We thank the following for their assistance: Dr. Dorothea Fiedler and Dr. Georg Seeber for stimulating discussions, Matthew N. Stavis and Dennis H. Leung for aid with the graphics, Dr. Ulla N. Andersen at the Mass Spectrometry Facility, and Don Harris at Waters Corporation for high-resolution electrospray mass spectrometry.

Supporting information for this article is available on the WWW under http://www.angewandte.org or from the author.

© 2006 Wiley-VCH Verlag GmbH & Co. KGaA, Weinheim
WILEY InterScience DISCOVER SOMETHING GREAT

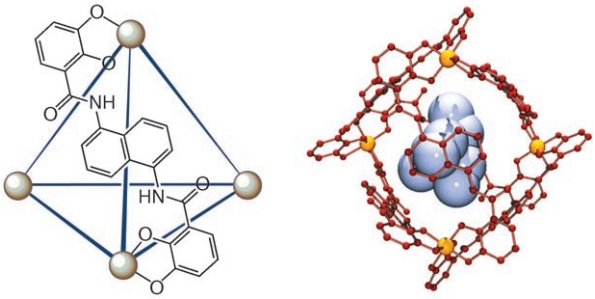
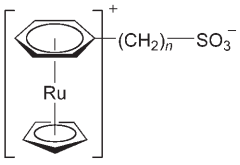


Figure 1. Left: Schematic structure of the M_4L_6 tetrahedral cluster which illustrates the structure of L^{4-} and its coordination to the metal-ion vertices. Right: Illustration of the host–guest complex $[Et_4N{\subset}Ga_4L_6]^{11-}$ based on the X-ray structure coordinates, with a Et_4N^+ guest shown in blue.

Recently, it was observed that $[Ga_4L_6]^{12-}$ and $[Ti_4L_6]^{8-}$ hosts facilitate guest exchange at essentially the same rate, thus demonstrating that the guest-exchange mechanism does not require a ligand-dissociation step. Small openings exist in the triangular faces of the host, and concerted cluster distortion is proposed as a means to enlarge these gaps for guests to pass through.[26] If a stable host–guest complex was synthesized with part of the guest protruding from the host through this opening, the aperture would have to expand to accommodate the steric bulk introduced by the protrusion. Such a system is analogous to the transition state proposed for nondissociative guest exchange. Rebek and co-workers have reported examples of linear molecules "partially" encapsulated in the hydrophobic pocket of an open-ended cavitand,[27] but no examples have been reported for "closed" self-assembled hosts, such as the M_4L_6 cluster. Herein, the synthesis and characterization of $[RuC_n{\subset}Ga_4L_6]^{12-}$ (RuC_n = $[CpRu\{\eta_6\text{-}C_6H_5(CH_2)_nSO_3\}]$, $n = 4$, 6, 8, 10; Cp = cyclopentadienyl) is reported in the solution state: a series of host–guest complexes with linear "arms" protruding from the host interior.

With the $[Ga_4L_6]^{12-}$ ion as the host, a suitable guest compound has to be designed with an appendage capable of protruding through the opening of the host into the bulk solvent. Such a guest should have three regions: a lipophilic monocationic head group which exhibits sufficient binding stability for encapsulation, a linear chain of variable length to protrude through the aperture, and a hydrophilic anionic end group to stabilize the arm in aqueous solution. The sandwich complex $[CpRu(\eta_6\text{-}C_6H_6)]^+$ is known to be encapsulated by the $[Ga_4L_6]^{12-}$ ion,[28] and was chosen as the cationic head group for RuC_n (Scheme 1). This series of compounds features linear alkyl chains, with one end bound to the cationic sandwich complex at the phenyl ligand, and the other bound to a sulfonate anion.



Scheme 1. Structural formula of RuC_n ($n = 4$, 6, 8, and 10).

Addition of a stoichiometric amount of RuC_n to $K_{12}[Ga_4L_6]$ in D_2O led to the encapsulation of the ruthenium head group for all chain lengths ($n = 4$–10). The ^1H NMR spectra of the resulting host–guest complexes display signals for the Cp and phenyl rings of the guest shifted to significantly higher fields relative to the values observed in the absence of the host (Figure 2). Such an upfield shift is a diagnostic

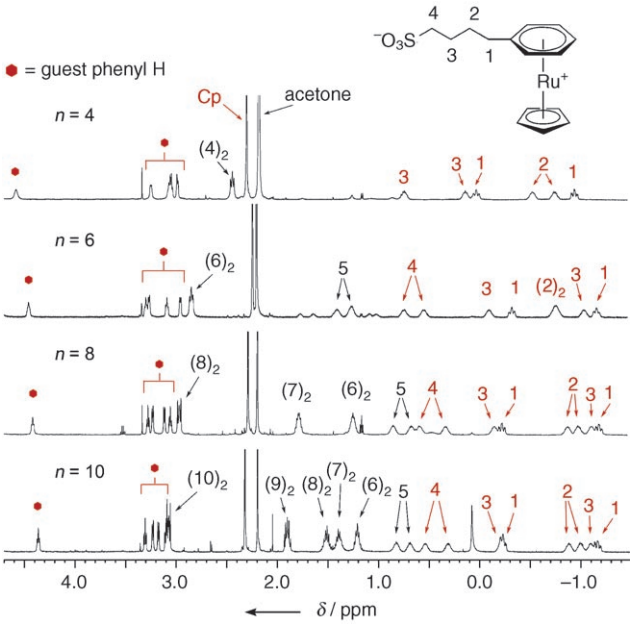


Figure 2. Portions of the ^1H NMR spectra (D_2O, 500 MHz) of the host–guest complexes $[RuC_n{\subset}Ga_4L_6]^{12-}$. Guest resonance assignments follow the labeling scheme illustrated for RuC_4 (top), with the same numbering pattern used for all chain lengths. Cp denotes the 5H singlet from the Ru-bound cyclopentadiene ring. Interior protons are highlighted with red labels, and signals that integrate to two protons are identified by subscripted labels.

feature observed for encapsulated guest protons and is caused by the magnetic shielding from the naphthalene groups surrounding the cavity of the $[Ga_4L_6]^{12-}$ ion.[16,18,20] Furthermore, the two sets of mirror-related phenyl protons become diastereotopic upon encapsulation of the sandwich complex by the host because of the chiral environment of the cavity.

Diastereotopic splitting is also observed for most, but not all, geminal methylene resonances, accompanied by varying upfield shifts. With the aid of 2D COSY and/or TOCSY NMR spectroscopic analysis, all chain protons were fully assigned (Figure 2). Methylene carbon atoms are numbered sequentially along the chain and begin with the carbon atom bound to the sandwich complex. For RuC_4, the geminal methylene protons on C1–C3 become diastereotopic upon encapsulation by the $[Ga_4L_6]^{12-}$ ion, and diastereotopic geminal methylene protons are observed for C1–C5 for encapsulated RuC_6, RuC_8, and RuC_{10}. Upfield shifts tend to increase for protons closer to the head group. In comparison, several methylene protons remain enantiotopic and show little, if any, upfield

 © 2006 Wiley-VCH Verlag GmbH & Co. KGaA, Weinheim

shift. The signal from the methylene group adjacent to the sulfonate moiety is unsplit and unshifted in all four $[RuC_n{\subset}Ga_4L_6]^{12-}$ host–guest spectra. These ^1H NMR observations indicate that part of the alkyl chain bound to the cationic sandwich complex resides within the chiral host and the rest of that alkyl chain lies outside the cavity with the terminal sulfonate group. At least one methylene group is found outside the host in all four systems. Thus, the $[Ga_4L_6]^{12-}$ cluster encapsulates only part of the RuC_n zwitterion.

The signals for the 72 host protons are typically observed as six sets of 12 protons (Figure 3a), as the catechol and naphthalene ring edges are interrelated in point group *T*, each

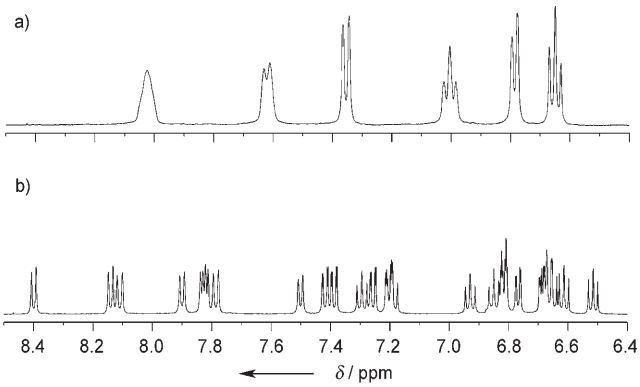


Figure 3. Portions of the ^1H NMR spectra (D_2O) that show the host resonances observed for a) point group *T* typically observed for most host–guest complexes and b) $[RuC_{10}{\subset}Ga_4L_6]^{12-}$ characteristic of C_3 symmetry.

with three adjacent nonequivalent protons. In the presence of the protruding arm, however, these resonances are split into 24 sets of three protons (Figure 3b). This observation indicates that the overall symmetry is reduced from point group *T* for the host alone to C_3 upon encapsulation of RuC_n. Such a symmetry reduction is expected to occur when the alkyl sulfonate arm of the guest protrudes through the opening in a triangular face of the tetrahedron. This action breaks the ligand twofold symmetry, but retains the C_3 axis running from a Ga^{III} vertex through the aperture of interest. The six ligands that span the edges of the tetrahedron separate into two chemically nonequivalent groups: three "base" ligands that surround the protruding arm and three "side" ligands connected to the Ga^{III} vertex opposite the protrusion, with 12 different protons for each. According to 2D COSY NMR spectroscopy, the 24 host signals originate from four sets of catechol protons and four sets of naphthyl protons (see the Supporting Information).

The 2D NOESY NMR spectra of the $[RuC_n{\subset}Ga_4L_6]^{12-}$ system provide additional information about the structures of the host–guest complexes. Figure 4 shows the spectrum of the $[RuC_6{\subset}Ga_4L_6]^{12-}$ system with focus on the cross section between the host and guest resonances. The phenyl and Cp signals of the guest show strong correlations with signals from three out of the four sets of host naphthalene protons. No cross peaks are observed between the phenyl or Cp reso-

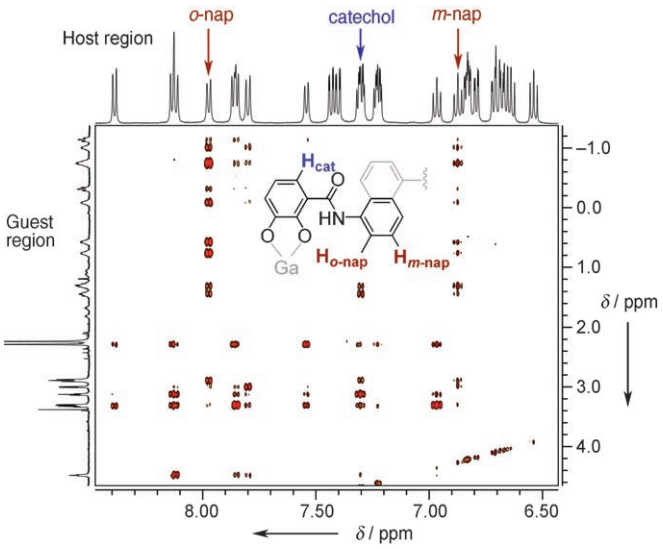


Figure 4. The 2D NOESY NMR spectrum (D_2O, 500 MHz) of the $[RuC_6{\subset}Ga_4L_6]^{12-}$ system shows cross peaks between host resonances (horizontal axis) and guest resonances (vertical axis). Resonances from naphthyl protons that border the aperture, *ortho* and *meta* to the amide nitrogen atom, are highlighted in red. The catechol resonance highlighted in blue shows cross peaks with signals from exterior methylene protons. nap = naphthyl, cat = catechol.

nances of the guest and catechol proton signals of the host, thus confirming that the cationic head group is buried deep within the host cavity, near the naphthyl ring walls. Similar 2D NOESY NMR spectroscopic observations have been reported for other guests within the $[Ga_4L_6]^{12-}$ cluster, such as Et_4N^+ and $[CpRu(\eta_6\text{-}C_6H_6)]^+$ ions.[18,28]

Cross peaks are also observed between several host resonances and most, if not all, methylene groups on the alkyl chain. The first six to eight methylene groups all show cross peaks with the same two host resonances—one doublet and one triplet, which are highlighted in Figure 4. According to molecular-modeling studies (Figure 5) and 2D COSY NMR spectra, these signals originate from two adjacent naphtha-

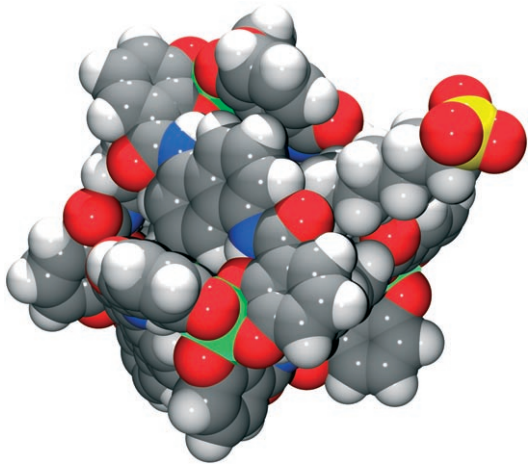


Figure 5. MM3 minimized structural model of the $[RuC_{10}{\subset}Ga_4L_6]^{12-}$ system

© 2006 Wiley-VCH Verlag GmbH & Co. KGaA, Weinheim

lene protons, located *ortho* and *meta* to the amide nitrogen atom. Because of the orientation of the naphthyl ring, the *para* proton is directed away from the alkyl chain and strong cross peaks are not observed with the guest. Relative distances between the host and guest protons in the $[RuC_6{\subset}Ga_4L_6]^{12-}$ system were determined from NOE interaction growth rates and show these two protons are the closest to the protruding alkyl chain on the C_3-related edges of the three naphthalene rings that surround the aperture. These hydrogen atoms are directed away from the cluster center and can be used as boundary markers to distinguish the host interior from the exterior. Methylene groups 4 and 5 are closest to the boundary, whereas methylene group 1 is the farthest. This difference suggests that the two naphthyl protons are situated between the C4 and C5 of the alkyl chain, with C4 on the interior side and C5 on the exterior side of the cavity boundary. C1, immediately adjacent to the encapsulated cationic head group, lies deep within the cluster. Future NOE interaction growth studies will address the specific conformations of the alkyl chain for guests with different chain lengths.

High-resolution negative ion electrospray mass spectrometry (ESI MS) confirmed the formation of host–guest complexes (Figure 6). Spectra were obtained for solutions of the

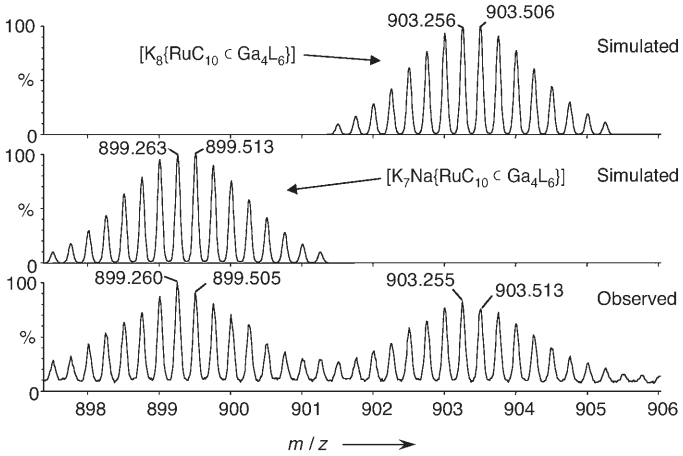


Figure 6. Portion of the electrospray mass spectrum of the $[RuC_{10}{\subset}Ga_4L_6]^{12-}$ system that shows two adjacent peaks for the $z=-4$ charge state, with predicted isotopic distribution patterns for two particular fragment ion formulae.

$[RuC_4{\subset}Ga_4L_6]^{12-}$, $[RuC_6{\subset}Ga_4L_6]^{12-}$, $[RuC_8{\subset}Ga_4L_6]^{12-}$, and $[RuC_{10}{\subset}Ga_4L_6]^{12-}$ systems, and the resulting spectra showed peaks for the $z=-3$ and -4 charge states of the host–guest complexes with K^+, Na^+, and/or H^+ counterions. The mass spectra of the $[RuC_4{\subset}Ga_4L_6]^{12-}$ and $[RuC_{10}{\subset}Ga_4L_6]^{12-}$ systems show additional peaks that correspond to the $z=-5$ charge state of the host–guest complex.

This study shows that the $[Ga_4L_6]^{12-}$ tetrahedron remains intact upon incorporation of the cationic head of a zwitterion, while the link to the anionic tail passes through one of the small openings at the centers of the triangular faces. This process is fully consistent with the nondissociative guest-exchange mechanism recently described.[26] If a guest can extend out of the cavity, new reactions may be envisioned, such as linear polymerizations, with the product extending out of the host cavity as it forms.

Received: June 23, 2005
Published online: November 22, 2005

Keywords: host–guest systems · sandwich complexes · supramolecular chemistry · zwitterions

[1] D. S. Lawrence, T. Jiang, M. Levett, *Chem. Rev.* **1995**, *95*, 2229.
[2] S. Leininger, B. Olenyuk, P. J. Stang, *Chem. Rev.* **2000**, *100*, 853.
[3] M. M. Conn, J. Rebek, Jr., *Chem. Rev.* **1997**, *97*, 1647.
[4] M. A. Manteos-Timoneda, M. Crego-Calama, D. N. Reinhoudt, *Chem. Soc. Rev.* **2004**, *33*, 363.
[5] T. D. Hamilton, L. R. MacGillvray, *Cryst. Growth Des.* **2004**, *4*, 419.
[6] M. Yoshizawa, Y. Takeyama, T. Kusukawa, M. Fujita, *Angew. Chem.* **2002**, *114*, 1403; *Angew. Chem. Int. Ed.* **2002**, *41*, 1347.
[7] M. Fujita, M. Tominaga, A. Hori, B. Therrien, *Acc. Chem. Res.* **2005**, *38*, 371.
[8] V. F. Slagt, J. N. H. Reek, P. C. J. Kamer, P. W. N. M. van Leeuwen, *Angew. Chem.* **2001**, *113*, 4401; *Angew. Chem. Int. Ed.* **2001**, *40*, 4271.
[9] V. F. Slagt, P. W. N. M. van Leeuwen, J. N. H. Reek, *Angew. Chem.* **2003**, *115*, 5777; *Angew. Chem. Int. Ed.* **2003**, *42*, 5619.
[10] V. F. Slagt, P. C. J. Kamer, P. W. N. M. van Leeuwen, J. N. H. Reek, *J. Am. Chem. Soc.* **2004**, *126*, 1526.
[11] F. Hof, S. L. Craig, C. Nuckolls, J. Rebek, Jr., *Angew. Chem.* **2002**, *114*, 1556; *Angew. Chem. Int. Ed.* **2002**, *41*, 1488.
[12] J. M. Kang, J. Rebek, Jr., *Nature* **1997**, *385*, 50.
[13] J. M. Kang, J. Santamaria, G. Hilmersson, J. Rebek, Jr., *J. Am. Chem. Soc.* **1998**, *120*, 3650.
[14] J. M. Kang, J. Santamaria, G. Hilmersson, J. Rebek, Jr., *J. Am. Chem. Soc.* **1998**, *120*, 7389.
[15] A. J. Terpin, M. Ziegler, D. W. Johnson, K. N. Raymond, *Angew. Chem.* **2001**, *113*, 161; *Angew. Chem. Int. Ed.* **2001**, *40*, 157.
[16] D. L. Caulder, R. E. Powers, T. N. Parak, K. N. Raymond, *Angew. Chem.* **1998**, *110*, 1940; *Angew. Chem. Int. Ed.* **1998**, *37*, 1840.
[17] M. Ziegler, J. J. Miranda, U. N. Andersen, D. W. Johnson, J. A. Leary, K. N. Raymond, *Angew. Chem.* **2001**, *113*, 755; *Angew. Chem. Int. Ed.* **2001**, *40*, 733.
[18] D. L. Caulder, C. Bruckner, R. E. Powers, S. Konig, T. N. Parak, J. A. Leary, K. N. Raymond, *J. Am. Chem. Soc.* **2001**, *123*, 8923.
[19] M. Ziegler, A. V. Davis, D. W. Johnson, K. N. Raymond, *Angew. Chem.* **2003**, *115*, 689; *Angew. Chem. Int. Ed.* **2003**, *42*, 665.
[20] T. N. Parak, D. L. Caulder, K. N. Raymond, *J. Am. Chem. Soc.* **1998**, *120*, 8003.
[21] T. N. Parac, M. Scherer, K. N. Raymond, *Angew. Chem.* **2000**, *112*, 1288; *Angew. Chem. Int. Ed.* **2000**, *39*, 1239.
[22] M. Ziegler, J. L. Brumaghim, K. N. Raymond, *Angew. Chem.* **2000**, *112*, 4285; *Angew. Chem. Int. Ed.* **2000**, *39*, 4119.
[23] D. H. Leung, D. Fiedler, R. G. Bergman, K. N. Raymond, *Angew. Chem.* **2004**, *116*, 981; *Angew. Chem. Int. Ed.* **2004**, *43*, 963.
[24] D. Fiedler, R. G. Bergman, K. N. Raymond, *Angew. Chem.* **2004**, *116*, 6916; *Angew. Chem. Int. Ed.* **2004**, *43*, 6748.
[25] D. Fiedler, D. H. Leung, R. G. Bergman, K. N. Raymond, *Acc. Chem. Res.* **2005**, *38*, 351.
[26] A. V. Davis, K. N. Raymond, *J. Am. Chem. Soc.* **2005**, *127*, 7912.
[27] L. Trembleau, J. Rebek, Jr., *Science* **2003**, *301*, 1219.
[28] D. Fiedler, D. Pagliero, J. L. Brumaghim, R. G. Bergman, K. N. Raymond, *Inorg. Chem.* **2004**, *43*, 846.

 © 2006 Wiley-VCH Verlag GmbH & Co. KGaA, Weinheim

Polymer Architectures

DOI: 10.1002/anie.200502306

Controlling Polymer Architecture through Host–Guest Interactions**

Liang Chen, Xinyuan Zhu, Deyue Yan,* Yan Chen, Qun Chen, and Yefeng Yao*

Structure and performance are two fundamental characteristics of a polymeric material. Therefore, controlling the structure to get a desired property remains one of the main goals of polymer chemistry.[1] Nowadays, supramolecular principles are also commonly utilized in the design and synthesis of polymer structures, with cyclodextrin (CD) being one of the most widely used hosts. However, most of these works concern the construction of novel supramolecular systems[2–4] rather than controlling the molecular structure of the guest polymer.[5] Herein we report a supramolecular method to control the architecture of polymers. The branched structure of a polymer can be adjusted conveniently using such a method. Moreover, this supramolecular approach is versatile and can be used for the design and preparation of materials with special topological structures, functionalities, and properties.

The polycondensation–addition of 1-(2-aminoethyl)piperazine (AP), a BB'_2 monomer, and divinylsulfone (DV), an A_2 monomer, is a typical reaction for preparing hyperbranched polymers[6] by monomer-coupling methods.[7] The difference in reactivity between primary amino and secondary amino groups makes it possible to form an $AabB'_2$-type intermediate rapidly; further polymerization gives hyperbranched poly(sulfone–amine) (PSA).

A ^{1}H NMR experiment in situ revealed that neither AP nor DV react with β-CD, despite its many active hydroxy groups (see Supporting Information). Interestingly, the similarities in the size and polarity of the AP molecule and the β-CD cavity induce complexation, and intermolecular hydrogen bonds between the amino and hydroxy groups also help to stabilize the inclusion compound (IC). ^{1}H NMR and elemental analysis confirmed that AP is located in the cavity of β-CD[8] and forms a 1:1 IC. The equilibrium constant between AP and β-CD was measured by two NMR methods, namely conventional NMR binding titration and NMR diffusion measurements.[9] Both experiments gave a value for K_a in the range of $(100 \pm 10)\ \text{M}^{-1}$. This value is similar to those for ICs between β-CD and various small organic molecules.[9d]

A series of PSA samples were then prepared by adjusting the amount of β-CD. The optical rotations of these samples (see Supporting Information) suggest the presence of β-CD in the final products. A comparison of the wide-angle X-ray diffraction (WAXD) and NMR spectra before and after polymerization reveals that reaction between AP and DV can be carried out successfully in the presence of β-CD: the diffractogram of the IC formed by AP and β-CD in a 1:1 ratio (Figure 1a) shows strong crystalline peaks and corresponds to a typical crystalline IC formed by β-CD and small guest molecules. It is different from the diffractograms of pure β-CD (Figure 1b) and polymerized samples (Figure 1c–f). Furthermore, in the ^{1}H NMR spectra of the polymerized samples the peaks at $\delta = 6.3$ and 7.0 ppm, assigned to the vinyl moiety, are no longer observed, which means that all of the vinyl groups have been transformed into dimethylenes ($-CH_2-CH_2-$) by polymerization and that the retro-Michael addition is negligible. A DEPT-135 experiment revealed that there are only secondary carbon atoms in the guest polymer chains, thereby further suggesting the complete conversion of the vinyl groups. These results confirm that the reaction between the vinyl and amino groups can take place even in the presence of an equimolar amount of β-CD.

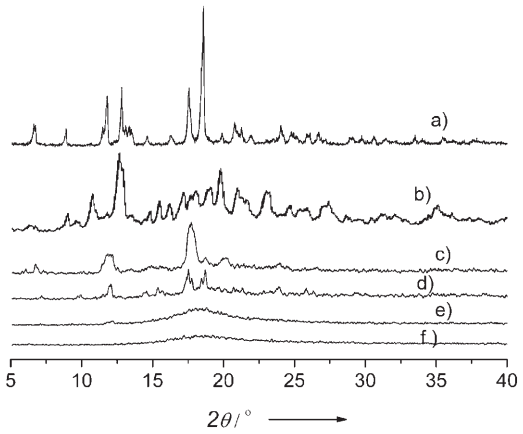


Figure 1. Diffractograms of a) IC formed by AP and β-CD; b) pure β-CD, and PSA samples with a β-CD to AP molar ratio of c) 1:1, d) 0.5:1, e) 0.14:1, and f) 0.02:1.

The WAXD spectra of polymerized samples are illustrated in Figures 1c–f. Figure 1c corresponds to the sample polymerized in the presence of an equimolar amount of β-CD. To our surprise, its diffractogram is identical to those of polyrotaxanes/pseudopolyrotaxanes formed by β-CD and

[*] L. Chen, Prof. Dr. X. Zhu, Prof. Dr. D. Yan, Y. Chen
School of Chemistry and Chemical Technology
State Key Laboratory of Metal Matrix Composites
Shanghai Jiao Tong University
800 Dongchuan Road, Shanghai 200240 (P.R. China)
Fax: (+86) 21-5474-1297
E-mail: xyzhu@sjtu.edu.cn
dyyan@sjtu.edu.cn
Prof. Dr. Q. Chen, Y. Yao
Key Laboratory of Education Ministry for Optical and Magnetic Resonance Spectroscopy
East China Normal University
Shanghai 200062 (P.R. China)

[**] This work was supported by the National Natural Science Foundation of China (grant nos. 20574044, 20104004, and 50233030). X. Z. thanks Prof. Reiko Saito for her helpful suggestion and Dr. Daniel Schmidt for his assistance in proofreading the manuscript.

Supporting information for this article is available on the WWW under http://www.angewandte.org or from the author.

© 2006 Wiley-VCH Verlag GmbH & Co. KGaA, Weinheim

linear polymers, and the characteristic reflections at $2\theta = 11.66°$ and 18.00° indicate that the β-CD molecules are threaded onto the polymer chain to form a channel-like structure.[10] It can be inferred from this result that linear PSA is obtained by polymerization in the presence of large amounts of β-CD. The intensities of the characteristic diffraction peaks reduce gradually with decreasing amounts of β-CD, and when the ratio of β-CD to AP is below 0.14:1 only a diffuse peak, which is close to that of pure, amorphous, hyperbranched PSA synthesized from AP and DV in the absence of β-CD, is observed (Figures 1 c–f).

Standard solid-state CP/MAS ^{13}C NMR spectra are shown in Figure 2. Split signals at $\delta = 94.6$ and 96.6 ppm assigned to

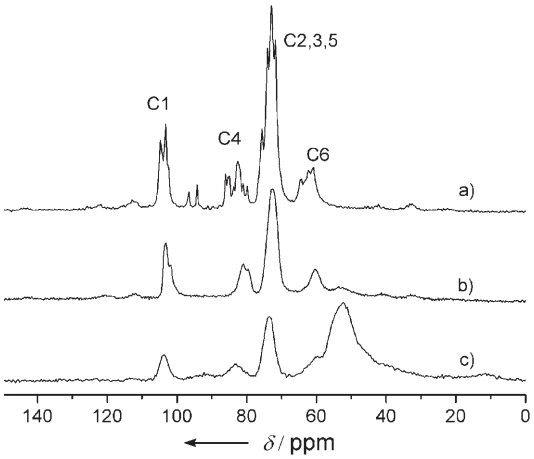


Figure 2. Solid-state CP/MAS ^{13}C NMR spectra of pure β-CD (a) and PSA samples with a β-CD to AP molar ratio of 1:1 (b) and 0.1:1 (c).

the conformationally strained α-1,4-glycosidic linkage are noticeable in the spectrum of natural β-CD (Figure 2 a); however, they are no longer observed in the spectra of polymerized samples (Figures 2 b and 2 c). This result reveals that the β-CD molecules in the polymerized samples have a more symmetric conformation than in pure β-CD. In other words, the β-CD host molecules are still threaded by the polymer chains after polymerization.[11]

The structural units of PSA can be distinguished completely with the help of $^{1}H,^{1}H$-COSY, and $^{13}C,^{1}H$-HSQC techniques. Consequently, the degree of branching (DB) of various products can be determined. Details of DB determination can be found in the Supporting Information. The relation between the DB and the β-CD:AP ratio is illustrated in Figure 3. From these results, it can be seen that the DB of the PSAs decreases with increasing β-CD.

The final products are very stable. The polymerized samples with CD have a higher decomposition temperature than pure PSA, which means that the polymer chains are stabilized by inclusion complexation with β-CD (see Supporting Information).

Now we have a clear image of how to control the branched structure of PSA by adjusting the amount of β-CD. Thus, 1) changing the amount of β-CD gives samples with various architectures, 2) the β-CD does not take part in the chemical

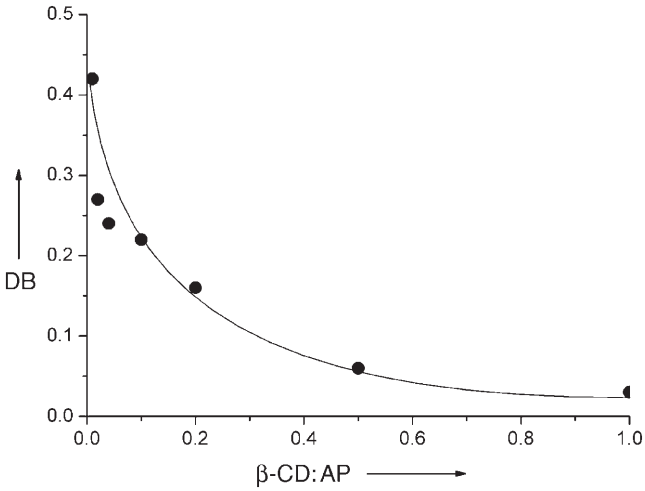
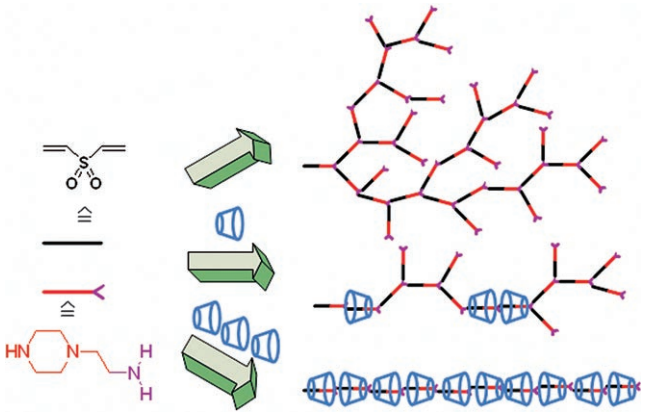


Figure 3. Relation between the molar ratio of β-CD and AP and the DB of the obtained PSA.

reaction itself, although it binds with guest molecules through host–guest interactions, and 3) β-CD remains threaded onto the polymer chains after polymerization. A diagram illustrating these concepts is given in Scheme 1.



Scheme 1. Proposed mechanism for an architecturally controlled polymerization.

Molecular simulations gave a possible explanation as to how β-CD controls the structure of the final products. They showed that an AP molecule matches the β-CD cavity perfectly. The primary amino group in the AP molecule has two hydrogen atoms, one in an equatorial position and the other in an axial position. The former can form a hydrogen bond with adjacent 6-OH groups in β-CD to stabilize the inclusion compound, and the latter, together with the secondary amine, can react with the vinyl groups of DV. Moreover, if an AP molecule is present in the CD cavity, steric effects also favor the formation of linear units. It seems that AP units encapsulated by β-CD molecules behave as bifunctional monomers during polymerization, and this explains why the DB of the PSAs decreases with increasing amounts of β-CD.

 © 2006 Wiley-VCH Verlag GmbH & Co. KGaA, Weinheim

Copolymerization of AP and DV is a typical ($A_2 + BB'_2$)-type reaction. In fact, this physical protection approach is also feasible for AB_2, AB_3, and other $A_n + B_m$ or A_nB_m polymerizations. For instance, CD can be used to control the cross-linking in a polymerization system. It is well known that if an A_2 monomer (DV) and a B_4 monomer (hexamethylenediamine; HDA) are mixed together, chemical cross-linking takes place. However, adding β-CD to such a system means that β-CD will form an inclusion complex with HDA, and this complex will behave as bifunctional monomer in the polymerization. Thus, upon adding a small amount of β-CD the product changes from a gel to a water-soluble polymer. Figure 4 shows that further increasing the amount of β-CD

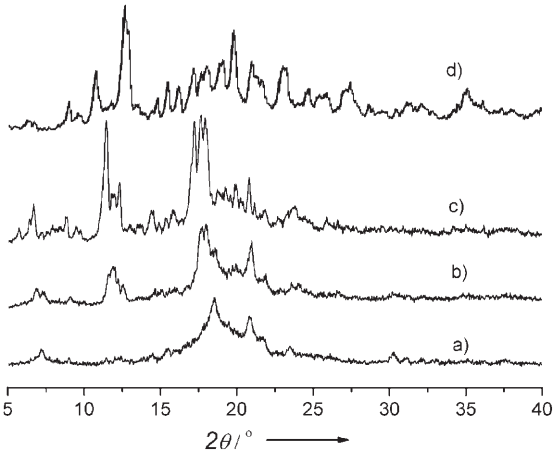


Figure 4. Diffractograms of copolymers of HDA and DV for different β-CD/HDA ratios: a) 0.2:1; b) 0.5:1; c) 1:1; d) 1:0.

reduces the area of the amorphous halo and that the characteristic reflections at $2\theta = 11.66°$ and 18.00°, which correspond to channel-like structures,[10] become stronger and stronger, thus indicating the formation of a linear polymer in the presence of large amounts of β-CD. Similarly, the solid-state CP/MAS ^{13}C NMR spectra (Figure 5) confirm that the β-CD molecules are threaded onto the polymer chains.[11] Therefore, the cross-linking of a polymerization system can be well controlled by adjusting the amount of β-CD.

In conclusion, a supramolecular method to control polymer architecture by merely adjusting the amount of host molecules present has been developed. Using this method, polymers with a large number of unreacted functional groups "inhibited" by β-CD have been obtained. These groups can be "re-activated" after removal of β-CD, thus allowing further modifications. For example, linear PSA can react with the intermediate $AabB'_2$ formed by AP and DV to form a dendronized polymer. Similarly, polymer brushes can be produced from the reaction of linear PSA with piperazine and DV. All the polymerizations described herein were carried out in aqueous solution, although the reactions can also be performed in organic solvents such as DMF and DMSO. However, we found that an aqueous solution is the most efficient system, thus illustrating that hydrophobic interactions have an important influence on the polymeri-

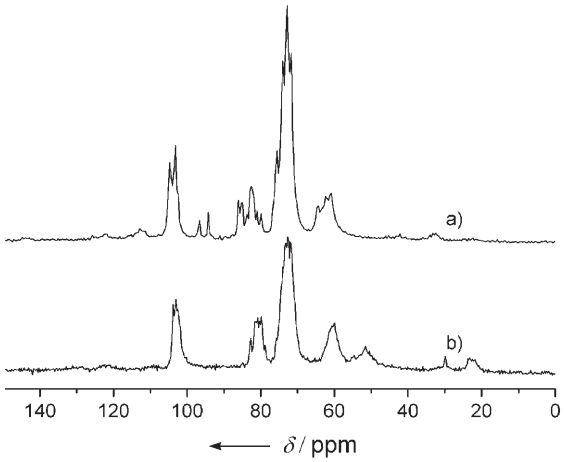


Figure 5. Solid-state CP/MAS ^{13}C NMR spectra of a) pure β-CD and b) a copolymer of HDA and DV (β-CD/HDA = 1:1).

zation. Although the scope of suitable monomers is limited by the aqueous medium, this is a green way to synthesize polymers, which is important for both science and industry.[4a,5a] Other compounds besides CD, such as crown ethers and calixarenes, can also be used as hosts. Therefore, this approach can be extended to organic solvents for some systems.

Experimental Section

Inclusion between AP and β-CD: Purified β-CD (5.675 g, 5 mmol) was added to 100 mL of distilled water. The mixture was heated to 50 °C to get a clear solution, and then AP (5.168 g, 40 mmol) was added. After stirring at this temperature for 30 min, the solution was further heated to 70 °C and stirred for another 5 h. The solution was then kept in a refrigerator at 5 °C for recrystallization. The filtered precipitate was washed with cold distilled water to remove free AP. Finally, the white precipitate was dried under vacuum at 100 °C for 24 h. Element analysis for one AP molecule encapsulated by one β-CD molecule ($C_{48}H_{85}N_3O_{35}$): calcd. C 44.98, H 6.91, N 3.48; found C 45.27, H 6.78, N 3.32.

Copolymerization of AP and DV: A typical copolymerization procedure (where the feed ratio of β-CD to AP is 0.1:1) is as follows. β-CD (113.5 mg, 0.1 mmol) was dissolved in 20 mL of distilled water and then AP (129.21 mg, 1 mmol) was added. This mixture was stirred at 70 °C for 5 h. After cooling the solution to room temperature, DV (118.15 mg, 1 mmol) was added. The reaction bulb was then sealed and filled with nitrogen to avoid oxidation. After stirring for 120 h at 40 °C, the reaction mixture was freeze-dried to remove the solvent. Dialysis was performed with a Cellu·Sep H1 membrane, with a nominal molecular weight cut-off of 2000 $g\,mol^{-1}$ (MFPI Inc.), in order to remove free β-CD and unreacted monomers. The dialysis procedure was carried out in distilled water for 48 h. β-CD can be removed by dialysis for linear polymers, whereas for those polymers with a high degree of branching an enzyme degradation method can be used.[5c] Further details of the experiments and analysis can be found in the Supporting Information.

Copolymerization of HDA and DV: A typical copolymerization procedure (β-CD:HDA = 0.1:1) is as follows. β-CD (113.5 mg, 0.1 mmol) and HDA (116.2 mg, 1 mmol) were dissolved in 20 mL of distilled water and the solution was kept at 70 °C for 5 h. After cooling the solution to room temperature, DV (118.15 mg, 1 mmol) was

 © 2006 Wiley-VCH Verlag GmbH & Co. KGaA, Weinheim

added. After stirring for 120 h at 50 °C, the mixture was dialyzed and freeze-dried to remove solvent and unreacted monomers.

Received: July 1, 2005
Revised: September 30, 2005
Published online: November 22, 2005

Keywords: cyclodextrins · polymers · supramolecular chemistry · synthesis design

[1] a) J. M. DeSimone, *Science* **1995**, *269*, 1060; b) J. M. J. Fréchet, M. Henmi, I. Gitsov, S. Aoshima, M. R. Leduc, R. B. Grubbs, *Science* **1995**, *269*, 1080.
[2] a) A. Harada, M. Kamachi, *Macromolecules* **1990**, *23*, 2821; b) A. Harada, J. Li, M. Kamachi, *Nature* **1993**, *364*, 516; c) T. Ooya, H. Mori, M. Terano, *Macromol. Rapid Commun.* **1995**, *16*, 259; d) C. C. Rusa, C. Luca, A. E. Tonelli, *Macromolecules* **2001**, *34*, 1318.
[3] a) L. Jullien, B. Canceill, J. M. Lehn, *J. Am. Chem. Soc.* **1996**, *118*, 5432; b) G. Wenz, B. Keller, *Angew. Chem.* **1992**, *104*, 201; *Angew. Chem. Int. Ed. Engl.* **1992**, *31*, 197; c) M. B. Steinbrunn, G. Wenz, *Angew. Chem.* **1996**, *108*, 2274; *Angew. Chem. Int. Ed. Engl.* **1996**, *35*, 2139; d) R. Breslow, J. B. Doherty, G. Guillot, C. Lipsey, *J. Am. Chem. Soc.* **1978**, *100*, 3227; e) J. P. Sylvestre, A. V. Kabashin, E. Sacher, M. Meunier, J. H. T. Luong, *J. Am. Chem. Soc.* **2004**, *126*, 7176.
[4] a) H. Ritter, M. Tabatabai, *Prog. Polym. Sci.* **2002**, *27*, 1713; b) H. Ritter, O. Sadowski, E. Tepper, *Angew. Chem.* **2003**, *115*, 3279; *Angew. Chem. Int. Ed.* **2003**, *42*, 3171; c) R. Saito, K. Yamaguchi, *Macromolecules* **2003**, *36*, 9005; d) Y. Liu, Y. L. Zhao, *Macromolecules* **2004**, *37*, 6362; e) J. Li, X. Ni, K. Leong, *Angew. Chem.* **2003**, *115*, 73; *Angew. Chem. Int. Ed.* **2003**, *42*, 69.
[5] a) V. Alupei, I. C. Alupei, H. Ritter, *Macromol. Rapid Commun.* **2005**, *26*, 40; b) V. Alupei, I. C. Alupei, H. Ritter, *Macromol. Rapid Commun.* **2003**, *24*, 527; c) T. Uyar, M. Rusa, A. E. Tonelli, *Macromol. Rapid Commun.* **2004**, *25*, 1382.
[6] a) Y. H. Kim, *J. Am. Chem. Soc.* **1992**, *114*, 4947; b) M. W. Weimer, J. M. J. Fréchet, I. Gitsov, *J. Polym. Sci. Part A: Polym. Chem.* **1998**, *36*, 955; c) H. Frey, D. Holter, *Polym. Mater.* **1997**, *77*, 220; d) C. Lach, H. Frey, *Macromolecules* **1998**, *31*, 2381.
[7] a) C. Gao, D. Yan, *Chem. Commun.* **2001**, 107; b) D. Yan, C. Gao, *Macromolecules* **2000**, *33*, 7693; c) P. Froehling, J. Brackman, *Macromol. Symp.* **2000**, *151*, 581; d) R. A. T. M. van Benthem, N. Meijerink, E. Gelade, C. G. de Koster, D. Muscat, P. E. Froehling, P. H. M. Hendriks, C. J. A. A. Vermeulen, T. J. G. Zwartkruis, *Macromolecules* **2001**, *34*, 3559.
[8] a) J. Szejtli, *Cyclodextrin Technology*, Kluwer, Dordrecht, **1998**, p. 130–134; b) M. Miyauchi, A. Harada, *J. Am. Chem. Soc.* **2004**, *126*, 11418; c) Y. Inoue, T. Okuda, Y. Miyada, R. Chujo, *Carbohydr. Res.* **1984**, *125*, 65; d) G. A. Webb, *Annu. Rep. NMR Spectrosc.* **1993**, *27*.
[9] a) R. Rydém, J. Carlfors, P. Stilbs, *J. Incl. Phenom.* **1983**, *1*, 159; b) K. S. Cameron, L. Fielding, *Magn. Reson. Chem.* **2002**, *40*, 106; c) R. Wimmer, F. L. Aachmann, K. L. Larsen, S. B. Petersen, *Carbohydr. Res.* **2002**, *337*, 841; d) J. Szejtli, *Chem. Rev.* **1998**, *98*, 1743.
[10] a) K. Harata, *Chem. Rev.* **1998**, *98*, 1803; b) A. Harada, M. Kamachi, *J. Chem. Soc. Chem. Commun.* **1990**, 1322; c) A. Harada, M. Okada, J. Li, *Macromolecules* **1995**, *28*, 8406.
[11] a) M. J. Gidley, S. M. Bociek, *J. Am. Chem. Soc.* **1988**, *110*, 3820; b) A. Harada, J. Li, M. Kamachi, *Macromolecules* **1993**, *26*, 5698.

 © 2006 Wiley-VCH Verlag GmbH & Co. KGaA, Weinheim

Biosensors

DOI: 10.1002/anie.200502589

Fast Colorimetric Sensing of Adenosine and Cocaine Based on a General Sensor Design Involving Aptamers and Nanoparticles**

*Juewen Liu and Yi Lu**

Aptamers are nucleic acid based binding molecules that are obtained through a combinatorial selection process known as systematic evolution of ligands by exponential enrichment (SELEX).[1,2] They are emerging as a new class of molecules that can rival antibodies in terms of the broad range of molecules they can selectively bind.[3,4] In comparison with antibodies, aptamers, particularly DNA aptamers, are relatively easy to obtain, more stable to biodegradation, and less vulnerable to denaturation. Therefore they are prime candidates as sensors in a number of applications, such as environmental monitoring and medical diagnostics. The key challenge to their successful application is transforming the aptamer-binding events into physically detectable signals. To meet the challenge, a number of methods have been developed, most of which involve fluorescence-based detection.[5–13] Simple colorimetric sensors can eliminate the use of analytical instruments and have attracted much attention recently.[14–17] For example, organic-dye replacement was employed to design a colorimetric cocaine sensor.[14] However, an appropriate dye has to be found for a designated aptamer, and a waiting time of 12 hours is needed to observe a color change. Cationic conjugated polymers form complexes of different color with aptamers in the presence or absence of a target analyte. A number of colorimetric sensors were made with this method.[15]

The high extinction coefficients and distance-dependent optical properties have made metallic nanoparticles very attractive in DNA-related colorimetric assays,[18–20] such as the detection of DNA with high sequence selectivity,[21,22] and the detection of metal ions[23,24] and other analytes.[16,17] Recently, aptamer-functionalized gold nanoparticles were employed to detect thrombin. This system took advantage of the fact that each thrombin molecule binds two aptamers, so nanoparticles

[*] J. Liu, Dr. Y. Lu
Department of Chemistry
Beckman Institute for Advanced Science and Technology
University of Illinois at Urbana–Champaign
Urbana, IL, 61801 (USA)
Fax: (+1) 217-333-2685
E-mail: yi-lu@uiuc.edu

[**] This work was supported by the US Army Research Laboratory and the US Army Research Office under grant number DAAD19-03-1-0227, the National Science Foundation through a Science and Technology Center of Advanced Materials for Purification of Water with Systems (WaterCAMPWS), and a Nanoscale Science and Engineering Center (NSEC) program.

Supporting information for this article is available on the WWW under http://www.angewandte.org or from the author.

WILEY InterScience DISCOVER SOMETHING GREAT
© 2006 Wiley-VCH Verlag GmbH & Co. KGaA, Weinheim

could be cross-linked by thrombin. Subsequent catalytic growth of the gold nanoparticles was needed for detection with this sensor.[16a] We have previously reported the use of effector-regulated DNA enzymes (aptazymes) for colorimetric adenosine detection.[17] As the aptazyme-cleavage reaction and the assembly of nanoparticles had to be carried out separately, more than one hour was needed for detection.

With the initial success in designing aptamer-based colorimetric sensors, it remains desirable to have a more general method to construct sensors for any aptamer of interest. Preferably, the sensors should be simple to design, easy to operate, give a fast color change, and have a minimal consumption of materials. We herein describe a general method for sensor design that can meet all of the above criteria. To demonstrate the generality of this method, sensors for adenosine and cocaine were constructed, both of which can produce a color change within seconds at room temperature.

We first constructed an adenosine sensor as shown in Figure 1. The sensor was made of nanoparticle aggregates containing three components: gold nanoparticles (13 nm diameter) functionalized with 3′-thiol-modified DNA (3′$Adap_{Au}$), or 5′-thiol-modified DNA (5′$Adap_{Au}$), and a linker DNA ($Linker_{Adap}$) molecule. 3′$Adap_{Au}$ and 5′$Adap_{Au}$ were assembled with $Linker_{Adap}$ to form aggregates, which displayed a faint purple color when suspended in solution. $Linker_{Adap}$ can be divided into three segments. The first segment (in purple) hybridized with a 3′$Adap_{Au}$ nanoparticle. The second segment (in gray) hybridized with the last five nucleotides of a 5′$Adap_{Au}$ nanoparticle. The third segment (in green), the aptamer sequence for adenosine,[25] hybridized with the other seven nucleotides on the 5′$Adap_{Au}$ nanoparticle. In the presence of adenosine, the aptamer changed its structure to bind adenosine.[9,26–28] As a result, only five base pairs were left to hybridize with 5′$Adap_{Au}$, which was unstable at room temperature. Therefore, the 5′$Adap_{Au}$ particles dissociated from the 3′$Adap_{Au}$ particles, resulting in disassembly of the aggregates. Upon disassembly, the color of the system changed from purple to red. Niemeyer and coworkers employed DNA base-pairing interactions, rather than adenosine/aptamer interactions, to disassemble nanoparticle aggregates.[29] The method involving adenosine-induced disassembly was inspired by the recent reports from Nutiu and Li, who discovered that an aptamer underwent a structure-switching process upon binding to target molecules. Fluorescent sensors based on this behavior were developed.[9,30,31]

To study disassembly of nanoparticle aggregates, it is helpful to know the size of an aggregate and the number of linkages among particles. The nanoparticle aggregates assembled by $Linker_{Adap}$ were first characterized by transmission electron microscopy (TEM). Most aggregates were composed of thousands of nanoparticles forming a compact structure of several micrometers. The plasmon frequency of such aggregated particles decreased, which was responsible for the purple color. Typical TEM images are presented in the Supporting Information. The number of thiol-modified DNA molecules attached to each 13-nm-diameter nanoparticle was calculated to be 94 on the basis of the average results reported by two independent groups by assuming the same surface coverage.[32,33] The concentrations of $Linker_{Adap}$ and nanoparticles when preparing the aggregates were 100 nM and 12 nM (6 nM each of 5′$Adap_{Au}$ and 3′$Adap_{Au}$), respectively. As a result, each nanoparticle was connected by approximately 17 $Linker_{Adap}$ aptamers to other nanoparticles.

Such aptamer-linked nanoparticle aggregates were used directly as a colorimetric sensor for the detection of adenosine. The absorbance spectrum of the purple-colored adenosine sensor is shown in Figure 2a (blue curve). The nanoparticle aggregates disassembled within 10 seconds of adding adenosine (2 mM) to give a red colored solution (red curve, Figure 2A). Upon disassembly of the aggregates, the absorbance at 522 nm increased, while the absorbance at 700 nm decreased. We chose to use the absorbance ratio at these two wavelengths to quantify the color of the system, with a high ratio associated with red colored dispersed particles and a low ratio associated with purple colored aggregates. The kinetics of the color change at various adenosine concentrations were monitored by UV/Vis spectroscopy. Faster rates of color change were observed at higher adenosine levels (Figure 2B). The color change was instantaneous in the presence of 2 mM adenosine. Quantitative analysis was performed by monitoring the absorbance ratio at one minute after the addition of adenosine

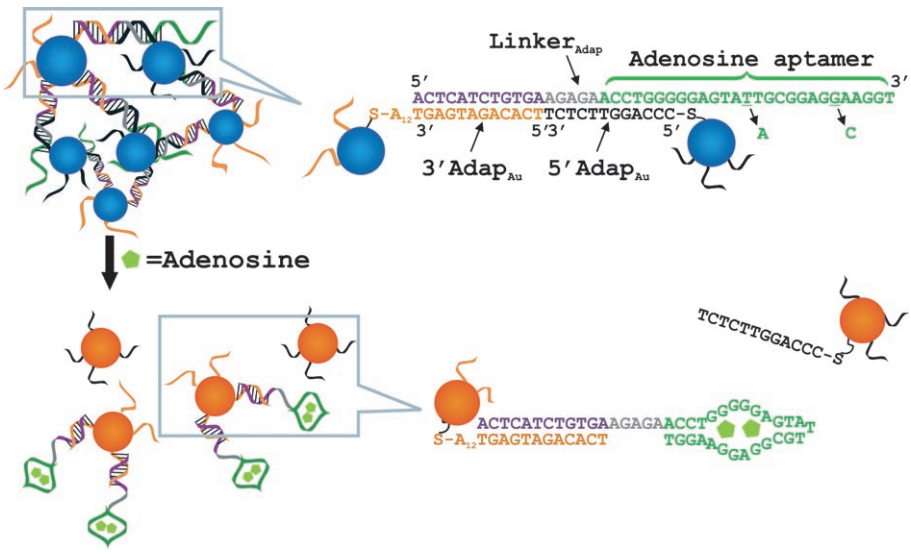


Figure 1. Schematic representation of colorimetric detection of adenosine. The DNA sequences are shown in the right side of the figure. The A_{12} in 3′$Adap_{Au}$ denotes a 12-mer polyadenine chain. In a control experiment, a mutated linker with the two mutations shown by the two short black arrows was used. Note: The drawing is not to scale.

© 2006 Wiley-VCH Verlag GmbH & Co. KGaA, Weinheim

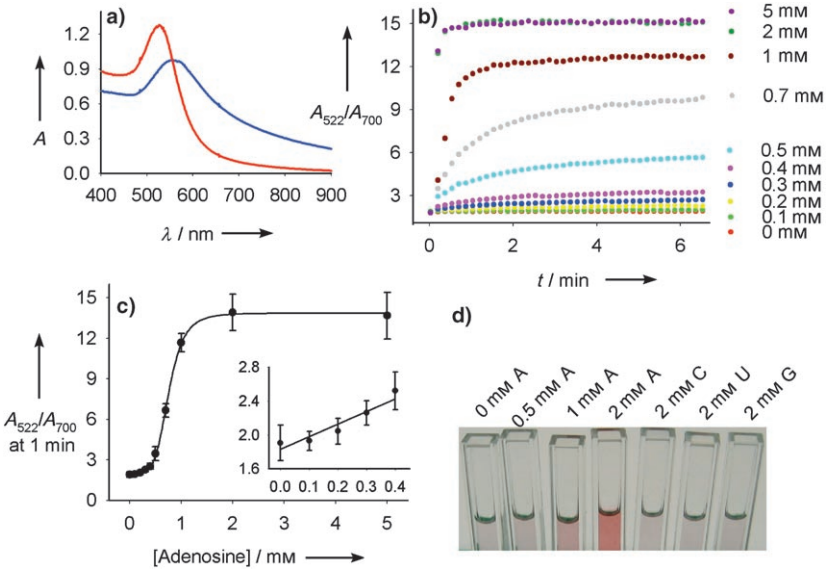


Figure 2. A) Absorbance spectra of the adenosine sensor before (blue) and 10 seconds after (red) the addition of adenosine (2 mM). B) Kinetics of the color change at various concentrations of adenosine. C) Quantification of adenosine concentration by monitoring the absorbance ratio one minute after the addition of adenosine. The data were obtained from three independent measurements and the error bars indicate the standard deviation. D) Photograph of solutions of the sensor one minute after the addition of adenosine or other nucleosides at room temperature. A = adenosine, C = cytidine, U = uridine, G = guanosine.

(Figure 2C), from which adenosine can be detected in concentrations from 0.3 to 2 mM. At low adenosine concentration, only a small fraction of the gold nanoparticles was released from the aggregates. This could be attributed to the fact that there were around 17 linkages for each nanoparticle. All of these linkages need to be broken before a nanoparticle can be released. Therefore, the change in absorbance was very small in the presence of the high background absorbance of the remaining aggregates. As a result, the sensitivity of the current detection method is not as high as that of fluorescence-based detection methods.[9,30,31] The color change was directly observed by the naked eye and allowed qualitative or semiquantitative analysis. An image taken one minute after the addition of nucleosides at different concentration levels is shown in Figure 2D. The color changed from faint purple to red with increasing concentrations of adenosine, whereas the color remained purple for samples with other nucleosides, which suggests that the sensor has high selectivity.

A control experiment was performed to support the mechanism of disassembly shown in Figure 1. Instead of the original linker ($Linker_{Adap}$), a mutated linker was employed to assemble nanoparticles. The sites of mutation are marked in Figure 1; aptamers with this mutated sequence had been shown to be incapable of binding ATP.[9] No color change was observed for aggregates linked by the mutated linker after adding adenosine (see Supporting Information), which strongly suggested that the observed color change was caused by adenosine/aptamer interactions rather than being an artifact. Structural studies by NMR spectroscopy indicated that each adenosine aptamer binds two AMP molecules.[26] As the aptamer has similar affinity for ATP, AMP, and adenosine, two adenosine molecules were drawn for each aptamer in Figure 1.

To test the generality of the method, we constructed a colorimetric sensor for cocaine based on a reported cocaine aptamer, with slight modifications.[7,8] The 3′ and 5′ ends did not form perfect Watson–Crick pairs in the reported aptamer, and no cocaine-induced color change was observed. When these bases were paired, the nanoparticle aggregates assembled with the new aptamer linker ($Linker_{Coc}$, Figure 3) showed a cocaine-induced color change (Figure 4). The rate of color change increased with increasing cocaine concentration (Figure 4A), from which cocaine could be quantified in the range from 50 to 500 μM. An image of the sensor alone and with either adenosine (1 mM) or cocaine (1 mM) is also shown (Figure 4B, inset). Similarly to the adenosine sensor, the colorimetric cocaine sensor can also produce an instantaneous color change.

In conclusion, we have demonstrated a general design of colorimetric sensors based on the disassembly of nanoparticle aggregates linked by aptamers. The sensors are easy to use

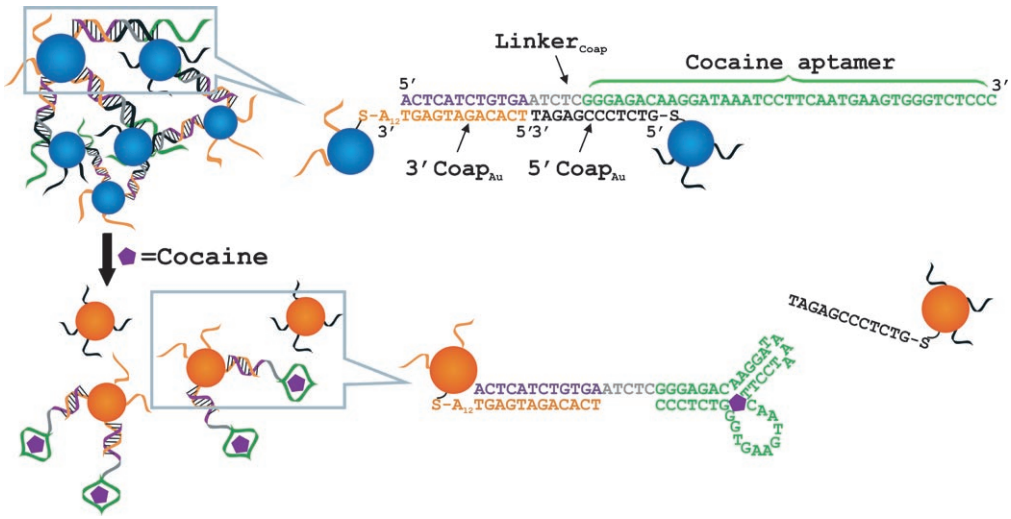


Figure 3. Schematic representation of the colorimetric detection of cocaine based on cocaine-induced disassembly of nanoparticle aggregates linked by a cocaine aptamer.

 © 2006 Wiley-VCH Verlag GmbH & Co. KGaA, Weinheim

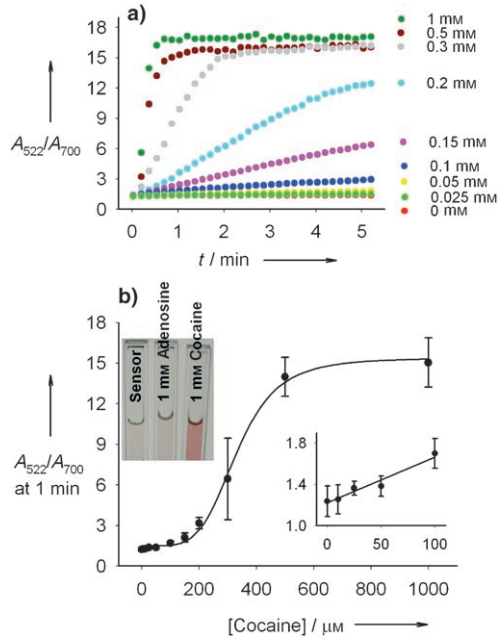


Figure 4. A) Kinetics of the color change of the cocaine sensor at various concentrations of cocaine. B) Quantification of cocaine concentration by monitoring the absorbance ratio one minute after the addition of cocaine. The data were obtained from three independent measurements and the error bars indicate the standard deviation. Inset: Photograph of a solution of the sensor one minute after the addition of cocaine or adenosine at room temperature.

and show a fast color change. As no special features on the aptamers are required, the design should be applicable to any aptamer of choice. Such simple colorimetric sensors should find applications in a diverse range of areas, such as medical diagnostics, environmental monitoring, and the electronic industry.

Experimental Section

Materials: All DNA samples were purchased from Integrated DNA Technologies Inc. (Coralville, IA). The linker DNA molecules were purified by gel electrophoresis, whereas the thiol-modified DNA molecules were purified by the standard desalting method. Adenosine, cytidine, uridine, guanosine, and cocaine hydrochloride were purchased from Aldrich (St. Louis, MO). Gold nanoparticles (13 nm diameter) were synthesized by the citrate reduction method.[22] Thiol-modified DNA was activated with two equivalents of tris(2-carboxyethyl)phosphine hydrochloride (TCEP). TCEP-activated thiol-modified DNA and gold nanoparticles were mixed at room temperature for 16 h or longer, and NaCl (100 mM) and tris(hydroxymethyl)aminomethane (tris) acetate (5 mM) were added to the solution to give a pH value of 8.2. The solution was left at room temperature for another 25 days, and the DNA-functionalized nanoparticles were purified by centrifugation and removal of supernatant before use.

Sensor preparation: Solutions of 5′-thiol-modified DNA (5′$Adap_{Au}$ or 5′$Coap_{Au}$; 500 μL; $A_{522\,nm} = 2.2$; ca. 12 nM) and 3′-thiol-modified DNA (3′$Adap_{Au}$ or 3′$Coap_{Au}$; 500 μL; $A_{522\,nm} = 2.2$; ca. 12 nM) were mixed in the presence of NaCl (300 mM), tris acetate buffer (25 mM; pH 8.2), and linker ($Linker_{Adap}$ or $Linker_{Coap}$; 100 nM). The samples were stored at 4 °C for 90 minutes. Nanoparticles aggregated and changed color from red to purple in this process. The samples were centrifuged, and the precipitates were collected and dispersed in the same buffer (300 mM NaCl; 25 mM tris acetate; pH 8.2).

Detection: To detect adenosine or cocaine, 100 μL of the sensor suspension described above was added to a small volume of concentrated adenosine solution. The buffer contained 300 mM NaCl for adenosine detection and 150 mM NaCl for cocaine detection. The color change was monitored with a UV/Vis spectrophotometer (Hewlett–Packard 8453) at 28 °C for adenosine detection and at 30 °C for cocaine detection. To monitor the color change with the naked eye, the experiments were performed at room temperature (ca. 23 °C).

Received: July 25, 2005
Published online: November 17, 2005

Keywords: aggregation · DNA structures · nanotechnology · nucleosides · sensors

[1] A. D. Ellington, J. W. Szostak, *Nature* **1990**, *346*, 818.
[2] C. Tuerk, L. Gold, *Science* **1990**, *249*, 505.
[3] S. D. Jayasena, *Clin. Chem.* **1999**, *45*, 1628.
[4] D. S. Wilson, J. W. Szostak, *Annu. Rev. Biochem.* **1999**, *68*, 611.
[5] S. D. Jhaveri, R. Kirby, R. Conrad, E. J. Maglott, M. Bowser, R. T. Kennedy, G. Glick, A. D. Ellington, *J. Am. Chem. Soc.* **2000**, *122*, 2469.
[6] X. Fang, Z. Cao, T. Beck, W. Tan, *Anal. Chem.* **2001**, *73*, 5752.
[7] M. N. Stojanovic, P. de Prada, D. W. Landry, *J. Am. Chem. Soc.* **2000**, *122*, 11547.
[8] M. N. Stojanovic, P. de Prada, D. W. Landry, *J. Am. Chem. Soc.* **2001**, *123*, 4928.
[9] R. Nutiu, Y. Li, *J. Am. Chem. Soc.* **2003**, *125*, 4771.
[10] J. J. Li, X. Fang, W. Tan, *Biochem. Biophys. Res. Commun.* **2002**, *292*, 31.
[11] N. Hamaguchi, A. Ellington, M. Stanton, *Anal. Biochem.* **2001**, *294*, 126.
[12] R. Yamamoto, T. Baba, P. K. Kumar, *Genes Cells* **2000**, *5*, 389.
[13] Y. Liu, C. Lin, H. Li, H. Yan, *Angew. Chem.* **2005**, *117*, 4407; *Angew. Chem. Int. Ed.* **2005**, *44*, 4333.
[14] M. N. Stojanovic, D. W. Landry, *J. Am. Chem. Soc.* **2002**, *124*, 9678.
[15] H.-A. Ho, M. Leclerc, *J. Am. Chem. Soc.* **2004**, *126*, 1384.
[16] a) V. Pavlov, Y. Xiao, B. Shlyahovsky, I. Willner, *J. Am. Chem. Soc.* **2004**, *126*, 11768; b) C. -C. Huang, Y. -F. Huang, Z. Cao, W. Tan, H. -T. Chang, *Anal. Chem.* **2005**, *77*, 5735.
[17] J. Liu, Y. Lu, *Anal. Chem.* **2004**, *76*, 1627.
[18] N. L. Rosi, C. A. Mirkin, *Chem. Rev.* **2005**, *105*, 1547.
[19] C. M. Niemeyer, *Angew. Chem.* **2001**, *113*, 4254; *Angew. Chem. Int. Ed.* **2001**, *40*, 4128.
[20] E. Katz, I. Willner, *Angew. Chem.* **2004**, *116*, 6166; *Angew. Chem. Int. Ed.* **2004**, *43*, 6042.
[21] R. Elghanian, J. J. Storhoff, R. C. Mucic, R. L. Letsinger, C. A. Mirkin, *Science* **1997**, *277*, 1078.
[22] J. J. Storhoff, R. Elghanian, R. C. Mucic, C. A. Mirkin, R. L. Letsinger, *J. Am. Chem. Soc.* **1998**, *120*, 1959.
[23] J. Liu, Y. Lu, *J. Am. Chem. Soc.* **2004**, *126*, 12298.
[24] J. Liu, Y. Lu, *J. Am. Chem. Soc.* **2003**, *125*, 6642.
[25] D. E. Huizenga, J. W. Szostak, *Biochemistry* **1995**, *34*, 656.
[26] C. H. Lin, D. J. Patel, *Chem. Biol.* **1997**, *4*, 817.
[27] T. Hermann, D. J. Patel, *Science* **2000**, *287*, 820.
[28] J. S. Hartig, S. H. Najafi-Shoushtari, I. Gruene, A. Yan, A. D. Ellington, M. Famulok, *Nat. Biotechnol.* **2002**, *20*, 717.
[29] P. Hazarika, B. Ceyhan, C. M. Niemeyer, *Angew. Chem.* **2004**, *116*, 6631; *Angew. Chem. Int. Ed.* **2004**, *43*, 6469.
[30] R. Nutiu, Y. Li, *Chem. Eur. J.* **2004**, *10*, 1868.

 © 2006 Wiley-VCH Verlag GmbH & Co. KGaA, Weinheim

[31] R. Nutiu, Y. Li, *Angew. Chem.* **2005**, *117*, 1085; *Angew. Chem. Int. Ed.* **2005**, *44*, 1061.
[32] L. M. Demers, C. A. Mirkin, R. C. Mucic, R. A. Reynolds III, R. L. Letsinger, R. Elghanian, G. Viswanadham, *Anal. Chem.* **2000**, *72*, 5535.
[33] C. M. Niemeyer, B. Ceyhan, P. Hazarika, *Angew. Chem.* **2003**, *115*, 5944; *Angew. Chem. Int. Ed.* **2003**, *42*, 5766.

 © 2006 Wiley-VCH Verlag GmbH & Co. KGaA, Weinheim

Seleno-Modified RNA

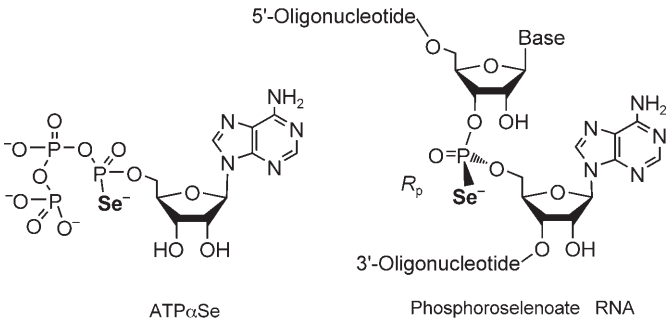
DOI: 10.1002/anie.200502215

Efficient Enzymatic Synthesis of Phosphoroselenoate RNA by Using Adenosine 5′-(α-*P*-Seleno)triphosphate**

*Nicolas Carrasco, Julianne Caton-Williams, Gary Brandt, Siming Wang, and Zhen Huang**

The discovery that RNA has a variety of biological functions in living organisms[1–3] has prompted the development of new methods to elucidate its structure and mechanism at the atomic level. X-ray crystallography is the method of choice for the elucidation of the three-dimensional structure of RNA macromolecules.[4,5] New developments in RNA X-ray crystallography have occurred due to advances in synchrotron radiation, diffraction data collection,[6,7] solid-phase synthesis of RNA oligonucleotides,[8] RNA crystallization,[9,10] and heavy-atom derivatization.[11] To further advance the field of RNA structure and function research, we have been working on the development of selenium derivatization for nucleic acid biochemistry and structure studies.[12–17]

The use of selenomethionyl proteins for multiwavelength anomalous-dispersion (MAD) phasing has revolutionized the field of protein X-ray crystallography.[18,19] This derivatization of proteins with Se has also been applied successfully in RNA structure determination through indirect derivatization of RNA that binds to the Se-derivatized protein.[11] Motivated by the phosphoroselenoate oligonucleotide structure and function studies with MAD phasing performed by Egli and co-workers,[20] we are developing the enzymatic synthesis of phosphoroselenoate nucleic acids for X-ray crystal structure studies. We report herein the first enzymatic synthesis of phosphoroselenoate RNA (Scheme 1), containing a selenium atom that replaces one of the nonbridging oxygen atoms on the phosphate group, by in vitro transcription with T7 RNA polymerase and adenosine 5′-(α-*P*-seleno)triphosphate (ATPαSe).



Scheme 1. Chemical structures of ATPαSe and phosphoroselenoate RNA. The suffix "P" indicates that the *R* or *S* nomenclature refers to the phosphorus center.

For this enzymatic synthesis, we first synthesized and characterized both diastereomeric monomers of adenosine triphosphate harboring the selenium functionality at the α-phosphate group (ATPαSe, Scheme 1) by using a modification of the procedures for the synthesis of nucleotide 5′-(α-*P*-thio)triphosphates (NTPαS)[21] and thymidine 5′-(α-*P*-seleno)triphosphate (TTPαSe).[17] The fast- and slow-moving ATPαSe isomers as represented by peaks on the reversed-phase (RP) HPLC profile were termed ATPαSe I and ATPαSe II, respectively. A DNA template (55 nucleotides) was designed to allow the incorporation of 12 A residues (Figure 1 a). The generated RNA transcript (35 nucleotides) was body-labeled by using α-[^{32}P]-cytidine 5′-triphosphate (α-[^{32}P]CTP) in the enzymatic reaction mixture for gel electrophoresis and autoradiography.

We first tested the incorporation of ATPαSe I and ATPαSe II. The results (Figure 1 b) indicated that ATPαSe I was incorporated into the RNA transcript as well as natural ATP; however, no full-length product was detected when ATPαSe II was used. Although the formation of short abortive fragments in in vitro transcription is normal,[22] surprisingly, ATPαSe I, which generated almost no short abortive sequences, led to a much cleaner reaction than natural ATP. A mixture of ATP and ATPαSe I also reduced the formation of nondesired short abortive sequences. These results suggest that ATPαSe I is an efficient substrate for T7 RNA polymerase, a finding that is consistent with an X-ray crystal structure study of the interaction between T7 RNA polymerase and NTP.[23] On the basis of the RNA polymerase recognition of the S_P diastereomer of nucleoside 5′-(α-*P*-thio)triphosphates as a substrate,[24,25] ATPαSe I is tentatively assigned as the S_P diastereomer and ATPαSe II as the R_P

[*] Dr. N. Carrasco, J. Caton-Williams, G. Brandt, S. Wang, Prof. Dr. Z. Huang
Department of Chemistry
Georgia State University
Atlanta, GA 30303 (USA)
and
Brooklyn College
Brooklyn, NY 11210 (USA)
Fax: (+1) 404-651-1416
E-mail: huang@gsu.edu

[**] This work was supported by the Georgia State University Research Program and the US National Institutes of Health (Grant no.: GM069703). We thank Dr. Martin Egli and Prof. Steven A. Benner for carefully reading this manuscript and Dr. Yanling Zhang and Sarah Shealy for assistance in MS data collection.

InterScience
© 2006 Wiley-VCH Verlag GmbH & Co. KGaA, Weinheim

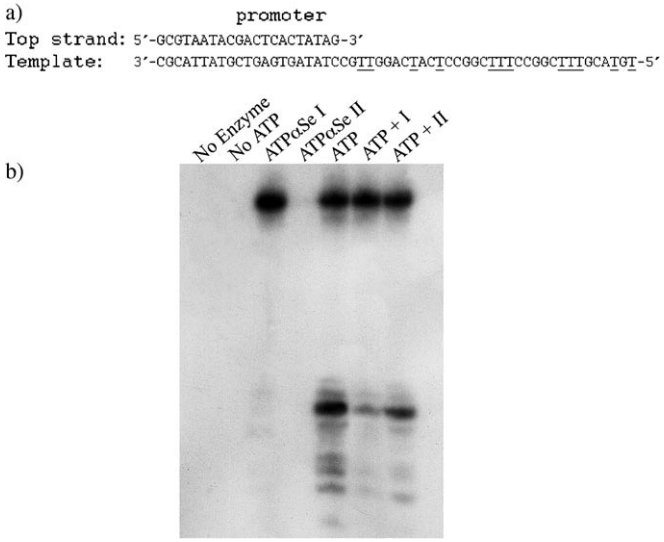


Figure 1. Enzymatic incorporation of ATPαSe into RNA by T7 RNA polymerase. a) The DNA sequences of the top strand and template. Underlined T residues in the template correspond to the locations of ATPαSe incorporated in the RNA transcript. b) Gel electrophoresis analysis of the transcription mixture after 1 h of incubation at 37 °C; each mix of ATP and ATPαSe I or II was prepared in a 1:1 ratio.

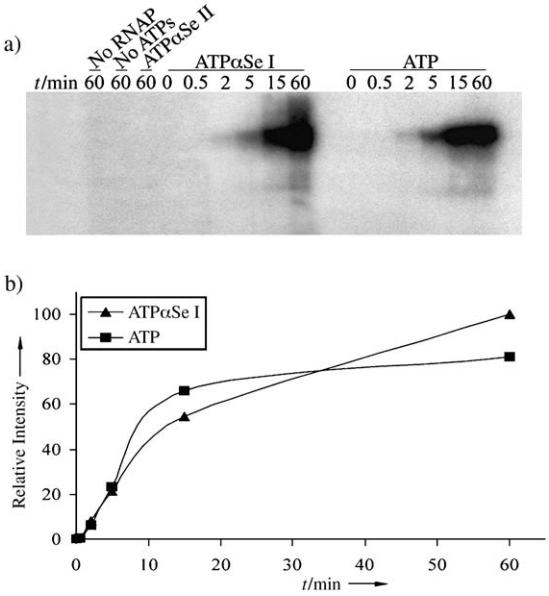


Figure 2. Time-course incorporation of ATPαSe I and ATPαSe II into RNA. Aliquots of the reaction mixture were taken at the indicated time points and quenched with 100 mM of ethylenediaminetetraacetate (EDTA); this was followed by immediate freezing in dry ice. The results are presented as a) gel electrophoresis autoradiography and b) the incorporation-versus-time plot.

diastereomer. Based on literature reports on the inversion of configuration at the phosphorous stereocenter during the enzymatic incorporation of NTPαS,[24–26] it is expected that the phosphoroselenoate RNA transcript is the R_P diastereomer.

This type of stereospecificity of T7 RNA polymerase has also been reported on the RNA incorporation of nucleoside triphosphate boranophosphates.[27] In addition, our experimental results (Figure 1b) of ATPαSe II nonincorporation and with a mixture of natural ATP and ATPαSe II indicated that ATPαSe II is neither an inhibitor nor a substrate. These results are consistent with the literature report on ATPα S II.[25] Therefore, it is possible to use ATPαSe directly for the transcription without separation of the S_P and R_P diastereomers. Since both diastereomers underwent the same treatments during their synthesis, purification, and polymerization, it is unlikely that the RNA transcript observed in the ATPαSe I reaction was due to oxidation of ATPαSe I to ATP.

To obtain more insight into the incorporation of ATPα Se I into RNA, we carried out a time-course experiment (Figure 2) with ATP as a positive control. The results indicate that incorporation of ATPαSe I is as efficient as that of natural ATP, and ATPαSe I gives approximately 20% more RNA product than ATP, probably due to formation of many fewer nondesired short abortive sequences. The minimum formation of nondesired short abortive sequences and the formation of more desired RNA product suggest a favorable interaction between T7 RNA polymerase and ATPαSe I.

To confirm the incorporation of ATPαSe I into RNA, the RNA transcript was subjected to digestion with snake venom phosphodiesterase I, which is an exonuclease that degrades both DNA and RNA successively in the 3′→5′ direction.[28] The result (Figure 3) indicates that the formed phosphoroselenoate RNA can indeed resist the enzymatic digestion. Its digestion was four to five times slower than that of the

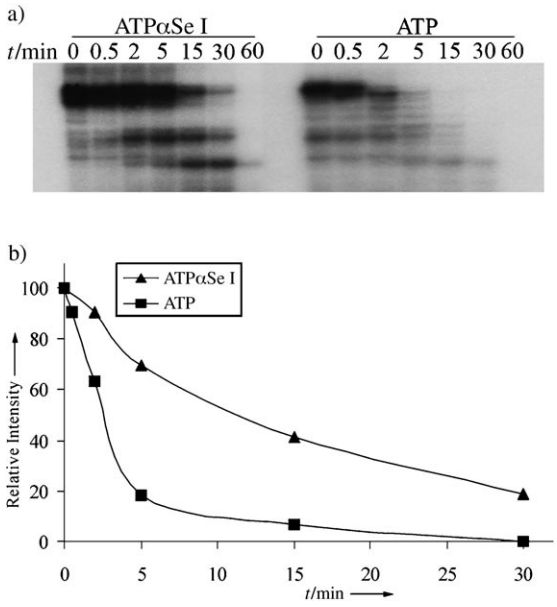


Figure 3. Time-course enzymatic digestion of phosphoroselenoate RNA with snake venom phosphodiesterase I. The results are presented as a) gel electrophoresis autoradiography and b) the digestion-versus-time plot.

corresponding nonmodified RNA. This finding is consistent with reports on the enzymatic digestion resistance of phosphoroselenoate DNA,[17] phosphorothioate DNA and RNA,[29] and boranophosphate DNA and RNA.[30]

In addition, the MALDI-TOF MS analysis[31] also confirms incorporation of 12 Se atoms per RNA molecule

 © 2006 Wiley-VCH Verlag GmbH & Co. KGaA, Weinheim

(Figure 4). The measured average mass difference between the nonmodified RNA (11 605 Da) and the Se-modified RNA (12 359 Da, containing 12 Se-modified A units) is 754 Da. As the theoretical mass difference between the modified and

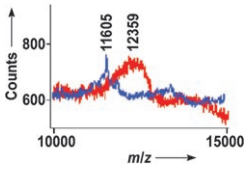


Figure 4. The MALDI-TOF MS analysis of Se-modified RNA transcription. Nonmodified RNA (blue) with a mass of 11 605 Da and Se-modified RNA (red) with an average mass of 12 359 Da. Their mass difference of 754 reflects incorporation of 12 Se-modified A units ($12\,Se-12\,O=12\times79-12\times16=756$).

nonmodified RNAs is 756 Da ($12\,Se-12\,O=12\times79-12\times16=756$), this experimental mass difference reflects the incorporation of 12 Se atoms per RNA molecule. The broad peak of the Se-modified RNA (average 12 359 Da) is probably caused by the satellite peaks from selenium isotopes (major ones: 76, 77, 78, 80, 82) and the formation of $N-1$ and $N+1$ minor products, which are commonly observed in RNA transcription.[22a] This minor 3′ heterogeneity of the transcribed RNA, also revealed by the gel electrophoresis analysis (Figure 2), can be removed by a ribozyme system.[32]

In summary, we have synthesized ATPαSe and enzymatically synthesized Se-modified RNA for the first time. We have found that only one diastereomer (ATPαSe I, presumably the S_P isomer) is efficiently recognized by T7 RNA polymerase for synthesizing diastereomerically pure phosphoroselenoate RNA (presumably R_P). As T7 RNA polymerase specifically recognizes just one diastereomer (ATPαSe I) and the other diastereomer (ATPαSe II) does not inhibit the transcription, prior separation of these two diastereomers is not necessary for preparation of diastereomerically pure RNA transcripts. In addition, our results suggest that ATPαSe I is an efficient substrate for T7 RNA polymerase and its use has shown advantages over ATP transcription: almost no short abortive sequences and a higher RNA transcription yield. Formation of almost no short abortive sequences also makes RNA purification by gel electrophoresis or HPLC easier. By following the established procedures,[9] this novel and efficient method can be used in particular for the preparation of long phosphoroselenoate RNA on a large scale (multimilligram quantity), which would be unattainable by using solid-phase synthesis. Introduction of multi-Se labels through transcription is very useful for studying RNA–protein complexes. Like the phosphorothioate[21] and boranophosphate[27] RNAs that have been previously synthesized, phosphoroselenoate RNAs are also expected to exhibit biochemical and biological properties that are closely related to those of natural RNA. Research in this area will undoubtedly open new frontiers in the fields of selenium chemistry and substrate recognition through RNA polymerase, in biochemistry studies of ribozyme catalysis, and in studies of the structures of functional RNAs and their complexes with proteins by using the MAD and/or single-wavelength anomalous-dispersion (SAD) methods.

Experimental Section

ATPαSe was synthesized by a modification of the procedures for the synthesis of NTPαS[21] and TTPαSe.[17] Briefly, 2′,3′-diacetyladenosine (35.13 mg, 0.10 mmol, Sigma) was placed in a 5-mL flask, dried under high vacuum overnight, and dissolved in a mixture of freshly distilled pyridine (0.10 mL) and dioxane (0.30 mL). The resultant solution was then injected dropwise over the course of about 5 min into a solution of 2-chloro-4*H*-1,3,2-benzodioxaphosphorin-4-one (21.0 mg, 0.10 mmol, 1 equiv, Aldrich) in dioxane (0.10 mL). The reaction was stirred at room temperature under dry argon for 10 min. A solution of tributylammonium pyrophosphate (64.1 mg, 0.14 mmol, 1.5 equiv, Sigma) in dry *N*,*N*-dimethylformamide (DMF, 0.28 mL) containing tributylamine (0.10 mL) was then injected, and the reaction was stirred for another 10 min. A solution of 3*H*-1,2-benzothiaselenol-3-one (43.0 mg, 0.20 mmol, 1.5 equiv) in dioxane (0.22 mL) was then added into the reaction mixture. Once selenization was completed (30 min, monitored by ^{31}P NMR spectroscopy), the reaction was quenched with water (1.0 mL) for 2 h.

The acetyl protecting groups were removed by hydrolysis with concentrated aqueous ammonia (3.0 mL) at 60 °C for 1.5 h. After most of the ammonia was removed by rotary evaporation, the pH value was adjusted to 7.0 by using an 80% acetic acid solution. A 100 mM solution of 1,4-dithiothreitol (DTT, 200 μL) was then added, and the crude product was transferred into a 15-mL centrifuge tube and spun for 3 min to remove the selenium metal. The supernatant was transferred into a 50-mL centrifuge tube, NaCl in water (3.0 M, 1.3 mL) was added, and the content was divided into two equal portions. Absolute ethanol (3 volumes, thoroughly purged with argon) was added to each portion, and the samples were placed in a −20 °C freezer for 10 min before centrifugation (10 min at 6000 rpm). After removal of the supernatant, the crude product was redissolved in water (500 μL) and purified by RP-HPLC with a Zorbax C18 column (9.4 × 250 mm). Samples were eluted (5 mL min^{-1}) with a linear gradient from buffer A (10 mM triethylammonium acetate (TEAAc), pH 7.0) to 20% buffer B (30% acetonitrile in water, 10 mM TEAAc, pH 7.0) over 20 min. The purified ATPαSe diastereomers were then analyzed by RP-HPLC (Figure 5a) and HR-MS (Figure 5b) and stored at −20 °C (13.78 mM in a solution of 10 mM tris(hydroxymethyl)aminomethane/HCl (Tris-HCl, pH 7.5) and 20 mM of DTT). The concentrations and quantities of the diastereomers were determined by UV analysis, which indicated 15% overall yield for each diastereomer (30% total yield), a satisfactory yield considering the many steps involved in the overall synthesis and HPLC purification. It is assumed that the selenium modification on the phosphate group does not alter the extinction coefficient of the modified nucleoside triphosphate.

Enzymatic synthesis of phosphoroselenoate 5′-*O*-adenosine-labeled RNA: The DNA top strand of the T7 RNA polymerase promoter (5′-GCGTAATACGACTCACTATAG-3′) and the DNA template (3′-CGCATTATGCTGAGTGATATCCGTTGGAC-TACTCCGGCTTTCCGGCTTTGCATGT-5′) were prepared by oligonucleotide solid-phase synthesis. AmpliScribe T7 Transcription Kits (Epicentre) were used for the in vitro transcription, where the DNA template and the top strand were added in equal molar amounts into a cocktail containing all the NTPs, except ATP, ATPαSe I, and ATPαSe II. α-[^{32}P]CTP (Perkin-Elmer) was included in the cocktail to body-label the RNA transcript. Equal amounts of the cocktail were then added to vials containing the appropriate amounts of ATPαSe I, ATPαSe II, ATP, or the negative control (water). The reaction was initiated by the addition of the T7 RNA polymerase solution (provided within the kit), and the mixtures were incubated at 37 °C.

For the time-course experiments, aliquots (4 μL) were withdrawn from the reaction mixtures at the appropriate time points and added to a loading dye containing 100 mM EDTA (4 μL); the samples were then placed on dry ice. The samples were analyzed by electrophoresis on a 12.5% gel, and quantitation was carried out on a BioRad phosphorimager (see, for example, Figure 2). A typical transcription

 © 2006 Wiley-VCH Verlag GmbH & Co. KGaA, Weinheim

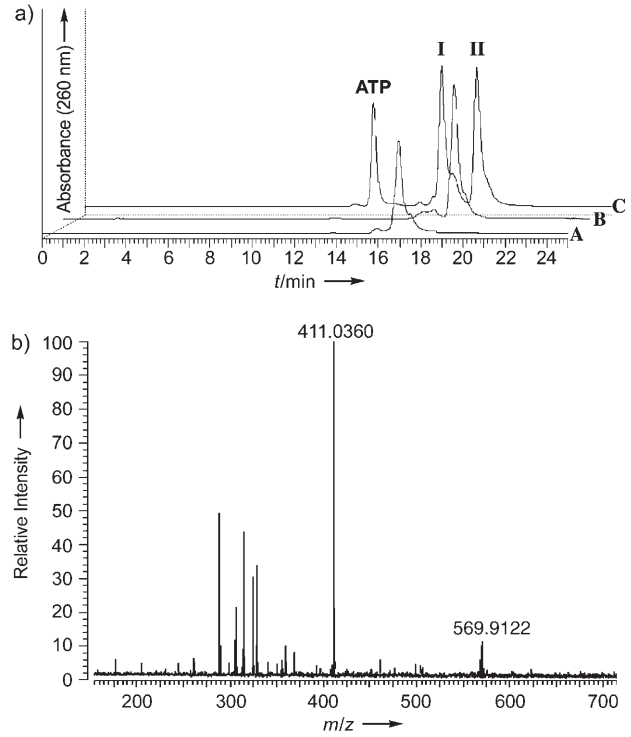


Figure 5. a) HPLC analysis of ATPαSe diastereomers: A) ATPαSe I; B) ATPαSe II; C) a mixture of ATP, ATPαSe I, and ATPαSe II. b) HR-MS analysis of ATPαSe I. (The spectrum for ATPαSe II is almost the same.) Molecular formula: $C_{10}H_{16}N_5O_{12}P_3Se$; calculated mass $[M-H^+]^-$: 569.9101; measured mass: 569.9122.

reaction contained the top strand (0.1 μM), the template (0.1 μM), all NTPs (1.0 mM, including ATPαSe I and II), α-[^{32}P]CTP, the polymerase (0.06 μL of T7 RNA polymerase per 1 μL of transcription reaction, Epicentre), and the buffer provided. By using the Epicentre kit, large-scale RNAs (6 mg) were prepared under the typical conditions of the template (1 μM) and with all NTPs (7.5 mM, including ATPαSe) in a transcription reaction (1 mL reaction volume) that took 2 h.

MALDI-TOF analysis of the RNAs: All mass spectra (with crude transcribed samples) were recorded on a biomass spectrometer in linear-negative mode with delayed extraction. 3-hydroxypicolinic acid (3-HPA)/diammonium citrate (9:1) in water was used as the matrix. A mixture (1 μL) of sample and matrix (1:30) was spotted and dried naturally before the analysis. 25 kV were applied as the acceleration voltage. A mass range of 1000–20000 was scanned. Each spectrum was summed from multiple spectra at different spots. Proteins, such as insulin, thioredoxin, and apomyoglobin, were used as external standards.

Exonuclease digestion analysis: The phosphoroselenoate RNA transcripts were digested with snake venom phosphodiesterase I (USB), following Se-modified RNA transcription by using the same protocol as that described above. The transcribed RNA was desalted by centrifugation (by using a membrane with a cut-off of 3000 Da, 3 times), and the RNA was digested with snake venom phosphodiesterase I (0.001 U μL^{-1}, USB) in its buffer over 60 min. The digested RNA samples were analyzed by PAGE (Figure 3).

Received: June 24, 2005
Revised: September 9, 2005
Published online: November 22, 2005

Keywords: nucleic acids · nucleotides · RNA synthesis · RNA transcription · selenium

[1] G. Storz, *Science* **2002**, *296*, 1260–1263.
[2] M. Mandal, R. R. Breaker, *Nat. Rev. Mol. Cell Biol.* **2004**, *5*, 451–463.
[3] M. T. McManus, P. A. Sharp, *Nat. Rev. Genet.* **2002**, *3*, 737–747.
[4] M. Egli, *Curr. Opin. Chem. Biol.* **2004**, *8*, 580–591.
[5] S. R. Holbrook, S. H. Kim, *Biopolymers* **1997**, *44*, 3–21.
[6] W. A. Hendrickson, *Trends Biochem. Sci.* **2000**, *25*, 637–643.
[7] W. A. Hendrickson, *J. Synchrotron Radiat.* **1999**, *6*, 845–851.
[8] W. S. Marshall, R. J. Kaiser, *Curr. Opin. Chem. Biol.* **2004**, *8*, 222–229.
[9] A. Ke, J. A. Doudna, *Methods* **2004**, *34*, 408–414.
[10] A. R. Ferre-D'Amare, K. Zhou, J. A. Doudna, *J. Mol. Biol.* **1998**, *279*, 621–631.
[11] A. R. Ferre-D'Amare, K. Zhou, J. A. Doudna, *Nature* **1998**, *395*, 567–574.
[12] N. Carrasco, D. Ginsburg, Q. Du, Z. Huang, *Nucleosides Nucleotides Nucleic Acids* **2001**, *20*, 1723–1734.
[13] Q. Du, N. Carrasco, M. Teplova, C. J. Wilds, M. Egli, Z. Huang, *J. Am. Chem. Soc.* **2002**, *124*, 24–25.
[14] M. Teplova, C. J. Wilds, Z. Wawrzak, V. Tereshko, Q. Du, N. Carrasco, Z. Huang, M. Egli, *Biochimie* **2002**, *84*, 849–858.
[15] Y. Buzin, N. Carrasco, Z. Huang, *Org. Lett.* **2004**, *6*, 1099–1102.
[16] N. Carrasco, Y. Buzin, E. Tyson, E. Halpert, Z. Huang, *Nucleic Acids Res.* **2004**, *32*, 1638–1646.
[17] N. Carrasco, Z. Huang, *J. Am. Chem. Soc.* **2004**, *126*, 448–449.
[18] W. A. Hendrickson, J. R. Horton, D. M. LeMaster, *EMBO J.* **1990**, *9*, 1665–1672.
[19] S. E. Ealick, *Curr. Opin. Chem. Biol.* **2000**, *4*, 495–499.
[20] C. J. Wilds, R. Pattanayek, C. Pan, Z. Wawrzak, M. Egli, *J. Am. Chem. Soc.* **2002**, *124*, 14910–14916.
[21] a) F. Eckstein, *Annu. Rev. Biochem.* **1985**, *54*, 367–402; b) J. Ludwig, F. Eckstein, *J. Org. Chem.* **1989**, *54*, 631–635; c) F. Eckstein, *Biochimie* **2002**, *84*, 841–848.
[22] a) J. F. Milligan, D. R. Groebe, G. W. Witherell, O. C. Uhlenbeck, *Nucleic Acids Res.* **1987**, *15*, 8783–8798; b) G. M. Cheetham, T. A. Steitz, *Science* **1999**, *286*, 2305–2309; c) G. M. Cheetham, D. Jeruzalmi, T. A. Steitz, *Nature* **1999**, *399*, 80–83.
[23] a) Y. W. Yin, T. A. Steitz, *Cell* **2004**, *116*, 393–404; b) D. Temiakov, V. Patlan, M. Anikin, W. T. McAllister, S. Yokoyama, D. G. Vassylyev, *Cell* **2004**, *116*, 381–391.
[24] P. M. Burgers, F. Eckstein, *Proc. Natl. Acad. Sci. USA* **1978**, *75*, 4798–4800.
[25] A. D. Griffiths, B. V. Potter, I. C. Eperon, *Nucleic Acids Res.* **1987**, *15*, 4145–4162.
[26] F. Eckstein, H. Gindl, *Eur. J. Biochem.* **1970**, *13*, 558–564.
[27] a) K. He, A. Hasan, B. Krzyzanowska, B. R. Shaw, *J. Org. Chem.* **1998**, *63*, 5769–5773; b) A. H. S. Hall, J. Wan, E. E. Shaughnessy, B. R. Shaw, K. A. Alexander, *Nucleic Acids Res.* **2004**, *32*, 5991–6000.
[28] L. Dolapchiev, E. Sulkowski, M. Laskowski, *Biochem. Biophys. Res. Commun.* **1974**, *61*, 274–279.
[29] F. Eckstein, H. Gindl, *FEBS Lett.* **1969**, *2*, 262–264.
[30] K. He, B. R. Shaw, *Nucleic Acids Res. Symp. Ser.* **1999**, *41*, 99–100.
[31] Y.-S. Kwon, K. Tang, C. R. Cantor, H. Koester, C. Kang, *Nucleic Acids Res.* **2001**, *29*, e11.
[32] A. R. Ferre-D'Amare, J. A. Doudna, *Nucleic Acids Res.* **1996**, *24*, 977–978.

 © 2006 Wiley-VCH Verlag GmbH & Co. KGaA, Weinheim

Tautomerism

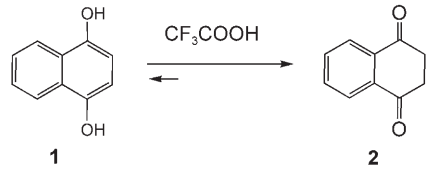
DOI: 10.1002/anie.200502588

Rediscovery, Isolation, and Asymmetric Reduction of 1,2,3,4-Tetrahydronaphthalene-1,4-dione and Studies of Its $[Cr(CO)_3]$ Complex**

E. Peter Kündig, Alvaro Enríquez García, Thierry Lomberget, and Gérald Bernardinelli*

Melting 1,4-dihydroxynaphthalene (**1**) under vacuum generates a 2:1 equilibrium (1 h, 200 °C) with its tautomer 1,2,3,4-tetrahydronaphthalene-1,4-dione (**2**).[1] The conversion of **1** into **2** can also be effected in neat CF_3COOH.[2] The dione is kinetically stable at room temperature but rapidly converts into the phenolic form in the presence of a base. The keto form is implicated in the acid-catalyzed monoalkylation of **1**,[2] but surprisingly no chemistry of isolated **2** has ever been reported to our knowledge. We herein detail our results on a) an efficient access to pure diketone **2**, b) preliminary studies of the isomerization of **1** in solution, c) the asymmetric reduction of **2**, and d) the study of the corresponding $[Cr(CO)_3]$ complexes.

As reported by Laatsch,[2] stirring **1** in trifluoroacetic acid afforded the tautomeric product **2** (Scheme 1). However, evaporation of this solvent from gram-amounts of **2** gave mixtures of **1** and **2.** As it is poorly soluble, **1** precipitates on concentration, which results in a displacement of the equilibrium. The addition of toluene to the reaction mixture before evaporation under vacuum solved this problem. The crude product consisted of a mixture of **1** and **2** in a ratio of 1:9, and recrystallization (iPr_2O) afforded pure diketone **2** in 72% yield. The structure of **2** was confirmed by X-ray diffraction studies (Figure 1).[3]



Scheme 1. The equilibrium of the tautomers **1** and **2** in CF_3CO_2H overwhelmingly favors **2**. Tautomers **1** and **2** do not interconvert in apolar solvents at room temperature.

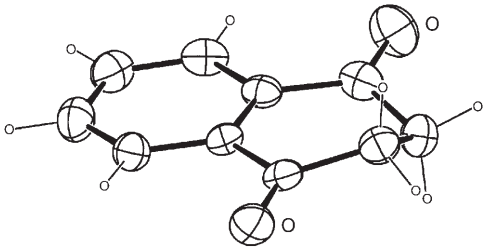
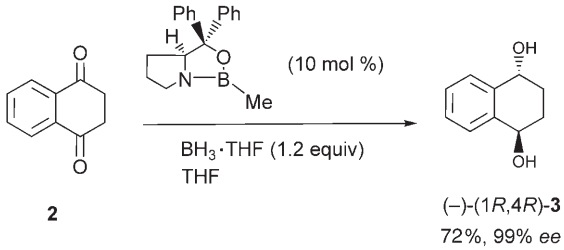


Figure 1. ORTEP view of the crystal structure of **2**. Ellipsoids are represented with 40% probability.

We also found that **1** equilibrates with **2** in degassed, dry benzene. This process requires heating to above 120 °C[6] and can be conveniently followed by ^1H NMR spectroscopic analysis at room temperature. Isomerization in benzene in a sealed NMR tube immersed in an oil bath at 150 °C exhibited first-order kinetics, and equilibrium was reached after 3 days (1:1 ratio).

Diketone **2** is an attractive and promising starting material for organic synthesis. Studies are ongoing, but a first example is shown in Scheme 2. The reduction of **2** with (*S*)-1-methyl-3,3-diphenyltetrahydropyrrolo[1,2-c][1,3,2]oxazaborole afforded the *trans*-diol (−)-(1*R*,4*R*)-**3** in 72% yield and with 99% *ee*.[7] To our knowledge, there is no viable alternative synthetic access to this C_2-chiral diol.[8]



Scheme 2. Reduction of dione **2** with CBS to give the *trans* diol **3**.

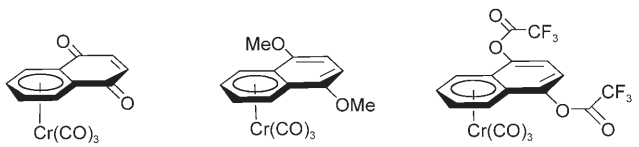
The facile isomerization of **1** into 1,4-tetralindione encouraged us to investigated the respective $[Cr(CO)_3]$ complexes **4** and **5**. We recently reported a synthesis of $[Cr(CO)_3(\eta^6\text{-}5,8\text{-naphthoquinone})]$ (**6**), its reduction to the corresponding *meso syn*-diol complex, and efficient desymmetrization by using new chiral diamine acyl-transfer catalysts.[9,10] In a further study of this chemistry, we investigated access to $[Cr(CO)_3(\eta^6\text{-}5,8\text{-dihydroxynaphthalene})]$ (**4**) by demethylation of the readily accessible $[Cr(CO)_3(\eta^6\text{-}5,8\text{-dimethoxynaphthalene})]$ (**7**),[11] mild hydrolysis of $[Cr(CO)_3(\eta^6\text{-}5,8\text{-bis(trifluoroacetoxy)naphthalene}]$[9] (**8**), or catalytic hydrogenation or radical-transfer reduction of **6**.[9]

Both the reactions of **7** with BBr_3 and **8** with Et_3N/SiO_2[9] afforded red oils. The first reaction afforded the monodemethylated complex as the major product. Compound **4**

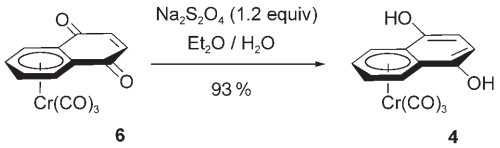
[*] Prof. Dr. E. P. Kündig, A. Enríquez García, Dr. T. Lomberget
Department of Organic Chemistry
University of Geneva
30 Quai Ernest Ansermet, 1211 Genève 4 (Switzerland)
Fax: (+41) 22-379-3215
E-mail: peter.kündig@chiorg.unige.ch
Dr. G. Bernardinelli
Laboratoire de Crystallographie
Université de Genève
24 Quai Ernest Ansermet, 1211 Genève 4 (Switzerland)

[**] Support of this work by the Swiss National Foundation is gratefully acknowledged (SNF grant 200020-103851).

InterScience
© 2006 Wiley-VCH Verlag GmbH & Co. KGaA, Weinheim



was the major product in the second reaction, which, however, proved difficult to isolate in pure form. Catalytic hydrogenation of **6** (benzene, Pd/C, H_2 50 bar),[12] also afforded **4** as the major product. The second, more soluble product, from these reactions proved to be the tautomer of **4**, [$Cr(CO)_3$(η^6-1,2,3,4-tetrahydronaphthalene-5,8-dione)] (**5**). Just as with **1** and **2**, the two tautomers appeared to be kinetically stable at ambient temperature (this point will be discussed later on). Finally, we found that the reduction[13] of **6** using sodium dithionite under biphasic conditions afforded **4** as the sole product in 93% yield (Scheme 3).



Scheme 3. Reduction of the naphthoquinone complex **6** with sodium dithionite yields the dihydroxynaphthalene complex **4** as the sole product.

The X-ray structure of **4**, which forms orange crystals, is shown in Figure 2.[3] In accord with other naphthalene complexes, the projection of the metal atom onto the arene

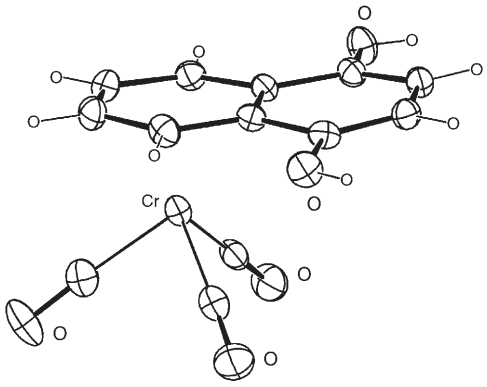
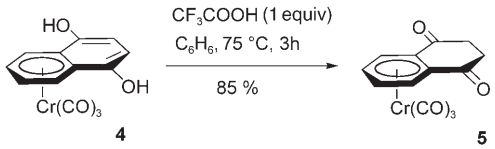


Figure 2. ORTEP view of the crystal structure of **4**. Ellipsoids are represented with 40% probability.

plane shows a displacement away from the central C–C bond, and the [$Cr(CO)_3$] tripod adopts a staggered conformation with respect to the arene carbons.

A solution of **4** in benzene at room temperature slowly changes from orange to red; this red color is characteristic of the diketone tautomer **5**. The tautomerization thus occurs far more readily than in uncomplexed **1**. Moreover, the equilibrium lies entirely on the side of the diketo form. Addition of a small amount of trifluoroacetic acid accelerates the tautomerization. The following protocol proved best for the synthesis of **5**: CF_3COOH (1 equiv) and **4** in degassed, dry benzene are stirred at 75 °C for 3 h to yield a mixture of **4** and **5** in a ratio of 8:92. Two successive recrystallizations from iPr_2O gave pure **5** in 85% yield (Scheme 4). Longer reaction times give rise to the formation of small quantities of [Cr(benzene)$(CO)_3$] by arene exchange in **4**, with concomitant appearance of free ligand **1**.



Scheme 4. High-yield conversion of **4** into its stable tautomer **5**.

The crystal structure of **5**, like that of **6**,[9] shows a displacement of the vertical projection of the metal onto the arene plane towards the ring junction. The Cr–C(5a) and Cr–C(8a) bonds are 0.04 Å shorter than the Cr–C(6) and Cr–C(7) bonds. Comparison of the structure of the metal-bound arene ligand in **5** with that of the free ligand **2** shows conformational change to be insignificant (Figure 3).[3]

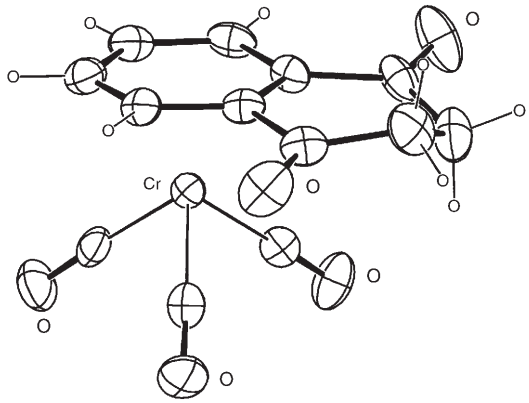
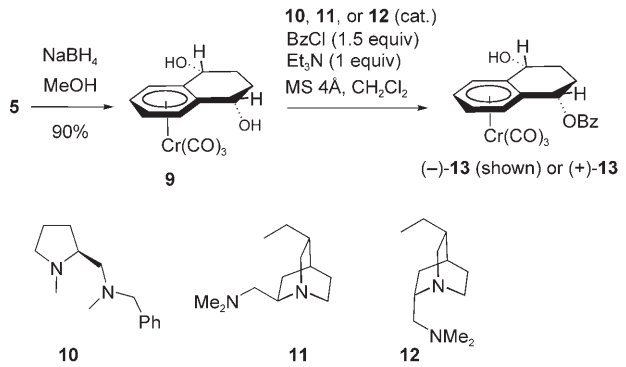


Figure 3. ORTEP view of the crystal structure of **5**. Ellipsoids are represented with 40% probability.

Reduction of the diketone complex **5** cleanly afforded the *cis* diol **9** (Scheme 5, Table 1).[3,9] Chiral-diamine-catalyzed acyl transfer efficiently desymmetrized the *meso* complex **9**. As in a previous report,[9] both the Oriyama catalyst **10**[15] and the readily synthesized quincorine- and quincoridine-derived diamines **11** and **12** performed well in this reaction. The 5*S*,8*R* configuration of (–)-**13** was assigned based on a comparison of its CD spectrum with that of (–)-[$Cr(CO)_3$]{(5*S*,8*R*)-(5,8-dihydro-5-benzoyloxy-8-hydroxynaphthalene)}].[9,16]

The chemistry described herein is based on the known fact that the two tautomers 1,4-dihydroxynaphthalene and tetrahydronaphthalene-1,4-dione are not in equilibrium at room

 © 2006 Wiley-VCH Verlag GmbH & Co. KGaA, Weinheim



Scheme 5. Highly asymmetric acyl-transfer reaction catalyzed by chiral diamines **10**–**12**.

Table 1: Asymmetric acylation of **9**.

Entry	Chiral diamine catalyst (10 mol%)	*T* [°C]	*t* [h]	**13** [%]	*ee* [%] (major prod)
1	**10**[15]	−60	22	78	95 (−)
2	**11**[9]	−60	23	80	94 (+)
3	**12**[9]	−60	22	76	99 (−)

temperature in apolar solvents. The rediscovery of this fact opens up new opportunities in organic synthesis and metal-mediated reactions. Future studies will delineate the scope of the transformations as well as the origin of the milder conditions for the conversion of the dihydroxynaphthalene system into the diketone tautomer in the case of the $[Cr(CO)_3]$ complex compared with the free ligand.

Experimental Section

2: 1,4-Dihydroxynaphthalene (**1**; 10.00 g, 62.43 mmol) was placed in a round-bottomed flask with CF_3CO_2H (200 mL). Stirring of the reaction mixture for 30 min at room temperature resulted in a clear solution. Toluene (800 mL) was added followed by removal of the solvents under vacuum at 35 °C. Recrystallization from hot iPr_2O (400 mL) afforded **2** (7.19 g, 72%) as a colorless crystalline solid. M.p. 94–95 °C; IR (solid): $\nu = 3352, 2971, 2910, 1683, 1585, 1425, 1282, 1200\ cm^{-1}$; ^1H NMR (300 MHz, $CDCl_3$, 25 °C, TMS): $\delta = 8.05$–8.01 (m, 2H), 7.76–7.71 (m, 2H), 3.08 ppm (s, 4H); ^{13}C NMR (75 MHz, $CDCl_3$, 25 °C, TMS): $\delta = 196.2, 135.5, 134.5, 126.9, 37.7$ ppm; TLC: $R_F = 0.26$ (ether/pentane = 1:6); ESI MS: *m*/*z* 161 (67) ([*M* + 1]), 150 (100), 118 (66), 106 (82), 84 (34), 72 (18); HRMS: *m*/*z* calcd for $C_{10}H_9O_2$: 161.0603; found 161.0597.

3: Dione **2** (2.48 g, 15.5 mmol) in dry THF (124 mL) was added over a period of 2 h (syringe pump) to a solution of BH_3·THF (18.6 mL (1 M solution in THF), 18.6 mmol) and (*S*)-1-methyl-3,3-diphenyltetrahydro-3H-pyrrolo[1,2-c][1,2,3]oxazaborole (1.56 mL (1 M solution in toluene), 0.156 mmol) in dry THF (95 mL) at −10 °C. TLC analysis showed complete conversion of **2** after stirring of the reaction mixture for an additional hour. The volatiles were removed under vacuum after addition of MeOH (50 mL) and the reaction mixture had been warmed up to room temperature. Two successive recrystallizations from iPr_2O afforded **3** (1.825 g, 72%; 99% *ee*) as a colorless solid. M.p. 141–142 °C; $[\alpha]_D^{20} = -73$ ($c = 0.305$, MeOH); IR (solid): $\nu = 3278, 2866, 1507, 1050, 761\ cm^{-1}$; ^1H NMR (400 MHz, $CDCl_3$, 25 °C, TMS): $\delta = 7.45$–7.43 (m, 2H), 7.35–7.31 (m, 2H), 4.80–4.84 (m, 2H), 2.33–2.27 (m, 2H), 1.86–1.79 (m, 2H), 1.55 ppm (br s, 2H); ^{13}C NMR (125 MHz, $CDCl_3$, 25 °C, TMS): $\delta = 138.5, 128.4, 128.3, 67.9, 28.3$ ppm; TLC: $R_F = 0.13$ (diethyl ether); EI MS: *m*/*z* 164 (1) ([M^+]), 146 (100) ([$M - H_2O$]), 131 (38), 120 (45), 105 (30), 77 (28); enantiomeric excess was determined by HPLC analysis on a Daicel Chiracel OJ-H column at $\lambda = 254$ nm; flow rate: 1 mL min^{-1}; eluent: hexane/*i*PrOH (99:1), $t_1 = 5.3$ min, $t_2 = 5.7$ min.

4: Complex **6**[9] (700 mg, 2.38 mmol) was placed in an schlenk tube with Et_2O (24.5 mL) under N_2 followed by the addition of an N_2-saturated aqueous solution of $Na_2S_2O_4$ (24 mL)). The reaction mixture was stirred at room temperature, and the color of the reaction mixture changed from deep violet to orange after 10 min. The organic phase was transferred by a cannula to another schlenk tube containing $MgSO_4$ and the aqueous phase was extracted three times with small portions of Et_2O. Filtration and evaporation under vacuum afforded a solid that was washed with pentane and then dried under vacuum to give **4** (651 mg, 93%) as an orange solid. M.p. 137–138 °C (under N_2); IR (CH_2Cl_2): $\nu = 3569, 3055, 1965, 1889, 1227, 1232\ cm^{-1}$; ^1H NMR (500 MHz, C_6D_6, 25 °C, TMS): $\delta = 6.10$–6.07 (m, 2H), 5.59 (s, 2H), 4.59–4.57 (m, 2H), 4.27 ppm (s, 2H); ^{13}C NMR (125 MHz, C_6D_6, 25 °C, TMS): $\delta = 233.0, 145.4, 108.1, 98.4, 91.9, 86.0$ ppm; EI MS: *m*/*z* 296 (11) ([M^+]), 240 (7), 212 (42), 160 (26), 131 (9), 104 (9), 77 (6), 52 (100); HRMS: *m*/*z* calcd for $C_{13}H_8CrO_5$: 295.9777; found: 295.9759.

5: Complex **4** (735 mg, 2.48 mmol) and degassed, dry benzene (37 mL) were placed in a schlenk tube under N_2. CF_3COOH (190 μL, 2.48 mmol) was added and the mixture was subjected to three freeze/pump/thaw cycles prior to heating to 75 °C for 3 h. On cooling to room temperature, the solvent was removed under vacuum, and two recrystallizations from hot iPr_2O (44 mL) yielded red complex **5** (624 mg, 85%). M.p. 100–101 °C (under N_2); IR (CH_2Cl_2): $\nu = 3569, 3055, 1965, 1889, 1630\ cm^{-1}$; ^1H NMR (400 MHz, C_6D_6, 25 °C, TMS): $\delta = 5.44$–5.40 (m, 2H), 4.36–4.32 (m, 2H), 2.32–2.22 (m, 2H), 2.01–1.91 ppm (m, 2H); ^{13}C NMR (100 MHz, C_6D_6, 25 °C, TMS): $\delta = 229.8, 193.8, 95.8, 92.5, 89.0, 35.6$ ppm; ESI MS: *m*/*z* 297 (8) ([$M + 1$]), 296 (24), 295 (100), 173 (88), 113 (68), 63 (8); HRMS: *m*/*z* calcd for $C_{13}H_8CrO_5$: 295.9777; found: 295.9777.

Received: July 24, 2005
Published online: November 22, 2005

Keywords: acylation · arene ligands · asymmetric catalysis · chromium · ketones

[1] a) R. H. Thomson, *J. Chem. Soc.* **1950**, 1737; b) R. H. Thomson, *Q. Rev. Chem. Soc.* **1956**, *10*, 27; c) M. S. Pearson, B. J. Jensky, F. H. Greer, J. P. Hagston, N. M. Wells, *J. Org. Chem.* **1978**, *43*, 4617.
[2] H. Laatsch, *Liebigs Ann. Chem.* **1980**, 140.
[3] Crystallographic data: Cell dimensions and intensities were measured at 200 K on a Stoe IPDS diffractometer with graphite-monochromated $Mo_{K\alpha}$ radiation ($\lambda = 0.71073$ Å). Data were corrected for Lorentz and polarization effects and for absorption. The structures were solved by direct methods (SIR97),[4] all other calculations were performed with XTAL system.[5] **2**: $C_{10}H_8O_2$, $M_r = 160.2$, monoclinic, $P2_1$, $a = 4.7167(8)$, $b = 7.4607(10)$, $c = 11.285(3)$ Å, $\beta = 96.95(3)°$, $V = 394.18(12)$ Å^3, $Z = 2$, $\mu = 0.094\ mm^{-1}$, $d_x = 1.349\ g\,cm^{-3}$, $R = 0.033$, $\omega R = 0.031$. **4**: $C_{13}H_8CrO_5 \cdot 1/2\,C_6H_6$, $M_r = 335.3$, monoclinic, $P2_1/c$, $a = 14.2611(9)$, $b = 7.2120(4)$, $c = 14.5831(9)$ Å, $\beta = 109.885(7)°$, $V = 1410.46(16)$ Å^3, $Z = 4$, $\mu = 0.83\ mm^{-1}$, $d_x = 1.579\ g\,cm^{-3}$, $R = \omega R = 0.032$. **5**: $C_{13}H_8CrO_5$, $M_r = 296.2$, orthorhombic, $Pna2_1$, $a = 11.2836(9)$, $b = 10.3052(10)$, $c = 10.3366(7)$ Å, $V = 1201.94(18)$ Å^3, $Z = 4$, $\mu = 0.96\ mm^{-1}$, $d_x = 1.637\ g\,cm^{-3}$, Flack parameter $x = -0.02(4)$, $R = \omega R = 0.027$. **9**: $C_{13}H_{12}CrO_5$, $M_r = 300.3$, triclinic, $P\bar{1}$, $a = 7.3157(7)$, $b = 13.3798(11)$, $c = 13.6957(11)$ Å, $\alpha = 101.996(9)$, $\beta = 105.332(10)$, $\gamma = 97.332(10)°$,

 © 2006 Wiley-VCH Verlag GmbH & Co. KGaA, Weinheim

$V = 1240.7(3)$ Å^3, $Z = 4$, $\mu = 0.935$ mm^{-1}, $d_x = 1.607$ g·cm^{-3}, $R = \omega R = 0.030$. CCDC 277444–277447 contain the supplementary crystallographic data for this paper. These data can be obtained free of charge from The Cambridge Crystallographic Data Centre via www.ccdc.cam.ac.uk/data_request/cif.

[4] A. Altomare, M. C. Burla, M. Camalli, G. Cascarano, C. Giacovazzo, A. Guagliardi, A. G. G. Moliterni, G. Polidori, R. Spagna, *J. Appl. Crystallogr.* **1999**, *32*, 115.

[5] S. R. Hall, H. D. Flack, J. M. Stewart, *XTAL3.2 User's Manual*, (Eds.: Universities of Western Australia and Maryland), **1992**.

[6] An earlier investigation found no evidence for equilibration of **1** and **2** at 25 °C in dioxane, $CHCl_3$, acetone, or dimethyl sulfoxide (DMSO).[1b]

[7] E. J. Corey, C. J. Helal, *Angew. Chem. Int. Ed.* **1998**, *37*, 1986.

[8] Compound (1*R*,4*R*)-**3** was previously obtained by HPLC separation of a 1:1 mixture of the *cis* and *trans* diols obtained in 55% yield from a four-step sequence from 1(*R*)-tetralol: D. R. Boyd, N. D. Sharma, N. A. Kerley, G. McConville, C. C. R. Allen, A. J. Blacker, *ARKIVOC* **2003**, *7*, 32.

[9] E. P. Kündig, T. Lomberget, R. Bragg, C. Poulard, G. Bernardinelli, *Chem. Commun.* **2004**, 1548.

[10] For a more recent, closely related synthesis of **6**, see: D. Möhring, M. Nieger, B. Lewall, K. H. Dötz, *Eur. J. Org. Chem.* **2005**, 2620.

[11] E. P. Kündig, V. Desobry, D. P. Simmons, *J. Am. Chem. Soc.* **1983**, *105*, 6962.

[12] A conversion of 32% was observed after 20 h at under 1 bar hydrogen pressure, whereas conversion was complete after 20 h at under 50 bar hydrogen pressure; ^{1}H NMR spectroscopic analysis of the crude product mixture showed free naphthoquinone, dihydroxy complex **4**, and diketo complex **5** in a ratio of 23:47:30.

[13] P. G. Gassman, O. M. Rasmy, T. O. Murdock, K. Saito, *J. Org. Chem.* **1981**, *46*, 5457.

[14] The reduction of $[Cr(CO)_3$(1-tetralone)] is known to occur *exo* to the $\{Cr(CO)_3\}$ unit and the reduction with *N*-cyclohexyl-2-benzothiazole sulfenamide (CBS) allows kinetic resolution of the racemic complex; see: H.-G. Schmalz, H. Jope, *Tetrahedron* **1998**, *54*, 3457, and references therein.

[15] T. Oriyama, K. Imai, T. Sano, T. Hosoya, *Tetrahedron Lett.* **1998**, *39*, 3529.

[16] X-ray structure to be published.

 © 2006 Wiley-VCH Verlag GmbH & Co. KGaA, Weinheim

Synthetic Methods

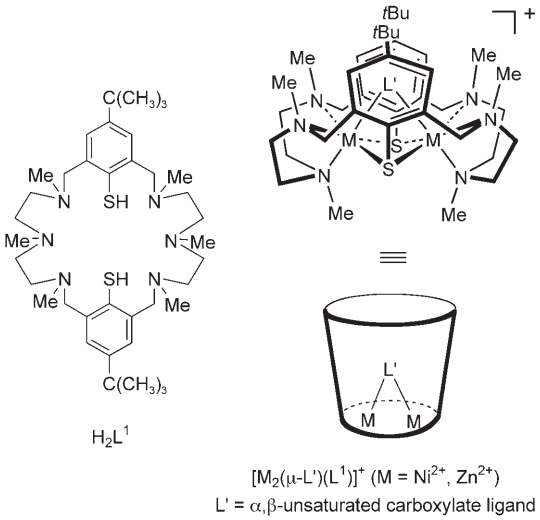
DOI: 10.1002/anie.200500683

Diels–Alder Reactivity of Binuclear Complexes with Calixarene-like Structures**

*Steffen Käss, Thomas Gregor, and Berthold Kersting**

Dedicated to Professor Heinrich Vahrenkamp on the occasion of his 65th birthday

The Diels–Alder reaction is one of the most useful reactions in organic synthesis.[1] As a consequence, a large number of strategies have been developed to control the course and rate of this transformation.[2] Recently, it has been found that the outcome of some cycloadditions can be altered remarkably when performed inside the cavity of cyclodextrines,[3,4] self-assembled molecular capsules,[5–7] or coordination cages.[8–10] This fact intrigued us greatly and awoke our interest in the Diels–Alder reactivity of the "calixarene-like" $[M_2(\mu\text{-}L')(L^1)]^+$ complexes bearing unsaturated carboxylate coligands L′ (Scheme 1).[11] We report herein the synthesis and



Scheme 1. Structures of H_2L^1 and its metal complexes. Compound labels are given in Schemes 2–4. The cavity representation of the complexes has been used for reasons of clarity. It should not be confused with the one used for the cyclodextrins.

[*] S. Käss, T. Gregor, Prof. Dr. B. Kersting
Institut für Anorganische Chemie
Universität Leipzig
Johannisallee 29, 04103 Leipzig (Germany)
Fax: (+49) 341-973-6199
E-mail: b.kersting@uni-leipzig.de

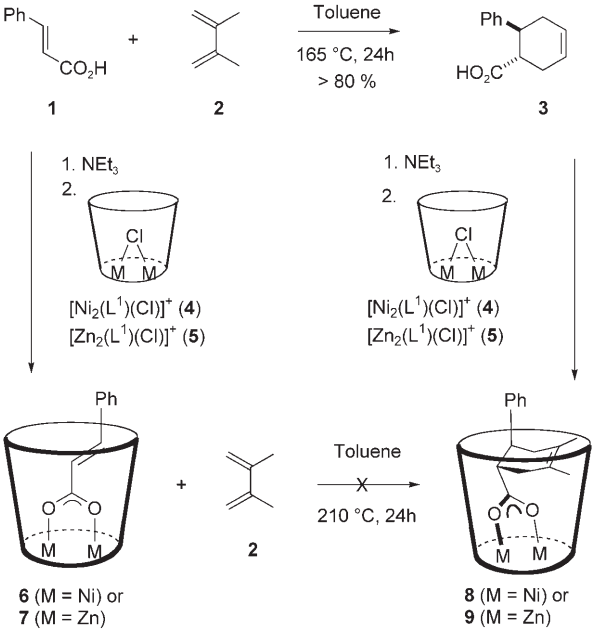
[**] This work was supported by the Deutsche Forschungsgemeinschaft (KE 585/3-1,2,3).

Supporting information for this article is available on the WWW under http://www.angewandte.org or from the author.

© 2006 Wiley-VCH Verlag GmbH & Co. KGaA, Weinheim

structures of a series of such complexes and demonstrate the remarkable effect of the binding pocket on the regioselectivity of the Diels–Alder reaction between sorbinic acid and acrylonitrile.

The observation that α,β-unsaturated carboxylate ligands can be readily incorporated in the binding pocket of our complexes[12] led us to focus our first investigation on the Diels–Alder reaction between the cinnamate ion in **6** and 2,3-dimethylbutadiene (**2**). The reaction between cinnamic acid **1** and **2** proceeds readily in solution with toluene at 165 °C to give the corresponding adduct **3** (Scheme 2).[13] However, the reaction of **6** with a large excess of **2** in solution with toluene did not occur, even when heated in a sealed glass tube at 210 °C for 24 h.[14] The same behavior was observed for the dizinc complex **7**.



Scheme 2. Preparation of **6**–**9**.

It has been possible to synthesize the expected products **8** and **9** of the above reactions by substituting the bridging chlorides in complexes **4** and **5** for triethylammonium cinnamate (Scheme 2) and to determine the X-ray crystal structure of complex **8** (Figure 1). This structure revealed the presence of an unusual conformation of cyclohexene derivative **3**, with both the phenyl and carboxylate residues in axial positions. In general, the substituents in cyclohexene rings assume equatorial positions.[15] The bisaxial arrangement in **8** is presumably enforced by the limited space in the binding pocket, which can be described by the distances between H38a···H33c (9.226 Å, diameter of the pocket) and C48···Ni1 (6.820 Å, depth of the pocket).[16] It is likely that these steric constraints also inhibit the Diels–Alder reaction of the coordinated cinnamate ion in **6**.

The above findings prompted us to study a Diels–Alder reaction between a coordinated dienoate ligand and an external alkene. We chose to study the reaction between

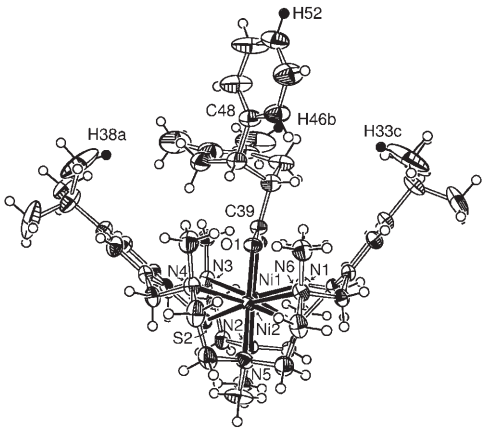
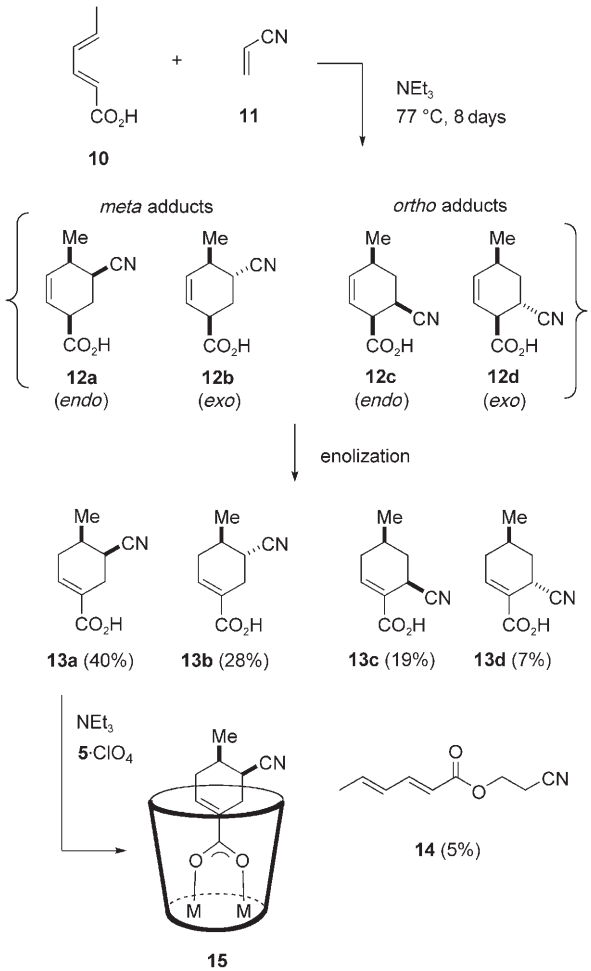


Figure 1. Structure of the dinickel complex **8**, with thermal ellipsoids drawn at the 30% probability level. Bond lengths and angles are given in the Supporting Information.

sorbinic acid **10** and acrylonitrile **11** (Scheme 3). The reaction of the free acid was investigated first. This reaction is rather slow (pseudo first-order rate constant $k' = 4.8 \times 10^{-6}\ s^{-1}$, $\tau_{1/2} \approx 2$ days) and produces a mixture of the four possible Diels–

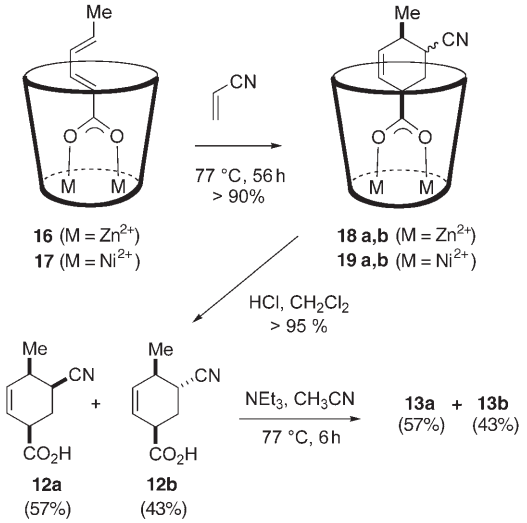


Scheme 3. Preparation of **13a**–**15**. Numbers in parentheses refer to the yields of the isolated products.

 © 2006 Wiley-VCH Verlag GmbH & Co. KGaA, Weinheim

Alder adducts **12a–d** and the by-product **14**. All acids **12a–d** isomerize under the basic reaction conditions to give the corresponding α,β-unsaturated derivatives **13a–d**. It was possible to separate **13a**, **13b**, and **13d** by fractional crystallization and to determine their structures by ^{1}H and ^{13}C NMR spectroscopic and X-ray crystallographic studies.[14] This analysis confirmed unambiguously the assignment of the regiochemistry as represented in Scheme 3. Complex **15** (prepared by a simple coligand exchange reaction) served as a reference compound.

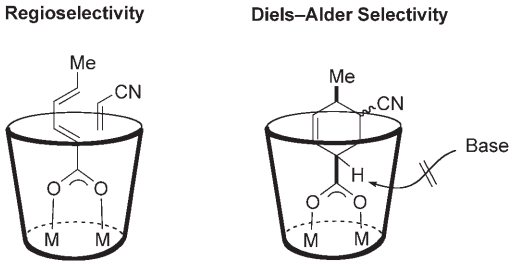
We then looked at the Diels–Alder reaction between the coordinated dienoate ligand in **16** and acrylonitrile (Scheme 4). Surprisingly, this reaction was already complete



Scheme 4. Preparation of complexes **18a,b**, **19a,b**, Diels–Alder products **12a,b**, and α,β-unsaturated acids **13a,b**. Numbers in parentheses refer to the yields of the isolated products.

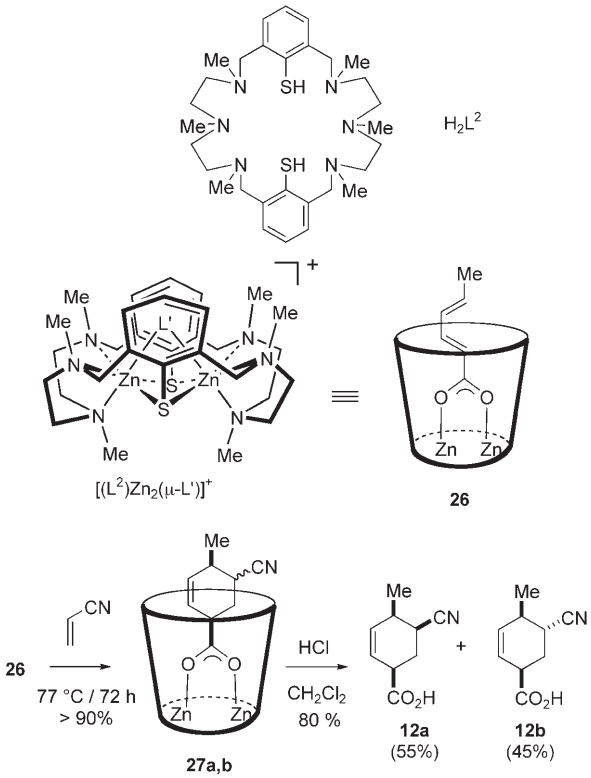
after 56 hours (pseudo first-order rate constant $k' = 1.4 \times 10^{-5}\ s^{-1}$, $\tau_{1/2} \approx 0.5$ days) and gave only two products **18a** and **18b** in nearly quantitative yield in a ratio of 57:43, as revealed by NMR spectroscopy. The dinickel complex **17** behaved in a similar manner, thus producing **19a** and **19b**. To establish the structures of the coligands, **18a** and **18b** (or **19a** and **19b**) were decomposed under mild acidic conditions. In both cases, this gave the hydrochloride of the macrocycle ($H_2L^1 \cdot 6HCl$), a metal(II) salt (M = Zn^{II} or Ni^{II}), and the free acids **12a** and **12b**. The latter isomerized in the presence of a base to the α,β-unsaturated derivatives **13a** and **13b**, respectively. This approach proved the structures of **12a** and **12b** and their complexes. Thus, in striking contrast to the low regioselectivity observed in the background reaction, the Diels–Alder reaction between coordinated **10** and acrylonitrile proceeds with strict "*meta*" regioselectivity. In addition, there are no detectable by-products, such as **14**.

This regioselectivity and the fact that the Diels–Alder adducts **12a,b** do not isomerize in the binding pocket of the complexes can be attributed to the directing and protecting effect of the binding cavity, as schematically represented in Scheme 5.



Scheme 5. Directing and protecting effect of the binding cavity.

Finally, to investigate the role played by the *tert*-butyl substituents of $(L^1)^{2-}$, we investigated the reactivity of the analogous complex $[Zn_2\{(2E,4E)\text{-hexa-2,4-dienoate}\}(L^2)]^+$ **26** of macrocycle $(L^2)^{2-}$ lacking *tert*-butyl groups (Scheme 6).



Scheme 6. Structure of H_2L^2 and reactivity of its dizinc complex **26**.

The reaction of **26** with acrylonitrile and the subsequent decomposition of the intermediate complexes **27a,b** produced the acids **12a,b** as the sole reaction products again in a similar 55:45 ratio. The pseudo first-order rate constant k' was determined to be $8.2 \times 10^{-6}\ s^{-1}$ ($\tau_{1/2} \approx 1$ day). This rate is slower than the reaction between **16** and acrylonitrile ($\tau_{1/2} \approx 0.5$ days), but still significantly faster than the background reaction ($\tau_{1/2} \approx 2$ days). Thus, the *tert*-butyl substituents do not affect the regiochemistry of this particular Diels–Alder reaction, but they clearly increase its rate. The observed trend is indicative of a small stabilization of the transition state by hydrophobic effects ($\Delta\Delta G^{\neq} \approx 3\ kJ\,mol^{-1}$; $k'_{complex}/k'_{background} = \exp(\Delta\Delta G^{\neq}/RT)$). This result would be consistent with our earlier observation that complexes bearing less polar carboxylate anions have higher stability constants.[17]

 © 2006 Wiley-VCH Verlag GmbH & Co. KGaA, Weinheim

The Diels–Alder reactivity of "calixarene-like" metal complexes supported by the ligands H_2L^1 and H_2L^2 has been described. The reaction between the coordinated sorbinate coligand and acrylonitrile is controlled by the binding cavity of the complexes and is highly regioselective. The new method is currently only applicable to dienes with anchoring carboxylate groups, but expansion of this approach to a general concept for the control of the regioselectivity of Diels–Alder reactions between unsymmetrical dienes and dienophiles appears to be in reach. We are currently probing the possibility whether the rate of these transformations can be enhanced by enlarging the binding pocket of the complexes.

Received: February 23, 2005
Revised: October 4, 2005
Published online: November 22, 2005

Keywords: binuclear complexes · calixarenes · Diels–Alder reaction · regioselectivity · synthetic methods

[1] J. Sauer, *Angew. Chem.* **1966**, *78*, 233 – 252; *Angew. Chem. Int. Ed. Engl.* **1966**, *5*, 211 – 230.
[2] S. Otto, J. B. F. N. Engberts, *Pure Appl. Chem.* **2000**, *72*, 1365 – 1372.
[3] D. C. Rideout, R. Breslow, *J. Am. Chem. Soc.* **1980**, *102*, 7816 – 7817.
[4] H. J. Schneider, N. K. Sangwan, *Angew. Chem.* **1987**, *99*, 924 – 925; *Angew. Chem. Int. Ed. Engl.* **1987**, *26*, 896 – 897.
[5] D. J. Cram, M. E. Tanner, R. Thomas, *Angew. Chem.* **1991**, *103*, 1048 – 1051; *Angew. Chem. Int. Ed. Engl.* **1991**, *30*, 1024 – 1027.
[6] J. Kang, J. Rebek, Jr., *Nature* **1997**, *385*, 50 – 52.
[7] T. Ooi, Y. Kondo, K. Maruoka, *Angew. Chem.* **1998**, *110*, 3213 – 3215; *Angew. Chem. Int. Ed.* **1998**, *37*, 3039 – 3041.
[8] C. J. Walter, J. K. M. Sanders *J. Chem. Soc. Chem. Commun.* **1993**, 458 – 460.
[9] T. Kusukawa, M. Yoshizawa, M. Fujita, *Angew. Chem.* **2002**, *114*, 1403 – 1405; *Angew. Chem. Int. Ed.* **2002**, *41*, 1403 – 1405.
[10] D. Fiedler, R. G. Bergman, K. N. Raymond, *Angew. Chem.* **2004**, *116*, 6916 – 6919; *Angew. Chem. Int. Ed.* **2004**, *43*, 6748 – 6751.
[11] G. Steinfeld, V. Lozan, B. Kersting, *Angew. Chem.* **2003**, *115*, 2363 – 2365; *Angew. Chem. Int. Ed.* **2003**, *42*, 2261 – 2263.
[12] B. Kersting, G. Steinfeld, *Inorg. Chem.* **2002**, *41*, 1140 – 1150.
[13] J. Monnin, *Helv. Chim. Acta* **1958**, *41*, 2112 – 2119.
[14] For details of the experimental procedures, characterization data, results of kinetic measurements, control experiments, and crystal-structure determinations, see the Supporting Information. CCDC-264275 (**8**·BPh_4), -264276 (**13a**), -264277 (**13b**), -264278 (**13d**), -264279 (**15**·BPh_4·EtOH), -264280 (**16**·BPh_4), and -278590 (**25**·BPh_4) contain the supplementary crystallographic data for this paper. These data can be obtained free of charge from The Cambridge Crystallographic Data Centre via www.ccdc.cam.ac.uk/data_request/cif.
[15] C. Pedone, E. Benedetti, A. Immirzi, G. Allegra, *J. Am. Chem. Soc.* **1970**, *92*, 3549 – 3552.
[16] The distances between H52 and H46 for the two conformers were calculated to be 9.062 Å (ax,ax) and 10.401 Å (eq,eq) by using the program Chem3D (CambridgeSoft); only the dimensions of the former conformer are compatible with those of the binding pocket of **8**.
[17] B. Kersting, *Angew. Chem.* **2001**, *113*, 4110 – 4112; *Angew. Chem. Int. Ed.* **2001**, *40*, 3988 – 3990.

 © 2006 Wiley-VCH Verlag GmbH & Co. KGaA, Weinheim

Nanostructures

DOI: 10.1002/anie.200500234

Hole-Doped Single-Walled Carbon Nanotubes: Ornamenting with Gold Nanoparticles in Water**

*Dong Sik Kim, Takhee Lee, and Kurt E. Geckeler**

Since the discovery of carbon nanotubes,[1] intensive studies of their unique electronic and mechanical properties have been performed,[2] and considerable potential applications in nanotechnology have been suggested.[3] It is advantageous or required to modify carbon nanotubes by physical or chemical methods to optimize their use in many applications. Nanohybrid materials based on carbon nanotubes with metal nanoparticles are promising materials because of their exciting features (which are different from their intrinsic physical properties) such as catalytic activity,[4] enhanced conductivity,[5] and hydrogen-sensing ability.[6] These properties of hybrid nanostructures could hold promise for a bright future in electronic, optical, and magnetic applications.[7]

A variety of different methods, such as physical evaporation,[8] thermal decomposition,[9] electroless deposition,[10] chemical immobilization using covalent coupling[11] and hydrophobic anchoring,[12] and polymer-assisted hybridization,[7] have been explored to obtain hybrids of carbon nanotubes and metal nanoparticles.

Recently, Au nanoparticles were generated on single-walled carbon nanotubes (SWNTs) through direct redox reactions by the immersion of SWNTs grown on a SiO_2 substrate in a solution of Au^{3+} ions.[5] This method is an attractive approach because it opens up a direct way to prepare Au nanoparticles on SWNTs without using high-temperature treatment, reducing agents, or anchoring functional groups. However, the reaction took place on a solid support and the final hybrid material was not soluble. In addition, the size of the nanoparticles was not uniform and the poorly wetted surface of the as-produced SWNTs required the use of an ethanol/water (1:1) mixture.

Herein, we report for the first time a simple and facile method to prepare water-soluble hybrid materials of Au nanoparticles and hole-doped SWNTs.[13] The SWNTs with uniformly arranged Au nanoparticles were obtained by the addition of metal salts to surfactant-suspended SWNTs in water by using the solution-phase dispersion technique.[14]

[*] D. S. Kim, Dr. T. Lee, Prof. Dr. Dr. K. E. Geckeler
Department of Materials Science and Engineering
Gwangju Institute of Science and Technology (GIST)
1 Oryong-dong, Buk-gu, Gwangju 500-712 (South Korea)
Fax: (+82) 62-970-2338
E-mail: keg@gist.ac.kr

[**] This work was financially supported by the "Brain Korea 21" (BK21) project from the Ministry of Education. We thank Ji Su Kim (Korea Basic Science Institute) for kind help with the HR-TEM (JEM-2100F) experiments.

Supporting information for this article is available on the WWW under http://www.angewandte.org or from the author.

WILEY InterScience DISCOVER SOMETHING GREAT
© 2006 Wiley-VCH Verlag GmbH & Co. KGaA, Weinheim

The method reported here is easy to scale-up and a uniform size of nanoparticles can be prepared. More importantly, as the method yields water-soluble products, a much greater variety of applications can be envisaged.

In a typical experiment, commercially available, highly pure SWNTs (1 mg, from Iljin Nanotech) were dispersed in an aqueous solution of the surfactant Tween-80 (0.1 wt%, 10 mL) by using an ultrasonic tip for 10 minutes. The dispersion was then ultracentrifuged at 80000 g for 3 h and the supernatant collected. The final concentration of nanotubes was determined to be 48 mg L^{-1} by UV/Vis spectroscopy. Subsequently, $KAuCl_4$ (0.3 mg) was added to the black solution of carbon nanotubes (1.2 mL) to yield the carbon nanotube/Au nanoparticle hybrid, which was comfirmed by Raman spectroscopy and transmission electron microscopy (TEM) images (see the Supporting Information). Furthermore, an optimized procedure for the high-resolution transmission electron microscopy (HRTEM) sample was used, in which the sample was incubated at 60°C for 1 h to yield uniformly distributed Au nanoparticles on the SWNTs.

As shown in Figure 1, the TEM studies confirmed the successful formation of the Au nanoparticles on the sidewalls of carbon nanotubes. Well-dispersed and isolated Au nanoparticles can be seen to decorate the walls of the nanotubes quite uniformly. The energy dispersive X-ray (EDX) spectrum (see the Supporting Information) identified the black dots as gold. No nanoparticles were observed in a blank experiment without treatment with the metal salt. The high-resolution TEM image (Figure 1b) indicates an average size of the Au nanoparticles of 2.94 ± 0.75 nm, which was determined from a statistical study with 36 nanoparticles. On the basis of the dimensions of the SWNT (length: 300 nm, diameter: 1.4 nm) and the assumption of a spherical shape of the nanoparticles, it can be calculated that 7.5×10^{-17} g of gold is coated on one individual nanotube and one tube contains about 300 Au nanoparticles. More interesting results were observed after increasing the metal salt concentration in the solution of the carbon nanotubes to 3.5 mM. Figure 2 shows the TEM image with Au nanoparticles of 9-nm diameter aligned on the carbon nanotubes.

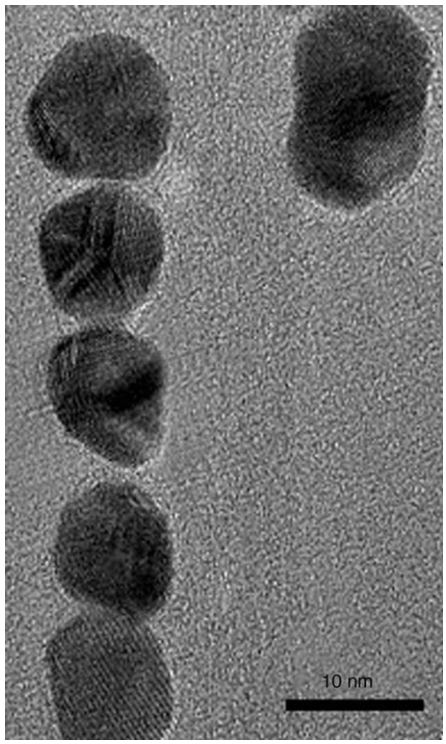


Figure 2. High-resolution TEM image of the carbon nanotube/Au nanoparticle hybrid obtained from a solution of carbon nanotubes suspended in Tween 80 (3.5 mM of $KAuCl_4$).

A frontier orbital picture describing the chemistry of carbon nanotubes suggested by Joselevich[15] could be used to explain these surprising experimental results. Carbon nanotubes have a rich electronic structure that stems from the quantization of the wave vector of the carbon nanotube along the circumferential direction. When $(n-m)/3$ is an integer (where both integers n and m define the nanotube chirality), the carbon nanotube is metallic, otherwise it is semiconducting. The frontier orbitals of semiconducting nanotubes are related to the first van Hove singularities in the valence and conduction bands, whereas those of metallic nanotubes correspond to the orbitals near the Fermi level. The frontier orbital picture of the reduction reaction of $AuCl_4^-$ at the surface of a carbon nanotube can be represented as shown in Figure 3. It is well known that the electrochemical potential measured with respect to a reference electrode is related to the absolute potential relative to the vacuum level. The potential scale versus the vacuum level can be calculated using the equation: V_{abs}(versus vacuum

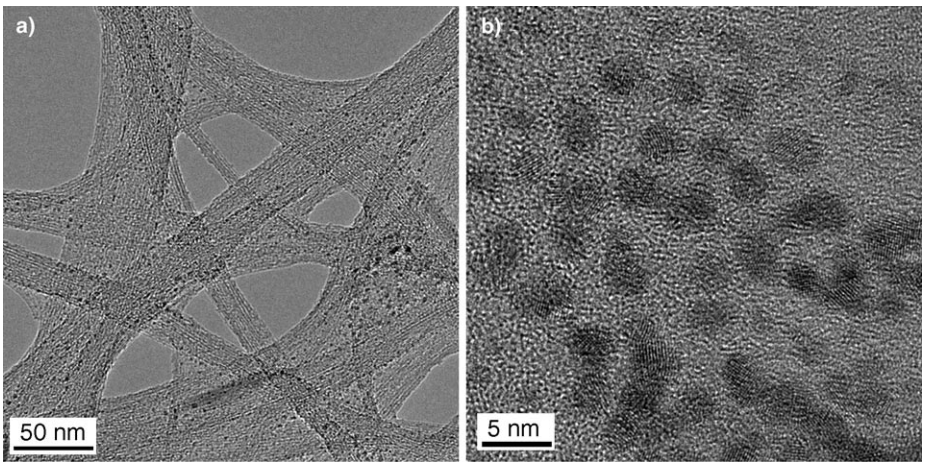


Figure 1. TEM images of the carbon nanotube/Au nanoparticle hybrid (a), and high-resolution TEM image of the carbon nanotube/Au nanoparticle hybrid (b) obtained from a solution of carbon nanotubes suspended in Tween 80 (0.46 mM of $KAuCl_4$; focusing on the Au nanoparticles prevents visibility of the SWNTs, Figure 1b).

 © 2006 Wiley-VCH Verlag GmbH & Co. KGaA, Weinheim

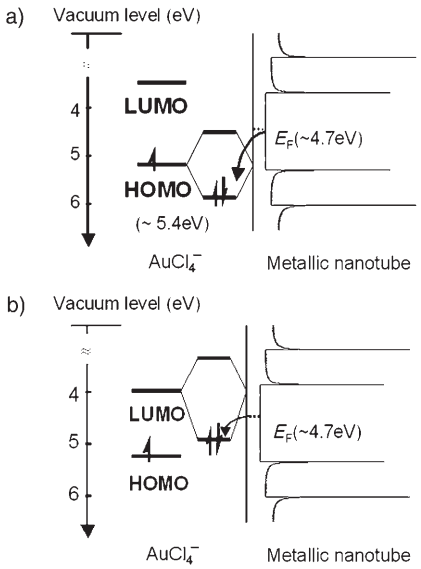


Figure 3. Frontier-orbital picture representation of four-electron interactions (a) and zero-electron interactions (b) between $AuCl_4^-$ and a metallic carbon nanotube. The $AuCl_4^-$ frontier orbitals are designated as HOMO and LUMO, and the nanotube orbitals are represented by the density of states plots. A similar picture can be applied for semiconducting carbon nanotubes (not shown). E_F = fermi level.

level) = V(versus normal hydrogen electrode (NHE))+4.44 V, as derived by Trasatti.[16] Since the reduction potential of $AuCl_4^-$ corresponds to 1.002 V,[17] the HOMO level is 5.44 eV. Here the work function of individual single-walled carbon nanotubes was chosen as approximately 4.7 eV.[18]

Since the relative position of the Fermi level of nanotubes with respect to the mixed metal ion/nanotube HOMO and LUMO is suitable for charge transfer, both semiconducting and metallic carbon nanotubes may establish attractive interactions with the metal ions, either by four-electron interactions involving two occupied orbitals (Figure 3a) or zero-electron interactions involving two empty orbitals (Figure 3b). It is worth noting that the HOMO level of $AuCl_4^-$ is partly occupied with electrons.

Figure 4a and b show the radial breathing mode (RBM) and tangential G-band of the Raman spectra, respectively, of carbon nanotubes suspended in Tween 80 after the successive addition of $KAuCl_4$ (excited at 532 nm). An increase in the concentration of the metal salt results in both the RBM and tangential G-band decaying significantly as a consequence of a depletion of singular features in the density of states of the carbon nanotubes. This observation is a strong indication of the removal of electrons from the conduction band of carbon nanotubes following the reduction of metal ions at the surface of nanotubes. Similar behavior was reported for chemical[19] and electrochemical redox doping.[20] It is also interesting to note that the peak of the tangential G-band shifted to a higher frequency. This shift can be interpreted as a stiffening of the graphene mode, caused by the introduction of holes into the conduction band of nanotubes as a result of the charge-transfer interaction.[20]

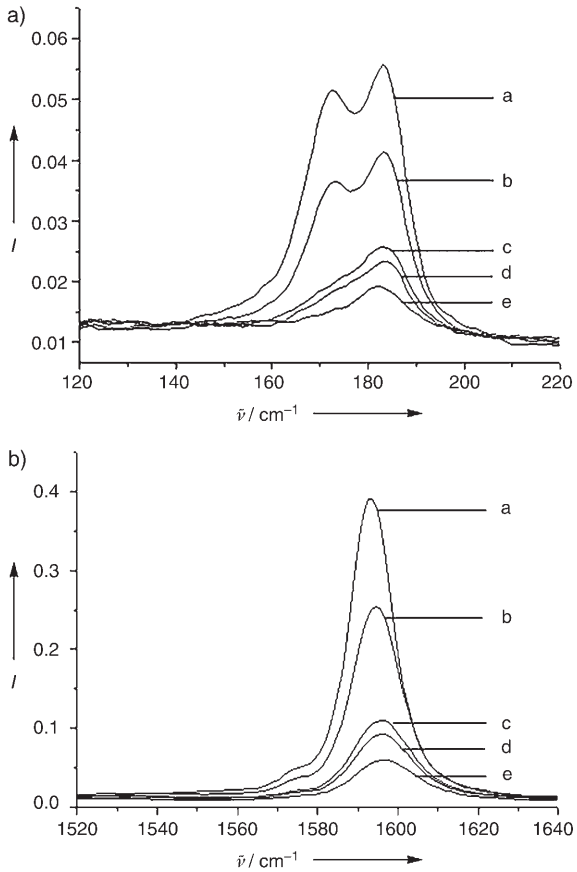


Figure 4. Raman spectra of SWNTs suspended in Tween 80 after the addition of various amounts of metal salt (0 mM, 0.1 mM, 0.5 mM, 1 mM, and 5 mM of $KAuCl_4$ (a–e)) with excitation at 532 nm. The plots display the region of RBM mode (a) and the region of tangential G-band (b). I = intensity, arbitrary units.

In summary, a novel carbon nanotube/Au nanoparticle hybrid material was prepared in a homogeneous phase by using the reduction reaction of gold salts with surfactant-suspended carbon nanotubes in water. It has been observed that well-dispersed Au nanoparticles were formed quite uniformly on the side walls of nanotubes. Frontier orbital pictures can explain this phenomenon. The process is easy to scale up and the size can be controlled. More importantly, a water-soluble and processable product is obtained. Further study is underway to align metal nanoparticles on individual carbon nanotubes, which is an attractive challenge in the generation of nanoscale building blocks.

Received: January 21, 2005
Revised: August 31, 2005
Published online: November 21, 2005

Keywords: carbon nanotubes · gold nanoparticles · nanostructures · redox chemistry · water

[1] S. Iijima, *Nature* **1991**, *354*, 56–58.
[2] M. S. Dresselhaus, G. Dresselhaus, P. Avouris, *Carbon Nanotubes: Synthesis Properties and Applications*, Springer, Berlin, **2001**.

 © 2006 Wiley-VCH Verlag GmbH & Co. KGaA, Weinheim

[3] a) P. G. Collins, A. Zettl, H. Bando, A. Thess, R. E. Smalley, *Science* **1997**, *278*, 100 – 102; b) T. Rueckes, K. Kim, E. Joselevich, G. Y. Tseng, C. Cheung, C. M. Lieber, *Science* **2000**, *289*, 94 – 97; c) D. J. Hornbaker, S. J. Kahng, S. Misra, B. W. Smith, A. T. Johnson, E. J. Mele, D. E. Luzzi, A. Yazdani, *Science* **2002**, *295*, 828 – 831; d) D. S. Kim, D. Nepal, K. E. Geckeler, Proceedings of the 2nd International Symposium on Macro- and Supramolecular Architectures and Materials (MAM-04): Functional and Nano-Systems, Missoula, USA, 13 – 17 June **2004**, p. 5; e) *Advanced Macromolecular and Supramolecular Materials and Processes* (Ed.: K. E. Geckeler), Academic/Plenum, New York, **2003**.
[4] G. L. Che, B. B. Lakshmi, E. R. Fisher, C. R. Martin, *Nature* **1998**, *393*, 346 – 349.
[5] H. C. Choi, M. Shim, S. Bangsaruntip, H. Dai, *J. Am. Chem. Soc.* **2002**, *124*, 9058 – 9059.
[6] J. Kong, M. Chapline, H. Dai, *Adv. Mater.* **2001**, *13*, 1384 – 1386.
[7] K. Jiang, A. Eitan, L. S. Schadler, P. M. Ajayan, R. W. Siegel, N. Grobert, M. Mayne, M. Reyes-Reyes, H. Terrones, M. Terrones, *Nano Lett.* **2003**, *3*, 275 – 277.
[8] Y. Zhang, H. Dai, *Appl. Phys. Lett.* **2000**, *77*, 3015 – 3017.
[9] B. Xue, P. Chen, Q. Hong, J. Lin, K. Tan, *J. Mater. Chem.* **2001**, *11*, 2378 – 2381.
[10] J. Li, M. Moskovits, T. Haslett, *Chem. Mater.* **1998**, *10*, 1963 – 1967.
[11] R. Azamian, K. Coleman, J. Davis, N. Hanson, M. Green, *Chem. Commun.* **2002**, 366 – 367.
[12] A. V. Ellis, K. Vijayamohanan, R. Goswami, N. Chakrapani, L. S. Ramanathan, P. M. Ajayan, G. Ramanath, *Nano Lett.* **2003**, *3*, 279 – 282.
[13] K. E. Geckeler, D. S. Kim, Internat. Patent application pending.
[14] M. J. O′Connell, S. M. Bachilo, C. B. Huffman, V. C. Moore, M. S. Strano, E. H. Haroz, K. L. Rialon, P. J. Boul, W. H. Noon, C. Kittrell, J. Ma, R. H. Hauge, R. B. Weisman, R. E. Smalley, *Science* **2002**, *297*, 593 – 596.
[15] E. Joselevich, *ChemPhysChem* **2004**, *5*, 619 – 624.
[16] S. Trasatti, *J. Electroanal. Chem.* **1974**, *52*, 313 – 329.
[17] *Handbook of Chemistry and Physics*, 81th ed., CRC Press, Boca Raton, **2000**, pp. 8 – 21.
[18] S. Satoru, W. Yoshio, H. Yoshikazu, F. Shin-ya, H. Stefan, L. Andrea, *Appl. Phys. Lett.* **2004**, *85*, 127 – 129.
[19] A. M. Rao, P. C. Eklund, S. Bandow, A. Thess, R. E. Smalley, *Nature* **1997**, *388*, 257 – 279.
[20] L. Kavan, P. Rapta, L. Dunsch, M. J. Bronikowski, P. Willis, R. E. Smalley, *J. Phys. Chem. B* **2001**, *105*, 10764 – 10771.

 © 2006 Wiley-VCH Verlag GmbH & Co. KGaA, Weinheim

Reaction Mechanisms

DOI: 10.1002/anie.200502415

In Situ NMR Spectroscopic Observation of a Catalytic Intermediate in Phosphine-Catalyzed Cyclo-Oligomerization of Isocyanates**

Zoltán Pusztai, Gábor Vlád, Andrea Bodor, István T. Horváth, Hans J. Laas, Reinhard Halpaap, and Frank U. Richter**

Dedicated to Dr. Josef Pedain on the occasion of his 70th birthday

Polyurethanes, manufactured from aromatic and aliphatic isocyanates (**1**),[1] are an important class of high-performance materials. Aliphatic polyisocyanates are the preferred building blocks for coatings and most are based on hexamethylene diisocyanate (HDI). For the majority of applications, oligomers of HDI with significantly lower vapor pressure than that of the monomer are required. These oligomers are predominantly cyclo-oligomers, such as uretdiones **2**,[2] isocyanurates **3**,[3] and iminooxadiazinediones **4**,[4] which can be prepared by catalytic cyclo-oligomerization of monomeric isocyanates.[5] Although phosphines, including tri-*n*-butylphosphine (**5**), have been used commercially as catalysts for more than 20 years,[6] no information is available on the mechanism of the reaction. Based on the reactivity of nucleophiles towards heterocumulenes,[7] the reaction may start by the nucleophilic attack of the phosphine on the carbonyl group of the isocyanate to form a zwitterionic intermediate **A**, followed by reaction with another isocyanate moiety to result in a second zwitterionic intermediate **B** (Scheme 1). Although an intramolecular nucleophilic attack by the $^{-}O(RN)^{-}$ ion on the carbonyl group of **B** could lead to the formation of **2** and **5**, the addition of another isocyanate moiety could result in the formation of zwitterionic intermediates $\mathbf{C_1}$ and $\mathbf{C_2}$. Similarly,

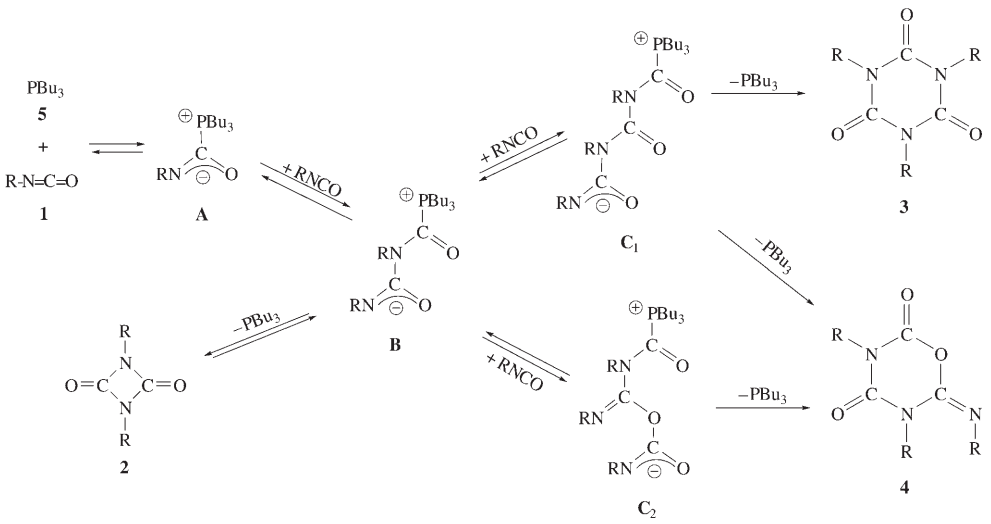
[*] Z. Pusztai,[+] G. Vlád, Dr. A. Bodor, Prof. Dr. I. T. Horváth
Eötvös University
Department of Chemical Technology and Environmental Chemistry
Pázmány Péter sétány 1/A, 1117 Budapest (Hungary)
Fax: (+36) 1209-0607
E-mail: istvan.t.horvath@hit-team.net
Dr. H. J. Laas, Dr. R. Halpaap, Dr. F. U. Richter
Bayer MaterialScience AG
Leverkusen, 51368 (Germany)
E-mail: frank.richter@bayermaterials.com

[+] This work was started by Zoltán Pusztai, a cherished colleague whose untimely death ended a brilliant career prematurely.

[**] This work was supported by Bayer MaterialScience AG (Leverkusen, Germany). The donation of the ReactIR 1000 instrument by Mettler Toledo AutoChem, Inc. is greatly appreciated. We thank the Department of Chemistry at Princeton University for the donation of a Bruker A 250 NMR spectrometer and the American Chemical Society for enabling it to be shipped from Princeton to Budapest.

Supporting information for this article is available on the WWW under http://www.angewandte.org or from the author.

 © 2006 Wiley-VCH Verlag GmbH & Co. KGaA, Weinheim



Scheme 1. Proposed mechanism of the phosphine-catalyzed oligomerization of isocyanates.

intramolecular nucleophilic attack by the $^{-}O(RN)-$ ion on the carbonyl group of $\mathbf{C_1}$ and $\mathbf{C_2}$ could lead to the formation of isocyanurates **3** or iminooxadiazinediones **4**, respectively, and the reformation of **5**. We report herein the first structural characterization of **B** by in situ spectroscopic studies.

The cyclo-oligomerization of alkyl isocyanates (RNCO: R = *n*-butyl and *n*-hexyl **1a** and **1b**, respectively) was studied by in situ IR spectroscopy in the presence of various amounts of **5** in the temperature range 20–80 °C.[8] Even in the presence of a slight excess of **5** (4.8 mmol) in relation to **1a** (4.4 mmol), only the peaks assigned to products **2a**, **3a**, and **4a** (1771; 1694; and 1791, 1719, and 1687 cm^{-1}, respectively) could be observed at 20 °C (Figure 1).[9] At the beginning of the

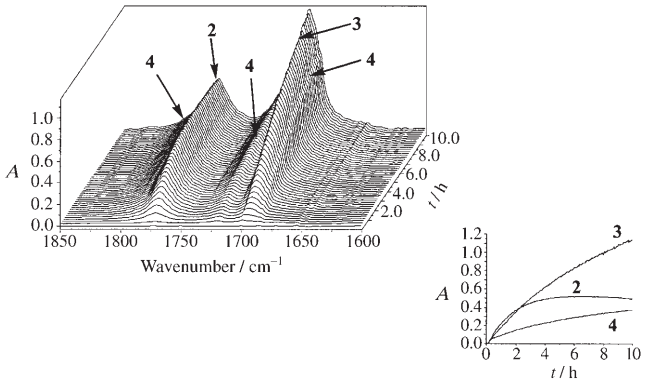


Figure 1. The IR spectra of the carbonyl region during the cyclo-oligomerization of **1a** with **5** at 20 °C.

reaction, the rate of the formation of **2a** is higher than that of **3a** and **4a**, but its concentration reaches a maximum after five hours, thus indicating that the reaction of **2a** with **1a** or yields **3a** and **4a** in almost constant ratios. When 12.2 mmol of **2a** was treated with 1.22 mmol of **5**, the formation of free isocyanates **1a**, **3a**, and **4a** was observed (Figure 2), thus providing direct evidence that the formation of **2a** is a reversible process.

As the in situ IR investigations only showed the formation of the products, we used in situ ^{1}H, ^{13}C, and ^{31}P NMR spectroscopy to confirm these results and to structurally characterize the intermediates. During the tri-*n*-butylphosphine-catalyzed cyclo-oligomerization of **1a**, we observed again the initial formation of **2a** followed by the appearance of **3a** and **4a**.[10] The concentration of **2a** goes to a maximum value, as expected, and at the end of the reaction the ratio of **2a**/**3a**/**4a** is always equal to 0.2:2:1. The in situ

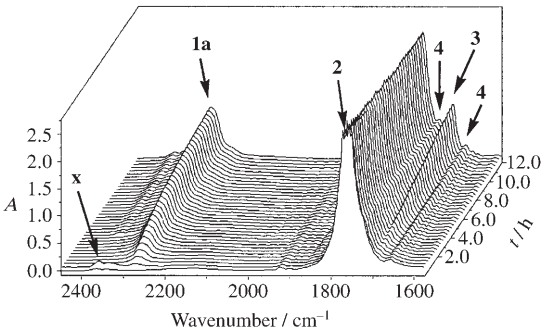


Figure 2. The IR spectra of the carbonyl region during the reaction of **2a** (12.2 mmol) with **5** (1.22 mmol) at 25 °C (the peaks marked with x are due to gaseous CO_2 in the arm of the ReactIR 1000 instrument).

NMR spectroscopic analysis of the reaction of **2a** with **5** also confirmed the formation of free **1a**, **3a**, and **4a**. On the contrary, no reaction was observed when the mixture of **3a** and **4a** was treated with **5**, thus indicating that neither the ring opening of **3** and **4** nor the interconversion between **3** and **4** occurs.[10] Similar results were obtained when **1b** was used as the monomer.

Next, we used ^{31}P NMR spectroscopy to observe the possible intermediate(s) in the reaction between **1b** and **5** in ratios of 1:1, 2:1, and 3:1, thus leading to **A**, **B**, and $\mathbf{C_1}$ and $\mathbf{C_2}$, respectively. Only one resonance at $\delta = -32.9$ ppm (linewidth (LW) = 1 Hz) was observed for **5** at 297 K (Figure 3). By lowering the temperature to 250 K, the appearance of a new, sharp peak is observed at $\delta = -54.0$ ppm (LW = 7 Hz). This peak begins to broaden when the temperature increases from 250 to 270 K (Figure 3) and finally disappears into the baseline at 275 K. It should be noted that below 250 K there is no change in the linewidth of this resonance and that there is no variation in the linewidth of free **5** over the whole temperature range studied. The observed dynamic phenomena can be explained by the fast exchange between the intermediate(s) and free isocyanate. The exact structure of the intermediate was delineated by using 99.0 % ^{13}C-labelled

 © 2006 Wiley-VCH Verlag GmbH & Co. KGaA, Weinheim

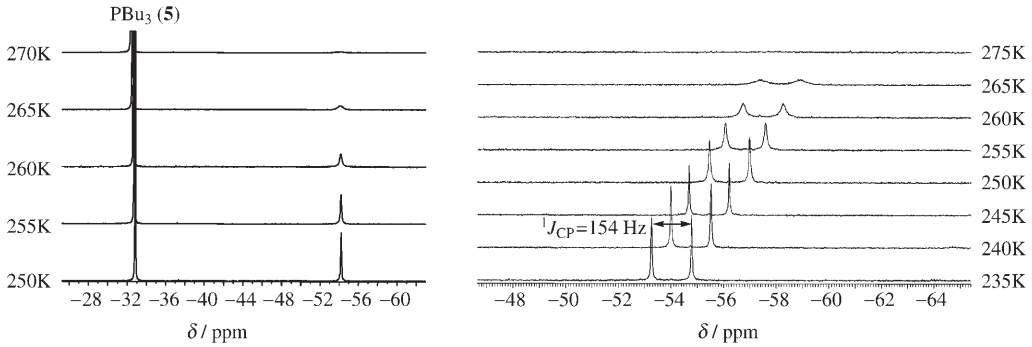


Figure 3. $^{31}P\{^1H\}$ NMR spectra at different temperatures of solutions containing: left: **1b** (3.4 mmol) and **5** (0.4 mmol); right: [^{13}C]*n*-hexyl isocyanate (3.4 mmol) and **5** (0.18 mmol).

n-hexyl isocyanate. The ^{31}P NMR spectrum shows a doublet at $\delta = -54.0$ ppm, with a coupling constant of $J = 154$ Hz, thus indicating P–C coupling over a single bond ($^1J_{PC}$; Figure 3). This observation was confirmed by a doublet of doublets at $\delta = 166.7$ ppm in the ^{13}C NMR spectrum. Besides the coupling constant exhibited by $^1J_{PC}$, a coupling constant of $^2J_{CC} = 2.5$ Hz indicates coupling to another C atom in a second -NC(O)- moiety. Accordingly, a doublet with the same $^2J_{CC}$ value appears at $\delta = 153.9$ ppm (Figure 4). The integral ratio of the

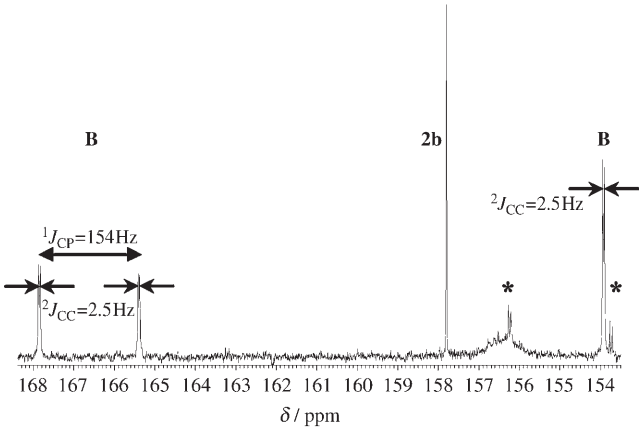


Figure 4. Part of the $^{13}C\{^1H\}$ NMR spectrum at 235 K of a solution containing [^{13}C]*n*-hexyl isocyanate (3.4 mmol) and **5** (0.18 mmol) showing the signals of **B** (* denotes an unidentified species).

peaks at $\delta = 166.7$ and 153.9 ppm is 1:1. These results confirm the presence of a P-^{13}C-N-^{13}C fragment and, thus, the formation of intermediate **B**. Finally, the temperature variation monitored by $^{13}C\{^1H\}$ spectra shows line broadening and disappearance for this intermediate at 275 K, as expected (Figure 5).

In conclusion, we have developed an understanding of the mechanism of the tri-*n*-butylphosphine-catalyzed cyclo-oligomerization of alkyl isocyanates at the molecular level and have structurally characterized one of the key catalytic intermediates for the first time. This information can be used to design new catalysts with built-in selectivity towards various oligomers. Finally, this reaction is a good example for

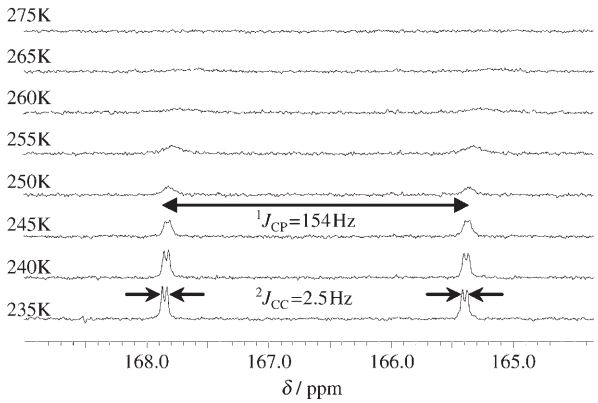


Figure 5. Temperature-dependent $^{13}C\{^1H\}$ NMR spectra for the signal of **B** at $\delta = 166.7$ ppm.

organocatalysis—a rapidly developing field of contemporary homogeneous catalysis.

Experimental Section

n-Butyl isocyanate, *n*-hexyl isocyanate, and tri-*n*-butylphosphine were purified by vacuum distillation. Preparation of [^{13}C]*n*-hexyl isocyanate: *n*-hexylamine (40.4 g, 0.4 mol) and triethylamine (121.4 g, 1.2 mol) were combined with CH_2Cl_2 (43.3 g, solvent) in a steel vessel, cooled to 0 °C, and pressurized with $^{13}CO_2$. The steel vessel containing the amine solution was connected with a lecture bottle containing 10 L of $^{13}CO_2$ (99.0 % isotopic purity, 0.45 mol; Cambridge Isotope) and occasionally shaken. The pressure dropped from 4 to 2.6 bar within 15 h and remained constant thereafter. The vessel containing the carbamate salt solution was 17 g heavier than before, thus indicating an uptake of 0.38 mol of $^{13}CO_2$. After cooling to −24 °C, the content of the steel vessel was transferred to a cooled (−20 °C) solution of $POCl_3$ (73.6 g, 0.48 mol) in CH_2Cl_2 (50 mL). The resulting yellow–orange turbid mixture was extracted with deionized water (3 × 250 mL), the organic phase was dried with sodium sulfate and distilled to yield 23.6 g of product (99.6 % pure, GC analysis; 0.18 mol, 48 % yield based on $^{13}CO_2$ uptake). B.p. 39–40 °C at 5 mbar; ^1H NMR ($CDCl_3$): $\delta = 3.3$ (t/d, $^3J_{HH} = 6.6$ Hz, $^3J_{CH} = 4.5$ Hz, 2H), 1.6 (quin, $^3J_{HH} = 7$ Hz, 2H), 1.25–1.45 (m, 6H), 0.9 (t, $^3J_{HH} = 7$ Hz, 3H); ^{13}C NMR ($CDCl_3$) intense signals at $\delta = 121.9$, 42.9 (d, $^2J_{CNC} = 3.7$ Hz), 31.2, 31.1, 26.2, 22.5, 13.9 ppm.

IR spectra were collected under nitrogen on a ReactIR 1000 instrument using a SiComp probehead.[8] A typical in situ IR experiment was performed by placing the alkyl isocyanate (**1**) onto a

 © 2006 Wiley-VCH Verlag GmbH & Co. KGaA, Weinheim

thermostated (±0.5 °C) schlenk flask fitted with the IR probehead, a nitrogen inlet, a magnetic stirrer, and a septum. Tri-*n*-butylphosphine (**5**) was syringed into the schlenk flask after the data collection of the ReactIR 1000 was started.

^{1}H, ^{13}C, and ^{31}P NMR spectra were recorded on a Bruker AC 250 spectrometer. In a typical in situ NMR experiment, **1** was added into an NMR tube under nitrogen and **5** was added by syringe. The tube was immediately capped with a rubber septum and placed into the magnet for measurements at the preset temperature (±0.05 °C) using standard Bruker pulse sequences.

Received: July 11, 2005
Published online: November 22, 2005

Keywords: IR spectroscopy · isocyanates · NMR spectroscopy · oligomerization · organocatalysis

[1] "Isocyanates, Organic": C. Six, F. Richter, *Ullman's Encyclopedia of Industrial Chemistry*, Wiley-VCH, **2002**.
[2] D. Liebsch, W. Altner, R. Kress (Bayer AG), DE-A 1 670 720, **1966**.
[3] M. Bock, J. Pedain, W. Uerdingen (Bayer AG), EP-A 10589, **1978**.
[4] F. Richter, J. Pedain, H. Mertes, C.-G. Dieris (Bayer AG), EP-A 798299, **1997**.
[5] H. J. Laas, R. Halpaap, J. Pedain, *J. Prakt. Chem.* **1994**, *336*, 196–198.
[6] Compounds of general formula $P(NR_2)_3$ are very selective catalysts for the formation of **2** (DE-A 3030513) but the carcinogenicity of their oxides prohibits a technical-scale application. Special aminopyridines (DE-A 3739549) selectively catalyze the formation of **2** from isophorone diisocyanate, but not for HDI or isocyanates containing exclusively NCO groups bound to a secondary carbon atom like hydrogenated methane diisocyanate or cyclohexyl isocyanate.
[7] H. Ulrich in *Organic Chemistry: A Series of Monographs* (Ed.: A. T. Blomquist), Academic Press, New York, **1967**, pp. 128–133.
[8] ReactIR 1000 Instrument, Mettler Toledo AutoChem, Inc., USA, http://www.mt.com/autochem.
[9] Compounds **2a**, **3a**, and **4a** were prepared and IR spectra (neat) were collected for the reference values.
[10] See the Supporting Information.

 © 2006 Wiley-VCH Verlag GmbH & Co. KGaA, Weinheim

Fullerene Chemistry

DOI: 10.1002/anie.200502556

Retro-Cycloaddition Reaction of Pyrrolidinofullerenes**

Nazario Martín, Margarita Altable, Salvatore Filippone, Angel Martín-Domenech, Luis Echegoyen,* and Claudia M. Cardona*

Dedicated to Professor David Schuster on the occasion of his 70th birthday

The 1,3-dipolar cycloaddition reaction of azomethine ylides to alkenes is one of the most important and elegant methods for the construction of nitrogen-containing five-membered ring compounds. This reaction has been successfully conducted with fullerenes and it is considered one of the most straightforward procedures for their functionalization.[1] The resulting C_{60}-fused pyrrolidines (pyrrolidino[3,4:1,2][60]fullerenes or simply pyrrolidinofullerenes) are easily prepared by reaction of the in situ generated azomethine ylides to [60]fullerene. Although azomethine ylides are reactive intermediates which can be generated in several ways by following efficient synthetic protocols, the decarboxylation of iminium salts, derived from condensation of α-amino acids with aldehydes or ketones, is the easiest and most general procedure commonly followed.[2] Other convenient methods for the synthesis of pyrrolidinofullerenes are based on the thermal ring opening of aziridines, acid-catalyzed or thermal desililation of trimethylsilylamino derivatives, or photochemical treatment of tertiary amines with C_{60}.[3] The isolation and characterization of all eight possible regioisomers of bis-adducts of pyrrolidinofullerene derivatives have also been reported.[4]

Pyrrolidinofullerene cycloadducts have proven to be chemically stable species and, therefore, they typically do

[*] Prof. Dr. N. Martín, M. Altable, Dr. S. Filippone, Dr. A. Martín-Domenech
Departamento de Química Orgánica I
Facultad de Ciencias Químicas
Universidad Complutense de Madrid
Ciudad Universitaria s/n, 28040 Madrid (Spain)
Fax: (+34) 91-394-4103
E-mail: nazmar@quim.ucm.es
Prof. Dr. L. Echegoyen, Dr. C. M. Cardona
Department of Chemistry
Clemson University
219 Hunter Laboratories, Clemson, SC 29634-0973 (USA)
Fax: (+1) 864-656-6613
E-mail: luis@clemson.edu

[**] These investigations were financially supported by the MEC of Spain (Project BQU2002-00855). S.F. thanks the CAM for a postdoctoral contract, and M.A. thanks the MEC for a research grant. L.E. and C.C. thank the US NSF (CHE-0509989) for generous financial support.

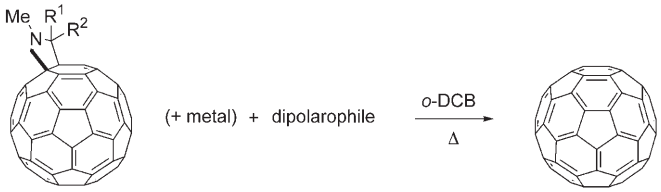
Supporting information for this article is available on the WWW under http://www.angewandte.org or from the author.

WILEY InterScience DISCOVER SOMETHING GREAT
© 2006 Wiley-VCH Verlag GmbH & Co. KGaA, Weinheim

not undergo further chemical transformations. In contrast to other well-known fullerene derivatives, such as Diels–Alder cycloadducts[5] or Bingel's methanofullerenes,[6] which can undergo their corresponding retro-cycloaddition reactions, pyrrolidinofullerenes are considered to be very stable cycloadducts. Herein, we describe the first highly efficient retro-cycloaddition reactions of differently substituted pyrrolidinofullerenes which quantitatively afford the parent unsubstituted fullerene.

It was previously reported that pyrrolidines undergo a retro-cycloaddition reaction which leads to the alkene and the azomethine ylide.[7] Although it is well-known that pyrrolidinofullerenes exhibit a much lower basic and nucleophilic character than pyrrolidines owing to the electronegative character of the fullerene core,[8] we decided to investigate the retro-cycloaddition reaction of pyrrolidinofullerenes under thermal and catalytic conditions.

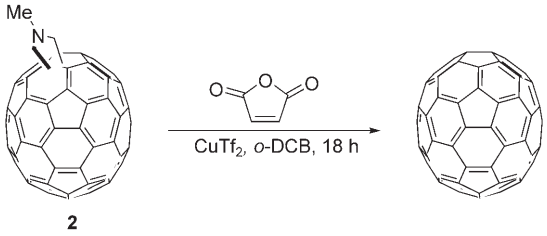
Following previously reported standard procedures,[9] pyrrolidinofullerenes **1a–e** were initially synthesized (Scheme 1). Compound **1a** ($R^1 = R^2 = H$) was heated at reflux in *o*-dicholorobenzene (*o*-DCB) for 24 h in the presence of an excess of a highly efficient dipolarophile, such as maleic anhydride, in order to trap the corresponding ylide that results from the thermal retro-cycloaddition reaction. However, under these conditions the reaction proceeded with a very low yield (Table 1, entry 1: 4.9% of recovered C_{60} as determined by HPLC). When compounds **1b–d** were treated under similar reaction conditions, significantly better yields were obtained (entries 2–4). Surprisingly, when compound **1e** was heated at reflux in *o*-DCB for 12 h under the same experimental conditions (entry 6), C_{60} was recovered quantitatively. In fact, the initial brown solution of the pyrrolidinofullerene **1e** recovered the magenta color typical of solutions of [60]fullerene. Furthermore, **1e** led to pristine C_{60} in 96.5% yield (determined by HPLC) after only 4 h at reflux in *o*-DCB (entry 5, Table 1). These results clearly indicate that the retro-cycloaddition reaction is strongly dependent on the nature of the substituents on the pyrrolidine ring which influence the stability of the thermally generated 1,3-dipole.



1a: $R^1 = R^2 = H$
1b: $R^1 = H$, $R^2 = Ph$
1c: $R^1 = H$, $R^2 = C_{16}H_{11}$
1d: $R^1 = R^2 = CH_3$
1e: $R^1 = H$, $R^2 = COOEt$

Scheme 1. Retro-cycloaddition reaction of pyrrolidinofullerenes **1a–e**.

To improve the efficiency of the removal of the pyrrolidine ring from the carbon sphere to yield pristine C_{60}, we carried out the thermal reaction in the presence of a metal Lewis acid to see if a possible coordination with the nitrogen atom could activate the retro-reaction. When compounds **1a–d** were heated at reflux in *o*-DCB for a variable time (8–18 h) in the presence of maleic anhydride (30 equiv) and copper(II) triflate (1 equiv), the reaction led in all cases (entries 7–10, Table 1) to the quantitative formation of the parent unsubstituted C_{60} (determined by HPLC), solutions of which were the typical magenta color. Interestingly, the reaction also proved to be highly efficient with the mono-adduct mixture of the three isomers of [70]pyrrolidinofullerene (**2**),[10] which afforded under these conditions pristine C_{70} in 95% yield (by HPLC; see entry 11 in Table 1 and Scheme 2).



Scheme 2. Retro-cycloaddition reaction of C_{70} derivative **2** catalyzed by a metal Lewis acid. $Tf = CF_3SO_2$.

The 1,3-dipolar retro-cycloaddition reaction appears to be quite general in terms of substitution on the pyrrolidine ring (unsubstituted **1a**, monosubstituted **1b**,**c**,**e**, and disubstituted **1d**) as well as with higher fullerenes, such as C_{70} and C_{80}.

Table 1: Experimental conditions of the retro-cycloaddition reaction.[a]

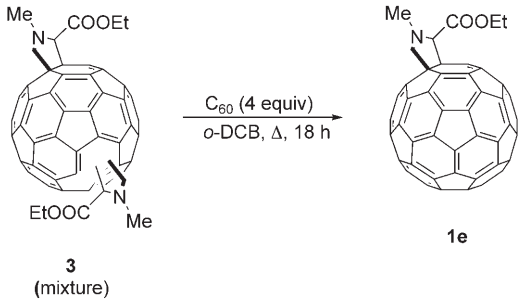
Entry	Compound	Dipolarophile[b]	Catalyst	*t* [h]	Conv. [%][c]
1	**1a**	maleic anhydride	–	24	4.9
2	**1b**	maleic anhydride	–	24	43.5
3	**1c**	maleic anhydride	–	12	35.0
4	**1d**	maleic anhydride	–	24	15.3
5	**1e**	maleic anhydride	–	4	96.5
6	**1e**	maleic anhydride	–	12	100.0
7	**1a**	maleic anhydride	$CuTf_2$[d]	8	100.0
8	**1b**	maleic anhydride	$CuTf_2$[d]	8	99.3
9	**1c**	maleic anhydride	$CuTf_2$[d]	18	100.0
10	**1d**	maleic anhydride	$CuTf_2$[d]	8	100.0
11	**2**	maleic anhydride	$CuTf_2$[d]	18	95.0
12	**1e**	*N*-phenylmaleimide	$(Ph_3P)_3RhCl$[e]	18	100.0
13	**1e**	maleic anhydride	$(Ph_3P)_3RhCl$[e]	18	97.2
14	**1e**	1,4-benzoquinone	$(Ph_3P)_3RhCl$[e]	18	79.9
15	**1e**	diethyl maleate	$(Ph_3P)_3RhCl$[e]	18	60.9
16	**3**	C_{60} (4 equiv)	–	18	100.0

[a] All the reactions were carried out in *o*-DCB at reflux (4–24 h); [b] 30 equiv dipolarophile used unless otherwise stated. [c] Conversion determined by HPLC. [d] 1 equiv $CuTf_2$ (copper(II) trifluoromethylsulfonate) used. [e] 0.1 equiv Wilkinson's catalyst ($(Ph_3P)_3RhCl$) used.

 © 2006 Wiley-VCH Verlag GmbH & Co. KGaA, Weinheim

To explore the use of other metals as well as the influence of the trapping dipolarophile on the reaction outcome, we carried out the thermal retro-cycloaddition reaction of **1e** in the presence of catalytic amounts of Wilkinson's catalyst (0.1 equiv) and using a variety of different efficient dipolarophiles (entries 12–15, Table 1). After heating at reflux in *o*-DCB for 18 h, the reaction gave good yields of C_{60} when *N*-phenylmaleimide (100%) or maleic anhydride (97.2%) was used as dipolarophiles. However, lower yields were observed when either 1,4-benzoquinone (79.9%) or diethyl maleate (60.9%) was used as the trapping dipolarophile (entries 14 and 15).

It is well-known that [60]fullerene is a very efficient dipolarophile, and, therefore, we decided to evaluate its effectiveness in the present reaction. To test this, a mixture of bis-cycloadducts **3** was heated at reflux in *o*-DCB for 18 h in the presence of an excess (4 equiv) of pristine C_{60} (Scheme 3).



3 (mixture) **1e**

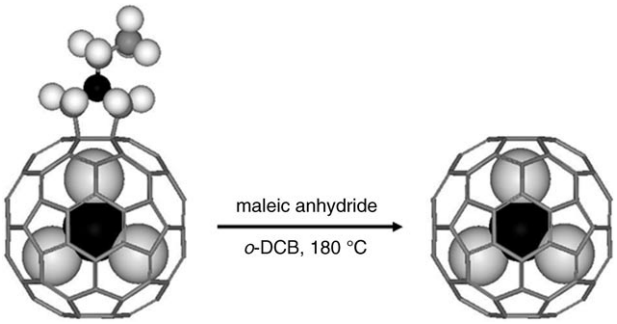
Scheme 3. Reaction of a mixture of bis-adducts **3** in the presence of C_{60} as dipolarophile.

The mono-adduct was recovered quantitatively (100% by HPLC) together with unreacted C_{60} (entry 16). This finding confirms the general scope of this thermal retro-cycloaddition reaction and opens new avenues for improving the yields of mono-adduct formation from the usually undesired bis-cycloadducts in many 1,3-dipolar cycloaddition reactions of differently substituted azomethine ylides.

Depending on the substitution pattern on the pyrrolidinofullerene moiety, we can use different protocols to quantitatively remove the pyrrolidine ring from the carbon sphere to recover the parent fullerene. This new reaction significantly enhances the utility of one of the most important and successful reactions in the chemistry of fullerenes, as it can now be used as a highly efficient protection/deprotection protocol. This new strategy will enable the preparation of unusual addition patterns on different fullerenes. Just as the cyclopropanation/retro-cyclopropanation protocol has been successfully used in the purification of higher fullerenes and their enantiomers,[11] the pyrrolidine/retro-pyrrolidine strategy described here has the potential for similar applications. We thus decided to apply this thermal retro-cycloaddition reaction to the separation of pyrrolidine derivatives of trimetallic nitride endohedral metallofullerenes, whose constitutional isomers are difficult to separate.[12]

Recently, some of us reported the synthesis and characterization of a mono-adduct derivative of $Sc_3N@C_{80}$, an *N*-ethylpyrrolidinofullerene.[13] ^1H, ^{13}C, and 2D NMR experiments of this mono-adduct confirmed that the cycloaddition occurred selectively at a corannulene-type site (a double bond at a [5,6] ring junction abutted by two hexagons) of the icosahedral (I_h) C_{80} cage, in the same position as that described previously for a Diels–Alder mono-adduct of the same compound.[14] In our synthesis, the 1,3-dipolar cycloaddition reaction was very selective, and only one regioisomer product of the I_h constitutional isomer of $Sc_3N@C_{80}$ was isolated, even when the reaction was conducted in the presence of $Sc_3N@C_{78}$ (and presumably D_{5h} $Sc_3N@C_{80}$).[12] Therefore, the cycloaddition selectively extracts the I_h constitutional isomer from the product mixture, and the subsequent retro-cycloaddition constitutes an efficient purification method for I_h-symmetric $Sc_3N@C_{80}$ by its separation from other endohedral metallofullerenes and other constitutional isomers.

The 1,3-dipolar retro-cycloaddition reaction was successfully carried out with *N*-ethylpyrrolidino-$Sc_3N@C_{80}$ (with a ^{13}C label incorporated in the pyrrolidine ring) by heating at reflux in *o*-dichlorobenzene (20–24 h) in the presence of maleic anhydride (30 equiv) in sealed NMR tubes in the dark (Scheme 4). The retro-cycloaddition reaction of this endohedral metallofullerene was followed by TLC, HPLC, and NMR spectroscopy. The heteronuclear multiple quantum coherence (HMQC) NMR spectrum of the derivative (Figure 1) clearly shows that the starting compound is a pure pyrrolidine mono-adduct derivative of $Sc_3N@C_{80}$. The ^{13}C NMR spectrum exhibits a single signal at $\delta = 69.56$ ppm in [D_4]-*o*-dichlorobenzene, indicating that both the methylene carbon atoms of the five-membered ring are equivalent. The complete disappearance of the single ^{13}C signal after heating this derivative at 180 °C in the presence of maleic anhydride for 22 h indicates that retro-cycloaddition occurred in high yield as the pyrrolidine adduct is no longer present (Figure 1).



Scheme 4. 1,3-Dipolar retro-cycloaddition of *N*-ethylpyrrolidino-$Sc_3N@C_{80}$.

The reaction proved to be quantitative upon analysis by TLC (93% recovered after column chromatography on SiO_2), and only $Sc_3N@C_{80}$ was isolated and characterized by HPLC (Figure 2, peak at 6.16 min) and MALDI mass spectrometry. We believe that the product must be the I_h isomer, as this was the only isomer of the pyrrolidine derivative present initially.

 © 2006 Wiley-VCH Verlag GmbH & Co. KGaA, Weinheim

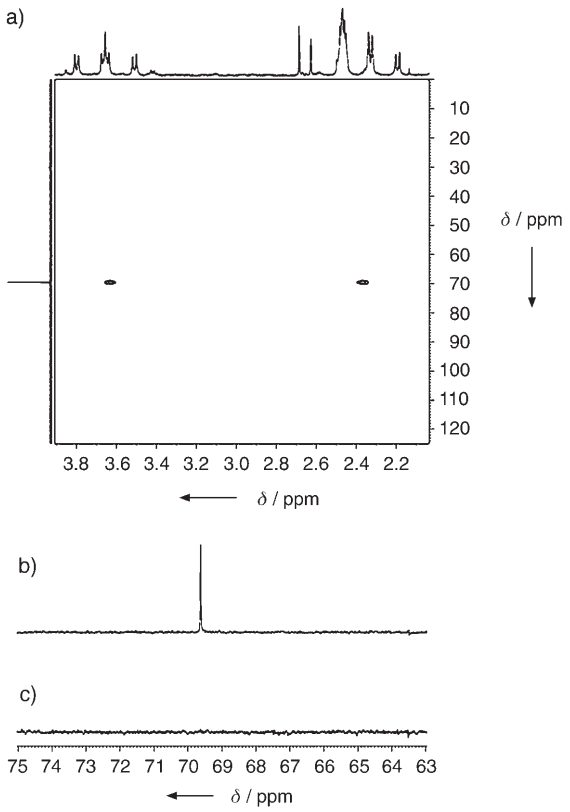


Figure 1. a) HMQC NMR spectrum of ^{13}C-labeled I_h-symmetric *N*-ethylpyrrolidino-$Sc_3N@C_{80}$ mono-adduct in [D_4]-*o*-dichlorobenzene, and b, c) ^{13}C NMR spectra recorded before (a) and after (b) heating the adduct at reflux in the presence of maleic anhydride in *o*-dichlorobenzene.

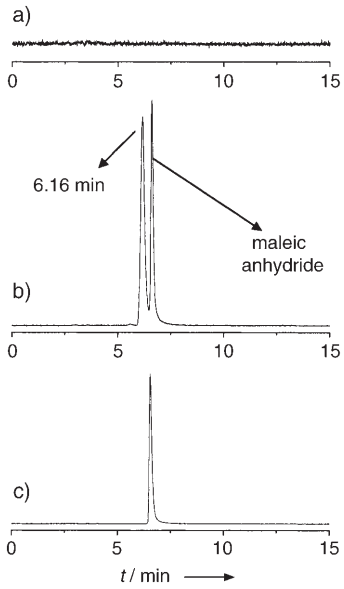


Figure 2. HPLC traces of a) the initial reaction mixture, b) the mixture after completion of the reaction, and c) maleic anhydride under identical conditions (Buckyclutcher column: 25 cm × 10 mm (Regis Chemical Company); toluene, flow rate: 4 mL min^{-1}; detection at $\lambda = 310$ nm).

The retro-cycloaddition proceeded in the presence of maleic anhydride as the dipolarophile in both dark aerobic and anaerobic conditions. ^{12}C- and ^{13}C-enriched formaldehyde was a noticeable by-product of the retro-cycloaddition reaction under oxygenated conditions when ^{13}C-labeled *N*-ethylpyrrolidinofullerene was employed, as shown by the ^{1}H NMR spectra (Figure 3) recorded before and after retro-

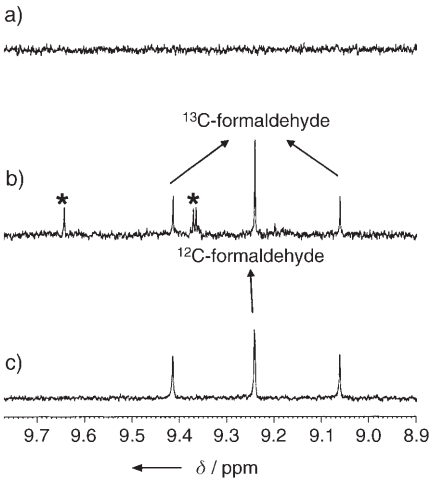
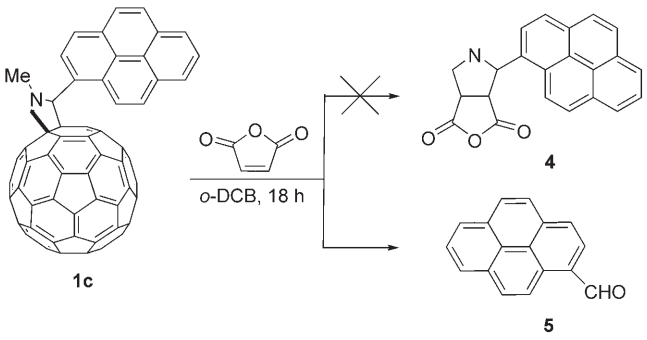


Figure 3. ^{1}H NMR spectrum of ^{13}C-enriched I_h-symmetric *N*-ethylpyrrolidino-$Sc_3N@C_{80}$ a) before the reaction and b) after 22 h at 180 °C in the presence of maleic anhydride, showing signals for the azomethine ylide product after retro-cycloaddition. c) ^{1}H NMR spectrum of a (control) solution of maleic anhydride and paraformaldehyde (both ^{12}C- and ^{13}C-enriched) in [D_4]-*o*-dichlorobenzene after 22 h at 180 °C. The asterisk (*) denotes unknown products.

cycloaddition. Such a strategy also worked successfully and quantitatively for the isolation of I_h-symmetric $Y_3N@C_{80}$ when *N*-ethylpyrrolidino-[5,6]-$Y_3N@C_{80}$[15] was subjected to the retro-cycloaddition conditions described above. We are currently analyzing the other by-products of the reaction and investigating the roles of oxygen and light in the reaction in order to elucidate the mechanism and compare it to the retro-cycloaddition of fullerene derivatives with empty cages. Our interest also lies in the isolation of other constitutional isomers such as D_{5h}-symmetric $Sc_3N@C_{80}$, which has eluded isolation thus far.

Although the reaction mechanism of the retro-cycloaddition reaction is not yet clear, the above experiments suggest that thermal treatment leads to the formation of the azomethine ylide, which is efficiently trapped by the dipolarophile that is present in the reaction medium. When pyrrolidinofullerene **1c**, which bears a fluorescent pyrene unit as substituent at C2 of the pyrrolidine ring, was heated at reflux in *o*-DCB under standard conditions (maleic anhydride (30 equiv), 18 h), formation of the corresponding pyrene-substituted pyrrolidine **4** was not observed. However, aldehyde **5** was isolated as the only characterizable compound instead (Scheme 5) which thus suggests that oxygen could play a role in the evolution of the 1,3-dipole, although the influence of the trace amounts of water present in the solvent cannot be ruled out. More studies are therefore required to

 © 2006 Wiley-VCH Verlag GmbH & Co. KGaA, Weinheim



Scheme 5. Retro-cycloaddition reaction of pyrene-substituted pyrrolidinofullerene **1c**.

determine if this is a simple thermal cycloreversion or a more-complex oxidative process. In this regard, preliminary investigations using oxidative controlled-potential electrolysis indicate that retro-cycloaddition is also efficiently obtained under these conditions. These experiments are ongoing and may shed additional information about the nature of the mechanism.

Experimental Section

In a typical experiment, pyrrolidinofullerene (0.02 mmol), dipolarophile (0.06 mmol), and metal catalyst (0.002 mmol) were heated at reflux in *o*-DCB (6 mL). The reaction was monitored by HPLC (Cosmosil Buckyprep column, 4.6 mm (i.d.) × 250 mm; toluene, flow rate: 1 mL min^{-1}). Retention times: 5.8–6.2 min for the pyrrolidinofullerenes; 8.0 min for C_{60}.

Received: July 21, 2005
Published online: October 20, 2005

Keywords: azomethine ylides · cycloaddition · fullerenes · nitrogen heterocycles · retro reactions

[1] a) A. Hirsch, M. Brettreich, *Fullerenes: Chemistry and Reactions*, Wiley-VCH, Weinheim, **2005**; b) *Fullerenes: From Synthesis to Optoelectronic Properties* (Eds.: D. M. Guldi, N. Martín), Kluwer Academic Publishers, Dordrech, **2002**.
[2] a) M. Prato, M. Maggini, *Acc. Chem. Res.* **1998**, *31*, 519–526; b) N. Tagmatarchis, M. Prato, *Synlett* **2003**, 768–779.
[3] M. Maggini, E. Menna in *Fullerenes: From Synthesis to Optoelectronic Properties* (Eds.: D. M. Guldi, N. Martín), Kluwer Academic Publishers, Dordrech, **2002**, pp. 1–50, chap. 1.
[4] K. Kordatos, S. Bosi, T. Da Ros, A. Zambon, V. Lucchini, M. Prato, *J. Org. Chem.* **2001**, *66*, 2802–2808.
[5] N. Martín, J. L. Segura, F. Wudl in *Fullerenes: From Synthesis to Optoelectronic Properties* (Eds: D. M. Guldi, N. Martín), Kluwer Academic Publishers, Dordrech, **2002**, chap. 3, pp. 81–120.
[6] a) C. Bingel, *Chem. Ber.* **1993**, *126*, 1957–1959; b) X. Camps, A. Hirsch, *J. Chem. Soc. Perkin Trans. 1* **1997**, 1595–1596.
[7] S. Sinbandhit, J. Hamelin, *J. Chem. Soc. Chem. Commun.* **1977**, 768–769.
[8] A. Bagno, S. Claeson, M. Maggini, M. L. Martini, M. Prato, G. Scorrano, *Chem. Eur. J.* **2002**, *8*, 1015–1023.
[9] a) M. Maggini, G. Scorrano, M. Prato, *J. Am. Chem. Soc.* **1993**, *115*, 9798–9799; b) D.-J. Zhou, L.-B. Gan, H.-S. Tan, C.-P. Luo, C.-H. Huang, J.-Q. Pan, M.-J. Lu, Y. Wu, *Chin. Chem. Lett.* **1995**, *6*, 1033–1036; c) K. Kordatos, T. Da Ros, M. Prato, D. Guldi, *Monatsh. Chem. E* **2001**, *132*, 63–70; d) Spectral data for **1d**: ^{1}H NMR (300 MHz, $CDCl_3/CS_2$): $\delta = 1.71$ (s, 6H, $2CH_3$), 2.56 (s, 3H, CH_3), 4.23 ppm (s, 2H, CH_2); ^{13}C NMR (300 MHz, $CDCl_3/CS_2$): $\delta = 22.5$, 33.9, 65.4, 68.6, 69.3, 79.1, 136.0, 136.4, 139.6, 140.0, 141.5, 141.7, 141.8, 141.9, 142.0, 142.2, 142.5, 143.0, 144.3, 144.4, 145.0, 145.1, 145.2, 145.5, 145.8, 145.9, 146.0, 146.1, 146.3, 147.2, 154.3, 156.0 ppm; MS (ESI): m/z: 805 $[M]^+$; e) L.-B. Gan, D.-J. Zhou, C.-P. Luo, H.-S. Tan, C.-H. Huang, M.-J. Lu, J.-Q. Pan, Y. Wu, *J. Org. Chem.* **1996**, *61*, 1954–1961.
[10] S. R. Wilson, Q. J. Lu, *J. Org. Chem.* **1995**, *60*, 6496–6498.
[11] M. Á. Herranz, F. Diederich, L. Echegoyen, *Eur. J. Org. Chem.* **2004**, 2299–2316, and references therein.
[12] a) J. C. Duchamp, A. Demortier, K. R. Flrtche, D. Dorn, E. B. Iezzi, T. Glass, H. C. Dorn, *Chem. Phys. Lett.* **2003**, *375*, 655–659; b) M. Krause, L. Dunsch, *ChemPhysChem* **2004**, *5*, 1445–1449.
[13] C. M. Cardona, A. Kitaygorodskiy, A. Ortiz, M. A. Herranz, L. Echegoyen, *J. Org. Chem.* **2005**, *70*, 5092–5097.
[14] a) E. B. Iezzi, J. C. Duchamp, K. Harich, T. E. Glass, H. M. Lee, M. M. Olmstead, A. L. Balch, H. C. Dorn, *J. Am. Chem. Soc.* **2002**, *124*, 524–525; b) H. M. Lee, M. M. Olmstead, E. Iezzi, J. C. Duchamp, H. C. Dorn, A. L. Balch, *J. Am. Chem. Soc.* **2002**, *124*, 3494–3495.
[15] a) C. M. Cardona, A. Kitaygorodskiy, L. Echegoyen, *J. Am. Chem. Soc.* **2005**, *127*, 10448–10453; b) C. M. Cardona, L. Echegoyen, unpublished results.

 © 2006 Wiley-VCH Verlag GmbH & Co. KGaA, Weinheim

DNA Structures

DOI: 10.1002/anie.200503110

Stabilization of the DNA I-Motif Structure by Incorporation of 3′-*S*-Phosphorothiolate Linkages**

John A. Brazier, Julie Fisher, and Richard Cosstick**

The telomeric regions of human chromosomes contain a cytosine-rich strand that can associate into a unique four-

[*] Dr. J. Fisher
Department of Chemistry
University of Leeds
Leeds, LS2 9JT (UK)
Fax: (+44) 113-343-656
E-mail: J.Fisher@chem.leeds.ac.uk
Dr. J. A. Brazier, Dr. R. Cosstick
Department of Chemistry
University of Liverpool
Crown Street, Liverpool, L69 7ZD (UK)
Fax: (+44) 151-794-3588
E-mail: rcosstic@liv.ac.uk

[**] This work was financially supported by the Biotechnology and Biological Sciences Research Council. We would like to thank Allan Mills (Liverpool) for obtaining mass spectra.

Supporting information for this article is available on the WWW under http://www.angewandte.org or from the author.

WILEY InterScience DISCOVER SOMETHING GREAT
© 2006 Wiley-VCH Verlag GmbH & Co. KGaA, Weinheim

stranded and intercalated structure, commonly known as an i-motif.[1–3] This structure is formed from two parallel-stranded duplexes containing hemiprotonated cytosine–cytosine ($C{\cdot}CH^+$) base pairs (C = cyt = cytosine). The two duplexes run antiparallel to each other and are intimately associated by base-pair intercalation.[4–6] Stoichiometrically, the i-motif can be assembled through the association of four strands,[4] by two hairpins each containing two cytosine-rich regions[7] or by the folding of a single strand containing four cytosine stretches[8] (as is the case in the human telomeric sequence d-[$(CCCTA_2)_3CCCT$]).[1,3] Consistent with the hemiprotonated base pairs, the stability of the i-motif is pH dependent and is at a maximum at a pH value close to the pK_a value of cytosine.[9] At a neutral pH value, the i-motif is much less stable although it can still be observed in intramolecular systems.[1,9] The recent discovery of proteins that specifically bind the cytosine-rich strand of human telomeric sequences, combined with the stability of an intramolecular i-motif at physiological pH values, implies a biological role.[10] Detailed structural features of the i-motif have been revealed by both NMR and X-ray crystallographic techniques.[9,11] Viewed along the helical axis, the i-motif displays two wide grooves and two narrow grooves with close sugar–sugar contacts in the narrow groove.[8] The deoxyribose sugars adopt an *endo* conformation at C3′, which is typical for RNA A-type duplexes.[1,9]

To probe the importance of some of the structural features, a number of 2′-deoxycytidine analogues have been substituted into the i-motif. Surprisingly, despite the C3′-*endo*-conformational preference of ribonucleosides, melting studies have shown that the RNA i-motif is much less stable than the analogous DNA structure.[12,13] Destabilization by the ribose sugar appears to result from a steric clash between 2′-hydroxy groups in the narrow groove. In support of this steric effect, replacement of a single 2′-hydroxy group by the bulkier 2′-*O*-methyl substituent abolishes formation of the i-motif,[12] whereas the incorporation of D-arabinocytidine (2′-hydroxy group pointing away from the narrow groove) has a neutral effect.[14] Other analogues of deoxycytidine that have been studied in this context include 5-methyldeoxycytidine [9,15] and the phosphorothioate,[15,16] methylphosphonate,[15] and 3′-*N*-phosphoramidate[15] backbone modifications. However, none of these modifications stabilize the i-motif relative to the natural sequences. In one report, an intramolecular i-motif (derived from TCCTCCTTTTCCTCCT) was stabilized through replacement of thymidine by 5-propynyl deoxyuridine.[15] This modification presumably acts by stabilization of the loop regions of the structure through hydrophobic interactions rather than stabilizing the unique structural features of the i-motif.

Our previous studies have shown that incorporation of a 3′-*S*-phosphorothiolate linkage into DNA shifts the conformational preference of the sugar to which the sulfur atom is attached to the C3′-*endo* (north) pucker (Figure 1a). This alteration thus mimics the RNA conformation without the introduction of a substituent at the C2′.[17] In this study we have introduced either one or two phosphorothiolate linkages (Figure 1b) into d(TCCCCC) and report the first example of a deoxycytidine analogue that stabilizes an i-motif.

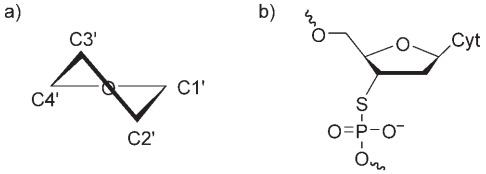


Figure 1. a) North (C3′-*endo*) sugar pucker. b) 3′-S-phosphorothiolate linkage. Cyt = cytosin-1-yl.

Oligonucleotides that contain phosphorothiolate linkages were synthesized by using a 3′-*S*-phosphorothioamidite derived from deoxycytidine and prepared as previously described.[18] The sequences studied are presented in Table 1. i-Motif structures were assembled in citrate buffer at pH 4.6 and the samples were stored, as previously described, at 4 °C for one week to give a single i-motif tetrad.[12]

Table 1: ESI mass spectrometry data and UV T_m data.

Sequence[a]	Mass calcd	Mass obs.[b]	T_m [°C][c]
d(TCCCCC)	1687.3221	1687.3330	46.0
d(TCC**Cs**CC)	1703.2993	1703.2780	48.5
d(TCC**Cs**C**Cs**C)	1719.2765	1719.2950	53.0
d(TC**Cs**C**Cs**CC)	1719.2765	1719.2991	54.5

[a] **Cs** indicates a cytidine phosphorothiolate analogue. [b] The measurement was carried out in negative mode and the sample prepared in aqueous methanol + diethylamine (0.1%). [c] Sodium citrate buffer (50 mM, pH 4.6), 5 μM strand concentration.

Both the natural and modified sequences exhibited melting behavior characteristic of an i-motif with an increase in absorption at 260 nm and a hypochromic transition at 295 nm. The melting temperature (T_m) of the unmodified i-motif is consistent with that previously reported for this sequence (48 °C) at a higher concentration (11.5 μM).[12] Incorporation of a single 3′-*S*-phosphorothiolate linkage at C4 [d(TCC**Cs**CC)] gave a modest increase in T_m (ΔT_m) of 2.5 °C but a much greater effect was seen when two modifications were introduced. The modifications of d(TCC**Cs**C**Cs**C) and d(TC**Cs**C**Cs**CC) resulted in ΔT_m values of 7.0 and 8.5 °C, respectively. The moderate increase of the singly modified i-motif may be related to the twofold symmetry axis of the tetrad present at C4. These data demonstrate the considerable stabilizing effect of the phosphorothiolate modification on the i-motif structure.

Although the hypochromic transition at 295 nm is supportive of an i-motif structure, further evidence was sought from solution NMR spectroscopic investigations. 1D ^{1}H NMR spectra recorded for d(TCC**Cs**CC) (Figure 2a) displayed four distinct imino proton resonances at chemical shifts greater than $\delta = 15$ ppm; the imino group at C6 was exchanged/broadened beyond observation under the conditions adopted. These signals arise from imino hydrogen atoms on protonated cytosines that are involved in hydrogen bonding and are thus characteristic of an i-motif. Non-hydrogen bonded imino protons of this type would be shifted

 © 2006 Wiley-VCH Verlag GmbH & Co. KGaA, Weinheim

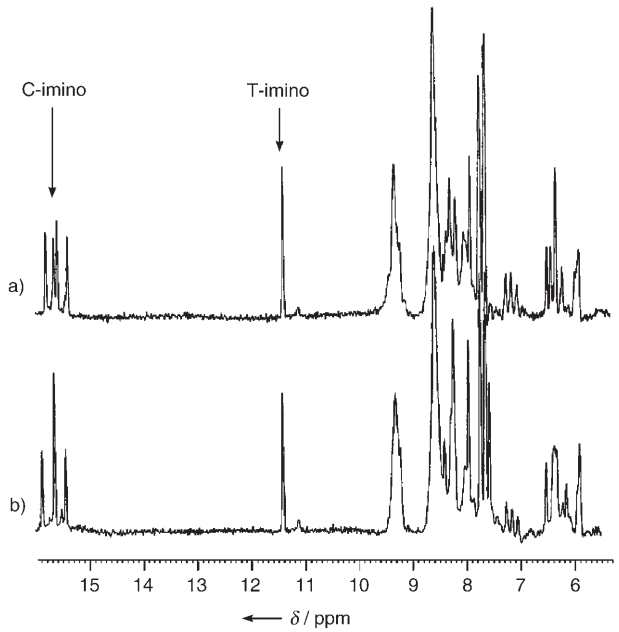


Figure 2. Downfield region of the 500 MHz 1D ^{1}H NMR spectra recorded for i-motifs a) d(TCC**Cs**CC) and b) d(TCCCCC). Conditions: 1 mM oligonucleotide in 50 mM citrate buffer, H_2O/D_2O solution (9:1), pH 4.6, 10 °C. The signal for water was suppressed by using the WATERGATE sequence.

several ppm upfield.[4,5] The single resonance at $\delta = 11.4$ ppm is due to the imino proton of the thymine residue and is consistent with the presence of a single i-motif structure. Overall, the spectrum is very similar to that obtained for the nonmodified sequence d(TCCCCC) (Figure 2b),[5] with some variation apparent in the midrange imino proton and the H1′ chemical shifts.

A comparison of NOESY spectra recorded for d(TCC**Cs**CC) with those obtained for d(TCCCCC)[4] enabled resonance assignments to be made, some of which are shown in Figure 3. It is interesting that the signal for the imino hydrogen atom at C3 is shifted downfield in d(TCC**Cs**CC) and likely reflects a change in conformation of the tetraplex in this region. The H1′ of C6 shifts downfield upon introduction of the phosphorothiolate linkage, which may reflect a tightening of the structure in this region. The NOESY data for d(TCC**Cs**CC) also exhibits nonsequential imino–imino and H1′–H1′ (Figure 3b) close-spatial relationships that are another characteristic of i-motif structures. These data are consistent with a fully intercalated structure with a base-pair stacking order of Thy1-Cyt6-Cyt2-Cyt5-Cyt3-Cyt4-Cyt4-Cyt3-Cyt5-Cyt2-Cyt6-Thy1 (bases from one duplex are underlined), which is the same base-pair order as that observed for the unmodified sequence.

In conclusion, the UV melting and NMR spectroscopic studies clearly demonstrate that phosphorothiolate incorporation stabilizes the i-motif with a minimum perturbation of the overall structure and is the first example of a deoxycytidine analogue that stabilizes the i-motif. This stabilization almost certainly arises from the preference of the phosphorothiolate residues for the C3′-*endo* sugar pucker, which is universally observed in solution for the cytidine sugars in the i-motif. These results also strongly suggest that the destabilization of the i-motif by ribose sugars is due to the 2′-substituent and not the C3′-*endo* sugar pucker.

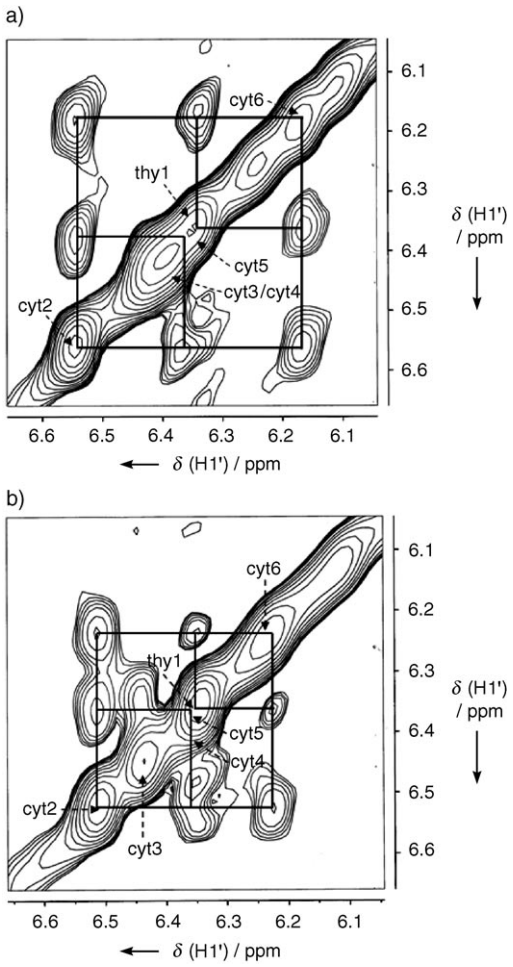


Figure 3. 500 MHz NOESY spectrum of the H1′–H1′ region, recorded for a) d(TCCCCC) and b) d(TCC**Cs**CC). Conditions are as described in Figure 2. NOESY spectra were recorded with $\tau_M = 200$ ms, 2048 points were collected in t_2 and 512 in t_1 by using TPPI phase cycling. Prior to Fourier transformation, a Gaussian function with gb = 0.02 and lb = −10 Hz was applied in both dimensions. The assignments shown for d(TCCCCC) were taken directly from reference [4], and those for d(TCC**Cs**CC) were made through comparison. Cyt = cytosine, Thy = thymine.

Received: September 1, 2005
Published online: November 21, 2005

Keywords: DNA structures · i-motif · NMR spectroscopy · nucleic acids · phosphorothiolates

[1] J. L. Leroy, M. Gueron, J. L. Mergny, C. Helene, *Nucleic Acids Res.* **1994**, *22*, 1600.
[2] S. Ahmed, A. Kintanar, E. Henderson, *Nat. Struct. Biol.* **1994**, *1*, 83.
[3] A. T. Phan, M. Gueron, J. L. Leroy, *J. Mol. Biol.* **2000**, *299*, 123.
[4] K. Gehring, J. L. Leroy, M. Gueron, *Nature* **1993**, *363*, 561.

 © 2006 Wiley-VCH Verlag GmbH & Co. KGaA, Weinheim

[5] J. L. Leroy, K. Gehring, A. Kettani, M. Gueron, *Biochemistry* **1993**, *32*, 6019.
[6] M. Gueron, J. L. Leroy, *Curr. Opin. Struct. Biol.* **2000**, *10*, 326.
[7] P. Catasti, X. Chen, L. L. Deaven, R. K. Moyzis, E. M. Bradbury, G. Gupta, *J. Mol. Biol.* **1997**, *272*, 369.
[8] X. G. Han, J. L. Leroy, M. Gueron, *J. Mol. Biol.* **1998**, *278*, 949.
[9] J. L. Mergny, L. Lacroix, X. G. Han, J. L. Leroy, C. Helene, *J. Am. Chem. Soc.* **1995**, *117*, 8887.
[10] a) E. Marsich, A. Piccini, L. E. Xodo, G. Manzini, *Nucleic Acids Res.* **1996**, *24*, 4029; b) L. Lacroix, H. Lienard, E. Labourier, M. Djavaheri-Mergny, J. Lacoste, H. Leffers, J. Tazi, C. Helene, J. L. Mergny, *Nucleic Acids Res.* **2000**, *28*, 1564.
[11] a) L. Q. Chen, L. Cai, X. H. Zhang, A. Rich, *Biochemistry* **1994**, *33*, 13540; b) C. H. Kang, I. Berger, C. Lockshin, R. Ratliff, R. Moyzis, A. Rich, *Proc. Natl. Acad. Sci. USA* **1995**, *92*, 3874.
[12] D. Collin, K. Gehring, *J. Am. Chem. Soc.* **1998**, *120*, 4069.
[13] K. Snoussi, S. Nonin-Lecomte, J. L. Leroy, *J. Mol. Biol.* **2001**, *309*, 139.
[14] S. Robidoux, M. J. Damha, *J. Biomol. Struct. Dyn.* **1997**, *15*, 529.
[15] L. Lacroix, J. L. Mergny, *Arch. Biochem. Biophys.* **2000**, *381*, 153.
[16] a) H. Kanehara, M. Mizuguchi, K. Tajima, K. Kanaori, K. Makino, *Biochemistry* **1997**, *36*, 1790; b) K. Kanaori, S. Sakamoto, H. Yoshida, P. Guga, W. Stec, K. Tajima, K. Makino, *Biochemistry* **2004**, *43*, 5672.
[17] a) A. P. G. Beevers, K. J. Fettes, I. A. O'Neil, S. M. Roberts, J. R. P. Arnold, R. Cosstick, J. Fisher, *Chem. Commun.* **2002**, 1458; b) A. P. G. Beevers, K. J. Fettes, G. Sabbagh, F. K. Murad, J. R. P. Arnold, R. Cosstick, J. Fisher, *Org. Biomol. Chem.* **2004**, *2*, 114.
[18] G. Sabbagh, K. J. Fettes, R. Gosain, I. A. O'Neil, R. Cosstick, *Nucleic Acids Res.* **2004**, *32*, 495.

 © 2006 Wiley-VCH Verlag GmbH & Co. KGaA, Weinheim

Aza-Henry Reaction

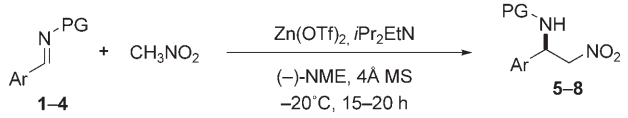
DOI: 10.1002/anie.200502674

Enantioselective Aza-Henry Reactions Assisted by Zn^{II} and *N*-Methylephedrine**

Claudio Palomo, Mikel Oiarbide, Rajkumar Halder, Antonio Laso, and Rosa López*

The addition reaction of nitro compounds to azomethine functions, known as the aza-Henry (or nitro-Mannich) reaction,[1] is a highly valuable C–C bond-forming process. The resulting 1,2-nitroamine adducts can be transformed into 1,2-diamines[2] by reduction[3] as well as α-amino acids by a Nef oxidation.[4] Whereas the production of both families of target molecules in nonracemic form bears considerable interest, the use of the aza-Henry approach in that endeavor remains largely unexplored because of the long-standing lack of (catalytic) asymmetric versions.[1,5] In this context, Shibasaki and co-workers[6] described the use of binaphthoxide (binol)-based heterobimetallic complexes of ytterbium and aluminum as catalysts of the reaction of nitro compounds with *N*-phosphinoyl imines derived from aromatic aldehydes, while Jørgensen and co-workers[7] used copper bis(oxazoline) complexes to catalyze the reaction of silyl nitronates with α-imino esters. These methods usually require a high catalyst loading (20 mol%), and the substrate scope is limited with regards to one or both of the reaction partners.[8] Three alternative organocatalytic aza-Henry reactions using unmodified nitro compounds have also appeared.[9] Johnston and co-workers[9a] reported a chiral bisamidine triflate salt that induced diastereoselective addition of nitroethane to several *N*-Boc-protected aryl imines (Boc = *tert*-butyloxycarbonyl), specifically those bearing electron-withdrawing groups, while Takemoto and co-workers described[9b] moderate enantioselectivities in reactions of nitromethane and aromatic *N*-phosphinoyl imines induced by bifunctional ureas. Most recently, Yoon and Jacobsen[9c] have documented a thiourea-based catalytic aza-Henry reaction of aromatic *N*-Boc imines leading to high enantioselectivities. Again, organocatalytic methods featured some important restrictions regarding the substrate scope and/or selectivity.

Some of us recently found[10] that cooperative activation[11] of nitro compounds and aldehydes towards the Henry reaction can be effected by combination of $Zn(OTf)_2$ (OTf = trifluoromethylsulfonate), (−)-*N*-methylephedrine (NME),[12] and a tertiary amine, all of which are available from commercial sources. This finding oriented new research towards establishing the validity of this activation model in related reactions. Our specific new finding is that the same system can effect highly enantioselective aza-Henry reactions (Scheme 1) of nitromethane and *N*-Boc aryl imines, thus providing a new entry to enantioenriched diamines and aryl glycines.



Scheme 1. The aza-Henry reaction between imines **1**–**4** and nitromethane. PG = protecting group, MS = molecular sieves.

Our initial aim was to identify the best-suited *N*-protecting group in the imine component in terms of both reaction conversion and enantioselection.[13] By using this activation system, *N*-sulphonyl and *N*-phosphinoyl imines **1** and **2**, respectively, led to the corresponding β-nitroamines **5** and **6** with poor enantioselectivity, if at all (Table 1). Gratifyingly,

[*] Prof. Dr. C. Palomo, Prof. Dr. M. Oiarbide, R. Halder, A. Laso, Dr. R. López
Departamento de Química Orgánica I
Facultad de Química
Universidad del País Vasco
Apdo. 1072, 20080 San Sebastián (Spain)
Fax: (+34) 943-015-270
E-mail: qoppanic@sc.ehu.es

[**] This work was financially supported by the University of the Basque Country (UPV) and the Ministerio de Educación y Ciencia (MEC, Spain). A Ramón y Cajal contract to R.L. from the MEC and predoctoral grants to R.H. and A.L. from UPV and MEC, respectively, are acknowledged.

Supporting information for this article is available on the WWW under http://www.angewandte.org or from the author.

 © 2006 Wiley-VCH Verlag GmbH & Co. KGaA, Weinheim

Table 1: Effect of the imine substituent (protecting group, PG) on the yield and enantioselectivity of the aza-Henry reaction.[a]

Imine	Ar	PG	Product	Yield [%]	*ee* [%][b]
1	Ph	$CH_3C_6H_4SO_2$	**5**	>99[c]	30
2	Ph	Ph_2PO	**6**	>99[c]	0
3	Ph	Cbz	**7**	82	82
4a	Ph	Boc	**8a**	80	94

[a] Reactions were conducted on a 1 mmol scale (**1**–**4**) in nitromethane (2 mL) using imine/$Zn(OTf)_2$/iPr_2EtN/(−)-NME in a 1:1:1:1.5 molar ratio at −20°C, except that for imine **2** which was conducted at room temperature. [b] Determined by HPLC. See Supporting Information for details. [c] Reaction conversion.

the *N*-Cbz-protected imine **3** (Cbz = carbobenzyloxy) afforded **7** with relatively much better *ee* values. The highest enantioselectivity (94% ee) was obtained in the reaction with *N*-Boc-protected imine **4a**, which furnished the corresponding protected β-nitroamine **8a** in 80% yield. A set of experiments in which the quantities of $Zn(OTf)_2$, iPr_2EtN, and (−)-NME were varied for the reaction between nitromethane and imine **4a** proved informative (Table 2). Importantly, substoichiometric quantities of the three activating reagents sufficed for full conversion of the starting imine into adduct **8a**, with yields of about 80% and generally high *ee* values. For example, a percentage mole (mol%) ratio of 30:30:45 and 20:20:30 for the three activating components gave selectivities of 94% *ee* and 92% *ee*, respectively (Table 2, entries 1 and 2). Loadings of $Zn(OTf)_2$ of 10 mol% or lower resulted in enantiomeric excesses below 90% (Table 2, entry 3). Interestingly, while (−)-NME alone (entry 4) or a combination of $Zn(OTf)_2$ and (−)-NME in a ratio of 30:45 (Table 2, entry 5) led to racemic product, combinations of $Zn(OTf)_2$ and (−)-NME in a ratio of 30:75 or higher (entries 6 and 7) led to high enantioselectivities again. These results demonstrate that the presence of a base is key for success and suggest that the amino alcohol ligand, when used in excess, may play a dual role as base and as chiral inductor. Additionally, as supported by results from entries 8 and 9 (Table 2), the reaction selectivity is essentially independent of the nature of the amine base employed.

Table 2: The effect of the quantities of metal triflate, amine base, and amino alcohol ligand on the reaction between *N*-Boc imine **1a** and nitromethane.[a]

Entry	$Zn(OTf)_2$ [%][b]	Base	Base [%][b]	(−)-NME [%][b]	*ee* [%][c]
1	30	iPr_2EtN	30	45	94
2	20	iPr_2EtN	20	30	92
3	10	iPr_2EtN	10	15	87
4	0	–	–	45	0
5	30	–	–	45	0[d]
6	30	–	–	75	97
7	30	–	–	90	95
8	30	Et_3N	30	45	92
9	30	Bu_3N	30	45	94

[a] Reactions conducted on a 1 mmol scale in nitromethane (2 mL) for 15–16 h at −20°C. Virtually complete conversion was observed in all experiments, except for entry 5. [b] Percentage values refer to the mole percentage (% mol) of the catalyst constituents with respect to the *N*-Boc-protected imine. [c] Determined by HPLC. [d] Reaction conversion: 40%.

A preliminary evaluation of the reaction scope was carried out by using a series of *N*-Boc-protected aryl imines that vary in electronic character (Table 3). Imines **4**, which bear electron-rich, electron-neutral, or electron-poor aryl substituents, were well tolerated to give *N*-Boc β-nitroamines **8** in generally good yields and with high levels of stereocontrol.[14] The standard reaction conditions involved nitromethane as solvent, but other solvent systems, such as mixtures of nitromethane and dichloromethane or toluene (1:1 v/v), can also be used. It was also observed that the presence of traces of moisture or protic contaminants in the reaction mixture were detrimental to the enantioselectivity. In this regard, the addition of 4 Å molecular sieves was beneficial and gave the highest enantioselectivity in the present aza-Henry reaction. A practical aspect of the method is that a single recrystallization of the crude nitroamine from hexane and or mixtures of ethyl acetate and hexane can provide products of increased enantiomeric purity.

Table 3: Aza-Henry reaction of *N*-Boc imines **4** with nitromethane.[a]

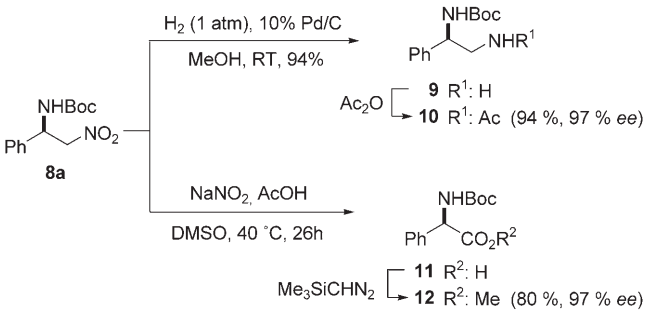
Imine **4**	Ar	Yield [%][b]	Product **8** *ee* [%][c]
a	C_6H_5	81	97
b	2-$CH_3C_6H_4$	75	99
c	4-$CH_3C_6H_4$	90	92 (94)
		92	88[d]
		85	86[e]
d	3-$CH_3OC_6H_4$	80	90 (99)
		86	88[d]
e	4-$CH_3OC_6H_4$	73	91
f	4-ClC_6H_4	97	96[f] (98)
g	4-$F_3CC_6H_4$	98	92 (94)
h	3-$NO_2C_6H_4$	59	90 (92)
i	4-$NO_2C_6H_4$	65	87
j	4-$CH_3O_2CC_6H_4$	78	94
k	1-Naphthyl	95	94 (98)
l	2-Naphthyl	70	93
m	3,5-Cl_2,4-$MeOC_6H_2$	66	87[e] (95)

[a] Reactions conducted on a 1 mmol scale in dry nitromethane (2 mL) for 15–16 h at −20°C using $Zn(OTf)_2$ (30%), iPr_2EtN (30%); (−)-NME (45%), and 4 Å MS (100 mg mmol^{-1}), unless otherwise noted. [b] Yield of the isolated product after column chromatography. [c] Determined by HPLC after removal of traces of (−)-NME by column chromatography (see Supporting Information for details). The number in parentheses refers to the *ee* value for the product after a single crystallization from hexane/ethyl acetate. [d] $Zn(OTf)_2$ (20%), iPr_2EtN (20%), and (−)-NME (30%). [e] $Zn(OTf)_2$ (30%) and (−)-NME (75%). [f] In the absence of 4 Å MS, 84% *ee* was attained.

The elaboration of thus-obtained aza-Henry products into 1,2-diamines and amino acids, respectively, could be performed using known procedures. For example, reduction of the nitro group in **8a** led to the known monoprotected diamine **9**,[15] while Nef oxidation under the conditions described by Mioskowski and co-workers[16] followed by methylation afforded the *N*-Boc-protected (*R*)-phenylglycine

 © 2006 Wiley-VCH Verlag GmbH & Co. KGaA, Weinheim

methyl ester **12** without apparent loss of optical integrity (Scheme 2).[17] Further acetylation of **9** to the known compound **10** allowed the absolute configuration of the adducts to be confirmed.



Scheme 2. Assignment of the configuration of the adducts by transformation into 1,2-diamines. DMSO = dimethyl sulfoxide.

In conclusion, the pool of available methods for the asymmetric aza-Henry (nitro-Mannich) reaction has been enhanced by the approach described here which features a) tolerance to imines that bear aryl groups of diverse electronic nature and substitution patterns, b) exclusive use of commercially available reagents, in particular the relatively low-cost *N*-methylephedrine as the recyclable chiral inductor, and c) flexibility on the effective loading of the triggering system, which varies from stoichiometric to about 10 mol% with respect to the transformed imine substrate.

Experimental Section

In a typical procedure, diisopropylethylamine (1.05 mL, 6 mmol) was added dropwise to a solution of anhydrous zinc triflate (2.18 g, 6 mmol) in nitromethane (40 mL) under a nitrogen atmosphere and the resulting mixture was stirred at 25 °C for 1 h. The mixture became yellow. After addition of (−)-(1*R*,2*S*)-*N*-methylephedrine (1.6 g, 9 mmol) and 4 Å molecular sieves (2.0 g), the resulting mixture was stirred for an additional 2 h at the same temperature. The reaction mixture was then kept for 10 min at −20 °C, imine **4a** (4.1 g, 20 mmol) was added, and the mixture was stirred for 21 h at −20 °C. The reaction was quenched with 0.1 M HCl (50 mL), and the mixture was extracted with dichloromethane (3 × 50 mL). The organic layer was dried over $MgSO_4$ and concentrated under reduced pressure. Purification of the crude product by flash column chromatography (ethyl acetate/hexane) afforded **8a** (4.3 g, 80% yield). From the late fractions of the column, 0.432 g of (1*S*,2*R*)-*N*-methylephedrine was recovered. Recovery of the chiral ligand that remained in the acidic aqueous phase was carried out by dropwise addition of a solution of NaOH (20% w/v) until pH 10. The mixture was extracted with CH_2Cl_2 (3 × 10 mL), the organic layer was dried over $MgSO_4$, and the solvent was evaporated to afford an additional 1.12 g of (−)-NME (1.55 g (97%) combined yield of chemically and optically pure (−)-NME ligand).

Received: July 29, 2005
Published online: November 17, 2005

Keywords: amines · asymmetric catalysis · enantioselectivity · nitro compounds

[1] For recent advances on this reaction, see: B. Westermann, *Angew. Chem.* **2003**, *115*, 161 – 163; *Angew. Chem. Int. Ed.* **2003**, *42*, 151 – 153.
[2] For a review on 1,2-diamines, see: D. Lucet, T. Le Gall, C. Mioskowski, *Angew. Chem.* **1998**, *110*, 2724 – 2772; *Angew. Chem. Int. Ed.* **1998**, *37*, 2580 – 2627.
[3] See, for instance: P. H. O'Brien, D. R. Sliskovic, C. J. Blankley, B. Roth, M. W. Wilson, K. L. Hamelehle, B. R. Krause, R. L. Stanfield, *J. Med. Chem.* **1994**, *37*, 1810 – 1822.
[4] For reviews, see: a) H. W. Pinnick, *Org. React.* **1990**, *38*, 655 – 792; b) R. Ballini, M. Petrini, *Tetrahedron* **2004**, *60*, 1017 – 1047. For the application of this approach to the synthesis of optically active α-amino acids; see: c) E. Foresti, G. Palmieri, M. Petrini, R. Profeta, *Org. Biomol. Chem.* **2003**, *1*, 4275 – 4281.
[5] For non-asymmetric aza-Henry reactions, see: a) J. C. Anderson, A. J. Blake, G. P. Howell, C. W. Ilson, *J. Org. Chem.* **2005**, *70*, 549 – 555; b) L. Bernardi, B. F. Bonini, E. Capitó, G. Dessole, M. Comes-Franchini, M. Fochi, A. Ricci, *J. Org. Chem.* **2004**, *69*, 8168 – 8171.
[6] a) K. Yamada, S. J. Harwood, H. Gröger, M. Shibasaki, *Angew. Chem.* **1999**, *111*, 3713 – 3715; *Angew. Chem. Int. Ed.* **1999**, *38*, 3504 – 3506; b) K. Yamada, G. Moll, M. Shibasaki, *Synlett* **2001**, 980 – 982.
[7] a) K. R. Knudsen, T. Risgaard, N. Nishiwaki, K. V. Gothelf, K. A. Jørgensen, *J. Am. Chem. Soc.* **2001**, *123*, 5843 – 5844. For latter versions using unmodified nitro compounds, see: b) N. Nishiwaki, K. R. Knudsen, K. V. Gothelf, K. A. Jørgensen, *Angew. Chem.* **2001**, *113*, 3080 – 3083; *Angew. Chem. Int. Ed.* **2001**, *40*, 2992 – 2995; c) K. R. Knudsen, K. A. Jørgensen, *Org. Biomol. Chem.* **2005**, *3*, 1362 – 1364.
[8] The aza-Henry reaction with *N*-*p*-methoxyphenyl imines using preformed nitropropane silyl nitronate in the presence of a Cu^{II}/*t*BOX catalyst with generally good diastereo- and enantioselectivities has been recently published, see: J. C. Anderson, G. P. Howell, R. M. Lawrence, C. S. Wilson, *J. Org. Chem.* **2005**, *70*, 5665 – 5670.
[9] a) B. M. Nugent, R. A. Poder, J. N. Johnston, *J. Am. Chem. Soc.* **2004**, *126*, 3418 – 3419; b) T. Okino, S. Nakamura, T. Furukawa, Y. Takemoto, *Org. Lett.* **2004**, *6*, 625 – 627; c) T. P. Yoon, E. N. Jacobsen, *Angew. Chem.* **2005**, *117*, 470 – 472; *Angew. Chem. Int. Ed.* **2005**, *44*, 466 – 468.
[10] C. Palomo, M. Oiarbide, A. Laso, *Angew. Chem.* **2005**, *117*, 3949 – 3952; *Angew. Chem. Int. Ed.* **2005**, *44*, 3881 – 3884.
[11] For recent reviews on cooperative activation of nucleophiles (or pronucleophiles) and electrophiles, see: a) J.-A. Ma, D. Cahard, *Angew. Chem.* **2004**, *116*, 4666 – 4683; *Angew. Chem. Int. Ed.* **2004**, *43*, 4566 – 4583; b) S. Kanemasa, K. Ito, *Eur. J. Org. Chem.* **2004**, 4741 – 4753.
[12] For other recent uses of *N*-methylephedrine, such as the addition of acetylides to aldehydes, see: a) N. K. Anand, E. M. Carreira, *J. Am. Chem. Soc.* **2001**, *123*, 9687 – 9688; b) D. E. Frautz, R. Fässler, E. M. Carreira, *J. Am. Chem. Soc.* **2000**, *122*, 1806 – 1807; for imino-Reformatsky reaction, see: c) P. G. Cozzi, E. Rivalta, *Angew. Chem.* **2005**, *117*, 3666 – 3669; *Angew. Chem. Int. Ed.* **2005**, *44*, 3600 – 3603.
[13] Benzaldehyde-derived imines from *p*-anisidine and benzylamine did not react under the conditions described. These kind of imines have been shown to be active against preformed silyl nitronates in the presence of a Lewis acid. See, for instance, reference [8].
[14] Apparently, heteroaromatic *N*-Boc-protected imines are less-suitable substrates for the reaction. For instance, the aza-Henry adduct from the furfuraldehyde *N*-Boc imine derivative was obtained in 96% yield and with 66% *ee*.

 © 2006 Wiley-VCH Verlag GmbH & Co. KGaA, Weinheim

[15] P. H. O'Brien, D. R. Sliskovic, C. J. Blankley, B. Roth, M. W. Wilson, K. L. Hamelehle, B. R. Krause, R. L. Stanfield, *J. Med. Chem.* **1994**, *37*, 1810 – 1822.
[16] a) C. Matt, A. Wagner, C. Mioskowski, *J. Org. Chem.* **1997**, *62*, 234 – 235. For the application of this method to the synthesis of α-hydroxy acids from β-nitro alcohols, see: b) B. M. Trost, V. S. C. Yeh, *Angew. Chem.* **2002**, *114*, 889 – 891; *Angew. Chem. Int. Ed.* **2002**, *41*, 861 – 863.
[17] Subjecting **8a** (97% *ee*) to the conditions reported in reference [4c] ($KMnO_4$, KOH, Na_2HPO_4) led to partially racemized **11a** (65% yield, 70% *ee*).

 © 2006 Wiley-VCH Verlag GmbH & Co. KGaA, Weinheim

DNA Devices

DOI: 10.1002/anie.200502568

High-Yield Generation of a Long-Lived Charge-Separated State in Diphenylacetylene-Modified DNA**

*Tadao Takada, Kiyohiko Kawai, Mamoru Fujitsuka, and Tetsuro Majima**

The development of macromolecular chemical systems that are capable of generating a long-lived charge-separated state is of particular interest for technological advances in solar-energy conversion and molecular devices.[1] DNA is a particularly important and promising molecule that can be used as a molecular scaffold for nanostructures and nanotechnology.[2] In addition, there is interesting potential for the use of DNA as a molecular wire as a result of the efficient charge-transport properties through the DNA π stack.[3] DNA-based electrochemical sensors to detect target DNA, protein analytes, and single nucleotide polymorphism have been developed by Barton and co-workers.[4] Recently, Okamoto, Saito, and co-workers reported the photochemical response of functionalized DNA on an electrochemical surface and its diagnostic application for the detection of mismatches.[5] However, the efficient generation of the photocurrent has not yet been achieved because of a rapid charge-recombination process in the charge-separated state after photoirradiation.[6] This process limits the application of DNA for photoelectrochemical devices. In this context, it is necessary to establish a system for the high-yield generation of the charge-separated state in DNA.

Generally, to generate a long-lived charge-separated state, the charge recombination must be slowed down by spatially separating positive and negative charges.[7] Previously, we showed that the rapid hole hopping over consecutive adenine (A) bases can be useful to generate the charge-separated state in DNA.[8,9] However, the yield is not sufficiently high as a result of the initial charge-recombination process within the contact ion pair. As predicted from electron-transfer theory, the rates of charge recombination between the electron donor and acceptor are dependent upon the energetics and, in particularly, the driving force of the process.[10] Lewis, Wasielewski, and co-workers reported on the electron-transfer process between diphenylacetylene (DPA) and DNA in which the charge-recombination process between the DPA radical anion and a neighboring A radical cation was quite slow ($7\times10^8\ s^{-1}$) because the back-electron transfer was deep within the Marcus inverted region ($\Delta G_{cr}=3.8$ eV, calculated from the reduction potential of DPA ($E_{red}=-2.1$ V vs SCE) and the oxidation potential of the A base ($E_{ox}=1.7$ V vs SCE); SCE = saturated calomel electrode).[11] Thus, a long-lived charge-separated state in DNA is anticipated to be generated in high yield by combining slow charge-recombination properties and rapid hole hopping through consecutive A bases. Herein, we report the high-yield generation of the long-lived charge-separated state in DPA-modified DNA.

The synthesis of DNA modified with DPA was carried out by conventional phosphoramidite chemistry using the DNA synthesizer as previously reported.[12] The chemical structures of DPA and the sequence of the synthetic DNA are shown in Figure 1a and Table 1, respectively. Two types of DPA-modified DNA derivatives were designed; namely, the hairpin (H-A*n*) and end-capped (E-A*n*) structures. Charge separation and the following hole-hopping process are schematically shown in Figure 1b. As mentioned above, DPA in the singlet excited state ($^1DPA^*$) is capable of

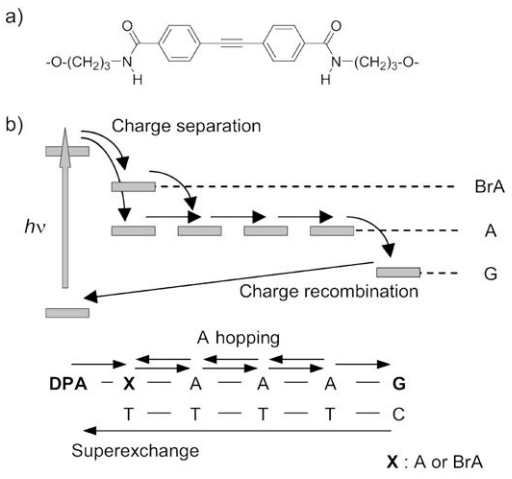


Figure 1. a) Structure of diphenylacetylene (DPA). b) Charge separation and subsequent hole-transfer process through A-base hopping.

[*] T. Takada, K. Kawai, M. Fujitsuka, Prof. T. Majima
The Institute of Scientific and Industrial Research (SANKEN)
Osaka University
Mihogaoka 8-1, Ibaraki, Osaka 567-0047 (Japan)
Fax: (+81) 6-6879-8499
E-mail: majima@sanken.osaka-u.ac.jp

[**] This work was partly supported by a Grant-in-Aid for Scientific Research (Project 17105005, Priority Area (417), 21st Century COE Research, and others) from the Ministry of Education, Culture, Sports, Science, and Technology (MEXT) of the Japanese Government.

Supporting information for this article is available on the WWW under http://www.angewandte.org or from the author.

InterScience
© 2006 Wiley-VCH Verlag GmbH & Co. KGaA, Weinheim

Table 1: Sequences of DNA modified with DPA, the yields of charge separation after photoexcitation, and the lifetimes of the charge-separated states.

DNA	Sequence[a]	Yield[b] [%]	τ[b,c] [μs]
H-A3	5′-AAA**G**-AAA-**DPA**-TTT-CTTT-3′	26	0.23 (86%), >50 (14%)
H-A4	5′-AA**G**-AAAA-**DPA**-TTTT-CTT-3′	18	7.6
H-A5	5′-A**G**-AAAAA-**DPA**-TTTTT-CT-3′	16	26
E-A3	5′-**DPA**-AAA-**G**TGTGTGT-3′	15	0.26 (75%), >50 (25%)
E-A4	5′-**DPA**-AAAA-**G**TGTGTGT-3′	13	>50
E-A5	5′-**DPA**-AAAAA-**G**TGTGTGT-3′	11	>50
E-A6	5′-**DPA**-AAAAAA-**G**TGTGTGT-3′	8.4	>50
E-A7	5′-**DPA**-AAAAAAA-**G**TGTGTGT-3′	7.1	>50
E-A8	5′-**DPA**-AAAAAAAA-**G**TGTGTGT-3′	6.2	>50
E-BrA	5′-**DPA**-BrA-AAAAA-**G**TGTGTGT-3′	13	>50

[a] DNA duplexes with hairpin (H-A*n*) and end-capped (E-A*n*) structures. Sequences of single-strand DNA modified with DPA are only shown for the E-A*n* series. [b] Determined by comparing the transient absorption of $DPA^{\bullet-}$ at 490 nm with that of benzophenone, which was used as an actinometer, observed after the laser-pulse excitation. [c] Lifetimes (τ) of charge-separated state were determined by the decay of the transient absorption monitored at 490 nm. Lifetimes that were longer than 50 μs could not be determined owing to the intermolecular charge recombination and the intrinsic decay of $DPA^{\bullet-}$.

oxidizing the A base as well as the guanine (G) base. After the photoexcitation of DPA, charge separation between $^1DPA^*$ and A takes place and a hole on the nearest A base can escape from the contact ion pair through A hopping. This provides a long-lived charge-separated state between DPA and the nearest G base (Figure 1b).

The charge-separation and -recombination processes in DPA-modified DNA were characterized by nanosecond time-resolved transient absorption measurements. The transient absorption spectra observed for the DPA-modified DNA (H-A4) upon excitation with a 308 nm laser pulse (FWHM = 50 ns, 8 mJ/pulse) are shown in Figure 2. A strong absorption peak around $\lambda = 500$ nm was observed after photoexcitation and assigned to the DPA radical anion ($DPA^{\bullet-}$). Transient species observed around 500 nm are almost completely quenched by molecular oxygen (see Supporting Information for details about quenching experiments). The quenching experiments confirmed that the transient absorption originated from $DPA^{\bullet-}$ and that the DPA radical cation generated by the two-photon ionization or reductive electron transfer can be excluded. $DPA^{\bullet-}$ was not observed for DNA that does not contain a guanine–cytosine (GC) base pair, indicating that the trapping of a hole at a G site leads to the long-lived charge-separated state. From the intensity of the absorption of $DPA^{\bullet-}$ monitored at $\lambda = 490$ nm, the yield of the charge-separated state was determined to be 18% for this sequence, which is quite high compared with previous results.[8] In earlier studies, we reported that the yields of charge separation for DNA modified with naphthaldiimide ($\Delta G_{cs} = 1.5$ eV) and naphthalimide ($\Delta G_{cs} = 3.0$ eV) were 2.1% and 3.3%, respectively, when these photosensitizers were separated from G by four adenine–thymine (AT) base pairs.[8,13] These results indicate that the yields are correlated with the driving force of the initial charge-recombination process.

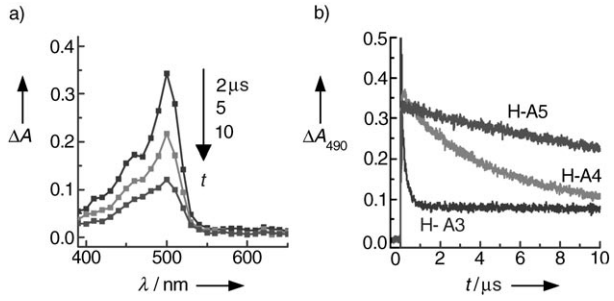


Figure 2. a) Transient absorption spectra for DPA-modified DNA (H-A4) monitored at 2, 5, and 10 μs after the excitation of DPA with a 308 nm laser pulse. b) Decay profiles for H-A3, H-A4, and H-A5 monitored at 490 nm after laser-pulse excitation. Sample solutions contained 20 μM DNA, 20 mM sodium phosphate buffer (pH 7.0), and 100 mM NaCl.

Decay profiles of the charge-separated state for H-A3, H-A4, and H-A5 are shown in Figure 2b. Yields of the charge-separated state and the lifetimes for these DNA duplexes are summarized in Table 1. The strong dependence of the lifetimes for the charge-separated states on the distance demonstrates that the charge recombination between $DPA^{\bullet-}$ and $G^{\bullet+}$ occurred through a superexchange type of mechanism owing to the higher oxidation potential of A relative to that of G. On the other hand, the weak distance dependence of the yields suggests that the long-lived charge-separated states were generated by A hopping. The high yields of the long-lived charge-separated states were also observed for the end-capped structures (E-A*n*). The yields of the charge-separated state obtained for E-A*n* are somewhat lower than those for H-A*n* when the number of A bases between DPA and the nearest G base is the same. This result may be attributed to the structural differences that cause the changes in the initial charge-recombination rate. The long lifetime of the charge-separated state was observed for all E-A*n* except E-A3, because the hole transfer between G bases over the $(GT)_4$ sequence increases with an increase in the distance between the positive and negative charges.[14]

In previous reports, Lewis, Wasielewski, and co-workers demonstrated that hole migration from a contact ion pair cannot occur because of Coulombic interactions.[12] Therefore, there may be a possibility that a hole generated by oxidizing the second A base from DPA migrates to a G base to provide a long-lived charge-separated state. However, on the basis of the superexchange mechanism, the yield of the direct oxidation of the second A base by $^1DPA^*$ should be less than 10% because of the strong dependence on distance. Charge-separation yields obtained for H-A3 and H-A4 were higher than 10%, confirming that the hole-escape reaction from the contact ion pair can take place to generate the long-lived charge separated state by A hopping.

To improve the yields of the charge-separated states by changing the oxidation potential of the bridge, an 8-bromo-substituted adenine base (BrA) was incorporated in place of

 © 2006 Wiley-VCH Verlag GmbH & Co. KGaA, Weinheim

A at the first position from DPA (E-BrA). As a result of the electron-withdrawing properties of the Br group, BrA shows a higher oxidation potential than A[15] and thus it is expected to facilitate the hole transfer from the contact radical ion pair to the next A base. When the A base nearest to DPA in E-A6 was replaced by BrA (E-BrA), the yield of charge separation was improved by about 50% relative to that of E-A6. This observation suggests that the gradual change in the redox potential over the bridge bases facilitates the hole-transfer reaction from the contact ion pair to the next A base and improves the yield of the charge-separated states.

In conclusion, we have demonstrated the high-yield generation of the long-lived charge-separated state through A-base hopping in DPA-modified DNA. On the basis of the effect of the driving force of the charge-recombination process and the redox gradient of the bridge bases, it was demonstrated that the modulation of the redox properties of the photosensitizer and bridge bases can improve the yield of the long-lived charge-separated state. This observation will be important in the development of DNA-based photoelectrochemical devices.

Received: July 22, 2005
Revised: September 29, 2005
Published online: November 21, 2005

Keywords: charge transfer · DNA · electrochemistry · time-resolved spectroscopy

[1] a) M. Lahav, V. Heleg-Shabtai, J. Wasserman, E. Katz, I. Willner, H. Duerr, Y.-Z. Hu, S. H. Bossmann, *J. Am. Chem. Soc.* **2000**, *122*, 11480; b) H. Imahori, M. Arimura, T. Hanada, Y. Nishimura, I. Yamazaki, Y. Sakata, S. Fukuzumi, *J. Am. Chem. Soc.* **2001**, *123*, 335; c) K. Ohkubo, H. Kotani, J. Shao, Z. Ou, K. M. Kadish, G. Li, R. K. Pandey, M. Fujitsuka, O. Ito, H. Imahori, S. Fukuzumi, *Angew. Chem.* **2004**, *116*, 871; *Angew. Chem. Int. Ed.* **2004**, *43*, 853; d) M. A. Fox, *Acc. Chem. Res.* **1999**, *32*, 201; e) M. Graetzel, *Nature* **2001**, *414*, 338.

[2] N. C. Seeman, *Angew. Chem.* **1998**, *110*, 3408; *Angew. Chem. Int. Ed.* **1998**, *37*, 3220.

[3] a) D. M. Ceres, J. K. Barton, *J. Am. Chem. Soc.* **2003**, *125*, 14964; b) S. Delaney, J. K. Barton, *J. Org. Chem.* **2003**, *68*, 6475; c) B. Giese, A. Biland, *Chem. Commun.* **2002**, 667; d) G. B. Schuster, *Acc. Chem. Res.* **2000**, *33*, 253; e) F. D. Lewis, R. L. Letsinger, M. R. Wasielewski, *Acc. Chem. Res.* **2001**, *34*, 159; f) K. Nakatani, C. Dohno, I. Saito, *J. Am. Chem. Soc.* **1999**, *121*, 10854; g) T. Takada, K. Kawai, M. Fujitsuka, T. Majima, *Proc. Natl. Acad. Sci. USA* **2004**, *101*, 14002.

[4] a) T. G. Drummond, M. G. Hill, J. K. Barton, *Nat. Biotechnol.* **2003**, *21*, 1192; b) E. M. Boon, D. M. Ceres, T. G. Drummond, M. G. Hill, J. K. Barton, *Nat. Biotechnol.* **2000**, *18*, 1096.

[5] A. Okamoto, T. Kamei, K. Tanaka, I. Saito, *J. Am. Chem. Soc.* **2004**, *126*, 14732.

[6] F. D. Lewis, T. F. Wu, Y. F. Zhang, R. L. Letsinger, S. R. Greenfield, M. R. Wasielewski, *Science* **1997**, *277*, 673.

[7] a) D. Gust, T. A. Moore, A. L. Moore, *Acc. Chem. Res.* **2001**, *34*, 40; b) H. Imahori, D. M. Guldi, K. Tamaki, Y. Yoshida, C. P. Luo, Y. Sakata, S. Fukuzumi, *J. Am. Chem. Soc.* **2001**, *123*, 6617; c) K. Kawai, X. Cai, A. Sugimoto, S. Tojo, M. Fujitsuka, T. Majima, *Angew. Chem.* **2004**, *116*, 2460; *Angew. Chem. Int. Ed.* **2004**, *43*, 2406.

[8] T. Takada, K. Kawai, X. Cai, A. Sugimoto, M. Fujitsuka, T. Majima, *J. Am. Chem. Soc.* **2004**, *126*, 1125.

[9] K. Kawai, T. Takada, T. Nagai, X. C. Cai, A. Sugimoto, M. Fujitsuka, T. Majima, *J. Am. Chem. Soc.* **2003**, *125*, 16198.

[10] F. D. Lewis, R. S. Kalgutkar, Y. S. Wu, X. Y. Liu, J. Q. Liu, R. T. Hayes, S. E. Miller, M. R. Wasielewski, *J. Am. Chem. Soc.* **2000**, *122*, 12346.

[11] a) F. D. Lewis, J. Q. Liu, W. Weigel, W. Rettig, I. V. Kurnikov, D. N. Beratan, *Proc. Natl. Acad. Sci. USA* **2002**, *99*, 12536; b) F. D. Lewis, X. Y. Liu, S. E. Miller, M. R. Wasielewski, *J. Am. Chem. Soc.* **1999**, *121*, 9746.

[12] F. D. Lewis, X. Liu, S. E. Miller, R. T. Hayes, M. R. Wasielewski, *J. Am. Chem. Soc.* **2002**, *124*, 14020.

[13] T. Takada, K. Kawai, M. Fujitsuka, T. Majima, *Chem. Eur. J.* **2005**, *11*, 3835.

[14] K. Kawai, Y. Osakada, T. Takada, M. Fujitsuka, T. Majima, *J. Am. Chem. Soc.* **2004**, *126*, 12843.

[15] K. Kawai, Y. Wata, M. Hara, S. Tojo, T. Majima, *J. Am. Chem. Soc.* **2002**, *124*, 3586.

 © 2006 Wiley-VCH Verlag GmbH & Co. KGaA, Weinheim

Asymmetric Synthesis

DOI: 10.1002/anie.200500469

Highly Enantioselective Synthesis of γ-Hydroxy-α,β-acetylenic Esters by Asymmetric Alkyne Addition to Aldehydes**

Ge Gao, Qin Wang, Xiao-Qi Yu, Ru-Gang Xie, and Lin Pu**

γ-Hydroxy-α,β-acetylenic esters containing three adjacent and structurally very different functional groups are very useful in the synthesis of highly functionalized organic molecules.[1,2] This class of compound is normally prepared by treatment of an alkyl propiolate with *n*BuLi at $\leq -78\,^{\circ}C$

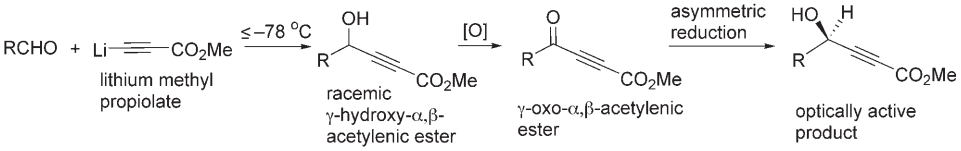
[*] Dr. G. Gao, Q. Wang, Prof. X.-Q. Yu, Prof. R.-G. Xie
Department of Chemistry
Key Laboratory of Green Chemistry and Technology (Ministry of Education)
Sichuan University, Chengdu 610064 (P.R. China)
Fax: (+86) 288-541-5886
E-mail: xqyu@tfol.com
Prof. L. Pu
Department of Chemistry
University of Virginia
Charlottesville, VA 22904-4319 (USA)
Fax: (+1) 434-924-3170
E-mail: lp6n@virginia.edu

[**] This work is supported by the National Natural Science Foundation of China (No. 20328203 and 20132020). L.P. thanks the US National Institute of Health for partial support of this work (R01M58454/R01EB002037-05).

Supporting information for this article is available on the WWW under http://www.angewandte.org or from the author.

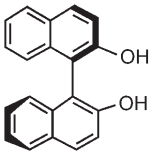
WILEY InterScience DISCOVER SOMETHING GREAT
© 2006 Wiley-VCH Verlag GmbH & Co. KGaA, Weinheim

followed by the addition of aldehydes,[1] as originally reported by Midland et al.[1a] Recently, Shahi and Koide reported a milder method in which AgC≡CCO$_2$Me was reacted with aldehydes in the presence of [Cp$_2$ZrCl$_2$] (Cp = cyclopentadienyl) and AgOTf (Tf = trifluoromethanesulfonyl) at room temperature.[3] Asymmetric reductions of γ-oxo-α,β-acetylenic esters have been used to synthesize optically active γ-hydroxy-α,β-acetylenic esters (Scheme 1).[2] This process first



Scheme 1. Synthesis of optically active γ-hydroxy-α,β-acetylenic esters by asymmetric reduction of γ-oxo-α,β-acetylenic esters.

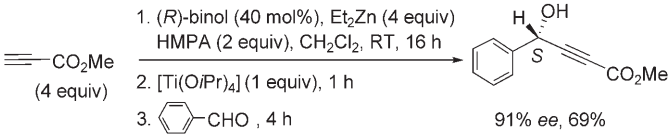
requires the synthesis of racemic γ-hydroxy-α,β-acetylenic esters, which are then oxidized to γ-oxo-α,β-acetylenic esters before asymmetric reduction. However, the most efficient way to prepare optically active γ-hydroxy-α,β-acetylenic esters should be the direct asymmetric addition of an alkyl propiolate to aldehydes, as this one-step reaction simultaneously produces both a carbon–carbon bond and a stereogenic propargylic alcohol center. Although major progress has been made in recent years in the area of asymmetric addition of alkynes to aldehydes,[4–7] no enantioselective reaction of alkynoates with aldehydes has been reported.[8,9] Herein, we report a highly enantioselective, as well as practical, method for the addition of methyl propiolate to aromatic aldehydes to generate optically active γ-hydroxy-α,β-acetylenic esters.



(*R*)-binol

Earlier, we discovered that 1,1′-bi-2-naphthol (binol) in combination with [Ti(O*i*Pr)$_4$] can catalyze the highly enantioselective addition of alkynes to both aliphatic and aromatic aldehydes with high enantioselectivity.[6a,b] However, this method cannot be used for the reaction of methyl propiolate with aldehydes because the solution of the alkyne in toluene needs to be heated with Et$_2$Zn at reflux, which leads to the decomposition of methyl propiolate. Later, we found that addition of hexamethylphosphoramide (HMPA) greatly accelerates the reaction of Et$_2$Zn with terminal alkynes at room temperature while maintaining the high enantioselectivity for the addition to aldehydes.[6c] When we initially tested the use of this method for the addition of methyl propiolate to benzaldehyde, the product was obtained only in low yield.

Further investigation revealed that prolonging the treatment of methyl propiolate with Et$_2$Zn in the presence of (*R*)-binol and HMPA at room temperature before the addition of [Ti(O*i*Pr)$_4$] and benzaldehyde led to the desired γ-hydroxy-α,β-acetylenic product both in good yield and with high enantioselectivity (Scheme 2): methyl 4-hydroxy-4-phenylbut-2-ynoate was obtained in 69% yield and with 91% *ee* (see the Experimental Section for further details). The specific



Scheme 2. Asymmetric addition of methyl propiolate to benzaldehyde.

optical rotation was found to be $[\alpha]_D^{28} = -3.56$ ($c = 0.73$, $CHCl_3$), and the absolute configuration was determined to be *S* by studying the ^{19}F NMR spectra of its Mosher ester.[10] This configuration assignment is consistent with other studies on the binol-catalyzed alkyne addition to aldehydes.[6a]

We applied this procedure to the reaction of methyl propiolate with a variety of aromatic and α,β-unsaturated aldehydes. The results summarized in Table 1 show that high enantioselectivities (85–95% *ee*) were achieved for the reaction of benzaldehyde derivatives with either electron-donating or -withdrawing substituents at the *ortho*, *meta*, or *para* positions in the presence of a substoichiometric amount of the chiral ligand (*R*)-binol (Table 1, entries 1–12). Other types of aromatic aldehydes, such as 1-naphthaldehyde, 2-naphthaldehyde, and 2-furaldehyde, also showed high enantioselectivity (87–95% *ee*; Table 1, entries 13–15). An excellent result was obtained as well when the α,β-unsaturated aldehyde cinnamaldehyde was used (91% *ee*; Table 1, entry 16).

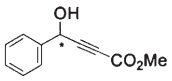
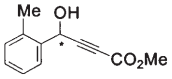
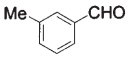
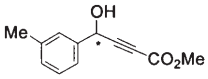
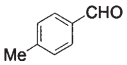
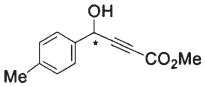
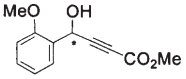
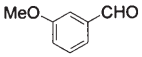
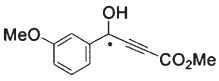
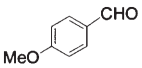
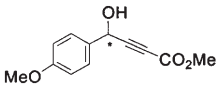
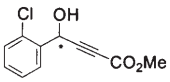
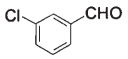
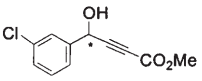
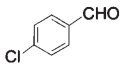
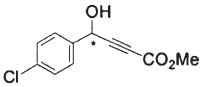
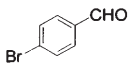
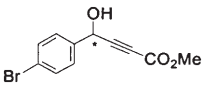
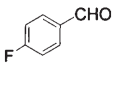
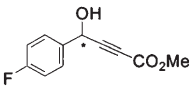
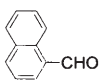
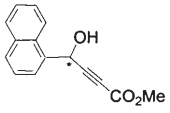
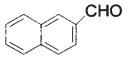
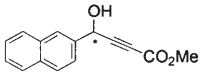
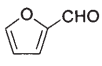
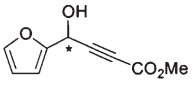
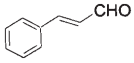
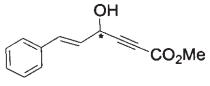
In summary, we have discovered the first highly enantioselective reaction of an alkynoate with aromatic and α,β-unsaturated aldehydes for the synthesis of optically active γ-hydroxy-α,β-acetylenic esters. This reaction can be carried out at room temperature by using a substoichiometric amount of the chiral binol ligand. The easy availability of the chiral ligand as well as the metal reagents and the mild reaction conditions make this process practically very useful. Currently, we are further expanding the scope of this reaction to include substrates such as aliphatic and other functionalized aldehydes.

Experimental Section

HMPA (88 μL, 0.50 mmol), methyl propiolate (85 μL, 1.0 mmol), and Et$_2$Zn (0.91 mL (1.1M in toluene), 1.0 mmol) were added sequentially to (*R*)-binol (28.6 mg, 0.10 mmol, 40 mol%) in dry CH_2Cl_2 (3 mL) in a 10-mL round-bottomed flask under argon. The reaction mixture was allowed to stir at room temperature for 16 h. After the addition of [Ti(O*i*Pr)$_4$] (74 μL, 0.25 mmol), the solution was stirred for another hour. Benzaldehyde (25.5 μL, 0.25 mmol) was then added and the reaction was allowed to proceed for 4 h. Saturated ammonium chloride was added to quench the reaction, and CH_2Cl_2 was used for extraction. After removal of the organic solvent under reduced pressure, the residue was purified by using a short column of silica gel with petroleum ether/ethyl acetate (9:1) as the eluant to afford methyl 4-hydroxy-4-phenylbut-2-ynoate in 69% yield with 91% *ee*, as

 © 2006 Wiley-VCH Verlag GmbH & Co. KGaA, Weinheim

Table 1: Enantioselective addition of methyl propiolate to aldehydes.

Entry	Aldehyde	Product	Yield of isolated product [%]	*ee* [%]
1			69	91
2			96	91
3			91	93
4			81	93
5			91	90
6			52	90
7			82	91
8			94	91
9			90	93
10			84	95
11			82	93
12			76	85
13			87	95
14			84	93
15			55[a]	87
16			65[a]	91

[a] Determined by NMR spectroscopic analysis.

determined with a HPLC-Diacel Chiralcel OD column; $[\alpha]_D^{28} = -3.56$ ($c = 0.73$, $CHCl_3$).

Received: February 7, 2005
Revised: September 12, 2005
Published online: November 21, 2005

Keywords: aldehydes · alkynes · asymmetric synthesis · binol ligands · esters

[1] a) M. M. Midland, A. Tramontano, J. R. Cable, *J. Org. Chem.* **1980**, *45*, 28–29; b) A. Arcadi, E. Bernocchi, A. Burini, S. Cacchi, F. Marinelli, B. Pietroni, *Tetrahedron* **1988**, *44*, 481–490; c) W. M. Grootaert, P. J. De Clercq, *Tetrahedron Lett.* **1986**, *27*, 1731–1734; d) B. M. Trost, S. Matsubara, J. J. Caringi, *J. Am. Chem. Soc.* **1989**, *111*, 8745–8746; e) F. De Corte, F. Nuyttens, S. Cauwberghs, P. De Clercq, *Tetrahedron Lett.* **1993**, *34*, 1831–1832; f) M. T. Crimmins, D. K. Jung, J. L. Gray, *J. Am. Chem. Soc.* **1993**, *115*, 3146–3155; g) B. M. Trost, Z. Shi, *J. Am. Chem. Soc.* **1994**, *116*, 7459–7460; h) H. Corlay, R. T. Lewis, W. B. Motherwell, M. Shipman, *Tetrahedron* **1995**, *51*, 3303–3318; i) M. K. E. Saïah, R. Pellicciari, *Tetrahedron Lett.* **1995**, *36*, 4497–4500; j) K. Mikami, A. Yoshida, *Tetrahedron* **2001**, *57*, 889–898; k) B. M. Trost, M. L. Crawley, *J. Am. Chem. Soc.* **2002**, *124*, 9328–9329; l) G. A. Molander, D. J. St. Jean, Jr., *J. Org. Chem.* **2002**, *67*, 3861–3865; m) B. M. Trost, Z. T. Ball, *J. Am. Chem. Soc.* **2004**, *126*, 13942–13944; n) D. Tejedor, F. Garcia-Tellado, J. J. Marrero-Tellado, P. de Armas, *Chem. Eur. J.* **2003**, *9*, 3122–3131; o) C. T. Meta, K. Koide, *Org. Lett.* **2004**, *6*, 1785–1787.

[2] a) M. M. Midland, D. C. McDowell, R. L. Hatch, A. Tramontano, *J. Am. Chem. Soc.* **1980**, *102*, 867–869; b) M. M. Midland, A. Tramontano, A. Kazubski, R. S. Graham, D. J. S. Tsai, D. B. Cardin, *Tetrahedron* **1984**, *40*, 1371–1380; c) R. Noyori, T. M. Yamada, M. Nishizawa, *J. Am. Chem. Soc.* **1984**, *106*, 6717–6725; d) T. Duvold, M. Rohmer, *Tetrahedron Lett.* **2000**, *41*, 3875–3878; e) J. Mulzer, M. Csybowski, J.-W Bats, *Tetrahedron Lett.* **2001**, *42*, 2961–2964; f) M. Johansson, B. Köpcke, H. Anke, O. Sterner, *Tetrahedron* **2002**, *58*, 2523–2528.

[3] S. P. Shahi, K. Koide, *Angew. Chem.* **2004**, *116*, 2579–2581; *Angew. Chem. Int. Ed.* **2004**, *43*, 2525–2527.

[4] Reviews: a) L. Pu, *Tetrahedron* **2003**, *59*, 9873–9886; b) P. Aschwanden, E. M. Carreira in *Acetylene Chemistry. Chemistry, Biology and Material Science* (Eds.: F. Diederich, P. J. Stang, R. R. Tykwinski), Wiley-VCH, Weinheim, **2005**, pp. 101–138.

[5] a) D. E. Frantz, R. Fassler, E. M. Carreira, *J. Am. Chem. Soc.* **2000**, *122*, 1806–1807; b) N. K. Anand, E. M. Carreira, *J. Am. Chem. Soc.* **2001**, *123*, 9687–9688.

 © 2006 Wiley-VCH Verlag GmbH & Co. KGaA, Weinheim

[6] a) D. Moore, L. Pu, *Org. Lett.* **2002**, *4*, 1855 – 1857; b) G. Gao, D. Moore, R.-G. Xie, L. Pu, *Org. Lett.* **2002**, *4*, 4143 – 4146; c) G. Gao, R.-G. Xie, L. Pu, *Proc. Natl. Acad. Sci. USA* **2004**, *101*, 5417 – 5420.

[7] a) G. Lu, X.-S. Li, X. Jia, W. L. Chan, A. S. C. Chan, *Angew. Chem.* **2003**, *115*, 5211 – 5212; *Angew. Chem. Int. Ed.* **2003**, *42*, 5057 – 5058; b) B. Jiang, Z.-L. Chen, W.-N. Xiong, *Chem. Commun.* **2002**, 1524 – 1525; c) Z. Q. Xu, R. Wang, J. K. Xu, C. S. Da, W. J. Yan, C. Chen, *Angew. Chem.* **2003**, *115*, 5925 – 5927; *Angew. Chem. Int. Ed.* **2003**, *42*, 5747 – 5749.

[8] The Carreira asymmetric alkyne addition to aldehydes[5] was found not to be suitable for this reaction.[3]

[9] The diastereoselective reactions of chiral aldehydes with LiC≡ CCO_2R were reported: a) C. Baldoli, P. Del Buttero, E. Licandro, S. Maiorana, A. Papagni, M. Torchio, *Tetrahedron Lett.* **1993**, *34*, 7943 – 7946; b) S. Cauwberghs, P. J. De Clercq, B. Tinant, J. P. Declercq, *Tetrahedron Lett.* **1988**, *29*, 2493 – 2496.

[10] G. R. Sullivan, J. A. Dale, H. S. Mosher, *J. Org. Chem.* **1973**, *38*, 2143 – 2147.

[11] Experimental details of the synthesis and characterization of the chiral γ-hydroxy-α,β-acetylenic esters and the assignment of the absolute configuration, determined by preparation of the Mosher esters, are given in the Supporting Information.

 © 2006 Wiley-VCH Verlag GmbH & Co. KGaA, Weinheim

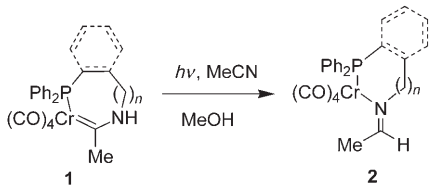
Carbene Complex Chemistry

DOI: 10.1002/anie.200501590

The Photochemical Reactivity of the "Photo-Inert" Tungsten (Fischer) Carbene Complexes**

Israel Fernández, Miguel A. Sierra, Mar Gómez-Gallego, María J. Mancheño, and Fernando P. Cossío**

The seminal discovery in 1982[1] of the sunlight-promoted reaction between chromium(0) carbene complexes and imines to yield β-lactams began the synthetically useful photochemistry of group 6 (Fischer) carbene complexes.[2,3] Both alkoxy- and aminocarbene complexes of chromium(0) are active in these reactions.[4] The reversible formation of chromium-bound ketenes by irradiation of chromium(0) carbene complexes with visible light was further postulated based on indirect evidence.[5] In contrast, tungsten(0) alkoxycarbene complexes do not carbonylate, and all the previous experimental data collected about the photochemical behavior of these compounds have led them to be considered as photo-inert.[6] Recently, we reported[7] a new photochemical dyotropic rearrangement from aminocarbenes **1** to imines **2** (Scheme 1), which unambiguously demonstrates the possibility of other reaction pathways in these organometallic complexes that do not necessarily involve a photocarbonylation step. According to our calculations, the first triplet state (T_1) in these compounds has a biradical character rather than the metallacyclopropanone structure proposed for the T_1 of alkoxycarbene complexes.[5,8] This short-lived species evolves stepwise to products **2** on the T_1 hypersurface.



1 2

Scheme 1. Dyotropic rearrangement from aminocarbene complexes **1** to imine complexes **2**.

The discovery of these new photochemical reactions in chromium(0) aminocarbene complexes led us to propose that tungsten(0) aminocarbene complexes may, in fact, experience reactions analogous to their chromium counterparts. Should this hypothesis be correct, the photo-inert tungsten(0) carbene complexes could be made photo-active by adequately modifying their structures. Herein we present the experimental confirmation of this hypothesis and show not only that tungsten(0) carbene complexes can be photo-active, but also that they undergo photocarbonylation processes.

The tungsten(0) carbene complexes **3a–c** were prepared following our previously reported procedure.[7] Thus, complexes **4a–c**, obtained by aminolysis of pentacarbonyl[ethoxy(methyl)carbene]tungsten(0) with the corresponding aminophosphanes, were heated in toluene to afford the desired products **3** in good yield (Scheme 2).

Irradiation of complexes **3a–c** in MeCN/MeOH yielded the *syn*-metalated imine complexes **5a–c** in acceptable yields (Scheme 3). The structures of the *syn*-metalated cyclic imines **5** were assigned by comparison of their spectroscopic data with those of their chromium analogues.[7] To the best of our knowledge, the 1,2-dyotropic rearrangement represented in Scheme 3 is the first photoreaction reported to date of the presumed photochemically unreactive tungsten(0) carbene complexes.[6]

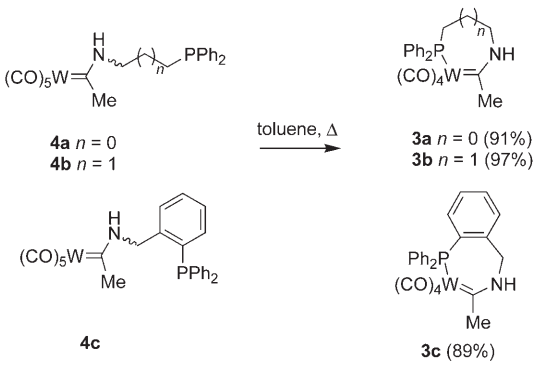
It may be possible that the dyotropic reaction represented in Scheme 3 is a particular process restricted to complexes **3**.

[*] I. Fernández, Prof. M. A. Sierra, Prof. M. Gómez-Gallego, Dr. M. J. Mancheño
Departamento de Química Orgánica
Facultad de Química
Universidad Complutense
28040 Madrid (Spain)
Fax: (+34) 91-394-4310
E-mail: sierraor@quim.ucm.es
Prof. F. P. Cossío
Kimika Fakultatea
Euskal Herriko Unibertsitatea, P.K. 1072
20080 San Sebastián–Donostia (Spain)
Fax: (+34) 943015270
E-mail: fp.cossio@ehu.es

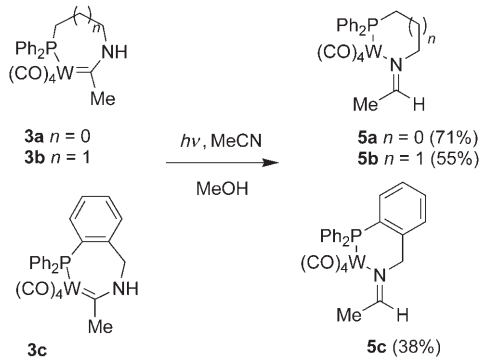
[**] Support for this work under grants CTQ2004-06250-C02-01/BQU (Madrid group) and CTQ2004-0681/BQU (San Sebastián–Donostia group) from the Ministerio de Ciencia y Tecnología (Spain), and the Euskal Herriko Unibertsitatea (9/UPV 00040.215-13548/2001) (San Sebastian–Donostia group) is gratefully acknowledged. I.F. thanks the Ministerio de Educación y Cultura (Spain) for a predoctoral (FPU) grant.

Supporting information for this article is available on the WWW under http://www.angewandte.org or from the author.

 © 2006 Wiley-VCH Verlag GmbH & Co. KGaA, Weinheim

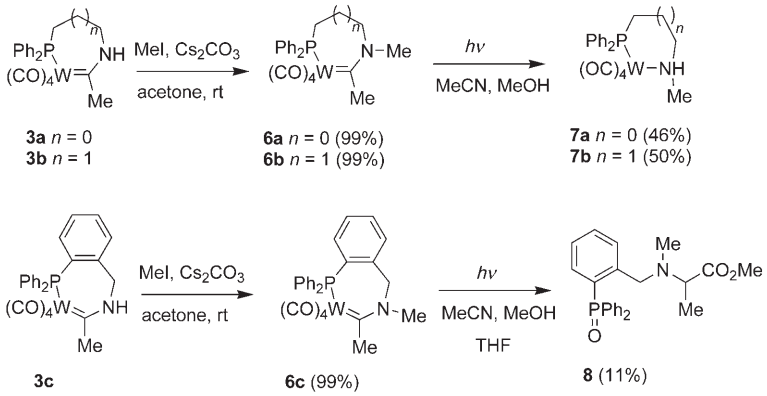


Scheme 2. Synthesis of cyclic tungsten(0) carbene complexes **3**. For details, see Experimental Section.



Scheme 3. Photochemical metalladyotropic type I rearrangement of complexes **3**. For details, see Experimental Section.

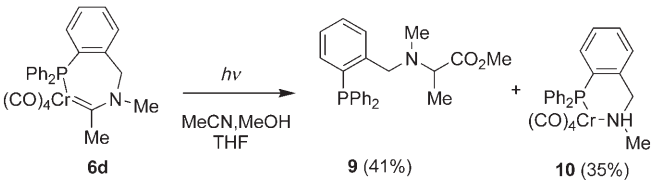
Therefore, to extend our knowledge of this reaction and to check the generality of tungsten(0)–carbene photochemistry, complexes **6** were prepared in almost quantitative yields by alkylation of complexes **3** with MeI/Cs_2CO_3, and irradiated in MeCN/MeOH (10:1; complexes **6a** and **6b**) or MeCN/THF/MeOH (5:5:1; complex **6c**; Scheme 4). Complexes **6** did not lead to the expected products analogous to **5** derived from a type I 1,2-dyotropic rearrangement.



Scheme 4. Photochemical α-fragmentation and carbonylation reactions of *N*-methylated complexes **6**. For details, see Experimental Section.

In fact, two different classes of compounds were obtained, either as mixtures (for complex **6c**) or as single products (for complexes **6a** and **6b**). The structure of a cyclic tetracarbonyl(phosphanylamino)tungsten complex was assigned to compounds **7a** and **7b** (derived from complexes **6a** and **6b**) on the basis of their spectroscopic data. Thus, complex **7a** shows a set of four ^{13}C NMR signals in the range $\delta = 202.9$–210.8 ppm as doublets (due to P–C coupling) corresponding to the $[W(CO)_4]$ fragment, while the signal for the *N*-Me moiety appears at $\delta = 56.1$ ppm. It should be pointed out that complexes **7** lack the Me group and the carbene carbon atom of the starting complexes **6**. The product isolated from **6c** lacks the metal moiety and has an amino ester structure.[9] The ^{13}C NMR spectrum of this compound contains a signal at $\delta =$ 174.0 ppm attributable to the ester carbonyl group. This feature shows unambiguously that carbonylation has occurred. The oxidation of the phosphorus atom was confirmed from the ^{31}P NMR spectrum ($\delta \approx 34$ ppm) and additionally by ESI mass spectrometry (*m*/*z* 407), thus confirming the presence of the phosphane oxide moiety (Scheme 4).

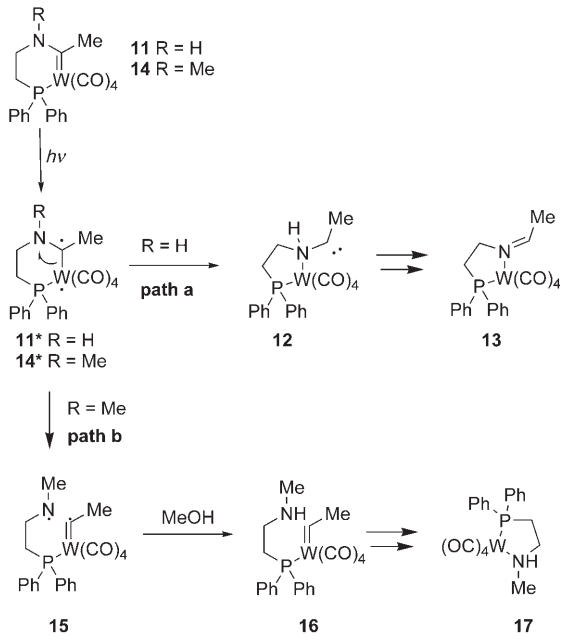
The UV-visible photochemistry of tungsten(0) aminocarbene complexes is therefore quite sensitive to the substitution at the nitrogen atom and can lead to up to three different photochemical reactions. This is remarkable for a class of compounds that had previously been considered as photo-inert. To confirm that this reactivity could also be observed in chromium(0) aminocarbene complexes, compound **6d** was prepared and irradiated under similar conditions. Now, in a very efficient process, both the *N*-methylamino ester **9** and the (aminophosphanyl)tetracarbonylchromium complex **10** were obtained (Scheme 5).



Scheme 5. Competitive α-fragmentation and carbonylation reactions of chromium(0) carbene **6d**.

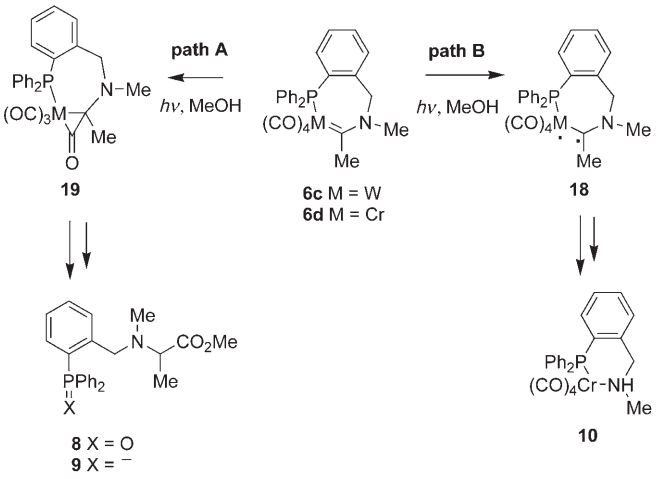
To rationalize the results obtained above we propose that the irradiation of complex **11** produces the biradical species **11*** (Scheme 6). This excited species evolves into the final *N*-metalated imine **13** via carbene **12**. This reaction pathway is analogous to that observed for chromium(0) carbene complexes.[7] In contrast, the biradical **14*** derived from the irradiation of **14**, which has a methyl substituent at nitrogen, evolves by fragmentation of the α-N–C=[W] bond to form a new biradical **15**. This process is similar to the α fragmentation of amides,[10] which are the isolobal analogues of aminocarbene complexes.[11] Capture of two hydrogen atoms from the solvent forms the species **16**. The evolution of this kind of complex into a metalated amine product like **17** has been previously observed by us and others.[12,13]

 © 2006 Wiley-VCH Verlag GmbH & Co. KGaA, Weinheim



Scheme 6. Proposed reaction pathways for the photoreaction of tungsten(0) aminocarbene complexes to yield *syn*-metalated imines **13** (path a) or α-fragmentation products **17** (path b).

The formation of α-amino ester **8** from tungsten(0) complex **6c** and the mixture of *N*-metalated amine **10** and the carbonylation product α-amino ester **9** from chromium(0) carbene **6d** indicate the co-existence of different activated species that are formed upon irradiation of these complexes (Scheme 7). It is reasonable to assume that compound **10**



Scheme 7. Proposed reaction pathways for the competitive processes observed in the irradiation of complexes **6c** and **6d**.

would arise from biradical intermediate **18**, while compounds **8** and **9** are formed from coordinated-ketene intermediates **19**.[13]

In conclusion, tungsten(0) carbene complexes, which were previously considered to be photo-inert, show a rich and complex photoreactivity when they are properly substituted, which may be of future interest both theoretically and synthetically. Thus, we have demonstrated experimentally that the excitation of tetracarbonyltungsten(0) (phosphanylamino)carbene complexes produces species having either a biradical structure or a tungstacyclopropanone structure. These species coexist and produce three different classes of products depending mainly on the substitution pattern on the nitrogen atom: *N*-unsubstituted complexes produce cyclic *syn*-metalated imine complexes through a type I metalladyotropic process, while *N*-methylated complexes produce pentacarbonyl(phosphanylamino)tungsten(0) complexes and α-amino esters. Further work in this emerging area of tungsten photochemistry as well as the study of other related processes in chromium(0) and molybdenum(0) carbene complexes is currently in progress.

Experimental Section

*General procedure for the synthesis of complexes **4***: A solution of stoichiometric amounts of pentacarbonyl[ethoxy(methyl)carbene]-tungsten(0) and the corresponding aminophosphane, in dry CH_2Cl_2, was stirred at room temperature until the disappearance of the starting material (checked by TLC). Then, the solvent was removed and the product was purified by flash column chromatography to yield pure compounds.

4a: yellow oil (58%). ^{1}H NMR (300 MHz, $CDCl_3$): $\delta = 1.75$ (m, 2H; CH_2P), 2.56 (s, 3H; CH_3), 3.95 (m, 2H; CH_2N), 7.32–7.72 (m, 10H; H_{Ar}), 8.46 ppm (br. s, 1H; NH). ^{13}C NMR (50 MHz, $CDCl_3$): $\delta =$ 28.1 (d, $J_{C,P} = 15.3$ Hz; CH_2P), 47.1 (CH_3), 52.7 (d, $J_{C,P} = 16.5$ Hz; CH_2N), 128.9 (d, $J_{C,P} = 6.4$ Hz; C_{Ar}), 129.4 (C_{Ar}), 132.7 (d, $J_{C,P} =$ 19.1 Hz; C_{Ar}), 136.5 (d, $J_{C,P} = 11.4$ Hz; C_{Ar}), 198.2 (*C*O), 203.2 (*C*O), 255.6 ppm (W=C). IR (CCl_4): $\tilde{\nu} = 2062$, 1965, 1927 cm^{-1}. $C_{21}H_{18}NO_5PW$: calcd. C 43.55, H 3.13, N 2.42; found C 43.69, H 3.00, N 2.28.

*General Procedure for the synthesis of complexes **3***: A solution of the (phosphanylamino)carbene complex was heated at reflux in toluene until the disappearance of the starting material (checked by TLC). The solvent was then removed under reduced pressure to yield pure compounds (unless otherwise specified).

3a: yellow solid (91%). ^{1}H NMR (300 MHz, $CDCl_3$): $\delta = 2.36$ (m, 2H; CH_2P), 2.77 (s, 3H; CH_3), 3.85 (m, 1H; CH_2N), 3.92 (m, 1H; CH_2N), 7.30–7.52 (m, 10H; H_{Ar}), 8.92 ppm (s, 1H; NH). ^{13}C NMR (75.5 MHz, $CDCl_3$): $\delta = 25.2$ (d, $J_{C,P} = 23.6$ Hz; CH_2P), 46.6 (d, $J_{C,P} =$ 4.1 Hz; CH_3), 48.9 (d, $J_{C,P} = 6.1$ Hz; CH_2N), 128.5 (d, $J_{C,P} = 9.3$ Hz; C_{Ar}), 129.8 (d, $J_{C,P} = 1.4$ Hz; C_{Ar}), 131.9 (d, $J_{C,P} = 12.0$ Hz; C_{Ar}), 137.0 (d, $J_{C,P} = 38.3$ Hz; C_{Ar}), 203.2 (d, $J_{C,P} = 7.0$ Hz; CO), 209.2 (d, $J_{C,P} =$ 26.8 Hz; CO), 213.4 (d, $J_{C,P} = 7.3$ Hz; CO), 261.4 ppm (d, $J_{C,P} =$ 9.6 Hz; W=C). IR (KBr): $\tilde{\nu} = 3304$, 2002, 1875, 1838 cm^{-1}. $C_{20}H_{18}NO_4PW$: calcd. C 43.58, H 3.29, N 2.54; found C 43.74, H 3.51, N 2.70.

*General Procedure for the synthesis of complexes **6**:* A solution of complex **3** in degassed acetone (0.025 M) was treated with two equivalents of MeI, three equivalents of Cs_2CO_3, and water (drops) at room temperature overnight. The crude reaction mixture was filtered through a short pad of celite and the solvent was removed under reduced pressure to yield pure compounds (unless otherwise specified).

6a: yellow solid (99%). ^{1}H NMR (300 MHz, $CDCl_3$): $\delta = 2.31$ (m, 2H; CH_2P), 2.67 (s, 3H; CH_3C), 3.26 (s, 3H; CH_3N); 4.05 (m, 1H; CH_2N), 4.14 (m, 1H; CH_2N), 7.26–7.46 ppm (m, 10H; H_{Ar}). ^{13}C NMR (75.5 MHz, $CDCl_3$): $\delta = 24.8$ (d, $J_{C,P} = 23.6$ Hz; CH_2P), 42.0 (d, $J_{C,P} =$ 37.2 Hz; CH_2N), 53.4 (CH_3C), 62.5 (d, $J_{C,P} = 7.1$ Hz; CH_3N), 128.5 (d, $J_{C,P} = 9.3$ Hz; C_{Ar}), 129.7 (d, $J_{C,P} = 1.6$ Hz; C_{Ar}), 131.9 (d, $J_{C,P} =$ 12.0 Hz; C_{Ar}), 137.3 (d, $J_{C,P} = 38.2$ Hz; C_{Ar}), 203.9 (d, $J_{C,P} = 6.9$ Hz; CO), 210.1 (d, $J_{C,P} = 28.1$ Hz; CO), 213.0 (d, $J_{C,P} = 6.7$ Hz; CO),

 © 2006 Wiley-VCH Verlag GmbH & Co. KGaA, Weinheim

259.7 ppm (d, $J_{C,P}=10.1$ Hz; W=C). IR (KBr): $\tilde{\nu}=2000$, 1902, 1857, 1842 cm^{-1}. $C_{21}H_{20}NO_4PW$: calcd. C 44.63, H 3.57, N 2.48; found C 44.44, H 3.40, N 2.55.

*General Procedure for the photochemical reactions of complexes **3** and **6***: Photochemical reactions were conducted with a 450-W medium-pressure Hg lamp through a Pyrex filter in dry, degassed MeCN containing MeOH (10:1 ratio) or in MeCN, THF, and MeOH (5:5:1 ratio) in a sealed Pyrex tube filled with argon. In a typical experiment, after irradiation for 10 h the solution (0.015 M) was filtered through a short pad of celite, the solvents were removed under reduced pressure, and the crude product was submitted to flash chromatography to give pure complexes, unless otherwise specified.

5a: yellow solid (71%). ^{1}H NMR (300 MHz, $CDCl_3$): $\delta=2.28$ (d, $J=5.2$ Hz, 3H; CH_3), 2.46 (m, 2H; CH_2P), 3.85 (m, 1H; CH_2N), 3.93 (m, 1H; CH_2N), 7.34–7.59 (m, 10H; H_{Ar}), 7.86 ppm (q, $J=5.2$ Hz, 1H; CH). ^{13}C NMR (75.5 MHz, $CDCl_3$): $\delta=26.0$ (CH_3), 30.7 (d, $J_{C,P}=21.2$ Hz; CH_2P), 69.6 (d, $J_{C,P}=10.1$ Hz; CH_2N), 128.8 (d, $J_{C,P}=9.9$ Hz; C_{Ar}), 130.2 (d, $J_{C,P}=1.7$ Hz; C_{Ar}), 131.9 (d, $J_{C,P}=12.2$ Hz; C_{Ar}), 135.5 (d, $J_{C,P}=40.4$ Hz; C_{Ar}), 172.9 (CH), 203.0 (d, $J_{C,P}=7.0$ Hz; CO), 210.1 (d, $J_{C,P}=32.0$ Hz; CO), 211.6 ppm (d, $J_{C,P}=5.1$ Hz; CO). IR (KBr): $\tilde{\nu}=2008$, 1867, 1838 cm^{-1}. $C_{20}H_{18}NO_4PW$: calcd. C 43.58, H 3.29, N 2.54; found C 43.39, H 3.33, N 2.41.

7a: yellow solid (46%). ^{1}H NMR (300 MHz, $CDCl_3$): $\delta=2.21$ (m, 1H; CH_2P), 2.48 (m, 1H; CH_2P), 2.76 (m, 1H; CH_2N), 2.89 (d, $J=5.9$ Hz, 3H; CH_3), 3.20 (m, 1H; CH_2N), 7.32–7.62 ppm (m, 10H; H_{Ar}). ^{13}C NMR (75.5 MHz, $CDCl_3$): $\delta=30.0$ (d, $J_{C,P}=21.6$ Hz; CH_2P), 48.1 (CH_3), 56.1 (d, $J_{C,P}=10.2$ Hz; CH_2N), 128.7 (d, $J_{C,P}=3.9$ Hz; C_{Ar}), 128.9 (d, $J_{C,P}=3.6$ Hz; C_{Ar}), 130.3 (C_{Ar}), 131.7 (d, $J_{C,P}=12.7$ Hz; C_{Ar}), 132.1 (d, $J_{C,P}=12.6$ Hz; C_{Ar}), 134.8 (d, $J_{C,P}=19.9$ Hz; C_{Ar}), 135.3 (d, $J_{C,P}=22.9$ Hz; C_{Ar}), 202.9 (d, $J_{C,P}=6.8$ Hz; CO), 204.0 (d, $J_{C,P}=7.8$ Hz; CO), 210.2 (d, $J_{C,P}=31.9$ Hz; CO), 210.8 ppm (d, $J_{C,P}=4.1$ Hz; CO). IR (CCl_4): $\tilde{\nu}=2012$, 1954, 1888 cm^{-1}. $C_{19}H_{18}NO_4PW$: calcd. C 42.33, H 3.37, N 2.60; found C 42.28, H 3.50, N 2.74.

8: pale-yellow oil (11%). The solvent was removed in vacuo and the residue was dissolved in a mixture of hexane and EtOAc (1:1) and exposed to direct sunlight until a clear solution was obtained. The solution was then filtered through a short pad of celite, the solvent eliminated, and the residue was purified by flash column chromatography to yield pure compound. ^{1}H NMR (300 MHz, $CDCl_3$): $\delta=0.86$ (d, $J=6.9$ Hz, 3H; CH_3C), 1.91 (s, 3H; CH_3N), 3.31 (q, $J=6.9$ Hz, 1H; C*H*CH_3), 3.54 (s, 3H; CH_3O), 3.92 (d, $J=10.6$ Hz, 2H; AB system, CH_2), 6.95–7.59 ppm (m, 14H; H_{Ar}). ^{13}C NMR (125 MHz, $CDCl_3$): $\delta=14.0$ (CH_3C), 36.5 (CH_3N), 51.1 (CH_3O), 56.9 (CH), 60.7 (CH_2), 126.1 (d, $J_{C,P}=13.2$ Hz; C_{Ar}), 128.4 (d, $J_{C,P}=9.1$ Hz; C_{Ar}), 130.1, 131.2 (d, $J_{C,P}=9.4$ Hz; C_{Ar}), 131.6 (C_{Ar}), 131.8 (d, $J_{C,P}=8.6$ Hz; C_{Ar}), 132.0 (C_{Ar}), 133.2 (C_{Ar}), 133.6 (d, $J_{C,P}=12.0$ Hz; C_{Ar}), 145.5 (d, $J_{C,P}=9.4$ Hz; C_{Ar}), 174.0 ppm (CO). ^{31}P NMR (internal H_3PO_4 reference): $\delta=34.2$ ppm. IR (CCl_4): $\tilde{\nu}=1736$, 1437, 1194, 1159, 1119 cm^{-1}. $C_{24}H_{20}NO_3P$: calcd. C 70.75, H 6.43, N 3.44; found C 70.60, H 6.61, N 3.59.

Received: May 10, 2005
Revised: September 23, 2005
Published online: November 22, 2005

Keywords: carbene ligands · carbonylation · photochemistry · rearrangement · tungsten

[1] a) M. A. McGuire, L. S. Hegedus, *J. Am. Chem. Soc.* **1982**, *104*, 5538; b) L. S. Hegedus, M. A. McGuire, L. M. Schultze, C. Yijun, O. P. Anderson, *J. Am. Chem. Soc.* **1984**, *106*, 2680.

[2] For reviews on the photochemistry of Group 6 metal–carbene complexes, see: a) L. S. Hegedus, *Tetrahedron* **1997**, *53*, 4105; b) L. S. Hegedus in *Comprehensive Organometallic Chemistry II, Vol. 12* (Eds.: E. W. Abel, F. G. A. Stone, G. Wilkinson), Pergamon, Oxford, **1995**, p. 549; c) M. A. Schwindt, J. R. Miller, L. S. Hegedus, *J. Organomet. Chem.* **1991**, *413*, 143.

[3] For reviews on different aspects of metal–carbene chemistry, see: a) K. H. Dötz, H. Fischer, P. Hofmann, R. Kreissel, U. Schubert, K. Weiss, *Transition Metal Carbene Complexes*, Verlag Chemie, Deerfield Beach, FL, **1983**; b) K. H. Dötz, *Angew. Chem.* **1984**, *96*, 573; *Angew. Chem. Int. Ed. Engl.* **1984**, *23*, 587; c) W. D. Wulff in *Comprehensive Organic Synthesis, Vol. 5* (Eds.: B. M. Trost, I. Fleming), Pergamon, Oxford, **1991**, p. 1065; d) H. Rudler, M. Audouin, E. Chelain, B. Denise, R. Goumont, A. Massoud, A. Parlier, A. Pacreau, M. Rudler, R. Yefsah, C. Alvarez, F. Delgado-Reyes, *Chem. Soc. Rev.* **1991**, *20*, 503; e) D. B. Grötjahn, K. H. Dötz, *Synlett* **1991**, 381; f) W. D. Wulff in *Comprehensive Organometallic Chemistry II, Vol. 12* (Eds.: E. W. Abel, F. G. A. Stone, G. Wilkinson), Pergamon, Oxford, **1995**, p. 470; g) D. F. Harvey, D. M. Sigano, *Chem. Rev.* **1996**, *96*, 271; h) R. Aumann, H. Nienaber, *Adv. Organomet. Chem.* **1997**, *41*, 163; i) B. Alcaide, L. Casarrubios, G. Domínguez, M. A. Sierra, *Curr. Org. Chem.* **1998**, *2*, 551; j) M. A. Sierra, *Chem. Rev.* **2000**, *100*, 3591; k) A. de Meijere, H. Schirmer, M. Duetsch, *Angew. Chem.* **2000**, *112*, 4124; *Angew. Chem. Int. Ed.* **2000**, *39*, 3964; l) J. Barluenga, J. Flórez, F. J. Fañanás, *J. Organomet. Chem.* **2001**, *624*, 5.

[4] A. Hafner, L. S. Hegedus, G. de Weck, B. Hawkins, K. H. Dötz, *J. Am. Chem. Soc.* **1988**, *110*, 8413.

[5] L. S. Hegedus, G. de Weck, S. D'Andrea, *J. Am. Chem. Soc.* **1988**, *110*, 2122.

[6] Strictly speaking tungsten(0) Fischer carbene complexes may experience loss of CO ligands as well as *syn–anti* isomerization upon irradiation. Nevertheless, to the best of our knowledge these complexes are photo-inert toward nucleophiles. The irradiation of chromium(0) carbene complexes with UV light also produces CO extrusion and *syn–anti* isomerization of the group tethered to the ligand. See: K. O. Doyle, M. L. Gallagher, M. T. Pryce, A. D. Rooney, *J. Organomet. Chem.* **2001**, *617*, 269. For the purposes of this work we will always refer to visible light photochemistry, using medium-pressure Hg lamps, a Pyrex filter, and a Pyrex well. Under these conditions medium-pressure Hg lamps radiate predominantly at 365–366 nm as well as significant amounts in the visible region at 404–408, 436, 546, and 577–579 nm. Under these experimental conditions, to the best of our knowledge, only photocarbonylation and carbene-transfer processes have been reported for chromium(0) and molybdenum(0) carbene complexes. See references [1] and [2].

[7] M. A. Sierra, I. Fernández, M. J. Mancheño, M. Gómez-Gallego, M. R. Torres, F. P. Cossío, A. Arrieta, B. Lecea, A. Poveda, J. Jiménez-Barbero, *J. Am. Chem. Soc.* **2003**, *125*, 9572.

[8] I. Fernández, M. A. Sierra, M. Gómez-Gallego, M. J. Mancheño, F. P. Cossío, *Chem. Eur. J.* **2005**, *20*, 5988.

[9] The ^{1}H NMR spectrum of the reaction mixture shows the presence of the cyclic phosphane–amine analogue to **7** (signals at $\delta=2.73$ (d) and 3.62 ppm (m)) as the main reaction product. However, all attempts to isolate this compound were fruitless. The crude reaction mixture was oxidized and chromatographed to isolate compound **8** (see Scheme 4).

[10] a) J. D. Coyle, *Chem. Rev.* **1978**, *78*, 97; b) A. G. Gilbert, J. Baggott, *Essentials of Molecular Photochemistry*, Blackwell Science, Oxford, **1991**, pp. 328–329.

[11] a) R. Hoffmann, *Science* **1981**, *211*, 995; b) R. Hoffmann, *Angew. Chem.* **1982**, *94*, 711; *Angew. Chem. Int. Ed. Engl.* **1982**, *21*, 711.

[12] a) C. K. Murray, B. P. Warner, V. Dragisich, W. D. Wulff, R. D. Rogers, *Organometallics* **1990**, *9*, 3142; b) I. Fernández, M. J. Mancheño, M. Gómez-Gallego, M. A. Sierra, T. Lejon, L. K. Hansen, *Organometallics* **2004**, *23*, 1851.

[13] Preliminary DFT calculations carried out at the uB3LYP/6-31 g(d)&LANL2DZ + ΔZPVE level of theory are consistent with these mechanistic proposals.

 © 2006 Wiley-VCH Verlag GmbH & Co. KGaA, Weinheim

Polymerization

DOI: 10.1002/anie.200502116

Cobalt-Catalyzed Carbonylative Copolymerization of *N*-Alkylazetidines and Tetrahydrofuran**

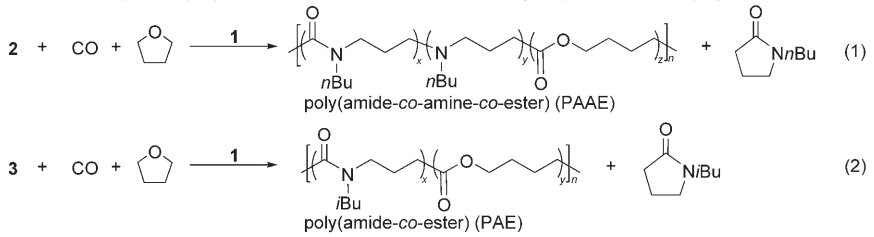
*Guosheng Liu and Li Jia**

The metal-catalyzed carbonylative polymerization of heterocycles (COPH) has received much attention in the last few years as a novel method for the synthesis of polyamides and polyesters.[1–7] Motivation for these research activities is the practical demand for polymers with heteroatom-containing backbones that are susceptible to hydrolytic and/or enzymatic attack in biological or ecological environments.[8,9] We are interested in the development of COPH using an approach based on single-site catalysts, under the idea that well-defined molecular catalysts would allow rational design and control of the chemical composition, molecular weight, and microstructure of the polymer product.

Herein, we report the carbonylative polymerization of azetidines catalyzed by $[Co(CH_3CO)(CO)_3P(o\text{-tol})_3]$ (**1**; tol = tolyl), and the participation of the tetrahydrofuran (THF) solvent in the polymerization to give ester units in the polymer products. The use of LiI as a cocatalyst eliminates the γ-lactam by-product and influences both the amount and distribution of the ester units in the polymer backbone. The well-controlled distribution of the ester units and the living character of the polymerization have allowed the synthesis of polymers with alternating amide blocks and ester segments, which undergo two-stage degradation.[10]

Herein, *N*-*n*-butylazetidine (**2**) and *N*-isobutylazetidine (**3**) are used as representative monomers. The polymerization was carried out in THF under CO (1000 psi) at 60–80 °C (Table 1). For **2**, in addition to the major carbonylative enchainment that resulted in the amide units, a simple ring-opening enchainment without carbonylation was also observed, which resulted in amine units in the polymer chain (entries 1 and 2).[7c] For the sterically bulkier and less nucleophilic **3**, selective carbonylative enchainment occurred, as assessed by NMR spectroscopy (entries 3–8).[11] Somewhat surprisingly, carbonylative enchainment of THF also took place and resulted in δ-oxyvaleroyl ester units in the polymer products.[12] Thus, the reactions of **2** and **3** in THF produced poly(amide-*co*-amine-*co*-ester)s (PAAEs) and poly(amide-*co*-ester)s (PAEs), respectively [Table 1, Eqs. (1) and (2)].

Table 1: Carbonylative polymerization of azetidine and THF (CO pressure 1000 psi).[a]



Entry	THF [mL]	Azetidine	Azetidine/**1** (molar ratio)	Cocatalyst	Selectivity[b]	Ester abundance [%]	$M_n \times 10^{-3}$ (PDI)[c]
1[d,e]	20	**2**	8:1	–	(81:9)[f]:10	8.3	2.16 (1.47)
2[d,e]	20	**2**	16:1	–	(84:8)[f]:8	4.7	3.78 (1.55)
3[d,e]	20	**3**	8:1	–	75:25	16	1.43 (1.18)
4[d,e]	20	**3**	16:1	–	82:18	9.4	2.68 (1.20)
5[d,e]	20	**3**	32:1	–	86:14	6.7	5.43 (1.20)
6[d,e]	30	**3**	48:1	–	83:17	4.3	7.42 (1.23)
7[d,g]	35	**3**	80:1	–	85:15	3.3	13.3 (1.22)
8[d,g]	40	**3**	100:1	–	82:18	2.4	15.5(1.25)
9[d,e]	30	**3**	18:1	LiI	>99:1	16.7	4.38 (1.12)
10[d,e]	30	**3**	18:1	$LiBPh_4$	84:16	8.5	2.63 (1.35)
11[d,e]	30	**3**	18:1	nBu_4NI	>99[h]:1	0	–
12[i]	65	**3**	(18×2):1	LiI	>99:1	15	7.51 (1.18)
13[i]	70	**3**	(18×3):1	LiI	>99:1	9.1	11.65 (1.21)
14[i]	75	**3**	(18×4):1	LiI	>99:1	8.7	14.92 (1.23)

[a] Catalyst **1** (0.12 mmol) used in all runs; cocatalyst (0.24 mmol) used for entries 9–14. Quantitative total conversion was achieved, except for entry 11. [b] Molar ratio of azetidine converted to polymer and γ-LA. [c] Determined by GPC with a refractive index detector against polystyrene standards with $CHCl_3$ as the eluent. [d] Oil-bath temperature 70 °C. [e] Reaction time 48 h. [f] Molar ratio of amide and amine units estimated by ^1H NMR spectroscopy. [g] Reaction time 72 h. [h] Monomer conversion 58 %. [i] Autoclave interior temperature 62 °C; 18 equiv of **3** added 10 h after the previously added **3** was exhausted.

The extent of THF carbonylative enchainment differed when **2** and **3** were used as the monomer: twofold as many ester units were incorporated with **3** than with **2** (entries 1 vs. 3, and 2 vs. 4).

The ester abundance, which is defined as the number of ester units divided by the total number of all monomer units, was also a function of the initial monomer-to-catalyst ratio. Higher monomer loadings resulted in a lower degree of ester incorporation (entries 3–8), which suggests that the reaction of THF was favored when the azetidine concentration was low. Directly monitoring the amide and ester growth by in situ IR spectroscopy confirmed that the ester abundance in the

[*] Dr. G. Liu, Prof. Dr. L. Jia[+]
Department of Chemistry
Lehigh University
6 East Packer Avenue, Bethlehem, PA 18015 (USA)
Fax: (+1) 610-758-6536
E-mail: ljia@rohmhaas.com

[+] Current address: Rohm and Haas Electronic Materials
455 Forest Street, Marlborough, MA 01752 (USA)

[**] This research was supported by the National Science Foundation (CHE 01-34285) and the Petroleum Research Fund (40241-AC1).

Supporting information for this article (polymerization procedures, plots of M_n versus conversion, NMR spectra of polymer products, and mechanistic hypotheses on γ-lactam formation) is available on the WWW under http://www.angewandte.org or from the author.

© 2006 Wiley-VCH Verlag GmbH & Co. KGaA, Weinheim

polymer increased as the reaction proceeded (Figure 1). The polymerization has a living character, as evidenced by the narrow polydispersity (Table 1, entries 3–8) and the linear

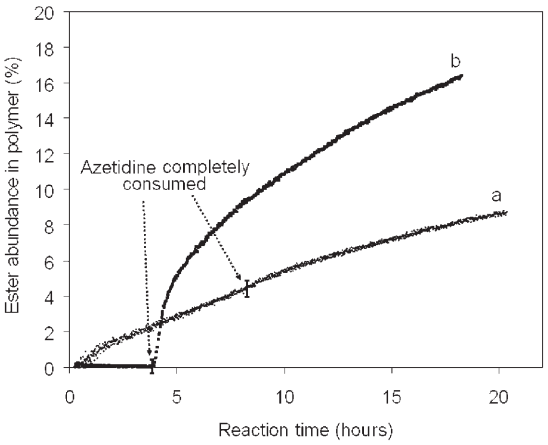
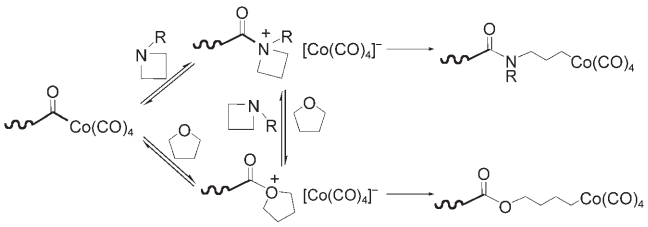


Figure 1. Change of ester abundance in the polymer chain as a function of reaction time. Line a: reaction in the absence of LiI; line b: reaction in the presence of LiI.

increase of molecular weight (M_n) with increasing monomer conversion,[11] and hence the ester units must populate the polymer chain in a gradient fashion that increases from the head to the tail. The gradient ester distribution and the variation in the ester abundance can likely be attributed to competition for the acyl site by THF, azetidine, and $[Co(CO)_4]^-$ ions and the relative ring-opening rates of azetidine and THF (Scheme 1).[12] Note that although the incorporation of THF was observed by Osakada and co-workers in the carbonylative polymerization of oxiranes,[5] we have never observed such reactivity in the carbonylative polymerization of aziridines.[7]



Scheme 1. Plausible mechanistic scenario affecting THF enchainment.

The selectivity of the polymerization of both **2** and **3** suffered from the ring-expanding side reaction that produced the γ-lactam (γ-LA). The selectivity did not deteriorate over a 12-fold increase in monomer loading (entries 3–8). The total conversions to the polymer and γ-LA were quantitative in all runs (entries 1–8). The formation of γ-LA did not annihilate the living character of the polymerization. Therefore, we tentatively attribute the formation of γ-LA to a process intrinsically coupled to the polymerization, most likely "back-biting"[6] as opposed to catalyst decomposition.[7a] We further hypothesize that back-biting happens at the stage of the acylazetidinium intermediate rather than that of the acyl-$Co(CO)_4$ intermediate.[13] Based on this hypothesis, one could formulate that the addition of nucleophiles, such as I^- ions, capable of opening the azetidium ring would bias the reaction toward polymerization. Indeed, the γ-LA by-product was eliminated with the addition of two equivalents of LiI relative to **1** (entry 9). The role of I^- in suppressing the formation of γ-LA was corroborated by the fact that the amount of **3** converted to γ-LA was hardly affected by the addition of $LiBPh_4$ (entry 10). Furthermore, nBu$_4$NI was also effective in suppressing the formation of γ-LA, although the polymerization was slower, and converted only 58% of **3** in 48 h under otherwise identical conditions (entries 9 vs. 11). The latter observation suggests that the Li^+ cation must also play a role in the polymerization.

In addition, LiI exerted an unexpected effect on the distribution and abundance of ester units in PAE. In situ IR spectroscopic monitoring of the polymerization revealed that in the presence of LiI, ester units did not form until complete consumption of **3** (Figure 1). The formation of the ester units began once the growth of the amide units stopped, and the final ester abundance was appreciably higher with LiI than without LiI for the same reaction time (entries 4 vs. 9). Thus, the PAEs produced in the presence of LiI are best characterized as consisting of an amide block followed by a very short ester segment. Note that again, Li^+ cations must play a role in the reaction of THF, as no ester units were formed in the presence of nBu$_4$NI (entry 11).

The combination of the segmental ester distribution and the living character of the polymerization provides an opportunity for the synthesis of PAEs with multiple, alternating amide blocks and ester segments. This was achieved by periodically feeding **3** into the reaction 10 hours after the previously added **3** was exhausted. The multiple additions under high pressure preserved the living polymerization, as demonstrated by the relatively narrow polydispersity indices (PDI; entries 12–14 in Table 1) and the linear increase of M_n with increasing number of monomer additions (Figure 2). Methanolysis of the PAEs at room temperature under acidic conditions completely eroded the ester linkages in the

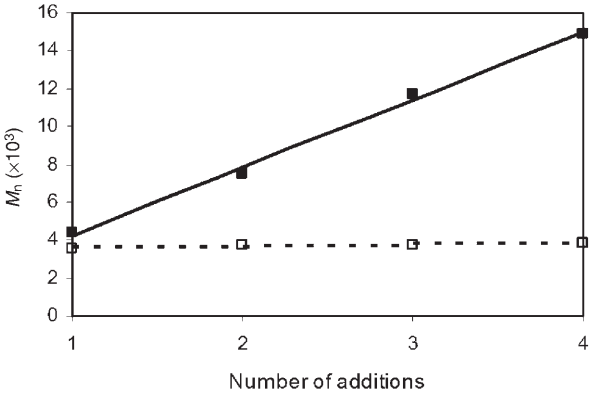


Figure 2. The linear increase of M_n values of PAEs with increasing number of additions of **3** (——; PAEs from entries 9, 12–14, Table 1). The dashed line shows the nearly constant M_n values of the methanolysis products independent of the M_n values of the original PAEs.

 © 2006 Wiley-VCH Verlag GmbH & Co. KGaA, Weinheim

backbone in 12 hours. The M_n values of the resulting polyamides were significantly reduced to the narrow range of 3570–3880 g mol^{-1}, and their PDI values were rather small in the range of 1.11–1.30. The uniform M_n and the narrow PDI of the methanolysis products are consistent with the anticipated microstructure of the PAEs, that is, amide blocks with uniform block length separated by segments of ester units. In comparison, the polyamides from the degradation of PAEs synthesized in the absence of LiI under otherwise identical conditions by multiple additions of **3** displayed a much broader molecular weight distribution.[11] Finally, the polyamides that resulted from methanolysis at room temperature can be completely degraded in refluxing water in one day under acidic conditions. Thus, the chemical compositions and their distributions in the above PAEs dictate that they would undergo two-stage degradation.

The Co-catalyzed living carbonylative polymerization of *N*-alkylazetidines provides a method that circumvents the thermodynamic problem for the synthesis of poly(γ-lactam)s via the ring-opening polymerization of γ-LAs.[13] The participation of THF in the polymerization is an interesting feature of this reaction. The ability of LiI to control the selectivity of the reaction and the microstructure of the polymer product is likely not limited to azetidines, but may also be applicable to other heterocyclic monomers. Combination of the above attributes has allowed the synthesis of PAEs with controlled molecular weight and microstructure that impart unique chemical degradation properties.

Experimental Section

Azetidine monomers were synthesized with modified methods from the literature,[14] and were dried with Bu_2Mg at room temperature. The synthesis of catalyst **1** was previously reported.[6] THF was refluxed over Na/benzophenone and freshly distilled.

The polymerizations were carried out in 300-mL stainless-steel reactors equipped with a stainless-steel tube as the reservoir for addition of azetidines. The tube was connected to the reactor by a stainless-steel ball-valve fitting. The reactor was located in a well-ventilated hood, around which CO detectors were placed. Catalyst **1** was dissolved in a small amount of THF and added to the stainless-steel tube with a syringe under a gentle flow of CO. After being charged with the solvent, the reactor was immediately pressurized with CO (1000 psi) and was heated with either an oil bath or a heating jacket. The stainless-steel tube holding the monomer was slightly overpressurized to allow the addition of azetidine. Multiple additions of monomer under high pressure could be performed in the same way. After the reaction was complete, the reactor was cooled to ambient temperature and the pressure was released into the fume hood. The polymer product was isolated by removal of solvent under vacuum, washing with ether/hexane (1:3 v/v), and drying under vacuum at room temperature.

Received: June 17, 2005
Published online: November 22, 2005

Keywords: azetidines · block copolymers · carbonylation · cobalt · polymerization

[1] N. Komine, S. Tanaka, S. Tsutsuminai, Y. Akahane, M. Hirano, S. Komiya, *Chem. Lett.* **2004**, *33*, 858–859.
[2] T. L. Lee, H. Alper, *Macromolecules* **2004**, *37*, 2417–2421.
[3] a) M. Allmendinger, M. Zintl, R. Eberhardt, G. Luinstra, F. Molnar, B. Rieger, *J. Organomet. Chem.* **2004**, *689*, 971–979; b) M. Allmendinger, R. Eberhardt, G. Luinstra, B. Rieger, *Macromol. Chem. Phys.* **2003**, *204*, 564–569; c) M. Allmendinger, R. Eberhardt, G. Luinstra, B. Rieger, *J. Am. Chem. Soc.* **2002**, *124*, 5646–5647.
[4] K. Nakano, K. Fumitaka, K. Nozaki, *J. Polym. Sci. A* **2004**, *42*, 4666–4670.
[5] D. Takeuchi, Y. Sakaguchi, K. Osakada, *J. Polym. Sci. A* **2002**, *40*, 4530–4537.
[6] D. J. Darensbourg, A. L. Phelps, N. Le Gall, L. Jia, *J. Am. Chem. Soc.* **2004**, *126*, 13808–13815.
[7] a) H. Xu, N. Le Gall, J. Zhao, L. Jia, W. W. Brennessel, B. E. Kucera, *J. Organmet. Chem.* **2005**, *690*, 5150–5158; b) G. Liu, L. Jia, *J. Am. Chem. Soc.* **2004**, *126*, 14716–14717; c) J. Zhao, E. Ding, L. Jia, *J. Polym. Sci. A* **2003**, *41*, 376–385; d) L. Jia, H. Sun, J. T. Shay, A. M. Allgerier, S. D. Hanton, *J. Am. Chem. Soc.* **2002**, *124*, 7282–7283; e) L. Jia, E. Ding, W. R. Anderson, *Chem. Commun.* **2001**, 1436–1437.
[8] E. S. Stevens, *Green Plastics*, Princeton University Press, Princeton, **2002**.
[9] *Biomedical Polymers and Polymer Therapeutics* (Eds.: E. Chiellini, R. M. Ottenbrite, D. Cohn, C. Migliaresi, J. Sunamoto), Kluwer, New York, **2001**.
[10] H. Abe, Y. Doi, *Macromol. Rapid Commun.* **2004**, *25*, 1303–1308.
[11] See the Supporting Information.
[12] THF can be carbonylatively oligomerized under identical conditions in the absence of azetidines but at a slower rate. Details of this finding will be reported in due course. No ether linkages were observed in any experiments with or without azetidine.
[13] a) V. P. Kolesov, I. E. Paukov, S. M. Skuratov, *Zh. Fiz. Khim.* **1962**, *36*, 770–779; b) S. K. Kakar, *Text. Res. J.* **1976**, *46*, 776–778; c) H. Sekiguchi, P. Tsourkas-Rapacoulia, F. Carriere, R. Andebert, *Eur. Polym. J.* **1974**, *10*, 1185–1193.
[14] a) A. T. Bottini, J. D. Roberts, *J. Org. Chem.* **1958**, *23*, 5203–5208; b) G. Lai, *Synth. Commun.* **2001**, *31*, 565–568; c) N. D. Kimpe, D. D. Smaele, *Tetrahedron Lett.* **1994**, *35*, 8023–8026.

 © 2006 Wiley-VCH Verlag GmbH & Co. KGaA, Weinheim

Dendrimers

DOI: 10.1002/anie.200502291

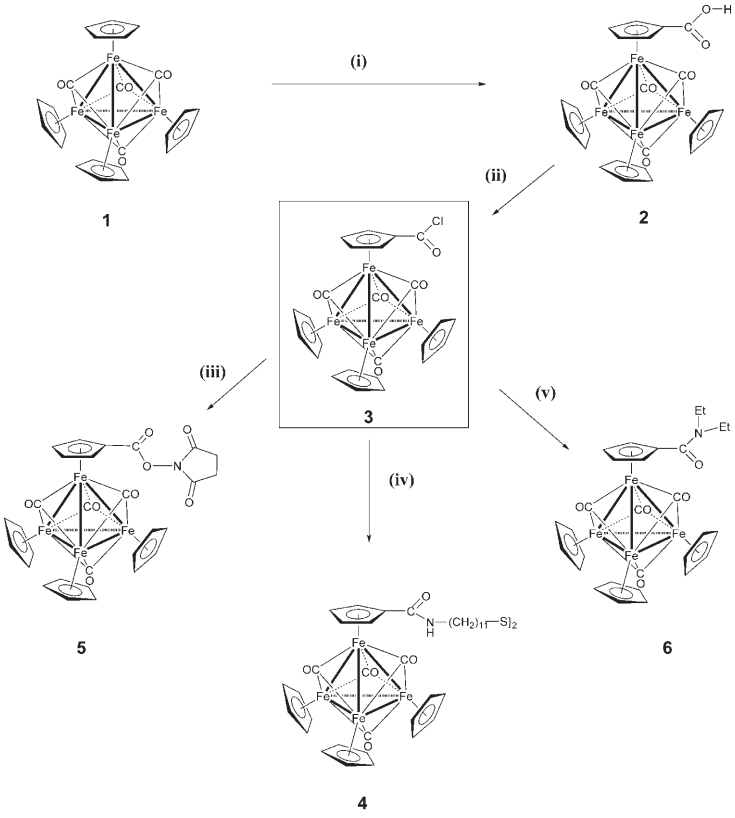
Assembly of Dendrimers with Redox-Active [{CpFe(μ_3-CO)}$_4$] Clusters at the Periphery and Their Application to Oxo-Anion and Adenosine-5′-Triphosphate Sensing**

*Jaime Ruiz Aranzaes, Colette Belin, and Didier Astruc**

Metallodendrimers[1–8] are well-established nanomaterials that have applications as electronic devices,[2] sensors,[3] and catalysts.[3,4] However, only a few examples are known with transition-metal clusters at the dendrimer periphery.[5] A star decorated with four polyoxometallate groups active in oxidation catalysis was reported,[6] and other redox-active transition-metal groups surrounding dendrimers at the periphery include metallocenes[7] and ruthenium polypyridine complexes.[2a] These molecular assemblies show promise as electronic devices and sensors which can be used by electrode modification.[8] Herein we report 1) functionalization of the long-known tetrairon cluster [{CpFe(μ_3-CO)}$_4$] (**1**),[9,10] the prototype of redox-rich organometallic clusters; 2) derivatization of 9-, 16-, and 27-branched dendrimers therewith; 3) redox behavior and redox robustness of these new metallodendrimers and formation of modified electrodes on which the cluster dendrimers are more strongly adsorbed with increasing size; 4) their application as selective sensors for oxo anions including adenosine-5′-triphosphate (ATP^{2-}); and 5) dendritic and structural effects on anion recognition, in particular the selectivity of recognition of ATP^{2-} in the presence of other anions and, for the first time, better recognition of ATP^{2-} than $H_2PO_4^-$.

Cluster **1** and its rich redox chemistry have been known for a long time.[9] We have synthesized its acyl chloride derivative **3** by reaction of the acid [$Fe_4Cp_3(\eta^5$-$C_5H_4CO_2H)$] (**2**)[9d] with $(COCl)_2$, the disulfide **4** by reaction of **3** with {$-S(CH_2)_{11}NH_3^+Cl^-$}$_2$, and the *N*-succinimidyl ester **5** by reaction of **3** with *N*-hydroxysuccinimide (Scheme 1).

Complex **3** reacts with 9-branched amino dendrimer **7** in the presence of NEt_3 to give the expected 9-branched amido cluster dendrimer **8** [Eq. (1)]. However, this is not the case for commercial (DSM) third-generation 16-branched amino dendrimer **9**,[11] probably for steric reasons. Compound **9** did not give the expected dendritic amide complex in the presence of NEt_3, but unexpected formation of the diethylamido cluster **6** was observed, presumably resulting from electron transfer from NEt_3 to **3** to generate the acyl radical



Scheme 1. i) a) LiN*i*Pr$_2$, −40 °C, 1 h, THF; b) CO_2, −40→20 °C; c) aq. 1 N HCl, 20 °C (30% yield); ii) $(COCl)_2$, CH_2Cl_2, 0 °C, 12 h (100% yield); iii) *N*-hydroxysuccinimide, NEt_3, CH_2Cl_2, 20 °C, 12 h (85% yield); iv) {$-SCH_2)_{11}NH_3^+Cl^-$}$_2$, NEt_3, CH_2Cl_2, 20 °C, 12 h (63% yield); v) NEt_3, CH_2Cl_2, 20 °C, 12 h (65% yield).

[$Fe_4(\mu_3$-$CO)_4Cp_3(\eta^5$-$C_5H_4CO^{\bullet})$], which further reacts with $NEt_3^{\bullet+}$ or $NEt_2^{\bullet}$. Successful functionalization of dendrimer **9** was performed by using *N*-succinimidyl ester **5**[12] to give 16-branched amido cluster dendrimer **10** [Eq. (2)].

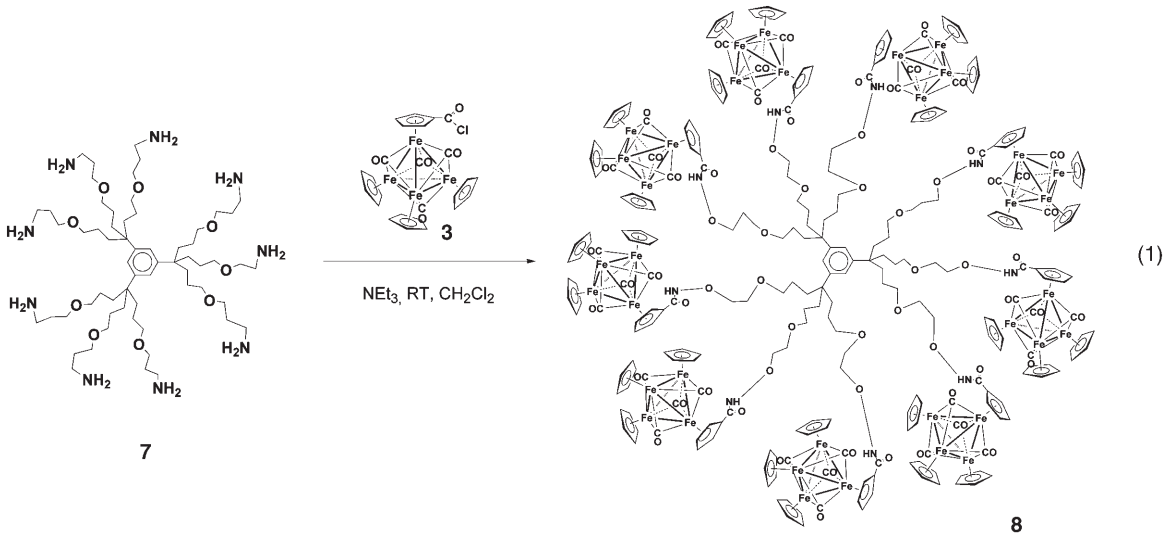
The reaction of **5** with the fourth-generation 32-branched amino dendrimer (DSM, following that of third-generation **9**) gave a dark green powder that was insoluble in all solvents, obviously due to excess steric bulk at the dendrimer periphery. However, the functionalization reaction worked smoothly with the new 27-NH_2 dendrimer **11**[13] to give 27-Fe_4 dendrimer **12** [Eq. (3)], because the interior and peripheral tethers are longer in **11** than in the diaminobutane dendrimers from DSM. The new metallodendrimers **8**, **10**,and **12** are air-stable, forest-green powders. They were characterized by

[*] Dr. J. R. Aranzaes, Prof. D. Astruc
Nanosciences and Catalysis Group
LCOO, UMR CNRS No 5802
Université Bordeaux I
33405 Talence Cedex (France)
Fax: (+33) 540-006-646
E-mail: d.astruc@lcoo.u-bordeaux1.fr
Dr. C. Belin
LPCM, UMR CNRS No 5803
Université Bordeaux I
33405 Talence Cedex (France)

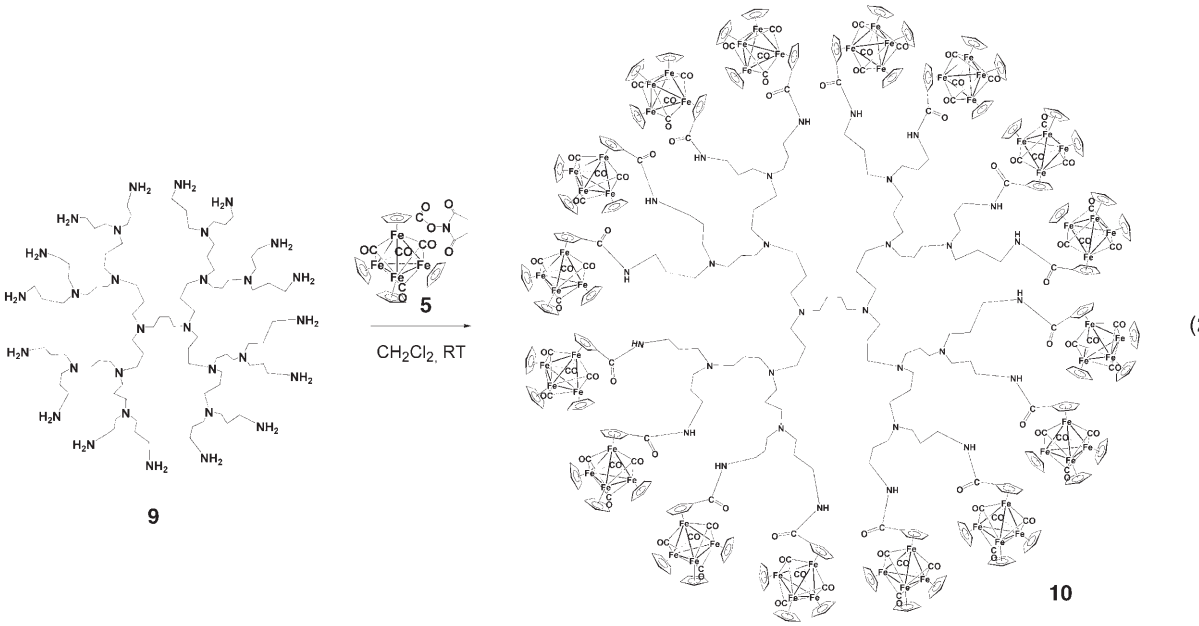
[**] Financial support from the Institut Universitaire de France (IUF, DA), the Université Bordeaux I, and the CNRS is gratefully acknowledged.

Supporting information for this article is available on the WWW under http://www.angewandte.org or from the author.

InterScience
© 2006 Wiley-VCH Verlag GmbH & Co. KGaA, Weinheim



(1)



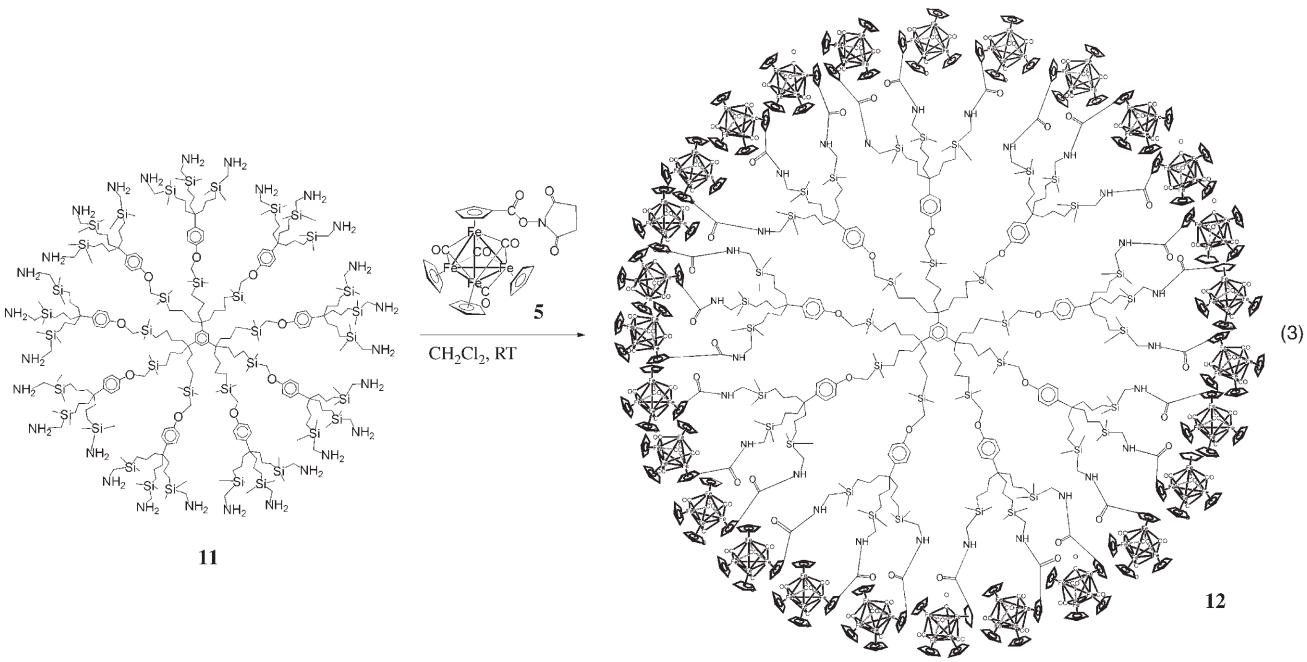
(2)

standard spectroscopic and elemental analyses, and atomic force microscopy (AFM) on **10** and **12** (Figure 1 and Supporting Information) showed monolayers of aggregated metallodendrimers are formed on the mica surface. Indeed, the heights of 1.5 nm for **10** and 2.4 nm for **12** are reproducibly obtained by AFM and correspond to the dimensions of slightly flattened molecular models.[14]

The cyclovoltammograms (CVs) of dendrimer clusters **8**, **10**,and **12** in CH_2Cl_2 (Pt, 0.1 M nBu_4NPF_6) resemble that of the monomeric cluster **1**,[9c] that is, the clusters are sufficiently remote from one another in the dendrimers to render the electrostatic factor almost nil. Therefore all the redox sites corresponding to the redox change $Fe_4 \rightarrow Fe_4^+$ appear in a single reversible wave (the other waves $Fe_4^+ \rightarrow Fe_4^{2+}$ and $Fe_4^0 \rightarrow Fe_4^-$ are also reversible, see Supporting Information).[15] For this wave, the Bard–Anson equation[15a] was applied to determine the number of electrons under conditions that avoid adsorption. This gave a result of 27 ± 3 electrons in CH_2Cl_2 and DMF with $[FeCp^*_2]$ ($Cp^* = \eta^5$-C_5Me_5) as internal reference. This stoichiometry could be confirmed by titration of **12** in CH_2Cl_2 with 27 equiv of green $[CpFe(\eta^5\text{-}C_5H_4COCH_3)]PF_6$, which generates $[CpFe(\eta^5\text{-}C_5H_4COCH_3)]$ and a dark green precipitate of $[\mathbf{12}](PF_6)_{27}$, characterized by the CO IR band at $\tilde{\nu}_{CO} = 1690\ cm^{-1}$, 55 cm^{-1} higher than $\tilde{\nu}_{CO}$ of **12** (1635 cm^{-1}). The color of the CH_2Cl_2 solution changes from dark green (**12**) to red (acetylferrocene) at the equivalence point.[9]

This property offers the possibility of recognizing anions, an area pioneered and deeply studied by Beer et al.,[16] then also by Moutet et al.,[17] with endoreceptors functionalized with various redox active species, although clusters have not yet been used for such sensing. We are dealing here with dendritic exoreceptors, a family that also proved successful for sensing, but only with metallocene units.[3b]

 © 2006 Wiley-VCH Verlag GmbH & Co. KGaA, Weinheim



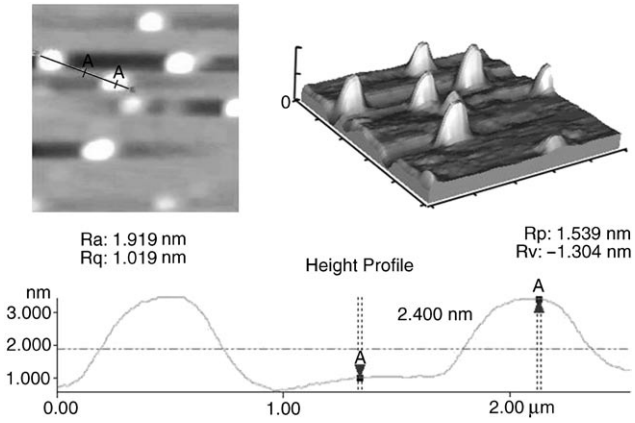


Figure 1. AFM pictures of 27-Fe_4 cluster dendrimer **12** on a mica surface.

Recognition of the oxo anions HSO_4^-, $H_2PO_4^-$, and adenosine-5′-triphosphate (ATP^{2-}) as their *n*-tetrabutylammonium salts by exoreceptors **8**, **10**, and **12** was investigated by adding their $n\mathrm{Bu_4N^+}$ salts to electrochemical cells containing a solution of the exoreceptor in CH_2Cl_2 at a Pt anode. Interestingly, for comparison, addition of these salts to a solution of the monomeric amido cluster **6** or $[Fe_4(CO)_4Cp_3(C_5H_4CONH\mathit{n}Pr)]$ did not provoke any change in the CV of the monomeric cluster. On the other hand, addition of $(n\mathrm{Bu_4N})_2(ATP)$ to one of these three dendritic clusters (even in the presence of HSO_4^- and Cl^-, vide infra) gave recognition features that were very different from one another and different from those of previous dendritic metallocenyl exoreceptors.[3b]

With $H_2PO_4^-$, a progressive wave shift was observed on titration, which was approximated according to the weak-interaction case in the Echegoyen–Kaifer model,[18] and the value of the apparent association constant was $K_{(+)} = 412 \pm 70$ (Supporting Information).

Contrary to the case of $(n\mathrm{Bu_4N})H_2PO_4$, addition of $(n\mathrm{Bu_4N})_2(ATP)$ to the electrochemical cell containing the solution of the host in CH_2Cl_2 provoked the appearance of a new CV wave, although with very different features for each dendrimer. In addition, the potential shifts are larger than those observed with $(n\mathrm{Bu_4N})H_2PO_4$ (Figure 2, Table 1), which contrasts with the behavior found for all metallocenyl dendrimers. The titration diagrams were recorded by using the decrease in intensity of the initial wave and increase in intensity of the new wave for both **10** and **12**. They show equivalence points for 0.5–0.6 equiv $(n\mathrm{Bu_4N})_2(ATP)$ per branch due to the double negative charges, which seemingly means that each phosphate monoanion unit of ATP^{2-} interacts with one Fe_4 cluster branch. Various other stoichiometries have been reported in such titrations.[17]

The addition of $(n\mathrm{Bu_4N})HSO_4$ to dendrimer **10** provokes a shift of the initial wave. This shift reaches 110 mV at saturation, which leads to an apparent association constant of $K_+ = (55 \pm 5) \times 10^3\ \mathrm{L\,mol^{-1}}$. The titration diagram shows an equivalence point at 0.75 equiv $(n\mathrm{Bu_4N})HSO_4$ per Fe_4 cluster branch, although saturation is obtained at 1 equiv $(n\mathrm{Bu_4N})HSO_4$ per branch (see Supporting Information). In this case the interaction is of the weak type, loose, and not selective.

The addition of equimolar amounts of $(n\mathrm{Bu_4N})_2(ATP)$, $(n\mathrm{Bu_4N})HSO_4$, and $(n\mathrm{Bu_4N})Cl$ to the electrochemical cell containing dendrimer **10** leads to a shift of the initial wave by 0.1 V. The equivalence point is reached at 0.7 equiv $(n\mathrm{Bu_4N})_2$ (ATP) (see Supporting Information), although no new CV wave is observed. This wave shift instead of the appearance of a new wave, when only $(n\mathrm{Bu_4N})_2(ATP)$ is added, and the slight increase in stoichiometry, can tentatively be taken into account by a dynamic equilibrium among the various ions of

 © 2006 Wiley-VCH Verlag GmbH & Co. KGaA, Weinheim

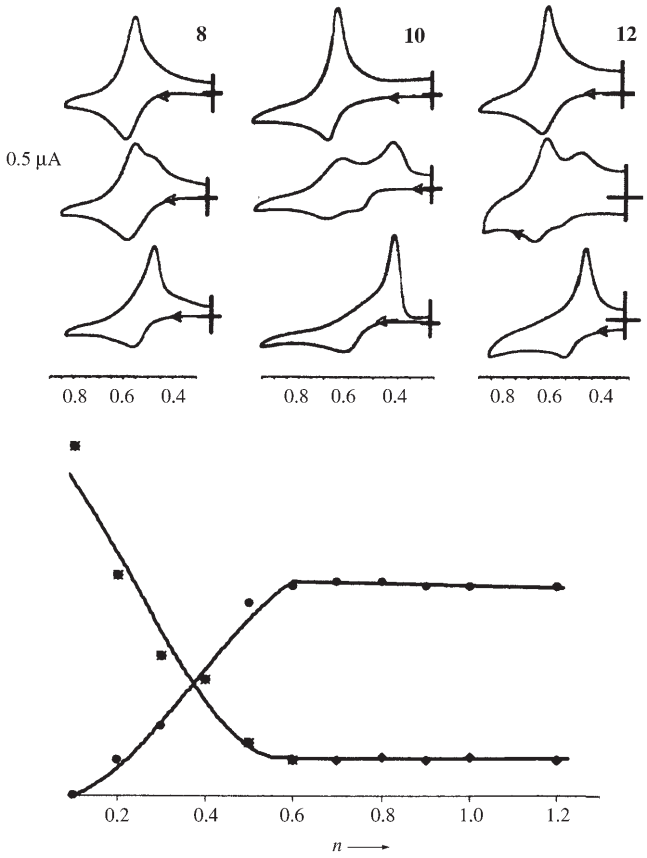


Figure 2. Titration of ATP^{2-} with **8**, **10**, and **12** (6×10^{-5} M) in CH_2Cl_2. Top: CVs before (bottom), during (middle), and after (top) addition of $(n\mathrm{Bu_4N})_2$(ATP) (x axis: voltage [V] vs [FeCp*$_2$]). Bottom: Decrease of the intensity of the initial CV wave (■) and increase of the intensity of the new CV wave (●) versus the number n of equivalents of $(n\mathrm{Bu_4N})_2$(ATP) added per cluster branch of **10**.

positive potential. After disappearance of the initial wave, the final chemically reversible wave has an $E_{pa}-E_{pc}$ value of 70 or 100 mV (Table 1), which signifies that electron transfer at the electrode surface is slow. This is due to structural reorganization of the dendritic host–guest supramolecular assembly that involves, as in solution, formation versus disruption of large ion pairs in synergy with double hydrogen bonding between the oxo anion and the amido group.[16] The shape of this wave is a fingerprint of the oxo anion. The salt $(n\mathrm{Bu_4N})_2$(ATP) can be washed away with CH_2Cl_2 to leave the modified electrode, which now only shows the initial wave of the dendritic cluster, although its current intensity is lower than initially. Subsequently, this washed, modified electrode can be used again.

The addition of equimolar amounts of $(n\mathrm{Bu_4N})_2$(ATP), $(n\mathrm{Bu_4N})HSO_4$, and $(n\mathrm{Bu_4N})Cl$ to the electrochemical cell containing dendrimer **12** leads to the appearance of a new wave, but the initial wave does not completely disappear after equivalence, consistent with the suggested hypothesis of a dynamic equilibrium (see below and Supporting Information).

In conclusion, we have successfully functionalized the cluster $[CpFe(\mu_3\text{-}CO)]_4$ for covalent attachment through a Cp ligand to the periphery of 9-, 16-, and 27-branched dendrimers and characterized the resulting cluster dendrimers inter alia by AFM on mica, which showed their flattening. Their cyclic voltammograms show a single reversible wave for the redox change $Fe_4\rightarrow Fe_4^+$, and this CV wave can be used for redox recognition and titration of oxo anions and in particular $(n\mathrm{Bu_4N})_2$(ATP) in CH_2Cl_2 solution. The larger cathodic wave shift with **10** than with **12** on ATP^{2-} addition is presumably due to the shorter distance between two clusters in **10** (12 bonds) than in **12** (16 bonds). Remarkably, and for the first time, $(n\mathrm{Bu_4N})_2$(ATP) is better recognized than $(n\mathrm{Bu_4N})H_2PO_4$, whereas the opposite holds with metallocenyl dendrimers. This specificity is certainly due to the mutual nanosize of the Fe_4 clusters and ATP^{2-}, which facilitates their interaction, whereas the smaller ferrocenyl groups do not exhibit this property. Dendritic effects (dendritic structure and compacity) are dramatic as is the replacement of metallocenes for cluster redox sensors. A Pt electrode modified with the 16-Fe_4 or 27-Fe_4 dendrimer provides selective ATP recognition. It is possible to wash the dendrimer with CH_2Cl_2 for recycling, and the quality of the modified electrode is optimum with the larger 27-Fe_4 dendrimer **12** due to better adsorption. Finally, given the known properties of **1** as a selective hydrogenation catalyst for various functional groups,[9h] this family of metallodendritic catalysts should also find use as recyclable catalysts.[4,20]

Table 1: Cyclic voltammetry data for **8**, **12** and **10** before, during, and after titration of $(n\mathrm{Bu_4N})_2$(ATP).

	$E_{1/2}$[a] ($E_{pa}-E_{pc}$)	$E_{1/2\,free}-E_{1/2\,new}$[b]	$E_{1/2\,bound}$[c] ($E_{Pa}-E_{Pc}$)	K_+/K_0[d]
monomer	0.630 (60)		0.610 (100)	
8	0.580 (30)	0.040	0.465 (100)	5
12	0.620 (30)	0.110	0.500 (100)	
10	0.590 (30)	0.165	0.385 (200)	700
modified Pt electrode with **12**	0.600 (10)	0.095	0.495 (70)	43
modified Pt electrode with **10**	0.590 (30)	0.070	0.500 (100)	16

[a] $E_{1/2}$ [V] vs [FeCp*$_2$] (internal reference) convertible into the value vs [$FeCp_2$] by subtracting 0.545 V;[19] electrolyte, $(n\mathrm{Bu_4N})PF_6$; working and counterelectrodes, Pt; solvent, CH_2Cl_2. The $E_{pa}-E_{pc}$ values are indicated in parentheses. [b] Difference of $E_{1/2}$ value [V] between the free wave and the new wave at half titration in order to observe and compare both waves (see Figure 1). [c] $E_{1/2}$ after addition of 0.5–0.6 equiv ATP^{2-} (equivalence point). [d] Ratio between the apparent association constants of the cationic (K_+) and neutral form (K_0) with ATP^{2-}.

the ion pairs and complexation kinetics that are different in the presence and absence of a mixture of anions.

Modification of a Pt electrode with dendrimers[6,7] such as **10** and **12** is possible (although not cleanly with the monocluster thiol derivative **4**); the best results were obtained with **12** due to its larger size ($E_{pa}-E_{pc}=10$ mV, see Supporting Information). Recognition of ATP^{2-} also then proceeds with the replacement of the initial wave by the new wave at less

 © 2006 Wiley-VCH Verlag GmbH & Co. KGaA, Weinheim

Experimental Section

27-cluster dendrimer **12**: The 27-NH_2 dendrimer **11** (0.020 g, 3.8×10^{-3} mmol) and triethylamine (0.029 mL, 0.2 mmol) were dissolved in dry CH_2Cl_2. Complex **5** (0.112 g, 0.152 mmol) in CH_2Cl_2 (10 mL) was added to this solution. The green solution was stirred at room temperature for 7 d under positive nitrogen pressure. The solution was then washed twice with a saturated sodium carbonate solution and twice with water, and the green organic solution was dried over sodium sulfate. The volume was reduced to 5 mL, and 25 mL of dry diethyl ether was added, which gave a green powder. This precipitate was dissolved in 5 mL of CH_2Cl_2, and the solution was poured over 25 mL of dry diethyl ether with stirring, which yielded a forest-green precipitate. The powdery 27-Fe_4 dendrimer **12** was finally dried under vacuum (0.030 g, 30% yield); dendrimer **10** was synthesized in the same way (see data in Supporting Information).

See the Supporting Information for the syntheses of all the clusters and dendrimers, AFM, and CVs including redox recognition and titration data.

Received: June 30, 2005
Revised: September 28, 2005
Published online: November 22, 2005

Keywords: anions · cluster compounds · dendrimers · iron · sensors

[1] Books on dendrimers: a) G. R. Newkome, C. N. Moorefield, F. Vögtle, *Dendrimers and Dendrons: Concepts, Synthesis, Applications*, Wiley-VCH, Weinheim, **2001**; b) *Dendrimers and Other Dendritic Polymers* (Eds.: J. M. J. Fréchet, D. A. Tomalia), Wiley, New York, **2002**; c) *Dendrimers and Nanosciences, Vol. 6* (issues 8–10: Guest Ed.: D. Astruc), Elsevier, Paris, **2003**.

[2] Reviews on metallodendrimers: a) V. Balzani, S. Campana, G. Denti, A. Juris, S. Serroni, M. Venturi, *Acc. Chem. Res.* **1998**, *31*, 26; b) G. R. Newkome, C. N. Moorefield, *Chem. Rev.* **1999**, *99*, 1689; c) M. A. Hershaw, J. R. Moss, *Chem. Commun.* **1999**, 1.

[3] Metallodendritic sensors: a) M. Albrecht, N. J. Hovestad, J. Boersma, G. van Koten, *Chem. Eur. J.* **2001**, *7*, 1289; A. W. Kleij, A. Ford, J. T. B. H. Jastrzebski, G. van Koten in ref. [1b], p. 185; b) D. Astruc, M.-C. Daniel, J. Ruiz, *Chem. Commun.* **2004**, 2637; see also refs. [7, 8].

[4] Metallodendritic catalysts: a) G. E. Oosterom, J. N. H. Reek, P. C. J. Kamer, P. W. N. M. van Leeuwen, *Angew. Chem.* **2001**, *113*, 1878; *Angew. Chem. Int. Ed.* **2001**, *40*, 1828; b) D. Astruc, F. Chardac, *Chem. Rev.* **2001**, *101*, 1991.

[5] a) Dendrimers with clusters at the periphery: G. R. Newkome, C. N. Moorefield, *Polym. Prepr. Am. Chem. Soc. Div. Polym. Chem.* **1993**, *34*, 75; b) M. Ferrer, R. Reina, O. Rossell, M. Seco, *Coord. Chem. Rev.* **1999**, *193–195*, 619; c) E. Alonso, D. Astruc, *J. Am. Chem. Soc.* **2000**, *122*, 3222.

[6] Dendrimers with redox-active clusters at the periphery: H. Zheng, G. R. Newkome, C. L. Hill, *Angew. Chem.* **2000**, *112*, 1841; *Angew. Chem. Int. Ed.* **2000**, *39*, 1772.

[7] Reviews on ferrocenyl dendrimers and their redox activity: ref. [3b] and C. M. Casado, I. Cuadrado, M. Moran, B. Alonso, B. Garcia, B. Gonzales, J. Losada, *Coord. Chem. Rev.* **1999**, *185–186*, 53.

[8] Dendritic redox-active assemblies modifying electrodes and their redox properties: refs. [3b, 7] and M. Yamada, I. Quieros, J. Mizutani, K. Kubo, I. Nishihara, *Phys. Chem. Chem. Phys.* **2001**, *3*, 3377; M. Yamada, H. Nishihara, *Chem. Commun.* **2002**, 2578.

[9] a) R. B. King, *Inorg. Chem.* **1966**, *5*, 2227; b) T. Toan, W. P. Felhammer, L. F. Dahl, *J. Am. Chem. Soc.* **1972**, *94*, 3389; c) J. A. Ferguson, T. J. Meyer, *J. Am. Chem. Soc.* **1972**, *94*, 3409; d) A. J. White, A. J. Cunningham, *J. Chem. Educ.* **1980**, *57*, 317; e) M. D. Westmeyer, M. A. Massa, T. B. Rauchfuss, S. R. Wilson, *J. Am. Chem. Soc.* **1998**, *120*, 114; f) W.-Y. Yeh, C.-Y. Wu, L.-W. Chiou, *Organometallics* **1999**, *18*, 3547; g) J. Ruiz, F. Ogliaro, J.-Y. Saillard, J.-F. Halet, F. Varret, D. Astruc, *J. Am. Chem. Soc.* **1998**, *120*, 1163; h) E. Alonso, J. Ruiz, D. Astruc, *C. R. Acad. Sci. Ser. IIc* **2001**, *3*, 189; i) cluster **1** is also a selective hydrogenation catalyst: see for instance j) C. U. Pittman, R. C. Ryan, J. McGee, J. P. O'Connor, *J. Organomet. Chem.* **1979**, *178*, C43.

[10] C. Valério, J.-L. Fillaut, J. Ruiz, J. Guittard, J.-C. Blais, D. Astruc, *J. Am. Chem. Soc.* **1997**, *119*, 2588.

[11] E. M. M. de Brabander-van den Berg, E. W. Meijer, *Angew. Chem.* **1993**, *105*, 1370; *Angew. Chem. Int. Ed. Engl.* **1993**, *32*, 1308; for examples of seminal applications of diaminobutane-based polyamine dendrimers using an amido linkage, see: J. F. G. A. Jansen, E. M. M. de Brabander-van der Berg, E. W. Meijer, *Science* **1994**, *266*, 1226.

[12] For previous syntheses of amides from *N*-succinimidyl esters, see: P. D. Beer, C. Harlewood, D. Hesek, J. Hodacova, S. E. Stokes, *J. Chem. Soc. Dalton Trans.* **1993**, 1327.

[13] J. Ruiz, G. Lafuente, S. Marcen, C. Ornelas, S. Lazarre, E. Cloutet, J.-C. Blais, D. Astruc, *J. Am. Chem. Soc.* **2003**, *125*, 7250.

[14] a) A. Hierlemann, J. K. Campbell, L. A. Baker, R. M. Crooks, A. J. Ricco, *J. Am. Chem. Soc.* **1998**, *120*, 5323; b) J. Li, L. T. Piehler, D. Qin, J. R. Baker, Jr., D. A. Tomalia, D. J. Meier, *Langmuir* **2000**, *16*, 5613.

[15] a) J. B. Flanagan, S. Margel, A. J. Bard, F. C. Anson, *J. Am. Chem. Soc.* **1978**, *100*, 4248; b) A. J. Bard, R. L. Faulkner, *Electrochemical Methods*, Wiley, New York, **1980**.

[16] P. D. Beer, *Adv. Inorg. Chem.* **1993**, *39*, 79; P. D. Beer, *Chem. Commun.* **1996**, 689 (feature article); P. D. Beer, *Acc. Chem. Res.* **1998**, *31*, 71; P. D. Beer, P. A. Gale, Z. Chen, *Adv. Phys. Org. Chem.* **1998**, *31*, 1; P. D. Beer, *Angew. Chem.* **2001**, *113*, 502; *Angew. Chem. Int. Ed.* **2001**, *40*, 486; J. H. R. Tucker, S. R. Collison, *Chem. Soc. Rev.* **2002**, *31*, 147; P. D. Beer, E. J. Hayes, *Coord. Chem. Rev.* **2003**, *240*, 167; W. W. H. Wong, D. Curiel, S.-W. Lai, M. G. B. Drew, P. D. Beer, *Dalton Trans.* **2005**, 774, and references therein.

[17] O. Reynes, J.-C. Moutet, J. Pecaut, G. Royal, E. Saint-Aman, *Chem. Eur. J.* **2000**, *6*, 2544; O. Reynes, G. Royal, E. Chainet, J.-C. Moutet, E. Saint-Aman, *Electroanalysis* **2002**, *15*, 65; O. Reynes, T. Gulon, J.-C. Moutet, G. Royal, E. Saint-Aman, *J. Organomet. Chem.* **2002**, *656*, 116; O. Reynes, J.-C. Moutet, J. Pecaut, G. Royal, E. Saint-Aman, *New J. Chem.* **2002**, *26*, 9; C. Bucher, D. H. Devillers, J.-C. Moutet, G. Royal, E. Saint-Aman, *New J. Chem.* **2004**, *28*, 1584; O. Reynes, C. Bucher, J.-C. Moutet, G. Royal, E. Saint-Aman, E.-M. Ungureanu, *J. Electroanal. Chem.* **2005**, *580*, 291.

[18] S. R. Miller, D. A. Gustowski, Z.-H. Chen, G. W. Gokel, L. Echegoyen, A. E. Kaifer, *Anal. Chem.* **1988**, *60*, 2021.

[19] D. Astruc in *Electron Transfer in Chemistry, Vol. 2* (Ed.: V. Balzani), Wiley-VCH, Weinheim, **2001**, Sec. 2, chap. 4, pp. 714–803.

[20] We are grateful to a reviewer for useful remarks concerning the redox-recognition aspects.

 © 2006 Wiley-VCH Verlag GmbH & Co. KGaA, Weinheim

Protein Photocleavage

DOI: 10.1002/anie.200502344

Site-Selective Photocleavage of Proteins by Uranyl Ions**

*Michael R. Duff, Jr. and Challa V. Kumar**

Dedicated to Professor J. C. Scaiano on the occasion of his 60th birthday

The uranyl ion (UO_2^{2+}) has a high affinity for the phosphate groups of DNA/RNA,[1] and this affinity was exploited to photocleave these biopolymers at the uranyl-binding sites.[2–5] Earlier success in our laboratory with site-specific photocleavage of proteins by organic molecules[6] and metal complexes[7] led to the idea that photoactive[8] metal–oxo species such as UO_2^{2+} should be capable of cleaving proteins with high selectivity. However, even though there is ample evidence to suggest that UO_2^{2+} binds to proteins,[9,10] it is not known if UO_2^{2+} can photocleave the peptide backbone. It is also not known if binding of UO_2^{2+} at specific sites would result in high selectivity for the protein cleavage. In addition, the ease with which UO_2^{2+} can be directed to metal-binding sites on proteins and the activation of the cation at visible wavelengths indicated that this would be a promising approach for footprinting metal-binding sites. In this report, high-affinity binding of UO_2^{2+} to proteins and their site-selective photocleavage, with visible light, is demonstrated for the first time.

Serum albumin (SA) and transferrin are known to bind UO_2^{2+},[11,12] and these proteins therefore provided good initial targets to test the above approach. Quantitative data on the binding of UO_2^{2+} to bovine SA (BSA), however, were lacking; these were obtained from calorimetric and spectroscopic studies. Isothermal titration calorimetry of the addition of a solution of UO_2^{2+} (0.5 mM) to BSA (0.1 mM; see Supporting Information) indicated exothermic binding (Figure 1). Best fits to the data required a two-site binding model[13] and indicated a high-affinity site (binding constant (K_b) of $(1.6 \pm 0.7) \times 10^7\,M^{-1}$) with moderate exothermicity (binding enthalpy (ΔH) of (-4.7 ± 0.7) kcal mol^{-1}) and a low-affinity site ($K_b = 2.8 \pm 2.5 \times 10^5\,M^{-1}$) with weak exothermicity ($\Delta H = -(1.2 \pm 0.8)$ kcal mol^{-1}).

Binding of UO_2^{2+} to BSA was also supported by absorption, circular dichroism (CD), and fluorescence studies. The CD spectra, for example, of a mixture of BSA (1 mM) and UO_2^{2+} in increasing concentrations (0–0.8 mM) showed the growth of new bands at 440 and 510 nm (Figure 2). These evidences established the binding of UO_2^{2+} to BSA.

Photocleavage of BSA by UO_2^{2+} was achieved by irradiating a mixture of BSA and UO_2^{2+} at 420 nm (Figure 3). Three distinct product bands at 35, 33 and 30 kDa were obtained in yields (11 ± 0.5), (4 ± 0.6), and (11 ± 1) % (lane 5), respectively. No photocleavage was noted without UO_2^{2+} (lane 3) or without light (lane 4). Photocleavage was observed at wavelengths up to 460 nm, although the yields were lower (data not shown).

To demonstrate the general nature of the photocleavage, other proteins such as human SA (HSA), porcine SA (PSA), glucose oxidase, and transferrin were also tested. These are cleaved with high selectivity (see Supporting Information). As negative controls, we also tested the photoreactivity with proteins such as α-lactalbumin, hemoglobin, and myoglobin, which do not bind the uranyl ion. These latter proteins are not cleaved by UO_2^{2+}, a result that is consistent with our expectations. Therefore, binding is essential for the cleavage

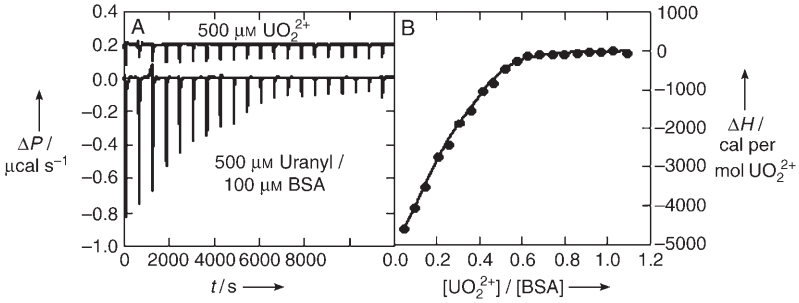


Figure 1. A) Exothermic binding of UO_2^{2+} to BSA (in water, pH 5.5); B) a two-site-binding fit to the data with binding constants of $1.6 \times 10^7\,M^{-1}$ and $2.8 \times 10^5\,M^{-1}$. ΔP = differential power.

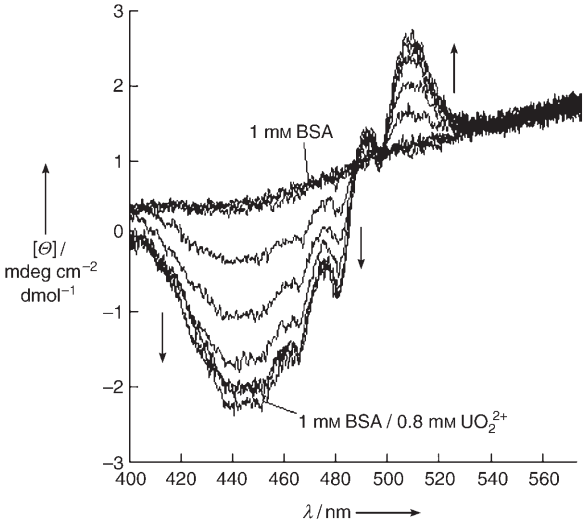


Figure 2. Circular dichroism spectra of BSA (1 mM) with increasing concentrations of UO_2^{2+} (0–0.8 mM).

[*] M. R. Duff, Jr., Prof. C. V. Kumar
Department of Chemistry
U-3060, Storrs CT 06269 (USA)
Fax: (+1) 860-486-2981
E-mail: Challa.Kumar@UCONN.edu

[**] The National Science Foundation is acknowledged for financial support (Grant no.: DMR-0300631).

Supporting information for this article is available on the WWW under http://www.angewandte.org or from the author.

© 2006 Wiley-VCH Verlag GmbH & Co. KGaA, Weinheim

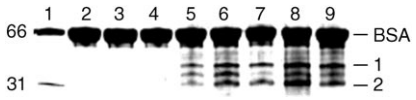


Figure 3. Visible-light induced cleavage of BSA (15 μM) by UO_2^{2+} (100 μM, 420 nm, 0.75 h, lane 5). Lane 1 contained molecular-weight markers (kDa), and all other lanes contained BSA. Lanes 4–9 contained UO_2^{2+}, lane 3 was the light control without UO_2^{2+}, and lane 4 was the dark control with UO_2^{2+}. The sample in lane 6 (100 μM UO_2^{2+}) was irradiated for 1.5 h. Lane 7 is similar to lane 5 but an additional portion of UO_2^{2+} (100 μM) was added after 0.75 h of irradiation. Lane 8 is similar to lane 7 except that the sample was irradiated for an additional 0.75 h after the second addition of UO_2^{2+}. The sample in lane 9 contained 200 μM UO_2^{2+} and was irradiated for 0.75 h. Labels 1 and 2 indicate the 35- and 30-kDa bands, respectively.

and free UO_2^{2+} is unlikely to be responsible for the observed photocleavage.

The reaction mixture was examined after photolysis to ascertain whether the uranyl ion is consumed during the reaction. The protein–uranyl complex retained its characteristic CD peaks, shown in Figure 2, even after the photoreaction; hence, the reaction is photocatalytic. This is consistent with the regeneration of the uranyl ion in its photoreactions with organic substrates.[14] The UV CD spectra of the BSA/uranyl mixture were also examined before and after irradiation (see Supporting Information). There was a decrease of only 8% in the 220-nm band between these spectra, a result indicating that the secondary structure of the protein is largely preserved. Even so, the product formation reached a maximum after around 0.75 h. Addition of fresh UO_2^{2+} to the reaction mixture and continued irradiation improved product yields (Figure 3, lane 8, yields of 20, 14, and 20%, respectively), but similar yields were also obtained when the same total concentration of UO_2^{2+} was used initially (lane 9, yields of 14, 9, and 14%, respectively).

To test the presence of photochemical intermediates in these reactions, quenching studies were carried out. Addition of 2-propanol quenched the reaction with a quenching constant of $0.35\,M^{-1}$. Since 2-propanol is known to quench the excited state of UO_2^{2+} at a rate constant (k_q) of $1.76\times10^9\,M^{-1}s^{-1}$,[15] interception of the excited state of free UO_2^{2+} (lifetime = 1.4 μs)[16] should have resulted in quenching constants greater than $10^3\,M^{-1}$ ($k_q\times$ lifetime). The much smaller value observed here ($0.35\,M^{-1}$) indicates that the cleavage results from UO_2^{2+} bound to the protein and not from free UO_2^{2+}.

In order to identify the cleavage site on BSA, amino acid sequencing of the photofragments was carried out (see Supporting Information). N-terminal sequencing of the 35-kDa fragment indicated the residues Asp-Thr-His-Lys-Ser, which match with the known N-terminal residues of BSA. Sequencing of the 30-kDa fragment indicated residues Lys-Asn-Tyr-Gln, which are internal to BSA. Thus, the newly formed N terminus is sequencible, and this is useful in the identification of the cleavage site. From the known primary sequence of BSA and the above sequencing data, we conclude that BSA is cleaved at Val314–Cys315.

The minor 33-kDa band (lane 5, Figure 3), which increases in intensity with extended irradiation time, is too small in yield to be sequenced, and this band is likely to be the secondary photoproduct from the 35-kDa fragment. The 2-kDa band, from the secondary cleavage of the 35-kDa band, is probably eluted out of the gel. If the 33-kDa band were the result of direct cleavage of BSA, then the corresponding 32-kDa band would be present; however, this is not observed.

To test whether UO_2^{2+}-induced photocleavage is useful for mapping metal-binding sites on BSA, the photocleavage was carried out in the presence of Ca^{II}, Zn^{II}, Cd^{II}, or Ni^{II} (2 mM metal ion). Only Ni^{II} completely inhibited the formation of the 35-, 33-, and 30-kDa bands, while Zn^{II} showed modest reductions in the product formation (see Supporting Information). This inhibition of photocleavage is not due to increased ionic strength because addition of 100 mM $NaNO_3$ to the reaction mixture had no effect on the yield. In addition, CD studies show that addition of Ni^{II} or Zn^{II} substantially reduced the intensities of the 440- and 510-nm CD bands of the UO_2^{2+}/BSA complex. Inhibition, therefore, is probably due to competitive binding of Ni^{II} or Zn^{II} to the metal-binding site or due to allosteric interactions across the protein. CD studies also show that UO_2^{2+} does not bind at the primary Cu^{II} site[17] on BSA.

From the above data and from the known 3D structure of HSA,[18] as a model for BSA, it is proposed that UO_2^{2+} binds to the cluster of ligands Asp311, Asp313, Cys315–disulfide, and His366. Among these, Asp311 and His366 appear to be essential for the photoreaction. For example, Asp311 of BSA is replaced by serine in HSA and this protein is not cleaved by UO_2^{2+} at Val314–Cys315. Similarly, His366 in BSA is replaced by Phe in PSA and this protein is also not cleaved by UO_2^{2+} at this site (see Supporting Information). The lack of cleavage of HSA and PSA at these sites strongly suggests that Asp311 and His366 in BSA are important for the observed photocleavage.

The protein cleavage most likely proceeds through steps which are similar to those proposed for DNA cleavage[1] and the photoxidation of hydrocarbons by the uranyl ion.[14] In our case, hydrogen-atom extraction from the Val314 side chain by the uranyl ion in the excited state is a strong possibility.[14,16] The reaction of the resulting alkyl radical with oxygen could lead to peptide-bond cleavage, as suggested earlier.[6,7] Further studies are in progress to consider these details.

In conclusion, UO_2^{2+} photocleaves a number of proteins, with high selectivity, and the primary cleavage site on BSA is Val314–Cys315. Ni^{II}, and to a lesser extent Zn^{II}, inhibit binding of UO_2^{2+} and the subsequent photocleavage. The binding site involved is likely to be the secondary Ni^{II} site on BSA and not the N-terminal site.[19] This is the first demonstration of protein photocleavage by a metal–oxo species with visible light. Photochemical footprinting with UO_2^{2+} is a promising method for investigating cohabitating metal-binding sites on proteins and biological interfaces.

Experimental Section

A VP-ITC isothermal titration calorimeter (MicroCal, Northampton, MA) was used to inject 20 portions of 500 μM UO_2^{2+} (14 μL) into 100 μM BSA at 15 min intervals (25°C, pH 5.5). The resulting data were fitted by using the Origin software (MicroCal, Northampton, MA). For the photoreactions, mixtures of 15 μM protein (see

 © 2006 Wiley-VCH Verlag GmbH & Co. KGaA, Weinheim

Supporting Information) and 200 μM $UO_2(NO_3)_2$ were prepared in 0.5–5 μM $NaNO_3$ (100 μL, pH 5.5) and irradiated at 420 nm for 0.75 h, and the products separated by 9% sodium dodecylsulfate PAGE as described previously.[6] The gels were stained by Coomassie Brilliant Blue, and the product bands were quantified by using NIH Image v1.1.6 software (NIH, U.S.A).

Additional information on the photocleavage of other proteins by UO_2^{2+}, BSA/UO_2^{2+} CD spectra before and after irradiation, and the cleavage inhibition by Ni^{II} and Zn^{II} are available in the Supporting Information.

Received: July 5, 2005
Revised: September 11, 2005
Published online: November 21, 2005

Keywords: cleavage reactions · photochemistry · proteins · uranyl ions

[1] P. E. Nielsen, *Methods Mol. Biol.* **2001**, *148*, 111–119.
[2] S. M. Fonseca, H. D. Burrows, M. G. Miguel, M. Sarakha, M. Bolte, *Photochem. Photobiol. Sci.* **2004**, *3*, 317–321.
[3] G. S. Bassi, N. E. Mollegaard, A. I. H. Murchie, D. M. J. Lilley, *Biochemistry* **1999**, *38*, 3345–3354.
[4] P. E. Nielsen, C. Jeppesen, O. Buchardt, *FEBS Lett.* **1988**, *235*, 122–124.
[5] D. Wittberger, C. Berens, C. Hammann, E. Westhof, R. Schroeder, *J. Mol. Biol.* **2000**, *300*, 339–352.
[6] C. V. Kumar, A. Buranaprapuk, *Angew. Chem.* **1997**, *109*, 2175–2177; *Angew. Chem. Int. Ed. Engl.* **1997**, *36*, 2085–2087.
[7] C. V. Kumar, J. Thota, *Inorg. Chem.* **2005**, *44*, 825–827.
[8] a) A. B. Yusov, V. P. Shilov, *Russ. Chem. Bull.* **2000**, *49*, 1925–1953; b) A. L. Buchachenko, I. V. Khudyakov, *Russ. Chem. Rev.* **1991**, *60*, 555–567.
[9] a) C. Monteilhet, C. Zelwer, J. L. Risler, *FEBS Lett.* **1974**, *46*, 101–105; b) J. Wang, R. S. Houk, D. Dreessen, D. R. Wiederin, *J. Am. Chem. Soc.* **1998**, *120*, 5793–5799.
[10] a) F. Takusagawa, S. Kamitori, S. Misaki, G. D. Markham, *J. Biol. Chem.* **1996**, *271*, 136–147; b) G. M. Ananyev, A. Murphy, Y. Abe, G. C. Dismukes, *Biochemistry* **1999**, *38*, 7200–7209.
[11] a) J. A. Muntz, E. S. G. Barron in *Toxicology of Uranium* (Ed.: A. E. Tannenbaum), McGraw-Hill, New York, **1951**, pp. 182–198.
[12] R. G. Reed in *Transport by Proteins* (Eds.: G. Blauer, H. Sund), de Gruyter, New York, **1978**, pp. 57–78.
[13] J. Tellinghuisen, *Anal. Biochem.* **2003**, *321*, 79–88.
[14] W.-D. Wang, A. Bakac, J. H. Espenson, *Inorg. Chem.* **1995**, *34*, 6034–6039.
[15] G. Sergeeva, A. Chibisov, L. Levshin, A. Karyakin, *J. Chem. Soc. Chem. Commun.* **1974**, 159–160.
[16] S. J. Formosinho, H. D. Burrows, M. G. Miguel, M. E. D. G. Azenha, I. M. Saraiva, A. C. D. N. Ribeirio, I. V. Khudyakov, R. G. Gasanov, M. Bolte, M. Sarakha, *Photochem. Photobiol. Sci.* **2003**, *2*, 569–575.
[17] CD studies with a mixture of Cu^{II} (2 mM) and BSA (1 mM) show that the CD bands that are assigned to Cu^{II} bound to the N terminus (a positive peak at 475 nm and a negative peak at 556 nm) are not diminished by the presence of UO_2^{2+} (2.2 mM).
[18] S. Sugio, A. Kashima, S. Mochizuki, M. Noda, K. Kobayashi, *Protein Eng.* **1999**, *12*, 439–446.
[19] W. Bal, J. Christodoulou, P. J. Sadler, A. Tucker, *J. Inorg. Biochem.* **1998**, *70*, 33–39.

 © 2006 Wiley-VCH Verlag GmbH & Co. KGaA, Weinheim

Polyoxometalates

DOI: 10.1002/anie.200502441

Step-by-Step Assembly of Trivacant Tungstosilicates: Synthesis and Characterization of Tetrameric Anions

*Nathalie Leclerc-Laronze, Mohamed Haouas, Jérôme Marrot, Francis Taulelle, and Gilbert Hervé**

Rational synthesis of large inorganic clusters from simple mononuclear or dinuclear metal complexes remains a challenge. Species with complex structures have been often obtained by a "one-pot" synthesis,[1] but their mechanism of formation is generally not known even if building units can be identified. Another approach, step-by-step control of the aggregation process, proved successful with reduced molybdenum compounds.[2] High-valent metal–oxo complexes are also especially suitable for such a strategy as the formation of highly reactive polyvacant intermediates is now well understood. For example, polyvacant polyoxotungstates have strongly basic oxygen atoms, which react with aquo-, oxo-, or thiometal complexes to give larger oligomeric species with new catalytic and magnetic properties.[3] However, we have recently shown with the trivacant ion A-α-$[SiW_9O_{34}]^{10-}$ (abbreviated as $\{SiW_9\}$; the A isomer results from the association of one tritungsten and three bitungsten groups) that protonation of oxygen atoms leads, in the first step and only in the presence of potassium cations, to a dimer by self-association of the two monomeric units.[4] Strongly basic oxygen atoms remain in the dimeric anion α-$[\{K(H_2O)_2\}Si_2W_{18}O_{66}]^{15-}$ (abbreviated as $\{Si_2W_{18}\}$), which can bind several transition-metal cations.[5] This anion can thus be the starting species for the construction of larger architectures through condensation reactions.

We report herein the synthesis and structural characterization of two polyanions: α-$[\{[K(H_2O)_2](\mu\text{-}H_2O)[Li(H_2O)_2]\}_2Si_4W_{36}O_{126}(H_2O)_4]^{16-}$ (**1**) and α-$[\{[K(H_2O)][K(H_2O)_4]\}_2Si_8W_{36}O_{136}]^{22-}$ (**2**). Anion **1** results from the direct association of two dimeric species, $[KSi_2W_{18}O_{66}]^{15-}$ and anion **2** through a $\{Si_4O_4\}$ cyclic assembling group. These two polyoxotungstate units can be considered as tetramers with respect to the initial A-α-$[SiW_9O_{34}]^{10-}$ ion.

The potassium salt of **1** was obtained by the addition of hydrochloric acid to an aqueous suspension of K_{15}α-$[KSi_2W_{18}O_{66}]$. Dissolution first occurs then precipitation of the hydrated potassium salt $K_{18}[K_2H_8Si_4W_{36}O_{130}]$. Crystals

[*] Dr. N. Leclerc-Laronze, Dr. M. Haouas, Dr. J. Marrot, Dr. F. Taulelle, Prof. G. Hervé
Institut Lavoisier, IREM UMR 8637
Université de Versailles Saint-Quentin-en-Yvelines
45 avenue des Etats-Unis
78035 Versailles Cedex (France)
Fax: (+33) 1-39-25-43-81
E-mail: herve@chimie.uvsq.fr

Supporting information for this article is available on the WWW under http://www.angewandte.org or from the author.

© 2006 Wiley-VCH Verlag GmbH & Co. KGaA, Weinheim

suitable for X-ray diffraction studies were obtained from a solution of this crude product in 2 M LiCl.[6] Crystal-structure analysis shows that anion **1** comprises the association of two dimeric subunits, $\{KLiSi_2W_{18}O_{64}(H_2O)_2\}$. The two $\{WO_6\}$ octahedra, which participate in the two W-O-W junctions, share a corner in each subunit (Figure 1). As for the parent

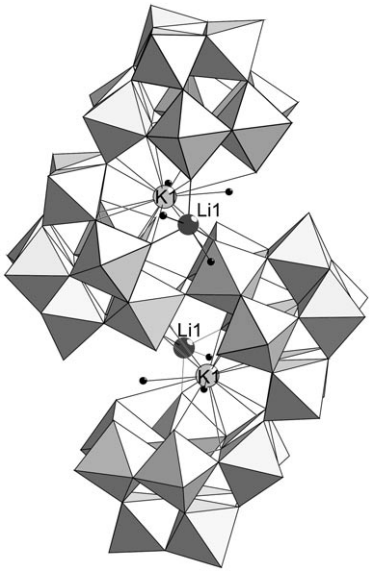


Figure 1. Combined polyhedra/ball-and-stick representation of **1**: $\{WO_6\}$ (gray polyhedra), potassium (gray ball), lithium (black ball), oxygen (small black ball).

dimeric anion,[4] there is a pocket in each subunit, which accommodates several cations: potassium, lithium, and protons. Two crystallographically non-equivalent subunits, **1a** and **1b**, have been found in the unit cell. In **1b**, there is no disorder on the positions of the potassium ion (K1), the lithium ion (Li1), and protons bound to the terminal oxygen atoms that surround the pocket. K1 and Li1 ions are arranged on each side of a $\{Si_2W_{18}\}$ subunit such that there is an inversion centre and the symmetry of the tetramer is *Ci*. In the external $\{SiW_9\}$ half of the $\{Si_2W_{18}\}$ subunit (Si3, W19–W27), three of the terminal oxygen atoms that surround the pocket are not bound to any metal cations. Bond lengths within the unit (W24–O90 = 2.12 Å, W25–O91 = 1.74 Å, W26–O97 = 2.05 Å; see Figure 2) show that the O atoms bound to W24 and W26 are protonated. Bond-valence calculations (see Supporting Information) reveal that O90 and O97 are biprotonated so that the pocket terminal ligands of W24 and W26 are water molecules.[7] Thus, there are eight protons bound to anion **1**, which is in good agreement with elemental analysis. The localization of the protons to only two of the three terminal oxygen atoms can be discussed by considering the lengths of the *trans*-W–O bonds between them (Figure 2). Starting from O85, which is bound to Li1 and K1 and must not be protonated (W23–O85 = 1.72 Å), the successive *trans*-W–O bonds are alternatively short (1.70 to 1.87 Å) and long (2.00 to 2.18 Å). This *trans*-influence explains why the last bond, W26–O97, is long as two protons are fixed on O97. The

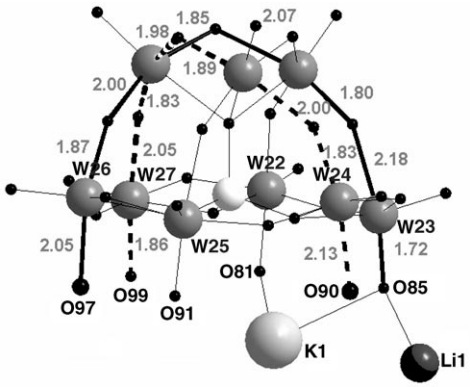


Figure 2. W–O bond lengths in the **1b** subunit; O90 and O97 correspond to water molecules.

neighboring terminal O91 atom associated with the same bitungsten group (with edge sharing tungsten octahedra) is not protonated, and in contrast to O90, which is associated with another bitungsten group, O91 is protonated. There are still alternate short (1.83 to 1.89 Å) and long (1.98 to 2.13 Å) *trans*-W–O bonds between the nonprotonated O99 and the protonated O90 atoms. Analogous coordination of water ligands in γ-$[SiW_{10}O_{34}(H_2O)_2]^{4-}$[8] to every second octahedron in the ring of six octahedra of the anion $[PMo_9O_{31}(H_2O)_3]^{3-}$ was reported previously.[9]

Inclusion of K1 in one side of the pocket results in a lateral distortion of the $\{Si_2W_{18}\}$ subunit. For example, the distance between O85 and O118 atoms is 3.23 Å on the side of K1 but the distance between the analogous O97 and O105 is 3.76 Å on the other side. For example, the O85-O118 distance is 3.23 Å on the side of K1, but the distance between the O97 and O105 is 3.76 Å on the other side. In the second $\{SiW_9\}$ half of the $\{Si_2W_{18}\}$ subunit, O118 and O105 correspond to O85 and O97, respectively. The O85–O118 distance is well adapted to the binding of a small cation such as Li^+, which thus bridges the two $\{SiW_9\}$ halves of $\{Si_2W_{18}\}$ on the same side as K1. This mode of binding of Li1 is analogous to the binding of one of the Co atoms in the $\{Co_2Si_2W_{18}\}$ complexes.[5] Spectrophotometric titration of **1** with Co^{2+} ions shows the formation of complexes with a Co/**1** ratio of about 2 and the corresponding complex has been synthesized. Unfortunately, the quality of the crystals was not sufficient to refine precisely the structure.

An interesting feature of the corner junction between the two $\{Si_2W_{18}\}$ subunits is the large value of the W30-O111-W31 angle (164°) in comparison with the corner junction between the two $\{SiW_9\}$ in $\{Si_2W_{18}\}$ (140°). Such a large angle is known in the association of the two $\{PW_9\}$ halves of the Dawson anion $[P_2W_{18}O_{62}]^{6-}$ and has important consequences in the localization of electrons in reduced derivatives.[10]

There is disorder in the positions of the potassium cation K2 and of the protonation sites for the independent unit **1a**; K2 occupies two positions, either in one side or the other of the pseudosymmetry plane comprising the Si1, Si2, W1, and W18 atoms (not shown). Due to the deformation of the anion resulting from the shift of the potassium atom out of this plane, all the atoms must be on two positions with occupation

 © 2006 Wiley-VCH Verlag GmbH & Co. KGaA, Weinheim

factors of 1/2. In addition to K2, only the tungsten atoms W5 and W8 can be refined on two positions (A and B); these positions are about 0.48 Å apart for W5 and about 0.56 Å apart for W8. These findings are in agreement with the structure of the non-disordered anion, **1b**, wherein W23 and W26, which correspond to W5 and W8 in **1a**, are strongly displaced owing to the deformation described above.

Anion **1** is kinetically stable in acidic solutions as shown by polarography (see Supporting Information) and ^{183}W NMR spectroscopy. The NMR spectrum shows seven resonance signals between −126 and −171 ppm with relative intensities 2:5:2:2:4:2:1 (Figure 3; see the Supporting Information for complete NMR characteristics). Signals with intensities of 5 and 4 result from fortuitous degeneracy, and for the latter two very close signals ($\delta = -166.14$ and −166.22 ppm) of equal intensities can be seen with enhanced resolution (inset of Figure 3). A very sharp signal at $\delta = -103.8$ ppm, attributed to the Keggin anion α-$[SiW_{12}O_{40}]^{4-}$, corresponds to 10% of the W atoms present in solution after 5 h and 16% after 29 h and is due to a very slow evolution of the anion **1**.

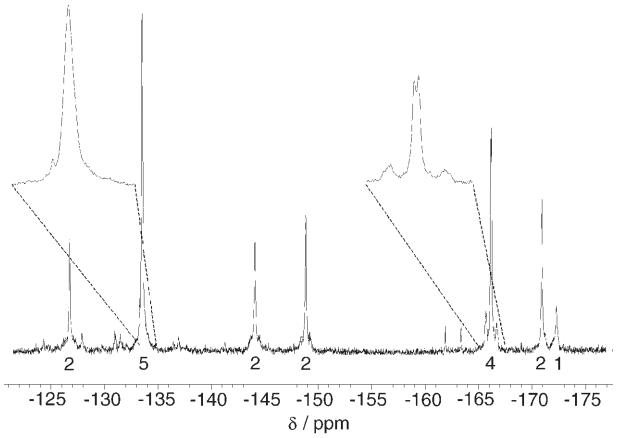


Figure 3. ^{183}W NMR spectrum of **1** (2×10^{-3} mol L^{-1} in H_2O/D_2O). The value underneath each signal indicates its relative intensity.

The apparent symmetry of **1** in solution is higher than that in the solid state as 18 resonance signals are expected from the structure of the non-disordered anion, **1b**. If we consider that the signal with a intensity of 5 is due to the superposition of three signals with intensities of 1, 2, and 2, then the ^{183}W NMR spectrum corresponds to ten non-equivalent tungsten atoms in **1**. Indeed, expansion of the spectrum around $\delta = 134$ ppm (see inset of Figure 3) shows a small signal for one W atom and a nonsymmetrical signal that could account for two equivalent plus another two equivalent W atoms. This observation can be explained by a rapid "jump" (compared with ^{183}W NMR time scale) of the potassium atom, K1, from left to right and right to left, that generates a pseudosymmetry plane. This dynamic behavior explains why only corner coupling (about 20 Hz) is observed but not the edge coupling (less than 10 Hz), thus preventing an assignment of the signals to tungsten atoms.

The potassium salt of **2** was obtained by adding hydrochloric acid to an aqueous suspension of the potassium salt $K_{15}\alpha$-$[KSi_2W_{18}O_{66}]$ in presence of potassium silicate. Anion **2** comprises the lateral association of two dimeric subunits, $\{KSi_2W_{18}O_{66}\}$, which are linked by a $\{Si_4O_4\}$ ring (Figure 4).[6] Since the cyclic species $[H_4Si_4O_{12}]^{4-}$ has been observed in aqueous silicate solution,[11] anion **2** can be considered as a condensation product of $[H_4Si_4O_{12}]^{4-}$ and two $\{Si_2W_{18}O_{66}\}$ units.

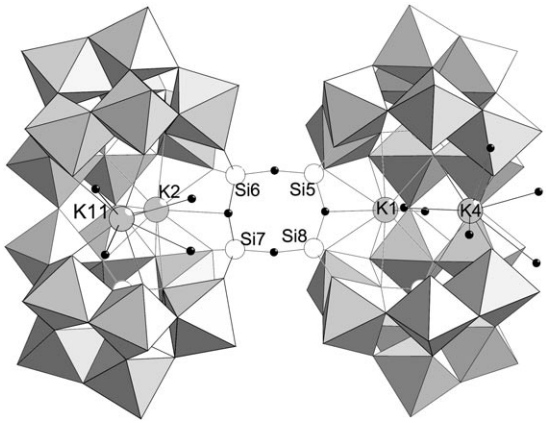


Figure 4. Combined polyhedra/ball-and-stick representation of **2:** labeling scheme as for Figure 1 except silicon (white ball).

The K1 potassium atom included in the pocket is on one side of the $\{Si_4O_4\}$ ring and another potassium atom, K4, is bound to the terminal oxygen atoms of the pocket on the other side. With M^{2+} transition-metal ions, anion **2** gives complexes in which M substitutes K4, but the quality of the crystals did not allow precise refinement of the structure.

In conclusion, condensation of $[SiW_9O_{34}]^{10-}$ anions in successive steps gives dimeric and tetrameric species. This strategy can be extended to other polyvacant polyoxotungsten structures. In **2**, the two subunits are linked by a tetraoxosilicate ring and we expect that new oligomeric anions can be obtained with other assembling groups such as polyphosphates and phosphonates.

Experimental Section

1: $K_{16}\alpha$-$[Si_2W_{18}O_{66}]\cdot25H_2O$[4] (12 g, 2.18 mmol) was suspended in water (65 mL). Dissolution of the solid occurred during addition of 1M HCl (12 mL; the pH was about 2.4). The solution was gently stirred and a white solid began to precipitate after 5 min. The reaction mixture was gently stirred for 12 h, then the solid was collected by filtration through a fine frit (yield: 5.4 g, 45%). This crude product was dissolved in 2M LiCl (5 g in 32 mL) and colorless crystals of **1** suitable for X-ray crystallography were obtained at room temperature within one day (yield: 30%). Elemental analysis (%) calcd for $K_{13}Li_3\alpha$-$[K_2Li_2H_8Si_4W_{36}O_{130}]\cdot74H_2O$: Li 0.32, K 5.44, W 61.44, Si 1.04; found: Li 0.39, K 5.40, W 61.18, Si 1.47. IR (KBr pellet): $\tilde{\nu} =$ 1004(w), 953(m), 877(s), 726(s), 637(m), 553(m), 528(sh), 374(w), 323(m) cm^{-1}.

Anion **1** can be characterized in solution by its polarogram. In formic acid/sodium formiate buffer (pH 3.4), it shows four successive

 © 2006 Wiley-VCH Verlag GmbH & Co. KGaA, Weinheim

waves at −0.58, −0.69, −0.78, and about −0.95 V versus the saturated AgCl/Ag reference electrode (see Supporting Information).

The ^{183}W NMR spectrum of **1** was recorded with a solution obtained by cation exchange of the potassium salt through a H^+-saturated Prolabo IRN-77 resin. A time-averaged Fourier-transform ^{183}W NMR (20.8 MHz) spectrum was recorded on a Bruker Avance 500 spectrometer (26 °C, 10 mm sample tube; chemical shifts were referenced to the ^{183}W resonance of an external 2 M Na_2WO_4 solution in alkaline D_2O and to dodecatungstosilicic acid as secondary standard ($\delta = -103.8$ ppm)).

2: $K_{16}\alpha$-$[Si_2W_{18}O_{66}]\cdot 25\,H_2O$ (4.7 g, 0.86 mmol) was added to water (100 mL). A solution of K_2SiO_3 was prepared by dissolving SiO_2 (0.1 g, 1.7 mmol) with KOH (0.4 g, 7.1 mmol) in water (50 mL) at room temperature. The solution of K_2SiO_3 was slowly added to a suspension of the dimer and 1 M HCl (9.3 mL) was then added (the pH was about 3.5). The solution was filtered, and colorless crystals of **2** suitable for X-ray crystallography were obtained at room temperature within 10 days (yield: 20 %). Elemental analysis (%) calcd for $K_{22}[K_2Si_8W_{36}O_{136}]\cdot 54\,H_2O$: K 8.58, W 60.55, Si 2.06; found: K 8.14, W 60.41, Si 2.42. IR (KBr pellet): $\tilde{\nu} = 1173$(w), 1048(sh), 1002(m), 944(s), 885(s), 836(s), 738(s), 675(s), 646(s), 601(sh), 553(m), 524(sh), 474(m), 357(m), 324(m) cm^{-1}.

Received: July 13, 2005
Revised: September 13, 2005
Published online: November 22, 2005

Keywords: anions · cluster compounds · polyoxometalates · self-assembly · tungsten

[1] a) C. du Peloux, P. Mialane, A. Dolbecq, J. Marrot, F. Sécheresse, *Angew. Chem.* **2002**, *114*, 2932 – 2934; *Angew. Chem. Int. Ed.* **2002**, *41*, 2808 – 2810; b) A. Müller, A. M. Todea, J. van Slageren, M. Dressel, H. Bögge, M. Schmidtmann, M. Luban, L. Engelhardt, M. Rusu, *Angew. Chem.* **2005**, *117*, 3925 – 3929; *Angew. Chem. Int. Ed.* **2005**, *44*, 3857 – 3861.

[2] a) A. Müller, F. Peters, M. T. Pope, D. Gatteschi, *Chem. Rev.* **1998**, *98*, 239 – 271; b) L. Cronin, C. Beugholt, E. Krickemeyer, M. Schmidtmann, H. Bögge, P. Kögerler, T. K. K. Luong, A. Müller, *Angew. Chem.* **2002**, *114*, 2929 – 2932; *Angew. Chem. Int. Ed.* **2002**, *41*, 2805 – 2808.

[3] Examples of recent work include: a) E. Cadot, M.-A. Pilette, J. Marrot, F. Sécheresse, *Angew. Chem.* **2003**, *115*, 2223 – 2226; *Angew. Chem. Int. Ed.* **2003**, *42*, 2173 – 2176; b) J. Marrot, M.-A. Pilette, F. Sécheresse, E. Cadot, *Inorg. Chem.* **2003**, *42*, 3609 – 3615; c) S. S. Mal, U. Kortz, *Angew. Chem.* **2005**, *117*, 3843 – 3846; *Angew. Chem. Int. Ed.* **2005**, *44*, 3777 – 3780; d) U. Kortz, F. Hussain, M. Reicke, *Angew. Chem.* **2005**, *117*, 3839 – 3843; *Angew. Chem. Int. Ed.* **2005**, *44*, 3773 – 3777.

[4] N. Laronze, J. Marrot, G. Hervé, *Chem. Commun.* **2003**, 2360 – 2361.

[5] a) N. Leclerc-Laronze, J. Marrot, G. Hervé, *Inorg. Chem.* **2005**, *44*, 1275 – 1281; b) L.-H. Bi, U. Kortz, *Inorg. Chem.* **2004**, *43*, 7961 – 7962.

[6] Crystals of **1** and **2** were mounted in a Lindemann tube. X-ray intensity data were collected on a Bruker X8-APEX2 CCD area-detector diffractometer by using $Mo_{K\alpha}$ radiation ($\lambda = 0.71073$ Å). Seven sets of narrow data frames (60 s per frame for **1** and 30 s for **2**) were collected at different values of θ (for 5 and 2 initial values of ϕ and ω, respectively for **1**; for 3 and 4 initial values of ϕ and ω, respectively for **2**) by using 0.5° increments of ϕ or ω. Crystal data and structure refinements: **1**: colorless crystal, $0.28 \times 0.26 \times 0.20$ mm^3, triclinic, space group $P\bar{1}$ (no. 2), $a =$ 18.7555(5), $b = 22.5419(5)$, $c = 23.7793(6)$ Å, $\alpha = 112.543(1)$, $\beta = 96.996(1)$, $\gamma = 104.136(1)$°, $V = 8739.8(4)$ Å^3, $Z = 2$, $\rho_{calcd} =$ 3.833 g cm^{-3}, $\mu(Mo_{K\alpha}) = 24.012$ mm^{-1}, $F(000) = 8782$, $T =$ 296(2) K. A total of 69677 independent reflections, 44418 observed with $I > 2\sigma(I)$, $R(\text{int}) = 0.057$, $R1 = 0.0492$, $wR2 =$ 0.1224, 2177 refined parameters. **2**: colorless crystal, $0.26 \times 0.14 \times 0.08$ mm^3, triclinic, space group $P\bar{1}$ (no. 2), $a =$ 18.5206(7), $b = 20.9506(7)$, $c = 24.5669(9)$ Å, $\alpha = 91.972(2)$, $\beta =$ 104.569(2), $\gamma = 96.615(2)$°, $V = 9144.5(6)$ Å^3, $Z = 2$, $\rho_{calcd} =$ 3.836 g cm^{-3}, $\mu(Mo_{K\alpha}) = 23.141$ mm^{-1}, $F(000) = 9250$, $T =$ 296(2) K. A total of 100269 independent reflections, 48690 observed with $I > 2\sigma(I)$, $R(\text{int}) = 0.0841$, $R1 = 0.0547$, $wR2 =$ 0.1242, 2206 refined parameters. Data reduction was accomplished by using SAINT V7.03. The substantial redundancy in data allowed a semiempirical absorption correction (SADABS V2.10) to be applied, on the basis of multiple measurements of equivalent reflections. The structure was solved by direct methods, developed by successive difference Fourier syntheses, and refined by full-matrix least-squares on all F^2 data with SHELXTL V6.12. Further details on the crystal-structure investigations may be obtained from the Fachinformationszentrum Karlsruhe, 76344 Eggenstein-Leopoldshafen, Germany (fax: (+49) 7247-808-666; e-mail: crysdata@fiz-karlsruhe.de), on quoting the depository number CSD 415593.

[7] N. E. Brese, M. O'Keeffe, *Acta Crystallogr. Sect. A* **1991**, *47*, 192 – 197.

[8] K. Kamata, K. Yonehara, Y. Sumida, K. Yamaguchi, S. Hikichi, N. Mizuno, *Science* **2003**, *300*, 964 – 966.

[9] B. Hedman, *Acta Chem. Scand. Ser. A* **1978**, *32*, 439 – 446.

[10] a) G. M. Varga, E. Papaconstantinou, M. T. Pope, *Inorg. Chem.* **1970**, *9*, 662 – 667; b) X. Lopez, C. Bo, J. M. Poblet, *J. Am. Chem. Soc.* **2002**, *124*, 12574 – 12582.

[11] R. K. Harris, C. T. G. Knight, *J. Chem. Soc. Faraday Trans. 2* **1983**, *79*, 1539 – 1561.

 © 2006 Wiley-VCH Verlag GmbH & Co. KGaA, Weinheim

Host–Guest Systems

DOI: 10.1002/anie.200502597

Simple and Quantitative Mechanochemical Preparation of a Porous Crystalline Material Based on a 1D Coordination Network for Uptake of Small Molecules**

Dario Braga, Marco Curzi, Anna Johansson, Marco Polito, Katia Rubini, and Fabrizia Grepioni**

Many research groups worldwide are engaged in the quest for nanoporous solids that are able to absorb and release small

[*] Prof. D. Braga, M. Curzi, Dr. A. Johansson, Dr. M. Polito, K. Rubini, Prof. F. Grepioni
Department of Chemistry, G. Ciamician
Via F. Selmi 2, 40126 Bologna (Italy)
Fax: (+39) 051-209-9456
E-mail: dario.braga@unibo.it
fabrizia.grepioni@unibo.it

[**] This work was supported by MIUR (PRIN2004, FIRB2001), the University of Bologna, and the Bertil Lundqvist Foundation.

Supporting information for this article is available on the WWW under http://www.angewandte.org or from the author.

WILEY InterScience DISCOVER SOMETHING GREAT
© 2006 Wiley-VCH Verlag GmbH & Co. KGaA, Weinheim

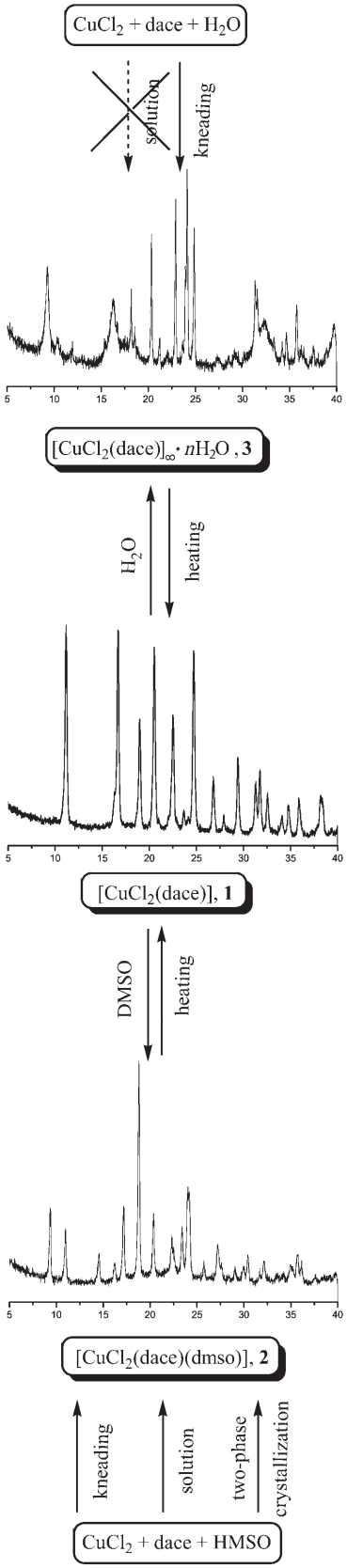
molecules in a controllable and selective fashion.[1] In many cases, coordination networks have been shown to allow formation of structures with channels and cavities (zeotypes), which can often be emptied and refilled without disruption of the crystalline edifice.[2] The preparation of zeotype compounds by hydrothermal methods or by reactions in solution, followed by crystallization, is often difficult because of the tendency of coordination networks to form highly insoluble materials. Recently we have begun to explore the use of solid-state, solvent-free methods for the preparation of molecular crystals[3] and more recently of coordination network compounds.[4,5]

It has long been known that co-grinding and co-milling of solid reactants are viable routes to molecular compounds or molecular crystals.[6] Early work dates back to the pioneering investigations of Etter and co-workers,[7] Rastogi and co-workers,[8] and Curtin, Paul, and co-workers.[9] Recently, mechanochemical methods have begun to be successfully applied also in the field of molecular crystal engineering[10] for solvent-free preparation of supramolecular aggregates,[11] cocrystals, and coordination networks.[12] Importantly, crystals formed by co-grinding of crystals in the absence of liquid can be different from those obtained from solutions or melts.[13]

Examples of the utilization of mechanochemical methods in coordination chemistry are not numerous, but these procedures are increasingly attractive because of environmental and sustainability issues. For example, *cis*-platinum complexes such as *cis*-$(Ph_3P)_2PtCl_2$ and *cis*-$(Ph_3P)_2PtCO_3$ have been prepared mechanochemically from solid reactants,[14] and the supramolecular self assembly of a number of two- or three-dimensional helicates has also been recently reported.[15]

Herein we describe the simple mechanochemical preparation of an inexpensive and versatile porous material based on the 1D coordination network $[CuCl_2(dace)]_\infty$ (**1**; dace = *trans*-1,4-diaminocyclohexane), which is able to absorb and release small molecules. Compound **1** can be obtained by mild thermal treatment of the hydrated compound $[CuCl_2(dace)]_\infty \cdot n H_2O$ (**3**) (see below), which is prepared as a polycrystalline material by manual kneading of solid $CuCl_2$ and dace in the presence of a small quantity of water (see Scheme 1). The system **1** reversibly absorbs small molecules either from solution or by simple kneading, whereas guest desorption invariably results in reversion to the unsolvated form **1**.

The structure of compound **1** is not known in crystallographic detail because the insolubility of the product does not permit the growth of X-ray crystallographic-quality single crystals. However, insight into the structure of **1** has been obtained from the knowledge of the structure of the dimethyl sulfoxide (DMSO) adduct $[CuCl_2(dace)(dmso)]_\infty$ (**2**), which has been fully characterized by single-crystal X-ray crystallographic diffraction (see the Experimental Section). As in the case of **3**, compound **2** can be easily and quantitatively prepared by kneading solid $CuCl_2$ and dace with a few drops of DMSO. Comparison of the X-ray powder diffractogram measured on the kneaded product with that calculated on the basis of the single crystal structure allowed unambiguous formulation of the former product as **2**.



Scheme 1. Preparation of compound **1** (middle) from its hydrated precursor **3** (top), and its behavior as a porous material to reversibly take up small guest molecules: in the example here (bottom) DMSO is absorbed to yield compound **2**.

 © 2006 Wiley-VCH Verlag GmbH & Co. KGaA, Weinheim

Figure 1 shows how compound **2** is formed out of 1D coordination networks in which the $CuCl_2$ units are bridged by dace ligands located in chains. Parallel 1D $CuCl_2$–dace

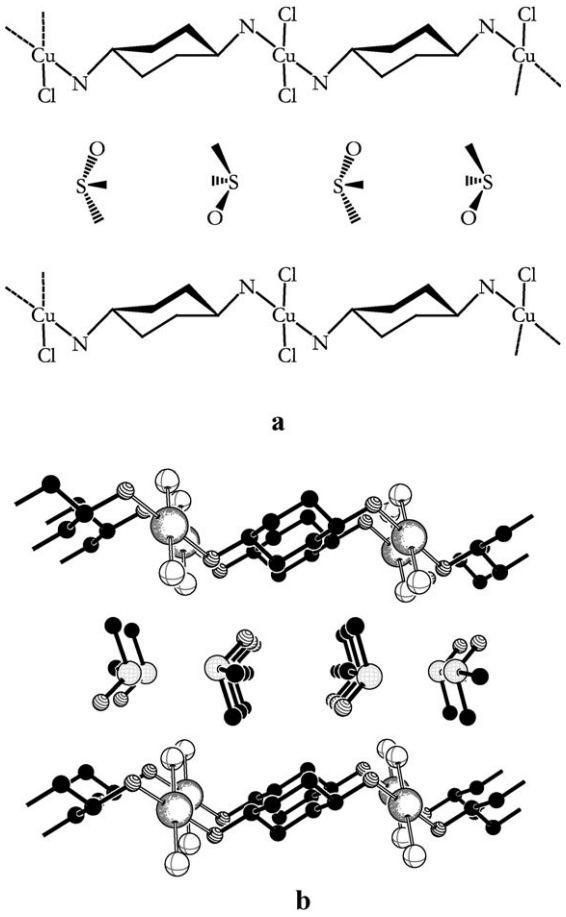
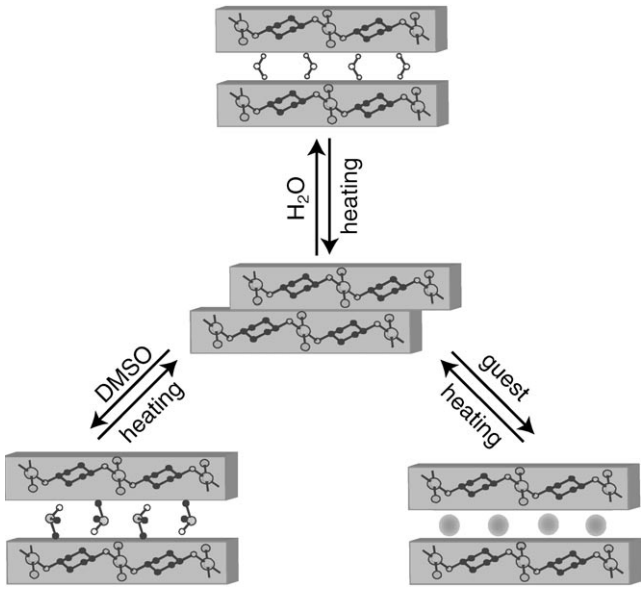


Figure 1. a) A schematic representation of the structure of **2**. b) A perspective view of the packing of **2**, showing the layers formed by parallel 1D networks of alternating $CuCl_2$ and dace units. H atoms omitted for clarity.

networks form layers, which host, in intercalation fashion, the cocrystallized DMSO molecules (see view of the packing in Figure 1b). The copper atoms in **2** adopt a square-planar coordination and the cyclohexane rings of dace are in the chair conformation. The earlier reported structure of *cis*-1,4-diaminocyclohexane, $PtCl_4$, and similar Pt compounds contain dace in the boat conformation.[16] Recently, we reported that solid-state and solution reactions between dace and silver acetate yield three isomeric forms of the coordination network $[Ag(H_2NC_6H_{10}NH_2)^+]_\infty$, all characterized by the presence of chevronlike Ag^+···dace···Ag^+···dace networks.[5]

The interest in compound **2** and its congeners stems not so much from their structures, but from their behavior upon thermal treatment. When polycrystalline **2**, which can be taken as a prototype of this family of compounds, is heated to 130 °C in TGA and DSC experiments, conversion into compound **1** is observed (Scheme 1). This was easily ascertained through comparison of X-ray powder diffractograms after and before DMSO absorption. The process is reversible, and the addition of a few drops of DMSO is sufficient to revert **1** into **2**. Compound **2** can also be obtained by mixing stoichiometric amounts of $CuCl_2$ and dace directly in DMSO with the resultant formation of an insoluble purple microcrystalline powder. In all cases, the products were identified unambiguously through comparison of X-ray powder diffraction patterns. From the structure of **2** and from the knowledge of its thermal behavior, it is possible to infer that the structure of **1** is based on a stacking sequence of layers as in **2**, but 'squeezed' at a shorter interlayer separation as a consequence of DMSO removal (Scheme 2). When the guest molecules enter between the layers, the spacing between the $CuCl_2$–dace chains is expanded and the layers are shifted back in position.



Scheme 2. Schematic representation of the stacking sequence of layers in compounds containing water (**3**), DMSO (**2**), and a generic guest molecule; in **1** a shorter interlayer separation is present, as a consequence of the guest removal.

Scheme 2 also shows that **1**, produced by guest removal, can in turn be used as a starting material in further uptake/release reactions. Table 1 lists the behavior of compound **1** towards a series of small molecules and how the formation of a host–guest compound depends on the preparation method, that is, kneading, suspension in the liquid guest, and kneading followed by suspension. This latter approach is the most productive; when suspended in the desired liquid guest, compound **1** only takes up relatively small molecules (DMSO, methanol, acetone, etc.). In contrast, kneading results in the uptake of other guest molecules as well, probably because the kneading procedure breaks crystallites and reduces surface clogging. Indeed, if polycrystalline **1** is first kneaded with a small amount of the desired liquid and then left to stir in the same liquid guest for 12 h, partial or complete filling of the compound is observed, independent of the guest molecule. Kneading is widely used in the pharmaceutical and food industry and also in the preparation of host–guest compounds

 © 2006 Wiley-VCH Verlag GmbH & Co. KGaA, Weinheim

Table 1: Guest uptake by **1** as a function of the preparation route.

Guest	Kneading	Suspension[a]	Kneading followed by suspension[a]
1-hexanol	–	–	x
1-pentanol	–	–	x
acetone	x	–	x
acetonitrile	–	–	x
cyclohexane	–	–	x
dichloromethane	–	–	x
dioxane	–	–	x
dimethylsulphoxide	x	x	x
dimethoxyethane	–	–	x
dimethylformamide	–	–	x
ethylacetate	–	–	x
ethanol	x	x	x
glyme[b]	x	-	x
H_2O	x	x	x
hexane	–	–	x
2-propanol	x	–	x
methanol	x	x	x
tert-butyl alcohol	–	–	x
tetrahydrofuran	x	x	x
TMEDA[c]	x	x	x
toluene	–	–	x

[a] Suspension occurs in the liquid guest. [b] Glyme = ethylene glycol dimethyl ether. [c] TMEDA = *N*,*N*,*N*′,*N*′-tetramethylethylenediamine

of cyclodextrins.[17] All uptake/release processes were monitored by powder diffraction (see Supporting Information).

In conclusion, we have found a simple way to prepare a relatively inexpensive material that absorbs and releases a variety of small molecules through an intercalation mechanism. Similar behavior is shown by intercalation compounds, such as metal calcogenides (TiS_2, ZrS_2, etc.) and metal oxides (MO_3, V_2O_5, $MOPO_4$, etc.). However, to the best of our knowledge, system **1** is the first example of a 1D coordination network with reversible intercalation capacity. Furthermore, guest uptake in **1** appears to be somewhat selective and depends on the method used.

Experimental Section

All starting materials were purchased from Aldrich. Reagent grade solvents and bidistilled water were used.

Kneading experiments; **1**: *trans*-1,4-Diaminocyclohexane (1.14 g, 1.0 mol) and $CuCl_2{\cdot}2H_2O$ (1.70 g, 1.0 mol) was ground together in an agate mortar to a fine powder, and water (0.5 mL) was then added. The mixture was kneaded for 5–10 min, and the water was then removed by thermal and vacuum treatment (100 °C under vacuum for 5 h).**2**: See synthesis of **1**, but DMSO was used instead of water.

3: In an agate mortar, **1** (0.2 g, 0.80 mmol) and water (0.5 mL) were kneaded for 5 min and left to stand for 1 h before measuring the powder diffractogram.

1·*n*(guest): see synthesis of **3**, with the exception that all the compounds listed in Table 1 were used instead of water.

Typical kneading experiment: See synthesis of **3**, but different solvents were used, and the product was left to stand for 1–6 h. Synthesis of **2** in DMSO: In a round-bottomed flask $CuCl_2{\cdot}2H_2O$ (1.70 g, 1 mol) was dissolved in DMSO (75 mL). A solution of *trans*-1,4-diaminocyclohexane (1.14 g, 1 mol) in DMSO (100 mL) was slowly added dropwise, and a blue-purple powder was formed in 92 % (2.86 g) yield.

A typical kneading experiment was followed by suspension in the same solvent that was used for the kneading process: After kneading, the powder mixture was left in suspension in the appropriate solvent for 12 h. In all cases, treatment of the product under vacuum and at 100 °C for 3 h quantitatively yields the solid reagent **1**.

Three-phase crystallization of **2**: In a sample tube, a saturated solution of *trans*-1,4-diaminocyclohexane in DSMO (0.5 mL), methanol/DMSO (1:1, 0.5 mL), and a saturated solution of $CuCl_2{\cdot}2H_2O$ in methanol (0.5 mL) was layered in three phases. A light-purple powder slowly formed between the DMSO layer and the methanol/DMSO layer after 3 days and in the powder a few single crystals of **1** of X-ray crystallographic quality were recovered.

Thermogravimetric measurements: Thermogravimetric investigations were carried out on dried samples by using a Perkin–Elmer TGA-7. Heating was performed under a nitrogen flow (20 $cm^3 min^{-1}$) by using a platinum crucible at a rate of 5 °C min^{-1} up to 450 °C. The weight of the samples was around 3 mg. Calorimetric measurements were performed by using a Perkin–Elmer DSC-7 equipped with a model PII intracooler. Temperature and enthalpy calibration were performed by using high purity standards (*n*-decane, benzene and indium). Heating was carried out at 5 °C min^{-1} in the temperature range 45–140 °C. Samples in the weight range from 5 to 10 mg were analyzed in open aluminum pans.

Crystal-structure determination: Data for **2** were collected at room temperature on an Enraf–Nonius CAD4 diffractometer, monochromator graphite. **2**: $C_6H_{14}Cl_2CuN_2\,2(C_2H_6OS)$, $M_r = 404.89$, light purple crystals, crystal dimensions: $0.2 \times 0.10 \times 0.10$ mm^3; triclinic $P\bar{1}$, $a = 5.911(2)$, $b = 8.515(2)$, $c = 9.621(4)$ Å, $\alpha = 86.81(3)$, $\beta = 78.09(4)$, $\gamma = 70.42(2)°$, $V = 446.4(3)$ $Å^3$, $Z = 1$, $\rho_{calcd} = 1.506$ g cm^{-3}, R_1 (wR_2) 0.0410 (0.0985) for 1547 observed independent reflections; $Mo_{K\alpha}$ radiation ($\lambda = 0.71073$ Å), 2θ range = 6.0–50.0. All non-hydrogen atoms were refined anisotropically. SHELXL97[18] was used for structure solution and refinement on F^2, and SCHAKAL[19] was used for the molecular graphics. CCDC-279106 contains the supplementary crystallographic data for this paper. These data can be obtained free of charge from The Cambridge Crystallographic Data Centre via www.ccdc.cam.ac.uk/data_request/cif. See Supporting Information for crystallographic data in CIF format, X-ray powder patterns for compounds **1**–**4**, and TGA and DSC measurements for **2**. Powder data were collected on a Philips X'Pert automated diffractometer with $Cu_{K\alpha}$ radiation, graphite monochromator. The program PowderCell 2.2 was used for calculation of X-ray crystallographic powder patterns.[20]

Received: July 25, 2005
Published online: November 21, 2005

Keywords: host–guest systems · mechanochemistry · porous materials · solid-state reactions

[1] a) M. Kruk, M. Jaroniec, *Chem. Mater.* **2001**, *13*, 3169–3183; b) P. J. Langley, J. Hulliger, *Chem. Soc. Rev.* **1999**, *28*, 279–291; c) D. Bradshaw, J. B. Claridge, E. J. Cussen, T. J. Prior, M. J. Rosseinsky, *Acc. Chem. Res.* **2005**, *38*, 273–282; d) S. Kitagawa, K. Uemura, *Chem. Soc. Rev.* **2005**, *34*, 109–119; e) B. Moulton, M. J. Zaworotko, *Chem. Rev.* **2001**, *101*, 1629–1658; f) S. Takamizawa, E.-i. Nakata, T. Saito, *CrystEngComm* **2004**, *6*, 39–41; g) S. Takamizawa, E.-i. Nakata, H. Yokoyama, K. Mochizuki, W. Mori, *Angew. Chem.* **2003**, *115*, 4367–4370; *Angew. Chem. Int. Ed.* **2003**, *42*, 4331–4334; h) P. Sozzani, S. Bracco, A. Comotti, L. Ferretti, R. Simonutti, *Angew. Chem.* **2005**, *117*, 1850–1854; *Angew. Chem. Int. Ed.* **2005**, *44*, 1816–1820.

[2] a) A. C. Sudik, A. R. Millward, N. W. Ockwig, A. P. Cote, J. Kim, O. M. Yaghi, *J. Am. Chem. Soc.* **2005**, *127*, 7110–7118; b) H. K. Chae, D. Y. Siberio-Perez, J. Kim, Y. B. Go, M. Eddaoudi, A. J.

 © 2006 Wiley-VCH Verlag GmbH & Co. KGaA, Weinheim

Matzger, M. O'Keeffe, O. M. Yaghi, *Nature* **2004**, *427*, 523 – 527; c) N. L. Rosi, J. Eckert, M. Eddaoudi, D. T. Vodak, J. Kim, M. O'Keeffe, O. M. Yaghi, *Science* **2003**, *300*, 1127 – 1130; d) L. C. Rowsell Jesse, R. Millward Andrew, S. Park Kyo, O. M. Yaghi, *J. Am. Chem. Soc.* **2004**, *126*, 5666 – 5667; e) O. Ohmori, M. Kawano, M. Fujita, *Angew. Chem.* **2005**, *117*, 1998 – 2000; *Angew. Chem. Int. Ed.* **2005**, *44*, 1962 – 1964; f) O. Ohmori, M. Kawano, M. Fujita, *J. Am. Chem. Soc.* **2004**, *126*, 16292 – 16293; g) M. Tominaga, K. Suzuki, M. Kawano, T. Kusukawa, T. Ozeki, S. Shakamoto, K. Yamaguchi, M. Fujita, *Angew. Chem.* **2004**, *116*, 5739 – 5743; *Angew. Chem. Int. Ed.* **2004**, *43*, 5621 – 5625; h) D.-L. Long, R. J. Hill, A. J. Blake, N. R. Champness, P. Hubberstey, D. M. Proserpio, C. Wilson, M. Schroeder, *Angew. Chem.* **2004**, *116*, 1887 – 1890; *Angew. Chem. Int. Ed.* **2004**, *43*, 1851 – 1854; i) A. N. Khlobystov, M. T. Brett, A. J. Blake, N. R. Champness, P. M. W. Gill, D. P. O'Neill, S. J. Teat, C. Wilson, M. Schroeder, *J. Am. Chem. Soc.* **2003**, *125*, 6753 – 6761.

[3] a) D. Braga, L. Maini, M. Polito, L. Mirolo, F. Grepioni, *Chem. Eur. J.* **2003**, *9*, 4362 – 4370; b) D. Braga, L. Maini, G. de Sanctis, K. Rubini, F. Grepioni, M. R. Chierotti, R. Gobetto, *Chem. Eur. J.* **2003**, *9*, 5538 – 5548; c) D. Braga, L. Maini, M. Polito, L. Mirolo, F. Grepioni, *Chem. Commun.* **2002**, 2960 – 2961.

[4] D. Braga, S. L. Giaffreda, F. Grepioni, M. Polito, *CrystEngComm* **2004**, *6*, 458 – 462.

[5] D. Braga, M. Curzi, F. Grepioni, M. Polito, *Chem. Commun.* **2005**, 2915 – 2917.

[6] a) G. W. V. Cave, C. L. Raston, J. L. Scott, *Chem. Commun.* **2001**, 2159 – 2169; b) K. Tanaka, F. Toda, *Chem. Rev.* **2000**, *100*, 1025 – 1074; c) G. Rothenberg, A. P. Downie, C. L. Raston, J. L. Scott, *J. Am. Chem. Soc.* **2001**, *123*, 8701 – 8708; d) F. Toda, *CrystEngComm* **2002**, *4*, 215 – 222; e) G. Kaupp, *Compr. Supramol. Chem.* **1996**, *8*, 381 – 423; f) G. Kaupp, *CrystEngComm* **2003**, *5*, 117 – 133.

[7] a) M. C. Etter, *J. Phys. Chem.* **1991**, *95*, 4601 – 4610; b) M. C. Etter, S. M. Reutzel, C. G. Choo, *J. Am. Chem. Soc.* **1993**, *115*, 4411 – 4412; c) W. H. Ojala, M. C. Etter, *J. Am. Chem. Soc.* **1992**, *114*, 10288 – 10293.

[8] a) R. P. Rastogi, P. S. Bassi, S. L. Chadha, *J. Phys. Chem.* **1963**, *67*, 2569 – 2573; b) T. P. Rastogi, N. B. Singh, *J. Phys. Chem.* **1966**, *70*, 3315 – 3324; c) R. P. Rastogi, N. B. Singh, *J. Phys. Chem.* **1968**, *72*, 4446 – 4449.

[9] a) I. C. Paul, D. Y. Curtin, *Acc. Chem. Res.* **1973**, *6*, 217 – 225; b) C. C. Chiang, C. T. Lin, H. J. Wang, D. Y. Curtin, I. C. Paul, *J. Am. Chem. Soc.* **1977**, *99*, 6303 – 6308; c) A. O. Patil, D. Y. Curtin, I. C. Paul, *J. Am. Chem. Soc.* **1984**, *106*, 348 – 353.

[10] D. Braga, *Chem. Commun.* **2003**, 2751 – 2754.

[11] a) V. R. Pedireddi, W. Jones, A. P. Chorlton, R. Docherty, *Chem. Commun.* **1996**, 987 – 988; b) R. Kuroda, Y. Imai, N. Tajima, *Chem. Commun.* **2002**, 2848 – 2849; c) A. V. Trask, W. D. S. Motherwell, W. Jones, *Chem. Commun.* **2004**, 890 – 891.

[12] a) P. J. Nichols, C. L. Raston, J. W. Steed, *Chem. Commun.* **2001**, 1062 – 1063; b) W. J. Belcher, C. A. Longstaff, M. R. Neckenig, J. W. Steed, *Chem. Commun.* **2002**, 1602 – 1603.

[13] D. Braga, F. Grepioni, *Angew. Chem.* **2004**, *116*, 4092 – 4102; *Angew. Chem. Int. Ed.* **2004**, *43*, 4002 – 4011.

[14] a) V. P. Balema, J. W. Wiench, M. Pruski, V. K. Pecharsky, *Chem. Commun.* **2002**, 724 – 725; b) V. P. Balema, J. W. Wiench, M. Pruski, V. K. Pecharsky, *Chem. Commun.* **2002**, 1606 – 1607.

[15] A. Orita, L. Jiang, T. Nakano, N. Ma, J. Otera, *Chem. Commun.* **2002**, 1362 – 1363.

[16] a) A. R. Khokhar, S. Shamsuddin, Q. Xu, *Inorg. Chim. Acta* **1994**, *219*, 193 – 197; b) S. Shamsuddin, C. C. Santillan, J. L. Stark, K. H. Whitmire, Z. H. Siddik, A. R. Khokhar, *J. Inorg. Biochem.* **1998**, *71*, 29 – 35; c) S. Shamsuddin, J. W. van Hal, J. L. Stark, K. H. Whitmire, A. R. Khokhar, *Inorg. Chem.* **1997**, *36*, 5969 – 5971; d) J. D. Hoeschele, H. D. H. Showalter, A. J. Kraker, W. L. Elliott, B. J. Roberts, J. W. Kampf, *J. Med. Chem.* **1994**, *37*, 2630 – 2636; e) S. Shamsuddin, A. R. Khokhar, *J. Coord. Chem.* **1994**, *33*, 83 – 91.

[17] a) J. Shailaja, S. Karthikeyan, V. Ramamurthy, *Tetrahedron Lett.* **2002**, *43*, 9335 – 9339; b) F. Taneri, T. Gueneri, Z. Aigner, M. Kata, *J. Inclusion Phenom. Macrocyclic Chem.* **2002**, *44*, 257 – 260; c) R. Saikosin, T. Limpaseni, P. Pongsawasdi, *J. Inclusion Phenom. Macrocyclic Chem.* **2002**, *44*, 191 – 196; d) L. R. Nassimbeni, *Acc. Chem. Res.* **2003**, *36*, 631 – 637.

[18] G. M. Sheldrick, University of Göttingen, Germany, **1997**.

[19] E. Keller, SCHAKAL99, Graphical Representation of Molecular Models, University of Freiburg, Germany, **1999**.

[20] PowderCell, program by W. Kraus and G. Nolze (BAM Berlin) subgroups derived by Ulrich Müller (Gh Kassel).

 © 2006 Wiley-VCH Verlag GmbH & Co. KGaA, Weinheim

Nucleobase–Metal Complexes

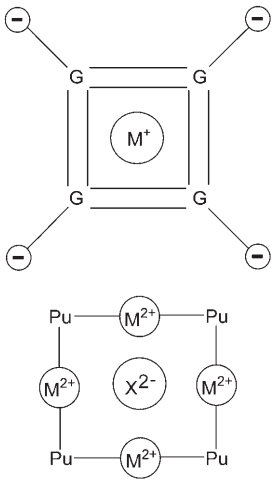
DOI: 10.1002/anie.200502878

Inverting the Charges of Natural Nucleobase Quartets: A Planar Platinum–Purine Quartet with Pronounced Sulfate Affinity**

*Michael Roitzsch and Bernhard Lippert**

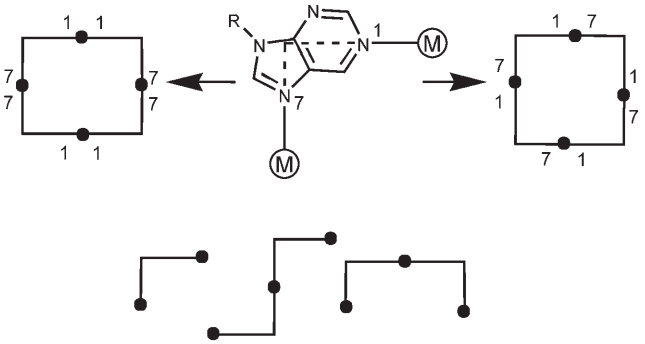
The formation of four-stranded nucleic acid structures like those in DNA and RNA is closely connected with the existence of guanine tetrads (G_4). In G_4 four purine bases are interconnected by eight hydrogen bonds, and the structure is further stabilized by a central cation.[1] The negative charges of the phosphate groups are located at the periphery of this motif. Similar tetrads consisting of uracil[2] or thymine[3] are based essentially on the same principle. The significance of tetrastranded DNA concerning its function in the telomeres as well as in regulatory regions of the DNA is presently the subject of intense investigations.[4]

Here we describe a non-natural quartet of 9-methylpurine, which differs from the natural nucleobase quartets in that cationic *trans*-$(NH_3)_2Pt^{II}$ moieties are located at the periphery of the quartet and an anion is trapped in the center (Scheme 1). The hydrogen bonds in the natural-base quartets



Scheme 1. G = guanine, Pu = 9-methylpurine, M^{2+} = *trans*-$[(NH_3)_2Pt^{II}]^{2+}$.

are replaced by coordinative Pt–nucleobase bonds in the artificial quartet, and the overall negative charge of the natural quartets is changed to positive in the artificial one. At the same time we report on the corresponding molecular triangle, the analogy of which to natural purine triplets is less obvious. As we have shown in a number of cases,[5] simultaneously N1- and N7-coordinated purine bases can behave as bridging ligands forming 90° angles. Complexes with linear coordinating metal ions M such as *trans*-$(NH_3)_2Pt^{II}$, Ag^+ or Hg^{2+} lead to diverse architectures containing right angles, for example, rectangles of the type *cyclo*-(*N1*-M-*N1*,*N7*-M-*N7*)$_2$ (Scheme 2).



Scheme 2. Possible architectures of purine–metal complexes.

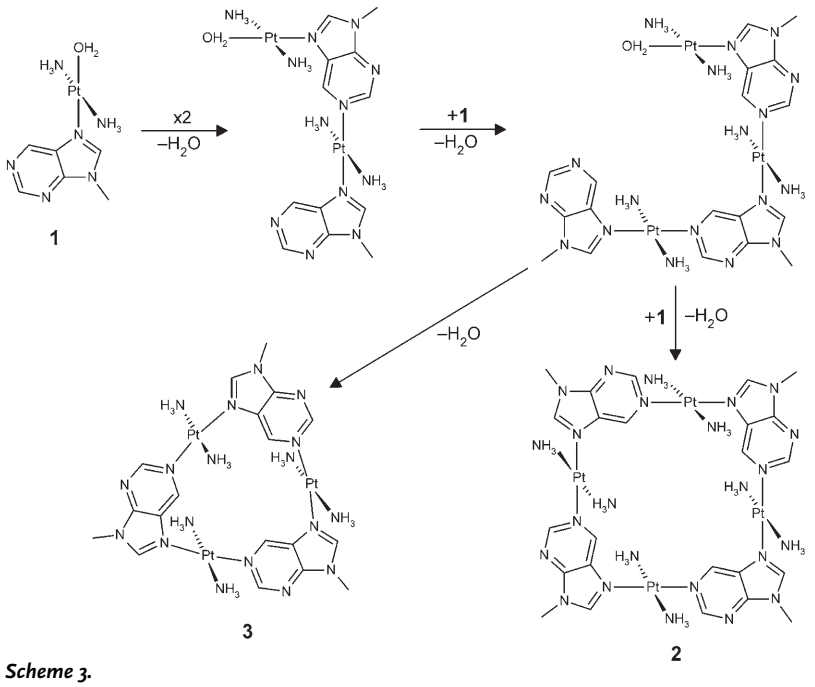
Using unsubstituted 9-methylpurine (Pu), we have now succeeded in preparing a molecular square with the coordination sequence *cyclo*-(*N1*-Pt-*N7*)$_4$. This compound, all-*trans*-$[\{(NH_3)_2Pt(\mu\text{-}N1\text{-Pu-}N7)\}_4]^{8+}$ (**2**), forms spontaneously from the 1:1 complex *trans*-$[(NH_3)_2Pt(Pu\text{-}N7)(H_2O)]^{2+}$ (**1**). Observation of the product formation by ^{1}H NMR spectroscopy shows that several molecules of **1** condense to form short chains, which undergo complete reaction at room temperature over five days to yield two distinct cyclic complexes (Scheme 3). Besides the molecular square **2**, a molecular triangle of composition all-*trans*-$[\{(NH_3)_2Pt(\mu\text{-}N1\text{-Pu-}N7)\}_3]^{6+}$ (**3**) is formed. In both compounds, the Pu ligands are symmetrically equivalent and hence in the ^{1}H NMR spectrum only a single set of signals can be observed for the respective species. According to signal integration, the formation of **3** is preferred over formation of **2** (**2**/**3** = 0.6:1). The situation changes when the reaction is carried out in the presence of sulfate, which acts as a template. In 100 mM Na_2SO_4, formation of **2** is preferred, and the **2**/**3** ratio increases to 2.5:1. In addition, the presence of sulfate anions speeds up the reaction, such that product formation is complete within three days at room temperature.

Crystallization of **2** and **3** proved to be difficult, and only very small crystals could be obtained, which have the composition **2**-$(ClO_4)_8\cdot 6H_2O$ (**2a**) and **3**-$(PF_6)_6\cdot 6H_2O$ (**3a**), respectively.[6] The cations of **2a** and **3a** are shown in Figure 1. In both compounds the purine ligands and the Pt^{II} atoms are essentially coplanar, and the ammine ligands are perpendicular to this plane. Pt–N distances are normal. In **2a**, the distances between the Pt^{II} atoms on opposing sides of the square are 9.03(1) Å (Pt1–Pt1a) and 9.09(1) Å (Pt2–Pt2a). The square has outer diagonals of 17.07(4) Å (C9a–C9aa) and 17.24(6) Å (C9b–C9ba). The diagonals in the center are

[*] Dr. M. Roitzsch, Prof. B. Lippert
Fachbereich Chemie, Universität Dortmund
44221 Dortmund (Germany)
Fax: (+49) 231-755-3797
E-mail: bernhard.lippert@uni-dortmund.de

[**] Support by the Deutsche Forschungsgemeinschaft is gratefully acknowledged.

 © 2006 Wiley-VCH Verlag GmbH & Co. KGaA, Weinheim



Scheme 3.

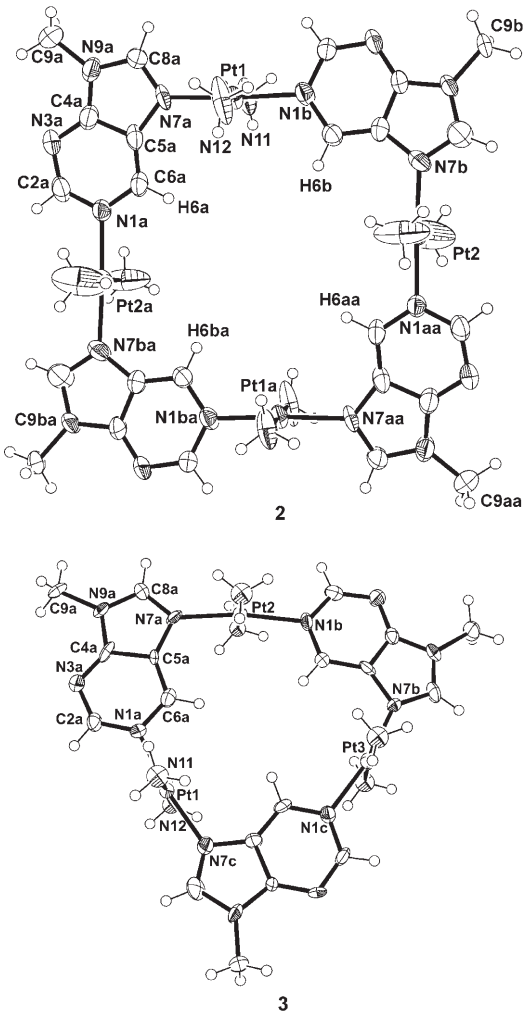


Figure 1. Cations of **2a** and **3a** with atomic numbering.

6.08 Å (H6a–H6aa) and 6.24 Å (H6b–H6ba). The N1-Pt-N7 angles deviate slightly from the ideal angle of 180° and measure 176.8(5)° (N1b-Pt1-N7a) and 177.4(5)° (N1aa-Pt2-N7b), respectively. As a consequence, the angle between the Pt^{II} atoms coordinated to the N1 and N7 sites of a purine ligand likewise deviate from the ideal 90°–88.1° in purine a and 85.1° in purine b. In the crystal structure, the cations are packed on top of each other in a slightly staggered manner with a stacking distance of 7.5 Å. Some of the perchlorate anions, which display pronounced positional disorder, are located between the cations yet appear not to be firmly fixed to these.

In **3a**, the distances between the Pt^{II} atoms are in the range of 5.91(1)–6.00(1) Å, while the distances between the C9 atoms are between 12.67(2) and 12.73(3) Å. The N1-Pt-N7 angles in **3a** deviate markedly from the ideal 180° and are in the range of 168.8(5)–170.8(4)°. The angles between the Pt^{II} atoms coordinated to the N1 and N7 sites of a purine ligand deviate strongly from 90° and range between 67.8° and 70.8°.

Of the six hexafluorophosphate anions in **3a**, one is located above and another below the center of each cation, and the C_3 axis of the anion points towards the cation. The other face of the PF_6^- anion is oriented toward a purine ligand of a parallel cation. This leads to a helical arrangement of the cations in the structure, making it chiral (Figure 2). The distance between the planes of the cations is 7.6 Å.

Both compounds show a pronounced affinity for sulfate anions. The binding of SO_4^{2-} was monitored by concentration-dependent ^1H NMR spectroscopy, where the concentration of

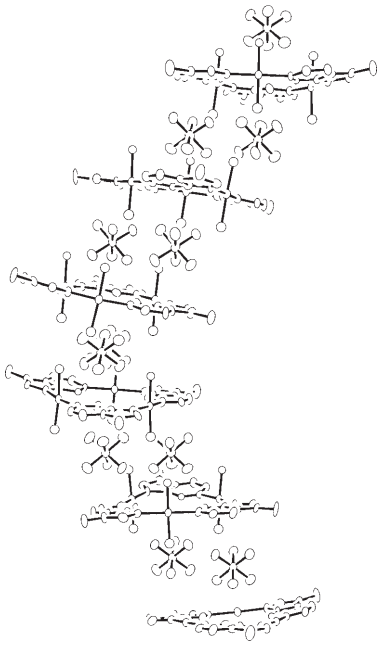


Figure 2. Section of the packing pattern of **3a**. The PF_6^- anions are layered between the cations, thereby producing a helix.

 © 2006 Wiley-VCH Verlag GmbH & Co. KGaA, Weinheim

the anion was varied, while the concentration of the respective cyclic compound was kept constant. In [D_6]DMSO, **2** shows a new signal set upon addition of nBu$_4$NHSO$_4$. The resonances of the H6 protons and those of the ammine ligands are strongly shifted towards low field, whereas the other signals of the purine ligands are scarcely influenced (Figure 3). In D_2O, the H6 signals shift downfield with increasing concentrations of Na_2SO_4 (Figure 4). The influence on the other resonances of the purine ligands is only very weak, and the resonances of the protons of the ammine ligands cannot be observed because of isotope exchange with the solvent.

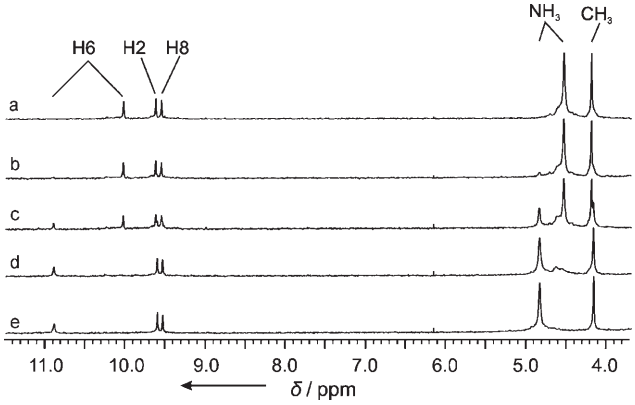


Figure 3. ^{1}H NMR spectra of **2** recorded in [D_6]DMSO. The uppermost spectrum was recorded in the absence of sulfate ions, the spectra below with increasing amounts of nBu$_4$NHSO$_4$: a) no HSO_4^-, b) 0.1 equiv HSO_4^-, c) 0.5 equiv HSO_4^-, d) 1.0 equiv HSO_4^-, e) 3.0 equiv HSO_4^-. Upon addition of sulfate a host–guest complex forms, which displays a new set of signals indicating the slow exchange of the sulfate ions. While the signals assigned to H6 and to the protons of the ammine ligands are strongly low-field shifted, the other resonances are only weakly affected. This is consistent with the view that the sulfate is trapped in the center of the molecular square and that the NH_3 ligands are involved in hydrogen bonding with sulfate.

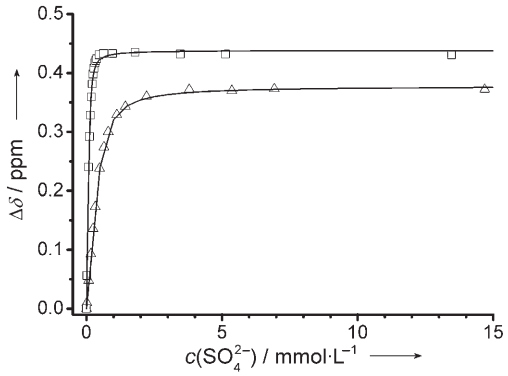


Figure 4. Change of the chemical shifts $\Delta\delta$ of the H6 signals of **2** (□) and **3** (△) in D_2O with increasing amounts of Na_2SO_4. In both cases the perchlorate salts (**2a** and **3b**) where used, since perchlorate ions appear to be only weakly bound to the cations. The solid lines where obtained by a least-squares fitting procedure,[7] which yielded the association constants discussed in the text. Concentrations of the host molecules were 0.40 mM **2** and 0.47 mM **3**.

The concentration dependence of the H6 signals can be used to determine the association constants.[7] For the binding of sulfate in D_2O, we have found association constants of $(7.2 \pm 1.2) \times 10^4$ L mol^{-1} for **2** and $(9.9 \pm 0.6) \times 10^3$ L mol^{-1} for **3**. These values indicate very strong sulfate binding in water and are in the range known for very strong anion receptors such as aza crown ethers and cryptands.[8,9] We are currently performing experiments to investigate the selectivity of **2** and **3** for different anions. These studies will be accompanied by DFT calculations in order to elucidate the mode of anion binding in more detail. Preliminary results suggest that the anion is trapped by **2** by means of multiple hydrogen bonds, with the S atom residing in the center of the cavity. In addition to the general aspect of sulfate binding, the templating effect of this anion during the formation of the square **2** is noteworthy, as is the topical issue of factors influencing equilibria of metallosupramolecular assemblies.[10] Finally, **2** represents the first example of a true purine square with four metal entities at the periphery and alternating N1,N7 coordination. Previously described cases of metal-containing purine quartets displayed rectangular shapes[5a,e] as a consequence of pairwise N7,N7 and N1,N1 metal binding. Another point of interest is whether these cationic nucleobase squares are capable of interacting with natural tetrastranded nucleic acid structures.[11]

Experimental Section

Preparation of *trans*-[$(NH_3)_2$Pt(9MePu-*N7*)Cl]ClO_4 (**1a**): A solution of Pu[12] (134 mg, 1.00 mmol) in 5 mL of 2.4 M $HClO_4$ was added at once to *trans*-[$(NH_3)_2$Pt(OH)Cl]·H_2O[13] (300 mg, 1.00 mmol). The mixture was stirred for 5 min, then the yellowish precipitate was filtered off and washed with ca. 20 mL of 1 M $NaClO_4$ and 2 mL of H_2O. The product was dried under vacuum. Yield: 275 mg, 55.2%; white powder. C,H,N analysis calcd (%): C 14.5, H 2.4, N 16.9; found: C 14.2, H 2.4, N 16.7. ^{1}H NMR: (D_2O, pD 2.4): $\delta = 9.56$ (s, H6), 9.12 (s, H2), 9.09 (s, H8), 4.06 ppm (s, CH_3).

Preparation of **2a** and *trans*-[{$(NH_3)_2$Pt(μ-*N1*-Pu-*N7*)}$_3$]-$(ClO_4)_6$·3H_2O (**3b**): A solution of **1a** (199 mg, 0.400 mmol) in 15 mL of H_2O was treated with 1 mL of 1 M HNO_3 and $AgNO_3$ (67.9 mg, 0.400 mmol), and the mixture was stirred for 3 d at 45 °C in the dark. Precipitated AgCl was removed by filtration, and the solution was concentrated at reduced pressure to a volume of 5 mL. The solution was cooled to 4 °C for 12 h, and the crude **2a** that precipitated was isolated by filtration. Addition of 800 μL of 1 M $NaClO_4$ to the remaining solution precipitated crude **3b**, which was isolated by filtration. The crude products were washed twice with 250 μL of H_2O and dried under vacuum. The products obtained were dissolved in 40 mL (**2a**) and 20 mL of H_2O (**3b**), respectively, and then precipitated by addition of 1 M $NaClO_4$, filtered off, and dried under vacuum. Yields of isolated products were 38 mg (16%) of **2a** and 39 mg (17%) of **3b**. C,H,N analysis calcd (%): **2a**: C 12.4, H 2.4, N 14.5; found: C 12.1, H 2.5, N 14.8; **3b**: C 12.2, H 2.6, N 14.3; found: C 12.1, H 2.5, N 14.3. ^{1}H NMR: (**2**, D_2O, pD 2.0): $\delta = 10.47$ (s, H6), 9.81 (s, H2), 9.60 (s, H8), 4.22 ppm (s, CH_3); (**3**, D_2O, pD 2.0): $\delta =$ 11.44 (s, H6), 9.49 (s, H2), 9.37 (s, H8), 4.18 ppm (s, CH_3). The hexafluorophosphate salt **3a** was prepared by precipitation from a solution of **3b** with 0.2 M solution of KPF_6 in H_2O. **3a** was characterized by X-ray crystallography.

Received: August 12, 2005
Published online: November 21, 2005

 © 2006 Wiley-VCH Verlag GmbH & Co. KGaA, Weinheim

Keywords: base quartets · guanine · nucleobases · platinum · purine

[1] J. T. Davis, *Angew. Chem.* **2004**, *116*, 684; *Angew. Chem. Int. Ed.* **2004**, *43*, 668, and references therein.
[2] a) C. J. Cheong, P. B. Moore, *Biochemistry* **1992**, *31*, 8406; b) J. Deng, Y. Xiong, M. Sundaralingam, *Proc. Natl. Acad. Sci. USA* **2001**, *98*, 13665; c) B. C. Pan, Y. Xiong, K. Shi, J. P. Deng, M. Sundaralingam, *Structure* **2003**, *11*, 815.
[3] a) P. K. Patel, R. V. Hosur, *Nucleic Acids Res.* **1999**, *27*, 2457; b) C. Cáceres, G. Wright, C. Gouyette, G. Parkinson, J. A. Subirana, *Nucleic Acids Res.* **2004**, *32*, 1097.
[4] a) J. Seenisamy, S. Bashyam, V. Gokhale, H. Vankayalapati, D. Sun, A. Siddiqui-Jain, N. Streiner, K. Shin-Ya, E. White, W. D. Wilson, L. H. Hurley, *J. Am. Chem. Soc.* **2005**, *127*, 2944; b) A. T. Phan, V. Kuryavyi, H. Y. Gaw, D. J. Patel, *Nat. Chem. Biol.* **2005**, *1*, 167.
[5] See, e.g.: a) I. B. Rother, M. Willermann, B. Lippert, *Supramol. Chem.* **2002**, *14*, 189; b) M. Roitzsch, I. B. Rother, M. Willermann, A. Erxleben, B. Costisella, B. Lippert, *Inorg. Chem.* **2002**, *41*, 5946; c) M. S. Lüth, M. Willermann, B. Lippert, *Chem. Commun.* **2001**, 2058; d) M. S. Lüth, E. Freisinger, B. Lippert, *Chem. Eur. J.* **2001**, *7*, 2104; e) M. S. Lüth, E. Freisinger, F. Glahé, B. Lippert, *Inorg. Chem.* **1998**, *37*, 5044.
[6] Crystal structure data for **2a**: C_{24} H_{60} N_{24} O_{38} Cl_8 Pt_4, $M_r = 2256.81$, colorless crystals, monoclinic $C2/c$, $a = 20.825(4)$, $b = 18.584(4)$, $c = 16.142(3)$ Å, $\alpha = \gamma = 90°$, $\beta = 98.67(3)°$, $V = 6176(2)$ Å^3, $Z = 2$, $\rho_{calcd} = 2.419$ Mg m^{-3}, $\mu = 9.485$ mm^{-1}, $T = 150$ K. 44983 data (7069 unique, 3675 observed, $R_{int} = 0.146$, $3.08 < \theta < 27.52°$) were collected. Final $R = 0.084$ ($wR_2 = 0.144$, GoF = 1.104). A major disorder of three of the four crystallographically independent perchlorate anions over two or three positions, respectively, made it necessary to use numerous constraints to fix the geometry of these ions. As a consequence, the R values are comparably poor and the assignment of crystal water molecules was not possible; the amount of crystal water given in the empirical formula therefore is based on elemental analysis data. Crystal structure data for **3a**: C_{18} H_{48} N_{18} O_6 F_{36} P_6 Pt_3, $M_r = 2067.71$, colorless crystals, hexagonal $P6_1$, $a = 15.085(2)$, $b = 15.085(2)$, $c = 42.280(9)$ Å, $\alpha = \beta = 90°$, $\gamma = 120°$, $V = 8332(2)$ Å^3, $Z = 6$, $\rho_{calcd} = 2.420$ Mg m^{-3}, $\mu = 7.881$ mm^{-1}, $T = 150$ K. 29176 data (9153 unique, 7118 observed, $R_{int} = 0.068$, $3.06 < \theta < 27.49°$) were collected. Final $R = 0.046$ ($wR_2 = 0.088$, GoF = 1.027). The reflections of both crystals were collected on a Nonius KappaCCD diffractometer using graphite-monochromated $Mo_{K\alpha}$ radiation ($\lambda = 0.71069$ Å) and were corrected empirically (SADABS: G. M. Sheldrick, Bruker AXS Inc., Madison, WI, **2000**) for absorption. The raw intensity data frames were integrated with the EVALCCD (Bruker AXS Inc., Madison, WI, **2000**) program. Both structures were solved by direct methods and refined by full-matrix least-squares methods based on F^2 using the SHELXTL-PLUS (G. M. Sheldrick, Siemens Analytical X-ray Instruments, Inc., Madison, WI, **1990**) and SHELXL-97 (G. M. Sheldrick, SHELXL-97, Universität Göttingen, Göttingen, Germany) programs. With the exception of the disordered perchlorate atoms in **2a** and the C6b atom, two fluorine atoms of a disordered PF_6^- anion, and the nitrogen atoms of the ammine ligands in **3a**, all non-hydrogen atoms in the structures were refined anisotropically. The hydrogen atoms were included in geometrically calculated positions and refined with isotropic displacement parameters. CCDC-280955 and 280954 (**2a** and **3a**) contain the supplementary crystallographic data for this paper. These data can be obtained free of charge from the Cambridge Crystallographic Data Centre via www.ccdc.cam.ac.uk/data_request/cif.
[7] H. Sigel, K. H. Scheller, V. M. Rheinberger, B. E. Fischer, *J. Chem. Soc. Dalton Trans.* **1980**, *7*, 1022.
[8] D. Grell, E. Grell, P. Bugnon, B. Dietrich, J. M. Lehn, *J. Therm. Anal. Calorim.* **2004**, *77*, 483.
[9] J. L. Sessler, E. Katayev, G. D. Pantos, Y. A. Ustynyuk, *Chem. Commun.* **2004**, 1276.
[10] See, e.g.: a) A. Sautter, D. G. Schmid, G. Jung, F. Würthner, *J. Am. Chem. Soc.* **2001**, *123*, 5424; b) M. Schweiger, S. R. Seidel, A. M. Arif, P. J. Stang, *Inorg. Chem.* **2002**, *41*, 2556; c) M. Ferrer, M. Mounir, O. Rossell, E. Ruiz, M. A. Maestro, *Inorg. Chem.* **2003**, *42*, 5890.
[11] E. Freisinger, I. B. Rother, M. S. Lüth, B. Lippert, *Proc. Natl. Acad. Sci. USA* **2003**, *100*, 3748.
[12] N. C. Gonnella, J. D. Roberts, *J. Am. Chem. Soc.* **1982**, *104*, 3162.
[13] J. Arpalahti, R. Sillanpää, M. Mikola, *J. Chem. Soc. Dalton Trans.* **1994**, 1499.

 © 2006 Wiley-VCH Verlag GmbH & Co. KGaA, Weinheim

Arsenic Metabolites

DOI: 10.1002/anie.200502706

Arsenic Fatty Acids Are Human Urinary Metabolites of Arsenolipids Present in Cod Liver**

*Ernst Schmeisser, Alice Rumpler, Manfred Kollroser, Gerald Rechberger, Walter Goessler, and Kevin A. Francesconi**

Arsenic has long attracted public interest because of the toxic properties of its inorganic forms such as arsenic trioxide. In the past, this arsenical was a favored homicidal agent because its benign physical properties (odorless, tasteless, and colorless) belied its high acute toxicity. Today, arsenic's association with toxicity persists owing to the presence of inorganic arsenic species in drinking water and the consequent chronic human health effects culminating in cancers, primarily skin and bladder cancers.[1] Less well-known in the public domain is the presence of many organoarsenic compounds in food-

[*] E. Schmeisser, A. Rumpler, Dr. W. Goessler, Prof. K. A. Francesconi
Institute of Chemistry—Analytical Chemistry
Karl-Franzens University Graz
Universitätsplatz 1, 8010 Graz (Austria)
Fax: (+43) 316-380-9845
E-mail: kevin.francesconi@uni-graz.at
Dr. M. Kollroser
Institute of Forensic Medicine
Medical University of Graz
Universitätsplatz 4, 8010 Graz (Austria)
Dr. G. Rechberger
Institute of Molecular Biosciences
Karl-Franzens University Graz
Heinrichstrasse 31a, 8010 Graz (Austria)

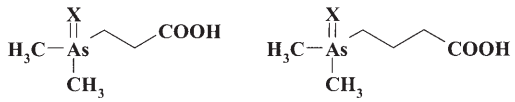
[**] Support by the Austrian Science Fund (FWF Project P16088-N03) is gratefully acknowledged.

WILEY InterScience DISCOVER SOMETHING GREAT
© 2006 Wiley-VCH Verlag GmbH & Co. KGaA, Weinheim

stuffs, particularly in seafoods.[2] Research during the last 30 years has identified over 40 naturally occurring organoarsenicals, and because some of these compounds can be present in seafoods at concentrations up to and exceeding 100 μg As g^{-1} (wet mass) there are human health concerns about the safety of such foods. Increasingly, these issues involve metabolic investigations[3,4] because the original, perhaps nontoxic, organoarsenical(s) present in the food may be metabolized to other arsenicals with currently unknown toxic effects.

Until recently, our knowledge of water-soluble arsenic species in biological samples was restricted to quaternary arsonio compounds (e.g. arsenobetaine) and oxodimethylarsenicals (e.g. arsenosugars).[2] Although much less studied, lipid-soluble arsenicals, hereafter termed arsenolipids, which can constitute 50% or more of the total arsenic in some samples,[5] were considered to be acylated derivatives of arsenosugars based on early work by Benson and co-workers,[6,7] and Morita and Shibata.[8] Research over the last two years, however, has extended our knowledge of arsenic speciation in two significant ways: first it has revealed the presence of a novel group of water-soluble compounds, namely thioarsenicals,[9] and second, it has shown arsenolipids present in fish oils comprise 10 or more unknown arsenic compounds, none of which appears to be an acylated arsenosugar.[5]

Our ongoing research on the human health consequences of arsenicals in foods has recently focused on the metabolic aspects of arsenolipids. These compounds are ingested through fatty fish and fish-oil supplements—foods thought to be beneficial against cardiovascular disease because they are rich in omega-3 fatty acids. We now report that arsenolipids present in cod liver are biotransformed in humans to four novel human urinary metabolites, namely two thioarsenic-containing fatty acids, thiodimethylarsenopropanoic acid (thio-DMAP) and thiodimethylarsenobutanoic acid (thio-DMAB), and their oxo analogues, oxodimethylarsenopropanoic acid (oxo-DMAP) and oxodimethylarsenobutanoic acid (oxo-DMAB). Furthermore, we present preliminary evidence suggesting the possible presence of a homologous series of dimethylated arsenic fatty acids originating from arsenolipids. Collectively these data suggest the widespread nature of thioarsenicals as human arsenic metabolites and provide the first insight into the chemical nature of arsenolipids present in fish.



oxo-DMAP: X = O **oxo-DMAB: X = O**

thio-DMAP: X = S **thio-DMAB: X = S**

The experiment was performed in two parts: the first involved ingestion of a known quantity of canned cod liver in its own oil by one volunteer, and in the second part, the same volunteer consumed only the pure oil from the canned cod liver product. The arsenolipid content, expressed as a percentage of total arsenic, for the two products was 73% (cod liver) and 100% (cod liver oil); the balance of arsenic in the cod liver comprised predominantly arsenobetaine, a water-soluble arsenical commonly found in marine animal tissues[2] and not metabolized by humans.[3] After ingestion of the cod liver product by the volunteer, urine samples were individually collected for 66 h and analyzed for total arsenic by inductively coupled plasma mass spectrometry (ICPMS) and for arsenic species by HPLC/ICPMS. The volunteer excreted most ($\approx$70%) of the ingested arsenic within 24 h ($\approx$90% over the course of the experiment).

Besides arsenobetaine (present in the cod liver and excreted unchanged) and dimethylarsinate, four unknowns (**U1**, **U2, U1***, **U2***) were present in the urine as significant arsenic compounds (Figure 1a solid line). After treatment of the sample with H_2O_2, the peaks for **U1** and **U2** disappeared, whereas those of the two other unknown arsenicals (**U1***, **U2***) increased quantitatively (Figure 1b solid line). Based on similar transformations reported in a recent study,[10] these results suggested that **U1*** and **U2*** could be oxo analogues of thioarsenic species corresponding to **U1** and **U2**. The first thio analogue of an oxoarsenical was reported in 2004 in sheep

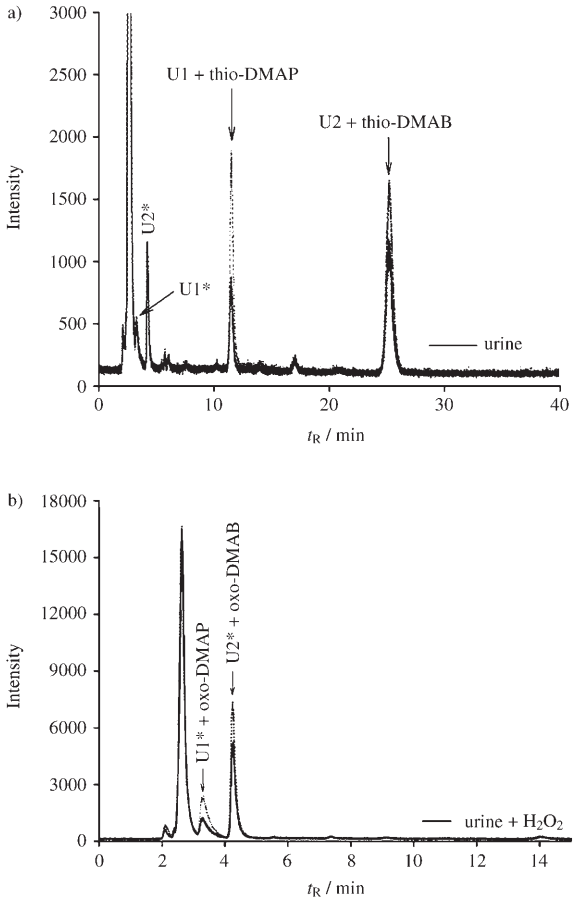


Figure 1. Reversed-phase chromatograms (Table 1, method D) of urine with ICPMS detection at *m/z* 75 of a) untreated urine (solid line) and urine spiked with thio-DMAP and thio-DMAB (dotted line); b) urine sample treated with H_2O_2 (solid line) and H_2O_2-treated urine spiked with oxo-DMAP and oxo-DMAB (dotted line).

 © 2006 Wiley-VCH Verlag GmbH & Co. KGaA, Weinheim

Table 1: Chromatographic conditions for identification of oxo-DMAP, oxo-DMAB, thio-DMAP, and thio-DMAB.

Method	Column	Column dimensions [mm]	Eluent	Flow rate [mL min^{-1}]	T [°C]	Species analyzed	t_R [min]	Detector
A	PRP-X100[b]	250×4.1	20 mM $NH_4H_2PO_4$, pH 5.6	1.5	40	oxo-DMAP	2.8	ICPMS
						oxo-DMAB	5.9	
B	PRP-X100[b]	100×4.1	20 mM NH_4HCO_3, pH 10.3, 3% MeOH	1.5	40	thio-DMAP	7.8	ICPMS
						thio-DMAB	12.3	
C	Zorbax 300 SCX[c]	150×4.6	20 mM pyridine, pH 2.6	1.5	30	oxo-DMAB	3.2	ICPMS
D	Atlantis C18[d]	150×4.6	20 mM $NH_4H_2PO_4$, pH 3.0	1	30	oxo-DMAP	3.3	ICPMS
						oxo-DMAB	4.2	
						thio-DMAP	11.7	
						thio-DMAB	25.5	
E	Atlantis C18[d]	150×4.6	20 mM $NH_4H_2PO_4$, pH 5.6	1	30	thio-DMAP	9.7	ICPMS
						thio-DMAB	14.5	
F	Atlantis C18[d]	150×4.6	20 mM NH_4COOH, pH 3.0, 3% MeOH	1	30	thio-DMAB	17.8	ICPMS ESMS
G[a]	Symmetry C18[d]	150×3.9	A: MeCN + 0.1% HCOOH B: 0.1% aq HCOOH	0.5	25	thio-DMAB	2.7	ESMS/MS

[a] Gradient elution during 0–10 minutes from 10% A to 100% A. [b] Hamilton, USA. [c] Agilent, Germany. [d] Waters, USA.

urine;[9] that work has generated considerable interest, and there have been several subsequent reports of thioarsenicals in shellfish[10–12] and in human urine as metabolites of an ingested arsenosugar.[4]

The retention behavior of the four unknowns under different chromatographic systems (Table 1, methods A–F) provided information on their relative acidities and polarities. A variety of systems was employed because, except for method D, no single system could adequately retain and separate the four target analytes. The results of these findings, and the recent identification of oxodimethylarsenopropanoic acid (oxo-DMAP) in a MeOH/water extract of cod liver,[13] suggested that the two unknowns **U1** and **U1*** may contain the dimethylarsenopropanoate moiety. Furthermore, comparison of the chromatographic behavior of the urine arsenicals with the two standard arsenic fatty acids available to us at that time, oxo- and thiodimethylarsenoacetic acid [$(CH_3)_2As(O)CH_2COOH$ and $(CH_3)_2As(S)CH_2COOH$], suggested that **U2** and **U2*** may be homologous compounds based on a dimethylarsenobutanoate moiety. Consequently, we then synthesized oxo-DMAP, thio-DMAP, oxo-DMAB, and thio-DMAB to serve as analytical standards for HPLC/ICPMS and later for HPLC/ESMS and HPLC/ESMS/MS (ESMS = electrospray mass spectrometry).

The chromatographic behavior of the four synthesized arsenicals, oxo-DMAP, thio-DMAP, oxo-DMAB, and thio-DMAB, under different chromatographic conditions (Table 1) matched those of the four new arsenicals **U1***, **U1**, **U2***, and **U2** respectively, present in the urine sample. Furthermore, spiking (addition) experiments under four different sets of chromatographic conditions (Table 1, methods A–D), whereby standard oxo-DMAP, thio-DMAP, oxo-DMAB, or thio-DMAB was added to the urine sample, could not distinguish the standard analyte from the urine analyte. Representative chromatograms from one of these systems (Table 1, method D) are shown in Figure 1a and b (dotted line).

As recently discussed,[14] structural assignments based solely on HPLC data with atomic mass spectrometric detection may not always provide sufficient proof of structure, particularly when novel compounds are involved. For this reason, we attempted to confirm our proposed structures with molecular mass spectrometric data, and focused on thio-DMAB, the most abundant (and structurally novel) of the metabolites in our samples. To reduce anticipated problems with the electrospray ionization process associated with the (salty) urine matrix, we performed a simple phenol partitioning prior to the analysis. Electrospray mass spectra (single quadrupole mass analyzer) for the standard thio-DMAB showed a clear signal at m/z 225 for the protonated molecular ion in addition to a signal at m/z 87 for the fragment ion ($[CH_2CH_2CH_2COOH]^+$) and signals at m/z 107 (AsS^+, assignment was supported by a small ^{34}S isotopic signal at m/z 109), and 91 (possibly $[MeAsH]^+$, or AsO^+ formed from traces of O_2 in the N_2 drying gas[15]). These ions were selectively monitored in the HPLC/ESMS analysis of the thio-DMAB standard and the phenol extract of the urine sample; the sample returned clear signals at m/z 225, 107, 91, and 87 at a retention time ($t_R = 17.8$ min) exactly matching that of the standard arsenical. Spiking experiments performed with comparable quantities of standard analyte and sample analyte produced single undistorted peaks for the monitored ions (m/z 225, 107, 91, 87).

Further evidence for the presence of thio-DMAB in the urine sample was obtained with HPLC/ESMS/MS. Retention ($t_R = 2.73$ min) of the compound was achieved on a reversed-phase HPLC column with gradient elution (Table 1, method G) and characteristic fragments at m/z 207 (loss of H_2O), 191 (loss of H_2S), 179, 109, 105, and 87 were obtained (Figure 2a). This method was then directly applied to the phenol extract of the urine sample. As shown in Figure 2b, the result was a clean chromatogram containing a major peak ($t_R = 2.74$ min) which matched that of the standard analyte. MS/MS spectra were achieved by performing HPLC and recording the product ions resulting from the m/z 225 precursor ion; the mass spectrum obtained from the sample analyte closely matched that obtained for the standard (Figure 2a and b). Collectively, the HPLC/mass spectrometric

 © 2006 Wiley-VCH Verlag GmbH & Co. KGaA, Weinheim

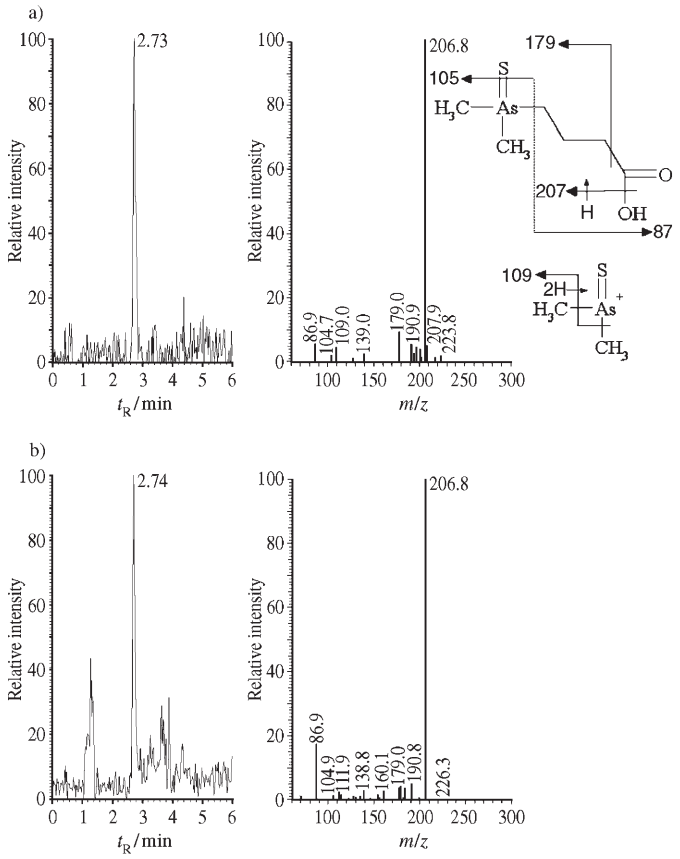


Figure 2. Product ion chromatograms and spectra of a) standard DMAB and b) phenol extract of urine. Data were obtained with an ion trap mass spectrometer by selecting ions with *m/z* 225 and scanning for product ions from *m/z* 60–300.

data presented here with both arsenic-selective and molecular-mass-selective detection provide strong evidence for the presence of four novel arsenic-containing fatty acids in human urine after ingestion of lipid-soluble arsenic species present in cod liver.

The fact that one of the compounds (oxo-DMAP) had been reported[13] in cod liver raised the question whether the compounds had been present originally in the cod liver before ingestion. Although the cod liver contained some water-soluble arsenicals (about 27% of the total comprising mainly arsenobetaine), HPLC/ICPMS analysis of the water-soluble fraction failed to produce detectable quantities ($<10\ \mu g\ As\ kg^{-1}$ dry mass; $<0.3\%$ of the total arsenic) of any of the fatty acid arsenicals, whereas these compounds represented 3 to 15% of the total urine arsenic. Furthermore, when the ingestion experiment was carried out with pure cod liver oil, which contains all of its arsenic as lipid-soluble species, the four metabolites oxo-DMAP, oxo-DMAB, thio-DMAP, and thio-DMAB were also detected in the urine in amounts comparable with those obtained after ingesting cod liver. We note that in the study of Sloth et al.,[13] oxo-DMAP was present in cod liver as a trace constituent only (0.4%), and, possibly, it may have arisen from partial hydrolysis of the lipids, either in vivo or during sample preparation, which involved extraction with aqueous methanol.

On the basis of the experiments reported here, it appears that arsenolipids in cod liver and cod liver oil are metabolized by humans to dimethylarsinate and two significant arsenic-containing fatty acids which are present as oxo and thio analogues. It is likely that the thio compounds are produced from the oxo analogues in the body, as suggested for other oxoarsenicals.[4] These data suggest that the native arsenolipids in cod liver and cod liver oil (and fish oils in general) contain a $(CH_3)_2As(O)$ moiety and may be bound into lipid-soluble species through esterification of a carboxylate group. The diversity of arsenolipids present in cod liver,[5] in contrast to the presence of significant amounts of just two fatty acids found as urinary metabolites in our study, may be largely explained by different moieties forming the ester linkage.

One final interesting observation, however, may also be relevant to the diversity of arsenolipids found in cod liver oil. Close inspection of the HPLC/ICPMS chromatogram (Figure 1b) for the urine sample treated with H_2O_2 revealed a regular succession of late-eluting peaks (e.g, $t_R = 3.3$, 4.2 5.5, 7.4, 9.2, 10.9, 12.1; and 14.0 min) suggesting a homologous series of arsenic-containing fatty acids of the form $(CH_3)_2As(O)(CH_2)_nCOOH$. A plot of retention time versus the number of methylene groups in the chain ($n = 2$–9) produced a straight line plot with a correlation coefficient of 0.99. We speculate that the multitude of observed arsenolipids in cod liver and other fish oils may, at least in part, be explained by the incorporation of arsenic-containing fatty acids of varying methylene chain length. In future work we will test this hypothesis by chemically synthesizing model arsenolipids with arsenic-containing fatty acid moieties of varying carbon chain length. The possible biological role of this novel group of arsenicals will also be investigated.

Experimental Section

As a source of arsenolipids we used a commercially available cod liver product in its own oil (Larsen, Denmark) and the separated oil from this product; arsenic concentrations were $3.0\ \mu g\ g^{-1}$ (cod liver, dry mass) and $1.0\ \mu g\ g^{-1}$ (cod liver oil). The total urine was collected as individual samples for 66 h, stored at 4 °C, and analyzed within ten days. Portions of those urine samples containing the unknowns **U1**, **U2**, **U1***, and **U2***, were stored at −80 °C.

The oxo derivative of dimethylarsenobutanoic acid (oxo-DMAB) was prepared according to Francesconi et al.,[16] and oxodimethylarsenopropanoic acid (oxo-DMAP) was prepared from 3-bromopropanoic acid and bis(dimethylarsenic) oxide (obtained from dimethyliodoarsine and NaOH); the thio analogues (thio-DMAB and thio-DMAP) were prepared by treating the respective oxoarsenical with H_2S.[10]

Phenol extraction was performed by extracting one sample of urine (25 mL) with a solution of phenol and water (15 mL, 9:1 *v*/*v*). The phenol layer was separated and diluted with ether (60 mL), and the mixture was washed with 1 mL of water. The aqueous phase was analyzed by HPLC/ICPMS, HPLC/ESMS, and HPLC/ES/MS/MS.

Analysis of the arsenicals by HPLC/ICPMS was carried out as recently described by Raml et al.[4] under ion-exchange and reversed-phase conditions as summarized in Table 1. HPLC/ESMS was performed under reversed-phase conditions (Table 1, method F). Electrospray ionization and mass detection was performed in positive-ion mode with an Agilent LC/MSD 1100 series single quadrupole MS of the SL type. Optimized fragmentor voltages for standard thio-DMAB for protonated molecular ions and product ions

 © 2006 Wiley-VCH Verlag GmbH & Co. KGaA, Weinheim

were: *m*/*z* 225 (100 V), *m*/*z* 107 (400 V), *m*/*z* 91 (400 V), and *m*/*z* 87 (200 V). HPLC/ESMS/MS analyses were performed using a TSP LC system consisting of a vacuum degasser, a P4000 quaternary pump, an AS3000 autosampler, and a Finnigan LCQ^{DUO} ion trap mass spectrometer equipped with an electrospray source (Finnigan MAT, USA) run by XCALIBUR 1.2 software. HPLC separation was performed according to Table 1, method G. Operating conditions for the electrospray source in the positive-ionization mode were: transfer capillary temperature 270 °C, spray voltage 4.5 kV, capillary voltage and tube lens offset of 20 V, and sheath gas flow of 80 units (units refer to arbitrary values set by the LCQ software). Nitrogen was used for sample nebulization.

Received: August 1, 2005
Published online: November 24, 2005

Keywords: arsenic · arsenolipids · fatty acids · mass spectrometry · thio-arsenicals

[1] T. Yoshida, H. Yamauchi, G. Fan Sun, *Toxicol. Appl. Pharmacol.* **2004**, *198*, 243 – 252.
[2] K. A. Francesconi, D. Kuehnelt in *Environmental Chemistry of Arsenic* (Ed.: W. T. Frankenberger), Marcel Dekker, New York, **2002**, pp. 51 – 94.
[3] R. M. Brown, D. Newton, C. J. Pickford, J. C. Sherlock, *Hum. Exp. Toxicol.* **1990**, *9*, 41 – 46.
[4] R. Raml, W. Goessler, P. Traar, T. Ochi, K. A. Francesconi, *Chem. Res. Toxicol.* **2005**, *18*, 1444 – 1450.
[5] E. Schmeisser, W. Goessler, N. Kienzl, K. A. Francesconi, *Analyst* **2005**, *130*, 948 – 955.
[6] R. V. Cooney, R. O. Mumma, A. A. Benson, *Proc. Natl. Acad. Sci. USA* **1978**, *75*, 4262 – 4264.
[7] A. A. Benson, *Proc. Natl. Acad. Sci. USA* **1989**, *86*, 6131 – 6132.
[8] M. Morita, Y. Shibata, *Chemosphere* **1988**, *17*, 1147 – 1152.
[9] H. R. Hansen, R. Pickford, J. T. Oates, M. Jaspars, J. Feldmann, *Angew. Chem.* **2004**, *43*, 341 – 344; *Angew. Chem. Int. Ed.* **2004**, *43*, 337 – 340.
[10] E. Schmeisser, R. Raml, K. A. Francesconi, D. Kuehnelt, A. L. Lindberg, C. Soeroes, W. Goessler, *Chem. Commun.* **2004**, 1824 – 1825.
[11] M. W. Fricke, P. A. Creed, A. N. Parks, J. A. Shoemaker, C. A. Schwegel, J. T. Creed, *J. Anal. At. Spectrom.* **2004**, *19*, 1454 – 1459.
[12] C. Soeroes, W. Goessler, K. A. Francesconi, E. Schmeisser, R. Raml, N. Kienzl, M. Kahn, P. Fodor, D. Kuehnelt, *J. Environ. Monit.* **2005**, *7*, 688 – 692.
[13] J. J. Sloth, E. H. Larsen, K. Julshamn, *Rapid Commun. Mass Spectrom.* **2005**, *19*, 227 – 235.
[14] K. A. Francesconi, M. Sperling, *Analyst* **2005**, *130*, 998 – 1001.
[15] D. Kuehnelt, W. Goessler, K. A. Francesconi, *Rapid Commun. Mass Spectrom.* **2002**, *16*, 654 – 659.
[16] K. A. Francesconi, J. S. Edmonds, R. V. Stick, *J. Chem. Soc. Perkin Trans. 1* **1992**, 1349 – 1357.

 © 2006 Wiley-VCH Verlag GmbH & Co. KGaA, Weinheim

Reductive Carbonylation

DOI: 10.1002/anie.200502697

A General and Efficient Method for the Formylation of Aryl and Heteroaryl Bromides**

Stefan Klaus, Helfried Neumann, Alexander Zapf, Dirk Strübing, Sandra Hübner, Juan Almena, Thomas Riermeier, Peter Groß, Martin Sarich, Wolf-Rüdiger Krahnert, Kai Rossen, and Matthias Beller**

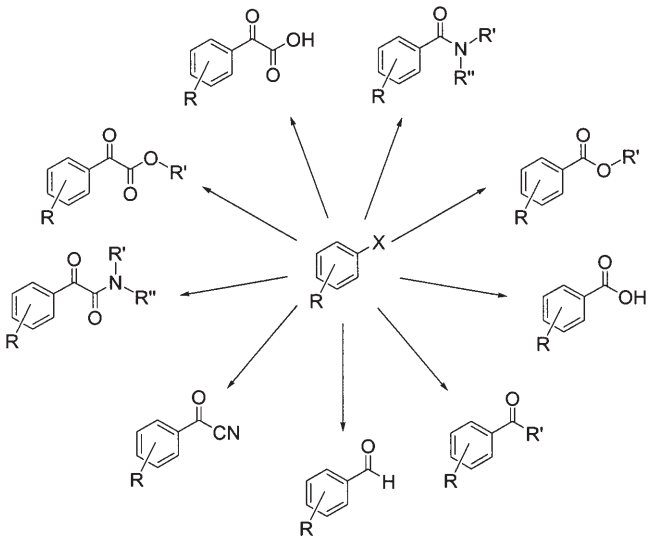
Functionalizations of aryl and heteroaryl halides are of major importance for modern organic synthesis since the resulting products are frequently present in agrochemicals, pharmaceuticals, fine chemicals, and new materials. Among the various catalytic transformations, the palladium-catalyzed coupling reactions such as the Heck, Suzuki, Kumada, and Sonogashira reactions, as well as Buchwald–Hartwig aminations have, in particular, become very popular in organic synthesis.[1] So far, mechanistically related catalytic carbonylation of aryl–X derivatives (X = Cl, Br, I, OTf, OMs, N_2^+) have found fewer applications in synthetic organic chemistry and industry. This is in part understandable, since reactions with carbon monoxide generally require specific high-pressure equipment.[2] On the other hand, these reactions offer numerous possibilities for the selective synthesis of various aromatic carbonyl compounds (Scheme 1).[3]

Aromatic aldehydes are probably the most useful class of products in regard to carbonylations as the highly reactive aldehyde group can be readily employed in numerous C–C and C–N coupling reactions, reductions, as well as other transformations. Traditionally, aromatic aldehydes have been synthesized by electrophilic formylation reactions, such as the Vilsmeier–Haack, Gattermann, Gattermann–Koch, Reimer–Tiemann, and Duff reactions, which use unacceptable amounts of reagents and produce large quantities of side products and waste.[4] In more advanced applications, toluene

[*] S. Klaus, Dr. H. Neumann, Dr. A. Zapf, D. Strübing, S. Hübner, Prof. Dr. M. Beller
Leibniz-Institut für Organische Katalyse an der Universität Rostock e.V. (IfOK)
Albert-Einstein-Strasse 29a, 18059 Rostock (Germany)
Fax: (+49) 381-1281-5000
E-mail: matthias.beller@ifok-rostock.de
Dr. J. Almena, Dr. T. Riermeier, P. Groß, M. Sarich, Dr. W.-R. Krahnert, Dr. K. Rossen
Degussa AG
Rodenbacher Chaussee 4, 63457 Hanau (Germany)
Fax: (+49) 6181-5978709
E-mail: juan.almena@degussa.com

[**] The authors thank Dr. H. Klein, S. Giertz, and S. Buchholz for excellent technical and analytical assistance, as well as Dr. R. Jackstell and Dr. T. Schareina (all at IfOK) for providing ligands and complexes. Generous financial support from Degussa AG, Mecklenburg-Vorpommern, the Fonds der Chemischen Industrie, and the Bundesministerium für Bildung und Forschung (BMBF) is gratefully acknowledged.

WILEY InterScience DISCOVER SOMETHING GREAT
© 2006 Wiley-VCH Verlag GmbH & Co. KGaA, Weinheim



Scheme 1. Palladium-catalyzed carbonylation reactions of aryl halides and pseudohalides. X = Cl, Br, I, OTf (Tf = trifluoromethanesulfonyl, Ms = methanesulfonyl), OMs, N_2^+.

derivatives are (photo)dichlorinated and subsequently hydrolyzed, alcohols are selectively oxidized,[5] and acid chlorides are reduced with specially deactivated catalysts in a hydrogen atmosphere. The classical conversion of aryl bromides into the corresponding aldehydes involves a halogen/metal exchange, frequently at low temperature using *n*BuLi, and a subsequent quench with a formylation agent, such as *N*,*N*-dimethylformamide (DMF). Clearly, such an approach requires expensive reagents and reaction conditions which are not compatible with sensitive functional groups.

A general catalytic formylation of readily available aryl halides using carbon monoxide would thus offer significant advantages over these rather limited and specific methods. The first example of the so-called reductive carbonylation was reported by Schoenberg and Heck in 1974 in which they used high pressures (80–100 bar), high temperatures (125–150 °C), and a large amount of $[PdX_2(PPh_3)_2]$ as a catalyst.[6] The use of expensive reagents such as silyl[7] and tin[8] hydrides was explored to achieve palladium-catalyzed formylations under a lower pressure of carbon monoxide. However, these reactions are often accompanied by overreduction of the aldehyde and other functional groups. To date, the use of formate salts is probably the best variant to perform palladium-catalyzed reductive carbonylations.[9] Recently, acetic formic anhydride has been used successfully as a formyl source in the palladium-catalyzed conversion of aryl iodides into benzaldehydes.[10]

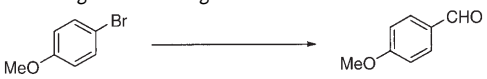
All known formylation procedures of aryl halides use either high catalyst loadings or expensive reagents, which makes the existing protocols inapplicable on a larger scale. It is also interesting to note that, despite the advantages, relatively little work has been done on using the most simple and environmentally benign formylation source CO/H_2 (synthesis gas).[11]

For some time we have been involved in the development of new ligands and catalysts for coupling reactions of aryl halides.[12,13] Recent examples include diadamantylalkylphosphines,[14,15] and *N*-aryl-substituted heteroaryldialkylphosphines,[16] which lead to highly active catalysts, but are comparably stable to air and moisture, and thus easy to handle.

Based on our experience of carbonylation reactions,[17] we started to explore the potential of our ligands in reductive carbonylations of aryl halides. Here, we describe the first results of our investigations, which led to the most general, active and productive palladium catalyst known to date for reductive carbonylations of aryl and heteroaryl bromides.

The formylation of 4-bromoanisole (deactivated aryl bromide) was initially investigated in a model system (Table 1). Typically, all experiments were carried out in a modified sixfold-parallel autoclave, which allows a rapid testing of catalysts and conditions. With regard to conditions suitable for practical applications, low catalyst loadings (< 0.5 mol %) and the presence of the most economical formyl source, which is synthesis gas, were applied. A threefold excess of the ligand (P/Pd = 3:1) was used to stabilize the palladium catalyst and to prevent the formation of palladium carbonyl clusters. More than 20 phosphine and carbene ligands (Scheme 2) were tested at 100 °C and low pressure (5 bar $CO/H_2 = 1:1$) in our study. Gratifyingly, under these conditions it is not necessary to use expensive high-pressure steel autoclave equipment, as it is also possible to perform the reactions in simpler glass autoclaves. Table 1 shows a summary of the results obtained.

Table 1: Screening of various ligands.[a]

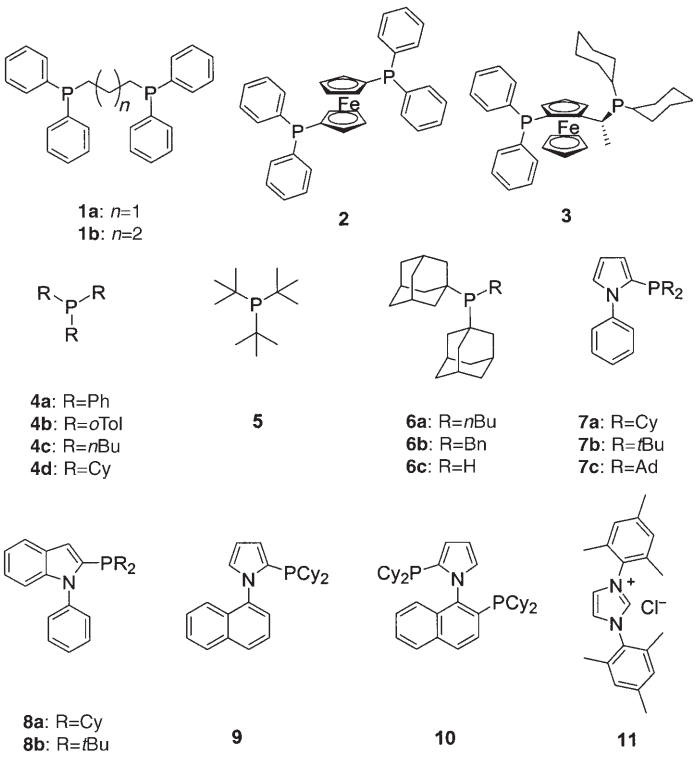


Entry	Ligand (mol %)	Conv. [%][b]	Yield [%][b]	Select. [%]
1	**1a** (0.75)	3	0	0
2	**1a** (0.375)	2	1	50
3	**1b** (0.75)	9	7	78
4	**2** (0.375)	6	3	50
5	**3** (0.75)	3	0	0
6	**4a** (0.75)	2	0	0
7	**4b** (0.75)	1	0	0
8	**4c** (0.75)	1	0	0
9	**4d** (0.75)	13	11	85
10	**5** (0.75)	22	18	82
11	**6a** (0.75)	97	92	95
12	**6b** (0.75)	26	19	73
13	**6c** (0.75)	7	4	57
14	**7a** (0.75)	9	6	67
15	**7b** (0.75)	2	0	0
16	**7c** (0.75)	2	1	50
17	**8a** (0.75)	4	2	50
18	**8b** (0.75)	1	0	0
19	**9** (0.75)	13	9	69
20	**10** (0.375)	3	0	0
21	**11** (0.75)	0	0	0

[a] Reaction conditions: 4-bromoanisole (2 mmol), TMEDA (0.75 equiv), $Pd(OAc)_2$ (0.25 mol %), toluene (2 mL), CO/H_2 (1:1, 5 bar), 100 °C, 16 h. [b] Determined by gas chromatography.

Standard bidentate ligands such as 1,3-bis(diphenylphosphanyl)propane (dppp, **1a**), 1,4-bis(diphenylphosphanyl)bu-

 © 2006 Wiley-VCH Verlag GmbH & Co. KGaA, Weinheim



Scheme 2. Ligands used for the model reaction.

tane (dppb, **1b**), and 1,1′-bis(diphenylphosphanyl)ferrocene (dppf, **2**), which are known to give good results in the alkoxycarbonylation of aryl bromides, do not lead to significant conversion (2–9%) and aldehyde formation (<7%; Table 1, entries 1–4). Not surprisingly, triarylphosphines were inactive (Table 1, entries 6, 7). Remarkably, di-1-adamantyl-*n*-butylphosphane (**6a**, cata*CX*ium A) allows for an unprecedented efficient reductive carbonylation of 4-bromoanisole (92%; Table 1, entry 11). However, even electronically and sterically comparable bulky ligands such as diadamantylbenzylphosphane (cata*CX*ium ABn, **6b**) and P(*t*Bu)$_3$ (**5**) gave only low yields of 4-anisaldehyde (<20%). Dialkylheteroarylphosphines were significantly less active or nearly inactive (Table 1, entries 14–20).

In addition to the ligand screening, the effects of different solvents, pressure, and bases were studied. In general, toluene gave better results than the more-polar solvents *N*-methylpyrrolidinone (NMP), 1,2-dimethoxyethane, and acetonitrile. The choice of synthesis gas pressure is a key parameter for the success of the reaction and a low pressure (<5 bar) is essential to achieve complete conversion. Apparently, a higher pressure of carbon monoxide impedes the oxidative addition of the aryl halide and/or sufficient ligand coordination on the palladium center. Among the different palladium sources tested, Pd(OAc)$_2$ proved to be the best. Fine tuning of the reductive carbonylation is possible by choosing the appropriate base for the reaction. The influence of seven different bases is shown in Table 2.

The low solubility and competing formation of 4-methoxy-,*N*′-tetramethylethylenediamine (TMEDA), NEt$_3$, and N(*n*Bu)$_3$. TMEDA, which has been used only rarely as a base

Table 2: Influence of different bases on the aldehyde yield.[a]

Entry	Base	Conv. [%][b]	Yield [%][b]	Select. [%]
1	K_2HPO_4	32	9	28
2	*N*,*N*-dimethylglycine ethylester	35	29	83
3	pyridine	1	0	0
4	DABCO	89	50	56
5	TMEDA	95	88	93
6	NEt_3	77	66	86
7	N(*n*Bu$_3$)	45	41	91

[a] Reaction conditions: 4-bromoanisole (2 mmol), base (1.5 equiv), Pd(OAc)$_2$ (0.33 mol%), cata*CX*ium A (1 mol%), toluene (2 mL), CO/H_2 (1:1, 2 bar), 100°C, 16 h. [b] Determined by gas chromatography.

for palladium-catalyzed coupling reactions, is the most active base for the model substrate.

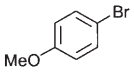
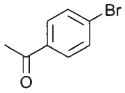
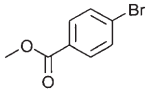
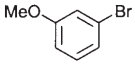
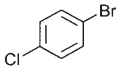
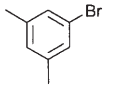
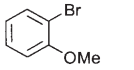
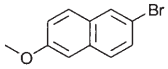
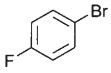
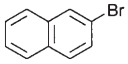
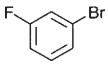
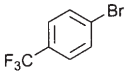
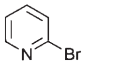
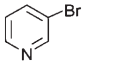
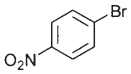
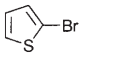
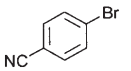
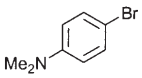
The promising results obtained with di-1-adamantyl-*n*-butylphosphane (**6a**, cata*CX*ium A) encouraged us to study the general scope and limitations of this catalyst system for the formylation of different aryl and heteroaryl bromides (Table 3).

High conversion and excellent selectivity (>88%) were observed for the formylation of various monosubstituted aryl bromides such as 3- and 4-bromoanisoles, 3- and 4-bromofluorobenzene, 4-bromobenzonitrile, 4-(dimethylamino)bromobenzene, ethyl 4-bromobenzoate, 4-bromoacetophenone, and 4-bromochlorobenzene (Table 3, entries 1–4, 6, 7, 12–16). In general, there is no significant difference between electron-rich substrates (for example, bromoanisoles, bromoanilines) and electron-deficient educts (for example, bromoacetophenone, bromobenzonitrile). However, *ortho*-substituted aryl bromides are less reactive than the corresponding *meta* and *para* isomers (see Table 3, entries 1–5). The carbonylation of 4-bromonitrobenzene is problematic because of deactivation of the catalyst (Table 3, entry 10). The new formylation protocol also works well with 1-bromo-3,5-xylene as well as different bromonaphthalenes (Table 3, entries 17–20). A key reagent in the synthesis of the analgesic nabumetone and a potential naproxen precursor (Table 3, entry 18) was produced in excellent yield (99%). In addition to the formylation of bromobenzenes, the reductive carbonylation of different heteroaryl halides (2- and 3-bromothiophene, 3-bromobenzothiophene, 3-bromopyridine) is also effective (Table 3, entries 22–25). This result is of special importance since heteroaromatic aldehydes are particularly useful intermediates for the synthesis of a number of biologically active molecules.[18] In the case of 2-bromopyridine, the catalyst seems to be deactivated by the formation of inactive dimers after the oxidative addition step (Table 3, entry 21).

It should be noted that the amount of palladium necessary can be reduced at constant ligand concentration by raising the temperature from 100°C to >120°C. This typically increases the conversion, but sometimes diminishes the chemoselectivity of the reaction, since reductive dehalogenation of the aryl bromide becomes faster now. On the other hand, decreasing the temperature retards the conversion, but increases the selectivity.

 © 2006 Wiley-VCH Verlag GmbH & Co. KGaA, Weinheim

Table 3: Scope and limitations of the formylation method.[a]

Entry	(hetero)Aryl bromide	$Pd(OAc)_2$ [mol%]	Cata*CX*ium A [mol%]	*T* [°C]	Conv. [%][b]	Yield [%][b]	Select. [%][b]	Entry	(hetero)Aryl bromide	$Pd(OAc)_2$ [mol%]	Cata*CX*ium A [mol%]	*T* [°C]	Conv. [%][b]	Yield [%][b]	Select. [%][b]
1		0.1	0.75	125	100	96	96	14		0.25	0.75	100	100	88	88
2		0.33	1	100	98	96	98	15		0.25	0.75	100	100	91	91
3		0.25	0.75	100	99	99	100	16		0.25	0.75	100	100	89	89
4		0.1	0.75	125	100	98	98	17		0.25	0.75	100	85	85	100
5		0.33	1	100	84	63	75	18		0.25	0.75	100	100	99	99
6		0.25	0.75	100	98	89	91	19		0.25	0.75	100	100	92	92
7		0.25	0.75	100	99	93	94	20		0.25	0.75	100	100	86	86
8		0.25	0.75	100	100	84	84	21		0.25	0.75	100	21	7	33
9		0.05	1	140	87	57	66	22		0.33	1	100	97	77	79
10		0.25	0.75	100	8	0	0	23		0.25	0.75	100	99	66	67
11		0.33	1	100	99	74	75	24		0.25	0.75	100	97	82	85
12		0.25	0.75	100	99	98	99	25		0.33	1	100	100	73	73
13		0.1	0.75	125	100	96	96								

[a] Reaction conditions: (hetero)aryl bromide (2 mmol), TMEDA (0.75 equiv), toluene (2 mL), CO/H_2 (1:1, 5 bar), 16 h. [b] Determined by gas chromatography.

In conclusion, we have presented a general formylation procedure for the synthesis of aromatic and heteroaromatic aldehydes from the corresponding bromides with unprecedented catalyst productivity. Advantageously, synthesis gas can be used as an environmentally benign formylation source at comparably low pressure (5 bar). The high air stability of the cata*CX*ium A ligand enables the autoclave to be loaded with all the reagents in the air and then to purge it with synthesis gas without decreasing the catalyst activity. The simplicity of the reaction conditions combined with the practicality and usefullness of this novel method allows such reactions to be performed for the first time on an industrial scale.[19]

Experimental Section

General information: All reactions were performed by using standard Schlenk techniques (argon). ^1H and ^{13}C NMR spectra were recorded on a Bruker ARX 300 spectrometer. Chemical shifts (δ) are given in ppm and refer to the residual undeuterated solvent as the internal standard ($CDCl_3$: 7.26/77.0). Gas chromatography was performed on a Hewlett Packard HP 6890 chromatograph with a HP1 column. Chemicals were purchased from Fluka, Aldrich, and Strem and used as received. The cata*CX*ium A ligand is available from Strem or directly from Degussa Homogenous Catalysts. Solvents were distilled from sodium and benzophenone.

General procedure for formylation of 4-bromoanisole: A 50-mL Schlenk flask was charged with $Pd(OAc)_2$ (22.2 mg, 0.33 mol%), cata*CX*ium A (108 mg, 1 mol%), and toluene (30 mL). Hexadecane (1.5 mL, internal GC standard), TMEDA (3.4 mL, 22.5 mmol), and 4-bromoanisole (3.8 mL, 30 mmol) were then added. The resulting clear yellow solution was transferred by means of a cannula to a 100-mL mini-bench-top reactor (4560 series from Parr Instruments). After 16 h at a constant pressure of 5 bar CO/H_2 (1:1) and 100 °C, an aliquot was taken from the reaction mixture and subjected to GC analysis for determination of the yield and conversion. The light yellow solution was separated from the solid TMEDA hydrobromide by filtration. The solvent was removed under reduced pressure and the residue was vacuum-distilled at 70 °C/0.15 mbar to yield 4-methoxybenzaldehyde (2.8 g, 71%). ^1H NMR (300 MHz, $CDCl_3$, 300 K): $\delta = 9.89$ (s, 1H,

 © 2006 Wiley-VCH Verlag GmbH & Co. KGaA, Weinheim

CHO), 7.84 (m, 2H, C*H*CCHO), 7.01 (m, 2H, C*H*COCH$_3$), 3.89 ppm (s, 3H, OCH$_3$); ^{13}C NMR (75 MHz, $CDCl_3$, 300 K): δ = 190.8 (CHO), 164.6 (*C*OCH$_3$), 132.0 (2*C*HCCHO), 129.9 (*C*CHO), 114.3 (2*C*HCOCH$_3$), 55.6 ppm (OCH$_3$).

Received: August 1, 2005
Published online: November 22, 2005

Keywords: aldehydes · aryl halides · carbon monoxide · formylation · palladium

[1] *Organopalladium Chemistry for Organic Synthesis* (Ed.: E.-i. Negishi), Wiley-Interscience, New York, **2002**.
[2] An exception is the use of metal carbonyl compounds as a carbon monoxide source; see for example: a) X. Wu, M. Larhed, *Org. Lett.* **2005**, *7*, 3327 – 3329; b) X. Wu, R. Roenn, T. Gossas, M. Larhed, *J. Org. Chem.* **2005**, *70*, 3094 – 3098; c) J. Georgsson, A. Hallberg, M. Larhed, *J. Comb. Chem.* **2003**, *5*, 350 – 352; d) N.-F. Kaiser, A. Hallberg, M. Larhed, *J. Comb. Chem.* **2002**, *4*, 109 – 111.
[3] Recent examples: a) C. Jimenez-Rodriguez, G. R. Eastham, D. J. Cole-Hamilton, *Dalton Trans.* **2005**, 1826 – 1830; b) S. Couve-Bonnaire, J.-F. Carpentier, A. Mortreux, Y. Castanet, *Tetrahedron* **2003**, *59*, 2793 – 2799; c) H.-U. Blaser, M. Diggelmann, H. Meier, F. Naud, E. Scheppach, A. Schnyder, M. Studer, *J. Org. Chem.* **2003**, *68*, 3725 – 3728; d) N. Tsukada, Y. Ohba, Y. Inoue, *J. Organomet. Chem.* **2003**, *687*, 436 – 443.
[4] a) F. Aldabbagh, *Compr. Org. Funct. Group Transform. II* **2005**, *3*, 99 – 133; b) L. P. Crawford, S. K. Richardson, *Gen. Synth. Methods* **1994**, *16*, 37 – 91.
[5] A. El-Ghayoury, R. Ziessel, *J. Org. Chem.* **2000**, *65*, 7757 – 7763.
[6] A. Schoenberg, R. F. Heck, *J. Am. Chem. Soc.* **1974**, *96*, 7761 – 7764.
[7] a) K. Kikukawa, T. Totoki, F. Wada, T. Matsuda, *J. Organomet. Chem.* **1984**, *207*, 283 – 287; b) I. Pri-Bar, O. Buchman, *J. Org. Chem.* **1984**, *49*, 4009 – 4011.
[8] a) V. P. Baillardgeon, J. K. Stille, *J. Am. Chem. Soc.* **1986**, *108*, 452 – 461; b) V. P. Baillard-Geon, J. K. Stille, *J. Am. Chem. Soc.* **1983**, *105*, 7175 – 7176.
[9] a) Y. Ben-David, M. Portnoy, D. Milstein, *J. Chem. Soc. Chem. Commun.* **1989**, 23, 1816 – 1817; b) I. Pri-Bar, O. Buchman, *J. Org. Chem.* **1988**, *53*, 624 – 626; c) T. Okano, N. Harada, J. Kiji, *Bull. Chem. Soc. Jpn.* **1994**, *67*, 2329 – 2332; d) M. Z. Cai, H. Zhao, J. Zhou, C.-S. Song, *Synth. Commun.* **2002**, *32*, 923 – 926.
[10] S. Cacchi, G. Fabrizi, A. Goggiamani, *J. Comb. Chem.* **2004**, *6*, 692 – 694.
[11] R. Mutin, C. Lucas, J. Thivole-Cazat, V. Dufaud, F. Dany, J. M. Basset, *J. Chem. Soc. Chem. Commun.* **1988**, *13*, 896 – 898.
[12] A. Zapf, M. Beller, *Chem. Commun.* **2005**, 431 – 440.
[13] a) A. Frisch, N. Shaikh, A. Zapf, M. Beller, O. Briel, B. Kayser, *J. Mol. Catal. A: Chem.* **2004**, *214*, 231 – 239; b) K. Selvakumar, A. Zapf, M. Beller, *Org. Lett.* **2002**, *4*, 3031 – 3033; c) K. Selvakumar, A. Zapf, A. Spannenberg, M. Beller, *Chem. Eur. J.* **2002**, *8*, 3901 – 3906; d) A. Zapf, M. Beller, *Chem. Eur. J.* **2001**, *7*, 2908 – 2915; e) M. Gómez Andreu, A. Zapf, M. Beller, *Chem. Commun.* **2000**, 2475 – 2476; f) A. Zapf, M. Beller, *Chem. Eur. J.* **2000**, *6*, 1830 – 1833; g) M. Beller, J. G. E. Krauter, A. Zapf, *Angew. Chem.* **1997**, *109*, 793 – 795; *Angew. Chem. Int. Ed. Engl.* **1997**, *36*, 772 – 774; h) W. A. Herrmann, C. Broßmer, C.-P. Reisinger, K. Öfele, M. Beller, T. H. Riermeier, *Chem. Eur. J.* **1997**, *3*, 1357 – 1364; i) M. Beller, H. Fischer, W. A. Herrmann, C. Broßmer, *Angew. Chem.* **1995**, *107*, 1992 – 1994; *Angew. Chem. Int. Ed. Engl.* **1995**, *34*, 1848 – 1849.
[14] For the preparation of adamantylphosphines see: a) J. R. Görlich, R. Schmutzler, *Phosphorus Sulfur Silicon Relat. Elem.* **1993**, *81*, 141 – 148; b) A. Aranyous, D. W. Old, A. Kiyomori, J. P. Wolfe, J. P. Sadighi, S. L. Buchwald, *J. Am. Chem. Soc.* **1999**, *121*, 4369 – 4378.
[15] These ligands are commercially available on an industrial scale under the trade name cata*CX*ium A; for catalytic applications of adamantylphosphines see: a) A. Ehrentraut, A. Zapf, M. Beller, *Synlett* **2000**, 1589 – 1592; b) A. Zapf, A. Ehrentraut, M. Beller, *Angew. Chem.* **2000**, *112*, 4315 – 4317; *Angew. Chem. Int. Ed.* **2000**, *39*, 4153 – 4155; c) A. Ehrentraut, A. Zapf, M. Beller, *J. Mol. Catal. A: Chem.* **2002**, 182 – 183; d) A. Ehrentraut, A. Zapf, M. Beller, *J. Mol. Catal. A: Chem.* **2002**, 515 – 523; e) A. Ehrentraut, A. Zapf, M. Beller, *Adv. Synth. Catal.* **2002**, *344*, 209 – 217.
[16] These ligands are commercially available up to multikilogram scale under the trade name cata*CX*ium P; for catalytic applications see: a) A. Zapf, R. Jackstell, F. Rataboul, T. Riermeier, A. Monsees, U. Dingerdissen, M. Beller, *Chem. Commun.* **2004**, 38 – 39; b) F. Rataboul, A. Zapf, R. Jackstell, S. Harkal, T. Riermeier, A. Monsees, U. Dingerdissen, M. Beller, *Chem. Eur. J.* **2004**, *10*, 2983 – 2990; c) S. Harkal, K. Kumar, D. Michalik, A. Zapf, R. Jackstell, F. Rataboul, T. Riermeier, A. Monsees, M. Beller, *Tetrahedron Lett.* **2005**, *46*, 3237 – 3240.
[17] a) W. Mägerlein, A. F. Indolese, M. Beller, *J. Organomet. Chem.* **2002**, *641*, 30 – 40; b) M. Beller, A. F. Indolese, *Chimia* **2001**, *55*, 684 – 687; c) A. Schnyder, M. Beller, G. Mehltretter, A. F. Indolese, T. Nsenda, M. Studer, *J. Org. Chem.* **2001**, *66*, 4311 – 4315; d) W. Mägerlein, A. Indolese, M. Beller, *Angew. Chem.* **2001**, *113*, 2940 – 2943; *Angew. Chem. Int. Ed.* **2001**, *40*, 2856 – 2859; e) W. Mägerlein, A. Indolese, M. Beller, *J. Mol. Catal. A: Chem* **2000**, *156*, 213 – 221.
[18] For the importance of heteroaromatic derivatives in agrochemicals see: J. Stetter, F. Lieb, *Angew. Chem.* **2000**, *112*, 1793 – 1812; *Angew. Chem. Int. Ed.* **2000**, *39*, 1724 – 1744.
[19] The reaction is currently applied on a >100 kg scale for the synthesis of aromatic aldehydes. To the best of our knowledge, this is the first industrial application of reductive carbonylations of aryl halides.

 © 2006 Wiley-VCH Verlag GmbH & Co. KGaA, Weinheim

Grignard Reagents

DOI: 10.1002/anie.200502220

Highly Efficient Reagents for Br/Mg Exchange**

Arkady Krasovskiy, Bernd F. Straub, and Paul Knochel**

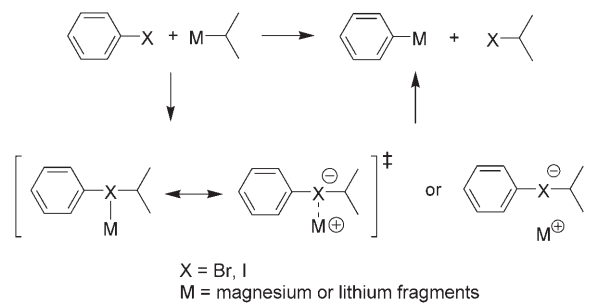
Dedicated to Professor Bernd Giese on the occasion of his 65th birthday

Functionalized aryl and heteroaryl magnesium compounds have become readily available from the corresponding organic iodides through an iodine–magnesium exchange by using *i*PrMgCl in THF.[1] Recently, we reported that aryl and heteroaryl bromides also undergo a bromine–magnesium exchange if the mixed complex *i*PrMgCl·LiCl (**1**) is used.[2a] Herein, we report the exceptional reactivity of the new exchange reagent *i*Pr_2Mg·LiCl (**2**) and the principles on which its reactivity is based. Synthetic applications as well as quantum-chemical calculations provide a rationalization for the reactivity differences and insight into the mechanism of the halogen–magnesium exchange.

We have speculated that the high reactivity of the bimetallic reagent **1** is due to the magnesiate character of this reagent solution in THF.[2,3] Indeed, our quantum-chemical model calculations of halogen–metal exchange reactions predict that the energy of the reaction barrier decreases with increased electronic saturation at the magnesium center.[4] Both a higher magnesium coordination number as well as more-strongly electron-donating ligands dramatically facilitate the formation of 10-valence-electron ate transition states (Scheme 1, Figure 1, and Table 1).

Experimentally, iodine ate complexes have been either observed or isolated as intermediates.[5] In contrast, quantum-chemical studies on halogen–metal exchange reactions with 'naked' lithium counter ions have so far only predicted hypervalent halogen ate transition states.[6] Our model calculations involve a more reasonable metal coordination environment (Figure 1 and Table 1). Both pathways now appear to be competitive alternatives (Figure 2).

The enthalpic stabilization of ate intermediates owing to the additional magnesium–solvent bond is, however, entropically unfavorable. Thus, low temperatures and strong donor



Scheme 1. Halogen–metal exchange reactions through a one-step transition-state pathway or a two-step ate complex intermediate mechanism.

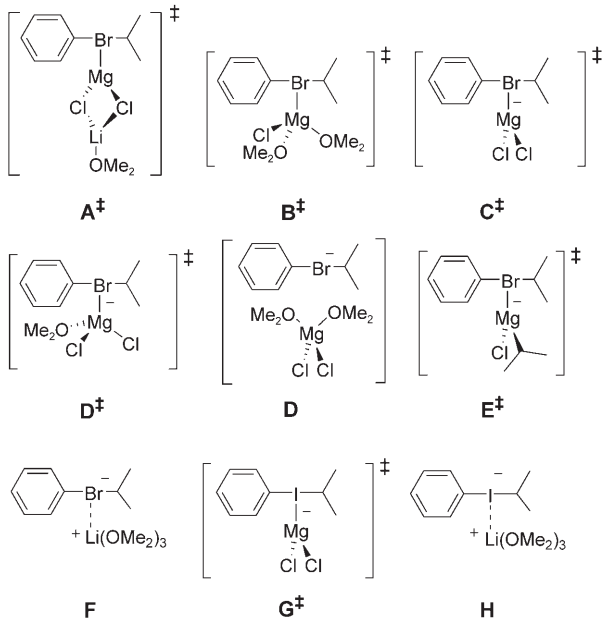


Figure 1. Calculated halogen ate transition states and intermediates.

Table 1: Calculated total electronic energies E_0 [kJ mol^{-1}] for aryl halides and organometallic substrates, hypervalent halides, and products.[a]

	X	M	Hypervalent halide $[C_6H_5X\,i\mathrm{Pr}]^-\ M^+$ transition state	Products $C_6H_5M + i\mathrm{PrX}$ ΔE_0(reaction)
A$^+$	Br	$Mg(\mu\text{-}Cl)_2Li(OMe_2)$	147.7	−42.7
B$^+$	Br	$Mg(OMe_2)_2Cl$	129.3	−37.3
C$^+$	Br	$MgCl_2^-$	99.2	−55.7
D$^+$	Br	$Mg(OMe_2)Cl_2^-$	84.5	−58.0
D	Br	$Mg(OMe_2)_2Cl_2^-$	(49.3)[b]	–
E$^+$	Br	$MgCl(i\mathrm{Pr})^-$	81.9	−57.5
F	Br	$Li(OMe_2)_3$	19.3[c]	−64.6
G$^+$	I	$MgCl_2^-$	69.1	−56.1
H	I	$Li(OMe_2)_3$	−11.5[c]	−65.0

[a] Gibbs free activation energies will be higher, as two substrate molecules have to combine in one entropically disfavored transition-state molecule. As a consequence, the Gibbs free activation energies are highly temperature-dependent. Energy values are given relative to the energies of the substrates C_6H_5X + *i*PrM; [b] Ion pair, local minimum (NIMAG 0), energy relative to $PrMgCl_2(OMe_2)^-$, PhBr, and Me_2O model structures. [c] Contact ion pair, local minimum (NIMAG 0).

[*] Dr. A. Krasovskiy, Dr. B. F. Straub, Prof. Dr. P. Knochel
Department Chemie und Biochemie
Ludwig-Maximilians-Universität München
Butenandtstrasse 5–13, Haus F, 81377 München (Germany)
Fax: (+49) 89-2180-77680
E-mail: bernd.f.straub@cup.uni-muenchen.de
paul.knochel@cup.uni-muenchen.de

[**] We thank the Fonds der Chemischen Industrie and Merck Research Laboratories (MSD) for financial support. We also thank Chemetall GmbH (Frankfurt) and BASF AG (Ludwigshafen) for generous gifts of chemicals.

Supporting information for this article is available on the WWW under http://www.angewandte.org or from the author.

© 2006 Wiley-VCH Verlag GmbH & Co. KGaA, Weinheim

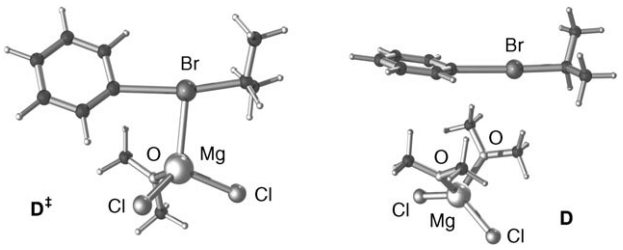
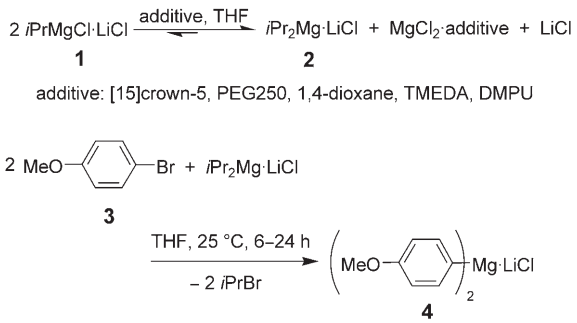


Figure 2. Ball-and-stick model structures of the transition state **D**‡ and the intermediate **D**.



Scheme 2. Preparation of iPr$_2$Mg·LiCl (**2**) by the reaction of iPrMgCl·LiCl (**1**) with additives, and the Br/Mg-exchange reaction with 4-bromoanisole (**3**).

solvents favor two-step pathways via ate intermediates, whereas high temperatures and weak donor ligands support one-step reactions with ate transition states.

To increase the effective negative charge at the magnesium center through separation of the lithium cation from the magnesiate anion, we added various strong σ donors, particularly chelating ethers. Li^+ selective [12]crown-4 is not, however, efficient, and only a small rate enhancement was observed. This therefore indicates that **1** is already an ionic reagent, presumably with the formula $[Li(thf)_4]^+[Mg(thf)(iPr)Cl_2]^-$. Nevertheless, other additives such as 1,4-dioxane or [15]crown-5 lead to a higher reactivity through the enforcement of an 'anionic Schlenk equilibrium' with the formation of a $MgCl_2$·additive precipitate and a solution containing **2**, presumably as $[Li(thf)_4]^+[Mg(thf)(iPr)_2Cl]^-$.[7] We prepared reagent **2** by mixing iPrMgCl (2 equiv), LiCl (1 equiv), and 1,4-dioxane (10 vol%) in THF, and the resultant precipitate was removed by filtration. The solution of **2** gave the same results as that prepared in situ. The new reagent **2** displays exceptional reactivity for the conversion of various aryl bromides into the corresponding Grignard reagents (Scheme 2 and Table 2).

Interestingly, no significant rate enhancements are observed in Br/Mg-exchange reactions with iPr$_2$Mg prepared from iPrMgCl and 1,4-dioxane relative to reactions with iPrMgCl. Apparently, the reactive species in solutions of iPrMgCl is iPr$_2$Mg, which is formed in a Schlenk equilibrium and thermodynamically shifted to the right side by the higher magnesium coordination number of the $MgCl_2$ by-product (Scheme 3).[8]

Whereas the reaction of **1** with 4-bromoanisole (**3**) produces the corresponding Grignard reagent **4** in 24 h with only 31% conversion, the addition of [15]crown-5 (1 equiv) to **1** leads to complete conversion within 6 h (Table 2, entries 1 and 2). The use of the larger [18]crown-6 leads to 77% conversion after 24 h. This correlates with a stronger complexation of $MgCl_2$ by [15]crown-5, which has the perfect size for a seven-coordinated Mg^{II} center (Scheme 3).[9] Conveniently, ethylene glycol derivatives such as PEG250, Me-$(OCH_2CH_2)_4$OMe, or dimethoxyethane (DME) also give significant rate enhancement (Table 2, entries 4–6). However, the addition of 1,4-dioxane ($\approx$1.2 equiv, 10 vol%) provides 100% conversion after 10 h (Table 2, entry 7). Finally,

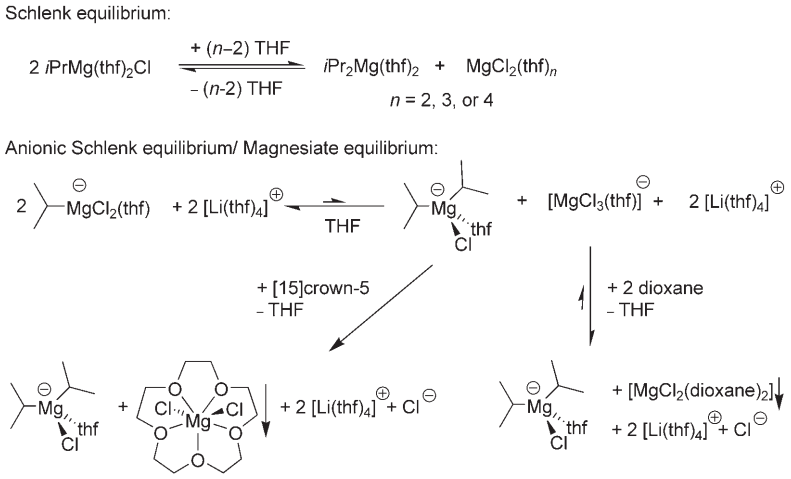
Table 2: Effect of chelating additives on the conversion of the Br/Mg-exchange reaction of 4-bromoanisole.[a]

Entry	Additive	Amount	Conversion [%][b]
1	–	–	31
2	[15]crown-5	1.0 equiv	100[c]
3	[18]crown-6	1.0 equiv	77
4	PEG250	10 vol%	55
5	Me(O $CH_2CH_2)_4$OMe	10 vol%	60
6	DME	10 vol%	70
7	1,4-dioxane	10 vol%	100[d]
8	DMPU	10 vol%	60
9	TMEDA	10 vol%	77

[a] After 24 h at 25 °C; [b] The conversion of the reaction was determined by gas chromatographic analysis of reaction aliquots; precision ±2%; [c] After 6 h; [d] After 10 h.

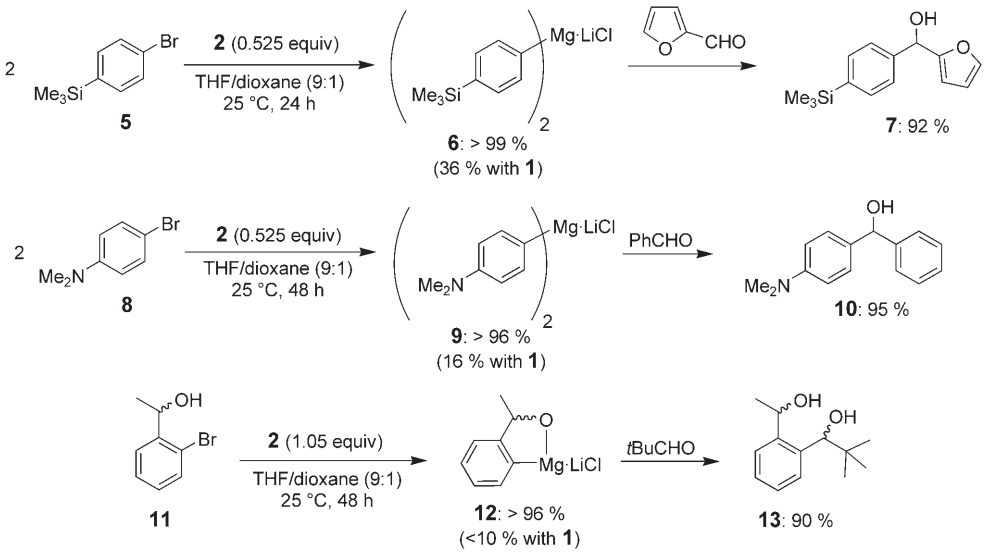
related complexing molecules such as *N*,*N*′-dimethyl-*N*,*N*′-propylene urea (DMPU) or *N*,*N*,*N*′,*N*′-tetramethylethylenediamine (TMEDA) similarly enhanced the exchange rate (Table 2, entries 8 and 9).[10]

Several electron-rich aryl bromides, which react only slowly with **1**, undergo a smooth Br/Mg-exchange reaction with **2**. Thus, the reaction of 1-bromo-4-trimethylsilylbenzene



Scheme 3. Schlenk equilibrium (without μ-chloro dimers) and the proposed magnesiate equilibrium.

 © 2006 Wiley-VCH Verlag GmbH & Co. KGaA, Weinheim



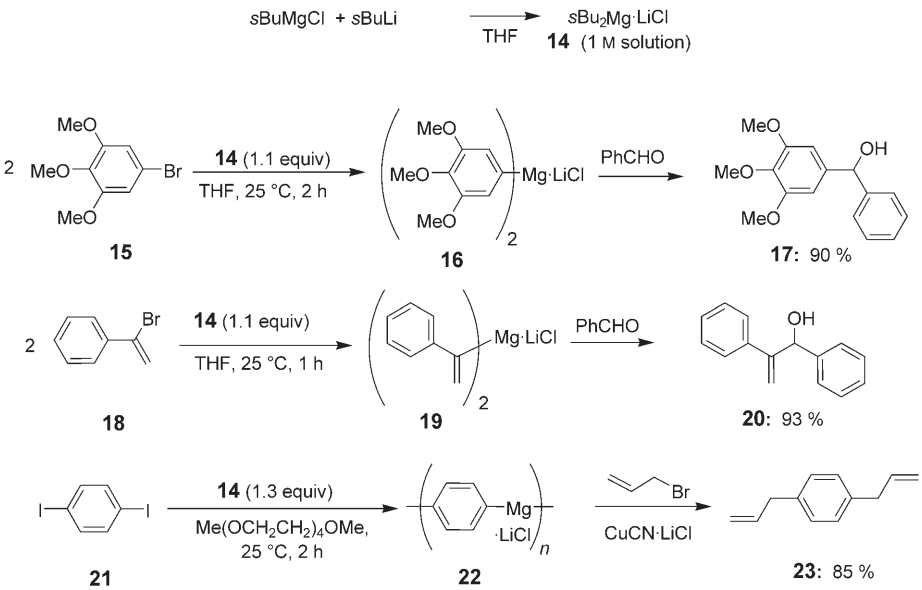
Scheme 4. Br/Mg exchanges with *i*Pr_2Mg·LiCl (**2**) generated by the addition of 1,4-dioxane (10 vol%) to *i*PrMgCl·LiCl (**1**).

(**5**) with **2** (0.525 equiv), generated by adding 1,4-dioxane (10 vol%) to **1** (1.05 equiv), is completed within 24 h at 25 °C (Scheme 4). The same exchange with **1** in THF led to a conversion of only 36%. The reaction of the resultant Grignard reagent **6** with furfural provided the alcohol **7** in 92% yield. Strongly electron-donating amine substituents slow down the Br/Mg exchange considerably. However, the reaction of 4-bromo-*N*,*N*-dimethylanilin (**8**) with **2**, prepared in the same way, furnishes the Grignard reagent **9** within 48 h at 25 °C, whereas the use of **1** results in only 16% conversion. Quenching of **9** with benzaldehyde leads to the benzhydrol **10** in 95% yield. For benzylic alcohols such as **11**, the Br/Mg exchange is nonselective with **1**. On the other hand, the reaction of the unprotected alcohol **11** with **2** in THF/dioxane (9:1) provides cleanly the Grignard reagent **12** within 24 h at 25 °C. Its reaction with *t*BuCHO furnishes the diol **13** in 90% yield and as a separable mixture of two diastereomers (1:1 ratio).

On the basis of these these results, we independently prepared the dialkyl magnesiate reagent *s*Bu_2Mg·LiCl (**14**) directly by combining *s*BuLi (1 equiv) with *s*BuMgCl (1 equiv) in THF at 25 °C (Scheme 5). No precipitate was formed, and the resulting clear solution (1.0 M in THF) is stable at 25 °C and again proved to be a superior reagent for of Br/Mg-exchange reactions. For example, the reaction of **3** with **14** (0.55 equiv) results in the formation of the corresponding diaryl magnesium reagent **4** within 6 h at 25 °C. Also, the highly electron-rich aryl bromide **15** is smoothly converted into the diaryl magnesium reagent **16**, which (after trapping with benzaldehyde) affords the alcohol **17** in 90% yield (Scheme 5). Alkenyl bromides do not undergo Br/Mg exchange with previously known magnesium reagents; however, the reaction of **14** (0.55 equiv) with α-bromostyrene (**18**) provides the desired magnesium reagent **19** within 1 h at 25 °C. Quenching with benzaldehyde leads to the allylic alcohol **20** in 93% yield. Finally, **14** allows the facile preparation of dimagnesium reagents. After 2 h at 25 °C in $Me(OCH_2CH_2)_4OMe$, the reaction of 1,4-diiodobenzene (**21**) with **14** (1.3 equiv) furnishes the corresponding magnesium reagent **22**,which in the presence of excess allyl bromide forms the 1,4-diallylbenzene (**23**) in 85% yield.

In summary, we have presented model calculations that correlate the structure of magnesium reagents and their reactivity in Br/Mg-exchange reactions. Efficient procedures for the shifting of alkyl magnesiate–dialkyl magnesiate equilibria by additives or the alternative direct preparations of dialkyl magnesiates have been developed. Compounds **2** and **14** display exceptional reactivities for otherwise challenging Br/Mg-exchange reactions, thus giving dialkyl magnesiates general synthetic value.

Received: June 24, 2005
Published online: November 24, 2005



Scheme 5. Preparation and reactivity of *s*Bu_2Mg·LiCl (**14**) in halogen–magnesium exchange reactions.

© 2006 Wiley-VCH Verlag GmbH & Co. KGaA, Weinheim

Keywords: bromine–magnesium exchange · density functional calculations · Grignard reaction · lithium · Schlenk equilibrium

[1] a) P. Knochel, W. Dohle, N. Gommermann, F. F. Kneisel, F. Kopp, T. Korn, I. Sapountzis, V. A. Vu, *Angew. Chem.* **2003**, *115*, 4438; *Angew. Chem. Int. Ed.* **2003**, *42*, 4302; b) A. E. Jensen, W. Dohle, I. Sapountzis, D. M. Lindsay, V. A. Vu, P. Knochel, *Synthesis* **2002**, 565.

[2] a) A. Krasovskiy, P. Knochel, *Angew. Chem.* **2004**, *116*, 3396; *Angew. Chem. Int. Ed.* **2004**, *43*, 3333; b) H. Ren, A. Krasovskiy, P. Knochel, *Chem. Commun.* **2005**, 543; c) H. Ren, A. Krasovskiy, P. Knochel, *Org. Lett.* **2004**, *6*, 4215.

[3] For the higher reactivity of triorganomagnesiates, see: a) K. Kitagawa, A. Inoue, H. Shinokubo, K. Oshima, *Angew. Chem.* **2000**, *112*, 2594; *Angew. Chem. Int. Ed.* **2000**, *39*, 2481; b) A. Inoue, K. Kitagawa, H. Shinokubo, K. Oshima, *J. Org. Chem.* **2001**, *66*, 4333; c) A. Inoue, K. Kitagawa, H. Shinokubo, K. Oshima, *Tetrahedron* **2000**, *56*, 9601.

[4] The B3LYP level of theory, with an SDD ECP and basis set on Br and I and a correlation-consistent basis set on Mg, O, C, and H, was used with the Gaussian 98 program package. a) Gaussian 98 (Revision A.11.1): M. J. Frisch et al., see Supporting Information; b) A. D. Becke, *J. Chem. Phys.* **1993**, *98*, 5648; c) S. H. Vosko, L. Wilk, M. Nusair, *Can. J. Phys.* **1980**, *58*, 1200; d) C. Lee, W. Yang, R. G. Parr, *Phys. Rev. B* **1988**, *37*, 785; e) J. M. L. Martin, A. Sundermann, *J. Chem. Phys.* **2001**, *114*, 3408; f) D. E. Woon, T. H. Dunning, Jr., *J. Chem. Phys.* **1993**, *98*, 1358; g) E. R. Davidson, *Chem. Phys. Lett.* **1996**, *260*, 514; h) M. Dolg, U. Wedig, H. Stoll, H. Preuss, *J. Chem. Phys.* **1987**, *86*, 866.

[5] a) W. B. Farnham, J. C. Calabrese, *J. Am. Chem. Soc.* **1986**, *108*, 2449; b) H. J. Reich, D. P. Green, N. H. Phillips, J. P. Borst, I. L. Reich, *Phosphorus Sulfur Silicon Relat. Elem.* **1992**, *67*, 83; c) M. Müller, M. Brönstrup, O. Knopff, V. Schulze, R. W. Hoffmann, *Organometallics* **2003**, *22*, 2931, and references therein.

[6] a) J. Cioslowski, P. Piskorz, M. Schimeczek, G. Boche, *J. Am. Chem. Soc.* **1998**, *120*, 2612; b) K. B. Wiberg, S. Sklenak, W. F. Baiky, *J. Org. Chem.* **2000**, *65*, 2014; c) B. Jedlicka, R. H. Crabtree, P. E. M. Siegbahn, *Organometallics* **1997**, *16*, 6021; d) G. Boche, M. Schimeczek, J. Cioslowski, P. Piskorz, *Eur. J. Org. Chem.* **1998**, 1851.

[7] A titration of the supernatant solution indicated that the base equivalents remain in solution (> 95 %).

[8] J. Tammiku-Taul, P. Burk, A. Tuulmets, *J. Phys. Chem. A* **2004**, *108*, 133.

[9] a) A. D. Pajerski, J. E. Chubb, R. M. Fabicon, H. G. Richey, Jr., *J. Org. Chem.* **2000**, *65*, 2231; b) S. Chadwick, U. Englich, K. Ruhland-Senge, *Inorg. Chem.* **1999**, *38*, 6289.

[10] Solutions of *t*BuMgCl·LiCl (1 M in THF) and $t\text{Bu}_2\text{Mg}$·LiCl (1 M in THF) were also prepared and applied in Br/Mg-exchange reactions with **3**. However, these *tert*-butylmagnesiates featured slightly lower reaction rates than the secondary reagents **1** and **14**. For full conversion of the aryl bromides into the Grignard reagents, 1.1 equiv of both types of reagents was enough, therefore indicating that no elimination of HBr from the *t*BuBr byproduct by magnesiates takes place. Further work on magnesiates with different alkyl groups is in progress in our laboratories.

 © 2006 Wiley-VCH Verlag GmbH & Co. KGaA, Weinheim

Iminoboryl Complexes

DOI: 10.1002/anie.200502825

Synthesis and Characterization of Palladium and Platinum Iminoboryl Complexes**

Holger Braunschweig, Krzysztof Radacki, Daniela Rais, and Katharina Uttinger*

The presence of a triple bond between boron and nitrogen renders iminoboranes, X−B≡N−R, isoelectronic to alkynes, X−C≡C−R. This relationship stimulated intense experimental[1,2] and theoretical[3] studies on these compounds. Indeed, their chemistry was extensively investigated for more than two decades, particularly in the research groups led by Paetzold[1] and Nöth.[2] Despite strong similarities in the structural properties of iminoboranes and alkynes, the polarity and relative weakness of the B≡N linkage[3] leads to its increased reactivity in comparison to that of the C≡C triple bond, and to the thermodynamic instability of iminoboranes towards cyclooligomerization.[1,2] Low temperature, high dilution, and the presence of sterically demanding substituents on either side of the triple bond are generally necessary to hinder the otherwise favorable cyclization process and allow for the isolation of monomeric compounds.

Among the numerous reactions of iminoboranes, 1,2-additions of polar reagents across the BN multiple bond were thoroughly investigated.[1,2] In particular, hydrometallations with transition-metal-containing reaction partners, such as $[Cp_2Zr(H)Cl]$[4a,c] and $[Cp_2NbH_3]$ ($Cp = \eta^5\text{-}C_5H_5$),[4b] afforded examples of transition-metal-bound iminoborane ligands. A coordination mode akin to that of side-on-bound alkynes was observed, with a varying degree of BN multiple bonding retained in the final compounds. Cyclodimerization of iminoboranes within the coordination sphere of different transition metals was also reported, yielding η^4-coordinated diazadiboretidines.[1,5a,c] [2+2] Cycloadditions of different X−B≡N−R compounds with the short-lived complex $[Cp_2Ti{=}CH_2]$ yielded 1-aza-2-bora-4-titanacyclobutanes.[5b] However, in contrast to the wealth of reported transition-metal alkynyl complexes $[L_nM{-}C{\equiv}C{-}R]$,[6] corresponding iminoboryl compounds $[L_nM{-}B{\equiv}N{-}R]$ are unknown.

We recently described the synthesis of *trans*-$[(Cy_3P)_2Pt(Br)\{B(Fc)Br\}]$ (Fc = ferrocenyl, Cy = cyclohexyl) upon reaction of $[Pt(PCy_3)_2]$ with $[FcBBr_2]$,[7a] and its facile conversion into the T-shaped three-coordinate complex *trans*-$[(Cy_3P)_2Pt\{B(Fc)Br\}][BAr^f{}_4]$ ($Ar^f = 3,5\text{-}(CF_3)_2C_6H_3$) which, in

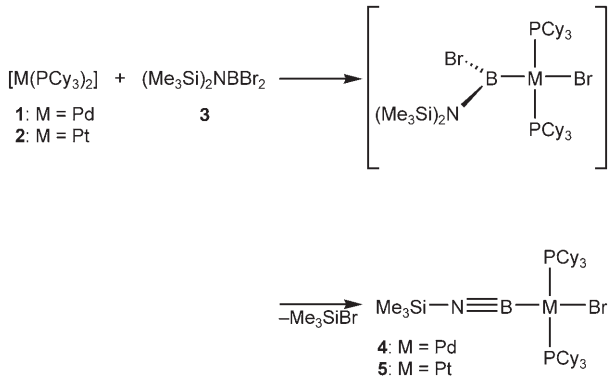
[*] Prof. H. Braunschweig, Dr. K. Radacki, Dr. D. Rais, K. Uttinger
Institut für Anorganische Chemie
Bayerische Julius-Maximilians-Universität Würzburg
Am Hubland, 97074 Würzburg (Germany)
Fax: (+49) 931-888-4623
E-mail: h.braunschweig@mail.uni-wuerzburg.de

[**] This work was supported by the Deutsche Forschungsgemeinschaft. D.R. thanks the Alexander von Humboldt Foundation for a postdoctoral fellowship.

WILEY InterScience DISCOVER SOMETHING GREAT
© 2006 Wiley-VCH Verlag GmbH & Co. KGaA, Weinheim

turn, served as a precursor to the base-stabilized borylene complex *trans*-[$(Cy_3P)_2Pt(Br)\{B(Fc)(NC_5H_4\text{-}4\text{-}Me)\}$]-[$BAr^f_4$].[7b] In continuation of this work, we explored analogous reactions employing differently substituted dibromoboranes. Herein, we report the unprecedented formation of the (trimethylsilyl)iminoboryl complexes *trans*-[$(Cy_3P)_2M(B{\equiv}N\text{-}SiMe_3)(Br)$] (M = Pd, Pt), obtained upon oxidative addition of the B–Br bond in $(Me_3Si)_2NBBr_2$ to $[M(PCy_3)_2]$ (M = Pd, Pt) and subsequent facile intramolecular elimination of Me_3SiBr at room temperature.

When $(Me_3Si)_2NBBr_2$[8] (**3**) was added to an equimolar amount of $[M(PCy_3)_2]$ (M = Pd,[9a] **1**; M = Pt,[9b] **2**) in C_6D_6, multinuclear NMR spectroscopy revealed gradual consumption of the starting materials over 24–36 h and predominant formation of products **4** and **5**, respectively, with concomitant liberation of Me_3SiBr (Scheme 1). The $^{11}B\{^1H\}$ NMR spectra



Scheme 1. Synthesis of iminoboryl complexes **4** and **5**.

of the reaction mixtures feature a signal at $\delta = 22.0$ ppm for **4** and one at $\delta = 25.9$ ppm for **5**, values that compare well with those of main-group-element-substituted (trimethylsilyl)iminoboranes, such as $(Me_3Si)_3CB{\equiv}NSiMe_3$[10] ($\delta_B = 21.0$ ppm) and $(Me_3Si)_3SiB{\equiv}NSiMe_3$[10] ($\delta_B = 21.9$ ppm).

In the $^{31}P\{^1H\}$ NMR spectra a singlet resonance is observed at $\delta = 34.3$ ppm for **4** (cf. $\delta = 39.2$ ppm for **1**)[9a] and one is found at 31.2 ($^1J(P,Pt) = 2389$ Hz) for **5**; the latter is strongly high-field-shifted with respect to that of **2** ($\delta =$ 62.3 ppm, $^1J(P,Pt) = 4161$ Hz).[9b] In the ^1H NMR spectra, a singlet at $\delta = 0.30$ ppm suggests the formation of the common by-product Me_3SiBr, while the presence of only one other singlet in the high-field region, at $\delta = 0.35$ ppm for **4** and at $\delta = 0.37$ ppm for **5**, and its integration (9H) with respect to the cyclohexyl protons (66H), indicate that only one trimethylsilyl group is retained in the new complexes.

The constitution of the two new compounds was determined unequivocally by an X-ray diffraction study performed on suitable single crystals.[11] Colorless crystals of **4** and **5** were obtained by slow evaporation of toluene/hexane mixtures at room temperature. The structural determinations indicate the presence of a (trimethylsilyl)iminoboryl ligand terminally bound through the boron atom to the transition metal of the *trans*-[$(Cy_3P)_2M(Br)$] complex fragment (Figures 1 and 2).

The B–N bond lengths are very similar in the two complexes (two independent molecules, **4a** and **4b**, are

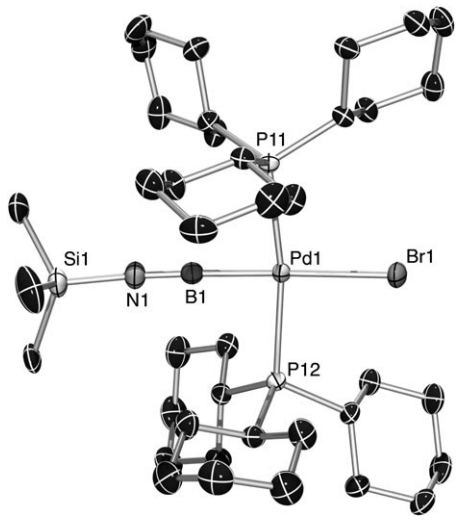


Figure 1. Molecular structure of **4a** (thermal ellipsoids at the 50% probability level). Bond lengths [Å] and angles [°]: **4a**: Pd1–B1 1.958(3), Pd1–Br1 2.5531(5), B1–N1 1.251(4); B1-N1-Si1 163.1(3); **4b**: Pd2–B2 1.967(3), Pd2–Br2 2.5224(5), B2–N2 1.262(3); B2-N2-Si2 166.1(2).

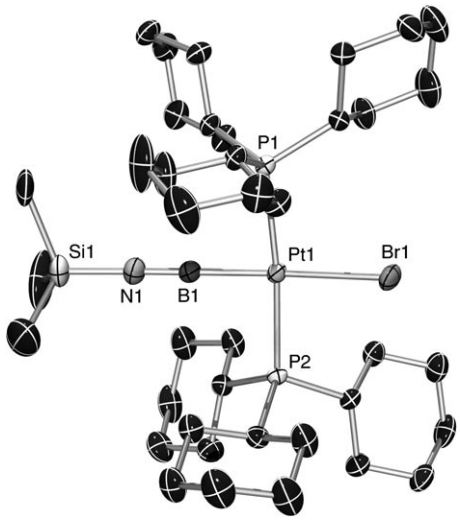


Figure 2. Molecular structure of **5** (thermal ellipsoids at the 50% probability level). Bond lengths [Å] and angles [°]: Pt1–B1 1.960(3), Pt1–Br1 2.5516(4), B1–N1 1.260(4); B1-N1-Si1 173.3(3).

present in the asymmetric unit of **4**: $d(B{-}N) = 1.251(4)$ Å, **4a**, 1.262(3) Å, **4b**; 1.260(4) Å, **5**) and are moderately longer than that reported for the only structurally characterized main group element substituted iminoborane $(Me_3Si)_3SiB{\equiv}NtBu$ (1.221(5) Å)[12] and comparable to that found in the (iminoboryl)borate $[Li(tmeda)_2][(Bu)(tBu)_2BB{\equiv}NtBu]$ (1.250(5) Å) (tmeda = *N*,*N*,*N*′,*N*′-tetramethylethylenediamine).[13] Since palladium and platinum terminal borylene complexes,[14] that is, complexes featuring a two-coordinate boron atom linked to the above metal centers, are not known, the M–B distances in **4** and **5** must be compared to those found in palladium and platinum boryl complexes, of which **4** and **5** represent special examples. The Pd–B bond lengths

 © 2006 Wiley-VCH Verlag GmbH & Co. KGaA, Weinheim

(1.958(3) Å, **4a**, 1.967(3) Å, **4b**) are shorter than those reported in boryl complexes of palladium (2.006(9)–2.077(6) Å),[15] while the Pt–B bond length in **5** (1.960(3) Å) is slightly shorter than the corresponding distance in *trans*-[$(Cy_3P)_2Pt(Br)\{B(Fc)Br\}$] (1.9963(34) Å)[7a] and comparable to that found in the three-coordinate T-shaped platinum boryl complex *trans*-[$(Cy_3P)_2Pt\{B(Fc)Br\}][BAr^f_4]$ (1.966(4) Å).[7b] A slight deviation of the B-N-Si bond angle from linearity (163.1(3)°, **4a**, 166.1(2)°, **4b**; 173.3(3)°, **5**) is observed, with a more pronounced distortion in the case of the palladium complex. Interestingly, the M–Br distances in compounds **4** and **5** (2.5531(5) Å, **4a**, 2.5224(5) Å, **4b**, 2.5516(4) Å, **5**) indicate a weaker *trans* influence of the iminoboryl ligand with respect to that of the (Fc)BrB boryl group (d(Pt–Br) = 2.6183(8) Å, in *trans*-[$(Cy_3P)_2Pt(Br)\{B(Fc)Br\}$])[7a] and that of the base-stabilized borylene ligand (Fc)(NC_5H_4-4-Me)B (d-(Pt–Br) = 2.6057(5) Å in *trans*-[$(Cy_3P)_2Pt(Br)\{B(Fc)(NC_5H_4$-4-Me)$\}][BAr^f_4]$).[7b] This finding is in line with the reduced p character of the boron-based orbital utilized in the formation of the M–B σ bond, leading to shorter M–B bonds and to a weaker σ-donating ability of the iminoboryl ligand compared to that of a boryl group.[16] This effect is further attenuated in **4** and **5** by the presence of the electronegative nitrogen atom.

Our previous results on the oxidative addition of the B–Br bond in $FcBBr_2$ to $[Pt(PCy_3)_2]$[7a] and the reported syntheses of iminoboranes upon elimination of Me_3SiX from suitable $R(X)B{\equiv}N(SiMe_3)R'$ precursors,[1] strongly suggest that formation of compounds **4** and **5** occurs by the intramolecular elimination of Me_3SiBr from the nonobserved intermediates *trans*-[$(Cy_3P)_2M(Br)\{B(Br)N(SiMe_3)_2\}$]. However, elimination of Me_3SiX from $R(X)B{\equiv}N(SiMe_3)R'$ compounds generally occurs at temperatures of 400–500 °C and low pressures; the halosilane is then separated by low-temperature evaporation in order to prevent recombination of the products.[17] Thus, the ease of Me_3SiBr elimination to form **4** and **5** is truly remarkable. A plausible reason might be the need to reduce the steric congestion resulting from the bulky tricyclohexylphosphine ligands and the bis(trimethylsilyl)-amino group.

Equally remarkable is the thermal stability of complexes **4** and **5** in comparison to the known tendency of most iminoboranes to oligomerize already at room temperature.[1,2] A solution of **5** in [D_8]-toluene gave no evidence for oligomerization or decomposition after heating at 100 °C for 14 h. Furthermore, irradiation of C_6D_6 solutions of the two complexes at room temperature for 12 h did not afford any change in their NMR spectra, proving that significant stabilization of the iminoboryl moiety is achieved upon coordination to the transition metals.

In conclusion, we have reported the unprecedented synthesis of palladium and platinum (trimethylsilyl)iminoboryl complexes, upon intramolecular elimination of Me_3SiBr from the putative *trans*-[$(Cy_3P)_2M(Br)\{B(Br)N(SiMe_3)_2\}$] intermediates, which are obtained by oxidative addition of a B–Br bond of $(Me_3Si)_2NBBr_2$ (**3**) to $[M(PCy_3)_2]$ (M = Pd, **1**; M = Pt, **2**). We are currently studying the reactivity of the new compounds with particular regard to their possible polymerization upon intermolecular elimination of Me_3SiBr.

Experimental Section

4: $(Me_3Si)_2NBBr_2$ (**3**; 0.025 g, 0.075 mmol) was added to a pale yellow solution of **1** (0.050 g, 0.075 mmol) in toluene (2 mL). The solution was stirred at room temperature for 24 h, and then it was layered with hexane (4 mL). The solvent mixture was left to evaporate slowly at room temperature. Colorless crystals of **4** were obtained within 48 h (0.035 g, 55 %). ^{1}H NMR (500 MHz, C_6D_6, 25 °C, TMS): δ = 2.92 (br m, 6H, Cy), 2.18–1.17 (m, 60H, Cy), 0.35 ppm (s, 9H, $SiMe_3$); $^{13}C\{^1H\}$ NMR (125.8 MHz, C_6D_6, 25 °C): δ = 35.4 (virtual triplet, $N^{[18]}$ = 22 Hz, C_1, Cy), 31.2 (s, C_3 and C_5, Cy), 27.9 (virtual triplet, $N^{[19]}$ = 11 Hz, C_2 and C_6, Cy), 27.0 (s, C_4, Cy), 3.4 ppm (s, $SiMe_3$); $^{31}P\{^1H\}$ NMR (202.4 MHz, C_6D_6, 25 °C): δ = 34.3 ppm (s); $^{11}B\{^1H\}$ NMR (160.5 MHz, C_6D_6, 25 °C): δ = 22.0 ppm. IR (toluene): $\tilde{\nu}$ = 1857 (w), 1812 cm^{-1} (m), (B≡N). Elemental analysis calcd for $C_{39}H_{75}NBBrP_2PdSi$: C 55.42, H 8.94, N 1.66; found: C 55.31, H 8.53, N 1.49.

5: $(Me_3Si)_2NBBr_2$ (**3**; 0.022 g, 0.066 mmol) was added to a pale yellow solution of **2** (0.050 g, 0.066 mmol) in toluene (2 mL). The solution was kept at room temperature for 36 h, and then it was layered with hexane (4 mL). The solvent mixture was left to evaporate slowly at room temperature. Colorless crystals of **5** were obtained within 48 h (0.038 g, 62 %). ^{1}H NMR (500 MHz, C_6D_6, 25 °C, TMS): δ = 3.08 (br m, 6H, Cy), 2.20–1.19 (m, 60H, Cy), 0.37 ppm (s, 9H, $SiMe_3$); $^{13}C\{^1H\}$ NMR (128.5 MHz, C_6D_6, 25 °C): δ = 34.9 (virtual triplet, $N^{[18]}$ = 30 Hz, C_1, Cy), 30.9 (s, C_3 and C_5, Cy), 27.8 (virtual triplet, $N^{[19]}$ = 11 Hz, C_2 and C_6, Cy), 27.1 (s, C_4, Cy), 3.6 ppm (s, $SiMe_3$); $^{31}P\{^1H\}$ NMR (202.4 MHz, C_6D_6, 25 °C): δ = 31.2 ppm (s, ^1J(Pt,P) = 2389 Hz); $^{11}B\{^1H\}$ NMR (64.2 MHz, C_6D_6, 25 °C): δ = 25.9. IR (toluene): $\tilde{\nu}$ = 1851 (w), 1809 cm^{-1} (m), (B≡N). Elemental analysis calcd for $C_{39}H_{75}NBBrP_2PtSi$: C 50.16, H 8.10, N 1.50; found: C 49.85, H 8.35, N 1.30.

Received: August 9, 2005
Published online: November 21, 2005

Keywords: boron · halosilane elimination · iminoboranes · palladium · platinum

[1] a) P. Paetzold, *Adv. Inorg. Chem.* **1987**, *31*, 123; b) P. Paetzold, *Pure Appl. Chem.* **1991**, *63*, 345; c) P. Paetzold, *Phosphorus Sulfur Silicon* **1994**, *93–94*, 39; d) J. Münster, P. Paetzold, E. Schröder, H. Schwan, T. von Bennigsen-Mackiewicz, *Z. Anorg. Allg. Chem.* **2004**, *630*, 2461, and references therein.

[2] a) H. Nöth, *Angew. Chem.* **1988**, *100*, 1664; *Angew. Chem. Int. Ed. Engl.* **1988**, *27*, 1603; b) U. Braun, B. Böck, H. Nöth, I. Schwab, M. Schwartz, S. Weber, U. Wietelmann, *Eur. J. Inorg. Chem.* **2004**, 3612, and references therein.

[3] a) D. R. Armstrong, T. D. Clark, *Theor. Chim. Acta* **1972**, *24*, 307; b) C. Baird, R. K. Datta, *Inorg. Chem.* **1972**, *11*, 17.

[4] a) D. Männig, H. Nöth, I. Schwab, M. Schwartz, S. Weber, U. Wietelmann, *Angew. Chem.* **1985**, *97*, 979; *Angew. Chem. Int. Ed. Engl.* **1985**, *24*, 998; b) E. Bulak, G. E. Herberich, I. Manners, H. Mayer, P. Paetzold, *Angew. Chem.* **1988**, *100*, 964; *Angew. Chem. Int. Ed. Engl.* **1988**, *27*, 958; c) E. Bulak, P. Paetzold, *Z. Anorg. Allg. Chem.* **2000**, *626*, 1277.

[5] a) K. Delpy, D. Schmitz, P. Paetzold, *Chem. Ber.* **1983**, *116*, 2994; b) P. Paetzold, K. Delpy, R. P. Hughes, W. A. Herrmann, *Chem. Ber.* **1985**, *118*, 1724; c) P. Paetzold, K. Delpy, R. Boese, *Z. Naturforsch. B* **1988**, *43*, 839.

[6] N. J. Long, C. K. Williams, *Angew. Chem.* **2003**, *115*, 2690; *Angew. Chem. Int. Ed.* **2003**, *42*, 2586.

[7] a) H. Braunschweig, K. Radacki, D. Rais, F. Seeler, *Organometallics* **2004**, *23*, 5545; b) H. Braunschweig, K. Radacki, D. Rais, D. Scheschkewitz, *Angew. Chem.* **2005**, *117*, 5796; *Angew. Chem. Int. Ed.* **2005**, *44*, 5651.

 © 2006 Wiley-VCH Verlag GmbH & Co. KGaA, Weinheim

[8] W. Haubold, U. Kraatz, *Z. Anorg. Allg. Chem.* **1976**, *421*, 105.
[9] a) W. Kuran, A. Musco, *Inorg. Chim. Acta* **1975**, *12*, 187; b) S. Otsuka, T. Yoshida, M. Matsumoto, K. Nakatsu, *J. Am. Chem. Soc.* **1976**, *98*, 5850.
[10] M. Haase, U. Klingebiel, *Angew. Chem.* **1985**, *97*, 335; *Angew. Chem. Int. Ed. Engl.* **1985**, *24*, 324.
[11] Crystal data for **4** and **5** were collected on a Bruker Apex diffractometer with CCD area detector and multilayer-mirror-monochromated $Mo_{K\alpha}$ radiation. The structures were solved using direct methods, refined with the Shelx software package (G. Sheldrick, University of Göttingen, **1997**) and expanded using Fourier techniques. All non-hydrogen atoms, except those in the solvent molecule in **5**, were refined anisotropically. Hydrogen atoms were assigned idealized positions and were included in structure factor calculations. Crystal data for **4**: $C_{39}H_{75}BBrNP_2PdSi$, $M_r = 845.15$, colorless needle, $0.150 \times 0.090 \times 0.045$ mm, monoclinic space group $P2(1)$, $a = 21.187(4)$, $b = 9.8472(16)$, $c = 21.806(4)$ Å, $\beta = 103.318(3)°$, $V = 4427.2(12)$ Å^3, $Z = 4$, $\rho_{calcd} = 1.268$ g cm^{-3}, $\mu = 1.447$ cm^{-2}, $F(000) = 1784$, $T = 173(2)$ K, $R_1 = 0.0249$, $wR^2 = 0.0625$, 17851 independent reflections [$2\theta = 52.9°$] and 835 parameters. Crystal data for **5**: $C_{42}H_{82}BBrNP_2PtSi$, $M_r = 976.93$, colorless plate, $0.23 \times 0.22 \times 0.20$ mm, orthorhombic space group $Fdd2$, $a = 36.389(2)$, $b = 40.126(2)$, $c = 12.9610(7)$ Å, $V = 18925.2(18)$ Å^3, $Z = 16$, $\rho_{calcd} = 1.371$ g cm^{-3}, $\mu = 3.930$ cm^{-2}, $F(000) = 8048$, $T = 173(2)$ K, $R_1 = 0.0200$, $wR^2 = 0.0494$, 9013 independent reflections [$2\theta = 52.96°$] and 437 parameters. CCDC-280498 (**4**) and CCDC-280497 (**5**) contain the supplementary crystallographic data for this paper. These data can be obtained free of charge from The Cambridge Crystallographic Data Centre via www.ccdc.cam.ac.uk/data_request/cif.
[12] a) M. Haase, U. Klingebiel, R. Boese, M. Polk, *Chem. Ber.* **1986**, *119*, 1117; b) The first structural characterization of an iminoborane was reported in: P. Paetzold, C. von Plotho, G. Schmid, R. Boese, B. Schrader, D. Bourgeard, U. Pfeiffer, R. Gleiter, W. Schäfer, *Chem. Ber.* **1984**, *117*, 1089. However, due to severe disorder, the structural values are not fully reliable.
[13] E. Eversheim, U. Englert, R. Boese, P. Paetzold, *Angew. Chem.* **1994**, *106*, 211; *Angew. Chem. Int. Ed. Engl.* **1994**, *33*, 201.
[14] a) H. Braunschweig, *Angew. Chem.* **1998**, *110*, 1882–1898; *Angew. Chem. Int. Ed.* **1998**, *37*, 1786–1801; b) H. Braunschweig, M. Colling, *Coord. Chem. Rev.* **2001**, *223*, 1–51; c) H. Braunschweig, M. Colling, *Eur. J. Inorg. Chem.* **2003**, 393–403; d) H. Braunschweig, *Adv. Organomet. Chem.* **2004**, *51*, 163–192; e) For a base-stabilized borylene complex of platinum, see Ref. [7b].
[15] a) S.-Y. Onozawa, Y. Hatanaka, T. Sakakura, S. Shimada, M. Tanaka, *Organometallics* **1996**, *15*, 5450; b) S.-Y. Onozawa, M. Tanaka, *Organometallics* **2001**, *20*, 2956.
[16] We thank Prof. T. B. Marder, University of Durham, UK, for the personal communication of his results prior to publication.
[17] For an example of Me_3SiF elimination at ca. 60 °C under vacuum, see Ref. [10].
[18] $N = |{}^1J(P,C) + {}^3J(P,C)|$.
[19] $N = |{}^2J(P,C) + {}^4J(P,C)|$.

 © 2006 Wiley-VCH Verlag GmbH & Co. KGaA, Weinheim

Boride Carbides

DOI: 10.1002/anie.200502325

$Li_2B_{12}C_2$ and $LiB_{13}C_2$: Colorless Boron-Rich Boride Carbides of Lithium**

*Natascha Vojteer and Harald Hillebrecht**

Dedicated to Professor Gerhard Thiele on the occasion of his 70th birthday

Because boron-rich borides and boride carbides contain a great variety of boron polyhedra, they form their own class of compounds and show a unique structure chemistry.[1] Furthermore they are of growing interest owing to a number of applications in material sciences, for example, as high-temperature materials,[2] abrasives,[3] composites,[4] and high-temperature semiconductors,[5] and in high-temperature thermoelectrics.[6] In the system Li/B/C LiBC[7] is the only well-characterized ternary compound that can be classified as a heterographite structure. Boron-rich boride carbides of lithium were previously unknown,[8] primarily because the high reactivity and vapor pressure of lithium make synthesis under the required high-temperature conditions quite difficult. In addition, boron and boron-rich borides tend to incorporate other elements, leading to problems in the unequivocal characterization of the reaction products (e.g. "KB_6"/KB_5C).[9]

Our previous investigations have shown that the use of molten metals allows synthetic access to new compounds not yielded by conventional high-temperature methods.[10,11] The reaction of boron and carbon in a Li/Sn melt using boron nitride crucibles welded in Ta ampules resulted in single crystals of $Li_2B_{12}C_2$und $LiB_{13}C_2$ (Figure 1), the first boron-rich boride carbides of lithium.

$Li_2B_{12}C_2$ forms nearly colorless, pale greenish yellow rectangular platelets and columns. The crystal structure (space group *Amm2*, $Z=2$, $a=4.706(1)$ Å, $b=9.010(2)$ Å, $c=5.652(1)$ Å)[12] represents a new structure type and contains B_{12} icosahedra arranged in the pattern of a hexagonal primitive packing (Figure 2). C_2 units and Li atoms are located between the layers. The connection of the icosahedra within a layer occurs through four apices with exohedral B–B distances of 1.756(2) Å. The connection between the layers by edges of the icosahedra is very unusual for boron-rich borides and was found only in monoclinic $MgB_{12}C_2$,[10d,11] in $Mg_3B_{50}C_8$,[11] and in $RE_{1-x}B_{12}Si_3$/$RE_{3-x}B_{36}Si_8C_2$ (RE = rare-

[*] Dipl.-Chem. N. Vojteer, Prof. Dr. H. Hillebrecht
Institut für Anorganische und Analytische Chemie
Albertstrasse 21, 79100 Freiburg (Germany)
Fax: (+49) 761-203-6012
E-mail: harald.hillebrecht@ac.uni-freiburg.de

[**] We thank Dr. H. Rotter and A. Becherer for the measurement of the Raman and IR spectra, and Dr. M. Ade and Dr. H. Müller-Sigmund, University of Freiburg, Institute for Mineralogy and Geochemistry, for support with the WDX measurements.

 © 2006 Wiley-VCH Verlag GmbH & Co. KGaA, Weinheim

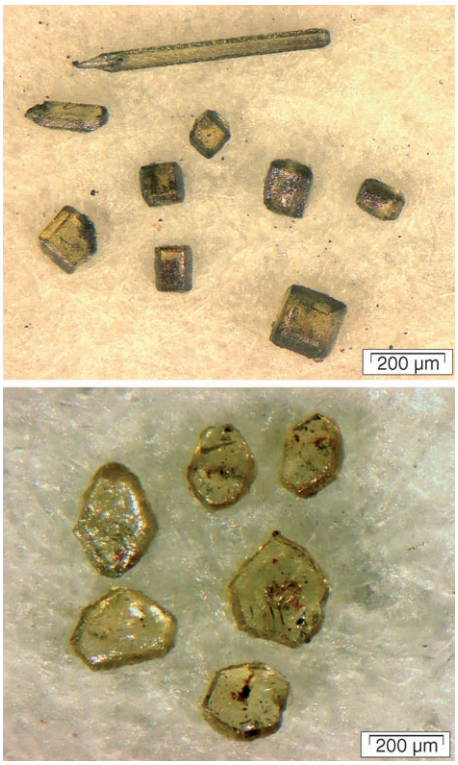


Figure 1. Single crystals of $Li_2B_{12}C_2$ (top) and $LiB_{13}C_2$ (bottom).

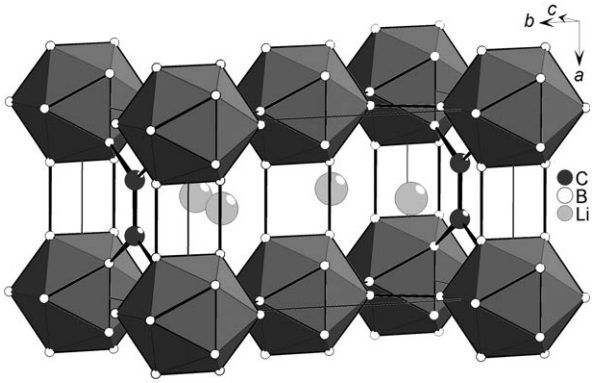


Figure 2. Crystal structure of $Li_2B_{12}C_2$ with B_{12} icosahedra, C_2 units (black), and Li atoms (gray).

earth element).[13] These exohedral distances are quite long (1.821(2) Å); typical values are between 1.70 and 1.75 Å. The B–B distances within the icosahedra are in the typical range from 1.717(4) to 1.842(2) Å with an average of 1.810 Å. The C_2 units between the layers of icosahedra have a C–C distance of 1.374(2) Å. Each C atom forms two additional C–B bonds, which are 1.587(3) and 1.599(3) Å in length and in agreement with the sum of the atomic radii. Because the bond angles at the C atoms are 119.3(1) and 120.7(1)°, sp^2 hybridization and a C–C double bond can be assumed. The Li atoms show two Li–C distances of 2.250(3) Å, and in all ten Li–B distances between 2.211(3) and 2.600(2) Å (average: 2.407 Å).

The framework of covalent bonds composed of B_{12} icosahedra and C_2 units can be assigned to the centrosymmetric space group *Ammm* (or *Cmmm* in the standard setting) with the same unit cell dimensions. The symmetry reduction to the noncentrosymmetric structure is caused only by the Li atoms. Each B_{12} icosahedron exhibits a total of 12 exohedral bonds, eight to neighboring icosahedra and four to C_2 units. According to Wade's rules for the stability and electronic structure of boron clusters, which were transferred to solid-state structures by Longuet-Higgins,[14] a *closo* cluster with exohedral two-electron, two-center (2e2c) bonds needs two additional electrons to achieve optimal stabilization. In $Li_2B_{12}C_2$ the two electrons are supplied by the Li atoms. The electronic situation can be described as $(Li^+)_2[(B_{12})^{2-}]C_2$ or alternatively as $(Li^+)_2[(B_{12})C_2]^{2-}$ if one considers the three-dimensional framework of covalent bonds.

The second compound, $LiB_{13}C_2$, forms nearly colorless crystals (Figure 1). It crystallizes orthorhombically in space group *Imma* with $a = 5.668(1)$, $b = 10.820(2)$, and $c = 8.040(1)$ Å (Figure 3).[12] Here, too, B_{12} icosaheda are

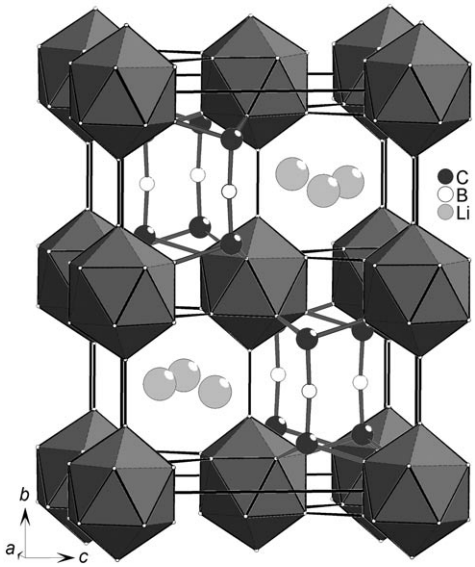


Figure 3. Crystal structure of $LiB_{13}C_2$ with B_{12} icosahedra, CBC units (C atoms black, B atoms white), and Li atoms (gray).

arranged in terms of a hexagonal primitive packing and connected to layers perpendicular to the *b* axis by four exohedral B–B bonds with a distance of 1.771(1) Å. The orientation of the icosahedra is different from that in $Li_2B_{12}C_2$, because the layers are connected through the apices (1.796(2) Å). Endohedral B–B distances range from 1.756(1) to 1.839(1) Å with an average of 1.808 Å. One-half of the trigonal-prismatic voids between the layers of icosahedra are occupied by the Li atoms, the other half by nearly linear CBC groups (C-B-C angle: 174.9(2)°). The CBC units are oriented parallel to the *b* axis. The C atoms are tetrahedrally coordinated by three boron atoms of the icosahedra with a distance of 1.617(1) Å (2×) and 1.629(1) Å and the central boron atom of the CBC group (1.413(1) Å). The latter distance is quite short but is observed quite similar to distances in Al_3BC_3 (1.441 Å),[10a] $Mg_3B_{50}C_8$ (1.450 Å),[11] Sc_2BC_2 (1.475 Å),[15] Lu_3BC_3 (1.446 Å),[16] and boron carbide

 © 2006 Wiley-VCH Verlag GmbH & Co. KGaA, Weinheim

$B_{13}C_2$ (1.429 Å).[17] The Li atoms are exclusively coordinated by boron with the coordination number 11. The Li–B distances between 2.500(3) and 2.751(1) Å (average: 2.617 Å) are significantly larger than those in $Li_2B_{12}C_2$.

The crystal structure of $LiB_{13}C_2$ is a new variant of the MgB_7 type,[18] which includes Na_2B_{29},[19] $MAlB_{14}$ (M = Li, Na, Mg, *RE*)[20] and orthorhombic $MgB_{12}C_2$.[11] Each B_{12} icosahedron forms 12 exohedral 2e2c bonds, six to neighboring icosahedra and six to carbon atoms of the CBC groups. Following the rules of Wade and Longuet-Higgins, the description of the electronic situation is $(Li^+)([B_{12}]^{2-})(CBC^+)$ or $Li^+(B_{12}CBC)^-$. Therefore the covalent framework is isoelectronic to that of the carbon-rich boron carbide $B_4C = (B_{11}C)CBC$.

Figure 4 shows the vibrational spectra of $Li_2B_{12}C_2$ and $LiB_{13}C_2$. A comparison with published spectra reveals that for boron-rich borides with B_{12} icosahedra frequencies up to ca. 1200 cm^{-1} occur (e.g. α-rhombohedral boron,[21] B_6As,[21] SiB_3,[22] $MgB_{12}Si_2$[23]), whereas the closest similarity should be to boron carbide B_4C and $B_{13}C_2$, respectively.[24] Therefore the strong Raman-active mode at 1477 cm^{-1} in the spectrum of $Li_2B_{12}C_2$ is clearly attributed to the C–C vibration. The comparison to published data for C_2H_4 (1619 cm^{-1}), C_2Cl_4 (1571 cm^{-1}), C_2Br_4 (1547 cm^{-1}), and C_2I_4 (1465 cm^{-1})[25] confirms both the double-bond character and the red shift of the band upon incorporation into the icosahedra framework as expected.

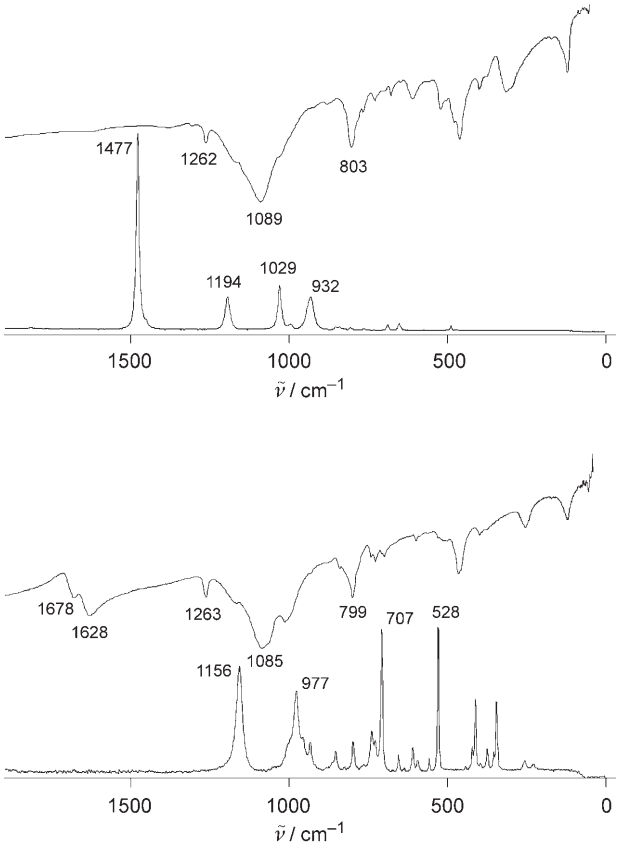


Figure 4. Vibrational spectra of $Li_2B_{12}C_2$ (top) and $LiB_{13}C_2$ (bottom).

Also unequivocal is the assignment of the strong IR band at 1628 cm^{-1} in the spectrum of $LiB_{13}C_2$ to the antisymmetric vibration of the CBC group. The weak shoulder at 1678 cm^{-1} is explained by isotopic splitting $^{10}B/^{11}B$ and supports this assignment. In $B_{13}C_2$ this band is observed at 1571 cm^{-1} (^{10}B: 1604 cm^{-1}; ^{11}B: 1558 cm^{-1}),[24b] in Al_3BC_3 at 1580 cm^{-1}.[10a] The lower frequencies reflect the slightly longer B–C distances ($B_{13}C_2$: 1.429 Å; Al_3BC_3: 1.441 Å). Because the modes are strongly coupled within the tight covalent framework of B_{12} icosahedra and C_2 and CBC units, a detailed assignment of the other bands is possible only on the basis of quantitative calculations, which are a part of our further investigations.[18b]

$Li_2B_{12}C_2$ and $LiB_{13}C_2$ are the first boron-rich boride carbides of lithium. As a distinct exception for this class of compounds, they are of stoichiometric composition and display a remarkably simple crystal structure. Both of the compounds can be separated by diluted aqueous HCl from the excess metallic melt, that is, in contrast to binary borides[7a,26] and carbides of lithium they are stable against acids and water. Both of the compounds are nearly colorless, which is also very unusual for boron-rich borides but agrees well with the simple electron-counting rules of Wade and Longuet-Higgins. The vibrational spectra can be explained based on the observed structural features. New properties can be expected, which are of great interest for the development of new materials for applications in, for example, ionic conductors (unusual long Li–B distances in $LiB_{13}C_2$), battery systems, thermoelectrics, superconductors (predicted for boron-rich borides[27]), nonoxidic ceramics, reactive ceramics, and composite materials.

Experimental Section

$Li_2B_{12}C_2$ and $LiB_{13}C_2$ were synthesized from the elements in a tin melt (molar ratio Sn/Li/B/C = 45:33:20:2 to 38:36:21:5, total mass: 1–1.5 g). BN crucibles (inner diameter: 12 mm, outer diameter: 14 mm; height: 3 cm) were welded into Ta ampules and heated up to 1300 °C for 70 h. The excess melt was removed with aqueous HCl. The residue contained in addition to black single crystals of Li_3B_{14}[7a,26] mainly well-developed, pale greenish single crystals of $Li_2B_{12}C_2$ (max. length: 1 mm) and a few colorless single crystals of $LiB_{13}C_2$ (max. 0.5 mm). For further investigations single crystals were separated manually under a microscope. Unlike $Li_2B_{12}C_2$, the crystals of $LiB_{13}C_2$ seemed to be attacked at the crystal edges and apices. Both compounds are stable against hydrolysis, which can be explained as follows. For kinetic reasons $LiB_{13}C_2$ is formed at the beginning of the synthesis; later on it is transformed to the thermodynamically more stable $Li_2B_{12}C_2$.

Characterization: Boron-rich borides have the tendency to take up additional elements. Because of the high reaction temperatures and the high reactivity of Li with contaminations (crucible, components of the melt, starting material) the incorporation of foreign elements must be taken into account. Therefore the composition of the single crystals was checked by WDX. For both of the compounds the absence of elements heavier than carbon was proved and the B/C ratio qualitatively confirmed.

The assignment of Li, B, and C on the basis of the structure refinement is clear. Refinements with free occupation factors for boron and carbon resulted in values between 99 and 102% with standard deviations of 1%. Thermal displacement parameters and *R* values confirm the assignment as well. Furthermore it is remarkable that the Li atoms can be localized unambiguously and refined

 © 2006 Wiley-VCH Verlag GmbH & Co. KGaA, Weinheim

with anisotropic thermal displacement parameters. There are no hints for disorder or incomplete occupation as is frequently observed for other compounds ($Li_2B_{12}C_2$: Li occupation 102(4)%; $LiB_{13}C_2$: Li occupation 102(4)%).

Vibrational spectra were recorded with a Bruker IFS66v FT-IR spectrometer equipped with a FT-Raman microscope (RFA106, Nd-YAG-Laser). WDX-measurements were conducted with a CAMECA SX 100 at the Institut für Mineralogie und Geochemie. The reference for the boron-to-carbon ratio was $Al_{2.7}B_{48}C_2$.[28] Special analyzer crystals for light elements were used, and the sample surface was treated with an oxygen jet to prevent contamination.

Received: July 4, 2005
Published online: November 22, 2005

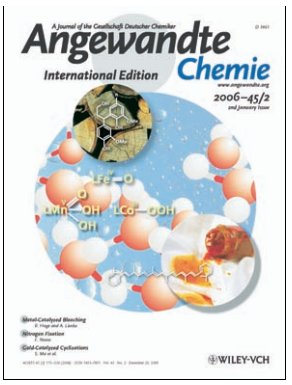
Keywords: boride carbides · lithium · solid-state structures · structure elucidation · vibrational spectroscopy

[1] a) V. I. Matkovich, *Boron and Refractory Borides*, Springer, Berlin, **1977**; b) T. Lundström in *Encyclopedia of Inorganic Chemistry* (Ed.: R. B. King), Wiley, New York, **1994**.
[2] a) K. K. Chawla, *Ceramic Composites*, Chapman & Hall, London, **1993**; b) "Structure and Properties of Composites": T. W. Chou in *Material Science and Technology, Vol. 13*, Verlag Chemie, Weinheim, **1993**.
[3] a) R. Riedel, *Adv. Mater.* **1994**, *6*, 549; b) R. Telle, *Chem. Unserer Zeit* **1988**, *22*, 93.
[4] a) D. C. Halverson, A. Pyzik, I. Aksay, *Ceram. Eng. Sci. Proc.* **1985**, *6*, 736; b) A. Pyzik, D. Beamon, *J. Am. Ceram. Soc.* **1995**, *78*, 305.
[5] a) D. Emin, *Phys. Today* **1987**, *40*, 55; b) G. A. Samara, H. L. Tardy, E. Venturini, T. L. Aselage, D. Emin, *Phys. Rev. B* **1993**, *48*, 1468.
[6] C. Wood, *Rep. Prog. Phys.* **1988**, *51*, 459.
[7] a) G. Mair, PhD Thesis, Universität Stuttgart, **1984**; b) M. Wöhrle, R. Nesper, G. Mair, M. Schwarz, H. G. von Schnering, *Z. Anorg. Allg. Chem.* **1995**, *621*, 1153.
[8] P. Rogl, *Phase Diagrams of Ternary Metal-Boron-Carbon Systems*, ASM, Ohio Park, **1998**.
[9] a) A. Ammar, M. Ménétrier, A. Villesuzanne, S. Matar, B. Chevalier, J. Etourneau, G. Villeneuve, J. Rodríguez-Carvajal, H.-J. Koo, A. I. Smirnov, M.-H. Whangbo, *Inorg. Chem.* **2004**, *43*, 4974; b) B. Albert, K. Schmitt, *Chem. Mater.* **1999**, *11*, 3406.
[10] a) H. Hillebrecht, F. Meyer, *Angew. Chem.* **1996**, *108*, 2655; *Angew. Chem. Int. Ed.* **1996**, *35*, 2499; b) H. Hillebrecht, M. Ade, *Angew. Chem.* **1998**, *110*, 981; *Angew. Chem. Int. Ed.* **1998**, *37*, 935; c) H. Hillebrecht, K. Gebhardt, *Angew. Chem.* **2001**, *113*, 1492; *Angew. Chem. Int. Ed.* **2001**, *40*, 1445; d) V. Adasch, K.-U. Hess, H. Hillebrecht, Ger. Offen. DE 102004014315A1 20050512, **2005** CAN 142:413894 AN 2005:408030.
[11] V. Adasch, PhD Thesis, Universät Bayreuth, **2005**.
[12] Structure solution and refinement: $Mo_{K\alpha}$ radiation, STOE-IPDS II, graphite monochromator, Lorentz and polarization corrections, no absorption correction, structure solution by direct methods in the programme package SHELXTL (G. M. Sheldrick, University Göttingen), refinement with SHELXTL; $Li_2B_{12}C_2$: orthorhombic, $a = 4.706(1)$, $b = 9.010(2)$, $c = 5.652(1)$ Å, space group $Amm2$, $Z = 2$, $2\theta_{max} = 70°$, $\mu = 0.09\ mm^{-1}$, 2658 measured reflections, 603 independent reflections with $I > 0$, 47 free parameters, $R_1(F) = 0.033$, $wR_2(I) = 0.082$, $+0.58/-0.30\ e^-\ Å^{-3}$; $LiB_{13}C_2$: orthorhombic, $a = 5.668(1)$, $b = 10.820(2)$, $c = 8.040(1)$ Å, space group $Imma$, $Z = 4$, $2\theta_{max} = 70°$, $\mu = 0.09\ mm^{-1}$, 6078 measured reflections, 607 independent reflections with $I > 0$, 46 free parameters, $R_1(F) = 0.041$, $wR_2(I) = 0.115$, $+0.84/-0.30\ e^-\ Å^{-3}$. Further details on the crystal structure investigation may be obtained from the Fachinformationszentrum Karlsruhe, 76344 Eggenstein-Leopoldshafen, Germany (fax: (+49) 7247-808-666; e-mail: crysdata@fiz-karlsruhe.de), on quoting the depository numbers CSD-415556 ($Li_2B_{12}C_2$) and -415557 ($LiB_{13}C_2$).
[13] a) F. X. Zhang, F. F. Xu, T. Mori, Q. L. Liu, T. Tanaka, *J. Solid State Chem.* **2003**, *170*, 75; b) J. R. Salvador, D. Bilc, S. D. Mahanti, M. G. Kanatzidis, *Angew. Chem.* **2002**, *114*, 872; *Angew. Chem. Int. Ed.* **2002**, *41*, 844.
[14] H. C. Longuet-Higgins, M. de V. Roberts, *Proc. R. Soc. London Ser. A* **1955**, *230*, 110.
[15] a) J.-F. Halet, J.-Y. Saillard, J. Bauer, *J. Less-Common Met.* **1990**, *158*, 239; b) Y. Shi, A. Leithe-Jasper, T. Tanaka, *J. Solid State Chem.* **1999**, *148*, 250.
[16] a) O. Oeckler, C. Jardin, H. Mattausch, A. Simon, J.-F. Halet, J.-Y. Saillard, J. Bauer, *Z. Anorg. Allg. Chem.* **2001**, *627*, 1389; b) C. Jardin, H. Hillebrecht, J. Bauer, J.-F. Halet, J.-Y. Saillard, R. Gaultier, *J. Solid State Chem.* **2003**, *176*, 609.
[17] A. Kirfel, A. Gupta, G. Will, *Acta Crystallogr. Sect. B* **1979**, *35*, 1052.
[18] a) R. Naslain, A. Guette, P. Hagenmüller, *J. Less-Common Met.* **1976**, *47*, 1; b) N. Vojteer, Diploma Thesis, Universität Freiburg, **2005**.
[19] B. Albert, K. Hofmann, C. Fild, H. Eckert, M. Schleifer, R. Gruehn, *Chem. Eur. J.* **2000**, *6*, 2531.
[20] a) I. Higashi, *J. Less-Common Met.* **1981**, *82*, 317; b) S. Okada, T. Tanaka, A. Sato, T. Shishido, K. Kudou, K. Nakajima, T. Lundström, *J. Alloys Compd.* **2005**, *395*, 231; c) V. Matkovich, J. Economy, *Acta Crystallogr. Sect. B* **1970**, *26*, 616; d) M. Korsukova, V. Gurin, *J. Alloys Compd.* **1992**, *187*, 39.
[21] D. R. Tallant, T. L. Aselage, A. N. Campbell, D. Emin, *Phys. Rev. B* **1989**, *40*, 5649.
[22] a) B. Hirsche, PhD Thesis, Universität Bayreuth, **2005**; b) J. R. Salvador, D. Blic, S. D. Mahanti, M. G. Kanatzidis, *Angew. Chem.* **2003**, *115*, 1973; *Angew. Chem. Int. Ed.* **2003**, *42*, 1929.
[23] T. Ludwig, H. Hillebrecht, *J. Solid State Chem.*, in press.
[24] a) H. Werheit, H. W. Rotter, F. D. Meyer, H. Hillebrecht, S. O. Shalamberidze, T. G. Abzianidze, G. G. Esadze, *J. Solid State Chem.* **2004**, *177*, 569; b) H. Werheit, T. Au, R. Schmechel, S. Shalamberidze, G. Kalandadze, A. Eristavi, *J. Solid State Chem.* **1999**, *145*, 79.
[25] J. Weidlein, U. Müller, K. Dehnicke, *Schwingungsfrequenzen I*, Thieme, Stuttgart, **1981**.
[26] G. Mair, R. Nesper, H.-G. von Schnering, *J. Solid State Chem.* **1988**, *75*, 30.
[27] S. Gunji, H. Kamimura, *Phys. Rev. B* **1996**, *54*, 13665.
[28] F. D. Meyer, PhD Thesis, Universität Freiburg, **1998**.

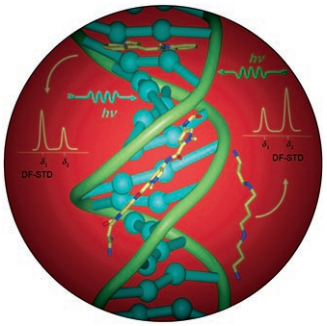
 © 2006 Wiley-VCH Verlag GmbH & Co. KGaA, Weinheim

Cover Picture

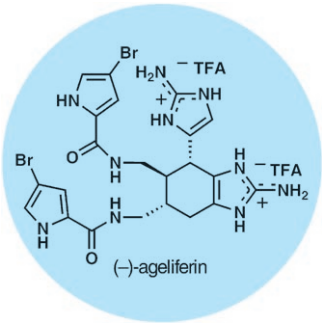
Ronald Hage* and Achim Lienke*



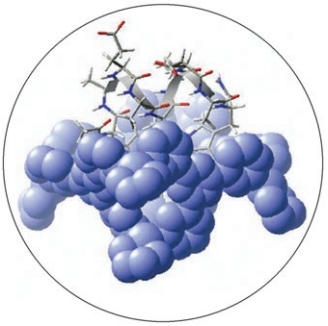
Bleaching catalysts accelerate the removal of a variety of unwanted chromophores present in stains or wood pulp. The cover picture shows the structures of lignin residues from wood pulp and of lycopene which is found in tomato stains. Peroxo–metal and oxo–metal species are proposed as intermediates in the various catalytic cycles. In their Review on page 206 ff. R. Hage and A. Lienke show that a large variety of transition-metal complexes enhance the activity of H_2O_2 or O_2 towards stain or wood-pulp bleaching.



NMR Analysis
A bioanalytical NMR spectroscopic method allows the coordination of small molecules to DNA to be investigated and differences in bonding to be determined. L. Gomez-Paloma and co-workers describe this approach in their Communication on p. 224 ff.



Natural Products Synthesis
The marine alkaloids sceptrin and ageliferin are prepared by an enantioselective total synthesis. The synthetic pathway, which does not require any auxiliaries, is described by P. S. Baran et al. in their Communication on p. 249 ff.



Host–Guest Complexes
Hydrophobic and electrostatic interactions stabilize the host–guest complex of a peptide in an organometallic bowl. M. Fujita and co-workers explain in their Communication on p. 241 ff. why the complexed peptide retains its α-helical conformation.

Contents

VIP *The following Communications have been judged by at least two referees to be "very important papers" and will be published online at www.angewandte.org soon:*

*J. Deschamp, O. Chuzel, J. Hannedouche, O. Riant**
Highly Diastereo- and Enantioselective Copper-Catalyzed Tandem Conjugated Reduction/Aldol Reaction to Ketones

J. W. Bode, R. M. Fox, K. D. Baucom*
Chemoselective Amide Ligations by Decarboxylative Condensations of *N*-Alkylhydroxylamines and α-Keto Acids

A. Oleksi, A. G. Blanco, R. Boer, I. Usón, J. Aymamí, A. Rodger, M. J. Hannon, M. Coll**
Molecular Recognition of a Three-Way DNA Junction by a Metallosupramolecular Helicate

J. E. Banham, C. R. Timmel, R. J. M. Abbott, S. M. Lea, G. Jeschke**
A New Tool for Characterization of Weak Protein–Protein Interactions: Evidence from DEER for the Trimerization of a von Willebrand Factor A Domain in Solution

B. H. Lipshutz, B. A. Frieman, A. E. Tomaso, Jr.*
Copper-in-Charcoal (Cu/C): Heterogeneous, Copper-Catalyzed Asymmetric Hydrosilylations

J. T. Shaw, J. M. Mitchell*
A Structurally Diverse Library of Polycyclic Lactams Resulting from the Systematic Placement of Proximal Functional Groups

Meeting Reviews

Asymmetric Synthesis from a Chemical and Biological View — *B. Plietker* — **190**

Obituary

Ivar K. Ugi (1930–2005): Multicomponent Reactions, Computer and Phosphorus Chemistry — *P. Lemmen, E. Fontain, J. Bauer* — **193**

Books

Handbook of Functionalized Organometallics — Paul Knochel — *reviewed by H. Yorimitsu* — **194**

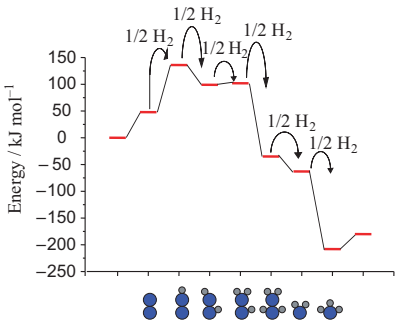
Highlights

Reaction Mechanisms

F. Neese* — **196–199**

The Yandulov/Schrock Cycle and the Nitrogenase Reaction: Pathways of Nitrogen Fixation Studied by Density Functional Theory

Doubling up: Converging results from theory and experiments on model systems as well as the nitrogenase active site have recently given new clues as to how it is possible to split the N≡N bond under ambient conditions during the conversion of nitrogen into ammonia. Quantum chemical methods have been shown to be key to studying reaction mechanisms and unstable intermediates (see graph) which are difficult to characterize experimentally.

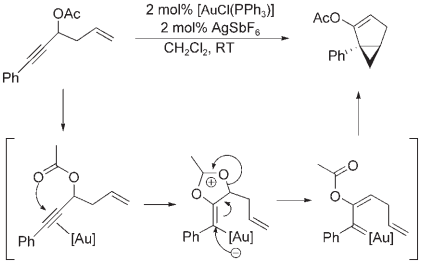


Homogeneous Catalysis

S. Ma,* S. Yu, Z. Gu — **200–203**

Gold-Catalyzed Cyclization of Enynes

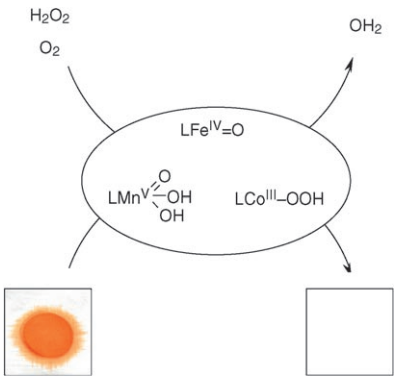
The key step in the gold-catalyzed cycloisomerization of enynes is the nucleophilic attack at the Au-coordinated C–C triple bonds to form a vinylic gold intermediate (see example). The homogeneous gold-catalyzed reaction of enynes under mild conditions has wide scope and high efficiency and gives access to complex or otherwise inaccessible products.



WILEY InterScience DISCOVER SOMETHING GREAT
© 2006 Wiley-VCH Verlag GmbH & Co. KGaA, Weinheim

Reviews

Stain removal: The bleaching of textiles and paper are amongst the most important industrial oxidation processes. Chlorine-based bleaching agents, however, can damage the fibers and lead to chlorinated waste products, and H_2O_2 is expensive and less efficient. Transition-metal catalysts based on Fe, Mn, or Co, which activate H_2O_2 or O_2 (see picture), offer an alternative. In this way, it should be possible to achieve savings both in terms of the amount of chemicals and the energy required for bleaching processes.



Bleaching Processes

R. Hage,* A. Lienke* ____ **206 – 222**

Applications of Transition-Metal Catalysts to Textile and Wood-Pulp Bleaching

Communications

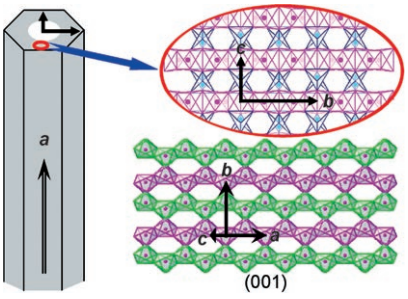


Vive la différence! The binding of small molecules of pharmaceutical interest to DNA can be screened by differential-frequency saturation transfer difference spectroscopy (DF-STD). The technique allows the probing of DNA recognition phenomena, such as those of base-pair intercalators, minor groove binders, and external backbone binders (see picture).

DNA Binding

S. Di Micco, C. Bassarello, G. Bifulco, R. Riccio, L. Gomez-Paloma* **224 – 228**

Differential-Frequency Saturation Transfer Difference NMR Spectroscopy Allows the Detection of Different Ligand–DNA Binding Modes



Carbon-assisted thermal coevaporation of In_2O_3 and GeO_2 generates monocrystalline, sub-micrometer $In_2Ge_2O_7$ tubes with a laminar crystal structure (see figure). Within an $In_2Ge_2O_7$ tube, the $\{InO_6\}$ octahedron laminae are parallel to the [100] growth direction. These structures may find applications in waveguides or microlasers since their diameters are close to the wavelength and mean free path of appropriate photons.

Nanotubes

J. Zhan,* Y. Bando, J. Hu, L. Yin, X. Yuan, T. Sekiguchi, D. Golberg ____ **228 – 231**

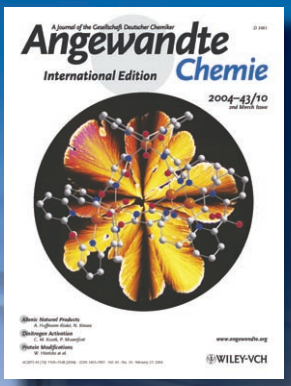
Hollow and Polygonous Microtubes of Monocrystalline Indium Germanate

For the USA and Canada:
ANGEWANDTE CHEMIE International Edition (ISSN 1433-7851) is published weekly by Wiley-VCH PO Box 191161, D 69451 Weinheim, Germany. Air freight and mailing in the USA by Publications Expediting Inc. 200 Meacham Ave., Elmont, NY 11003. Periodicals postage paid at Jamaica NY 11431. US POSTMASTER: send address changes to *Angewandte Chemie*, Wiley-VCH, 111 River Street, Hoboken, NJ 07030. Annual subscription price for institutions: US$ 5685/5168 (valid for print and electronic / print or electronic delivery); for individuals who are personal members of a national chemical society prices are available on request. Postage and handling charges included. All prices are subject to local VAT/sales tax.

© 2006 Wiley-VCH Verlag GmbH & Co. KGaA, Weinheim

The best in chemistry –

for more than a hundred years



A Journal of the Gesellschaft Deutscher Chemiker

Angewandte
International Edition Chemie

www.angewandte.org

1888: ***The beginning of a success story***

Constant Innovations

1962: *First issue of the International Edition*
1976: *Graphical abstracts*
1979: *Cover pictures*
1988: *Centenary of Angewandte*
1989: *Routine use of color*
1991: *New section: Highlights*
1992: *Computerized editorial tracking system*
1995: *Internet service for readers*
1998: *Regular press service; full-text online*
2000: *New section: Essays; EarlyView: Communications available online ahead of the printed version*
2001: *New section: Minireviews*
2002: *Online submission of manuscripts*
2003: *Weekly publication; new section: News; new layout*
2004: *Backfiles (1962-1997); ManuscriptXpress: Online system for authors and referees*



Angewandte's advisors...

Roald Hoffmann
Cornell University
(Photo: Lois Anshus)

» As an applied theoretical chemist, I love it that the best chemical journal in the world has „applied" in its title. It's history, I know. But there is also the implication in this adjective that these sterling accounts of the new, these just-in-time reviews, these incisive essays that ***Angewandte Chemie*** *contains – that they all are of true utility, and are really used, by the finest chemists of our time. «*

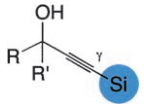
Angewandte Chemie International Edition *is a journal of the German Chemical Society (GDCh)*

GDCh

WILEY InterScience® DISCOVER SOMETHING GREAT

WILEY-VCH

11951404_gu

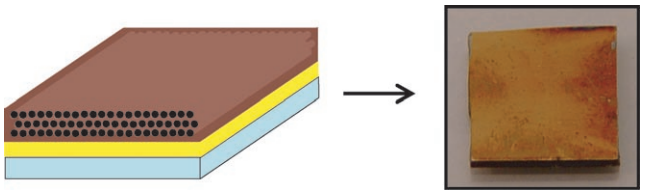


Making the right substitution: A remarkable acceleration effect of phenyl-substituted silyl groups in hydroalumination and carbolithiation reactions of propargylic alcohols (see formula) is described. The results show that an aryl silyl group can act not only as a protecting group but also as an activating group of the alkynyl moiety. This work provides an efficient group-selective approach to multifunctionalized alkenes.

Hydroalumination

K. Igawa, K. Tomooka* ——— **232 – 234**

γ-Silyl Group Effect in Hydroalumination and Carbolithiation of Propargylic Alcohols

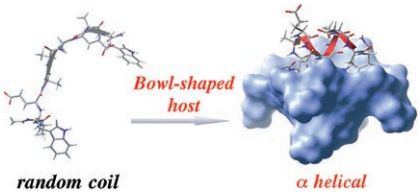


Inorganic cluster anions (Zintl ions) have been cross-linked by transition metals in the presence of alkyl ammonium surfactants and gold substrates to produce nanostructured thin films (see picture). These films display a variety of phases, including hexagonal, cubic, lamellar, and wormlike. Optical measurements show that the films are semiconductors, and *I*–*V* measurements indicate rectifying behavior.

Nanostructures

A. E. Riley, S. D. Korlann, E. K. Richman, S. H. Tolbert* ——— **235 – 241**

Synthesis of Semiconducting Thin Films with Nanometer-Scale Periodicity by Solution-Phase Coassembly of Zintl Clusters with Surfactants

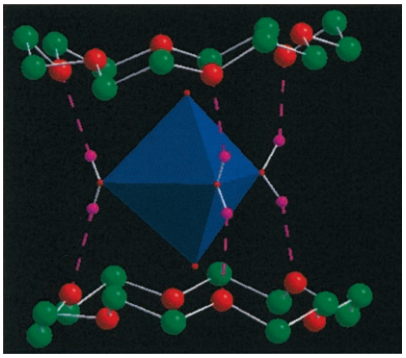


In a twist: Encapsulation of a nine-residue peptide (Trp-Ala-Glu-Ala-Ala-Ala-Glu-Ala-Trp) within a bowl-shaped coordination host in water induces and stabilizes the α-helical conformation. The α-helical peptide is recognized through two types of host–guest interactions: a hydrophobic interaction with both terminal Trp residues and electrostatic interactions between the Glu residues and the high positive charge of the host (12+).

Host–Guest Systems

S. Tashiro, M. Tominaga, Y. Yamaguchi, K. Kato, M. Fujita* ——— **241 – 244**

Folding a De Novo Designed Peptide into an α Helix through Hydrophobic Binding by a Bowl-Shaped Host



Copper crowned: A trigonal-bipyramidal $[Cu(H_2O)_5]^{2+}$ ion, which is inserted between two crown ether molecules ([18]crown-6) to form a unique supramolecular sandwich, $[Cu(H_2O)_5([18]crown\text{-}6)_2]^{2+}$ (see picture), has been characterized unambiguously by single-crystal X-ray diffraction. Isopolyanions, $[Mo_6O_{19}]^{2-}$, facilitate the formation of this new structure.

Supramolecular Chemistry

V. Shivaiah, S. K. Das* ——— **245 – 248**

Fivefold Coordination of a Cu^{II}–Aqua Ion: A Supramolecular Sandwich Consisting of Two Crown Ether Molecules and a Trigonal-Bipyramidal $[Cu(H_2O)_5]^{2+}$ Complex

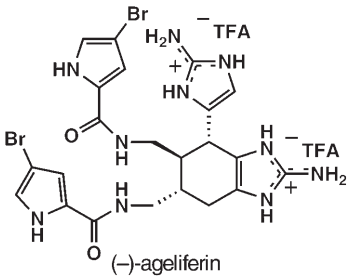
© 2006 Wiley-VCH Verlag GmbH & Co. KGaA, Weinheim

Contents

Asymmetric Synthesis

P. S. Baran,* K. Li, D. P. O'Malley, C. Mitsos ——— **249 – 252**

Short, Enantioselective Total Synthesis of Sceptrin and Ageliferin by Programmed Oxaquadricyclane Fragmentation

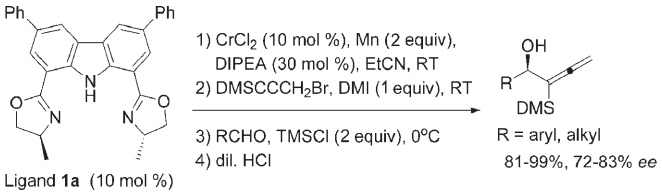


Absolutely without auxiliaries: The enantioselective syntheses of both enantiomers of the dimeric pyrrole–imidazole alkaloids sceptrin and ageliferin have been achieved by a non-auxiliary-based route, which allows assignment of the absolute configuration of natural ageliferin. The "programming" of the oxaquadricyclane fragmentation leading to enantiopure tetrasubstituted cyclobutanes is the crucial step in the synthesis.

Asymmetric Catalysis

M. Inoue, M. Nakada* ——— **252 – 255**

Studies into Asymmetric Catalysis of the Nozaki–Hiyama Allenylation

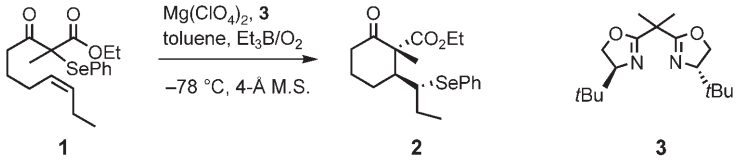


From aldehydes to allenic alcohols: Studies into the asymmetric catalysis of the Nozaki–Hiyama allenylation are described. Ligand **1a** is effective for the enantioselective allenylations of various aldehydes, with the generation of products with *ee* values ranging from 72–83%. The products can be easily desilylated or used as allenylsilanes. DIPEA = diisopropylethylamine, DMI = 1,3-dimethyl-2-imidazolidinone, DMS = dimethylsilyl, TMS = trimethylsilyl.

Radical Cyclization

D. Yang,* B.-F. Zheng, Q. Gao, S. Gu, N.-Y. Zhu ——— **255 – 258**

Enantioselective PhSe-Group-Transfer Tandem Radical Cyclization Reactions Catalyzed by a Chiral Lewis Acid



1 2 3

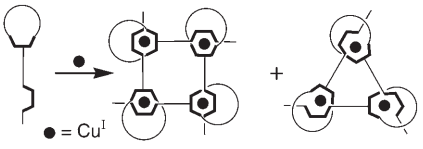
A radical change: α-Phenylselenyl-β-ketoesters (e.g., **1**) undergo radical cyclization in the presence of a chiral Lewis acid complex $Mg(ClO_4)_2$–**3** with Et_3B/O_2 as the radical initiator. Monocyclic compounds, such as **2** (or bicyclic products from diene precursors), were obtained in good yields (33–82%) with 65–97% *ee* in this first enantioselective PhSe-group-transfer radical cyclization.

Supramolecular Chemistry

T. Kraus, M. Buděšínský, J. Cvačka, J.-P. Sauvage* ——— **258 – 261**

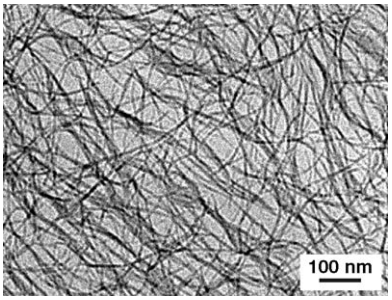
Copper(I)-Directed Formation of a Cyclic Pseudorotaxane Tetramer and Its Trimeric Homologue

A matter of concentration: Cyclic pseudorotaxanes are formed by the addition of copper(I) ions to a ligand consisting of a ring containing a chelating unit and, appended to the ring, a rigid fragment containing another chelating unit. The tetramer is formed as the major product in concentrated solution, and the analogous trimer prevails in more dilute solution; both species are connected through a concentration-dependent slow equilibrium.



© 2006 Wiley-VCH Verlag GmbH & Co. KGaA, Weinheim

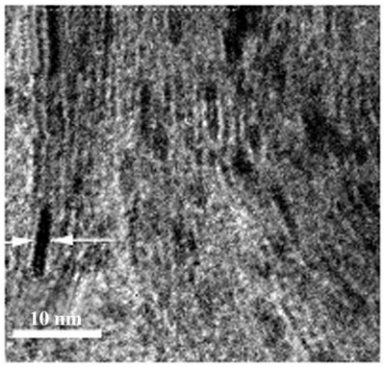
A nonaqueous approach that involves the reaction of tungsten isopropoxide with benzyl alcohol leads to tungsten oxide nanowire bundles without the use of any additional structure-directing templates. The bundles consist of crystalline nanowires with highly uniform diameters of about 1 nm and aspect ratios exceeding 500 (see picture). Gas-sensing tests show a high sensitivity to NO_2.



Nanostructures

J. Polleux, A. Gurlo, N. Barsan, U. Weimar, M. Antonietti, M. Niederberger* ——— **261 – 265**

Template-Free Synthesis and Assembly of Single-Crystalline Tungsten Oxide Nanowires and their Gas-Sensing Properties



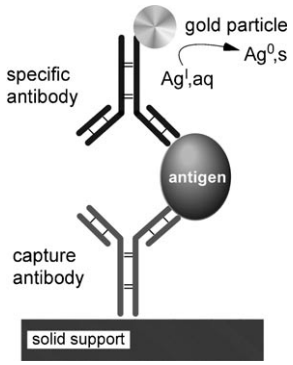
In three steps to ruthenium-based heterogeneous catalysts: The central element of this novel and simple route is the immobilization of Ru^0 nanoparticles on montmorillonite (see picture; the arrows indicate a Ru nanoparticle intercalated in the interlaminar space of montmorillonite) with the help of an ionic liquid. The resulting catalyst is highly efficient for the hydrogenation of benzene.

Catalytic Hydrogenation

S. Miao, Z. Liu,* B. Han, J. Huang, Z. Sun, J. Zhang, T. Jiang ——— **266 – 269**

Ru Nanoparticles Immobilized on Montmorillonite by Ionic Liquids: A Highly Efficient Heterogeneous Catalyst for the Hydrogenation of Benzene

Read the fine print: Biomolecular binding events can be counted with a readout system based on compact disc (CD) pickup technology. An immunoassay of C-reactive protein was performed by microcontact printing of antibodies onto a support, autometallography, and imaging by a CD reader mounted on an optical microscope (see picture). The dynamic range was four orders of magnitude with a detection limit of 1 pM.

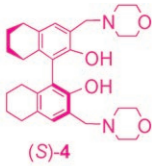


Bioassay Imaging

S. A. Lange, G. Roth, S. Wittemann, T. Lacoste, A. Vetter, J. Grässle, S. Kopta, M. Kolleck, B. Breitinger, M. Wick, J. K. H. Hörber, S. Dübel, A. Bernard* ——— **270 – 273**

Measuring Biomolecular Binding Events with a Compact Disc Player Device





All sorts of aldehydes **2** (R = aryl, vinyl, branched, and linear alkyl) undergo the highly enantioselective addition of diphenylzinc (**1**) in the presence of catalytic (*S*)-**4** to give α-substituted benzyl alcohols **3** in high yields. In contrast to previous catalysts, no additive is required, the reaction is carried out at room temperature, and the reaction is equally effective with linear aldehydes.

Asymmetric Addition

Y.-C. Qin, L. Pu* ——— **273 – 277**

Highly Enantioselective Addition of Diphenylzinc to Aliphatic and Aromatic Aldehydes Catalyzed by a Readily Available H_8-Binol Derivative

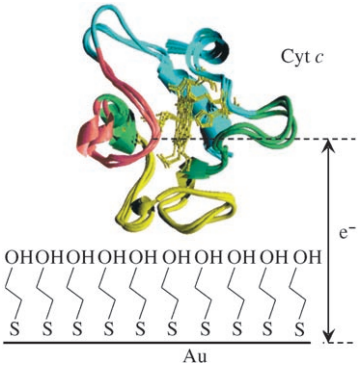
© 2006 Wiley-VCH Verlag GmbH & Co. KGaA, Weinheim

Contents

Charge Transfer

D. E. Khoshtariya,* T. D. Dolidze, D. Sarauli, R. van Eldik* ——— **277 – 281**

High-Pressure Probing of a Changeover in the Charge-Transfer Mechanism for Intact Cytochrome *c* at Gold/Self-Assembled Monolayer Junctions



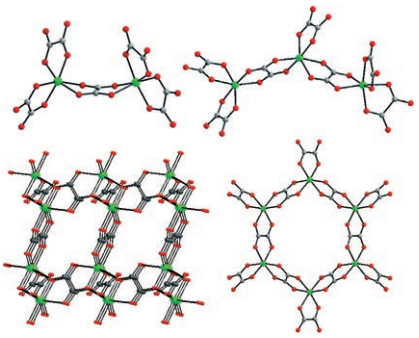
Free trade: The electron exchange of cytochrome *c* freely diffusing to gold electrodes modified by hydroxy-terminated alkanethiol self-assembled monolayers (SAMs; see picture) is examined by high-pressure kinetic studies. The SAM thickness, solution viscosity, and hydrostatic pressure influence a changeover in the charge-transfer mechanism and the corresponding kinetic response.

Open-Framework Structures

M. Dan, C. N. R. Rao* ——— **281 – 285**

A Building-Up Process in Open-Framework Metal Carboxylates that Involves a Progressive Increase in Dimensionality

Zero- and one-dimensional metal carboxylates are shown to transform into higher-dimensional structures (see figure), thereby indicating the presence of a progressive building-up process.

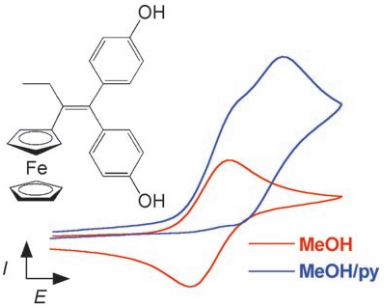


Antitumor Agents

E. Hillard, A. Vessières, L. Thouin, G. Jaouen,* C. Amatore* ——— **285 – 290**

Ferrocene-Mediated Proton-Coupled Electron Transfer in a Series of Ferrocifen-Type Breast-Cancer Drug Candidates

A double-barreled approach: The addition of ferrocene to an antiestrogen drug skeleton was found to induce cytotoxicity towards breast-cancer cells that are resistant to the common antiestrogen drug. The efficacy of this drug has been related to the proton-coupled electron transfer observed in the presence of pyridine as a base (see picture).

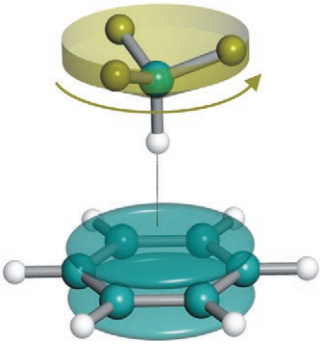


Molecular Complexes

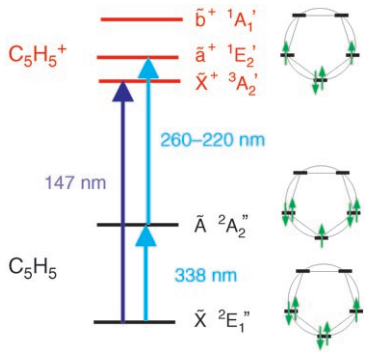
J. C. López, W. Caminati, J. L. Alonso* ——— **290 – 293**

The C–H···π Hydrogen Bond in the Benzene–Trifluoromethane Adduct: A Rotational Study

Free to rotate: The rotational spectrum of unlabeled and ^{13}C-labeled benzene species reveals that the benzene–trifluoromethane complex is stabilized by a CH···π weak hydrogen bond and undergoes an almost-free rotation of the two subunits with respect to each other (see picture). The estimated dissociation energy is 8.4 kJ mol^{-1}.



© 2006 Wiley-VCH Verlag GmbH & Co. KGaA, Weinheim

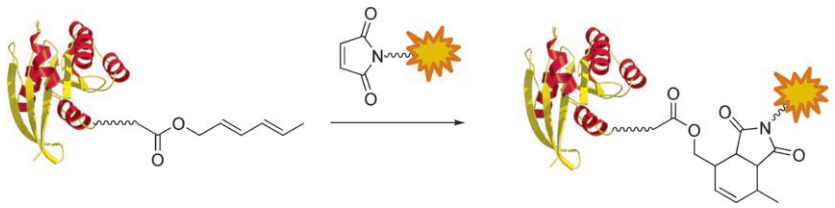


From radical to biradical: The pulsed-field-ionization zero-kinetic-energy photoelectron spectrum of the C_5H_5 radical is recorded after direct excitation from the $\tilde{X}\,{}^2E_1''$ ground state and two-photon excitation via the $\tilde{A}\,{}^2A_2''$ electronically excited state. The intensity distributions of the spectra enables the characterization of the energetics, symmetry, and structure of the lowest two electronic states of the cation (see picture).

Photoelectron Spectroscopy

H. J. Wörner, F. Merkt* ——— **293 – 296**

Photoelectron Spectroscopic Study of the First Singlet and Triplet States of the Cyclopentadienyl Cation

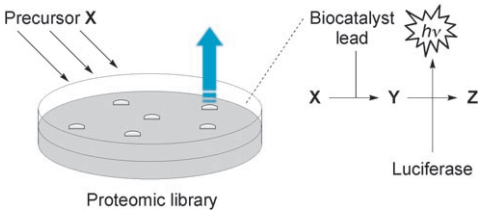


Mild attachment: Proteins can be ligated chemoselectively and immobilized on functionalized glass surfaces by means of Diels–Alder cycloadditions (see scheme).

Protein Ligation

A. D. de Araújo, J. M. Palomo, J. Cramer, M. Köhn, H. Schröder, R. Wacker, C. Niemeyer, K. Alexandrov, H. Waldmann* ——— **296 – 301**

Diels–Alder Ligation and Surface Immobilization of Proteins

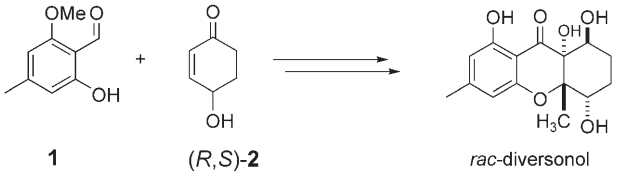


Seeing the light: The use of a coupled assay with bacterial luciferase results in a common light-emission screen for a variety of potential biotransformations. Screening the *E. coli* proteome for the oxidation of simple alcohols to good and bad luciferase substrates reveals examples of substrate ambiguity and catalytic promiscuity. Reactions leading to aldehydes can easily be screened by this method.

Biocatalysis

G. Krebs, L. Hugonet, J. D. Sutherland* ——— **301 – 305**

Substrate Ambiguity and Catalytic Promiscuity Within a Bacterial Proteome Probed by an Easy Phenotypic Screen for Aldehydes



Mission accomplished. The fungal metabolite diversonol has been synthesized for the first time. A key step in the total synthesis was the domino oxa-Michael–aldol condensation of salicylic aldehyde **1** and 4-hydroxycyclohexenone (**2**) that afforded the tricyclic scaffold of the target compound.

Natural Product Synthesis

C. F. Nising, U. K. Ohnemüller (née Schmid), S. Bräse* ——— **307 – 309**

The Total Synthesis of the Fungal Metabolite Diversonol

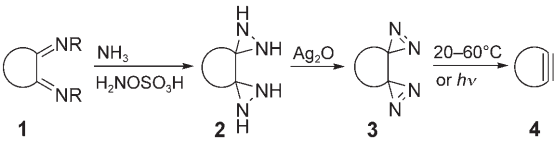
© 2006 Wiley-VCH Verlag GmbH & Co. KGaA, Weinheim

Contents

Strained Molecules

M. Al-Omari, K. Banert,*
M. Hagedorn ——— 309 – 311

Bi-3*H*-diazirin-3-yls as Precursors of Highly Strained Cycloalkynes



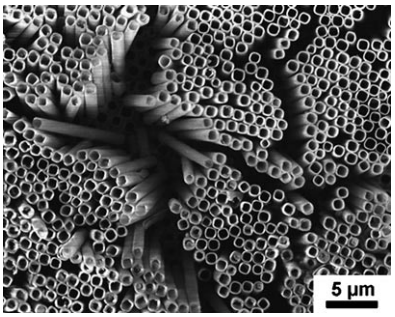
No reagents and very mild conditions are required for the transformation of isolable precursors **3** into highly strained cycloalkynes **4** (cycloheptyne, cycloheyxne, norbornyne), which can be trapped by cycloaddition reactions.

Inorganic Nanotubes

L. Zhao, M. Yosef, M. Steinhart, P. Göring, H. Hofmeister, U. Gösele, S. Schlecht* ——— 311 – 315

Porous Silicon and Alumina as Chemically Reactive Templates for the Synthesis of Tubes and Wires of SnSe, Sn, and SnO_2

Three in one: Ordered nanostructures of SnSe, SnO_2, and elemental tin (see SEM image) were prepared by template-assisted synthesis in porous alumina and macroporous silicon. The use of the templates as chemical reactants allowed the preparation of all three target materials from the same single-source precursor, $Sn(SePh)_4$.

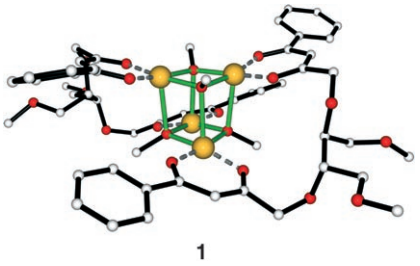


Chiral Cubanes

R. W. Saalfrank,* C. Schmidt, H. Maid, F. Hampel, W. Bauer, A. Scheurer* ——— 315 – 318

Enantiomerically Pure Copper(II) Cubanes $[Cu_4L_2(OMe)_4]$ from Chiral Bis-(1,3-diketones) H_2L through Diastereoselective Self-Assembly

Loaded dice: Copper cubanes **1** and *ent*-**1** were generated in a one-pot reaction by diastereoselective self-assembly, starting from ligands derived from L- and D-tartaric acid, respectively. Both structures were confirmed by X-ray structure analysis.

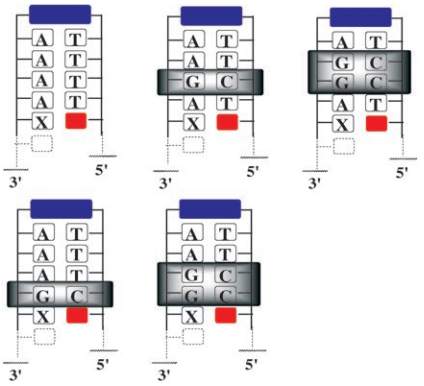


Electron Transfer

A. Manetto, S. Breeger, C. Chatgilialoglu, T. Carell* ——— 318 – 321

Complex Sequence Dependence by Excess-Electron Transfer through DNA with Different Strength Electron Acceptors

An independent jump: Excess electrons move through DNA by using a hopping-type mechanism in which the pyrimidine bases dT and dC act as 'stepping stones'. It was shown that GC base pairs, in contrast to AT base pairs, lower the efficiency of the excess-electron transfer through the duplex. Through the use of the shown DNA hairpins, three different electron acceptors (■) were investigated with the electron donor, reduced flavin (■).



© 2006 Wiley-VCH Verlag GmbH & Co. KGaA, Weinheim

Sources

Product and Company Directory

You can start the entry for your company in "Sources" in any issue of *Angewandte Chemie*.

If you would like more information, please do not hesitate to contact us.

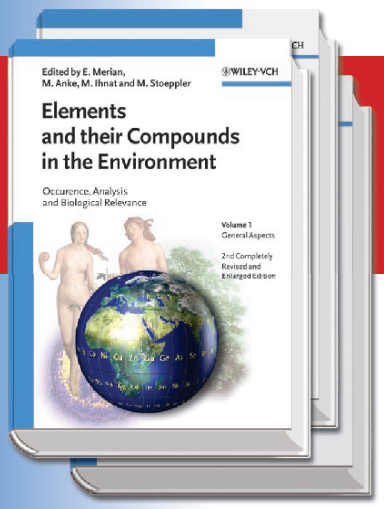
Wiley-VCH Verlag – Advertising Department
Tel.: 0 62 01 - 60 65 65
Fax: 0 62 01 - 60 65 50
E-Mail: MSchulz@wiley-vch.de

Service

Keywords ____ 322

Authors ____ 323

Preview ____ 325



The Second Edition!

Elements and their Compounds in the Environment

Occurrence, Analysis and Biological Relevance

2nd completely revised and enlarged edition
3 Volume Set

Edited by E. MERIAN, M. ANKE, M. IHNAT and M. STOEPPLER

- The "Merian" is the established standard reference on this topic.
- This new edition is more clearly and concisely structured, with more emphasis on nutritional aspects.
- All contributions are revised and updated to present the current state of knowledge.
- Further elements, including some non-metals of nutritional importance, have been added.
- Essential information for chemists, biologists, geologists, food scientists, toxicologists and physiologists involved in environmental research and remediation, risk assessment, food research and industrial hygiene.

For your order:

3527-30459-2 2004
1774pp with 97 figs and 377 tabs
Hbk
€ 599.00 /£ 415.00 /US$ 810.00

Wiley-VCH,
Customer Service Department,
Fax: +49 (0) 6201 606-184,
E-Mail: service@wiley-vch.de,
www.wiley-vch.de

John Wiley & Sons, Ltd., Customer Services Department, Fax: +44 (0) 1243-843-296,
E-Mail: cs-books@wiley.co.uk,
www.wiley.com

John Wiley & Sons, Inc., Customer Care,
Fax: +1 800-597-3299,
E-Mail: custserv@wiley.com,
www.wiley.com

WILEY-VCH

WILEY

i6122412_gu

© 2006 Wiley-VCH Verlag GmbH & Co. KGaA, Weinheim



Asymmetric Synthesis from a Chemical and Biological View**

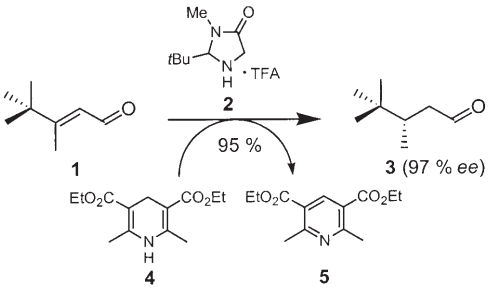
*Bernd Plietker**

On October 10–11, 2005, the Collaborative Research Center (Sonderforschungsbereich, SFB) in Aachen (Germany) held its 9th SFB Symposium. This meeting marked the endpoint of the ten-year-long research program at the Collaborative Research Center entitled "Asymmetric Synthesis with Chemical and Biological Methods". Nearly 700 participants from 20 countries attended the meeting, which featured outstanding lectures from both the fields of organic and bioorganic chemistry as well as various poster presentations.

After a short welcome note by the spokesman of the Collaborative Research Center, Dieter Enders (RWTH Aachen), the scientific program was opened with a lecture by Dieter Seebach (ETH Zürich, Switzerland) on peptide chemistry. His talk spanned his early investigations on asymmetric synthesis to the structure of β- and γ-peptides. The question posed with a wink of the eye in the title "*Peptide Chemistry—A Synthetic Organic Chemist Gone Astray?*" was answered in many ways. Besides answering the question of the stereoselective formation of non-natural β-amino acids, he provided details of his investigations on the structure of substituted β-peptides.[1] He described the selective generation of new helical structures that display low biological activity but remain for long periods of time in eucaryontic cells. He emphasized the fact that only this cell type experienced an enrichment of the new peptide structures. Their persistence in these cells may hint at an irreversible binding of these novel peptides to the DNA of the cell.

This excursion into the complex world of peptides and macromolecules was followed by a lecture by Hisashi Yamamoto (University of Chicago, USA) on the possibilities of acid-assisted Lewis and Brønsted acid catalysis in asymmetric synthesis. The focus was placed on the description of cooperative effects between both types of acid. Examples from the field of Brønsted acid assisted activation of Lewis acids, Brønsted acid assisted activation of Brønsted acids, Lewis acid assisted activation of Brønsted acids, and Lewis acid assisted activation of Lewis acids were discussed in detail. Yamamoto demonstrated that activation of the acid catalyst by an acid is a fundamental requirement for a high degree of asymmetric induction. The field of organocatalysis was complemented by the subsequent lecture given by David MacMillan (California Institute of Technology, USA), who presented a chronological overview of his work starting from the amine-catalyzed Diels–Alder reaction to new reactions in the presence of amine catalysts. He also highlighted the organocatalytic enantioselective reductions of α,β-unsaturated carbonyl compounds **1** using a Hantzsch ester **4** as a hydride source, as developed almost simultaneously by his group and that of List (Scheme 1).[2] Further examples of hydride transfers in organocatalytic reductive aminations in the presence of chiral phosphoric acid diesters concluded his lecture.

Manfred Reetz (Max Planck Institute for Coal Research, Germany) reflected on organocatalytic procedures in his talk on the directed evolution of enzymes. He reported the development of fast and more-efficient directed evolution techniques and underlined the importance of this methodology for asymmetric catalysis. Nowadays, the structural variation of wild-type enzymes in combination with the use of new high-throughput screening methods allows the generation of a variety of mutants and their evaluation in a minimum amount of time. To further decrease the timeframes, Reetz and coworkers have used the CAST process (combinatorial active-site saturation test). The basic requirement for a directed mutagenesis within a CAST process is the localization of the active binding site (based upon 3D models), the subsequent identification of spatially close amino acid residues pointing into the active site, and the concluding randomization of two to three amino acid residues (Figure 1).[3] This technology may be regarded as a practical compromise between single- and multisite mutagenesis and guarantees both a good structural diversity and a useful amount of new mutants.



Scheme 1. Asymmetric reduction of α,β-unsaturated aldehydes.

[*] Priv.-Doz. Dr. B. Plietker
Organische Chemie II, FB Chemie
Universität Dortmund
Otto-Hahn-Strasse 6
D-44221 Dortmund (Germany)
E-mail: bernd.plietker@uni-dortmund.de

[**] 9th International SFB Symposium "Asymmetric Synthesis with Chemical and Biological Methods", Aachen, Germany, October 10–11, 2005.

WILEY InterScience DISCOVER SOMETHING GREAT
© 2006 Wiley-VCH Verlag GmbH & Co. KGaA, Weinheim

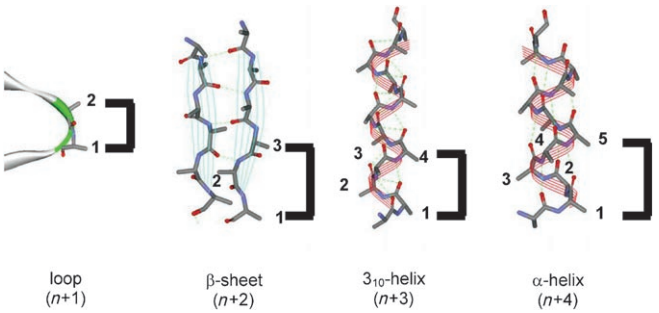
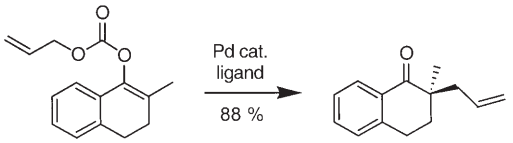


Figure 1. Design of enzyme libraries by CAST.

Chi Huey Wong (Scripps Research Institute, USA) presented a talk on protein glycosidations, with an emphasis on the important role of carbohydrates in molecular recognition processes in proteins and the synthesis of protein–carbohydrate conjugates. He showed how a variation in the carbohydrate unit can influence biological functions as well as signal cascades. Besides the modification of molecular recognition processes, the biological activity of carbohydrate-containing natural products can also be changed by a simple variation of the sugar moiety. Vancomycine serves as a prominent example for this fact. A change in the carbohydrate unit led to high cytotoxic activity against vancomycine-resistant bacteria such as *Enterococci*.[4]

Günther Helmchen (University of Heidelberg, Germany) and Barry Trost (Stanford University, USA) both discussed the chemistry of allyl–transition-metal complexes. Helmchen guided the audience into the depth of this field in organometallic chemistry. Detailed investigations on the mechanism of palladium- and iridium-catalyzed allylic alkylations highlighted the complexity of these reactions. Iridium-catalyzed, regioselective allylic alkylation and amination reactions in the presence of chiral phosphoramidite ligands as developed by Helmchen and co-workers impressively underlined the importance of mechanistic investigations.[5] In contrast, Trost focused on the role of the nucleophile rather than the allyl moiety in his talk. He demonstrated different strategies for the selective formation of a stereocenter at the nucleophile by means of a palladium-catalyzed allylic alkylation, such as the selective α-allylation of alloc-substituted enol ethers such as **6** (Scheme 2). The allyl moiety of the carbonate functions as a electrophile. However, investigations indicated



6 **7** (99 % *ee*)

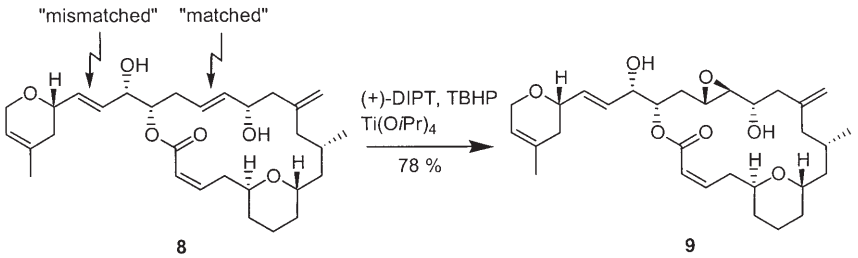
Scheme 2. Palladium-catalyzed allylation of allyl enol carbonates.

an alternative π-allyl–palladium mechanism to take place in which the nucleophile adds to the allyl moiety from the palladium in a reductive elimination process.[6]

Steven Ley (University of Cambridge, UK) dealt with immobilized reagents and their application in the development of "synthesis machines". Completely mechanical purification allows a variety of processes to be automated and assembled to give indeed a synthesis machine. Ley discussed the technology, such as reactors, reagents, and reactions, that is necessary for such assemblies. A highlight of the lecture was the discussion of the fully automated synthesis of epothilone with high overall yield (55% over all steps) and the renunciation of purification procedures such as crystallization or chromatography.[7]

Masakatsu Shibasaki (University of Tokyo, Japan) discussed new catalytic asymmetric reactions for the generation of quaternary stereocenters. By using either aluminum or gadolinium catalysts in the presence of identical chiral-carbohydrate-based ligands in the cyanosilylation of ketones, Shibasaki and co-workers were able to generate opposite enantiomers.[8] The application of these asymmetric methods allowed the synthesis of different biologically active compounds in a few steps and in an efficient manner. The formation of complex molecular architectures was the central topic of the concluding lecture given by Johann Mulzer (University of Vienna, Austria). He demonstrated natural product synthesis to be the guideline for the evaluation of the synthetic utility of a new chemical method, using the asymmetric Sharpless epoxidation of laulimalide precursor **8** for the elegant and regioselective formation of the oxirane in the natural product **9** for illustration. The stereodifferentiation led to an impressive stereo- and regioselectivity in the oxidation process in the presence of an alternative allyl alcohol moiety (Scheme 3).[9]

In summary, the 9th SFB Symposium in Aachen gave an overview of the current state of the art in asymmetric synthesis. Handcrafted metal complexes as well as small organic molecules or randomized enzymes open the way



8 **9**

Scheme 3. Stereodifferentiation in asymmetric epoxidations as the regioselectivity-determining factor. DIPT = diisopropyltartrate; TBHP = *tert*-butylhydroperoxide.

© 2006 Wiley-VCH Verlag GmbH & Co. KGaA, Weinheim

synthetically to chiral building blocks with almost perfect enantiopurity. However, the synthesis of complex molecular structures still remains the guideline for the evaluation of the synthetic utility of a new method. In summary, the lectures presented during this symposium made one point very clear: asymmetric synthesis in the future will be characterized by perfect stereocontrol, easily accessible catalysts, and simple workup procedures. In short, it has to fulfill the criteria of "sustainability".

Besides the excellent scientific content of this symposium, the attendance fees for students to participate at the meeting were affordable and this should set a precedent for future symposia. In this context, Aachen set a new standard and it seems justified to call this symposium a "finale furioso". Da capo …

[1] X. Daura, K. Gademann, H. Schäfer, B. Jaun, D. Seebach, W. F. van Gunsteren, *J. Am. Chem. Soc.* **2001**, *123*, 2393.

[2] a) S. G. Ouellet, J. B. Tuttle, D. W. C. MacMillan, *J. Am. Chem. Soc.* **2005**, *127*, 32; b) J. W. Yang, M. T. Hechavarria Fonseca, N. Vignola, B. List, *Angew. Chem.* **2005**, *117*, 110; *Angew. Chem. Int. Ed.* **2005**, *44*, 108.

[3] M. T. Reetz, M. Bocola, J. D. Carballeira, D. Zha, A. Vogel, *Angew. Chem.* **2005**, *117*, 4264; *Angew. Chem. Int. Ed.* **2005**, *44*, 4192.

[4] R. Süssmuth, *ChemBioChem* **2002**, *3*, 295.

[5] G. Lipowsky, N. Miller, G. Helmchen, *Angew. Chem.* **2004**, *116*, 4695; *Angew. Chem. Int. Ed.* **2004**, *43*, 4595.

[6] B. M. Trost, J. Xu, *J. Am. Chem. Soc.* **2005**, *127*, 2846.

[7] R. I. Storer, T. Takemoto, P. S. Jackson, D. S. Brown, I. R. Baxendale, S. V. Ley, *Chem. Eur. J.* **2004**, *10*, 2355.

[8] a) Y. Hamashima, M. Kanai, M. Shibasaki, *J. Am. Chem. Soc.* **2000**, *122*, 7412; b) K. Yabu, S. Masumoto, S. Yamasaki, Y. Hamashima, M. Kanai, W. Du, D. P. Curran, M. Shibasaki, *J. Am. Chem. Soc.* **2001**, *123*, 9908.

[9] A. Ahmed, E. K. Hoegenauer, V. S. Enev, M. Hanbauer, H. Kaehlig, E. Öhler, J. Mulzer, *J. Org. Chem.* **2003**, *68*, 3026.

DOI: 10.1002/anie.200503995



 © 2006 Wiley-VCH Verlag GmbH & Co. KGaA, Weinheim

Reaction Mechanisms

DOI: 10.1002/anie.200502667

The Yandulov/Schrock Cycle and the Nitrogenase Reaction: Pathways of Nitrogen Fixation Studied by Density Functional Theory

*Frank Neese**

Keywords:
cofactors · DFT calculations · nitrogen fixation · nitrogenase · reaction mechanisms

The catalytic synthesis of ammonia is of fundamental importance not only because of its technical relevance but also because it is a key reaction in biology.[1] It is noteworthy that to date there are three known pathways of catalytic ammonia synthesis: the biological process, the industrially widely used Haber–Bosch process, and the recently achieved catalytic conversion developed by Yandulov and Schrock.[2] These processes, however, are understood mechanistically to very different degrees. The oldest of these pathways forms the basis of biological nitrogen fixation, that is, the conversion of atmospheric N_2 into NH_3 under ambient conditions, which provides the basic source of nitrogen for all forms of life.[3] The corresponding enzyme, nitrogenase, consists of two proteins—an iron protein which delivers the necessary electrons and a molybdenum–iron protein which contains the iron–molybdenum cofactor (FeMoco), a unique Mo/Fe/S cluster that binds N_2 and transforms it to NH_3.[4,5] The energy requirement of the reaction is high—as many as 16 ATP molecules are consumed to drive the enzyme through a single cycle. In the Haber–Bosch process invented about 100 years ago, ammonia is synthesized from dinitrogen and hydrogen over catalytic particles (mostly iron, but also ruthenium) at high temperatures (ca. 500 °C) and pressures (ca. 200 atm).[6] Both the industrial and the biological process account for the production of several tens to several hundred millions of tons of ammonia per year (4×10^7 and 10×10^7 tons per year, respectively).[7] However, whereas the Haber–Bosch process is probably the most intensively studied and best understood reaction of heterogeneous catalysis, the details of N_2 binding and conversion into NH_3 at the FeMoco are still not well understood from the available experimental data. In particular, the question whether the primary chemistry takes place at the iron or molybdenum centers of the FeMoco has been very controversially discussed in the literature.[8]

Given the many open questions about the nitrogenase reaction cycle and the enormous experimental challenges associated with obtaining detailed information about it, the discovery of the first truly catalytic room temperature synthesis of ammonia from N_2 by Yandulov and Schrock must be considered as a major advance in the field.[2] Irrespective of the question whether the iron or molybdenum centers are the sites of N_2 reduction in the FeMoco, the importance of this development is that it provides a well-defined chemical precedence. Thus, this process serves as a basis for detailed mechanistic studies that are expected to provide important hints of how N_2 activation can, in principle, be achieved under ambient conditions. The Yandulov/Schrock cycle is based on a Mo^{III} complex with a specifically designed ligand that provides a sterically shielded site for dinitrogen binding and reduction (Figure 1a). Schrock et al. succeeded in generating ammonia from N_2 in six cycles with an overall yield of 65% by using the strong reductant decamethylchromocene ($E^0\approx-1.5$ V versus the ferrocene/ferrocenium (Fc/Fc^+) couple) and the weak acid lutidinium $BAr^F{}_4$

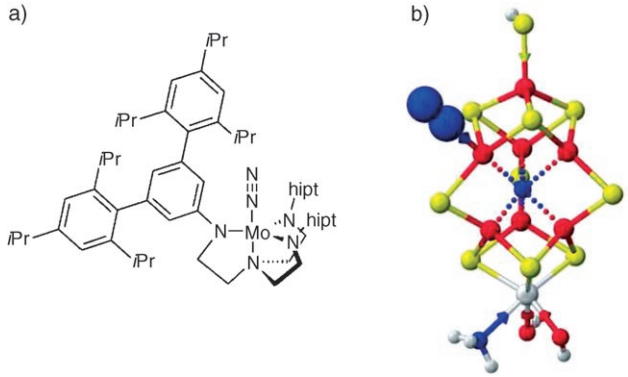


Figure 1. a) Mo^{III} complex involved in the Yandulov/Schrock cycle; hipt = hexaisopropylterphenyl. b) Molecular model of FeMoco; color code: blue N, red Fe, yellow S, gray Mo (large) or H (small).

[*] Priv. Doz. Dr. F. Neese
Max-Planck Institut für Bioanorganische Chemie
Stiftstrasse 34–36
45470 Mülheim/Ruhr (Germany)
Fax: (+49) 208-306-3951
E-mail: neese@mpi-muelheim.mpg.de

InterScience
© 2006 Wiley-VCH Verlag GmbH & Co. KGaA, Weinheim

($Ar^F = 3,5\text{-}(CF_3)_2C_6H_3$) as a proton source.

Evidently, such a complicated reaction must proceed through several intermediate steps. It is intriguing to ask what the chemical identity of these intermediates is and to identify the most energetically and kinetically demanding steps. While Yandulov and Schrock succeeded in stabilizing and structurally characterizing several of the presumed intermediates, a precise energetic profile of the reaction was not determined by experimental means. The use of contemporary theoretical methods, in particular those based on density functional theory (DFT), can provide important new insights. One must, however, always keep in mind that even modern quantum chemical methods only provide approximate solutions, which occasionally fail. Nevertheless, a well-calibrated theoretical investigation which carefully takes into account all constraints provided by the available experimental data can be of considerable help in interpreting experiments, closing gaps where there is no experimental information, and providing the necessary framework to design new and decisive experiments. An insightful computational study of the Yandulov/Schrock cycle has recently been published by Studt and Tuczek. Their findings are in agreement with the available experimental results, and basically support the mechanism proposed by Schrock et al. (Figure 2).[9] The theoretically derived pathway involves a strictly alternating sequence of protonation and reduction steps and offers a detailed picture of the room-temperature conversion of N_2 into ammonia on a specially designed transition-metal center.

Following the study of Studt and Tuczek, it is highly instructive to compare the overall energetics of this reaction with the nitrogenase reaction cycle. Calculations carried out by correlating the Yandulov/Schrock cycle with the (intrinsically exergonic) reaction $N_2 + 3H_2 \rightarrow 2NH_3$ ($\Delta G^0 = -7.7$ kcal mol^{-1} at 298 K and 1 atm pressure) predicted a required energy input of approximately 180 kcal mol^{-1} to mediate the synthesis of 2 moles of ammonia at room temperature and normal pressure. This high energy input is mostly contained in the supplied reductant (that is, decamethylchromocene). While at first glance this seems to be an excessively large energy requirement, Studt and Tuczek have pointed out that the situation in the biological system is quite similar and a major part of the energy expenditure is used for the synthesis of 16 moles of ATP. These ATP molecules are used to effectively lower the reduction potential of the iron protein and are consumed in one catalytic turnover.[4] Furthermore, the energy profile of the Schrock cycle derived from DFT calculations pinpoints two stages in the ammonia forming reaction where this negative redox potential is essential: 1) the first protonation of coordinated N_2 and 2) the final reduction of the NH_3 complex. According to the theoretical results, the first protonation is the most difficult step of the whole process; it is strongly endergonic for free N_2[10] and therefore requires "activation" of N_2 by binding to the Mo complex. The comparatively endergonic character of this step in the Schrock cycle reflects a "moderate" activation achieved by the ligand system used.[11] This moderate activation is in agreement with vibrational spectroscopic data.[12] The second demanding step is the last reduction, which reconstitutes the initial oxidation state of the metal center. Only through this reduction does the the metal become sufficiently electron rich to bind N_2 and close the catalytic cycle. All other elementary reactions of the cycle (reductions and protonations[13]) are exergonic, with the most exergonic step being the splitting of the N–N bond that is predicted to occur spontaneously after electron transfer to the $[Mo(NNH_3)]^+$ complex.

The calculations on the model system nicely illustrate the power and capacity of modern DFT methods. Since only a single metal center is involved, the model system is of reasonable size and allows the explicit calculation of zero-point energy and thermal corrections to the reaction energetics. The solvent can be modeled through the popular dielectric continuum methods, thus approaching energetic predictions close to the limit of what is possible with contemporary DFT methods and what can be achieved with reasonable computational effort. The same level of accuracy for the nitrogenase active site is currently very difficult to achieve. Such calculations would require the explicit modeling of the surrounding protein and its solvent-filled pockets, which is feasible with modern combined QM/MM methods. More importantly, however, proper account should be taken of the intricacies of the very complicated spin couplings between the open-shell metal centers constituting the FeMoco that lead to a very high density of states in close contact with the ground state. To do this rigorously is impossible with DFT methods, which cannot yield spin eigenfunctions for magnetically interacting systems. Moreover, systems of the size and complexity of the FeMoco are far out of reach of

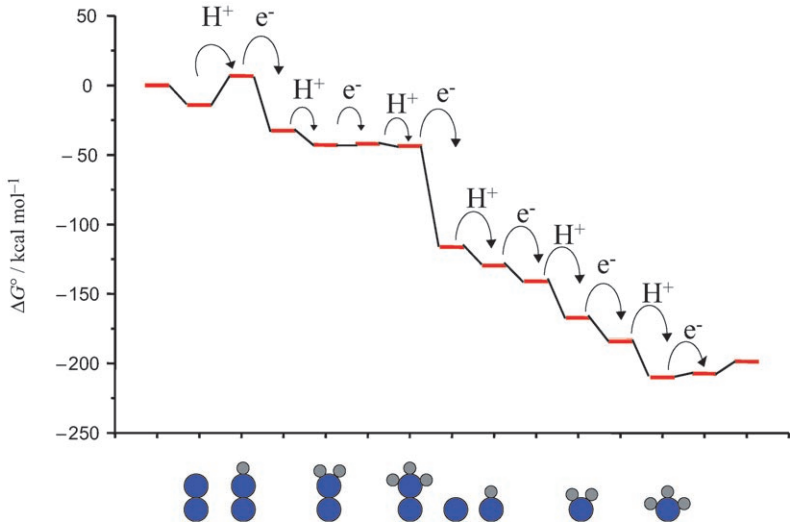


Figure 2. Energetic profile of the Yandulov/Schrock cycle as predicted by the DFT calculations of Studt and Tuczek.

© 2006 Wiley-VCH Verlag GmbH & Co. KGaA, Weinheim

correlated ab initio methods, which could "in principle" provide more correct solutions. The subject of spin couplings is, however, an important issue for reactivity, as exemplified by the fascinating recent insights into the reaction cycle of cytochrome P450 enzymes.[14] Of the many theoretical studies which have been published on the FeMoco, the results of Noodleman and co-workers perhaps address this issue most rigorously and are also the most comprehensive with respect to the size of the model system used to approximate this cluster.[15]

It is nevertheless very interesting to relate the results obtained for the Yandulov/Schrock cycle to recent detailed theoretical work of Nørskov and coworkers. These authors have applied DFT to the catalytic ammonia synthesis both on the surface of a Haber–Bosch catalyst and in nitrogenase.[16–18] In their investigation of FeMoco,[17] Hinnemann and Nørskov first deal with the possible insertion and extraction of the recently discovered central atom X of this cluster,[19] which has stimulated considerable activity in the theoretical community.[15,17,20] Consensus from these studies appears to be that X is a nitrogen atom (for example, a bridging μ_6-nitrido ligand).[26] The authors conclude on the basis of extensive calculations that a thermally accessible pathway for N insertion is unlikely to exist under turnover conditions. The central ligand X is thus an integral part of the FeMoco and is present at all times of the catalytic reaction, which is in agreement with spectroscopic findings.[21] In the next step, the bonding of N_2 to the central iron atoms of the FeMoco, coordinated in a trigonal-pyramidal geometry by three equatorial sulfides and X in an apical position, was simulated. The authors proposed an end-on terminal coordination of dinitrogen to one of these iron atoms as the most favorable binding position (Figure 1b). However, the binding of N_2 was calculated to be endothermic ($+38$ to $+65\,kJ\,mol^{-1}$, depending on the number n of protons and electrons already present in the cluster; $n=1$ in Figure 3).[22] Finally a sequence of combined protonation/reduction steps was proposed to achieve turnover. Interestingly, the authors found—in analogy to the theoretical

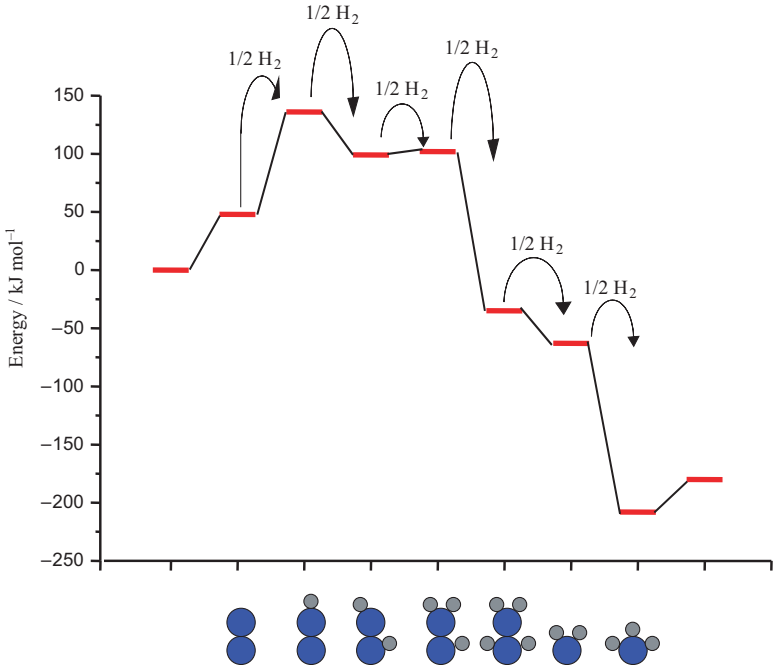


Figure 3. Energetic profile of the nitrogenase reaction as predicted by the DFT calculations of Hinnemann and Nørskov.

results obtained for the Schrock cycle—that the first hydrogenation of N_2 is the most energy-demanding step in the entire reaction sequence ($+66$ to $+119\,kJ\,mol^{-1}$, depending on n).[23] All subsequent hydrogenation steps were predicted to lead to lower energy intermediates with exception of the last step of the cycle. Here the desorption of NH_3 was calculated to be endothermic.

Thus, the theoretical results obtained for two very different systems which catalyze the same chemistry show surprisingly strong parallels, and the overall shape of the energy profile for the nitrogenase reaction appears to be quite similar to that of ammonia synthesis in the Yandulov/Schrock system. A closer look at the details of these reactions, however, also reveals important differences. In particular, the first three protonations in the Schrock system were predicted to exclusively occur on the N_β atom, thus leading to a coordinated hydrazidium ($-NNH_3^-$) ligand, which under splitting of the N–N bond generates the first molecule of NH_3 and coordinated nitride (N_α^{3-}). Successive protonation of the nitrido complex then produces the second molecule of NH_3. In contrast, the two N atoms of N_2 were calculated to be hydrogenated in an alternating fashion in the FeMoco system, thus leading to the sequence of -NNH, -N(H)NH, $-N(H)NH_2$, and $-NH_2$-NH_2 intermediates. It is not until after the fifth hydrogenation (leading to a coordinated hydrazinium ($-NH_2$-NH_3^+) ligand) that the N–N bond is cleaved, and NH_3 as well as coordinated amide (NH_2) are generated. In a final hydrogenation step the amido ligand is converted into a second molecule of NH_3 and then released. The reactivity differences between the FeMoco and the Yandulov/Schrock systems derive from the fact that the bonding of nitride to the cluster appears to be unfavorable, thus leading to a mechanistic pathway in which coordinated nitrido species are avoided. Indeed, the stabilization of a high-valent iron–nitrido species in nitrogenase appears to be unlikely on the basis of recent results obtained on model systems, which required the input of almost 3 eV (ca. $70\,kcal\,mol^{-1}$) of photon energy to produce such a species.[24] The avoidance of a high-valent nitrido species in the biological system is particularly noteworthy since the formation of a metal–N_α double or triple bond is an important driving force in the protonation and reduction of end-on-coordinated dinitrogen in mononuclear transition-metal complexes.[25]

 © 2006 Wiley-VCH Verlag GmbH & Co. KGaA, Weinheim

In summary, the converging results from theory and experiments on model systems as well as the nitrogenase active site have recently given new clues as to how it is possible to split the N≡N bond, the strongest bond known in chemistry for a homonuclear diatomic species, under ambient conditions. A key component of the evolving picture is certainly the use of quantum chemical methods to study reaction mechanisms and unstable intermediates which are difficult to characterize experimentally. There is every reason to believe that combined studies of the type described will see even more widespread application in the immediate future. With respect to the problem of catalytic N_2 reduction to ammonia, plausible scenarios have now been developed for the reactivity of the FeMoco of nitrogenase and the first synthetic realization of such a system by Yandulov and Schrock. It is to be expected that these studies will form the framework for new experimental and theoretical studies on nitrogenase leading to a greatly enhanced understanding of its reaction mechanism at an atomic or even sub-atomic level.

[1] R. Schlögl, *Angew. Chem.* **2003**, *115*, 2050; *Angew. Chem. Int. Ed.* **2003**, *42*, 2004.

[2] a) D. V. Yandulov, R. R. Schrock, *J. Am. Chem. Soc.* **2002**, *124*, 6252; b) D. V. Yandulov, R. R. Schrock, *Science* **2003**, *301*, 76; c) D. V. Yandulov, R. R. Schrock, A. L. Rheingold, C. Ceccarelli, W. M. Davis, *Inorg. Chem.* **2003**, *42*, 796; d) V. Ritleng, D. V. Yandulov, W. W. Weare, R. R. Schrock, A. S. Hock, W. M. Davis, *J. Am. Chem. Soc.* **2004**, *126*, 6150; e) D. V. Yandulov, R. R. Schrock, *Inorg. Chem.* **2005**, *44*, 1103.

[3] *Prokaryotic Nitrogen Fixation* (Ed.: E. W. Triplett), Horizon Scientific, Wymondham, **2000**.

[4] a) B. K. Burgess, D. J. Lowe, *Chem. Rev.* **1996**, *96*, 2983; b) J. B. Howard, D. C. Rees, *Chem. Rev.* **1996**, *96*, 2965.

[5] It should be noted that nitrogenase also produces one molecule of H_2 per two molecules of NH_3 as an obligatory side product of the reaction.

[6] a) *Catalytic Ammonia Synthesis* (Ed.: J. R. Jennings), Plenum, Oxford, **2002**; b) *Ammonia*, *Catalysis and Manufacture* (Ed.: R. Nielsen), Springer, Heidelberg, **1995**.

[7] L. Stryer, *Biochemistry*, 4. ed., Freeman, New York, **1995**.

[8] a) L. C. Seefeldt, I. G. Dance, D. R. Dean, *Biochemistry* **2004**, *43*, 1401; b) C. J. Pickett, *J. Biol. Inorg. Chem.* **1996**, *1*, 601.

[9] F. Studt, F. Tuczek, *Angew. Chem.* **2005**, *117*, 5783; *Angew. Chem. Int. Ed.* **2005**, *44*, 5639.

[10] The protonation of N_2 by lutidinium is predicted to be ca. 89 kcal mol^{-1} uphill using analogous methods and basis sets as in Ref. [9].

[11] F. Tuczek, N. Lehnert, *Angew. Chem.* **1998**, *110*, 2780; *Angew. Chem. Int. Ed.* **1998**, *37*, 2636.

[12] a) K. H. Horn, N. Bores, N. Lehnert, K. Mersmann, K. C. Näther, G. Peters, F. Tuczek, *Inorg. Chem.* **2005**, *44*, 3016; b) K. Mersmann, K. H. Horn, N. Bores, N. Lehnert, F. Studt, F. Paulat, G. Peters, I. Ivanovic-Burmazovic, R. van Eldik, F. Tuczek, *Inorg. Chem.* **2005**, *44*, 3031.

[13] One important feature of the calculations by Studt and Tuczek is that they have explicitly included the electron- and proton-donating reagents in their calculations to arrive at realistic energetic predictions.

[14] S. Shaik, S. D. Kumar, S. P. de Visser, A. Altun, W. Thiel, *Chem. Rev.* **2005**, *105*, 2279.

[15] a) T. Lovell, J. Li, D. A. Case, L. Noodleman, *J. Am. Chem. Soc.* **2001**, *123*, 4546; b) T. Lovell, T. Liu, D. A. Case, L. Noodleman, *J. Am. Chem. Soc.* **2003**, *125*, 8377.

[16] K. Honkala, A. Hellman, I. N. Remediakis, A. Logadottir, A. Carlsson, S. Dahl, Ch. H. Christensen, J. K. Nørskov, *Science* **2005**, *307*, 555.

[17] B. Hinnemann, J. K. Nørskov, *J. Am. Chem. Soc.* **2004**, *126*, 3920.

[18] There are other calculations of the FeMoco, the bonding of N_2 to the FeMoco, and the conversion of N_2 into NH_3 on the FeMoco available in the literature, see Ref. [10] and T. H. Rod, J. K. Nørskov, *J. Am. Chem. Soc.* **2000**, *122*, 12751, as well as J. Kästner, P. E. Blöchl, *Inorg. Chem.* **2005**, *44*, 4568.

[19] O. Einsle, F. A. Tezcan, S. L. A. Andrade, B. Schmid, M. Yoshida, J. B. Howard, D. C. Rees, *Science* **2002**, *297*, 1696.

[20] a) I. Dance, *Chem. Commun.* **2003**, 324; b) J. Schimpl, H. M. Petrill, P. E. Blöchl, *J. Am. Chem. Soc.* **2003**, *125*, 15772; c) J. Kästner, P. E. Blöchl, *Inorg. Chem.* **2005**, *44*, 4568; d) U. Huniar, R. Ahlrichs, D. Coucouvanis, *J. Am. Chem. Soc.* **2004**, *126*, 2588.

[21] H. I. Lee, P. M. Benton, M. Laryukim, R. Y. Igarashi, D. R. Dean, L. C. Seefeldt, B. M. Hoffman, *J. Am. Chem. Soc.* **2003**, *125*, 5974.

[22] The equal number of protons (m) and electrons (n) present in the resting cluster state in the calculations of Nørskov and co-workers is a consequence of the technical constraint that the cluster be neutral overall (that is, $q = m - n = 0$) On the basis of other theoretical studies,[15b,20b] the likely resting state has $n = 3$ and $m = 0$ if the central ligand X is represented by a nitrido nitrogen.

[23] The experimental literature indicates that an additional two to four electrons and probably two to four protons are added to the cluster prior to N_2 binding (B. K. Burgess, D. J. Lowe, *Chem. Rev.* **1996**, *96*, 2983; K. Fisher, W. Newton, D. Lowe, *Biochemistry* **2001**, *40*, 3333); see also Ref. [20b].

[24] N. Aliaga-Alcalde, S. DeBeer-George, E. Bill, K. Wieghardt, F. Neese, *Angew. Chem.* **2005**, *117*, 2968; *Angew. Chem. Int. Ed.* **2005**, *44*, 2908.

[25] B. A. MacKay, M. D. Fryzuk, *Chem. Rev.* **2004**, *104*, 385.

[26] Note added in proof (14. 11. 2005): Very recent spectroscopic results have indicated that the central atom X of FeMoco may not be nitrogen (T.-C. Yang, N. K. Maeser, M. Laryukhin, H.-I. Lee, D. R. Dean, L. C. Seefeldt, B. M. Hoffman, *J. Am. Chem. Soc.* **2005**, *127*, 12804–12805).

 © 2006 Wiley-VCH Verlag GmbH & Co. KGaA, Weinheim

Homogeneous Catalysis

DOI: 10.1002/anie.200502999

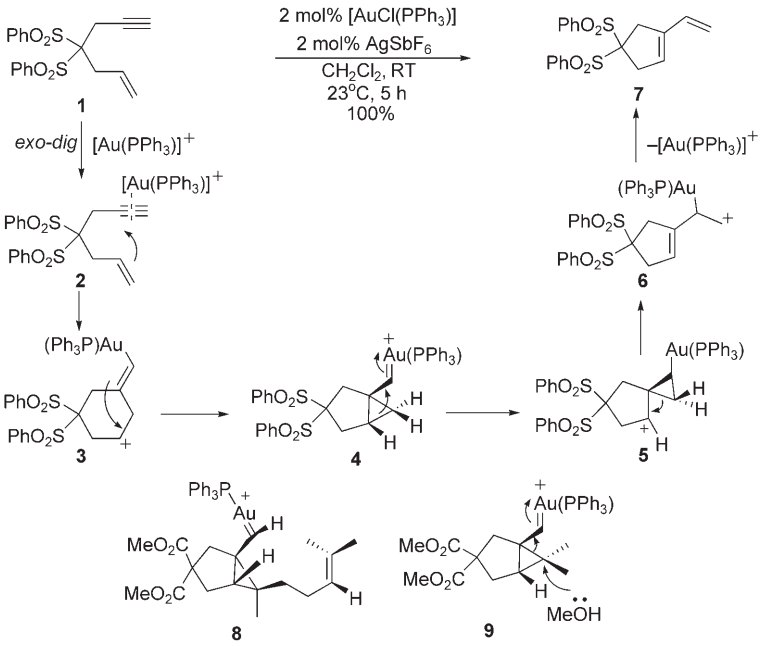
Gold-Catalyzed Cyclization of Enynes

Shengming Ma, Shichao Yu, and Zhenhua Gu*

Keywords:
alcohols · cycloisomerization · enynes · gold · homogeneous catalysis

Gold is a "soft" transition metal that shows high electrophilic affinity for alkynes, arenes, allenes, and even alkenes. It can also act simultaneously as a Lewis acid for the activation of electrophiles.[1a,b] Carbon–gold bonds are labile to protonolysis but undergo β-hydride elimination reactions only with difficulty. Reactions catalyzed by gold generally proceed under mild conditions and can be performed in the presence of water or even in pure water.[1] Although there are some new developments in this area,[2] this Highlight is concerned with the gold-catalyzed cycloisomerization of enynes.

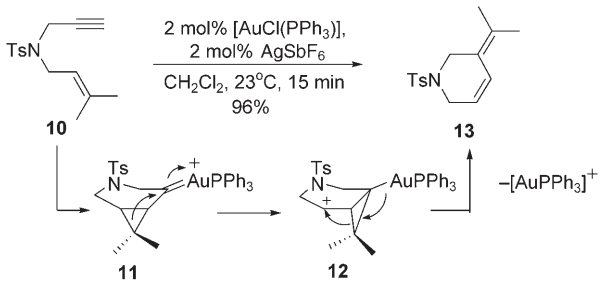
Cycloisomerizations of 1,*n*-enynes have emerged as attractive tools for the synthesis of various types of cyclic compounds in an easy one-pot process in which a wide range of transition-metal complexes can be used, either in a catalytic or stoichiometric manner.[3] Pioneering work by Echavarren and co-workers has shown that Au^+ is a versatile catalyst for the intramolecular enyne metathesis of substrates with a terminal carbon–carbon triple bond (Scheme 1).[3c,4] The intermediate **4** formed by the nucleophilic attack of the C=C bond at the terminal C–C triple bond was generally proposed as the key intermediate, as is common for other electrophilic transition metals such as platinum,[5,6] rhodium,[6,7] and ruthenium,[7] for this type of reaction. Intermediates such as **8** and **9** can undergo intramolecular cyclopropanation with another C–C double bond or trapped by the nucleophilic addition of MeOH (Scheme 1).[5,7] An asymmetric version of such a cyclization with moderate *ee* values has also been realized by using different chiral ligands.[6]



Scheme 1.

However, the reaction of tosylated, nitrogen-tethered enyne **10** with [Au(PPh$_3$)]SbF$_6$ afforded methylenecyclohexene derivative **13** through the double carbon–carbon bond cleavage of the cyclopropane rings in intermediates **11** and **12** (Scheme 2).[4]

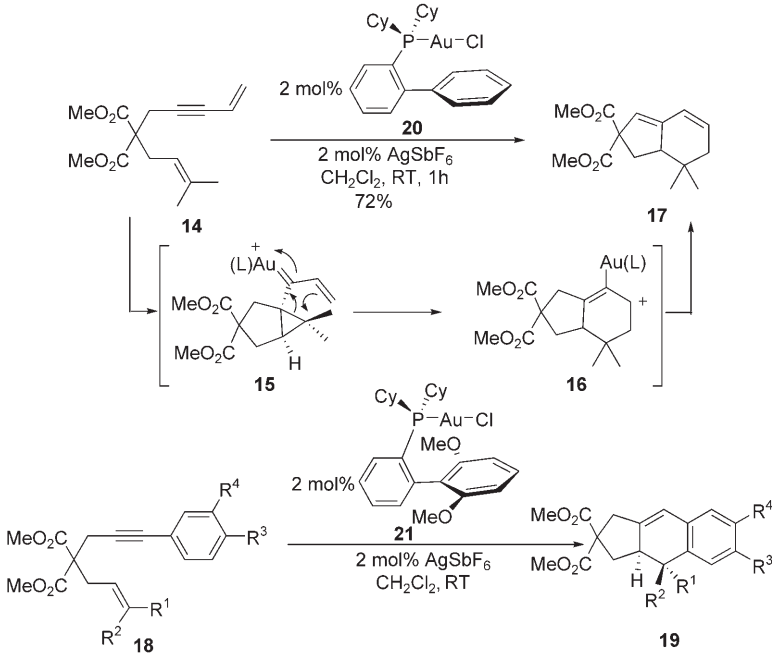
Such metallocarbene intermediates may also be formed from substrates bearing a vinyl- or aryl-substituted carbon–carbon triple bond. Treatment of 1,8-dien-3-yne **14** or 1-aryl-6-enyne **18** with 2 mol% of gold complex **20** or **21** and AgSbF$_6$ afforded hydrindane **17** or the tricyclic product **19** by an intramolecular interaction of the Au carbene moiety with the carbon–carbon double bond and the carbon–carbon bond in the



Scheme 2. Ts = toluene-4-sulfonyl.

[*] Prof. Dr. S. Ma, Dr. S. Yu, Z. Gu
State Key Laboratory of Organometallic Chemistry
Shanghai Institute of Organic Chemistry
Chinese Academy of Sciences
354 Fenglin Lu
Shanghai 200032 (P.R. China)
Fax: (+86) 21-6416-7510
E-mail: masm@mail.sioc.ac.cn

InterScience
© 2006 Wiley-VCH Verlag GmbH & Co. KGaA, Weinheim



Scheme 3. Cy = cyclohexyl.

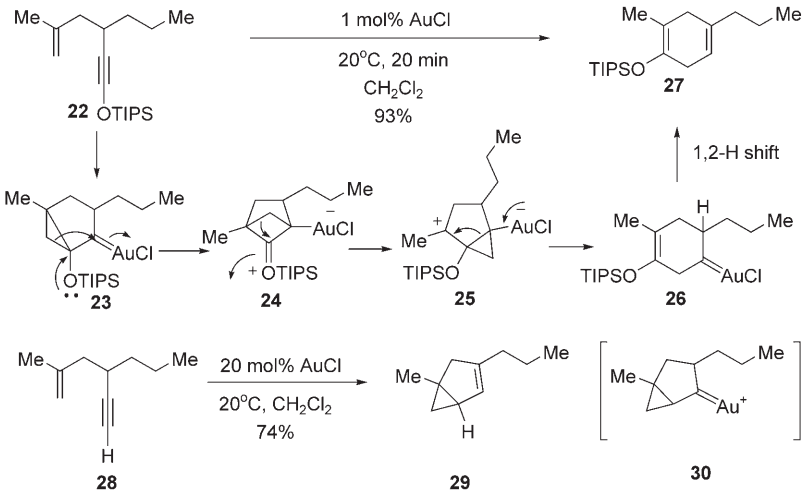
three-membered ring in an intermediate of type **15** (Scheme 3).[4b,8]

Zhang and Kozmin observed that a series of carbon–carbon bond cleavages induced by the lone pair of electrons on the oxygen atom in cyclopropyl gold carbene **23** led to the formation of 1,4-cyclohexadiene **27**. The silyl group is believed to stabilize the oxocarbenium intermediate **24**. Treatment of the enyne **28** without this silyl group with 20 mol % of AuCl in CH_2Cl_2 gave 5-methyl-3-propylbicyclo[3.1.0]hex-2-ene (**29**) through a 1,2-hydrogen shift of the metallocarbene intermediate **30** (Scheme 4).[9] Similar reaction pathways of metallocarbenes were also observed by Fürstner et al. as well as Gagosz,[10] and Toste et al.[11]

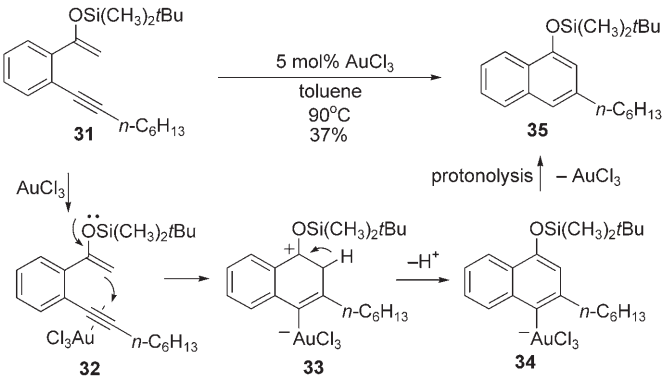
Dankwardt found that gold-mediated cyclization of *o*-alkynylphenylvinyl silyl ether **31** constitutes an efficient method for the construction of substituted naphthalene **35** through the nucleophilic addition of the enol silyl ether to the Au-coordinated triple bond[11,12] to form the vinylic gold intermediate **33** (Scheme 5).[13]

Sherry and Toste observed that treatment of propargylic vinyl ether **36** with a catalytic amount of $[\{Au(PPh_3)\}_3O]BF_4$ effected a skeletal rearrangement that afforded 3,4-allenols **39** through a β-heteroatom elimination of intermediate **38**, which was formed by the nucleophilic attack of the vinyl ether moiety at the coordinated C–C triple bond, and reduction. The chirality can be completely transferred to the final product **41** by using the enantiomerically enriched propargyl vinyl ether **40** (Scheme 6).[14]

Bicyclo[3.1.0]hexanone **47** was formed from propargylic acetate **42** as shown in Scheme 7. Coordination of the cationic gold(I) complex to the alkyne induces an intramolecular nucleophilic attack of the carbonyl oxygen atom of the ester group at the carbon–carbon triple bond to afford a zwitterionic vinylic gold intermediate **44**, which was converted into a new type of carbene intermediate **45** by the subsequent cleavage of the C–O bond. Intramolecular cyclopropanation would then lead to the formation of bicyclic vinylic ester



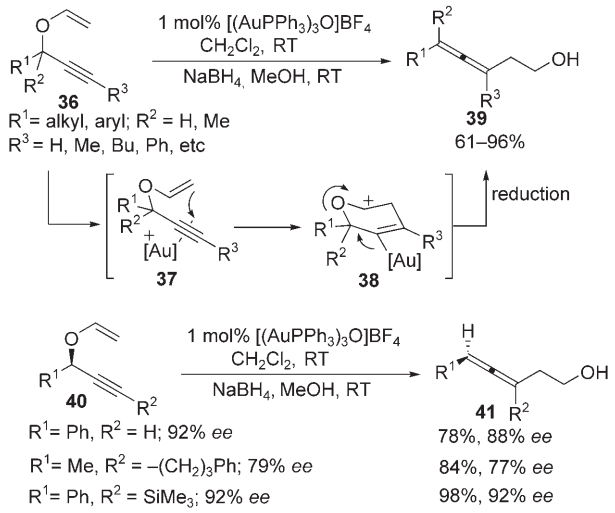
Scheme 4. TIPS = triisopropylsilyl.



Scheme 5.

© 2006 Wiley-VCH Verlag GmbH & Co. KGaA, Weinheim

46.[10,15] This mild and efficient method has been applied as a key step for the diastereoselective total synthesis of the natural product sesquicarene (**48**).[16]



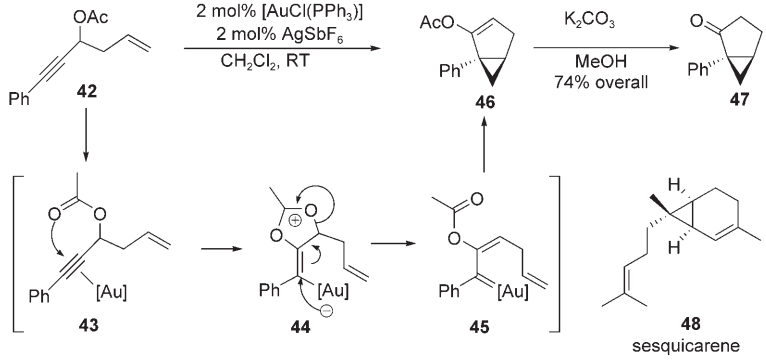
Scheme 6.

The Au-catalyzed skeletal rearrangement proceeds stereospecifically, and translates the configuration of the reacting alkene into the stereochemistry of the emerging cyclopropane unit.

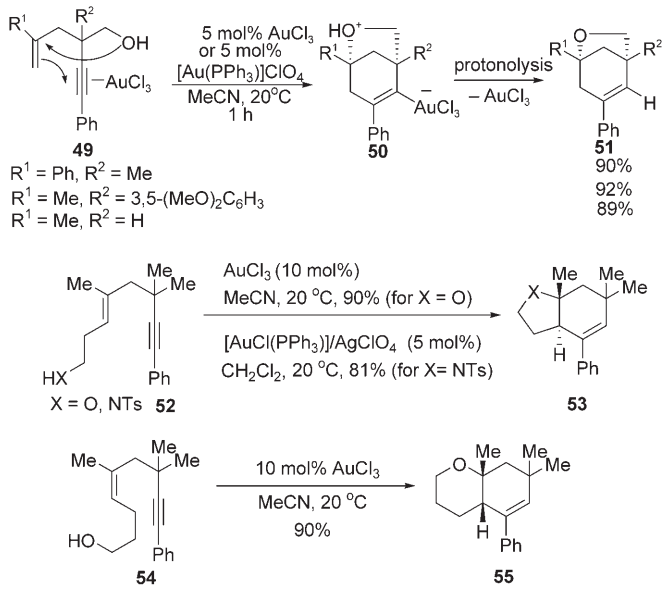
Similarly, 2-cyclopentenones and bicyclic 2-cyclopentenones were produced in the presence of 2–5 mol% of [Au(PPh$_3$)]OTf in CH_3CN at room temperature from the cycloisomerization of 1-ethynyl-2-propenyl pivaloates in 45–85% yields.[17] The reaction proceeded by a subsequent intramolecular Nazarov-type cyclization of similarly structured vinylic gold(I) species, elimination of cationic gold(I), and hydrolysis. Excellent chirality transfer was observed when enantioenriched propargyl pivaloates were treated with 5 mol% of [Au(PPh$_3$)]SbF$_6$ in CH_3CN at −20 °C, which strongly suggests the formation of vinylic gold(I) species as intermediates instead of gold–carbene species.[17]

Kozmin and co-workers observed that the treatment of a 1,5-enyne with catalytic amounts of $AuCl_3$ triggered the double cyclization of **49** to produce intermediate **50**,[12l,18] which underwent subsequent protonolysis to afford the heterobicyclic product **51**. The remarkable diastereoselective nature of this double cyclization is decipted in Scheme 8: Compound **52**, which contains an *E*-alkene moiety, afforded the *trans*-oxabicyclic product **53** whereas compound **54**, with a *Z* alkene, produced the *cis*-oxabicyclic product **55** exclusively. The tosyl amine moiety behaved similarly in the presence of the [Au(PPh$_3$)]ClO$_4$ catalyst.[19]

Gold catalysis represents a new frontier in catalysis which has substantial benefits to organic synthesis. The wide scope and high efficiency demonstrated by the gold-catalyzed reaction of enynes under mild conditions to access complex or hitherto inaccessible products are particularly appealing. There is still an urgent need to characterize reaction intermediates so that plausible mechanisms and catalytic cycles can be proposed. It is hoped that this Highlight will provide the basis for the development of new reactions.



Scheme 7.



Scheme 8.

[1] For recent reviews on Au-catalyzed oxidation, carbonylation, aldol reactions, hydroarylation, hydration, hydroamination, and intramolecular cyclizations see: a) A. S. K. Hashmi, *Gold Bull.* **2004**, *37*, 51; b) A. Arcadi, S. Di Giuseppe, *Curr. Org. Chem.* **2004**, *8*, 795; c) G. Dyker, *Angew. Chem.* **2000**, *112*, 4407; *Angew. Chem. Int. Ed.* **2000**, *39*, 4237; d) D. E. De Vos, B. F. Sels, *Angew. Chem.* **2005**, *117*, 30; *Angew. Chem. Int. Ed.* **2005**, *44*, 30; e) A. S. K. Hashmi, *Gold Bull.* **2003**, *36*, 3; f) A. Hoffmann-Röder, N. Krause, *Org. Biomol. Chem.* **2005**, *3*, 387; for general surveys of organogold chemistry, see: g) R. J. Puddephatt in *Comprehensive Organometallic Chemistry, Vol. 2*, 1st ed. (Eds.: G. Wilkinson, F. G. A. Stone, E. W. Abel), Pergamon, Oxford, **1982**, p. 765; h) R. J. Puddephatt, *The Chemistry of Gold*, Elsevier, Amsterdam, **1978**.

[2] A. S. K. Hashmi, *Angew. Chem.* **2005**, *117*, 7150; *Angew. Chem. Int. Ed.* **2005**, *44*, 6990.

 © 2006 Wiley-VCH Verlag GmbH & Co. KGaA, Weinheim

[3] For recent reviews on cycloisomerizations, see: a) C. Aubert, O. Buisine, M. Malacria, *Chem. Rev.* **2002**, *102*, 813; b) B. M. Trost, F. D. Toste, A. B. Pinkerton, *Chem. Rev.* **2001**, *101*, 2067; c) C. Bruneau, *Angew. Chem.* **2005**, *117*, 2380; *Angew. Chem. Int. Ed.* **2005**, *44*, 2328.

[4] a) C. Nieto-Oberhuber, M. P. Muñoz, E. Buñuel, C. Nevado, D. J. Cárdenas, A. M. Echavarren, *Angew. Chem.* **2004**, *116*, 2363; *Angew. Chem. Int. Ed.* **2004**, *43*, 2402; b) N. Mézailles, L. Ricard, F. Gagosz, *Org. Lett.* **2005**, *7*, 4133.

[5] a) M. Méndez, M. P. Muñoz, A. M. Echavarren, *J. Am. Chem. Soc.* **2000**, *122*, 11549; b) M. Méndez, M. P. Muñoz, C. Nevado, D. J. Cárdenas, A. M. Echavarren, *J. Am. Chem. Soc.* **2001**, *123*, 10511; c) A. Fürstner, H. Szillat, F. Stelzer, *J. Am. Chem. Soc.* **2000**, *122*, 6785; d) A. Fürstner, F. Stelzer, H. Szillat, *J. Am. Chem. Soc.* **2001**, *123*, 11863; e) C. Nevado, C. Ferrer, A. M. Echavarren, *Org. Lett.* **2004**, *6*, 3191; f) L. Charruault, V. Michelet, R. Taras, S. Gladiali, J.-P. Genêt, *Chem. Commun.* **2004**, 850.

[6] M. P. Muñoz, J. Adrio, J. C. Carretero, A. M. Echavarren, *Organometallics* **2005**, *24*, 1293.

[7] N. Chatani, K. Kataoka, S. Murai, N. Furukawa, Y. Seki, *J. Am. Chem. Soc.* **1998**, *120*, 9104.

[8] C. Nieto-Oberhuber, S. López, A. M. Echavarren, *J. Am. Chem. Soc.* **2005**, *127*, 6178.

[9] L. Zhang, S. A. Kozmin, *J. Am. Chem. Soc.* **2004**, *126*, 11806.

[10] V. Mamane, T. Gress, H. Krause, A. Fürstner, *J. Am. Chem. Soc.* **2004**, *126*, 8654; for a very recent report, see: F. Gagosz, *Org. Lett.* **2005**, *7*, 4129.

[11] M. R. Luzung, J. P. Markham, F. D. Toste, *J. Am. Chem. Soc.* **2004**, *126*, 10858.

[12] For some of the most typical examples of Au-catalyzed addition of nucleophiles to alkynes, see: a) Y. Fukada, K. Utimoto, H. Nozaki, *Heterocycles* **1987**, *25*, 297; b) Y. Fukuda, K. Utimoto, *J. Org. Chem.* **1991**, *56*, 3729; c) Y. Fukuda, K. Utimoto, *Bull. Chem. Soc. Jpn.* **1991**, *64*, 2013; d) Y. Fukuda, K. Utimoto, *Synthesis* **1991**, 975; e) R. Lok, R. E. Leone, A. J. Williams, *J. Org. Chem.* **1996**, *61*, 3289; f) J. H. Teles, S. Brode, M. Chabanas, *Angew. Chem.* **1998**, *110*, 1475; *Angew. Chem. Int. Ed.* **1998**, *37*, 1415; g) T. E. Muller, A.-K. Pleier, *J. Chem. Soc. Dalton Trans.* **1999**, 583; h) E. Mizushima, K. Sato, T. Hayashi, M. Tanaka, *Angew. Chem.* **2002**, *114*, 4745; *Angew. Chem. Int. Ed.* **2002**, *41*, 4563; i) R. Casado, M. Contel, M. Laguna, P. Romero, S. Sanz, *J. Am. Chem. Soc.* **2003**, *125*, 11925; j) J. P. Markham, S. T. Staben, F. D. Toste, *J. Am. Chem. Soc.* **2005**, *127*, 9708; k) S. T. Staben, J. J. Kennedy-Smith, F. D. Toste, *Angew. Chem.* **2004**, *116*, 5464; *Angew. Chem. Int. Ed.* **2004**, *43*, 5350; l) M. Alfonsi, A. Arcadi, M. Aschi, G. Bianchi, F. Marinelli, *J. Org. Chem.* **2005**, *70*, 2265; m) S. Antoniotti, E. Genin, V. Michelet, J.-P. Genêt, *J. Am. Chem. Soc.* **2005**, *127*, 9976; n) D. J. Gorin, N. R. Davis, F. D. Toste, *J. Am. Chem. Soc.* **2005**, *127*, 11260.

[13] J. W. Dankwardt, *Tetrahedron Lett.* **2001**, *42*, 5809.

[14] B. D. Sherry, F. D. Toste, *J. Am. Chem. Soc.* **2004**, *126*, 15978.

[15] For an intermolecular reaction, see: K. Miki, K. Ohe, S. Uemura, *J. Org. Chem.* **2003**, *68*, 8505.

[16] A. Fürstner, P. Hannen, *Chem. Commun.* **2004**, 2546.

[17] X. Shi, D. J. Gorin, F. D. Toste, *J. Am. Chem. Soc.* **2005**, *127*, 5802.

[18] For some of the most recent examples of Au-catalyzed addition of nucleophiles to alkenes, see: a) X. Yao, C.-J. Li, *J. Am. Chem. Soc.* **2004**, *126*, 6884; b) R.-V. Nguyen, X. Yao, D. S. Bohle, C.-J. Li, *Org. Lett.* **2005**, *7*, 673; c) C. Yang, C. He, *J. Am. Chem. Soc.* **2005**, *127*, 6966.

[19] L. Zhang, S. A. Kozmin, *J. Am. Chem. Soc.* **2005**, *127*, 6962.

 © 2006 Wiley-VCH Verlag GmbH & Co. KGaA, Weinheim

R. Hage and A. Lienke

DOI: 10.1002/anie.200500525

Bleaching Processes

Applications of Transition-Metal Catalysts to Textile and Wood-Pulp Bleaching

Ronald Hage and Achim Lienke**

Keywords:
bleaching · catalysts · lignin · peroxides · stains



© 2006 Wiley-VCH Verlag GmbH & Co. KGaA, Weinheim

From an economic perspective, textile and paper bleaching are amongst the most important oxidation processes. The removal of unwanted chromophores, be it stains on cloths or residual lignin in wood pulp, consumes more than 60% of the world production of hydrogen peroxide. However, existing technologies have their limitations. At ambient temperature, hydrogen peroxide gives little stain bleaching and is used inefficiently. Hence the high product dosages and washing temperatures required limit its application to predominantly European markets, to the exclusion of the majority of the world's population. In paper manufacture, the use of chlorine-based oxidants results in the formation of chlorinated waste products, which show poor biodegradability. On the other hand, hydrogen peroxide requires higher temperatures, longer reaction times and is more expensive. Transition-metal catalysts offer an alternative. This review discusses the main classes of known bleach catalysts and their possible modes of action.

From the Contents

1. Introduction 207
2. Current Bleaching Processes 207
3. Manganese Bleaching Catalysts 210
4. Iron Bleaching Catalysts 215
5. Cobalt-Based Catalysts for Hydrogen Peroxide Activation 218
6. Catalysts for O_2-Induced Delignification 218
7. Outlook 219

1. Introduction

Bleaching agents are widely used to bleach paper, pulp, raw cotton, and stains.[1] A common feature of these very different substrates is the presence of various chromophores that need to be whitened. A bleaching agent whitens a substrate through oxidative or reductive processes, either by degradation of the chromophore and thereby rendering it water-soluble or by shifting the wavelength of absorbance outside the visible region. The main bleaching systems used for laundry cleaning, raw cotton bleaching and pulp-paper bleaching are chlorine-based bleaches, hydrogen peroxide, ozone, and peracids. Bleaching processes are of major economic importance. For example, the annual world production of hydrogen peroxide is approximately 2.2 million metric tons, of which 50% is used for pulp/paper bleaching and 10% for textile bleaching.

A number of factors have spurred the attempt to find improved methods for the bleaching of stains and pulp. 1) Decreasing the temperature of the bleaching processes will lead to general savings in energy consumption. For laundry applications new markets might be opened, as a large majority of domestic detergent users still do laundry at ambient temperature. 2) The application of hydrogen peroxide rather than chlorine-based bleaches will lead to the avoidance of halogenated products in the waste streams from pulp bleaching. However, as the kinetics of these oxidants are more sluggish, it is desirable to activate hydrogen peroxide through transition-metal catalysts. 3) Replacement of peracid precursors by a hydrogen peroxide/catalyst combination will reduce the amount of chemicals used. Application of atmospheric oxygen would lead to a further decrease in the chemical loading and a reduction in costs.[2a] For laundry applications a bleaching system based on the activation of oxygen could also have a larger social impact. Most detergents sold at present do not contain bleaching agents, simply because they are unaffordable for most consumers in developing countries and emerging markets.

Various technologies to enhance the efficiency of hydrogen peroxide or oxygen are known. Technologies, such as those based on laccases, peroxidases,[3,4] or activated imines will not be presented.[5] Instead, this review focuses on the potential use of transition-metal bleach catalysts for pulp bleaching and laundry cleaning applications. Several iron and manganese compounds patented as bleaching catalysts will be discussed in more detail as mechanistic investigations have also been published. Other transition-metal compounds will also be discussed, including cobalt catalysts that activate hydrogen peroxide for laundry and hard-surface cleaning applications and vanadium-based polyoxometalates to enhance delignification by dioxygen. Although an overview of paper-pulp bleach catalysts research has been recently published, to date the development of bleach catalysts for detergent applications has not been reviewed.[6]

2. Current Bleaching Processes

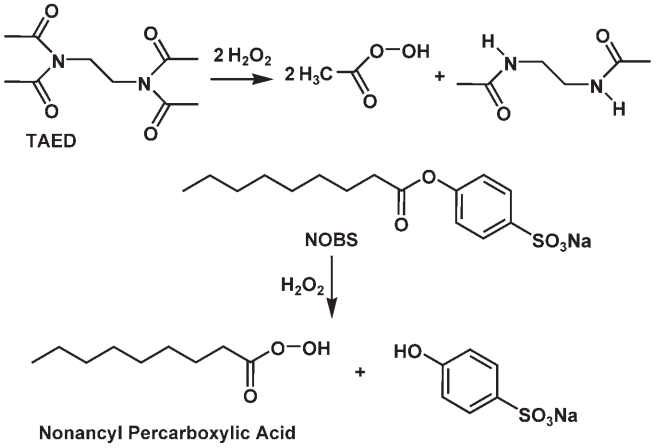
2.1. Stain Bleaching

Various bleaches are employed in stain removal. Hydrogen peroxide has widely been applied in detergent products since the introduction of sodium perborate in the early 20th century. Nearly 90 years later sodium percarbonate as a solid "hydrogen peroxide" delivering agent was introduced to

[*] Dr. R. Hage, Dr. A. Lienke
Unilever R&D Vlaardingen
Olivier van Noortlaan 120, 3133 AT Vlaardingen (The Netherlands)
Fax: (+31) 10-460-5166
E-mail: ronald.hage@unilever.com
achim.lienke@unilever.com

 © 2006 Wiley-VCH Verlag GmbH & Co. KGaA, Weinheim

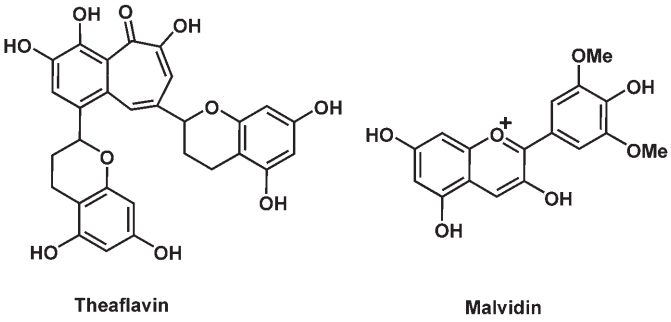
detergents. Upon dissolution of sodium percarbonate in water the carbonate buffer and hydrogen peroxide are released quickly. High washing temperatures (70–90 °C) are required to obtain good bleaching;[2a] however, wash temperatures can be decreased to between 40 and 60 °C by employing peracids, and they are nowadays widely used for domestic laundry cleaning. Peracids are incorporated in detergents primarily in the form of precursors, as the peracids themselves are often not sufficiently stable. Tetraacetylethylenediamine (TAED) and nonanoyloxybenzene sulfonate (NOBS) are amongst the most commonly applied precursors (see Scheme 1). Peracids



Scheme 1. Bleach precursors applied in detergents: TAED and NOBS.

with different carbon chain lengths and therefore different hydrophobicities can be applied, which can be useful in improving bleaching of oily stains.[2a] A further improvement in bleaching activity can be achieved by using hypochlorite-based bleaches, however, this bleach is often associated with undesired fabric and/or dye damage, and consequently its application is quite limited.[1]

There are a wide variety of stains encountered by consumers around the globe, and not all of them react to bleaching. Stains requiring bleach for efficient removal can be divided into two classes: hydrophilic stains, such as tea, wine, fruit stains as well as hydrophobic stains, such as oily-food stains. The color of hydrophilic stains originates from polyphenolic compounds. Black tea, for example, contains mainly the yellow-orange theaflavins and thearubigins that have a red-brown color and are formed during the fermentation process (Scheme 2). The theaflavin backbone may be esterified at various positions with gallic acids. However, the exact



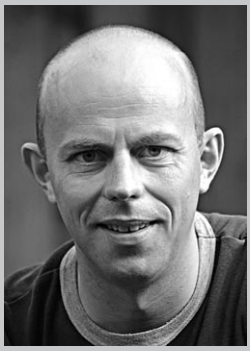
Scheme 2. Structures of theaflavin present in tea as well as malvidin as a model for anthocyanins present in fruit.

chemical composition of thearubigins remains poorly understood.[7] Intensely colored fruits, such as cherries, blackberries, and strawberries, derive their color chiefly from a class of chromophores called anthocyanins (Scheme 2). Anthocyanins display a pH-dependent structure and color. Often sugars are attached at the OH groups on the 3- and/or 5-positions and can be part of a larger polymeric structure. Stacking interactions between anthocyanins and especially flavonoids and hydroxycinnamoyl esters can lead to stabilization of the chromophore and a shift of the λ_{max} of the absorbance band. Anthocyanins are a main component of red wine, which also contains large amounts of oligomeric procyanidins.[7] Stains based on polyphenolic compounds frequently polymerize and in time form quinonoic structures, a phenomenon referred to as ageing. This polymerization might include the fabric matrix, so that the chromophore of the stain will become chemically bound to the textile.

Relatively few studies into the mechanism by which current bleaching technologies remove such hydrophilic stains have been reported. While there were no indications that $^1O_2$ leads to bleaching reactions and the involvement of radical species is unlikely,[2b] hydrogen peroxide and peracids can deprotonate and attack the chromophore as a nucleophile.[2a,b] This would eventually form epoxides, which would give



Ronald Hage received his Masters and PhD (1991) from Leiden University (The Netherlands). Since 1990 he has carried out research at Unilever (The Netherlands) on bleaches and bleach catalysts for detergent applications. His interest focuses on the development of new manganese and iron oxidation catalysis for applications in industry. In the field of biomimetic oxidation catalysis he works with the Stratingh Institute at Groningen University and the Leiden Institute of Chemistry. Since 2003 he is a part-time senior lecturer at Leiden University. Ronald Hage is co-author of more than 80 research publications and holds 59 patents.

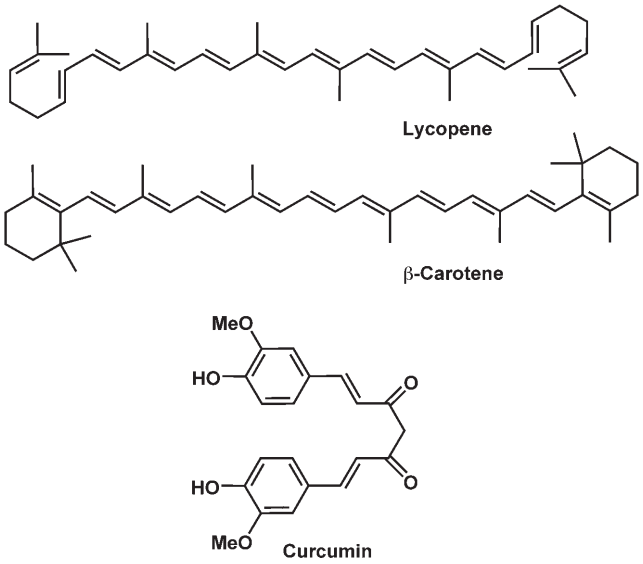


Achim Lienke studied in Heidelberg (Germany) and Canterbury (UK) and received his Ph.D. in 1998 from the University of Heidelberg. After postdoctoral studies at the University of Cape Town, South Africa, he joined Unilever Research in Vlaardingen (The Netherlands) in 2000. He is interested in fast methods to evaluate, optimize, and understand catalytic activity in applied systems.

 © 2006 Wiley-VCH Verlag GmbH & Co. KGaA, Weinheim

diols after ring-opening. Griffith and co-workers have proposed such a mechanism.[2b]

Oily-based food stains, which are chemically distinct from polyphenolic stains, derive from a variety of sources and can therefore contain quite different chromophores. A large number of very stubborn hydrophobic stains derive their color either from carotenoids such as β-carotene and lycopene or curcumin (Scheme 3). Carotenoids can be found in



Scheme 3. Structures of lycopene present in tomato, β-carotene present in carrots, and curcumin present in curries.

tomatoes, red peppers, carrots, and certain curries, whereas curcumin is a constituent of (yellow) curries and mustard. Remarkably, carotenoids and curcumin are quite labile compounds. Carotenoids are sensitive to light and highly reactive towards oxygen, even in the dark. The oxidation is autocatalytic, possibly involving peroxyl radicals and yielding, amongst other products, ketones of reduced molecular weight.[8,9] Such reactivity is very different from the nucleophilic reactivity of deprotonated hydrogen peroxide or peracids, required for hydrophilic stain bleaching. However, nucleophilic attack has been proposed for the carotene derivative crocetin (8,8-diapo-ψ,ψ-carotenedioic acid), which contains an electron-poor alkene adjacent to the carboxylate group,[2b] but it remains unknown whether such reactivity is of relevance for the neutral lycopene-type of substrates present in various oily-food stains. Curcumin exhibits antioxidant activity, most likely by reacting with reactive oxygen species, as well as by chelation of the transition-metal ions.[10] It is very quickly hydrolyzed at the pH of wash solutions to yield feruloyl methane, ferulic acid, and vanillin,[11] though additional experiments indicated that also trace metal ions induce the curcumin degradation at high pH.[12a] However, in the hydrophobic matrix of food oil, curcumin and carotenoids can be persistent chromophores, barely responsive to hydrogen peroxide or short chain peracids, such as peracetic acid. Most of the food oils used, such as sunflower, soya, or olive oil, contain long-chain esters that are sparingly soluble in water. These oils contain one or more unsaturated double bonds that are prone to oxidation.[7] Hydrophobic peracids, such as nonanoyl percarboxylic acid (Scheme 1), exhibit improved stain removal capabilities on such stains.[13]

Assessment of the stain removal capabilities by bleaches is often done on standardized stained fabrics, such as the BC-1 stain. This stain, which is made by extensive boiling of a tea solution in the presence of cotton, is difficult to remove by ordinary detergents, but responsive to bleaches such as hydrogen peroxide and peracids. Other stain systems have been standardized and are commercially available. These stains are not necessarily representative of real stains and researchers often prefer to use homemade stains, as exemplified in some of the patents discussed below. The extent of stain bleaching is assessed predominantly by measuring the reflectance at 460 nm before and after the wash or by measuring the change of color after the bleaching process.

A disadvantage of the conventional bleaches is that they may lead to dye damage on cloths or even to fiber damage, especially following repeated washing.[14,15] The most widely used textile is cotton, which consists of cellulose, a polymer of anhydro-D-glucose.[16,17] Oxidative processes have been described, such as H•-abstraction by free radicals to yield glucopyranose units that react with O_2. After β-elimination, depolymerization of the chain takes place.[16,17] Various other oxidative degradation pathways have also been described.[16] Depolymerization of cellulose is often accelerated under alkaline conditions.[16] The oxidative degradation of cellulose weakens the textile and damage may occur.[16,17]

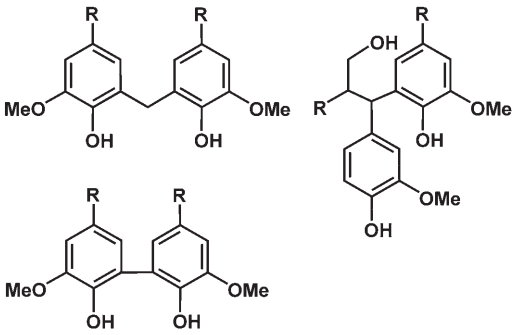
The presence of transition-metal ions in tap water, garments, and/or detergent products influences the reactivity of hydrogen peroxide and peracids. They may react with hydrogen peroxide to form oxygen-based radicals, such as superoxide and hydroxyl radicals and/or high-valent metal–oxo species.[15] These species are very reactive and bleach stains by electrophilic reactions (hydroxylation of aromatic rings), but also result in more dye- and textile damage. To decrease the damage induced by the transition-metal ions, sequestrants are frequently added to bind iron and copper salts. Often they are polyphosphonate- or polycarboxylate-based ligands such as EDTA. It remains a technological challenge, however, to bleach stains selectively, as various dyes contain phenolic groups and therefore resemble the chromophores of stains.

2.2. Pulp Bleaching

The paper industry produces high-quality lignin-free pulp for applications such as magazine and office paper.[1,18] Wood pulp is the most important raw material for this purpose and mainly consists of polysaccharides (cellulose and hemicellulose) and up to 20–30% of lignin. Lignin in plants/trees is derived from mainly coniferyl alcohol (4-hydroxy-3-methoxycinnamyl alcohol), which forms ill-defined, cross-linked hydroxylated and methoxylated phenylpropane polymers upon oxidative coupling. Chemical pulp is wood pulp that has undergone a delignification process. Most of the lignin is

 © 2006 Wiley-VCH Verlag GmbH & Co. KGaA, Weinheim

extracted at high temperatures (150–180 °C) in highly alkaline media with added sodium sulfide (Kraft process) or acidic solutions containing sodium sulfite. The Kraft pulping process reduces the lignin content to 2–5 %, and its structure changes considerably. Some of the key structural features of post-pulping lignin are depicted below; these features are often part of larger entities (Scheme 4).



Scheme 4. Representative structures present in lignin after the pulping process. R denotes various side groups including lignin polymers.

Several processes have been developed to bleach Kraft pulp. Chlorine-based bleaches have been applied since the 1930s. Initially, hypochlorite-based bleaches were used, but it was subsequently found that the amount of bleaching chemicals could be reduced in a multistage process by applying elemental chlorine followed by hypochlorite. Processes employing these oxidants are under environmental pressure, as there is concern about the release of chlorinated organic compounds in their waste streams. Chlorine dioxide has been found to be an excellent pulp-bleaching agent. It gives good whitening and very little cellulose damage, whilst the amount of chlorinated materials in the waste streams is much reduced compared to the use of Cl_2 or ClO^- and, as a result, ClO_2 has been applied since the 1940s.

Oxygen-based bleaching processes have been developed to further decrease the amount of chlorine-based chemicals, and they are used on large scale. The main chemicals used are dioxygen, ozone, and hydrogen peroxide. Dioxygen is being applied to improve delignification directly after the Kraft pulp process. This process takes place under fairly high pressure (5–10 atm) and at high temperatures (80–120 °C). It removes about 50 % of the residual lignin, and less bleaching chemicals are needed in subsequent stages. More extensive delignification using the O_2 process leads, however, to more cellulose damage and thus paper of poorer quality. Cellulose degradation is thought to be caused by transition-metal-induced auto-oxidation/radical reactions, very similar to those described for cotton degradation observed in detergents.

Ozone is a very powerful oxidizing agent and is employed at relatively low temperatures (20–40 °C). The process conditions require careful monitoring, as non-selective hydroxyl radicals are formed at higher temperatures that reduce the pulp strength.

Hydrogen peroxide is applied at higher temperatures than the other bleaching chemicals (90–110 °C). In alkaline media the hydroperoxyl anion eliminates various chromophores in the lignin structures. In particular, the carbonyl structures are prone to react with nucleophilic HOO^-, in a similar way to that described for tea stain bleaching. Further degradation products of lignin are formed during these processes, leading to formation of carboxylic acids that are more soluble. Trace metal ions present in the pulp may also play a role in the bleaching reactions. It has been suggested that due to activation of hydrogen peroxide by Cu and Fe ions, hydroxyl radicals are formed that subsequently lead to bleaching and cellulose damage in poorly stabilized bleaching systems.[18]

The lignin content in pulp is commonly determined by titrating the lignin with potassium permanganate solutions that gives the so-called kappa value.[18] The brightness of pulp/paper is determined by measuring the reflectance at 457 nm.[18] The chemical damage of the cellulose material is determined, typically, from the viscosity of the cellulose, which gives an indication of the polymer chain length. In general, cellulose with lower viscosity gives a paper of reduced strength.[18]

In addition to chemical pulp, there are two other major sources of paper. Mechanical pulp is a different type of wood pulp, in which the lignin is still largely present. Mechanical pulp requires bleaching, and H_2O_2 is the most commonly employed reagent for this. Recycle-pulp is made out of old paper and cartons. Apart from colored lignin residues originating from chemical and mechanical pulp, the removal of dyes used in the printing process is necessary. This is frequently achieved through a combination of H_2O_2 and reductive bleaching steps using sodium dithionite.

Related to paper and pulp bleaching is the application of bleaching agents to the bleaching of raw cotton.[1,17,19] Chlorine-based bleaches (elemental chlorine or hypochlorite), chlorine dioxide, hydrogen peroxide, or ozone are applied to produce white cotton; however, as few patents have been published on the application of transition-metal based catalysts in raw cotton bleaching, no further discussions on this topic will be given here.

3. Manganese Bleaching Catalysts

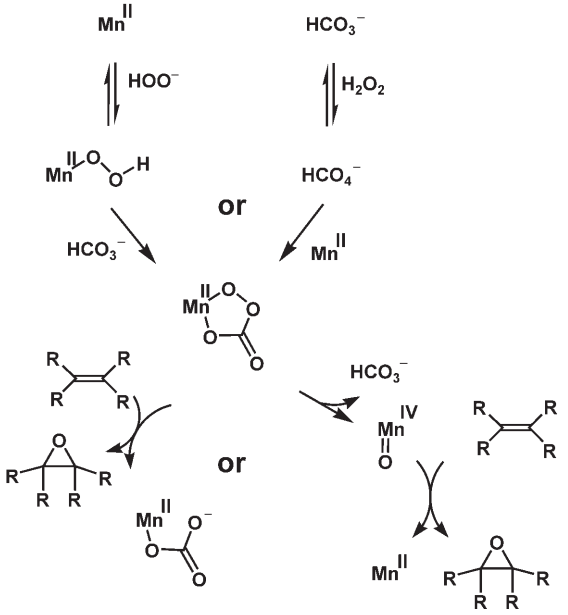
3.1. Manganese Salts

Since the mid 1980s several patents have been published, which deal with the application of metal salts in laundry cleaning. Manganese salts have been claimed as activators of hydrogen peroxide in detergent formulations containing sodium carbonate.[20] Reasonably good bleaching activity at 40 °C was reported by using the tea-model stain BC-1. However, the potential application is limited due to occasional staining, which originates from the deposition of manganese dioxide on the fabrics. It is interesting to note that many years later Burgess et al. reported the high activity of manganese salts in bicarbonate buffers towards epoxidation of a wide variety of alkenes using H_2O_2.[21] When additives such as sodium acetate are employed, both electron-rich and electron-poor alkenes are epoxidized. Burgess proposed the initial formation of a peroxycarbonate–manganese species. This species either attacks the alkene directly or

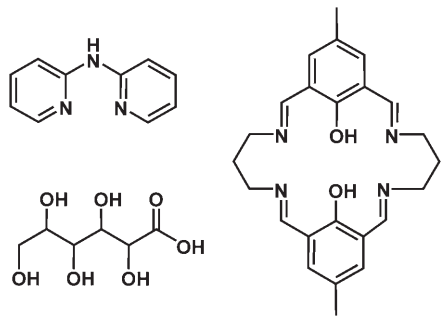
 © 2006 Wiley-VCH Verlag GmbH & Co. KGaA, Weinheim

forms an intermediate high-valent manganese–oxo species that transfers the oxygen atom to the substrate (Scheme 5).

The deposition of manganese dioxide on the fabrics can be inhibited by releasing manganese ions slowly using manganese-exchanged zeolites.[22] Another approach, initially taken, was the use of transition-metal salts in combination with sequestering agents such as EDTA, heptonic acids, and gluconates to either deliver the appropriate amounts of free metal ions in the wash solutions or to use the complex formed in the wash solution.[23] Subsequently several other patents were published that describe manganese, iron, copper, and cobalt compounds coordinated to various classes of organic ligands to activate H_2O_2 (Scheme 6).[24–26] The activity towards stain bleaching was in all cases low, and none of the compounds patented have seen application.



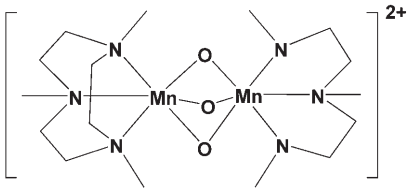
Scheme 5. Postulated mechanisms for the epoxidation of alkenes by the manganese-carbonate-hydrogen peroxide system.[21]



Scheme 6. Ligands patented as bleach catalysts in combination with Mn, Fe, Cu, and Co.

3.2. Manganese–Triazacyclononane Complexes

The first bleach catalyst employed in commercial detergent products was a dinuclear manganese compound containing 1,4,7-trimethyl-1,4,7-triazacyclononane (Me_3tacn) ligands (Scheme 7).[27] The compound was first published in 1988 as a model for manganese-containing enzymes by Wieghardt and co-workers.[29–32] According to the examples



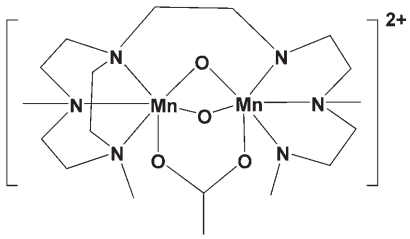
Scheme 7. Dinuclear Mn–Me_3tacn catalyst. Me_3tacn = 1,4,7-trimethyl-1,4,7-triazacyclononane.

given in the original patent, the bleaching activity at 40 °C on tea-model stains is very high.[27] Other stains such as wine, fruit, and curry stains were also bleached efficiently, in all cases using hydrogen peroxide. The efficiency of tea stain bleaching is optimal between pH 9 and 11. However, the detergent product containing this catalyst was withdrawn from the market after it was alleged that the product yields increased fabric- and dye-damage.[28] The catalyst is still applied in various machine-dishwashing products and is responsible for superior removal of tea residues.

The mechanism of the oxidation process was investigated by using phenolic compounds and catechol as models for tea stains.[33,34] Based on EPR spectroscopic measurements, it was suggested that the first step involves a one-electron-transfer process from the phenolate ion to the EPR-silent $[Mn^{IV}_2(\mu\text{-}O)_3(Me_3tacn)_2]^{2+}$, which yields an EPR-active $Mn^{III}Mn^{IV}$ species.[33,34] After the initial reduction, additional EPR signals were found that are typical for mononuclear Mn^{IV} compounds[33] and electrospray mass spectrometry (ES-MS) measurements support this.[35] The dinuclear complex itself is stable against hydrolysis, thus reduction is required for monomer formation. The initial reduction seems to involve one electron or H•, and phenoxyl radicals are formed when using Trolox, a water-soluble phenol derivative. This is observed in both the absence and presence of H_2O_2.[34a]

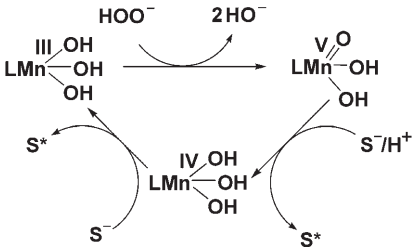
As the second step, oxidation to Mn^{IV} or Mn^{V} species is assumed, which can be either mono- or dinuclear. Comparison with the pH-dependent stain bleaching activity of $[Mn^{IV}Mn^{III}(\mu\text{-}O)_2(\mu\text{-}CH_3COO)(Me_4dtne)]^{2+}$, which contains a stable dinuclear $Mn^{III}Mn^{IV}$ core, led to the conclusion that both mononuclear and dinuclear Mn-Me_3tacn species are operative (Scheme 8).[33] This compound was originally synthesized and studied by Wieghardt and co-workers.[37] On the other hand, ES-MS experiments indicated that only a mononuclear species is formed, formulated as [(2,2-bisphenolato)-$(Me_3tacn)Mn^{V}$=O], when $[Mn^{IV}_2(\mu\text{-}O)_3(Me_3tacn)_2]^{2+}$ is allowed to react with H_2O_2 and 4-methoxyphenol.[34b,35] A more recent paper by the same group discusses the oxidation of azo-containing dyes catalyzed by $[Mn^{IV}_2(\mu\text{-}O)_3$-$(Me_3tacn)_2]^{2+}$.[36] The involvement of mononuclear $\{Mn^{V}=O\}$ species was again postulated. The authors indicate in the paper that the oxomanganese species gives rise to two, one-electron oxidations of the azo dye, and therefore it mimics the

© 2006 Wiley-VCH Verlag GmbH & Co. KGaA, Weinheim



Scheme 8. Dinuclear manganese complex with Me_4dtne for stain and pulp bleaching; Me_4dtne = 1,2-bis(4,7-dimethyl-1,4,7-triazacylonone-1-yl)ethane.

activity of heme-peroxidases (Scheme 9). EPR-sensitive spin traps did not give indications for the formation of hydroxyl radicals.[36]



Scheme 9. Mechanistic cycle postulated for oxidation of azo dyes by the Mn–Me_3tacn catalyst in the presence of hydrogen peroxide.[36]

Contrary to this, Meunier and co-workers came to the conclusion that hydroxyl radicals are responsible for the oxidation. They studied the reactivity of $[Mn^{IV}_2(\mu\text{-}O)_3(Me_3tacn)_2]^{2+}$ and H_2O_2 with catechol in the absence and presence of mannitol and found that the quinone formed degrades faster in the absence of mannitol than in the presence of it.[38] They interpreted this as the trapping of hydroxyl radicals by mannitol, though no additional measurements were conducted such as EPR spin-trapping experiments. Therefore other explanations may be valid, such as binding of mannitol to the active species that may prevent oxidation activity in this system.

Selective epoxidation by $[Mn^{IV}_2(\mu\text{-}O)_3(Me_3tacn)_2]^{2+}$ and H_2O_2 was reported for styrene and 4-vinylbenzoic acid.[33] Additionally, the two mononuclear complexes $[Mn^{IV}(Me_3tacn)(CH_3O)_3]^+$ and $[Mn^{IV}(L)]^+$ (H_3L = 1,4,7-tris(hydroxyethyl)-1,4,7-triazacyclononane) were studied with regard to their epoxidation activity on the water-soluble olefins 4-vinylbenzoic acid and styrylbenzoic acid.[33,40] At pH 8 both complexes have total turnovers of at least 400 for the formation of the epoxide, concomitant with decomposition of the H_2O_2 added. Mechanistic studies using $H_2{}^{18}O_2$ and $[Mn^{IV}(L)]^+$ revealed that the epoxide is fully labelled; this shows, that oxygen transfer takes place from the coordinated hydrogen peroxide species or a species derived thereof.[41] No hydroxylation of the aromatic group of styrene was observed and thus hydroxyl radicals are unlikely to form under these conditions.

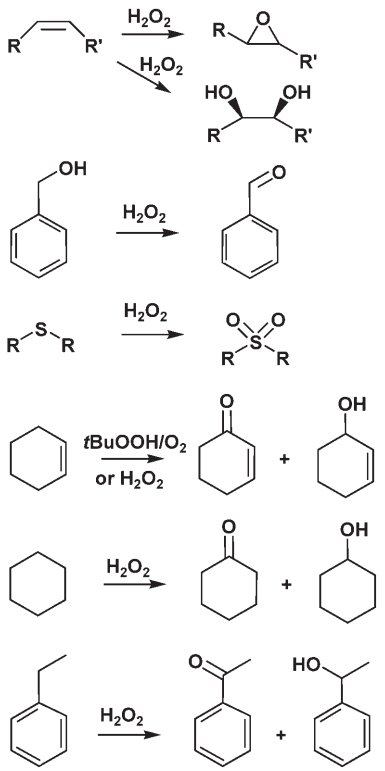
More surprising though is the fact that $[Mn^{IV}(L)]^+$, in contrast to $[Mn^{IV}_2(\mu\text{-}O)_3(Me_3tacn)_2]^{2+}$, does not catalyze stain bleaching.[33] This seems to indicate that the chemistry required to oxidize polyphenolic chromophores is distinct from the chemistry required for oxygen transfer to an alkene. However, this observation might be explained by the different pH values at which the reactions have been carried out (pH 8 versus pH 10–10.5), the stability of the catalyst in the detergent formulation, or specific interactions with the stain.

$[Mn^{IV}_2(\mu\text{-}O)_3(Me_3tacn)_2]^{2+}/H_2O_2$ in a buffer/acetone mixture also epoxidizes cinnamic acid.[42] As observed for the manganese compound with tris(hydroxyethyl)-tacn,[40] the epoxide becomes fully ^{18}O-labeled when using $[Mn^{IV}_2(\mu\text{-}O)_3(Me_3tacn)_2]^{2+}$ with $H_2{}^{18}O_2$.[42] Again, ES-MS signals of mononuclear species were detected, which were assigned to $[(Me_3tacn)Mn^{IV}(OH)_3]^+$ and $[(Me_3tacn)Mn^{IV}(O)(OH)]^+$. The latter species would imply a pentacoordinate Mn^{IV} species, which is unusual for a low-spin d^3 system. Be that as it may, these studies led to the suggestion that the same $\{Mn^{V}{=}O\}$ species is involved in the catalysis as described for the oxidation of phenol and styrene. Electron-rich derivatives of cinnamic acid are converted most efficiently, which is indicative of an electrophilic {Mn=O} center.

High epoxidation activities of manganese Me_3tacn species have been reported in nonaqueous media, too.[48–53] Depending on the conditions, total turnover numbers as high as 4000 are achievable. When acetone is used as solvent, the decomposition of hydrogen peroxide can be suppressed and selectivity towards epoxidation increased.[48b,49] High epoxidation activity was also observed in acetonitrile, provided that additives such as oxalate or ascorbic acid are present, but no information on the active species is available.[48c,50] Enantioselective epoxidation of substitued styrenes was achieved by Bolm and co-workers by using a chiral tacn derivative, 1,4,7-*S*,*S*,*S*-tris(2-hydroxypropyl)-1,4,7-triazacyclononane.[53] Other oxidation reactions (Scheme 10) include *cis*-dihydroxylation of cyclooctene,[52a,54] oxidation of benzyl alcohol to benzaldehyde,[55] oxidation of sulfides to sulfoxides and sulfones,[56,61,62] allylic CH oxidation of cyclohexene to the alcohol and ketone,[57] and alkane oxidations by radical reactions.[39,58–60] Frequently $\{Mn^{V}{=}O\}$ intermediates are assumed, but a coherent mechanistic understanding is still lacking. It is clear, however, that both typical oxygen-transfer and hydrogen-abstraction reactions are catalyzed. Based on the reactivity of $[Mn^{IV}_2(\mu\text{-}O)_3(Me_3tacn)_2]^{2+}/H_2O_2$ in aqueous solutions, it is assumed that the bleaching activity observed primarily originates from epoxidation/oxo transfer, though there is no definitive proof for this hypothesis.

The aforementioned dinuclear tacn-bridged compound, $[Mn^{IV}Mn^{III}(\mu\text{-}O)_2(\mu\text{-}CH_3COO)(Me_4dtne)]^{2+}$, was later claimed for pulp bleaching/delignification in combination with H_2O_2 by Patt and co-workers.[43] The examples given in the patent mentioned good bleaching of Kraft pulp at moderate temperatures (50 °C as compared to 90 °C in conventional hydrogen peroxide bleaching).[44] The degree of viscosity loss of cellulose was very low, indicating that efficient pulp bleaching, without concomitant cellulose damage, can be achieved with this catalyst. In contrast, $[Mn^{IV}_2(\mu\text{-}O)_3(Me_3tacn)_2]^{2+}$ did exhibit cellulose damage as

 © 2006 Wiley-VCH Verlag GmbH & Co. KGaA, Weinheim



Scheme 10. Examples of substrate conversions catalyzed by the Mn–Me_3tacn system.

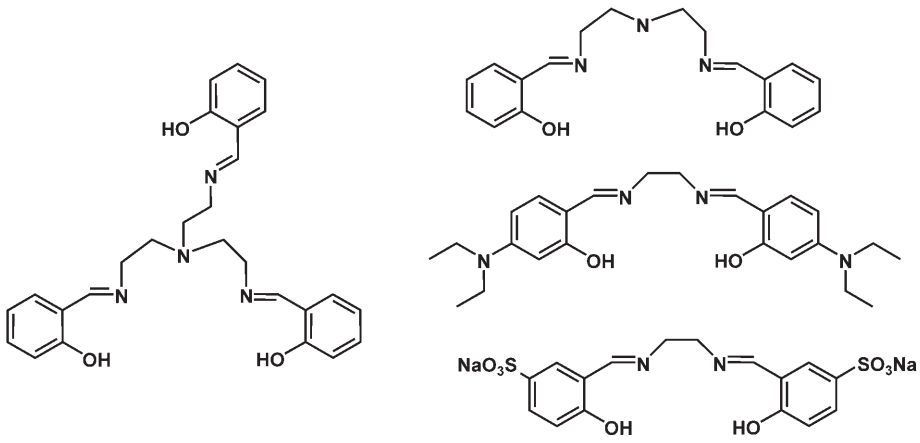
well as pulp bleaching.[43] $[Mn^{IV}_2(\mu\text{-}O)_3(Me_3tacn)_2]^{2+}$ was subsequently found to show a similar or even higher activity than the bridged catalyst for bleaching and delignification of wood pulp,[45] whilst in another study it became apparent that the extent of lignin bleaching depends very much on the conditions applied (temperature, hydrogen peroxide and NaOH dosage, and catalyst concentration).[47]

In various subsequent papers, the conditions of the pulp bleaching processes and proposals for mechanisms using the Mn–Me_4dtne complex were given.[44–46] For the pulp bleaching process a dinuclear Mn–hydroperoxo species is thought to oxidize the lignin. However, this contradicts various mechanistic schemes discussed for the Mn–Me_3tacn complexes, where mainly mononuclear high-valent oxomanganese species were postulated. Based on reactions with model substrates for lignin, Chen and coworkers suggested that an initial one-electron oxidation takes place by the hydroperoxomanganese species, whilst in the second step a hydroxyl radical is released, which results in further degradation.[45b] No evidence was given for the involvement of either species in the lignin-degradation reactions. Subsequently, the oxidation products obtained in the catalytic bleaching were analyzed in detail.[45c] A combination of electron transfer and reactions with hydroxyl radicals was proposed to account for the lignin degradation products observed,[45c] which was further supported by kinetic data.[45d] Hydroxyl radicals, however, are generally assumed to be extremely powerful oxidizing species that react unselectively with rate constants close to diffusion. Therefore their involvement would lead to cellulose degradation, as observed previously using unstabilized hydrogen peroxide at high temperatures.[12,46] As the Mn–Me_4dtne catalyst does not show cellulose damage, these hydroxyl radicals are unlikely to be relevant. A comparison with $[Mn^{IV}_2(\mu\text{-}O)_3(Me_3tacn)_2]^{2+}$ was also made.[45e] The reaction products observed were very similar, and a suggestion was made that a similar mechanism is operative. A difference noted was that $[Mn^{IV}Mn^{III}(\mu\text{-}O)_2(\mu\text{-}CH_3COO)(Me_4dtne)]^{2+}$ shows a slower oxidation reaction towards Kraft pulp and lignin model substrates than $[Mn^{IV}_2(\mu\text{-}O)_3(Me_3tacn)_2]^{2+}$.[45e]

3.3. Manganese Schiff-Base complexes

A variety of manganese complexes containing Schiff-base ligands were patented for stain bleaching and dye-transfer inhibition by Ciba, Clariant, and Henkel.[63–65] In most cases the oxidation state of the manganese center is III. Scheme 11 depicts the structures of some of the ligands in these complexes. The catalysts generally activate hydrogen peroxide to yield an improved tea stain bleaching, and in some cases they outperform the conventional TAED/percarbonate bleaching system.[64,65] Compounds patented by Ciba inhibit dye-transfer, too, which sometimes occurs when colored garments are combined with white articles. This is prevented by dye oxidation in solution.[63] The manganese Schiff-base compounds are less efficient catalysts than the Mn–Me_3tacn complexes in Section 3.2, but according to the patents, they cause less dye-fading on the cloths and are easier to synthesize.[63] Ciba has marketed one of the manganese Schiff-base compounds as a bleach catalyst, depicted in Scheme 11, left, especially suitable for low-temperature bleaching,[66] but no public information is available whether it is incorporated in any laundry product.

None of the patents give details on the mechanism, but the reactivity of manganese Schiff-base compounds has been



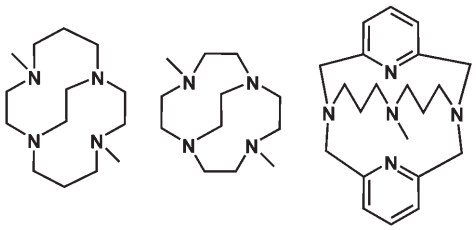
Scheme 11. Examples of Schiff-base ligands, which together with manganese have been patented as bleach catalysts.

© 2006 Wiley-VCH Verlag GmbH & Co. KGaA, Weinheim

studied in nonaqueous solutions.[67–71] Highly enantioselective oxidations have been obtained by using hypochlorite, iodosobenzene, or hydrogen peroxide in the presence of nitrogen donors such as imidazole. The involvement of an electrophilic {Mn^{V}=O} intermediate has been postulated, which yields a substrate radical intermediate.

3.4. Manganese Cross-Bridged Macrocyclic Complexes

D. H. Busch and co-workers synthesized and studied manganese and iron complexes with cross-bridged tetraaza- and pentaaza macrocyclic ligands (Scheme 12).[72–74] This class



Scheme 12. Cross-bridged macrocyclic ligand, together with manganese have been patented as bleach and oxidation catalysts.

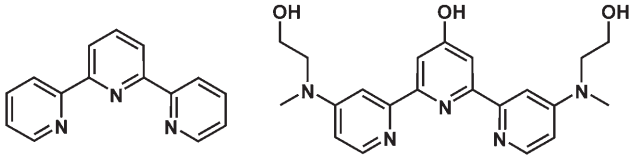
of ligands was originally reported by Weisman and co-workers.[75] Procter & Gamble patented manganese and iron complexes with both classes of ligands for stain bleaching.[72,73a] Initially, the patents claimed detergent compositions containing peroxy bleaches, that is, hydrogen peroxide, whilst in a later patent this was extended to detergent formulations without any peroxy compound.[73b] Examples of formulation mixtures with the catalyst are given, but none of these patents report stain-bleaching data. The most preferred ligand is the left structure given in Scheme 12, abbreviated as biscyclam. The Mn^{II} and Fe^{II} complexes with the biscyclam ligand show extremely high kinetic stabilities, as no formation of MnO_2 was observed, even after leaving the manganese complexes for several weeks in a 2 N NaOH solution. The Fe^{II} complex is stable for at least one month in very acidic (pH 1) and basic (pH 13) solutions.[74b] The [$MLCl_2$] complexes (M = Fe, Mn) undergo rapid exchange of the chloride ligands for aqua ligands in aqueous solution.

No details of the bleaching mechanism have been published, but Busch and co-workers reported that presumably a Mn^{IV} species epoxidizes carbamazepine in methanol/water in the presence of hydrogen peroxide or monopersulfate as oxidant.[74e] A high activity was, however, also observed when 1,4-cyclohexadiene was used as model substrate, which is indicative for H·-abstraction reactions.[74e] This shows that this compound catalyzes a variety of reactions.

Reactivity studies with the manganese complex with the cross-bridged pentadendate ligand depicted in Scheme 12, right, revealed that both with *t*BuOOH and hydrogen peroxide mainly radical species are formed. By using EPR-sensitive radical traps, *t*BuOO· radicals are trapped, whilst with H_2O_2 the hydroperoxyl radical was detected. No indications for the formation of high-valent metal species or metal–peroxo species were obtained,[74a] but this does not exclude that these species are present.

3.5. Manganese Complexes with 2,2′:6,2″-Terpyridine

Ciba published two patents on the application of manganese complexes with various terpy ligands for stain-bleaching, which stated that they activate hydrogen peroxide and enhanced tea stain bleaching (Scheme 13).[76] Perfor-



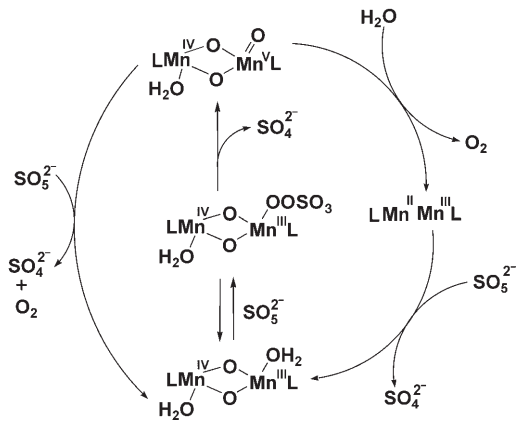
Scheme 13. Structure of 2,2′:6′,2″-terpyridine (terpy; left) and the example of a modified terpy ligand (right).

mance exceeding that of the TAED/percarbonate bleaching system is reported without significant dye-fading on cotton. Examples of epoxidation activity were also given. A later patent was filed which claimed that similar compounds also have a bleaching effect on stains using molecular oxygen. This was exemplified by tea stain bleaching in a detergent formulation without any peroxy-bleaching agent added.[77]

In two recent papers, Wieprecht et al. published mechanistic studies using homogeneous model substrates such as Morin (3,5,7,2′,4′-pentahydroxyflavon) as a flavonoid substrate and Trolox (a water-soluble vitamin E analogue).[78] The ligands with the greatest activity contain electron-donating amino substituents. The homogeneous bleaching activities of these catalysts in the presence of hydrogen peroxide were compared with those of $[Mn^{IV}_2(\mu\text{-}O)_3(Me_3tacn)_2]^{2+}$, and on Morin two of the Mn–terpy catalysts outperform the latter Mn–Me_3tacn catalyst. When using Trolox, only one of the catalysts remains active with an activity similar to that of $[Mn^{IV}_2(\mu\text{-}O)_3(Me_3tacn)_2]^{2+}$. The redox potentials of Morin and Trolox are similar, and it was suggested that the less active Mn–terpy complex reacts by a different pathway. Trolox can be oxidized by one-electron transfer or coupled proton/electron transfer only, whilst Morin can be oxidized by a variety of oxidation mechanisms.[78]

Interestingly, Mn–terpy bis-μ-oxo dimers catalyze the oxidation of water with monopersulfate as oxidant.[79] A {$Mn^{IV}Mn^{V}$=O} species was suggested as an intermediate on the basis of the results of labeling experiments, EPR, resonance Raman spectroscopy, electrospray mass spectrometry, and kinetic analyses. Brudvig et al. proposed that upon reaction of this intermediate with water a $Mn^{II}Mn^{III}$ intermediate is formed (four-electron transfer), which upon reaction with two equivalents of monopersulfate regenerates the high-valent active species (Scheme 14).[79b]

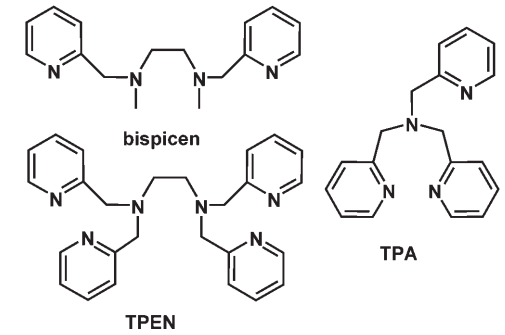
 © 2006 Wiley-VCH Verlag GmbH & Co. KGaA, Weinheim



Scheme 14. Proposed scheme for the oxidation of water catalyzed by the Mn–terpy dimer with monopersulfate.

3.6. Manganese Complexes with Polypyridineamine Ligands

Henkel claimed that the application of manganese complexes with TPA ligands (Scheme 15) yielded improved stain bleaching.[80] No stain-bleaching examples are included in the patent, but the data reported show accelerated homogeneous bleaching of Morin using $[Mn^{II}_2(TPA)_2(\mu\text{-}CH_3COO)_2]^{2+}$. Clariant claimed that manganese complexes with TPEN ligands (Scheme 15) were suitable for detergent applications.[81] In combination with hydrogen peroxide this compound catalyzes the bleaching of tea, red beetroot, and curry stains. Increased bleaching was also obtained in the presence of various peracids. Elf-Atochem patented the use of dinuclear manganese complexes with bispicen (Scheme 15) and TPA for pulp-bleaching with hydrogen peroxide.[82] The examples show an increased delignification of chemical pulp on using $[Mn^{III}Mn^{IV}(\mu\text{-}O)_2(TPA)_2]^{3+}$ at acidic pH values. Further it was shown that the depolymerization of cellulose by these complexes is low. It should be noted that the amount of catalyst used was high (e.g., 75 mmol complex per kg pulp or 18 g Mn-TPA per ton of pulp). Clearly, these conditions are quite different from the detergent experiments, which were conducted at about pH 10 using much lower concentrations of catalyst. Based on electrochemical studies on $[Mn^{III}Mn^{IV}(\mu\text{-}O)_2(TPA)_2]^{3+}$ the conclusion was drawn that electron-transfer processes from the lignin to the oxidized Mn species explain the enhanced pulp-bleaching activity. Kinetic studies indicated that diffusion of the complex into the pulp fibers may be the limiting step in the bleaching process.[83] No studies have been published to date that explain the oxidation activity under detergent conditions.



Scheme 15. Ligands, which together with manganese have been patented for pulp bleaching. TPA = (tris(pyridin-2-ylmethyl)amine; TPEN = tetrakis(pyridin-2-ylmethyl)ethylenediamine; bispicen = *N*,*N*′-bis(pyridin-2-ylmethyl)-1,2-diaminoethane.

Feringa and co-workers reported that manganese complexes containing TPPN (TPPN = *N*,*N*,*N*′,*N*′-tetrakis(pyridin-2-ylmethyl)-proponane-1,3-diamine) catalyze the epoxidation of alkenes and the oxidation of alcohols into aldehydes and ketones, efficiently using hydrogen peroxide as oxidant and acetone as solvent.[84] *N*-Benzyl-*N*,*N*′,*N*′-tris(pyridin-2-ylmethyl)-1,2-diaminopropane in combination with manganese(III)acetate yields a much faster rate of alcohol oxidation, which further improved by using the 3-methylated pyridine analogues. EPR and ES-MS experiments revealed that both mononuclear and dinuclear species are formed upon mixing these ligands with the manganese salts, but no mechanistic proposal was given.[84b]

4. Iron Bleaching Catalysts

4.1. Iron Complexes with Tris(pyridin-2ylmethyl)amine (TPA)

Iron complexes with TPA as ligand were patented to be activators for peroxy compounds and thus to yield substrate oxidation. This includes dye-bleaching in solution as well as a modest stain-bleaching, both in the presence of hydrogen peroxide.[85] No mechanistic details have been published so far on the specific bleaching chemistry of the Fe–TPA system in aqueous solution, but Que and co-workers have studied the oxidation chemistry of the Fe–TPA system in organic solvents. When cyclohexane was used as substrate, cyclohexanol and cyclohexanone are formed, whereby the alcohol was formed in large excess when H_2O_2 was added carefully under O_2-depleted conditions.[86] From detailed mechanistic investigations, it was inferred that the active intermediate is a high-valent metal–oxygen-based oxidant. The same catalysts convert alkenes both to epoxides and *cis*-diols.[87] Using a variety of approaches, it was suggested that the reaction with hydrogen peroxide generates $[(TPA)Fe^{III}(OOH)(CH_3CN)]^{2+}$, which upon ligand exchange with water forms $[(TPA)Fe^{III}(OH_2)(OOH)]^{2+}$. Heterolytic cleavage of the O–O bond generates a high-valent $\{HO\text{-}Fe^{V}{=}O\}$ species, which then reacts with the substrates (Scheme 16). The analogous catalyst with tris(6-methylpyridin-2ylmethyl)amine is assumed to generate a nucleophilic side-on Fe^{III}-peroxo species that gives efficient diol formation using electron-poor olefins (Scheme 16).[87b–d] A dinuclear complex, $[(TPA)Fe^{IV}(\mu\text{-}O)_2Fe^{III}(TPA)]^{3+}$, was shown to react very



Scheme 16. Postulated reactive intermediates in the hydroxylation and epoxidation reactions observed for Fe–TPA/H_2O_2.

 © 2006 Wiley-VCH Verlag GmbH & Co. KGaA, Weinheim

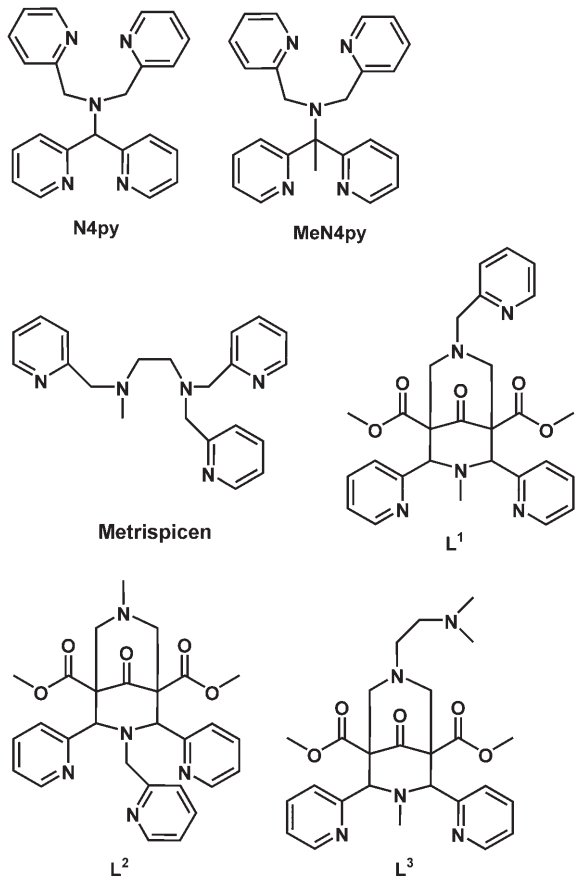
differently; phenolic substrates yield the phenoxy radicals and cumene forms cumylhydroperoxide via a radical intermediate.[88]

The mechanism differs when alkyl hydroperoxides are used as oxidant. Fe–TPA complexes are assumed to form an alkyl hydroperoxo intermediate with *t*BuOOH,[89] which cleaves the O–O bond homolytically to yield an alkoxy radical and a putative {Fe^{IV}=O} species. As a consequence, this system elicits radical-based processes,[89a] such as the formation of ketones and alcohols, mainly in a ratio of about 1:1 from cyclohexane. However, in addition to alkoxy radicals, the mononuclear {Fe^{IV}=O} species was proposed to be involved in the reactions. Reactivity studies have revealed that this species reacts with substrates such as thioanisole, cyclohexanol, and cyclooctene by two-electron oxidations, provided that the high-valent metal center is in close proximity to the substrate.[89b] Direct spectroscopic evidence for the formation of the {Fe^{IV}=O} species was more recently reported and characterized by using a variety of techniques.[90] Using arene-substituted TPA ligands, it was shown that the putative {Fe^{IV}=O} species reacts as an electrophilic oxidant, as hydroxylation at the *ortho* position of the phenyl ring was observed.[91]

4.2. Iron Complexes with Pentadentate Nitrogen-Donor Ligands

Various classes of iron complexes containing pentadentate nitrogen-based ligands have been studied in recent years. A patent filed by Unilever claimed the application of the iron complexes of N4py (Scheme 17) in combination with hydrogen peroxide.[92] Compared with the Fe–TPA complexes, the Fe–N4py system is a superior catalyst, as exemplified on model tea stains.[92] In addition, homogeneous azo-dye bleaching and alkane functionalization are mentioned in this patent. The derivative Fe–MeN4py (Scheme 17) shows an even higher activity for bleaching tea stains,[93] which is most likely associated with its higher intrinsic stability, since in this case the sensitive benzylic CH position is protected by a methyl group.[94] The same compounds were also claimed in various patents to yield stain bleaching by employing atmospheric oxygen only.[95a,b] Examples mentioned in these patents show complete removal of tomato stains and improved bleaching of curry-type stains. As is the case with most patents, no information on the mechanism is included. However, these claims are quite novel for this type of compounds, as most of the reactivity studies published were conducted in combination with hydrogen peroxide or alkyl hydroperoxide. Subsequently, the combination of catalysts with unsaturated soaps has been protected by Unilever. This patent also claims that air bleaching could be extended to hydrophilic stains.[95c] A patent filed later suggested that the reactivity on stains containing unsaturated oils is due to the formation of hydroperoxides.[95d]

Although the detergent compositions are free of hydroperoxides or hydrogen peroxide precursor (percarbonate or perborate), the chemistry observed for this catalyst can be explained on the basis of hydroperoxide chemistry, as outlined below.[95e] Also iron complexes with pentadentate



Scheme 17. Structures of representative examples of pentadentate nitrogen-donor ligands discussed in the text.

ligands based on 1,4,7-triazacyclononane groups containing two heteroaromatic rings, such as pyridin-2-ylmethyl and quinolin-2-ylmethyl, have been patented as bleaching catalysts both in detergent formulations without peroxy bleaches and with peroxy bleaches.[95f–h]

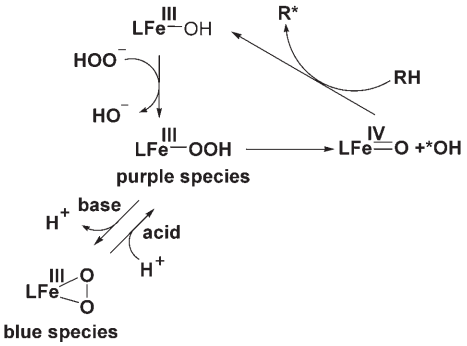
Elf-Atochem published a patent on the application of iron and manganese complexes with ligands based on Metrispicen (Scheme 17) for pulp bleach catalysts in combination with H_2O_2 (see Section 3.6).[82] Similar compounds were claimed by the same researchers to catalyze other oxidation reactions such as alkane hydroxylation.[96] Some years later, Unilever published a series of iron complexes with trispicen analogues that were methylated at the 3- or 5-positions of the pyridine rings. These compounds bleach tea stains more efficiently than the parent trispicen complexes using hydrogen peroxide as oxidant.[97]

Bispidon ligands L^1–L^3 (Scheme 17) belong to another class of iron complexes with N5 donors patented for stain bleaching.[98,99] These complexes also bleach tomato and curry stains efficiently using atmospheric oxygen only.[98,99b] The iron complex of ligand L^3 together with hydrogen peroxide was also reported to have a wide stain-removal profile, that is, on hydrophilic stains such as tea as well as oily tomato and curry stains.[99c]

 © 2006 Wiley-VCH Verlag GmbH & Co. KGaA, Weinheim

The pentadentate iron complexes have been studied extensively in nonaqueous media.[100–109] The Fe–N4py, Fe–trispicen and Fe–bispidon complexes react quite differently with H_2O_2 compared to $[(TPA)Fe^{II}(CH_3CN)_2]^{2+}$. Commonly purple intermediates are formed that are described as $[LFe^{III}OOH]^{2+}$. This intermediate has been characterized spectroscopically for Fe–N4py,[100a] Fe–Metrispicen,[104,105] and Fe–bispidin complexes with L^1 and L^2 (Scheme 17).[109a] The species formed are similar to the one proposed for bleomycin.[110] Although analysis by X-ray crystallography of such an adduct has not been reported for these complexes, their properties were studied by using a wide variety of spectroscopic techniques.[100a,104,105,106b,108] It was concluded that the hydroperoxide anion is bound in an end-on fashion to the low-spin iron(III) center. Addition of base to the purple intermediate species of the Fe–N4py, Fe–trispicen, and Fe–bispidon complexes leads to the formation of a blue intermediate that has been suggested to be a high-spin Fe^{III} side-on peroxo adduct based on UV/Vis absorption, ES-MS, resonance Raman, and EPR spectroscopy.[102a,106b,109a]

The purple {Fe^{III}–OOH} species of N4py and Metrispicen induce radical-based oxidations,[100d,107a] whilst the blue side-on {$Fe^{III}O_2$} species exhibits a very weak reactivity. Feringa, Que, and co-workers suggested that the oxidation chemistry observed for Fe–N4py originates from two different species that result from the homolytic cleavage of the purple {Fe^{III}–OOH}, namely an {Fe^{IV}=O} and a hydroxyl radical. Both species are hydrogen atom abstractors, but {Fe^{IV}=O} is more selective.[100d] A summarizing reaction scheme has been proposed tor the reactivity of Fe–N4py/hydrogen peroxide (see Scheme 18).



Scheme 18. Reactions of Fe–N4py and Fe–trispicen complexes with hydrogen peroxide.

The {(N4py)Fe^{IV}=O} species was obtained independently by reacting the $[Fe(N4py)(CH_3CN)]^{2+}$ with iodosylbenzene. This species induces CH abstraction,[101b] in agreement with the studies discussed above.[100d] Alkanes with quite strong C–H bonds of 99.3 kcal mol^{-1} can be hydroxylated. The kinetic isotope effect observed is large, indicating that the H$^{\bullet}$-transfer is rate limiting. The {Fe^{IV}=O} species is assumed to be the only active species when hydrogen peroxide is replaced by peracids in the catalytic oxidation of cyclohexane.[111a] The reaction is efficient under anaerobic conditions giving an increased alcohol/ketone reaction. However, the presence of oxygen very much decreases the yields, which is explained by an Fe^{II}/Fe^{IV} cycle that is only operative in the absence of oxygen. The same {Fe^{IV}=O} species was also obtained in aqueous media by reacting Fe–N4py with monopersulfate or iodosylbenzene and is, at low pH, relatively stable.[111b] It has electrophilic character and transfers an oxygen atom to sulfide substrates.

For Metrispicen a {Fe^{IV}=O} species has been identified and characterized by reacting the Fe^{II} complex with hypochlorite. This species hydroxylates cyclohexane and epoxidizes cyclooctene. *cis*-Stilbene is oxidized to *trans*-stilbene epoxide, which led to the suggestion that a long-lived radical intermediate is formed.[108b]

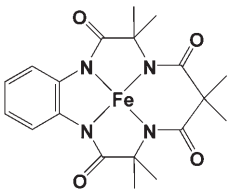
The Fe–bispidon complex with L^1 epoxidizes cyclooctene selectively under aerobic conditions using hydrogen peroxide as oxidant. The oxygen atom in the epoxide originates primarily from molecular oxygen rather than hydrogen peroxide, which is explained by radical reactions involving perhydroxyl-radicals.[109c] The Fe–bispidon complex with L^1 and L^2 form end-on and side-on hydroperoxide and peroxo species.[109a] The X-ray structures of two isomeric iron complexes with pentadentate bispidin ligands L^1 and L^2 (Scheme 17) with chloride and sulfate anions as co-ligands were determined and reveal distinct differences in the bond lengths of the co-ligands with the metal center.[109b] Though the redox potentials of the two L^1 and L^2 isomers are very similar, the iron–peroxo intermediates differ in their relative stability and physical properties.[109a] The isomer with the pyridine on the top of the bispidin moiety (L^1) shows a lower-energy resonance Raman vibration for the Fe–OOH bond, suggesting a weaker O–O bond. The principal difference between the complexes is observed when they are deprotonated. Whilst in the isomer with the pyridine below the bispidin unit (L^2) shows a stable side-on peroxo intermediate, this species could be formed only with difficulty for the other isomer with L^1.

The reactivity described for the iron catalysts containing pentadentate nitrogen donor ligands is dominated by radical chemistry and therefore quite different from that described for the manganese triazacyclononane based complexes. This might explain their reactivity towards oily food stains that are not susceptible to attack by the manganese catalysts.[95e] The aqueous bleaching chemistry with hydrogen peroxide is complicated by the different peroxo species that, at least for Fe–N4py, have been described in aqueous media.[12b] At the typical pH range of bleach-containing powders (9.5–10.5), the Fe–peroxide adducts mainly exist in their inactive side-on deprotonated form (blue species).[12b] However, as discussed in the introduction, many stains contain phenolic OH groups and become easier to oxidize at high pH. This effect may counter-balance the decreased reactivity of the iron–peroxo species. There is little information available to suggest which is the active intermediate oxidizing the chromophore of polyphenolic stains, but based on the studies in organic solvent, it is likely to be associated with {Fe^{III}OOH} or {Fe^{IV}=O} species. No indications were found that Fe–N4py type complexes generate hydroxyl-radical chemistry under alkaline conditions.[12b]

 © 2006 Wiley-VCH Verlag GmbH & Co. KGaA, Weinheim

4.3. Iron Complexes with Macrocyclic Tetraamidate Ligands

T. J. Collins developed Fe-based catalysts based on a class of macrocyclic tetraamide ligands (Scheme 19).[112–116] A number of applications are claimed, mostly in connection with solution bleaching such as waste water treatment and dye transfer inhibition for laundry cleaning.[113] A variety of dyes, relevant for detergents and waste water treatment, can be bleached in solution by employing hydrogen peroxide as oxidant.[116a] Stain removal and enhanced delignification has also been reported for this catalyst, the latter without significant loss of viscosity.[113b]



Scheme 19. An iron tetraamidate bleaching catalyst.

The tetraamidate ligands have a formal charge of −4 and stabilize high-valent metal species. For example, a $\{Mn^{V}=O\}$ complex was characterized by X-ray and spectroscopic analyses.[115] The electrophilicity of the oxomanganese center can be increased by replacing the benzene ring with pyridine, and then binding cations such as lithium to the pyridine.[115d] Oxygen-transfer reactions were studied by using triphenylphosphine. Addition of a scandium salt to the oxomanganese compound yielded an increase of the formation of triphenylphosphine oxide by more than three orders of magnitude as compared to the compound without added cation.

The mechanism of the catalytic bleaching action with hydrogen peroxide has not been published in detail, however, model reactions using *t*BuOOH as oxidant showed that ligand degradation takes place, most probably via an $\{Fe^{IV}=O\}$ species, which abstracts a hydrogen atom. By judicious choice of the side chains, the lifetime of the catalyst precursor can be altered significantly. The first generation of catalysts contained ethyl groups next to the carbonyl moieties. By replacing them with methyl groups the oxidative stability increased and with it the efficiency of this catalyst.[116a] Additionally, improvements to the hydrolytic stability were attained by changing the methyl groups next to the carbonyl moieties for fluorine groups or by introducing electron-withdrawing groups on the phenyl ring.[113a,116b]

More recently, it has been shown that the mononuclear Fe^{III} tetraamidato complex reacts with dioxygen to yield an oxo-bridged Fe^{IV} dinuclear complex.[116b] This species oxidizes PPh_3 to PPh_3O, benzyl alcohols to the corresponding aldehydes and the azo-dye Methyl Orange. The authors suggested that oxygen transfer for the oxidation of PPh_3 and two-electron transfer reactions for the conversion of the alcohol to the aldehyde takes place. No indications for free-radical autooxidation reactions were found.

5. Cobalt-Based Catalysts for Hydrogen Peroxide Activation

5.1. Cobalt Pentaammine Complexes

In the late 1980s, Interox disclosed the application of cobalt pentaammine complexes for the activation of hydrogen peroxide.[117] Procter and Gamble subsequently filed selection patents with specific claims on the sixth ligand being a carboxylic acid group.[118,119] One of the compounds has the potential for application in product formulations for use in dishwasher machines.[119] Griffith and co-workers have discussed some mechanistic aspects on hydrogen peroxide activation by $[Co(NH_3)_5Cl]Cl_2$.[120] They postulated that first ligand exchange takes place in alkaline aqueous solution to generate $[Co(NH_3)_5(OH)]^{2+}$ and subsequently ligand substitution occurs to yield $[Co(NH_3)_5(OOH)]^{2+}$. No further information concerning the subsequent bleaching reactions has been given.

5.2. Cobalt Complexes with Polypyridineamine Ligands

A series of cobalt and manganese catalysts complexes with tetradentate and pentadentate TPA, trispicen, and N4py ligands (Scheme 17) as bleach/delignification catalysts were patented by Degussa.[121] $[Co^{III}(N4py)(\mu\text{-}O_2)Co^{III}(N4py)]^{4+}$ induces delignification of Kraft pulp, however, quite large amounts of catalyst are needed to attain optimal activity (> 600 ppm). In the patent it was suggested that peroxocobalt(III) species are involved in the bleaching process. To the best of our knowledge no publications have appeared that deal with the mechanisms of hydrogen peroxide activation by this type of cobalt catalysts. Therefore, a meaningful discussion is not possible yet.

6. Catalysts for O_2-Induced Delignification

Weinstock, Hill et al. reported a novel way of delignifying pulp by using only oxygen as oxidant.[122,123] This process makes use of vanadium-containing polyoxometalates (POMs). Delignification is carried out under an inert atmosphere and the POMs act as the stoichiometric oxidant for the lignin. The POMs are filtered off and in a second vessel the POMs are re-oxidized by atmospheric oxygen. In the same process the solubilized lignin fragments are further oxidized and degraded. A one-step process using POMs and oxygen is possible but results in unacceptable damage of cellulose.[122] Initially, it was proposed that the POMs initiate auto-oxidation of the dissolved lignin species, although later studies suggested that the phenolic moieties are oxidized by the vanadium(v)–POM species directly, and subsequent hydrolysis of the cationic lignin intermediates leads to the lignin polymer degradation.[122b] As the POM can be reused, the system can be considered to be of interest, even though large amounts of POM are required per cycle. On the other hand, major capital investment is needed to accommodate such delignification processes in pulp bleaching factories.

A related system developed by Evtuguin and Pascoal Neto employs POMs to achieve delignification under aerobic conditions.[124] They have developed a vanadium-containing polymolybdate compound that reacts selectively with the lignin in air if the reaction is carried out in an ethanol/water mixture. Most studies were carried out using $Na_8[PMo_7V_5O_{40}]$. It should be noted that about 2 mM of the POM

 © 2006 Wiley-VCH Verlag GmbH & Co. KGaA, Weinheim

was used to obtain the desired bleaching effects, which implies a requirement of about 100 kg of catalyst per ton of oven dry pulp. Unless a system can be developed to re-use the spent liquor after the bleaching process, it is unlikely that this system can be applied on a large scale. Another polyoxometallate has been studied to enhance delignification by the same group, that is, $Na_5[SiW_{11}Mn(H_2O)O_{39}]$, and based on lignin model degradation studies, it was proposed that one-electron transfer degrades the lignin.[125] The Mn–POMs were shown to accelerate the oxygen delignification, and model studies using homovanillyl alcohol and homoveratryl alcohol suggested that phenoxy radicals are formed by reaction of the substrate with the oxidized POM. Similar reaction schemes were postulated for various manganese-based catalysts as described in Section 3.

7. Outlook

In the last two decades a wide variety of transition-metal complexes have been patented for bleaching applications. Undoubtedly, many more have been tested and not found to be active. Despite the numerous patents and intense research in this area, the use of bleaching catalysts is still limited.

One chemical hurdle in the development of bleaching catalysts is the hydrolytic stability in alkaline aqueous media, especially when the compound is iron- or manganese-based. Various approaches have led to more stable/robust bleaching catalysts, such as the use of 1,4,7-triazacyclononane ligands for manganese, the cross-bridged macrocyclic ligands with manganese or pentadentate ligands with iron, such as N4py. Sufficient catalytic activity in alkaline media is, however, just one of several criteria that need to be met. Others are robustness of performance under a wide variety of conditions, high selectivity for the chromophores to be bleached without oxidative damage to other dyes, textiles, or cellulose (cotton, wood pulp), and safety towards humans and the environment. Another main challenge is cost. Though the costs of bleaching chemicals are huge if summed up, hydrogen peroxide or chlorine-based oxidants are bulk chemicals and cheap on a molar basis. An overall saving on bleach chemicals can only be achieved with catalysts that have an excellent cost/efficiency ratio. A similar argument applies to catalysts in laundry products. The biggest opportunity for bleach catalysts is in developing countries and emerging markets. However, as many consumers can only afford a few cents per wash, there is little room for a technology that would make the product more expensive. Few of these criteria on various bleaching catalysts have been published, and consequently no further information concerning the likelihood of applicability can be given.

It is nonetheless expected that the area of catalytic bleaching will remain a field of active industrial research, despite all the challenges mentioned above. A bleaching catalyst, if successfully implemented, will have a considerable economic impact, providing new opportunities for better products as well as savings in bleaching chemicals and energy.

We thank Unilever R&D Vlaardingen and the Dutch Economy, Ecology, Technology (EET) programme, a joint programme of the Ministry of Economic Affairs, the Ministry of Education, Culture and Science, and the Ministry of Housing, Spatial Planning. and the Environment for financial support. We also thank Dr. Wesley Browne for useful comments. The authors especially thank the reviewers of the manuscript for their helpful suggestions.

Received: February 11, 2005
Published online: December 8, 2005

[1] Kirk-Othmer, *Encyclopedia of Chemical Technology*, 4rd ed. (Ed.: J. I. Kroschwitz, M. Howe-Grant), Wiley, New York, **1991**.
[2] a) N. J. Milne, *J. Surfactants Deterg.* **1998**, *1*, 253; b) K. M. Thompson, W. P. Griffith, M. Spiro, *J. Chem. Soc. Faraday Trans.* **1993**, *89*, 4035.
[3] E. I. Solomon, U. M. Sundaram, T. E. Manchonkin, *Chem. Rev.* **1996**, *96*, 2563.
[4] C. Hansch, H. Hao, *Chem. Rev.* **1997**, *97*, 2995.
[5] D. J. Pocalylko, J. L. Coope, A. J. Carchi, L. Boen, S. A. Madison, *J. Chem. Soc. Perkin Trans. 2* **1997**, 117.
[6] M. Suchy, D. S. Argyropoulos, *Tappi J.* **2002**, *1*, 1.
[7] E. Haslam, *Pratical Polyphenolics*, Cambridge University Press, Cambridge, UK **1998**.
[8] S.-J. Kim, E. Nara, H. Kobayashi, J. Terao, A. Nagao, *Lipids* **2001**, *36*, 191.
[9] R. C. Mordi, J. C. Walton, G. W. Burton, L Hughes, K. U. Ingold, D. A. Lindsay, *Tetrahedron Lett.* **1991**, *32*, 4203.
[10] a) A. C. Pulla Reddy, B. R. Lokesh, *Mol. Cell. Biochem.* **1992**, *111*, 117; b) A. C. Pulla Reddy, B. R. Lokesh, *Mol. Cell. Biochem.* **1994**, *137*, 1.
[11] H. H. Tonnesen, J. Karlsen, *Z. Lebensm.-Unters. Forsch.* **1985**, *180*, 132.
[12] a) R. Appel, R. Hage, unpublished results; b) W. Browne, R. Hage, unpublished results.
[13] K. D. Moe, *Am. Assoc. Text. Chem. Color.* **2000**, 79.
[14] a) D. Phillips, J. Taylor, R. Lakhanpal, R. Hall, J. Bailey, G. Bevan, J. Lloyd, J. Hoffmeister, D. McKelvey, *J. Soc. Dyers Color.* **2000**, *116*, 229; b) D. Phillips, M. Duncan, E. Jenkins, G. Bevan, J. Lloyd, J. Hoffmeister, *J. Soc. Dyers Color.* **1996**, *112*, 287.
[15] K. Fukatsu, S. Kokot, D. P. Schweinsberg, *Text. Res. J.* **1999**, *69*, 769.
[16] A. Meller, *Holzforschung* **1960**, *14*, 129.
[17] *Chemistry and Chemical Technology of Cotton* (Ed.: K. Ward), Interscience Publishers, London, **1955**.
[18] *Pulp bleaching principles and practice* (Eds.: C. W. Dence, D. W. Reeve), TAPPI, Atlanta, **1996**.
[19] *Chemical Technology of Fibrous Materials* (Eds.: F. Sadov, M. Korchagin, A. Matestky), Mir Publishers, Moscow, **1978**.
[20] J. Oakes (Unilever), EP-A-0082563, **1981** [*Chem. Abstr.* **1983**, *99*, 72622].
[21] B. S. Lane, M. Vogt, V. J. DeRose, K. Burgess, *J. Am. Chem. Soc.* **2002**, *124*, 11946.
[22] J. Oakes (Unilever), EP-A-0111963, **1982** [*Chem. Abstr.* **1984**, *101*, 93290].
[23] a) C. D. Bragg (Procter and Gamble), EP-B-72166, **1981** [*Chem. Abstr.* **1983**, *98*, 181584]; b) C. D. Bragg, P. A. Hardy (Procter and Gamble), EP-B-0124341, **1983** [*Chem. Abstr.* **1984**, *102*, 80782].
[24] C. G. van Kralingen, R. J. Martens, M. E. Rerek, T. Swarthoff, M. R. P. van Vliet (Unilever), EP-B-392592, **1989** [*Chem. Abstr.* **1990**, *114*, 231053].

 © 2006 Wiley-VCH Verlag GmbH & Co. KGaA, Weinheim

[25] R. J. Martens, E. K. Poels, L. H. Staal, M. R. P. van Vliet, M. M. J. van Zandvoort (Unilever), EP-B-0408131, **1989** [*Chem. Abstr.* **1991**, *115*, 13680].
[26] M. Rerek (Unilever), EP-B-0237111, **1986** [*Chem. Abstr.* **1987**, *108*, 23743].
[27] F. Favre, R. Hage, K. van der Helm-Rademaker, J. H. Koek, R. J. Martens, T. Swarthoff, M. R. P. van Vliet (Unilever), EP-B-0458397, **1990** [*Chem. Abstr.* **1991**, *116*, 154241].
[28] M. Verrall, *Nature* **1995**, *373*, 181.
[29] K. Wieghardt, U. Bossek, B. Nuber, J. Weiss, J. Bonvoisin, M. Corbella, S. E. Vitols, J.-J. Girerd, *J. Am. Chem. Soc.* **1988**, *110*, 7398.
[30] *Manganese Redox Enzymes* (Ed.: V. L. Pecoraro), VCH Publisher, New York, **1992**.
[31] R. Hage, *Recl. Trav. Chim. Pays-Bas* **1996**, *115*, 385.
[32] A. Zouni, H.-T. Witt, J. Kern, P. Fromme, N. Krauß, W. Saenger, P. Orth, *Nature* **2001**, *409*, 739.
[33] R. Hage, J. E. Iburg, J. Kerschner, J. H. Koek, E. L. M. Lempers, R. J. Martens, U. S. Racherla, S. W. Russell, T. Swarthoff, M. R. P. van Vliet, J. B. Warnaar, L. van der Wolf, L. B. Krijnen, *Nature* **1994**, *369*, 637.
[34] a) B. C. Gilbert, N. W. J. Kamp, J. R. Lindsay Smith, J. Oakes, *J. Chem. Soc. Perkin Trans. 2* **1997**, 2161; b) B. C. Gilbert, N. W. J. Kamp, J. R. Lindsay Smith, J. Oakes, *J. Chem. Soc. Perkin Trans. 2* **1998**, 1841.
[35] B. C. Gilbert, N. W. J. Kamp, J. R. Lindsay Smith, J. Oakes, *Org. Biomol. Chem.* **2004**, *2*, 1176.
[36] B. C. Gilbert, J. R. Lindsay Smith, M. S. Newton, J. Oakes, R. Pons i Prats, *Org. Biomol. Chem.* **2003**, *1*, 1568.
[37] a) U. Bossek, T. Weyhermüller, K. Wieghardt, *J. Inorg. Biochem.* **1991**, *43*, 371; b) K. O. Schafer, R. Bittl, W. Zweygart, F. Lendzian, G. Haselhorst, T. Weyhermüller, K. Wieghardt, W. Lubitz, *J. Am. Chem. Soc.* **1998**, *120*, 13104.
[38] A. Sorokin, L. Fraisse, A. Rabion, B. Meunier, *J. Mol. Catal. A* **1997**, *117*, 103.
[39] *Metal-catalyzed Oxidations of Organic Compounds* (Eds.: R. A. Sheldon, J. K. Kochi), Academic Press, New York, **1981**.
[40] V. Chin Quee-Smith, L. DelPizzo, S. H. Jureller, J. L. Kerschner, R. Hage, *Inorg. Chem.* **1996**, *35*, 6461.
[41] R. Hage, J. Kerschner, Research Trends, *Trends in Inorganic Chemistry* **1998**, *5*, 145.
[42] B. C. Gilbert, J. R. Lindsay Smith, A. Mairata, I. Payeras, J. Oakes, R. Pons i Prats, *J. Mol. Catal. A* **2004**, *219*, 265.
[43] R. Patt, H. J. Mielisch, J. Odermatt, K. Wieghardt, T. Weyhermüller, US-A-0025695, **1997** [*Chem. Abstr.* **2001**, *128*, 49695].
[44] a) T. Jaschinksi, J. Odermatt, R. Patt, H. Bachus, O. Korsdachia, *Pulp Pap. Can.* **1998**, *99*, 52; b) L. Kuhne, J. Odermatt, R. Patt, O. Korsdachia, *Pulp Pap. Can.* **2001**, *102*, 26.
[45] a) J. Odermatt, O. Kordsachia, L. Kuhne, C.-L. Chen, J. S. Gratzl, *ACS Symp. Ser.* **2001**, 235; b) Y. Cui, P. Puthson, C.-L. Chen, J. S. Gratzel, A. G. Kirkman, *Holzforschung* **2000**, *54*, 413; c) C.-L. Chen, E. A. Capanema, H. S. Gracz, *J. Agric. Food Chem.* **2003**, *51*, 1932; d) V. Alves, E. A. Capanema, C.-L. Chen, H. S. Gracz, *J. Mol. Catal. A* **2003**, *206*, 37; e) C.-L. Chen, E. A. Capanema, H. S. Gracz, *J. Agric. Food Chem.* **2003**, *51*, 6223.
[46] a) T. Reitberger, J. Gierer, *Holzforschung* **1988**, *42*, 351; b) J. Gierer. T. Reitberger, E. Yang, B.-H. Yoon, *J. Wood Chem. Technol.* **2001**, *21*, 313.
[47] R. Hage, A. Lienke, L. Chen, P. de Hoog, C. Luijendijk, C. Whiteoak, N. Keskinen, K. Ebeling, unpublished results.
[48] a) D. E. De Vos, T. Bein, *Chem. Commun.* **1996**, 917; b) D. E. De Vos, T. Bein, *J. Organomet. Chem.* **1996**, *520*, 195; c) D. E. De Vos, B. F. Sels, M. Reynaers, Y. V. Subba Rao, P. A. Jacobs, *Tetrahedron Lett.* **1998**, *39*, 3221.
[49] M. V. C. Sauer, J. O. Edwards, *J. Phys. Chem.* **1971**, *75*, 3004.
[50] A. Berkessel, C. A. Sklorz, *Tetrahedron Lett.* **1999**, *40*, 7965.
[51] a) D. E. De Vos, J. Meinershagen, T. Bein, *Angew. Chem.* **1996**, *108*, 2355; *Angew. Chem. Int. Ed. Engl.* **1996**, *35*, 2211; b) D. E. De Vos, T. Bein, *J. Am. Chem. Soc.* **1997**, *119*, 9460.
[52] a) D. De Vos, S. de Wildeman, B. F. Sels, P. J. Grobet, P. A. Jabobs, *Angew. Chem.* **1999**, *111*, 1033; *Angew. Chem. Int. Ed.* **1999**, *38*, 980; b) S. Y. V. Rao, D. E. De Vos, T. Bein, P. A. Jacobs, *Chem. Commun.* **1997**, 355.
[53] C. Bolm, D. Kadereit, M. Valacchi, *Synlett* **1997**, 687.
[54] J. Brinskma, L. Schmieder, G. van Vliet, R. Boaron, R. Hage, D. E. De Vos, P. L. Alsters, B. L. Feringa, *Tetrahedron Lett.* **2002**, *43*, 2619.
[55] C. Zondervan, R. Hage, B. L. Feringa, *Chem. Commun.* **1997**, 419.
[56] D. H. R. Barton, S.-Y. Choi, B. Hu, J. A. Smith, *Tetrahedron* **1998**, *54*, 3367.
[57] J. M. Vincent, A. Rabion, V. K. Yachandra, R. H. Fish, *Angew. Chem.* **1997**, *109*, 2438; *Angew. Chem. Int. Ed. Engl.* **1997**, *36*, 2346.
[58] T. H. Bennur, S. Sabne, S. S. Deshpande, D. Srinivas, S. Sivasanker, *J. Mol. Catal. A* **2002**, *185*, 71.
[59] M. Klopstra, R. Hage, R. M. Kellogg, B. L. Feringa, *Tetrahedron Lett.* **2003**, *44*, 4581.
[60] a) G. B. Shul'pin, G. V. Nizova, Y. N. Kozlov, I. G. Pechenkina, *New J. Chem.* **2002**, *26*, 1238; b) J. R. Lindsay Smith, G. Shul'pin, *Tetrahedron Lett.* **1998**, *39*, 4909; c) C. B. Woitiski, Y. N. Kozlov, D. Mandelli, G. V. Nizova, U. Schuchardt, G. B. Shul'pin, *J. Mol. Catal. A* **2004**, *222*, 103.
[61] J. Brinksma, R. La Crois, B. L. Feringa, M. I. Donnoli, C. Rosini, *Tetrahedron Lett.* **2001**, *42*, 4049.
[62] J. E. Barker, T. Ren, *Tetrahedron Lett.* **2004**, *45*, 4681.
[63] a) D. Reinehr, G. Metzger (Ciba), WO-A-9719162, **1995** [*Chem. Abstr.* **1997**, *127*, 67687]; b) F. Bachmann, J. Dannacher, M. Hazenkamp, G. Schlingloff, G. Richter, H. Dbaly, R. H. Traber (Ciba), WO-A-200105925, **1999** [*Chem. Abstr.* **2001**, *134*, 133329]; c) M. Hazenkamp, F. Bachmann, C. Makowka, M.-J. Dubs, G. Richter, G. Schlingloff, J. Dannacher, P. Weingartner (Ciba), WO-A-200053712, **1999** [*Chem. Abstr.* **2000**, *133*, 239758].
[64] B. Nestler (Clariant), EP-B-869171, **1997** [*Chem. Abstr.* **1998**, *129*, 291445].
[65] H. Blum, C. Nitsch, P. Jeschke, J. Haerer, U. Pegelow (Henkel), WO-A- 9707191, **1997** [*Chem. Abstr.* **1997**, *126*, 239902].
[66] *Chem. Eng. News* **2003**, *81*, January 20.
[67] a) T. Schwenkreis, A. Berkessel, *Tetrahedron Lett.* **1993**, *34*, 4785; b) A. Berkessel, M. Frauenkron, T. Schwenkreis, A. Steinmetz, G. Baum, D. Fenske, *J. Mol. Catal. A* **2002**, *113*, 321.
[68] T. Katsuki, *Coord. Chem. Rev.* **1995**, *140*, 189.
[69] B. S. Lane, K. Burgess, *Chem. Rev.* **2003**, *103*, 2457.
[70] C. Linde, N. Koliai, P.-O. Norrby, B. Akermark, *Chem. Eur. J.* **2002**, *8*, 2568.
[71] P. J. Pietikainen, *J. Mol. Catal. A* **2001**, *165*, 73.
[72] D. H. Busch, S. R. Collinson, T. Hubin (University of Kansas), WO-A-9839098, **1998** [*Chem. Abstr.* **1998**, *129*, 246918].
[73] a) C. M. Perkins, R. Labeque, B. K. Williams, J. P. Johnston, D. J. Kitko, J. C. Burckett-St. Laurent, M. E. Burns (Procter & Gamble), WO-A-9839405, **1997** [*Chem. Abstr.* **1998**, *129*, 246906]; b) M. E. Burns, A. R. Graydon, R. Labeque, C. M. Perkins, E. S. Sadlowski, B. K. Williams (Procter & Gamble), WO-A-0029537, **2000** [*Chem. Abstr.* **2000**, *132*, 349318].
[74] a) T. J. Hubin, J. M. McCormick, S. R. Collinson, N. W. Alcock, D. H. Busch, *Chem. Commun.* **1998**, 1675; b) T. J. Hubin, J. M. McCormick, N. W. Alcock, D. H. Busch, *Inorg. Chem.* **2001**, *40*, 435; c) S. R. Collinson, N. W. Alcock, T. J. Hubin, D. H. Busch, *J. Coord. Chem.* **2001**, *52*, 317; d) S. R. Collinson, N. W. Alcock, A. Raghunathan, P. K. Kahol, D. H. Busch, *Inorg. Chem.* **2000**, *39*, 757; e) T. J. Hubin, J. M. McCormick, S. R. Collinson, M.

 © 2006 Wiley-VCH Verlag GmbH & Co. KGaA, Weinheim

Buchalova, C. M. Perkins, N. W. Alcock, P. K. Kahol, A. Raghunathan, D. H. Busch, *J. Am. Chem. Soc.* **2000**, *122*, 2512.
[75] G. R. Weisman, M. E. Rogers, E. H. Wong, J. P. Jasinski, E. S. Paight, *J. Am. Chem. Soc.* **1990**, *112*, 8604.
[76] a) G. Schlingloff, T. Wieprecht, F. Bachmann, J. Dannacher, M.-J. Dubs, M. Hazenkamp, G. Richter (Ciba), WO-A-2002088289, **2001** [*Chem. Abstr.* **2002**, 137, 354716]; b) G. Schlingloff, T. Wieprecht, F. Bachmann, J. Dannacher, M.-J. Dubs, M. Hazenkamp, U. Heinz, M. Frey, A. Schneider (Ciba), WO-A-2004007657, **2004** [*Chem. Abstr.* **2004**, *140*, 113271].
[77] T. Wieprecht, G. Schlingloff, J. Xia, U. Heinz, A. Schneider, M.-J. Dubs, F. Bachman (Ciba), WO 2004039933, **2002** [*Chem. Abstr.* **2004**, *140*, 392559].
[78] a) T. Wieprecht, J. Xia, U. Heinz, J. Dannacher, G. Schlingloff , *J. Mol. Catal. A* **2003**, *203*, 113; b) T. Wieprecht, U. Heinz, J. Xia, G. Schlingloff, J. Dannacher, *J. Surfactants Deterg.* **2004**, *7*, 59.
[79] a) J. Limburg, J. S. Vrettos, L. M. Liable-Sands, A. L. Rheingold, R. H. Crabtree, G. W. Brudwig, *Science* **1999**, *283*, 1524; b) J. Limburg, J. S. Vrettos, H. Chen, J. C. de Paula, R. H. Crabtree, G. W. Brudwig, *J. Am. Chem. Soc.* **2001**, *123*, 423.
[80] H. Blum, B. Mayer, U. Pegelow, H.-D. Speckmann, B. Krebs, M. Duda, C. Nazikkol, J. Reim (Henkel), WO-A-9730144, **1996** [*Chem. Abstr.* **1997**, *127*, 222261].
[81] A. Tafesh, M. Beller, V. Friderichs, G. Reinhardt (Clariant), EP-B-0783035, **1996** [*Chem. Abstr.* **1997**, *127*, 137378].
[82] J. F. Boe, J. J. Girerd, C. Guignard, J. L. Seris, J. B. Verlhac (Elf-Atochem), WO-A-9400234, **1992** [*Chem. Abstr.* **1994**, *122*, 33783].
[83] a) T. Tzedakis, Y. Benzada, M. J. Comtat, *J. Electroanal. Chem.* **1997**, *421*, 187; b) T. Tzedakis, Y. Benzada, M. J. Comtat, *Ind. Eng. Chem. Res.* **2001**, *40*, 3435.
[84] a) J. Brinksma, R. Hage, J. Kerschner, B. L. Feringa, *Chem. Commun.* **2000**, 537; b) J. Brinksma, M. Rispens, R. Hage, B. L. Feringa, *Inorg. Chim. Acta* **2002**, *337*, 75.
[85] L. Que, Jr., C. Kim, J. Kim, Y. Zang, WO-A-9748710, **1996** [*Chem. Abstr.* **1997**, *128*, 90357].
[86] K. Chen, L. Que, Jr., *J. Am. Chem. Soc.* **2001**, *123*, 6327.
[87] a) J. Yeon Ryu, J. Kim, M. Costas, K. Chen, W. Nam, L. Que, Jr., *Chem. Commun.* **2002**, 1288; b) K. Chen. M. Costas, J. Kim, A. K. Tipton, L. Que, Jr., *J. Am. Chem. Soc.* **2003**, *124*, 3026; c) M. Fujita, M. Costas, L. Que, Jr., *J. Am. Chem. Soc.* **2003**, *125*, 9912; d) K. Chen, M. Costas, L. Que, Jr., *J. Chem. Soc. Dalton Trans.* **2002**, 672; e) C. Kim, K. Chen, J. Kim, L. Que, Jr., *J. Am. Chem. Soc.* **1997**, *119*, 5964; f) A. M. I. Payeras, R. Y. N. Ho, M. Fujita, L. Que, Jr., *Chem. Eur. J.* **2004**, *10*, 1.
[88] a) Y. Dong, H. Fujii, M. P. Hendrich, R. A. Leising, G. Pan, C. R. Randall, E. C. Wilkinson, Y. Zang, L. Que, Jr., B. G. Fox, K. Kauffmann, E. Münck, *J. Am. Chem. Soc.* **1995**, *117*, 2778; b) H.-F. Hsu, Y. Dong, L. Shu, V. G. Young, L. Que, Jr., *J. Am. Chem. Soc.* **1999**, *121*, 5230; c) Y. Zang, J. Kim, Y. Dong, E. Wilkinson, E. H. Appelman, L. Que, Jr., *J. Am. Chem. Soc.* **1997**, *119*, 4197.
[89] a) P. A. MacFaul, K. U. Ingold, D. D. M. Wayner, L. Que, Jr., *J. Am. Chem. Soc.* **1997**, *119*, 10594; b) H. Miyake, K. Chen, S. J. Lange, L. Que, Jr., *J. Am. Chem. Soc.* **2001**, *40*, 3534.
[90] a) J. Kaizer, M. Costas, L. Que, Jr., *Angew. Chem.* **2003**, *115*, 3799; *Angew. Chem. Int. Ed.* **2003**, *42*, 3671; b) M. H. Lee, J.-U. Rode, A. Stubna, M. R. Bukowski, M. Costas, R. Y. N. Ho, E. Münck, W. Nam, L. Que, Jr., *Proc. Natl. Acad. Sci. USA* **2003**, *100*, 3665.
[91] M. P. Jensen, S. J. Lange, M. P. Mehn, E. L. Que, L. , Que, Jr., *J. Am.Chem. Soc.* **2003**, *125*, 2113.
[92] B. L. Feringa, M. Lubben, R. M. Hermant, R. S. Twisker, L. Que, Jr., (Unilever), WO-A-9534268, **1994** [*Chem. Abstr.* **1995**, *124*, 205657].
[93] O. C. P. Beers, M. C. M. Gribnau, R. Hage, R. M. Hermant, R. E. Kalmeijer, J. H. Koek, C. Lamers, S. W. Russell, R. S. Twisker, B. L. Feringa, J. G. Roelfes (Unilever), EP-B-0 909 809, **1999** [*Chem. Abstr.* **1999**, *130*, 313501].
[94] R. H. Hermant, R. Hage, unpublished results.
[95] a) A. C. M. Appel, R. F. Carina, M. G.J Delroisse, B. L. Feringa, J.J Girerd, R. Hage, R. Kalmeijer, C.F Martens, J. C. J. Peelen, L. Que, T. Swarthoff, D. Tetard, D. Thornthwaite, L. Tiwari, R. Thijssen, R. S. Twisker, S. M. Veerman, G. van der Voet (Unilever), WO-A-0012667, **1998** [*Chem. Abstr.* **2000**, *132*, 209503]; b) A. C. M. Appel, R. F. Carina, M. G.J Delroisse, B. L. Feringa, J.J Girerd, R. Hage, R. Kalmeijer, C.F Martens, J. C. J. Peelen, L. Que, R. G. Smith, T. Swarthoff, D. Tetard, D. Thornthwaite, L. Tiwari, R. Thijssen, R. S. Twisker, S. M. Veerman, G. van der Voet (Unilever), WO-A-0012808, **1998** [*Chem. Abstr.* **2000**, *132*, 209505]; c) A. C. M. Appel, R. Hage, P. van der Hoeven, A. Lienke, R. G. Smith (Unilever), WO-A-0250229, **2001** [*Chem. Abstr.* **2002**, *137*, 64938]; d) A. C. M. Appel, R. Hage, A. Lienke (Unilever), EP-A-1326074, **2002** [*Chem. Abstr.* **2003**, *139*, 529396]; e) R. Hage, R. M. Hermant, S. M. Veerman (Unilever), WO-A-02072746, **2002** [*Chem. Abstr.* **2002**, *137*, 234406]; f) D. Nühlen, T. Weyhermüller, K. Wieghardt, WO-A-0164697, **2001** [*Chem. Abstr.* **2001**, *135*, 212627]; g) D. Nühlen, T. Weyhermüller, K. Wieghardt, R. Hage (Unilever), WO-A-0164826, **2001** [*Chem. Abstr.* **2001**, *135*, 244102]; h) A. C. M. Appel, R. Hage, D. Tetard, R. S. Twisker (Unilever), WO-A-0116272, **2001** [*Chem. Abstr.* **2001**, *134*, 224344].
[96] L. Fraisse, J.-J. Girerd, F. Perie, A. Rabion, D. Tetard, J. B. Verlhac, A. Nivorozhkin (Elf-Atochem), WO-A-9718035, **1995** [*Chem. Abstr.* **1997**, *127*, 67657].
[97] M. G. J. Delroisse, R. Hage, R. Kalmeijer, R. E. Lamers, S. W. Russell, J. Whittaker, B. L. Feringa, R. M. Hermant, J. H. Koek, M. T. Rispens, R. T. L. van Vliet (Unilever), WO-A-0027975, **1998** [*Chem. Abstr.* **2000**, *132*, 336136].
[98] H. Börzel, P. Comba, R. Hage, M. Kerscher, J. Lienke, M. Merz (Unilever), WO-A-0248301, **2000** [*Chem. Abstr.* **2002**, *137*, 48918].
[99] a) P. Comba, J. H. Koek, J. Lienke, M. Merz, L. Tsymbal (Unilever), WO-A-2003104234, **2002** [*Chem. Abstr.* **2003**, *140*, 28783]; b) R. Hage, J. Lienke, P. Petersen (Unilever), US-A-2003230732, **2002** [*Chem. Abstr.* **2003**, *140*, 29873]; c) R. Hage, J. Lienke, P. Petersen (Unilever), US-A-2003230736, **2002** [*Chem. Abstr.* **2003**, *140*, 28780].
[100] a) M. Lubben, A. Meetsma, E. C. Wilkinson, B. L. Feringa, L. Que, Jr., *Angew. Chem.* **1995**, *107*, 1610; *Angew. Chem. Int. Ed. Engl.* **1995**, *34*, 1512; b) G. Roelfes, M. Lubben, K. Chen, R. Y. N. Ho, A. Meetsma, S. Genseberger, R. H. Hermant, R. Hage, S. K. Mandal, V. G. Young, Jr, Y. Zang, H. Kooijman, A. L. Spek, L. Que Jr, B. L. Feringa, *Inorg. Chem.* **1999**, *38*, 1929; c) R. Y. N. Ho, G. Roelfes, B. L. Feringa, L. Que, Jr., *J. Am. Chem. Soc.* **1994**, *121*, 264; d) G. Roelfes, M. Lubben, R. Hage, L. Que, Jr., B. L. Feringa, *Chem. Eur. J.* **2000**, *6*, 2152.
[101] a) N Lehnert, F. Neese, R. Y. N. Ho, L. Que, Jr., E. I. Solomon, *J. Am. Chem. Soc.* **2002**, *124*, 10810; b) J. Kaizer, E. J. Klinker, N. Young Oh, J.-U. Rohde, W. J. Song, A. Stubna, J. Kim, E. Münck, W. Nam, L. Que, Jr., *J. Am. Chem. Soc.* **2004**, *126*, 472.
[102] a) R. Y. N. Ho, G. Roelfes, R. Hermant, R. Hage, B. L. Feringa, L. Que, Jr., *Chem. Commun.* **1999**, 2161; b) G. Roelfes, V. Vrajmasu, K. Chen, R. Y. N. Ho, J.-U. Rohde, C. Zondervan, R. M. La Crois, E. P. Schudde, M. Lutz, A. L. Spek, R. Hage, B. L. Feringa, E. Munck, L. Que, Jr., *Inorg. Chem.* **1999**, *38*, 1929.
[103] G. Roelfes, PhD thesis, University of Groningen (The Netherlands), **2000**.

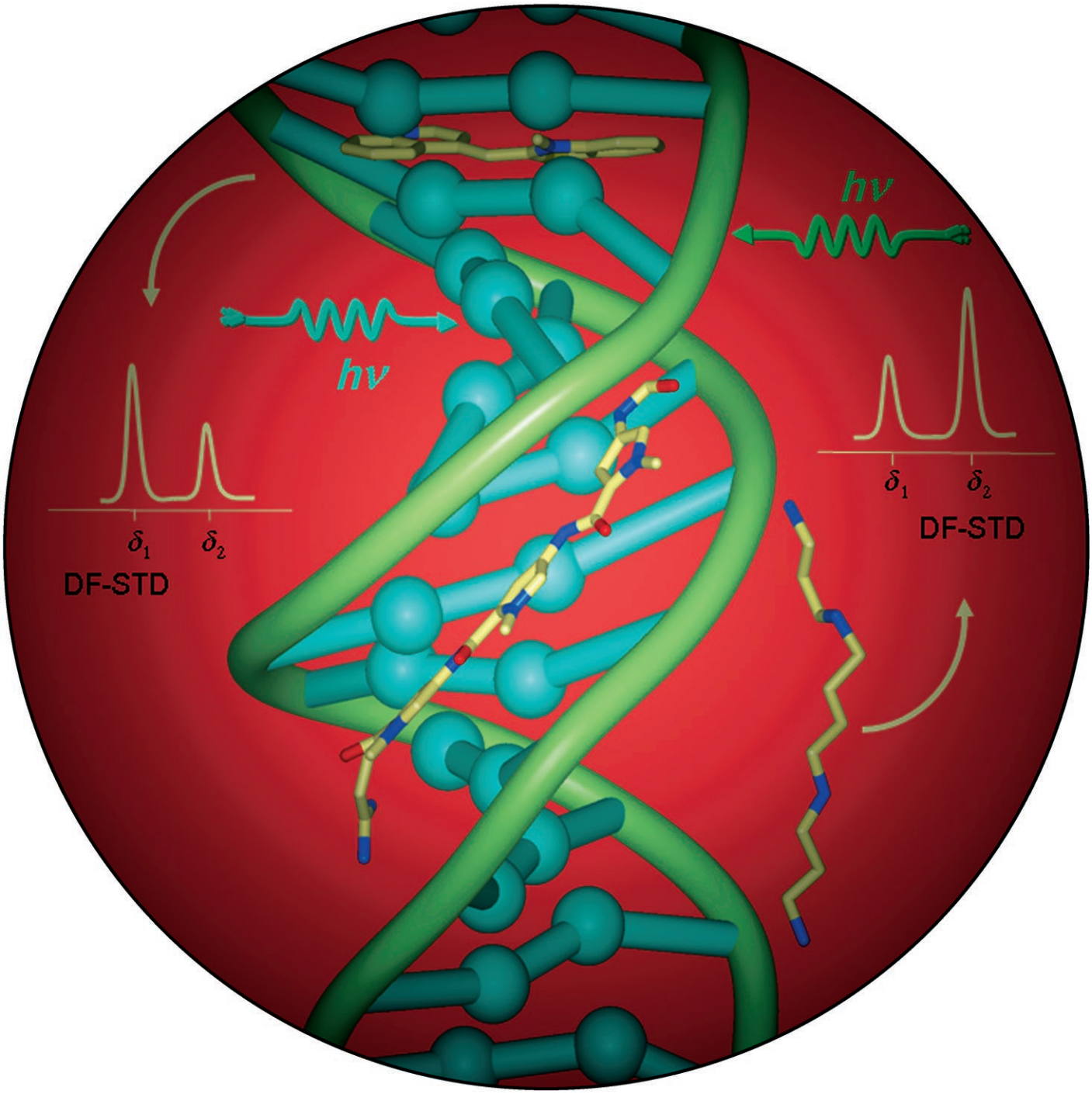
 © 2006 Wiley-VCH Verlag GmbH & Co. KGaA, Weinheim

[104] I. Bernal, I. M. Jensen, K. B. Jensen, C. J. McKenzie, H. Toftlund, J. P. Tuchagues, *J. Chem. Soc. Dalton Trans.* **1995**, 3667.
[105] J. J. Girerd, F. Banse, A. J. Simaan, *Struct. Bonding (Berlin)* **2000**, *97*, 145.
[106] a) A. J. Simaan, F. Banse, P. Mialane, A. Boussac, S. Un, T. Kargar-Grisel, G. Bouchoux, J.-J. Girerd, *Eur. J. Inorg. Chem.* **1999**, 993; b) A. J. Simaan, F. Banse, J.-J. Girerd, K. Wieghardt, E. Bill, *Inorg. Chem.* **2001**, *40*, 6538.
[107] a) K. Jensen, C. J. McKenzie, L. Preuss Nielsen, J. Zacho Pedersen, H. Molina Svendson, *Chem. Commun.* **1999**, 1313; b) A. Hazell, C. J. McKenzie, L. P. Nielsen, S. Schindler, M. Weitzer, *J. Chem. Soc. Dalton Trans.* **2002**, 310.
[108] a) V. Balland, F. Banse, E. Anxolabehere-Mallart, M. Ghiladi, T. A. Mattioli, C. Pilouze, G. Blondin, J.-J. Girerd, *Inorg. Chem.* **2003**, *42*, 2470; b) V. Balland, M.-F. Charlot, F. Banse, J.-J. Gired, T. A. Mattioli, E. Bill, J.-F. Bartoli, P. Battioni, D. Mansuy, *Eur. J. Inorg. Chem.* **2004**, 301; c) P. Mialane, A. Novorojkine, G. Pratviel, L. Azema, M. Slany, F. Godde, A. J. Simaan, F. Banse, T. Kargar-Grisel, G. Bouchoux, J. Saiton, O. Horner, J. Guilheim, L. Tchertanov, B. Meunier, J.-J. Girerd, *Inorg. Chem.* **1999**, *38*, 1085.
[109] a) M. R. Bukowksi, P. Comba, C. Limberg, M. Merz, L. Que, Jr., T. Wistuba, *Angew. Chem.* **2004**, *116*, 1303; *Angew. Chem. Int. Ed.* **2004**, *43*, 1283; b) H. Börzel, P. Comba, K. S. Hagen, Y. D. Lampeka, A. Lienke, G. Linti, M. Merz, H. Pritzkow, L. V. Tsymbal, *Inorg. Chim. Acta* **2002**, *337*, 407; c) P. Comba, A. Lienke, C. Limberg, C. Lopez de Laorden, M. Merz, L. Que, Jr., unpublished results.
[110] a) K. E. Loeb, J. M. Zaleski, T. E. Westre, R. J. Guajardo, P. K. Mascharak, B. Hedman, K. O. Hodgson, E. I. Solomon, *J. Am. Chem. Soc.* **1995**, *117*, 4545; b) R. M. Burger, J. Peisach, S. B. Horwitz, *J. Biol. Chem.* **1981**, *256*, 11636; c) J. W. Sam, X. J. Tang, J. Peisach, *J. Am. Chem. Soc.* **1994**, *116*, 5250.
[111] a) T. A. van den Berg, J. W. de Boer, W. R. Browne, G. Roelfes, B. L. Feringa, *Chem. Commun.* **2004**, 2550; b) C. V. Sastri, M. S. Seo, M. J. Park, K. M. Kim, W. Nam, *Chem. Commun.* **2005**, 1405.
[112] T. J. Collins C. P. Horwitz, WO-A-9803625, **1996** [*Chem. Abstr.* 1998, 128, 155724].
[113] a) T. J. Collins, *Acc. Chem. Res.* **2002**, *35*, 782; b) T. J. Collins, *ACS Symp. Ser.* **2002**, 47.
[114] T. J. Collins, K. M. Costa, E. Münck, E. S. Uffelman, *J. Am. Chem. Soc.* **1990**, *112*, 5637.
[115] a) T. J. Collins, S. W. Gordon-Wylie, *J. Am. Chem. Soc.* **1989**, *111*, 4511; b) T. J. Collins, R. D. Powell, C. Slebodnick, E. S. Uffelman, *J. Am. Chem. Soc.* **1990**, *112*, 899; c) J. M. Workman, R. D. Powell, A. D. Procyk, T. J. Collins, D. F. Bocian, *Inorg. Chem.* **1992**, *31*, 1550; d) C. M. Miller, S. W. Gordon-Wylie, C. P. Horwitz, S. A. Strazisar, D. K. Peraino, G. R. Clark, S. T. Weintraub, T. J. Collins, *J. Am. Chem. Soc.* **1998**, *120*, 11540.
[116] a) C. P. Horwitz, D. R. Fooksman, L. D. Vuocolo, S. W. Gordon-Wylie, N. J. Cox, T. J. Collins, *J. Am. Chem. Soc.* **1998**, *120*, 4867; b) A. Ghosh, A. D. Ryabov, S. M. Mayer, D. C. Horner, D. E. Prasuhn, Jr., S. S. Gupta, L. Vuocolo, C. Culver, M. P. Hendrich, C. E. F. Rickard, R. E. Norman, C. P. Horwitz, T. J. Collins, *J. Am. Chem. Soc.* **2003**, *125*, 12379; c) A. Ghosh, F. Tiago de Oliveira, T. Yano, T. Nishioka, E. Beach, I. Kinoshita, E. Münck, A. D. Ryabov, C. P. Horwitz, T. J. Collins, *J. Am. Chem. Soc.* **2005**, *127*, 2505.
[117] E. M. Diakun, C. T. Wright (Interox), EP-A-272030, **1986** [*Chem. Abstr.* **1988**, *110*, 97591].
[118] C. M. Perkins, W. M. Scheper, (Procter and Gamble), WO-A-9623859, **1996** [*Chem. Abstr.* **1996**, *125*, 225188].
[119] W. M. Scheper, M. R. Sivik, C. M. Perkins, F. V. Bielen, N. J. Gorelick, V. Vandepitte, *Household Pers. Prod. Ind.* **1998**, *35*, 58.
[120] a) K. M. Thompson, W. P. Griffith, M. Spiro, *J. Chem. Soc. Faraday Trans.* **1994**, *90*, 1105; b) K. M. Thompson, M. Spiro, W. P. Griffith, *J. Chem. Soc. Faraday Trans.* **1996**, *92*, 2535.
[121] H. Jakob, U. Kunz (Degusssa), EP-A-1199402, **2001** [*Chem. Abstr.* **2000**, *136*, 31157].
[122] a) I. A. Weinstock, R. H. Atalla, R. S. Reiner, M. A. Moen, K. E. Hammel, C. J. Houtmam, C. L. Hill, M. K. Harrup, *J. Mol. Catal. A* **1997**, *116*, 59; b) I. A. Weinstock, K. E. Hammel M. A. Moen, L. L. Landucci, S. Ralph, C. E. Sullivan, R. S. Reiner, *Holzforschung* **1998**, *52*, 311.
[123] I. A. Weinstock, R. H. Attala, C. Hill, WO-A-9526438, **1994** [*Chem. Abstr.* **1995**, *124*, 59630].
[124] a) D. V. Evtuguin, C. Pascoal Neto, J. D. Pedrosa de Jesus, *J. Pulp Pap. Sci.* **1998**, *24*, 133; b) D. V. Evtuguin, C. Pascoal Neto, *Holzforschung* **1997**, *51*, 338.
[125] A. Gaspar, D. V. Evtuguin, C. Pascoal Neto, *Appl. Catal.* **2003**, *239*, 157.

 © 2006 Wiley-VCH Verlag GmbH & Co. KGaA, Weinheim

Communications

DOI: 10.1002/anie.200501344



Differential-frequency saturation transfer diifference spectroscopy (DF-STD) is a new NMR spectroscopic approach for the screening of small molecules binding to DNA. The convenient probing of different binding modes between ligands and DNA is allowed and is described by Gomez-Paloma and co-workers in their Communication on the following pages.

WILEY InterScience DISCOVER SOMETHING GREAT
© 2006 Wiley-VCH Verlag GmbH & Co. KGaA, Weinheim

DNA Binding

DOI: 10.1002/anie.200501344

Differential-Frequency Saturation Transfer Difference NMR Spectroscopy Allows the Detection of Different Ligand–DNA Binding Modes**

*Simone Di Micco, Carla Bassarello, Giuseppe Bifulco, Raffaele Riccio, and Luigi Gomez-Paloma**

Ligand-based NMR spectroscopic approaches that allow the convenient probing of ligand–biomolecule binding phenomena have recently gained high visibility in the fields of chemical biology and medicinal chemistry.[1] In particular, saturation transfer difference (STD) spectroscopy[2] offers several advantages: a modest requirement of an unlabeled biological target, virtually without upper limits on its size; amenability to screening mixtures of putative ligands in the presence of non-ligands, molecules that target viruses,[3] and membrane-bound receptors on living cells;[4] and rapid access to relevant information on ligand epitope maps.[5] A main limitation, common to all ligand-based approaches for NMR screening, is that no direct information can be gathered on the intervening receptor surface, and therefore on the mode and site of binding, even if an indirect method (SOS-NMR; SOS: *s*tructural information using *O*verhauser effects and *s*elective labeling) based on selective protein labeling has been devised.[6] Indeed, the high efficiency in diffusing NMR saturation, which is typically observed in globular macromolecules (usually welcomed for the general applicability of STD methods), prevents the observation of any local effect that might be used to monitor the mode and site of binding of the ligand to the receptor surface.

Although such a consideration applies to most biological macromolecules, long tracts of helical DNA may be expected as a notable exception, as they are characterized by a marked difference in their vertical and horizontal dimensions. This effect, in turn, translates into a remarkable anisotropy in the efficiency of saturation diffusion along the two axes. Actually, we were at first surprised to observe important anisotropic effects in saturation diffusion, in the form of different experimental outcomes that depended on the chosen saturation frequency (and therefore DNA region), as such effects are normally not seen in the context of ligand–protein STD spectra.[7] We have found that such an intrinsic feature of STD-NMR experiments employing duplex DNA as receptor allows, at least partly, a differential monitoring of binding events that occur at specific regions of duplex DNA.

Herein, we report a novel STD-based approach that proved particularly valuable for the NMR screening of DNA binders, thus providing key information on their binding mode and allowing the convenient probing of DNA recognition phenomena such as those of base-pair intercalators, minor groove binders, and external backbone binders.[8] The impact of such a technique on drug-discovery processes may be appreciated by taking into account the great importance of small molecules specifically targeting nucleic acids, in the context of anticancer, antifungal, and antiviral drugs. In essence, our approach takes advantage of the difference in STD effect arising from the saturation of protons located in different DNA regions. Data from preliminary STD spectra on ligand–DNA complexes showed that saturation diffusion is far from being isotropic in long tracts of DNA.

The approach described herein is based on two parallel sets of STD experiments performed under the same experimental conditions, in which saturation is elicited by irradiating at a suitable frequency chosen from specific DNA resonances. The signal-to-noise (S/N) ratios of all the protons showing STD effects are measured with reference to an STD spectrum with an off-resonance irradiation. A comparative analysis of such effects in the two sets is then performed. For this reason, we named the method differential-frequency STD (DF-STD) spectroscopy. Besides presenting all the typical advantages of STD spectroscopy, DF-STD spectroscopy has the distinct attribute of providing direct information on the mode of binding of the ligand onto the DNA molecule. To devise our approach, we considered a poly(dG-dC)·poly(dG-dC) copolymer as receptor[9] and the following ligands, each of them characterized by a well-known DNA binding mode: spermine (**1**), a polyamine external binder; distamycin (**2**) and netropsin (**3**), two minor groove binders; and thiazole orange (**4**), doxorubicin (**5**), and ethidium bromide (**6**), three base-pair intercalators.

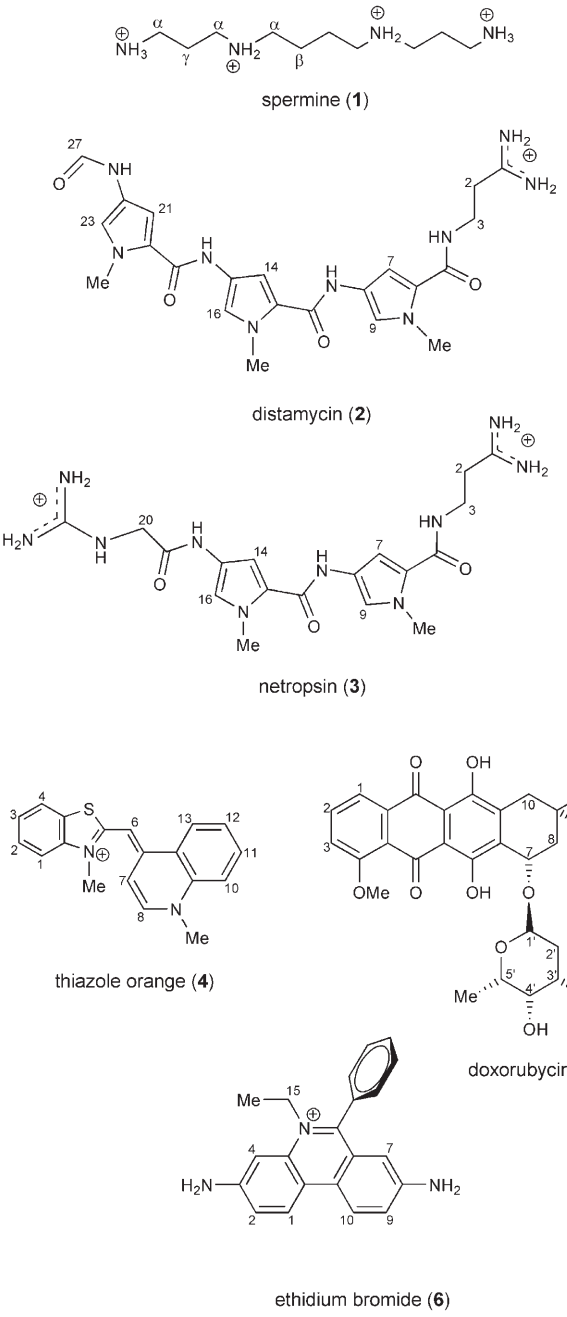
In particular, the two sets of STD spectra were recorded with saturation by a train of single 50-ms Gaussian pulses, centered either in the aromatic or in the low-field aliphatic spectral regions, where the proton resonances of purine/pyrimidine bases and deoxyribose/backbone,[10] respectively, can be found. This selection reflects the need to propagate saturation to the ligand starting from nuclei lying in different regions of the DNA helix. In this scenario, a ligand making proximate contacts with aromatic base protons, such as an intercalator sandwiched by consecutive base pairs, would receive more saturation upon irradiation of DNA aromatic protons rather than irradiation of deoxyribose protons. Conversely, an external ligand presenting the majority of its binding surface in contact with the DNA phosphodiester backbone should be more affected by irradiation in the deoxyribose region (especially H5′/H5″ in the DNA backbone) rather than by irradiation in the DNA aromatic region.

[*] S. Di Micco, Dr. C. Bassarello, Prof. G. Bifulco, Prof. R. Riccio, Prof. L. Gomez-Paloma
Dipartimento di Scienze Farmaceutiche
Università di Salerno
via Ponte don Melillo, 84084 Fisciano, Salerno (Italy)
Fax: (+39) 089-962-828
E-mail: gomez@unisa.it

[**] Financial support by the University of Salerno and by MIUR (Rome) is gratefully acknowledged. The authors also wish to acknowledge the use of the instrumental (NMR spectroscopy and mass spectrometry) facilities of the Center of Competence in Diagnostics and Molecular Pharmaceutics supported by Regione Campania (Italy) through POR funds.

Supporting information for this article is available on the WWW under http://www.angewandte.org or from the author.

 © 2006 Wiley-VCH Verlag GmbH & Co. KGaA, Weinheim InterScience



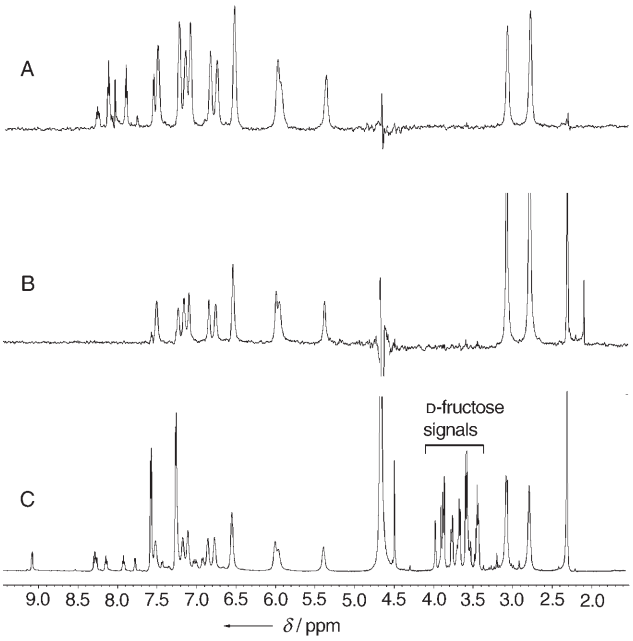


Figure 1. DF-STD spectra of the **4**–DNA complex. A, B) STD spectra recorded upon saturation in the aromatic (8.1 ppm) and deoxyribose/backbone (2.1 ppm) spectral regions, respectively. C) Reference STD spectrum with an off-resonance irradiation. D-Fructose, a non-ligand, was employed as a spy molecule to ensure that only actual STD effects were observed. S/N ratios for all individual proton resonances in both DF-STD spectra can be found in the Supporting Information.

In this respect, minor groove binders are unusual in that they make close contact with both the DNA backbone and base pairs, as the positioning of such ligands, which are often deeply inserted into the DNA minor groove, warrants their proximity to both DNA aromatic and deoxyribose/backbone functionalities. Therefore, for this category of DNA binders we should not expect, at least in principle, a sensitive difference in the outcome of the two sets of STD spectra.

Actually, a comparative analysis of the DF-STD spectra of the six ligands used in the present study confirmed our expectations, to the extent that each ligand with a given DNA binding mode showed a clear-cut DF-STD profile. For instance, Figure 1 shows reference and DF-STD spectra for the **4**–DNA complex. The different response of ligand protons to the two kinds of saturation, and in particular the higher intensity of STD effects upon saturation of DNA base protons, can be appreciated even by visual inspection. This result suggests a close proximity of ligand nuclei to base-pair functionalities, as expected for an intercalative mode of binding. The DF-STD spectral data for all the ligand–DNA complexes examined are reported in Table 1 (for the full data set, see the Supporting Information). To facilitate analysis of the DF-STD data, we propose the introduction of the binding mode index (BMI), a numerical parameter that expresses the relative sensitivity of ligand protons to the perturbation arising from each type of saturation (that is, base versus sugar/

Table 1: BMI values for ligands **1**–**6** computed by using Equation (1).

Ligand	Binding mode	BMI
1	external binder	0.40
2	minor groove binder	1.10
3	minor groove binder	0.90
4	base-pair intercalator	1.40
5	base-pair intercalator	1.33[a]/0.20[b]
6	base-pair intercalator[c]	0.90

[a] BMI calculated for the sole polyaromatic portion (base-pair intercalator). [b] BMI calculated for the sole sugar portion (external binder). For the role of the sugar domain of **5** in DNA binding, see reference [11]. [c] Ethidium bromide is an unusual type of intercalator, which also establishes interactions with the phosphodiester backbone.[12]

 © 2006 Wiley-VCH Verlag GmbH & Co. KGaA, Weinheim

backbone saturation). The BMI is computed as given in Equation (1), where $SN_{aromatic}$ and $SN_{aliphatic}$ are the signal-to-

$$BMI = \frac{\sum_i \left(\frac{SN_{aromatic}/SN_{ref}}{SN_{aliphatic}/SN_{ref}} \right)}{n_i} \quad (1)$$

noise ratios relative to STD peaks elicited by saturation of the aromatic bases and deoxyribose/backbone, respectively, SN_{ref} is the signal-to-noise ratio of STD peaks in the reference spectrum, and n_i is the number of ligand peaks considered. On the basis of the data gathered in our tests (see Table 1), we can extrapolate three BMI ranges: $0 < BMI < 0.50$ for external (nonspecific) electrostatic backbone binding; $0.90 < BMI < 1.10$ for minor groove binding; and $1.20\ (0.90) < BMI < 1.50$ for base-pair intercalation.

One point that deserves special comment concerns the BMI values found for base-pair intercalators. In fact, the DF-STD data show that at least two cases of intercalation can be identified. Simple intercalators, such as **4** (BMI = 1.40) or the tricyclic chromophoric portion of **5** (BMI = 1.33), whose interaction with DNA is exclusively based on extended van der Waals contacts with base-pair aromatic rings, can be clearly differentiated from more unusual intercalators. These include ligand **6** (BMI = 0.9), which is also involved in secondary electrostatic interactions with the DNA backbone. The apparent inconvenience of a potential overlap of BMI values between minor groove binders and some intercalators, such as ligand **6** and possibly others, does not seem, in our opinion, a major drawback of the DF-STD approach. Conversely, as DNA intercalators can usually be recognized by their typical structural fingerprint, DF-STD data can add fine details to the big picture of a general base-pair intercalation, the latter often being predicted on the sole basis of the structural features of the ligand. Another interesting case is offered by ligand **5**, which is characterized by two portions that exert two different DNA binding modes. In fact, an intercalative mode of binding is sustained by its tricyclic chromophoric core, and an external electrostatic phosphate binding is attributed to its amino sugar moiety. Again, the DF-STD data, with the two BMI values of 1.33 and 0.20, respectively, seem to describe a pattern perfectly in line with the previously acquired knowledge on **5**–DNA binding characteristics (see Supporting Information).

In conclusion, we have devised a novel STD-based approach that allows the convenient study of small molecule–DNA binding phenomena. We believe that such studies extend in a useful way the application of STD spectroscopy to the realm of chemical biology and medicinal chemistry of nucleic acids.

Experimental Section

STD-NMR experiments were performed on a Bruker Avance DRX 600-MHz spectrometer at 300 K. NMR samples were prepared by dissolving the ligand and the poly(dG-dC)·poly(dG-dC) copolymer in D_2O (500 μL, 99.996%, CIL Laboratories) containing phosphate-buffered saline at pH 7.1. A high ligand–receptor molar excess (20:1) was used for the best STD effects. In particular, the concentration of ligands **1**, **2**, **3**, **5**, and **6** was set at 1.8 mM, whereas that for **4** was 1.5 mM. The concentration of D-fructose was 1 mM. All compounds were purchased from Sigma-Aldrich and used without further purification. The concentration of the double-stranded DNA copolymer (purchased from Pharmacia Biochemicals) was 90 μM, expressed as molarity of phosphate groups.

The STD effects of the individual protons were calculated for each compound relative to a reference spectrum with off-resonance saturation at $\delta = -16$ ppm. Typically, 64 scans were recorded for the reference STD spectrum, whereas 128 scans were recorded for each DF-STD spectrum (saturation time = 4 sec). The relative STD effect was calculated for each signal as the difference between the intensity (expressed as S/N ratio) of one signal in the on-resonance STD spectrum and that of the same signal in the off-resonance NMR spectrum divided by the intensity of the same signal in the off-resonance spectrum. BMI values were obtained by using Equation (1).

Received: April 18, 2005
Revised: September 30, 2005
Published online: November 22, 2005

Keywords: DNA binding · DNA recognition · drug design · NMR spectroscopy · saturation transfer difference

[1] a) C. A. Lepre, J. M. Moore, J. W. Peng, *Chem. Rev.* **2004**, *104*, 3641–3675; b) S. W. Homans, *Angew. Chem.* **2004**, *116*, 292–303; *Angew. Chem. Int. Ed.* **2004**, *43*, 290–300; c) X. Salvatella, E. Giralt, *Chem. Soc. Rev.* **2003**, *32*, 365–372; d) M. Coles, M. Heller, H. Kessler, *Drug Discovery Today* **2003**, *8*, 803–810; e) B. J. Stockman, C. Dalvit, *Prog. Nucl. Magn. Reson. Spectrosc.* **2002**, *38*, 187–231; f) M. Pellecchia, D. S. Sem, K. Wüthrich, *Nat. Rev. Drug Discovery* **2002**, *1*, 211–219; g) P. Neri, C. Tringali, *Bioact. Compd. Nat. Sources* **2001**, 69–127; h) D. S. Sem, M. Pellecchia, *Curr. Opin. Drug Discovery Dev.* **2001**, *4*, 479–492; i) T. Diercks, M. Coles, H. Kessler, *Curr. Opin. Chem. Biol.* **2001**, *5*, 285–291.

[2] a) M. Mayer, B. Meyer, *Angew. Chem.* **1999**, *111*, 1902–1906; *Angew. Chem. Int. Ed.* **1999**, *38*, 1784–1788; b) M. Mayer, B. Meyer, *J. Am. Chem. Soc.* **2001**, *123*, 6108–6117; for a review, see: c) B. Meyer, T. Peters, *Angew. Chem.* **2003**, *115*, 890–918; *Angew. Chem. Int. Ed.* **2003**, *42*, 864–890.

[3] A. J. Benie, R. Moser, E. Bäuml, D. Blaas, T. Peters, *J. Am. Chem. Soc.* **2003**, *125*, 14–15.

[4] a) B. Claasen, M. Axmann, R. Meinecke, B. Meyer, *J. Am. Chem. Soc.* **2005**, *127*, 916–919; b) S. Mari, D. Serrano-Gomez, F. J. Canada, A. L. Corbi, J. Jimenez-Barbero, *Angew. Chem.* **2005**, *117*, 300–302; *Angew. Chem. Int. Ed.* **2005**, *44*, 296–298.

[5] C. Sandström, O. Berteau, E. Gemma, S. Oscarson, L. Kenne, A. M. Gronenborn, *Biochemistry* **2004**, *43*, 13926–13931.

[6] P. J. Hajduk, J. C. Mack, E. T. Olejniczak, C. Park, P. J. Dandliker, B. A. Beutel, *J. Am. Chem. Soc.* **2004**, *126*, 2390–2398.

[7] STD-NMR has largely been employed for detecting small molecules interacting with protein targets, whereas very few applications focus on RNA receptors and, to the best of our knowledge, none on DNA systems.

[8] Small molecules binding noncovalently to DNA are usually classified into the cited three main classes: external binders, often polyamines making nonspecific electrostatic contacts with the DNA backbone; minor groove binders, the most sequence-selective class thanks to a network of specific H bonds to base-pair and backbone functions; and base-pair intercalators, which establish extended, and partly specific, van der Waals contacts with the floor of aromatic base pairs.

[9] We also performed test STD experiments on small oligonucleotides. These tests confirmed the importance of having a long

 © 2006 Wiley-VCH Verlag GmbH & Co. KGaA, Weinheim

DNA sequence as receptor to give good-quality STD spectra. Accordingly, the DF-STD data were of poor quality in this case. Thus, a short DNA or RNA oligonucleotide (length <20 bp), even if containing a high-affinity binding site for a given ligand, should not be used for STD-NMR experiments.

[10] When saturation within the 4.8–5.5 ppm range, where backbone H5′/H5″ can be found, is prevented by the presence of ligand resonances, irradiation in the 1.5–3.0 ppm range is an alternative that also proved to be similarly valid. We believe that in this case saturation is propagated starting from the resonances of H2′/H2″ of deoxyribose and 5-Me of thymine.

[11] C. Baily, J. B. Chaires, *Bioconjugate Chem.* **1998**, *9*, 513–538.

[12] Ethidium bromide establishes secondary electrostatic interactions by extending its two positively charged amino groups toward the phosphate backbone; see: a) N. W. Luedtke, Q. Liu, Y. Tor, *Chem. Eur. J.* **2005**, *11*, 495–508; b) E. McLaughlin, *How Ethidium Bromide Interacts with DNA*, can be found under http://www.madsci.org/posts/archives/Jun2003/1054573405.Mb.r.html.

 © 2006 Wiley-VCH Verlag GmbH & Co. KGaA, Weinheim

Nanotubes

DOI: 10.1002/anie.200502870

Hollow and Polygonous Microtubes of Monocrystalline Indium Germanate

Jinhua Zhan, Yoshio Bando, Junqing Hu, Longwei Yin, Xiaoli Yuan, Takashi Sekiguchi, and Dmitri Golberg*

Since the identification of carbon nanotubes in 1991,[1] a challenging research field has been launched in materials science, solid-state physics, and chemistry, ensuring a wide range of exciting practical applications. Over the last decades there has been a continuous interest in exploring layered or nonlayered materials that form tubular structures. Generally, the generation of inorganic tubular forms has been based on layered binary inorganic compounds, such as BN, MoS_2, WS_2, VS_2, GaS, VO_x, TiO_2 etc.[2] The tubular forms of elemental or binary inorganic compounds with 3D nonlayered crystal structures have usually been fabricated by using carbon nanotubes, porous membranes, or removable nanowires as templates[3] to give amorphous or polycrystalline nanotubes. Single-crystalline tubes have occasionally been generated based on epitaxial casting. Germanates have attracted attention as important catalyst materials, scintillators for detection of low-energy solar neutrinos in agreement with Raghavan's nuclear reaction, and porous ceramic materials for humidity sensors.[4] Indium germanate ($In_2Ge_2O_7$) has a specific laminar thortveitite-type ($Sc_2Si_2O_7$) structure.[5] Herein, we demonstrate the successful synthesis of ternary indium germanate tubes with sub-micrometer diameters and present a thorough analysis of their morphological and structural characteristics.

Carbon-assisted thermal evaporation of an In_2O_3/GeO_2 powder mixture under a stream of Ar in a horizontal resistance furnace results in the formation of a white product on the inner wall of the tube (downstream), where the temperature is around 600 °C during heating. As shown in the scanning electron microscopy (SEM) image (Figure 1 a), the product is composed of numerous whiskers whose length reaches hundreds of micrometers. High-magnification SEM images (Figure 1 b) reveal that these whiskers have open tips and display tubular geometries. The cylinder pores of the tubular whiskers are either hexagonal or round. The powder X-ray diffraction (XRD) pattern of the product (Figure 1 c) suggests that it is composed of pure monoclinic $In_2Ge_2O_7$ (JCPDS card 26-0768: $a = 6.658$, $b = 8.784$, $c = 4.927$ Å, $\beta = 102.48°$; space group: $C2/m$). No characteristic peaks from other impurities, such as In_2O_3, GeO_2, In, or Ge, are detected in the XRD pattern.

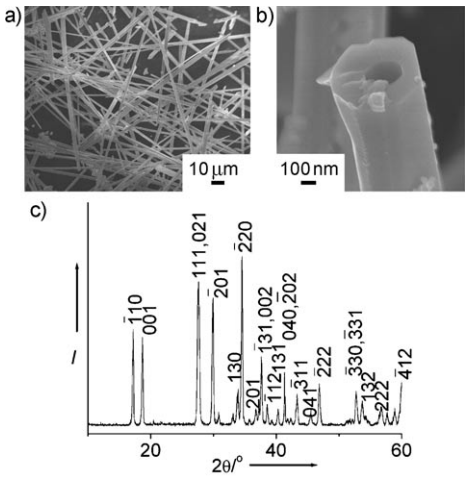


Figure 1. a) SEM image of $In_2Ge_2O_7$ tubes; b) high-magnification SEM image of a single tube revealing the open tip; c) XRD pattern of the product.

Detailed structural and chemical analyses of the products were carried out by TEM, high-resolution TEM, electron diffraction (ED), and energy-dispersive X-ray spectroscopy (EDS). Figure 2 shows a TEM micrograph of a typical $In_2Ge_2O_7$ tube. The diameter of this tube is about 600 nm and its cavity width is about 200 nm. Energy-dispersive X-ray spectra generated with an electron nanoprobe (diameter of around 50 nm) were collected from various regions of the

[*] Dr. J. Zhan, Prof. Y. Bando, Dr. L. Yin, Prof. D. Golberg
Advanced Materials Laboratory
National Institute for Materials Science (NIMS)
Namiki 1-1, Tsukuba, Ibaraki 305-0044 (Japan)
Fax: (+81) 29-851-6280
E-mail: ZHAN.Jinhua@nims.go.jp
Dr. J. Hu
International Center for Young Scientists (ICYS), NIMS
Namiki 1-1, Tsukuba, Ibaraki 305-0044 (Japan)
Dr. X. Yuan, Prof. T. Sekiguchi
Nanomaterials Laboratory, NIMS
Namiki 1-1, Tsukuba, Ibaraki 305-0044 (Japan)

Supporting information for this article is available on the WWW under http://www.angewandte.org or from the author.

InterScience
© 2006 Wiley-VCH Verlag GmbH & Co. KGaA, Weinheim

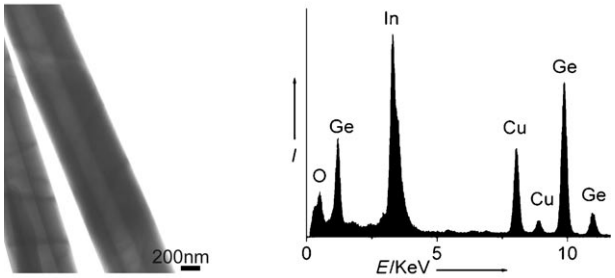


Figure 2. Typical TEM image of hollow $In_2Ge_2O_7$ microtubes (left) and a representative EDS spectrum (right) of a hollow $In_2Ge_2O_7$ microtube.

$In_2Ge_2O_7$ tube. They verify the uniformity of the indium and germanium compositions—the overall ratio of indium to germanium is close to 1:1. A typical EDS spectrum is shown in Figure 2.

Figure 3a clearly demonstrates that the tip of the $In_2Ge_2O_7$ tube is open. The corresponding selected-area electron diffraction (SAED) pattern is depicted in Figure 3b. This pattern can be indexed as that recorded along the $[\bar{1}10]$ zone axis of a monoclinic $In_2Ge_2O_7$ crystal. Electron diffraction (ED) patterns taken from various domains of the tube were strikingly similar, which clearly suggests its single-crystalline nature. Other $In_2Ge_2O_7$ tubes were also confirmed to be perfect single crystals. Streaking of the reflections in the

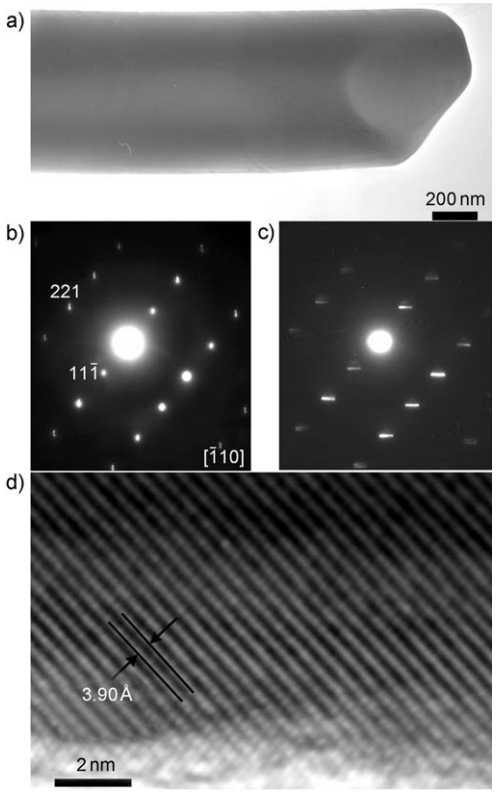


Figure 3. a) TEM image of an isolated open-ended hollow $In_2Ge_2O_7$ microtube; b) SAED pattern of a hollow $In_2Ge_2O_7$ microtube recorded along the $[\bar{1}10]$ zone axis, and c) its corresponding underfocused SAED pattern; d) a high-resolution TEM image of the hollow $In_2Ge_2O_7$ microtube along the $[\bar{1}10]$ direction.

underfocused electron diffraction pattern (Figure 3c) implies that the preferred tube growth direction is parallel to the (003) plane. High-resolution TEM images additionally reveal that the as-obtained $In_2Ge_2O_7$ tubes are structurally uniform single crystals. An HRTEM image taken at the edge of a $In_2Ge_2O_7$ tube (Figure 3d), shows clearly resolved fringes separated by 3.90 and 2.15 Å, which correspond to the (221) and $(11\bar{1})$ lattice spacings of a monoclinic $In_2Ge_2O_7$ crystal, respectively.

Another SAED pattern (Figure 4a), obtained after the $In_2Ge_2O_7$ tube was tilted inside the TEM, is shown in Figure 3a. The latter agrees well with the [110] zone axis of monoclinic $In_2Ge_2O_7$. As before, streaking of the reflections

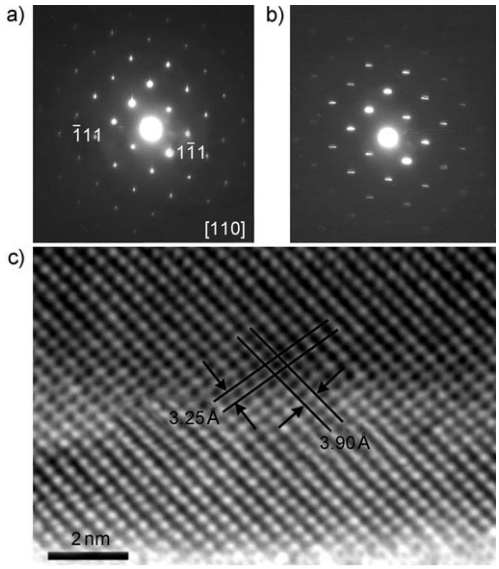


Figure 4. a) SAED pattern of a hollow $In_2Ge_2O_7$ microtube recorded along the [110] zone axis, and b) its corresponding underfocused SAED pattern, which reveals that the preferential growth direction is nearly parallel to the (002) plane; c) a high-resolution TEM image of the microtube wall along the [110] direction ($d_{\bar{1}11} = 3.90$ Å; $d_{1\bar{1}1} = 3.25$ Å, as marked by double lines).

in the underfocused ED pattern (Figure 4b) implies that the preferred growth direction is parallel to the (002) plane. Figure 4c depicts the HRTEM image corresponding to the [110] zone axis. The lattice fringes of the $(\bar{1}11)$ and $(1\bar{1}1)$ planes, with a d spacing of 3.90 and 3.25 Å, respectively, can be clearly seen. This indicates that the (002) plane is parallel to the edge of the $In_2Ge_2O_7$ tube. As seen from these images, this tube is a structurally uniform single crystal, the tube edge is clean, and there is no amorphous layer covering the surface. Upon taking the ED patterns and HRTEM images into account, one can suggest that the preferred growth direction of the tube is close to the [100] axis of the $In_2Ge_2O_7$ crystal.

Apart from the anisotropic growth of inorganic compounds in a solution modified by specific molecules,[6] anisotropic growth in the vapor phase generally results from the vapor–solid (VS) or vapor–liquid–solid (VLS) growth mechanisms.[7,8] The key feature of the VLS growth mechanism is that one end of a 1D nanostructure is capped with an alloy droplet. During the VLS growth process, this metal

 © 2006 Wiley-VCH Verlag GmbH & Co. KGaA, Weinheim

particle may act as a preferential site for the absorption of incoming vapors to form a liquid alloy. Once the absorbed reactant is supersaturated within the liquid alloy droplet at a given temperature, it nucleates. Further condensation of the reactant vapors results in the continuous axial growth of a 1D structure. In contrast, the anisotropic growth during the VS growth process might be controlled by some kinetic and intrinsic crystallographic properties. Temperature and supersaturation are therefore the two dominant factors affecting the morphology of the products during the VS growth process.

As there are no metal-containing caps at the single-crystalline $In_2Ge_2O_7$ tubes, it is assumed that a VS growth process lies behind the present growth. During the synthesis, In_2O_3 and GeO_2 can react with the carbon powder to produce gaseous In_2O and GeO. From a thermodynamic point of view, the equilibrium pressures of gaseous In_2O and GeO at 1000 °C are similar to each other and reach over 100 kPa. In_2O and GeO, which are brought by the Ar flow to the lower-temperature furnace zone ($\approx$600 °C), can recombine with the residual oxygen in the furnace to form $In_2Ge_2O_7$—a stable ternary oxide of indium and germanium at ambient pressure.[9] Figure 5 displays a schematic illustration of a mono-

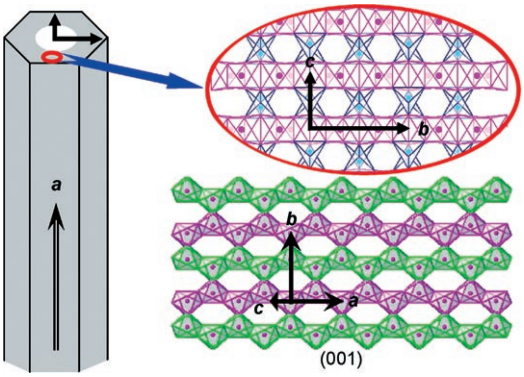


Figure 5. Network structure in of a hollow $In_2Ge_2O_7$ microtube.

crystalline $In_2Ge_2O_7$ tube. In the $In_2Ge_2O_7$ crystals, each In atom is coordinated to six O atoms to form an $\{InO_6\}$ octahedron. These $\{InO_6\}$ octahedra lie in a nearly hexagonal arrangement in the (001) plane and share edges to form a distorted honeycomb ensemble with the composition $\{[In_2O_6]^{6-}\}_n$. Each Ge atom is coordinated to four O atoms to form a tetrahedron. Two $\{GeO_4\}$ tetrahedra share one corner to form a $[Ge_2O_7]^{6-}$ group. The monoclinic $In_2Ge_2O_7$ lattice can therefore be described as a stacking of alternating parallel sheets of InO_6 octahedra and isolated $[Ge_2O_7]^{6-}$ groups (see Supporting Information). As demonstrated in the right-hand bottom panel of Figure 5, a honeycomb sheet of $\{InO_6\}$ octahedra can be viewed as a building block composed of edge-sharing, one-dimensional $\{In_nO_{4n+2}\}$ chains along the [100] axis. This anisotropic crystallographic feature may lead to the one-dimensional growth along the [100] axis. Analogous preferential growth patterns have also been frequently documented in some elemental or binary compounds composed of chain-like building blocks.[11–14] The formation of a specific tubular form may be attributed to several kinetic factors. When the evaporation temperature increases, the pores of tubular $In_2Ge_2O_7$ become larger. During the VS growth process, the interplay between the rates of deposition and surface diffusion becomes important. Generally, raising the temperature increases the growth rate exponentially according to the Arrhenius relation ($k = A\,e^{-Q/RT}$). At a higher growth temperature, the edge-growth rate prevails over the diffusion rate, giving rise to the growth of tubular $In_2Ge_2O_7$. An analogous growth mechanism has also been proposed for Sb_2S_3, AlN, GaN, InP, and MgO nanotubes.[14–18] It is notable that this growth scenario is quite different from that of layered compounds (such as C, BN, and MoS_2), which form nanotubes by molecular layer rolling.[1,2]

Finally, the optical properties of $In_2Ge_2O_7$ tubes were analyzed by means of high-spatial-resolution cathodoluminescence (CL) spectroscopy and imaging. To visualize the spatial distribution of the luminescence from a single $In_2Ge_2O_7$ tube, a CL image was recorded at room temperature and at a wavelength of 560 nm. Figure 6a shows the SEM image of an individual $In_2Ge_2O_7$ tube. Its corresponding CL image is depicted in Figure 6b. These images suggest that

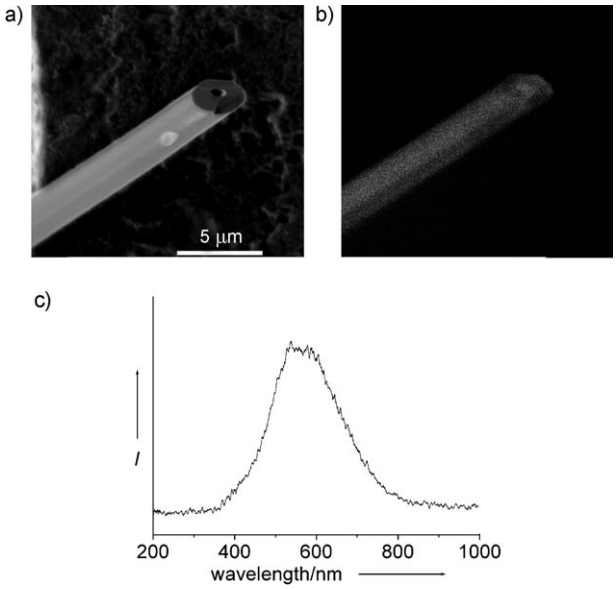


Figure 6. a) Thermal field emission SEM image of a hollow $In_2Ge_2O_7$ microtube; b) monochromatic CL image recorded at room temperature; c) CL spectrum of a hollow $In_2Ge_2O_7$ microtube.

the $In_2Ge_2O_7$ tube is optically uniform except for a small, bright dot within the pore region. The CL spectra collected from the various points over the $In_2Ge_2O_7$ tube show similar emissions (see Supporting Information). The CL spectrum (Figure 6c) recorded over the entire $In_2Ge_2O_7$ tube at room temperature shows a broad emission centered at around 560 nm. This luminescence may originate from the honeycomb sheets of $\{InO_6\}$ octahedra since the germanate groups most likely do not behave as luminescent centers in $In_2Ge_2O_7$, as was confirmed during a study on $Sc_2Ge_2O_7$ crystals with a very similar structure.[5]

In summary, monocrystalline, sub-micrometer $In_2Ge_2O_7$ tubes have been generated by carbon-assisted thermal co-

 © 2006 Wiley-VCH Verlag GmbH & Co. KGaA, Weinheim

evaporation of In_2O_3 and GeO_2. Within an $In_2Ge_2O_7$ tube, the InO_6 octahedra laminae are parallel to the [100] preferential growth axis. The tube generation has been discussed from both thermodynamic and kinetic points of view. It is notable that the diameter of these $In_2Ge_2O_7$ tubes is similar to the wavelength and mean free path of photons.[19–22] Therefore, these novel tubular structures may find interesting potential applications as waveguides or microlasers.

Experimental Section

The indium germanate tubes were synthesized by a vapor transport and condensation process. A quartz crucible containing a ground mixture of In_2O_3 (1.11 g), GeO_2 (0.84 g), and activated carbon (0.20 g) powders was placed in the center of a quartz tube within a tube furnace. The furnace was heated to 1000 °C at a rate of 20 K min^{-1}, kept at this temperature for 2 h, and then allowed to cool to room temperature. The whole process was carried out under a constant flow of pure Ar at a rate of 200 std cm^3 min^{-1}. A white product was collected from the inner wall of the quartz tube. The overall yield was around 10% based on the amount of In_2O_3. The product was characterized by powder XRD (RINT 2200) with $Cu_{K\alpha}$ radiation (λ = 1.5418 Å), scanning electron microscopy (SEM, JSM-6700F), and by means of a high-resolution transmission electron microscope (HRTEM; JEM-3000F) equipped with an energy-dispersive X-ray spectrometer (EDS). Cathodoluminescence (CL) spectra were collected at room temperature with a high-spatial-resolution CL system attached to a thermal field-emission scanning electron microscope (TFE-SEM, Hitachi S4200) performing at 5 kV and 1.2 nA.

Received: August 12, 2005
Published online: November 29, 2005

Keywords: crystal growth · germanium · indium · nanotubes · semiconductors

[1] S. Iijima, *Nature* **1991**, *354*, 56–58.
[2] a) N. G. Chopra, R. J. Luyken, K. Cherrey, V. H. Crespi, M. L. Cohen, S. G. Louie, A. Zettl, *Science* **1995**, *269*, 966–967; b) K. Suenaga, C. Colliex, N. Demoncy, A. Loiseau, H. Pascard, F. Willaime, *Science* **1997**, *278*, 653–655; c) Y. Feldman, E. Wasserman, D. J. Srolovitz, R. Tenne, *Science* **1995**, *267*, 222–225; d) R. Tenne, *Angew. Chem.* **2003**, *115*, 5280–5289; *Angew. Chem. Int. Ed.* **2003**, *42*, 5124–5132; e) J. M. Macak, H. Tsuchiya, P. Schmuki, *Angew. Chem.* **2005**, *117*, 2136–2139; *Angew. Chem. Int. Ed.* **2005**, *44*, 2100–2102; f) Y. Q. Zhu, T. Sekine, K. S. Brigatti, S. Firth, R. Tenne, R. Rosentsveig, H. W. Kroto, D. R. W. Walton, *J. Am. Chem. Soc.* **2003**, *125*, 1329–1333; g) U. K. Gautam, S. R. C. Vivekchand, A. Govindaraj, G. U. Kulkarni, N. R. Selvi, C. N. R. Rao, *J. Am. Chem. Soc.* **2005**, *127*, 3658–3659; h) M. Nath, C. N. R. Rao, *Angew. Chem.* **2002**, *114*, 3601–3604; *Angew. Chem. Int. Ed.* **2002**, *41*, 3451–3454; i) H. A. Therese, F. Rocker, A. Reiber, J. X. Li, M. Stepputat, G. Glasser, U. Kolb, W. Tremel, *Angew. Chem.* **2005**, *117*, 267–270; *Angew. Chem. Int. Ed.* **2005**, *44*, 262–265; j) F. S. Cai, G. Y. Zhang, J. Chen, X. L. Gou, H. K. Liu, S. X. Dou, *Angew. Chem.* **2004**, *116*, 4308–4312; *Angew. Chem. Int. Ed.* **2004**, *43*, 4212–4216.
[3] a) P. M. Ajayan, O. Stephan, P. Redlich, C. Colliex, *Nature* **1995**, *375*, 564–567; b) K. J. C. van Bommel, A. Friggeri, S. Shinkai, *Angew. Chem.* **2003**, *115*, 1010–1030; *Angew. Chem. Int. Ed.* **2003**, *42*, 980–999; c) C. R. Martin, *Science* **1994**, *266*, 1961–1965; d) J. Goldberger, R. He, Y. Zhang, S. Lee, H. Yan, H. Choi, P. Yang, *Nature* **2003**, *422*, 599–602; e) J. Hu, Y. Bando, Z. Liu, J. Zhan, D. Golberg, T. Sekiguchi, *Angew. Chem.* **2004**, *116*, 65–68; *Angew. Chem. Int. Ed.* **2004**, *43*, 63–66; f) R. Ma, Y. Bando, D. Golberg, T. Sato, *Angew. Chem.* **2003**, *115*, 1880–1882; *Angew. Chem. Int. Ed.* **2003**, *42*, 1836–1838; g) A. R. Armstrong, J. Canales, P. G. Bruce, *Angew. Chem.* **2004**, *116*, 5007–5010; *Angew. Chem. Int. Ed.* **2004**, *43*, 4899–4902; h) X. Wang, J. Zhuang, J. Chen, K. Zhou, Y. Li, *Angew. Chem.* **2004**, *116*, 2051–2054; *Angew. Chem. Int. Ed.* **2004**, *43*, 2017–2020; i) Y. G. Sun, Y. N. Xia, *Adv. Mater.* **2004**, *16*, 264–268.
[4] a) T. E. Gier, X. Bu, P. Feng, G. D. Stucky, *Nature* **1998**, *395*, 154–157; b) D. Pitzschke, W. Bensch, *Angew. Chem.* **2003**, *115*, 4525–4528; *Angew. Chem. Int. Ed.* **2003**, *42*, 4389–4391; c) Y. Zhou, H. Zhu, Z. Chen, M. Chen, Y. Xu, H. Zhang, D. Zhao, *Angew. Chem.* **2001**, *113*, 2224–2226; *Angew. Chem. Int. Ed.* **2001**, *40*, 2166–2168; d) H. Li, M. Eddaoudi, O. M. Yaghi, *Angew. Chem.* **1999**, *111*, 682–685; *Angew. Chem. Int. Ed.* **1999**, *38*, 653–655; e) M. Avenier, G. Bagieu, R. Brissot, J. F. Cavaignac, J. Collot, D. H. Koang, D. Lebrun, F. Minot, A. Stutz, *Nucl. Phys. B* **1992**, *A28*, 496–499; f) M. J. Hogan, A. W. Brinkman, T. Hashemi, *Appl. Phys. Lett.* **1998**, *72*, 3077–3079.
[5] T. Gaewdang, J. P. Chaminade, P. Gravereau, A. Garcia, C. Fouassier, M. Pouchard, P. Hagenmuller, *Z. Anorg. Allg. Chem.* **1994**, *620*, 1965–1970.
[6] a) G. R. Patzke, F. Krumeich, R. Nesper, *Angew. Chem.* **2002**, *114*, 2554–2571; *Angew. Chem. Int. Ed.* **2002**, *41*, 2446–2461; b) X. Wang, Y. Li, *Angew. Chem.* **2002**, *114*, 4984–4987; *Angew. Chem. Int. Ed.* **2002**, *41*, 4790–4793; c) A. R. Armstrong, G. Armstrong, J. Canales, P. G. Bruce, *Angew. Chem.* **2004**, *116*, 2336–2338; *Angew. Chem. Int. Ed.* **2004**, *43*, 2286–2288; d) S. H. Yu, M. Antonietti, H. Cölfen, M. Giersig, *Angew. Chem.* **2002**, *114*, 2462–2466; *Angew. Chem. Int. Ed.* **2002**, *41*, 2356–2360.
[7] a) Z. R. Dai, Z. W. Pan, Z. L. Wang, *Adv. Funct. Mater.* **2003**, *13*, 9–24; b) R. Q. Zhang, Y. Lifshitz, S. T. Lee, *Adv. Mater.* **2003**, *15*, 635–640.
[8] a) Y. Wu, P. Yang, *J. Am. Chem. Soc.* **2001**, *123*, 3165–3166; b) J. Zhan, Y. Bando, J. Hu, T. Sekiguchi, D. Golberg, *Adv. Mater.* **2005**, *17*, 225–230; c) C. N. R. Rao, F. L. Deepak, G. Gundiah, A. Govindaraj, *Prog. Solid State Chem.* **2003**, *31*, 5–147.
[9] R. D. Shannon, A. W. Sleight, *Inorg. Chem.* **1968**, *7*, 1649–1651.
[10] R. D. Shannon, C. T. Prewitt, *J. Solid State Chem.* **1970**, *2*, 199–202.
[11] B. Gates, B. Mayers, A. Grossman, Y. N. Xia, *Adv. Mater.* **2002**, *14*, 1749–1752.
[12] H. K. Edwards, P. A. Salyer, M. J. Roe, G. S. Walker, P. D. Brown, D. H. Gregory, *Angew. Chem.* **2005**, *117*, 3621–3624; *Angew. Chem. Int. Ed.* **2005**, *44*, 3555–3558.
[13] J. Liu, Q. Li, T. Wang, D. Yu, Y. Li, *Angew. Chem.* **2004**, *116*, 5158–5162; *Angew. Chem. Int. Ed.* **2004**, *43*, 5048–5052.
[14] J. Yang, Y. C. Liu, H. M. Lin, C. C. Chen, *Adv. Mater.* **2004**, *16*, 713–716.
[15] Q. Wu, Z. Hu, X. Wang, Y. Lu, X. Chen, H. Xu, Y. Chen, *J. Am. Chem. Soc.* **2003**, *125*, 10176–10177.
[16] J. Zhan, Y. Bando, J. Hu, D. Golberg, *Inorg. Chem.* **2004**, *43*, 2462–2464.
[17] J. Hu, Y. Bando, J. Zhan, F. Xu, T. Sekiguchi, D. Golberg, *Adv. Mater.* **2004**, *16*, 1464–1468.
[18] E. P. A. M. Bakkers, M. A. Verheijen, *J. Am. Chem. Soc.* **2003**, *125*, 3440–3441.
[19] M. Law, D. J. Sirbuly, J. C. Johnson, J. Goldberger, R. J. Saykally, P. Yang, *Science* **2004**, *305*, 1269–1273.
[20] L. M. Tong, R. R. Gattass, J. B. Ashcom, S. L. He, J. Y. Lou, M. Y. Shen, I. Maxwell, E. Mazur, *Nature* **2003**, *426*, 816–819.
[21] R. Yang, G. Chen, *Nano Lett.* **2005**, *5*, 1111–1115.
[22] J. S. Foresi, P. R. Villeneuve, J. Ferrera, E. R. Thoen, G. Steinmeyer, S. Fan, J. D. Joannopoulos, L. C. Kimerling, H. I. Smith, E. P. Ippen, *Nature* **1997**, *390*, 143–145.

 © 2006 Wiley-VCH Verlag GmbH & Co. KGaA, Weinheim

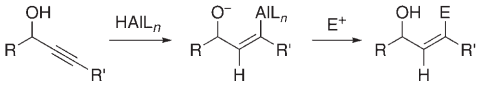
Hydroalumination

DOI: 10.1002/anie.200503176

γ-Silyl Group Effect in Hydroalumination and Carbolithiation of Propargylic Alcohols**

*Kazunobu Igawa and Katsuhiko Tomooka**

The hydrometalation reaction of an alkynyl group is a valuable process, not only for functionalized alkene synthesis but also for alkenyl metal preparations.[1] Among the numerous variants of this class of reaction, hydroalumination of propargylic alcohols is especially well utilized in many facets of organic synthesis owing to its promising chemo- and stereoselectivity [Eq. (1); L = ligand, E = electrophile].[2,3]



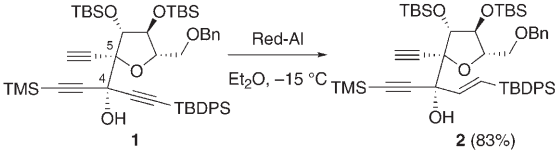
(1)

Herein, we report a noticeable accelerating effect of a γ-silyl substituent on the hydroalumination reaction, an effect that can substantially enhance the synthetic utility of this classical transformation. By proper choice of the silyl group, highly group-selective functionalization in polyalkynyl alcohols **A** has been accomplished by overcoming the steric influences, to provide valuable multifunctionalized alcohols **B** through hydroalumination and also carbolithiation [Eq. (2)].



(2)

We have found this unprecedented silyl effect during the course of our synthetic study of zaragozic acid A.[4] As one of the key steps in this total synthesis, we faced the problem of group-selective functionalization of intermediate **1**, which has three alkynyl groups on C4 and C5 [Eq. (3); Bn = benzyl, TBDPS = *tert*-butyldiphenylsilyl, TBS = *tert*-butyldimethylsilyl, TMS = trimethylsilyl]. Surprisingly enough, hydroalumination of alcohol **1** with sodium bis(2-methoxyethoxy) aluminum hydride (Red-Al) provides vinylsilane **2** exclusively.[5]

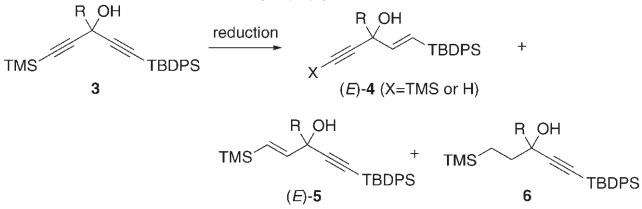


(3)

Our purpose for the total synthesis was achieved by this group-selective transformation; however, a question that immediately arose was why the reaction preferentially occurred at the alkyne substituted with the bulkier TBDPS group, rather than one substituted with the less bulky TMS group.[6] At an earlier stage, we suspected an influence of the multiple oxy functionalities on **1** to be the origin of the peculiar selectivity; these functionalities may exert chelation control on the aluminum reagent.[7] Thus, in order to eliminate this confusing factor, we examined a competitive hydroalumination in a series of simplified 1,1-bis(alkynyl) alcohols **3** bearing TBDPS and TMS groups at the γ and γ′ positions (Table 1).

The reaction of *sec*-alcohol **3a** (R = H) with Red-Al in toluene at 0 °C provides vinylsilane (*E*)-**4a** (95%) predominantly, along with a trace amount of (*E*)-**5a** (3%; TBDPS side/TMS side 97:3; Table 1, entry 1).[8] Similar selectivity was

Table 1: Reduction of 1,1-bis(alkynyl) alcohol **3**.



Entry	3	R	Reagent (equiv)	Solvent, *T*	Yield [%][a] 4[b]	5[b]	6	TBPS side/TMS side 4/(5+6)
1	**3a**	H	Red-Al (1.1)	toluene, 0 °C	95[c]	3	n.d.[d]	97:3
2	**3a**	H	$LiAlH_4$ (3.0)	THF, −78 to −10 °C[e]	58[c]	6	n.d.[d]	91:9
3	**3b**	Me	Red-Al (1.1)	toluene, 0 °C	88	5	n.d.[d]	95:5
4	**3b**	Me	H_2, Lindlar cat. (0.11)	MeOH, RT	n.d.[d]	70[f]	19	<1:99

[a] Yield of isolated product. [b] >95% *E* by ^{1}H NMR analysis. [c] The product with the TMS group removed (X = H) was obtained in 7–16% yield. [d] n.d. = not detected by ^{1}H NMR and TLC analyses. [e] THF = tetrahydrofuran. [f] The *E*/*Z* ratio was determined by ^{1}H NMR analysis to be 83:17.

[*] Dr. K. Igawa, Prof. Dr. K. Tomooka
Department of Applied Chemistry
Graduate School of Science and Engineering
Tokyo Institute of Technology
Meguro-ku, Tokyo 152-8552 (Japan)
Fax: (+81) 3-5734-3931
E-mail: ktomooka@apc.titech.ac.jp

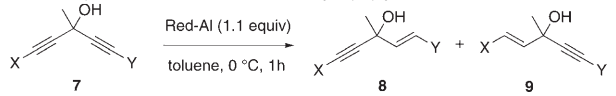
[**] This research was supported in part by a Grant-in-Aid for Scientific Research on Priority Areas (A) "Creation of Biologically Functional Molecules" (Grant No. 16073209), by an Exploratory Research grant (Grant No. 17655038), and by The 21st Century COE Program "Creation of Molecular Diversity and Development of Functionalities" of the Ministry of Education, Culture, Sports, Science, and Technology, Japan.

Supporting information for this article is available on the WWW under http://www.angewandte.org or from the author.

InterScience
© 2006 Wiley-VCH Verlag GmbH & Co. KGaA, Weinheim

observed when $LiAlH_4$ was employed instead of Red-Al (TBDPS side/TMS side 91:9; entry 2) and also in the reaction of *tert*-alcohol **3b** (TBDPS side/TMS side 95:5; entry 3). From these results, it was clarified that the peculiar selectivity of the reaction of **1** was caused by the γ-silyl group of the propargylic moiety. In sharp contrast with the above-mentioned hydroalumination, a partial reduction of **3b** by catalytic hydrogenation (H_2/Lindlar catalyst) preferentially gave product **5b**, from reduction of the less-hindered TMS-substituted alkyne, and the overreduced product **6b** (TBDPS side/TMS side < 1:99; entry 4). These results obviously show that the TBDPS substituent, rather than the TMS group, accelerates hydroalumination on the attached ethyne functionality, despite its steric disadvantage. A stereoelectronic effect of the phenyl group on silicon (see below) is regarded as the origin of this TBDPS effect. Based on this postulate, we anticipated that a triphenylsilyl group (TPS) would have a much higher ability to accelerate hydroalumination than that of TBDPS. To confirm this idea and to determine the order of magnitude of the rate acceleration by various substituents, we examined the competitive hydroalumination of 1,1-bis(alkynyl) alcohols **7a–g**, which have various combinations of γ substituents; the results are summarized in Table 2.[8]

Table 2: Hydroalumination of 1,1-bis(alkynyl) alcohol **7**.



7 **8** **9**

Entry	**7**	X	Y	Yield (**8**+**9**) [%][a]	**8**/**9**[b]
1	**7a**	*t*Bu	TMS	91	> 99:1
2	**7b**	TMS	TIPS[c]	97	55:45
3	**7c**	TIPS[c]	TBDPS	100	88:12
4	**7d**	TBDPS	TPS	93	72:28
5	**7e**	TMS	Ph	89	94:6
6	**7f**	TBDPS	Ph	40[d]	55:45
7	**7g**	Ph	TPS	79	78:22

[a] Yield of isolated product. [b] Determined by ^{1}H NMR analysis. [c] TIPS = triisopropylsilyl. [d] 1,1-Bis(alkenyl) alcohol (doubly reduced product) was obtained as a byproduct in 18% yield.

As can be seen from the results of **7a** and **7e** (Table 2, entries 1 and 5), the acceleration effect of TMS is higher than that of the alkyl group, but lower than that of the phenyl group.[9] Among the examined substituents, the TPS group shows the highest aptitude, as we expected (see results for **7d** and **7g**; entries 4 and 7). From these results, the order of the magnitude of the rate enhancement was determined to be: TPS > Ph ≈ TBDPS > TIPS ≈ TMS ≫ alkyl. Thus, the observed significant acceleration effect of TBDPS and TPS is explainable by the increase of electrophilicity of the β-carbon atom on the alkynyl group caused by the phenyl groups on the silicon atom. The alkynyl group acts as an electrophile (hydride acceptor) in a hydroalumination with an aluminum ate complex,[2a,3i] and the phenyl groups on the TBDPS and TPS moieties should raise the electrophilicity of the ethyne due to a hyperconjugation of the phenyl and ethyne π orbitals through a Si–C σ* bond.[10] This supposition was well supported by DFT calculations of the simple TPS- or TBDPS-substituted propargyl alcohols **10** and **11**, in which the lowest unoccupied molecular orbital (LUMO) of the alcohol consists of the π* orbital of the phenyl groups, the σ* orbital of the Si–C bond, and the π* orbital of the ethyne moieties (Figure 1).[11] The calculated LUMO energy levels of **10** and **11** are significantly lower than that of the TMS-substituted counterpart **12** (**10**: −0.9965 eV, **11**: −0.9954 eV, **12**: −0.4438 eV).[12–15]

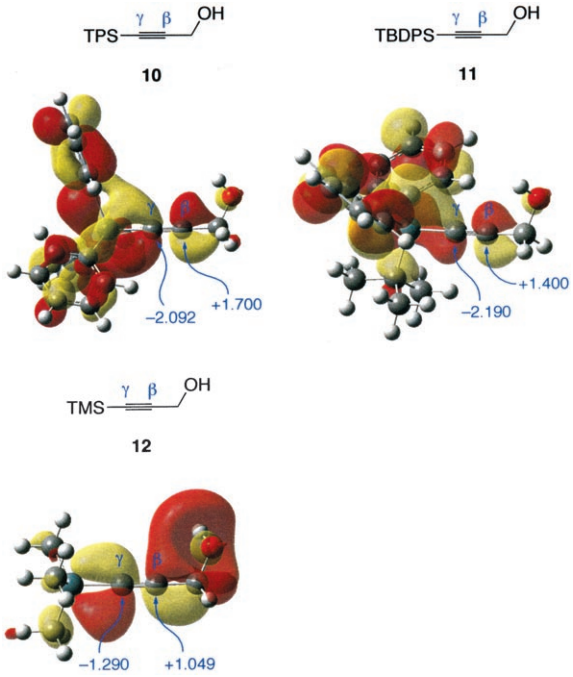
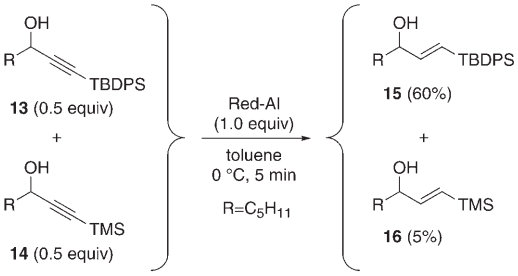


Figure 1. LUMOs of silyl-substituted propargyl alcohols **10**–**12** and Mulliken charges on the alkyne carbon atoms.

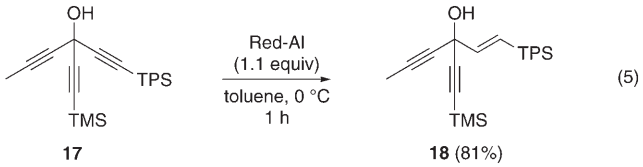
A similar accelerating effect was observed in an intermolecularly competitive variant, in which the reaction of an equimolar mixture of TBDPS- and TMS-substituted propargylic alcohols **13** and **14** with Red-Al gave vinylsilane **15** as the major product after 5 min (TBDPS side/TMS side 92:8) [Eq. (4)].



(4)

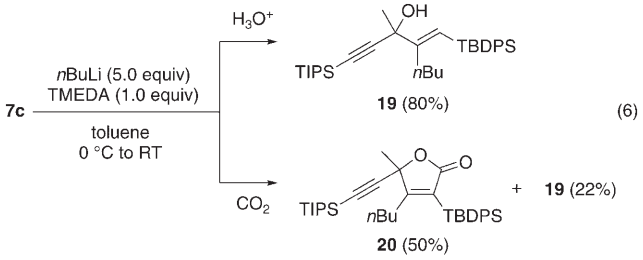
Moreover, proper combination of silyl groups may also enable group-selective functionalization in 1,1,1-tris(alkynyl)alcohol systems. For instance, the reaction of alcohol **17**, having TPS, TMS, and methyl groups at the γ positions, with Red-Al provided vinylsilane **18** as the sole product in 81% yield [Eq. (5)].

 © 2006 Wiley-VCH Verlag GmbH & Co. KGaA, Weinheim



17 18 (81%) (5)

Finally, we examined expansion of this methodology to a carbon–carbon bond-forming reaction, that is, carbolithiation of propargylic alcohol.[16] The reaction of alcohol **7c** with *n*BuLi in the presence of *N*,*N*,*N*′,*N*′-tetramethylethylenediamine (TMEDA) gave allylic alcohol **19**, with a trisubstituted alkene moiety, in 80% yield with excellent group selectivity. The stereochemistry of the resulting alkene was determined as the *E* configuration by transformation to the γ-lactone **20** through CO_2 trapping of vinyl lithium [Eq. (6)].



(6)

In summary, we have described a remarkable acceleration effect of phenyl-substituted silyl groups in hydroalumination and carbolithiation reactions of propargylic alcohols. These results clearly show that an arylsilyl group can act not only as a protecting group but also as an activating group of the alkynyl moiety. This work provides an efficient group-selective approach to multifunctionalized alkenes. Further work is underway in our group to expand the utility of this interesting phenomenon.

Received: September 7, 2005
Published online: November 28, 2005

Keywords: alkenes · carbolithiation · hydroalumination · hyperconjugation · substituent effects

[1] For leading reviews of hydrometalation, see: a) J. A. Labinger in *Comprehensive Organic Synthesis, Vol. 8* (Eds.: B. M. Trost, I. Fleming), Pergamon, Oxford, **1991**, pp. 667–702; b) N. Asao, Y. Yamamoto, *Bull. Chem. Soc. Jpn.* **2000**, *73*, 1071–1087.

[2] For reviews of hydroalumination, see: a) G. Zweifel, J. A. Miller in *Organic Reactions, Vol. 32* (Ed.: W. G. Dauben), Wiley, New York, **1984**, pp. 375–517; b) J. J. Eisch in *Comprehensive Organic Synthesis, Vol. 8* (Eds.: B. M. Trost, I. Fleming), Pergamon, Oxford, **1991**, pp. 733–761.

[3] For representative studies on hydroalumination of propargylic alcohols, see: a) J. D. Chanley, H. Sobotka, *J. Am. Chem. Soc.* **1949**, *71*, 4140–4141; b) E. B. Bates, E. R. H. Jones, M. C. Whiting, *J. Chem. Soc.* **1954**, 1854–1860; c) B. Franzus, E. I. Snyder, *J. Am. Chem. Soc.* **1965**, *87*, 3423–3429; d) E. I. Snyder, *J. Org. Chem.* **1967**, *32*, 3531–3534; e) E. J. Corey, J. A. Katzenellenbogen, G. H. Posner, *J. Am. Chem. Soc.* **1967**, *89*, 4245–4247; f) W. T. Borden, *J. Am. Chem. Soc.* **1970**, *92*, 4898–4901; g) B. Grant, C. Djerassi, *J. Org. Chem.* **1974**, *39*, 968–970; h) S. E. Denmark, T. K. Jones, *J. Org. Chem.* **1982**, *47*, 4595–4597; i) K. Kakinuma, T. Matsuzawa, T. Eguchi, *Tetrahedron* **1991**, *47*, 6975–6982; j) B. Caro, M.-C. Sénéchal-Tocquer, F. R.-L. Guen, P. LePoul, *J. Organomet. Chem.* **1999**, *585*, 43–52; k) K. Ohmori, T. Suzuki, K. Taya, D. Tanabe, T. Ohta, K. Suzuki, *Org. Lett.* **2001**, *3*, 1057–1060; l) T. Suzuki, K. Ohmori, K. Suzuki, *Org. Lett.* **2001**, *3*, 1741–1744; m) K. Ohmori, Y. Hachisu, T. Suzuki, K. Suzuki, *Tetrahedron Lett.* **2002**, *43*, 1031–1034.

[4] K. Tomooka, M. Kikuchi, K. Igawa, M. Suzuki, P.-H. Keong, T. Nakai, *Angew. Chem.* **2000**, *112*, 4676–4679; *Angew. Chem. Int. Ed.* **2000**, *39*, 4502–4505.

[5] It is well known that hydroalumination of a propargylic alcohol system proceeds significantly faster than that of a homopropargylic alcohol system; a) S. Ma, F. Liu, E. Negishi, *Tetrahedron Lett.* **1997**, *38*, 3829–3832; b) B. Crousse, M. Alami, G. Linstrumelle, *Synlett* **1997**, 992–994.

[6] The difference in bulkiness between TMS and TBDPS plays an important role in the diastereoselectivity of the [1,2]-Wittig rearrangement which forms a C–C bond between C4 and C5; see ref. [4].

[7] Quite recently, Suzuki's group has developed a chelation-controlled diastereoselective hydroalumination in a 1,1-bis-(alkynyl) alcohol system. They performed stereoselective construction of continuous pseudoquaternary chiral centers by using this method; see ref. [3k–m].

[8] The produced alcohols (that is, **4** and **5**) were easily distinguished by ^1H and ^{13}C NMR analysis after selective desilylation at the alkyne terminal.

[9] It has been reported that a phenyl substituent increases the electrophilicity of alkynes. For example, Slaugh's group reported that the reaction of diphenylacetylene with $LiAlH_4$ proceeds markedly faster than the same reaction of dialkylacetylene: E. F. Magoon, L. H. Slaugh, *Tetrahedron* **1967**, *23*, 4509–4515.

[10] Hyperconjugative interaction between the Si–C σ* orbitals and the π* orbitals of the phenyl and alkynyl moieties was observed by electron transmission spectroscopy in trimethylsilylbenzene and trimethylsilylacetylene: a) A. Modelli, D. Jones, G. Distefano, *Chem. Phys. Lett.* **1982**, *86*, 434–437; b) J. C. Giordan, J. H. Moore, *J. Am. Chem. Soc.* **1983**, *105*, 6541–6544; c) J. C. Giordan, *J. Am. Chem. Soc.* **1983**, *105*, 6544–6546.

[11] It has been reported that hydroalumination of alkynes with an ate-complex aluminum reagent is strongly dependent on the electrophilicity of the alkyne. Kakinuma, Matsuzawa, and Eguchi discussed the relationship between the LUMO level of the alkyne and the reactivity of the propargylic alcohols in hydroalumination with $LiAlH_4$; see ref. [3i].

[12] These calculations were performed at the B3LYP/6–31 + G(d)//B3LYP/6–31G(d) level with Gaussian 98.

[13] For more detailed discussion, calculation of a transition-state model is needed.

[14] We have found that measurement of the Δδ value of the ethyne carbon atoms ($\delta_{\beta\text{-carbon}}-\delta_{\gamma\text{-carbon}}$) in ^{13}C NMR analysis can predict the reactivity of silyl-substituted propargylic alcohols. Actually, the Δδ value of **10** was higher than that of the less reactive one (**10**: 22.4; **11**: 21.8; **12**: 13.1), which means that the Δδ value shows a polarization of the ethyne carbon atoms and electrodeficiency on the β-carbon atom.

[15] Recently, Gevorgyan's group reported that regiochemistry of the palladium-catalyzed hydrostannation is predictable from the Δδ value of the ethyne carbon atoms in a diarylacetylene system; M. Rubin, A. Trofimov, V. Gevorgyan, *J. Am. Chem. Soc.* **2005**, *127*, 10243–10249.

[16] Carbolithiation of propargylic alcohols has been reported in only a few cases of highly activated alkynyl systems. For the reaction of γ-phenylpropargyl alcohol, see: L.-I. Olsson, A. Claesson, *Tetrahedron Lett.* **1974**, 2161–2162.

 © 2006 Wiley-VCH Verlag GmbH & Co. KGaA, Weinheim

Nanostructures

DOI: 10.1002/anie.200501361

Synthesis of Semiconducting Thin Films with Nanometer-Scale Periodicity by Solution-Phase Coassembly of Zintl Clusters with Surfactants**

*Andrew E. Riley, Scott D. Korlann, Erik K. Richman, and Sarah H. Tolbert**

The cooperative self-assembly of inorganic precursors with organic surfactants or polymeric structure-directing agents has led to the synthesis of many oxide-based, nanostructured composite materials that show periodicity. Oxide powders, monoliths, and thin films with a diverse range of compositions (TiO_2, ZrO_2, Nb_2O_5, SnO_2, Mn_xO_y, Al_2O_3, and others) have been prepared following the work on surfactant-templated silicas (MCM-41-type materials).[1–17] Although the powdered forms of these materials have many proposed uses, including catalysis and size-selective separation, the thin-film forms have significantly expanded their potential.[18–23] The thin-film morphology has several applications for which bulk materials are not useful, including low-k dielectric coatings, optical waveguides, and membranes.[24–27]

Despite the many exciting potential applications of these periodic surfactant-templated thin films, there are still significant limitations to oxide-based materials. The most significant of these limitations is that most oxides are insulators, or wide-band-gap semiconductors, which limits their use in applications based on electrical conductivity because of their high intrinsic resistance and low carrier densities.

The development of self-assembled inorganic/organic composites based on non-oxide precursors has led to the synthesis of a variety of semiconducting composites with nanoscale periodicity.[28–36] These composite materials use highly reduced soluble metal clusters, or Zintl clusters, as an inorganic building block. The Zintl clusters can self-assemble with organic structure-directing agents in solution with the help of transition-metal cross-linkers. The resulting material is a highly periodic inorganic alloy with ordering similar to liquid-crystalline systems. These materials, which were initially designed to be analogues of silica and other oxide composites, have an advantage over most oxide systems for optoelectronic applications in that their range of band gaps can be tuned between 0.6 and 3.4 eV depending on their chemical composition.[28–37] Unfortunately, although composites with a wide range of electronic properties have been synthesized, their macroscale morphology has been limited to bulk powders, thus restricting their usefulness in some applications.

As with the oxide materials mentioned previously, knowledge of the macroscale morphology of this class of non-oxide materials helps to determine the optimal applications of the composites. Many of the proposed applications for the non-oxide composite materials, such as photovoltaics, ambipolar field-effect transistors (FETs), and chemical sensing, rely on the electrical conductivity of the composite. Bulk powders present several problems for the effective assembly of an electronic device, most notably the contact resistance between the powder and the electrode as well as between grains within the powder. A thin-film morphology should be able to overcome these obstacles if the film can be grown in intimate contact with a substrate that can double as an electrical contact.

To address this fundamental need, we report here the synthesis of semiconducting non-oxide thin films with a variety of compositions and structures by coassembly of Zintl clusters with cationic surfactants. Interestingly, in some cases, thin films form with phases that have not been observed in bulk composite powders. The phases formed range in nanoscale architecture from a partly disordered wormlike phase, to a periodic, hexagonal, honeycomb structure, and on to a highly ordered cubic geometry. The surface-nucleated growth mechanism used to synthesize these thin films appears to stabilize both new compositions and phases that are otherwise inaccessible in these systems. Furthermore, our results indicate that the optical homogeneity of the films can be modified by adding reagents that chelate the cross-linking transition metal. Layered thin films can also be synthesized in the absence of a metal cross-linking agent. UV/Vis/NIR reflectance data indicate that materials with a broad range of band gaps can be created. Finally, as expected for a semiconducting thin film, diode characteristics are observed in the current–voltage measurements when asymmetric electrodes are employed.

The solution-phase self-assembly of these non-oxide thin films was carried out under inert conditions. The Zintl cluster, a surfactant (cetyltriethylammonium bromide), and the transition-metal salt were all dissolved in formamide. A gold substrate was then placed in contact with the solution such that the gold was inverted to prevent sedimentation on the surface. This mixture was held at 60 °C for one hour during which time the films grew on the surface. Profilometry indicates that films could be formed with a range of thicknesses. The data indicate that films ranging from 90 to about 500 nm thick could be produced, depending on the reactivity of the cross-linking metal, the growth time of film, and the surfactant concentration. Films could also be prepared without a transition-metal cross-linking agent by taking advantage of the self-oligomerization of tin telluride ($SnTe_4^{4-}$). Such films were synthesized in a similar manner, although in this case room temperature and a growth time of 8 hours were employed.

Figure 1 shows typical low-angle X-ray diffraction patterns for thin films of five different phases and compositions.

[*] Dr. A. E. Riley, S. D. Korlann, E. K. Richman, Prof. S. H. Tolbert
Department of Chemistry and Biochemistry
The University of California, Los Angeles
Los Angeles, CA 90095-1569 (USA)
Fax: (+1) 310-206-4038
E-mail: tolbert@chem.ucla.edu

[**] This work was supported by the National Science Foundation under grant CHE-9985259 and by the Office of Naval Research under grant N00014-04-1-0410. S.H.T. is an Alfred P. Sloan Foundation Research Fellow.

 © 2006 Wiley-VCH Verlag GmbH & Co. KGaA, Weinheim

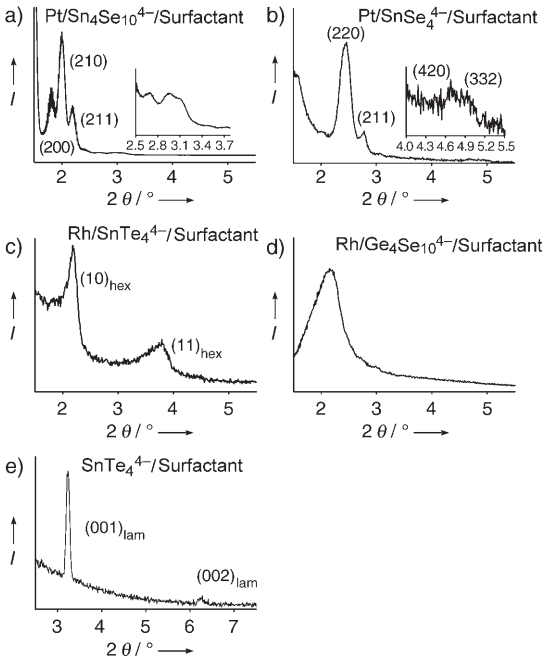


Figure 1. Low-angle X-ray diffraction patterns of nanostructured semiconducting inorganic/surfactant composite thin films: a) a thin film synthesized using Pt-coupled $Sn_4Se_{10}^{4-}$ clusters demonstrates a cubic *Pm*3*n* morphology (peak-position ratio $1:\sqrt{5}/2:\sqrt{6}/2$); b) a thin film synthesized using Pt-coupled $SnSe_4^{4-}$ clusters demonstrates a cubic *Ia*3*d* morphology (peak-position ratio $1:\sqrt{8}/\sqrt{6}:\sqrt{4}/\sqrt{6}:\sqrt{20}/\sqrt{6}$); c) a thin film synthesized from Rh-coupled $SnTe_4^{4-}$ clusters has a 2D hexagonal *P*6*mm* morphology (peak position ratio $1:\sqrt{3}$); d) a thin film synthesized from Rh-coupled $Ge_4Se_{10}^{4-}$ clusters has a disordered, probably wormlike geometry; e) a thin film synthesized by the self-oligomerization of $SnTe_4^{4-}$ clusters in the presence of surfactant has a layered lamellar structure.

The labels for each composite are based on the precursors used to synthesize the films, and are not indicative of the exact final stoichiometry of the films. In Figure 1a, a Pt-coupled $Sn_4Se_{10}^{4-}$/surfactant composite shows the (200), (210), and (211) diffraction peaks of a cubic *Pm*3*n* architecture.[38] The bulk analogue of this system has been shown to form either a 2D hexagonal (*P*6*mm*) or a cubic (*Ia*3*d*) phase.[30] The formation of a thin film with a periodicity different from those of the bulk analogues demonstrates the importance of surface stabilization to the nanoscale architecture. Figure 1b shows the (211), (220), (420), and (332) diffraction pattern of a cubic *Ia*3*d* phase of a Pt-coupled $SnSe_4^{4-}$/surfactant composite. While *Ia*3*d* phases have been observed previously in related bulk composites based on Zintl clusters,[30] this phase has not been observed previously for any nanostructured thin film, including silica-based composite thin films.[18–22] The absence of this phase likely stems from the fact that a flat substrate does not provide a good interfacial nucleation site for the *Ia*3*d* phase. The observation of this phase for Zintl cluster based systems suggests that the nucleation process is fundamentally different in these materials compared to oxide-based systems. This point will be discussed further below.

Figure 1c shows the low-angle diffraction pattern for a Rh-coupled $SnTe_4^{4-}$/surfactant composite thin film. This composite has a 2D hexagonal (*P*6*mm*) architecture as evidenced by the (10) and (11) peaks of this phase with a position ratio of $1:\sqrt{3}$. This material has a unit-cell parameter *a* of 46.1 Å. This repeat distance is slightly larger than the distances that have been observed in bulk composites of similar composition. A direct comparison of the structure with a bulk system, however, can not be made because the Rh/$SnTe_4^{4-}$/surfactant system has not been successfully synthesized as a bulk nanostructured composite. The presence of both a fundamental $(10)_{hex}$ and a $(11)_{hex}$ reflection indicates that although the film does have hexagonal order it is not constrained to the plane of the substrate, which would be lead to an absence of the $(11)_{hex}$ reflection in a θ–θ diffraction geometry. Low-angle X-ray diffraction studies on the bulk precipitate (not shown) indicate that the corresponding bulk system has no such structure. The lack of structure in the bulk precipitate again emphasizes the fact that the surface-growth mechanism allows the synthesis of composite films whose compositions are not accessible in powder form.

Figure 1d shows the low-angle X-ray diffraction pattern for a Rh-coupled $Ge_4Se_{10}^{4-}$/surfactant composite thin film. This film exhibits only one peak, which is indicative of a phase with a characteristic repeat distance, but no long-range order. This wormlike phase has a fundamental repeat distance of 42 Å. Finally, Figure 1e shows the diffraction pattern for a thin film prepared through Zintl-cluster auto-oligomerization without a transition-metal cross-linking agent. The $SnTe_4^{4-}$/surfactant composite has the (001) and (002) peaks at a 1:2 position ratio which would be expected for a layered composite.

Table 1 is a summary of the various compositions of thin films that have been synthesized thus far. Whereas in some cases, such as in the Rh/$SnTe_4^{4-}$/surfactant and Pt/$Sn_4Se_{10}^{4-}$/surfactant films described above, the films demonstrate hexagonal or cubic order, in many cases the films demonstrate a more disordered "wormlike" structure similar to that observed in Figure 1d. Such a single peak can be observed even for materials in which long range periodicity is not present. The position of these single peaks ranges from 34 to 43 Å for the wormlike structures. Hexagonal materials exhibit similar fundamental peak positions in the range between 38 and 42 Å. These peak positions correspond to hexagonal unit-cell parameters *a* that range from 44 to 49 Å. These values are reasonable compared to those of powders of non-oxide hexagonal composite systems prepared with similar surfactants.[28] The agreement between the patterns of the hexagonal and wormlike materials further emphasizes the fact that the disordered materials are likely to be composed of randomly assembled cylindrical micelles. The cubic *Pm*3*n* Pt/$Sn_4Se_{10}^{4-}$/surfactant composite has a unit-cell parameter *a* of 98 Å, whereas the cubic *Ia*3*d* Pt/$SnSe_4^{4-}$/surfactant composite has a unit-cell parameter *a* of 86 Å. Both of these values are in reasonable agreement with those of analogous silica-based cubic structures.[2,39] Finally, the lamellar $SnTe_4^{4-}$/surfactant system has a layer spacing of 28 Å, a value which has been observed previously for layered phases formed with cetyltriethylammonium bromide.[2]

Table 1 also includes the elemental data obtained from energy-dispersive spectroscopy (EDS) for the majority of

 © 2006 Wiley-VCH Verlag GmbH & Co. KGaA, Weinheim

Table 1: Summary of the compositions, phases, and average fundamental repeat distances of the thin film composites.

Composite[a]	Unit-cell parameter *a* [Å][b]	Bulk analogue[c]	Elemental analysis[d]
wormlike			
$Rh/Ge_4Se_{10}^{4-}$	42	no	
$Pt/Ge_4Se_{10}^{4-}$	35	yes	$Pt_{0.8}Ge_4Se_{10.4}$
$Pd/Sn_4Se_{10}^{4-}$	41	no	$Pd_{0.9}Sn_4Se_{12.6}$
$Ni/Sn_4Se_{10}^{4-}$	40	no	$Ni_{1.4}Sn_4Se_{12.4}$
$Rh/Sn_4Se_{10}^{4-}$	42	no	$Rh_{1.3}Sn_4Se_{11}$
$Ir/Sn_4Se_{10}^{4-}$	42	no	
$Ni/SnSe_4^{4-}$	37	no	$Ni_{1.1}SnSe_4$
$Pt/SnSe_4^{4-}$	37	no	$Pt_{1.3}SnSe_{4.6}$
$Zn/SnSe_4^{4-}$	43	yes	
$Pt/SnTe_4^{4-}$	34	no	$Pt_{1.4}SnTe_{4.2}$
hexagonal			
$Ni/Ge_4Se_{10}^{4-}$	49	yes	$Ni_{0.8}Ge_4Se_{10.4}$
$Pt/Sn_4Se_{10}^{4-}$	44	yes	$Pt_{1.3}Sn_4Se_{9.7}$
$Rh/SnTe_4^{4-}$	48	no	$Rh_{0.7}SnTe_{3.4}$
cubic Pm3n			
$Pt/Sn_4Se_{10}^{4-}$	98	no	$Pt_{1.2}Sn_4Se_{9.4}$
cubic Ia3d			
$Pt/SnSe_4^{4-}$	86	no	$Pt_{1.3}SnSe_{3.6}$
lamellar			
$SnTe_4^{4-}$	28	yes	

[a] The composites are listed according to phase, and all compositions should be assumed to include surfactant. The wormlike phases have one peak, which is indicative of a characteristic repeat distance and no long-range order. Hexagonal refers to a 2D *P6mm* hexagonal, honeycomb architecture. Lamellar is a layered phase. The diffraction patterns for all five phases are shown in Figure 1. [b] Although *a* is listed for each phase, it is however, actually just a characteristic repeat distance for the wormlike phase, rather than a unit-cell parameter. [c] This indicates if a nanostructured-powder analogue has been synthesized from the same precursors. [d] Determined by energy-dispersive spectroscopy (EDS) X-ray analysis. The ratio of cross-linking metal to precursor chalcogenide cluster in the mesostructure is approximately one in all cases. More importantly, the elemental data suggests that the initial tetrahedral or adamantine cluster is incorporated into the composite as an intact unit.

composites produced. In all cases, the 1:4 or 4:10 (Group 14 element:chalcogen) stoichiometry of the initial tetrahedral or adamantane-like clusters is preserved in the final composite. Moreover, all the materials show an approximately 1:1 transition-metal:Zintl-cluster ratio, which supports the assertion that the −4 charge on the clusters is not significantly altered during the synthesis. The results of elemental analysis provide strong evidence that the overall composition of the thin film can be simply and reproducibly tuned by merely changing the nature of the solution used in the synthesis.

Beyond controlling the nanoscale structure and elemental composition, there is also an interest in producing films that are continuous on a large scale. While most of the films described here are optically quite homogeneous, there are some synthetic combinations that lead to films that have surface inhomogeneity. This surface inhomogeneity is observed visually as islands of dark material, which appears to be bulk composite material, adhered to the surface. Although the diffraction pattern of the bulk precipitate yields no structural information, it is desirable to make the thin films as homogeneous as possible. In an effort to control the homogeneity of the product, we attempted to slow down the formation of the bulk film. This was accomplished by ligating the transition-metal cross-linking ion. For example, the addition of ethylenediamine (en) to a solution of $RhCl_3$ is accompanied by a color change as the rhodium ion is complexed by the bidentate ligand. Although the addition of $RhCl_3$ to a solution of surfactant and $SnTe_4^{4-}$ yields a precipitate immediately, the addition of $[Rh(en)_x]Cl_3$ yields no precipitate until the mixture is heated. Free Rh^{3+} ions are slowly released upon heating.

Figure 2 shows the low-angle X-ray diffraction patterns and pictures of $Rh/SnTe_4^{4-}$/surfactant thin films formed with

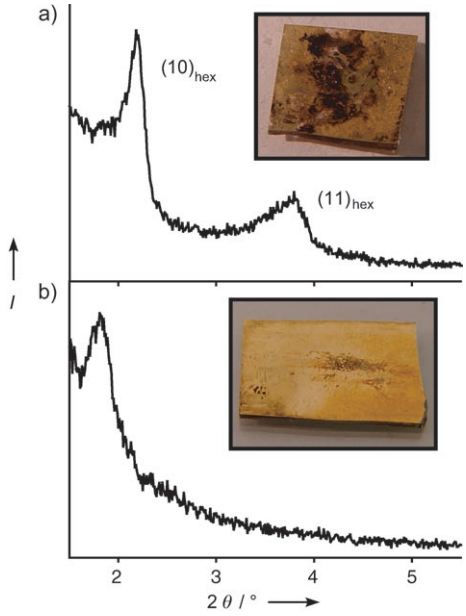


Figure 2. Low-angle diffraction patterns and pictures of $Rh/SnTe_4^{4-}$/surfactant composite thin films: a) an inhomogeneous film with hexagonal *P6mm* order (peak-position ratio $1:\sqrt{3}$); b) a film prepared by ligating the transition metal used to cross-link the structure. This film, while less ordered, is much more homogeneous.

$RhCl_3$ (Figure 2a) and $[Rh(en)_x]Cl_3$ (Figure 2b), respectively, as the Rh source. Figure 2a shows a diffraction pattern characteristic of a 2D hexagonal architecture whereas Figure 2b show a characteristic diffraction pattern of a less-ordered, wormlike structure. Also, the fundamental repeat distance of the disordered phase is 48.1 Å for this structure versus 41.5 Å for the hexagonal phase. The larger repeat distance for the en-containing phase may be indicative of a lower density of inorganic cross-links in the en-containing film or may be due to swelling of the nonpolar organic domains by en. Similarly, the lower order in the en-containing material may also be related to any reduction in the cross-linking density. Alternatively, it may be related to hydrophobic swelling by the en or more generally to the nonpolar nature of en, which is less effective than formamide at promoting amphiphilic assembly.[40,41] The insets in Figure 2, however, show that the film formed with the ligated transition

 © 2006 Wiley-VCH Verlag GmbH & Co. KGaA, Weinheim

metal is much more homogeneous than the nonligated film because of the slower formation kinetics.

To understand how these films differ from oxide-based materials produced previously, some discussion of the mechanism of film formation is desirable. In bulk composites of this class of materials, the self-assembly process is the result of inorganic oligomerization coupled with electrostatic attraction to the organic surfactant. Although the surfactant generally forms multiply charged micelles in solution, the clusters initially do not associate with the micelles as a result of entropic considerations. Upon addition of a transition-metal ion, which cross-links the inorganic species, the entropic barrier to self-assembly is lowered and the composite can form. This mechanism must be different for film formation. The bulk material forms quickly because of strong electrostatic interactions, but after the bulk powder precipitates, the concentration of reactants left in solution reaches a steady state. This state is more representative of an equilibrium composition, and may even involve some dissolution of already formed powders. The thin films grow at the metal surface using the reactants that are left in solution. Confirmation of these ideas comes from cases in which the inorganic oligomerization leads to extremely rapid precipitation of the precursors—in this situation, thin films are not formed. In this case, the concentrations of the precursors remaining in solution were probably too low for appreciable film growth to take place. A similar mechanism is involved in the interface-nucleated growth of silica films from aqueous solution.[18,42]

There is, however, one distinctive difference between interface-nucleated silica films and the films presented here. For silica-based materials, the surfactant first associates with the interface and then the silica oligomers associate with the surfactant.[43,44] This process results in materials with a well-defined orientation of the nanometer-scale structure relative to that of the substrate. For example, the hexagonal *c* axis of hexagonal honeycomb-structured materials lies in the plane of the film.[18,42] For these Zintl ion based films, however, it appears that formation of the film is driven by the attraction between the Zintl cluster and the noble-metal surface, rather than by the surfactant and the surface. Contrary to the results obtained for silica-based films, this produces films that do not have a well defined orientation of the nanometer-scale structure with respect to the interface. This same effect is likely to be responsible for the fact that the *Ia3d* cubic structure, which can not produce a favorable interaction of the surfactant with the substrate, can be produced for Zintl ion based composites, even though it has not been produced in silica-based materials.

Other synthetic parameters to consider include the redox activity of the transition-metal ion used in the inorganic oligomerization. Attempts to synthesize thin films using Au^{3+} ions resulted in the gold/titanium layers delaminating from the glass, probably because of oxidation of the adherence layer by the transition-metal ion.[45] Similarly, Pd^{2+}-coupled, mesostructured films could only be produced if very short growth times were employed to minimize degradation of the metallic substrate. The Au^{3+} and Pd^{2+} ions have the largest standard reduction potentials of the transition-metal ions that were used for cross-linking, which indicates that above a certain threshold, oxidation of the substrate is a factor that needs to be considered.

Although transition-metal cross-linking is the most commonly employed method for inorganic polymerization in this class of materials, there are other means of polymerization available. One of the thin-film compositions in Table 1 and Figure 1e is synthesized without a cross-linking transition-metal ion. The formation of the tin telluride film is based on the self-oligomerization of the $SnTe_4^{4-}$ cluster.[46] Tellurium elimination condenses the cluster into larger oligomers ($Sn_2Se_7^{4-}$, $Sn_2Se_6^{4-}$), which can then self-assemble with the surfactant in an analogous manner to the model proposed above for self-assembly based on transition-metal cross-linking.[46,47]

We next consider the electronic properties of these nanoscale semiconductor thin films. The bulk analogues of these thin films are semiconductors with band gaps that range from narrow (0.6 eV) to wide (3.4 eV).[28–30,32–37] Figure 3 shows the relative absorptivity calculated from specular reflectivity data for thin films of four different compositions. The four composites show a range of band gaps from 1.1 eV ($Ir/SnSe_4^{4-}$/surfactant) to 1.5 eV ($Rh/SnTe_4^{4-}$/surfactant), as determined by Tauc plot fits to this absorptivity data.[48,49] The tunability of the band gap is believed to stem from the variable elemental composition of the composites (Table 1). Although many nanoscale semiconductors show strong quantum-confinement effects, one might expect that these amorphous semiconductors would have fairly localized excitations, which are not expected to be very sensitive to the nanometer-scale periodicity of the composite. In agreement with this idea, studies of both bulk chalcogenide glass based semiconductors and Zintl cluster based inorganic/surfactant

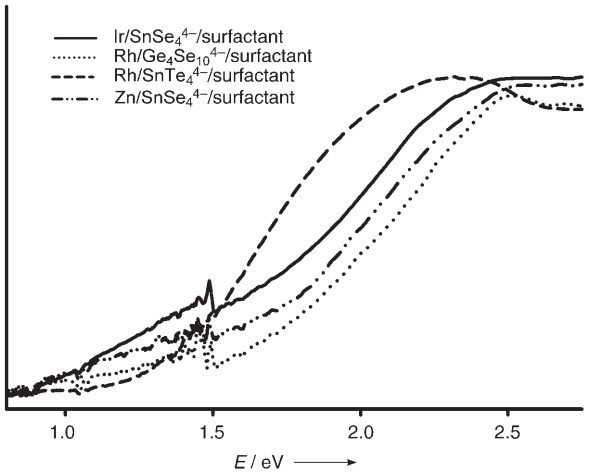


Figure 3. Relative absorptivity (α) calculated from Vis/NIR reflectance data for nanostructured, semiconducting thin films of different elemental composition. The optical band gaps of the materials were determined by using Tauc plots. All four of these materials are midgap semiconductors with band gaps of 1.1 eV ($Ir/SnSe_4^{4-}$/surfactant), 1.3 eV ($Rh/Ge_4Se_{10}^{4-}$/surfactant), 1.5 eV ($Rh/SnTe_4^{4-}$/surfactant), and 1.2 eV ($Zn/SnSe_4^{4-}$/surfactant). The noise at ca. 1.5 eV is due to a detector change in the spectrometer.

 © 2006 Wiley-VCH Verlag GmbH & Co. KGaA, Weinheim

composites have shown that changes in elemental composition are primarily responsible for shifts in band gaps. This includes both changes in the transition-metal and main-group elements that make up the composite,[28–30,32–37] and changes in the stoichiometric ratios of those elements.[37,50,51] We note that depending on the exciton size in these semiconductors, there could be some quantum-confinement effects on top of this elemental tuning, but because we can not make bulk analogues with stoichiometries that are identical to these thin-film composites, such size effects can not be clearly observed.

Interestingly, examination of the data in Figure 3 shows two distinct curve shapes: concave for the Rh/$SnTe_4^{4-}$/surfactant composite and convex for the other three compositions. Concave absorption curves are expected for a direct-band-gap material, while a convex curve would be expected for an indirect-band-gap semiconductor. In agreement with this assignment, the best linear fits to the data were achieved by using the direct-band-gap form of the Tauc plot for the Rh/$SnTe_4^{4-}$/surfactant composite (E vs $E^2 \times \alpha$) and the indirect-band-gap form of the Tauc plot for the other three compositions (E vs $\sqrt{E} \times \alpha$).[48,49] In chalcogenide glasses, tellurides tend to have different electronic properties than selenides and sulfides,[52] and, in direct agreement with our reflectance data, work on tin chalcogenides shows that the telluride composite has a direct band gap whereas the selenide, sulfide, and oxide composites all have indirect band gaps.[52]

Finally, to exemplify the potential for electronic applications for these nanostructured thin films, we produced a simple rectifier. Rectifiers are semiconductor-based devices that exhibit nonlinear current–voltage characteristics. These devices can be constructed by connecting a semiconductor with two electrodes that have different work functions. Figure 4a shows the current–voltage (I–V) characteristics, as determined by scanning tunneling spectroscopy, for a nanostructured Pt/$Sn_4Se_{10}^{4-}$/surfactant thin film grown on gold. The gold makes up one electrode, and the Pt/Ir STM tip provides the second electrode in the system. The device shows a small leakage current in this sample from -2.0 to $+0.4$ V on the order of nanoamps. There is an order-of-magnitude increase in the current traveling through the system at 0.4 V, the turn-on voltage. Figure 4b shows similar I–V data for a Ni/$Ge_4Se_{10}^{4-}$/surfactant nanostructured thin-film composite. This sample shows a turn-on voltage of -0.5 V. Both samples show large asymmetry, which is expected for rectification. Notably, these two films of different composition also show significantly different turn-on voltages. The difference of almost 1 V between the turn-on voltages in the two samples indicates that the data arises from a real material-based phenomenon and that the electronic properties of these films can be tuned over a large range through changes in the elemental composition.

In summary, in this work we have reported the synthesis of periodic, surfactant-templated thin films of Zintl clusters with nanoscale periodicity and cubic, hexagonal honeycomb, lamellar, and wormlike structures. The thin-film morphology holds several advantages for the design and synthesis of devices that utilize the semiconducting nature of these non-oxide composites. The variety of compositions synthesized not only demonstrates the breadth of the synthetic method, but also provides a means of tailoring the properties of the inorganic semiconducting framework. Moreover, work is currently underway to remove the surfactant from these materials and produce periodic nanoporous semiconductors. Preliminary results suggest that the substrate stabilizes the nanometer-scale architecture of these composites and makes removal of the surfactant without collapse of the inorganic framework possible.[53] We are also working on the incorporation of semiconducting, structure-directing agents into the organic phase, which could make these materials good candidates for device applications such as photovoltaics and ambipolar FETs.[54] The synthesis of thin-film rectifiers based on these materials is the first step toward developing functional devices that can take advantage of the nanoscale periodicity present in these films.

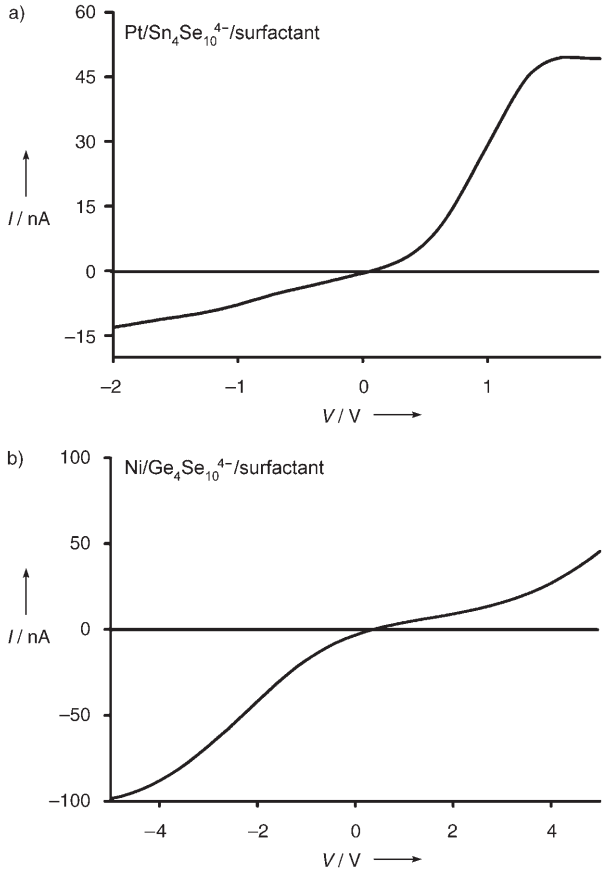


Figure 4. Current–voltage curves for two inorganic/surfactant composite thin film samples as measured by scanning tunneling spectroscopy. a) A Pt/$Sn_4Se_{10}^{4-}$/surfactant nanostructured thin film shows a turn-on voltage of approximately 0.4 V. b) A Ni/$Ge_4Se_{10}^{4-}$/surfactant nanostructured thin film shows a turn-on voltage near -0.5 V. Both curves are asymmetric, which is expected for semiconductor rectifiers. Furthermore, the turn-on voltages vary significantly depending on the composition of the thin film.

Experimental Section

The raw materials for our film growth were prepared by established methods.[55–59] The Zintl clusters ($K_4Ge_4Se_{10}$, $K_4Sn_4Se_{10}$, K_4SnSe_4, K_4SnTe_4) were prepared by direct combination of the constituent elements at high temperature (750 °C) under inert conditions.[55–58]

 © 2006 Wiley-VCH Verlag GmbH & Co. KGaA, Weinheim

The surfactant cetyltriethylammonium bromide was prepared by treating triethylamine with 1-bromohexadecane in refluxing ethanol for 3 days.[59] The product was evaporated and then purified by dissolution in chloroform and precipitation with diethyl ether. The white powder was recovered by filtration and then recrystallized from warm acetone.

Non-oxide composite films were synthesized through surface-nucleated growth from a gold substrate. The gold substrates consisted of a glass microscope slide with a thin adherence layer of titanium and a thin layer of gold deposited on the adherence layer. For most composites, the slides were inverted and supported in a synthesis solution consisting of Zintl cluster (0.1 mmol), cetyltriethylammonium bromide (0.3 or 0.6 mmol), and transition metal (0.1 mmol) in formamide (1 mL). For the *Ia3d* cubic phase, these ratios were adjusted slightly to contain Zintl cluster (0.2 mmol), cetyltriethylammonium bromide (0.95 mmol), and transition metal (0.065 mmol) in formamide (1 mL). All of the film mixtures were prepared under an inert atmosphere. The growing films were maintained at 60 °C under inert conditions for 1 h in all cases except for palladium, which was grown for only 25 min to minimize the Pd^{2+} degradation of the gold substrate. After synthesis, the films were washed with copious amounts of formamide under ambient conditions to remove any adhered bulk precipitate. After washing the films in formamide, they were rinsed with acetone and air-dried.

Some Rh-coupled $SnTe_4^{4-}$ thin films were also prepared by using a slightly altered procedure in which $[Rh(en)_x]Cl_3$ was employed as the cross-linking agent. These films were prepared in a similar manner to the method describe above. A solution (0.5 mL) was prepared containing formamide, $SnTe_4^{4-}$, and surfactant. In a second solution, $RhCl_3$ (0.1 mmol) was dissolved in formamide (1 mL) at 60 °C. Ethylenediamine (en; ca. 0.1 mL) was added to the $RhCl_3$ solution. Additional ethylenediamine was subsequently added to the solution dropwise until the color changed from red to colorless. The $[Rh(en)_x]Cl_3$ solution was then added to the Zintl/surfactant solution and placed in an oven at 60 °C for 1 h with a gold-coated substrate. The film was then recovered as described above.

Pure $SnTe_4$ thin films were prepared by using the standard procedure without the addition of a cross-linking transition metal. This Zintl/surfactant solution was mixed and left overnight at room temperature in an inert atmosphere in the presence of a gold-coated substrate. The product was collected the next day and washed with formamide.

The NIR/UV/Vis reflectance data were collected with a Shimadzu UV-3100 spectrophotometer. The reflectance data were measured by utilizing an ISR-3100 integrating sphere attachment because of the optical density of the samples. The collection was made over the wavelength range 2400–200 nm. Low-angle X-ray diffraction (XRD) patterns were collected with a home-built theta-theta powder diffractometer operating with $Cu_{K\alpha}$ radiation.

Scanning tunneling spectroscopy measurements were performed by using a Digital Instruments Nanoscope III in STM mode. After stabilizing a Pt/Ir tip above the sample, the bias of the tip was ramped from −5 to 5 V while holding the tip position constant. In imaging mode, which is used to stabilize the tip position, a bias and current determine the separation. For all scans, the tip position was taken at a bias of 1.135 mV and 100 pA.

Energy-dispersive spectroscopy (EDS) X-ray analysis was carried out on a JEOL TSM-6700F field-emission scanning electron microscope equipped with a liquid-nitrogen-cooled EDAX Super UTW Detector. All elemental spectra were obtained with the scanning electron microscope operating at 25 keV and 20 mA, except that of the platinum composite, which was measured operating at 5–6 keV and 20 mA. All spectra were analyzed with EDAX inc. Genesis Spectrum SEM Quant ZAF Software (version 3.60).

The film thickness was measured by using a Veeco Dektak 6M Profiler. The height of the sample film was assigned as the difference between the height of the film and the height of the bare-gold substrate on which the film was grown.

Received: April 19, 2005
Revised: August 8, 2005
Published online: November 28, 2005

Keywords: nanostructures · self-assembly · surfactants · thin films · Zintl phases

[1] C. T. Kresge, M. E. Leonowicz, W. J. Roth, J. C. Vartulli, J. S. Beck, *Nature* **1992**, *359*, 710.
[2] Q. Huo, D. I. Margolese, U. Clesa, P. Feng, T. E. Gier, P. Sieger, R. Leon, P. M. Petroff, F. Schuth, G. D. Stucky, *Nature* **1994**, *368*, 317.
[3] A. Monnier, F. Schuth, Q. Huo, D. Kumar, D. Margolese, R. S. Maxwell, G. D. Stucky, M. Krishnamurty, P. Petroff, A. Firouzi, M. Janicke, B. F. Chmelka, *Science* **1993**, *261*, 1299.
[4] D. M. Antonelli, J. Y. Ying, *Angew. Chem.* **1996**, *108*, 461; *Angew. Chem. Int. Ed. Engl.* **1996**, *35*, 426.
[5] S. A. Bagshaw, T. J. Pinnavaia, *Angew. Chem.* **1996**, *108*, 1180; *Angew. Chem. Int. Ed. Engl.* **1996**, *35*, 1102.
[6] Z. R. Tian, W. Tong, J.-Y. Wang, N.-G. Duan, V. K. Krishnan, S. L. Suib, *Science* **1997**, *276*, 926.
[7] U. Ciesla, S. Schacht, G. D. Stucky, K. K. Unger, F. Schuth, *Angew. Chem.* **1996**, *108*, 579; *Angew. Chem. Int. Ed. Engl.* **1996**, *35*, 541.
[8] P. Yang, D. Zhao, D. I. Margolese, B. F. Chmelka, G. D. Stucky, *Nature* **1998**, *396*, 152.
[9] M. S. Wong, D. M. Antonelli, J. Y. Ying, *Nanostruct. Mater.* **1997**, *9*, 165.
[10] M. S. Wong, J. Y. Ying, *Chem. Mater.* **1998**, *10*, 2067.
[11] T. Sun, J. Y. Ying, *Angew. Chem.* **1998**, *110*, 690; *Angew. Chem. Int. Ed.* **1998**, *37*, 664.
[12] M. Linden, S. Schunk, F. Schuth in *Mesoporous Molecular Sieves* (Eds.: L. Bonneviot, F. Beland, C. Danumah, S. Giasson, S. Kaliaguine), Elsevier, Amsterdam, **1998**.
[13] G. J. de A. A. Soler-Illia, A. Louis, C. Sanchez, *Chem. Mater.* **2002**, *14*, 750.
[14] L. Pidol, D. Grosso, G. J. A. A. Soler-Illia, E. L. Crepaldi, C. Sanchez, P. A. Albouy, H. Amenitsch, P. Euzen, *J. Mater. Chem.* **2002**, *12*, 557.
[15] E. L. Crepaldi, G. J. de A. A. Soler-Illia, D. Grosso, F. Cagnol, F. Ribot, C. Sanchez, *J. Am. Chem. Soc.* **2003**, *125(32)*, 9770.
[16] D. Grosso, G. J. de A. A. Soler-Illia, E. L. Crepaldi, F. Cagnol, C. Sinturel, A. Bourgeois, A. Brunet-Bruneau, H. Amenitsch, P. A. Albouy, C. Sanchez, *Chem. Mater.* **2003**, *15(24)*, 4562.
[17] D. Grosso, C. Boissiere, B. Smarsly, T. Brezesinski, N. Pinna, P. A. Albouy, H. Amenitsch, M. Antonietti, C. Sanchez, *Nat. Mater.* **2004**, *3*, 787.
[18] H. Yang, A. Kuperman, N. Coombs, S. Mamiche-Afara, G. A. Ozin, *Nature* **1996**, *379*, 703.
[19] H. Yang, N. Coombs, I. Sokolov, G. A. Ozin, *Nature* **1996**, *381*, 589.
[20] C. A. Alberius, K. L. Frindell, R. C. Hayward, E. J. Kramer, G. D. Stucky, B. F. Chmelka, *Chem. Mater.* **2002**, *14*, 3284.
[21] D. Grosso, A. R. Balkenende, P. A. Albouy, M. Lavergne, L. Mazerolles, F. Babonneau, *Mater. Chem.* **2000**, *10*, 2085.
[22] A. Gibaud, D. Grosso, B. Smarsly, A. Baptiste, J. F. Bardeau, F. Babonneau, D. A. Doshi, Z. Chen, C. J. Brinker, C. Sanche, *J. Phys. Chem. B* **2003**, *107*, 6114.
[23] H. Yang, N. Coombs, I. Sokolov, G. A. Ozin, *J. Mater. Chem.* **1997**, *7*, 1285.
[24] T. Nassivera, A. G. Eklund, C. C. Landry, *J. Chromatogr.* **2002**, *973*, 97.
[25] A. Sayari, *Chem. Mater.* **1996**, *8*, 1840.

 © 2006 Wiley-VCH Verlag GmbH & Co. KGaA, Weinheim

[26] B. J. Scott, M. H. Bartl, G. Wirnsberger, G. D. Stucky, *J. Phys. Chem. A* **2003**, *107*, 5499.
[27] T.-Q. Nguyen, J. Wu, V. Doan, B. J. Schwartz, S. H. Tolbert, *Science* **2000**, *288*, 652.
[28] A. E. Riley, S. H. Tolbert, *J. Am. Chem. Soc.* **2003**, *125*, 4551.
[29] K. K. Rangan, P. N. Trikalitis, C. Canlas, T. Bakas, D. P. Weliky, M. G. Kanatzidis, *Nano Lett.* **2002**, *2*, 513.
[30] P. N. Trikalitis, K. K. Rangan, M. G. Kanatzidis, *J. Am. Chem. Soc.* **2002**, *124*, 2604.
[31] P. N. Trikalitis, K. K. Rangan, T. Bakas, M. G. Kanatzidis, *Nature* **2001**, *410*, 671.
[32] K. K. Rangan, P. N. Trikalitis, M. G. Kanatzidis, *J. Am. Chem. Soc.* **2000**, *122*, 10230.
[33] M. Wachhold, K. K. Rangan, M. Lei, M. F. Thorpe, S. J. L. Billinge, V. Petkov, J. Heising, M. G. Kanatzidis, *J. Solid State Chem.* **2000**, *152*, 21.
[34] M. J. MacLachlan, N. Coombs, G. A. Ozin, *Nature* **1999**, *397*, 681.
[35] K. K. Rangan, S. J. L. Billinge, V. Petkov, J. Heising, M. G. Kanatzidis, *Chem. Mater.* **1999**, *11*, 2629.
[36] P. N. Trikalitis, K. K. Rangan, T. Bakas, M. G. Kanatzidi, *J. Am. Chem. Soc.* **2002**, *124*, 12255.
[37] S. D. Korlann, A. E. Riley, B. L. Kirsch, B. S. Mun, S. H. Tolbert, *J. Am. Chem. Soc.* **2005**, *127*, 12516.
[38] D. T. Cromer, R. L. Mills, D. Schiferl, L. A. Schwalbe, *Acta Crystallogr. Sect. B* **1981**, *37*, 8.
[39] J. C. Vartuli, K. D. Schmitt, C. T. Kresge, W. J. Roth, M. E. Leonowicz, S. B. McCullen, S. D. Hellring, J. S. Beck, J. L. Schlenker, D. H. Olson, E. W. Sheppard, *Chem. Mater.* **1994**, *6*, 2317.
[40] J. E. Gordon, *The Organic Chemistry of Electrolyte Solutions*, New York, Wiley, **1975**.
[41] D. F. Evans, D. D. Miller, *Water Sci. Rev.* **1989**, *4*, 1.
[42] I. A. Aksay, M. Trau, S. Manne, I. Honma, N. Yao, L. Zhou, P. Fenter, P. M. Eisenberger, S. M. Gruner, *Science* **1996**, *273*, 892.
[43] S. Manne, T. E. Schaeffer, Q. Huo, P. K. Hansma, D. E. Morse, G. D. Stucky, I. A. Aksay, *Langmuir* **1997**, *13*, 6382.
[44] S. Manne, *Prog. Colloid Polym. Sci.* **1997**, *103*, 226.
[45] $Pd^{2+} \rightarrow Pd^{0}$ 0.92 V, $Au^{3+} \rightarrow Au^{0}$ 1.36 V, $Ti^{2+} \rightarrow Ti^{0}$ −1.63 V; from: D. F. Shriver, P. Atkins, C. H. Langford, *Inorganic Chemistry*, 2nd ed., W. H. Freeman, New York, **1994**.
[46] A. E. Riley, S. H. Tolbert, *Res. Chem. Intermed.*, in press.
[47] J. C. Huffman, J. P. Haushalter, A. M. Umarji, G. K. Shenoy, R. C. Haushalter, *Inorg. Chem.* **1984**, *23*, 2312.
[48] J. Tauc, R. Grigorovici, A. Vancu, *Phys. Status Solidi* **1966**, *15*, 627.
[49] A. Rantzer, H. Arwin, J. Birch, B. Hjorvarsson, J. W. P. Bakker, K. Jarrendahl, *Thin Solid Films* **2001**, *394*, 256.
[50] R. M. Mehra, S. Kohli, A. Pundir, V. K. Sachdev, P. C. Mathur, *J. Appl. Phys.* **1997**, *87*, 7842.
[51] T. Gomi, Y. Hirose, T. Kurosu, T. Shiraishi, M. Iida, Y. Gekka, A. Kunioka, *J. Non-Cryst. Solids* **1980**, *41*, 37.
[52] I. Lefebvre, M. A. Szymanski, J. Olivier-Fourcade, J. C. Jumas, *Phys. Rev. B* **1998**, *58*, 1896.
[53] S. D. Korlann, S. H. Tolbert, unpublished results.
[54] A. P-Z. Clark, K.-F. Shen, Y. F. Rubin, S. H. Tolbert, *Nano Lett.* **2005**, *5*, 1647.
[55] O. Palchik, A. Gedanken, V. Plachik, M. A. Slifkin, A. M. Weiss, *J. Solid State Chem.* **2002**, *165*, 125.
[56] J. C. Hauffman, J. P. Haushalter, A. M. Umarji, G. K. Shenoy, R. C. Haushalter, *Inorg. Chem.* **1984**, *23*, 2312.
[57] A. M. Pirani, H. P. A. Mercier, D. A. Dixon, H. Bormann, G. J. Schrobligen, *Inorg. Chem.* **2001**, *40*, 4823.
[58] K. O. Klepp, F. Fabian, *Z. Naturforsch. B* **1999**, *54*, 1499.
[59] F. M. Menger, C. A. Littau, *J. Am. Chem. Soc.* **1993**, *115*, 10083.

 © 2006 Wiley-VCH Verlag GmbH & Co. KGaA, Weinheim

Host–Guest Systems

DOI: 10.1002/anie.200502802

Folding a De Novo Designed Peptide into an α-Helix through Hydrophobic Binding by a Bowl-Shaped Host**

*Shohei Tashiro, Masahide Tominaga, Yoshiki Yamaguchi, Koichi Kato, and Makoto Fujita**

Spontaneous folding of polypeptides into their latent secondary structures such as the α helix and β sheet is both a chemically and biologically important process. It is anticipated that studies on peptide folding will lead to the construction of functional architectures with peptide backbones and help the understanding of protein folding in nature.[1] Extensive studies have thus been made on the formation of peptide secondary structures from de novo designed oligopeptides.[2,3] However, secondary structures from synthetic peptides are normally ephemeral unless fixed by covalent links or metal coordination between the residues.[4–6] Fragmental units remain stable in proteins as they are sustained by protein scaffolds through weak interactions (hydrophobic, electrostatic, etc.). We anticipated that the large hydrophobic cavity of a synthetic host could replace the protein scaffolds and stabilize the secondary structures of oligopeptides.

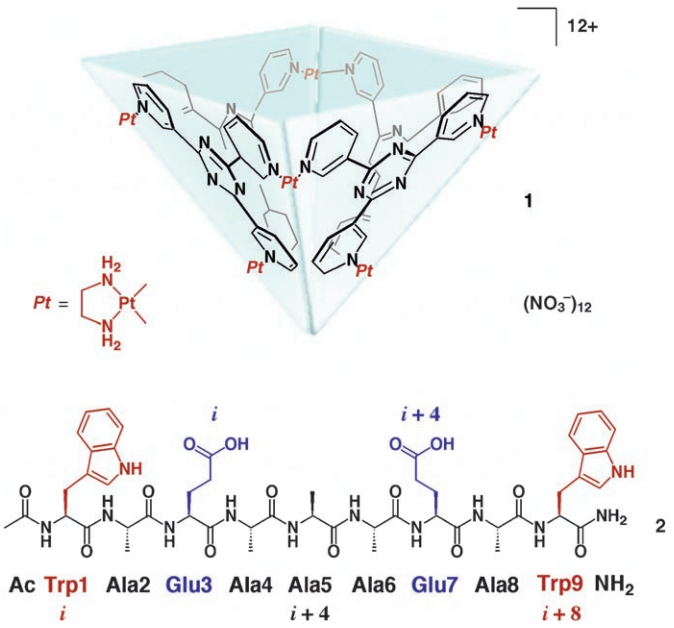
Bowl-shaped host **1**, assembled from $[Pt(en)(NO_3)_2]$ (en = ethylene-1,2-diamine) and a triazine-cored tridentate ligand, has a large hydrophobic pocket,[7] and is potentially capable of accommodating two or more amino acid residues.[8] De novo designed oligopeptide **2** consists of only nine residues with a Trp group at the two terminals.[9] Assuming that **2** has an α-helical conformation, the hydrophobic indole rings of the i and $i+8$ Trp residues are oriented on the same face of the helix,[10] whereas the negative charges of the i and $i+4$ Glu

[*] S. Tashiro, Dr. M. Tominaga, Prof. Dr. M. Fujita
Department of Applied Chemistry
School of Engineering
The University of Tokyo
Hongo, Bunkyo-ku, Tokyo 113-8656 (Japan)
Fax: (+81) 3-5841-7257
E-mail: mfujita@appchem.t.u-tokyo.ac.jp
Dr. Y. Yamaguchi, Prof. Dr. K. Kato
Graduate School of Pharmaceutical Sciences
Nagoya City University
Mizuho-ku, Nagoya, Aichi 467-8603 (Japan)
Prof. Dr. K. Kato
Institute for Molecular Science
Okazaki National Research Institutes
Higashiyama Myodaiji, Okazaki, Aichi 444-8787 (Japan)

[**] This work was supported by a CREST (Core Research for Evolution Science and Technology) project from the Japan Science and Technology Agency, and by the "Nanotechnology Support Project" of the Ministry of Education, Culture, Sports, Science, and Technology (MEXT), Japan.

Supporting information for this article is available on the WWW under http://www.angewandte.org or from the author.

© 2006 Wiley-VCH Verlag GmbH & Co. KGaA, Weinheim
WILEY InterScience DISCOVER SOMETHING GREAT



Job plot supported the formation of a 1:1 complex between **1** and **2**. The association constant was estimated from NMR titration experiments to be about $1 \times 10^3\,\text{M}^{-1}$.

The α-helical conformation of **2** in the cavity of **1** was elucidated by careful NMR spectroscopic analysis. We noted that the upfield shifts of the Hβ signals of the Trp 1, Trp 9, and Ala 5 residues ($\Delta\delta$ = ca. −1.2 ppm) were somewhat larger than those of the others, thus suggesting that these residues were co-enclathrated in the cavity of **1**, namely, Trp 1, Ala 5, and Trp 9 in the *i*-, *i* + 4-, and *i* + 8-positions were oriented on the same face and in good agreement with the α-helical conformation of peptide **2**.

The α-helical conformation was more reliably confirmed by analyzing NOE cross-peaks of peptide **2**. Several medium-range NOE interactions, for example, $d_{\alpha\beta}(i,i+3)$, $d_{\alpha N}(i,i+3)$, and $d_{\alpha N}(i,i+4)$ were observed in the NOESY spectrum and are characteristic of a typical α-helical conformation (Figure 2). Some sequential $d_{NN}(i, i+1)$ NOESY cross-peaks also supported the presence of helical structure.

residues are on the opposite face. Accordingly, the bowl complex **1** is expected to bind **2** in an α-helical conformation through two types of host–guest interactions: primarily by hydrophobic interactions between the Trp residues and the pocket of **1** and, secondarily through electrostatic interactions between the Glu residues and the high positive charge of **1** (12+).[11] The remaining Ala residues have latent propensity for an α-helical conformation.[2c]

Compounds **1** and **2** were mixed in an aqueous solution in the expectation of an induction of the α helix. Disappointingly, a somewhat complex NMR spectrum was obtained when **1** (3 equiv) was added to a solution of **2** (2.5 mM) in phosphate buffer (100 mM) and the conformation of **2** could not be determined. However, the addition of a small amount of chloroform (1 v/v %) resulted in the signals of **2** becoming simpler (Figure 1) and all nine residues of **2** could be assigned by TOCSY and NOESY measurements. Most signals of **2** were shifted upfield, thus indicating the encapsulation of **2** within the hydrophobic pocket of **1**. Indeed, some NOE interactions between **1** and **2** were observed. The

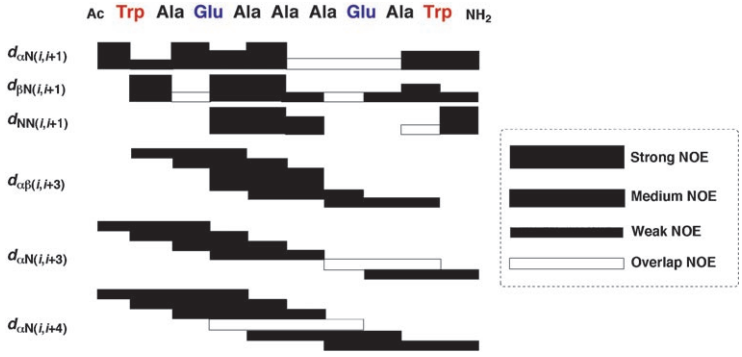


Figure 2. NOE correlations for bound peptide **2** in H_2O/D_2O (9:1; 100 mM phosphate buffer, pH 6.8). The black bars indicate the intensity of each NOE signal. The white bars indicate ambiguous NOE signals arising because of overlapping of the cross-peaks.

The conformation of **2** was also studied by a molecular dynamics (MD) simulation with the CNS program[12] that contains NOE distance restraints (39 intra-residue + sequential constraints, 25 medium-range constraints).[13] The 15 lowest energy structures for **2** all predicted an α-helical conformation (Figure 3). These ensembles showed low back-

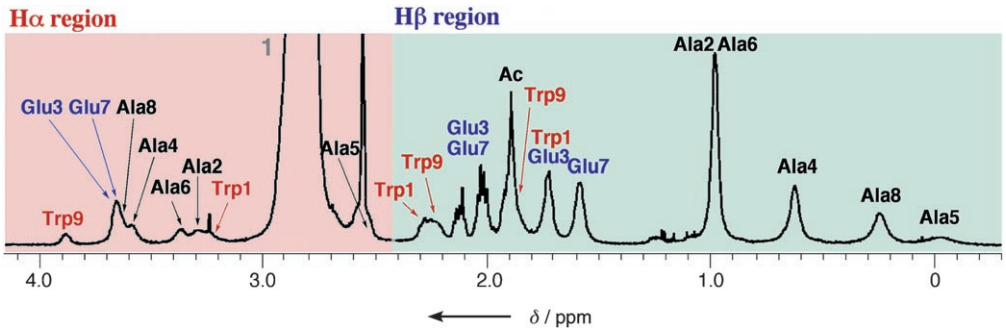


Figure 1. ^{1}H NMR spectrum (600 MHz) of **1**·**2** in H_2O/D_2O (9:1; 100 mM phosphate buffer, pH 6.8). The pale red and green backgrounds represent the regions of the Hα and Hβ signals of bound peptide **2**.

 © 2006 Wiley-VCH Verlag GmbH & Co. KGaA, Weinheim

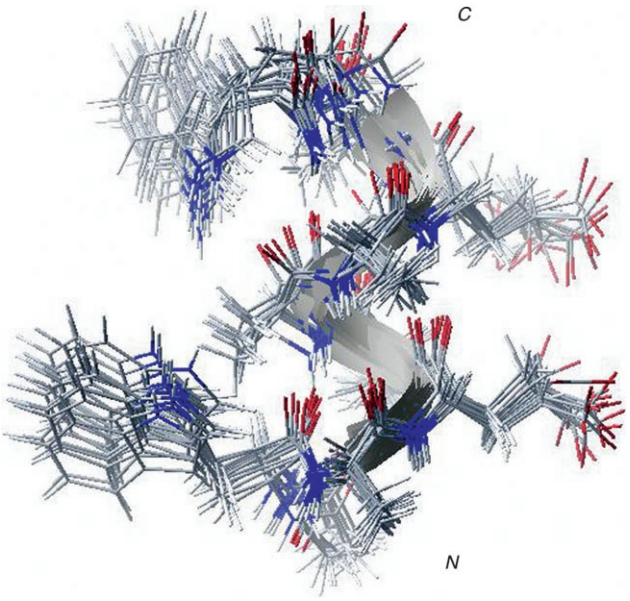


Figure 3. Superposition of the 15 lowest energy structures by CNS[12] for bound peptide **2**.

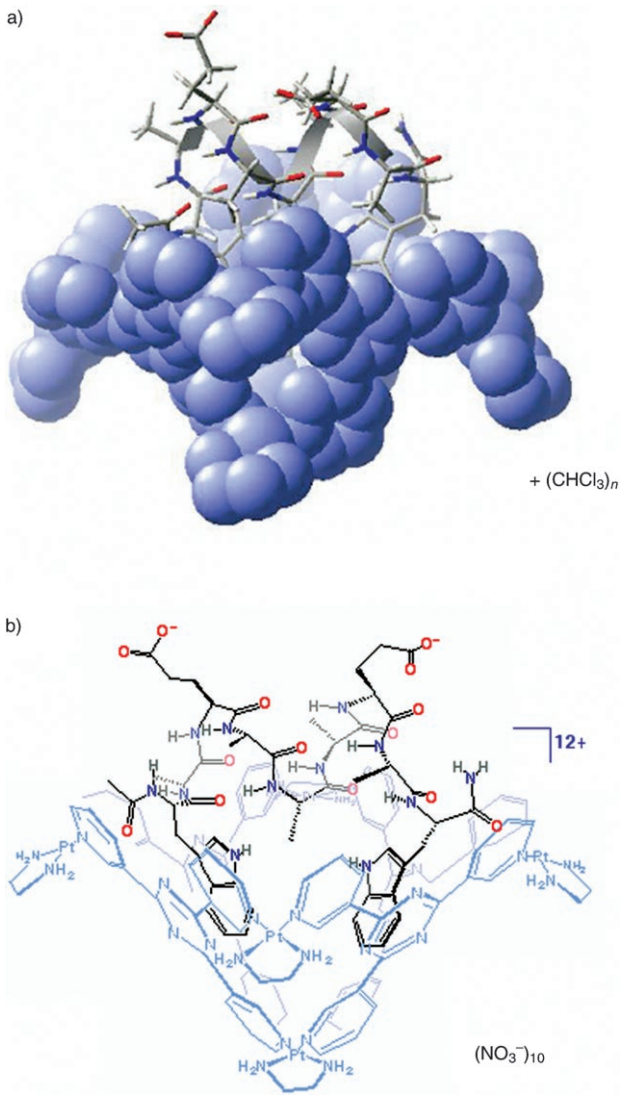


Figure 4. The proposed structure of complex **1**·**2**. a) The bowl-shaped cavity of **1** and peptide **2** are represented by space-filling and cylindrical models, respectively. b) Schematic representation of complex **1**·**2**.

bone pairwise root-mean-square deviation (0.68 Å) and no violation of the ideal bond lengths and angles.[14] The observation of some NOE interactions between the Ala 5 methyl group and the indole rings of both Trp residues illustrate the two indole rings were on the same face.

From the NMR studies, Job's plot, and the MD simulation, we conclude that oligopeptide **2** adopts an α-helical conformation and the Trp 1, Ala 5, and Trp 9 residues are on the same face of the helix and deeply accommodated in the cavity of **1** to form the stable **1**·**2** complex (Figure 4).[10] Chloroform, which is essential to induction of the α helix, is probably co-enclathrated in a small void surrounded by Trp 1, Ala 5, and Trp 9 in the **1**·**2** complex, although we could not specify the number and position of the co-enclathrated chloroform molecules by NMR spectroscopic analysis.[15]

In summary, we have demonstrated that bowl **1** has the ability to induce and stabilize the α-helix conformation of a de novo designed peptide. It is noteworthy that the stabilization of secondary structures by the hydrophobic environment is what nature does. Our bio-inspired method has potential applications for stabilizing not only other secondary structures but, ultimately, tertiary structures of proteins.

Experimental Section

Peptide **2** was synthesized with an automated peptide synthesizer (ABI 433A, Applied Biosystems) by using standard 9-fluorenylmethoxycarbonyl (Fmoc) based FastMoc coupling chemistry (0.1 mmol scale). Peptides were cleaved from the resin with trifluoroacetic acid (TFA, 10 mL) containing 5% (v/v) water and 5% (v/v) 1,2-ethanedithiol as a scavenger at room temperature for 3 h. Free peptides were washed from the resin with TFA (3 mL) followed by dichloromethane (5 mL), and then evaporated. A large volume of Et_2O was added to the residue and the precipitate was collected by filtration. Crude peptides were purified by reversed-phase HPLC on an Inertsil Peptides C18 (GL Sciences Inc.) semipreparative column (20 mm × 250 mm) using 10 mM ammonium hydrogencarbonate solution with a 0.05% TFA (pH 6.0) and acetonitrile gradient. The peptide was obtained as a white powder by lyophilization. Characterization of the peptide was carried out by ^{1}H NMR spectroscopy and MALDI-TOF mass spectrometry (Voyager-DE STR, Applied Biosystems).

1: 2,4,6-Tris(3-pyridyl)-1,3,5-triazine (0.20 mmol), $[Pt(en)(NO_3)_2]$ (0.30 mmol), and 2-naphthoic acid (0.25 mmol) as a template were combined in H_2O (10 mL) and stirred for 6 days at 90 °C. After filtration of the mixture, a small amount of nitric acid was added to the solution and the slightly acidic solution was washed five times with chloroform and then the solution was concentrated. A large volume of acetone was added to the concentrated solution to give a white precipitate, which was collected and then washed with acetone. After drying the white powder, it was dissolved in water, and then this solution was lyophilized (for complete evaporation of residual acetone). Yield 90%. ^{1}H NMR (500 MHz, D_2O, 300 K, tetramethylsilane (TMS) as external standard): $\delta = 10.63$ (s, 8H), 9.90 (s, 4H), 9.25 (d, $J = 5.0$ Hz, 8H), 9.19–9.14 (m, 16H), 7.87–7.81 (m, 12H), 3.02–2.86 ppm (m, 24H); ^{13}C NMR (125 MHz, D_2O, 300 K, TMS as

 © 2006 Wiley-VCH Verlag GmbH & Co. KGaA, Weinheim

external standard): $\delta = 169.2$ (Cq), 169.1 (Cq), 155.6 (CH), 155.2 (CH), 153.5 (CH), 153.0 (CH), 140.6 (CH), 140.3 (CH), 134.3 (Cq), 134.2 (Cq), 127.7 (CH), 127.4 (CH), 47.7 (CH_2), 47.2 ppm (CH_2); IR (KBr, cm^{-1}): 3066, 1608, 1587, 1533, 1384, 1320, 1192, 1175, 1053; m.p. $>250\,^{\circ}C$ (decomp); elemental analysis calcd for $C_{84}H_{96}N_{48}O_{36}Pt_6 \cdot 16\,H_2O$: C 26.46, H 3.38, N 17.63; found: C 26.72, H 3.44, N 17.37. The structure of **1** was the same as that of the Pd-bowl[7a] as determined by ^1H NMR spectroscopy.

Received: August 8, 2005
Published online: November 28, 2005

Keywords: helical structures · host–guest systems · NMR spectroscopy · peptides · self-assembly

[1] For reviews on the folding of secondary structures, see a) R. Parthasarathy, S. Chaturvedi, K. Go, *Prog. Biophys. Mol. Biol.* **1995**, *64*, 1–54; b) S. H. Gellman, *Curr. Opin. Chem. Biol.* **1998**, *2*, 717–725; c) J. Venkatraman, S. C. Shankaramma, P. Balaram, *Chem. Rev.* **2001**, *101*, 3131–3152.

[2] For de novo design of helices, see a) K. R. Shoemaker, P. S. Kim, E. J. York, J. M. Stewart, R. L. Baldwin, *Nature* **1987**, *326*, 563–567; b) S. Marqusee, R. L. Baldwin, *Proc. Natl. Acad. Sci. USA* **1987**, *84*, 8898–8902; c) P. C. Lyu, M. I. Liff, L. A. Marky, N. R. Kallenbach, *Science* **1990**, *250*, 669–673; d) S. Padmanabhan, S. Marqusee, T. Ridgeway, T. M. Laue, R. L. Baldwin, *Nature* **1990**, *344*, 268–270; e) D. H. Appella, L. A. Christianson, D. A. Klein, D. R. Powell, X. Huang, J. J. Barchi, Jr., S. H. Gellman, *Nature* **1997**, *387*, 381–384.

[3] For the de novo design of β-sheet structures, see a) M. R. Ghadiri, J. R. Granja, R. A. Milligan, D. E. McRee, N. Khazanovich, *Nature* **1993**, *366*, 324–327; b) F. J. Blanco, M. A. Jiménez, J. Herranz, M. Rico, J. Santoro, J. L. Nieto, *J. Am. Chem. Soc.* **1993**, *115*, 5887–5888; c) T. S. Haque, S. H. Gellman, *J. Am. Chem. Soc.* **1997**, *119*, 2303–2304; d) N. Sakai, N. Majumber, S. Matile, *J. Am. Chem. Soc.* **1999**, *121*, 4294–4295; e) N. Sakai, S. Matile, *Chem. Commun.* **2003**, 2514–2523.

[4] For covalent links, see a) D. Y. Jackson, D. S. King, J. Chmielewski, S. Singh, P. G. Schultz, *J. Am. Chem. Soc.* **1991**, *113*, 9391–9392; b) C. Bracken, J. Gulyás, J. W. Taylor, J. Baum, *J. Am. Chem. Soc.* **1994**, *116*, 6431–6432; c) E. Cabezas, A. C. Satterthwait, *J. Am. Chem. Soc.* **1999**, *121*, 3862–3875; d) C. E. Schafmeister, J. Po, G. L. Verdine, *J. Am. Chem. Soc.* **2000**, *122*, 5891–5892; e) R. N. Chapman, G. Dimartino, P. S. Arora, *J. Am. Chem. Soc.* **2004**, *126*, 12252–12253.

[5] For metal coordination, see a) M. R. Ghadiri, C. Choi, *J. Am. Chem. Soc.* **1990**, *112*, 1630–1632; b) F. Ruan, Y. Chen, P. B. Hopkins, *J. Am. Chem. Soc.* **1990**, *112*, 9403–9404; c) M. J. Kelso, H. N. Hoang, W. Oliver, N. Sakolenko, D. R. March, T. G. Appleton, D. P. Fairlie, *Angew. Chem.* **2003**, *115*, 437–440; *Angew. Chem. Int. Ed.* **2003**, *42*, 421–424; d) A. Ojida, M. Inoue, Y. Mito-oka, I. Hamachi, *J. Am. Chem. Soc.* **2003**, *125*, 10184–10185.

[6] For other interactions, see a) M. W. Peczuh, A. D. Hamilton, J. Sánchez-Quesada, J. de Mendoza, T. Haack, E. Giralt, *J. Am. Chem. Soc.* **1997**, *119*, 9327–9328; b) Y. Inai, K. Tagawa, A. Takasu, T. Hirabayashi, T. Oshikawa, M. Yamashita, *J. Am. Chem. Soc.* **2000**, *122*, 11731–11732; c) D. Wilson, L. Perlson, R. Breslow, *Bioorg. Med. Chem.* **2003**, *11*, 2649–2653; d) A. Verma, H. Nakade, J. M. Simard, V. M. Rotello, *J. Am. Chem. Soc.* **2004**, *126*, 10806–10807.

[7] For the Pd–bowl complex, see a) M. Fujita, S.-Y. Yu, T. Kusukawa, H. Funaki, K. Ogura, K. Yamaguchi, *Angew. Chem.* **1998**, *110*, 2192–2196; *Angew. Chem. Int. Ed.* **1998**, *37*, 2082–2085; b) S.-Y. Yu, T. Kusukawa, K. Biradha, M. Fujita, *J. Am. Chem. Soc.* **2000**, *122*, 2665–2666; c) M. Yoshizawa, T. Kusukawa, M. Fujita, S. Sakamoto, K. Yamaguchi, *J. Am. Chem. Soc.* **2001**, *123*, 10454–10459. Here, we used the Pt–bowl complex because of its high stability against phosphate buffer solution.

[8] S. Tashiro, M. Tominaga, M. Kawano, B. Therrien, T. Ozeki, M. Fujita, *J. Am. Chem. Soc.* **2005**, *127*, 4546–4547.

[9] Circular dichroism spectra showed that free peptide **2** took an almost unordered structure. The conformation of complexed **2** could not be determined from CD measurements because strong absorption of **1** around 200–250 nm interfered with the CD spectrum of **2**. The unordered structure of free **2** is also elucidated by comparison of the ^{13}C chemical shifts of the Cα carbon atoms; See the Supporting Information.

[10] Ideally, the Trp resides should be located at the *i*- and *i*+7-positions. We originally designed peptide **2** so that it would be encapsulated within the dimeric capsule of **1**, which we have previously reported.[7b] In this study, we unexpectedly observed the binding of **2** by monomeric **1**. Despite the subtle mismatch in the location of the Trp residues, the α-helical conformation of **2** was sufficiently stabilized because of flexible orientation of the terminal Trp residues.

[11] The importance of two interactions (hydrophobic and electrostatic) for peptide binding has been discussed in one of our previous papers.[8] Namely, a related Pd^{II}-linked host compound recognized the Trp-Trp-Ala sequence strongly, whereas the non-aromatic peptide Gly-Gly-Ala and cationic peptide Trp-His-Ala were much less strongly bound by the host.

[12] A. T. Brünger, P. D. Adams, G. M. Clore, W. L. DeLano, P. Gros, R. W. Grosse-kunstleve, J.-S. Jiang, J. Kuszewski, M. Nilges, N. S. Pannu, R. J. Read, L. M. Rice, T. Simonson, G. L. Warren, *Acta Crystallogr. Sect. A* **1998**, *54*, 905–921.

[13] We could not estimate the $^3J_{NHC\alpha}$ coupling constants for the CNS restraint because of broadening of the signals of the bound peptide.

[14] From the observed 68 NOE correlations, four unreasonable correlations presumably arising from very minor conformational isomers were eliminated for the CNS calculation.

[15] Titration experiments were difficult since chloroform shows very low solubility in water. Stabilization of the α-helical conformation of **2** was observed when more than approximately 10 equivalents of chloroform were added to the solution.

 © 2006 Wiley-VCH Verlag GmbH & Co. KGaA, Weinheim

Supramolecular Chemistry

DOI: 10.1002/anie.200503096

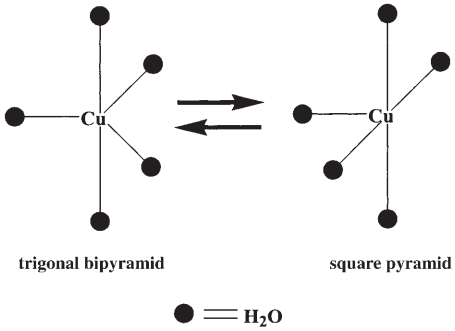
Fivefold Coordination of a Cu^{II}–Aqua Ion: A Supramolecular Sandwich Consisting of Two Crown Ether Molecules and a Trigonal-Bipyramidal $[Cu(H_2O)_5]^{2+}$ Complex**

*Vaddypally Shivaiah and Samar K. Das**

Copper ions play an important role in biological systems; for example, a normal human body contains between 80 and 120 mg of copper as one of the essential elements.[1] The more common oxidation state of copper is +2. However, the simplest aqueous form of the Cu^{II} ion is still not clearly understood. More than 40 years ago, aqueous solution-state divalent copper ions were presumed to have a tetragonal four-coordinate structure.[2,3] It was subsequently considered to be a distorted octahedral hexaqua ion,[4–7] based on ESR experiments and single-crystal spectroscopy of hexaqua copper(II) complexes.[8,9]

It is generally assumed that a Cu^{II} ion in an aqueous solution forms an octahedral $[Cu(H_2O)_6]^{2+}$ complex that undergoes Jahn–Teller distortion with elongated axial bonds because of its d^9 electronic configuration.[10–22] The shorter (equatorial) Cu–O bonds lengths in aqueous solution have been characterized by several experimental techniques including EXAFS (extended X-ray absorption fine structure),[13–16] XANES (X-ray absorption near-edge structure),[15] and isotropic substitution in neutron diffraction.[17–19] These physical studies provide consistent values for the equatorial Cu–O bond lengths in the range from 1.94 to 2.00 Å. The longer axial bond lengths obtained experimentally range from 2.12 to 2.60 Å,[19] because experimental techniques such as EXAFS and XANES require fitting procedures that incorporate some a priori assumptions about the structure.[10–16]

In 2001, Pasquarello and co-workers reported their combined experimental and theoretical investigation on the structure and dynamics of hydrated copper(II) in aqueous solution.[23] They determined the structure by both neutron diffraction and first principles molecular dynamics. The major breakthrough is that, in contrast to the generally accepted picture that assumes the Cu^{II} ion has an octahedral environment of solvent molecules, their experimental and theoretical results favor fivefold coordination around a copper center, $[Cu(H_2O)_5]^{2+}$. The solvated complex, $[Cu(H_2O)_5]^{2+}$, undergoes frequent transformations between square-pyramidal and trigonal-bipyramidal (tbp) configurations by a Berry twist mechanism (Scheme 1).[24] Fivefold coordination of water



Scheme 1. Interconversion between square-pyramidal and tbp configurations by a Berry twist mechanism.

molecules around a Cu^{2+} ion in a tbp geometry is one of the possible conformations.[23] However, to date there is no crystallographic evidence of a tbp $[Cu(H_2O)_5]^{2+}$ ion to confirm unambiguously its existence. We report herein the crystal structure of a "supramolecular sandwich" consisting of two crown ether molecules ([18]crown-6) that stabilize a tbp $[Cu(H_2O)_5]^{2+}$ cation with a polyoxomolybdate ion, $[Mo_6O_{19}]^{2-}$, in the compound $[Cu(H_2O)_5([18]crown\text{-}6)_2][Mo_6O_{19}]$ (**1**), which was obtained according to Equation (1).

$$Cu(NO_3)_2\cdot 3H_2O + 2\,[18]crown\text{-}6 + (Bu_4N)_2[Mo_6O_{19}] + 2H_2O \rightarrow [Cu(H_2O)_5([18]crown\text{-}6)_2][Mo_6O_{19}]\,(\mathbf{1}) + 2\,[Bu_4N]NO_3 \quad (1)$$

This is the first metal–aqua complex that is perfectly sandwiched by two crown ether molecules through well-defined hydrogen bonds that involve metal-coordinated water molecules and oxygen atoms of the crown ether molecules.

Compound **1** was characterized by elemental analysis, thermogravimetric analysis (TGA), single-crystal X-ray structure analysis,[25] and spectroscopic methods (IR, UV/Vis, EPR). In its crystal structure $[Cu(H_2O)_5([18]crown\text{-}6)_2]^{2+}$ and $[Mo_6O_{19}]^{2-}$ ions are present as shown in Figure 1. In the isopolyanion $[Mo^{VI}{}_6O_{19}]^{2-}$ (also known as Lindqvist type polyoxometalate (POM) anion) each Mo atom is surrounded by a distorted octahedron consisting of one central (O_c), one terminal (O_t), and four bridging (O_b) oxygen atoms (Figure 1). The Mo–O bond lengths can be grouped into three sets: Mo–O_t 1.677–1.694, Mo–O_b 1.851–2.021, and Mo–O_c 2.308–2.329 Å. The bond angle of Mo-O_b-Mo is 116.0–117.1°, while that of Mo-O_c-Mo is 179.5–179.7°.

The most exciting feature of the structure is the presence of a hitherto elusive tbp $[Cu(H_2O)_5]^{2+}$ ion that is flawlessly sandwiched by two crown ether molecules through O–H···O hydrogen-bonding interactions (Figure 2). The exactness of

[*] V. Shivaiah, Dr. S. K. Das
School of Chemistry
University of Hyderabad
Hyderabad 500046 (India)
Fax: (+91) 40-2301-2460
E-mail: skdsc@uohyd.ernet.in

[**] We thank DST, Government of India, for financial support (Project No. SR/S1/IC-18/2002). The National X-ray Diffractometer Facility at University of Hyderabad funded by the Department of Science and Technology, Government of India, is gratefully acknowledged. We are grateful to UGC, New Delhi, for providing the infrastructure facility at University of Hyderabad under UPE grant. We thank Professor M. V. Rajashekaran for helpful discussions. V.S. thanks CSIR, New Delhi, for a fellowship.

Supporting information for this article is available on the WWW under http://www.angewandte.org or from the author.

 © 2006 Wiley-VCH Verlag GmbH & Co. KGaA, Weinheim

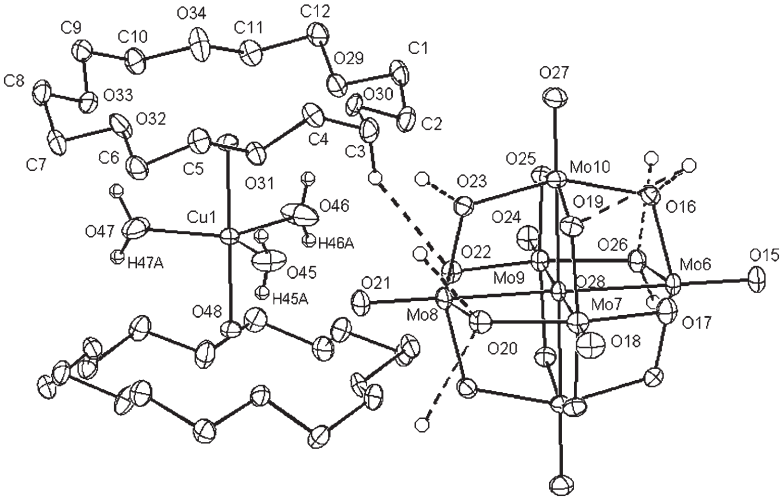


Figure 1. X-ray crystal structure of **1** as a thermal ellipsoidal plot (hydrogen atoms of the crown ether molecules are omitted for clarity). Oxygen atoms O16, O19, O20, O22, and O26 of the isopolyanion $[Mo_6O_{19}]^{2-}$ are involved in C–H···O hydrogen-bonding interactions. White circles are hydrogen atoms from surrounding crown ether molecules (see also Figure 3 in the context of molecular clipping).

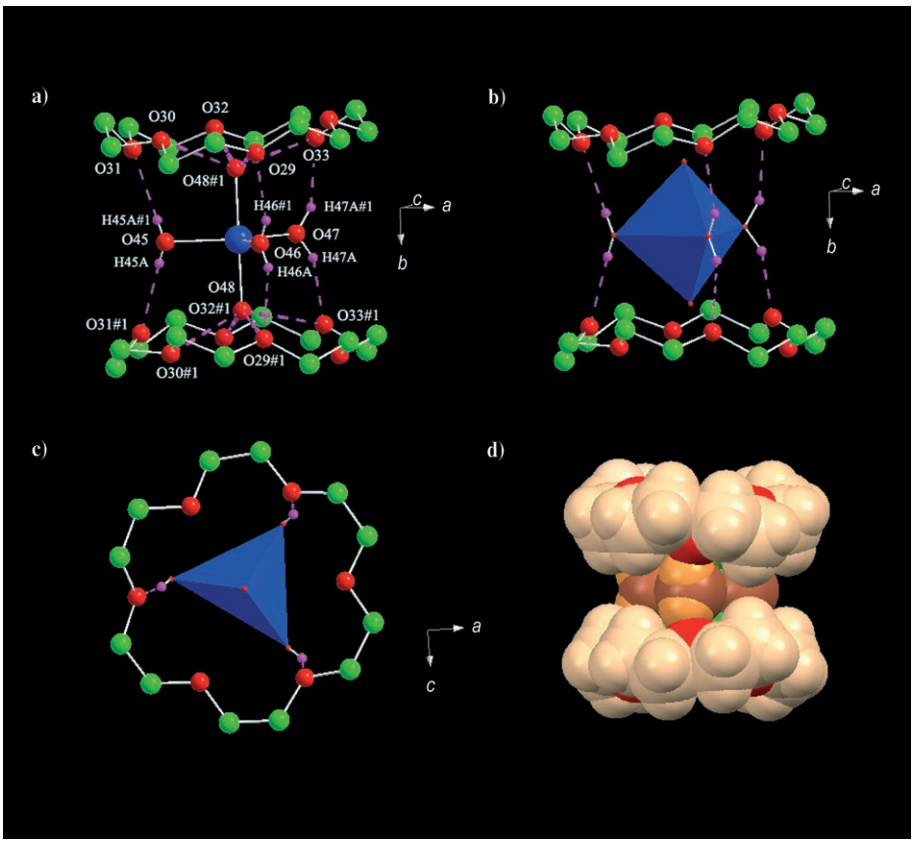


Figure 2. Supramolecular sandwich $[Cu(H_2O)_5([18]crown\text{-}6)_2]^{2+}$ consisting of two crown ether molecules and a tbp pentaaqua copper(II) ion: a) ball-and-stick representation; b) polyhedral representation of the $[Cu(H_2O)_5]^{2+}$ ion; c) view along the crystallographic *b* axis showing the exactness of the sandwich. Cu blue; O red; C green; H purple; hydrogen bonds are shown as purple dashed lines; d) space-filling plot of the sandwich. Hydrogen bonds between axial water and crown ether molecules are shown in Figure 2a but not in Figure 2b)–d) for clarity. Hydrogen-bonding parameters: O45–H45A···O31#1: 0.68(3), 2.05(3), 2.714(2), 169(5); O46–H46A···O29#1: 0.74(3), 1.99(3), 2.684(2), 157(3); O47–H47A···O33#1: 0.83(3), 1.94(3), 2.709(2), 155(3); O48···O29#1: 2.975(2); O48···O30#1: 2.833(2); O48···O32#1: 2.946(3); O48···O33#1: 2.976(2).

the sandwich with respect to the crown ether molecules is clearly evident when it is viewed down the crystallographic *b* axis (Figure 2c). The local molecular structure of $[Cu(H_2O)_5]^{2+}$ in the supramolecular sandwich $[Cu(H_2O)_5([18]crown\text{-}6)_2]^{2+}$ involves a five-coordinate $\{CuO_5\}$ chromophore with tbp geometry. The two out-of-plane Cu1–O48 bond lengths (related by a symmetry operation) are identical (1.936 Å) and form an almost perfect line, with O48-Cu1-O48 179.7°. The in-plane Cu–O distances are not significantly different (av = 2.012 Å) and longer than the out-of-plane Cu–O bonds by 0.076 Å.

The out-of-plane angle of exactly 90° (Figures 1 and 2) is rarely observed, as previously reported tbp copper complexes showed out-of-plane angular distortions of (90 ± 10)°.[26] However, the in-plane angles show very significant deviations from the 120° necessary for ideal tbp geometry: O45-Cu1-O46 113.43(16)°; O46-Cu1-O47 112.86(18)°; O45-Cu1-O47 133.72(16)° (Figure 1). This deviation, which is not significantly reflected in the in-plane Cu–O bond lengths, may be due to the fact that each axial water molecule, having two hydrogen atoms, cannot interact in a highly symmetrical fashion with the crown ether molecules (see Figure 2a). The sense of this deviation can also be rationalized in terms of the pathway of the Berry twist mechanism (Scheme 1), which describes the interconversion of a complex of regular tbp geometry to that of regular square-pyramidal geometry through bonding modes of vibration of a $\{CuO_5\}$ chromophore of C_{2v} symmetry. This interconversion occurs because the tbp and square-planar forms are energetically comparable.[27]

In the present study, the tbp coordination geometry around the Cu center in the $[Cu(H_2O)_5]^{2+}$ ion is governed by the participation of the ion in forming a supramolecular sandwich with two crown ether molecules that involves hydrogen-bonding interactions of copper-coordinated water molecules and oxygen atoms of the crown ether molecules (Figure 2). The formation of the sandwich can be explained by the fact that each of the equatorial water molecules of the tbp $[Cu(H_2O)_5]^{2+}$ ion forms hydrogen bonds with both upper and lower crown ether molecules, thus bringing the crown ether molecules closer together. This interaction accounts for the significant deviations of H-O-H angles (111.6, 119, and 121.4°) in the copper-coordinated equatorial water molecules from the ideal (≈109°). The relevant hydrogen-bonding parameters are provided as Supporting Information.

The Lindqvist type anion $[Mo_6O_{19}]^{2-}$ plays an important role in arranging the

 © 2006 Wiley-VCH Verlag GmbH & Co. KGaA, Weinheim

crown ether molecules in the crystal of **1** and therefore may be called a sandwich "clipper" (Figure 3). In the crystal, each sandwich is anchored—through C–H···O hydrogen bonds—by four surrounding isopolyanions and, similarly, each isopolyanion is hydrogen-bonded to four surrounding sandwich complexes. It is remarkable that each polyanion extends its four pairs of C–H···O hydrogen-bonding "hands" towards four sandwich complexes in such a way that each pair of hands uses one hand to attach the upper and the other hand to fasten the lower crown ether molecule of the sandwich (the relevant C–H···O hydrogen-bonding parameters are described in the Supporting Information). This situation is equivalent to each sandwich being clipped by four surrounding isopolyanions. The clipping of the sandwich by surrounding isopolyanions is presented in Figure 3.

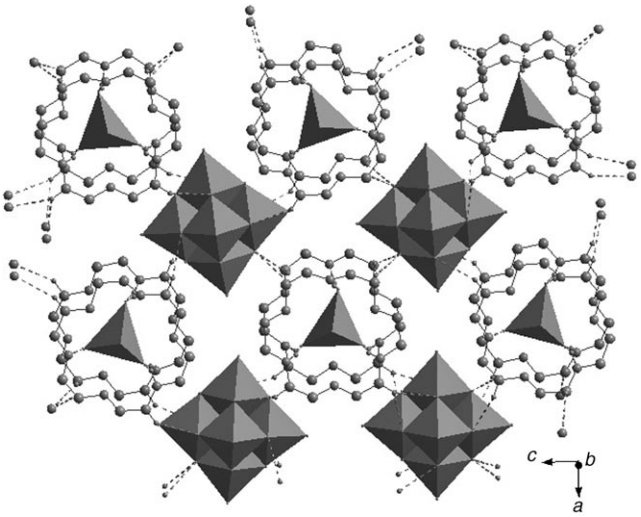


Figure 3. Representation of the clipping of the sandwich by the isopolyanions $[Mo_6O_{19}]^{2-}$. Isopolyanions and copper–aqua ions are shown in polyhedral representation.

Two independent $[Mo_6O_{19}]^{2-}$ isopolyanions and two independent sandwich complexes appear in the crystal structure of **1**. The oxygen atoms of one of the polyanions involved in molecular clipping through the C–H···O hydrogen bonds include O16, O19, O20, O22, and O26 (Figure 1). A similar pictorial representation of the other isopolyanion in the crystal of **1**, which shows four oxygen atoms (O2, O5, O9, and O12) interacting with surrounding crown ether molecules through C–H···O hydrogen bonds, is presented in the Supporting Information. The tbp $[Cu(H_2O)_5]^{2+}$ ion sandwiched by two crown ether molecules shows a tetragonal compression (see above) instead of a tetragonal elongation toward the apical positions. The fact that the tbp $[Cu(H_2O)_5]^{2+}$ ion is sandwiched by two crown ether molecules, which in turn are supported by surrounding polyoxometalate anions, is seemingly the driving force for the formation of a compressed tbp $[Cu(H_2O)_5]^{2+}$ complex cation.

ESR spectra of the complex also indicate the presence of an axially compressed trigonal geometry, as characterized by a d_{z^2} electronic ground state. Both room-temperature and liquid-nitrogen-temperature powder ESR spectra of compound **1** exhibit an inverse $g_\perp > g_\parallel > g_e$ pattern (g_e: g factor of the free electron (= 2.0023)) (Figure 4; $g_\perp = 2.235$, $g_\parallel = 2.04$). The solid-state electronic reflectance spectrum of **1** shows a broad peak centered at about 820 nm (see the Supporting Information). This spectrum is comparable with the visible/near-IR spectrum of an aqueous solution of Cu^{II} ions, which exhibits a broad band at around 820 nm. Is this result consistent with fivefold coordination of a Cu center? Pasquarello and co-workers calculated the joint density between the relevant filled and empty d states. For comparison, they also calculated such a density of states for a $[Cu(H_2O)_6]^{2+}$ ion and found that the two calculated spectra were essentially indistinguishable, which suggests that the transition energies are not substantially affected by the different bonding hybridizations in the five- and six-coordinated Cu^{II} complexes. Their calculated spectra showed a fair agreement with the experimental absorption spectrum.[23]

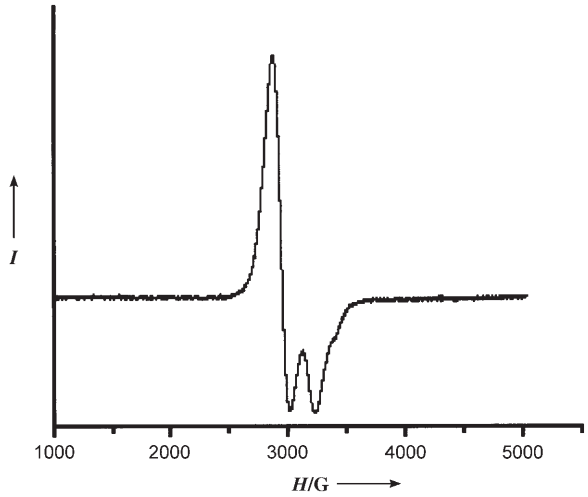


Figure 4. ESR spectrum of a powdered sample of **1** at liquid-nitrogen temperature.

TGA performed on **1** showed a weight loss (3.42 %) at around 100 °C that corresponds to the loss of three water molecules (calcd 3.46 %). We argue that these three water molecules are the equatorially coordinated of the tbp $[Cu(H_2O)_5]^{2+}$ ion. The other two water molecules (axially coordinated) are lost along with two crown ether molecules at around 200 °C. This is reflected in the second loss of the TGA curve (weight loss = 35.70 %; calcd weight loss 36.17 %; see the Supporting Information).

To conclude, the structure of a hydrated Cu^{II} complex was determined recently by both neutron diffraction (experimental) and first-principles molecular dynamics (theoretical) and these results favor fivefold coordination of water molecules around the Cu^{II} ion. This conclusion is in contrast with the generally accepted picture of an octahedrally solvated Cu^{II} ion. We have described here unambiguous crystallographic evidence of fivefold coordination of a aqua–Cu^{II} ion with tbp geometry, which is sandwiched by two crown ether molecules. We have named this a supramolecular sandwich. The polyoxometalate anion $[Mo_6O_{19}]^{2-}$ plays an important role

 © 2006 Wiley-VCH Verlag GmbH & Co. KGaA, Weinheim

in stabilizing the unique supramolecular ion $[Cu(H_2O)_5([18]crown\text{-}6)_2]^{2+}$.

Experimental Section

[18]Crown-6 ($C_{12}H_{24}O_6$; 0.06 g, 0.227 mmol) was dissolved in glacial acetic acid (10 mL), then acetonitrile was added (50 mL). To this reaction mixture, $(Bu_4N)_2[(Mo_6O_{19}]$ (0.03 g, 0.022 mmol) was added to give a light yellow solution to which $Cu(NO_3)_2{\cdot}3H_2O$ (0.125 g, 0.51 mmol) was added, and the resulting reaction mixture was stirred at room temperature for 24 h in an open reaction vessel. The resulting bluish-green solution was filtered and left to stand. Light green crystals were rendered by the solution; these crystals were isolated by filtration and washed with water (100 mL). Yield: 0.03 g (87% based on the quantity of molybdenum cluster used).

C,H analysis calcd (%) for $C_{24}H_{58}CuMo_6O_{36}$ (**1**): C 18.45, H 3.74; found: C 18.61, H 3.65. IR (KBr pellet): $\tilde{\nu}$ = 794 (s), 954 (vs), 1107 (s), 1253 (m), 1288 (m), 1352 (s), 1469 (s), 1612 (w), 2874 (m), 2910 (m), 3252 cm^{-1} (br).

Received: August 31, 2005
Published online: November 28, 2005

Keywords: copper · crown compounds · polyanions · sandwich complexes · supramolecular chemistry

[1] E. Ochiai, *Bioinorganic Chemistry, An Introduction*, Allen Bacon, Boston, **1977**.
[2] W. M. Latimer, J. H. Hildebrand, *Reference Book of Inorganic Chemistry*, 3rd ed., Maxmillan, New York, **1951**.
[3] C. S. G. Phillips, R. J. P. Williams, *Inorganic Chemistry, Vol. 2*, Oxford University, Oxford, UK, **1966**.
[4] F. Basolo, R. G. Pearson, *Mechanisms of Inorganic Chemistry: A Study in Metal Complexes in Solution*, 2nd ed., Wiley, New York, **1967**.
[5] F. A. Cotton, G. Wilkinson, *Basic Inorganic Chemistry*, Wiley, New York, **1976**.
[6] F. A. Cotton, G. Wilkinson, C. A. Murillo, M. Bochman, *Advanced Inorganic Chemistry*, 6th ed., Wiley-Interscience, New York, **1999**.
[7] E. Wiberg, A. F. Holleman, *Inorganic Chemistry*, 1st English ed., Academic Press, San Diego, CA, **2001**.
[8] T. J. Swift, R. E. Connick, *J. Chem. Phys.* **1962**, *37*, 307–320.
[9] S. N. Andreev, O. V. Sapozhnikova, *Dokl. Akad. Nauk SSSR* **1964**, *156*, 855–857.
[10] H. Ohtaki, M. Maeda, *Bull. Chem. Soc. Jpn.* **1974**, *47*, 2197–2199.
[11] M. Magini, *Inorg. Chem.* **1982**, *21*, 1535–1538.
[12] G. Licheri, A. Musinu, G. Paschina, G. Piccaluga, G. Pinna, A. F. Sedda, *J. Chem. Phys.* **1984**, *80*, 5308–5311.
[13] T. K. Sham, J. B. Hastings, M. L. Perlman, *Chem. Phys. Lett.* **1981**, *83*, 391–396.
[14] Y. Tajiri, H. Wakita, *Bull. Chem. Soc Jpn.* **1986**, *59*, 2285–2291.
[15] J. Garcia, M. Benfalto, C. R. Natoli, A. Bianconi, A. Fontaine, H. Tolentino, *Chem. Phys.* **1989**, *132*, 295–302.
[16] B. Beagley, A. Eriksson, J. Limgren, T. Persson, L. G. M. Petterson, M. Sandstrom, U. Wahlgren, E. W. White, *J. Phys. Condens. Matter* **1989**, *1*, 2395–2408.
[17] P. S. Salmon, G. W. Neilson, J. E. Enderby, *J. Phys. C.* **1988**, *21*, 1335–1349.
[18] P. S. Salmon, G. W. Neilson, *J. Phys. Condens. Matter* **1989**, *1*, 5291–5295.
[19] S. E. Okan, P. S. Salmon, *Mol. Phys.* **1995**, *85*, 981–998.
[20] P. S. Salmon, W. S. Howells, R. Mills, *J. Phys. C* **1987**, *20*, 5727–5747.
[21] R. Poupko, Z. Luz, *J. Chem. Phys.* **1972**, *57*, 3311- 3318.
[22] D. H. Powell, L. Helm, A. E. Merbach, *J. Chem. Phys.* **1991**, *95*, 9258–9265.
[23] A. Pasquarello, I. Petri, P. S. Salmon, O. Parisel, R. Car, E. Toth, D. H. Powell, H. E. Fischer, L. Helm, A. E. Merbach, *Science* **2001**, *291*, 856–859.
[24] a) B. J. Hathaway in *Comprehensive Coordination Chemistry, Vol. 5* (Ed.: G. Wilkinson), Pergamon, Oxford, **1987**, pp. 533–774; b) J. E. Huheey, E. A. Keiter, R. L. Keiter, *Inorganic Chemistry*, 4th ed., Pearson Education, Singapore, **2000**, pp. 240–243; c) N. N. Greenwood, A. Earnshaw, *Chemistry of the Elements*, Pergamon, Oxford, **1989**, pp. 572–573.
[25] Crystal data for **1**: $C_{24}H_{58}CuMo_6O_{36}$, M = 1561.88 g mol^{-1}, orthorhombic, space group *Pnma*, a = 22.5866(11), b = 18.1787(9), c = 22.5402(11) Å, V = 9254.9(8) $Å^3$, Z = 8, ρ = 2.242 Mg m^{-3}, μ = 2.132 mm^{-1}, $F(000)$ = 6168, crystal size = 0.34 × 0.32 × 0.13 mm^3. Crystals of **1** were removed from mother liquor and washed with distilled water cooled to 183(2) K on a Bruker SMART APEX CCD area detector system [$\lambda(Mo_{K\alpha})$ = 0.71073 Å], graphite monochromator, 1315 frames were recorded with an ω scan width of 0.3°, each for 10 s, crystal–detector distance 60 mm, collimator 0.5 mm. A total of 57892 reflections ($1.44 < \theta < 28.28°$) were collected of which 11495 reflections were unique (R_{int} = 0.0848). An empirical absorption correction using equivalent reflections was performed with the program SADABS.[28] The structure was solved with the program SHELXS-97[29] and refined using SHELXL-97[30] to R = 0.0325 for 9901 reflections with $I > 2\sigma(I)$, R = 0.0383 for all reflections; max/min residual electron density 1.160 and −1.968 e $Å^{-3}$. Two independent $[Mo_6O_{19}]^{2-}$ clusters and two independent $[Cu(H_2O)_5(C_{12}H_{24}O_6)_2]^{2+}$ ions appear in the crystal structure of **1**. All equatorial water-hydrogen atoms were located in one tbp $[Cu(H_2O)_5]^{2+}$ ion; in the other tbp $[Cu(H_2O)_5]^{2+}$ ion, two equatorial water-hydrogen atoms could be located. The hydrogen atoms of the axial water ligands could not be located in both cases. The located hydrogen atoms were picked up from differential Fourier maps and their positions were refined using isotropic thermal parameters. CCDC-282495 (**1**) contains the supplementary crystallographic data for this paper. These data can be obtained free of charge from The Cambridge Crystallographic Data Centre via www.ccdc.cam.ac.uk/data_request/cif.
[26] W. D. Harrison, B. J. Hathaway, *Acta Crystallogr. Sect. B* **1980**, *36*, 1069–1074.
[27] A. Bérces, T. Nukada, P. Margl, T. Ziegler, *J. Phys. Chem. A* **1999**, *103*, 9693–9701.
[28] G. M. Sheldrick, *SHELXS/L*, *SADABS*, University of Göttingen, Germany, **1997**.
[29] G. M. Sheldrick, *Program for Structure Solution*, University of Göttingen, Germany, **1997**.
[30] G. M. Sheldrick, *Program for Crystal Structure Analysis*, University of Göttingen, Germany, **1997**.

 © 2006 Wiley-VCH Verlag GmbH & Co. KGaA, Weinheim

Asymmetric Synthesis

DOI: 10.1002/anie.200503374

Short, Enantioselective Total Synthesis of Sceptrin and Ageliferin by Programmed Oxaquadricyclane Fragmentation**

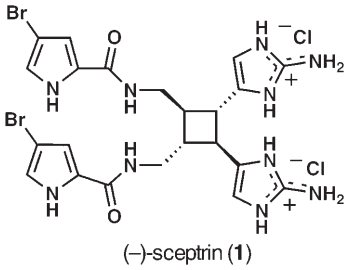
Phil S. Baran, Ke Li, Daniel P. O'Malley, and Christos Mitsos*

Dedicated to Professor David I. Schuster on the occasion of his 70th birthday.

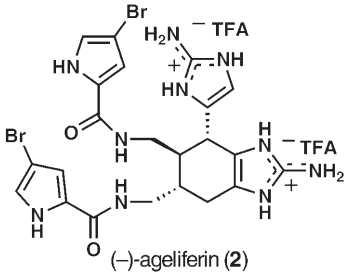
The marine-derived dimeric pyrrole-imidazole alkaloids sceptrin (**1**) and ageliferin (**2**) are endowed with intriguing molecular architectures and a range of useful bioactivities (Scheme 1).[1] The enantioselective synthesis of a dimeric pyrrole-imidazole alkaloid has yet to be reported, partly because of the intrinsic difficulty associated with handling multiply charged nitrogen-containing intermediates.[2]

We recently described practical syntheses of both **1** and **2** in their racemic form[3,4] by the use of an oxaquadricyclane fragmentation to generate the cyclobutane core of **1**. Since the mechanism of this reaction remained ill-defined,[5] it was unclear how, or even if, stereochemical information in an oxaquadricyclane could be transferred to the product cyclobutane. Indeed, preliminary screens using numerous enantioenriched oxaquadricyclanes (**3**, Scheme 2) under a variety of acidic conditions led to cyclobutanes which were either racemic or showed a considerable loss of optical activity. Racemic oxaquadricyclanes were also evaluated with chiral acids and auxiliaries, but to no avail. Further investigation was warranted because of the lack of viable alternatives for the enantioselective synthesis of tetrasubstituted cyclobutanes.[6]

Herein, we report the details of a unique method for the enantioselective synthesis of tetrasubstituted cyclobutanes by programmed fragmentation of an oxaquadricyclane, and the application of this method to the first asymmetric synthesis of both enantiomers of sceptrin and ageliferin.

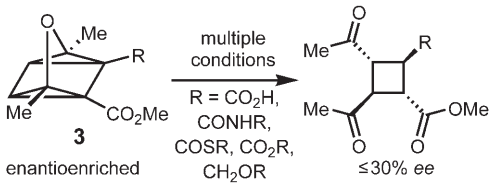


(–)-sceptrin (**1**)



(–)-ageliferin (**2**)

Scheme 1. The structures of sceptrin (**1**) and ageliferin (**2**). TFA=trifluoroacetate.



Scheme 2. Unsuccessful attempts at enantioselective fragmentation of an oxaquadricyclane.

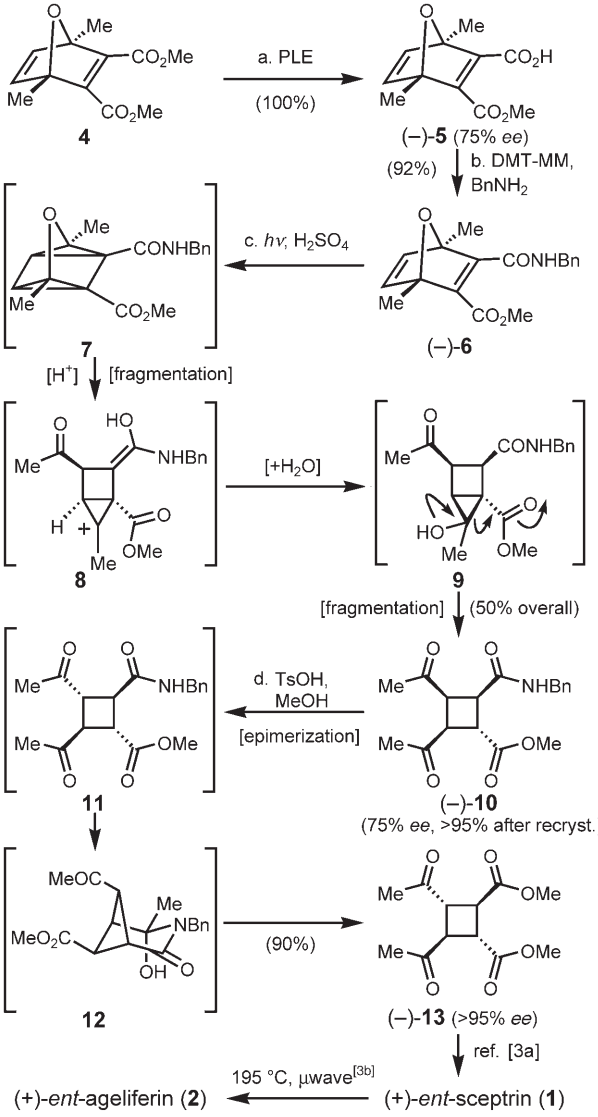
The synthesis commenced with the enzymatic desymmetrization[7] of *meso*-diester **4**[3a] using pig liver esterase (PLE) to provide monoester **5** in quantitative yield and 75% *ee* (Scheme 3). The *ee* value was determined by ^{1}H NMR spectroscopic analysis of the amide derived from (*S*)-α-methylbenzylamine (absolute configuration determined by X-ray analysis of the ammonium salt derived from the same amine and **5**). Formation of a benzylamide using DMT-MM[8] afforded the monobenzylamide **6** in 92% yield. Remarkably, *cis,trans,trans*-cyclobutane **10** was formed in 50% overall yield and 75% *ee* when amide **6** was irradiated to form oxaquadricyclane **7** and directly treated with H_2SO_4 in THF/MeOH (1:1). Amide (–)-**10** is nearly enantiopure (> 95% *ee*) after a single recrystallization. The use of a benzylamide was critical to achieve complete transfer of chirality. A mild and chemoselective debenzylation/esterification of the robust secondary amide in **10** and epimerization to the all-*trans* stereochemistry were necessary to access (–)-**13**. Treatment of **10** with TsOH and MeOH in toluene at 105 °C[9] accomplished all three tasks in a single pot to afford (–)-**13** in 90% yield. The ease with which this amide is hydrolyzed is likely due to assistance by the nearby *cis*-methyl ketone, as depicted in structure **12** (simple secondary amides are not converted into methyl esters under these conditions).

[*] Prof. Dr. P. S. Baran, Dr. K. Li, D. P. O'Malley, Dr. C. Mitsos
Department of Chemistry
The Scripps Research Institute
10550 North Torrey Pines Road, La Jolla, California 92037 (USA)
Fax: (+1) 858-784-7375
E-mail: pbaran@scripps.edu

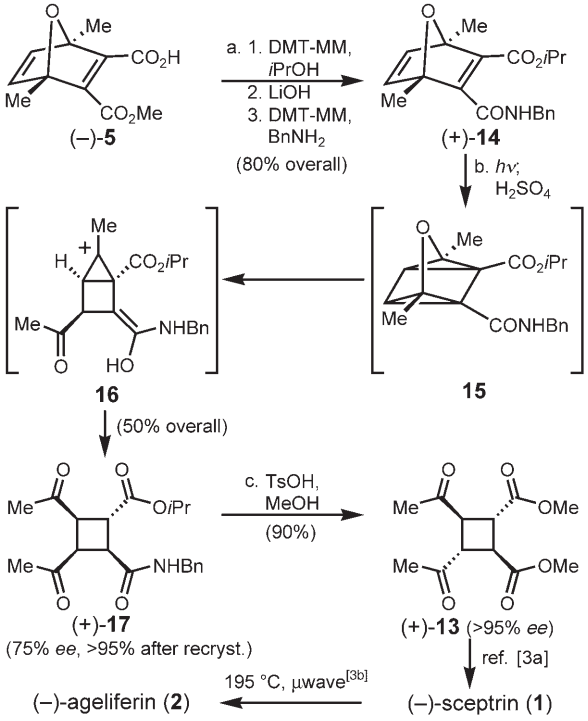
[**] We thank Dr. D. H. Huang and Dr. L. Pasternack for NMR spectroscopic assistance, and Dr. G. Siuzdak and Dr. R. Chadha for mass spectrometric and X-ray crystallographic assistance, respectively. We are grateful to Biotage for a generous donation of microwave process vials that were used extensively during these studies and to the Department of Defense and the Hertz Foundation for pre-doctoral fellowships (D.P.O.). Financial support for this work was provided by The Scripps Research Institute, Amgen, Dupont, Eli Lilly, GlaxoSmithKline, Roche, the Searle Scholarship Fund, and NIH/NIGMS (GM-073949).

Supporting information for this article (detailed experimental procedures, copies of all spectral data, and full characterization) is available on the WWW under http://www.angewandte.org or from the author.

 © 2006 Wiley-VCH Verlag GmbH & Co. KGaA, Weinheim



Scheme 3. Enantioselective Synthesis of *ent*-**1** and *ent*-**2**. Reagents and conditions: a) PLE (50 unit mmol^{-1}), acetone/phosphate buffer (pH 8), 23 °C, 1 week, 100%, 75% *ee*; b) $BnNH_2$ (1.05 equiv), DMT-MM (1.05 equiv), THF, 3 h, 92%; c) *hν*, THF, 72 h, then H_2SO_4, THF/MeOH (1:1), 3 h, 45–50%; d) recrystallization from hexanes/EtOAc (1:1), then TsOH (4.0 equiv), MeOH (20 equiv), toluene, 105 °C, sealed tube, 12 h, 50%. Bn = benzyl, THF = tetrahydrofuran; TsOH = toluenesulfonic acid, DMT-MM = 4-(4,6-dimethoxy-1,3,5-triazin-2-yl)-4-methylmorpholinium chloride.



Scheme 4. Enantioselective Synthesis of *nat*-**1** and *nat*-**2**. Reagents and conditions: a) 1. DMT-MM (1.05 equiv), DMAP (0.05 equiv), *i*PrOH, 55 °C, 3 h; 2. LiOH (1.2 equiv), THF/H_2O (1:1), 2 h; 3. DMT-MM (1.05 equiv), $BnNH_2$ (1.05 equiv), THF, 3 h, 80% (3 steps); b) *hν*, THF, 72 h, then H_2SO_4, THF/MeOH (1:1), 3 h, 45–50%; c) recrystallization from hexanes/EtOAc (1:1), then *p*TsOH (4.0 equiv), MeOH (20 equiv), toluene, 105 °C, sealed tube, 12 h, 50%. DMAP = 4-dimethylaminopyridine.

The absolute configuration of (−)-**13** was verified by conversion into sceptrin[3a] and comparison with a natural sample, which revealed that *ent*-sceptrin (**1**) had been synthesized ($[\alpha]_D = +16.0$ (MeOH, $c = 0.25$, HCl salt), lit. [1] $[\alpha]_D = -7.4$ (MeOH, $c = 1.2$, HCl salt)). Exposure of *ent*-sceptrin (**1**) to microwave irradiation[3b] led to *ent*-ageliferin (**2**; $[\alpha]_D = +8.0$ (MeOH, $c = 0.05$, TFA salt), natural product $[\alpha]_D = -10.0$ (MeOH, $c = 0.1$, TFA salt)).[3] The absolute configuration of **2** can now be assigned as depicted in Scheme 1.

The naturally occurring forms of **1** and **2** could be prepared as outlined in Scheme 4. Thus, monoacid **5** was directly converted into the amide **14** in 80% overall yield, without purification, by sequential formation of an ester, selective saponification of the methyl ester, and formation of an amide. Amide **14** was amenable to the same reaction sequence used for **6** (Scheme 3) and furnished cyclobutane **17** with complete conservation of optical activity. Following recrystallization (> 95% *ee*), epimerization, and transesterification to (+)-**13**, the synthesis of *nat*-(−)-sceptrin ($[\alpha]_D = -11.7$ (MeOH, $c = 0.12$, HCl salt)) and (−)-ageliferin ($[\alpha]_D = -10.0$ (MeOH, $c = 0.03$, TFA salt)) was completed. Both the sign and magnitude of the optical rotation of sceptrin changes depending on the counteranion (synthetic *ent*-sceptrin bishydrochloride had $[\alpha]_D = +16.0$ (MeOH, $c = 0.25$, HCl salt), while the bistrifluoroacetate salt had $[\alpha]_D = -23.5$ (MeOH, $c = 0.75$, no literature value available). This unusual reversal of optical rotation and the fact that the literature measurements for **1** and **2** are variable necessitated the use of circular dichroism to verify the assignments (Figure 1). The fact that (−)-**2** can be derived from (−)-**1** is consistent with the suggestion that the former may be produced from the latter in nature or that they share common intermediates in the biosynthetic pathway.[2,3b]

The cascade rearrangement of oxaquadricyclanes to cyclobutanes was initially discovered by McInnes and coworkers,[5a] who proposed a mechanism involving the initial fragmentation of the oxa bridge with water. The cascade was

 © 2006 Wiley-VCH Verlag GmbH & Co. KGaA, Weinheim

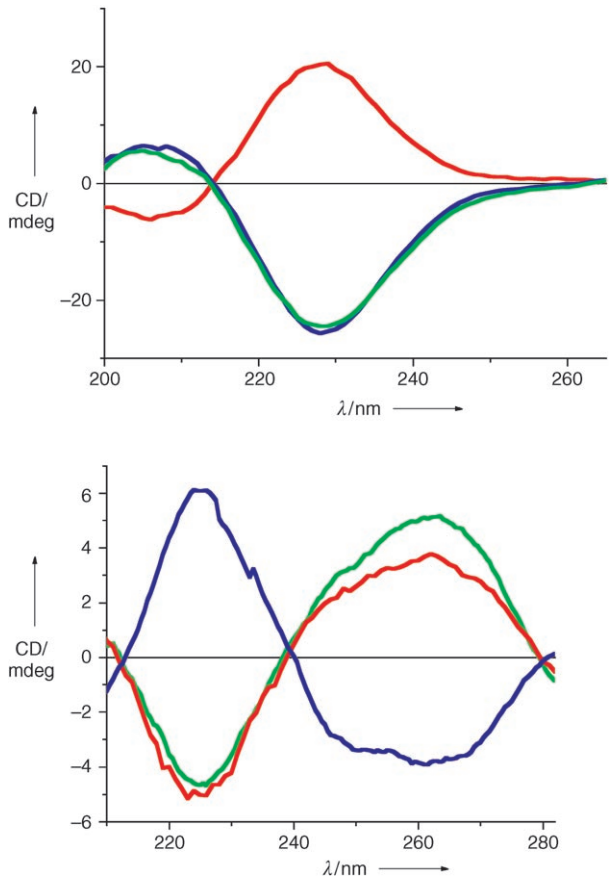


Figure 1. Top: Circular dichroism (CD) spectra of natural (−)-sceptrin (green), synthetic (−)-sceptrin (blue), and synthetic (+)-sceptrin (red) in water (0.2 mM). Bottom: Circular dichroism (CD) spectra of natural (−)-ageliferin (green), synthetic (−)-ageliferin (red), and synthetic (+)-ageliferin (blue) in water (0.35 mM). All measurements were recorded at 25 °C.

later studied by Nelsen and Calabrese,[5b] who posited an alternative mechanism initiated by fragmentation of a cyclopropyl ring to form an oxocarbonium ion (see **8** and **16**). After the work of Nelsen and Calabrese, little notice was taken of this reaction until it was adopted in the synthesis of sceptrin.[3] Success of an enantioselective variant relied on the assumption that the configuration of the final product is controlled by the order of the enolization (or protonation) of the carbonyl groups in the first fragmentation. For example, the major enantiomer (**10**) resulting from the fragmentation of **7** is produced by initial enolization of the benzylamide (Scheme 3), whereas the minor enantiomer (*ent*-**10**) would be produced by initial enolization of the ester. This result fits with the results of theoretical predictions that have found that enols of amides are more stable than those of carboxylic acids or esters.[10] The selective fragmentation of **7** to amide enol **8** is followed by tautomerization (protonation from the convex face) and capture by water to furnish **9**. Immediate fragmentation leads to the stable *cis*,*trans*,*trans*-cyclobutane **10**. The efficiency and complete transfer of chirality observed in these reactions (**6**→**10** and **14**→**17**) is surprising given the complexity of this mechanism, the difficulties encountered at the outset (see above), and the fact that oxaquadricyclanes are prone to a variety of other rearrangements under acidic conditions.[5c] This method proceeds in an operationally simple, scalable, and direct manner and represents the first solution for the nontrivial problem of the enantioselective construction of a tetrasubstituted cyclobutane which does not rely upon chiral auxiliaries.[6,11]

In summary, the first enantioselective syntheses of the dimeric pyrrole-imidazole alkaloids sceptrin (**1**) and ageliferin (**2**) have been accomplished (18% overall for (−)-**1** from commercially available compounds). Notably, column chromatography (on **10** and **17**) and HPLC (to separate **1** from **2**) only need to be performed once during the entire sequence. These syntheses have enabled the assignment of the absolute configuration of **2**, provided insight into the mechanism of the remarkable oxaquadricyclane→cyclobutane rearrangement, and opened up an enantioselective route to other complex alkaloids in this family.[12]

Received: September 23, 2005
Published online: November 30, 2005

Keywords: asymmetric synthesis · cascade reactions · enantioselectivity · natural products · rearrangement

[1] a) Sceptrin: R. P. Walker, D. J. Faulkner, D. Van Engen, J. Clardy, *J. Am. Chem. Soc.* **1981**, *103*, 6772–6773; b) Ageliferin: P. A. Keifer, R. E. Schwartz, M. E. S. Koker, R. G. Hughes, Jr., D. Rittschof, K. L. Rinehart, *J. Org. Chem.* **1991**, *56*, 2965–2975.

[2] For reviews, see H. Hoffmann, T. Lindel, *Synthesis* **2003**, 1753–1783; D. E. N. Jacquot, T. Lindel, *Current Org. Chem.* **2005**, *9*, 1551–1565.

[3] a) P. S. Baran, A. L. Zografos, D. P. O'Malley, *J. Am. Chem. Soc.* **2004**, *126*, 3726–3727; b) P. S. Baran, D. P. O'Malley, A. L. Zografos, *Angew. Chem.* **2004**, *116*, 2728–2731; *Angew. Chem. Int. Ed.* **2004**, *43*, 2674–2677.

[4] For a recent synthesis of (±)-**1**, see V. B. Birman, X.-T. Jiang, *Org. Lett.* **2004**, *6*, 2369–2371; for studies toward **2**, see Ref. [2] and Y. He, Y. Chen, H. Wu, C. J. Lovely, *Org. Lett.* **2003**, *5*, 3623–3626; I. Kawasaki, N. Sakaguchi, N. Fukushima, N. Fujioka, F. Nikaido, M. Yamashita, S. Ohta, *Tetrahedron Lett.* **2002**, *43*, 4377–4380.

[5] a) J. Laing, A. W. McCulloch, D. G. Smith, A. G. McInnes, *Can. J. Chem.* **1971**, *49*, 574–582; b) S. F. Nelsen, J. C. Calabrese, *J. Am. Chem. Soc.* **1973**, *95*, 8385–8388; c) for a review of oxaquadricyclane chemistry, see W. Tochtermann, G. Olsson, *Chem. Rev.* **1989**, *89*, 1203–1214.

[6] The use of chiral auxiliaries in [2+2] cycloadditions was shown to be only partially stereoselective with cinnamate derivatives, see D. Haag, H.-D. Sharf, *J. Org. Chem.* **1996**, *61*, 6127–6135; for a review, see E. Lee-Ruff, G. Mladenova, *Chem. Rev.* **2003**, *103*, 1449–1483.

[7] a) M. Ohno, Y. Ito, T. Shibata, K. Adachi, H. Sawai, *Tetrahedron* **1984**, *40*, 145–151; b) R. Bloch, E. Guibe-Jampel, C. Girard, *Tetrahedron Lett.* **1985**, *26*, 4087–4090; for a review of *meso* compounds in synthesis, see R. Hoffmann, *Angew. Chem.* **2003**, *115*, 1128–1142; *Angew. Chem. Int. Ed.* **2003**, *42*, 1096–1109.

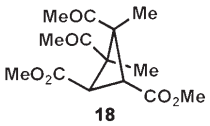
[8] 4-(4,6-Dimethoxy-1,3,5-triazin-2-yl)-4-methylmorpholinium chloride: M. Kunishima, C. Kawachi, J. Morita, K. Terao, F. Iwasaki, S. Tani, *Tetrahedron* **1999**, *55*, 13159–13170.

[9] C.-Y. Chern, Y.-P. Huang, W. M. Kan, *Tetrahedron Lett.* **2003**, *44*, 1039–1041.

 © 2006 Wiley-VCH Verlag GmbH & Co. KGaA, Weinheim

[10] N. Heinrich, W. Koch, G. Frenking, H. Schwarz, *J. Am. Chem. Soc.* **1986**, *108*, 593 – 600; R. E. Rosenberg, *J. Org. Chem.* **1998**, *63*, 5562 – 5567.

[11] For an example of a cyclobutane with vicinal quaternary centers (**18**) that can be made using this method, see the Supporting Information.



18

[12] CCDC-281469 (chiral ammonium salt of **5**) contains the supplementary crystallographic data for this paper. These data can be obtained free of charge from The Cambridge Crystallographic Data Centre via www.ccdc.cam.ac.uk/data_request/cif.

 © 2006 Wiley-VCH Verlag GmbH & Co. KGaA, Weinheim

Asymmetric Catalysis

DOI: 10.1002/anie.200502871

Studies into Asymmetric Catalysis of the Nozaki–Hiyama Allenylation**

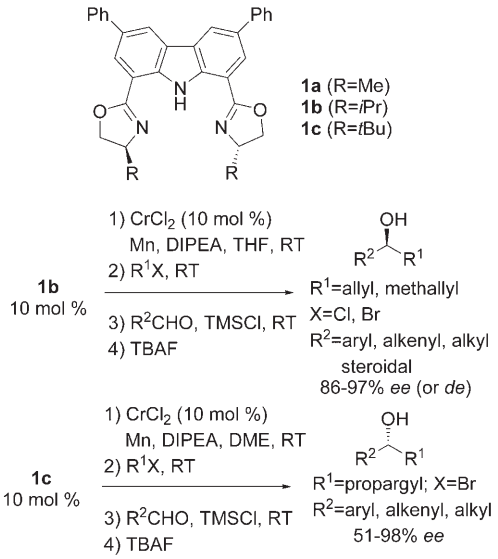
*Masahiro Inoue and Masahisa Nakada**

The allene moiety represents a versatile and useful functional group in organic synthesis because of its unique reactivity.[1] Recent developments in the chemistry of allenes suggest that allenic alcohols are important synthetic intermediates because they can be stereoselectively converted into compounds with other functional groups, for example, the amino alcohols[2] and 2,5-dihydrofurans,[1a,3] and they can also be used as substrates for Pauson–Khand reactions[1a,4] and Pd-mediated reactions.[1a,5]

Allenic alcohols are generally prepared by allenylation of carbonyl compounds,[1b,e,6] and chiral ones have been elaborated by asymmetric synthesis.[1a,7,8] Among the enantioselective methods, catalytic asymmetric synthesis[1a,9] is important in terms of efficiency; however, most of the asymmetric catalysis of allenylation reported so far requires preparation of propargyltin or propargylsilane compounds in advance, thereby rendering the asymmetric catalysis of allenylation inconvenient.

On the other hand, allenylations with low-valent metals and propargyl halides are advantageous with regard to their ease of manipulation; thus, the required operation is just mixing the commercially available reagents.[6a] The allenylation with Cr^{II} and a propargyl halide is particularly useful due to its easy operation, high chemoselectivity, and excellent compatibility with various functional groups; hence, this method has been developed by some research groups.[10]

We have reported highly enantioselective Nozaki–Hiyama allylations[11] and propargylations[12a] by utilizing a new carbazole tridentate ligand and have shown the wide applicability of this ligand (Scheme 1). Since no enantioselective allenylation with a low-valent metal and propargyl halide has been reported, we have examined the asymmetric catalysis of the Nozaki–Hiyama allenylation, and we report herein the first successful results.



Scheme 1. Asymmetric catalysis of the Nozaki–Hiyama allylation, methallylation, and propargylation. DIPEA = diisopropylethylamine, TMS = trimethylsilyl, TBAF = tetrabutylammonium fluoride, DME = 1,2-dimethoxyethane.

It has been shown that an equilibrium between the allenylchromium(III) and propargylchromium(III) intermediates exists in the reaction with Cr^{II} and a propargylic halide and that the ratio of these intermediates depends on their structure and/or additives.[10b,12–14] Consequently, these intermediates deliver the homopropargylic alcohol and the allenic alcohol, respectively.

Allenylations of carbonyl compounds with Cr^{II} and the terminally substituted propargyl halides afford allenic alcohols as the major products;[10b,12–14] hence, we surmised that the terminally silylated propargyl halide would generate the 2-silylated secondary allenic alcohol,[15] which can be easily desilylated[8c] and can also be used as the allenylsilane.

[*] M. Inoue, Prof. M. Nakada
Department of Chemistry
Faculty of Science and Engineering
Waseda University
3-4-1, Ohkubo, Shinjuku, Tokyo 169-8555 (Japan)
Fax: (+81) 3-5286-3240
E-mail: mnakada@waseda.jp

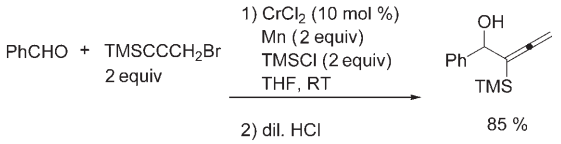
[**] This work was financially supported in part by a Waseda University Grant for Special Research Projects, a Grant-in-Aid for Scientific Research on Priority Areas "Creation of Biologically Functional Molecules" (Grant no.: 17035082), and a Grant-in-Aid for Scientific Research (C) from the Ministry of Education, Culture, Sports, Science, and Technology (MEXT), Japan. We are also indebted to 21COE "Practical Nano-Chemistry".

Supporting information for this article is available on the WWW under http://www.angewandte.org or from the author.

InterScience
© 2006 Wiley-VCH Verlag GmbH & Co. KGaA, Weinheim

Therefore, we focused our attention on the study of the asymmetric catalysis of the Nozaki–Hiyama allenylation with terminally silylated propargyl halides.

First, a Cr^{II}-mediated reaction of commercially available 1-trimethylsilyl-3-bromopropyne[16] with benzaldehyde in the absence of the chiral ligand under catalytic conditions[11,13a] was carried out (Scheme 2). The reaction was complete after 4 h and afforded the allenic alcohol as the sole product in 85% yield.



Scheme 2. The catalytic Nozaki–Hiyama allenylation without ligand.

Consequently, a Cr^{II}/chiral-ligand-mediated reaction of 1-trimethylsilyl-3-bromopropyne with benzaldehyde was carried out. This catalytic asymmetric allenylation followed the same procedure as that used for the catalytic asymmetric allylation and propargylation.[11]

The reaction with ligand **1a** was complete after 6 h and generated the *R* product in 90% yield with 64% *ee* (Table 1, entry 1).[17] The reaction with **1b** took 8 h to finish and generated the *R* product in 92% yield with 52% *ee* (entry 2). Interestingly, the enantioselectivity in the reaction with **1c** was reversed to afford the *S* product in 92% yield with 29% *ee* after 12 h.[18] It is noteworthy that the least bulky ligand **1a** gave the best result and only allenic alcohols were generated in all the reactions described in entries 1–3. The reaction with the propargyl chloride and **1a** did not improve the result (entry 4; 85%, 47% *ee*).

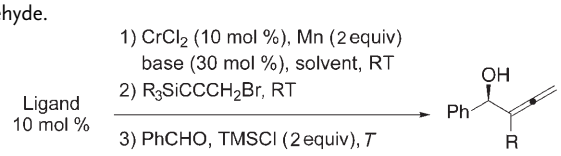
Next, the reaction was carried out in various solvents by using the most effective ligand, that is, **1a**, and propargyl bromide. The reactions in DME (entry 5) and acetonitrile (entry 6) required 12 h for completion and the *ee* values were slightly decreased. Although the reaction time was not shortened, propionitrile increased the *ee* value to 71% (entry 7). Other solvents gave fruitless results; for example, the reaction in CH_2Cl_2 required much more time and both the yield and the *ee* value were decreased (entry 8; 24 h, 49%, 57% *ee*). DMF generated the allenic alcohol (36%, 74% *ee*) along with the propargylic alcohol (20%, 4% *ee*).

The reaction at 0°C delayed the reaction time (16 h); however, the *ee* value was increased to 76% (entry 10). Hence, all the reactions were carried out at 0°C after this. Use of molecular sieves did not affect the *ee* value and merely prolonged the reaction time (entry 11).

The base used to prepare the chiral catalyst was also surveyed.[11b] Potassium carbonate (entry 12) and bulky γ-collidine (entry 13), which would not coordinate to chromium, gave results comparable with those obtained by the use of DIPEA; however, pyridine (entry 12) gave diminished results in all respects (reaction time, yield, and *ee* value), probably due to its strongly coordinating nature.

We found that the silyl group of the propargyl halide affected the enantioselectivity; that is, while silyl groups bulkier than the TMS group (TES, TIPS, DMPS, and MDPS) did not improve the enantioselectivity (entries 15–18), the smaller DMS group (entry 19) afforded the best result (81%, 80% *ee*).

Table 1: Asymmetric catalysis of the Nozaki–Hiyama allenylation of benzaldehyde.



Entry	Ligand	Solvent	*T* [°C]	Base[a]	R_3Si[b]	*t* [h]	Yield [%]	*ee* [%][c]
1	**1a**	THF	RT	DIPEA	TMS	6	90	64
2	**1b**	THF	RT	DIPEA	TMS	8	92	52
3	**1c**	THF	RT	DIPEA	TMS	12	92	−29[d]
4[e]	**1a**	THF	RT	DIPEA	TMS	8	85	47
5	**1a**	DME	RT	DIPEA	TMS	12	72	61
6	**1a**	CH_3CN	RT	DIPEA	TMS	12	74	60
7	**1a**	EtCN	RT	DIPEA	TMS	12	83	71
8	**1a**	CH_2Cl_2	RT	DIPEA	TMS	24	49	57
9	**1a**	DMF	RT	DIPEA	TMS	48	56[f]	74[g]
10	**1a**	EtCN	0	DIPEA	TMS	16	80	76
11[h]	**1a**	EtCN	0	DIPEA	TMS	20	81	76
12	**1a**	EtCN	0	K_2CO_3	TMS	16	72	76
13	**1a**	EtCN	0	γ-collidine	TMS	16	65	76
14	**1a**	EtCN	0	pyridine	TMS	30	64	65
15	**1a**	EtCN	0	DIPEA	TES	24	81	74
16	**1a**	EtCN	0	DIPEA	TIPS	30	49	66
17	**1a**	EtCN	0	DIPEA	DMPS	24	66	73
18	**1a**	EtCN	0	DIPEA	MDPS	30	79	73
19	**1a**	EtCN	0	DIPEA	DMS	16	81	80

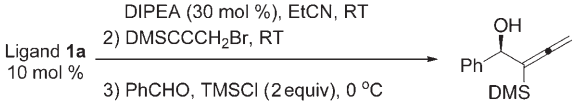
[a] 30 mol% was used. [b] TES = triethylsilyl, TIPS = triisopropylsilyl, DMPS = dimethylphenylsilyl, MDPS = methyldiphenylsilyl. [c] The *ee* value as determined by HPLC. [d] The minus sign indicates that the enantioselectivity of the reaction was reversed in this case to afford the *S* product. [e] 1-trimethylsilyl-3-chloropropyne was used instead of 1-trimethylsilyl-3-bromopropyne. [f] A mixture of allenic alcohol and homopropargylic alcohol (1.8:1) was obtained and the combined yield is given. [g] The *ee* value of the allenic alcohol as determined from the corresponding α-methoxy-α-(trifluoromethyl)phenylacetyl (MTPA) ester. The *ee* value of the homopropargylic alcohol was 4%. [h] 4 Å molecular sieves (200 wt%) were added.

As noted above, when DMF was the solvent (Table 1, entry 9), the *ee* value of the allenic alcohol was high (74% *ee*). Consequently, the reaction in the presence of an additive possessing a polar functional group was examined. The additives possessing an oxygen–phosphine bond (Table 2, entries 1–4) or oxygen–sulfur bond (entry 5) had no effect on the enantioselectivity; however, some ureas improved the *ee* value. Thus, the reaction in the presence of DMPU afforded the product in 91% yield with 82% *ee* (entry 6), and the reaction in the presence of DMI gave the best enantioselectivity (entry 7; 97%, 83% *ee*). Other ureas (entries 8–11) did not improve upon the result given in entry 7.

Under the optimized conditions (Table 2, entry 7), various aldehydes were successfully allenylated with high enantioselectivity. *p*-Methoxybenzaldehyde and *p*-chlorobenzaldehyde were allenylated in 90% yield with 80% *ee* (Table 3, entry 1) and in 91% yield with 82% *ee* (entry 2), respectively. Hydrocinnamaldehyde (entry 3; 99%, 72% *ee*), cyclohexyl-

 © 2006 Wiley-VCH Verlag GmbH & Co. KGaA, Weinheim

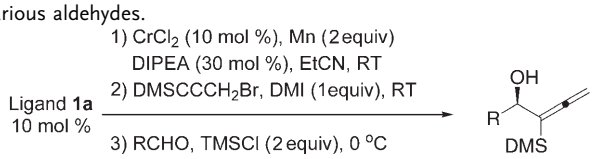
Table 2: Effect of additive on the catalytic asymmetric Nozaki–Hiyama allenylation of benzaldehyde.



Entry	Additive[a] (1 equiv)	*t* [h]	Yield [%]	*ee*[b] [%]
1	HMPA	24	75	76
2	$Ph_3P(O)$	24	69	80
3	$nBu_3P(O)$	36	23	77
4	$(PhO)_3P(O)$	48	20	55
5	DMSO	30	73	79
6	DMPU	24	91	82
7	DMI	24	97	83
8	DMI[c]	36	17[d]	73
9	TMU	48	21[e]	67
10	DEDPU	36	71	75
11	DTBI	16	73	81

[a] HMPA = hexamethyl phosphoramide, DMSO = dimethylsulfoxide, DMPU = *N*,*N*′-dimethylpropylene urea, DMI = 1,3-dimethyl-2-imidazolidinone, TMU = *N*,*N*,*N*′,*N*′-tetramethylurea, DEDPU = *N*,*N*′-diethyl-*N*,*N*′-diphenylurea, DTBI = 1,3-di-*tert*-butyl-2-imidazolidinone. [b] The *ee* value as determined by HPLC. [c] 10 equivalents of DMI were used. [d] A large amount of pinacol coupling product was formed (52% yield). [e] Homopropargylic alcohol was identified by ^{1}H NMR spectroscopy; the ratio of products was allenic alcohol:homopropargylic alcohol = 50:1.

Table 3: Asymmetric catalysis of the Nozaki–Hiyama allenylation of various aldehydes.



Entry	R	*t* [h]	Yield [%]	*ee*[a] [%]
1	*p*-MeOPh	36	90	80
2	*p*-ClPh	24	91	82
3	$PhCH_2CH_2$	24	99	72
4	*c*-C_6H_{11}	24	95	74
5	*n*-C_5H_{11}	24	81	75

[a] The *ee* value as determined by HPLC.

aldehyde (entry 4; 95%, 74% *ee*), and pentanal (entry 5; 81%, 75% *ee*) were also allenylated with good enantioselectivity, thereby revealing the generality of this catalytic asymmetric allenylation.

The absolute configurations of the products were determined by comparing the sign of the specific rotation with known compounds;[19] this disclosed that all the aldehydes showed the same enantioface selectivity. Thus, all the aldehydes were allenylated predominantly at the *si* face.

Compared with the previously reported catalytic asymmetric propargylation,[12a] in which the aldehydes showed *re*-face selectivity (Scheme 1), the enantioface selectivity in the allenylation is reversed. This reversal is well explained, as shown in Figure 1. Thus, since the terminally silylated propargyl group was positioned at the less-hindered apical

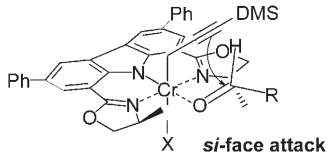
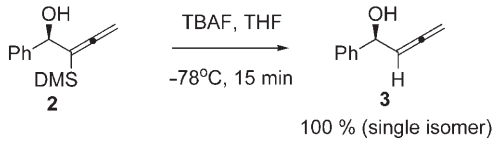


Figure 1. Proposed model for the catalytic asymmetric Nozaki–Hiyama allenylation. DMS = dimethylsilyl.

position of the asymmetric catalyst, the aldehyde coordinated at the equatorial position and was allenylated from the *si* face under the influence of the asymmetric circumstances.

However, several other explanations for the enantioselectivity are possible. For example, the possibilities of the reaction proceeding intermolecularly or the Cr–**1** complex being a dinuclear complex[20] cannot be ruled out. Furthermore, the stereochemical outcome of this allenylation reaction could derive from different chromium complexes. Hence, further studies on the structure of the Cr–**1a** complex and the mechanism of this reaction are in progress.

The product obtained through this asymmetric catalysis would be a good synthetic intermediate because the silyl group can be easily desilylated.[8c] For example, as shown in Scheme 3, the allenylated product **2** was easily desilylated to afford **3** in 100% yield without diminishing the *ee* value.



Scheme 3. Desilylation of the products.

In summary, ligand **1a** was found to realize the catalytic asymmetric allenylation of various aldehydes with high enantioselectivity. To the best of our knowledge, this is the first successful example of the asymmetric catalysis of the Nozaki–Hiyama allenylation. The product obtained from this reaction would be a useful synthetic intermediate because the 2-silylated secondary allenic alcohol can be easily desilylated or can be used as the allenylsilane; hence, we will investigate the utility of this allenic alcohol for the total synthesis of natural products.

Received: August 12, 2005
Published online: November 30, 2005

Keywords: allenes · allenic alcohols · asymmetric catalysis · chromium · enantioselectivity

[1] a) *Modern Allene Chemistry* (Eds.: N. Krause, A. S. K. Hashmi), Wiley-VCH, Weinheim, **2004**; b) N. Krause, A. Hoffmann-Röder, *Tetrahedron* **2004**, *60*, 11671–11694; A. Barbero, F. J. Pulido, *Acc. Chem. Res.* **2004**, *37*, 817–825; c) A. Barbero, F. J. Pulido, *Synthesis* **2004**, 779–785; d) S. Ma, *Acc. Chem. Res.* **2003**, *36*, 701–712; e) H. Yamamoto in *Comprehensive Organic Synthesis, Vol. 2* (Eds.: B. M. Trost, I. Fleming), Pergamon, Oxford, **1991**, Chap. 1.3, pp. 81–131.

 © 2006 Wiley-VCH Verlag GmbH & Co. KGaA, Weinheim

[2] R. W. Friesen, *Tetrahedron Lett.* **1990**, *31*, 4249 – 4252.
[3] a) N. Krause, A. Hoffmann-Röder, J. Canisius, *Synthesis* **2002**, 1759 – 1774; b) A. Hoffmann-Röder, N. Krause, *Org. Lett.* **2001**, *3*, 2537 – 2538; c) L. I. Olsson, A. Claesson, *Synthesis* **1979**, *9*, 743 – 745.
[4] a) C. Mukai, I. Nomura, S. Kitagaki, *J. Org. Chem.* **2003**, *68*, 1376 – 1385; b) B. Alcaide, P. Almendros, C. Aragoncillo, *Chem. Eur. J.* **2002**, *8*, 1719 – 1729.
[5] a) D. Xu, Y. Xu, L. Li, S. Ma, *Chem. Eur. J.* **2002**, *8*, 5012 – 5018; b) S. Ma, S. Zhao, *J. Am. Chem. Soc.* **2001**, *123*, 5578 – 5579; c) S. Ma, W. Gao, *Tetrahedron Lett.* **2000**, *41*, 8933 – 8936; d) S. Ma, S. Zhao, *J. Am. Chem. Soc.* **1999**, *121*, 7943 – 7944; e) S.-K. Kang, T. Yamaguchi, S.-J. Pyun, Y.-T. Lee, T.-G. Baik, *Tetrahedron Lett.* **1998**, *39*, 2127 – 2130.
[6] a) M.-J. Lin, T.-P. Loh, *J. Am. Chem. Soc.* **2003**, *125*, 13042 – 13043; b) T. Nishikawa, H. Shinokubo, K. Oshima, *Tetrahedron* **2003**, *59*, 9661 – 9668; c) T. Hamada, R. Mizojiri, H. Urabe, F. Sato, *J. Am. Chem. Soc.* **2000**, *122*, 7138 – 7139; d) S. Kobayashi, K. Nishio, *J. Am. Chem. Soc.* **1995**, *117*, 6392 – 6393.
[7] For a review, see: S. E. Denmark, J. Fu, *Chem. Rev.* **2003**, *103*, 2763 – 2793.
[8] a) C. Schultz-Fademrecht, B. Wibbeling, R. Froehlich, D. Hoppe, *Org. Lett.* **2001**, *3*, 1221 – 1224; b) A. Marshall, N. D. Adams, *J. Org. Chem.* **1997**, *62*, 8976 – 8977; c) H. C. Brown, U. R. Khire, G. Narla, *J. Org. Chem.* **1995**, *60*, 8130 – 8131; d) E. J. Corey, G. B. Jones, *Tetrahedron Lett.* **1991**, *32*, 5713 – 5716.
[9] a) M. Nakajima, M. Saito, S. Hashimoto, *Tetrahedron: Asymmetry* **2002**, *13*, 2449 – 2452; b) K. Iseki, Y. Kuroki, Y. Kobayashi, *Tetrahedron: Asymmetry* **1998**, *9*, 2889 – 2894; c) C.-M. Yu, S.-K. Yoon, K. Baek, J.-Y. Lee, *Angew. Chem.* **1998**, *110*, 2504 – 2506; *Angew. Chem. Int. Ed.* **1998**, *37*, 2392 – 2395.
[10] a) P. Knochel, *J. Org. Chem.* **1992**, *57*, 4070 – 4074; b) J. Gore, *Tetrahedron* **1981**, *37*, 1359 – 1367.
[11] a) M. Inoue, T. Suzuki, M. Nakada, *J. Am. Chem. Soc.* **2003**, *125*, 1140 – 1141; b) T. Suzuki, A. Kinoshita, H. Kawada, M. Nakada, *Synlett* **2003**, 570 – 572.
[12] a) M. Inoue, M. Nakada, *Org. Lett.* **2004**, *6*, 2977 – 2980. We obtained an allenyl alcohol as a minor product in the catalytic asymmetric propargylation under certain conditions. The same result had been obtained by Umani-Ronchi's group; see: b) M. Bandini, P. G. Cozzi, P. Melchiorre, R. Tino, A. Umani-Ronchi, *Tetrahedron: Asymmetry* **2001**, *12*, 1063 – 1069.
[13] For recent progress in chromium-mediated reactions, see: a) A. Fürstner, *Chem. Rev.* **1999**, *99*, 991 – 1045; b) L. A. Wessjohann, G. Scheid, *Synthesis* **1991**, 1 – 36.
[14] a) P. Wipf, S. Lim, *J. Chem. Soc. Chem. Commun.* **1993**, 1654 – 1656; b) K. Belyk, M. J. Rozema, P. Knochel, *J. Org. Chem.* **1992**, *57*, 4070 – 4074; c) B. Le Doussal, A. Le Coq, A. Gorgues, A. Meyer, *Tetrahedron* **1983**, *39*, 2185 – 2192; d) T. Hiyama, Y. Okude, K. Kimura, H. Nozaki, *Bull. Chem. Soc. Jpn.* **1982**, *55*, 561 – 568; e) B. Cazes, C. Vernière, J. Gorè, *Tetrahedron Lett.* **1982**, *23*, 3501 – 3504; f) P. Place, F. Delbecq, J. Gorè, *Tetrahedron Lett.* **1978**, 3801 – 3802.
[15] To the best of our knowledge, this is the first example of the use of the terminally silylated propargylic halide for the regioselective allenylation.
[16] H. D. Verkruijsse, L. Brandsma, *Synth. Commun.* **1990**, *20*, 3375 – 3378.
[17] The allenylation of benzaldehyde with 1-bromo-2-butyne was examined under the same conditions as those described in entry 1 of Table 1; however, a mixture of the allenic alcohol and the homopropargylic alcohol was obtained in a ratio of 2.7:1 in 90% combined yield, and the *ee* values were 22 and 14%, respectively.
[18] This change of enantioselectivity has also been observed in the catalytic asymmetric propargylation. For the results and the proposed explanation, see reference [12a].
[19] (*S*)-1-phenyl-2,3-butadien-1-ol: $[\alpha]_D^{26} = +28.7$ ($c = 0.72$, $CHCl_3$) (*R* form:[19a] $[\alpha]_D^{20} = -55.4$ ($c = 0.82$, $CHCl_3$)); (*R*)-1-phenyl-2,3-hexadien-1-ol: $[\alpha]_D^{26} = +3.04$ ($c = 0.77$, $CHCl_3$) (*S* form:[19b] $[\alpha]_D^{23} = -2.4$ ($c = 1.41$, $CHCl_3$)); (*R*)-1,2-nonadien-4-ol: $[\alpha]_D^{26} = -5.00$ ($c = 0.73$, $CHCl_3$) (*S* form:[19c] $[\alpha]_D^{23} = +4.5$ ($c = 0.2$, $CHCl_3$)); (*R*)-1-cyclohexyl-2,3-butadien-1-ol: $[\alpha]_D^{26} = -7.7$ ($c =$ 0.40, benzene) (*S* form:[19b] $[\alpha]_D^{24} = +10.5$ ($c = 1.02$, benzene)); a) C.-M. Yu, C. Kim, J.-H. Kweon, *Chem. Commun.* **2004**, 2494 – 2495; b) K. Iseki, Y. Kuroki, Y. Kobayashi, *Tetrahedron: Asymmetry* **1998**, *9*, 2889 – 2894; c) E. J. Corey, G. B. Jones, *Tetrahedron Lett.* **1991**, *32*, 5713 – 5716. With regard to the products of *p*-methoxybenzaldehyde and *p*-chlorobenzaldehyde, the absolute configurations were determined by analogy because these products showed the same sign (minus) as that of the product of benzaldehyde.
[20] For example, see: R. Ruck, E. N. Jacobsen, *J. Am. Chem. Soc.* **2002**, *124*, 2882 – 2883.

 © 2006 Wiley-VCH Verlag GmbH & Co. KGaA, Weinheim

Radical Cyclization

DOI: 10.1002/anie.200503056

Enantioselective PhSe-Group-Transfer Tandem Radical Cyclization Reactions Catalyzed by a Chiral Lewis Acid**

Dan Yang, Bao-Fu Zheng, Qiang Gao, Shen Gu, and Nian-Yong Zhu*

Tandem radical cyclization, which is a powerful method for the synthesis of polycyclic compounds, is used widely in the syntheses of natural products.[1] Only a few asymmetric tandem radical cyclization reactions are known,[2,3a] however, and no enantioselective group-transfer radical reactions have been reported.[4] Herein we report a catalytic enantioselective group-transfer radical cyclization reaction and its applications in tandem reactions.

[*] Prof. D. Yang, B.-F. Zheng, Q. Gao, S. Gu, N.-Y. Zhu
Department of Chemistry
The University of Hong Kong
Pokfulam Road, Hong Kong (P. R. China)
Fax: (+852) 2859-2159
E-mail: yangdan@hku.hk
Prof. D. Yang
Department of Chemistry
Fudan University
Shanghai, 200433 (P. R. China)

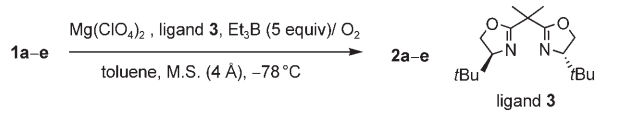
[**] This study was supported by the University of Hong Kong, the Hong Kong Research Grants Council (Project No. HKU7121/02P), and the National Natural Science Foundation of China (Project No. 20229201). D.Y. thanks the Bristol-Myers Squibb Foundation for an Unrestricted Grant in Synthetic Organic Chemistry and the Croucher Foundation for a Senior Research Fellowship.

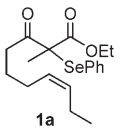
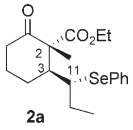
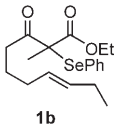
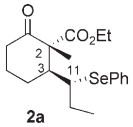
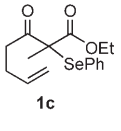
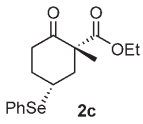
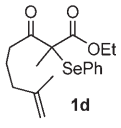
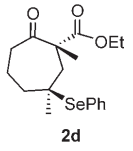
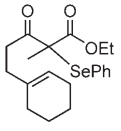
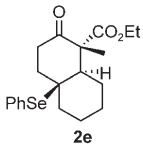
Supporting information for this article is available on the WWW under http://www.angewandte.org or from the author.

 © 2006 Wiley-VCH Verlag GmbH & Co. KGaA, Weinheim InterScience

To investigate the enantioselective PhSe-group-transfer radical cyclization reactions of unsaturated α-phenylseleno-β-ketoesters, we prepared compounds **1a–e** and subjected them to cyclization conditions, with Et_3B/O_2 as the radical initiator (Table 1). In the absence of a Lewis acid, no cyclization reaction occurred, and only reductive dephenylselenate products were obtained (data not shown). Clearly Lewis acids promoted this phenylseleno-transfer radical cyclization reaction. We found that the complex formed between $Mg(ClO_4)_2$ and the bisoxazoline ligand[5] **3** was the most suitable catalyst for the cyclization reaction.[6]

Table 1: Chiral Lewis acid catalyzed group-transfer radical monocyclization reactions.[a]



Entry	Substrate	LA[b] [equiv]	*t* [h]	Product	Yield [%][c]	*ee* [%][d]
1	 **1a**	1.0	6	 **2a**	82	89
2[e]		1.0	8		80	89
3		0.3	10		81	84
4[e]		0.3	12		< 5	
5	 **1b**	1.0	7	 **2a**	71	81
6		0.3	10		66	87
7	 **1c**	1.0	8	 **2c**	63	69
8	 **1d**	1.0	9	 **2d**	65	66
9	 **1e**	1.0	8	 **2e**	75	87
10		0.3	9		62	58

[a] Unless otherwise indicated, all reactions were performed with 0.2 mmol of the substrate at a concentration of 0.025 M in toluene in the presence of activated 4-Å molecular sieves (powder, 500 mg mmol^{-1} substrate) and the indicated amount of $Mg(ClO_4)_2$ and (*S*,*S*)-**3** (ligand/Lewis acid = 1.1:1). [b] LA = Lewis acid. [c] Yield of isolated product. [d] The enantiomeric excess was determined through HPLC analysis by using a Chiralcel AD column. [e] In the absence of the 4-Å molecular sieves (M.S.).

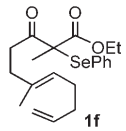
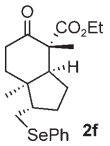
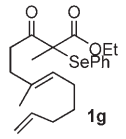
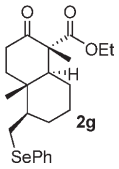
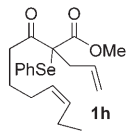
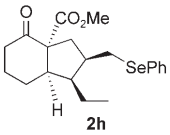
As Table 1 indicates, cyclization of **1a,** after purification by column chromatography, gave the 6-*exo* product **2a** as a single diastereoisomer in 82% yield with 89% *ee* (Table 1, entry 1). Although the addition of activated 4-Å molecular sieves did not improve the *ee* value, it accelerated the reaction dramatically and made it possible to use a catalytic amount of the chiral catalyst (Table 1, entries 2–4).[7] Substrate **1b**, the *trans* olefin analogue of **1a**, gave the same product (+)-**2a** in comparable yield and enantioselectivity (Table 1, entries 5 and 6). When we used a catalytic amount (0.3 equiv) of the chiral Lewis acid, the yield decreased slightly but the enantioselectivity increased to 87% *ee* (Table 1, entry 6). The absolute configuration of (+)-**2a** was determined to be (2*R*,3*S*,11*R*).[8] The excellent control of the configuration at the contiguous stereogenic centers is in contrast to the results obtained from the corresponding bromine-atom-transfer radical cyclization reactions, in which two diastereomeric products were obtained in a poor ratio.[3b] Substrate **1c** gave exclusively the 6-*endo* product **2c** in 63% yield with 69% *ee* (Table 1, entry 7). For the cyclization of **1d**, the α-radical center attacked the less-substituted side of the alkene to form the seven-membered ring product **2d** exclusively in moderate yield and enantioselectivity (Table 1, entry 8). The cyclization of substrate **1e** proceeded smoothly to produce the bicyclic product **2e** with 87% *ee*. A lower catalyst loading (0.3 equiv) led to a large decrease in the *ee* value (Table 1, entries 9 and 10). These results represent the first known enantioselective group-transfer radical cyclization reactions catalyzed by chiral Lewis acids.

Because PhSe-transfer radical cyclization reactions have been demonstrated previously to have great potential for use in tandem cyclization reactions,[9] we expected to obtain bicyclic PhSe-transfer products when applying our new method to a series of diene substrates (Table 2). In contrast to the low yields and enantioselectivities (< 33%) in the corresponding Br-transfer radical cyclization,[3a] substrate **1f** gave the *cis*-6,5-fused ring product **2f** in 70% yield with 73% *ee* (Table 2, entry 1). The use of 0.3 equivalents of chiral Lewis acid did not decrease the yield or the *ee* value significantly (Table 2, entry 2). Substrate **1g** underwent 6-*endo*/6-*exo* cyclization (Table 2, entry 3) to give the 6,6-*trans*-fused ring product **2g** with excellent enantioselectivity (97% *ee*) albeit in low yield (31%); high selectivity (87% *ee*) was attained even when using 0.3 equivalents of the chiral Lewis acid catalyst (Table 2, entry 4). In this case we also isolated approximately of the monocyclization product because the 1,3-diaxial interactions of two methyl groups rendered the second cyclization unfavorable. Substrate **1h**, which has an allyl substituent in the α-position, underwent sequential 6-*exo* and 5-*exo* cyclizations in the presence of a stoichiometric amount of the chiral Lewis acid to give the bicyclic product **2h** in 44% yield with 91% *ee* (Table 2, entry 5). Each of these tandem cyclization reactions successfully creates four stereogenic centers in a single step with moderate to high enantioselectivity, which further demonstrates the power of this chiral Lewis acid promoted PhSe-group-transfer radical cyclization.

The model proposed to account for the high stereoselectivity is similar to that for the corresponding Br-transfer

 © 2006 Wiley-VCH Verlag GmbH & Co. KGaA, Weinheim

Table 2: Chiral Lewis acid catalyzed group-transfer radical tandem cyclization reactions.[a]

Entry	Substrate	LA[b] [equiv]	*t* [h]	Product	Yield [%][c]	*ee* [%][d]
1	 **1f**	1.0	9	 **2f**	70	73
2		0.3	10		70	67
3	 **1g**	1.0	12	 **2g**	31	97
4		0.3	12		33	87
5	 **1h**	1.0	12	 **2h**	44	91

[a] Unless otherwise indicated, all reactions were performed with 0.2 mmol of the substrate at a concentration of 0.025 M in toluene in the presence of activated 4-Å molecular sieves (powder, 500 mg mmol^{-1} substrate) and the indicated amounts of $Mg(ClO_4)_2$ and (*S*,*S*)-**3** (ligand/Lewis acid = 1.1:1). [b] LA = Lewis acid. [c] Yield of isolated product. [d] The enantiomeric excess was determined through HPLC analysis by using a Chiralcel OD or AD column.

radical cyclizations we reported earlier (Figure 1). We assume that the dicarbonyl moiety of substrate **1a** chelates to the magnesium center, which adopts an octahedral geometry in which ClO_4^- ions occupy the two axial positions.[10] To avoid steric interactions with the α-*tert*-butyl group, the olefin moiety prefers to approach from the *Re* face of the α-radical center (transition states **A** and **B**). In TS **B**, steric interactions are found between the olefin group and the β-*tert*-butyl group. Thus TS **A** would be favored over TS **B**, affording the cyclic radical intermediate **C**. For the most stable conformer of radical intermediate **C**, SePh abstraction takes place preferentially from the less-hindered *Re* face to yield product **2a** as a single diastereoisomer. Thus, the lower transfer rate of the SePh group to the alkyl radical—relative to that of Br-atom transfer—and its bulk cause the SePh abstraction to be more stereoselective.[11]

In conclusion, we have developed Lewis acid catalyzed, highly enantioselective PhSe-group-transfer radical cyclization reactions for the construction of a variety of monocyclic and bicyclic compounds that include the core structures of many biologically interesting natural products.

Received: August 27, 2005
Revised: September 30, 2005
Published online: November 28, 2005

Keywords: asymmetric synthesis · enantioselectivity · ketoesters · Lewis acids · tandem cyclization

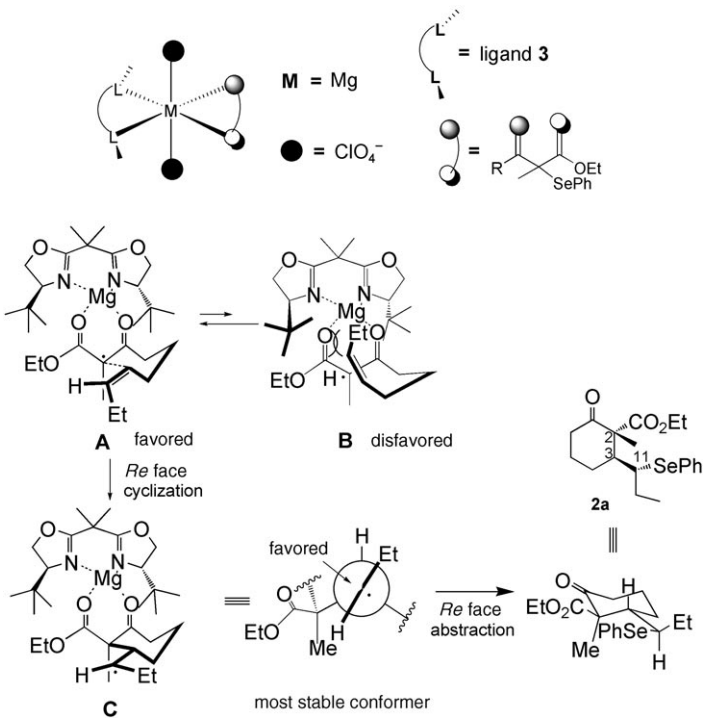


Figure 1. Transition-state model proposed for the enantioselective group-transfer radical cyclization.

[1] For recent reviews on tandem radical cyclization reactions, see: a) M. Malacria, *Chem. Rev.* **1996**, *96*, 289–306; b) B. B. Snider, *Chem. Rev.* **1996**, *96*, 339–363; c) P. J. Parsons, C. S. Penkett, A. J. Shell, *Chem. Rev.* **1996**, *96*, 195–206; d) A. J. McCarroll, J. C. Walton, *Angew. Chem.* **2001**, *113*, 2282–2307; *Angew. Chem. Int. Ed.* **2001**, *40*, 2224–2248; for recent reviews on free radical reactions used in the synthesis of natural products, see: e) C. P. Jasperse, D. P. Curran, T. L. Fevig, *Chem. Rev.* **1991**, *91*, 1237–1286; f) P. J. Parsons, C. S. Penkett, A. J. Shell, *Chem. Rev.* **1996**, *96*, 195–206.

[2] For excellent reviews on enantioselective radical reactions and Lewis acid catalyzed radical reactions, see: a) B. Guérin, W. W. Ogilvie, Y. Guindon in *Radicals in Organic Synthesis, Vol. 1* (Eds.: P. Renaud, M. P. Sibi), Wiley-VCH, Weinheim, **2001**, chap. 4.4; b) M. P. Sibi, N. A. Porter, *Acc. Chem. Res.* **1999**, *32*, 163–171; c) P. Renaud, M. Gerster, *Angew. Chem.* **1998**, *110*, 2704–2722; *Angew. Chem. Int. Ed.* **1998**, *37*, 2562–2579; d) M. P. Sibi, S. Manyem, J. Zimmerman, *Chem. Rev.* **2003**, *103*, 3263–3296.

[3] a) D. Yang, S. Gu, Y.-L. Yan, H.-W. Zhao, N.-Y. Zhu, *Angew. Chem.* **2002**, *114*, 3140–3143; *Angew. Chem. Int. Ed.* **2002**, *41*, 3014–3017; b) D. Yang, S. Gu, Y.-L. Yan, N.-Y. Zhu, K.-K. Cheung, *J. Am. Chem. Soc.* **2001**, *123*, 8612–8613.

[4] For references on atom- and group-transfer radical reactions, see: a) D. P. Curran, M.-H. Chen, D. Kim, *J. Am. Chem. Soc.* **1986**, *108*, 2489–2490; b) D. P. Curran, C.-T. Chang, *J. Org. Chem.* **1989**, *54*, 3140–3157; c) D. P. Curran, M.-H. Chen, D. Kim, *J. Am. Chem. Soc.* **1989**, *111*, 6265–6276; d) D. P. Curran, M.-H. Chen, E. Spletzer, C. M. Seong, C.-T. Chang, *J. Am. Chem. Soc.* **1989**, *111*, 8872–8878; e) D. P. Curran, J. Tamine, *J. Org. Chem.* **1991**, *56*, 2746–2750; f) for a recent review, see: J. Byers in *Radicals in Organic Synthesis, Vol. 1* (Eds.: P. Renaud, M. P. Sibi), Wiley-VCH, Weinheim, **2001**, chap. 1.5.

[5] For reviews on the use of C_2-symmetric chiral bisoxazoline ligands in asymmetric catalysis, see: a) J. S. Johnson, D. A. Evans, *Acc. Chem. Res.* **2000**, *33*, 325–335; b) A. K. Ghosh, P.

 © 2006 Wiley-VCH Verlag GmbH & Co. KGaA, Weinheim

Mathivanan, J. Cappiello, *Tetrahedron: Asymmetry* **1998**, *9*, 1 – 45.

[6] We found that the use of other Lewis acids, including $Yb(OTf)_3$, $Cu(OTf)_2$, and $Sc(OTf)_3$, was ineffective.

[7] The role of activated molecular sieves in the cyclization reactions is not yet fully understood. One possibility is that molecular sieves absorb water, as $Mg(ClO_4)_2$ is moisture sensitive. A similar effect was found in our Br-atom-transfer radical cyclization reactions.[3b]

[8] The relative configuration of **2a** was determined by X-ray crystallographic analysis of a 2,4-DNP (DNP = dinitrophenylhydrazine derivative of (±)-**2a**; the absolute configurations of the stereogenic centers C2 and C3 were determined by comparison of optical rotation data of the reductive dephenylseleno product of (+)-**2a** with those of the reductive debromo product of a known compound (see Supporting Information for details).

[9] a) D. Yang, Q. Gao, O.-Y. Lee, *Org. Lett.* **2002**, *4*, 1239 – 1241; b) D. Yang, Q. Gao, B.-F. Zheng, N.-Y. Zhu, *J. Org. Chem.* **2004**, *69*, 8821 – 8828.

[10] For a Mg^{II}–bisoxazoline complex with octahedral geometry, see: a) G. Desimoni, G. Faita, P. P. Righetti, *Tetrahedron Lett.* **1996**, *37*, 3027 – 3030; b) G. Desimoni, G. Faita, A. G. Invernizzi, P. P. Righetti, *Tetrahedron* **1997**, *53*, 7671 – 7688; c) J. M. Takacs, E. C. Lawson, M. J. Reno, M. A. Youngman, D. A. Quincy, *Tetrahedron: Asymmetry* **1997**, *8*, 3073 – 3078; d) S. Yao, M. Johannsen, R. G. Hazell, K. A. Jorgensen, *J. Org. Chem.* **1998**, *63*, 118 – 121.

[11] D. P. Curran, A. A. Martin-Esker, S.-B. Ko, M. Newcomb, *J. Org. Chem.* **1993**, *58*, 4691 – 4695.

 © 2006 Wiley-VCH Verlag GmbH & Co. KGaA, Weinheim

Supramolecular Chemistry

DOI: 10.1002/anie.200503163

Copper(I)-Directed Formation of a Cyclic Pseudorotaxane Tetramer and Its Trimeric Homologue**

*Tomáš Kraus, Miloš Buděšínský, Josef Cvačka, and Jean-Pierre Sauvage**

In the past decade, catenanes and rotaxanes[1] have been extensively exploited as functional units of molecular assemblies related to controlled dynamic systems ("molecular machines"[2]) or polymers. Several multicomponent assemblies have been reported in which the ring is covalently attached to a filament-like fragment threaded through the same ring[3] or through the cyclic unit belonging to another ring–filament conjugate. Particularly significant examples are the purely organic systems prepared by Huang and Gibson,[4] which lead to the formation of supramolecular polymers, or those reported by Stoddart and co-workers[5] and termed "daisy chains". Interesting cyclodextrin-based assemblies have also been reported by Harada and co-workers[6] as well as by other research groups.[7]

Transition-metal-based systems have only rarely been used to generate cyclic rotaxane or pseudorotaxane oligomers, with the only example being that of a dicopper(I) rotaxane dimer,[8] the precursor of a molecular "muscle" which is able to stretch or contract under the action of an external signal.[9] We now report that multinuclear cyclic pseudorotaxanes can be generated by copper(I)-mediated assembly of a ligand in which a chelate-containing macrocycle is rigidly attached to a filament bearing another bidentate ligation site (Figure 1).

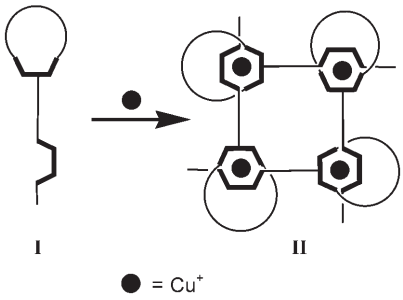


Figure 1. Formation of multinuclear cyclic rotaxane tetramer (**II**) from the two-chelate ligands (**I**) and a templating metal center.

The reaction relies on the gathering and threading process described long ago to make catenanes[10] and rotaxanes.[11] The success of this step is mostly due to the fact that one of the chelates is incorporated in a ring and cannot, therefore, form a metal bischelate complex without the threading of another chelate (not belonging to a cycle) through the ring in which it is incorporated. The two bidentate chelates of **I** are disposed in such a way that their coordination axes are orthogonal to each other. This arrangement implies that a tetrameric species **II** should be formed provided the metal center forms a tetrahedral complex.

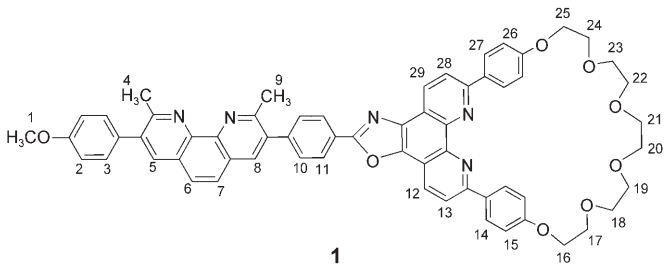
We used the copper(I)/1,10-phenanthroline system to build the cyclic rotaxane tetramer analogous to **II**. It is preferable to use 1,10-phenanthroline (phen) ligands bearing substituents at their 2- and 9-positions to stabilize the 4-coordinate tetrahedral copper(I) complex. We have thus incorporated a 2,9-diphenyl-1,10-phenanthroline (dpp) fragment into the ring and a 2,9-dimethyl-1,10-phenanthroline (dmp) chelate into the filament. The ligand **1** (Scheme 1) containing two bidentate chelates was prepared[12] in 13 steps from 1,10-phenanthroline and other commercially available compounds. Its chemical structure should provide strict control over the geometry of the whole system: the molecule is highly rigid and, as a consequence of the oxazole unit used

[*] Dr. J.-P. Sauvage
Laboratoire de Chimie Organo-Minérale, UMR 7513 du CNRS
Institut Le Bel
Université Louis Pasteur
4 rue Blaise Pascal, 67000 Strasbourg Cedex (France)
Fax: (+33) 3-9024-1368
E-mail: sauvage@chimie.u-strasbg.fr
Dr. T. Kraus, Dr. M. Buděšínský, Dr. J. Cvačka
Institute of Organic Chemistry and Biochemistry
Academy of Sciences of the Czech Republic
Flemingovo nám. 2, 166 10 Prague 6 (Czech Republic)

[**] We thank the European Commission for a Marie Curie fellowship (HMPF-CT-2002-01684) to T.K. and for financial support.

Supporting information for this article is available on the WWW under http://www.angewandte.org or from the author.

InterScience
© 2006 Wiley-VCH Verlag GmbH & Co. KGaA, Weinheim



1

Scheme 1. Structure of ligand **1** with the numbering of the protons.

as a spacer, the coordination axes of the phen chelates are, in an ideal case, orthogonal to one another. Furthermore, the two methyl groups attached *ortho* to the nitrogen atoms of the phen units should favor a tetrahedral geometry of the corresponding complexes.

Addition of an equimolar amount of $[Cu(CH_3CN)_4]PF_6$ in acetonitrile to a suspension of **1** in the same solvent resulted in rapid formation of a brown-red solution. Samples of concentration 10^{-2} M and 10^{-5} M were prepared from this solution and analyzed by high-resolution ESI-MS.

The ESI mass spectrum (see Supporting Information) of a solution of the complex at 10^{-5} M in acetonitrile revealed only one significant peak at *m*/*z* 1059.29 with an isotope spacing corresponding to the triply charged species $[(\mathbf{1}+Cu)_3]^{3+}$. At the highest concentration measured (10^{-2} M) two significant peaks were present above *m*/*z* 1000: a major peak at *m*/*z* 1059.32, with an isotope spacing corresponding to the species $[(\mathbf{1}+Cu)_4]^{4+}$, and a peak at *m*/*z* 1461.15 corresponding to $[(\mathbf{1}+Cu)_4PF_6]^{3+}$. These results strongly suggest that the complex is a mixture of the cyclic trimeric and tetrameric species **3** and **4** (Scheme 2), respectively, in which the former prevails at low concentration whereas the latter homologue is more abundant at high concentration.

$$\underset{\mathbf{2}}{\mathbf{1} + [Cu(CH_3CN)_4]^+} \longrightarrow \underset{\mathbf{3}}{[(\mathbf{1}\cdot Cu)_3]^{3+}} + \underset{\mathbf{4}}{[(\mathbf{1}\cdot Cu)_4]^{4+}}$$

Scheme 2. Reaction of ligand **1** with $[Cu(CH_3CN)_4]^+$ (**2**) in CH_3CN leads to a mixture of trimeric and tetrameric complex, with their relative proportion depending strongly on the solution concentration.

The ^{1}H NMR spectra of the complex in CD_3CN in the measurable range of concentrations (5×10^{-3} to 5×10^{-5} M) were recorded to gain a deeper insight into the structure of the complexes as well as into their mutual composition. Complete assignment of all the protons was achieved by 2D COSY and ROESY methods.

Spectra acquired at the upper concentration limit (5×10^{-3} M) revealed one major set of signals together with a set of less-intense signals that were attributed to tetrameric and trimeric species, respectively, which is in accordance with the ESI-MS results. Comparison of the ^{1}H NMR spectra with that of the free ligand **1** revealed typical shifts in the protons of the Cu^I-complexed dpp units; for example, H-15 and H-26 of the phenyl moiety are shifted upfield by $\Delta\delta = 1.2$ ppm in tetramer **4**. The initially minor signals of the trimer **3** intensify as the concentration is decreased, and dominate over signals of the tetramer **4** at 5×10^{-5} M. The singlets of the terminal methoxy groups (H-1 which resonates at $\delta = 3.92$ and 3.90 ppm for the trimer and tetramer, respectively) are suitable labels for the determination of the ratios of the two species in solution. Thus, by integration of the two signals (Figure 2), the ratio

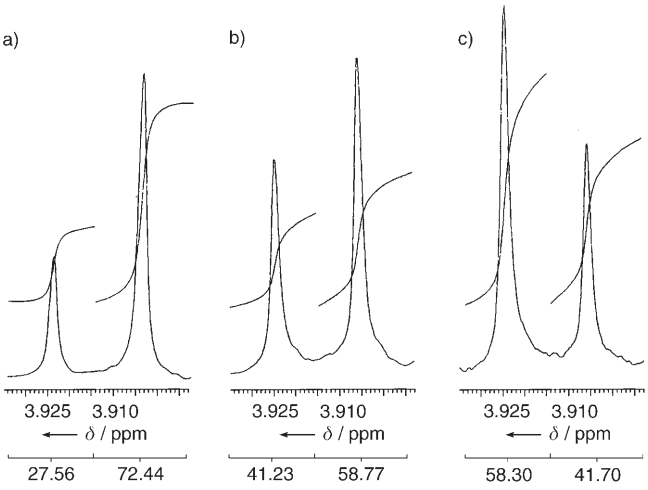


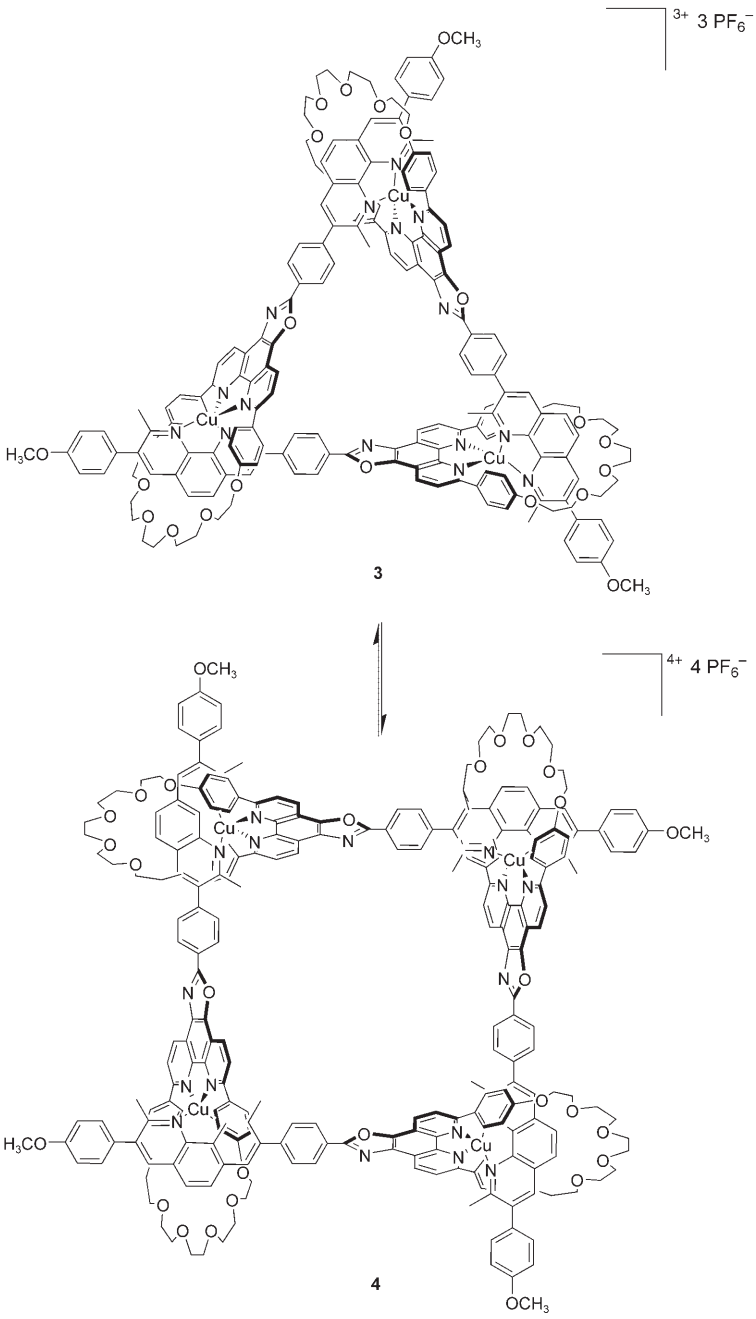
Figure 2. ^{1}H NMR spectrum of the -OCH_3 groups (H-1) as a function of concentration; the signals corresponding to the trimer (left) and the tetramer (right) are sufficiently shifted from one another to allow determination of the relative proportion of each compound with good accuracy: a) 5×10^{-3} M, b) 10^{-3} M, c) 5×10^{-5} M.

tetramer/trimer was found to be 72:28 and 42:58 at 5×10^{-3} and 5×10^{-5} M, respectively. Significant NOE interactions between the CH_3 protons of the dmp unit (H-4, H-9) and protons of the phenyl rings of the macrocycle (H-14, H-27) were observed, thus proving convincingly that the dmp unit threads through the dpp-containing ring upon complexation.

The presence of the oxazol moiety results in each copper(I) center becoming stereogenic in the triangular and squarelike complexes. Accordingly, the presence of diastereomers could be expected in the solution of the complex. We found that protons H-12 and H-29 of the dpp units are particularly sensitive to diastereoisomerism and their resonances appear as doublets at different chemical shifts in the ^{1}H NMR spectra. Whereas these differences are very small (at 500 MHz) for the tetrameric complex and do not allow for the resolution of the individual diastereoisomers, the two possible diastereomers of the trimer could be readily observed by NMR spectroscopy.

It is particularly noteworthy that the tetrameric complex, which was expected to be the sole product because of the structure of ligand **1**, was formed in 72% yield only in concentrated solutions and was the minor compound in more dilute solutions. This phenomenon once again demonstrates the importance of entropic factors in such complexation reactions. For entropic reasons the smallest assembly (the trimer, in the present case) is expected to be formed preferentially. On the other hand, the strainless tetrahedral geometry of the squarelike copper(I) complex should be favored in terms of enthalpy. Thus, the delicate balance of the two factors determines the ratio of the two species in the reaction mixture (Scheme 3) and can be tuned by changing

 © 2006 Wiley-VCH Verlag GmbH & Co. KGaA, Weinheim



Scheme 3. Representation of the equilibrium between the trimer and the tetramer (only one diastereomer is depicted for each trimer and tetramer); in dilute solution (5×10^{-5} M) the trimer is the major component, whereas in concentrated solution (5×10^{-3} M) the tetramer proportion is 72%.

the concentration of the solution. Related observations were made a few years ago by Fujita et al. on nonthreaded species containing palladium(II) ions and 4,4′-bipyridine (square/triangle).[13]

The equilibration in the present system is remarkably slow: dilution of the 5×10^{-3} M sample to 5×10^{-5} M resulted in the tetramer/trimer ratio changing from an initial 72:28 to only 64:36 after 20 h (at the end of the first 20-hour period of ^{1}H signal accumulation). The ratio was only 51:49 after 72 h, and it took 10 days to reach the final ratio of 42:58. This slow ligand exchange, which involves decoordination of the Cu^{I} center and threading/dethreading processes, has already been observed in the formation of a related dimer.[8,9] It has also been exploited in the isolation of non-stoppered copper(I)-complexed threaded species containing different rings threaded on a two-site linear fragment.[14]

The two cyclic pseudorotaxanes presented herein can be regarded as higher homologues of the rotaxane dimer[8] that was used in the preparation of a musclelike compound.[9] The incorporation of additional chelates of the 2,2′,6′,2″-terpyridine (terpy) type into the filament should lead to novel cyclic dynamic species, "expanding squares", thus extending the concept of linear motion of the previous "muscle" into two dimensions.

Experimental Section

Preparation of the copper(I) complexes: A solution of $[Cu(CH_3CN)_4]PF_6$ (3.73 mg, 0.01 mmol) in CH_3CN (0.5 mL) was added in an argon atmosphere to a stirred suspension of ligand **1** (9.96 mg, 0.01 mmol) in degassed CH_3CN (0.5 mL). The solids disolved within 5 min and a brown-red solution was formed. For ESI-MS studies, the solution was diluted with CH_3CN to final concentrations of 10^{-2} M and 10^{-5} M. Samples for NMR spectroscopic analysis were prepared by evaporation of the concentrated solution under a stream of argon and subsequent dilution with CD_3CN. The chemical shifts marked with an asterisk below correspond to the averaged values for given protons that appear at slightly different positions because of their symmetry non-equivalence in the diastereoisomers.

Trimer **3**: ^{1}H NMR (500 MHz; CD_3CN): $\delta\approx2.0$ overlapped with solvent (s, 9H; H-9), 2.46 (s, 9H; H-4), 3.38 (m, 2H; H-16, H-25), 3.45 (m, 2H; H-17, H-24), 3.59 (m, 2H; H-18, H-23), 3.66 (m, 2H; H-19, H-22), 3.74 (s, 2H; H-20, H-21), 3.92 (s, 9H; H-1), 6.11* (m, 12H; H-15, H-26), 7.16 (m, $J_{2,3}=8.8$ Hz, 6H; H-2), 7.54* (m, 12H; H-14, H-27), 7.54 (m, $J_{3,2}=8.8$ Hz, 6H; H-3), 7.68* (m, 6H; H-10), 8.11 (d, $J_{7,6}=8.8$ Hz, 3H; H-7), 8.31 (d, $J_{6,7}=8.8$ Hz, 3H; H-6), 8.35* (5 × d, $J_{13,12}=J_{28,29}=8.4$ Hz, 6H; H-13, H-28), 8.49 (s, 3H; H-5), 8.57* (m, 6H; H-11), 8.63 (s, 3H; H-8), 9.13* (4 × d, $J_{12,13}=8.4$ Hz, 3H; H-12), 9.22* ppm (3 × d, $J_{29,28}=8.8$ Hz, 3H; H-29).

Tetramer **4**: ^{1}H NMR (500 MHz; CD_3CN): $\delta=2.21$ (s, 12H; H-9), 2.25 (s, 12H; H-4), 3.38 (m, 16H; H-16, H-25), 3.45 (m, 16H; H-17, H-24), 3.59 (m, 16H; H-18, H-23), 3.66 (m, 16H; H-19, H-22), 3.74 (s, 16H; H-20, H-21), 3.90 (s, 12H; H-1), 6.08* (m, 16H, H-15, H-26), 7.14 (m, $J_{2,3}=8.8$ Hz, 8H; H-2), 7.47 (m, $J_{3,2}=8.8$ Hz, 8H; H-3), 7.60* (m, 16H; H-14, H-27), 7.81 (m, $J_{10,11}=8.4$ Hz, 8H; H-10), 8.24 (d, $J_{7,6}=8.8$ Hz, 4H; H-7), 8.26 (d, $J_{6,7}=8.8$ Hz, 4H; H-6), 8.39* (3 × d, $J_{13,12}=J_{28,29}=8.8$ Hz, 8H; H-13, H-28), 8.47 (s, 4H; H-5), 8.56 (s, 4H; H-8), 8.64 (m, $J_{11,10}=8.4$ Hz, 8H; H-11), 9.17* (4 × d, $J_{12,13}=8.5$ Hz, 4H; H-12), 9.26* ppm (3 × d, $J_{29,28}=8.8$ Hz, 4H; H-29).

Received: September 6, 2005
Published online: November 28, 2005

Keywords: copper · multinuclear assemblies · rotaxanes · template synthesis · thermodynamic control

[1] a) G. Schill, *Catenanes, Rotaxanes and Knots,* Academic Press, New-York, **1971**; b) C. O. Dietrich-Buchecker, J.-P. Sauvage, *Chem. Rev.* **1987**, *87*, 795; c) D. B. Amabilino, J. F. Stoddart, *Chem. Rev.* **1995**, *95*, 2725; d) *Molecular Catenanes, Rotaxanes and Knots* (Eds.: J.-P. Sauvage, C. Dietrich-Buchecker), Wiley-VCH, Weinheim, **1999**; e) F. Vögtle, T. Dünnwald, T. Schmidt, *Acc. Chem. Res.* **1996**, *29*, 451; f) M. Fujita, *Acc. Chem. Res.* **1999**,

 © 2006 Wiley-VCH Verlag GmbH & Co. KGaA, Weinheim

32, 53; g) T. Hoshimo, M. Miyauchi, Y. Kawaguchi, H. Yamaguchi, A. Harada, *J. Am. Chem. Soc.* **2000**, *122*, 9876; h) A. Bogdan, M. O. Vysotsky, T. Ikai, Y. Okamoto, V. Boehmer, *Chem. Eur. J.* **2004**, *10*, 3324.

[2] a) V. Balzani, M. Venturi, A. Credi, *Molecular Devices and Machines*, Wiley-VCH, Weinheim, **2003**; b) "Molecular Machines and Motors": J.-P. Sauvage, *Struct. Bonding (Berlin)* **2001**, *99*; c) V. Balzani, A. Credi, F. M. Raymo, F. J. Stoddart, *Angew. Chem.* **2000**, *112*, 3484; *Angew. Chem. Int. Ed.* **2000**, *39*, 3348; d) B. L. Feringa, *Molecular Switches*, Wiley-VCH, Weinheim, **2001**; e) L. Fabbrizzi, M. Licchelli, P. Pallavicini, *Acc. Chem. Res.* **1999**, *32*, 846; f) T. R. Kelly, H. de Silva, R. A. Silva, *Nature* **1999**, *401*, 150; g) N. Koumura, R. W. J. Zijistra, R. A. van Delden, N. Harada, B. L. Feringa, *Nature* **1999**, *401*, 152; h) D. A. Leigh, J. K. Y. Wong, F. Dehez, F. Zerbetto, *Nature* **2003**, *424*, 174; i) M. C. Jimenez-Molero, C. Dietrich-Buchecker, J.-P. Sauvage, *Chem. Commun.* **2003**, 1613; j) E. Katz, O. Lioubashevsky, I. Wilner, *J. Am. Chem. Soc.* **2004**, *126*, 15520; k) A. Harada, *Acc. Chem. Res.* **2001**, *34*, 456; l) J.-P. Sauvage, *Chem. Commun.* **2005**, 1507.

[3] a) V. Balzani, P. Ceroni, A. Credi, C. Hamers, M. Gomez-Lopez, J. F. Stoddart, R. Wolf, *New J. Chem.* **2001**, *25*, 25, and references therein; b) C. Reuter, W. Wienand, C. Schmuck, F. Vögtle, *Chem. Eur. J.* **2001**, *7*, 1728.

[4] F. Huang, H. W. Gibson, *J. Am. Chem. Soc.* **2004**, *126*, 14738.

[5] a) P. R. Ashton, I. Baxter, S. J. Cantrill, M. C. T. Fyfe, P. T. Glink, J. F. Stoddart, A. J. P. White, D. J. Williams, *Angew. Chem.* **1998**, *110*, 1344; *Angew. Chem. Int. Ed.* **1998**, *37*, 1294; b) P. R. Ashton, I. W. Parsons, F. M. Raymo, J. F. Stoddart, A. J. P. White, D. J. Williams, R. Wolf, *Angew. Chem.* **1998**, *110*, 2016; *Angew. Chem. Int. Ed.* **1998**, *37*, 1913.

[6] T. Hoshimo, M. Miyauchi, Y. Kawaguchi, H. Yamaguchi, A. Harada, *J. Am. Chem. Soc.* **2000**, *122*, 9876.

[7] a) T. Fujimoto, Y. Sakata, T. Kaneda, *Chem. Commun.* **2000**, 2143; b) H. Onagi, C. J. Easton, S. F. Lincoln, *Org. Lett.* **2001**, *3*, 10041.

[8] M.-C. Jimenez, C. Dietrich-Buchecker, J.-P. Sauvage, A. De Cian, *Angew. Chem.* **2000**, *112*, 1351; *Angew. Chem. Int. Ed.* **2000**, *39*, 1295.

[9] a) M.-C. Jimenez, C. Dietrich-Buchecker, J.-P. Sauvage, *Angew. Chem.* **2000**, *112*, 3422; *Angew. Chem. Int. Ed.* **2000**, *39*, 3284; b) M. C. Jimenez-Molero, C. Dietrich-Buchecker, J.-P. Sauvage, *Chem. Eur. J.* **2002**, *8*, 1456.

[10] C. O. Dietrich-Buchecker, J.-P. Sauvage, J. P. Kintzinger, *Tetrahedron Lett.* **1983**, *24*, 5095.

[11] J.-C. Chambron, V. Heitz, J.-P. Sauvage, *J. Chem. Soc. Chem. Commun.* **1992**, 1131.

[12] The synthesis of ligand **1** will be described elsewhere. Structural characterization: ^{1}H NMR (500 MHz; $CDCl_3$): $\delta = 2.93$ (s, 3H; H-4), 2.98 (s, 3H; H-9), 3.72 (m, 4H; H-19, H-21), 3.77 (m, 4H; H-18, H-23), 3.78 (s, 4H; H-20, H-21), 3.88 (m, 4H; H-17, H-24), 3.91 (s, 3H; H-1), 4.37 (m, 4H; H-16, H-25), 7.06 (m, $J_{2,3} =$ 8.8 Hz, 2H; H-2), 7.21 (m, $J_{15,14} = 8.9$ Hz, 2H; H-15), 7.22 (m, $J_{26,27} = 8.9$ Hz, 2H; H-26), 7.42 (m, $J_{3,2} = 8.8$ Hz, 2H; H-3), 7.71 (m, $J_{10,11} = 8.4$ Hz, 2H; H-10), 7.792 (d, $J_{7,6} = 8.8$ Hz, 1H; H-7), 7.794 (d, $J_{6,7} = 8.8$ Hz, 1H; H-6), 8.07 (s, 1H; H-5), 8.17 (s, 1H; H-8), 8.21 (d, $J_{13,12} = 8.5$ Hz, 1H; H-13), 8.23 (d, $J_{28,29} = 8.4$ Hz, 1H; H-28), 8.461 (m, $J_{27,26} = 8.9$ Hz, 2H; H-27), 8.465 (m, $J_{14,15} =$ 8.9 Hz, 2H; H-14), 8.52 (m, $J_{11,10} = 8.4$ Hz, 2H; H-11), 8.72 (d, $J_{12,13} = 8.5$ Hz, 1H; H-12), 8.98 ppm (d, $J_{29,28} = 8.4$ Hz, 1H; H-29), see also the Supporting Information; ESI-MS: m/z 996.5 $[M+H]^+$.

[13] M. Fujita, O. Sasaki, T. Mitsuhashi, T. Fujita, J. Yazaki, K. Yamaguchi, K. Ogura, *J. Chem. Soc. Chem. Commun.* **1996**, 1535.

[14] D. B. Amabilino, C. O. Dietrich-Buchecker, J.-P. Sauvage, *J. Am. Chem. Soc.* **1996**, *118*, 3285.

 © 2006 Wiley-VCH Verlag GmbH & Co. KGaA, Weinheim

Nanostructures

DOI: 10.1002/anie.200502823

Template-Free Synthesis and Assembly of Single-Crystalline Tungsten Oxide Nanowires and their Gas-Sensing Properties**

*Julien Polleux, Alexander Gurlo, Nicolae Barsan, Udo Weimar, Markus Antonietti, and Markus Niederberger**

The controlled synthesis and characterization of crystalline objects with reduced dimensionality is a fascinating objective in modern materials science, physics, and chemistry. One-dimensional systems such as nanowires and nanotubes are especially attractive building blocks for nanodevices because they represent the smallest dimension for efficient transport of electrons and excitons.[1] A wide variety of synthetic methodologies, ranging from vapor-phase techniques to solution-growth processes, have been used to produce nanowires of elements, oxides, nitrides, carbides, and chalcogenides.[2,3] Although transition metal oxides are an important class of materials,[4] soft-chemistry routes to crystalline metal-oxide nanowires under mild reaction conditions are not yet available. The reason for this is that sol-gel derived materials formed at low temperature are amorphous, and that the heat treatment necessary to induce crystallization is usually accompanied by an undesired alteration of the particle morphology.

In addition to the spontaneous self-assembly of preformed nanocrystals into nanowires by oriented attachment,[5–8] template techniques relying on the use of surfactants[9] or solids[10] as structure-directing agents have been reported for the soft-chemistry fabrication of anisotropic oxide nanomaterials. However, simpler systems avoid the use of additional templates, thereby enabling control over the dimensionality of the nanoparticles solely by the solvent, and thus offering the advantage that the amount of impurities in the final product can be kept low. The reaction of benzyl alcohol with metal alkoxides, for example, allows the controlled synthesis of metal oxide nanoparticles with a large variety of compo-

[*] Dr. J. Polleux, Prof. M. Antonietti, Dr. M. Niederberger
Max-Planck-Institute of Colloids and Interfaces
Research Campus Golm
14424 Potsdam (Germany)
Fax: (+49) 331-567-9502
E-mail: markus.niederberger@mpikg.mpg.de
Dr. A. Gurlo, Dr. N. Barsan, Dr. U. Weimar
University of Tuebingen
Institute of Physical and Theoretical Chemistry
Auf der Morgenstelle 15, 72076 Tuebingen (Germany)

[**] We thank Marc Willinger and Dr. Dangsheng Su (Fritz-Haber-Institute Berlin) for the HRTEM and Rona Pitschke for SEM measurements. Financial support by the Max-Planck-Society and by the DFG (priority program SPP 1165) is gratefully acknowledged.

Supporting information for this article is available on the WWW under http://www.angewandte.org or from the author.

© 2006 Wiley-VCH Verlag GmbH & Co. KGaA, Weinheim

sitions and particle shapes.[11–19] Similarly, benzylamine and *n*-butylamine can also act as shape-controlling agents.[20,21]

Herein, we report a soft-chemistry route to crystalline tungsten oxide nanowires self-assembled into bundles that is performed in a simple glass beaker at low temperature. Among the transition metal oxides, tungsten oxide offers a particularly wide spectrum of useful properties, including high structural flexibility,[22] switchable optical properties,[23] and catalytic behavior.[24] Accordingly, tungsten oxide is a good candidate for applications in electrochromic[25] and gas-sensing devices.[26,27] Anisotropic tungsten oxide nanorods have been prepared before using soft-chemistry approaches[28] and surfactant mixtures,[29–31] and additives such as oxalic acid or deferoxamine enabled the synthesis of self-assembled, highly oriented one-dimensional tungsten oxide nanostructures.[32,33] However, the absence of any structure-directing agents and the use of a halide-free precursor in our synthetic protocol, in combination with the outstanding aspect ratio of the nanowires, allows the preparation of a particularly promising nanomaterial for gas-sensing applications.

Tungsten isopropoxide in benzyl alcohol provides a versatile reaction system for the nonaqueous preparation of crystalline tungsten oxide nanowires. This one-pot synthetic procedure resulted in the formation of a blue powder, which was subsequently analyzed by XRD in the 2θ range of 2–60°. The corresponding powder pattern exhibits three sharp reflections (Figure 1 a): the first reflection, centered at 4.68°

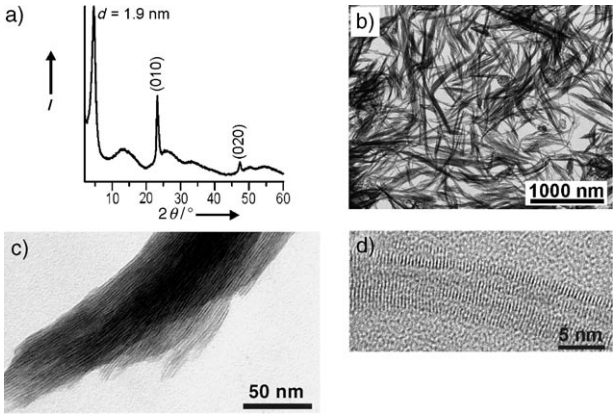


Figure 1. a) XRD powder pattern and b) TEM overview image of the as-synthesized tungsten oxide nanobundles. c) TEM image of a tip of one bundle consisting of individual nanowires. d) HRTEM image of a nanowire bundle.

in the small-angle range, corresponds to a *d*-value of 1.9 nm. The sharpness and intensity of the peak point to a highly ordered mesostructure. The other two reflections at $2\theta =$ 23.2° and 47.3° match best with the (010) and (020) planes of the monoclinic $W_{18}O_{49}$ (or $WO_{2.72}$) structure (JCPDS 36-101). All other reflections are much weaker, thus indicating that the nanowires grow along the [010] direction. Although it is difficult to assign the powder pattern unambiguously to a specific crystal structure as various stoichiometric and non-stoichiometric tungsten oxide compounds have rather similar structures,[22] the pattern is similar to that reported recently for $W_{18}O_{49}$ nanorods.[31]

A representative overview of the nanowire bundles is displayed in Figure 1 b. Their length ranges typically from 300 to 1000 nm, although longer species were also found in the sample, and the width is between 20 and 100 nm. It is interesting to note that the entire sample consists of this anisotropic nanomaterial, with no indication of other products. The higher-magnification TEM image in Figure 1 c gives evidence that the fibers consist of individual nanowires which appear with a dark contrast. Interestingly, the nanowires are mostly oriented parallel to each other with an equal distance almost throughout the whole length of the nanowires, giving rise to the intense reflection at $2\theta = 4.68°$. Accordingly, the constant interwire distance has to be a direct consequence of an ordered arrangement of the organic molecules between the inorganic nanowires. The high-resolution TEM image in Figure 1 d shows lattice fringes characteristic of a crystalline material. The diameter of all nanowires is highly uniform, typically (1 ± 0.1) nm. This tiny size is comparable to the diameter of single-walled carbon nanotubes (typically around 1.2 nm).[34]

In order to learn more about the attractive forces between the individual nanowires, the tungsten oxide sample dispersed in ethanol was mixed with formamide. TEM investigations showed that the bundles are completely transformed into separate nanowires (Figure 2 a), and only nanowires can be observed over a large area of the TEM grid (several square micrometers). A TEM image at higher magnification shows individual nanowires that are bent, sometimes forming circular structures (Figure 2 b). The high flexibility of the nanowires can be explained by their small cross-section, as well as by the construction principle of tungsten oxide. Obviously, bending stress can be reduced by tilting the octahedra with respect to each other. Nevertheless, the

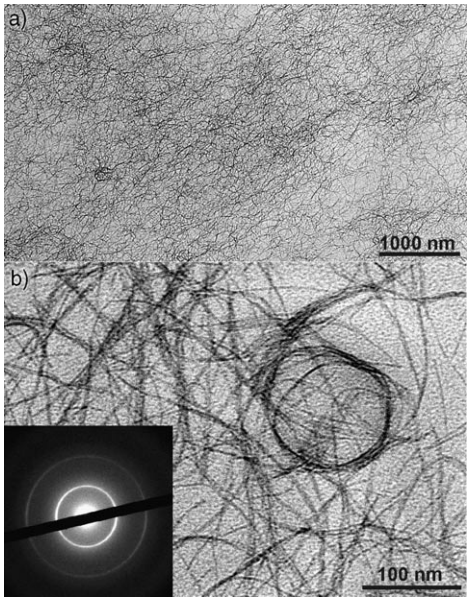


Figure 2. a) Overview TEM image of isolated nanowires. b) TEM image at higher magnification (inset: SAED pattern).

 © 2006 Wiley-VCH Verlag GmbH & Co. KGaA, Weinheim

nanowires are crystalline, as proven by selected-area electron diffraction, which exhibits the two rings assigned to the (010) and (020) reflections (Figure 2b, inset).

The organization of the nanowires into bundles is directed by specific interactions between the organic species present in the reaction system, and the uniform distance between the nanowires indicates an ordered supramolecular arrangement of intercalated organic molecules. FTIR spectroscopy clearly proves the presence of an organic–inorganic hybrid structure in the nanowire bundles (see Supporting Information). The typical bands for W=O and bridging oxygens (O–W–O) appear in the region of 1000–500 cm^{-1} in the IR spectrum.[24] The bands at 1595, 1580, 1500, and 1451 cm^{-1} are characteristic of the skeletal vibrations of an aromatic ring,[24,35] whereas the band at 1207 cm^{-1} is typical of the C–C vibration.[35] However, the lack of a band at 1018 cm^{-1}, which represents the C–O stretch of benzyl alcohol,[35] and the presence of a strong band at 1690 cm^{-1}, assignable to C=O stretching, points to the possibility that benzyl alcohol has been partly oxidized to benzaldehyde or benzoic acid during nanowire growth. As a matter of fact, the position of the C=O band corresponds exactly to benzaldehyde adsorbed to the surface of metal oxides.[36] This value is shifted slightly to lower frequency in comparison to free benzaldehyde due to coordination to Lewis acid sites present at the surface of the tungsten oxide.[24] This observation is further supported by the fact that the bands for a carboxylate group, expected to be at around 1550 and 1410 cm^{-1},[24] are missing. Oxidation of benzyl alcohol to benzaldehyde with WO_3 powder as a catalyst is well known and occurs at low temperatures.[24] A similar oxidation step has also been observed in the reaction of benzyl alcohol with WCl_6 in the presence of deferoxamine mesylate,[33] although it is interesting to note that in the case of yttrium oxide synthesized in benzyl alcohol, the final inorganic–organic hybrid material consists of yttrium oxide layers with intercalated benzoic acid molecules.[19] In that example, the oxidation of benzyl alcohol did not stop at the aldehyde stage but proceeded to the acid. Thermogravimetric analysis of the fiber bundles shows a weight loss of about 16% in the range of room temperature to 540°C (see Supporting Information).

Chemical sensors play a profound role in the areas of public safety, emission control, and environmental protection. The ubiquitous presence of contaminants in the environment as well as the rigorous regulations on the emission of toxic gases demand local monitoring of low concentrations of polluting gases at many locations. The practical application of local monitoring requires the development of small and cheap sensing devices, with high sensitivities in the sub parts-per-million range. Semiconducting metal oxides as sensing elements feature several advantages, such as simplicity in device structure, low fabrication cost, robustness in practical applications, and adaptability to a wide variety of reducing and oxidizing gases.[26] The reduction of power consumption is gaining more and more importance in sensing applications, and demands for further miniaturization of sensor devices, and, consequently, the question of how sensors can be integrated with modern electronic fabrication technologies, becomes a serious issue. One-dimensional nanostructures such as nanowires and nanotubes are particularly promising in this regard because they provide a large surface-to-volume ratio, which should result in excellent sensitivities and fast recovery and response times. They are also easily configurable as field-effect transistors and integrable with conventional devices and device-fabrication techniques.[37] However, investigations on the gas-sensing properties of metal oxide nanowires are basically restricted to SnO_2[38–41] and In_2O_3,[40] mainly due to the lack of simple synthetic procedures for other crystalline and high-purity metal oxide nanowires.

The gas-sensing properties of the tungsten oxide nanowire bundles were studied, especially with regard to the assessment of the performance of the nanobundle-based sensors as potential candidates for detection of low levels of NO_2. The peculiar morphology of the tungsten oxide nanomaterial, combined with its small size, requires the optimization of many parameters for effective sensor generation. The thermal stability of the nanobundles, the compatibility of the deposition techniques with the "fragile" nanowire morphology, their conductivity, which is directly related to the stoichiometry and the crystallinity of the nanowires, as well as the right choice of the transducer/substrate structure have to be taken into account and still leave room for optimization. For the gas-sensing tests (see Supporting Information), a suspension of the tungsten oxide nanobundles in ethanol was deposited onto alumina substrates by drop-coating and subsequently calcined at 500°C in air, resulting in the formation of a highly porous network as sensing layers. According to SEM results, the morphology of the nanowire bundles prior to (Figure 3a) and after heat treatment at 500°C (Figure 3b) is similar, although the annealed sample should be free of organic residues according to the TGA measurement. Obviously, the removal of the organic components from between the nanowires leads to more compact structures, although without changing the macroscopic fibrous morphology. At temperatures of 700°C the nanowire bundles start to transform into pearl-necklace-like structures (Figure 3c) due to Rayleigh instability.[42] Whereas the crystal structure and the nanowire morphology remain unaltered in the sample annealed at 500°C, a calcination temperature of 700°C induces a change in the crystal structure to monoclinic WO_3 (see XRD and TEM data in the Supporting Information). Therefore, only the nanobundles after thermal treatment at 500°C were investigated with respect to their gas-sensing properties.

In general, CO and NO_2 are used as probe molecules to assess the gas-sensing properties of a new sensing material, mainly due to the simplicity of their detection mechanism, i.e., CO oxidation by adsorbed oxygen species to CO_2 and NO_2 ionosorption and formation of surface electron traps $NO^-_{2,ads}$, respectively. In our case, the tungsten oxide nanowires were nearly insensitive to CO in the concentration range between 1 and 10 ppm at all operating temperatures studied (the sensor signal R_{air}/R_{CO} was less than 2).

Figure 4a shows that the tungsten oxide nanowire sensors exhibit a high signal (≈ 9) at particularly low NO_2 concentrations of about 50 ppb (100 $\mu g\,m^{-3}$), which is a much better sensitivity than the recently reported SnO_2 and In_2O_3 nanowires.[37,39,40] This behavior can be explained by their high surface area and good crystallinity, combined with an

 © 2006 Wiley-VCH Verlag GmbH & Co. KGaA, Weinheim

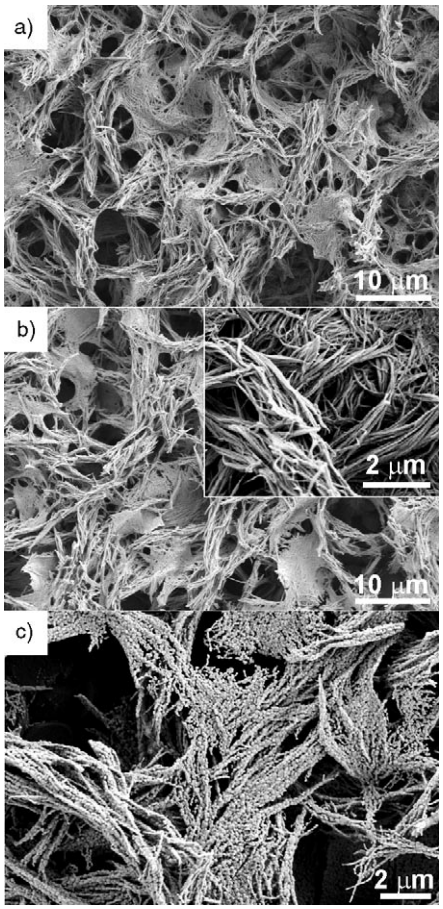


Figure 3. SEM images of the nanowire bundles deposited on the substrate at a) room temperature, b) after annealing at 500 °C (inset: higher magnification), and c) 700 °C.

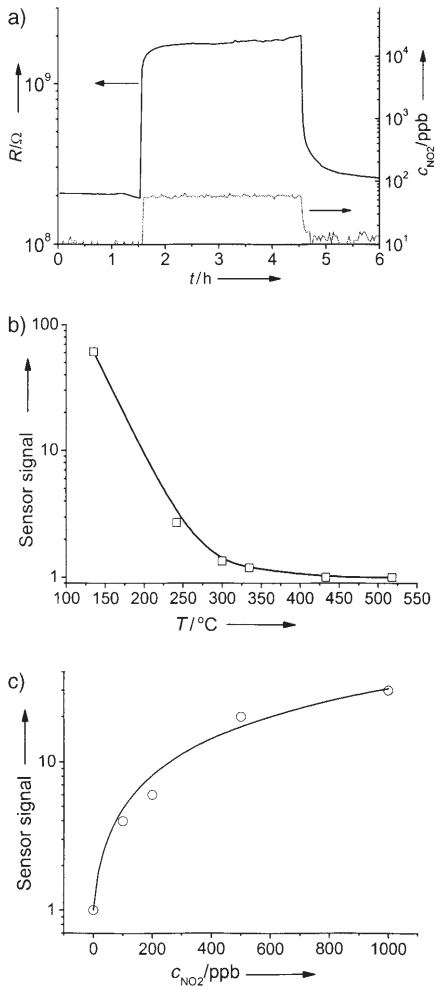


Figure 4. a) Black curve: change of the resistance R of the tungsten oxide nanowire bundles upon exposure to NO_2 ($\approx$50 ppb) at 150 °C in dry air; grey curve: NO_2 concentration measured simultaneously with an NO_x chemiluminescence analyzer. b) Dependence of the sensor signal ($S = R_{NO_2}/R_{air}$) to $\approx$100 ppb NO_2 on the operating temperature of the sensor in humid air (50% r.h. at 25 °C). c) Dependence of the sensor signal on NO_2 concentration in humid air (50% r.h. at 25 °C) (operating temperature of the sensors: 225 °C): experimental data points (○) and fitting curve based on the model from ref. [43]: $S = 1 + a\,c_{NO_2}^{b}$, fitting parameters: $a = (0.06 \pm 0.05)$ and $b = (0.89 \pm 0.13)$.

appropriate porosity of the deposited nanowire film, which provides good accessibility of the gases to the sensing layers. One should note, however, that at low operating temperatures of 150 °C the sensor is characterized by a relatively slow response and long recovery time. The sensor follows the profile of the NO_2 concentration as indicated by an on-line NO_x chemiluminescence analyzer (Figure 4a). Although the resistance of the layers (typically about 5 mm in diameter and several hundreds of nanometers thick) on conventional alumina substrates with low aspect ratio ($\approx$30) is very high ($\approx 10^8$ Ohm), this problem can be solved by using substrates with higher aspect ratios. The sensor signal of the tungsten oxide nanobundles is strongly dependent on the temperature (Figure 4b). Interestingly, the intensity of the signals decreases drastically with increasing operating temperature, leading to the observation that above 300 °C the nanobundles are nearly insensitive to NO_2. This behavior potentially enables the selective detection of reducing gases at higher temperatures. Generally, in the temperature range of 350–400 °C metal oxide sensors are sensitive to reducing gases such as hydrocarbons and volatile organic compounds. The calibration curves and the corresponding sensor signals and their dependence on NO_2 concentration can be approximated by power laws, as illustrated for an operating temperature of 200 °C in Figure 4c. The dependence of the sensor signal (S) on the NO_2 concentration (c_{NO_2}) can be described as $S = 1 + a\,c_{NO_2}^{b}$, where a and b are variables that can be fitted to $a = (0.06 \pm 0.05)$ and $b = (0.89 \pm 0.13)$. The experimental results correspond to the model developed by Gurlo et al.,[43] thus indicating the formation of surface-trapped states $NO_2^{-}{}_{,ads}$ (see also Figure 4c) with no evidence of dissociative NO_2 adsorption. The ionosorption of nitrogen dioxide at the surface of the tungsten oxide nanowires leads to the upward bending of the bands ($\approx$120 meV for 50 ppb NO_2 at 150 °C) and accordingly to an increase of the resistance, thus giving evidence for the n-type semiconducting properties of the tungsten oxide nanowires.

The controlled synthesis of one-dimensional tungsten oxide nanowires is particularly fascinating because bulk tungsten oxide exhibits manifold properties, including elec-

 © 2006 Wiley-VCH Verlag GmbH & Co. KGaA, Weinheim

trochromism, semiconductivity, catalytic activity, and sensing properties. The present synthetic route can easily be performed in regular laboratory glassware and leads, at a low reaction temperature, directly to highly crystalline nanowires in good yields. This unique synthetic approach avoids any structure-directing agents as templates in the preparation of a high-purity nanomaterial. The nanobundles, which consist of self-assembled nanowires, can be separated into individual wires, thereby enabling dispersion as well as a rational interfacing of these nanobuilding blocks, either to other functional organic units or for chemical assembly into patterned arrays.

Their high surface-to-volume ratio combined with the high purity of the material makes these nanowire bundles ideal candidates for gas-sensing devices. This assumption is supported by initial results, which show an extraordinarily high sensitivity to low NO_2 concentrations. One major advantage of the good performance of the tungsten oxide sensor at low temperature is not only the possibility to fabricate low energy consuming devices, but also to tailor the gas-sensing properties of the nanobundles by in situ functionalization of the surface with specific organic and bioorganic receptors in order to provide high selectivity.

Received: August 9, 2005
Published online: November 28, 2005

Keywords: nanowires · organic–inorganic hybrid composites · oxides · sensors · tungsten

[1] X. F. Duan, Y. Huang, Y. Cui, J. F. Wang, C. M. Lieber, *Nature* **2001**, *409*, 66.
[2] C. N. R. Rao, F. L. Deepak, G. Gundiah, A. Govindaraj, *Prog. Solid State Chem.* **2003**, *31*, 5.
[3] Y. N. Xia, P. D. Yang, Y. G. Sun, Y. Y. Wu, B. Mayers, B. Gates, Y. D. Yin, F. Kim, Y. Q. Yan, *Adv. Mater.* **2003**, *15*, 353.
[4] C. N. R. Rao, B. Raveau, *Transition Metal Oxides*, VCH, New York, **1995**.
[5] Z. Y. Tang, N. A. Kotov, M. Giersig, *Science* **2002**, *297*, 237.
[6] J. Polleux, N. Pinna, M. Antonietti, M. Niederberger, *Adv. Mater.* **2004**, *16*, 436.
[7] J. Polleux, N. Pinna, M. Antonietti, C. Hess, U. Wild, R. Schlögl, M. Niederberger, *Chem. Eur. J.* **2005**, *11*, 3541.
[8] Z. Tang, N. A. Kotov, *Adv. Mater.* **2005**, *17*, 951.
[9] X. G. Peng, L. Manna, W. D. Yang, J. Wickham, E. Scher, A. Kadavanich, A. P. Alivisatos, *Nature* **2000**, *404*, 59.
[10] C. R. Martin, *Chem. Mater.* **1996**, *8*, 1739.
[11] M. Niederberger, M. H. Bartl, G. D. Stucky, *Chem. Mater.* **2002**, *14*, 4364.
[12] M. Niederberger, M. H. Bartl, G. D. Stucky, *J. Am. Chem. Soc.* **2002**, *124*, 13642.
[13] M. Niederberger, G. Garnweitner, F. Krumeich, R. Nesper, H. Cölfen, M. Antonietti, *Chem. Mater.* **2004**, *16*, 1202.
[14] M. Niederberger, N. Pinna, J. Polleux, M. Antonietti, *Angew. Chem.* **2004**, *116*, 2320; *Angew. Chem. Int. Ed.* **2004**, *43*, 2270.
[15] M. Niederberger, G. Garnweitner, N. Pinna, M. Antonietti, *J. Am. Chem. Soc.* **2004**, *126*, 9120.
[16] N. Pinna, G. Garnweitner, M. Antonietti, M. Niederberger, *Adv. Mater.* **2004**, *16*, 2196.
[17] N. Pinna, G. Neri, M. Antonietti, M. Niederberger, *Angew. Chem.* **2004**, *116*, 4445; *Angew. Chem. Int. Ed.* **2004**, *43*, 4345.
[18] N. Pinna, M. Antonietti, M. Niederberger, *Colloids Surf. A* **2004**, *250*, 211.
[19] N. Pinna, G. Garnweitner, P. Beato, M. Niederberger, M. Antonietti, *Small* **2005**, *1*, 113.
[20] N. Pinna, G. Garnweitner, M. Antonietti, M. Niederberger, *J. Am. Chem. Soc.* **2005**, *127*, 5608.
[21] J. Yang, C. Xue, S. H. Yu, J. H. Zeng, Y. T. Qian, *Angew. Chem.* **2002**, *114*, 4891; *Angew. Chem. Int. Ed.* **2002**, *41*, 4697.
[22] G. L. Frey, A. Rothschild, J. Sloan, R. Rosentsveig, R. Popovitz-Biro, R. Tenne, *J. Solid State Chem.* **2001**, *162*, 300.
[23] C. G. Granqvist, *Sol. Energy Mater. Sol. Cells* **2000**, *60*, 201.
[24] A. Tocchetto, A. Glisenti, *Langmuir* **2000**, *16*, 6173.
[25] W. Cheng, E. Baudrin, B. Dunn, J. I. Zink, *J. Mater. Chem.* **2001**, *11*, 92.
[26] G. Eranna, B. C. Joshi, D. P. Runthala, R. P. Gupta, *Crit. Rev. Solid State Mater. Sci.* **2004**, *29*, 111.
[27] O. Berger, T. Hoffmann, W.-J. Fischer, V. Melev, *J. Mater. Sci. Mater. Electron.* **2004**, *15*, 483.
[28] H. G. Choi, Y. H. Jung, D. K. Kim, *J. Am. Ceram. Soc.* **2005**, *88*, 1684.
[29] X. W. Lou, H. C. Zeng, *Inorg. Chem.* **2003**, *42*, 6169.
[30] K. Lee, W. S. Seo, J. T. Park, *J. Am. Chem. Soc.* **2003**, *125*, 3408.
[31] J.-W. Seo, Y.-W. Jun, S. J. Ko, J. Cheon, *J. Phys. Chem. B* **2005**, *109*, 5389.
[32] Z. Gu, Y. Ma, W. Yang, G. Zhang, J. Yao, *Chem. Commun.* **2005**, 3597
[33] J. Polleux, N. Pinna, M. Antonietti, M. Niederberger, *J. Am. Chem. Soc.* **2005**, *127*, 15595–15601.
[34] S. Iijima, T. Ichihashi, *Nature* **1993**, *363*, 603.
[35] M. Caravati, J.-D. Grunwaldt, A. Baiker, *Phys. Chem. Chem. Phys.* **2005**, *7*, 278.
[36] V. Augugliaro, S. Coluccia, V. Loddo, L. Marchese, G. Martra, L. Palmisano, M. Schiavello, *Appl. Catal. A* **1999**, *20*, 15.
[37] A. Kolmakov, M. Moskovits, *Annu. Rev. Mater. Res.* **2004**, *34*, 151.
[38] M. Law, H. Kind, B. Messer, F. Kim, P. D. Yang, *Angew. Chem.* **2002**, *114*, 2511; *Angew. Chem. Int. Ed.* **2002**, *41*, 2405.
[39] E. Comini, G. Faglia, G. Sberveglieri, Z. Pan, Z. L. Wang, *Appl. Phys. Lett.* **2002**, *81*, 1869.
[40] C. Li, D. Zhang, X. Liu, S. Han, T. Tang, J. Han, C. Zhou, *Appl. Phys. Lett.* **2003**, *82*, 1613.
[41] Y. L. Wang, X. C. Jiang, Y. N. Xia, *J. Am. Chem. Soc.* **2003**, *125*, 16176.
[42] M. E. T. Molares, A. G. Balogh, T. W. Cornelius, R. Neumann, C. Trautmann, *Appl. Phys. Lett.* **2004**, *85*, 5337.
[43] A. Gurlo, N. Bârsan, M. Ivanovskaya, U. Weimar, W. Göpel, *Sens. Actuators B* **1998**, *47*, 92.

 © 2006 Wiley-VCH Verlag GmbH & Co. KGaA, Weinheim

Catalytic Hydrogenation

DOI: 10.1002/anie.200502632

Ru Nanoparticles Immobilized on Montmorillonite by Ionic Liquids: A Highly Efficient Heterogeneous Catalyst for the Hydrogenation of Benzene**

Shiding Miao, Zhimin Liu, Buxing Han, Jun Huang, Zhenyu Sun, Jianling Zhang, and Tao Jiang*

The design of nanocomposites consisting of functional metals and different matrices is a promising research area for the fabrication of a variety of catalysts, adsorbents, and optical and electrical devices. Montmorillonite (MMT), which is a type of naturally occurring clay, can be structurally defined as layers of negatively charged two-dimensional silicate sheets that are separated by interlayer cationic species with a high exchange ability for other cations.[1] Such layered materials have been used as host materials for the preparation of composites and have potential applications in catalysis, separation, and the optical and electrical fields.[2] For example, Pd nanoparticles deposited on MMT with surfactants exhibit a high selectivity for the partial hydrogenation of 1-phenyl-1-pentyne to 1-phenyl-*cis*-1-pentene,[3] and Sc^{3+}-exchanged MMT has been demonstrated to function as an efficient catalyst for the Michael reaction.[4] For MMT-based catalysts, the catalytic nanoparticles are generally intercalated into the interlayer spaces or deposited on the outer surfaces of MMT with the aid of surfactants or polymers.[3,5]

In recent years, room-temperature ionic liquids (ILs) have attracted much attention due to their unusual properties, especially their extremely low vapor pressure, high thermal and good chemical stability, and excellent solvent power for organic and inorganic compounds, and they have been widely utilized as environmentally benign solvents for different processes, including chemical reactions[6] and separations.[7] ILs are also attractive media to stabilize metal nanoparticles.[8] Recently, Pd nanoparticles immobilized on the molecular sieve SBA-15 by 1,1,3,3-tetramethylguanidinium lactate have been found to exhibit high catalytic activity for hydrogenation reactions.[9]

Ruthenium catalysts are important catalysts for the hydrogenation of aromatic compounds, and have been extensively investigated.[10] However, the development of a simpler and more efficient method for the preparation of Ru catalysts is still a challenge in nanocatalysis. As mentioned above, MMT possesses negatively charged, two-dimensional silicate sheets with cationic species, and ILs are composed entirely of ions. The combination of MMT and ILs may therefore provide a new way to prepare highly efficient catalysts. Herein, we report the immobilization of Ru nanoparticles onto MMT using the IL 1,1,3,3-tetramethylguanidinium trifluoroacetate ([TMG][TFA]) and their application in the catalytic hydrogenation of benzene. To the best of our knowledge, this is the first synthesis of a nanocatalyst that involves loading catalytic metal nanoparticles onto MMT with an IL.

The IL used was synthesized by following previously reported procedures.[11] To synthesize the catalyst, Na-MMT was first treated three times with an aqueous solution of [TMG][TFA] to exchange the Na cations with those of the IL (TMG-MMT). After filtration and washing three times with distilled water, TMG-MMT was dispersed in an aqueous solution of $RuCl_3$ with stirring in order to adsorb Ru^{3+} and form TMG-MMT/$RuCl_3$ composites. The solvent was then removed from the solution by evaporation and the Ru/MMT catalyst (catalyst A) was obtained after hydrogenation at 220 °C for 2 h.

The as-prepared catalyst A was used for the hydrogenation of benzene. The results are listed in Table 1. It is clear that catalyst A is very active for the hydrogenation of benzene to cyclohexane, with a catalytic activity that is comparable or superior to Ru-cluster-based catalysts. For comparison, the TOFs of $[(\eta_6\text{-}C_6H_6)(\eta_6\text{-}C_6Me_6)_2Ru_3(\mu_3\text{-}O)(\mu_2\text{-}H)_3][BF_4]$ at 110 °C[12] and $[(\eta_6\text{-}C_6H_6)_4Ru_4(\mu_3\text{-}H)_4]Cl_2$ at 90 °C and a hydrogen pressure of 6.0 MPa[13] in ionic liquids are 3644 and 364 mol benzene per mol Ru per hour, respectively.

Our Ru/MMT nanocatalyst is a heterogeneous catalyst, which means that it is superior to homogeneous catalysts in that it can be easily separated from the products and can be used in a fixed-bed process. Catalyst A was reused for a further four runs under the same reaction conditions without any significant loss of activity (entries 6–9). This confirms that it is very stable. We also performed benzene hydrogenation with the traditional Ru/C and Ru/Al_2O_3 catalysts under the same conditions; these results are also given in Table 1 (entries 15–18). Comparing entries 2 and 17, it can be seen that our Ru/MMT catalyst has a much higher activity than Ru/Al_2O_3. The Ru/MMT catalyst is also more active than Ru/C (see entries 3 and 16).

We carried out additional experiments that allowed us to obtain useful information about the very high activity and stability of catalyst A. First, the IR spectrum of the catalyst was recorded (Bruker Tensor 27). The bands at 1614 and 1419, 1456, and 2945 cm^{-1} can be attributed to the C=N and CH_3 groups in the TMG cation, thus indicating that this cation is present in the catalyst.

The X-ray photoelectron spectrum of the as-prepared catalyst A was collected on an ESCALab220i-XL spectrometer operating at 15 kV and 20 mA at a pressure of about 3×10^{-9} mbar with $Al_{K\alpha}$ radiation as the excitation source ($h\nu$ = 1486.6 eV). In the survey XPS analysis for catalyst A no Cl could be detected, which suggests that $RuCl_3$ is completely

[*] S. Miao, Dr. Z. Liu, Prof. B. Han, Dr. J. Huang, Z. Sun, Dr. J. Zhang, Dr. T. Jiang
Center for Molecular Science
Institute of Chemistry
Chinese Academy of Sciences
Beijing 100080 (P.R. China)
Fax: (+86) 10-6256-2821
E-mail: liuzm@iccas.ac.cn

[**] This work was financially supported by the National Natural Science Foundation of China (20374057, 50472096) and the Opening Research Fund of the State Key Laboratory of Heavy Oil Processing (2004-10).

InterScience
© 2006 Wiley-VCH Verlag GmbH & Co. KGaA, Weinheim

Table 1: Hydrogenation of benzene with different catalysts.

Entry	Catalyst	Benzene/Ru [mol/mol]	T [°C]	$P(H_2)$ [MPa]	t [h]	Yield [%][a]	TOF[b]
1	A	1000	40	2.0	2.5	84.5	–
2	A	1000	40	4.0	2.5	100	400
3	A	1000	40	6.0	1.8	100	555
4	A	1000	40	8.0	1.5	100	667
5	A	10000	110	8.0	2.5	100	4000
6[c]	A	10000	110	8.0	2.5	100	4000
7[c]	A	10000	110	8.0	2.5	100	4000
8[c]	A	10000	110	8.0	2.5	100	4000
9[c]	A	10000	110	8.0	2.5	100	4000
10	B	1000	40	4.0	2.5	100	400
11	B	10000	110	8.0	2.5	100	4000
12	C	1000	40	4.0	2.5	54.0	–
13	C	1000	40	6.0	2.5	94.2	376
14	D	1000	40	4.0	2.5	44.5	–
15	Ru/C[d]	1000	40	4.0	5.0	99.5	200
16	Ru/C[d]	1000	40	6.0	2.5	98.5	394
17	Ru/Al_2O_3[e]	1000	40	4.0	3.5	35.6	102
18	Ru/Al_2O_3[e]	1000	60	4.0	4.5	79.5	177

[a] Yield of cyclohexane. [b] TOF (turnover frequency) was calculated as conversion of mols of benzene per mol of Ru per hour. [c] Catalyst A was reused for a further four runs. [d] Ru/C, 5% Ru on carbon powder, from ICI Co., Japan. [e] Ru/Al_2O_3, 5% Ru on Al_2O_3 powder, provided by XiAA Catal. Chem. Tech. Co. Ltd., China.

converted into the metal under the conditions used. Figure 1 shows the Ru 3d spectrum of the composite. It can be seen that although the Ru 3d signal is obscured by the C 1s signal of a carbon contaminant at 284.6 eV, the deconvoluted spectrum shows a doublet for two chemically different Ru entities with peak binding energies of 280.3 (Ru $3d_{5/2}$) and 284.5 eV (Ru $3d_{3/2}$), which confirms the presence of Ru^0 in catalyst A.[14] Moreover, the peak at 281.1 eV suggests the presence of a Ru–O component, which probably results from oxidation of the ruthenium nanoparticles upon exposure to air.

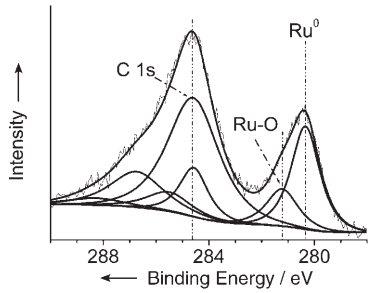


Figure 1. XPS spectra at the Ru 3d edge of catalyst A. The three vertical lines indicate the peak positions of the binding energies of C 1S, Ru–O, and Ru, respectively.

Similar phenomena have also been reported by other groups.[10c,d] The XPS results indicate that the $RuCl_3$ loaded on MMT is reduced to Ru^0 by hydrogen at 220 °C within 2 h. This reaction temperature is lower than those commonly used.[10e] The reduction in the reaction temperature probably results from the interaction of $RuCl_3$ with the IL and/or the substrate. A similar phenomenon has also been reported by Zhuang and co-workers, who reduced $RuCl_3$ and H_2PtCl_6 dispersed on activated carbon with hydrogen at 120 °C.[15]

The N_2 sorption isotherms of pristine MMT, TMG-exchanged MMT, and catalyst A were determined with an ASAP-2405N instrument at liquid-nitrogen temperature after degassing the samples at 200 °C and 10^{-4} Torr for 12 h. They show type-IV characteristics, thereby indicating the mesoporous structures of these samples. According to the nitrogen-desorption data, the specific surface area increases from 37 $m^2 g^{-1}$ for pristine MMT to 43 $m^2 g^{-1}$ for TMG-exchanged MMT and 57 $cm^2 g^{-1}$ for catalyst A due to the loading of Ru nanoparticles.

We also characterized the catalysts by means of X-ray diffraction (XRD) with an X'PERT SW diffractometer (40 kV, 40 mA, $Cu_{K\alpha}$ radiation) in the small-angle range of $2\theta = 1$–$12°$ and the wide-angle range of $2\theta = 4$–$70°$. On the basis of the XRD analysis in the small-angle range (Figure 2), the basal spacing of pristine MMT is 0.966 nm, while the spacing of TMG-exchanged MMT is enlarged to $d_{001} = 1.42$ nm due to the incorporation of the organic cations of the IL into the galleries of MMT upon ion exchange. The characteristic peak of catalyst A is shifted slightly to wider angle relative to the peak of TMG-MMT, which suggests the intercalation of Ru nanoparticles in the interlayers of MMT. However, there is no diffraction peak for Ru nanoparticles in the XRD pattern in the wide-angle range (not shown), which implies that the Ru particles are either very small or amorphous.

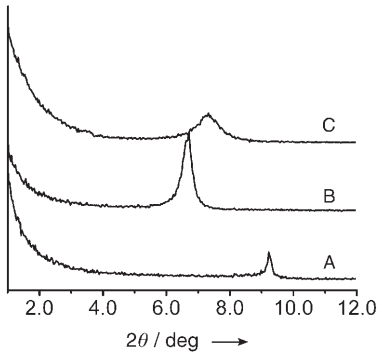


Figure 2. XRD patterns of A) pristine MMT, B) TMG-exchanged MMT, C) TMG-MMT/Ru (catalyst A).

The morphology of catalyst A was investigated with a transmission electron microscope (TEM, JEOL, JEM-2010) equipped with an energy-dispersive X-ray spectrometer (EDS) at an accelerating voltage of 200 kV. It can be seen that irregular nanoparticles with a size of less than 3 nm are uniformly distributed on the MMT surfaces (Figure 3a). These were confirmed as Ru particles by EDS analysis during

 © 2006 Wiley-VCH Verlag GmbH & Co. KGaA, Weinheim

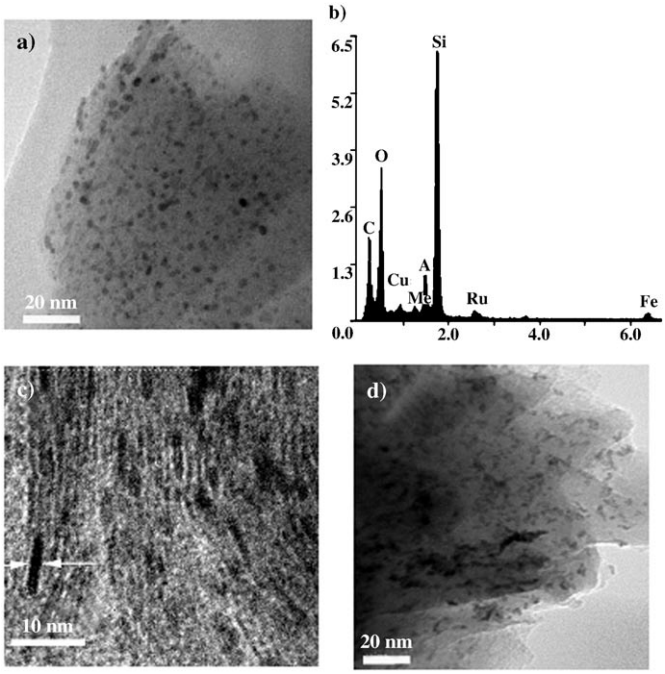


Figure 3. a) TEM image of fresh catalyst A, b) EDS analysis of catalyst A, c) HRTEM image of a cross-section of catalyst A. The white arrows indicate the interlaminar space of montmorillonite intercalated with an Ru nanoparticle, d) TEM image of catalyst A after five runs.

the TEM observation (Figure 3b). No large particles were found on MMT. The nanoparticles are firmly immobilized on MMT and could not be removed from the substrate even when the catalyst was treated ultrasonically for a long time.

To detect whether Ru nanoparticles are present in the interlayers of MMT, we embedded catalyst A in epoxy resin to form a solid specimen, and cut the specimen with an ultramicrotome to get an ultrathin section of the catalyst, which was examined by high-resolution TEM (HRTEM). Figure 3c shows an HRTEM image of the section of catalyst A. The layered structure of MMT in catalyst A can be clearly seen from this image, and the interlaminar spacing is about 1.2 nm (as indicated by the white arrows in Figure 3c), which is consistent with the XRD results. Moreover, there are many nanoparticles of less than 1.2 nm in the interlaminar spaces of MMT, thus indicating that Ru nanoparticles are intercalated into the MMT interlayers. This means that the Ru nanoparticles exist in the catalyst in two forms: some are present on the outer surfaces and others are embedded in the interlayers. We believe that both these kinds of Ru nanoparticles catalyze the hydrogenation of benzene. We also obtained the morphology of catalyst A after five catalytic cycles by TEM (Figure 3d). It can be seen that the nanoparticles on the MMT surface tend to aggregate. However, as discussed above, the activity of catalyst A does not decrease significantly after five runs. This may imply that the Ru particles in the interlayers play the main role in the high activity of the catalyst, and that most of the Ru particles are in the interlayers.

Using a similar procedure to that used to prepare catalyst A, we prepared catalyst B by thoroughly washing the TMG-MMT/$RuCl_3$ composite with water to remove the soluble Ru^{3+} before hydrogen reduction. In other words, the only difference in the procedures for preparing catalyst A and catalyst B is that the water-soluble Ru^{3+}, which could be precipitated and mixed with the MMT/Ru composite during the vaporization process, is removed before hydrogen reduction when preparing catalyst B, while all of the Ru^{3+} is reduced when preparing catalyst A. Catalyst B displays a similar catalytic activity for benzene hydrogenation to catalyst A, which suggests that the Ru^{3+} in the $RuCl_3$ aqueous solution is firmly fixed onto the TMG-exchanged MMT during the soaking process.

We also treated pristine MMT directly with the aqueous solution of $RuCl_3$ in the absence of the IL (catalyst C), and we synthesized catalyst D by treating MMT with 1-*n*-butyl-3-methylimidazolium tetrafluoroborate ([bmim][BF_4]), another IL, in a similar manner to catalyst A. Both catalysts C and D exhibit much lower activity for the hydrogenation of benzene than catalysts A and B, as shown in Table 1. Therefore, it can be deduced that the TMG cations present in catalysts A and B play an important role in immobilizing the Ru nanoparticles on MMT.

It has been reported that guanidine and guanidinium readily form coordination complexes.[16] On the basis of results reported in the literature and our experimental results we can propose a possible mechanism for the formation of catalyst A. During the treatment of MMT with the aqueous solution of [TMG][TFA] the cations of the IL exchange with the Na^+ ions present in the interlayers of pristine MMT to form the TMG-exchanged MMT, which has a larger interlayer spacing than MMT, as confirmed by XRD analysis. In the subsequent process to load Ru^{3+} onto the TMG-exchanged MMT, some Ru^{3+} ions could diffuse into the enlarged MMT interlayers , whilst others are distributed on the outer surface, due to the coordination between TMG and Ru^{3+}. This coordination between TMG and Ru^{3+} is favorable to the loading of Ru^{3+}. Finally, Ru^0 nanoparticles are produced by reduction of Ru^{3+} with H_2. Thus, for catalyst A, the TMG cations interact strongly with the surface of MMT by electrostatic forces and at the same time they stabilize Ru nanoparticles by coordination due to their electron-donor ability.[16]

In this way, Ru^0 nanoparticles could be prepared on an MMT support by a combination of electrostatic forces and coordination. Both the electrostatic and coordination forces are very strong, which results in a very stable catalyst. The Ru^0 nanoparticles in the interlayers of MMT are very small, which may be a reason for the very high activity for benzene hydrogenation. The TEM study clearly showed that some Ru nanoparticles are distributed on the outer MMT surfaces, and that these could not be separated from the MMT even after lengthy ultrasonic treatment. Therefore, the nanoparticles on the outer surface may also be stabilized by the IL.

In summary, we presented a method to prepare Ru nanocatalysts using [TMG][TFA] and MMT. In this method the IL is first exchanged with the ions in the clay, and then Ru^{3+} ions are loaded onto the IL-exchanged MMT. The final Ru/MMT nanocatalyst is obtained after hydrogen treatment. This catalyst shows very high activity for the hydrogenation of

 © 2006 Wiley-VCH Verlag GmbH & Co. KGaA, Weinheim

benzene and is very stable, due to the excellent synergistic effects of TMG, MMT, and Ru nanoparticles. We believe that other transition metals, such as Rh, Pd, and Ir, could also be supported on MMT using this method and the resulting materials could be used as efficient nanocatalysts.

Experimental Section

Preparation of the catalyst: Na montmorillite with a cation-exchange capacity (CEC) of 1.0 meq g^{-1} was supplied by Hongyan Mining Co. We only describe the preparation of catalyst A because the procedures to prepare catalysts B, C, and D are nearly the same and have been described briefly above. In the experiment to synthesize catalyst A, about 1.0 g of MMT was dispersed in an aqueous solution of the IL by stirring for about 4 h. The molar ratio of IL to the CEC of MMT was 1.1:1. The MMT was then separated from the solution by centrifugation and was treated again with an aqueous solution of the IL. This procedure was repeated three times. The IL-exchanged MMT was then washed several times with distilled water. The exchanged MMT was dispersed in 5 mL of an aqueous solution of $RuCl_3$ with a concentration of 8 mg mL^{-1}. The water was then removed by evaporation. The final Ru/MMT catalyst was obtained after hydrogenation of the solid at 220 °C for 2 h. The mass content of Ru in the composite was 3.3 wt.%, which was calculated based on the amounts of clay and $RuCl_3$ added.

Hydrogenation of benzene: The reactions were carried out in a 20-mL, stainless-steel autoclave equipped with a magnetic stirrer. In a typical experiment, 87 mg of Ru nanocatalyst and 2.0 g of benzene were placed in the autoclave and the air was replaced by H_2 within 10 min. The reaction mixture was stirred (300 rpm) at the desired temperature. More hydrogen was added to reach the pressure of interest. After the appropriate time the temperature was lowered to room temperature quickly in an ice-water bath and the hydrogen pressure was released. The products were analyzed by GC (Agilent 4890 D).

Received: July 27, 2005
Revised: October 10, 2005
Published online: November 28, 2005

Keywords: clays · heterogeneous catalysis · hydrogenation · ionic liquids · ruthenium

[1] a) J. Dale, M. Kowalska, D. L. Cocke, *Chemosphere* **1991**, *22*, 769; b) J. Sterte, *Clays Clay Miner.* **1986**, *34*, 658.
[2] a) T. J. Pinnavaia, *Science* **1983**, *220*, 365; b) A. Gil, L. M. Gandia, M. A. Vicente, *Catal. Rev. Sci. Eng.* **2000**, *42*, 145; c) "Pillared Clays": R. Burch in *Catalysis Today, Vol. 2*, Elsevier, New York, **1988**, p. 185; d) J. L. Valverde, A. de Lucas, P. Sánchez, F. Dorado, A. Romero, *Appl. Catal. B* **2003**, *43*, 43; e) B. M. Choudary, M. L. Kantam, K. V. S. Ranganath, K. K. Rao, *Angew. Chem.* **2005**, *117*, 326; *Angew. Chem. Int. Ed.* **2005**, *44*, 322; f) B. Veisz, Z. Király, L. Tóth, B. Pécz, *Chem. Mater.* **2002**, *14*, 2882; g) M. D. Nikalje, A. Sudalai, *Tetrahedron* **1999**, *55*, 5903; h) D. Dolmazon, R. Aldea, H. Alper, *J. Mol. Catal. A: Chem.* **1998**, *136*, 147; i) L. X. Shao, M. Shi, *Adv. Synth. Catal.* **2003**, *345*, 963; j) J. S. Yadav, B. V. S. Reddy, A. K. Raju, D. Gnaneshwar, *Adv. Synth. Catal.* **2002**, *344*, 938; k) Z. H. Han, H. Y. Zhu, S. R. Bulcock, S. P. Ringer, *J. Phys. Chem. B* **2005**, *109*, 2673.
[3] Z. Király, B. Veisz, Á. Mastalir, Gy. Köfaragó, *Langmuir* **2001**, *17*, 5381–5387.
[4] T. Kawabata, T. Mizugaki, K. Ebitani, K. Kaneda, *J. Am. Chem. Soc.* **2003**, *125*, 10486.
[5] S. Papp, J. Szél, A. Oszkó, I. Dékány, *Chem. Mater.* **2004**, *16*, 1674.
[6] a) T. Welton, *Chem. Rev.* **1999**, *99*, 2071; b) P. Wasserscheid, W. Keim, *Angew. Chem.* **2000**, *112*, 3926; *Angew. Chem. Int. Ed.* **2000**, *39*, 3772; c) M. J. Earle, K. R. Seddon, *Pure Appl. Chem.* **2000**, *72*, 1391; d) "Ionic Liquids as Green Solvents: Progress and Prospects", *ACS Symp. Ser.* **2003**, *856*.
[7] L. A. Blanchard, D. Hancu, E. J. Beckman, J. F. Brennecke, *Nature* **1999**, *399*, 28.
[8] a) J. Dupont, G. S. Fonseca, A. P. Umpierre, P. F. P. Fichtner, S. R. Teixeira, *J. Am. Chem. Soc.* **2002**, *124*, 4228; b) Y. Zhou, M. Antonietti, *J. Am. Chem. Soc.* **2003**, *125*, 14960; c) K. S. Kim, D. Demberelnyamba, H. Lee, *Langmuir* **2004**, *20*, 556.
[9] J. Huang, T. Jiang, H. Gao, B. Han, Z. Liu, W. Wu, Y. Chang, G. Zhao, *Angew. Chem.* **2004**, *116*, 1421; *Angew. Chem. Int. Ed.* **2004**, *43*, 1397.
[10] a) T. Naota, H. Takaya, S.-I. Murahashi, *Chem. Rev.* **1998**, *98*, 2599; b) O. Vidoni, K. Philippot, C. Amiens, B. Chaudret, O. Balmes, J. O. Malm, J. O. Bovin, F. Senocq, M. J. Casanove, *Angew. Chem.* **1999**, *111*, 3950; *Angew. Chem. Int. Ed.* **1999**, *38*, 3736; c) K. Pelzer, O. Vidoni, K. Philippot, B. Chaudret, V. Colliere, *Adv. Funct. Mater.* **2003**, *13*, 118; d) E. T. Silveira, A. P. Umpierre, L. M. Rossi, G. Machado, J. Morais, G. V. Soares, I. J. R. Baumvol, S. R. Teixeira, P. F. P. Fichtner, J. Dupont, *Chem. Eur. J.* **2004**, *10*, 3734; e) V. A. Mazzieri, P. C. L'Argentière, F. Coloma-Pascual, N. S. Fígoli, *Ind. Eng. Chem. Res.* **2003**, *42*, 2269; f) C. M. Hagen, L. Vieille-Petit, G. Laurenczy, G. Süss-Fink, R. G. Finke, *Organometallics* **2005**, *24*, 1819; g) L. M. Rossia, G. Machadoa, P. F. P. Fichtnerb, S. R. Teixeirac, J. Duponta, *Catal. Lett.* **2004**, *92*, 149; h) G. S. Fonseca, E. T. Silveira, M. A. Gelesky, J. Dupont, *Adv. Synth. Catal.* **2005**, *347*, 847.
[11] H. X. Gao, B. X. Han, J. C. Li, T. Jiang, Z. M. Liu, W. Z. Wu, Y. H. Chang, J. M. Zhang, *Synth. Commun.* **2004**, *34*, 3083.
[12] G. Süss-Fink, M. Faure, T. R. Ward, *Angew. Chem.* **2002**, *114*, 105; *Angew. Chem. Int. Ed.* **2002**, *41*, 99.
[13] P. J. Dyson, D. J. Ellis, D. G. Parker, T. Welton, *Chem. Commun.* **1999**, 25.
[14] J. F. Moulder, W. F. Stickle, P. E. Sobol, K. D. Bomben in *Handbook of X-ray Photoelectron Spectroscopy*, Perkin-Elmer, Eden Prairie, MN, **1992**.
[15] B. Yang, Q. Y. Lu, Y. Wang, L. Zhuang, J. T. Lu, P. F. Liu, *Chem. Mater.* **2003**, *15*, 3552.
[16] a) S. Aoki, K. Iwaida, N. Hanamoto, M. Shiro, E. Kimura, *J. Am. Chem. Soc.* **2002**, *124*, 5256; b) P. J. Bailey, S. Pace, *Coord. Chem. Rev.* **2001**, *214*, 91.

 © 2006 Wiley-VCH Verlag GmbH & Co. KGaA, Weinheim

Bioassay Imaging

DOI: 10.1002/anie.200501243

Measuring Biomolecular Binding Events with a Compact Disc Player Device**

*Sebastian A. Lange, Günter Roth, Silke Wittemann, Thilo Lacoste, Andreas Vetter, Jürgen Grässle, Susanne Kopta, Matthias Kolleck, Beate Breitinger, Manfred Wick, J. K. Heinrich Hörber, Stefan Dübel, and André Bernard**

Binding events in state-of-the-art parallel solid-phase binding assays, such as DNA arrays or protein chips, are quantified by using fluorescence labeling techniques.[1,2] Furthermore, immunoassays are one of the principal methods of measuring clinically relevant parameters in blood samples.[3] Herein, we demonstrate that inexpensive classical silver staining and standard compact disc (CD) reader technology can be combined into a novel binding-assay system as a substitute for the established, but expensive, signal tags and detection systems used for array-based assays. We constructed an assay reader using CD pickup technology, and determined the concentration of the important and versatile inflammation marker C-reactive protein (CRP)[4–6] in a test sample over a dynamic range of four orders of magnitude with a limit of detection (LOD) of 1 pM. We present a method of quantifying binding in a "binary" manner by counting individual binding events, potentially down to the single-molecule level, with an inexpensive readout system.

The principle of a CD or DVD (digital versatile disc) player relies on measuring the intensity of light reflected from a surface[7] (Figure 1). CDs have been applied in a biological context for some years.[8–16] However, most of these approaches merely use the CD as a cheap support medium and employ various detection mechanisms, such as colorimetry and external-signal or image processing. They do not adapt biological reactions to the high-density binary format of the information content of the CD, thus leaving the true density and simplicity of that system unused. In contrast, we demonstrate that the signal of a protein–protein interaction can be read in a format that is functionally identical to a CD information pit.

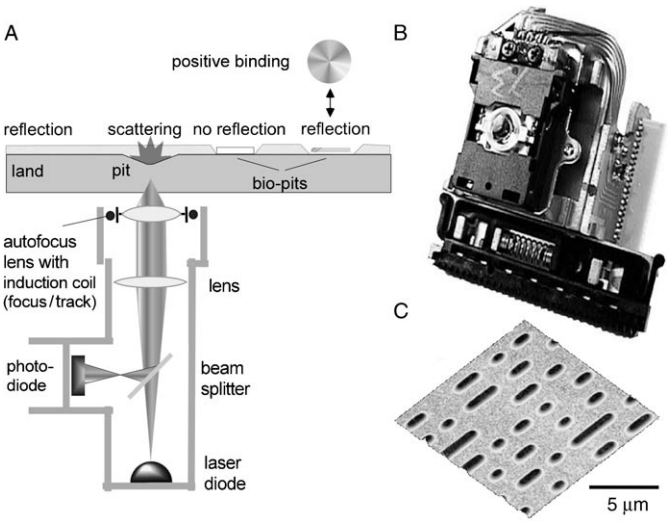


Figure 1. CD pickup for biomolecular-recognition detection. A) Operating principle. The light of a laser diode (standard wavelength of 780 nm) is passed through a beam splitter and focused through an electronically movable lens onto the disc surface. The metal-coated CD contains small impressions called pits, which encode the stored data in a spiral track. When following this spiral, the beam is reflected from the zones between the pits, and travels through the lens onto a photodiode. The intensity of the reflected light falls as a result of scattering when the beam of the pickup hits the sidewalls of the pits. An autotracking and autofocusing function, incorporated in the pickup head, keeps the beam centered on the spiral track. B) Photograph of a conventional CD pickup head. C) Topographic AFM image of a standard CD surface, which reveals the pit structure (the protective layer has been removed).

To obtain a versatile and flexible test system, we constructed the PickupImager, which was made of a CD reading head (pickup) mounted on the stage of an optical microscope,[17] and explored its application as a bioassay reader. As the CD reading principle is based on reflectivity (Figure 1 A), for a bioassay to be interpreted by original CD technology the perfect signal to be measured would be increased reflection, for example, from a tiny mirror. Therefore, we used silver precipitation catalyzed by colloidal-gold-labeled antibodies in a sandwich immunoassay format (Figure 2 A). The chemical process, called autometallographic precipitation,[18–20] is well-known from the staining of electrophoresis gels or tissue sections for electron microscopy. Silver reduction has already proved successful for use in DNA binding assays[21–23] and low-cost immunoassays.[24] We used specific antibodies coupled to colloidal gold particles with diameters of 1, 5, and 40 nm. However, the size of the

[*] Dr. S. A. Lange,[+] [#] G. Roth,[#] Dr. S. Wittemann, Dr. T. Lacoste, A. Vetter, J. Grässle, Dr. S. Kopta, M. Kolleck, B. Breitinger, Dr. M. Wick, Dr. A. Bernard
Indigon GmbH
Sindelfinger Strasse 3, 72070 Tübingen (Germany)
Fax: (+49) 531-3915763
E-mail: a.bernard@indigon.de
Prof. Dr. J. K. H. Hörber
Department of Physiology
Wayne State University School of Medicine
540 E. Canfield Ave., Detroit, MI 48201 (USA)
Prof. Dr. S. Dübel
Institut für Biochemie und Biotechnologie
Technische Universität Braunschweig
Spielmannstrasse 7, 38106 Braunschweig (Germany)
[+] Also at the European Molecular Biology Laboratory, Meyerhofstrasse 1, 69117 Heidelberg (Germany).
[#] S. A. Lange and G. Roth contributed equally to this work.
[**] We gratefully acknowledge D. Kern, U. Rexhausen, and P. Ruppersberg for stimulating ideas and helpful discussions, as well as A. Bietsch and L.-M. Pavka for carefully reading the manuscript. We also thank our colleagues S. Panwinkler, C. Sinner, Y. Ott, and M. Wacker for their continuous support.

Supporting information for this article is available on the WWW under http://www.angewandte.org or from the author.

InterScience
© 2006 Wiley-VCH Verlag GmbH & Co. KGaA, Weinheim

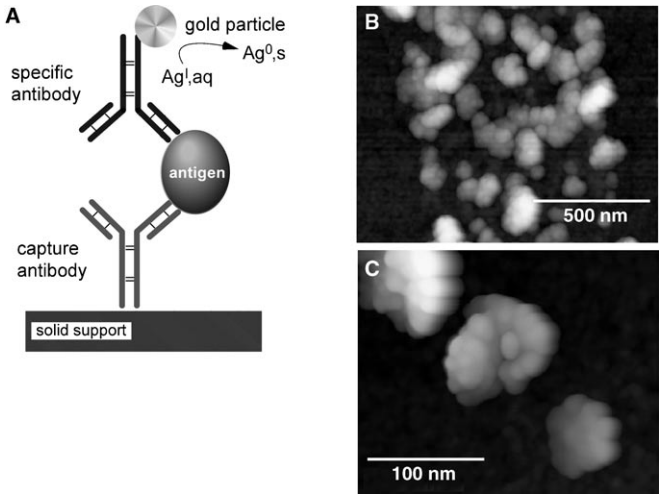


Figure 2. Signal enhancement using autometallography. A) Schematic of the sandwich immunoassay and signal generation. An immobilized capture antibody binds its target antigen. A gold-labeled specific detection antibody subsequently binds to the captured antigen and a silver grain is generated by gold-mediated catalysis. B) AFM image of silver grains grown on 1-nm colloidal gold particles in a patterned 1-μm-wide line of the immunoassay. C) Magnification of single growing silver grains reveals their shape and size.

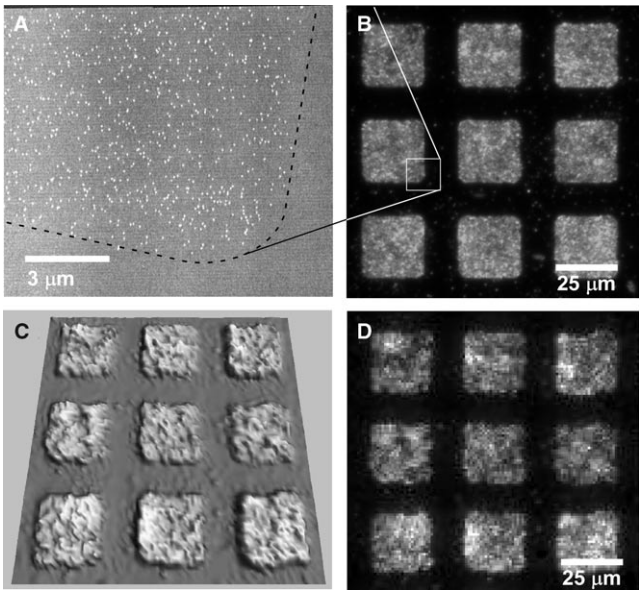


Figure 3. Imaging of the microcontact-printed recognition pads formed by colloidal-gold-labeled anti-biotin antibodies before and after silver development. A) Scanning electron microscope image of the gold beads in the binding assay before amplification by silver enhancement. B) Darkfield microscope image of the silver-enhanced array with a resolution of ca. 0.3 μm. C,D) CD-pickup image of the same array of recognition pads after silver enhancement with a resolution of approximately 1 μm (C) is an artificial 3D representation of the pickup data).

precipitated elementary silver particles, measured by AFM, was not significantly dependent on the size of the initiating colloidal gold particles attached to the antibodies: a larger size of the gold particles initiates and promotes a faster start and higher growth rate, but, from a certain size of the silver grains on the influence of the initial gold size fades and becomes negligible.

After brief metal enhancement (< 10 min), a particle-size distribution between 50 and 250 nm was observed (Figure 2B, C). Longer incubation times resulted in higher background noise and large clusters of grains. The average grain diameter achieved after prolonged enhancement (> 15 min) was (505 ± 140) nm under continuous exchange of the enhancement solution. Without exchange, the particles grew larger, to an average size of (795 ± 200) nm. Notably, grains grown under continuous exchange of the solution had a much smoother surface (see the Supporting Information).[17] Of practical relevance, we found no significant influence of ambient light exposure on the size of the silver grains.

To apply the PickupImager as a quantitative bioassay reader, we fabricated an array of squares (each 25×25 μm) of biotinylated bovine serum albumin (bBSA) by microcontact printing[25] onto a CD support made of polycarbonate, and blocked the surface with BSA to prevent nonspecific interactions. These squares acted as antigen-loaded test areas to bind Au-labeled anti-biotin antibodies from solution, and were subsequently enhanced by autometallography of the colloidal particles.

The electron microscope image (Figure 3A) of the treated surface before metal enhancement reveales that no bound gold particles were found outside the square pattern. As only the squares presented antigens (binding sites), the silver grains found outside these areas could be attributed to nonspecific background induced by autoprecipitation of silver. This array was recorded by the PickupImager with a precision and fidelity comparable to those of the optical microscope (Figure 3B–D). The smallest particles that were detectable and distinguished from background noise with the CD pickup had a diameter of roughly 300 nm (determined by AFM). For this type of single grain the acquired signal output voltage reached up to 2500 mV, within the full dynamic range of the output voltage of the PickupImager of 0–4000 mV.

Knowledge of the average density of binding partners on the surface allows the concentration of the analyte to be determined by counting a large population of single grains on a given surface area. The result will then be a concentration of grains (positive biotests) per unit surface area. At higher surface densities, when the silver grains become optically inseparable, the fractional surface coverage is determined by the PickupImager software.[17] To confirm this concentration dependence of the recorded signal, we patterned surfaces with a range of ratios of bBSA and unlabeled BSA molecules (Figure 4, insets), which conveniently simulated the varying density of captured antigens in a real-life assay.

Here, by using the ratio parameter bBSA/[bBSA+BSA], it might be appropriate to talk of single-molecule sensitivity: when decreasing the density of capture molecules to an average occupancy of the surface smaller than the size of the detecting silver grains, a single binding event is detected by an isolated grain. At the ratio of 0.01% (one bBSA molecule in 10000 BSA molecules, fractional coverage $= 0.16 \pm 0.01$, Figure 4) each bBSA ligand is separated from its nearest neighbor by about 1 μm, and at the ratio of 0.1% (0.23 ± 0.01) the average distance between ligands is still > 300 nm. Both

 © 2006 Wiley-VCH Verlag GmbH & Co. KGaA, Weinheim

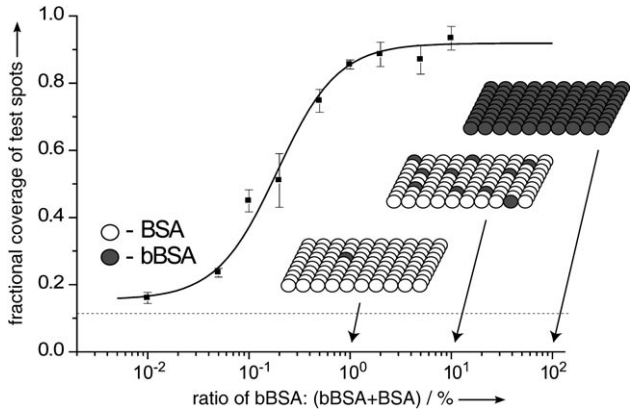


Figure 4. Two-component test assay set up by patterning surfaces with various ratios of bBSA molecules to the total number of BSA molecules. The fractional coverage of the test spots with silver precipitate was plotted against the surface ratio of capture molecules. The inset sketches illustrate different surface ratios of the molecules. At a ratio of 0.01 %, there is statistically one bBSA ligand on an area of 1000×1000 BSA molecules occupying ca. 1 μm^2 (size of BSA: $4\times4\times14$ nm^3). The dotted line marks the measured zero-dose value (0.13 ± 0.02), which is in good agreement with the parameter of the sigmoid fit ($A1=0.13\pm0.05$ and $A2=0.92\pm0.03$).

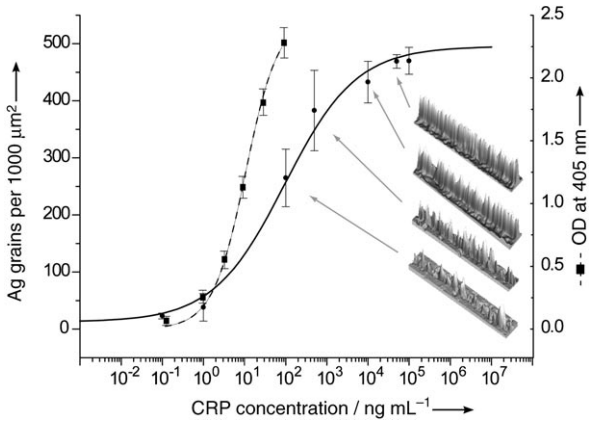


Figure 5. CRP-ELISA measured by the PickupImager and compared with standard ELISA. The number of counted silver grains per test area versus the antigen concentration (●) gives a classical binding curve (——). A classical standard CRP-ELISA measurement (■) with antigen concentration of 0.1–100 ng mL^{-1} was recorded photometrically (OD = optical density). The insets show line scans of dose–response experiments recorded by the PickupImager. Concentration-dependent reflectivity translates into a topographic map after applying different concentrations of CRP antigen and subsequent silver enhancement (100 ng mL^{-1}, 500 ng mL^{-1}, 1 µg mL^{-1}, and 5 µg mL^{-1}). The width of the structures is approximately 1 µm.

data points are above the zero-dose value (0.13 ± 0.02). Bearing in mind that the size of the average particle is 500–800 nm, these observations point toward single-molecule measurements.

We then applied our PickupImager to a sandwich immunoassay of CRP, for which the capture antibodies were deposited by microcontact printing onto glass or polycarbonate carriers. A range of different concentrations of analyte (100 pg mL^{-1}–100 µg mL^{-1} CRP spiked into serum) was applied, each on a separate carrier. The resulting reflective pattern of the precipitated metal particles was imaged with the PickupImager, and the measured density was plotted against the applied antigen concentration (Figure 5, filled circles). Significantly, these measurements showed that different analyte concentrations could easily be distinguished over at least four orders of magnitude. This is a truly remarkable value compared to the two orders of magnitude for conventional ELISA (Figure 5, filled squares). The sensitivity (LOD) of the CD pickup–ELISA was 0.1 ng mL^{-1} ((23 ± 5) grains per 1000 μm^2, which is distinguishable from the zero-dose value of (2.7 ± 0.8) grains per 1000 μm^2). This result corresponds to a LOD of about 1 pM for a molecular mass of 114 kDa.

The adaptation of a biological test to the CD format with pit structures that are 0.6 um wide and 1.5–6 µm long (Figure 1 C) was our final goal. A CD for molecular diagnostics should be readable in a standard PC laptop CD player. The ability to comply with the standard Philips CD coding format[7] requires that the bioactive receptor sites are of the same size (see the Supporting Information).[17] We also achieved this by microcontact printing. The capture antibodies for CRP were printed onto a polycarbonate disc by using stamps that consisted of parts of the pattern of a complete CD relief. Then a CRP assay was performed on the disc at a concentration of 100 ng mL^{-1} antigen, subsequently silver-enhanced, and analyzed (Figure 6). The measured concentration value corresponded well with that obtained from the same assays performed on glass slides (Figure 5).

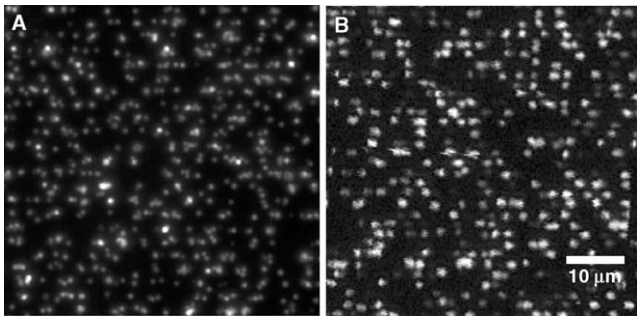


Figure 6. Microscope image (A) and pickup image (B) of a microcontact-printed CRP assay in CD format after Au enhancement. The two images show different areas on the same surface at the same magnification. Both images reveal the pit structure created by the printing stamp. This CRP disc (100 ng mL^{-1}) analyzed by the PickupImager yielded a value of (270 ± 30) grains per 1000 μm^2.

In conclusion, we have demonstrated that a CD pickup can be used to measure biomolecular binding quantitatively within a large dynamic range, and ultimately down to the single-molecule level. The lowest concentration detected with the PickupImager and distinguished from the background signal (samples without antigen) was 1 pM for the CRP antigen. Microcontact printing of proteins[25] or DNA[26] generates large numbers of separate immunoassay "spots". In a regime with a low concentration of analytes adjusted to yield statistically less than one detected binding event per

 © 2006 Wiley-VCH Verlag GmbH & Co. KGaA, Weinheim

individual spot on the surface, the number of silver grains detected would in principle allow quantification as a "binary decision"—that is, either a spot carries a silver grain or it does not. The number of "positive" spots measured in a series of many (> hundreds) identical spots then directly correlates to the concentration of the analyte in solution. As the number of binary information units available on a single CD exceeds six billion, the implementation of multiplex tests seems to be limited only by the logistics of receptor-molecule application and fluidic handling. In light of the demand for parallel analysis of multiple binding partners, this "binary biochemistry" detection method could add a novel approach to the microarray technology available today.

Received: April 8, 2005
Revised: September 11, 2005

Keywords: biomolecule binding · CD reader · immunoassays · proteins · single-molecule studies

[1] R. A. Irving, P. J. Hudson, *Nat. Biotechnol.* **2000**, *18*, 932.
[2] R. M. T. de Wildt, C. R. Mundy, B. D. Gorick, I. M. Tomlinson, *Nat. Biotechnol.* **2000**, *18*, 989.
[3] J. E. Buttler in *Immunoassays* (Eds.: E. P. Diamandis, T. K. Christopoulos), Academic Press, San Diego, CA, **1996**, pp. 205–223.
[4] L. J. Powell, *Am. J. Med. Technol.* **1979**, *87*, 138.
[5] H. Gewurz, C. Mold, J. Siegel, B. Fiedel, *Adv. Intern. Med.* **1982**, *27*, 345.
[6] M. B. Pepys, A. Berger, *Br. Med. J.* **2001**, *322*, 4.
[7] Philips International B. V., *Compact Disc System Description* "*Red and Yellow Book*", **1999**.
[8] R. P. Ekins, *J. Pharm. Biomed. Anal.* **1989**, *8*, 155.
[9] R. P. Ekins, F. W. Chu, E. M. Biggart, *J. Clin. Immunoassay* **1990**, *13*, 169.
[10] P. Becker, J. K. H. Hörber, PCT Int. Appl. WO 00/46600, **1998**.
[11] M. Gustafsson, D. Hirschberg, C. Palmberg, H. Jornvall, T. Bergman, *Anal. Chem.* **2004**, *76*, 345.
[12] D. C. Duffy, H. L. Gillis, J. Lin, N. F. Sheppard, G. J. Kellogg, *Anal. Chem.* **1999**, *71*, 4669.
[13] I. Alexandre, Y. Houbion, J. Collet, S. Hamels, J. Demarteau, J. L. Gala, J. Remacle, *Biotechniques* **2002**, *33*, 435.
[14] R. Barathur, J. Bookout, S. Sreevatsan, J. Gordon, M. Werner, G. Thor, M. Worthington, *Psychiatr. Genet.* **2002**, *12*, 193.
[15] F. Perraut, A. Lagrange, P. Poteau, O. Peyssonneaux, P. Puget, G. McGall, L. Menou, R. Gonzalez, P. Labeye, F. Ginot, *Biosens. Bioelectron.* **2002**, *17*, 803.
[16] J. J. La Clair, M. D. Burkart, *Org. Biomol. Chem.* **2003**, *1*, 3244.
[17] The Supporting Information includes experimental protocols, a description of the PickupImager, a discussion on the particle size/morphology, and further details of the data interpretation.
[18] G. Danscher, G. W. Hacker, L. Grimelius, J. O. R. Norgaard, *J. Histotechnol.* **1993**, *16*, 201.
[19] G. W. Hacker, G. Danscher, *Cell Vision* **1994**, *1*, 102.
[20] G. W. Hacker, I. Zehbe, J. F. Hainfeld, J. Sällström, C. Hauser-Kronberger, A.-H. Graf, H. Su, O. Dietze, O. Bagasra, *Cell Vision* **1996**, *3*, 209.
[21] T. A. Taton, C. A. Mirkin, R. L. Letsinger, *Science* **2000**, *289*, 1757.
[22] J. Reichert, A. Csaki, J. M. Kohler, W. Fritzsche, *Anal. Chem.* **2000**, *72*, 6025.
[23] W. Fritzsche, *J. Biotechnol.* **2001**, *82*, 37.
[24] S. K. Sia, V. Linder, B. A. Parviz, A. Siegel, G. M. Whitesides, *Angew. Chem.* **2004**, *116*, 504; *Angew. Chem. Int. Ed.* **2004**, *43*, 498.
[25] A. Bernard, E. Delamarche, H. Schmid, B. Michel, H. R. Bosshard, H. Biebuyck, *Langmuir* **1998**, *14*, 2225.
[26] S. A. Lange, V. Benes, D. P. Kern, J. K. Hörber, A. Bernard, *Anal. Chem.* **2004**, *76*, 1641.

 © 2006 Wiley-VCH Verlag GmbH & Co. KGaA, Weinheim

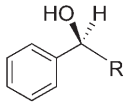
Asymmetric Addition

DOI: 10.1002/anie.200503206

Highly Enantioselective Addition of Diphenylzinc to Aliphatic and Aromatic Aldehydes Catalyzed by a Readily Available H_8-Binol Derivative**

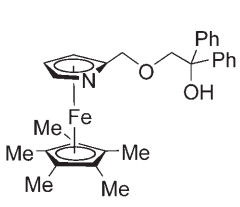
*Ying-Chuan Qin and Lin Pu**

Chiral α-substituted benzyl alcohols are ubiquitous in the structure of organic compounds. A straightforward synthesis of these compounds involves the nucleophilic addition of a phenyl–metal reagent to an aldehyde which produces a carbon–carbon bond and a stereogenic center simultaneously. Because of the high activity of phenyllithium and phenyl Grignard reagents, their asymmetric reactions with aldehydes need to be conducted in the presence of stoichiometric or excess amount of chiral reagents.[1–5]

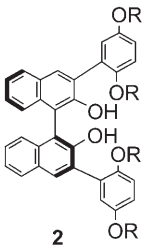


α-substituted benzyl alcohol

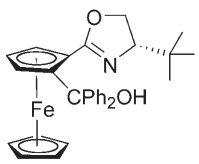
Among the catalytic asymmetric additions of the phenyl group to aldehydes,[6–16] the use of diphenylzinc has received much attention in recent years as the reagent is readily available.[10–16] In 1997, Fu and co-workers reported the addition of diphenylzinc to aldehydes catalyzed by **1** with



1



2



3

[*] Y.-C. Qin, Prof. L. Pu
Department of Chemistry
University of Virginia
Charlottesville, VA 22904-4319 (USA)
Fax: (+1) 434-924-3710
E-mail: lp6n@virginia.edu

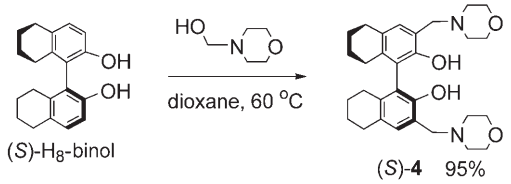
[**] The partial support of this work from the National Institutes of Health (R01M58454/R01EB002037-05) is gratefully acknowledged.

Supporting information for this article is available on the WWW under http://www.angewandte.org or from the author.

© 2006 Wiley-VCH Verlag GmbH & Co. KGaA, Weinheim

moderate enantioselectivity.[10] In 1999, we found that compound **2** showed high enantioselectivity for this reaction.[11] At about the same time, Bolm and co-workers reported good results with the use of **3**.[12] Other chiral ligands were also developed for the asymmetric addition of diphenylzinc.[13–16] A few of these compounds catalyze the addition of diphenylzinc to aromatic and α-branched aliphatic aldehydes with high enantioselectivity (>90% *ee*). However, the enantioselectivity for the addition to linear aliphatic aldehydes is generally lower, and no catalyst has been reported to give over 90% ee for the addition of diphenylzinc to a linear aliphatic aldehyde. Thus, the search for generally applicable catalysts for the asymmetric addition of diphenylzinc to aldehydes continues.

We have been interested in using 2,2′-dihydroxy-1,1′-binaphthyl (binol) and its derivatives in asymmetric processes such as catalysis and sensing. Recently, we reported a one-step synthesis of the 3,3′-substituted partially hydrogenated binol compound (*S*)-**4** from the reaction of (*S*)-H_8-binol with morpholinomethanol (Scheme 1).[17,18] This compound is a



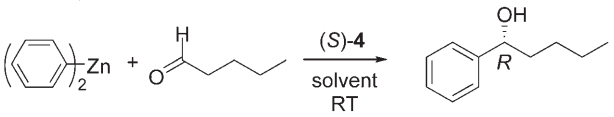
Scheme 1. Synthesis of the 3,3′-bismorpholinylmethyl H_8-binol (*S*)-**4**.

precursor to a class of bifunctional Lewis acid–base catalysts.[19] That is, the dihydroxy groups of (*S*)-**4** can produce a Lewis acidic center by reacting with a metal alkyl and the 3,3′-morpholinylmethyl groups of (*S*)-**4** can provide two Lewis basic nitrogen atoms. We found that (*S*)-**4** in combination with diethylzinc and $Ti(OiPr)_4$ catalyzed the addition of phenylacetylene to aldehydes with high enantioselectivity.[17] Herein we disclose that this compound also catalyzes the reaction of diphenylzinc with aldehydes with excellent enantioselectivity, especially in the case of linear aliphatic aldehydes.

We modified the preparation of (*S*)-**4**[18] and studied its application in the addition of diphenylzinc to valeraldehyde under various conditions at room temperature (Table 1). In solvents such as dichloromethane, toluene, and diethyl ether, (*S*)-**4** showed very low enantioselectivity (Table 1, entries 1–3; 35–39% *ee*). However, a dramatic increase in enantioselectivity was observed when the reaction was carried out in THF (Table 1, entry 4; 92% *ee*). The absolute configuration of the alcohol product was determined to be *R* by comparing its optical rotation with that reported in the literature.[20] Slow addition of the aldehyde did not change the enantioselectivity significantly (Table 1, entry 5). The use of diethylzinc and/or methanol as an additive decreased the enantioselectivity slightly (Table 1, entries 6, 7, and 8). Both increasing and decreasing the amount of the chiral ligand gave lower *ee* values (Table 1, entries 9 and 10).

We then used (*S*)-**4** to catalyze the reaction of diphenylzinc with various aliphatic and aromatic aldehydes by

Table 1: Results for the (*S*)-**4**-catalyzed addition of diphenylzinc to valeraldehyde under various conditions.[a]



Entry	(*S*)-**4** [mol%]	Solvent	Ph_2Zn [equiv]	*ee* [%][b,c]
1	10	CH_2Cl_2	1.2	35
2	10	toluene	1.2	38
3	10	Et_2O	1.2	39
4	10	THF	1.2	92
5[d]	10	THF	1.2	93
6[e]	10	THF	1.0	91
7[f]	10	THF	1.6	89
8[e,f]	10	THF	1.6	91
9	5	THF	1.2	84
10	20	THF	1.4	87

[a] Unless indicated otherwise, the following procedure was used: Solvent (2 mL, dried) was added under nitrogen to a flask containing (*S*)-**4** (12.3 mg, 0.025 mmol) and diphenylzinc (66.0 mg, 0.3 mmol). The solution was stirred at room temperature for 1 h. Valeraldehyde (0.25 mmol) was then added, and the resulting solution was stirred for 12 h. Aqueous workup and column chromatography on silica gel gave 1-phenyl-1-pentanol. [b] The products were isolated in 82–89% yield in all these reactions. [c] The *ee* values were determined by HPLC-Chiral OD column. [d] Valeraldehyde was added dropwise over 2 h. [e] (*S*)-**4** was pretreated with diethylzinc (20 mol%) for 1 h followed by the addition of diphenylzinc and aldehyde. [f] MeOH (40 mol%) was added after (*S*)-**4** was treated with diphenylzinc or diethylzinc.

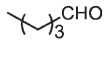
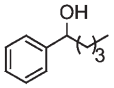
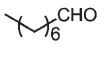
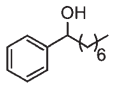
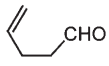
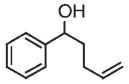
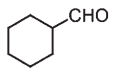
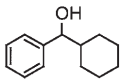
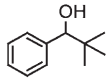
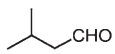
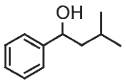
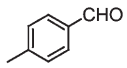
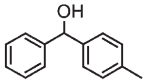
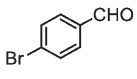
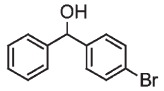
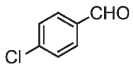
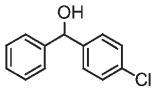
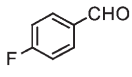
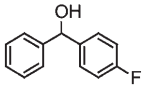
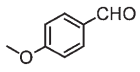
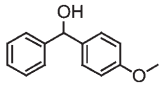
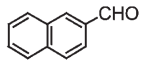
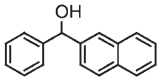
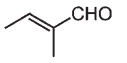
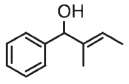
applying the conditions of entry 4 in Table 1. As summarized in Table 2, (*S*)-**4** exhibited generally high enantioselectivity for all the substrates. For the reactions of linear (Table 2, entries 1–3), α-branched (Table 2, entries 4 and 5) and β-branched (Table 2, entry 6) aliphatic aldehydes, selectivities in the range 92–98% *ee* were attained. Selectivities of 89–96% *ee* were found for the reactions of aromatic aldehydes and an α,β-unsaturated aldehyde (Table 2, entries 6–13). In all cases, the products were isolated in yields of 75–97%. Optical rotation measurements showed that the addition to aliphatic aldehydes gave *R* alcohols (Table 2, entries 1 and 5)[20a,b] and the addition to aromatic aldehydes gave *S* alcohols (Table 2, entries 9 and 10).[11,20c]

The relationship between the enantiomeric composition of the chiral ligand (*S*)-**4** and those of the products of the addition of diphenylzinc was investigated. Figure 1 displays the results obtained for the reactions of valeraldehyde and 4-fluorobenzaldehyde with diphenylzinc in the presence of (*S*)-**4** at various enantiomeric compositions. Both reactions gave a linear relationship between the *ee* value of the chiral ligand and that of the product. This suggests that the addition of diphenylzinc to either aliphatic or aromatic aldehydes might be catalyzed by a monomeric H_8-binol catalyst.

We conducted an NMR spectroscopic study for the catalytic addition of diphenylzinc to trimethylacetaldehyde in the presence of (*S*)-**4**. Trimethylacetaldehyde was chosen as the substrate for its simple ^{1}H NMR spectrum. We first monitored the interaction of (*S*)-**4** with diphenylzinc in [D_8]toluene by using ^{1}H NMR spectroscopy. Addition of diphenylzinc (1 equiv with respect to (*S*)-**4**) gave only partial

 © 2006 Wiley-VCH Verlag GmbH & Co. KGaA, Weinheim

Table 2: Diphenylzinc addition to various aldehydes catalyzed by (*S*)-**4**.

Entry	Aldehyde	Product	*t* [h]	Yield [%][a]	*ee* [%][b]
1			12	87	92
2			12	78	93
3			12	75	92
4			8	96	98
5			6	93	98
6			16	82	92
7			16	90	89
8			16	91	89
9			16	90	89
10			16	92	94
11			16	91	91
12			16	97	89
13			12	88	96

[a] Yield of isolated products. [b] Determined by HPLC-chiral column or GC-chiral column (see the Supporting Information for details).

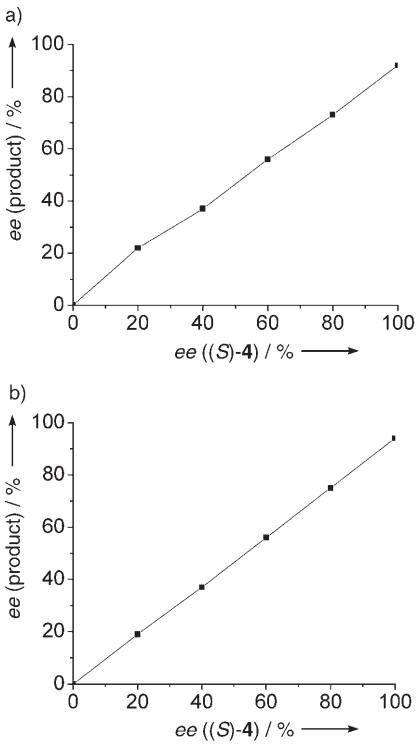
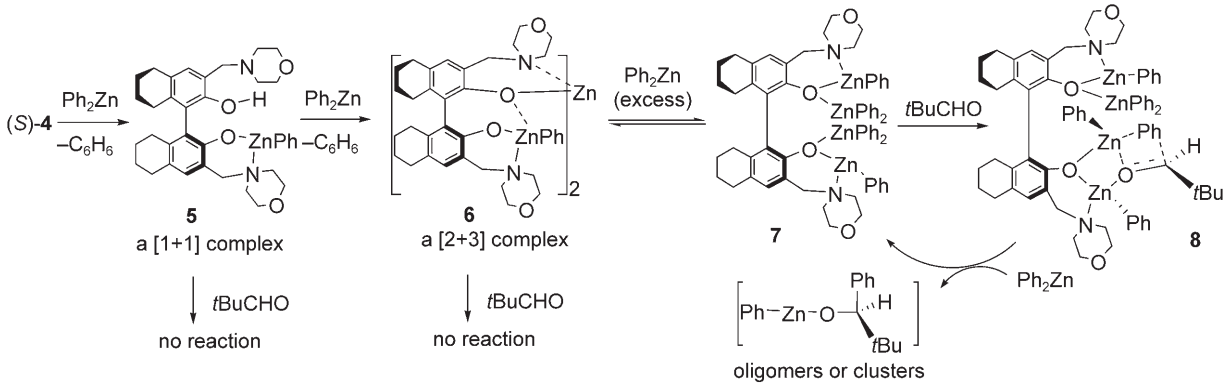


Figure 1. Relationship between *ee* values of (*S*)-**4** and those of the products of addition of diphenylzinc to a) valeraldehyde and b) 4-fluorobenzaldehyde.

deprotonation of (*S*)-**4**. The original singlet at $\delta = 9.99$ ppm for the dihydroxy protons of (*S*)-**4** diminished but multiple peaks appeared in the range of $\delta = 9.45$–9.96 ppm together with a signal indicating the formation of free benzene. Besides the signal for free benzene, the aromatic region displayed additional complicated peaks. This indicates that only one of the two hydroxy groups of (*S*)-**4** could be deprotonated by 1 equivalent of diphenylzinc and the resulting complex should contain a monophenylzinc unit {ZnPh} and a hydroxy group with a number of isomeric structures. This is understandable since the multiple Lewis basic sites of (*S*)-**4** could coordinate to the Lewis acidic {ZnPh} unit in various patterns. In Scheme 2, compound **5** represents one such [1+1] complex. When diphenylzinc (1.5 equiv with respect to (*S*)-**4**) was



Scheme 2. Tentative mechanism for the catalytic addition of diphenylzinc.

 © 2006 Wiley-VCH Verlag GmbH & Co. KGaA, Weinheim

added, all the hydroxy proton signals disappeared and the aromatic region gave sharp, clean signals at $\delta = 7.68$ (d, $J =$ 7.2 Hz, 2H); 7.55 (s, 1H); 7.48 (d, $J = 7.2$ Hz, 2H); 7.27 (t, $J =$ 7.2 Hz, 2H); 7.20 (t, $J = 7.2$ Hz, 2H); 7.18–7.10 (m, overlapping with the free benzene signal); 6.56 (s, 1H); 6.47 (s, 1H); 6.45 ppm (s, 1H). On the basis of gradient double-quantum-filtered (gDQ-COSY) and gradient heteronuclear single-quantum (gHSQC) correlation spectroscopy experiments, this complex was characterized as a [2+3] complex containing two H_8-binol ligands, three Zn centers, and a total of two phenyl groups on the Zn atoms. The four singlets in the aromatic region were assigned to the aromatic protons of two unsymmetrical H_8-binol ligands. The two doublets, two triplets, and the multiplet were assigned to the two unsymmetrical phenyl groups on the Zn centers. The ^{13}C NMR spectrum of this compound displayed six downfield singlets at $\delta = 160.1$, 158.5, 157.1, 156.7, 156.0 and 154.8 ppm: four were assigned to the aryl carbon atoms bearing the oxygen atom in the two unsymmetrical ligands and two are due to the *ipso* phenyl carbon atom connected to the Zn atom in the {ZnPh} units.[21] Compound **6** in Scheme 2 is proposed as a possible structures for the [2+3] complex generated from the reaction of diphenylzinc with the proposed [1+1] complex **5**.

Addition of trimethylacetaldehyde to the above [1+1] or [2+3] complex separately showed no reaction. This demonstrates that the phenyl group in the {ZnPh} units of **5** and **6** cannot migrate to the aldehyde. With the addition of up to 12 equivalents (with respect to (*S*)-**4**) of diphenylzinc in the absence of the aldehyde, the [2+3] complex probably dissociated completely to form a compound that may contain only one H_8-binol ligand and multiple coordinated {$ZnPh_2$} units. Its ^1H NMR spectrum showed only one singlet at $\delta =$ 6.65 ppm for the aromatic hydrogen atom of the ligand, indicating the formation of a C_2-symmetric complex as represented by **7**. The conversion of **6** into **7** may involve a metathesis process between diphenylzinc and the zinc center in **6** that contains no phenyl group to form the monophenylated zinc centers in **7**. Addition of trimethylacetaldehyde to this complex immediately led to phenyl migration to the aldehyde. Catalysis by this monomeric H_8-binol complex is consistent with the observed linear relationship between the *ee* value of the ligand and that of the product. The transition state **8** is proposed for this reaction on the basis of previous mechanistic work in the area of catalytic asymmetric organozinc additions.[22] Multiple peaks at $\delta = 4.85$–4.25 (*t*BuC*H*Ph) and at 0.95–0.60 ppm ($(CH_3)_3C$) suggest the formation of various zinc alkoxide products from the addition of phenyl to the aldehyde. These zinc alkoxides probably existed as oligomers or clusters. After complete consumption of diphenylzinc by excess trimethylacetaldehyde, the [2+3] complex reappeared. Addition of D_2O to the reaction mixture converted the zinc alkoxide products into 2,2-dimethyl-1-phenyl-1-propanol with two singlets observed at $\delta = 4.01$ and 0.89 ppm in the ^1H NMR spectrum. The ligand (*S*)-**4** was also regenerated. The mechanism depicted in Scheme 2 on the basis of the NMR study illustrates our current understanding of this catalytic process and more work will be conducted.

In summary, (*S*)-**4** allows high enantioselectivity in the reaction of diphenylzinc with both aliphatic and aromatic aldehydes and, especially, is the most enantioselective catalyst for linear aliphatic aldehydes. Unlike other catalysts developed for the addition of diphenylzinc—which often require the addition of a significant amount of diethylzinc with cooling (or heating) the reaction mixture to ensure high enantioselectivity—the use of (*S*)-**4** avoids the need for additive and gives excellent results at room temperature. The one-step synthesis of this ligand from H_8-binol and the mild asymmetric reaction conditions make this chiral catalyst practically useful for general synthesis. The NMR study has also revealed a few interesting mechanistic characteristics of this catalytic process.

Received: September 8, 2005
Published online: November 29, 2005

Keywords: alcohols · aldehydes · asymmetric synthesis · nucleophilic addition · zinc

[1] D. Seebach, A. K. Beck, S. Roggo, A. Wonnacott, *Chem. Ber.* **1985**, *118*, 3673–3682.
[2] R. Noyori, S. Suga, K. Kawai, S. Okada, M. Kitamura, *Pure Appl. Chem.* **1988**, *60*, 1597–1606.
[3] M. Nakajima, K. Tomioka, K. Koga, *Tetrahedron* **1993**, *49*, 9751–9758.
[4] J.-T. Wang, X. Fan, X. Feng, Y.-M. Qian, *Synthesis* **1989**, 291–292.
[5] M. Kaino, K. Ishihara, H. Yamamoto, *Bull. Chem. Soc. Jpn.* **1989**, *62*, 3736–3738.
[6] B. Weber, D. Seebach, *Tetrahedron* **1994**, *50*, 7473–7484.
[7] M. Sakai, M. Ueda, N. Miyaura, *Angew. Chem.* **1998**, *110*, 3475–3477; *Angew. Chem. Int. Ed.* **1998**, *37*, 3279–3281.
[8] a) C. Bolm, M. Kesselgruber, A. Grenz, N. Hermanns, J. P. Hildebrand, *New J. Chem.* **2001**, *25*, 13–15; b) J. Rudolph, F. Schmidt, C. Bolm, *Synthesis* **2005**, 840–842; c) C. Bolm, J. Rudolph, *J. Am. Chem. Soc.* **2002**, *124*, 14850–14851.
[9] a) J. X. Ji, J. Wu, T. T. L. Au-Yeung, C. W. Yip, R. K. Haynes, A. S. C. Chan, *J. Org. Chem.* **2005**, *70*, 1093–1095; b) X. Y. Wu, X. Y. Liu, G. Zhao, *Tetrahedron: Asymmetry* **2005**, *16*, 2299–2305.
[10] a) P. I. Dosa, J. C. Ruble, G. C. Fu, *J. Org. Chem.* **1997**, *62*, 444–445; b) P. I. Dosa, G. C. Fu, *J. Am. Chem. Soc.* **1998**, *120*, 445–446.
[11] a) W.-S. Huang, L. Pu, *J. Org. Chem.* **1999**, *64*, 4222–4223; b) W. S. Huang, L. Pu, *Tetrahedron Lett.* **2000**, *41*, 145–149.
[12] a) C. Bolm, K. Muñiz, *Chem. Commun.* **1999**, 1295–126; b) C. Bolm, N. Hermanns, J. P. Hildebrand, K. Muñiz, *Angew. Chem.* **2000**, *112*, 3607–3609; *Angew. Chem. Int. Ed.* **2000**, *39*, 3465–3467; c) C. Bolm, M. Kesselgruber, N. Hermanns, J. P. Hildebrand, G. Raabe, *Angew. Chem.* **2001**, *113*, 1536–1538; *Angew. Chem. Int. Ed.* **2001**, *40*, 1488–1490.
[13] a) G. Zhao, X.-G. Li, X.-R. Wang, *Tetrahedron: Asymmetry* **2001**, *12*, 399–403; b) D.-H. Ko, K. H. Kim, D.-C. Ha, *Org. Lett.* **2002**, *4*, 3759–3762.
[14] M. G. Pizzuti, S. Superchi, *Tetrahedron: Asymmetry* **2005**, *16*, 2263–2269.
[15] J. M. Betancort, C. Garcia, P. J. Walsh, *Synlett* **2004**, 749–760.
[16] M. Fontes, X. Verdaguer, L. Solà, M. A. Pericàs, A. Riera, *J. Org. Chem.* **2004**, *69*, 2532–2543.
[17] L. Liu, L. Pu, *Tetrahedron* **2004**, *60*, 7427–7430.
[18] See the Supporting Information.
[19] Selected references on 1,1′-binaphthyl-based bifunctional catalysts: a) M. Kanai, N. Kato, E. Ichikawa, M. Shibasaki, *Synlett* **2005**, 1491–1508; b) K. Matsui, S. Takizawa, H. Sasai, *J. Am.*

 © 2006 Wiley-VCH Verlag GmbH & Co. KGaA, Weinheim

Chem. Soc. **2005**, *127*, 3680 – 3681; c) Y. Hamashima, D. Sawada, M. Kanai, M. Shibasaki, *J. Am. Chem. Soc.* **1999**, *121*, 2641 – 2642; d) J. Casas, C. Nájera, J. M. Sansano, J. M. Saá, *Org. Lett.* **2002**, *4*, 2589 – 2592; e) E. F. DiMauro, M. C. Kozlowski, *Org. Lett.* **2001**, *3*, 1641 – 1644.

[20] a) K. H. Yong, N. J. Taylor, J. M. Chong, *Org. Lett.* **2002**, *4*, 3553 – 3556; b) A. M. Hayes, D. J. Morris, G. J. Clarkson, M. Wills, *J. Am. Chem. Soc.* **2005**, *127*, 7318 – 7319; c) G. E. Job, A. Shvets, W. H. Pirkle, S. Kuwahara, M. Kosaka, Y. Kasai, H. Taji, K. Fujita, M. Watanabe, N. Harada, *J. Chromatogr. A* **2004**, *1055*, 41 – 53.

[21] The ^{13}C NMR spectrum of diphenylzinc in [D_8]toluene showed a singlet at $\delta = 148.4$ ppm for the carbon atom connected to the Zn center.

[22] Selected references on the mechanistic studies of the asymmetric organozinc additions: a) S. Itsuno, J. M. J. Frèchet, *J. Org. Chem.* **1987**, *52*, 4142 – 4143; b) M. Kitamura, S. Suga, H. Oka, R. Noyori, *J. Am. Chem. Soc.* **1998**, *120*, 9800 – 9809; c) B. Goldfuss, K. N. Houk, *J. Org. Chem.* **1998**, *63*, 8998 – 9006; d) T. Rasmussen, P.-O. Norrby, *J. Am. Chem. Soc.* **2003**, *125*, 5130 – 5138; e) J. Rudolph, C. Bolm, P.-O. Norrby, *J. Am. Chem. Soc.* **2005**, *127*, 1548 – 1552; f) A review: L. Pu, H.-B. Yu, *Chem. Rev.* **2001**, *101*, 757 – 824.

 © 2006 Wiley-VCH Verlag GmbH & Co. KGaA, Weinheim

Charge Transfer

DOI: 10.1002/anie.200502386

High-Pressure Probing of a Changeover in the Charge-Transfer Mechanism for Intact Cytochrome *c* at Gold/Self-Assembled Monolayer Junctions**

Dimitri E. Khoshtariya, Tina D. Dolidze, David Sarauli, and Rudi van Eldik**

High-pressure (HP) kinetic studies provide unique information about the activation volumes for various processes and add a new dimension to the development of fundamental mechanistic understanding.[1–3] Application of this technique along (or in combination) with other kinetic approaches also seems to be promising for biological processes, including charge-transfer (CT) reactions.[4–6] However, even for small and well-characterized proteins such as cytochrome *c* (CytC),[7,8] an intrinsic CT mechanism in "homogeneous" systems is difficult to recognize conclusively as a consequence of the extra structural and dynamic environmental complexity introduced by the participating redox partner.[4,5,9–11] The covalent attachment of "small" complex ions as the redox counterparts at different external sites of CytC[12,13] does not warrant sufficiently smooth variation of intrinsic parameters, such as an electronic coupling (correlated with the CT distance; see below), because of the highly inhomogeneous nature of the protein interior. In this context, artificial bioelectrochemical devices made of electrode-deposited self-assembled monolayer (SAM) films of variable composition and thickness, and CytC or other redox proteins attached or freely diffusing to the SAM terminal groups (also subject to wide variations), were proven to be systems with well-controlled variable parameters, and hence suitable for fundamental studies[8,14–18] and some technological applications.[7,8]

Previous work that exploited SAM-implicated bioelectrochemical systems revealed kinetic behavior and a distinct change in mechanism with the CT distance for cases with CytC irreversibly attached (probably heavily altered in the native structure) to SAM terminal groups.[15–18] Only fragmentary work has been performed for totally intact CytC freely diffusing to electrode/SAM junctions,[8,19,20] which includes our pioneering HP kinetic study of CytC at "primitively" modified Au electrodes.[6] In the latter work, however, it was demonstrated for the first time that the application of hydrostatic pressure allows a variation of the internal viscosity (conformational mobility) of the protein without significant variation of the properties of the aqueous medium.

Herein, we report a changeover in the intrinsic mechanism for freely diffusing, unbound CytC as clearly observed in HP kinetic experiments, which reveal an evident trend in the activation volume from essentially positive (for short-range CT) to essentially negative (for long-range CT) values through an intermediate zero magnitude. By exploiting bioelectrochemical devices that comprise CytC weakly interacting with hydroxy-terminated alkanethiol SAMs of variable thickness ($[-S-(CH_2)_n-OH]$, where $n = 2$, 3, 4, 6, 11) deposited on Au disk electrodes, we took advantage of independent and gradual variation of the electron-transfer (ET) distance (directly affecting electronic coupling[12,13,21–23]), hydrostatic pressure (directly affecting the intrinsic friction of the protein[6,24]), and solution viscosity (externally affecting the intrinsic friction of the protein,[25–27] and applied here for the purposes of cross-testing). Fast-scan cyclic voltammetry (CV)[28,29] was applied in most cases (for $n = 2$, 3, 4, 6) to determine the heterogeneous standard rate constant. This method has been proven to be fully adequate for both the determination of the physical condition (structural accomplishment) of composite systems and the accurate determi-

[*] Prof. Dr. D. E. Khoshtariya, D. Sarauli, Prof. Dr. R. van Eldik
Institute for Inorganic Chemistry
University of Erlangen-Nürnberg
Egerlandstr. 1, 91058 Erlangen (Germany)
Fax: (+49) 913-185-27387
E-mail: dimitri.k@joker.ge
vaneldik@chemie.uni-erlangen.de
Prof. Dr. D. E. Khoshtariya, Dr. T. D. Dolidze
Institute of Molecular Biology and Biophysics
and Institute of Inorganic Chemistry and Electrochemistry
Georgian Academy of Sciences
Gotua 12, 0160 Tbilisi (Georgia)
Fax: (+995) 32-959-157

[**] Resumption of the Alexander von Humboldt Fellowship for D.E.K. is kindly acknowledged. R.v.E. gratefully acknowledges financial support from the Deutsche Forschungsgemeinschaft as part of SFB 583 on "Redox-Active Metal Complexes". D.E.K. is grateful to Prof. W. Schmickler for helpful comments.

Supporting information for this article is available on the WWW under http://www.angewandte.org or from the author.

 © 2006 Wiley-VCH Verlag GmbH & Co. KGaA, Weinheim

nation of dynamic characteristics, such as heterogeneous kinetic constants and diffusion coefficients, under variable experimental conditions.[6,8,30,31] The methods for preparation of the SAM-modified electrodes,[19,20] the instrumentation,[6] and the HP setup[2,6] were similar to those reported elsewhere, and are also briefly described in the Supporting Information.

For freely diffusing reactant species such as CytC, the experimentally determined standard heterogeneous rate constant is obtained at zero overvoltage (zero driving force) within the framework of the conventional encounter pre-equilibrium model with the accuracy of a scaling factor, that is, the pre-equilibrium term that could be assumed to be constant within the series of SAMs with identical terminal groups.[6,8,31–34] This heterogeneous rate constant can be associated with the intrinsic unimolecular rate constant representative of either nonadiabatic (long-range) or adiabatic (short-range) CT processes.[6,31] Theoretical work that accounts for both mechanisms and the smooth changeover between them is available.[35–40] The recently updated[18] expression is shown in Equation (1), where H_{if} is the

$$k_{ET}^{0} = \frac{(H_{if})^2}{\hbar}\frac{\rho_m}{1+g}\left(\frac{\pi^3 RT}{\lambda}\right)^{1/2}\exp\left(-\frac{\Delta G_a}{RT}\right) \quad (1)$$

electronic coupling matrix element, λ is the reorganization free energy, and ρ_m is the density of electronic states in the metal (electrode). The activation free energy under the experimental conditions of the present work can be defined as $\Delta G_a \approx \lambda/4$.[6,8,22,30,31]

The adiabaticity criterion g, which acts as a control parameter, is given by Equation (2),[18,34,36,39,40] where the

$$g = \frac{\pi^3 RT(H_{if})^2\rho_m}{\hbar\nu_{eff}\lambda} \quad (2)$$

effective frequency ν_{eff} is related to a single or several relaxation process(es) in the vicinity of the reaction zone, which are intrinsically coupled to electron transfer (actually, $\nu_{eff} \approx \eta$, where η is the effective viscosity of the medium[35–40]). With either $g \ll 1$ or $g \gg 1$, which depends on the values of intrinsic parameters from Equation (1) (especially of H_{if}, the value of which can be varied greatly in our experiments), one arrives at two different expressions for the intrinsic rate constant. These equations include phenomenological extensions for the long-range CT [Eq. (3)], where R_e is the CT

$$k_{ET} \propto \exp[-\beta(R_e - R_0)] \quad (3)$$

distance and β is the decay parameter, which is normally of the order of about 1 $Å^{-1}$,[12–18,23,31] and for the short-range CT [Eq. (4)], where δ is an "empirical" solvent–protein coupling

$$k_{ET} \propto \eta^{-\delta} \quad (4)$$

parameter with values between 0 and 1, and $\delta \approx 1$ represents full solvent–protein coupling.[25–27,32,35–40]

A general expression for the activation volume of any kind of microscopic barrier-crossing process, including ET, can be defined as shown in Equation (5).[1–3] By substitution of

$$\Delta V_a = -RT\left[\frac{\partial(\ln k)}{\partial P}\right]_T \quad (5)$$

Equations (1) and (3), and omitting minor terms, one obtains Equation (6).[41–43] This equation indicates that the experimentally measurable volume of activation [Eq. (5)] may originate from the effects of pressure on the ET distance as a result of shrinking of the reactive (SAM/protein) system and/or a change in the medium (SAM/protein/solvent) reorganization energy (Franck–Condon factor).

$$\Delta V_{a(NA)} = \beta RT\left(\frac{\partial R_e}{\partial P}\right)_T + \frac{1}{4}\left(\frac{\partial\lambda}{\partial P}\right)_T \quad (6)$$

On considering the effect of pressure on the adiabatic, viscosity-dependent ET process [Eqs. (1) and (4)], and again omitting the minor terms, one arrives at Equation (7),[3,44]

$$\Delta V_{a(AD)} = \beta RT\left(\frac{\partial\ln\eta}{\partial P}\right)_T + \frac{1}{4}\left(\frac{\partial\lambda}{\partial P}\right)_T \quad (7)$$

from which it follows that in the case of full dynamic control [Eq. (4); $\delta \approx 1$], viscosity changes arising from increasing pressure may result in a large positive contribution provided that viscosity is affected by pressure. This is the case for all known liquids except water.[3,6,44] Actually, for most solvents, η increases exponentially with pressure and yields a maximum net viscosity-related contribution as high as $+20\ cm^3\ mol^{-1}$ (as the upper limit[3,44]).

In addition, we assume that for composite multicomponent systems, as in the present case, the overall medium reorganization energy can be roughly reproduced by summation over individual components [Eq. (8)],[45–47] where the

$$\lambda = \lambda_{solv} + \lambda_{prot} + \lambda_{SAM} \quad (8)$$

three contributions to λ represent the solvent, protein, and SAM interior, respectively (see below).

Figure 1a shows the dependence of the experimental standard heterogeneous rate constant, k_{ET}^{0}, on the number of SAM methylene units. The matching numerical values, the data obtained at different concentrations of glucose (0, 100, 200, 300, and 400 $g\,L^{-1}$), and the corresponding viscosity values are available in the Supporting Information. The upper curve, clearly distinguishable for SAMs with $n = 2$, 3, and 4, represents kinetic data obtained in the absence of a viscous additive, and the two other curves that merge with the former one at $n = 6$ and 11 represent kinetic data obtained at a higher solution viscosity in the presence of 200 and 400 $g\,L^{-1}$ glucose, respectively. Kinetic data obtained at $n = 6$ and 11, which give larger electrode–reactant separations, demonstrate an exponential decay of the rate constant with increasing distance [Eq. (3)] in all three cases, with a slope of about 1 per CH_2 unit. This finding is in excellent agreement with previous results obtained for various composite systems.[12–18,23,31] Meanwhile, SAMs with $n = 2$ and 3 clearly demonstrate a

 © 2006 Wiley-VCH Verlag GmbH & Co. KGaA, Weinheim

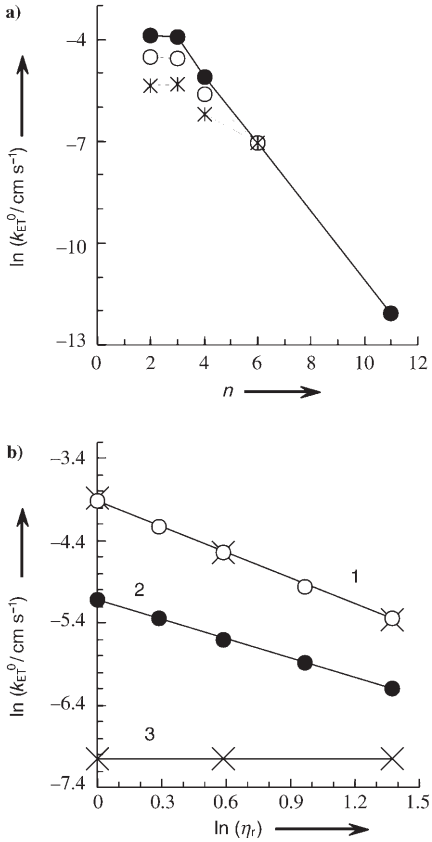


Figure 1. a) Natural logarithm of the heterogeneous standard rate constant for the CytC electron exchange at Au electrodes modified by hydroxy-terminated *n*-alkanethiol SAMs ($n=2$, 3, 4, 6, 11) versus number of methylene units *n* at different solution viscosities. Upper curve (●): no viscous additive, $\eta_r=1$; middle curve (○), $\eta_r=1.80$; lower curve (*), $\eta_r=3.96$. Note that all three curves merge at $n=6$ and 11, and form a single sloped line. b) Natural logarithm of the heterogeneous standard rate constant for the CytC electron exchange at Au electrodes modified by hydroxy-terminated *n*-alkanethiol SAMs versus logarithm of solution relative viscosity (η_r). Plot 1: two coinciding plots for $n=2$ (×) and $n=3$ (○); plot 2: $n=4$ (●); plot 3: $n=6$ (×). Note that the numerical values are averaged over three to five independent experiments. The symbols are larger than actual error bars throughout.

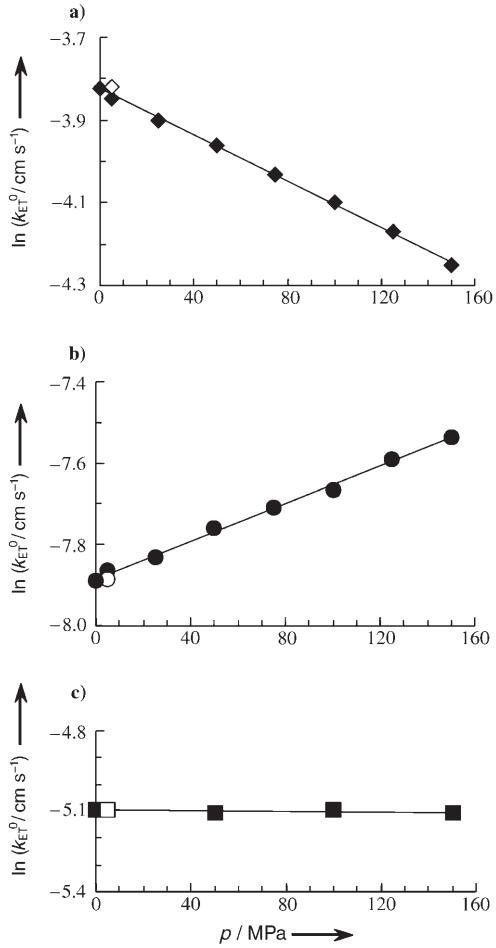


Figure 2. Natural logarithm of the heterogeneous standard rate constant for the CytC electron exchange at Au electrodes modified by hydroxy-terminated *n*-alkanethiol SAMs ($n=3$,4,6) versus hydrostatic pressure *p*: a) $n=3$: ◇, ◆; b) $n=6$: ○, ●; c) $n=4$: □, ■. The symbols are larger than actual error bars for each pressure-cycle experiment. The reported numerical values for the activation volumes are averaged over three to five independent pressure cycles.

plateau region. The data for the SAM with $n=4$ fall in the intermediate region.

Figure 1b shows the standard heterogeneous rate constant, k_{ET}^0, versus the relative solution viscosity for SAMs with $n=2$, 3, 4, and 6. Phenomenologically, these dependencies can be approximated by Equation (4) with power indexes (the actual slopes in Figure 2b) of $\delta=1$ ($n=2, 3$), 0.7 ($n=4$), and 0 ($n=6$, 11; the latter case is not shown in Figure 2b; see Supporting Information). The "limiting" value of about 0.6 was detected in the case of specific adsorption on the pyridine-terminated thin SAMs (plateau region).[18] Somewhat larger slopes were found for an ET within the "homogeneous" system involving zinc-substituted CytC, and wild-type and mutant cupriplastocyanin, which ranged from 0.7 to 0.9.[9–11] Interestingly, full viscosity control ($\delta\approx1$) has been observed for photoinduced CT from the artificial Ru-coordinated polypeptide electron donor to ferri-CytC,[48] which occurs through the loosely bound (encounter) complex as opposed to the "preformed" (tight) complex involving the same reactants ($\delta\approx0.6$); both patterns occur simultaneously. The latter findings closely match the whole pattern of CytC bioelectrochemical CT in both the tightly bound and freely diffusing (to Au-deposited SAMs comprising ω-COOH and ω-OH) regimes, respectively.

In addition, recent experimental and computational results obtained for a related system—a "charge-modified" complex of a photosynthetic reaction center (PRC) and cytochrome c_2[49,50]—together with our detailed analysis[51] for the case of CytC freely diffusing to hydroxy-terminated SAMs, strongly suggest the formation of a solvent-separated, softly stabilized complex as an encounter-reactive associate (see below).

The dependence of $\ln(k_{ET}^0)$ on the hydrostatic pressure up to 150 MPa for SAMs with $n=3$, 4, and 6 is shown in Figure 2a–c, respectively. It can be seen that for a SAM with $n=3$, the value of $\ln(k_{ET}^0)$ decreases linearly with pressure and yields a positive volume of activation of $+6.7\pm0.5$ cm^3 mol^{-1}

 © 2006 Wiley-VCH Verlag GmbH & Co. KGaA, Weinheim

(Figure 3a, and the Supporting Information). This value is very close to $+6.1 \pm 0.5\ cm^3 mol^{-1}$ which is found in the case of Au electrodes modified by 4,4′-bipyridyl and 4,4′-bipyridyl disulfide (the case of "primitive" thin SAMs).[6] On the contrary, for a much thicker SAM with $n = 6$, we found that the value of $\ln(k_{ET}^0)$ increases linearly with increasing pressure to yield a negative volume of activation of $-5.5 \pm 0.5\ cm^3 mol^{-1}$ (Figure 2b). In the case of a SAM with $n = 4$, an intermediate behavior is displayed with no effect of pressure on k_{ET}^0, to give $\Delta V_a \approx 0$ (Figure 2c and Supporting Information). To our knowledge, this is the first observation of a changeover of the HP kinetic response for a given bio(electro)chemical system. Hence, it is demonstrated that the HP studies provide direct, adequate, and fully complementary kinetic information suitable for the mechanistic analysis, as compared to more conventional experimental approaches.

In summary, three different strategies, namely, variation of the SAM thickness, solution viscosity, and hydrostatic pressure, all clearly indicate a definite switch in the intrinsic mechanism behind the change in specific performance with the change in CT distance. Importantly, this general conclusion is model-free, that is, independent of the theoretical interpretation. Consecutively, it is reasonable to attribute the observed kinetic effects that result from the alkane chain length, viscosity, and pressure variations to respective changes of the intrinsic unimolecular rate constant. Indeed, it is very unlikely that some variation of the internal order of the SAMs with the alkane chain length[52,53] would cause significant changes in the pre-equilibrium term, to exactly mimic three kinds of effects theoretically predictable *specifically* for the intrinsic CT constant. This argument, above all, is valid in the case of a "bulky" reactant such as CytC reacting in the free regime at the solvent-separated distance from the SAM "surface", as it is presumably almost insensitive to the extent of the SAM disorder (which is actually unimportant in many practical cases[8,15,16,31]). Furthermore, this natural assumption allows one to rationalize the whole variety of experimental results in terms of the self-consistent unified (extended) CT theory [Eqs. (1), (2), (6), and (7)].[54]

To this extent, within the framework of the generalized theoretical model adopted here, the HP kinetic results fully conform with two types of intrinsic mechanisms of CT, namely, nonadiabatic (long-range) and adiabatic (short-range) processes, in good accordance with two other experimental manifestations fully exhibited by our experiments. The individual components that contribute to the experimental volumes of activation (see Supporting Information) can be estimated on the basis of Equations (6) and (7) by assuming that the overall value of $\lambda = 0.6$–$0.8\ eV$[8,17–20] (representing the Franck–Condon term) is roughly composed of about 50% "outer-sphere" (solution) component, which can contribute about half of the activation volume, and about 50% "inner-sphere" protein reorganization component that is negligibly altered by pressure (resulting in a zero activation volume contribution).[42] Moreover, the reorganizational component due to the SAM interior seems to be negligible ($\lambda_{SAM} \approx 0$),[47] which also yields the zero activation volume increment. Further bioelectrochemical HP kinetic experiments with the participation of other, less well-studied redox proteins are planned to extend profound CT mechanistic studies.

Finally, this is the first time that the CT mechanism changeover has been clearly detected by a HP kinetic strategy. The changeover in CT mechanism has been cross-tested and proven by three independent experimental approaches. Furthermore, two distinct CT mechanisms and their changeover have been detected for freely diffusing, intact CytC molecules. The exponential decrease in the standard rate constant with increasing CT distance at larger CytC–electrode separations ($n = 6$, 11) has been shown to be in full accord with the well-established signature of nonadiabatic CT. Full viscosity control has been detected for freely diffusing CytC, presumably operating in the extreme adiabatic, "friction-controlled" regime in the case of thinner SAMs ($n = 2$, 3). The "intermediate" regime for the CT of CytC ($n = 4$) has been detected by using all three approaches. In addition, all the experimental results can be nicely described within the unified theoretical framework (extended CT theory).

Received: July 8, 2005
Revised: September 15, 2005
Published online: November 28, 2005

Keywords: charge transfer · cytochromes · gold · high-pressure chemistry · kinetics · monolayers

[1] *High Pressure Chemistry* (Eds.: R. van Eldik, F.-G. Klärner), Wiley-VCH, Weinheim, **2002**.
[2] A. Drljaca, C. D. Hubbard, R. van Eldik, T. Asano, M. V. Basilevsky, W. J. Le Noble, *Chem. Rev.* **1998**, *98*, 2167–2290.
[3] a) T. W. Swaddle, P. A. Tregloan, *Coord. Chem. Rev.* **1999**, *187*, 255–289; b) T. W. Swaddle, *Chem. Rev.* **2005**, *105*, 2573–2608.
[4] M. Meier, J. Sun, J. F. Wishart, R. van Eldik, *Inorg. Chem.* **1996**, *35*, 1564–1570.
[5] J. Sun, C. Su, M. Meier, S. S. Isied, J. F. Wishart, R. van Eldik, *Inorg. Chem.* **1998**, *37*, 6129–6135.
[6] T. D. Dolidze, D. E. Khoshtariya, D. H. Waldeck, J. Macyk, R. van Eldik, *J. Phys. Chem. B* **2003**, *107*, 7172–7179.
[7] *Cytochrome c: A Multidisciplinary Approach* (Eds.: R. A. Scott, A. G. Mauk), University Science Books, Sausalito, CA, **1996**.
[8] M. Fedurco, *Coord. Chem. Rev.* **2000**, *209*, 263–331.
[9] L. Qin, N. M. Kostić, *Biochemistry* **1994**, *33*, 12592–12599.
[10] M. M. Crnogorac, C. Shen, S. Young, Ö. Hansson, N. M. Kostić, *Biochemistry* **1996**, *35*, 16465–16474.
[11] M. M. Ivković-Jensen, G. M. Ullmann, S. Young, Ö. Hansson, M. M. Crnogorac, M. Ejdeback, N. M. Kostić, *Biochemistry* **1998**, *37*, 9557–9569.
[12] J. R. Winkler, A. J. Di Bilio, N. A. Farrow, J. H. Richards, H. B. Gray, *Pure Appl. Chem.* **1999**, *71*, 1753–1764.
[13] H. B. Gray, J. R. Winkler, *Proc. Natl. Acad. Sci. USA* **2005**, *102*, 3534–3539.
[14] M. J. Tarlov, E. F. Bowden, *J. Am. Chem. Soc.* **1991**, *113*, 1847–1849.
[15] A. Avila, B. W. Gregory, K. Niki, T. M. Cotton, *J. Phys. Chem. B* **2000**, *104*, 2759–2766.
[16] K. Niki, W. R. Hardi, M. G. Hill, H. Li, J. R. Sprinkle, E. Margoliash, K. Fujita, R. Tanimura, N. Nakamura, H. Ohno, J. H. Richards, H. B. Gray, *J. Phys. Chem. B* **2003**, *107*, 9947–9949.

 © 2006 Wiley-VCH Verlag GmbH & Co. KGaA, Weinheim

[17] J. Wei, H. Liu, D. E. Khoshtariya, H. Yamamoto, A. Dick, D. H. Waldeck, *Angew. Chem.* **2002**, *114*, 4894 – 4897; *Angew. Chem. Int. Ed.* **2002**, *41*, 4700 – 4703.
[18] D. E. Khoshtariya, J. Wei, H. Liu, H. Yue, D. H. Waldeck, *J. Am. Chem. Soc.* **2003**, *125*, 7704 – 7714.
[19] S. Terrettaz, J. Cheng, C. J. Miller, R. D. Guiles, *J. Am. Chem. Soc.* **1996**, *118*, 7857 – 7858.
[20] J. Cheng, S. Terrettaz, C. J. Blankman, C. J. Miller, R. D. Dangi, R. D. Guiles, *Isr. J. Chem.* **1997**, *37*, 259 – 266.
[21] R. R. Dogonadze, A. M. Kuznetsov, J. Ulstrup, *J. Theor. Biol.* **1977**, *69*, 239 – 263.
[22] R. A. Marcus, N. Sutin, *Biochim. Biophys. Acta* **1985**, *811*, 265 – 322.
[23] D. N. Beratan, J. N. Betts, J. N. Onuchic, *Science* **1991**, *252*, 1286 – 1288.
[24] H. Frauenfelder, N. A. Alberding, A. Ansari, D. Braunstein, B. Cowen, M. K. Hong, I. E. T. Iben, J. B. Johnson, S. Luck, M. C. Marden, J. R. Mourant, P. Ormos, L. Reinisch, R. Scholl, A. Schulte, E. Shyamsunder, L. B. Soremen, P. J. Steinbach, A. Xie, R. D. Young, K. T. Yue, *J. Phys. Chem.* **1990**, *94*, 1024 – 1037.
[25] D. Beece, L. Eisenstein, H. Frauenfelder, D. Good, M. C. Marden, L. Reinisch, A. H. Reynolds, L. B. Sorensen, K. T. Yue, *Biochemistry* **1980**, *19*, 5147 – 5157.
[26] N. G. Goguadze, D. E. Khoshtariya, J. M. Hammerstad-Pedersen, J. Ulstrup, *Eur. J. Biochem.* **1991**, *200*, 423 – 429.
[27] B. Gavish, S. Yedgar in *Protein–Solvent Interactions* (Ed.: R. B. Gregory), Marcel Dekker, New York, **1995**, pp. 343 – 373.
[28] a) R. S. Nicholson, *Anal. Chem.* **1965**, *37*, 1351 – 1355; b) R. S. Nicholson, I. Shain, *Anal. Chem.* **1964**, *36*, 706 – 723.
[29] A. J. Bard, L. R. Faulkner, *Electrochemical Methods: Fundamentals and Applications*, 2nd ed., Wiley, New York, **2001**, pp. 226 – 260.
[30] A. M. Bond, *Inorg. Chim. Acta* **1994**, *226*, 293 – 340.
[31] D. E. Khoshtariya, T. D. Dolidze, L. D. Zusman, D. H. Waldeck, *J. Phys. Chem. A* **2001**, *105*, 1818 – 1829.
[32] M. D. Newton, H. L. Friedman, *J. Chem. Phys.* **1985**, *83*, 5210 – 5218.
[33] J. T. Hupp, M. J. Weaver, *J. Electroanal. Chem.* **1983**, *152*, 1 – 14.
[34] A. Gochev, G. E. McManis, M. J. Weaver, *J. Chem. Phys.* **1989**, *91*, 906 – 916.
[35] H. A. Kramers, *Physica (Utrecht)* **1940**, *7*, 284 – 304.
[36] a) L. D. Zusman, *Chem. Phys.* **1980**, *49*, 295 – 304; b) L. D. Zusman, *Chem. Phys.* **1987**, *112*, 53 – 59; c) L. D. Zusman, *Z. Phys. Chem.* **1994**, *186*, 1 – 29.
[37] D. F. Calef, P. G. Wolynes, *J. Phys. Chem.* **1983**, *87*, 3387 – 3400.
[38] J. T. Hynes, *J. Phys. Chem.* **1986**, *90*, 3701 – 3706.
[39] D. N. Beratan, J. N. Onuchic, *J. Chem. Phys.* **1988**, *89*, 6195 – 6203.
[40] M. Bixon, J. Jortner, *Adv. Chem. Phys.* **1999**, *106*, 35 – 202.
[41] N. A. Lewis, R. R. McNeer, D. V. Taveras, *Inorg. Chim. Acta* **1994**, *225*, 89 – 93.
[42] O. Miyashita, N. Go, *J. Phys. Chem. B* **1999**, *103*, 562 – 571.
[43] V. Furukawa, K. Ishimori, I. Moroshima, *J. Phys. Chem. B* **2000**, *104*, 1817 – 1825.
[44] Y. Fu, A. S. Cole, T. W. Swaddle, *J. Am. Chem. Soc.* **1999**, *121*, 10410 – 10415.
[45] Y. I. Kharkats, L. I. Krishtalik, *J. Theor. Biol.* **1985**, *112*, 221 – 249.
[46] I. Muegge, P. X. Qi, A. J. Wand, Z. T. Chu, A. Warshel, *J. Phys. Chem. B* **1997**, *101*, 825 – 836.
[47] Y.-P. Liu, M. D. Newton, *J. Phys. Chem.* **1994**, *98*, 7162 – 7169.
[48] R. C. Lacey, L. Liu, L. Zang, M. Y. Ogawa, *Biochemistry* **2003**, *42*, 3904 – 3910.
[49] M. Tetreault, S. H. Rongey, G. Feher, M. Y. Okamura, *Biochemistry* **2001**, *40*, 8452 – 8462.
[50] O. Miyashita, M. Y. Okamura, J. N. Onuchic, *Proc. Natl. Acad. Sci. USA* **2005**, *102*, 3558 – 3563.
[51] D. E. Khoshtariya, T. D. Dolidze, R. van Eldik, et al., unpublished results.
[52] M. D. Porter, T. B. Bright, D. L. Allara, C. E. D. Chidsey, *J. Am. Chem. Soc.* **1987**, *109*, 3559 – 3568.
[53] a) V. Bindu, T. Pradeep, *Vacuum* **1998**, *49*, 63 – 66; b) N. Sandhyarani, T. Pradeep, *Int. Rev. Phys. Chem.* **2003**, *22*, 221 – 262.
[54] An attempt to ascribe the observed effects (or one of the effects) to the variation of the pre-equilibrium term unavoidably gives rise to a cascade of rather strained and controversial assumptions; for example, that the kinetic viscosity effects for CytC CT in the cases of "homogeneous"[48] and electrochemical, namely, tightly bound[15,18] and freely diffusing (this work), regimes are of totally different origin. Similarly, the designation of the onset of the plateau region in Figure 1a to some disorder in short SAMs ($n = 2, 3, 4$) makes the explanation of analogous occurrences for the cases of ω-Py[17,18] and ω-COOH[15,18] SAMs (which occur at $n \approx 8$ and 12, respectively) very confusing, as the alkanethiol SAMs with $n = 6$–12 are known to be the most stable within the sequence[53]. Further extended analysis of these and related mechanistic aspects will be presented elsewhere.[51]

 © 2006 Wiley-VCH Verlag GmbH & Co. KGaA, Weinheim

Open-Framework Structures

DOI: 10.1002/anie.200502413

A Building-Up Process in Open-Framework Metal Carboxylates that Involves a Progressive Increase in Dimensionality**

*Meenakshi Dan and C. N. R. Rao**

Dedicated to Professor Herbert W. Roesky on the occasion of his 70th birthday

Extensive research work has been carried out in the last few years on the synthesis and characterization of several families of open-framework materials, including aluminosilicates,[1] phosphates,[2] and carboxylates.[3] These studies have shown the occurrence of a variety of three-dimensional (3D) architectures containing channels and other features. A crucial problem with these materials relates to the mechanism of formation, an aspect that assumes special significance because these materials are generally synthesized under

[*] M. Dan, Prof. Dr. C. N. R. Rao
Chemistry and Physics of Materials Unit and
CSIR Centre of Excellence in Chemistry
Jawaharlal Nehru Centre for Advanced Scientific Research
Jakkur P. O., 560064 Bangalore (India)
and
Solid State and Structural Chemistry Unit
Indian Institute of Science
560012 Bangalore (India)
Fax: (+91) 80-2208-2766
E-mail: cnrrao@jncasr.ac.in

[**] M.D. thanks the CSIR (India) for a Senior Research Fellowship.

© 2006 Wiley-VCH Verlag GmbH & Co. KGaA, Weinheim
WILEY InterScience DISCOVER SOMETHING GREAT

hydro- or solvothermal conditions. An important suggestion in this context is the role of the secondary building units (SBUs) in the building-up of the 3D structures.[4] Recent studies of open-framework metal phosphates have shown how low-dimensional structures transform into higher-dimensional ones under mild conditions.[5] Thus, a zero-dimensional zinc phosphate comprising a four-membered ring has been shown to transform into a 3D sodalite-related structure, thereby providing an example of a molecule-to-material transformation.[6] While these studies are of significance, the question regarding the mode of formation of these structures still remains, since a given set of polyhedra can, in principle, generate a variety of three-dimensional structures through different rearrangements.[7] We therefore considered it important to investigate the process of formation of three-dimensional, open-framework structures that do not contain polyhedral anions, and chose to study the transformations of metal carboxylates.

We started with the zero-dimensional molecular zinc oxalate, $(C_4N_2H_{12})_3[Zn_2(C_2O_4)_5]\cdot 8H_2O$ (**1**), which has the dimeric structure shown in Figure 1a. On heating **1** in the presence of piperazine (PIP) at 100 °C for 48 h, we obtained a compound of the formula $(C_4N_2H_{12})_2[Zn_2(C_2O_4)_4]\cdot 3H_2O$ (**2**). Heating **1** at 165 °C in the presence of PIP for 48 h gave $(C_4N_2H_{12})_3[Zn_4(C_2O_4)_7]\cdot 4H_2O$ (**3**), whereas heating **1** at 180 °C for the same time period gave $(C_4N_2H_{12})[Zn_2(C_2O_4)_3]$ (**4**). We illustrate these transformations by showing the powder XRD patterns of the products recorded at different temperatures (Figure 2). Significantly, we did not find the presence of any other compounds during the transformations, as evidenced from the powder XRD patterns recorded periodically as the transformation progressed. A crystallographic study of **2**–**4** indicated that **2** has a linear-chain structure (Figure 1b), while **3** has a structure with honeycomb apertures (Figure 1c). Compound **4** is three-dimensional with a network of interconnected channels (Figure 3). Thus, as the reaction temperature is increased, the overall dimensionality of the product increases. Furthermore, the water content decreases as we go from **1** to **4**, and this is accompanied by an increase in the relative proportion of Zn with respect to the oxalate or the amine.

A brief description of the structures of **2**–**4** is in order. In the one-dimensional helical chain structure of **2**, each zinc atom is surrounded by six oxygen atoms from three oxalate units. There are two types of oxalate units, one of which binds to a Zn atom and has two terminal O atoms, and another which is a bis-chelating, bridging oxalate unit that binds to two Zn atoms. The one-dimensional helical chains run parallel to the *c*-axis of the unit cell (Figure 1b). The transformation product of the dimer at 165 °C, **3**, has a double-stranded 1D structure and contains two types of oxalate units just as in **2**. The two Zn atoms in the asymmetric unit are in different coordination environments: one is surrounded by six O atoms of the two bridging and one hanging oxalate molecules, whereas the other is surrounded by six O atoms of three bridging oxalate units. This results in condensation of the single-stranded, one-dimensional zinc oxalate chains to form a pseudo-two-dimensional zinc oxalate structure, with a honeycomb aperture, parallel to the *bc*-plane

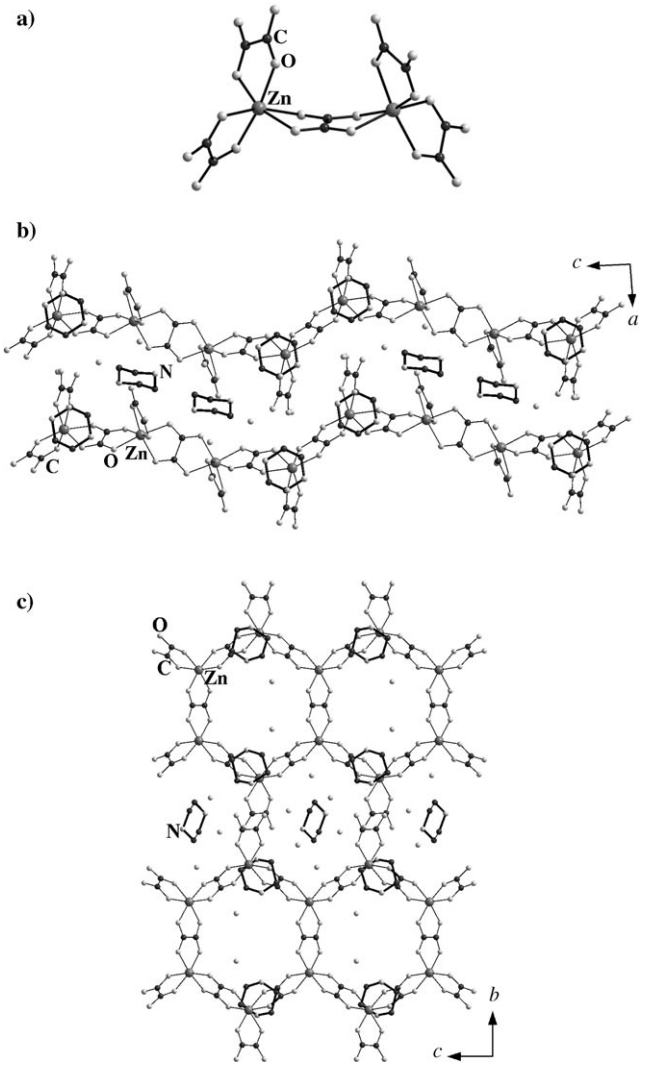


Figure 1. a) Structure of the zero-dimensional zinc oxalate dimer **1**. b) The helical chains in **2** viewed down the *b*-axis of the unit cell. Amine and interstitial water molecules are also shown. c) The pseudo-two-dimensional zinc oxalate **3** viewed down the *a*-axis of the unit cell. Note the honeycomb apertures.

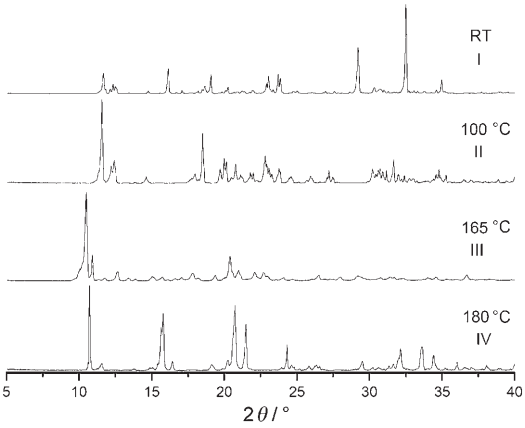


Figure 2. Powder XRD patterns of the products obtained by heating **1** at different temperatures for 48 h in the presence of piperazine.

 © 2006 Wiley-VCH Verlag GmbH & Co. KGaA, Weinheim

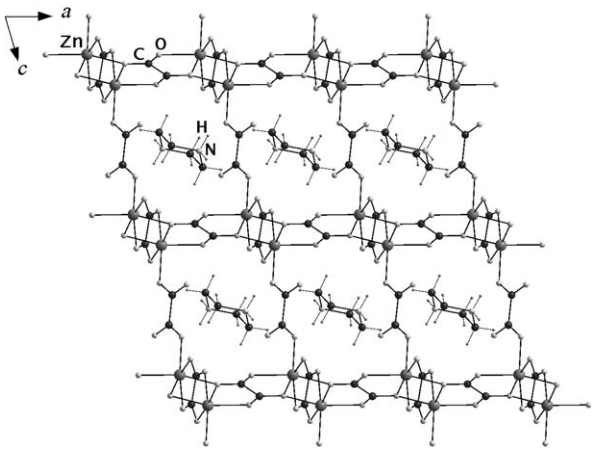


Figure 3. The three-dimensional structure of **4** formed by the pillaring of the layers by bridging oxalate groups. Protonated piperazine molecules are located in cages formed by the intersection of the channels running along the three crystallographic directions of the unit cell.

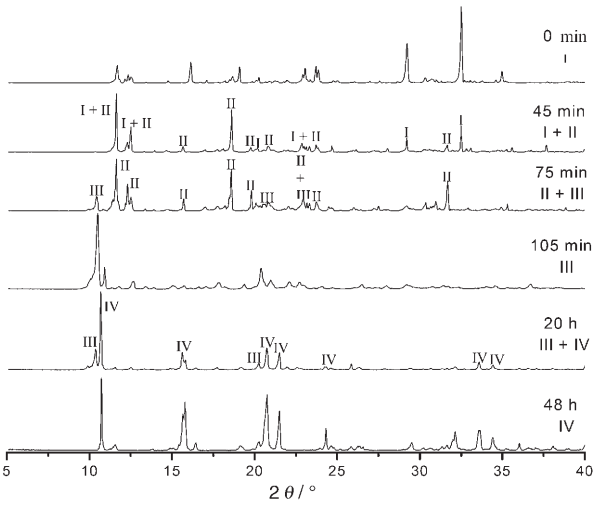


Figure 4. Changes of **1** during heating at 180 °C. Powder XRD patterns show the evolution of different phases with increasing dimensionality as a function of time.

of the unit cell (Figure 1 c). There are three types of oxalates in the three-dimensional structure of **4**: one bis-chelating and bridging oxalate moiety binding to two Zn atoms, a monodentate bridging oxalate which binds two Zn atoms and has two terminal O atoms, and another bis-chelating and triply bridging oxalate unit with three coordinated O atoms that binds four Zn atoms. The Zn atoms are connected by bridging oxalate units and three-coordinate O atoms to form layers parallel to the *ab*-plane of the unit cell. These layers are cross-linked by bridging oxalate units to form a three-dimensional architecture with a network of interconnected channels running along all the three crystallographic directions of the unit cell (Figure 3).

In order to understand the formation of the higher-dimensional oxalates from zero-dimensional **1** the progress of the conversion was monitored after different reaction times. On heating **1** at 100 °C with PIP for 9 h, the chain structure **2** appears, its proportion increasing progressively with time. After 48 h, **1** has been entirely transformed into **2**. When the reaction is carried out at 165 °C, formation of **2** is observed within 4 h, with the transformation to **2** being complete in 16 h. After 20 h, we noticed the appearance of **3**, accompanied by a decrease in the proportion of **2**. After 48 h, we obtained **3** as the sole product. When the study was carried out at 180 °C, we obtained all the three structures progressively, as shown by the powder XRD patterns in Figure 4. Thus, within 45 min, **1** starts transforming into **2** and as this transformation nears completion **2** starts transforming into **3**, as can be seen after 75 min of the reaction when a mixture of both **2** and **3** is present. After 105 min of the reaction **2** has been completely transformed into **3**, which then starts to transform into **4**. Thus, after 20 h of the reaction both **3** and **4** are present. After about 48 h, **3** has been transformed entirely into **4**. This study demonstrates that the three-dimensional structure emerges from the building-up of the lower-dimensional structures. This transformation involves hydrolysis and condensation, wherein the oxalate moiety is eliminated to form the higher-dimensional structures, accompanied by dehydration (Figure 5). On increasing the reaction temperature, the dimensionality of the structure increases as the total water content decreases, and this is accompanied by an increase in the number of zinc atoms bonding to the oxalate units (Zn/oxalate ratio).

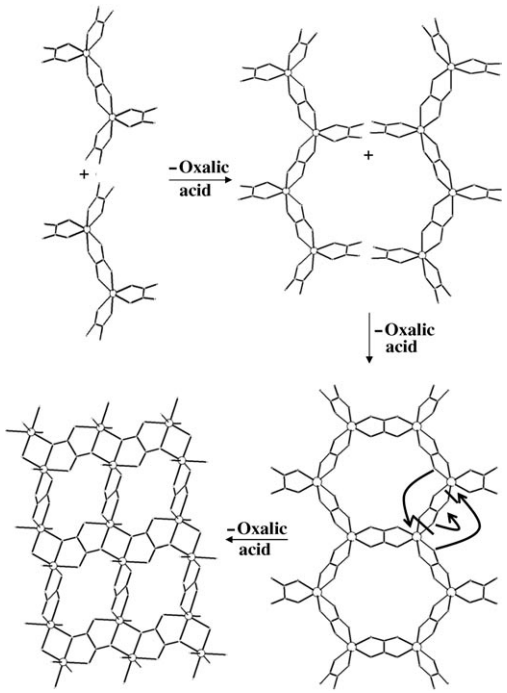


Figure 5. Formation of chain (**2**), pseudo-two-dimensional (**3**), and three-dimensional (**4**) structures from zero-dimensional **1** by hydrolysis/condensation.

We have also found that the nickel propionate dimer $[Ni(CH_3CH_2CO_2)_2(H_2O)]$ (**5**) transforms into a one-dimensional chain structure $[Ni(CH_3CH_2CO_2)_2]$ (**6**) at 25 °C within 24 h (Figure 6). The dimer has two Ni atoms connected by

 © 2006 Wiley-VCH Verlag GmbH & Co. KGaA, Weinheim

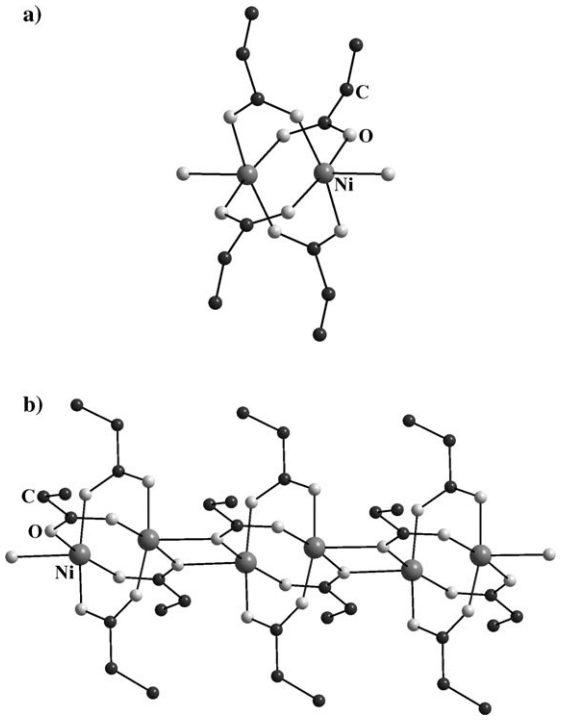


Figure 6. a) The nickel propionate dimer **5**. b) The nickel propionate chain **6**.

four bridging propionate groups in a paddlewheel-type architecture similar to that found in copper and other metal acetate dimers, as well as in many metal carboxylates.[8] The facile formation of the chain structure from the dimer can be visualized as a result of the self-assembly of the dimers followed by the elimination of water. The chain structure of **6** is formed by the joining of the dimer through the three-coordinate propionate oxygen atoms. Thus, there are two types of propionate units in **6**, one bridging the two Ni atoms and the other joining the dimers through the three-coordinate oxygen atoms as well as bridging the two Ni atoms to form chains running parallel to the *a*-axis. The metal-to-ligand ratio increases as the dimer transforms into the chain, with a concomitant decrease in the water content.

We found a similar building-up process in the cobalt succinates described by Férey and coworkers.[9] Accordingly, $[Co(H_2O)_4(C_4H_4O_4)]$, with a linear-chain structure, transforms into the layered complex $[Co_4(OH)_2(H_2O)_2(C_4H_4O_4)_3]\cdot 2H_2O$ on heating in water at 150 °C, as evidenced from XRD studies. It would therefore appear that the progressive formation of higher-dimensional structures of cobalt succinates with increasing temperature reported recently by Forster and Cheetham[10] occurs through such molecular transformations.

In the case of the transformation of **5** into **6**, we recognize that the aggregation of paddlewheel clusters is known,[11] but the transformation described by us has features comparable to those of the zinc oxalates. In conclusion, we feel that the low-D to high-D transformations discussed by us are likely to occur by a building-up process in solution, rather than by a decomposition or reformation process. The kinetic data lend some support to this observation. It is noteworthy that a 1,4-benzenedicarboxylate has recently been shown to undergo a 1D to 3D transformation.[12]

Experimental Section

The zinc oxalate dimer **1** was synthesized by the procedure described earlier.[13] The transformation reactions were carried out in a 7-mL, PTFE-lined acid digestion bomb. Heating of **1** (121.1 mg) with piperazine (10.8 mg; ratio **1**/PIP = 2:1) in H_2O (2 mL) at 100 °C, 165 °C, or 180 °C for 48 h yielded **2**, **3**, and **4**, respectively. The products were generally single-crystalline, although the starting zinc oxalate dimer was used in the form of a fine powder.

In a typical synthesis of nickel propionates **5** and **6**, NiO (1 g) was dispersed in propionic acid/water (4 mL, 1:1 (v/v)) and the mixture was heated in a 23-mL, PTFE-lined acid digestion bomb at 75 °C for 48 h. The reaction resulted in the formation of deep-green, rod-shaped crystals of **6**. The filtrate at room temperature gave green crystals **5**.

Single-crystal structure determination by X-ray diffraction was performed with a Siemens Smart-CCD diffractometer equipped with a normal focus, 2.4-kW, sealed-tube X-ray source ($Mo_{K\alpha}$ radiation, $\lambda = 0.71073$ Å) operating at 40 kV and 40 mA. The structure was solved by direct methods using SHELXS-86.[14] An empirical absorption correction based on symmetry-equivalent reflections was applied using the SADABS program.[15] All the hydrogen positions were initially located in the difference Fourier maps and the hydrogen atoms were placed geometrically and held in the riding mode for the final refinement. Full-matrix least-squares structure refinement against $|F^2|$ was carried out using the SHELXTL-PLUS package of programs.[16]

Crystal data: **2**: $C_{16}H_{30}N_4O_{19}Zn_2$, $M_r = 713.18$; monoclinic, space group $C2/c$, $a = 15.2706(3)$, $b = 9.0584(1)$, $c = 38.2638(1)$ Å, $\beta = 90.40°$; $V = 5292.8(1)$ Å^3; $Z = 8$; $\rho_{calcd} = 1.790$ g cm^{-3}, $T = 298$ K, $\mu = 1.907$ mm^{-1}; 10672 reflections measured with 3799 independent reflections; $R_{int} = 0.0399$; $R_1 = 0.0457$, $wR_2 = 0.1113$ (observed data) and $R_1 = 0.0633$, $wR_2 = 0.1233$ (all data). **3**: $C_{26}H_{44}N_6O_{32}Zn_4$, $M_r = 584.9$; monoclinic, space group $P2_1/m$, $a = 8.7924(9)$, $b = 35.595(4)$, $c = 9.2583(10)$ Å, $\beta = 96.602(2)°$; $V = 2878.3(5)$ Å^3; $Z = 4$. While the structure of the compound could be solved, the R values were large due to the rather poor quality of the crystals. **4**: $C_{10}H_{12}N_2O_{12}Zn_2$, $M_r = 241.48$; triclinic, space group $P\bar{1}$, $a = 5.8208(9)$, $b = 7.6266(11)$, $c = 8.5782(13)$ Å, $\alpha = 88.272(3)°$, $\beta = 73.81°$, $\gamma = 86.599(3)°$; $V = 365.02(9)$ Å^3; $Z = 2$; $\rho_{calcd} = 2.197$ g cm^{-3}, $T = 298$ K, $\mu = 3.362$ mm^{-1}; 1562 reflections measured with 1040 independent reflections; $R_{int} = 0.0291$; $R_1 = 0.0418$, $wR_2 = 0.0921$ (observed data) and $R_1 = 0.0577$, $wR_2 = 0.1006$ (all data). **5**: $C_6H_{12}NiO_5$, $M_r = 885.42$; monoclinic, space group $P2_1/c$, $a = 15.384(1)$, $b = 17.381(1)$, $c = 15.174(1)$ Å, $\beta = 94.407(1)°$; $V = 4045.4(3)$ Å^3; $Z = 4$; $\rho_{calcd} = 1.454$ g cm^{-3}, $T = 298$ K, $\mu = 1.902$ mm^{-1}; 16311 reflections measured with 5771 independent reflections; $R_{int} = 0.0808$; $R_1 = 0.0480$, $wR_2 = 0.1279$ (observed data) and $R_1 = 0.0557$, $wR_2 = 0.1404$ (all data). **6**: $C_6H_{10}NiO_4$, $M_r = 204.85$; triclinic, space group $P\bar{1}$, $a = 5.1954(2)$, $b = 8.4555(1)$, $c = 9.5431(4)$ Å, $\alpha = 91.720(2)$, $\beta = 91.789(2)$, $\gamma = 105.078(2)°$; $V = 404.28(2)$ Å^3; $Z = 2$; $\rho_{calcd} = 1.683$ g cm^{-3}, $T = 298$ K, $\mu = 2.362$ mm^{-1}; 1691 reflections measured with 1135 independent reflections; $R_{int} = 0.0202$; $R_1 = 0.0313$, $wR_2 = 0.0785$ (observed data) and $R_1 = 0.0377$, $wR_2 = 0.0820$ (all data).

CCDC-276975 (**2**), -277863 (**3**), -276977 (**4**), -276978 (**5**), and -276979 (**6**) contain the supplementary crystallographic data for this paper. These data can be obtained free of charge from The Cambridge Crystallographic Data Centre via www.ccdc.cam.ac.uk/data_request/cif.

Received: July 11, 2005
Revised: September 28, 2005
Published online: November 30, 2005

 © 2006 Wiley-VCH Verlag GmbH & Co. KGaA, Weinheim

Keywords: carboxylate ligands · materials science · solid-state structures · supramolecular chemistry · zinc

[1] W. M. Meier, D. H. Oslen, C. Baerlocher, *Atlas of Zeolite Structure Types*, Elsevier, London, **1996**.
[2] A. K. Cheetham, G. Férey, T. Loiseau, *Angew. Chem.* **1999**, *111*, 3466; *Angew. Chem. Int. Ed.* **1999**, *38*, 3268.
[3] C. N. R. Rao, S. Natarajan, R. Vaidhyanathan, *Angew. Chem.* **2004**, *116*, 1490; *Angew. Chem. Int. Ed.* **2004**, *43*, 1466.
[4] G. Férey, *J. Solid State Chem.* **2000**, *152*, 37; G. Férey, C. Serre, C. Mellot-Draznieks, F. Millange, S. Surblé, J. Dutour, I. Margiolaki, *Angew. Chem.* **2004**, *116*, 6456; *Angew. Chem. Int. Ed.* **2004**, *43*, 6296; M. E. Eddaoudi, D. B. Moler, H. Li, B. Chen, T. M. Reineke, M. O'Keeffe, O. M. Yaghi, *Acc. Chem. Res.* **2001**, *34*, 319; M. E. Eddaoudi, J. Kim, D. Vodak, A. Sudik, J. Wachter, M. O'Keeffe, O. M. Yaghi, *Proc. Natl. Acad. Sci. USA* **2002**, *99*, 4900; O. M. Yaghi, M. O'Keeffe, N. W. Ockwig, H. K. Chae, M. Eddaoudi, J. Kim, *Nature* **2003**, *423*, 705.
[5] S. Oliver, A. Kuperman, G. A. Ozin, *Angew. Chem.* **1998**, *110*, 48; *Angew. Chem. Int. Ed.* **1998**, *37*, 46; C. N. R. Rao, S. Natarajan, A. Choudhury, S. Neeraj, A. A. Ayi, *Acc. Chem. Res.* **2003**, *36*, 80; A. Choudhury, S. Neeraj, S. Natarajan, C. N. R. Rao, *J. Mater. Chem.* **2001**, *11*, 1537; A. A. Ayi, A. Choudhury, S. Natarajan, S. Neeraj, C. N. R. Rao, *J. Mater. Chem.* **2001**, *11*, 1181; R. I. Walton, F. Millange, A. L. Bail, T. Loiseau, C. Serre, D. O'Hare, G. Férey, *Chem. Commun.* **2000**, 203; A. J. Norquist, D. O'Hare, *J. Am. Chem. Soc.* **2004**, *126*, 6673.
[6] M. Dan, D. Udayakumar, C. N. R. Rao, *Chem. Commun.* **2003**, 2212; R. Murugavel, M. G. Walawalkar, M. Dan, H. W. Roesky, C. N. R. Rao, *Acc. Chem. Res.* **2004**, *37*, 763.
[7] C. Mellot-Draznieks, J. Dutour, G. Férey, *Angew. Chem.* **2004**, *116*, 6450; *Angew. Chem. Int. Ed.* **2004**, *43*, 6290.
[8] M. E. Eddaoudi, J. Kim, J. B. Wachter, H. K. Chae, M. O'Keeffe, O. M. Yaghi, *J. Am. Chem. Soc.* **2001**, *123*, 4368; M. J. Rosseinsky, *Microporous Mesoporous Mater.* **2004**, *73*, 15.
[9] C. Livage, C. Egger, G. Férey, *Chem. Mater.* **2001**, *13*, 410.
[10] P. M. Forster, A. R. Burbank, C. Livage, G. Férey, A. K. Cheetham, *Chem. Commun.* **2004**, 368.
[11] F. A. Cotton, E. A. Hillard, C. A. Murillo, H.-C. Zhou, *J. Am. Chem. Soc.* **2000**, *122*, 416.
[12] A. Thirumurugan, C. N. R. Rao, *J. Mater. Chem.* **2005**, *15*, 3852.
[13] R. Vaidhyanathan, S. Natarajan, C. N. R. Rao, *J. Chem. Soc. Dalton Trans.* **2001**, 699.
[14] G. M. Sheldrick, *SHELXS-86 Program for Crystal Structure Determination*, University of Göttingen, Germany, **1986**; G. M. Sheldrick, *Acta Crystallogr. Sect. A* **1990**, *46*, 467.
[15] G. M. Sheldrick, *SADABS: Siemens Area Detector Absorption Correction program*, University of Göttingen, Germany, **1994**.
[16] G. M. Sheldrick, *SHELXS-93 Program for Crystal Structure Solution and Refinement*, University of Göttingen, Germany, **1993**.

 © 2006 Wiley-VCH Verlag GmbH & Co. KGaA, Weinheim

Antitumor Agents

DOI: 10.1002/anie.200502925

Ferrocene-Mediated Proton-Coupled Electron Transfer in a Series of Ferrocifen-Type Breast-Cancer Drug Candidates**

Elizabeth Hillard, Anne Vessières, Laurent Thouin, Gérard Jaouen, and Christian Amatore**

The archetypical selective estrogen receptor modulator (SERM) tamoxifen, (*Z*)-2-[4-(1,2-diphenyl-1-butenyl)phenoxy]-*N*,*N*-dimethylethanamine, is widely prescribed for patients diagnosed with hormone-dependent breast cancer, that is, cancer in which the estrogen receptor (ER) is present (ER(+)). The antiproliferative action in the breast of the hydroxylated form of tamoxifen (OH-Tam) arises primarily from an antiestrogenic effect caused by competitive binding to the ER, which represses estradiol-mediated DNA transcription.[1] Unfortunately, some breast-cancer cells are resistant to tamoxifen because they either do not express ER (classified as ER(−)) or have developed resistance following prolonged exposure to the drug. To fight both ER(+) and ER(−) breast cancer, we have focused on the creation of dual-function drugs that combine antiestrogenicity and estrogen-independent cytotoxicity in the same molecule.

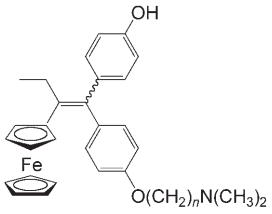
The discovery of the inorganic complex cisplatin (*cis*-$[PtCl_2(NH_3)_2]$) has revolutionized the treatment of testicular cancer[2] and has led to increased research into organometallic complexes as antitumor agents.[3] Our strategy, therefore, has been to incorporate a potentially cytotoxic moiety, ferrocene, by grafting it onto the tamoxifen skeleton. A series of these molecules, called "hydroxyferrocifens" by analogy, have been prepared (Scheme 1) and their antiproliferative effects have been studied in ER(+) and ER(−) breast-cancer cell lines.[4] In the ER(+) MCF7 cells, the hydroxyferrocifens behave similarly to OH-Tam in that they express an antiestrogenic effect, although they also possess a cytotoxic component.[5] However, the hydroxyferrocifens present a remarkable anti-

[*] Dr. E. Hillard, Dr. A. Vessières, Prof. Dr. G. Jaouen
Laboratoire de Chimie et Biochimie des Complexes Moléculaires
Ecole Nationale Supérieure de Chimie de Paris
11, Rue Pierre et Marie Curie, 75231 Paris Cedex 05 (France)
Fax: (+33) 1-4326-0061
E-mail: gerard-jaouen@enscp.fr

Dr. L. Thouin, Prof. Dr. C. Amatore
Ecole Normale Supérieure
Département de Chimie
24 rue Lhomond, 75231 Paris Cedex 05 (France)
Fax: (+33) 1-4432-3863
E-mail: christian.amatore@ens.fr

[**] This work was supported by the CNRS (UMR 7576 and UMR 8640), the French Ministry of Research, ENSCP, and ENS. E.A.H. thanks the National Science Foundation (USA) for a Postdoctoral Grant (No. 0302042) and acknowledges Dr. J. Wadhawan for useful discussions. The authors also thank K. Kowalski, F. Le Bideau, P. Pigeon, and D. Plazuk for providing the compounds.

 © 2006 Wiley-VCH Verlag GmbH & Co. KGaA, Weinheim InterScience



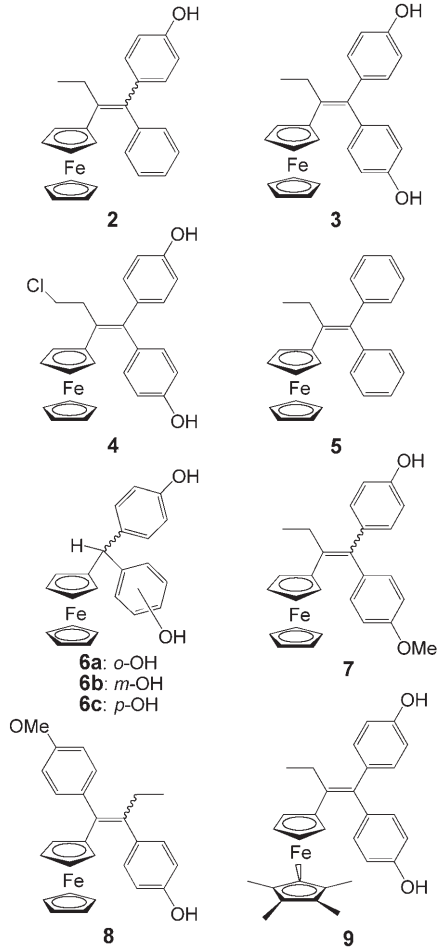
Z + *E*
1a: *n* = 2
1b: *n* = 3
1c: *n* = 5

Scheme 1. Hydroxyferrocifens.

proliferative behavior on the ER(−) MDA-MB231 cell line, with IC_{50} values on the order of 0.5 μM, whereas OH-Tam is completely inactive at this concentration range; this effect can be attributed only to cytotoxicity of the ferrocenyl complexes. Thus, the observed antiproliferative effect of the hydroxyferrocifens can be divided into two components: antiestrogenic in ER(+) cells and cytotoxic in both ER(+) and ER(−) cells; the cytotoxicity likely arises from the oxidation in situ of Fe^{2+} to Fe^{3+} ions.[6]

Although hydroxytamoxifen does not show cytotoxic activity towards MCF7 or MDA-MB231 breast-cancer cell lines at sub-micromolar concentrations, a cytotoxic effect has been observed at higher concentrations (IC_{50} = 34 μM for the ER(−) MDA-MB231 cell line).[7] The fact that hydroxyferrocifens show cytotoxic activity at much lower concentrations than hydroxytamoxifen suggests that the ferrocene group somehow modulates this effect. We have synthesized several compounds based on the hydroxyferrocifen structure (Scheme 2) and assessed their antiproliferative effects in vitro to further understand the role of ferrocene and the structure–activity relationship in the cytotoxicity of these molecules in both hormone-dependent (MCF7) and hormone-independent (MDA-MB231) breast-cancer cell lines. In the MDA-MB231 cell line, an antiproliferative effect was observed for **1**, **2**, **3**, and **4**, whereas the remaining compounds showed little or no effect towards the MDA-MB231 cells. These results are compiled in Table 1.

As cell death has been linked with the oxidation in situ of phenol groups and the ferrocenium cation, we have used electrochemistry to monitor the reactivity of these compounds in a model environment. First, the cyclic voltammograms were obtained in methanol, and then pyridine was added to determine the reactivity of the electrochemically generated cations towards nucleophiles; the standard potentials ($E°$) are shown in Table 2. In pure MeOH, the compounds exhibited voltammograms that are essentially due to the ferrocene/ferrocenium (Fc/Fc^+) redox couple, often followed by the irreversible oxidation of the phenolic moiety.[8] However, two distinct types of electrochemical behavior were observed when pyridine was added. Very little change was observed in the cyclic voltammograms upon the addition of pyridine for the compounds that showed slight or no cytotoxic effects in vitro. However, the addition of pyridine caused two major changes to the voltammograms of the biologically active compounds. Firstly, the Fc/Fc^+ couple became irreversibile at low scan rates, which indicates



Scheme 2. Hydroxyferrocifen-type molecules used for electrochemical and bioactivity screening.

Table 1: Biological and electrochemical results for the ferrocenyl derivatives.

Compound	Antiproliferative effect on MDA-MB231 cells [% of inhibition][a]	Cytotoxic effect?[b]	Electron transfer?[c]
OH-Tam	none[g]	–	n.a.
1a	53[g]	+	Y
1b	77[g]	+	Y
1c	80[g]	+	Y
2	35[h]	+	Y
3	71[i]	+	Y
4[d]	49[j]	+	Y
6a[e]	26[k]	slight	N
6b[e]	18[k]	slight	N
6c[e]	16[k]	slight	N
7[d]	16[j]	slight	Y
8[d]	3[j]	–	N
9[f]	none[j]	–	N

[a] Defined as the effect of 1 μM of the compound after 6 days of culturing relative to the control, set by definition at 100%. [b] The cytotoxic effect is considered positive (+) for an antiproliferative effect (% inhibition) greater than 30%, slight for an effect 10–30%, and negative (−) for an effect less than 10%. [c] Observed by the loss of the ferrocenium reduction wave in the presence of pyridine. [d] Prepared as described in Ref. [17]. [e] Prepared as described in Ref. [18]. [f] Prepared as described in Ref. [19]. [g] Ref. [4c]. [h] Ref. [4b]. [i] Ref. [16]. [j] Ref. [17]. [k] Ref. [20].

 © 2006 Wiley-VCH Verlag GmbH & Co. KGaA, Weinheim

Table 2: Standard oxidation potentials in methanol and methanol/pyridine (6:1 v/v).

Compound	Solvent	E°, (Fc/Fc^+) [V vs. SCE][a]	Second-wave peak potential [V vs. SCE][a]
ferrocene	MeOH	0.417(2)	–
	MeOH/py	*0.432(2)*	–
1a	MeOH	0.395(3)	very broad
	MeOH/py	*0.393(3)*	*0.482(3)*
1b	MeOH	0.401(2)	0.92(3)
	MeOH/py	*0.420(3)*	*0.513(3)*
1c	MeOH	0.385(2)	0.93(4)
	MeOH/py	*0.383(3)*	*0.476(2)*
2	MeOH	0.397(2)	0.96(3)
	MeOH/py	*0.423(4)*	*0.510(3)*
3	MeOH	0.373(2)	0.88(3)
	MeOH/py	*0.387(3) (sh)*	*0.480(2)*
4	MeOH	0.413(2)	0.87(4)
	MeOH/py	*0.460(2)*	*0.584(3)*
5	MeOH	0.421(3)	–
	MeOH/py	*0.442(3)*	–
6a	MeOH	0.379(3)	not observed
	MeOH/py	*0.408(3)*	*not observed*
6b	MeOH	0.404(3)	not observed
	MeOH/py	*0.428(3)*	*not observed*
6c	MeOH	0.391(2)	not observed
	MeOH/py	*0.414(2)*	*not observed*
7	MeOH	0.387(2)	0.93(3)
	MeOH/py	*0.407(2) (sh)*	*0.513(3)*
8	MeOH	0.39(2)	not observed
	MeOH/py	*0.461(2)*	*1.03(4)*
9	MeOH	0.153(3)	not observed
	MeOH/py	*0.164(2)*	*0.83(4)*

[a] The uncertainty of last digit given in parentheses.

that the ferrocenium cation was scavenged chemically prior to the reverse sweep. The loss of reversibility was accompanied by an increase of the Fc oxidation wave, which is indicative of secondary electron transfer following a chemical reaction of the primary cation radical. Secondly, any phenol-oxidation waves present in the cyclic voltammogram in MeOH underwent a dramatic cathodic shift. An example of this phenomenon for **3** is shown in Figure 1. The fact that all of the compounds displaying significant cytotoxic effects in vitro also showed reactivity with pyridine in the electrochemical experiments (Table 1) validates the use of this electrochemical model.

The ferrocenium group appears to play the role of an intramolecular electron acceptor in the cytotoxicity in vitro, as evidenced by the transience of the electrochemically produced Fe^{3+} center in the presence of pyridine. The inertness of the non-phenolic compound **5** to pyridine in our electrochemical model system shows that a phenolic group is necessary for electron transfer to take place (Figure 2). Furthermore, the fact that chemical reduction of the Fe^{3+} centers was not observed for the nonconjugated compounds **6a–c** suggests that the electron-transfer process is intramolecular and occurs through a slight coupling in the molecular π system. A further electrochemical experiment to support this interpretation was performed using a mixture of ferrocene and 1,1-di-*p*-hydroxyphenyl-2-phenylbut-1-ene in pyridine/MeOH. The Fc/Fc^+ couple was conventional and reversible, and the phenol-oxidation wave was observed at a potential typical of the hydroxyferrocifens when pyridine is not present. These results confirm the conclusion that the electron transfer from the phenol moiety to the ferrocenyl group is intramolecular and relies on weak electron delocalization within the π system. It is important to note, however, that the π electron delocalization in the initial cation radical is quite weak. This is attested to by the observation that the standard oxidation potentials of the Fc/Fc^+ couple of the hydroxyfer-

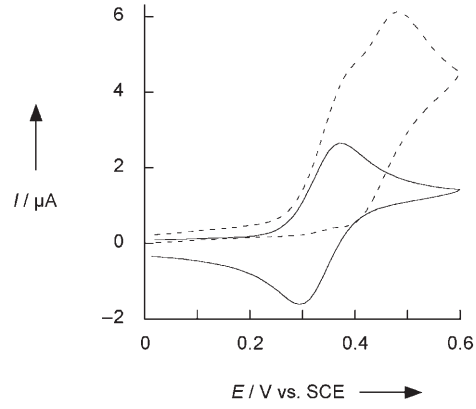


Figure 1. Cyclic voltammograms of **3** (2 mM in 0.1 M Bu_4NBF_4/MeOH) in the absence (solid line) and presence (dashed line) of pyridine in 1:6 volume ratio. Scan rate 0.5 Vs^{-1}. Pt electrode of 0.5 mm diameter. The oxidations of the phenol groups in MeOH occur at 0.88 and 1.17 V versus SCE (not shown).

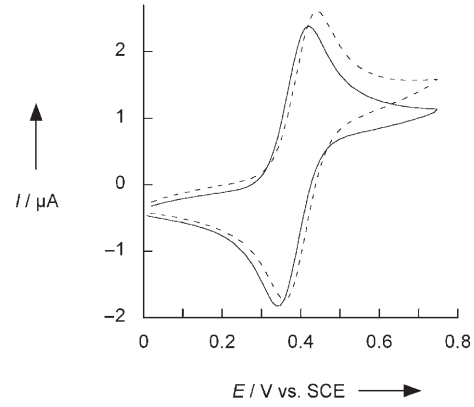


Figure 2. Cyclic voltammograms of **5** in the absence (solid line) and presence (dashed line) of added pyridine. Same conditions as for Figure 1.

 © 2006 Wiley-VCH Verlag GmbH & Co. KGaA, Weinheim

rocifens **2** (0.397 V), **3** (0.373 V), and **7** (0.387 V) are not very much lower than that of the non-hydroxylated analogue **5** (0.421 V). The standard oxidation potentials of the non-conjugated compounds **6a** (0.379 V), **6b** (0.404 V), and **6c** (0.391 V) suggest that any stabilization of the radical species in the hydroxyferrocifens is due to inductive effects, rather than resulting from extended electron-delocalization effects, and that the cation radical is primarily ferrocene-centered. However, weak delocalization is sufficient to allow significant interaction between the phenolic and ferrocenium substituents during intramolecular electron transfer. Thus, as soon as an adequate base is present, a relatively fast intramolecular electron transfer may occur, thereby leading to the oxidation of the phenolic moiety becoming easier because of its displacement by the reaction of the phenoxy cation with the pyridine base.[9–11]

Pyridine could conceivably contribute to the irreversible electron-transfer process either by proton abstraction or nucleophilic attack. To rule out a nucleophilic mechanism, the nucleophilic, but nonbasic, electrolyte Me_4NCl was substituted for pyridine and Bu_4NBF_4. In this experiment, the ferrocene moiety displayed a reversible redox event, which suggests that pyridine acts as a base, not as a nucleophile. Further experiments have shown that the pKa value of the added base influences the reaction pathway. For example, dimethylformamide (DMF) and pyrazole are too weak to deprotonate the phenol moiety in the activated molecule, as the cyclic voltammograms are not qualitatively different from those in MeOH, whereas pyridine ($pK_a = 5.14$)[12a] and imidazole ($pK_a = 6.95$)[12b] are sufficiently basic. In this respect, it may be envisioned that DNA bases act as proton scavengers in vitro. Alternatively, the relatively high pK_a values (>7) of α-NH_2 groups present in most peptides suggest that these groups could also act as bases in vitro in proteinic environments.[12c] However, this point was not tested in this work because the low solubility of the ferrocenyl compounds precludes electrochemical experiments in aqueous solution.

Finally, the importance of the position of the ethyl group with respect to the ferrocene moiety was assessed by comparing the electrochemical results for the geometric isomers **7** and **8**. Only the compound in which the ethyl group and the ferrocene group are attached to the same carbon atom (**7**) showed the characteristic irreversible Fc oxidation and shift of the phenol oxidation wave upon addition of pyridine (Figure 3). These results strongly suggest the participation of the ethyl group in the mechanism.

In view of the role of the ferrocene moiety as an intramolecular hole reservoir,[10] the conjugated π system, the basic action of pyridine, and the interesting constraints on the placement of the ethyl group, we propose the mechanism shown in Scheme 3 for the generation of the quinone methide species most likely responsible for the cytotoxicity in the MDA-MB231 cell line. The ferrocene moiety is electrochemically oxidized, and the electron may to a small extent be delocalized over the π system. This imparts a partial positive charge to the hydroxy group, thus acidifying the proton, which may then be easily abstracted by pyridine.[11] The small delocalization is almost not observable in the absence of

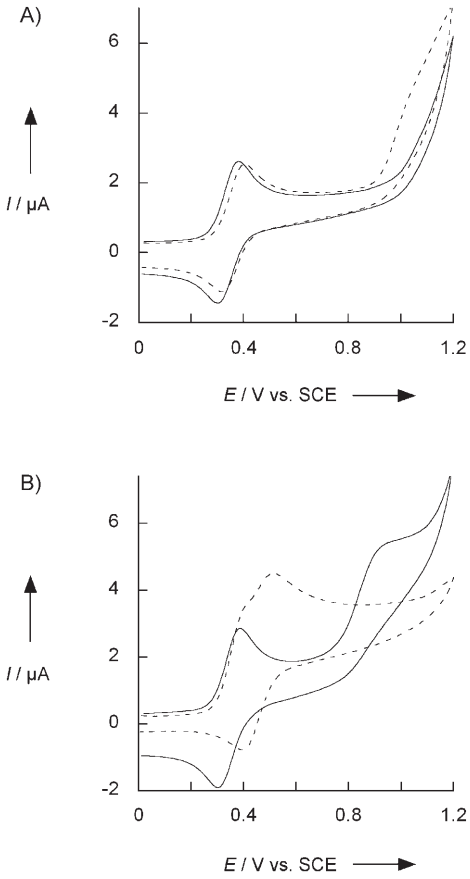
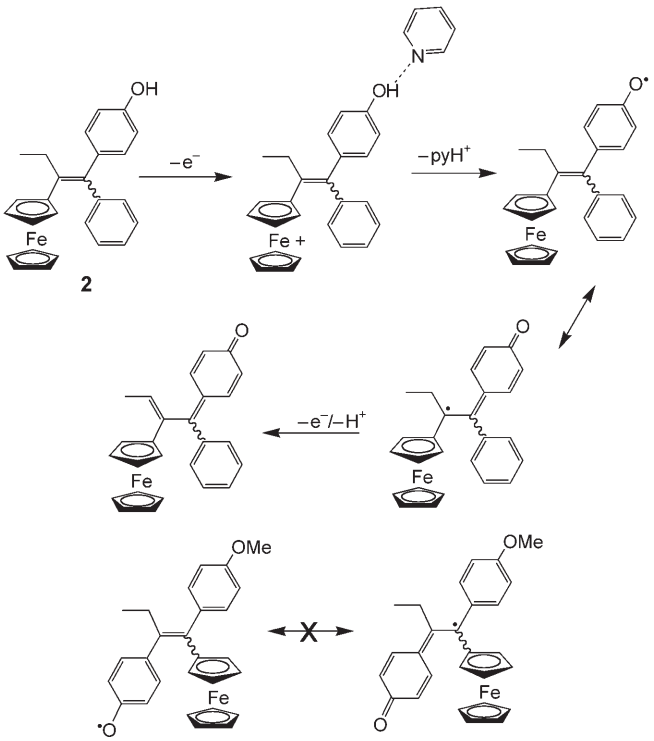


Figure 3. Cyclic voltammograms of A) **8** and B) **7** in the absence (solid line) and presence (dashed line) of added pyridine. Same conditions as for Figure 1.

pyridine, as evidenced by the small change in the oxidation potential of the ferrocene moiety. In the presence of pyridine, the transient existence of an adduct may encourage a strong coupling in the deprotonated transition state. The resulting phenoxy radical species can be described by many mesomeric structures, one of the most stable being the quinoid in which the radical is positioned on the α carbon atom with respect to the ferrocene moiety. This species may then be oxidized, observed as the second oxidation wave at slightly higher potential than the ferrocene oxidation wave. This second oxidation may then be followed by another proton abstraction from the ethyl group, which results in a quinone methide structure. This mechanism is the only possibility that we can envision to account for the difference in reactivity between **7** and **8**. In the latter case, there is no possibility to stabilize the α-carbenium radical through back-bonding into the iron d orbital, and simultaneously abstract an adjacent proton to form a double bond (see bottom of Scheme 3).[13]

The potential cell-damaging pathways for tamoxifen include metabolism to electrophilic *o*-quinones, quinone methides, or carbocations, which may form adducts with DNA, GSH, or proteins.[14] We believe that the biologically active ferrocifen-type compounds undergo similar oxidative metabolism, which is enhanced by the easier oxidation of ferrocene in comparison to phenol. Thus, the ferrocene

 © 2006 Wiley-VCH Verlag GmbH & Co. KGaA, Weinheim



Scheme 3. Proposed mechanism for transformation of **2** to a quinone methide species in the presence of pyridine. As indicated in the lower part of the Scheme, compound **8** cannot follow the same mechanism.

moiety may be oxidized far from the biological target and may thus serve as an intramolecular carrier of the hole while the activated drug finds its way to its target. Furthermore, the small degree of coupling between the ferrocenium-centered radical and the oxo radical yields a relatively high energy transition state, which may stabilize the ferrocenium species on its path to the target.[15] In this way the ferrocene acts as a kind of intramolecular oxidation "antenna" and may oxidize the phenol group through a intramolecular pathway, thus producing cytotoxic species in milder oxidizing conditions. Only when an adequate base is present will the electron transfer proceed, presumably in a concerted fashion with deprotonation, to yield the neutral phenoxy radical. DMF, for example, is not basic enough to allow such electron transfer. Therefore, the drug will only be activated to form the quinone methide species in the presence of basic species such as DNA nucleobases or peptides, the harm of which may lead to cell death.

Received: August 17, 2005
Published online: November 28, 2005

Keywords: antitumor agents · electrochemistry · electron transfer · hormones · metallocenes

[1] a) S. Bardon, F. Vignon, D. Derocq, H. Rochefort, *Mol. Cell. Endocrinol.* **1984**, *35*, 89; b) for recent reviews on the biological mechanisms of SERMs, see: V. C. Jordan, *J. Med. Chem.* **2003**, *46*, 883 and V. C. Jordan, *J. Med. Chem.* **2003**, *46*, 1081.

[2] B. K. Keppler, *Metal Complexes in Cancer Chemotherapy*, VCH, Weinheim, **1993**.

[3] a) M. J. Clarke, F. Zhu, D. R. Frasca, *Chem. Rev.* **1999**, *99*, 2511; b) P. Köpf-Maier, *Eur. J. Clin. Pharmacol.* **1994**, *47*, 1.

[4] a) S. Top, J. Tang, A. Vessières, D. Carrez, C. Provot, G. Jaouen, *Chem. Commun.* **1996**, 955; b) S. Top, A. Vessières, C. Cabestaing, I. Laios, G. Leclercq, C. Provot, G. Jaouen, *J. Organomet. Chem.* **2001**, *637*, 500; c) S. Top, A. Vessières, G. Leclercq, J. Quivy, J. Tang, J. Vaissermann, M. Huché, G. Jaouen, *Chem. Eur. J.* **2003**, *9*, 5223; d) G. Jaouen, S. Top, A. Vessières, G. Leclercq, M. J. McGlinchey, *Curr. Med. Chem.* **2004**, *11*, 2505.

[5] Herein, Cytotoxicity is defined as an antiproliferative effect that, in contrast to an antihormonal effect, is not reversed by the addition of estradiol.

[6] a) A. M. Joy, D. M. L. Goodgame, J. I. Stratford, *Int. J. Radiat. Oncol. Biol. Phys.* **1989**, *16*, 1053; b) D. Osella, M. Ferrali, P. Zanello, F. Laschi, M. Fontani, C. Nervi, G. Cavigiolio, *Inorg. Chim. Acta* **2000**, *306*, 42; c) H. Tamura, M. Miwa, *Chem. Lett.* **1997**, *11*, 1177.

[7] a) R. L. Sutherland, C. K. W. Watts, R. E. Hall, P. C. Ruenitz, *J. Steroid Biochem.* **1987**, *27*, 891, and references therein; b) D. Yao, F. Zhang, L. Yu, Y. Yang, R. B. van Breeman, J. L. Bolton, *Chem. Res. Toxicol.* **2001**, *14*, 1643.

[8] The wave of the phenol moiety was shifted to higher potential, as expected, because of the positive charge on the Fc^+ moiety.

[9] In our system, phenol oxidation waves occurred at potentials higher than 0.8 V vs. SCE.

[10] a) C. Amatore, A. Thiébault, J.-N. Verpeaux, *J. Chem. Soc. Chem. Commun.* **1989**, 1543; b) C. Amatore, M. Bayachou, F. Boutejengout, J.-N. Verpeaux, *Bull. Soc. Chim. Fr.* **1993**, *130*, 371.

[11] C. J. Schlesener, C. Amatore, J. K. Kochi, *J. Am. Chem. Soc.* **1984**, *106*, 7472.

[12] a) H. C. Brown, D. H. McDaniel, O. Hafliger in *Determination of Organic Structures by Physical Methods* (Eds.: E. A. Braude, F. C. Nachod), Academic Press, New York, **1955**; b) T. C. Bruice, G. L. Schmir, *J. Am. Chem. Soc.* **1958**, *80*, 148; c) E. Ellenbogen, *J. Am. Chem. Soc.* **1952**, *74*, 5198.

[13] The involvement of a quinone methide species subsequent to the electron-transfer activation is further supported by the observation that the *meta*-OH-substituted analogues that have been tested did not show any reactivity following their initial one-electron oxidation in the presence of base (comparable to Figure 3a), whereas intramolecular electron transfer was observed electrochemically when a *para*-phenol was added to the *meta*-substituted derivative, (comparable to Figure 3b). (P. Pigeon, A. Vessières, E. Hillard, G. Jaouen, unpublished results).

[14] a) P. W. Fan, F. Zhang, J. L. Bolton, *Chem. Res. Toxicol.* **2000**, *13*, 45; b) F Zhang, P. W. Fan, X. Liu, L. Shen, R. B. van Breeman, J. L. Bolton, *Chem. Res. Toxicol.* **2000**, *13*, 53; c) S. S. Dehal, D. Kupfer, *Cancer Res.* **1995**, *55*, 1283; d) I. R. Hardcastle, M. N. Horton, M. R. Osborne, A. Hewer, M. Jarman, D. H. Phillips, *Chem. Res. Toxicol.* **1998**, *11*, 369; e) S. Shibutani, L. Dsaradhi, I. Terashima, E. Banoglu, M. W. Duffel, *Cancer Res.* **1998**, *58*, 647; f) L. Dasaradhi, S. Shibutani, *Chem. Res. Toxicol.* **1997**, *10*, 189.

[15] C. J. Schlesener, C. Amatore, J. K. Kochi, *J. Phys. Chem.* **1986**, *90*, 3747.

[16] A. Vessières, S. Top, P. Pigeon, E. A. Hillard, L. Boubeker, D. Spera, G. Jaouen, *J. Med. Chem.* **2005**, *48*, 3937.

[17] A. Vessières, E. A. Hillard, P. Pigeon, S. Top, K. Kowalski, J. Zakrzewski, G. Jaouen, unpublished results. Compounds **4**, **7**, and **8** were synthesized by McMurry cross-coupling reactions between 3-chloropropionylferrocene and 4,4′-dihydroxybenzophenone, ferrocene ethyl ketone and 4-hydroxy,4′-methoxybenzophenone, and 4-hydroxyphenylethyl ketone and 4-methoxyphenylferrocenyl ketone, respectively, and characterized by NMR spectroscopy and HRMS.

 © 2006 Wiley-VCH Verlag GmbH & Co. KGaA, Weinheim

[18] D. Plaźuk, A. Vessières, F. Le Bideau, G. Jaouen, J. Zakrzewski, *Tetrahedron Lett.* **2004**, *45*, 5425.
[19] K. Kowalski, A. Vessières, S. Top, G. Jaouen, J. Zakrzewski, *Tetrahedron Lett.* **2003**, *44*, 2749.
[20] E. A. Hillard, F. Le Bideau, A. Vessières, D. Plazuk, D. Spera, G. Jaouen, *ChemMedChem* **2005**, submitted.

 © 2006 Wiley-VCH Verlag GmbH & Co. KGaA, Weinheim

Molecular Complexes

DOI: 10.1002/anie.200503097

The C–H···π Hydrogen Bond in the Benzene–Trifluoromethane Adduct: A Rotational Study**

*Juan C. López, Walther Caminati, and José L. Alonso**

Herein, we report the structural and energetic features of the C–H···π interaction obtained from the analysis of the pure rotational spectra of the benzene–trifluoromethane molecular complex in its normal and ^{13}C-benzene species. The complexes were generated in a supersonic jet and characterized by Fourier transform microwave spectroscopy (FTMW).

Weak hydrogen bonds (WHB) are a major topic in hydrogen-bond research. The energies of these interactions lie within a few kJ mol^{-1} and approach those of van der Waals forces, but have the same directional properties of "classical" hydrogen bonds.[1] This behavior was recently shown for the C–H···O, C–H···F–C, and CH···S WHB interactions from investigations of the rotational spectra of several hydrogen-bonded molecular complexes generated in supersonic jets.[2–3] With this technique, precise information on the energetics and structural and dynamical aspects of such interactions is obtained in an environment free of the intermolecular interactions that take place in condensed media.

A special type of weak hydrogen bond is that in which the proton acceptor is a π system, its role as Lewis base being well established after the pioneering work of Pimentel and co-workers.[4] In recent years, there has been an increasing interest in C–H···π interactions.[5] The C–H group can display a wide range of polarities, and C–H···π interactions have been suggested to play important roles in many aspects of organic, biological, and supramolecular chemistry.[5] There is, however, a small amount of rotational information concerning weak C–H···π linkages.[6–8]

Benzene is the prototype of an aromatic π-system proton acceptor, and, indeed, O–H···π_{arom} and N–H···π_{arom} interactions have been characterized through rotational spectroscopy for C_6H_6–H_2O[9] and C_6H_6–NH_3.[10] Trifluoromethane (fluoroform, CHF_3) represents the prototype of a weak proton donor owing to the polarized character of its aliphatic C–H bond, which lies adjacent to three electron-withdrawing fluorine atoms. Within this role, it has been used as a partner to different proton-acceptor molecules to study C–H···O, C–H···S, and C–H···F weak hydrogen bonds.[3] Herein, we investigated the rotational spectrum of the benzene–trifluoromethane (C_6H_6–HCF_3) complex, which is probably an ideal model to analyze the energetics and structure of the C–H···π interaction.

The complex C_6H_6–HCF_3 was generated in a supersonic expansion, and its rotational spectrum was characterized by FTMW spectroscopy (see Experimental Section). After scans over a wide frequency range, six evenly spaced bands with the typical features of a symmetric top were observed, consistent with the C_{3v} configuration of the complex depicted in Figure 1. In Figure 2 we report the $J = 8 \leftarrow 7$ transition,

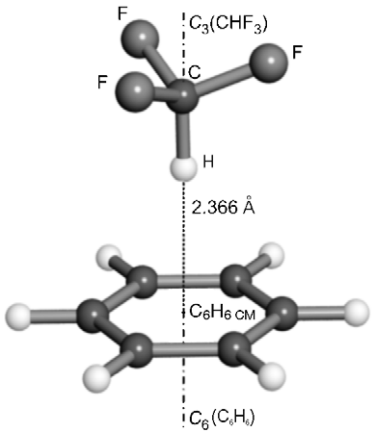


Figure 1. Drawing of the benzene–trifluoromethane adduct showing the collinearity of the symmetry axes of the two moieties and the distance $r(H\cdots C_{6}H_{6\,CM})$. CM = center of mass.

which, at high resolution, shows the complex pattern that arises from the practically free internal rotation of CHF_3 with respect to C_6H_6. Such a motion has been observed in several molecules[11] and complexes[12] with two internal symmetric rotors. In the present case, considering the C_6H_6 moiety as the framework, the internal rotation state of the complex is specified by the quantum number m, which gives the projection of the angular momentum of the CHF_3 unit on

[*] Prof. Dr. J. C. López, Prof. Dr. W. Caminati,[+] Prof. Dr. J. L. Alonso
Grupo de Espectroscopía Molecular (GEM)
Departamento de Química Física y Química Inorgánica
Facultad de Ciencias
Universidad de Valladolid
47005 Valladolid (Spain)
Fax: (+34) 983-423-204
E-mail: jlalonso@qf.uva.es

[+] Permanent address:
Dipartimento di Chimica "G. Ciamician" dell'Università
Via Selmi 2, 40126 Bologna (Italy)

[**] We would like to thank the Dirección General de Investigación, Ministerio de Educación y Ciencia, (project BQU2003-03275) and the Junta de Castilla y León—Fondo Social Europeo (project VA012C05) for financial support. W.C. thanks J.L.A. and co-workers for their very kind hospitality.

Supporting information for this article is available on the WWW under http://www.angewandte.org or from the author.

InterScience
© 2006 Wiley-VCH Verlag GmbH & Co. KGaA, Weinheim

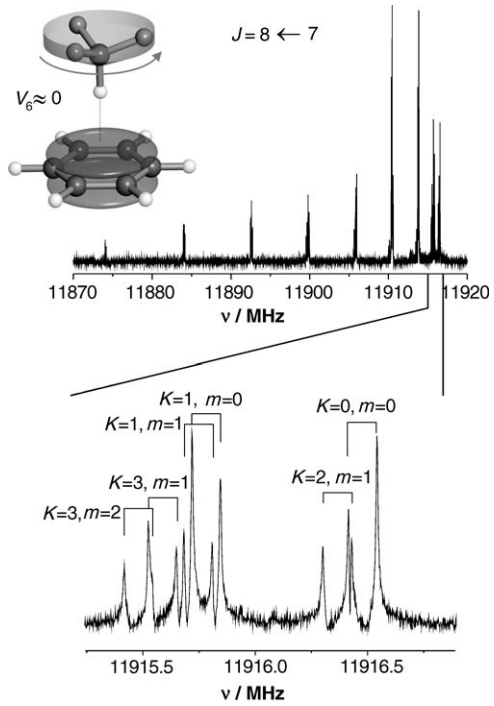


Figure 2. The $J+1 \leftarrow J=8 \leftarrow 7$ band of the benzene–trifluoromethane complex (upper trace). The high-resolution details (lower trace) show the complex patterns due to free internal rotation. Each rotational transition, split by the Doppler effect ($\lceil\ \rceil$), is labeled with the quantum numbers K and m.

the symmetry axis of the complex. In this way, the rotational transitions are uniquely labeled by J, $|K|$, and $\pm m$.[11,12] The observed frequencies were interpreted using the expression shown in Equation (1).

$$\nu = 2(J+1)[B - D_{JK}K^2 + H_{KJ}K^4 - D_{Jm}m^2 + H_{mJ}m^4 - D_{JKm}Km + L_{JK^3m^3}K^3m^3] - 4(J+1)^3[D_J - H_{JK}K^2 - H_{Jm}m^2 - H_{JKm}Km] \quad (1)$$

D_{JK}, D_{Jm}, and D_{JKm} are quartic centrifugal distortion constants. Higher order constants such as H_{JK}, H_{KJ}, H_{Jm}, H_{mJ}, H_{JKm}, or $L_{JK^3m^3}$ were found necessary to fit the data, given the extreme flexibility of the adduct. The parameters determined from the least-squares fit of a total of 125 lines are provided in Table 1.

As the benzene ring contains six equivalent carbon atoms, the spectrum of the [1-^{13}C]C_6H_6 species in natural abundance is expected to display an intensity of 6% of that of the most abundant species and the features of a slightly asymmetric top because the asymmetric isotopic substitution breaks down the C_{3v} symmetry of the complex. In addition, as typical of molecular systems with free internal rotation[13] in the ground state ($m=0$), the internal rotor (the CHF_3 subunit in our case) does not rotate. Consequently, the moment of inertia I_a does not take into account its mass contributions. This means that the value of the rotational constant A' should be coincident with the value of the rotational constant $C=$ 2813.8 MHz calculated for bare mono-^{13}C-substituted benzene.[14,15] Following this model, we could identify 34 transitions of the $m=0$ spectrum of the [1-^{13}C]C_6H_6–HCF_3

Table 1: Spectroscopic constants of the two isotopomers of C_6H_6–HCF_3.

Parameter	C_6H_6–HCF_3	[1-^{13}C]C_6H_6–HCF_3
A' [MHz]	–	2837(6)[a]
B [MHz]	744.840122(65)	741.33150(6)
C [MHz]		739.19544(6)
D_J [kHz]	0.46995(54)	0.4640(4)
D_{JK} [kHz]	42.3923(68)	41.792(8)
D_{Jm} [kHz]	166.820(18)	–
D_{JKm} [kHz]	−164.702(18)[b]	–
H_{JK} [Hz]	1.775(55)	1.49(6)
H_{KJ} [Hz]	−1.00(15)	–
H_{Jm} [Hz]	7.27(14)	–
H_{mJ} [Hz]	−37.17(83)	–
H_{JKm} [Hz]	7.48(12)[b]	–
$L_{JK^3m^3}$ [Hz]	1.96(38)[b]	–
σ[c] [kHz]	1.9	0.9
N[d]	125	34

[a] Standard errors in parentheses are given in units of the last digit. [b] The sign given for these constants is arbitrary. The sign given here corresponds to the choice of the sign of m given in Table 1 of frequencies (see Supporting Information). [c] Root-mean-square deviation of the fit. [d] Number of fitted transitions.

asymmetric-top species. These were fitted to the I^r representation of Watson's "S"-reduced Hamiltonian,[16] producing the spectroscopic constants reported in the second column of Table 1. The agreement between the rotational and centrifugal distortion constants for the parent and [1-^{13}C]C_6H_6–HCF_3 species supports the assignments. (All measured rotational frequencies are available in the Supporting Information.)

The experimental evidence that the normal species is a symmetric top and that the [1-^{13}C]C_6H_6–HCF_3 species is an asymmetric top leaves little doubt about the conformation of the complex shown in Figure 1. By assuming that the structures of the monomers[14,15,17] are not altered upon formation of the complex, the distances between the hydrogen atom of CHF_3 and the center of mass (CM) of benzene, $r(H\cdots C_6H_{6\,CM}) = 2.366(2)$ Å, and that between the two centers of mass, $r_{CM} = 3.8286$ Å, were calculated from the rotational constants.

The experimental evidence of an almost-free internal rotation are consistent with ab initio computations[18] at the MP2/6-311++G(d,p) level, including BSSE CP (basis-set superposition error counterpoise) corrections, which predict a V_6 barrier of less than 0.2 cm^{-1}.

Six low-energy vibrational modes take origin from the formation of the adduct, as the three translational and the three rotational degrees of freedom of one subunit disappear. We have already seen the effects on the spectra of one of these motions, the internal rotation of the CHF_3 subunit. Also, the stretching between the centers of mass of the two constituent molecules can be, in a first approximation, separated from the remaining vibrational modes. For symmetric-top complexes, such as C_6H_6–HCF_3, the stretching-force constant (k_s) can be estimated by approximating the complex to a molecule made of two rigid parts. This can be

 © 2006 Wiley-VCH Verlag GmbH & Co. KGaA, Weinheim

done by using the so-called pseudodiatomic approximation, expressed by Equation (2).[19]

$$k_s = 128\,\pi^4\,(\mu\, r_{CM})^2\, B^4/(h\, D_J) \quad (2)$$

where μ, r_{CM}, and D_J are the reduced mass, the distance between the centers of mass, and the first-order centrifugal distortion constant, respectively. Contributions to the D_J parameter from the free internal rotation of the CHF_3 group were calculated to be zero as a consequence of the collinearity between the principal axis *a* of the complex and the internal rotation axis.[20] By using $r_{CM} = 3.8286$ Å in Equation (2), we obtained $k_s = 6.8\ N\,m^{-1}$ and $\nu_{str} = 56\ cm^{-1}$. The dissociation energy (E_D) was evaluated to be 8.4 kJ mol^{-1} by assuming a Lennard-Jones potential function, according to the approximation shown as Equation (3).[21]

$$E_D = 1/72\, k_s\, r_{CM}^2 \quad (3)$$

The value of 8.4 kJ mol^{-1} is in reasonable agreement with the MP2/6-311++G(d,p) ab initio CP-corrected dissociation energy of 12.6 kJ mol^{-1} calculated in this work and with that calculated previously for the C–H···π-bonded form of C_6H_5F–HCF_3 ($E_D = 8.6$ kJ mol^{-1}).[22]

Structural data obtained from the rotational spectra, such as distances and dissociation energies, can be used to infer the nature of the WHB interactions. In the case of C–H···π interactions, no atom–atom distances are given but we can take $r(H\cdots C_6H_{6CM})$ as the C–H···π hydrogen-bond distance. Its value of 2.366(2) Å in C_6H_6–HCF_3 is remarkably shorter than those of 2.78 Å and 2.74 Å determined for the acetylene dimer[6] and the acetylene–ethylene complex,[7] respectively. The dissociation energy (8.4 kJ mol^{-1}) of the C_6H_6–HCF_3 complex is higher than those observed for the acetylene dimer (5.6 kJ mol^{-1})[6] and ethylene–acetylene (4.1 kJ mol^{-1})[7]. Both structural and energetic data support that the C–H···π_{arom} WHB bonds to aromatic rings are stronger than C–H···$\pi_{\equiv}$ or C–H···$\pi_{=}$ WHB interactions to triple or double bonds, respectively.

Let us discuss the C–H···C hydrogen bonds. The C_6H_6–HCF_3 complex could be considered as formed by a hexafurcated C–H···C_6 hydrogen bond. From the distance $r(H\cdots C_6H_{6CM}) = 2.366$ Å and the structure of benzene, the atom–atom distance $r_{H\cdots C} = 2.738$ Å is obtained which is similar to the C–H···O, C–H···S, and C–H···F–C WHB distances.[2,3] The dissociation energy for C_6H_6–HCF_3 is also of the same order of magnitude as determined for complexes formed by a combination of those bonds.[2,3] The individual energies of the C–H···O, C–H···S, or C–H···F–C interactions, which are calculated to be approximately 2.0 kJ mol^{-1},[2,3] are lower than that of the C–H···π_{arom} linkage. However, if this energy is interpreted as a sum of contributions from six C–H···C WHB interactions, it appears that each C–H···C contact (1.4 kJ mol^{-1}) would be weaker than each of the C–H···O, C–H···S, or C–H···F–C interactions.

The most interesting results of our investigation are:

1) The unrivalled resolving power and precision of molecular beam (MB)-FTMW spectroscopy allowed the detailed analysis of the spectrum of C_6H_6–HCF_3 and the determination of accurate spectroscopic parameters which supplied important chemical information, such as the structure or dissociation energy.
2) Here we show that in the complex C_6H_6–HCF_3, the CHF_3 moiety undergoes an almost fully free rotation.
3) The structural and energetic data obtained in this work on C_6H_6–HCF_3 reveal that the C–H···π_{arom} WHB bonds to aromatic rings are stronger than C–H···$\pi_{\equiv}$ or C-H···$\pi_{=}$ WHB interactions to triple or double bonds, respectively.
4) We note that while in previous WHB-linked adducts, a cooperative effect of some WHBs was required to stabilize them, for C_6H_6–HCF_3 a single C–H···π_{arom} bridge reaches the stability of maybe three or four C–H···O or C–H···F–C weak interactions. One could consider that the energy of the interaction between the benzene crown π system with the CHF_3 hydrogen atom is equivalent in magnitude to the sum of three or four of these weak interactions.

Experimental Section

Commercial samples of benzene and CHF_3 (Aldrich) were used without further purification. The spectrum of the monosubstituted [1-^{13}C]C_6H_6–HCF_3 isotopic species was measured in natural abundance.

The MB-FTMW spectrum in the 5–14 GHz frequency region was measured by using a molecular beam Fourier transform microwave spectrometer, as described previously.[23] A gas mixture of 2% of C_6H_6 and 2% HCF_3 in He at a total pressure of 1.5 bar was expanded through the solenoid valve (General Valve, Series 9, nozzle diameter 0.8 mm) into the Fabry-Pérot cavity. The frequencies were determined after Fourier transformation of the 8k data points time-domain signal, recorded at 100-ns intervals. Each rotational transition is split by a Doppler effect owing to the coaxial arrangement of the supersonic jet and resonator axes. The rest frequency is calculated as the arithmetic mean of the frequencies of the Doppler components. The estimated accuracy of frequency measurements is better than 3 kHz. Lines separated by more than 7 kHz are resolvable.

Received: August 31, 2005
Published online: November 28, 2005

Keywords: hydrogen bonding · molecular complexes · molecular dynamics · rotational spectroscopy

[1] G. R. Desiraju, T. Steiner, *The Weak Hydrogen Bond*, Oxford University Press, Oxford, **1999**.
[2] W. Caminati, S. Melandri, P. Moreschini, P. G. Favero, *Angew. Chem.* **1999**, *111*, 3105; *Angew. Chem. Int. Ed.* **1999**, *38*, 2924; S. Blanco, J. C. López, A. Lesarri, J. L. Alonso, *J. Mol. Struct.* **2002**, *612*, 255; Y. Tatamitani, B. Liu, J. Shimada, T. Ogata, P. Ottaviani, A. Maris, W. Caminati, J. L. Alonso, *J. Am. Chem. Soc.* **2002**, *124*, 2739; S. Blanco, J. C. López, A. Lesarri, W. Caminati, J. L. Alonso, *ChemPhysChem* **2004**, *5*, 1779; Y. Tatamitami, T. Ogata, *J. Mol. Spectrosc.* **2003**, *222*, 102.
[3] J. L. Alonso, S. Antolínez, S. Blanco, A. Lesarri, J. C. López, W. Caminati, *J. Am. Chem. Soc.* **2004**, *126*, 3244; E. J. Cocinero, R. Sánchez, S. Blanco, A. Lesarri, J. C. López, J. L. Alonso, *Chem. Phys. Lett.* **2005**, *402*, 4; W. Caminati, J. C. López, J. L. Alonso, J.-U. Grabow, *Angew. Chem.* **2005**, *117*, 3908; *Angew. Chem. Int. Ed.* **2005**, *44*, 3840.

 © 2006 Wiley-VCH Verlag GmbH & Co. KGaA, Weinheim

[4] W. Klemperer, M. W. Cronyn, A. M. Maki, G. C. Pimentel, *J. Am. Chem. Soc.* **1954**, *76*, 5846.
[5] M. Nishio, M. Hirota, Y. Umezawa, *The CH/π Interaction. Evidence, Nature, and Consequences*, Wiley, New York, **1998**.
[6] J. T. Fraser, R. D. Suenram, F. C. Lovas, A. S. Pine, J. T. Hougen, W. J. Lafferty, J. S. Muenter, *J. Chem. Phys.* **1988**, *89*, 6028.
[7] J. T. Fraser, F. C. Lovas, R. D. Suenram, J. Z. Gillies, C. W. Gillies, *Chem. Phys.* **1992**, *163*, 91.
[8] E. Arunan, H. S. Gutowsky, *J. Chem. Phys.* **1993**, *98*, 4294.
[9] S. Suzuki, P. G. Green, P. E. Bumgarner, S. Dasgupta, W. A. Goddard III, G. A. Blake, *Science* **1992**, *257*, 942.
[10] D. A. Rodham, S. Suzuki, R. D. Suenram, F. D. Lovas, S. Dasgupta, W. A. Goddard III, G. A. Blake, *Nature* **1993**, *362*, 735.
[11] W. Kirchhoff and D. R. Lide, Jr., *J. Chem. Phys.* **1965**, *43*, 2203; S. Blanco, M. E. Sanz, A. Lesarri, J. C. López, J. L. Alonso, *Chem. Phys. Lett.* **2004**, *397*, 379.
[12] G. T. Fraser, F. J. Lovas, R. D. Suenram, D. D. Nelson, Jr., W. Klemperer, *J. Chem. Phys.* **1986**, *84*, 5983; S. E. Forest, R. L. Kuczkowski, *Chem. Phys. Lett.* **1994**, *218*, 349.
[13] See, for example: W. Caminati, G. Cazzoli D. Troiano, *Chem. Phys. Lett.* **1976**, *43*, 65, and references therein.
[14] W. Caminati, S. Di Bernardo, L. Schäfer, S. Q. Kulp-Newton, K. Siam, *J. Mol. Struct.* **1990**, *240*, 263.
[15] M. Oldani, A. Bauder, *Chem. Phys. Lett.* **1984**, *108*, 7; M. Oldani, R. Widmer, G. Grassi, A. Bauder, *J. Mol. Struct.* **1988**, *190*, 31.
[16] J. K. G. Watson in *Vibrational Spectra and Structure, Vol. 6* (Ed.: J. R. Durig), Elsevier, New York, **1977**, p. 1.
[17] C. Hirose, *Bull. Chem. Soc. Jpn.* **1974**, *47*, 976; Y. Kawashima, A. P. Cox, *J. Mol. Spectrosc.* **1978**, *72*, 423.
[18] Gaussian 03 (Revision B.04), M. J. Frisch, G. W. Trucks, H. B. Schlegel, G. E. Scuseria, M. A. Robb, J. R. Cheeseman, J. A. Montgomery, Jr., T. Vreven, K. N. Kudin, J. C. Burant, J. M. Millam, S. S. Iyengar, J. Tomasi, V. Barone, B. Mennucci, M. Cossi, G. Scalmani, N. Rega, G. A. Petersson, H. Nakatsuji, M. Hada, M. Ehara, K. Toyota, R. Fukuda, J. Hasegawa, M. Ishida, T. Nakajima, Y. Honda, O. Kitao, H. Nakai, M. Klene, X. Li, J. E. Knox, H. P. Hratchian, J. B. Cross, C. Adamo, J. Jaramillo, R. Gomperts, R. E. Stratmann, O. Yazyev, A. J. Austin, R. Cammi, C. Pomelli, J. W. Ochterski, P. Y. Ayala, K. Morokuma, G. A. Voth, P. Salvador, J. J. Dannenberg, V. G. Zakrzewski, S. Dapprich, A. D. Daniels, M. C. Strain, O. Farkas, D. K. Malick, A. D. Rabuck, K. Raghavachari, J. B. Foresman, J. V. Ortiz, Q. Cui, A. G. Baboul, S. Clifford, J. Cioslowski, B. B. Stefanov, G. Liu, A. Liashenko, P. Piskorz, I. Komaromi, R. L. Martin, D. J. Fox, T. Keith, M. A. Al-Laham, C. Y. Peng, A. Nanayakkara, M. Challacombe, P. M. W. Gill, B. Johnson, W. Chen, M. W. Wong, C. Gonzalez, J. A. Pople, Gaussian, Inc., Pittsburgh, PA, **2003**.
[19] D. J. Millen, *Can. J. Chem.* **1985**, *63*, 1477; W. G. Read, E. J. Campbell, G. Henderson, *J. Chem. Phys.* **1983**, *78*, 3501.
[20] W. Caminati, *J. Mol. Spectrosc.* **1982**, *90*, 315.
[21] A. C. Legon, *Chem. Phys. Lett.* **1995**, *247*, 24.
[22] B. Reimann, K. Buchhold, S. Vaupel, B. Brutschy, Z. Havlas, V. Spirko, P. Hobza, *J. Phys. Chem. A* **2001**, *105*, 5560.
[23] J. L. Alonso, F. J. Lorenzo, J. C. López, A. Lesarri, S. Mata, H. Dreizler, *Chem. Phys.* **1997**, *218*, 267.

 © 2006 Wiley-VCH Verlag GmbH & Co. KGaA, Weinheim

Photoelectron Spectroscopy

DOI: 10.1002/anie.200503032

Photoelectron Spectroscopic Study of the First Singlet and Triplet States of the Cyclopentadienyl Cation**

*Hans Jakob Wörner and Frédéric Merkt**

The cyclopentadienyl cation ($C_5H_5^+$) is of fundamental importance in the study of diradicals and in the understanding of antiaromaticity and its effects on structure and chemical reactivity.[1–4] $C_5H_5^+$ is also predicted to be involved as an intermediate in the first steps of soot formation[5] and in the oxidation of aromatic hydrocarbons. The determination of the structure and energetics of the low-lying states in diradicals is a major goal of experimental and theoretical research in physical organic chemistry.[6,7]

Very little experimental information is available on the cyclopentadienyl cation. It has been observed by mass spectrometry,[8,9] but neither optical nor photoelectron spectra have been reported yet. The spectroscopic information on $C_5H_5^+$ is currently limited to an ESR spectrum in an SbF_5 matrix, which led to the conclusion that the electronic ground state is a triplet state with a small-to-negligible distortion from D_{5h} symmetry.[10]

The low-lying electronic configurations and corresponding states of $C_5H_5^+$ are given in Scheme 1 in which the symbols

$$\text{I: } (a_2'')^2(e_1'')^2(e_2'')^0 \;:\; {}^1A_1',\ {}^3A_2',\ {}^1E_2'$$
$$\text{II: } (a_2'')^1(e_1'')^3(e_2'')^0 \;:\; {}^1E_1',\ {}^3E_1'$$
$$\text{III: } (a_2'')^0(e_1'')^4(e_2'')^0 \;:\; {}^1A_1'$$

Scheme 1. The low-lying electronic configurations and corresponding states of $C_5H_5^+$.

in parentheses represent the symmetry of the five π molecular orbitals in the D_{5h} point group. The Hartree–Fock energies of the three electronic states of configuration I at D_{5h} geometry are $(2h+J_{23}-K_{23})$ for ${}^3A_2'$, $(2h+J_{23}+K_{23}, 2h+J_{22}-K_{23})$ for ${}^1E_2'$, and $(2h+J_{22}+K_{23})$ for ${}^1A_1'$, in which h, J_{ij}, and K_{ij} represent the one-electron orbital energy, the Coulomb, and the exchange integrals, respectively, and the indices designate the π molecular orbitals of $C_5H_5^+$ in order of increasing energy.[11] By symmetry, $J_{22}-J_{23}=2K_{23}$ and hence the three states are equally spaced by $2K_{23}$. The spacing of the

[*] H. J. Wörner, Prof. Dr. F. Merkt
Laboratorium für Physikalische Chemie
ETH Zürich
8093 Zürich (Switzerland)
Fax: (+41) 446-321-021
E-mail: frederic.merkt@ethz.ch

[**] We thank Vasiliy Goncharov (Emory University, Atlanta) for his contributions to the experimental work. This work was supported financially by the Swiss National Science Foundation and the ETH Zürich.

 © 2006 Wiley-VCH Verlag GmbH & Co. KGaA, Weinheim

electronic states of $C_5H_5^+$ also depends on vibronic and configuration interactions. The $^1E_2'$ state can be stabilized by a linear Jahn–Teller effect in the vibrational modes of e_1' symmetry, by a quadratic effect in the e_2' and e_2'' modes, or by a pseudo-Jahn–Teller coupling to the $^1A_1'$ state mediated by the e_2' modes.[12] The published ab initio calculations usually predict a ground state of $^3A_2'$ symmetry and D_{5h} structure,[1–3] with few exceptions.[5,13]

Two types of photoelectron spectroscopic experiments were performed: one involving single-photon vacuum-ultraviolet (VUV) excitation, the other with a $(1+1')$ two-photon ionization scheme via the $\tilde{A}\,^2A_2''$ intermediate state.[14] All electronic states belonging to configuration I are accessible in the VUV experiment. In contrast, ionization from the $\tilde{A}$ state of configuration $(a_2'')^1(e_1'')^4(e_2'')^0$ leads to the excited configurations II and III of Scheme 1 and the states of configuration I can only be observed through vibronic or configuration interactions. The $\tilde{A}\,^2A_2''$ state contains a contribution from the close-lying $^2A_2''$ state of configuration $(a_2'')^2(e_1'')^2(e_2'')^1$. If the admixture of this state is significant, all three electronic states of configuration I become accessible in the two-color experiment.

The only state of configuration I that can gain intensity in a photoelectron spectrum from excited states of configurations II and III is the $^1A_1'$ state (Scheme 1). The $^1E_2'$ state of configuration I can be accessed from the $\tilde{A}\,^2A_2''$ state through vibronic interactions, either by a coupling to the low-lying $^1E_1'$ state[15] of configuration II mediated by modes of symmetry e_1' or e_2', or by coupling to the $^1A_1'$ state of configuration I according to the strong pseudo-Jahn–Teller effect predicted by theory. The observation or nonobservation of certain ionic states in the two-color photoelectron spectroscopic experiment thus enables one to distinguish between the intensity-borrowing mechanisms listed above.

Figure 1 shows the VUV photoionization (dashed line) and the pulsed-field-ionization zero-kinetic-energy (PFI-ZEKE) photoelectron spectra (full line) of C_5H_5. The step observed in the photoionization spectrum at the position of the first photoelectron band marks the first adiabatic ionization threshold. From a comparison with the two-color photoelectron spectrum (see below), the photoelectron band is assigned to the transition to the vibrationless $\tilde{X}\,^3A_2'$ cationic ground state. The inset of Figure 1 shows a simulation of the rotational envelope of that band based on a rotational temperature of 8 K and the orbital ionization model described previously[16,17] assuming that ionization occurs from an orbital of d_π character. The simulation used neutral ground-state parameters previously reported,[14] Boltzmann population factors (including spin-statistical weights), and ionic rotational constants of the $\tilde{X}\,^3A_2'$ state taken from the ab initio equilibrium geometry reported elsewhere.[2] No further vibronic structure was observed in the spectral region 67800–71500 cm^{-1}, indicating almost diagonal Franck–Condon factors.

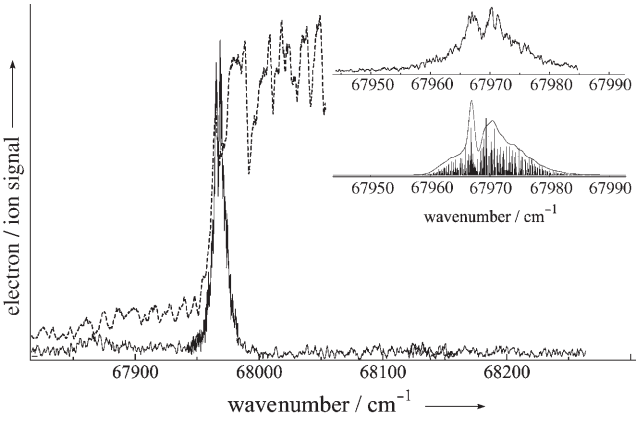


Figure 1. Single-photon photoionization (dashed line) and PFI-ZEKE photoelectron spectrum (full line) of the cyclopentadienyl radical in the region corresponding to the vibrationless $\tilde{X}\,^2E_1'' \rightarrow \tilde{X}\,^3A_2'$ transition. The inset shows a comparison of the rotational contour of the origin band (upper trace) with a simulation (lower trace) discussed in the text.

To record the two-color photoionization and PFI-ZEKE photoelectron spectra displayed in Figure 2, the first laser was kept fixed at the intensity maximum of the origin band of the $\tilde{X} \leftarrow \tilde{A}$ transition (29573.3 cm^{-1}) and the second laser was scanned across the ionization thresholds. The first PFI-ZEKE photoelectron band was observed 1600 cm^{-1} above the $^3A_2'$ origin together with a sharp increase in the photoionization signal. The absence of a sharp onset of the photoionization signal at the $\tilde{X}\,^3A_2'$ threshold indicates a negligible direct ionization to the $^3A_2'$ state which, in turn, rules out configurational mixing in the $\tilde{A}\,^2A_2''$ state as a significant intensity-borrowing mechanism. We attribute the structured photoionization signal between the $^3A_2'$ origin and the onset of the two-photon PFI-ZEKE photoelectron spectrum at ≈ 69500 cm^{-1} to electronic autoionization of low-n Rydberg states associated with series converging on electronically excited states of the cation.

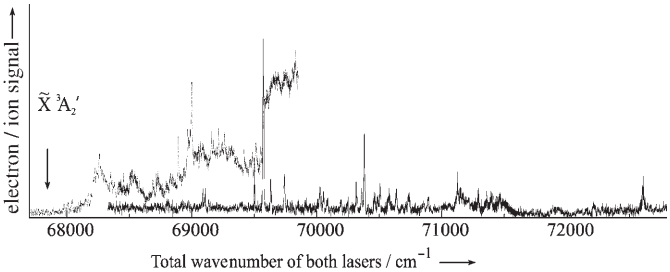


Figure 2. Photoionization (dotted line) and PFI-ZEKE photoelectron spectrum (full line) of the cyclopentadienyl radical recorded following resonance-enhanced two-photon ionization via the $\tilde{A}\,^2A_2''$ intermediate state. The wave number axis corresponds to the sum of the wave numbers of both lasers. The spectrum has not been corrected for the slow variation of the dye laser intensity with wave number.

Striking features of the two-color photoelectron spectrum are the presence of three bands located very close to the main band at 69567 cm^{-1} (see Figure 2) and an extended vibrational structure. The low-frequency structure must arise from a pseudorotational motion[18] because sequence bands can be ruled out and the wave numbers are too low to correspond to vibrational normal modes. It renders the identification of the origin of the photoelectron band difficult and at present only an upper bound of 69567 cm^{-1} can be given.

 © 2006 Wiley-VCH Verlag GmbH & Co. KGaA, Weinheim

The intensity of the transition to the upper electronic state is likely to originate from vibronic and configuration interactions (see above). Alternatively, it could stem from electronic channel interactions involving the low-*n* Rydberg states observed in the photoionization spectrum.[19]

The following conclusions can be drawn:

1. The higher of the two states must be $\tilde{a}\,^1E_2'$ because it displays both a pseudorotational motion and a strong Franck–Condon activity resulting from a Jahn–Teller distortion. The other singlet state ($^1A_1'$) of configuration I is predicted to lie more than 1 eV above the triplet ground state.[1,2]
2. Being only observed in the single-photon experiment, the lower of the two observed states must be the $\tilde{X}\,^3A_2'$ state. The almost diagonal Franck–Condon factors imply a D_{5h} structure.[*]
3. The adiabatic ionization energy corresponding to the formation of the $\tilde{X}\,^3A_2'$ state amounts to $(67969.2 \pm 4)\ cm^{-1}$ and the singlet–triplet interval is estimated to be less than $1600\ cm^{-1}$. As discussed in reference [6], this interval is a key quantity in the characterization of diradicals and an important test for the quality of ab initio calculations. Recent calculations at the highest levels of theory overestimate this interval (see Table 1).

Table 1: Adiabatic ionization thresholds (IE) of photoionizing transitions[a] of the cyclopentadienyl radical and first singlet–triplet interval of $C_5H_5^+$.[b]

	This work	Other work
$IE(C_5H_5, {}^3A_2')/(hc\,cm^{-1})$	67969.2 ± 4	67830 ± 800[8]
$IE(C_5H_5, {}^1E_2')/(hc\,cm^{-1})$	≤ 69570	
$\Delta E(S_0-T_0)/(hc\ cm^{-1})$	≤ 1600	2275[2] [c]

[a] $\tilde{X}\,^2E_1'' \rightarrow \tilde{X}\,^3A_2'$ and $\tilde{X}\,^2E_1'' \rightarrow \tilde{a}\,^1E_2'$. [b] $\Delta E(S_0-T_0)$. [c] CCSD(T)/cc-pVTZ//QCISD/6-31G** value.

4. From a measurement of the adiabatic ionization energy of cyclopentadiene ($(69094.5 \pm 3)\ cm^{-1}$)[21] and the known dissociation energy of cyclopentadiene, $D_0(C_5H_5{-}H)$ ($(22874 \pm 350)\ cm^{-1}$),[22] the dissociation energy of the cyclopentadiene radical cation, $D_0(C_5H_5^+{-}H)$, can be estimated to be $(21748 \pm 350)\ cm^{-1}$ and the 0-K appearance threshold of $C_5H_5^+$ in the photoionization of cyclopentadiene to be $(90843 \pm 350)\ cm^{-1}$. This value is more than 0.3 eV lower than the lowest value reported to date (11.57 eV).[23]
5. The ground state is a nondegenerate $^3A_2'$ state of D_{5h} structure and must therefore have five equivalent C–C bonds, a property usually expected for aromatic molecules.[24] The antiaromatic nature of the ground-state configuration manifests itself in the lowest degenerate singlet $\tilde{a}\,^1E_2'$ state. The Jahn–Teller effect allows the molecule to avoid by distortion the unfavorable antiaromatic electronic structure and favors other conjugatively more stable structures such as the allylic or dienylic structures.[3,25] The stabilization gained by circumventing antiaromaticity is however less than the destabilization by electron repulsion in the singlet state. This situation is in contrast to that of the next member of the cyclic $4n\pi$-electron family of antiaromatic molecules, cyclooctatetraene, the lowest singlet state of which lies below the triplet state.[7] Both results are in accordance with an early prediction of Borden and Davidson that planar $D_{(4n+1)h}$-symmetric $4n\pi$-electron annulenes have a triplet ground state because the repulsion between the unpaired electrons in the nondisjoint, nonbonding MOs increases the energy of the singlet configurations.[25]

The present measurements provide a stringent test for future ab initio calculations of structural and dynamical properties of diradicals. $C_5H_5^+$ is an ideal system to study the relationship between antiaromaticity, symmetry, and the Jahn–Teller effect. A full analysis of these effects will necessitate experimental studies with rotational resolution.

Experimental Section

The spectra were recorded by using a tunable UV/VUV laser system[26] coupled to a photoion/photoelectron time-of-flight (TOF) mass spectrometer and a pulsed source of jet-cooled radicals,[27], based on excimer laser photolysis of cyclopentadiene at 248 nm in a quartz capillary. Cyclopentadiene was produced from dicyclopentadiene (Fluka) through distillation and stored at −78 °C until used. It was introduced in a stream of neat helium into the nozzle reservoir at a stagnation pressure of 5 bar.

VUV radiation was generated by two-photon resonance-enhanced difference-frequency mixing ($\nu_{VUV} = 2\nu_1 - \nu_2$) in Kr by using a previously described procedure.[28] In the two-photon, two-color experiment, the outputs of the two dye lasers were combined on a dichroic mirror and crossed the molecular beam at right angles.

The photoelectron spectra were recorded by monitoring the pulsed-field ionization of high Rydberg states ($n \gg 200$) by using a technique known as PFI-ZEKE photoelectron spectroscopy.[29] An electric-field pulse sequence consisting of a discrimination pulse of $0.1\ V\,cm^{-1}$ and a detection pulse of $0.4\ V\,cm^{-1}$ delayed by 3 μs with respect to photoionization was used, which resulted in a resolution of $1\ cm^{-1}$. A correction of $1.6\ cm^{-1}$ was applied to compensate for the field-induced shift of the ionization thresholds. The photoionization spectra were obtained by measuring the $C_5H_5^+$ ion signal mass selectively as a function of the laser wavenumber. The ions were extracted by using a pulsed electric field of $336\ V\,cm^{-1}$ delayed by 200 ns with respect to the laser pulses.

Received: August 25, 2005
Published online: November 30, 2005

Keywords: antiaromaticity · ionization potentials · Jahn–Teller distortion · photoelectron spectroscopy · radicals

[*] The ground state of the radical undergoes a weak Jahn–Teller distortion with free pseudorotation[20] and has a time-averaged D_{5h} structure. The vibrational structure of the $\tilde{X}\,^2E_1'' \rightarrow \tilde{X}\,^3A_2'$ transition is reminiscent of the $\tilde{X}\,^2E_1'' \rightarrow \tilde{A}\,^2A_2''$ transition of the radical that is dominated by the origin band and only shows weak vibrational structure.

[1] W. T. Borden, E. R. Davidson, *J. Am. Chem. Soc.* **1979**, *101*, 3771.
[2] E. P. F. Lee, T. G. Wright, *Phys. Chem. Chem. Phys.* **1999**, *1*, 219.
[3] S. Zilberg, Y. Haas, *J. Am. Chem. Soc.* **2002**, *124*, 10683.
[4] A. D. Allen, M. Sumonja, T. T. Tidwell, *J. Am. Chem. Soc.* **1997**, *119*, 2371.

 © 2006 Wiley-VCH Verlag GmbH & Co. KGaA, Weinheim

[5] J. Feng, J. Leszczynski, B. Weiner, M. C. Zerner, *J. Am. Chem. Soc.* **1989**, *111*, 4648.
[6] W. T. Borden, E. R. Davidson, *Acc. Chem. Res.* **1981**, *14*, 69.
[7] P. G. Wenthold, D. A. Hrovat, W. T. Borden, W. C. Lineberger, *Science* **1996**, *272*, 1456.
[8] F. P. Lossing, J. C. Traeger, *J. Am. Chem. Soc.* **1974**, *97*, 1579.
[9] "Carbon Skeletal Rearrangements via Pyramidal Carbocations": H. Schwarz, H. Thies, W. Franke in *Ionic Processes in the Gas Phase* (Ed.: M. A. A. Ferreira), Reidel Publishing, Dordrecht, The Netherlands, **1984**, p. 267–286.
[10] M. Saunders, R. Berger, A. Jaffe, J. M. McBride, J. O'Neill, R. Breslow, J. M. Hoffman, Jr., C. Perchonock, E. Wasserman, R. S. Hutton, V. J. Kuck, *J. Am. Chem. Soc.* **1973**, *95*, 3017.
[11] T. W. Borden, *Diradicals*, Wiley, New York, **1982**.
[12] P. C. Engelking, W. C. Lineberger, *J. Chem. Phys.* **1977**, *67*, 1412.
[13] M. N. Glukhovtsev, R. D. Bach, S. Laiter, *J. Phys. Chem.* **1996**, *100*, 10952.
[14] L. Yu, S. C. Foster, J. M. Williamson, M. C. Heaven, T. A. Miller, *J. Phys. Chem.* **1988**, *92*, 4263.
[15] H. C. Longuet-Higgins, K. L. McEwen, *J. Chem. Phys.* **1957**, *26*, 719.
[16] A. D. Buckingham, B. J. Orr, J. M. Sichel, *Philos. Trans. R. Soc. London Ser. A* **1970**, *268*, 147.
[17] S. Willitsch, F. Merkt, *Int. J. Mass Spectrom.* **2005**, *245*, 14.
[18] H. C. Longuet-Higgins, U. Öpik, M. H. L. Pryce, R. A. Sack, *Proc. R. Soc. London Ser. A* **1958**, *244*, 1.
[19] F. Merkt, T. P. Softley, *Int. Rev. Phys. Chem.* **1993**, *12*, 205.
[20] B. E. Applegate, A. J. Bezant, T. A. Miller, *J. Chem. Phys.* **2001**, *114*, 4869.
[21] H. J. Wörner, F. Merkt, still unpublished, **2005**.
[22] K. Roy, M. Braun-Unkhoff, P. Frank, T. Just, *Int. J. Chem. Kinet.* **2001**, *33*, 821.
[23] J. L. Occlowitz, G. L. White, *Aust. J. Chem.* **1968**, *21*, 997.
[24] V. Gogonea, P. von R. Schleyer, P. R. Schreiner, *Angew. Chem.* **1998**, *110*, 2045; *Angew. Chem. Int. Ed.* **1998**, *37*, 1945.
[25] W. T. Borden, E. R. Davidson, *J. Am. Chem. Soc.* **1977**, *99*, 4587.
[26] P. Rupper, F. Merkt, *Rev. Sci. Instrum.* **2004**, *75*, 613.
[27] S. Willitsch, J. M. Dyke, F. Merkt, *Helv. Chim. Acta* **2003**, *86*, 1152.
[28] F. Merkt, A. Osterwalder, R. Seiler, R. Signorell, H. Palm, H. Schmutz, R. Gunzinger, *J. Phys. B* **1998**, *31*, 1705.
[29] G. Reiser, W. Habenicht, K. Müller-Dethlefs, E. W. Schlag, *Chem. Phys. Lett.* **1988**, *152*, 119.

 © 2006 Wiley-VCH Verlag GmbH & Co. KGaA, Weinheim

Protein Ligation

DOI: 10.1002/anie.200502266

Diels–Alder Ligation and Surface Immobilization of Proteins**

*Aline Dantas de Araújo, Jose M. Palomo, Janina Cramer, Maja Köhn, Hendrik Schröder, Ron Wacker, Christof Niemeyer, Kirill Alexandrov, and Herbert Waldmann**

The site-specific equipment of proteins and other biomolecules with additional functional groups for subsequent biochemical and biological investigations, for example, fluorophores, spin probes, photoactivatable groups, and affinity tags, is among the most frequently employed and important methods of research in the life sciences. A number of techniques for protein derivatization are now established.[1] Recently, in particular, aldehyde-assisted ligations,[2] native chemical ligation,[3] expressed protein ligation,[4] expressed enzymatic ligation,[5] Staudinger ligation,[6] and the application of the Huisgen azide cycloaddition[7] have been developed as powerful new methods, thereby advancing the field significantly. However, due to the multifunctionality of biomacromolecules in general and proteins in particular and the manifold applications of such techniques, there is a major and continuing demand for the development of new technology providing alternatives to the methods mentioned above. The chemistry required must be compatible with the functional groups found in proteins and proceed chemoselectively under mild conditions and in aqueous solution, preferably in

[*] Dr. A. D. de Araújo, Dr. J. M. Palomo, Dr. M. Köhn, Prof. H. Waldmann
Department of Chemical Biology
Max-Planck-Institut für Molekulare Physiologie
Otto-Hahn-Strasse 11, 44227 Dortmund (Germany)
and
Fachbereich 3, Chemische Biologie
Universität Dortmund (Germany)
Fax: (+49) 231-133-2499
E-mail: herbert.waldmann@mpi-dortmund.mpg.de

Dr. J. Cramer, Dr. K. Alexandrov
Department of Physical Biochemistry
Max-Planck-Institut für molekulare Physiologie
Otto-Hahn-Strasse 11, 44227 Dortmund (Germany)

Prof. C. Niemeyer
Fachbereich 3, Chemische Biologie
Biologisch-Chemische Mikrostrukturtechnik
Universität Dortmund (Germany)

Dr. H. Schröder, Dr. R. Wacker
Chimera Biotec GmbH
Emil-Figge-Strasse 76a, 44227 Dortmund (Germany)

[**] This research was supported by the Max-Planck Gesellschaft and the Fonds der Chemischen Industrie. J.M.P. would like to thank the European Molecular Biology Organization (EMBO) for a long term Fellowship.

Supporting information for this article is available on the WWW under http://www.angewandte.org or from the author.

WILEY InterScience DISCOVER SOMETHING GREAT
© 2006 Wiley-VCH Verlag GmbH & Co. KGaA, Weinheim

the absence of any potentially denaturating cosolvent. The Diels–Alder reaction is a highly selective transformation and can proceed in water with a higher velocity and selectivity than in organic solvents.[8] Its compatibility with biomolecules has been explored elegantly in the bioconjugation and/or immobilization of oligonucleotides and other biomolecules.[9]

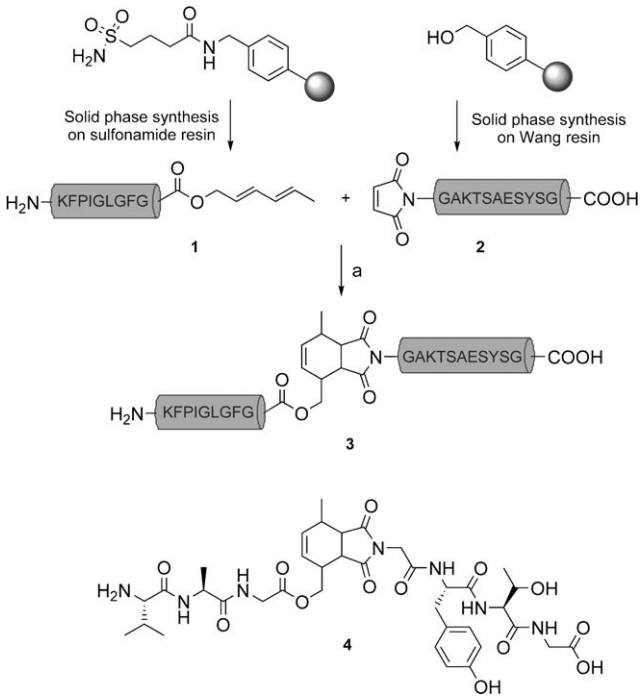
Herein, we demonstrate that the Diels–Alder reaction can be used for efficient ligation reactions of peptides and entire functional proteins.

In order to develop the underlying methodology, several peptides were initially equipped with a diene and dienophile, respectively. For instance, nonapeptide **1** (Scheme 1) was synthesized on the solid phase by employing a sulfonamide resin.[10] The *trans*,*trans*-2,4-hexadienyl ester was introduced by alkylation of the acylsulfonamide linker and subsequent treatment with the corresponding alcohol.[11] The maleimido peptide **2** was synthesized on Wang resin by applying the 9-fluorenylmethoxycarbonyl (Fmoc)/*t*Bu protocol.[11]

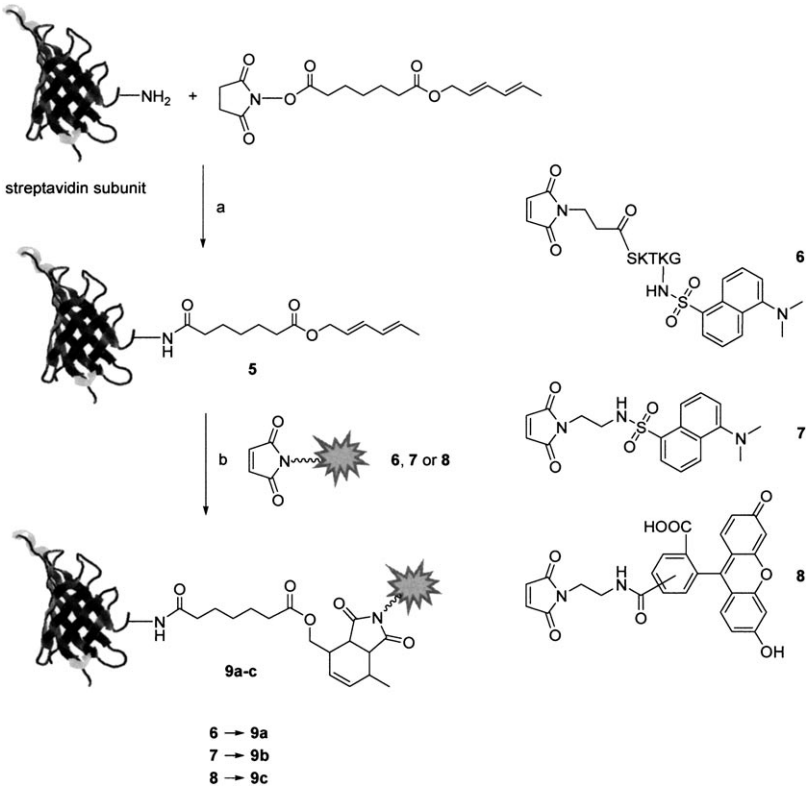
Upon exposure of the peptides to each other at 25 °C in water, the desired cycloaddition proceeded smoothly with a conversion of 92 % after 47 h. Peptide **3** was isolated in 67 % yield and identified by NMR spectroscopy and ESI-MS (calculated mass: *m*/*z* 2153.1; observed mass: *m*/*z* 2153.0). Spectroscopic and chromatographic analysis of Diels–Alder adduct **3** did not allow the stereoselectivity of the cycloaddition to be conclusively determined. However, peptide **4**, which was synthesized by analogy, was obtained as a single *endo* stereoisomer.[12] This observation indicates that in this transformation the peptides function as efficient stereodirecting groups to yield a cycloadduct with at least 95 % diastereomeric excess.

These results demonstrate that the Diels–Alder process is fully compatible with the nucleophilic side chains incorporated into the amino acids lysine, serine, threonine, and tyrosine. We note, however, that free SH groups of cysteine residues undergo conjugate addition to the maleimide and, therefore, they require protection (data not shown; see also below).

The applicability of the method and the reaction conditions described above to protein labeling was initially investigated by employing streptavidin as a model protein. Streptavidin is composed of four biotin-binding subunits containing lysine but not cysteine residues.[13] The protein was acylated with a hexadienyl bifunctional linker on the lysine side chains (Scheme 2). MALDI-TOF analysis indicated that, on average, each subunit was acylated once if a linker/protein ratio of 6:1 was chosen (see the Supporting Information). After purification by ultrafiltration, the modified protein **5** was treated with maleimide-functionalized fluorescent peptide **6** or maleimide-functionalized fluorophores **7** or **8** at 25 °C in water. After removal of unligated peptide dienophile by ultrafiltration, analysis of the reaction products by sodium dodecylsulfate (SDS) PAGE (Figure 1) and MALDI-MS (see the Supporting Information) showed that the desired cycloadducts had been formed. If nonfunctionalized streptavidin was combined with dienophile **6** at pH values of 5.5–



Scheme 1. Peptide ligation by means of a Diels–Alder cycloaddition. a) 10 mM Peptide, H_2O, 25 °C, 47 h.



Scheme 2. Diels–Alder ligation of the streptavidin-derived diene **5** with dienophiles **6**–**8**. a) 2 mg mL^{-1} Streptavidin (1 equiv) in H_2O, hexadienyl cross-linker (6 equiv), 2 h, 25 °C; b) 100 μM **5** (1 equiv) in H_2O or 10 mM sodium phosphate buffer (pH 5.5–6.5), **6**, **7**, or **8** (30 equiv), 24 h, 25 °C.

 © 2006 Wiley-VCH Verlag GmbH & Co. KGaA, Weinheim

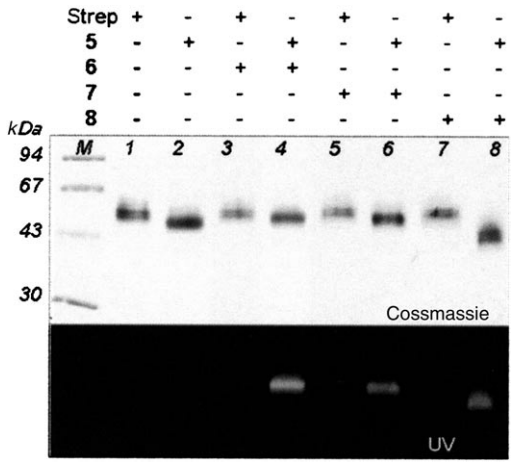


Figure 1. SDS PAGE analysis of the streptavidin conjugates **9a–c** obtained by Diels–Alder ligation of streptavidin-diene **5** (lane 2) with maleimides **6** (lane 4), **7** (lane 6), and **8** (lane 8), respectively. Control experiments showed that no binding occurs when wild-type streptavidin (lane 1) is combined with maleimides **6** (lane 3), **7** (lane 5), or **8** (lane 7) in water under slightly acidic conditions (pH 5.5–6.5). The 15% SDS PAGE gel was photographed while exposed to UV light (lower part) prior to Coomassie Blue staining (upper part). Strep: streptavidin, M: molecular-weight marker.

6.5, coupling to the protein through nucleophilic attack to the α,β-unsaturated imide could not be detected, whereas this side reaction occurs at pH 7. Thus, under slightly acidic conditions, the Diels–Alder ligation employing maleimido-modified peptides and fluorescent probes is chemoselective. The labeling of streptavidin by the cycloaddition method did not impair the biotin-binding activity of the protein,[14] a fact indicating that it remains fully functional after the Diels–Alder ligation process.

The stability of the diene unit incorporated into proteins in aqueous solutions and its compatibility with the functional groups found in these biopolymers opens up an opportunity to combine the Diels–Alder ligation method with other ligation techniques. In such a combined strategy, the protein of interest is initially functionalized by a general strategy with a diene unit and then the resulting protein-derived diene can be further functionalized site specifically, that is, at the C terminus, by Diels–Alder reactions with different dienophiles under very mild conditions.

This approach was successfully implemented by employing the Rab7 protein as a representative biologically relevant example. The Rab proteins are key regulators of vesicular transport that control budding, transport, and fusion of intracellular vesicles.[15] Many aspects of these multistep processes including, for instance, the timing of the cellular events and the localization of the proteins involved are only partly understood; differently and site-specifically labeled Rab proteins are considered to be versatile probes for the study of such biological events.[16–18]

Initial functionalization of Rab7 was achieved by means of expressed protein ligation.[4] To this end, recombinant truncated Rab7 thioester **10** was expressed as described[17] and then ligated with peptide hexadienyl ester **11** under reducing conditions[16] to yield Rab hexadienyl ester **12** (Scheme 3). The ligation process generates a nucleophilic cysteine side chain in addition to the three cysteines that are buried in the core of the Rab protein. To avoid undesired modification of these mercapto groups in the subsequent reaction with the maleimide, the accessible cysteine side chains were protected as disulfides by treatment with Ellmann's reagent[19] immediately after the ligation reaction to yield masked protein ester **13**.[20]

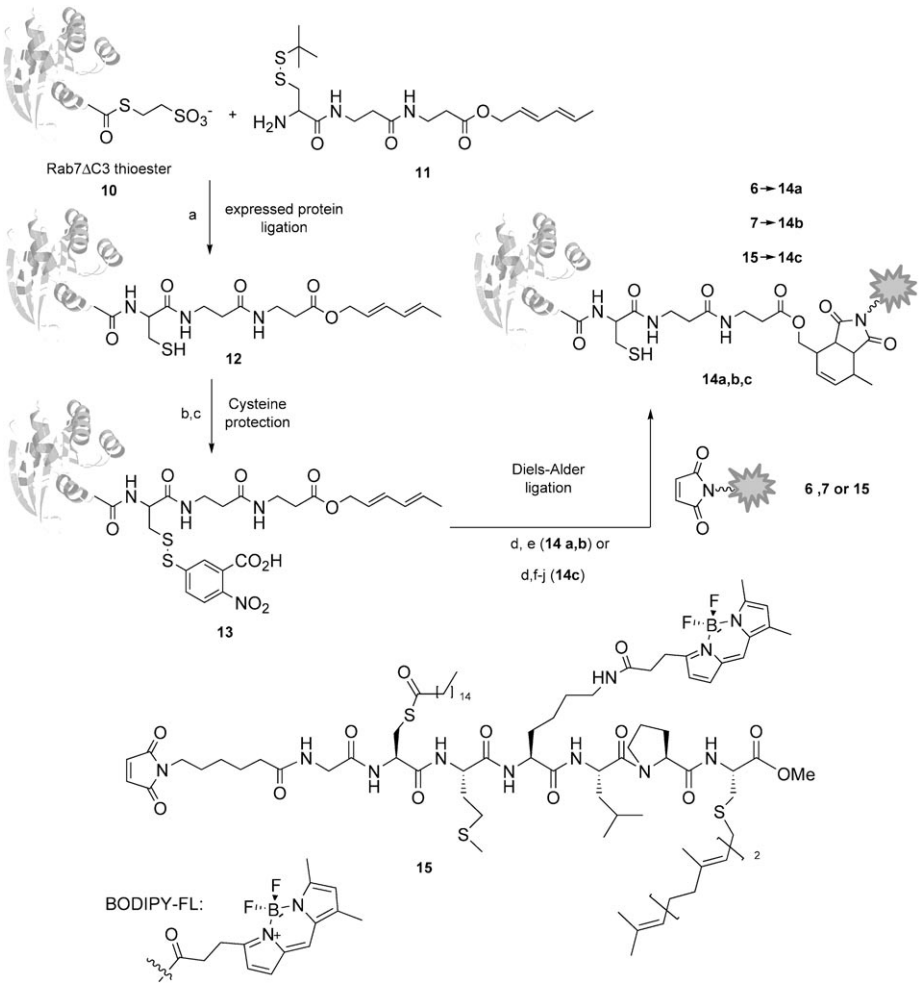
Protein hexadienyl ester **13** was then dialyzed against phosphate buffer (pH 6) to remove all small molecules (MESNA, Ellmann's reagent, dienyl peptide **11**) and subjected to a Diels–Alder reaction with peptide-derived dienophile **6** or dansyl derivative **7** for 24 h. The coupling reactions were terminated by addition of excess dithiothreitol which traps the dienophile and simultaneously converts the disulfides into unmasked thiols.

The ligation products **14a** and **14b** were analyzed by SDS PAGE (Figure 2A), and all intermediates and final products were identified by ESI-MS (see the Supporting Information). In the presence of a 100-fold excess of dienophile the hexadienyl protein is converted into the expected fluorescent conjugates with high efficiency (approximately 90%). In the presence of 30 equivalents of dienophile the ligation proceeds as well; however, in this case a longer reaction time is required to reach complete transformation. Undesired multiple labeling of Rab7 could not be detected. The purification of the ligated Rab proteins was carried out as previously described.[16a]

Upon UV illumination a distinct fluorescence band is observed that cannot be detected for wild-type Rab7 prefunctionalized with Ellman's reagent prior to ligation. Treatment of dienophile **6** with wild-type Rab that was not protected at the cysteine SH groups leads to the incorporation of the fluorescent label. Likewise treatment of dienophile **6** with wild-type Rab that was protected at the cysteine SH groups does not lead to incorporation of the fluorescent label (see the Supporting Information).

In order to establish whether the generated proteins remain natively folded and functionally active, we analyzed the interaction of semisynthetic protein **14a** with Rab escort protein 1 (REP-1). REP-1 is an accessory factor that facilitates prenylation of Rab guanosine triphosphatases (GTPases) by presenting them to Rab geranylgeranyltransferase and subsequently by delivering them to the target membranes. Recognition of Rab proteins by REP-1 occurs through a large protein–protein interface and requires integrity of the Rab GTPase ternary structure.[17] To analyze the interaction of Rab7 with REP-1 we took advantage of the dansyl label attached to the flexible C terminus of Rab7; this label enables the use of fluorescence spectroscopy to monitor the interaction of both proteins. When the solution of semisynthetic Rab7 **14a** fluorescently excited at 333 nm was titrated with increasing concentrations of REP-1a, a dose-dependent and saturable increase of the fluorescence emission at 440 nm was observed (Figure 3). Titration data could be fitted by using a quadratic equation describing the binding curve and were consistent with a 1:1 stoichiometry and a K_d value of 2 nM. This K_d value is very close to the one determined earlier with mant-GDP-bound Rab7.[21] The

 © 2006 Wiley-VCH Verlag GmbH & Co. KGaA, Weinheim



Scheme 3. Combination of expressed protein ligation and Diels–Alder ligation for site-specific modification of the Rab7 protein. a) 0.3 mM Thioester-tagged Rab7ΔC3 **10** in 5 mM sodium phosphate buffer (pH 7.5), 20 mM NaCl, 20 mM MESNA, 0.4% CHAPS, 10 μM GDP, 0.2 mM $MgCl_2$, and 6 mM peptide **11**, overnight, 16°C; b) DTNB, 30 min, 25°C; c) dialysis against DA buffer (5 mM sodium phosphate buffer (pH 6.0), 20 mM NaCl, 0.2 mM $MgCl_2$, 20 μM GDP); d) 40 μM Rab7 **13** (1 equiv) in DA buffer, maleimide **6** or **7** (100 equiv), 24 h, 25°C; e) DTT, 2 h, 25°C: f) 40 μM Rab7 **13** (1 equiv) in DA buffer, maleimide **15** (100 equiv) in $MeOH/CH_2Cl_2$ (3:1), 24 h, 25°C (ligated product precipitates); g) centrifugation and washing of the pellet with MeOH (×3) to remove excess peptide; h) dissolution of the precipitate in denaturation buffer (100 mM Tris-HCl (pH 8.0), 6 M guanidinium-HCl, 100 mM DTE, 1% CHAPS, 1 mM EDTA) overnight at 4°C; i) protein renaturation by 25-fold dilution dropwise into refolding buffer (50 mM HEPES (pH 7.5), 2.5 mM DTE, 2 mM $MgCl_2$, 10 μM GDP, 1% CHAPS, 400 mM arginine-HCl, 400 mM trehalose, 0.5 mM PMSF, 1 mM EDTA) with stirring, 25°C, 3 h; j) protein concentration to approximately 40 μM by ultracentrifugation (Amicon 10 kDa cut-off). MESNA = sodium 2-mercaptoethane sulfonate, CHAPS = 3-[(3-cholamidopropyl)-dimethyl-ammonio]-1-propane sulfonate, GDP = guanosine 5′-diphosphate, DTNB = 5,5′-dithiobis-(2-nitrobenzoic acid), DA = Diels–Alder, DTT = dithiothreitol, Tris = tris(hydroxymethyl)aminomethane, DTE = dithioerythritol, EDTA = ethylenediaminetetraacetate, HEPES = 2-[4-(2-hydroxyethyl)-1-piperazinyl]ethanesulfonic acid, PMSF = phenylmethylsulfonyl fluoride.

obtained data prove that the developed procedure yields fully active functionalized Rab7 protein.

Our results demonstrate that the Diels–Alder ligation offers an advantageous new opportunity for the site-selective functionalization and labeling of proteins and peptides. It proceeds under very mild conditions with high selectivity and is compatible with most functional groups found in proteins. Its combination with other ligation methods, particularly expressed protein ligation, is feasible and allows a given protein to be rapidly equipped with different functional groups in a site-specific manner, that is, at the C terminus.

The use of the two-step ligation strategy delineated above is particularly indicated if reporter groups or tags need to be introduced into proteins that are not stable under the conditions of expressed protein ligation. For instance, in the course of a different research program, we observed that the fluorescence of the BODIPY label (Scheme 3), one of the most advantageous and very often used fluorophores, is lost during attempted ligation of BODIPY-functionalized peptides to proteins by means of expressed protein ligation. However, fluorescently labeled Rab proteins are formed if diene-modified Rab protein **13** is subjected to Diels–Alder ligation with BODIPY-labeled peptides.

Thus, upon treatment of protein dienyl ester **13** with maleimide-tagged doubly lipidated peptide **15**, the desired lipid-modified protein **14c** was formed and isolated (Scheme 3 and Figure 2B). The ligated protein was identified by ESI-MS (calculated mass for $[M^+]$: 25496 Da; found: 25495 Da). Lipidated peptide **15** represents a fluorescently labeled analogue of the *S*-palmitoylated and *S*-farnesylated C terminus of the human Ras protein and was synthesized as described.[22] Notably, the synthesis of chimeric lipoprotein **14c** also demonstrates that the Diels–Alder ligation is applicable to the synthesis of sensitive protein conjugates like acid- and base-sensitive lipoproteins.[23]

In order to further demonstrate the scope of applications of the Diels–Alder reactions with dienyl-modified proteins, we investigated the possibility of employing this transformation for the immobilization of proteins on glass slides.[24] Streptavidin was chosen as a model protein and was first ligated to a cyclopentadiene derivative by analogy to the procedure described above to yield protein **16** (Scheme 4 A). On average, each streptavidin subunit was acylated with one dienyl linker, as indicated by the mass spectrum (data not shown). The protein–cyclopentadiene conjugate was then

 © 2006 Wiley-VCH Verlag GmbH & Co. KGaA, Weinheim

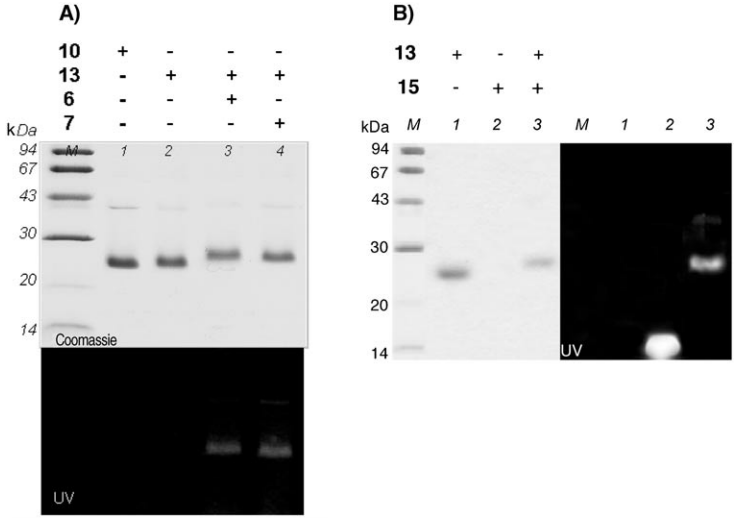


Figure 2. SDS PAGE analysis of the Diels–Alder ligation products. A) **14a** (lane 3) and **14b** (lane 4) obtained from masked Rab7 hexadienyl ester **13** (lane 2) with maleimide probes **6** and **7**, respectively. B) **14c** (lane 3) obtained from masked Rab7 hexadienyl ester **13** (lane 1) with BODIPY-labeled maleimide peptide **15** (lane 2).

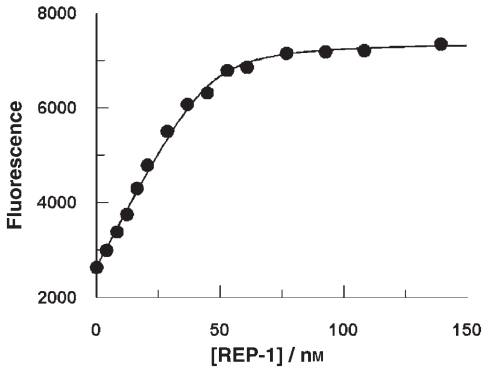
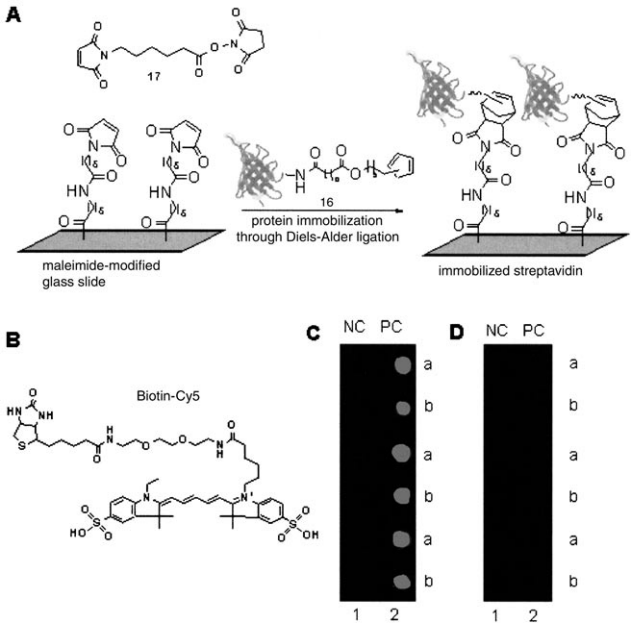


Figure 3. Spectrofluorometric titration of **14a** with REP-1. Conditions: 25 °C, 25 mM HEPES (pH 7.2), 40 mM NaCl, 2 mM $MgCl_2$, 2 mM DTE, and 20 μM GDP. The concentration of **14a** complex was 50 nM. The excitation/emission wavelengths were fixed at 333/440 nm. Data were fitted to a quadratic equation as implemented in the program Grafit 5.1 (Erithacus software) leading to a dissociation constant (K_d) value of 1.9 ± 0.5 nM, which is consistent with a 1:1 stoichiometry.

subjected to immobilization on a maleimide-functionalized surface. To this end, glass slides with an amino-functionalized surface were decorated with the functionalized maleimide **17** (Scheme 4 A). For the preparation of the maleimide-functionalized surface, an aminocaproic acid linker was introduced to establish distance between the functional groups and the surface; this was followed by coupling of the maleimide through amide formation.[25]

For the immobilization experiments, the diene-modified streptavidin (positive control) and the nonmodified streptavidin as a negative control were dissolved in double-distilled water (pH ≈ 6) at 7 μM concentration and spotted to the maleimide-modified surface by using a piezo-driven spotting robot.[26] After 8 h the slides were washed with water (3 times for 5 min) and buffer (3 times for 5 min). The slides were then



Scheme 4. A) Immobilization of the diene-functionalized streptavidin **16** on maleimide-functionalized glass slides. B) Structure of biotin–Cy5. C) Binding of Cy5-labeled biotin to immobilized diene-functionalized streptavidin (lane 2) as a positive control (PC) and nonmodified streptevidin (lane 1) as a negative control (NC). a = without glycerol (15%), b = with glycerol. D) Same as (C) but with the maleimide-functionalized surface blocked by 5% mercaptoethanol.

treated with Cy5-labeled biotin (10 nM, 30 min at room temperature; Scheme 4 B), and the fluorescence signals were recorded and quantified after removal of excess reagent. The results for the immobilization of diene-modified streptavidin are shown in Scheme 4 C. The immobilization of diene-modified streptavidin, either without or in the presence of 15 vol% of glycerol in the spotting solution, gave clear fluorescence signals, whereas no signal was observable for the negative control. If the maleimide-modified surface was blocked by treatment with mercaptoethanol prior to application of the protein-derived diene no signal was observable (Scheme 4 D), a result showing that the immobilization was due to covalent-bond formation with the immobilized dienophile. These results clearly demonstrate that the Diels–Alder reaction provides a new method for the immobilization of proteins on glass slides.

Received: June 28, 2005
Revised: August 3, 2005
Published online: November 29, 2005

Keywords: Diels–Alder reaction · immobilization · ligation · protein synthesis · proteins

[1] G. T. Hermanson, *Bioconjugate Techniques*, Academic Press, San Diego, **1996**.
[2] J. P. Tam, J. Xu, K. D. Eom, *Biopolymers* **2001**, *60*, 194–205.
[3] P. E. Dawson, S. B. H. Kent, *Annu. Rev. Biochem.* **2000**, *69*, 923–960.
[4] T. W. Muir, *Annu. Rev. Biochem.* **2003**, *72*, 249–289.

 © 2006 Wiley-VCH Verlag GmbH & Co. KGaA, Weinheim

[5] Z. Machova, R. von Eggelkraut-Gottanka, N. Wehofsky, F. Bordusa, A. G. Beck-Sickinger, *Angew. Chem.* **2003**, *115*, 5065 – 5067; *Angew. Chem. Int. Ed.* **2003**, *42*, 4916 – 4918.
[6] E. Saxon, C. R. Bertozzi, *Science* **2000**, *287*, 2007 – 2010.
[7] H. C. Kolb, K. B. Sharpless, *Drug Discovery Today* **2004**, *9*, 1128 – 1137.
[8] a) P. A. Grieco, *Organic Reactions in Aqueous Media*, Wiley, New York, **1997**; b) U. M. Lindström, *Chem. Rev.* **2002**, *102*, 2751 – 2772; c) S. Otto, J. B. F. N. Engberts, *Org. Biomol. Chem.* **2003**, *1*, 2809 – 2820.
[9] a) K. W. Hill, J. Tauton-Rigby, J. D. Carter, E. Kropp, K. Vagle, W. Pieken, D. P. C. McGee, G. M. Husar, M. Leuck, D. J. Anziano, D. P. Sebesta, *J. Org. Chem.* **2001**, *66*, 5352 – 5358; b) G. M. Husar, D. J. Anziano, M. Leuck, D. P. Sebesta, *Nucleosides Nucleotides Nucleic Acids* **2001**, *20*, 559 – 566; c) H. A. Latham-Timmons, A. Wolter, J. S. Roach, R. Giare, M. Leuck, *Nucleosides Nucleotides Nucleic Acids* **2003**, *22*, 1495 – 1497; d) B. T. Houseman, J. H. Huh, S. J. Kron, M. Mrksich, *Nat. Biotechnol.* **2002**, *20*, 270 – 274; e) W. Yeo, M. N. Yousaf, M. Mrksich, *J. Am. Chem. Soc.* **2003**, *125*, 14994 – 14995; f) W. S. Dillmore, M. N. Yousaf, M. Mrksich, *Langmuir* **2004**, *20*, 7223 – 7231; g) B. T. Houseman, M. Mrksich, *Chem. Biol.* **2002**, *9*, 443 – 454; h) A. Berkin, B. Coxon, V. Pozsgay, *Chem. Eur. J.* **2002**, *8*, 4424 – 4433; i) V. Pozsgay, N. E. Vieira, A. Yergey, *Org. Lett.* **2002**, *4*, 3191 – 3194.
[10] B. J. Backes, J. A. Ellman, *J. Am. Chem. Soc.* **1999**, *121*, 2322 – 2330.
[11] Details concerning the synthesis of the peptides are available from the authors upon request.
[12] The relative configuration of the cycloadduct was determined by NOE spectroscopic techniques. The absolute configuration of compound **4** was not determined.
[13] B. A. Katz, *J. Mol. Biol.* **1997**, *274*, 776 – 800.
[14] The streptavidin conjugate **9** and wild-type streptavidin have the same biotin-binding capacity (14 units per mg protein), as determined by means of titrimetric assays according to the method in N. M. Gree, *Meth. Enzymol.* **1970**, *18*, 418 – 427.
[15] M. Zerial, H. McBride, *Nat. Rev. Mol. Cell Biol.* **2001**, *2*, 107 – 117.
[16] a) K. Alexandrov, I. Heinemann, T. Durek, V. Sidorovitch, R. S. Goody, H. Waldmann, *J. Am. Chem. Soc.* **2002**, *124*, 5648 – 5649; b) T. Durek, K. Alexandrov, R. S. Goody, A. Hildebrand, I. Heinemann, H. Waldmann, *J. Am. Chem. Soc.* **2004**, *126*, 16368 – 16378.
[17] A. Rak, O. Pylypenko, A. Niculae, K. Pyatkov, R. S. Goody, K. Alexandrov, *Cell* **2004**, *117*, 749 – 760.
[18] A. Rak, O. Pylypenko, T. Durek, A. Watze, S. Kushnir, L. Brunsveld, H. Waldmann, R. S. Goody, K. Alexandrov, *Science* **2003**, *302*, 646 – 650.
[19] G. L. Ellman, *Arch. Biochem. Biophys.* **1959**, *82*, 70 – 77.
[20] ESI-MS analysis of protein intermediate **13** revealed that two cysteines were masked as disulfides (see the Supporting Information). Two further cysteine residues are buried inside the protein and not accessible.
[21] K. Alexandrov, I. Simon, A. Iakovenko, B. Holz, R. S. Goody, A. Scheidig, *FEBS Lett.* **1998**, *425*, 460 – 464.
[22] M. Lumbierres, J. M. Palomo, G. Kragol, S. Röehrs, O. Müller, H. Waldmann, *Chem. Eur. J.* in press, DOI: 10.1002/chem..200500476.
[23] For the synthesis of Ras and Rab proteins by other methods, see: a) T. Durek, K. Alexandrov, R. S. Goody, A. Hildebrand, I. Heinemann, H. Waldmann, *J. Am. Chem. Soc.* **2004**, *126*, 16368 – 16378; b) O. Rocks, A. Peyker, M. Kahms, P. J. Verveer, C. Koerner, M. Lumbierres, J. Kuhlmann, H. Waldmann, A. Wittinghofer, P. I. H. Bastiaens, *Science* **2005**, *307*, 1746 – 1752; c) R. Reents, M. Wagner, S. Schlummer, J. Kuhlmann, H. Waldmann, *ChemBioChem* **2005**, *6*, 86 – 94; d) L. Brunsveld, A. Watzke, T. Durek, K. Alexandrov, R. S. Goody, H. Waldmann, *Chem. Eur. J.* **2005**, *11*, 2756 – 2772; e) A. Watzke, L. Brunsveld, T. Durek, K. Alexandrov, A. Rak, R. S. Goody, H. Waldmann, *Org. Biomol. Chem.* **2005**, *3*, 1157 – 1164.
[24] For a review of methods for the immoblization of proteins on glass slides, see: K.-Y. Tomizaki, K. Usui, H. Mihara, *ChemBioChem* **2005**, *6*, 1 – 18.
[25] M. Köhn, Dissertation, University of Dortmund, Germany, **2005**.
[26] The spotting process was carried out with a Gesim Nanoplotter (Gesim, Dresden, Germany) by spotting of 0.25-nL droplets of protein solutions (in buffer; spot size: 400 μm diameter) followed by incubation for 8 h.

 © 2006 Wiley-VCH Verlag GmbH & Co. KGaA, Weinheim

Biocatalysis

DOI: 10.1002/anie.200503031

Substrate Ambiguity and Catalytic Promiscuity Within a Bacterial Proteome Probed by an Easy Phenotypic Screen for Aldehydes**

*Guillaume Krebs, Laure Hugonet, and John D. Sutherland**

Economic and environmental considerations are driving efforts to produce biocatalysts for organic synthesis. Fermentation and the use of whole cells and enzymes are becoming increasingly common in the industrial manufacture of chemicals, but many reactions cannot be catalyzed at present.[1] In those cases where a slight activity can be found by screening, directed evolution is proving a powerful way to improve the activity,[2] but in many cases the starting activity cannot be found. We are interested in finding, and evolving, background activities for a diverse range of reactions, some of which have precedence in nature, and some not. Our approach is based upon the expectation that amongst the proteome, and its mutational variants, there must exist the catalytic potential for many new reactions, either through substrate ambiguity, or catalytic promiscuity.[3] Developing screens for a range of different reactions by using a conventional approach is time consuming, however, so we have been attracted by the idea of using one screen for many reactions. One way in which this could be achieved is by building biosynthetic trees to a

[*] G. Krebs, L. Hugonet, Professor Dr. J. D. Sutherland
School of Chemistry
The University of Manchester
Oxford Road, Manchester M13 9PL (UK)
Fax: (+44) 161-275-4939
E-mail: john.sutherland@manchester.ac.uk

[**] We thank Nicola Glynn and Fabien Buchet for assistance, Dr. Matti T. Karp, University of Turku, Finland, for his kind gift of the *luxDCABE* vector pTetLux1, and The University of Manchester for financial support.

Supporting information for this article is available on the WWW under http://www.angewandte.org or from the author.

© 2006 Wiley-VCH Verlag GmbH & Co. KGaA, Weinheim

common intermediate, or class of intermediates, for which an easy assay exists (Figure 1 a). Thus, if a screen for the reaction of **Y** to **Z** exists, then the same screen can be used for the conversion of precursors **V**, **W**, and **X** into **Y**. If **Y** is carefully

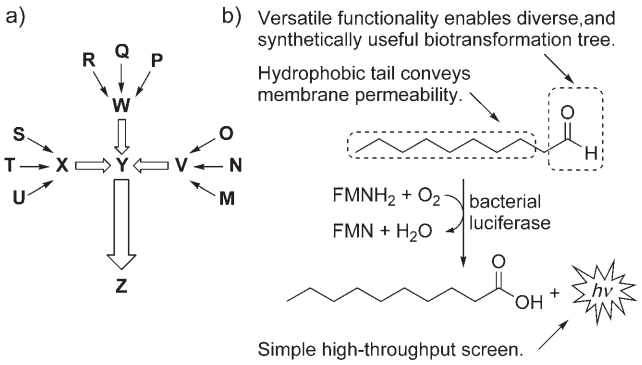


Figure 1. Building a biosynthetic product tree from a screenable reaction. a) Product tree based on the reaction **Y**→**Z**. b) The advantages of a screen using bacterial luciferase and light emission.

chosen, then it should be possible for different types of chemical reaction to be associated with these conversions. By optimizing the discovered activities and integrating them into the screening host, the process could be iterated to screen for additional chemical reaction types in the conversion of, for example, **M**, **N**, and **O** into **V** (Figure 1 a). In addition to the careful choice of **Y**, an easy screen as well as membrane-permeable precursors are crucial for this approach. Light emission is a very simple phenotype to screen, and bioluminescent bacteria can either be detected as colonies on plates or by fluorescence-assisted cell sorting (FACS).[4] The simplicity of a screen based on light emission made us consider a luciferase enzyme as our reporter, and the corresponding luciferin as the pivotal intermediate **Y**. In particular, the use of long-chain aldehydes as substrates for bacterial luciferase[5] was attractive given the central role of the carbonyl group in organic synthesis and the expected membrane permeability of such compounds (Figure 1 b).

An *Escherichia coli* luciferase expression system was developed to evaluate this approach (Figure 2). Our plan was then to introduce random fragments of the *E. coli* genome into pLH1 to generate a library of plasmids all encoding luciferase and over-expressing different *E. coli* genes. We hoped that this over-expression would mean that any trace activity of a particular protein would be amplified to the extent that it would be detectable. If the trace activity corresponded to the conversion of an aldehyde precursor into the aldehyde, then that aldehyde would be oxidized by luciferase, and light would be emitted. If this wild-type library did not yield the desired starting activities, then we planned to mutagenize it.

Before constructing and screening the library, we investigated whether different aldehydes would cause *E. coli*:pLH1 to emit light under inducing conditions. This was deemed important because the light emission would depend upon both membrane permeability and the substrate specif-

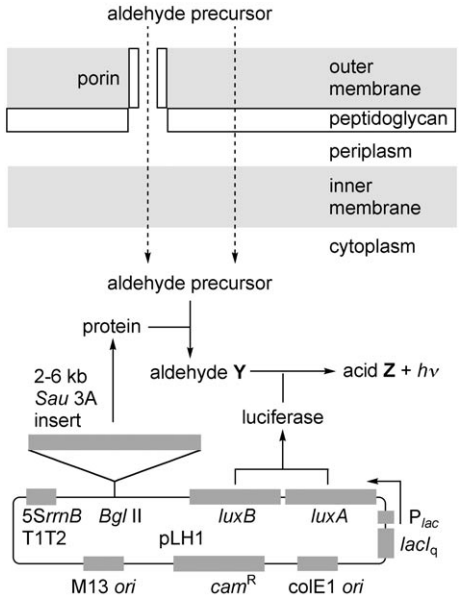
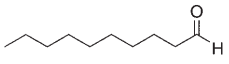
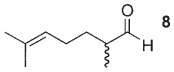
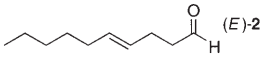
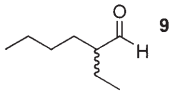
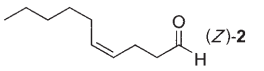
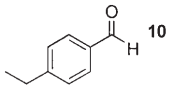
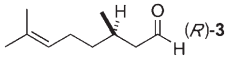
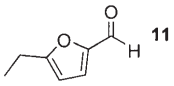
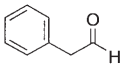
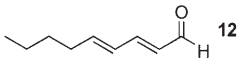
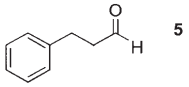
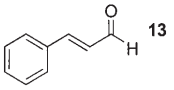
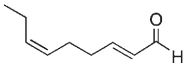
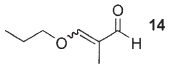
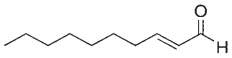
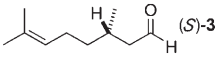


Figure 2. *E. coli* assay system. Based on the assumption that long-chain aldehydes and their precursors might freely diffuse into bacterial cells through the outer and inner membranes (and porins), a luciferase expression plasmid was used to transform *E. coli*. The plasmid pLH1 contains the *luxA* and *luxB* genes under the control of the strong inducible P_{lac} promoter. Upon induction with isopropylthio-β-D-galactoside, these genes direct the synthesis of the two subunits of bacterial luciferase. We used this basic system to investigate light emission caused by aldehydes; we used a library of *E. coli* genomic fragments cloned into the *Bgl* II site of pLH1 to screen the *E. coli* proteome for the oxidation of alcohols to aldehydes.

icity of luciferase. If many different aldehydes were to cause light emission in the assay then a greater range of chemical reactions could be screened for in subsequent evaluations of precursors. In the event, we found a wide range of aldehydes to cause light emission, as measured by luminometry (Table 1). The natural substrate for bacterial luciferase is a saturated long-chain aldehyde, most likely tetradecanal.[6] We have used shorter chain aldehydes to give slightly higher aqueous solubility, and we found excellent light emission from *E. coli*:pLH1 using decanal (**1**). Unsaturation is tolerated to varying degrees, depending on the position of the C=C bond, as shown by compounds **2**, **3**, **6**, **7**, and **12**. Branching is not accepted at the α-position (**8**, **9**, and **14**), but is at the β-position, although with a strong dependency on stereochemistry ((*R*)-**3** versus (*S*)-**3**). Aromatic substituents are tolerated at both the α- and β-positions (**4** and **5**), but conjugated aromatic aldehydes are not detectable substrates (**10**, **11**, and **13**), nor is the vinylogous ester **14**. Since all the compounds tested are nonpolar, and presumably membrane-permeable, we suspect that these trends in light emission reflect specificity for the luciferase substrate. Whatever the case, the wide range of substrates for the system suggests that a broad range of organic reactions could be screened through the use of appropriately chosen precursors. We are currently in the process of doing this, but herein report the results of some experiments on simple precursors because they validate the approach and provide evidence of substrate ambiguity, as

 © 2006 Wiley-VCH Verlag GmbH & Co. KGaA, Weinheim

Table 1: Light emission from *E. coli*:pLH1 in the presence of various aldehydes.

Substrate	Light emission (RLU[a])	Not detectable as a substrate
 **1**	2.13	 **8**
 (*E*)-**2**	1.54	 **9**
 (*Z*)-**2**	1.15	 **10**
 (*R*)-**3**	0.20	 **11**
 **4**	0.18	 **12**
 **5**	0.07	 **13**
 **6**	0.04	 **14**
 **7**	0.03	
 (*S*)-**3**	0.01	

[a] Value of light emission at the maximum luminescence wavelength of 490 nm in luminescence units divided by the absorption of the sample at 600 nm (OD_{600}; see the Supporting Information for experimental procedures).

well as a remarkable example of catalytic promiscuity, in the proteome of *E. coli*.

The oxidation of an alcohol is one of the simplest ways in which an aldehyde can be synthesized, either chemically or biochemically, and we chose this reaction to evaluate screening of the *E. coli* proteome. Grossman and co-workers have also used bioluminescence to detect the oxidation of a long-chain alcohol to an aldehyde by *E. coli*.[7] In that work, however, the *Pseudomonas oleovorans* alcohol dehydrogenase, which is active on C_5–C_{12} linear alcohols, was heterologously expressed in *E. coli* because of the lack of such activity in the host. Our hope was that there would be trace activity of endogenous long-chain alcohol oxidation that would be amplified, and thus detectable, if the corresponding genes were over expressed. We selected the alcohol precursors to a good aldehyde substrate (**1**) and a poor one (**7**) to probe the sensitivity of our system. A genomic library was then constructed by cloning random 2–6 kb *E. coli Sau* 3A fragments into the *Bgl* II site of pLH1. 23000 colonies were grown on plates under inducing conditions, sprayed with *n*-decanol ($CH_3(CH_2)_9OH$, **15**), and examined for light emission in the dark with a CCD device attached to a sensitive camera. From this process 14 light-emitting colonies were selected, grown in a liquid medium, and the light emission in the presence of **15** checked by luminometry. The precise location of the selected DNA sequence in the *E. coli* genome, and, where possible, the size, were determined by sequencing both ends of the inserts (Table 2). In this way we found that over expression of three different genes caused light emission in the presence of **15**. The most commonly selected gene (*fucO*) encodes L-1,2-propanediol oxidoreductase, an enzyme involved in fucose metabolism.[8] The substrate specificity of this iron-containing alcohol dehydrogenase has not been fully mapped out, but it was previously thought to include 1,2-diols and short-chain alcohols only. The second class of insert contains genes from the ethanolamine utilization operon, and we think it likely that the product of the *eutG* gene is responsible for oxidation of **15** since it is homologous to the C terminus of *E. coli* alcohol dehydrogenase AdhE,[9] although, interestingly, none of our selected clones contained the *adhE* gene despite its likely representation in the library (see the Supporting Information). The last insert we isolated contains the *yphC* gene which encodes a putative member of the large class of zinc metalloenzyme medium-chain dehydrogenases;[10] however, light emission from these clones was lower. These results suggest that a number of alcohol dehydrogenases have a trace, low-level activity towards **15**, and it is likely that directed evolution could be used to increase this. We chose not to do this, however, and instead focused on screening our library for the precursor to the poor substrate **7**. Approximately 17000 colonies were screened for light emission in the presence of (*E*)-2-decenol (**16**), and one weakly bioluminescent clone was obtained. After purification of the colony and verification of the light-emitting phenotype in the presence of **16**, the sequence of the insert was determined. To our surprise, we found that the sequence (126809–129811) corresponded to the *lpd* gene, which encodes the E3 subunit of pyruvate dehydrogenase.[11] In the course of the action of pyruvate dehydrogenase, acetyl groups are transferred from the lipoyl domains (LDs) of the E2 subunit to coenzyme A, and the resultant LD dithiols are then oxidized to disulfides by the E3 subunit (Figure 3).[12] The lipoic acid is attached to a lysine residue of E2-LD, which itself is attached to the main body of E2 by a "swinging arm".[13] The dehydrogenase active site of E3 is at the end of a long, hydrophobic substrate-binding channel which accomodates the lipoyl lysine group of E2-LD,[14] and by implication,

Table 2: Inserts of plasmids obtained by screening the *E. coli*:pLH1-(*Sau* 3 A fragment) library for light emission in the presence of *n*-decanol (**15**).

Genome region[a]	Number of clones	Gene	Gene product
2926083–2937591	11[b]	*fucO*	L-1,2-propanediol oxidoreductase
2566061–2569982	1	*eutG*	putative alcohol dehydrogenase similar to the iron-containing alcohol dehydrogenase family
2671927–2675820	2[c]	*yphC*	hypothetical zinc-type alcohol dehydrogenase

[a] Region of the *E. coli* genome spanned by the insert or the range of inserts [http://genolist.pasteur.fr/Colibri/]. [b] Eight different clones plus three repeats. [c] One clone plus one repeat.

 © 2006 Wiley-VCH Verlag GmbH & Co. KGaA, Weinheim

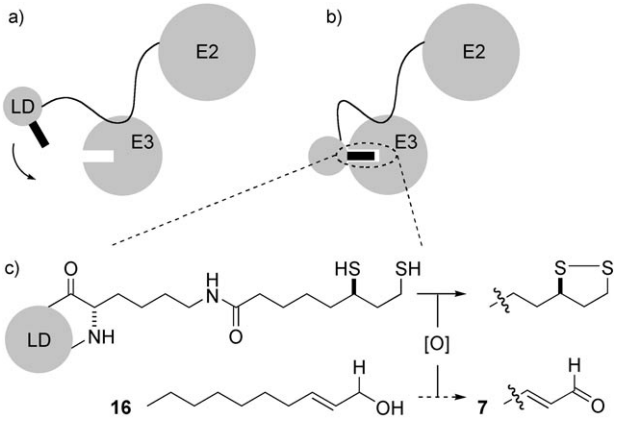


Figure 3. Catalytic promiscuity of lipoamide dehydrogenase. a) Schematic representation of part of the pyruvate dehydrogenase complex. The E3 subunit of the complex functions to oxidize the dihydrolipoamide group of a lipoyl domain (LD) of the E2 subunit.[13] b) A swinging arm[14] of E2 brings the LD into a position where the dihydrolipoamide group can dock into the active site of the E3 subunit. c) Molecular detail of the oxidative transformation of the LD dihydrolipoyllysine residue in comparison with the conversion of **16** into **7**. Although both transformations are oxidations, the conversion of **16** into **7** must be mechanistically distinct from the dithiol oxidation since it is known that the latter proceeds by way of a mixed disulfide with the enzyme.[15]

according to our results, the long chain of **16**, as a result of structural resemblance (Figure 3c)). However, the dehydrogenase uses a redox relay triad comprising an enzyme dithiol/disulfide, $FADH_2$/FAD, and NADH/NAD^+, and a mechanism not apparently adaptable to oxidation of an allylic alcohol such as **16**.[15] Thus, we wanted to prove that **16** was indeed oxidized directly to **7**, and not, for example, isomerized to **1**, which would also have resulted in light emission in the initial screen. Accordingly, we prepared a crude extract from the cell carrying the *lpd* clone and incubated it with **16** and NAD^+. ^{1}H NMR spectroscopic analysis after extraction into an organic phase clearly demonstrated the direct oxidation of **16** to **7** by the crude extract (Figure 4). We also found that the oxidation of **16** to **7** was inhibited by reduced lipoamide, a close analogue of the natural substrate for the *lpd* gene product (see the Supporting Information). These observations, coupled with the mechanism of the oxidation of the natural dithiol substrate,[15] suggest that the oxidation of the alcohol is an example of catalytic promiscuity. The actual mechanism by which **16** is oxidized to **7**, and the directed evolution of this activity will be addressed in future studies.

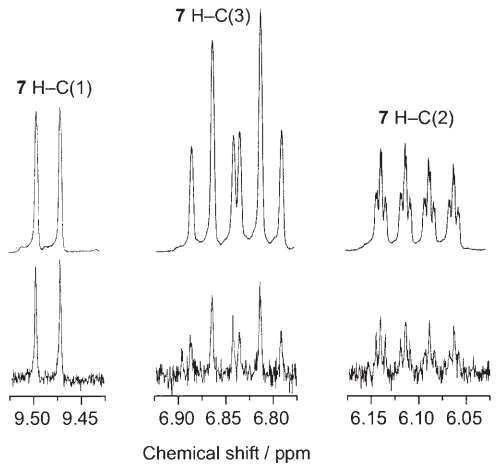


Figure 4. ^{1}H NMR analysis (300 MHz, $CDCl_3$) of the reaction of **16** with NAD^+ catalyzed by a cell-free extract of *E. coli* over-expressing the *lpd* gene. Comparison of the downfield region of the spectrum with that of a standard sample of **7** (upper) clearly shows that **16** is oxidized to **7**, and not isomerized to **1**.

The substrate ambiguity of the enzymes found to oxidize **15** to **1**, and the catalytic promiscuity observed in the oxidation of **16** to **7** by the *lpd* gene product were easily found by using the bacterial luciferase screen, and add to the growing number of reports concerning the metabolic plasticity of microbial proteomes. It is now hoped that other biocatalyst leads of use in mainstream organic chemistry can be obtained from this rich source of catalytic diversity.[16]

Received: August 25, 2005
Published online: November 29, 2005

Keywords: biocatalysis · biotechnology · enzymes · luminescence · oxidation

[1] A. Schmidt, J. S. Dordick, B. Hauer, A. Kiener, M. Wubbolts, B. Witholt, *Nature* **2001**, *409*, 258; M. Breuer, K. Ditrich, T. Habicher, B. Hauer, M. Kesseler, R. Stürmer, T. Zelinski, *Angew. Chem.* **2004**, *116*, 806; *Angew. Chem. Int. Ed.* **2004**, *43*, 788.

[2] W. P. C. Stemmer, *Nature* **1994**, *370*, 389; J. D. Sutherland, *Curr. Opin. Chem. Biol.* **2000**, *4*, 263; K. A. Powell, S. W. Ramer, S. B. del Cardayré, W. P. C. Stemmer, M. B. Tobin, P. F. Longchamp, G. W. Huisman, *Angew. Chem.* **2001**, *113*, 4068; *Angew. Chem. Int. Ed.* **2001**, *40*, 3948; M. T. Reetz, *Angew. Chem.* **2001**, *113*, 292; *Angew. Chem. Int. Ed.* **2001**, *40*, 284; S. Brakmann, K. Johnsson, *Directed Molecular Evolution of Proteins (or How to Improve Enzymes for Biocatalysis)*, Wiley-VCH, Weinheim, **2002**; M. T. Reetz, M. Bocola, J. D. Carballeira, D. Zha, A. Vogel, *Angew. Chem.* **2005**, *117*, 4264; *Angew. Chem. Int. Ed.* **2005**, *44*, 4192.

[3] P. J. O'Brien, D. Herschlag, *Chem. Biol.* **1999**, *6*, R91; S. Raillard, A. Krebber, Y. Chen, J. E. Ness, E. Bermudez, R. Trinidad, R. Fullem, C. Davis, M. Welch, J. Seffernick, L. P. Wackett, W. P. C. Stemmer, J. Minshull, *Chem. Biol.* **2001**, *8*, 891; U. T. Bornscheuer, R. Kazlauskas, *Angew. Chem.* **2004**, *116*, 6156; *Angew. Chem. Int. Ed.* **2004**, *43*, 6032; A. Aharoni, L. Gaidukov, O. Khersonsky, S. McQ. Gould, C. Roodveldt, D. S. Tawfik, *Nat. Genet.* **2005**, *37*, 73.

[4] M. J. Olsen, D. Stephens, D. Griffiths, P. Daugherty, G. Georgiou, B. L. Iverson, *Nat. Biotechnol.* **2000**, *18*, 1071; S. W. Santoro, L. Wang, B. Herberich, D. S. King, P. G. Schultz, *Nat. Biotechnol.* **2002**, *20*, 1044.

[5] a) T. O. Baldwin, T. Berends, T. A. Bunch, T. F. Holzman, S. K. Rausch, L. Shamansky, M. L. Treat, M. M. Ziegler, *Biochemistry* **1984**, *23*, 3663; b) M. T. Korpela, J. S. Kurittu, J. T. Karvinen, M. T. Karp, *Anal. Chem.* **1998**, *70*, 4457.

[6] S. Ulitzur, J. W. Hastings, *Proc. Natl. Acad. Sci. USA* **1979**, *76*, 265; W. A. Francisco, H. M. Abu-Soud, T. O. Baldwin, F. M. Raushel, *J. Biol. Chem.* **1993**, *268*, 24734.

[7] V. Minak-Bernero, R. E. Bare, C. E. Haith, M. J. Grossman, *Biotechnol. Bioeng.* **2004**, *87*, 170.

 © 2006 Wiley-VCH Verlag GmbH & Co. KGaA, Weinheim

[8] A. Boronat, J. Aguilar, *J. Bacteriol.* **1979**, *140*, 320; C. Montella, L. Bellsolell, R. Pérez-Luque, J. Badía, L. Baldoma, M. Coll, J. Aguilar, *J. Bacteriol.* **2005**, *187*, 4957.
[9] I. Stojiljkovic, A. J. Bäumler, F. Heffron, *J. Bacteriol.* **1995**, *177*, 1357.
[10] J. Shafqat, J.-O. Höög, L. Hjelmqvist, U. C. T. Opperman, C. Ibàñez, H. Jörnvall, *Eur. J. Biochem.* **1999**, *263*, 305.
[11] D. J. Carothers, G. Pons, M. S. Patel, *Arch. Biochem. Biophys.* **1989**, *268*, 409.
[12] S. S. Mande, S. Sarfaty, M. D. Allen, R. N. Perham, W. G. J. Hol, *Structure* **1996**, *4*, 277.
[13] R. N. Perham, *Annu. Rev. Biochem.* **2000**, *69*, 961.
[14] A. Mattevi, A. J. Schierbeek, W. G. J. Hol, *J. Mol. Biol.* **1991**, *220*, 975; A. Mattevi, G. Oblomova, K. H. Kalk, W. J. H. van Berkel, W. G. J. Hol, *J. Mol. Biol.* **1993**, *230*, 1200.
[15] K. D. Wilkinson, C. H. Williams, Jr., *J. Biol. Chem.* **1979**, *254*, 852; A. Argyrou, J. S. Blanchard, B. A. Palfey, *Biochemistry* **2002**, *41*, 14580.
[16] M. Müller, *Curr. Opin. Biotechnol.* **2004**, *15*, 591.

 © 2006 Wiley-VCH Verlag GmbH & Co. KGaA, Weinheim

Natural Product Synthesis

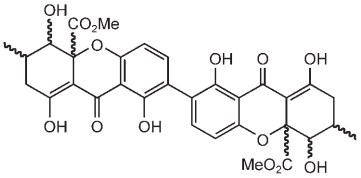
DOI: 10.1002/anie.200502913

The Total Synthesis of the Fungal Metabolite Diversonol**

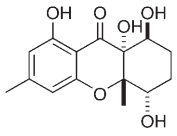
*Carl F. Nising, Ulrike K. Ohnemüller (née Schmid) , and Stefan Bräse**

Dedicated to Professor Burchard Franck

Mycotoxins, which are secondary metabolites produced by fungi, are a source of substances with interesting biological activity.[1] The secalonic acids (**1**) represent a class of substances produced by *Claviceps purpurea* as well as various other fungi.[2] The secalonic acids are symmetrical or unsymmetrical tetrahydroxanthenone dimers possessing a 2,2′-biaryl unit. Since other mycotoxins with a similar structure have been isolated recently, many of which show promising biological activity, an efficient synthetic access to this substance class would be very useful.[3] In the course of our studies towards the total synthesis of the secalonic acids, we were also interested in the synthesis of the secondary metabolite diversonol (**2**), which was isolated by Turner from *Penicillium diversum* and whose structural motif can also be found in some of the substances mentioned above. The absolute configuration of naturally occurring diversonol is not known to date.[4]

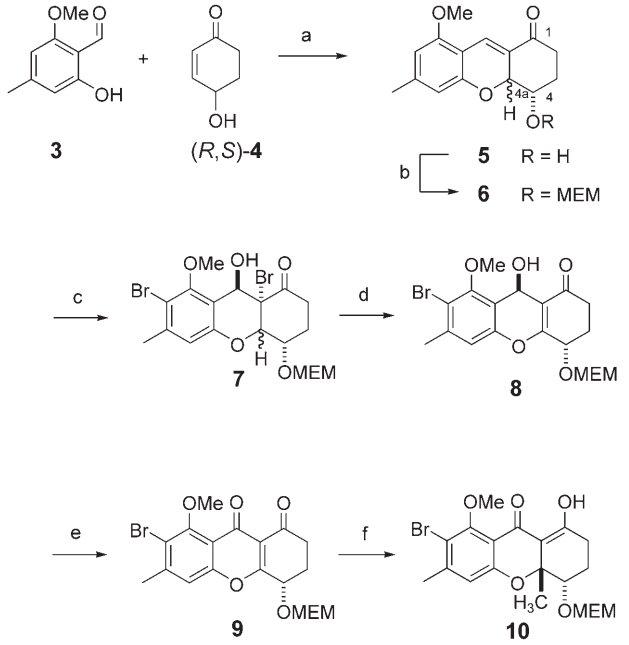


secalonic acids (**1**)



diversonol (**2**)

As the structure of diversonol is very similar to that of the secalonic acid monomers, the total synthesis of diversonol would also be a step towards the total synthesis of the secalonic acids. The synthesis of diversonol was expected to be challenging owing to the high density of functional groups—all four hydroxy groups are located close to each other—which would require an efficient protecting-group strategy. Furthermore, control over the relative stereochemistry of the substituents is mandatory for a successful synthesis. Based on the synthetic access to tetrahydroxanthenones developed in our group, diversonol (**2**) can be reduced retrosynthetically to a substituted salicylic aldehyde and 4-hydroxycyclohexenone (**4**).[5] The tetrahydroxanthenone **5** formed by a domino oxa-Michael–aldol condensation should then be transformed to diversonol (**2**) in few steps (Scheme 1).[6]



Scheme 1. Modification of tetrahydroxanthenone **5**: a) imidazole, dioxane/H_2O, sonication, 7 d, 61%; b) MEMCl, iPr_2NEt, CH_2Cl_2, RT, 3 h, 75%; c) tetrabutylammonium tribromide, THF/H_2O, RT, 5 h, 52%; d) DABCO, dioxane, RT, 16 h, 53%; e) TPAP, NMO, CH_2Cl_2/CH_3CN, sonication, 40%; f) MeLi, CuCN, Et_2O, −78°C, 5 h, 52%. MEMCl = (2-methoxyethoxy)methyl chloride, DABCO = 1,4-diazabicyclo-[2.2.2]octane, TPAP = tetrapropylammonium perruthenate.

We now report on the first total synthesis of diversonol in racemic form. Starting from orcinol, salicylic aldehyde **3** could be prepared in a three-step procedure with excellent yields.[7] 4-Hydroxycyclohexenone (**4**) could be synthesized on a multigram-scale according to a procedure optimized in our group and starting from *p*-benzoquinone.[8]

With these building blocks in hand, we set out to optimize the key domino oxa-Michael–aldol condensation. When imidazole was used as the base, tetrahydroxanthenone **5** could be isolated in a yield of 61% and as a 1.5:1 mixture of the two possible diastereoisomers, whereas the bases DABCO and K_2CO_3 used in former tetrahydroxanthenone syntheses[5] only led to decomposition of the cyclohexenone.

Protection of the free hydroxy functionality as a MEM ether,[9] followed by the stereoselective formation of bromohydrin **7** now set the stage for the synthesis of the conjugated system **8** by elimination of hydrogen bromide from **7**. The moderate yields of steps b–d in Scheme 1 result from the fact

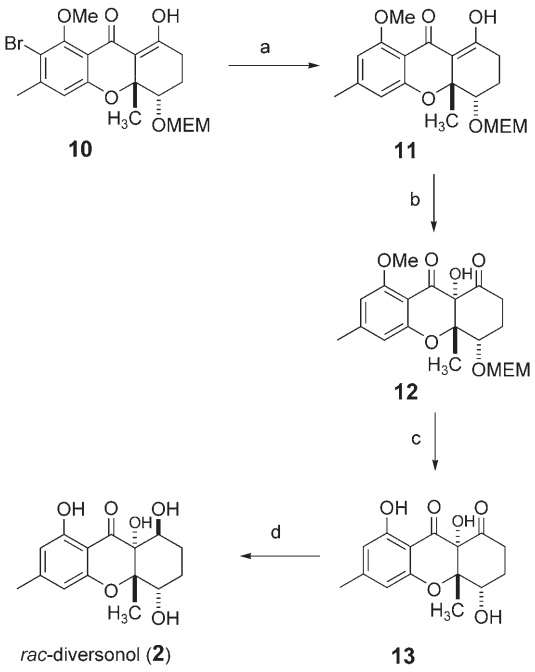
[*] Dipl.-Chem. C. F. Nising, Dipl.-Chem. U. K. Ohnemüller (née Schmid) , Prof. Dr. S. Bräse
Institut für Organische Chemie
Universität Karlsruhe (TH)
Fritz-Haber-Weg 6, 76131 Karlsruhe (Germany)
Fax: (+49) 721-608-8581
E-mail: braese@ioc.uka.de

[**] We thank the Fonds der Chemischen Industrie (grant for C.F.N.) and the Landesgraduiertenförderung Baden-Württemberg (grant for U.K.O.).

Supporting information for this article is available on the WWW under http://www.angewandte.org or from the author.

 © 2006 Wiley-VCH Verlag GmbH & Co. KGaA, Weinheim

that the *trans* diastereoisomers (C4-OR and H4a *trans*) of tetrahydroxanthenones **5**–**7** are almost unreactive; after elimination of HBr from **7** allylic alcohol **8** was isolated as a single diastereoisomer. The halogenation of the aromatic moiety, which inevitably takes place during bromohydrin formation, could be used for palladium-catalyzed aryl–aryl coupling since dimeric analogues of diversonol bearing a biaryl unit have been reported recently.[10] The subsequent oxidation of compound **8** was unexpectedly difficult since the allylic alcohol proved to be acid- and base-sensitive. Of a number of different oxidation protocols, only oxidation under Ley conditions[11] using tetrapropylammonium perruthenate (TPAP) as a catalytic oxidizing agent gave diketone **9** in acceptable yield. The subsequent cuprate addition could be performed diastereoselectively and with good yield by a protocol developed by Gabbutt et al.[12] After dehalogenation of **10** by halogen–metal exchange followed by protonation, the hydroxy functionality on C9a was introduced by diastereoselective hydroxylation of enol **11** using magnesium monoperoxophthalate (Scheme 2).



Scheme 2. Concluding stages of the total synthesis of *rac*-diversonol (**2**): a) *t*BuLi, THF, −78°C, $NaHCO_3$, 4 h, 93%; b) magnesium monoperoxophthalate, EtOH, RT, 5 h, 57%; c) BBr_3, CH_2Cl_2, RT, 7 h, 40%; d) $NaBH_4$, MeOH, −78°C, 20 min, 66%.

To our delight, the diastereoselectivity of this step could be influenced by varying the reaction conditions.[13] After deprotection of compound **12** at the phenolic and secondary hydroxy functionalities, diversonol (**2**) was obtained by diastereoselective reduction of the unconjugated carbonyl function using sodium borohydride. The analytical data are in complete agreement with those reported for the natural product[4] except for the optical rotation, which remains unknown to date.

In summary, we have developed a flexible route to tetrahydroxanthenone mycotoxins by applying a domino oxa-Michael–aldol condensation.[5] In this context, we were able to achieve the first total synthesis of the secondary metabolite diversonol (**2**) in racemic form and in a sequence of 14 synthetic steps. The application of this methodology to the total synthesis of the secalonic acids (**1**) and an evaluation of the biological activity of diversonol (**2**) are currently underway in our laboratory.

Received: August 16, 2005
Revised: October 4, 2005
Published online: December 9, 2005

Keywords: diversonol · domino reactions · fungal metabolites · natural products · total synthesis

[1] a) B. Franck, *Angew. Chem.* **1984**, *96*, 462–474; *Angew. Chem. Int. Ed. Engl.* **1984**, *23*, 493–505; b) L. Roth, H. Frank, K. Kormann, *Pilzgifte*, Nikol, Hamburg, **1990**; c) I. F. H. Purchase, *Mycotoxins*, Elsevier, Amsterdam, **1974**; d) W. B. Turner, *Fungal Metabolites*, Academic Press, New York, **1971**; e) W. B. Turner, D. C. Aldridge, *Fungal Metabolites II*, Academic Press, New York, **1983**; f) K. Krohn, J. Dai, U. Flörke, H.-J. Aust, S. Dräger, B. Schulz, *J. Nat. Prod.* **2005**, *68*, 400–405.

[2] a) B. Franck, G. Baumann, U. Ohnsorge, *Tetrahedron Lett.* **1965**, 2031–2037; b) B. Franck, E. M. Gottschalk, U. Ohnsorge, G. Baumann, *Angew. Chem.* **1964**, *76*, 438–439; *Angew. Chem. Int. Ed. Engl.* **1964**, *3*, 441–442; c) B. Franck, E. M. Gottschalk, U. Ohnsorge, F. Hüper, *Chem. Ber.* **1966**, *99*, 3842–3862; d) "The Biosynthesis of the Ergochromes": B. Franck in *The Biosynthesis of Mycotoxins: A Study in Secondary Metabolism* (Ed.: P. S. Steyn), Academic Press, New York, **1980**.

[3] a) M. Wagenaar, J. Clardy, *J. Nat. Prod.* **2001**, *64*, 1006–1009; b) M. Isaka, A. Jaturapat, K. Rukseree, K. Danwisetkanjana, M. Tanticharoen, Y. Thebtaranonth, *J. Nat. Prod.* **2001**, *64*, 1015–1018; biological activity: c) I. Kurobane, S. Iwahashi, A. Fukuda, *Drugs Exp. Clin. Res.* **1987**, *13*, 339–344; d) A. Stoll, J. Renz, A. Brack, *Helv. Chim. Acta* **1952**, *35*, 2022–2034; e) F. McPhee, P. S. Caldera, G. W. Bemis, A. F. McDonagh, I. D. Kuntz, C. S. Craik, *Biochem. J.* **1996**, *320*, 681–686.

[4] a) W. B. Turner, *J. Chem. Soc. Perkin Trans. 1* **1978**, 1621; in this publication, the question whether the isolated compound was a racemate or an enantiomerically pure compound remains unanswered; b) diversonolic esters: J. S. Holker, E. O'Brien, T. J. Simpson, *J. Chem. Soc. Perkin Trans. 1* **1983**, 1365–1368.

[5] B. Lesch, S. Bräse, *Angew. Chem.* **2004**, *116*, 118–120; *Angew. Chem. Int. Ed.* **2004**, *43*, 115–118; benzpyran synthesis: B. Lesch, J. Toräng, S. Vanderheiden, S. Bräse, *Adv. Synth. Cat.* **2005**, *4*, 555–562; for an independent study see: K. Y. Lee, J. M. Kim, J. N. Kim, *Bull. Korean Chem. Soc.* **2003**, *24*, 17–18.

[6] For a review of domino reactions see: L. F. Tietze, *Chem. Rev.* **1996**, *96*, 115–136.

[7] Details of this synthesis can be found in the Supporting Information.

[8] M. Oda, T. Kawase, T. Okada, T. Enomoto, *Org. Synth.* **1996**, *73*, 253–261; A. P. Marchand, D. Xing, Y. Wang, S. G. Bott, *Tetrahedron: Asymmetry* **1995**, *6*, 2709–2714; U. K. Ohnemüller, S. Bräse, unpublished results.

[9] E. J. Corey, J.-L. Gras, P. Ulrich, *Tetrahedron Lett.* **1976**, 809–812.

[10] M. Stewart, R. J. Capon, J. M. White, E. Lacey, S. Tennant, J. H. Gill, M. P. Shaddock, *J. Nat. Prod.* **2004**, *67*, 728–730; for the

 © 2006 Wiley-VCH Verlag GmbH & Co. KGaA, Weinheim

synthesis of symmetrical biaryls see: C. F. Nising, U. K. Schmid, M. Nieger, S. Bräse, *J. Org. Chem.* **2004**, *69*, 6830 – 6833.
[11] S. V. Ley, J. Norman, W. P. Griffith, S. P. Marsden, *Synthesis* **1994**, 639 – 666.
[12] C. D. Gabbutt, J. D. Hepworth, M. W. J. Urquhart, L. M. Vazquez de Miguel, *J. Chem. Soc. Perkin Trans. 1* **1997**, 1819 – 1824.
[13] Both of the two possible diastereoisomers could be synthesized selectively by using either *meta*-chloroperbenzoic acid or magnesium monoperoxophthalate as the oxidizing agent. The possibility of controlling the diastereoselectivity could be proved by X-ray structure analyses of model compounds; C. F. Nising, M. Nieger, S. Bräse, unpublished results.

 © 2006 Wiley-VCH Verlag GmbH & Co. KGaA, Weinheim

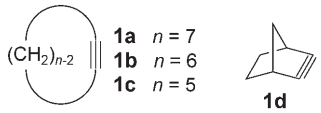
Strained Molecules

DOI: 10.1002/anie.200503124

Bi-3*H*-diazirin-3-yls as Precursors of Highly Strained Cycloalkynes**

Mohammad Al-Omari, Klaus Banert, and Manfred Hagedorn*

Several methods for the generation of highly strained non-isolable cycloalkynes, for example, **1a–c**, have been developed within the last decades (Scheme 1).[1] These methods



Scheme 1.

typically rely on the use of metals, metal salts or complexes, organometallic compounds, strong bases, fluoride salts, or oxidizing reagents. High temperatures or irradiation of the starting material are sometimes also necessary. After their generation, the highly reactive cycloalkynes **1a–c** can be trapped by cycloaddition reactions. Norbornyne (**1d**)[2–5] and related bicyclic compounds[6] are the limiting cases of strained cyclic alkynes that be proved experimentally by trapping reactions.

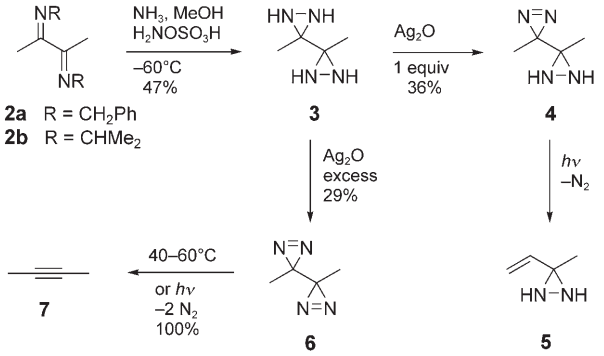
[*] Dr. M. Al-Omari, Prof. Dr. K. Banert, Dr. M. Hagedorn
Lehrstuhl für Organische Chemie
Technische Universität Chemnitz
Strasse der Nationen 62, 09111 Chemnitz (Germany)
Fax: (+49) 371-531-1839
E-mail: klaus.banert@chemie.tu-chemnitz.de

[**] Strained Rings, Part 1. This research was supported by the Deutsche Forschungsgemeinschaft and the Fonds der Chemischen Industrie.

Supporting information for this article is available on the WWW under http://www.angewandte.org or from the author.

We now report on the isolable diazirine derivatives **6**, **12**, **13**, and **26**, which lead to the alkyne **7** and the short-lived cycloalkynes **1a**, **1b**, and **1d**, respectively, already at room temperature or slightly above without the need of other reagents and without formation of any side product except nitrogen. Originally, we planned to prepare the title compounds in order to investigate the possible valence isomerization yielding tetraazabenzenes. Analogous rearrangement reactions of bi-2*H*-azirin-2-yls to give diazabenzenes occur already at surprisingly low temperatures.[7]

We obtained bidiaziridin-3-yl **3** as a mixture of diastereomers (ca. 10:1) upon treatment of a solution of bisimine **2a**[8] in anhydrous methanol with liquid ammonia and hydroxylamine-*O*-sulfonic acid (Scheme 2). If one assumes that N-



Scheme 2.

bonded substituents (here H atoms) in a diaziridine ring always adopt a *trans* configuration,[9] the formation of both a C_2-symmetrical (*rac*, *R*,*R*,*R*,*R* and *S*,*S*,*S*,*S*) and an achiral (*meso*, *R*,*R*,*S*,*S*) stereoisomer should occur. Starting with **2b**,[10] similar results were found. Although the workup is more convenient, the yield of **3** is significantly lower. Early attempts[11] to prepare **3** from butane-2,3-dione were unsuccessful, and our own efforts to synthesize the bidiaziridines **3**, **9**, and **24** from the corresponding α-diketones, their dioximes, or α-iminoketones also failed.[12] The structure of **3** was supported by the usual spectroscopic methods including ^{15}N NMR data (Table 1) as well as by its oxidation to give the diazirine **4**. Reaction of **3** with an excess of freshly generated silver oxide afforded the isolable[13] product **6**. This compound as well as the bi-3*H*-diazirin-3-yls described below slowly eliminated nitrogen at room temperature. They can be handled conveniently in solution and stored at −30 °C for a long period. On warming or irradiation a solution of **6** in chloroform, the alkyne **7** was formed quantitatively. When this transformation was monitored by NMR spectroscopy, no intermediate could be observed. The mild conditions of the thermal reaction and the high yield of **7** may be the outcome of a cooperative effect between both 3*H*-diazirine units of **6**. When **6** was photolyzed in the presence of a great excess of hex-3-yne, exclusively alkyne **7** and thus no product of intermolecular carbene trapping results. However, product **5**, which was generated in only moderate yield (36 % based on ^1H NMR) by irradiation of **4**, can be explained by insertion of a carbene into the neighboring C–H bond.

 © 2006 Wiley-VCH Verlag GmbH & Co. KGaA, Weinheim

Table 1: Selected physical data of compounds **3**, **4**, **6**, **9**, **10**, **12**, **13**, **24**, and **26**.[a]

3:[b] White crystals; m.p. 149–151 °C (CH_3OH or CH_2Cl_2); major isomer: ^{1}H NMR ([D$_6$]DMSO): $\delta = 1.34$ (s, 6H, CH_3), 2.36 (d, $^3J = 8.1$ Hz, 2H, NH), 2.58 ppm (d, $^3J = 8.1$ Hz, 2H, NH); ^{13}C NMR ([D$_6$]DMSO): $\delta = 19.71$ (q, CH3), 56.51 ppm (s, C-3); ^{15}N NMR ([D$_3$]$MeNO_2$, also as standard with $\delta = 0$): $\delta = -314.8$ (d, $^1J = 64$ Hz), −308.9 ppm (d, $^1J = 62$ Hz); minor isomer: ^{1}H NMR ([D$_6$]DMSO): $\delta = 1.31$ (s), 2.42 ppm (br); ^{13}C NMR ([D$_6$]DMSO): $\delta = 20.52$ (q), 56.22 ppm (s).

4: Pale yellow crystals; m.p. = 56–58 °C; ^{1}H NMR ([D$_6$]DMSO): $\delta = 0.98$ (s, 3H, CH_3), 1.13 (s, 3H, CH_3), 2.57 (d, $J = 8.1$ Hz, 1H, NH), 2.68 ppm (d, $J = 8.1$ Hz, 1H, NH); ^{13}C NMR ([D$_6$]DMSO): $\delta = 15.28$ (q, CH_3), 19.95 (q, CH_3), 28.04 (s, C-3), 54.45 ppm (s, C-3′).

6: Brown oil; IR (C_6D_6): $\tilde{\nu} = 2963$, 2928, 1580, 1436, 1384, 1103 cm^{-1}; ^{1}H NMR ($CDCl_3$): $\delta = 0.85$ ppm (s, CH_3); ^{13}C NMR ($CDCl_3$): $\delta = 15.30$ (q, CH_3), 26.55 ppm (s, C-3); ^{15}N NMR ($CDCl_3$): $\delta = 69.7$ ppm.

9:[b] Yellow crystals; m.p. 120–125 °C (hexane/Et_2O); major isomer: ^{1}H NMR ([D$_6$]DMSO): $\delta = 1.50$–1.85 (m, 10H, CH_2), 2.37 (d, $^3J = 8.1$ Hz, 2H, NH), 2.60 ppm (d, $^3J = 8.1$ Hz, 2H, NH); ^{13}C NMR ([D$_6$]DMSO): $\delta = 23.59$ (t), 26.69 (t), 34.10 (t), 59.09 ppm (s); minor isomer: ^{1}H NMR ([D$_6$]DMSO): $\delta = 1.50$–1.85 (m, 10H, CH_2), 2.01 (d, $^3J = 7.8$ Hz, 2H, NH), 2.59 ppm (d, $^3J = 7.8$ Hz, 2H, NH); ^{13}C NMR ([D$_6$]DMSO): $\delta = 25.26$ (t), 29.26 (t), 35.75 (t), 57.92 ppm (s).

10:[b] Brown solid; m.p. 152–154 °C; IR (KBr): $\tilde{\nu} = 3427$, 3178, 2946, 2923, 2863, 2366, 1652, 1399, 1201, 855 cm^{-1}; ^{1}H NMR ([D$_6$]DMSO): $\delta = 1.62$ (br s, 8H, CH_2), 2.23 (d, $^3J = 7.8$ Hz, 2H, NH), 2.63 ppm (d, $^3J = 7.8$ Hz, 2H, NH); ^{13}C NMR ([D$_6$]DMSO): $\delta = 24.14$ (t), 33.79 (t), 58.06 ppm (s).

12: Brown oil; ^{1}H NMR ($CDCl_3$): $\delta = 1.30$ (m, 4H, CH_2), 1.70–1.86 ppm (m, 6H, CH_2); ^{13}C NMR ($CDCl_3$): $\delta = 24.43$ (t), 29.91 (s, C-3/C-4), 30.29 (t, C-9), 32.84 ppm (t).

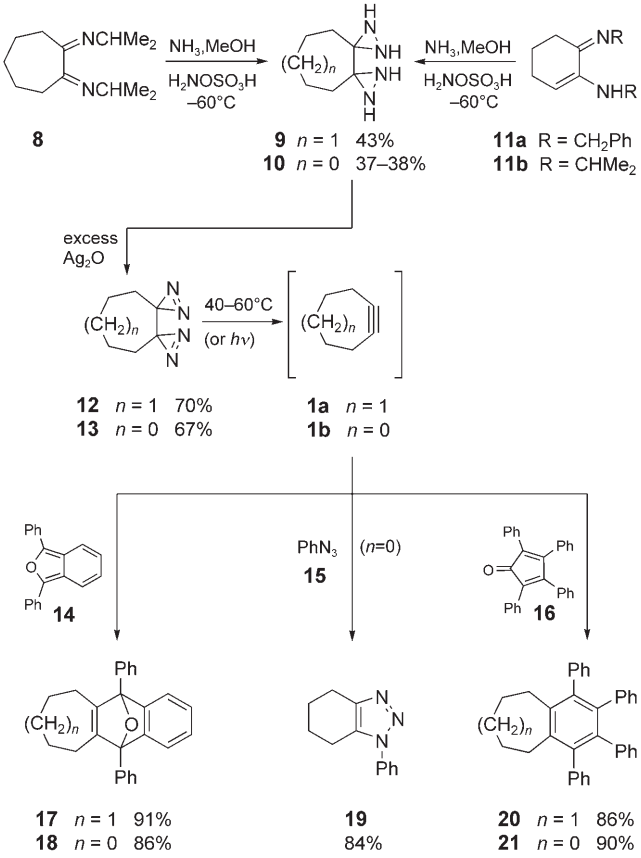
13: Brown oil; ^{1}H NMR ($CDCl_3$): $\delta = 1.36$ (m, 4H, CH_2), 1.86 ppm (m, 4H, CH_2); ^{13}C NMR ($CDCl_3$): $\delta = 23.72$ (t), 27.99 (s), 30.68 ppm (t).

24:[b] Yellow oil; IR ($CDCl_3$): $\tilde{\nu} = 3176$, 3124, 2970, 2878, 1670, 1591, 1406, 1125 cm^{-1}; ^{1}H NMR ($CDCl_3$): $\delta = 1.05$–2.55 (m), 2.60–3.80 ppm (m); ^{13}C NMR ($CDCl_3$): $\delta = 23.51$ (t), 24.95 (t), 34.77 (t), 43.00 (d), 43.20 (d), 64.34 (s), 64.79 ppm (s).

26: Brown oil; ^{1}H NMR ($CDCl_3$): $\delta = 1.50$ (m, 2H, 7-H/10-H), 1.54 (dt, $^2J = 9.9$ Hz, $^4J = 1.8$ Hz, 1H, 11_{syn}-H), 1.75 (m, 2H), 2.02 (m, 2H), 2.37 ppm (dm, $^2J = 9.9$ Hz, 1H, 11_{anti}-H); ^{13}C NMR ($CDCl_3$): $\delta = 24.53$ (t, C-8/C-9), 37.28 (t, C-11), 37.88 (s, C-3/C-4), 40.19 ppm (d, C-7/C-10).

[a] ^{1}H NMR: 300 MHz; ^{13}C NMR: 75 MHz; ^{15}N NMR; 30 MHz. [b] The bidiaziridines **3**, **9**, **10**, and **24** were treated with an excess of PhNCO to yield urea derivatives which were completely characterized (including combustion analyses).

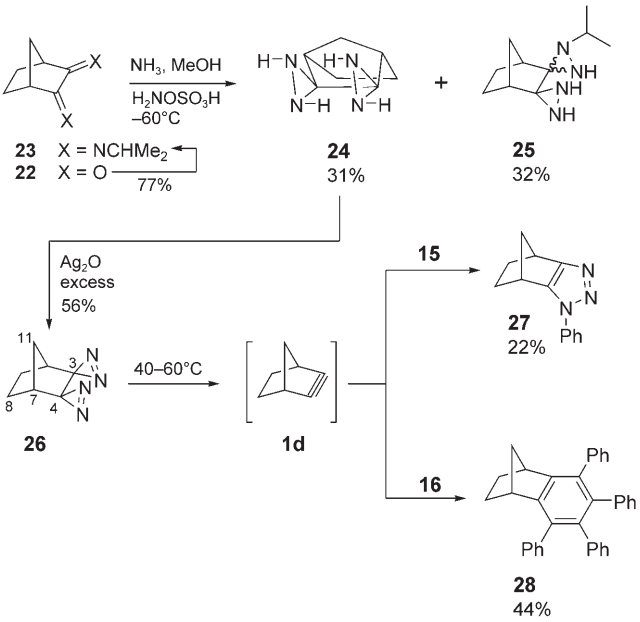
The spirocyclic diaziridines **9** and **10** were accessible from the bisimines **8**[14] and **11a**[14] or **11b**,[15] respectively. The spectroscopic data of **9** (Table 1) point to a mixture of diastereomers (ca. 9:5). The isolable title compounds **12** and **13**, which function as precursors of cycloheptyne (**1a**) and cyclohexyne (**1b**), were obtained by oxidation of **9** and **10**, respectively. When **12** or **13** were warmed in the presence of the reaction partners **14**, **15**, or **16**, the trapping products of cycloalkynes **17**–**21**[16] were formed in excellent yields (Scheme 3). Similar results were achieved on irradiation of precursors **12** or **13** in the presence of **14** or **16**. Lower yields of



Scheme 3.

20 (25–35 %) were obtained when trapping reagent **16** was added *after* photolysis of **12** at low temperature (−90 °C in CD_2Cl_2 or −120 °C in CD_2ClF).

The bisimine **23**, which is easily accessible from diketone **22**, can also be transformed into bidiaziridines. After workup



Scheme 4.

 © 2006 Wiley-VCH Verlag GmbH & Co. KGaA, Weinheim

by chromatography (neutral alumina), we isolated the desired product **24** and also the isopropyl derivative **25**. Based on the ^{13}C NMR data (Table 1) and supposing that both H-N-N-H units have a *trans* arrangement, we assume either an all-*R* configuration (see Scheme 4) or an all-*S* configuration for the four nitrogen atoms of **24**. Oxidation of **24** afforded the norbornyne precursor **26**. Thermolysis of the latter compound in the presence of **15** led to cycloadduct **27**, whereas **28**[17] was formed in the presence of **16**.

This clean and reagent-free generation of highly strained cycloalkynes from bi-3*H*-diazirin-3-yls, which occurs under very mild reaction conditions, could lead to new applications for these compounds.

Received: September 2, 2005

Keywords: cycloaddition · cycloalkynes · reactive intermediates · spiro compounds · strained molecules

[1] Reviews: a) H. Hopf, *Classics in Hydrocarbon Chemistry*, Wiley-VCH, Weinheim, **2000**, chap. 8.2; b) R. Gleiter, R. Merger in *Modern Acetylenic Chemistry*, (Eds.: P. J. Stang, F. Diederich), VCH, Weinheim, **1995**, pp. 285 – 319; c) H. Meier in *Advances in Strain in Organic Chemistry, Vol. 1* (Ed.: B. Halton), JAI, London, **1991**, pp. 215 – 272; d) A. Krebs, J. Wilke, *Top. Curr. Chem.* **1983**, *109*, 189 – 233.

[2] D. W. Laird, J. C. Gilbert, *J. Am. Chem. Soc.* **2001**, *123*, 6704 – 6705.

[3] In early attempts to generate **1d**,[4] trapping by means of a Diels–Alder reaction was not successful (see Ref. [5]).

[4] a) P. G. Gassman, I. Gennick, *J. Am. Chem. Soc.* **1980**, *102*, 6863 – 6864; b) P. G. Gassman, I. Gennick, *J. Org. Chem.* **1980**, *45*, 5211 – 5213.

[5] H. Hart, S. Shamouilian, Y. Takehira, *J. Org. Chem.* **1981**, *46*, 4427 – 4432, see footnote [27].

[6] T. Kitamara, M. Kotani, T. Yokoyama, Y. Fujiwara, K. Hori, *J. Org. Chem.* **1999**, *64*, 680 – 681.

[7] K. Banert, F. Köhler, *Angew. Chem.* **2001**, *113*, 173 – 176; *Angew. Chem. Int. Ed.* **2001**, *40*, 174 – 177.

[8] H. Bock, H. tom Dieck, *Chem. Ber.* **1967**, *100*, 228 – 246.

[9] A. Mannschreck, W. Seitz, *Angew. Chem.* **1969**, *81*, 224; *Angew. Chem. Int. Ed. Engl.* **1969**, *8*, 212.

[10] H. tom Dieck, K.-D. Franz, W. Majunke, *Z. Naturforsch. B* **1975**, *30*, 922 – 925.

[11] E. Schmitz, C. Hörig, C. Gründemann, *Chem. Ber.* **1967**, *100*, 2093 – 2100.

[12] Reviews on the synthesis of diaziridines and diazirines: a) E. Schmitz in *Comprehensive Heterocyclic Chemistry, Vol. 7* (Ed.: W. Lwowski), Pergamon, Oxford, **1984**, pp. 195 – 236; b) R. G. Kostyanovsky, R. Murugan, M. Sutharchanadevi in *Comprehensive Heterocyclic Chemistry II, Vol. 1A* (Ed.: A. Padwa), Pergamon, New York, **1996**, pp. 347 – 364.

[13] Caution should be exercised during isolation of diazirines which may be explosive. However, our bidiazirinyls did not explode even when samples were hit with a hammer.

[14] Compounds **8** and **11a** can be prepared easily from the corresponding α-diketones and primary amines.

[15] R. van Asselt, C. J. Elsevier, W. J. J. Smeets, A. L. Spek, R. Benedix, *Recl. Trav. Chim. Pays-Bas* **1994**, *113*, 88 – 98.

[16] a) G. Wittig, R. Pohlke, *Chem. Ber.* **1961**, *94*, 3276 – 3286; b) G. Wittig, P. Fritze, *Angew. Chem.* **1966**, *78*, 905; *Angew. Chem. Int. Ed. Engl.* **1966**, *5*, 846; c) K. L. Erickson, J. Wolinsky, *J. Am. Chem. Soc.* **1965**, *87*, 1142 – 1143; d) T. Harada, K. Iwazaki, T. Otani, A. Oku, *J. Org. Chem.* **1998**, *63*, 9007 – 9012; e) G. Wittig, A. Krebs, *Chem. Ber.* **1961**, *94*, 3260 – 3275; f) R. Breslow, L. J. Altman, A. Krebs, E. Mohacsi, I. Murata, R. A. Peterson, J. Posner, *J. Am. Chem. Soc.* **1965**, *87*, 1326 – 1331; g) F. G. Willey, *Angew. Chem.* **1964**, *76*, 144; *Angew. Chem. Int. Ed. Engl.* **1964**, *3*, 138.

[17] Alternative synthesis of **28**: D. W. Macomber, A. G. Verma, R. D. Rogers, *Organometallics* **1988**, *7*, 1241 – 1253.

 © 2006 Wiley-VCH Verlag GmbH & Co. KGaA, Weinheim

Inorganic Nanotubes

DOI: 10.1002/anie.200502665

Porous Silicon and Alumina as Chemically Reactive Templates for the Synthesis of Tubes and Wires of SnSe, Sn, and SnO_2**

*Lili Zhao, Maekele Yosef, Martin Steinhart, Petra Göring, Herbert Hofmeister, Ulrich Gösele, and Sabine Schlecht**

Highly ordered porous templates such as alumina membranes[1] and macroporous silicon[2] are valuable and versatile tools for the fabrication of arrays of one-dimensional nanostructures with high aspect ratios and narrow diameter distributions.[3] With templates of macroporous silicon and porous alumina, pore diameters from 25 nm up to 1000 nm are accessible. Here, we report on a new synthetic approach where these templates are not simply inert shape-defining molds but also chemical reagents for the oxidation or reduction of tin(II) selenide. For a given template system, the reduction or oxidation can be initiated easily by increasing the temperature to $\approx 650\,^{\circ}C$. Starting from tin(II) selenide nanotubes with tin in a medium oxidation state, single-crystalline nanotubes of elemental tin were produced in a high-temperature reaction with the macroporous silicon template as a reducing environment. In an analogous manner single-crystalline nanowires of tin(IV) oxide (SnO_2) were obtained using the high-temperature oxidizing proper-

[*] Dr. M. Yosef, Prof. Dr. S. Schlecht
Institut für Chemie und Biochemie
Freie Universität Berlin
Fabeckstrasse 34–36, 14195 Berlin (Germany)
Fax: (+49) 30-838-53310
E-mail: schlecht@chemie.uni-marburg.de
L. Zhao, Dr. M. Steinhart, Dr. P. Göring, H. Hofmeister, Prof. Dr. U. Gösele
Max-Planck-Institut für Mikrostrukturphysik
Halle (Germany)

[**] This research was supported financially by the Deutsche Forschungsgemeinschaft (SPP1165 "Nanowires and Nanotubes", STE1127/2-1 and SCHL529/2-1) and the Fonds der Chemischen Industrie. We thank T. Geppert, K. Sklarek, and S. Grimm for preparing the templates.

© 2006 Wiley-VCH Verlag GmbH & Co. KGaA, Weinheim
InterScience

ties of the pore walls of alumina templates etched with sulfuric acid.

It is known that SnSe forms as the primary thermolytic product of the precursor $Sn(SePh)_4$[4] at temperatures above 300 °C. SnSe is a narrow-band-gap semiconductor with an optical band gap of ≈ 1 eV. In particular, nanoscale thin films of the tin(II) chalcogenides SnS and SnSe are promising materials for photoelectric conversion.[5,6] Polycrystalline films of SnSe can be used in energy-conversion devices[6] and in memory switching.[7] Ordered structures of tin nanotubes can be used for the preparation of nanostructures of catalytically active binary intermetallics such as Pt–Sn[8] and Au–Sn.[9] Tin nanowires also exhibit superconducting properties.[10] Nanoribbons, nanowires, and nanoboxes[11] of tin(IV) oxide were produced by template-assisted routes or by addition of surface-capping additives and showed excellent sensing properties. The different types of templates we used for the preparation of nanowires and nanotubes of SnSe, Sn, and SnO_2 are listed in Table 1.

Table 1: Redox properties of different template types at elevated temperatures.

Template type	Pore diameter	Redox properties
alumina (etched with sulfuric acid)	25 nm, 30 nm	oxidizing
alumina (etched with phosphoric acid)	180 nm, 400 nm	mostly inert
silicon	1000 nm	reducing

Self-ordered porous alumina is currently accessible with pore diameters ranging from 25 nm to 400 nm and pore depths up to 100 μm. The pore walls are amorphous and also contain tetrahedrally coordinated aluminum atoms, defects, and electrolyte anions.[12,13] Commonly used electrolytes are sulfuric acid,[1c] yielding pores with a diameter of 25 nm, and phosphoric acid,[1d] yielding pores with a diameter of 180 nm. The latter pores can be widened to 400 nm by an isotropic wet-etching step. The properties of the pore walls depend to a great extent on the electrolyte, and the more acidic medium of sulfuric acid together with a higher defect concentration in thin pore walls should enhance the reactivity of the templates with small pore diameters (Table 1). Macroporous silicon templates cover the diameter range from 370 nm up to few microns. Their pore depths are limited only by the thickness of the wafers used as substrates and can reach several hundreds of microns,[2] thus leading to excellent aspect ratios of the pores.

Independent of the produced target material, solid wires formed in narrow pores with diameters of 25 nm, whereas tubes were obtained when pores with diameters of 180, 400, or 1000 nm were used. All products resulting from a thermolysis at 350 °C showed a granular, polycrystalline morphology. When higher temperatures of 600 °C to 650 °C were applied, the formation of single-crystalline wires and tubes was achieved. The transition from wires to tubular structures depending on the pore diameter of the templates also occurs in the case of the template-assisted thermolysis of hydrogen tetrachloroaurate leading to gold nanostructures.[3i]

In the wetting procedure applied here, the single-source precursor $Sn(SePh)_4$ is infiltrated into the pores. In a low-temperature thermolysis at about 350 °C SnSe forms as the initial thermolytic product and no chemical reaction involving the template and the precursor or the template and the produced SnSe takes place. Nanowires consisting of orthorhombic SnSe (space group *Pbnm*)[14] with a diameter of 25 nm, corresponding to the diameter of the template pores, were obtained when the wetted samples were annealed at 350 °C for 36 h. A transmission electron microscopic (TEM) image of a bundle of released polycrystalline SnSe nanowires is shown in Figure 1 a, and the corresponding selected area electron diffraction pattern (SAED) is shown in Figure 1 b. An X-ray diffraction pattern of the SnSe nanowires, which indicates the formation of single-phase SnSe, is represented in Figure 1 c.

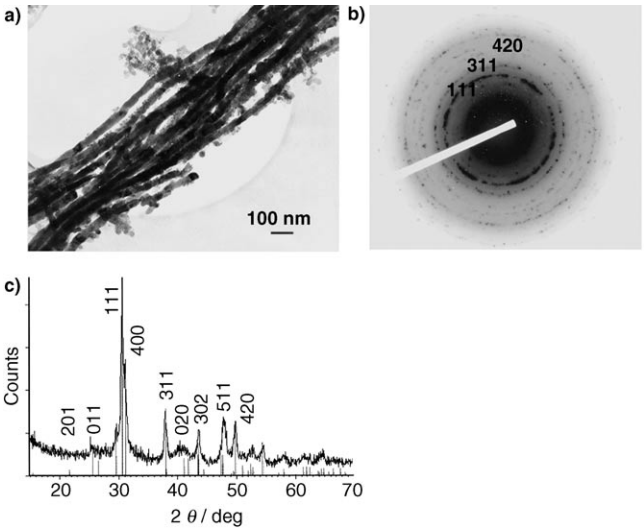


Figure 1. a) TEM image of a bundle of released SnSe nanowires with a diameter of 25 nm; b) electron diffraction pattern of a bundle of SnSe nanowires; c) XRD pattern of SnSe nanowires in the template (reflections are calculated as a line pattern and indexed according to JCPDS card no. 88-0287).

Nanotubes of SnSe with polycrystalline walls formed when porous alumina with a pore diameter of 180 nm was used as a template. The scanning electron micrographic (SEM) images in Figure 2 a and b show an overview and a magnified image of an array of aligned SnSe nanotubes released from the template. In Figure 2 b it can be seen that the nanotubes have terminating caps at their ends, resulting from the bottom dimple of the template pores. This detail nicely shows that the pores were filled in their full depth and that the excellent aspect ratio of the pores can be transferred quantitatively to the one-dimensional nanostructures. The grain structure of the tube walls is apparent in Figure 2 c, where an individual polycrystalline SnSe tube released from a template with a pore diameter of 400 nm is depicted. The crystallites have diameters on the order of 10–20 nm. The thickness of the tube walls is also in the range of 20 nm. The SAED pattern depicted in Figure 2 d shows the characteristics

 © 2006 Wiley-VCH Verlag GmbH & Co. KGaA, Weinheim

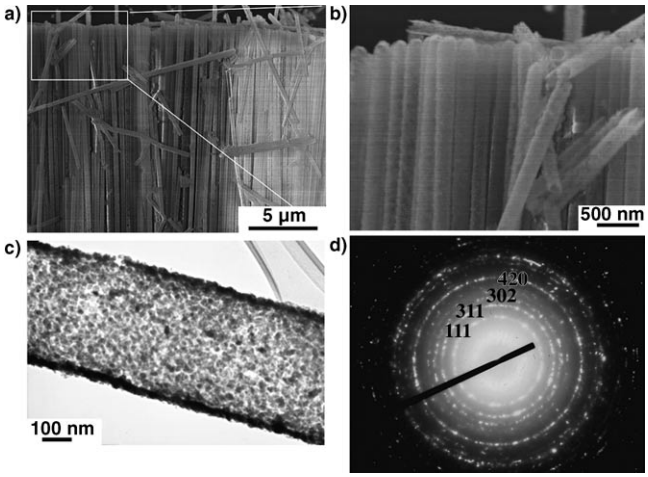


Figure 2. SEM images of an ordered array of SnSe nanotubes with a diameter of 180 nm: a) overview; b) magnified image showing granular wall morphology and terminating caps; c) TEM image of a single SnSe nanotube with a diameter of 400 nm and polycrystalline walls; d) electron diffraction pattern of the tube section seen in (c).

of polycrystalline tubes of single-phase orthorhombic SnSe (space group *Pbnm*).

The intermediate oxidation state of Sn^{II} in SnSe offers the opportunity of either a reduction or an oxidation of the SnSe nanostructures by appropriate pore walls with reducing or oxidizing properties. Such selective redox chemistry within the pores requires that the pore walls of the alumina templates have sufficient oxidizing power and that the pores of the macroporous silicon have good reducing ability, as these two template materials are the most readily accessible ones with complementary redox properties.

To model the redox chemistry of $Sn(SePh)_4$ and SnSe with macroporous silicon and with the pore walls of porous alumina, the two tin compounds were reacted with commercial silicon powder under different conditions (Table 2), and

Table 2: Overview of reactions of $Sn(SePh)_4$ and SnSe with silicon (reaction time: 15 h).

Tin compound	Silicon source	Reaction temperature	Product
$Sn(SePh)_4$	Si template	650 °C	Sn
$Sn(SePh)_4$	Si powder	500 or 600 °C	SnSe
$Sn(SePh)_4$	Si powder	650 °C	Sn
SnSe (nanopart.)	Si powder	650 °C	Sn
SnSe (microcryst.)	Si powder	650 °C	SnSe, very little Sn

the molecular precursor $Sn(SePh)_4$ was heated in boiling wet diethylene glycol solvent, a system with hydroxy groups and a small water content just like the amorphous wall structure of the pores in ordered alumina membranes.[12,13,15] Under these conditions $Sn(SePh)_4$ did not thermolyze into SnSe but was converted into nanoparticles of SnO_2 with a diameter of about 10 nm, as could be shown by X-ray powder diffraction. In a series of experiments with silicon powder the formation of elemental tin was observed at reaction temperatures higher than 600 °C (Table 2). The reduction can be performed as a quantitative conversion either starting directly from molecular $Sn(SePh)_4$ or from independently produced nanoparticles of SnSe with a particle size of ≈50 nm. In both reactions elemental tin was formed under the reaction conditions and crystallized from its liquid state under cooling. Owing to the large surface area of the pore walls of macroporous silicon templates and a relevant number of defects and distortions that form in the structure of the pore walls of macroporous silicon during annealing,[3h] the reaction of $Sn(SePh)_4$ with the template pores should be even more effective than its reaction with microcrystalline silicon powder. Accordingly, single-crystalline microtubes consisting of elemental Sn with a diameter of 1 μm were obtained by infiltrating macroporous silicon molds with $Sn(SePh)_4$, annealing the wetted templates at temperatures in the range of 600–650 °C for 5 h, and subsequently cooling the samples to room temperature at a rate of 2 K min^{-1}. Figure 3a shows an array of aligned Sn

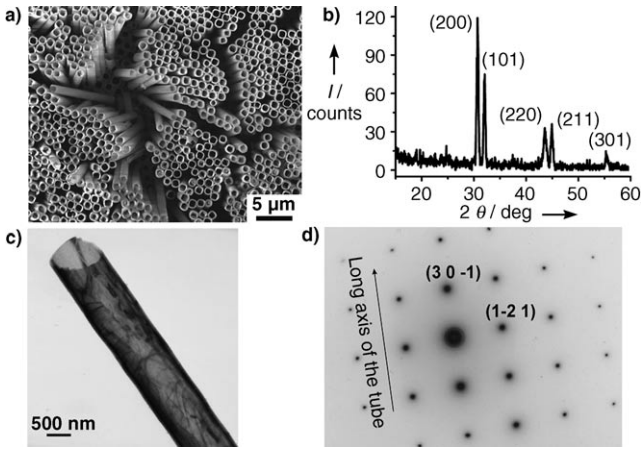


Figure 3. a) SEM image of a laterally extended array of Sn nanotubes with a diameter of 1000 nm, protruding from the macroporous silicon matrix; b) XRD pattern of aligned, partially released tin tubes. All reflections are indexed on the basis of JCPDS card no. 04-673; c) tin nanotube after removal of the silicon template; d) indexed SAED pattern of a single tin nanotube (zone axis [123]), indicating its single-crystalline character.

tubes protruding from a partially removed template. They are uniform in size and have a wall thickness of approximately 150 nm. All reflections in the X-ray diffraction pattern (Figure 3b) can be indexed for tetragonal β-Sn[16] without ambiguity, indicating that the reduction of tin(II) selenide is quantitative. Figure 3c shows an individual tin tube (d = 1000 nm) after removal of the silicon template, and an indexed SAED pattern is depicted in Figure 3d.

When $Sn(SePh)_4$ was infiltrated into porous alumina and annealed at 650 °C a big difference in the oxidizing power of the walls of small pores etched with sulfuric acid and the walls of larger pores etched with phosphoric acid became apparent. Whereas the thicker, less acidic walls of the larger pores did not lead to the oxidation of SnSe, single-crystalline SnO_2 nanowires with a high aspect ratio and diameters of 25 nm were obtained from porous alumina templates etched with sulfuric acid. This is in accordance with the higher defect

 © 2006 Wiley-VCH Verlag GmbH & Co. KGaA, Weinheim

concentration, the increased acidity, and the presence of electrolyte anions and residual water in the pore walls of templates etched with sulfuric acid.[12] Figure 4a shows a TEM image of SnO_2 nanowires at low magnification. They typically

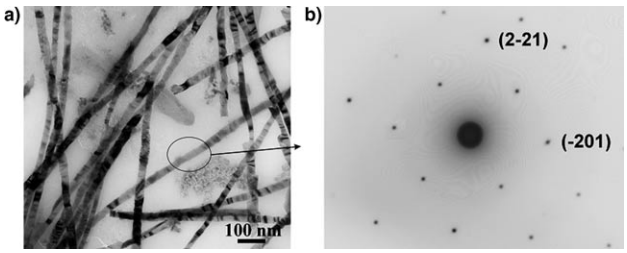


Figure 4. a) TEM image of single-crystalline SnO_2 nanowires with a diameter of 25 nm; b) indexed SAED pattern (zone axis [122]) of the marked section of the SnO_2 nanowire seen in (a).

have aspect ratios (length over diameter) greater than 100. The nonuniform contrast of these nanowires is due to bending contours, thickness fringes, and planar defects.[17] An indexed SAED pattern of part of a section of a single-crystalline SnO_2 nanowire (Figure 4a) is depicted in Figure 4b.

A high-resolution TEM micrograph of a selected area of an individual nanowire of tetragonal SnO_2 (Figure 5) again shows the single-crystalline nature of the wires. The interplanar spacing of $d = 3.34$ Å (Figure 5c) could be assigned to {110} planes of the SnO_2 lattice described in space group $P4_2/mnm$.[18]

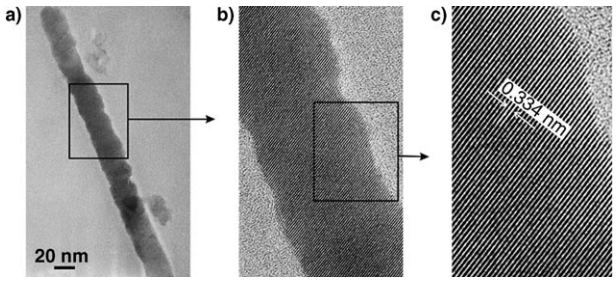


Figure 5. a) Segment of an individual SnO_2 nanowire with a diameter of 25 nm; b) enlarged section of the nanowire, indicating the good homogeneity and crystallinity; c) high-resolution image of a part of (b), showing {110} lattice fringes of SnO_2.

In conclusion, the selective reactivity of the pore walls of porous alumina and macroporous silicon, which leads not just to a surface modification but to a complete conversion of the one-dimensional nano-objects, allows the preparation of monodisperse tubes and nanowires of three different target materials—SnSe, SnO_2, and Sn—from a single-source precursor, $Sn(SePh)_4$. The enhanced reaction temperature for the oxidation within the pores facilitated the formation of single-crystalline nanowires of SnO_2.

Experimental Section

Synthetic procedures: The precursor compound $Sn(SePh)_4$ was synthesized according to a literature procedure.[4]

Sample preparation: The templates were prepared according to procedures described elsewhere.[1,2] For the SnSe and SnO_2 wires, as well as for the Sn tubes shown in Figure 1 and Figures 3–5, the $Sn(SePh)_4$ was melted on the template surface at a temperature of 110 °C. For the SnSe tubes shown in Figure 2, a solution of 5 wt % $Sn(SePh)_4$ in chloroform was applied dropwise onto the template surface. Subsequently, thermolysis was performed at 350 °C, and or alternatively, SnSe was converted into SnO_2 or Sn at 650 °C. All thermolytic reactions and annealing procedures were performed in corundum crucibles under argon. The templates were selectively removed either partially or completely by etching with a 20 wt % aqueous solution of potassium hydroxide at 70 °C. The resulting suspension was washed with deionized water several times until it was neutral.

X-ray diffraction measurements: XRD measurements were performed with a Philips X'pert MRD diffractometer with a $Cu_{K\alpha}$ radiation source, cradle, and secondary monochromator in a $\theta/2\theta$ geometry. The wires and tubes were aligned within the pores of the templates. Their long axes were parallel, and the template surface was perpendicular to the plane defined by the incident beam and the detector.

Electron microscopy: SEM images of both the completely released tubes, which were deposited on conductive substrates (highly doped silicon wafers), and the partially liberated tubes standing in the matrix of the partially etched templates were obtained using a field-emission scanning electron microscope JEOL JSM 6300F at an accelerating voltage of 5 kV. For TEM imaging and electron diffraction recording, aqueous suspensions of the nano- and micro-objects were applied dropwise onto copper grids coated with a holey carbon film. The samples were investigated in a JEM 1010 microscope operated at 100 kV. High-resolution TEM images shown in Figure 5 were recorded with a high-resolution TEM (JEM 4010 operating at 400 kV).

Received: July 29, 2005
Published online: November 30, 2005

Keywords: nanostructures · selenides · template synthesis · tin

[1] a) H. Masuda, K. Fukuda, *Science* **1995**, *268*, 1466; b) H. Masuda, M. Satoh, *Jpn. J. Appl. Phys.* **1996**, *35*, L126; c) H. Masuda, F. Hasegawa, S. Ono, *J. Electrochem. Soc.* **1997**, *144*, L127; d) H. Masuda, K. Yada, A. Osaka, *Jpn. J. Appl. Phys. Part 2* **1998**, *37*, L1340; e) P. Braunstein, H.-P. Kormann, W. Meyer-Zaika, R. Pugin, G. Schmid, *Chem. Eur. J.* **2000**, *6*, 4637; f) K. Nielsch, J. Choi, K. Schwirn, R. B. Wehrspohn, U. Gösele, *Nano Lett.* **2002**, *2*, 677.

[2] a) V. Lehmann, *J. Electrochem. Soc.* **1993**, *140*, 2836; b) A. Birner, U. Grüning, S. Ottow, A. Schneider, F. Müller, V. Lehmann, H. Föll, U. Gösele, *Phys. Status Solidi A* **1998**, *165*, 111.

[3] a) C. R. Martin, *Science* **1994**, *266*, 1961; b) C. A. Huber, T. E. Huber, M. Sadoqi, J. A. Lubin, S. Manalis, C. B. Prater, *Science* **1994**, *263*, 800; c) B. B. Lakshmi, P. K. Dorhout, C. R. Martin, *Chem. Mater.* **1997**, *9*, 857; d) M. Steinhart, J. H. Wendorff, A. Greiner, R. B. Wehrspohn, K. Nielsch, J. Schilling, U. Gösele, *Science* **2002**, *296*, 1997; e) M. Steinhart, Z. Jia, A. Schaper, R. B. Wehrspohn, U. Gösele, J. H. Wendorff, *Adv. Mater.* **2003**, *15*, 706; f) N. I. Kovtyukhova, T. E. Mallouk, T. S. Mayer, *Adv. Mater.* **2003**, *15*, 780; g) M. Steinhart, R. B. Wehrspohn, U. Gösele, J. H. Wendorff, *Angew. Chem.* **2004**, *116*, 1356; *Angew. Chem. Int. Ed.* **2004**, *43*, 1334; h) L. Zhao, M. Steinhart, M. Yosef, S. K. Lee, T. Geppert, E. Pippel, R. Scholz, U. Gösele, S. Schlecht, *Chem. Mater.* **2005**, *17*, 3; i) P. Göring, E. Pippel, H. Hofmeister, R. B. Wehrspohn, M. Steinhart, U. Gösele, *Nano Lett.* **2004**, *4*, 1121.

[4] S. Schlecht, M. Budde, L. Kienle, *Inorg. Chem.* **2002**, *41*, 6001.

 © 2006 Wiley-VCH Verlag GmbH & Co. KGaA, Weinheim

[5] M. T. S. Nair, P. K. Nair, *Semicond. Sci. Technol.* **1991**, *6*, 132.
[6] a) A. Bennouna, P. Y. Tessier, M. Priol, Q. Dang Tran, S. Robin, *Phys. Status Solidi B* **1983**, *117*, 51; b) K. Bindu, P. K. Nair, *Semicond. Sci. Technol.* **2004**, *19*, 1348.
[7] T. Subba Rao, B. K. Samanata Ray, A. K. Chaudhuri, *Thin Solid Films* **1988**, *165*, 257.
[8] Y.-G. Gao, J.-S. Hu, H.-M. Zhang, H.-P. Liang, L.-J. Wan, C.-L. Bai, *Adv. Mater.* **2005**, *17*, 746.
[9] J.-G. Wang, M.-L. Tian, T. E. Mallouk, M. H. W. Chan, *Nano Lett.* **2004**, *4*, 1313.
[10] M. L. Tian, J. Wang, J. Snyder, J. Kurtz, Y. Liu, P. Schiffer, T. E. Mallouk, M. H. W. Chan, *Appl. Phys. Lett.* **2003**, *83*, 1620.
[11] a) D.-F. Zhang, D.-L. Sun, J.-L. Yin, C.-H. Yan, *Adv. Mater.* **2003**, *15*, 1022; b) M. Law, H. Kind, B. Messer, F. Kim, P. Yang, *Angew. Chem.* **2002**, *114*, 2511; *Angew. Chem. Int. Ed.* **2002**, *41*, 2405; c) Y. Liu, J. Dong, M. Liu, *Adv. Mater.* **2004**, *16*, 353; d) Z. R. Dai, J. L. Gole, J. D. Sout, Z. L. Wang, *J. Phys. Chem. B* **2002**, *106*, 1274; e) B. Liu, H. C. Zeng, *J. Phys. Chem. B* **2004**, *108*, 5867; f) M. Zheng, G. Li, X. Zhang, S. Huang, Y. Lei, L. Zhang, *Chem. Mater.* **2001**, *13*, 3859.
[12] J. Choi, Y. Luo, R. B. Wehrspohn, R. Hillebrand, J. Schilling, U. Gösele, *J. Appl. Phys.* **2003**, *94*, 4757.
[13] R. Kniep, P. Lamparter, S. Steeb, *Angew. Chem.* **1989**, *101*, 975; *Angew. Chem. Int. Ed. Engl.* **1989**, *28*, 951.
[14] H. G. von Schnering, H. Wiedemeier, *Z. Kristallogr.* **1981**, *156*, 143.
[15] T. Krieg, M. Yosef, S. Schlecht, unpublished results. A 250-mg sample of $Sn(SePh)_4$ was suspended in 50 mL of wet diethylene glycol and heated under reflux for 20 h. The reaction mixture was allowed to cool to room temperature, and the resulting off-white solid was washed filtered, washed with acetone, and air dried. An XRD pattern of the product showed the formation of SnO_2 in $>90\%$ yield with some SnSe present.
[16] β-Sn: JCPDS entry no. 04-673.
[17] Y. Ding, Z. L. Wang, *J. Phys. Chem. B* **2004**, *108*, 12280.
[18] SnO_2: JCPDS entry no. 21-1250.

 © 2006 Wiley-VCH Verlag GmbH & Co. KGaA, Weinheim

Chiral Cubanes

DOI: 10.1002/anie.200502477

Enantiomerically Pure Copper(II) Cubanes $[Cu_4L_2(OMe)_4]$ from Chiral Bis-1,3-diketones H_2L through Diastereoselective Self-Assembly**

Rolf W. Saalfrank, Christine Schmidt, Harald Maid, Frank Hampel, Walter Bauer, and Andreas Scheurer**

Dedicated to Professor Rudi van Eldik on the occasion of his 60th birthday

The bis-1,3-diketo dianion $(L^1)^{2-}$ proved to be an excellent ligand for copper(II) ions, and owing to the extra oxygen donors of the glycolate spacer, most suitable for the synthesis of racemic *P*/*M* metallacoronates $\{M\subset[Cu_2(L^1)_2(MeOH)_2]\}OAc$ (**1**, $M = K^+$, Rb^+, Cs^+) (Figure 1).[1] In an

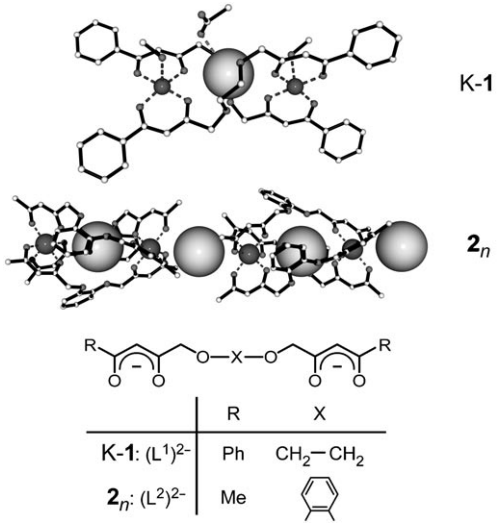


Figure 1. Top: View of (*M*)-$[\{K\subset[Cu_2(L^1)_2(MeOH)_2]\}OAc]$ (K-**1**) in the crystal. Bottom: View of the repeating unit $(\Delta,\Delta)/(\Lambda,\Lambda)$-*fac* in *meso*-$[\{Cs\subset[Ni_2(L^2)_3]\}Cs]_n$ $(\mathbf{2})_n$. Povray presentation: C white, O gray (small), Cu and Ni gray (medium), Cs gray (large); hydrogen atoms omitted for clarity.

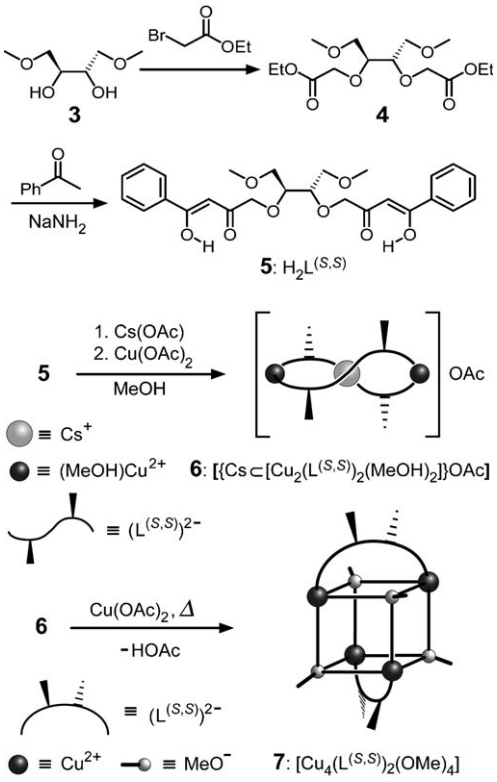
[*] Prof. Dr. R. W. Saalfrank, Dipl.-Chem. C. Schmidt, Dr. H. Maid, Dr. F. Hampel, Prof. Dr. W. Bauer, Dr. A. Scheurer
Institut für Organische Chemie
Universität Erlangen-Nürnberg
Henkestrasse 42, 91054 Erlangen (Germany)
Fax: (+49) 9131-852-1165
E-mail: saalfrank@chemie.uni-erlangen.de
andreas.scheurer@chemie.uni-erlangen.de

[**] Chelate Complexes, Part 31. This research was supported by the Deutsche Forschungsgemeinschaft (Sa 276/27-1-2, SPP 1137, SFB 583, GK 312) and the Fonds der Chemischen Industrie. We thank F. Pointillart, Dr. C. Train, and Prof. M. Verdaguer for performing preliminary CD measurements and for fruitful discussions. Part 30: R. W. Saalfrank, A. Scheurer, K. Pokorny, H. Maid, U. Reimann, F. Hampel, F. W. Heinemann, V. Schünemann, A. X. Trautwein, *Eur. J. Inorg. Chem.* **2005**, 1383–1387.

© 2006 Wiley-VCH Verlag GmbH & Co. KGaA, Weinheim

extension of this strategy, starting from the bis-1,3-diketone dianion $(L^2)^{2-}$ with catecholate spacer and hexacoordinate nickel(II), instead of tetra-or pentacoordinate copper(II), we prepared neutral homochiral {2}-metallacryptate {Cs⊂$[Ni_2(L^2)_3]$}Cs (**2**) with either (Δ,Δ)-*fac* or (Λ,Λ)-*fac* stereochemistry. The building blocks **2** are self-complementary and aggregate alternating across the external cesium ions to give the one-dimensional coordination polymer *meso*-[{Cs⊂$[Ni_2(L^2)_3]$}Cs]$_n$ (**2**$_n$) (Figure 1).[1]

In the course of our studies on supramolecular coordination chemistry, we focused on developing stereoselective syntheses for **1** and (**2**$_n$). To this end we prepared enantiomerically pure $H_2L^{(S,S)}$ (**5**), in which the chirality is incorporated in the spacer backbone (Scheme 1). Commercially



Scheme 1. Generation of cubane **7** via coronate **6** (not isolable as a solid).

available (2*S*,3*S*)-1,4-dimethoxy-2,3-butanediol (**3**), derived from L-tartaric acid, was etherified with ethyl bromoacetate in the presence of sodium hydride to afford (2*S*,3*S*)-1,4-dimethoxy(2,3-ethylacetoxy)butane (**4**). Subsequent Claisen condensation of **4** with acetophenone and sodium amide led to the C_2-symmetric ligand $H_2L^{(S,S)}$ (**5**).[2] As expected, reaction of equimolar amounts of $H_2L^{(S,S)}$ (**5**), copper(II) acetate, and 0.5 equivalents of cesium acetate in methanol readily yielded {Cs⊂$[Cu_2(L^{(S,S)})_2(MeOH)_2]$}OAc (**6**), which was identified in solution by FAB mass spectrometry (*m*/*z* 1197 (100%) $[M-2MeOH-OAc]^+$) (Scheme 1). All efforts to crystallize **6** remained unsuccessful, however. Besides large quantities of blue copper acetate, we isolated a few green crystals which turned out to be copper(II) cubane (*C*,*C*,*C*,*C*)-$[Cu_4(L^{(S,S)})_2(OMe)_4]$ (**7**) according to X-ray analysis (Scheme 1; Figure 2).[3–6]

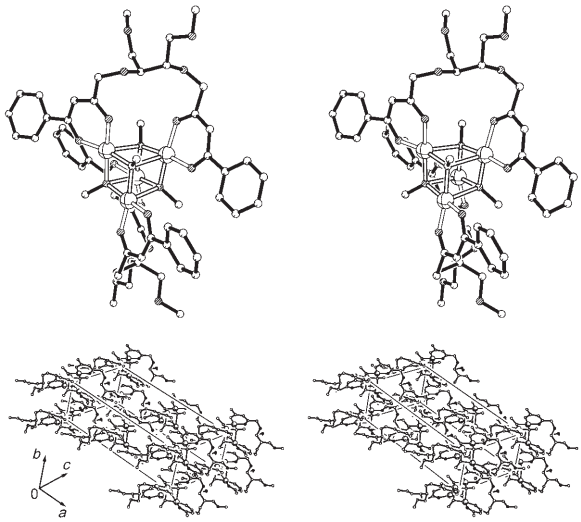


Figure 2. Top: Stereoview of **7**. C shaded, O hatched, Cu marked with a cross; hydrogen atoms omitted for clarity. Bottom: Stereoview of the crystal packing of **7**. The ordered parallel strands running through the corners and the *ab* plane of the unit cell are evident. Hydrogen atoms and phenyl groups omitted for clarity.

On the basis of the composition of **7**, we modified the synthetic procedure by changing the ratio of $Cu(OAc)_2$ to $H_2L^{(S,S)}$ to 2:1 (instead of 1:1 for **6**). The subsequent reaction in methanol with one equivalent of cesium acetate resulted in a higher yield of **7** of 84%. As a result of the asymmetric induction of the stereogenic centers of $(L^{(S,S)})^{2-}$, cubane **7** is generated by diastereoselective self-assembly.[7,8] The crucial step of the reaction is the removal of the acetic acid formed during the reaction, which is achieved simply by repeated evaporation and renewed addition of methanol.

Cubane **7** exists as a single enantiomer, crystallizes in the chiral monoclinic space group *C*2, and possesses a $[Cu_4(\mu_3\text{-}O)_4]$ cubane core unit[9] consisting of two interpenetrating tetrahedra: one made up of four copper ions and one of four μ_3-OMe ligands. The metal–metal separations in **7** are 2.98 Å and 3.25 Å. Each copper ion has approximate square-pyramidal coordination with a total of five oxygen donors (two μ_1-O ions from the ligand and three μ_3-OMe donors). Consequently, the two bisbidentate ligands bridge opposite edges of the copper tetrahedron (Figure 2).

All cubane molecules **7** in the crystal are packed identically and are located in the corners of two interpenetrating lattices. One lattice is constructed of cubanes placed in the corners of the unit cell, giving rise to strands running along the *b* and *c* axis (midpoint distances: $d_b = 7.08$ Å, $d_c = 14.52$ Å), whereas the second, analogous lattice is formed from the *ab*-face-centered cubanes (Figure 2).

Similarly, (*A*,*A*,*A*,*A*)-$[Cu_4(L^{(R,R)})_2(OMe)_4]$ (*ent*-**7**) was prepared from $H_2L^{(R,R)}$ (*ent*-**5**) and characterized by X-ray diffraction analysis.[3–6] Unlike the racemic metallacoronate (*P*,*M*)-{M⊂$[Cu_2(L^1)_2(MeOH)_2]$}OAc (M-**1**), in which metha-

 © 2006 Wiley-VCH Verlag GmbH & Co. KGaA, Weinheim

nol acts solely as extra ligand at the pentacoordinated copper, methanol is a reagent in the synthesis of **7**, and the methanolate ions are part of the cubic scaffold. Whereas in metallacoronate Cs-**1** the Cs^+ ion is encapsulated, the decisive role of the Cs^+ ions for the formation of cubane **7** is not yet clear. But it is worth mentioning that in the absence of cesium ions only polymeric material, insoluble in standard solvents, is isolated.

Transition-metal complexes with a cubane structure, in which the four metal ions are located in the apices of a tetrahedron, are an extensively examined class of compounds with intriguing magnetostructural properties.[9,10] For that reason, the synthesis of chiral, enantiomerically pure single-molecule magnets is of special interest (e.g. for magneto-dichroism[11]), and complexes like cubane **7** and *ent*-**7** are potential candidates.

In conclusion, we have developed a convenient route for the diastereoselective synthesis of cubane (*C*,*C*,*C*,*C*)-[$Cu_4(L^{(S,S)})_2(OMe)_4$] (**7**) and its enantiomer (*A*,*A*,*A*,*A*)-[$Cu_4(L^{(R,R)})_2(OMe)_4$] (*ent*-**7**), starting from the L- and D-tartaric acid derived enantiomerically pure ligands $(L^{(S,S)})^{2-}$ and $(L^{(R,R)})^{2-}$, respectively.

Experimental Section

$H_2L^{(S,S)}$ (**5**): A solution of acetophenone (4.19 mL, 35.3 mmol) in THF (50 mL) was added dropwise to a stirred suspension of sodium amide (2.75 g, 70.4 mmol, 95%) in THF (50 mL) at room temperature. After 10 min the resulting orange mixture was treated with a solution of **4** (5.16 g, 16.0 mmol) in THF (50 mL) which was added dropwise within 5 min. The color changed to dark brown, and the mixture was refluxed for 4 h. After the solution had cooled to room temperature, the solvent was removed. The dark residue was hydrolyzed with 1M hydrochloric acid (100 mL) and extracted with ethyl acetate (3× 100 mL). The combined extracts were washed with H_2O (2× 100 mL), dried over anhydrous Na_2SO_4, and filtered. Removal of the solvent gave a brown oil which crystallized at low pressure (oil pump) to give **5**. Yield: 2.30 g (31%), colorless needles from methanol; m.p. 85–86°C; IR ($CHBr_3$): $\tilde{\nu}$ = 2924, 1603, 1574 cm^{-1}; ^1H NMR (di-/monoenol 7:1, dienol, 400 MHz, $CDCl_3$): δ = 16.55–15.21 (br s, 2H, O*H*), 7.92–7.83 (m, 4H, Ar-CH_{ortho}), 7.57–7.36 (m, 6H, Ar-C$H_{meta,\ para}$), 6.61 (s, 2H, =C*H*), 4.38 (d, 2H, O-CH_AH$_B$, J = 16.6 Hz), 4.34 (d, 2H, O-CH$_A$$H_B$, J = 16.6 Hz), 3.85–3.79 (m, 2H, O-C*H*),[12] 3.69 (pseudo dd, 2H, J = 10.4, 2.8 Hz, CH_2-O-CH$_3$),[12] 3.57 (pseudo dd, 2H, J = 10.4, 5.6 Hz, CH_2-O-CH$_3$),[12] 3.37 ppm (s, 6H, O-CH_3); ^{13}C NMR (100 MHz, $CDCl_3$): δ = 194.64 (2C, *C*=O), 182.89 (2C, *C*H-OH), 134.43 (2C, Ar-C_{ipso}), 132.45 (2C, Ar-*C*H$_{para}$), 128.59 (4C, Ar-*C*H$_{ortho}$), 127.07 (4C, Ar-*C*H$_{meta}$), 93.58 (2C, =*C*H), 79.88 (2C, O-*C*H), 72.66 (2C, O-*C*H$_2$), 72.07 (2C, *C*H$_2$-O-CH$_3$), 59.22 ppm (2C, O-*C*H$_3$); FAB-MS (3-nitrobenzyl alcohol matrix) *m*/*z* (%): 471 (100) $[M+H]^+$, 439 (6) $[M-OCH_3]^+$, 293 (8) $[M-CH(OH)CHCOPh]^+$, 235 (5) $[M/2]^+$; $[\alpha]_D^{25}$ = +6.5, $[\alpha]_{578}^{25}$ = +6.7, $[\alpha]_{546}^{25}$ = +8.3, $[\alpha]_{436}^{25}$ = +29.8 (c = 0.005 in $CHCl_3$); elemental analysis calcd for $C_{26}H_{30}O_8$ (470.52): C 66.37, H 6.43; found: C 66.32, H 6.46.

$H_2L^{(R,R)}$ (*ent*-**5**): Prepared in analogy to **5**, starting from D-tartaric acid: $[\alpha]_D^{24}$ = −5.8, $[\alpha]_{578}^{24}$ = −6.3, $[\alpha]_{546}^{24}$ = −8.1, $[\alpha]_{436}^{24}$ = −29.0 (c = 0.01 in $CHCl_3$).

7: A solution of copper(II) acetate monohydrate (80 mg, 0.40 mmol) in methanol (8.0 mL) was added to a refluxing solution of $H_2L^{(S,S)}$ (**5**) (94 mg, 0.20 mmol) and cesium acetate (39 mg, 0.20 mmol) in methanol (4.0 mL). The reaction mixture was allowed to cool to room temperature and stirred for 30 min. Analysis of the deep green solution by FAB mass spectrometry showed the formation of **6**. FAB-MS (3-nitrobenzyl alcohol matrix) *m*/*z* (%): 1197 (100) $[Cs{\subset}Cu_2(L^{(S,S)})_2]^+$, 1127 (4) $[Cu_3(L^{(S,S)})_2]^+$, 1087 (6) $[Na{\subset}Cu_2(L^{(S,S)})_2]^+$, 727 (13) $[Cs{\subset}Cu_2(L^{(S,S)})]^+$, 659 (10) $[Cu_3(L^{(S,S)})]^+$, 619 (3) $[Na{\subset}Cu_2(L^{(S,S)})]^+$. After removal of the solvent (rotary evaporator, 40°C), the deep green, oily residue was treated repeatedly (6×) with methanol (12 mL), which was removed by evaporation. The crude reaction product was suspended in methanol (12 mL), and the green powder was filtered off. After drying under vacuum (oil pump), the solid material was dissolved in dichloromethane, and green crystals of cubane **7** suitable for X-ray analysis were obtained by layering with methanol. Yield: 110 mg (84%); m.p. 185–188°C (decomp); IR (neat): $\tilde{\nu}$ = 2923, 2904, 2811, 1594, 1563, 1520, 1488, 1453, 1410, 1345, 1310 cm^{-1}; FAB-MS (3-nitrobenzyl alcohol) *m*/*z* (%): 1197 (24) $[Cs{\subset}Cu_2(L^{(S,S)})_2]^+$ (Cs^+ from the matrix), 1127 (66) $[Cu_3(L^{(S,S)})_2]^+$, 1088 (32) $[Na{\subset}Cu_2(L^{(S,S)})_2]^+$ (Na^+ from the matrix), 1065 (100) $[Cu_2(L^{(S,S)})_2]^+$, 659 (31) $[Cu_3(L^{(S,S)})]^+$, 595 (65) $[Cu_2(L^{(S,S)})]^+$, 533 (47) $[Cu(L^{(S,S)})]^+$; CD measurements;[13] elemental analysis calcd for $C_{56}H_{68}Cu_4O_{20}$ (1315.26): C 51.14, H 5.21; found: C 50.97, H 5.25.

Received: July 15, 2005
Published online: November 28, 2005

Keywords: chirality · copper · cubanes · oxo ligands · X-ray diffraction

[1] R. W. Saalfrank, H. Maid, N. Mooren, F. Hampel, *Angew. Chem.* **2002**, *114*, 323–326; *Angew. Chem. Int. Ed.* **2002**, *41*, 304–307.
[2] J. T. Adams, C. R. Hauser, *J. Am. Chem. Soc.* **1944**, *66*, 1220–1222; R. Levine, J. A. Conroy, J. T. Adams, C. R. Hauser, *J. Am. Chem. Soc.* **1945**, *67*, 1510–1512.
[3] For the description of the chirality of **7**: see: M. F. Brown, B. R. Cook, T. E. Sloan, *Inorg. Chem.* **1975**, *14*, 1273–1278; T. Damhus, C. E. Schäffer, *Inorg. Chem.* **1983**, *22*, 2406–2412; A. von Zelewsky, *Stereochemistry of Coordination Compounds*, Wiley, Chichester, **1996**, p. 70.
[4] Crystal structure analyses: Nonius KappaCCD diffractometer, $Mo_{K\alpha}$ radiation (λ = 0.71073 Å); T = 173(2) K; graphite monochromator; empirical absorption correction (scalepack). Structure solution by direct methods using SHELXS-97 and refinement with all data (361 parameters) by full-matrix least-squares on F^2 using SHELXL97;[5] all non-hydrogen atoms were refined anisotropically. Crystal data for (*C*,*C*,*C*,*C*)-[$Cu_4(L^{(S,S)})_2(OMe)_4$] (**7**): $C_{56}H_{68}Cu_4O_{20}$, M = 1315.26 g mol^{-1}; crystal dimensions 0.20 × 0.20 × 0.20 mm^3; monoclinic, space group *C*2, a = 28.3417(7), b = 7.0841(2), c = 14.5185(3) Å, β = 103.2680(16)°, V = 2837.15(12) Å^3; Z = 2; $F(000)$ = 1360, ρ_{calcd} = 1.540 g cm^{-3}; 2.88° < θ < 27.49°; section of the reciprocal lattice: $-35 \le h \le 36$, $-9 \le k \le 8$, $-18 \le l \le 18$; of 6044 measured reflections, 6044 were independent and 5637 with $I > 2\sigma(I)$; linear absorption coefficient 1.555 mm^{-1}; $R1$ = 0.0279 for $I > 2\sigma(I)$ and $wR2$ = 0.0688 (all data); largest peak (0.264 e Å^{-3}) and hole (−0.356 e Å^{-3}).[5,6] Crystal data for (*A*,*A*,*A*,*A*)-[$Cu_4(L^{(R,R)})_2(OMe)_4$] (*ent*-**7**): $C_{56}H_{68}Cu_4O_{20}$, M = 1315.26 g mol^{-1}; crystal dimensions 0.35 × 0.30 × 0.20 mm^3; monoclinic, space group *C*2, a = 28.3337(4), b = 7.0760(1), c = 14.5128(2) Å, β = 103.309(1)°, V = 2831.51(7) Å^3; Z = 2; $F(000)$ = 1360, ρ_{calcd} = 1.543 g cm^{-3}; 2.29° < θ < 27.49°; section of the reciprocal lattice: $-35 \le h \le 36$, $-9 \le k \le 9$, $-18 \le l \le 18$; of 6449 measured reflections, 6449 were independent and 6184 with $I > 2\sigma(I)$; linear absorption coefficient 1.558 mm^{-1}; $R1$ = 0.0238 for $I > 2\sigma(I)$ and $wR2$ = 0.0634 (all data); largest peak (0.266 e Å^{-3}) and hole (−0.394 e Å^{-3}).[5,6] Refinement of the correct absolute structure was ensured through refinement of the Flack parameter (−0.002(9) for **7** and 0.000(7) for *ent*-**7**).[14]
[5] G. M. Sheldrick, C. Krüger, P. Goddard, *Crystallographic Computing 3*, Oxford University Press, Oxford **1985**, p. 175;

 © 2006 Wiley-VCH Verlag GmbH & Co. KGaA, Weinheim

G. M. Sheldrick, SHELXL-97, *Program for Crystal Structure Refinement*, University of Göttingen, **1997**.

[6] CCDC-253582 (**7**) and CCDC-275185 (*ent*-**7**) contain the supplementary crystallographic data for this paper. These data can be obtained free of charge from The Cambridge Crystallographic Data Centre via www.ccdc.cam.ac.uk/data_request/cif.

[7] For asymmetric induction through stereogenic centers during self-assembly, see: O. Mamula, A. von Zelewsky, P. Brodard, C.-W. Schläpfer, G. Bernardinelli, H. Stoeckli-Evans, *Chem. Eur. J.* **2005**, *11*, 3049 – 3057; H.-R. Tseng, S. A. Vignon, P. C. Celestre, J. F. Stoddart, A. J. P. White, D. J. Williams, *Chem. Eur. J.* **2003**, *9*, 543 – 556; G. Baum, E. C. Constable, D. Fenske, C. E. Housecroft, T. Kulke, *Chem. Eur. J.* **1999**, *5*, 1862 – 1873; E. J. Enemark, T. D. P. Stack, *Angew. Chem.* **1998**, *110*, 977 – 981; *Angew. Chem. Int. Ed.* **1998**, *37*, 932 – 935.

[8] For definition of diastereoselectivity, see: G. Helmchen, *Enantiomer* **1997**, *2*, 315 – 318.

[9] J. K. Eberhardt, T. Glaser, R.-D. Hoffmann, R. Fröhlich, E.-U. Würthwein, *Eur. J. Inorg. Chem.* **2005**, 1175 – 1181; E. A. Buvaylo, V. N. Kokozay, O. Y. Vassilyeva, B. W. Skelton, J. Jezierska, L. C. Brunel, A. Ozarowski, *Inorg. Chem.* **2005**, *44*, 206 – 216; A. Mukherjee, M. Nethaji, A. R. Chakravarty, *Angew. Chem.* **2004**, *116*, 89 – 92; *Angew. Chem. Int. Ed.* **2004**, *43*, 87 – 90; H. Oshio, Y. Saito, T. Ito, *Angew. Chem.* **1997**, *109*, 2789 – 2791; *Angew. Chem. Int. Ed. Engl.* **1997**, *36*, 2673 – 2675; J. Sletten, A. Sørensen, M. Julve, Y. Journaux, *Inorg. Chem.* **1990**, *29*, 5054 – 5058; L. Schwabe, W. Haase, *J. Chem. Soc. Dalton Trans.* **1985**, 1909 – 1913; L. Merz, W. Haase, *J. Chem. Soc. Dalton Trans.* **1978**, 1594 – 1598; J. W. Hall, W. E. Estes, E. D. Estes, R. P. Scaringe, W. E. Hatfield, *Inorg. Chem.* **1977**, *16*, 1572 – 1574.

[10] J. F. Berry, F. A. Cotton, C. Y. Liu, T. Lu, C. A. Murillo, B. S. Tsukerblat, D. Villagrán, X. Wang, *J. Am. Chem. Soc.* **2005**, *127*, 4895 – 4902; G. Aromí, A. S. Batsanov, P. Christian, M. Helliwell, O. Roubeau, G. A. Timco, R. E. P. Winpenny, *Dalton Trans.* **2003**, 4466 – 4471; T. K. Paine, E. Rentschler, T. Weyhermüller, P. Chaudhuri, *Eur. J. Inorg. Chem.* **2003**, 3167 – 3178; E.-C. Yang, D. N. Hendrickson, W. Wernsdorfer, M. Nakano, L. N. Zakharov, R. D. Sommer, A. L. Rheingold, M. Ledezma-Gairaud, G. Christou, *J. Appl. Phys.* **2002**, *91*, 7382 – 7384; H. Oshio, N. Hoshino, T. Ito, *J. Am. Chem. Soc.* **2000**, *122*, 12602 – 12603; A. Escuer, M. Font-Bardía, S. B. Kumar, X. Solans, R. Vicente, *Polyhedron* **1999**, *18*, 909 – 914; M. S. El Fallah, E. Rentschler, A. Caneschi, D. Gatteschi, *Inorg. Chim. Acta* **1996**, *247*, 231 – 235; H.-J. Mai, R. Meyer zu Köcker, S. Wocadlo, W. Massa, K. Dehnicke, *Angew. Chem.* **1995**, *107*, 1349 – 1350; *Angew. Chem. Int. Ed. Engl.* **1995**, *34*, 1235 – 1236; M. A. Halcrow, J. C. Huffman, G. Christou, *Angew. Chem.* **1995**, *107*, 971 – 973; *Angew. Chem. Int. Ed. Engl.* **1995**, *34*, 889 – 891; K. L. Taft, A. Caneschi, L. E. Pence, C. D. Delfs, G. C. Papaefthymiou, S. J. Lippard, *J. Am. Chem. Soc.* **1993**, *115*, 11753 – 11766.

[11] H. Imai, K. Inoue, K. Kikuchi, Y. Yoshida, M. Ito, T. Sunahara, S. Onaka, *Angew. Chem.* **2004**, *116*, 5736 – 5739; *Angew. Chem. Int. Ed.* **2004**, *43*, 5618 – 5621; R. Andrés, M. Brissard, M. Gruselle, C. Train, J. Vaissermann, B. Malézieux, J.-P. Jamet, M. Verdaguer, *Inorg. Chem.* **2001**, *40*, 4633 – 4640; R. Andrés, B. Malézieux, M. Brissard, M. Gruselle, C. Train, M. Verdaguer, *Chirality* **2001**, *13*, 712 – 714; G. L. J. A. Rikken, E. Raupach, *Nature* **2000**, *405*, 932 – 935; G. L. J. A. Rikken, E. Raupach, *Nature* **1997**, *390*, 493 – 494.

[12] The ^{1}H NMR spectra of the tartaric acid derived ligands $H_2L^{(S,S)}$ (**5**) and $H_2L^{(R,R)}$ (*ent*-**5**) are consistent with a symmetrical AA′BB′CC′ six-spin system; see: A. Scheurer, H. Maid, F. Hampel, R. W. Saalfrank, L. Toupet, P. Mosset, R. Puchta, N. J. R. van Eikema Hommes, *Eur. J. Org. Chem.* **2005**, 2566 – 2574; A. Scheurer, P. Mosset, R. W. Saalfrank, *Tetrahedron: Asymmetry* **1999**, *10*, 3559 – 3570.

[13] CD spectroscopic data of **5** and **7** were recorded in various solvents in the laboratory of Prof. M. Verdaguer (Université Pierre et Marie Curie at Paris, France). However, dichroism transitions above 400 nm, induced by the chirality of the metal centers of **7**, could not be observed. Measurements below 400 nm were rendered impossible due to the strong absorption of ligand **5** in the range of wavelengths investigated.

[14] H. D. Flack, *Acta Crystallogr. Sect. A* **1983**, *39*, 876 – 881.

 © 2006 Wiley-VCH Verlag GmbH & Co. KGaA, Weinheim

Electron Transfer

DOI: 10.1002/anie.200502551

Complex Sequence Dependence by Excess-Electron Transfer through DNA with Different Strength Electron Acceptors**

*Antonio Manetto, Sascha Breeger, Chryssostomos Chatgilialoglu, and Thomas Carell**

Numerous studies of the long-distance hole-migration process through a DNA double strand have revealed detailed insight into the distance and sequence dependence of charge-movement processes.[1–4] In contrast to the wealth of information now available on the long-distance hole transfer,[5–9] less is known about the complementary excess-electron-transfer process in which an anion, instead of a cation, moves through the duplex. We,[10–13] and others,[14–19] have recently shown that excess electrons move through DNA by a hopping-type mechanism in which the pyrimidine bases dT and dC act as 'stepping stones'.[17]

Although the hopping of excess electrons through DNA is now a generally accepted model, conflicting data on the sequence dependence of this process were reported. The charge-transfer process was investigated by using DNA that was modified with either arylamines,[14–16] pyrenes, or phenothiazines[18,19] as the electron donor, or 5-bromouracil as the electron acceptor. It was shown that GC base pairs, in contrast to AT base pairs, reduce the efficiency of the excess-electron transfer through the duplex. Our studies with a reduced flavin

[*] Dipl.-Chem. A. Manetto, Dipl.-Chem. S. Breeger, Prof. Dr. T. Carell
Department of Chemistry and Biochemistry
LMU Munich
Butenandtstrasse 5–13, 81377 Munich (Germany)
Fax: (+49) 89-2189-77756
E-mail: thomas.carell@cup.uni-muenchen.de
Dr. C. Chatgilialoglu
ISOF
Consiglio Nazionale delle Ricerche
Via P. Gobetti 101, 40129 Bologna (Italy)

[**] We thank the Deutsche Forschungsgemeinschaft, the Volkswagen Foundation, and the EU Marie Curie training and mobility program , project number MRTN-CT-2003-505086 [CLUSTOXDNA], for financial support. S.B. thanks the Fonds der Chemischen Industrie for a predoctoral fellowship.

WILEY InterScience DISCOVER SOMETHING GREAT
© 2006 Wiley-VCH Verlag GmbH & Co. KGaA, Weinheim

as the electron donor and a thymine dimer as the electron acceptor—a system that mimics the repair of UV-induced thymine dimer DNA lesions by photolyases[20,21]—showed, in contrast, no sequence dependence.[13] Based on the likely reductive opening of the thymine dimer at a rate of approximately $10^6\ s^{-1}$ [22] and under the assumption that electron-hopping rate could be 10^8–$10^9\ s^{-1}$, we speculated that the dimer opening might be the rate-determining step. Through the use of DNA duplexes that contain two thymine dimers in a row, we recently provided evidence that the electron is able to hop over a thymine dimer without cleaving it. This lends support to the assumption that dimer cleavage is slower than electron hopping.[23]

To investigate in more detail how the rate of reaction of an acceptor with excess electrons influences the observed sequence dependence of charge movement in DNA, we prepared a series of 15 DNA hairpins (**1**–**5** depicted in Figure 1). Within these hairpins, we have placed the light-dependent flavin electron injector **6** ($E^*_{flav\text{-}red} = -2.6$ V against NHE)[24] in the loop region of the hairpin, and three electron acceptors (5-bromouracil[14–16] = series **a**, 8-bromoadenine = series **b**, and 8-bromoguanine[25] = series **c**) positioned in the stem region at a distance of about 17.5 Å from the donor.

The bimolecular rates of reaction of a solvated electron, with all three electron acceptors (BrdA, BrdG and BrdU), are known but they are in the diffusion controlled environment[26] with approximately 1×10^{10}–$2\times10^{10}\ M^{-1}s^{-1}$.[27–29] The primary reduction is followed by a release of Br^-.[27,30–32] Although the redox potential of the Br-substituted bases are not all known, we can assume, based on the reduction potentials of the unmodified nucleobases, a sequence of BrdU > BrdA ≥ BrdG, with BrdU being the easiest to reduce, followed by BrdA and BrdG.[33] All the hairpins depicted in Figure 1 show melting points above room temperature. CD measurements of the hairpins **1**–**5** are, in all cases, in agreement with a B-DNA conformation. All of the hairpins were prepared and purified in accordance with standard phosphoramidite automated solid-phase-synthesis protocols.

In previous studies the flavin was reduced with sodium dithionite ($Na_2S_2O_4$).[10–12] Recently we, and Ito and Rokita,[15] observed that the dithionite reduction inhibits the excess-electron-transfer process after some time. Therefore, in this study we used a more stable EDTA-based photoreduction process.[34] Although the initial yields determined with dithionite and EDTA are similar, EDTA allowed us to establish a stable, fully reduced system for more than 1 h.

In a typical irradiation experiment, EDTA (0.02 M) was added to a solution of DNA ($c_{DNA} = 20\ \mu M$, 0.01 M Tris, pH 7.4, 0.15 M NaCl) and irradiated with white light for 1 min in fluorescence cuvettes and under anaerobic conditions to photoreduce the flavin (monitored by fluorescence spectroscopy). After photoreduction, we further irradiated the samples with a 1000-W Xe lamp, equipped with a cooled 340-nm cut-off filter. For analysis, 10-μL samples were removed from the assay solution after defined time intervals, aerated for 30 min, desalted, and analyzed. Analysis of the data was performed by capillary gel electrophoresis. In the past, excess-electron transfer through DNA with 5BrdU, was evaluated by observation of strand cleavage that was induced by the neutral dU radical after heating of the DNA with piperidine.[35] Capillary electrophoresis (CE), in contrast, allowed us to detect directly the loss of the Br anion within the intact 19-mer hairpins after electron capture. An example of the CE analysis of an irradiation experiment performed with the hairpin (**1a**) is given in Figure 2.

The fractions were collected and the corresponding peaks were analyzed by MALDI-TOF mass spectrmetry to prove the formation of the expected product strands. The yield data obtained for all 15 hairpins are depicted as bar graphs in Figure 3. They show the time-dependent formation of the debrominated 19-mer hairpins as average values that

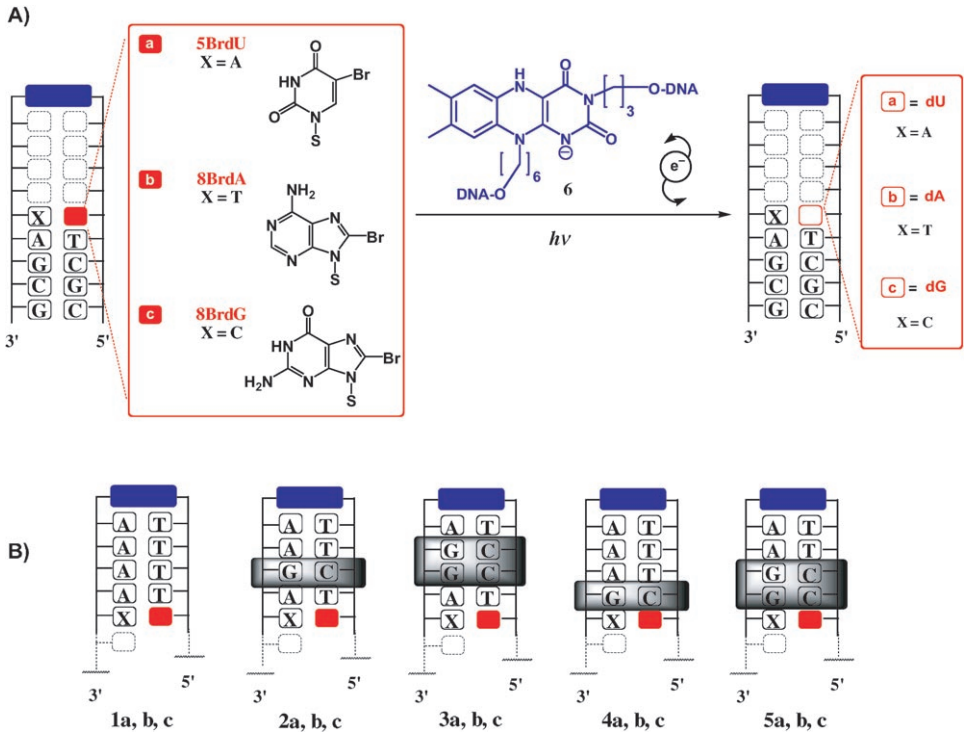


Figure 1. DNA-hairpin models (**1**–**5**) for the excess-electron-transfer study through DNA depending on the acceptor strength. A) ■ = Flavin electron donor **6** in the reduced and deprotonated form; ■ = electron acceptor (**a** = 5BrdU, **b** = 8BrdA, **c** = 8BrdG); □ = dibrominated electron acceptors (a = dU, b = dA, c = dG); X = the acceptor counter bases. B) Sequence of hairpins **1**–**5** for the three acceptors (**a**, **b**, and **c**); ■ = flavin **6**; ■ = electron acceptor. Highlighted in gray are the number and the position of GC base pairs.

© 2006 Wiley-VCH Verlag GmbH & Co. KGaA, Weinheim

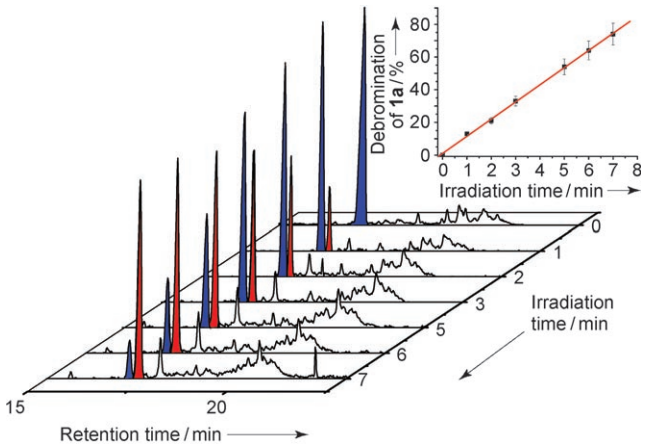


Figure 2. Irradiation of hairpin (**1a**). Time-dependent debromination of the acceptor within hairpin **1a**. The signals for the parent and the debrominated strand are highlighted in blue and red, respectively. Their identity was confirmed after collection of the fractions by MALDI-MS analysis. The inset shows the debromination rate (10.5% min^{-1}) as calculated by peak-area integration and linear approximation of the data (Beckman Coulter P/ACE-MDQ DNA system, UV detection at 254 nm, 30-cm fused-silica capillary filled with 6% polyacrylamide gel in 0.1 M tris-borate, 2 mM EDTA, pH 8.4, electrokinetic injection by applying 10 kV for 2–10 s, separation at 9 kV for 45 min).[36]

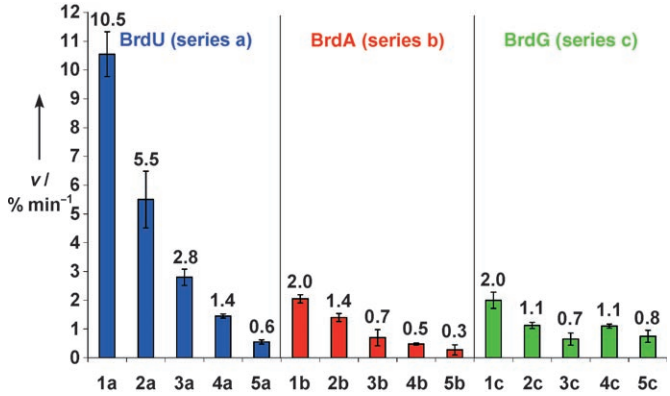


Figure 3. Debromination rates υ for the hairpins **1**–**5**. The calculated repair rates are given as % Br-anion loss per minute. Analysis was performed by CE of at least three independent measurements per strand. Calculation was carried out on the data of up to 5 minutes of irradiation time by peak area integration followed by linear approximation (for an example, see the inset in Figure 2).

were obtained from at least three independent experiments. We believe that the hydrogen atom needed for the reduction of the nucleobase radicals may be efficiently donated from the EDTA in our experiments.

We first investigated how the type of acceptor influences the debromination yield within the hairpin series **1a**–**c**, which have only AT base pairs between the flavin donor and acceptor. These data show that the yield of debromination depends strongly on the kind of acceptor. The fastest debromination was observed with BrdU (**1a**), followed by BrdA (**1b**), and BrdG (**1c**), which reflects the ease of reduction of these acceptors. This shows that in the process of electron migration through DNA, which involves electron injection, migration, and capture, the reduction of the acceptor can indeed be the rate-determining step! Next, we studied **2a**–**c** and **3a**–**c** and how the system reacts if we replace one or two AT base pairs by GC base pairs. For the BrdU acceptor strands **2a** and **3a**, we observe that the yield drops by 50% with every GC base pair. For the weaker purine acceptors, BrdA and BrdG, a much smaller influence is observed, which indicates that in these systems the acceptor is not strong enough to fully report the sequence effect. In our explanation, reduction of the acceptor is the rate-determining step with BrdA and BrdG. More important, however, is the observation that the position of the GC base pair, relative to the acceptor, is more important than the number of GC base pairs. If we shift either one or both GC base pairs so that they stack directly on top of the acceptor, dramatic decreases in the yields are observed. In the 5BrdU series (**a**), the yield drops from 10.5% min^{-1} to about 1.4% min^{-1} with one GC base pair (**4a**) and again to 0.6% min^{-1} with two GC base pairs (**5a**). The same was observed when the BrdA or BrdG acceptors were used, although the yield reductions were in these cases much less pronounced (series **b** and **c**). This is again in agreement with our idea that reduction of the acceptor is rate determining if the weaker Br-purine acceptors are used.

From these studies it becomes clear, that a GC base pair between the donor and acceptor reduces the excess-electron-transfer efficiency by a factor of approximately 2. This is, however, only observable with very efficient acceptors such as BrdU. Weaker electron acceptors provide systems with rate-determining electron-capture steps. More important, however, is our observation that the position of the GC base pairs between the donor and the acceptor plays a larger role than the number of GC base pairs. Although this is difficult to explain, one reason could be modulation of the redox potential of the acceptors by the stacking of the GC base pairs on top of the acceptor. This situation is similar to that observed in the hole-transfer process, in which the stacking of guanine makes the oxidation of nucleobases more efficient.

Received: July 21, 2005
Published online: November 29, 2005

Keywords: DNA damage · electron transfer · nucleobases · redox potential

[1] S. Hess, M. Götz, W. B. Davis, M.-E. Michel-Beyerle, *J. Am. Chem. Soc.* **2001**, *123*, 10046–10055.
[2] B. Giese, M. Spichty, *ChemPhysChem* **2000**, *1*, 195–198.
[3] M. Bixon, J. Jortner, *J. Am. Chem. Soc.* **2001**, *123*, 12556–12567.
[4] M. B. J. Jortner, T. Langenbacher, M. E. Michel-Beyerle, *Proc. Natl. Acad. Sci. USA* **1998**, *95*, 12759–12765.
[5] F. D. Lewis, T. Wu, Y. Zhang, R. L. Letsinger, S. R. Greenfield, M. R. Wasielewski, *Science* **1997**, *277*, 673–676.
[6] F. D. Lewis, R. L. Letsinger, M. R. Wasielewski, *Acc. Chem. Res.* **2001**, *34*, 159–170.
[7] G. B. Schuster, *Acc. Chem. Res.* **2000**, *33*, 253–260.
[8] C. J. Murphy, M. R. Arkin, Y. Jenkins, N. D. Ghatlia, S. H. Bossmann, N. J. Turro, J. K. Barton, *Science* **1993**, *262*, 1025–1029.
[9] M. Nunez, D. B. Hall, J. K. Barton, *Chem. Biol.* **1999**, *6*, 85–97.

 © 2006 Wiley-VCH Verlag GmbH & Co. KGaA, Weinheim

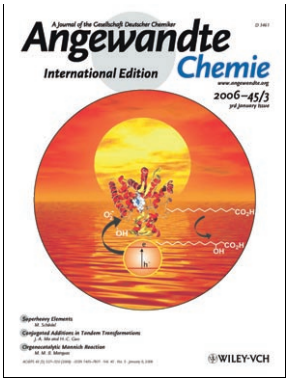
[10] C. Behrens, L. T. Burgdorf, A. Schwögler, T. Carell, *Angew. Chem.* **2002**, *114*, 1841 – 1844; *Angew. Chem. Int. Ed.* **2002**, *41*, 1763 – 1766.
[11] C. Behrens, M. Ober, T. Carell, *Eur. J. Org. Chem.* **2002**, 3281 – 3289.
[12] C. Behrens, T. Carell, *Chem. Commun.* **2003**, 1632 – 1633.
[13] S. Breeger, U. Hennecke, T. Carell, *J. Am. Chem. Soc.* **2004**, *126*, 1302 – 1303.
[14] T. Ito, S. E. Rokita, *J. Am. Chem. Soc.* **2003**, *125*, 11480 – 11481.
[15] T. Ito, S. E. Rokita, *Angew. Chem.* **2004**, *116*, 1875 – 1878; *Angew. Chem. Int. Ed.* **2004**, *43*, 1839 – 1842.
[16] T. Ito, S. E. Rokita, *J. Am. Chem. Soc.* **2004**, *126*, 15552 – 15559.
[17] H.-A. Wagenknecht, *Angew. Chem.* **2003**, *115*, 2558 – 2565; *Angew. Chem. Int. Ed.* **2003**, *42*, 2454 – 2460.
[18] C. Wagner, H.-A. Wagenknecht, *Chem. Eur. J.* **2005**, *11*, 1871 – 1876.
[19] P. Kaden, E. Mayer-Enthart, A. Trifonov, T. Fiebing, H.-A. Wagenknecht, *Angew. Chem.* **2005**, *117*, 1662 – 1666; *Angew. Chem. Int. Ed.* **2005**, *44*, 1636 – 1639.
[20] A. Sancar, *Chem. Rev.* **2003**, *103*, 2203 – 2238.
[21] A. Mees, T. Klar, P. Gnau, U. Hennecke, A. P. M. Eker, T. Carell, L. O. Essen, *Science* **2004**, *306*, 1789 – 1793.
[22] S.-R. Yeh, D. E. Falvey, *J. Am. Chem. Soc.* **1991**, *113*, 8557 – 8558.
[23] B. Giese, B. Carl, T. Carl, T. Carell, C. Behrens, U. Hennecke, O. Schiemann, E. Feresin, *Angew. Chem.* **2004**, *116*, 1884 – 1887; *Angew. Chem. Int. Ed.* **2004**, *14*, 1848 – 1851.
[24] S.-R. Yeh, D. E. Falvey, *J. Am. Chem. Soc.* **1992**, *114*, 7313 – 7314.
[25] T. Kimura, K. Kawai, S. Tojo, T. Majima, *J. Org. Chem.* **2004**, *69*, 1169 – 1173.
[26] K. H. Schmidt, P. Han, D. M. Bartels, *J. Phys. Chem.* **1995**, *99*, 10530 – 10539.
[27] C. Chatgilialoglu, M. Guerra, Q. G. Mulazzani, *J. Am. Chem. Soc.* **2003**, *125*, 3839 – 3848.
[28] M. Ioele, R. Bazzanini, C. Chatgilialoglu, Q. G. Mulazzani, *J. Am. Chem. Soc.* **2000**, *122*, 1900 – 1907.
[29] L. K. Patterson, K. M. Bansal, *J. Phys. Chem.* **1972**, *76*, 2392 – 2399.
[30] E. Rivera, R. H. Schuler, *J. Phys. Chem.* **1983**, *87*, 3966 – 3971.
[31] G. P. Cook, M. M. Greenberg, *J. Am. Chem. Soc.* **1996**, *118*, 10025 – 10030.
[32] C. Chatgilialoglu, C. Caminal, M. Guerra, Q. G. Mulazzani, *Angew. Chem.* **2005**, 117. 6184 – 6186; *Angew. Chem. Int. Ed.* **2005**, *44*, 6030 – 6032.
[33] The redox potential $E°$ of the nucleobases are reported as $E^0_T = 1.7$ V, $E^0_C = 1.6$ V, $E^0_A = 1.4$ V, $E^0_G = 1.3$ V versus NHE (C. A. M. Seidel, A. Schulz, M. H. M. Sauer, *J. Phys. Chem.* **1996**, *100*, 5541 – 5553), whereas their rate constants (dT, dC, dA, and dG) with solvated electrons are also in the diffusion-controlled region $0.6–1.8 \times 10^{10}\,M^{-1}s^{-1}$ (G. V. Buxton, C. L. Greenstock, W. P. Helman, A. B. Ross, *J. Phys. Chem. Ref. Data* **1988**, *17*, 513 – 886). BrdU is reported to be easier to reduce than dT by 40–50 mV (S. T. Gaballah, G. Collier, T. L. Netzel, *J. Phys. Chem. B* **2005**, *109*, 12175 – 12181).
[34] R. Traber, H. E. A. Kramer, P. Hemmerich, *Biochemistry* **1982**, *21*, 1687 – 1693.
[35] T. Chen, G. P. Cook, A. T. Koppisch, M. M. Greenberg, *J. Am. Chem. Soc.* **2000**, *122*, 3861 – 3866.
[36] The debrominated yield in the case of BrdA and BrdG are 100%. For BrdU, up to 10% additional degradation peaks are observed.

 © 2006 Wiley-VCH Verlag GmbH & Co. KGaA, Weinheim

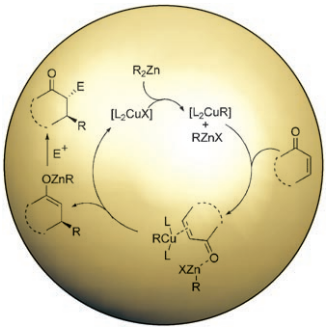
Cover Picture

Binil Itty Ipe and Christof M. Niemeyer*

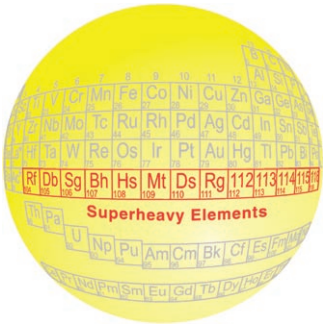
Sunlight does chemistry in nanohybrids composed of CdS quantum dots (QDs) and enzyme $P450_{BS\beta}$. The hybrids, which are self-assembled through electrostatic interactions between the negatively charged QDs and the positively charged His_6-marked P450, produce hydroxyl and superoxide radicals upon irradiation. In their Communication on page 504 ff., B. I. Ipe and C. M. Niemeyer report that these reactive oxygen species activate P450 to catalyze the monooxygenation of myristic acid. (Graphic prepared by P. Alhorn, B. Ipe, and K. Rabe.)



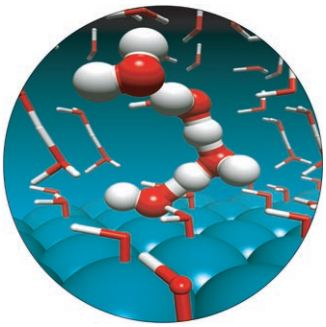
Tandem Transformations
In their Minireview on page 354 ff., J.-A. Ma and H.-C. Guo discuss the latest developments in catalytic asymmetric tandem transformations initiated by conjugate additions to construct complex molecules with several stereogenic centers.



Superheavy Elements
The heaviest artificially generated elements lie in the area of the transactinides. Experimental and theoretical work aimed at understanding these superheavy elements is reported by M. Schädel in his Review on page 368 ff.



Electrocatalysis
The properties of a water/Pd(111) interface change as a function of the applied potential. In their Communication on page 402 ff., M. Neurock and J.-S. Filhol analyze this problem through ab initio methods.



Contents

The following Communications have been judged by at least two referees to be "very important papers" and will be published online at www.angewandte.org soon:

*J. Deschamp, O. Chuzel, J. Hannedouche, O. Riant**
Highly Diastereo- and Enantioselective Copper-Catalyzed Tandem Conjugated Reduction/Aldol Reaction to Ketones

J. W. Bode, R. M. Fox, K. D. Baucom*
Chemoselective Amide Ligations by Decarboxylative Condensations of *N*-Alkylhydroxylamines and α-Keto Acids

A. Oleksi, A. G. Blanco, R. Boer, I. Usón, J. Aymamí, A. Rodger, M. J. Hannon, M. Coll**
Molecular Recognition of a Three-Way DNA Junction by a Metallosupramolecular Helicate

J. E. Banham, C. R. Timmel, R. J. M. Abbott, S. M. Lea, G. Jeschke**
Characterization of Weak Protein–Protein Interactions: Evidence from DEER for the Trimerization of a von Willebrand Factor A Domain in Solution

B. H. Lipshutz, B. A. Frieman, A. E. Tomaso, Jr.*
Copper-in-Charcoal (Cu/C): Heterogeneous, Copper-Catalyzed Asymmetric Hydrosilylations

J. T. Shaw, J. M. Mitchell*
A Structurally Diverse Library of Polycyclic Lactams Resulting from the Systematic Placement of Proximal Functional Groups

Meeting Reviews

Chembiogenesis 2005 and Systems Chemistry Workshop — *J. Stankiewicz, L. H. Eckardt* — **342**

Obituary

Heinrich Zollinger (1919–2005): Renovator of Dyestuff and Textile Chemistry — *P. Skrabal* — **345**

Books

Silicon-Mediated Transformations of Functional Groups — Helmut Vorbrüggen — *reviewed by T. Müller, N. Auner* — **346**

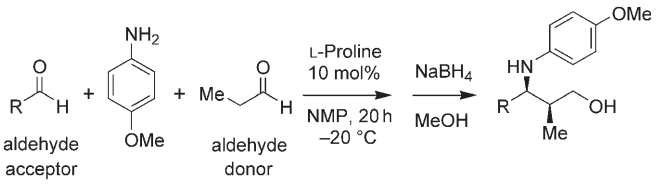
Charge Transfer in DNA — Hans-Achim Wagenknecht — *reviewed by T. von Feilitzsch* — **346**

Highlights

Asymmetric Catalysis

M. M. B. Marques* — **348 – 352**

Catalytic Enantioselective Cross-Mannich Reaction of Aldehydes

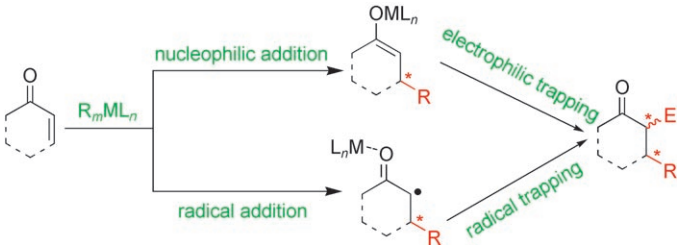


A wide variety of optically active compounds as well as active compounds such as amino acid derivatives can be accessed by the cross-Mannich reaction of aldehydes, particularly by the direct catalytic asymmetric version, in which C–C bonds are formed. Remarkable advancements have been reported, including one-pot, three-component procedures with absolute stereocontrol and high yields (see example, NMP = *N*-methylpyrrolidine).

InterScience

© 2006 Wiley-VCH Verlag GmbH & Co. KGaA, Weinheim

Minireviews



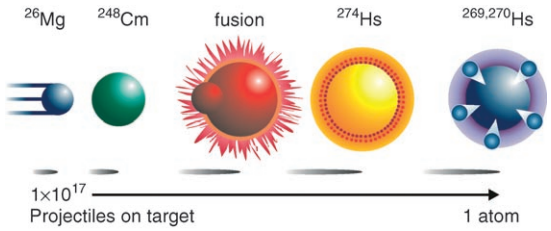
Tandem Transformations

H.-C. Guo, J.-A. Ma* ——— **354 – 366**

Catalytic Asymmetric Tandem Transformations Triggered by Conjugate Additions

Conjugate additions lead the way in catalytic asymmetric tandem transformations, which allow rapid access to complex molecular structures from readily available starting compounds. The advantage of such transformations is the formation of several bonds and the creation of two or more contiguous stereogenic centers by using a single catalyst in one pot (see scheme).

Reviews



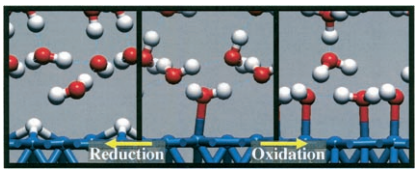
Superheavy Elements

M. Schädel* ——— **368 – 401**

Chemistry of Superheavy Elements

Man-made atoms: Experimental techniques, such as hot fusion (see scheme) and theoretical calculations on the superheavy elements (the transactinides) are now shedding light on the chemistry of these elements. Nuclear chemistry, performed at the ultimate one-atom-at-a-time limit, has reached element 108, hassium, and the elements 112 and beyond are now under investigation.

Communications



Electrocatalysis

J.-S. Filhol, M. Neurock* ——— **402 – 406**

Elucidation of the Electrochemical Activation of Water over Pd by First Principles

Structural changes that occur at the palladium(111)/water interface during the electrocatalytic oxidation and reduction of water (see picture) have been calculated by ab initio methods. These results have been used to construct an electrochemical phase diagram, and demonstrate the influence of the polarization of the water/metal interface on surface properties.

For the USA and Canada:
ANGEWANDTE CHEMIE International Edition (ISSN 1433-7851) is published weekly by Wiley-VCH PO Box 191161, D 69451 Weinheim, Germany. Air freight and mailing in the USA by Publications Expediting Inc. 200 Meacham Ave., Elmont, NY 11003. Periodicals postage paid at Jamaica NY 11431. US POSTMASTER: send address changes to *Angewandte Chemie*, Wiley-VCH, 111 River Street, Hoboken, NJ 07030. Annual subscription price for institutions: US$ 5685/5168 (valid for print and electronic / print or electronic delivery); for individuals who are personal members of a national chemical society prices are available on request. Postage and handling charges included. All prices are subject to local VAT/sales tax.

© 2006 Wiley-VCH Verlag GmbH & Co. KGaA, Weinheim

The best in chemistry – for more than a hundred years



A Journal of the Gesellschaft Deutscher Chemiker

Angewandte
International Edition **Chemie**

www.angewandte.org

1888: ***The beginning of a success story***

Constant Innovations

1962: *First issue of the International Edition*
1976: *Graphical abstracts*
1979: *Cover pictures*
1988: *Centenary of Angewandte*
1989: *Routine use of color*
1991: *New section: Highlights*
1992: *Computerized editorial tracking system*
1995: *Internet service for readers*
1998: *Regular press service; full-text online*
2000: *New section: Essays; EarlyView: Communications available online ahead of the printed version*
2001: *New section: Minireviews*
2002: *Online submission of manuscripts*
2003: *Weekly publication; new section: News; new layout*
2004: *Backfiles (1962-1997); ManuscriptXpress: Online system for authors and referees*



Angewandte's advisors ...

Martin Jansen
Max-Planck-Institut für Festkörperforschung, Stuttgart

»Professional presentation of the latest research in all fields of chemistry is the distinguishing characteristic that makes ***Angewandte Chemie*** *indispensable. This journal leads students to the cutting edge of chemical knowledge.«*

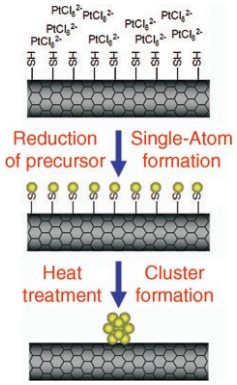
Angewandte Chemie International Edition *is a journal of the German Chemical Society (GDCh)*

GDCh

WILEY InterScience® DISCOVER SOMETHING GREAT

WILEY-VCH

18941504_gu

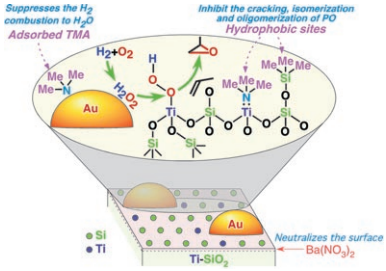


Bond formation between single Pt atoms and surface thiol groups is the result of the reduction of a Pt precursor in the presence of surface-thiolated carbon nanotubes. By setting the temperature of the following heat treatment, finely size-controlled and monodispersed Pt clusters were obtained from the dispersed single atoms (see picture).

Electrocatalyst Design

Y.-T. Kim, K. Ohshima, K. Higashimine, T. Uruga, M. Takata, H. Suematsu, T. Mitani* ——— **407 – 411**

Fine Size Control of Platinum on Carbon Nanotubes: From Single Atoms to Clusters



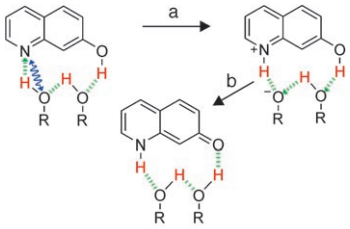
The probable reaction pathways for propylene epoxidation with O_2 and H_2 in the presence of trimethylamine on trimethylsilylated Au-$Ba(NO_3)_2$/titanosilicate catalyst are discussed (see figure). The use of trimethylamine as a gas-phase promoter for nanoparticulate gold catalysts leads to a direct one-stage production of propylene oxide (PO) with steady space–time yields comparable to values for current industrial ethylene oxide production.

Epoxidation Catalysts

B. Chowdhury, J. J. Bravo-Suárez, M. Daté, S. Tsubota, M. Haruta* ——— **412 – 415**

Trimethylamine as a Gas-Phase Promoter: Highly Efficient Epoxidation of Propylene over Supported Gold Catalysts

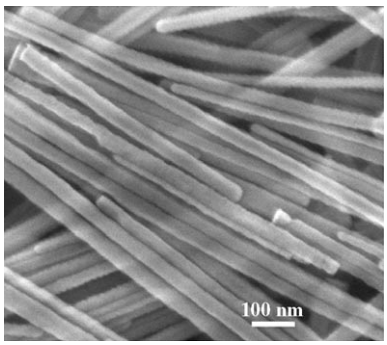
Proton relay in cyclic 7-hydroxyquinoline–$(alcohol)_2$ complexes (see picture) has been explored in nonpolar solvents. The asymmetric triple proton transfer has an unusually large, temperature-independent, and viscosity-dependent kinetic isotope effect. Heavy-atom motions (wavy arrow) of solvent and bridging molecules allow proton tunneling by assisting the complex to reach the optimal precursor configuration.



Proton Transfer

O.-H. Kwon, Y.-S. Lee, B. K. Yoo, D.-J. Jang* ——— **415 – 419**

Excited-State Triple Proton Transfer of 7-Hydroxyquinoline along a Hydrogen-Bonded Alcohol Chain: Vibrationally Assisted Proton Tunneling



Bring in the substitute! $Zn_{1-x}Co_xO$ nanowires are prepared by using a solution-based synthetic route. Structural, optical, and spectroscopic characterizations indicate that the cobalt atoms substitute the zinc cations in the host lattice as a result of the cobalt doping (the picture shows prepared Co-doped ZnO nanowires).

Semiconductors

B. D. Yuhas, D. O. Zitoun, P. J. Pauzauskie, R. He, P. Yang* ——— **420 – 423**

Transition-Metal-Doped Zinc Oxide Nanowires

© 2006 Wiley-VCH Verlag GmbH & Co. KGaA, Weinheim

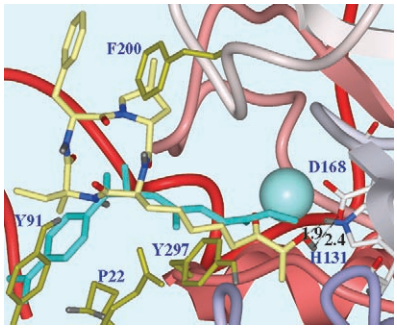
Contents

Total Synthesis

M. Rodriquez, S. Terracciano, E. Cini, G. Settembrini, I. Bruno, G. Bifulco, M. Taddei,* L. Gomez-Paloma* ——— **423 – 427**

Total Synthesis, NMR Solution Structure, and Binding Model of the Potent Histone Deacetylase Inhibitor FR235222

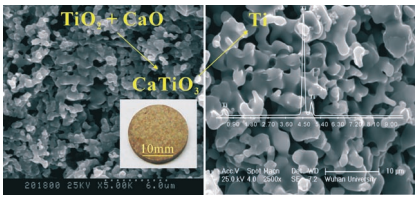
An alternative route: The fungal metabolite FR235222, a potent inhibitor of mammalian histone deacetylase (HDAC), has been synthesized. Key steps are the preparation of unusual amino acids Ahoda and (2*R*,4*S*)-MePro. A 3D model for cyclopeptide inhibitor interaction with the HDAC active site (see picture) highlights the differences between the binding mode of small-molecule and cyclopeptide inhibitors.



Materials Science

K. Jiang, X. H. Hu, M. Ma, D. H. Wang,* G. H. Qiu, X. B. Jin, G. Z. Chen* ——— **428 – 432**

"Perovskitization"-Assisted Electrochemical Reduction of Solid TiO_2 in Molten $CaCl_2$



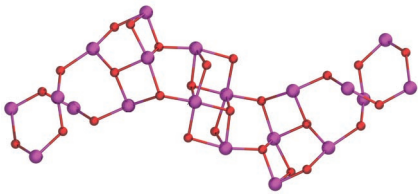
Speed up: In situ formation of perovskite phases ($Ca_\delta TiO_x$, $x/\delta \geq 2$) during electroreduction of porous TiO_2 pellets to Ti metal in molten $CaCl_2$ kinetically retards the process. Ex situ perovskitization of TiO_2 with CaO (see picture) can prevent in situ perovskitization during electrolysis, thereby significantly increasing the electroreduction speed.

Cluster Compounds

A. K. Boudalis,* C. P. Raptopoulou, B. Abarca, R. Ballesteros, M. Chadlaoui, J.-P. Tuchagues, A. Terzis ——— **432 – 435**

Co^{II} Chemistry of 2,6-Bis(2-pyridylcarbonyl)pyridine: An Icosanuclear Co Cluster Exhibiting Superparamagnetic Relaxation

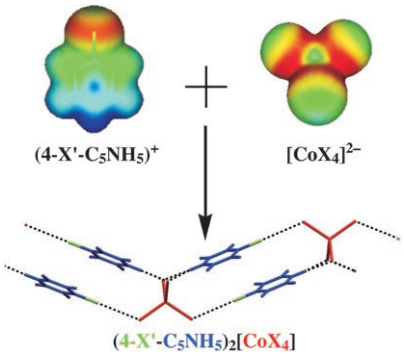
Giant clusters: Metal-assisted hydrolysis of 2,6-bis(2-pyridylcarbonyl)pyridine with $Co(O_2CMe)_2 \cdot 4H_2O$ in hot DMF yielded an icosanuclear Co^{II} complex containing the triply deprotonated bis(*gem*-diol) form of the ligand and exhibiting superparamagnetic relaxation of its magnetization. The picture shows the central Co–O core of the complex (Co violet, O red).



Electrostatic Interactions

G. Mínguez Espallargas, L. Brammer,* P. Sherwood ——— **435 – 440**

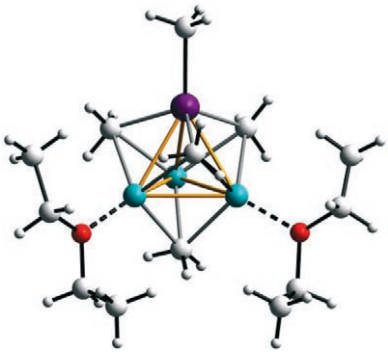
Designing Intermolecular Interactions between Halogenated Peripheries of Inorganic and Organic Molecules: Electrostatically Directed M–X···X′–C Halogen Bonds



Complementary electronic properties of inorganic and organic halogen species are exploited in the design of molecular networks that employ M–X···X′–C halogen bonds. The dominance of electrostatic effects in this type of interaction over other energy terms, such as charge transfer, is demonstrated by the study of a series of eight isostructural compounds $(4\text{-}X'pyH)_2[CoX_4]$ (see picture; X = Cl, Cl/Br, Br, I; X′ = Cl, Br).

© 2006 Wiley-VCH Verlag GmbH & Co. KGaA, Weinheim

The additional molecule of methyllithium present in $[(Me_4Fe)(MeLi)][Li(OEt_2)]_2$ (**1**), the first structurally characterized ate complex of Fe^{II} bearing only alkyl substituents without any further stabilizing ligands (see picture: Fe: magenta; Li: cyan; O: red; C and H: gray), is a particularly remarkable structural feature and contributes to the fascinating reactivity profile of **1** in the title reactions.

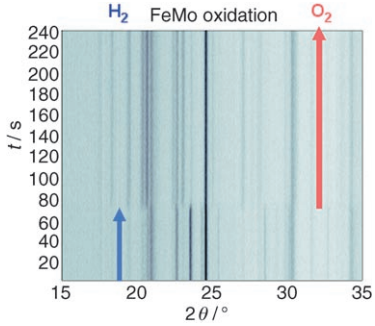


Synthetic Methods

A. Fürstner,* H. Krause, C. W. Lehmann ——— 440 – 444

Unusual Structure and Reactivity of a Homoleptic "Super-Ate" Complex of Iron: Implications for Grignard Additions, Cross-Coupling Reactions, and the Kharasch Deconjugation

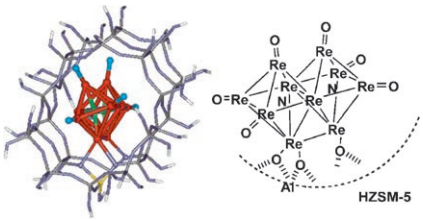
Hot air in a hurry: An industrial Fe-Mo-O catalyst, used in the production of formaldehyde has been studied under redox conditions using rapid in situ powder diffraction studies (see contour image). Surprisingly, the oxidation step is fastest as it is completed within 15 s at 472 °C.



Oxidation Reactions

S. D. M. Jacques, O. Leynaud, D. Strusevich, A. M. Beale, G. Sankar, C. M. Martin, P. Barnes* ——— 445 – 448

Redox Behavior of Fe-Mo-O Catalysts Studied by Ultrarapid In Situ Diffraction

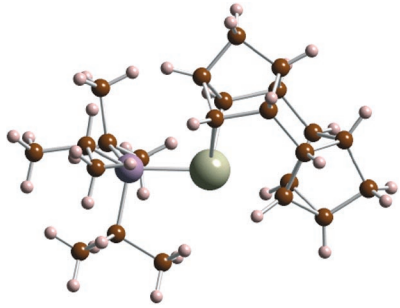


Remarkable selectivity (88 % in the steady-state reaction and 94 % in the pulse reaction) is observed in the direct synthesis of phenol from benzene with molecular oxygen over a Re/zeolite catalyst prepared by chemical-vapor deposition. The novel interstitial-N/Re clusters are formed with NH_3 and are essential for the activity in the selective oxidation reaction.

Phenol Synthesis

R. Bal, M. Tada, T. Sasaki, Y. Iwasawa* ——— 448 – 452

Direct Phenol Synthesis by Selective Oxidation of Benzene with Molecular Oxygen on an Interstitial-N/Re Cluster/Zeolite Catalyst



Hidden qualities: $[Rh(PiPr_3)(C_{14}H_{16})][BAr^F_4]$ (**1**; see picture of the cation; P violet, Rh olive green), which was synthesized by treatment of $[RhCl(nbd)(PiPr_3)]$ with $Na[BAr^F_4]$ ($BAr^F_4 = B\{C_6H_3(CF_3)_2\}_4$) and norbornadiene (nbd) in fluorobenzene, contains an organic fragment derived from Binor-S as well as agostic Rh···CC and Rh···HC interactions. In solution, **1** undergoes rapid, reversible C–C activation/reductive elimination.

C–C Activation

S. K. Brayshaw, J. C. Green, G. Kociok-Köhn, E. L. Sceats, A. S. Weller* ——— 452 – 456

A Rhodium Complex with One Rh···C–C and One Rh···H–C Agostic Bond

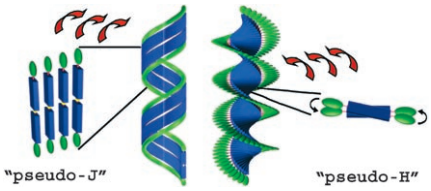
© 2006 Wiley-VCH Verlag GmbH & Co. KGaA, Weinheim

Contents

Helical Structures

A. Ajayaghosh,* C. Vijayakumar, R. Varghese, S. J. George ——— **456 – 460**

Cholesterol-Aided Supramolecular Control over Chromophore Packing: Twisted and Coiled Helices with Distinct Optical, Chiroptical, and Morphological Features

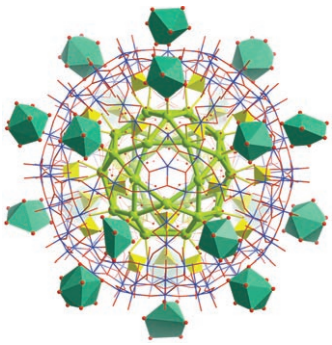


Good cholesterol: Oligo(*p*-phenylenevinylene)s (OPVs) that are mono- or disubstituted with cholesterol moieties form pseudo-J and pseudo-H aggregates, respectively (see picture), which lead to coiled and twisted helical structures with distinct optical, chiroptical, and morphological properties.

Supramolecular Chemistry

A. Müller,* Y. Zhou, H. Bögge, M. Schmidtmann, T. Mitra, E. T. K. Haupt, A. Berkle ——— **460 – 465**

"Gating" the Pores of a Metal Oxide Based Capsule: After Initial Cation Uptake Subsequent Cations Are Found Hydrated and Supramolecularly Fixed above the Pores

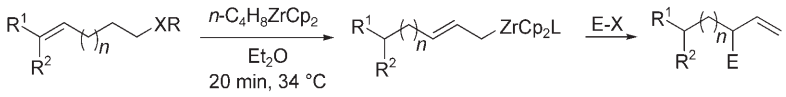


Artificial cells: A polyoxomolybdate capsule, in which the cavity is linked to surface pores by channels, can take up Pr^{3+} ions. Each uptake reduces the negative charge on the capsule so that eventually no more Pr^{3+} ions enter the capsule, instead they remain bound on the surface (see structure: external hydrated Pr^{3+} green polyhedra, encapsulated Pr^{3+} light green, Mo blue, O red, SO_4^{2-} yellow). This process models voltage gating of the ion channels of cells.

Organometallic Chemistry

N. Chinkov, A. Levin, I. Marek* ——— **465 – 468**

Unsaturated Fatty Alcohol Derivatives as a Source of Substituted Allylzirconocene

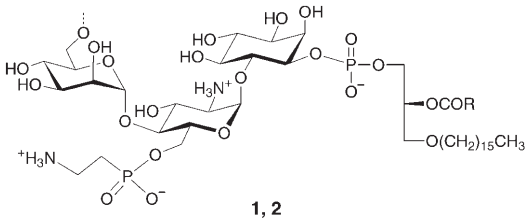


From A to Z: Allylzirconocenes have been easily prepared in a one-pot procedure through a tandem allylic C–H activation–β-elimination reaction from unsaturated fatty alcohol and ether starting materials (see scheme). The reaction proceeds rapidly under mild condition and is insensitive to the length of the carbon tether between the double bond and the alcohol moiety.

Synthetic Methods

D. V. Yashunsky, V. S. Borodkin, M. A. J. Ferguson, A. V. Nikolaev* ——— **468 – 474**

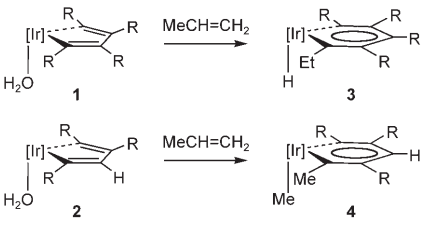
The Chemical Synthesis of Bioactive Glycosylphosphatidylinositols from *Trypanosoma cruzi* Containing an Unsaturated Fatty Acid in the Lipid



1, 2

Protection strategy: Glycosylphosphatidylinositols (GPIs) from the *Trypanosoma cruzi* parasite (a causative agent of Chagas' disease) that contain an unsaturated fatty acid in the lipid moiety (see partial structure of **1**, R = $(CH_2)_7CH{=}CH$-$(CH_2)_7CH_3$, and **2**, R = $(CH_2)_7CH{=}CHCH_2CH{=}CH(CH_2)_4CH_3$) were prepared by a strategy that employs non-benzyl-type protecting groups. The synthetic GPIs show similar biological activity to their natural counterparts.

© 2006 Wiley-VCH Verlag GmbH & Co. KGaA, Weinheim

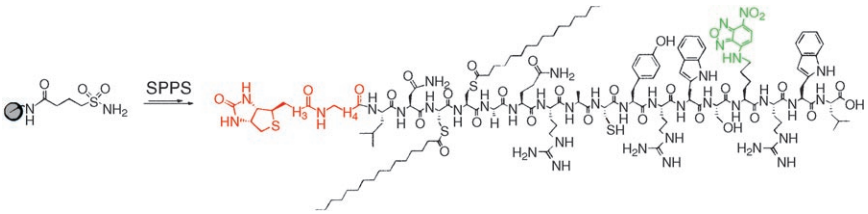


A new synthesis of iridabenzene species involves the coupling of $MeCH{=}CH_2$ with iridacycles **1** and **2**. Surprisingly, the structure of the coupling product of the iridacyclopentadienes with propene (**3** or **4**) is highly susceptible to the nature of the substituents in the starting metallacycle.

Metallabenzenes

E. Álvarez, M. Paneque,* M. L. Poveda,* N. Rendón ——— **474 – 477**

Formation of Iridabenzenes by Coupling of Iridacyclopentadienes and Alkenes

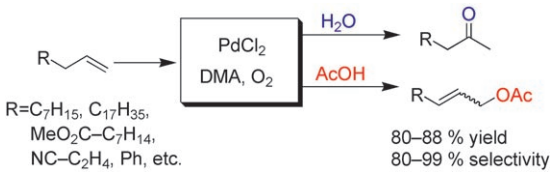


Anchored down: Long lipopeptides (up to 26 amino acids) that carry multiple sensitive lipid residues as well as different reporter groups and tags can be synthesized efficiently by employing the Ellman sulfonamide linker as an anchoring group to the solid support (SPPS = solid-phase peptide synthesis).

Peptide Synthesis

J. M. Palomo, M. Lumbierres, H. Waldmann* ——— **477 – 481**

Efficient Solid-Phase Lipopeptide Synthesis Employing the Ellman Sulfonamide Linker

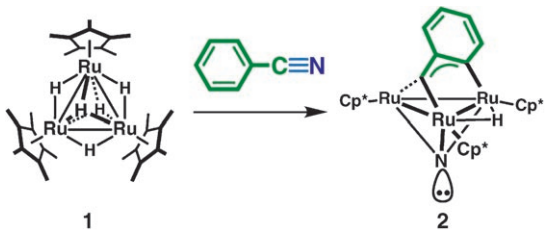


Just the one: The combination of palladium dichloride and *N*,*N*-dimethylacetamide (DMA) constitutes a highly efficient and reusable catalytic system, which uses molecular oxygen as the sole reoxidant for liquid-phase Wacker oxidation and acetoxylation of terminal olefins to the corresponding methyl ketones and linear allylic acetates, respectively (see scheme).

Synthetic Methods

T. Mitsudome, T. Umetani, N. Nosaka, K. Mori, T. Mizugaki, K. Ebitani, K. Kaneda* ——— **481 – 485**

Convenient and Efficient Pd-Catalyzed Regioselective Oxyfunctionalization of Terminal Olefins by Using Molecular Oxygen as Sole Reoxidant



Broken bonds: The reaction of $[(Cp^*Ru)_3(\mu\text{-}H)_3(\mu_3\text{-}H)_2]$ (**1**, $Cp^* = \eta^5\text{-}C_5Me_5$) with an equimolar amount of benzonitrile yields the μ_3-nitrido-μ_3-allyl complex **2** as a result of the C≡N bond cleavage (see scheme). The C≡N bond cleavage proceeds through the formation of $\mu_3(\perp)$-iminoacyl complex $[(Cp^*Ru)_3(\mu_3\text{-}\eta^2{:}\eta^2(\perp)\text{-}PhCNH)(\mu\text{-}H)_2]$.

Cleavage Reactions

T. Kawashima, T. Takao, H. Suzuki* ——— **485 – 488**

Cleavage of the C≡N Bond on a Triruthenium Cluster: Synthesis and Structure of a Triruthenium Complex Containing a μ_3-Nitrido Ligand

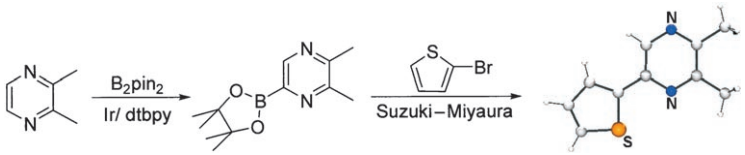
© 2006 Wiley-VCH Verlag GmbH & Co. KGaA, Weinheim

Contents

Synthesis Design

I. A. I. Mkhalid, D. N. Coventry, D. Albesa-Jove, A. S. Batsanov, J. A. K. Howard, R. N. Perutz, T. B. Marder* ——— **489 – 491**

Ir-Catalyzed Borylation of C–H Bonds in N-Containing Heterocycles: Regioselectivity in the Synthesis of Heteroaryl Boronate Esters

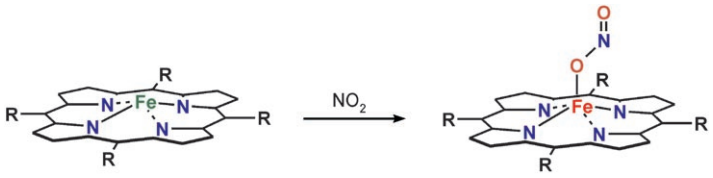


Blocking the way: Substitution at the 2-position in pyridines and other N-heterocycles blocks N-coordination to an Ir center. This steric hindrance provides a substrate-design criterion that allows the Ir-catalyzed borylation of C–H bonds, which can be followed by Suzuki–Miyaura cross-coupling in a one-pot reaction (see scheme; B_2pin_2 = bis(pinacolato-*O*,*O*′)diboron, dtbpy = 4,4′-*t*Bu_2-2,2′-bipyridine).

Porphyrin Complexes

T. S. Kurtikyan,* P. C. Ford* — **492 – 496**

Reactions of Nitrogen Oxides with Heme Models: Spectral Characterization of an Elusive Five-Coordinate Fe^{III}(porphyrin) Nitrito Intermediate

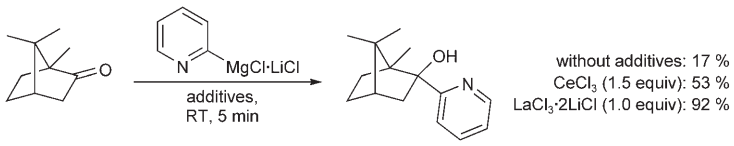


The famous five: The elusive five-coordinate nitrito complexes [Fe^{III}(por)(ONO)] (por = *meso*-tetraphenylporphyrinato dianion or *meso*-tetra-*p*-tolylporphyrinato dianion) have been obtained by interaction of low-pressure NO_2 with sublimed layers of [Fe^{II}(por)]. Spectral data confirm that the NO_2^- ligand prefers to bind through O coordination but adopts the N-bonded configuration when the second axial site is occupied (R = Ph, *p*-tolyl).

Grignard Reactions

A. Krasovskiy, F. Kopp, P. Knochel* ——— **497 – 500**

Soluble Lanthanide Salts ($LnCl_3$·2 LiCl) for the Improved Addition of Organomagnesium Reagents to Carbonyl Compounds

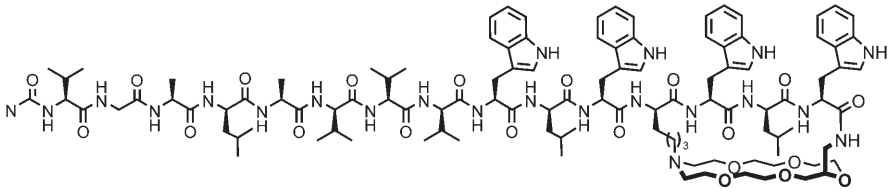


Easy-to-prepare solutions of $LnCl_3$·2 LiCl (Ln = La, Ce, Nd) (0.3–0.5 M in THF) are a unique source of soluble lanthanide salts with versatile applications in organic synthesis. These salts can serve as promoters or catalysts for the addition of organometallic compounds to sterically hindered, enolizable or α,β-unsaturated ketones or imines.

Ion Channels

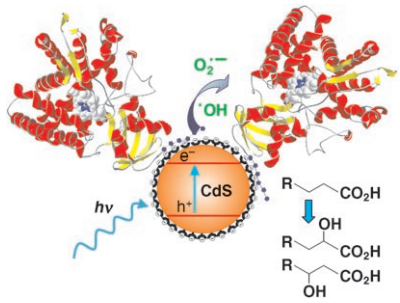
J. R. Pfeifer, P. Reiß, U. Koert* **501 – 504**

Crown Ether–Gramicidin Hybrid Ion Channels: Dehydration-Assisted Ion Selectivity



Predictable ion selectivity is a major goal for the use of synthetic channels in biological systems. Gramicidin A (**gA**) is a suitable lead structure for the design of such channels. The crown ether–**gA** hybrid structure shown forms ion channels with a higher ion selectivity for K^+ than for Cs^+.

© 2006 Wiley-VCH Verlag GmbH & Co. KGaA, Weinheim

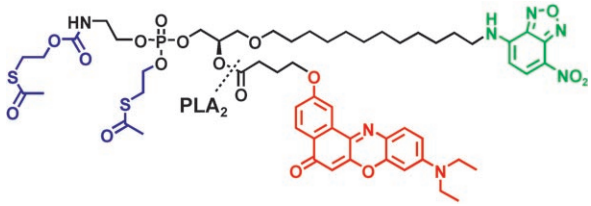


Synthesis with light: CdS quantum dots (QDs) generate superoxide and hydroxyl radicals upon UV irradiation in aqueous solution. The radicals are used for activating $P450_{BS\beta}$ enzymes attached at the QD surface, effecting the catalytic transformation of myristic acid into α- and β-hydroxymyristic acid (see picture, $R = (CH_2)_{10}CH_3$).

Photocatalysis

B. I. Ipe, C. M. Niemeyer* ____ **504 – 507**

Nanohybrids Composed of Quantum Dots and Cytochrome P450 as Photocatalysts



Watching live: The FRET reporter PENN/SATE (see picture; FRET = fluorescence resonance energy transfer) is membrane permeant and enters cells and small organisms by using a prodrug approach. Once inside cells the reporter is cleaved by phospholipases, which results in a 30-fold change in the emission ratio

Fluorescent Probes

O. Wichmann, J. Wittbrodt, C. Schultz* ____ **508 – 512**

A Small-Molecule FRET Probe To Monitor Phospholipase A_2 Activity in Cells and Organisms

Looking for outstanding employees?

Do you need another expert for your excellent team?
... Chemists, PhD Students, Managers, Professors, Sales Representatives...

Place an advert in the printed version and have it made available online for 1 month, free of charge!

Angewandte Chemie International Edition
Advertising Sales Department: Marion Schulz
Phone: 0 62 01 - 60 65 65
Fax: 0 62 01 - 60 65 50
E-Mail: MSchulz@wiley-vch.de

Service

Keywords ____ *514*

Authors ____ *515*

Angewandte's Sister Journals *516 – 517*

Preview ____ *519*

© 2006 Wiley-VCH Verlag GmbH & Co. KGaA, Weinheim

Corrigenda

Aqueous Fe^{IV}=O: Spectroscopic Identification and Oxo-Group Exchange

O. Pestovsky, S. Stoian, E. L. Bominaar, X. Shan, E. Münck,* L. Que, Jr.,* A. Bakac* _____ **6871–6874**

Angew. Chem. Int. Ed. **2005**, *44*

DOI 10.1002/anie.200502686

In Figure 1, the Mössbauer spectrum measured at 8.0 T was inadvertently also shown as that measured at 4.0 T. The revised Figure 1 shown herein contains the correct spectrum obtained at 4.0 T. The authors apologize for this oversight and would like to emphasize that the error has no bearing on any parameter reported in the manuscript and does not affect the discussion of the results.

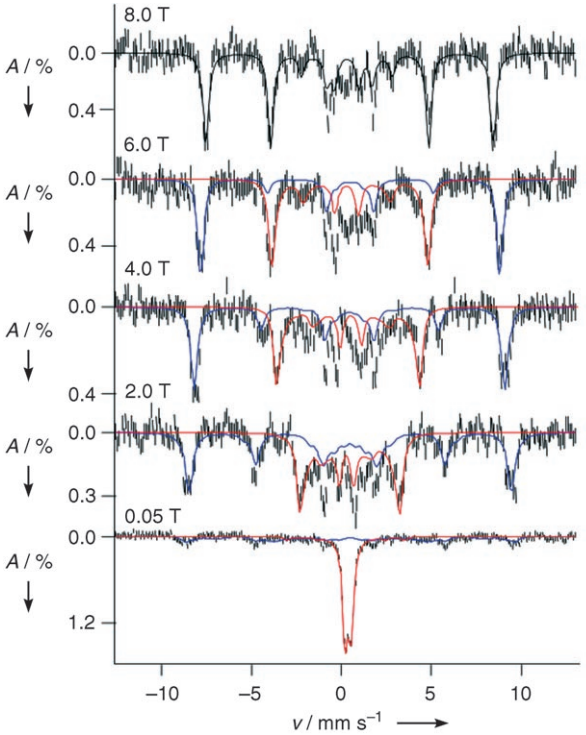


Figure 1. Mössbauer spectra of a sample at 4.2 K containing 250 μM **Z**, prepared by the rapid freeze–quench technique (see Supporting Information). The solid lines (red for **Z**, representing ca. 50% of total Fe) are simulations based on Equation (2). The contribution from $[Fe(H_2O)_6]^{3+}$ is shown in blue. We found the following parameters for **Z**: $D = 9.7(7)$ cm^{-1}, $A_x/g_n\beta_n = A_y/g_n\beta_n = -20.3(3)$ T, $\Delta E_Q = -0.33(3)$ mm s^{-1}, $\delta = 0.38(2)$ mm s^{-1}. For the 8.0-T spectrum, the theoretical curves for **Z** and $[Fe(H_2O)_6]^{3+}$ were added (black).

In addition, the authors would like to acknowledge the Stanford Synchrotron Radiation Laboratory (SSRL), a national user facility operated by Stanford University on behalf of the US Department of Energy, for the X-ray absorption measurements. The SSRL Structural Molecular Biology Program is supported by the Department of Energy, Office of Biological Environmental Research, and by the NIH, National Center for Research Resources, Biomedical Technology Program.

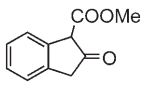
Organocatalytic Asymmetric α-Halogenation of 1,3-Dicarbonyl Compounds

G. Bartoli,* M. Basco, A. Carlone, M. Locatelli, P. Melchiorre,* L. Sambri _____ **6219–6222**

Angew. Chem. Int. Ed. **2005**, *44*

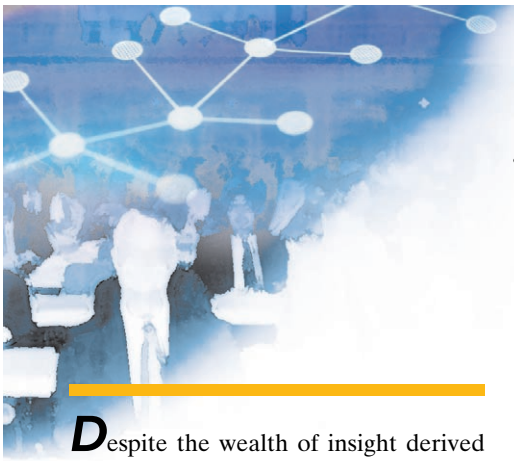
DOI 10.1002/anie.200502134

In this Communication, the structure of methyl-2-oxo-1-indanecarboxylate (**1d**) was rendered incorrectly; the correct structure is shown. The authors apologize for this oversight.



1d

 © 2006 Wiley-VCH Verlag GmbH & Co. KGaA, Weinheim



Chembiogenesis 2005 and Systems Chemistry Workshop**

Johanna Stankiewicz and Lars Henning Eckardt*

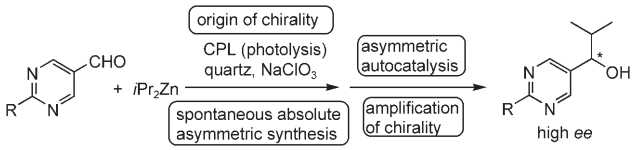
Despite the wealth of insight derived from existing forms of life, biology by itself has not been able so far to answer the question concerning the origin of its subject. Finding the roots of biology in chemical systems calls for an integrated endeavor in which chemistry interfaces with molecular biology, theoretical biology, and complex systems research. COST Chemistry Action D27 was founded in early 2002, and its main objective was seen in the development of the chemistry connected with the origin of life and early evolution of life on earth, while giving special emphasis on self-replicating systems, prebiotic synthesis of nucleic acids and polypeptides, as well as simple protocells as early models of biological cells.

Two meetings on these topics, organized by Günter von Kiedrowski (Bochum, Germany) and his team, were held at Venice International University located on the small island of San Servolo in the Laguna of Venice. The first of these meetings, "Chembiogenesis 2005", was the midterm evaluation conference of the European Chemistry Action COST D27 "Prebiotic Chemistry and Early Evolution" and was attended by nearly 90 participants. The second, "Systems Chemistry", was another occasion to unite the main speakers of Chembiogenesis in a workshop aiming to define a new field of chemistry seen as the offspring of prebiotic and supramolecular chemistry on the one hand and theoretical biology and complex systems research on the other.

During the course of Chembiogenesis 2005, members of six European workgroups reported on their activities, embedded into a framework of keynote and invited lectures from internationally leading scientists. The four-day conference was divided into eight sessions with 40 lectures and about 20 poster presentations by young scientists. A splendid opening by Albert Eschenmoser (Zürich, Switzerland, and La Jolla, CA, USA) addressed the question of why nature selected the structures of DNA and RNA from a plethora of structurally and functionally conceivable alternatives that a grand master of organic chemistry is able to realize by design and synthesis. According to Eschenmoser the postulate of prebiotic robustness deserves a serious reconsideration, at least when it comes to the development of new chemistry that aims to take advantage of a higher level of systems dynamics.

The session continued with an overview of the COST working group "*Etiology, Replication, and Persistence of RNA*" given by Marie-Christine Maurel (Paris, France) followed by workgroup highlight presentations from John Sutherland (Manchester, UK) on potentially prebiotic formation and reactions of activated nucleotides and from Michael Göbel (Frankfurt, Germany) on the prospects and limitations of nonenzymatic oligomerization of ribonucleotides. The unifying theme of the session was genetic biomolecules and their possible ancestors, such as peptide nucleic acids (PNAs) as introduced and discussed by Peter Nielsen (Copenhagen, Denmark). The afternoon saw contributions on a remarkably efficient template-directed synthesis of polynucleotides in artic ice (Christof Biebricher, Göttingen, Germany), twin ribozymes (Sabine Müller, Bochum, Germany), and the role of boric acid as a prebiotic catalyst of peptide formation (Benoit Prieur, Paris, France). The Los Alamos Protocell Project was introduced by Hans Ziok (Los Alamos, NM, USA) and Arvydas Tamulis (Vilnius, Lithuania). The closing lecture of the first day was delivered by Zbigniew Zagorski (Warsaw, Poland), who discussed considerations on the unprobability of panspermia.

The spontaneous generation of homochirality, which is a signature of life, was the subject of theoretical research for a long time until Kenso Soai (Tokyo, Japan) came up with the first example of a chiral-symmetry-breaking reaction almost 15 years ago in the style of the Frank model (1953); for a recent example, see Scheme 1.[1] Much impressive work has been elaborated since then including the kinetic study by Donna Blackmond (London, UK) which shows that chiral amplification is a second-order reaction with respect to the chiral autocatalyst. As a consequence of the latter, the Soai reaction follows a hyperbolic growth law that holds many promises for the discovery of unusual spatiotemporal patterns, whose design may be a future subject of systems chemistry. Chiral-



Scheme 1. One aspect of systems chemistry: the origin of chirality.

[*] J. Stankiewicz, L. H. Eckardt
Bioorganic Chemistry
Ruhr-Universität Bochum
Universitätsstrasse 150, NC2/173
44780 Bochum (Germany)
E-mail: johanna.stankiewicz@oc1.rub.de

[**] Chembiogenesis 2005, COST Action D27: Prebiotic Chemistry and Early Evolution, Midterm Evaluation Conference, Venice, September 28–October 1, 2005. Systems Chemistry Workshop, Venice, October 3–4, 2005.

InterScience
© 2006 Wiley-VCH Verlag GmbH & Co. KGaA, Weinheim

symmetry-breaking processes may, however, also involve crystallization processes, a point that was clarified by Meir Lahav (Rehovot, Israel) before he introduced the COST workgroup on "*The Use of Surfaces and Vesicles for the Amplification of Homochirality in Polypeptide Chains*". Ben Feringa (Groningen, Netherlands), a key contributor to this workgroup, presented a variety of experimental systems which showed that the question of breaking chiral symmetry has many facets, ranging from molecular motors to materials nanotechnology.

The second half of the proceedings on the second day was dedicated to the issue of self-reproduction of protocells. Tadashi Sugawara (Tokyo, Japan) gave a brilliant keynote lecture about a continuously self-reproducing giant vesicle system in which a bipolar amphiphile (membrane precursor) sustains the autocatalytic growth of giant multilamellar vesicles (GMVs). This precursor is hydrolyzed to a membrane molecule and a division-inducing agent. The originator of this field of research is Pier-Luigi Luisi (Rome, Italy), whose COST workgroup on "*Functionalized Self-Reproducing Vesicles as Precursors for Early Cells*" was highlighted by experimental contributions from Christiano Chiarabelli and Pasquale Stano (both Rome). The theory behind vesicle self-reproduction, explaining observable geometrical distortions of vesicle shape, was outlined in the lecture by Saša Svetina (Ljubljana, Slovenia) and put forward by Doron Lancet (Rehovot, Israel). His "lipid world" scenario claims that compositional information encoded in lipid mixtures which express different catalytic phenotypes may be the subject of a primitive way of evolution.

Vesicular models of early cells was the subject of the morning session on the third day opened by Antonio Lazcano (Mexico City) who reconsidered early stages of lipid biosynthesis in evolutionary history. Following an overview of the workgroup by Vesna Nöthig-Laslo (Zagreb, Croatia), Constantinos Paleos (Athens, Greece) presented his work on the interaction of liposomes equipped with complementary functional groups as models for cellular aggregation. The richness of lipid nanoscale phases and their dependence on pH as well as lipid composition was introduced by Peter Walde (Zürich, Switzerland), who raised the question about potentially primordial lipid structures and the range of conditions for vesicle formation. How vesicles could have exhibited the influence of a template for the formation of peptides from thioglutamic acid was the subject of a model study by Helmut Zepik (Zürich). A somehow similar study, namely, the role of surfaces and particles as organizational templates for the formation of lipid bilayers, was presented by Martin Hanczyc (Venice, Italy).

"*Chembiogenesis: A Meteoritic Perspective*" was the title of the keynote lecture given by Sandra Pizzarello (Tempe, AZ, USA) to open the afternoon session. Interestingly, the Soai reaction has found an application in the amplification of chirality in the low enantiomeric excesses from non-proteinogenic amino aids observed in meteorites. The workgroup on "*Dynamic Coevolution of Peptides and Chemical Energetics, A Gate towards the Emergence of Homochirality and Nucleotides*" was introduced by Laurent Boiteau (Montpellier, France) and followed by a contribution on the polymerization of Leuchs' anhydride by Hans Kricheldorf (Hamburg, Germany). The utilization of the latter anhydride for the aminoacylation of nucleotides was highlighted by Alastair L. Parkes (Manchester, UK) as a prebiotic model of tRNA loading. Theoretical contributions in this workgroup came from Tom Lenaerts (Brussels, Belgium) and Jean Claude Micheau (Toulouse, France), who presented an alternative mechanistic interpretation for the autocatalysis in the Soai reaction. Whereas in Blackmond's kinetic investigations the Soai reaction was found to be second order with respect to the homochiral autocatalyst, Micheau reinterpreted the kinetic data using a model that is based on the conventional interpretation of nonlinear effects caused by a strong association in heterochiral complexes. This model, however, contradicts NMR studies according to which homo- and heterochiral complexes are nearly equally populated. The lively discussions between Blackmond, Micheau, Soai, von Kiedrowski, Szathmary, Lahav, and Schuster on these matters continued in the Systems Chemistry Workshop and contributed very much to the style and spirit of both meetings.

The keynote lecture by Peter Schuster (Vienna, Austria), on the fourth day of the meeting, on the evolutionary dynamics of RNA folding included an impressive visualization of the influence of mutations on the secondary structure of RNA. In a similar spirit, Peter F. Stadler (Leipzig, Germany) introduced the work carried out by the workgroup on "*Emergence and Selection of Networks of Catalytic Species*". Mauro Santos (Barcelona, Spain) presented recent work with Eörs Szathmáry (Budapest, Hungary) on a possible resolution of the error catastrophe paradox, which is based on Eigen's insight that the error rate of replication must be smaller than the inverse genome size. The resolution is found in real ribozyme structures, in which not each position has the same probability for a deleterious mutation. Szathmáry summarized his reflections on the integration of metabolic subsystems into minimal cells and the problems concerning systems integration that had to be solved in order to achieve its goal. The session was completed by Peter Strazewski (Lyon, France) with a provocative reconsideration of the enthalpy–entropy compensation problem. His concept of group thermodynamics and his insight that both quantities, enthalpy and entropy, are fundamentally linked by a mathematical function that describes a hyperbolic paraboloid may open a new point of view in the future.

The afternoon session on the last day began with a keynote lecture by Reza Ghadiri (La Jolla, CA, USA) that summarized remarkable success at the frontier of self-replicating peptides and self-organizing catalytic networks by employing peptides. The synthesis of dynamic networks as signal-processing entities was outlined and will certainly be an issue of design that a field such as systems chemistry is able to address in the future. Synthesis was also the theme of the lecture by Dieter Schinzer (Magdeburg, Germany), who revealed the fascination in the hunt for the total synthesis of a million-dollar drug. Both epothilones and sorangicins still are such candidates in the race between

 © 2006 Wiley-VCH Verlag GmbH & Co. KGaA, Weinheim

laboratories that are focused on the synthesis of natural products.

The Systems Chemistry Workshop provided two further days of exciting brainstorming dedicated to creating links between the groups of researchers who are interested in template self-replication, asymmetric autocatalysis, vesicle self-reproduction, and protocell formation. The main speakers focused their lectures, giving insight into unpublished results and future perspectives. This was particularly evident in the lecture given by Albert Eschenmoser which made clear that his published studies on the aetiology of nucleic acid structure are just the tip of an iceberg. So many new informational oligomers await to be discovered in the future.

As a result of the workshop, two facets of systems chemistry were established. First, it can be understood in terms of the integration of kinetic studies, dynamic modeling, structural studies, and computational chemistry to obtain a better understanding of complex dynamic phenomena such as chemical self-replication and chiral-symmetry breaking. The second facet can be seen in the integration of dynamic subsystems into higher ordered supersystems such as protocells. Systems chemistry deals with complex dynamic phenomena such as chemical self-replication and chiral-symmetry breaking as well as with the integration of dynamic subsystems into higher ordered supersystems.

Steen Rasmussen (Los Alomos, NM, USA) reported on new experimental findings towards the implementation of the Los Alamos protocell. Eörs Szathmáry and Timoteo Carlotti (Namur, Belgium) reconsidered another scheme of subsystem integration that is based on the chemoton theory of Tibor Ganti.

Systems chemistry deals with complex dynamic phenomena such as chemical self-replication and chiral-symmetry breaking as well as with the integration of dynamic subsystems into higher ordered supersystems.

Surprising dynamic self-organization processes leading to a non-Brownian motion of self-reproducing vesicles as well as the spontaneous formation of helical mesophases were discussed by Tadashi Sugawara. These phenomena go clearly beyond a thermodynamic description by lipid phase diagrams, as beautifully outlined by Peter Walde. The experimental aspect was covered by Peter Strazewski, talking about peptidyl RNAs from lipophilic peptides, and Ludovic Jullien (Paris, France), who gave an introduction on the engineering of dynamic properties in chemical systems with examples from his laboratory.

In a final discussion, von Kiedrowski outlined where the future of systems chemistry may lie. The creation of coupled autocatalytic systems starting from well-characterized subsystems, such as self-replicating templates and vesicles, and the Soai reaction is clearly a challenge. For example, the coupling of templated self-replication and vesicle self-reproduction may be achievable if the template-directed synthesis proceeds with the liberation of a lipid leaving group. Other opportunities as outlined by Szathmary are seen in the coupling of self-replication and chromatography processes. The Soai reaction is expected to exhibit interesting spatio-temporal pattern formation such as traveling or spiral waves. An experimental approach towards Lancet's lipid world is clearly feasible today and calls for suitable experimental systems. The same holds for an experimental implementation of Ganti's chemoton (a supersystem composed of a metabolic, a genetic, and a compartment-forming subsystem), which may start from a systematic investigation of couplings between two subsystems. All this could be the future of systems chemistry.

[1] T. Kawasaki, M. Sato, S. Ishiguro, T. Saito, Y. Morishita, I. Sato, H. Nishino, Y. Inoue, K. Soai, *J. Am. Chem. Soc.* **2005**, *127*, 3274 – 3275.

DOI: 10.1002/anie.200504139

 © 2006 Wiley-VCH Verlag GmbH & Co. KGaA, Weinheim

Asymmetric Catalysis

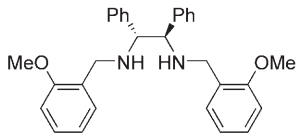
DOI: 10.1002/anie.200502630

Catalytic Enantioselective Cross-Mannich Reaction of Aldehydes

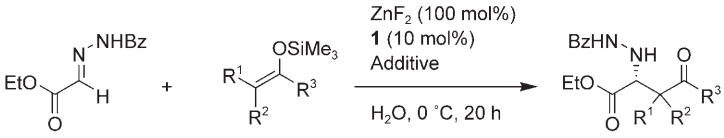
*Maria Manuel B. Marques**

Keywords:
asymmetric catalysis · C–C coupling · enantioselectivity · homogeneous catalysis · Mannich reaction

The Mannich reaction is one of the most useful reactions for the synthesis of nitrogen-containing compounds as well as an effective method for the construction of C–C bonds.[1] A wide variety of natural products and drugs possessing optically active, nitrogen-containing molecules (proteins, nucleic acids, biologically active compounds) have attracted considerable attention from synthetic chemists and the pharmaceutical industry, which has stimulated the development of asymmetric Mannich reactions.[1,2] Mannich and aldol reactions are both highly atom economic and address the problem of stereocontrol, and are therefore often used as key steps in modern organic synthesis. Control over the three components of the Mannich reaction (carbonyl donor, amine, and aldehyde acceptor) constitutes one of the main challenges, since side reactions such as the corresponding aldol reaction might occur, thus lowering the yield. Impressive achievements have recently been made, in particular in asymmetric catalysis, with regard to the versatility of this reaction. Catalytic direct and indirect enantioselective methodologies have been developed. While the direct Mannich reaction requires unmodified ketone donors, amines, and aldehydes, the indirect Mannich reaction uses preformed enolate equivalents and/or imines. Many catalytic asymmetric Mannich methods have been reported over the last few years.[3] Excellent indirect catalytic methods, which involve the addition of enolates to imines in the presence of metal catalysts, have been reported by the Kobayashi, Sodeoka, and Lectka research groups, who used chiral zirconium/binol, palladium(II)/binap, and copper(I)/binap complexes, respectively (binol = 1,1′-binaphthol, binap = 2,2′-bis(diphenylphosphanyl)-1-1′-binaphthyl).[4] Recently, Kobayashi and co-workers developed an efficient catalytic, enantio- and diastereoselective Mannich-type reaction of a hydrazono ester with silicon enolates using water as the solvent (Scheme 1). It should be noted that this method provides access to either the *syn* or *anti* adducts stereospecifically from (*E*) or (*Z*)-enolates.[5]



1



2 **3** **4**

Yield (%)	*syn*/*anti*	*ee* (%)
≤ 94	8:92–92:8	67–95

R^1 = H, Me, Et
R^2 = H, Me
R^3 = 4-MeC_6H_4, Ph, Et, S*i*Bu
Additive (mol %) = TfOH (1), SDS (5), Triton X-405 (5), CTAB (5 or 2), CPB (2)

Scheme 1. Enantio- and diastereoselective Mannich-type reactions in water. Bz = benzoyl, SDS = sodium dodecyl sulfate, CTAB = cetyltrimethylammonium bromide, CPB = cetylpyridinium bromide.

Most of these methods have the disadvantage that the preformed enolates are unstable. Thus, a direct methodology based on unmodified ketone donors would enhance the efficiency of the Mannich reaction. Direct and highly enantioselective catalytic asymmetric Mannich reactions were reported by Trost and Terrell as well as by Shibasaki and co-workers, who used a dinuclear zinc catalyst and zinc combined with (*S*,*S*)-linked-binol as the catalyst, respectively.[6] A new approach to α,β-

[*] Prof. Dr. M. M. B. Marques
REQUIMTE—Departamento de Química
Faculdade de Ciências e Tecnologia
Universidade Nova de Lisboa
2829-516 Caparica (Portugal)
Fax: (+351) 21-294-8300
E-mail: mmbmarques@dq.fct.unl.pt

InterScience
© 2006 Wiley-VCH Verlag GmbH & Co. KGaA, Weinheim

diamino acid derivatives from imines of glycine esters, catalyzed by a chiral copper(I)/phosphanyloxazoline complex, was recently developed by Jørgensen and co-workers.[7]

Asymmetric organocatalysis has received much attention since it avoids the use of expensive and/or toxic metals. Moreover, Shibasaki and co-workers very recently reported a highly efficient *syn*-selective enantio- and diastereoselective catalytic Mannich-type reaction of a glycine Schiff base using the chiral two-center phase-transfer catalyst (*S*,*S*)-tadias (**5**, Scheme 2).[8] This method represents a simple and mild procedure for the preparation of *syn*-α,β-diamino acids, with the advantage of the facile removal of the pivotal imine-protecting group instead of the *p*-tosyl group used by Jørgensen and co-workers.[7]

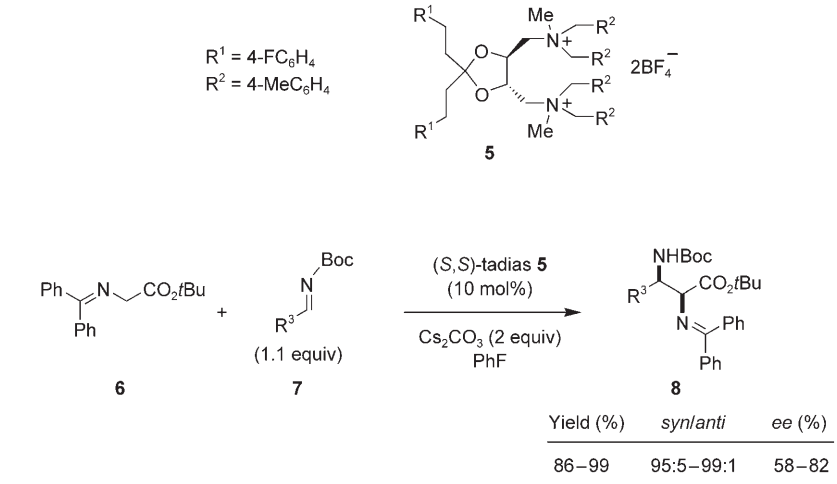
The use of unmodified ketones as donors and metal-free catalysts—in particular amine catalysts—appeared to be an excellent strategy and a promising alternative. However, the use of amino acid derivatives as catalysts has been the method of choice. Proline was first used as the catalyst in the Hajos–Parrish–Eder–Sauer–Wiechert reaction,[9] and was subsequently employed in a broad range of intermolecular aldol and cross-aldol reactions.[10] During the last five years, many research groups have applied this strategy to the Mannich reaction. Thus, organocatalytic asymmetric Mannich reactions involving amino acid derivatives as catalysts have been reported by the research groups of List, Barbas, Córdova, and Jacobsen.[11] Some of these methods involve a catalytic indirect asymmetric Mannich reaction, while others involve direct methods.

Encouraged by the results obtained by Kobayashi and co-workers in the three-component Mannich reaction, and the fact that L-proline promoted the direct enantioselective aldol reaction, List et al. explored the first L-proline-catalyzed asymmetric three-component Mannich reaction of a free aldehyde (instead of preformed imine equivalents or paraformaldehyde) with an unmodified ketone and an imine, which is a more atom-economic process. This approach led to the development of highly enantioselective and efficient syntheses of 1,2-amino alcohols using ketones as donors. The main advantage of the three-component procedure is that it does not require any preformed imine and enol equivalents; on the other hand, the direct aldol and Mannich reaction compete and are dependent on the equilibrium ratio between the aldehyde and imine (K_{aldol} versus $K_{Mannich}$).

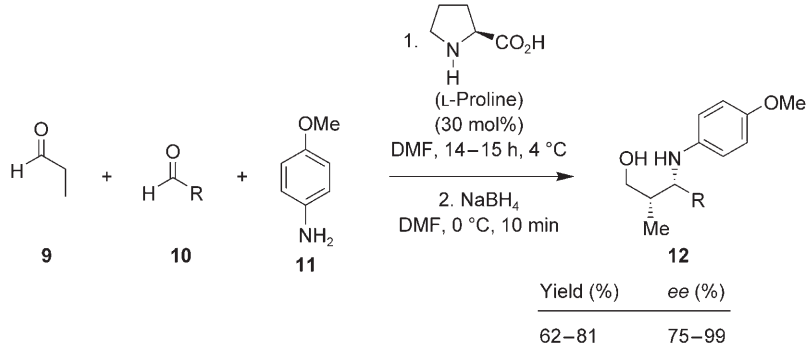
Recently, the scope of the proline-catalyzed asymmetric Mannich reaction has been expanded[12] by applying a one-pot, three-component procedure to unmodified aldehydes as donors. The 3-amino adducts were reduced with $NaBH_4$ to the corresponding γ-amino alcohols to avoid epimerization and racemization during the purification process. A Mannich-type reaction to afford γ-amino alcohol derivatives **12** with high stereocontrol and in high yield was also described (Scheme 3).

Moreover, Christmann and co-workers[13] recently developed a new and efficient protocol for the construction of azetidines, piperidines, and pyrrolidines by using a highly selective proline-catalyzed Mannich reaction of functionalized aldehydes.

The development of a cross-Mannich reaction between two different unmodified aldehydes provided a significant advancement to the synthetic methodology. However, the use of an aldehyde as the Mannich donor and another aldehyde as the Mannich acceptor has associated problems (Scheme 4).

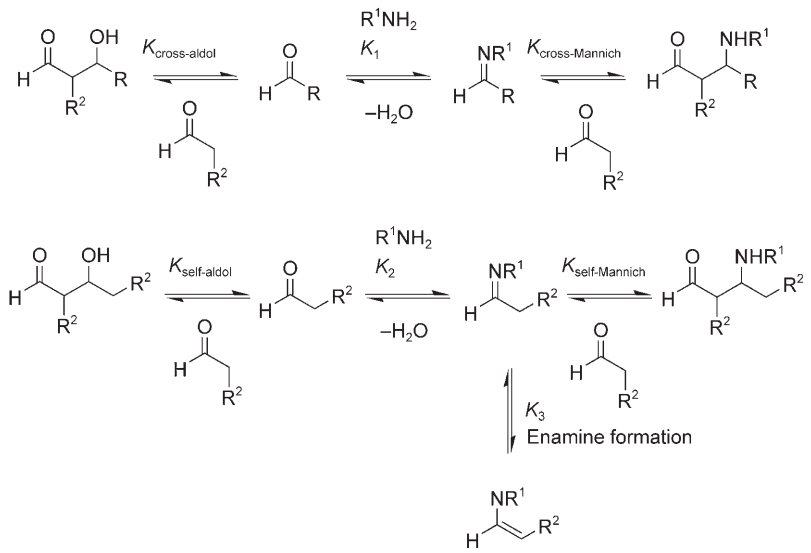


Scheme 2. Enantio- and diastereoselective catalytic Mannich-type reactions of a glycine Schiff base using (*S*,*S*)-tadias **5** as a phase-transfer catalyst. Boc = *tert*-butoxycarbonyl.



Scheme 3. One-pot direct asymmetric synthesis of γ-amino alcohol derivatives catalyzed by proline.

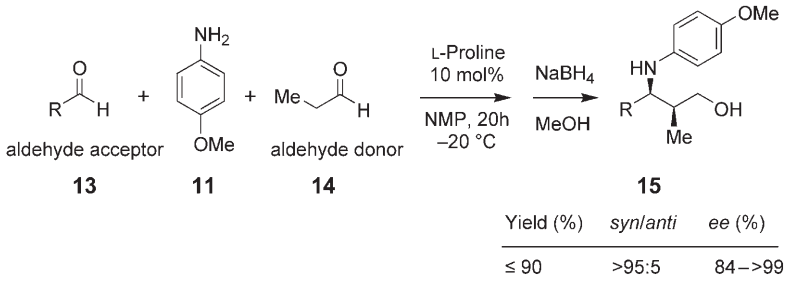
© 2006 Wiley-VCH Verlag GmbH & Co. KGaA, Weinheim



Scheme 4. Possible different reaction pathways that might occur during the reaction between two different unmodified aldehydes.

The challenge and fundamental problem of a cross-Mannich reaction consists of finding the right reaction conditions (temperature, solvent, catalyst) that favors the cross-Mannich reaction and equilibrium rather than the side pathways: cross-aldol, self-aldol, self-Mannich, and enamine formation (K_3). The equilibrium constants as well as the relative stability—the energy gap—of the competing transition states are extremely important and determine the course of the reaction. Imine formation must be specific for the aldehyde acceptor and the formation of an enamine from an aldehyde donor must be avoided.

Nevertheless, Hayashi et al. and Córdova reported the one-pot, three-component enantioselective cross-Mannich reaction of aldehydes not only with high *syn* diastereo- and enantioselectivity but also with low catalyst loading.[14,15] Stimulated by the excellent results reported by the research groups of List and Barbas on proline-mediated reactions, Hayashi and co-workers explored a new system for the reaction between two different aldehydes. They found higher reaction efficiency when the reactions were performed at a lower temperature: higher yields and enantioselectivities were achieved at −20 °C (Scheme 5), and only the *syn* isomer was observed. Indeed, lower temperature favors the Mannich reaction and suppresses the aldol reaction (favored at 4 °C). Thus, proline was found to activate aldimines preferentially to aldehydes. The best results were reported when aromatic and heteroaromatic acceptors were used instead of the aliphatic ones. The desired cross-Mannich adducts were isolated after reduction to the corresponding β-amino alcohol **15** to avoid decomposition during purification.

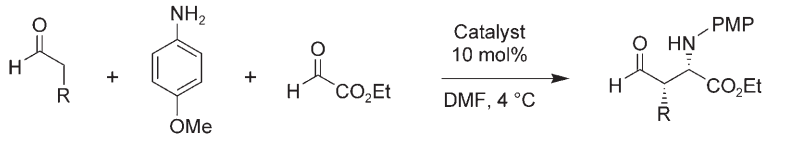


Scheme 5. One-pot, direct cross-Mannich reaction of two different aldehydes with high *syn* diastereo- and enantioselectivity by proline catalysis.

The scope, mechanism, applications, and limitations of the cross-Mannich reaction between two different unmodified aldehydes has been fully explored.[15] On the basis of previous results and investigations,[12] it was later realized that both (*S*)- and (*R*)-proline could be used as catalysts for the cross-Mannich reaction. The chemoselectivity was sometimes low when unmodified ketones were used, however, absolute stereocontrol was achieved when aldehydes were tested as acceptors and donors, and the Mannich adducts could be isolated in high yield (>99% *ee* and >19:1 d.r.). The role of the aldehyde acceptor was also investigated, and it was observed that proline exhibited a higher selectivity for the cross-Mannich instead of the cross-aldol reaction for aromatic acceptors (lacking electron-withdrawing groups). In contrast, aliphatic acceptors only gave trace amounts of the desired adduct. Thus, the increased reactivity of the acceptor results in a higher yield, as well as a higher enantioselectivity of the Mannich adducts. Another interesting observation was that a stable acceptor imine favors the cross-Mannich reaction rather than the self-Mannich reaction. The structural features of the aldehyde donor were also explored. The chain length of the nucleophilic aldehyde influenced the diastereoselectivity: lower *ee* valuess were observed as the chain length of the aldehyde donor increased. The results obtained motivated the study of a one-pot, direct catalytic asymmetric synthesis of each enantiomer of the unnatural amino acid **18** using ethyl glyoxylate (**17**, Scheme 6). The reaction proceeded with excellent chemo- and enantioselectivities, and could be readily scaled up.

Different organic amines were also tested, although the best results were obtained with proline (>90% *ee*). However, all the catalysts exhibited *syn* selectivity. It should be emphasised that the main difference between the proline-catalyzed Mannich and aldol reactions in regard to stereoselectivity is that

 © 2006 Wiley-VCH Verlag GmbH & Co. KGaA, Weinheim



Yield (%)	d.r.	*ee* (%)
≤ 80	1.5:1 – > 19:1	>99

R = Me, Bu, CH_2=$CHCH_2$, pentyl, isopropyl, $CH_3(CH_2)CH$=$CHCH_2$
Catalyst = (*S*)-proline, (*R*)-proline

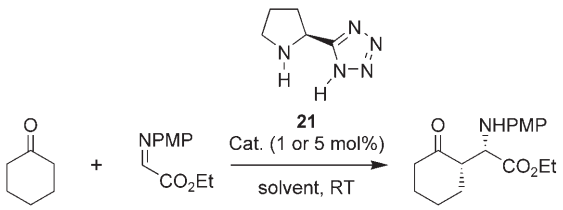
Scheme 6. One-pot, three-component, direct catalytic asymmetric synthesis of functional α-amino alcohol derivatives. PMP = *para*-methoxyphenyl.

the Mannich reaction affords the *syn*-adduct whereas the aldol reaction gives the *anti* adduct (Scheme 7). List et al. and Córdova explored certain mechanistic features and found that a single proline molecule is involved in the transition state as well as in the mechanism. Since proline is a bifunctional acid/base catalyst that acts like a Lewis base type catalyst, and allows enamine formation, and also like a general acid (because of its increased pK_a value relative to primary amino acids) it is regarded as an artificial enzyme.

A plausible explanation was proposed for the observed diastereoselectivity in the (*S*)-proline-catalyzed direct asymmetric Mannich reactions. They were proposed to occur by the attack of the *si* face of the enamine on the *si* face of an imine with an *E* configuration, rather than the proposed *re*-face attack in the cross-aldol reaction. Similar to the cross-aldol reaction, the trasition state—a six-membered metal-free Zimmermann–Traxler system—is stabilized by hydrogen bonding between the nitrogen atom (imine) and the carboxylic acid (proline). The attack of the imine at the *re* face was considered disfavored because of steric congestion between the PMP group and the pyrrolidine unit.

One of the drawbacks of using proline as the catalyst is the limited choice of solvent, since only polar solvents such as DMSO, DMF, *N*-methylpyrrolidine (NMP), and *N*,*N*-dimethylacetamide (DMA) can be used. More recently, Ley and co-workers screened new catalysts and solvents for the catalytic asymmetric Mannich reaction.[16] Among the catalysts tested, a new catalyst—tetrazole **21** (Scheme 8)—was found to catalyze the asymmetric Mannich reactions of ketone **19** and *N*-PMP-protected α-imino ethyl glyoxalate **20** with high enantioselectivity and high yield. This catalyst is compatible with organic solvents such as dichloromethane and THF and requires low catalyst loadings (1 mol%), without affecting the enantioselectivety.

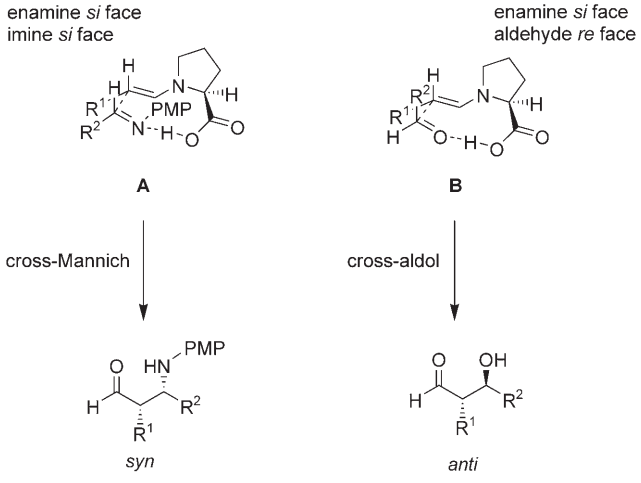
All the examples of the cross-Mannich reaction described herein are highly enantioselective (*ee* values up to 99%), and under optimized reaction conditions gave only the *syn* adduct, although in only moderate to good yields.



Yield (%)	*syn*/*anti*	*ee* (%)
≤ 70	> 19:1	>99

Solvent = CH_2Cl_2, aqueous MeCN, aqueous THF

Scheme 8. Asymmetric Mannich reaction using **21** as the catalyst.



Scheme 7. Proposed transition states of the cross-Mannich and cross-aldol reactions.

Despite all the efforts devoted to asymmetric organocatalysis during the last few years, the search for a catalyst that permits access to both *syn* and *anti* adducts is still a problem waiting to be solved, maybe the search for a catalyst that stabilizes a *Z* configuration of the imine in the transition state will allow the formation of an *anti*-Mannich adduct. Another problem concerns the search for other imine protecting groups, since removal of the PMP group requires oxidative procedures. Also the scope of the aldehyde acceptor has to be increased, since it is limited to aromatic moieties.

A non-enantioselective version of the cross-Mannich reactions of aldehydes was recently applied to an efficient and elegant synthesis of symmetrically and unsymmetrically substituted pyridines.[17]

The cross-Mannich reaction of aldehydes, particularly the direct catalytic asymmetric version, is a new valuable method for the formation of C–C bonds

 © 2006 Wiley-VCH Verlag GmbH & Co. KGaA, Weinheim

and permits access to a wide variety of optically active compounds as well as active compounds such as amino acid derivatives. Remarkable advancements have been reported over the last five years, including one-pot, three-component procedures with absolute stereocontrol and high yields, and the competition between cross-aldol and cross-Mannich reactions could be overcome by controlling the reaction conditions. The success of this reaction will unquestionably prompt chemists to develop new catalysts that will overcome the limitations presented in this Highlight.

Published online: December 12, 2005

[1] Reviews: a) E. F. Kleinmann in *Comprehensive Organic Synthesis, Vol. 2* (Ed.: B. M. Trost), Pergamon, New York, **1991**, Chap. 4.1; b) M. Arend, B. Westermann, N. Risch, *Angew. Chem.* **1998**, *110*, 1096; *Angew. Chem. Int. Ed.* **1998**, *37*, 1044.

[2] Review: S. Denmark, O. J.-C. Nicaise in *Comprehensive Asymmetric Catalysis, Vol. 2* (Eds.: E. N. Jacobsen, A. Pfaltz, H. Yamamoto), Springer, Berlin, **1999**, p. 93.

[3] Review: S. Kobayashi, H. Ishitani, *Chem. Rev.* **1999**, *99*, 1069, and references therein; for indirect methods employing stoichiometric amounts of chiral enol equivalents see: a) M. R. Naimi-Jamal, S. A. Webb, M. R. Saidi, J. Ipaktschi, *Eur. J. Org. Chem.* **1998**, 197; b) D. Enders, S. Oberbörsch, J. Adam, *Synlett* **2000**, 644; E. J. Corey, C. P. Cecicco, R. C. Newbold, *Tetrahedron Lett.* **1991**, *32*, 5287; C. Palomo, M. Oiarbide, M. C. Gonzalez-Rego, A. K. Sharma, J. M. Garcia, A. Gonzalez, C. Landa, A. Linden, *Angew. Chem.* **2000**, *112*, 1105; *Angew. Chem. Int. Ed.* **2000**, *39*, 1063.

[4] a) S. Kobayashi, T. Hamada, K. Manabe, *J. Am. Chem. Soc.* **2002**, *124*, 5640; b) S. Kobayashi, R. Matsubara, H. Kitagawa, *Org. Lett.* **2002**, *4*, 143; c) Y. Hamashima, K. Yagi, H. Tamas, M. Sodeoka, *J. Am. Chem. Soc.* **2002**, *124*, 14530; d) Y. Hamashima, M. Hotta, M. Sodeoka, *J. Am. Chem. Soc.* **2002**, *124*, 11240; e) D. Ferraris, B. Young, C. Cox, T. Dudding, W. J. Drury III, L. Ryhkov, T. Taggi, T. Lectka, *J. Am. Chem. Soc.* **2002**, *124*, 67.

[5] T. Hamda, K. Manabe, S. Kobayashi, *J. Am. Chem. Soc.* **2004**, *126*, 7768.

[6] a) B. M. Trost, L. R. Terrell, *J. Am. Chem. Soc.* **2003**, *125*, 338; b) S. Matsunaga, N. Kumagai, S. Harada, M. Shibasaki, *J. Am. Chem. Soc.* **2003**, *125*, 4712.

[7] L. Bernardi, A. S. Gothelf, R. G. Hazell, K. A. Jørgensen, *J. Org. Chem.* **2003**, *68*, 2583.

[8] A. Okada, T. Shibuguchi, T. Ohshima, H. Masu, K. Yamaguchi, M. Shibasaki, *Angew. Chem.* **2005**, *117*, 4640; *Angew. Chem. Int. Ed.* **2005**, *44*, 4564.

[9] a) "Asymmetric Synthesis of Optically Active Polycyclic Organic Compounds": Z. G. Hajos, D. R. Parrish, German patent DE 2102623, July 29, **1971**; b) "Optically Active 1,5-Indanone and 1,6-Naphthaledione": U. Eder, G. Sauer, R. Wiechert, German patent DE 2014757, Oct 7, **1971**.

[10] For a review on proline-catalyzed asymmetric reactions see: B. List, *Tetrahedron* **2002**, *58*, 5573.

[11] a) B. List, *J. Am. Chem. Soc.* **2000**, *122*, 9336; B. List, P. Pojarliev, W. T. Biller, H. Martin, *J. Am. Chem. Soc.* **2002**, *124*, 827; b) W. Notz, K. Sakthievel, T. Bui, G. Zhong, C. F. Barbas III, *Tetrahedron Lett.* **2001**, *42*, 199; S.-I. Watanabe, A. Córdova, F. Tanaka, C. F. Barbas III, *Org. Lett.* **2002**, *4*, 4519; A. Córdova, W. Notz, G. Zhong, J. M. Betancort, C. F. Barbas III, *J. Am. Chem. Soc.* **2002**, *124*, 1842; A. Córdova, C. F. Barbas III, *Tetrahedron Lett.* **2003**, *44*, 1923; c) A. G. Wenzel, E. N. Jacobsen, *J. Am. Chem. Soc.* **2002**, *124*, 12964; d) for a review of asymmetric aminocatalysis see: B. List, *Synlett* **2001**, 1675.

[12] A. Córdova, *Synlett* **2003**, 1651.

[13] A. Münch, B. Wendt, M. Christmann, *Synlett* **2004**, 2751.

[14] Y. Hayashi, W. Tsuboi, I. Ashimine, T. Urushima, M. Shoji, K. Sakai, *Angew. Chem.* **2003**, *115*, 3805; *Angew. Chem. Int. Ed.* **2003**, *42*, 3677.

[15] A. Córdova, *Chem. Eur. J.* **2004**, *10*, 1987.

[16] A. J. A. Cobb, D. M. Shaw, D. A. Longbottom, J. B. Gold, S. V. Ley, *Org. Biomol. Chem.* **2005**, *3*, 84.

[17] A. Winter, N. Risch, *Synthesis* **2003**, 2667.

 © 2006 Wiley-VCH Verlag GmbH & Co. KGaA, Weinheim

DOI: 10.1002/anie.200500195

Tandem Transformations

Catalytic Asymmetric Tandem Transformations Triggered by Conjugate Additions

*Hong-Chao Guo and Jun-An Ma**

Keywords:
asymmetric catalysis · conjugate addition · enantioselectivity · organocatalysts · tandem transformations

The development of efficient methods to access complex molecules with multistereogenic centers has been a substantial challenge in both academic research and industrial applications. One approach to this challenge is catalytic asymmetric tandem transformations, which allow a rapid increase in molecular complexity from readily available starting materials to produce enantiopure compounds. In recent years, considerable efforts have been directed towards the development of asymmetric tandem transformations. This Minireview highlights recent developments and the applications of metal-catalyzed and organocatalytic asymmetric tandem transformations triggered by conjugate additions.

1. Introduction

Catalytic asymmetric synthesis has developed significantly over the past decades, as evident by the large number of publications in this field and the award of the Nobel Prize in 2001 to Knowles, Noyori, and Sharpless.[1] Today a considerable number of catalytic systems that provide enantioselectivities in excess of 95% are known, and several highly selective procedures are used in the industrial production of enantiomerically enriched compounds.[2] Despite this remarkable success, there still remain many challenges for organic chemists. For instance, as expensive metals and chiral ligands are often employed in asymmetric syntheses, a high efficiency of the asymmetric catalyst becomes a particularly important requirement as the scale of the reaction or the cost of the catalyst increases. The solution to this challenge would not only be favorable for the environment but also allow a reduction in production costs.

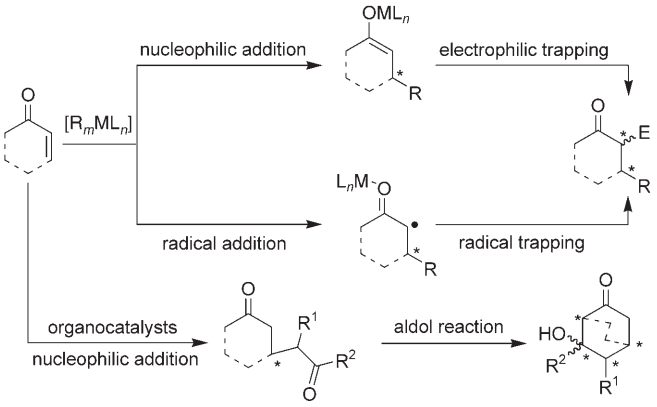
[*] Prof. Dr. J.-A. Ma
Department of Chemistry
School of Chemistry, Tianjin University,
Tianjin 300072 (P.R. China)
Fax: (+86) 22-2740-3475
E-mail: majun_an68@yahoo.com
Dr. H.-C. Guo
Max-Planck-Institut für Kohlenforschung
Kaiser-Wilhelm-Platz 1
45470 Mülheim/Ruhr (Germany)

Catalytic enantioselective carbon–carbon bond-forming reactions such as Diels–Alder and ene reactions, additions of organometallic reagents to carbonyl compounds, aldol and related transformations, coupling reactions, allylic substitutions, and cyclopropanations have been a central tenet of modern asymmetric synthesis.[1a,b,3] Among the most widely used methods for the construction of carbon–carbon bonds are conjugate addition reactions of nucleophiles or nucleophilic radicals to α,β-unsaturated compounds. The broad potential of this approach, combined with the large variety of donor and acceptor substrates that can be employed, has been embodied in the synthesis of numerous biologically active compounds, including steroids, prostaglandins, and terpenes.[4] These conjugate additions to acceptor-substituted olefins can be catalyzed not only by metal complexes but also by various small organic molecules. Many asymmetric catalytic systems that exhibit high reactivity and stereoselectivity have been reported.[5] Moreover, recent advances have demonstrated that catalytic asymmetric transformations mediated by conjugate additions are feasible.

Asymmetric tandem transformation is a very appealing strategy as it involves a multistep transformation that enables a rapid increase in molecular complexity from readily available starting compounds.[6] The advantage of these transformations is the formation of several bonds and the creation of two or more contiguous stereogenic centers by using a single catalyst in one pot, without the need for isolation of the intermediates. Furthermore, the increase in efficiency favors the economic and ecological feasibility of this type of process. In recent years, considerable efforts have been made to develop catalytic asymmetric tandem transformations initiated by conjugate additions (Scheme 1). For

WILEY InterScience DISCOVER SOMETHING GREAT

© 2006 Wiley-VCH Verlag GmbH & Co. KGaA, Weinheim



Scheme 1. Tandem transformations triggered by conjugate additions. E = electrophile; L = ligand; M = metal; R = alkyl/aryl group; * = stereogenic center.

example, the use of prochiral substrates and an enantiomerically pure catalyst provides enantioselectivity in the first step, after which the chiral catalyst and/or the newly generated stereocenter(s) determine the subsequent transformation(s). According to the mechanism of the addition step, these tandem conversions are divided into anionic and radical processes.

Some tandem transformations have been reviewed previously,[7] and stoichiometric (and/or diastereoselective) tandem conjugate additions followed by α functionalization have been known for a long time.[8] Herein, we present recent developments such as metal-catalyzed and metal-free organocatalytic asymmetric tandem transformations triggered by conjugate additions.

2. Metal-Catalyzed Asymmetric Tandem Transformations

2.1. Conjugate Additions of Nucleophiles to α,β-Unsaturated Compounds

Metal-catalyzed asymmetric conjugate additions of nucleophiles to α,β-unsaturated compounds and subsequent transformation of the products is an extensively studied procedure and is applied to the preparation of a variety of optically active compounds. Broadly speaking, conjugate reductions may be considered as conjugate addition reactions of hydrogen, and thus tandem conjugate reduction/aldol reactions are also discussed in this section.

2.1.1. Copper-Catalyzed Tandem Transformations

Over the past decade, highly enantioselective copper-catalyzed conjugate addition reactions of organozinc reagents to α,β-unsaturated ketones have been reported.[7b–d,9] Typically starting with a chiral copper(I) complex (or preferably the Cu^{II} precatalyst), transfer of an alkyl fragment from R_2Zn to the copper center takes place. Complexation of the alkylzinc fragment to the enone carbonyl group and formation of the π complex of the alkylcopper species with the C–C double bond of the enone results in a heterobimetallic complex. As high levels of stereocontrol are attained in the catalytic cycle, the heterobimetallic complex leads to a fixed conformation of the enone. Subsequent alkyl transfer generates a zinc enolate, which can be trapped conveniently by various electrophiles such as aldehydes, ketones, oxocarbenium ions (by way of acetal decomposition), carboxylates, nitriles, alkyl halides, or tosylates for the construction of complex molecular frameworks in tandem protocols (Figure 1).

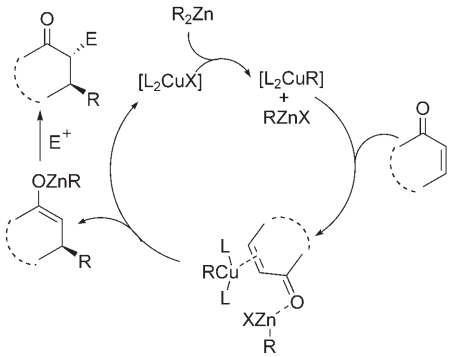


Figure 1. Catalytic cycle of copper-catalyzed conjugate additions of organozinc reagents to α,β-unsaturated compounds.

In 1997, Feringa and co-workers reported the first catalytic regio- and enantioselective three-component cou-



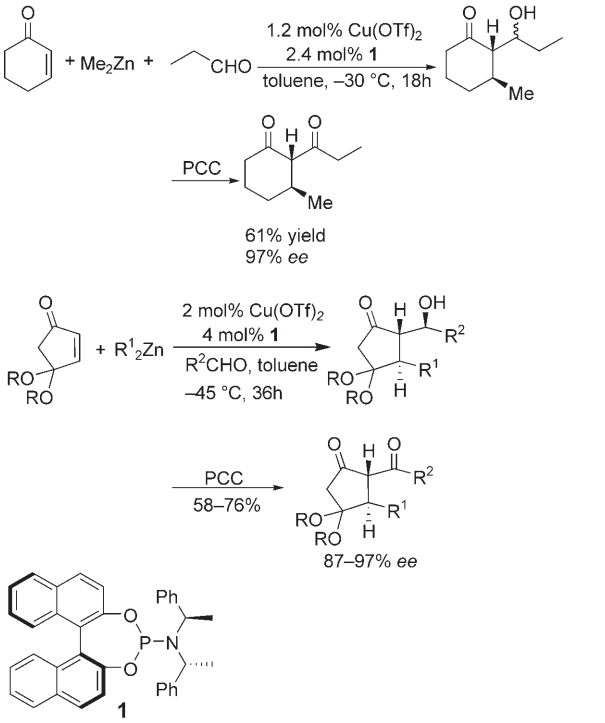
Jun-An Ma received his BS degree from He'nan University (1991) and his MS degree from Nankai University (1994). He then joined Guangzhou Baihua Flavor & Fragrance Co. as a senior research fellow. From 1996 to 1999, he completed his PhD under the supervision of Prof. R.-Q. Huang at Nankai University. He remained there as a collaborator with Prof. Q.-L. Zhou and was appointed associate professor in December 2001. He was a research fellow in the groups of Dr. D. Cahard (France) and Prof. M. T. Reetz (Germany), and since July 2005 he is professor at Tianjin University. His research interests are focused on asymmetric synthesis and catalysis as well as fluorine chemistry.



Hong-Chao Guo received his BS degree from China Agricultural University in 1997. In 2002, he graduated from the same university with a PhD in organic chemistry carried out under the guidance of Prof. M. Wang. After a postdoctoral stay with Prof. K. Ding at the Shanghai Institute of Organic Chemistry, he joined the group of Prof. M. T. Reetz at the Max-Planck-Institut für Kohlenforschung (Germany) as a postdoctoral fellow. His research interests include the development of new methods in synthesis and the study of metal-catalyzed carbon–carbon and carbon–heteroatom bond-forming transformations, with particular emphasis on asymmetric catalysis and combinatorial chemistry.

© 2006 Wiley-VCH Verlag GmbH & Co. KGaA, Weinheim

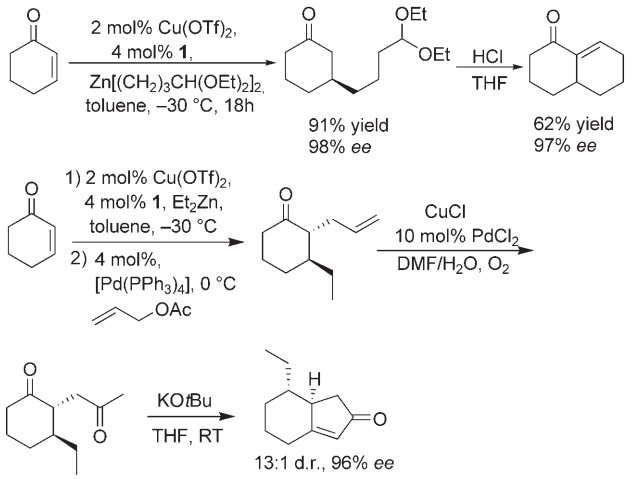
pling of organozinc reagents with α,β-unsaturated ketones and aldehydes, for example, tandem 1,4-addition/aldol reactions involving organozinc reagents to 2-cyclohexenone to afford *trans*-2,3-disubstituted cyclohexanones with more than 90% *ee* in all cases examined (Scheme 2).[10a–b] A few years later, the authors reported catalytic enantioselective tandem reactions of cyclopentene-3,5-dione monoacetals.[10c–e] With only 2 mol% of a chiral catalyst, which was prepared in situ from $Cu(OTf)_2$ and chiral phosphoramidite ligand **1**, the reaction gave β-hydroxy ketones with three consecutive stereocenters (Scheme 2). Nearly complete stereocontrol was achieved in the formation of the consecutive stereocenters in the subsequent aldol step to provide enantiomerically pure multifunctional cyclopentanones. The nature of the acetal had a strong influence on the stability and *ee* values of the reaction products. The stability and *ee* values of the reaction products with 2,2-dimethyl- and 2,2-diphenyl-substituted 1,3-dioxane acetal functionalities were superior to those for 1,3-dioxolane and acyclic acetal functionalities.



Scheme 2. Copper-catalyzed asymmetric conjugate addition/aldol reactions. R,R = -$CH_2CMe_2CH_2$-, -$CH_2CPh_2CH_2$-; R^1 = Et, Bu; R^2 = Ph, *p*-BrC_6H_4; OTf = trifluoromethylsulfonate; PCC = pyridinium chlorochromate.

In the absence of an aldehyde, the homocondensation side product from the aldol reaction between a zinc enolate (produced by 1,4-addition) and cyclopentenone was obtained in moderate yield (Scheme 2). However, for the copper-catalyzed conjugate addition of diethylzinc to 2-cyclohexenone, this side product was not detected even at higher temperatures. The results demonstrate the difference in reactivity between the five- and six-membered-ring zinc enolates.

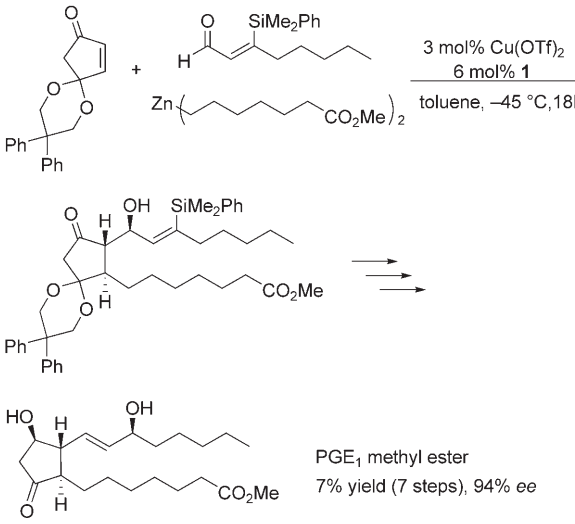
Feringa and co-workers also reported a catalytic enantioselective annulation through a tandem 1,4-addition/aldol cyclization, in which 2-cyclohexenone was treated with acetal-functionalized organozinc reagents in the presence of a copper catalyst prepared in situ from $Cu(OTf)_2$ and chiral ligand **1**.[11] Under these conditions, the cyclohexenone underwent 1,4-addition to form a 3-substituted cyclohexanone, which subsequently underwent acetal hydrolysis in situ and ring closure (aldol cyclization) under acidic conditions to give a bicyclic decalone (Scheme 3). The reaction proceeded for a series of cyclic enones to construct 6,6-, 6,7-, and 6,8-annulated ring systems in good yields and with over 96% *ee* in all the cases examined. However, this protocol was unsatisfactory for the formation of carbobicyclic structures that incorporate a five- as well as a six-membered ring (bicyclo[4.3.0]nonenone skeleton) owing to a lack of highly enantioselective catalysts for the 1,4-addition of organozinc reagents to 2-cyclopentenone at that time. As shown in Scheme 3, a new procedure for 5,6-annulated ring systems was developed. The zinc enolate intermediate from the conjugate addition of diethylzinc to cyclohexenone was treated with allyl acetate and a palladium catalyst to produce the 2,3-disubstituted cyclohexanone in high yield and with 96% *ee*. Subsequent Wacker oxidation of the allyl moiety to the corresponding methyl ketone followed by aldol cyclization provided the 5,6-annulated product in good yield and with 96% *ee* for the major isomer (13:1 d.r.).



Scheme 3. Copper-catalyzed enantioselective tandem 1,4-addition/aldol cyclization versus 1,4-addition/allylation followed by annulation. DMF = *N*,*N*-dimethylformamide.

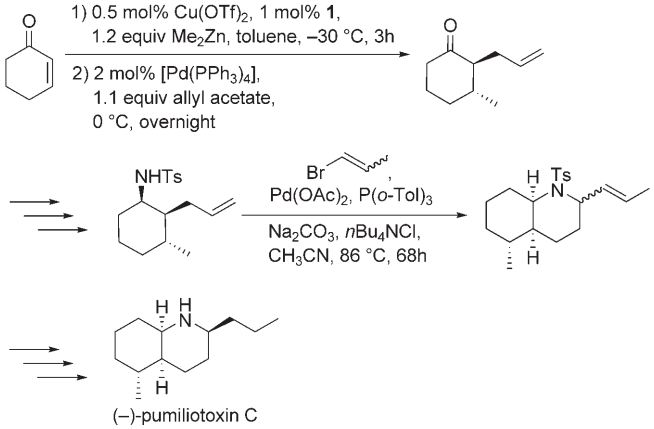
The versatility of the tandem conjugate addition/electrophilic trapping reaction was demonstrated by the application of the catalytic system to the total synthesis of two natural products. With catalytic enantioselective 1,4-addition/aldol tandem reactions as the key step, PGE_1 (prostaglandin E1) methyl ester was obtained with 94% *ee* in 7% overall yield (Scheme 4).[10c,e] In another example, two tandem reactions were carried out for the synthesis of pumiliotoxin C,[12] a potent neurotoxin that acts as a noncompetitive blocker for acetylcholine receptor channels and was first isolated from

© 2006 Wiley-VCH Verlag GmbH & Co. KGaA, Weinheim



Scheme 4. Asymmetric tandem conjugate addition/aldol reaction as the key step in the total synthesis of PGE_1 methyl ester.

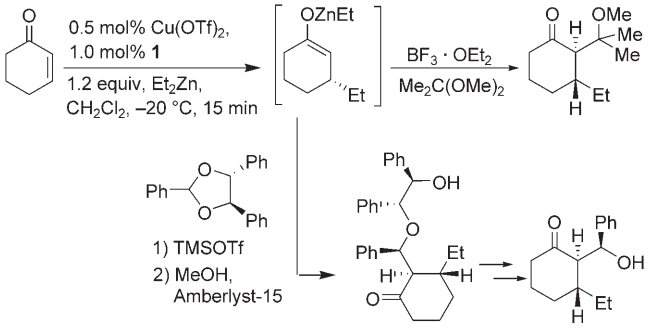
Dendrobates pumilio. The stereoselective construction of the central decahydroquinoline unit of pumiliotoxin C was the major synthetic challenge. However, on the basis of retrosynthetic analysis, the decahydroquinoline unit could be readily and enantioselectively synthesized by initially performing an asymmetric conjugate addition/allylation reaction of 2-cyclohexenone (Scheme 5). After modification of the



Scheme 5. Tandem asymmetric conjugate addition/allylation and tandem Heck/allylation reactions in the total synthesis of (−)-pumiliotoxin C. Ts = p-$CH_3C_6H_4SO_2$; Tol = tolyl.

carbonyl group, a powerful Heck/allylic substitution reaction was applied to initiate the construction of the nitrogen-containing six-membered ring and to create the decahydroquinoline skeleton. A few additional steps completed the total synthesis of pumiliotoxin C.

Alexakis et al. reported that besides aldehydes, Lewis acid activated acetals, ketals, and ortho esters could also be used to functionalize the zinc enolate intermediate to afford aldol-type products.[13a] As shown in Scheme 6, the trapping of the zinc enolate intermediate was carried out with 2,2-dimethoxypropane and $BF_3{\cdot}OEt_2$ to provide the dimethyl-substituted methyl ether product as a single diastereomer. When $PhCH(OMe)_2$ was utilized as electrophile, poor diastereocontrol was observed. To overcome this hurdle and obtain complete stereocontrol, the zinc enolate intermediate was treated with chiral acetals in the presence of TMSOTf. Following cleavage of the trimethylsilyl ether, the alcohol was obtained as a single diastereomer in 66% yield. After removal of the chiral auxiliary in a mild, highly efficient two-step procedure, the *trans,anti* aldol product was obtained in quantitative yield.

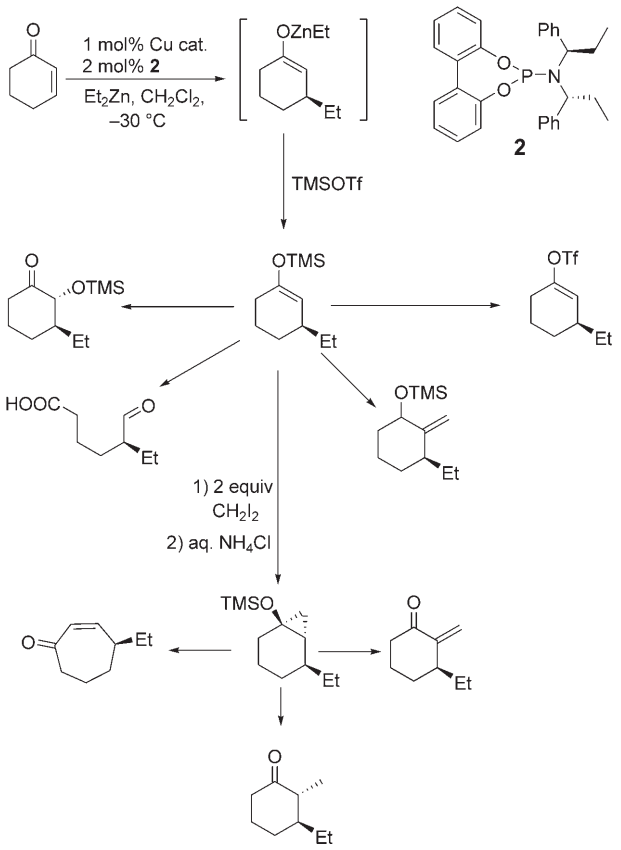


Scheme 6. Tandem asymmetric conjugate addition/aldol reaction using acetals as electrophiles. TMS = trimethylsilyl.

Alexakis and co-workers also utilized silylating agents such as TMSCl and TMSOTf to trap the enantiomerically enriched zinc enolate ($ee > 99\%$) and demonstrated a tandem asymmetric conjugate addition/silylation reaction.[13b] This finding considerably widened the scope of tandem conjugate addition/electrophilic trapping reactions. Many transformations can be readily performed on these silyl enol ethers to prepare many interesting optically active synthons (Scheme 7). Especially when using the double bond of the silyl enol ether as a starting point, the ether generated in situ can be treated with diiodomethane to produce enantiomerically pure cyclopropyl silyl ether.[13c] By this tandem asymmetric conjugate addition/cyclopropanation, a cyclic or linear enone can be converted directly in one pot into a TMS-protected trisubstituted cyclopropanol, which can then be selectively cleaved to yield other useful synthons. This methodology was also successfully applied to the total synthesis of (−)-(*S*,*S*)-clavukerin A and (+)-(*R*,*S*)-isoclavukerin.

Hoveyda and co-workers used the peptidic compounds **3** and **4** as chiral ligands for copper-catalyzed asymmetric conjugate additions of dialkylzinc reagents to afford the desired products in high yields and with high enantioselectivity. Compounds **3** and **4** are among the most efficient and enantioselective ligands for copper-catalyzed conjugate additions reported to date. The catalytic asymmetric procedure delivers zinc enolate intermediates, which can be functionalized with alkyl halides and tosylates to give complex molecules with consecutive stereocenters. As shown in Scheme 8, sequential catalytic conjugate addition/alkylation of cyclic enones gave the tandem products.[14a] Compared with aldehydes, less-reactive electrophiles such as alkyl chlorides and bromides react with difficulty and even the use of alkyl iodides works only under particular reaction conditions

 © 2006 Wiley-VCH Verlag GmbH & Co. KGaA, Weinheim

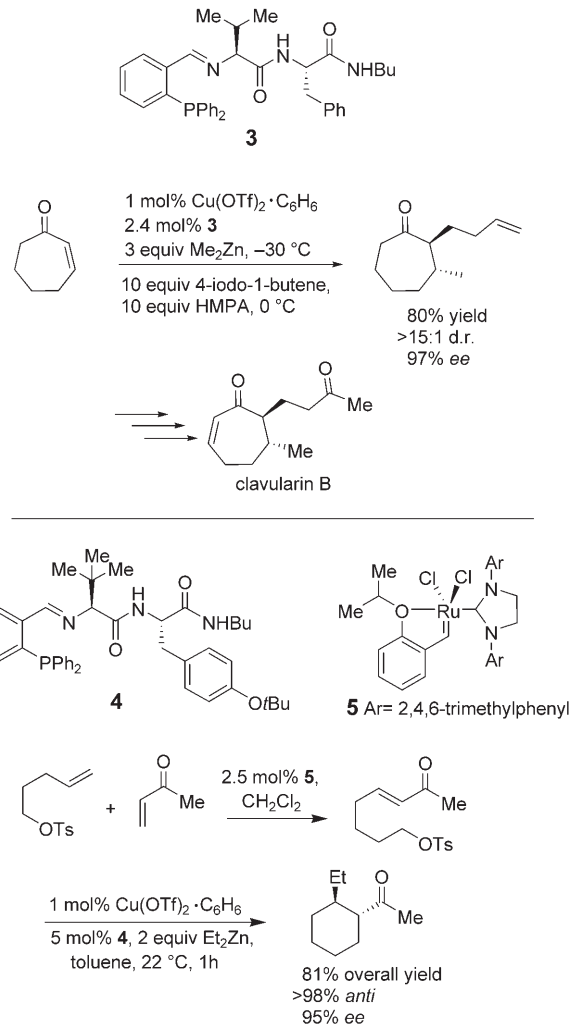


Scheme 7. Copper-catalyzed tandem asymmetric conjugate addition/silylation and conjugate addition/cyclopropanation reactions on the route to various chiral building blocks.

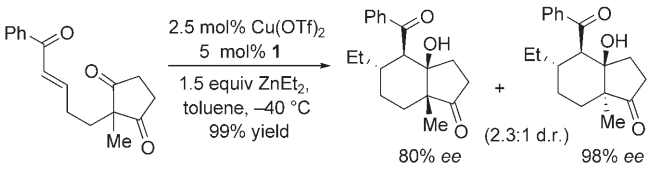
(excess reagent; HMPA additive). After two oxidation steps, the enantioselective synthesis of anticancer drug clavularin B was completed in 42% overall yield from commercially available cycloheptenone (Scheme 8).

By using two different catalysts, sequential catalytic cross-metathesis, asymmetric conjugate addition, and alkylation could also be achieved. In the presence of ruthenium catalyst **5**, 5-tosylpent-1-ene reacted with methyl vinyl ketone to give the corresponding α,β-unsaturated enone, which was treated with a copper catalyst and diethylzinc to provide a cyclohexyl ketone with two vicinal stereogenic centers in high yield and with excellent enantio- and diastereoselectivity. In this process, the zinc enolate intermediate was trapped with the tosylate (Scheme 8).[14b]

Krische and co-workers reported the use of ketones, esters, and nitriles as electrophiles in copper-catalyzed conjugate addition/intramolecular electrophilic trapping reactions.[15] In the presence of catalytic $Cu(OTf)_2/P(OEt)_3$, enone substrates containing pendant ketone, ester, and nitrile moieties reacted with organozinc reagents to afford cyclized products in good to excellent yields and with moderate diastereoselectivities. By using Feringa's phosphoramidite ligand **1** instead of $P(OEt)_3$, the tandem carbon–carbon bond formation was enantioselective under the standard reaction conditions (Scheme 9). Although diastereoselectivity of the reaction was not optimized, a high level of asymmetric induction was nonetheless observed.



Scheme 8. Copper-catalyzed asymmetric conjugate addition/alkylation reactions. HMPA = hexamethylphosphoric triamide.



Scheme 9. Copper-catalyzed asymmetric conjugate addition/aldol reaction.

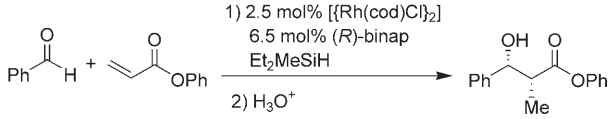
2.1.2. Rhodium-Catalyzed Tandem Transformations

In the copper-catalyzed asymmetric 1,4-addition of organozinc reagents and electrophilic trapping sequence, it is generally recognized that the catalyst operates in the first step (1,4-addition) but is not involved with the second step (electrophilic trapping). Furthermore, the organic groups introduced are limited to alkyl groups (sp^3-hybridized carbon atoms) in most cases, and the reactions must be carried out at very low temperatures, usually below 0 °C. Since Miyaura and co-workers reported non-asymmetric 1,4-addition reactions of organoboron reagents with a phosphine–rhodium complex

 © 2006 Wiley-VCH Verlag GmbH & Co. KGaA, Weinheim

as a catalytic system,[16] many efforts have been directed towards the development of rhodium-catalyzed asymmetric 1,4-addition reactions.[7e–g] These reactions provide a complementary method for the enantioselective introduction of aryl and alkenyl groups (sp^2-hybridized carbon atoms) or hydrogen atoms at the β position of electron-deficient olefins.

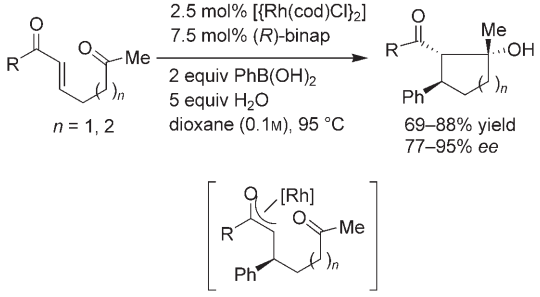
In 2000, Morken and co-workers reported the first rhodium-catalyzed asymmetric conjugate reduction/aldol reaction.[17] A complex derived from $[Rh(cod)Cl]_2$ and (*R*)-binap catalyzed the diastereoselective and enantioselective conjugate reduction/aldol reaction between acrylate esters and aldehydes. The acrylate and aldehyde structure also had an impact on the stereoselectivity. Phenyl acrylate, diethylmethylsilane, and aldehydes were employed, and the *syn* products were preferred over the *anti* products with *syn/anti* ratios of up to 5.1:1. The reaction gave good yields (48–82%) with good to moderate enantioselectivities (45–91% *ee*; Scheme 10). This procedure is believed to proceed by a catalytic cycle that involves an (oxa-π-allyl)rhodium intermediate generated by the hydrometalation of enones. That is, insertion of the acrylate into a Rh–H bond is followed by aldol addition of the derived rhodium enolate to the aldehyde.[18]



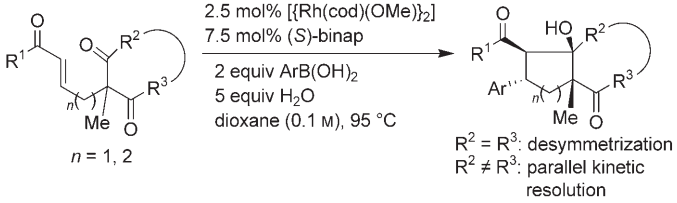
Scheme 10. Rhodium-catalyzed asymmetric reductive aldol reaction. cod = cycloocta-1,5-diene; binap = 2,2′-bis(diphenylphosphianoyl)-1,1′-binaphthyl.

Recently, Krische and co-workers showed that tandem 1,4-addition/aldol reactions of keto-enones with phenylboronic acid could be conducted in the presence of an excess of water.[19a] This is an attractive procedure for the creation of three contiguous stereogenic centers in a single manipulation with high levels of relative and absolute stereochemical control. The optimized conditions are effective for the formation of five- and six-membered-ring products derived from aromatic and aliphatic mono-enone, mono-ketone precursors. High enantioselectivities were observed for methyl-substituted enone precursors (R = Me; Scheme 11), which provided cyclized products with up to 95% *ee*. The reaction is likely to proceed through the (oxa-π-allyl)rhodium intermediate, as established by Hayashi et al.[18b] As the intramolecular reaction of the intermediate with the ketone moiety is faster than protonolysis, the aldol product is obtained in high yields even in the presence of water (Scheme 11).

In light of these promising results, Krische and co-workers explored the applicability of this methodology in the desymmetrization of prochiral diketones by tandem conjugate addition/aldol cyclization.[19b] Gratifyingly, by using the methoxy-bridged dimer $[\{Rh(cod)(OMe)\}_2]$ as a precatalyst (Scheme 12), the desired conjugate addition/aldol products were obtained in high yields (65–95%) with excellent levels of



Scheme 11. Rhodium-catalyzed enantioselective carbometalative aldol cycloreduction.



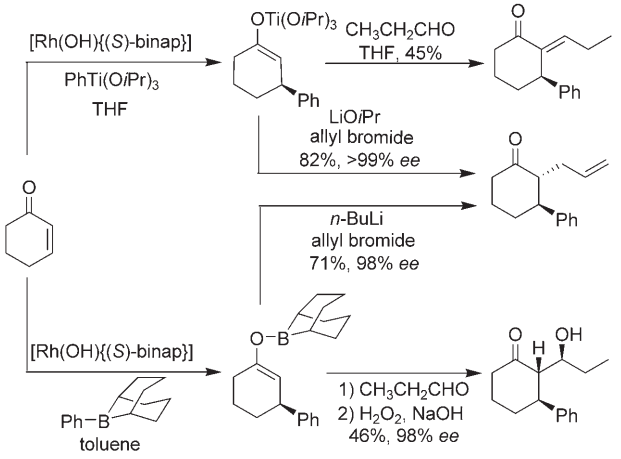
Scheme 12. Enone-dione desymmetrization and parallel kinetic resolution by diastereo- and enantioselective catalytic tandem conjugate addition/aldol cyclization reactions.

diastereo- (> 99:1 d.r.) and enantioselectivities (85–92% *ee*). This highly enantioselective desymmetrization of terminal dione-based electrophiles suggests the feasibility of performing a parallel kinetic resolution of chiral racemic enone-diones. Here, the absolute stereochemistry of the substrate dictates which of the two nonequivalent carbonyl moieties of the appended dione participates in aldolization. These tandem transformations, which result in the formation of two carbon–carbon bonds and four contiguous stereogenic centers, enables the rapid assembly with high levels of stereocontrol of complex polycyclic ring systems from simple precursors.

In the rhodium-catalyzed 1,4-addition of organoboron reagents to α,β-unsaturated ketones as described above, the use of water as a cosolvent plays a key role in the catalytic cycle, which involves hydrolysis of (oxa-π-allyl)rhodium to give hydroxorhodium species and the hydrolyzed 1,4-addition product. However, one major drawback is that the 1,4-addition product is hydrolyzed only at a high temperature. Another limitation is the competing hydrolysis of the organoboronic acid which means that an excess of the boronic acid is required to obtain a reasonable yield of the adduct product. Interestingly, Hayashi and co-workers disclosed a new variant of the tandem 1,4-addition/electrophilic trapping reactions.[20] In these procedures, aryltitanium and arylboron compounds were employed as arylating reagents in a rhodium-catalyzed asymmetric 1,4-addition in nonprotic solvents to form titanium and boron enolates, which are versatile intermediates for the synthesis of enantiomerically enriched compounds with different electrophilic trapping reagents (Scheme 13).[20]

As shown in Scheme 13, the titanium enolate salt from cyclohexenone was treated with lithium isopropoxide and allyl bromide to give (2*R*,3*S*)-*trans*-3-phenyl-2-allylcyclohexanone in 82% yield as a single diastereomer whose enantio-

 © 2006 Wiley-VCH Verlag GmbH & Co. KGaA, Weinheim



Scheme 13. Rhodium-catalyzed enantioselective tandem conjugate addition/electrophilic trapping reactions.

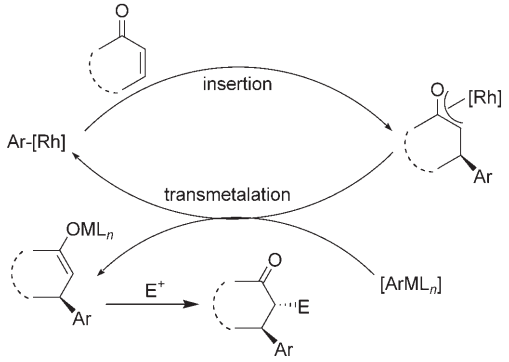
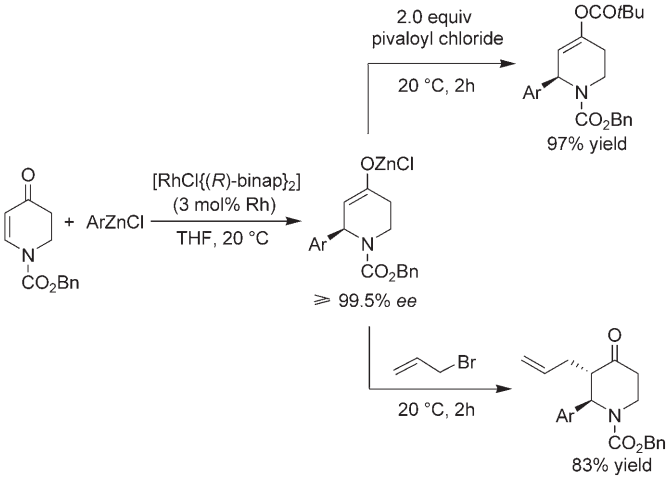


Figure 2. Catalytic cycle of tandem conjugate addition/electrophilic trapping reactions. [Rh] = Rh{(*S*)-binap}; M = Ti(O*i*Pr)$_3$ or 9-(9-borabicyclo[3.3.1]nonyl).

meric purity was over 99%. In the reaction of the titanium enolate with pivaloyl chloride, *O*-acylation took place selectively to give a high yield of the enol ester. Treatment of the titanium enolate with propanal resulted in the formation of the *E*-enone by aldol addition and elimination. Additionally, rhodium-catalyzed asymmetric 1,4-addition with boron reagents that contained substituted phenyl groups successfully led to the formation of chiral boron enolates. Treatment of the boron enolate with *n*-butyllithium at −78 °C followed by reaction with allyl bromide gave (2*R*,3*S*)-*trans*-3-phenyl-2-allylcyclohexanone, as also obtained through the titanium enolate, in 71% yield. One of the most useful reactions of the resulting boronates is the aldol reaction with aldehydes (such as propanal) which is known to proceed through a well-organized transition state to give the *anti* aldol product as a single diastereoisomer (2*S*,3*S*,1′*S*). This aldol reaction of the boron enolate has advantages over the reaction of the corresponding chiral titanium enolate, which gives the dehydration product of the β-hydroxy ketone (see Scheme 13).

Hayashi et al. identified a hydroxorhodium species as the key intermediate in the catalytic cycle of rhodium-catalyzed 1,4-additions in water which is generated by the hydrolysis of an (oxa-π-allyl)rhodium intermediate and undergoes transmetalation to give a phenylrhodium species.[18b] Further mechanistic studies indicated that the catalytic cycle of these new tandem transformations consists of two steps (Figure 2): 1) transmetalation of the aryl group from titanium (or boron) to the (oxa-π-allyl)rhodium intermediate to form an arylrhodium species and the titanium (or boron) enolate and 2) insertion of an enone into the arylrhodium species to form the (oxa-π-allyl)rhodium complex. Finally, reaction of the titanium (or boron) enolate with electrophiles gives *trans* products.

Somewhat later, the same group developed another rhodium-catalyzed asymmetric 1,4-addition reaction of organozinc reagents to 2,3-dihydro-4-pyridones.[21] Note that the asymmetric 1,4-addition of organozinc reagents to 2,3-dihydro-4-pyridones tolerates a sterically and electronically diverse array of arylzinc reagents to afford the products in good yields with excellent enantioselectivities (87–100% yield, *ee* ≥ 99% (*R*)), whereas the addition of [PhTi(O*i*Pr)$_3$] to these substrates gives mixtures of 1,2- and 1,4-adducts. As a zinc enolate is the primary product in this 1,4-addition reaction as established above, it could be further functionalized in one pot by the addition of an electrophile to the reaction mixture. For example, the addition of allyl bromide provided the α-allylated product as a single diastereomer in the *trans* form in high yield (Scheme 14). The use of pivaloyl chloride as the electrophile, however, afforded the *O*-acylated product in excellent yield (97%).



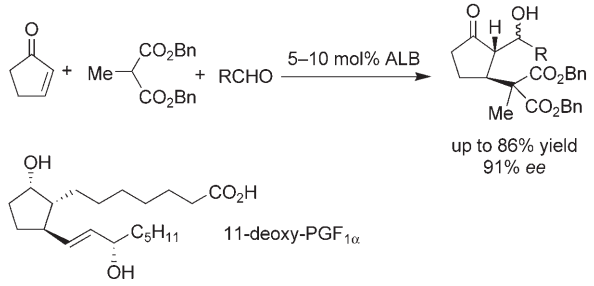
Scheme 14. Rhodium-catalyzed 1,4-addition of organozinc reagents and electrophilic trapping reactions. Bn = benzyl; Ar = Ph.

2.1.3. Other Metal-Catalyzed Asymmetric Tandem Transformations

The strategy of dual activation of the electrophile and the nucleophile has been extensively developed in catalytic asymmetric synthesis over the past decade.[22] Shibasaki and co-workers employed a variety of heterobimetallic complexes as dual-activation catalysts that efficiently promote many asymmetric reactions.[23] Among these heterobimetallic complexes, [AlLi(binol)$_2$] (ALB; binol = binaphthoxide) shows

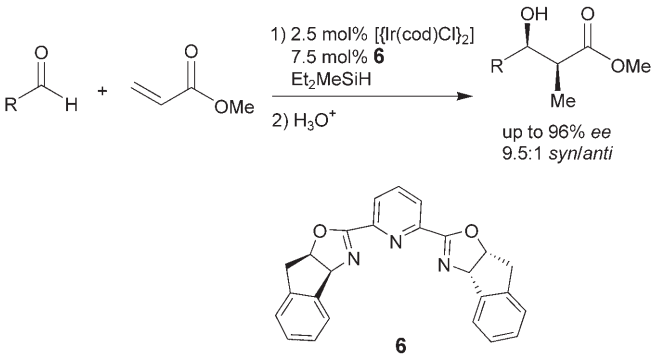
© 2006 Wiley-VCH Verlag GmbH & Co. KGaA, Weinheim

the most interesting chemical reactivities. In particular, this complex catalyzes a tandem Michael/aldol reaction, which gives rise to three-component coupling products with high enantioselectivity even at room temperature.[24] However, other complexes such as $[LaNa_3(binol)_3]$, the alkali-metal-free lanthanum complex, or $[GaNa(binol)_2]$ do not promote this tandem Michael/aldol reaction effectively and give rise only to highly enantiomerically enriched Michael adducts as major products. It was thought that an aluminum enolate would be more stable and undergo much slower protonation. Indeed, the extended lifetime of the aluminum enolate favors the aldol reaction, which proceeds with excellent regiocontrol and considerable selectivity at the newly formed hydroxy group (Scheme 15). Furthermore, this catalytic asymmetric tandem Michael/aldol reaction was employed as the key step in the synthesis of biologically significant compounds, such as the prostaglandin (PG) derivative 11-deoxy-$PGF_{1\alpha}$.[24b]



Scheme 15. Heterobimetallic catalysis of an asymmetric tandem reaction and its application to the synthesis of 11-deoxy-$PGF_{1\alpha}$. R = Ph, $PhCH_2CH_2$, $(CH_2)_5CO_2Me$; ALB = $[AlLi(binol)_2]$.

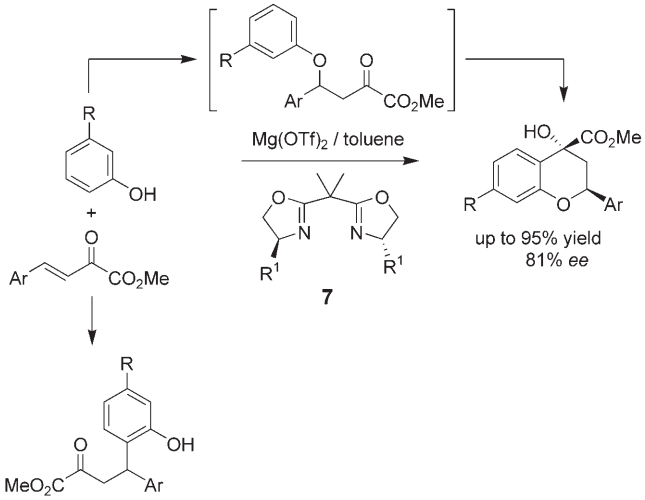
Morken and co-workers extended enantioselective conjugate reduction/aldol reactions to catalytic systems other than rhodium complexes.[17] 2,6-Bis(oxazolinyl)pyridine (PyBox) ligands were used complexed with iridium salts,[25] and the corresponding aminoindanol-derived Indane-PyBox ligand **6** (Scheme 16) was found to be a good ligand. For example, conjugate reduction/aldol reactions catalyzed by $[\{Ir(cod)Cl\}_2]$/Indane-PyBox showed remarkable enantioselectivity with benzaldehyde and α-alkoxy aldehydes, but with simple aldehydes the reaction was less efficient (Scheme 16). The reaction may occur through a similar catalytic cycle as



Scheme 16. Asymmetric reductive aldol reaction catalyzed by Ir/PyBox.

that with rhodium complexes and involve (oxa-π-allyl)iridium intermediates generated by the hydrometalation of enones and subsequent electrophilic trapping.

Jørgensen and co-workers developed an enantio- and diastereoselective catalytic tandem reaction that involves an oxa-Michael addition and subsequent Friedel–Crafts alkylation to provide facile access to optically active functionalized chromanes (Scheme 17).[26] The oxa-Michael reaction is



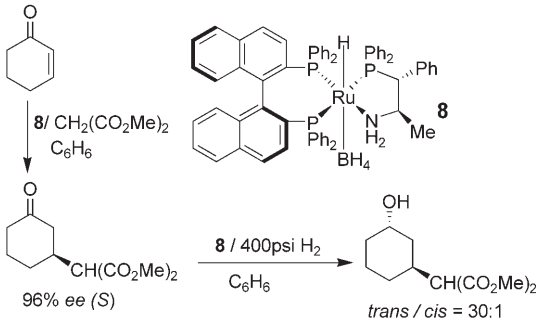
Scheme 17. Catalytic asymmetric tandem transformation versus *C*-conjugate addition. R = MeO, Me_2N; R^1 = *t*Bu, Ph, 1-Naphthyl; Ar = Ph, *p*-FPh, *p*-ClPh, *p*-BrPh.

reversible owing to an equilibrium that favors the starting materials. The second step, the Friedel–Crafts alkylation, is completely diastereoselective as the tandem products are formed as single diastereoisomers. Magnesium triflate was found to be better than other Lewis acids tested, while toluene was the most appropriate solvent. Additionally, bulky 1-naphthyl (1-Nap) bis(oxazolinyl) (NapBox) ligands gave superior results than other ligands. The use of certain bases such as proton sponge—1,8-bis(dimethylamino)naphthalene—led to enhanced enantioselectivities. Unfortunately, the rate of competing *C*-nucleophilic 1,4-addition reactions also increased. Replacement of the methoxy substituent in the nucleophile by the more electron-donating dimethylamine group resulted in a dramatic decrease in enantioselectivity. The more nucleophilic *m*-methoxy-*N*-methylaniline afforded diastereoselectively, but non-enantioselectively, the desired tetrahydroquinoline as the exclusive product.

Following the findings of Noyori and co-workers[27] came reports from two groups that chiral ruthenium amido complexes are active catalysts for the Michael addition of malonates to α,β-unsaturated compounds.[28] In one example, Morris and co-workers employed the borohydride complex [*trans*-RuH(η^1-BH_4){(*S*)-binap}{(*R*,*R*)-Pnor}] (**8**; (*R*,*R*)-Pnor = (1*R*,2*R*)-$PPh_2CHPhCHMeNH_2$) as an enantioselective catalyst for the asymmetric addition of dimethyl malonate to 2-cyclohexenone under mild conditions to produce the corresponding Michael adduct with 96% *ee*.[28c] Note that this system allows a one-pot, tandem asymmetric Michael addi-

 © 2006 Wiley-VCH Verlag GmbH & Co. KGaA, Weinheim

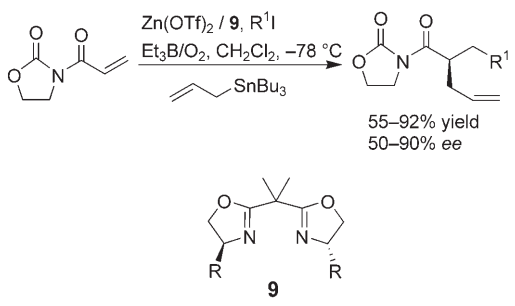
tion/ketone hydrogenation protocol to create two stereogenic centers. The hydrogenation of the Michael addition product of 2-cyclohexene-1-one catalyzed by **8** occurred with excellent diastereoselectivity (*trans/cis* = 30:1) in benzene (Scheme 18).



Scheme 18. Tandem Michael addition/hydrogenation catalyzed by ruthenium complex **8**.

2.2. Conjugate Additions of Nucleophilic Radicals to α,β-Unsaturated Compounds

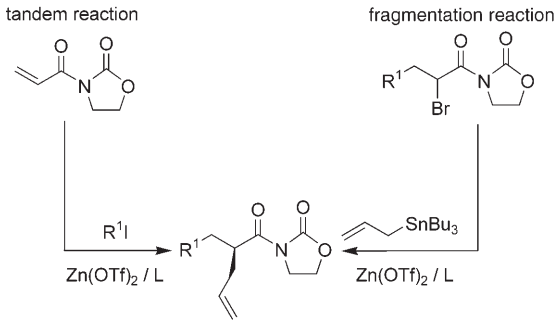
Although radicals are highly reactive short-lived species, their synthetic utility has been properly recognized. Radical reactions have been shown to be compatible with many functional groups, and tedious protection/deprotection steps can quite often be avoided. Recently, enantioselective radical processes have been approached in various ways. Intermolecular conjugate additions of nucleophilic radicals to α,β-unsaturated compounds have been carried out enantioselectively by using chiral Lewis acids.[29] α-Acyl radicals form as intermediates in the conjugate addition of nucleophilic radicals to α,β-unsaturated substrates and can further react with allystannanes. In principle, two stereocenters can be created in this tandem reaction. Porter and co-workers reported an example involving the creation of a single chiral center through the addition of radicals to oxazolidinone acrylate followed by trapping with a stannane (Scheme 19).[30] Zinc triflate was the ideal Lewis acid, whereas zinc chloride, magnesium triflate, and scandium triflate were ineffective, while diethyl ether proved to be better than dichloromethane as the solvent. Further experiments were carried out with CH_2Cl_2/pentane (40:60) mixtures, and the addition of *tert*-



Scheme 19. Introduction of stereocenter at α position through radical addition/trapping sequence. R = Ph; R[1] = *c*Hex, *t*Bu.

butyl radicals gave up to 90% *ee*. High selectivity could be obtained with diethyl ether, although two equivalents of the chiral Lewis acid were required. Tributyltin iodide, which is a weaker Lewis acid than its bromide analogue, did not have a detrimental impact on selectivity. A tetrahedral zinc complex with bidentate chelation to the substrate and the ligand was proposed to account for the observed stereochemistry.

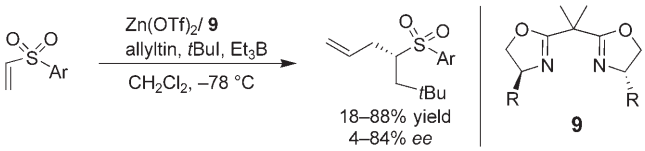
Porter and co-workers made a direct comparison of the stereochemical efficiency of the fragmentation reaction versus the tandem reaction as a function of the steric effect (based on the Taft parameters) for different substituents (Scheme 20).[31a] The results indicated that the tandem



Scheme 20. Influence of steric effects on radical addition/trapping sequence versus fragmentation reactions.

reactions performed better and provided higher levels of enantioselectivity than the fragmentation reactions. This effect could be a result of the tin bromide byproduct catalyzing a nonstereoselective process, as previously observed by the same authors[31b] as well as by Sibi and Ji in their studies.[32]

Sulfones are an interesting class of substrates and have been used in tandem reactions with the generation of a chiral center adjacent to the sulfonyl group (Scheme 21).[33] To



Scheme 21. Enantioselective radical addition/allylation reactions of vinyl sulfones. Ar = 2-pyridyl, 2-(1-methylbenzimidazolyl), 2-(1-benzylbenzimidazolyl); R = *i*Pr, Bn, Ph.

achieve bidentate chelation with a metal center, either pyridyl or benzimidazolyl moieties were also introduced in the substrates. The effect of the N substituent was not apparent. The reaction efficiency was dependent on the amount and nature of the trapping agents employed. Diallyldibutylstannane performed better than all the other stannanes tested, and the use of 10 equivalents of the stannane gave the best results in terms of yield and selectivity. To account for the observed selectivity, a chiral relay model was proposed

© 2006 Wiley-VCH Verlag GmbH & Co. KGaA, Weinheim

(Figure 3). As the sulfonyl oxygen atoms are enantiotopic, they can form diastereotopic complexes with the chiral Lewis acid. Selection at this level, combined with discrimination from the ligand, is then translated into the final enantioselectivities observed in the reactions.[34]

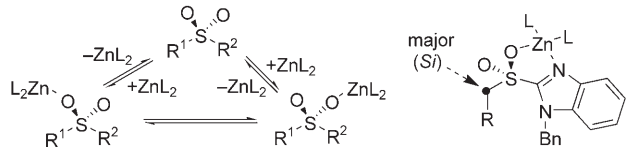
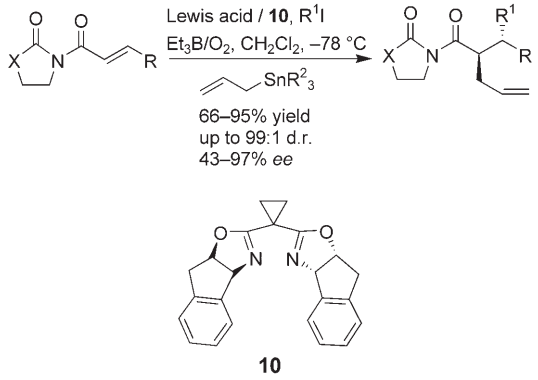


Figure 3. A chiral relay model for the radical addition/trapping sequence with sulfones.

Sibi and Chen demonstrated that the relative and absolute configuration at both the α and β positions could be controlled in intermolecular radical addition/trapping experiments (Scheme 22).[35] Magnesium and copper salts in combination with a chiral bisoxazoline **10** performed better than



Scheme 22. Radical addition/trapping reactions for vicinal stereocenters. X = O, CH_2; R = Ph, Me; R^1 = *c*Hex, *t*Bu, Et, *i*Pr; R^2 = *n*Bu, Ph.

when their zinc/**10** counterparts were used. The use of 30 mol% of the chiral Lewis acid (Mg^{II}/**10** or Cu^{II}/**10**) led to higher selectivities than when stoichiometric amounts were used. Among the magnesium salts, those with an iodide counterion were found to be more effective than those with bromide or perchlorate counterions. Interestingly, copper triflate led to better selectivities with allyltriphenylstannane relative to other stannanes, whereas no such difference was observed with magnesium Lewis acids. The products obtained predominantly have *anti* stereochemistry. Note also that copper triflate and magnesium iodide gave enantiomeric products with the same ligand. The selectivity was dependent on both the size of the radical added and the size of the β substituent. The best selectivities were obtained when a *tert*-butyl radical was added to the β-phenyl-substituted substrate. In the case of crotonate substrates, a change in the template from oxazolidinone to pyrrolidinone led to higher selectivities. The *anti* selectivity was shown to depend mainly on the configuration at the β stereocenter.

3. Organocatalytic Asymmetric Tandem Transformations

In the past few years, asymmetric organocatalytic reactions have emerged as one of the most attractive areas in synthetic organic chemistry.[36] Extensive research into the design and synthesis of small organic molecules and their application in asymmetric catalysis has resulted in a rapid increase in the availability of such organocatalysts. Many examples of diverse organocatalytic reactions with high catalytic activity and enantioselectivity have been reported in recent years. The scope of organocatalytic reactions has been extended considerably, and the "golden age" has already dawned with respect to asymmetric organic catalysis.[36h]

Generally, one organocatalyst can often promote several types of chemical transformations. Therefore, the organocatalytic reaction is ideally suited for the design of tandem processes. Some tandem reactions based on organocatalysis have been reported and are becoming powerful tools in the construction of complex molecular structures in the absence of metals. Among the most widely used organocatalysts are chiral small molecular amines. For catalytic asymmetric Michael addition reactions, chiral amines serve either to activate the Michael acceptor through the formation of an iminium species (Figure 4a) or as bases such that the salt

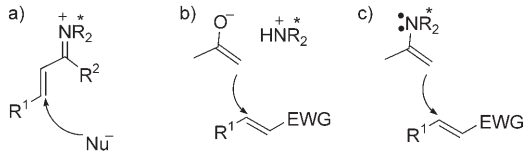
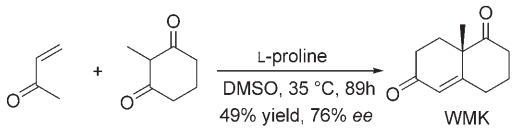


Figure 4. Proposed mechanisms for amine-catalyzed Michael reactions.

formed between the amine and the enolate reacts with the acceptor (Figure 4b). A third mechanism could involve transient activation of the ketone donor through formation of an enamine intermediate (Figure 4c).

In the early 1970s, enantiopure Wieland–Miescher ketone (WMK), which had proven to be a particularly useful building block for the synthesis of a variety of biologically active compounds, was prepared in a two-step processes by treating 2-methylcyclohexane-1,3-dione with methyl vinyl ketone in aqueous acetic acid in a Michael reaction to give 2-methyl-2-(3-oxobutyl)-1,3-cyclohexanedione, which was then subjected to cyclodehydration catalyzed by L-proline to afford WMK with 70% *ee*.[37] Inspired by antibody aldolase-catalyzed one-flask Robinson annulation reactions,[38] Bui and Barbas investigated proline-catalyzed asymmetric tandem Robinson annulation reactions.[39] In the presence of L-proline, a single-operation annulation provided WMK in 49% yield with 76% *ee* (Scheme 23). Thus, by using an enamine-based reaction mechanism, proline could catalyze the entire annulation in one pot to afford the desired ketone with an overall yield and enantiomeric purity similar to that of the original two-step reaction sequence. From the examination of structure–activity relationships, chiral compounds that contain a

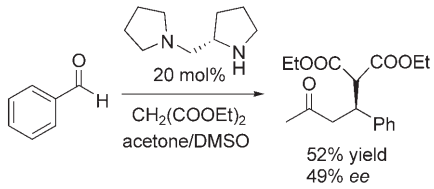
 © 2006 Wiley-VCH Verlag GmbH & Co. KGaA, Weinheim



Scheme 23. L-Proline-catalyzed asymmetric Robinson annulation reaction to form Wieland–Miescher ketone (WMK). DMSO = dimethyl sulfoxide.

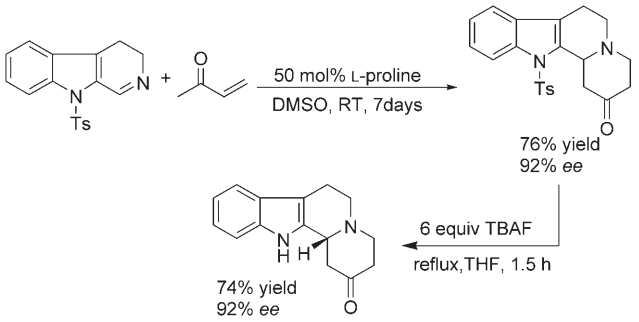
secondary pyrrolidine-type amine and carboxylic acid functionality were found to be the most efficient catalysts for this asymmetric annulation reaction. The carboxylic acid functionality appears to play an important role in the dehydration step.

Barbas and co-workers also reported a tandem Knoevenagel/Michael reaction. Chiral (*S*)-1-(2-pyrrolidinyl)methylpyrrolidine catalyzes the Knoevenagel reaction of aldehydes to yield the alkylidene malonate, which reacts with nucleophiles to afford the final Michael adduct with moderate yield and enantioselectivity in one pot (Scheme 24).[40]



Scheme 24. Organocatalytic asymmetric tandem Knoevenagel/Michael reaction.

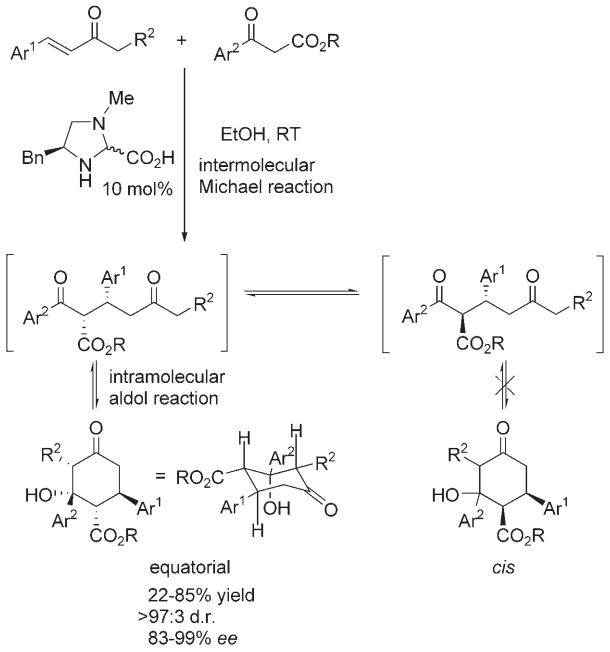
Ohsawa and co-workers presented a proline-catalyzed asymmetric tandem Mannich/Michael reaction (Scheme 25).[41] Asymmetric tandem reaction of methyl vinyl



Scheme 25. L-Proline-catalyzed asymmetric tandem Mannich/Michael reaction. TBAF = tetra-*n*-butylammonium fluoride.

ketone with 9-tosyl-3,4-dihydro-β-carboline promoted by L-proline afforded the tetracyclic precursor, in 76% yield and with 92% *ee*, which was derivatized to provide detosylated product—a versatile precursor for the synthesis of some indole alkaloids such as yohimbine and deserpidine. The presence of water in this system resulted in only retardation of the reaction progress without variation of the stereoselectivity.

Jørgensen and co-workers demonstrated that an imidazolidine catalyst, which is easily prepared from phenylalanine, could promote the tandem Michael/aldol reaction of α,β-unsaturated ketones and a broad range of aromatic and heteroaromatic β-keto esters to provide cyclohexanones that comprise three or four contiguous stereogenic centers with excellent enantio- and diastereoselectivity, although the yields obtained were only moderate (Scheme 26).[42] Fortu-

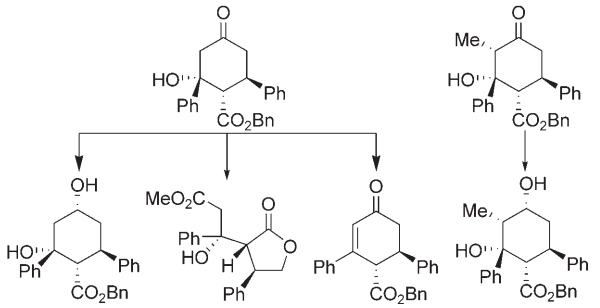


Scheme 26. Asymmetric tandem Michael/aldol reaction catalyzed by a chiral imidazolidine.

nately, in all cases only a single diastereomer of the tandem adduct was formed. In this tandem sequence, the intermolecular Michael reaction was followed by an intramolecular aldol reaction step. For two stereogenic carbon centers of the adduct formed from the initial Michael addition step, only the Ar^1-substituted stereogenic carbon center is stable. As the proton is highly acidic, another stereogenic carbon center, which comprises the ester substituent, undergoes epimerization in the reaction mixture. Therefore the initial Michael adduct exists as a mixture of *syn* and *anti* isomers. Interestingly, the intramolecular aldol reaction proceeds highly diastereoselectively to form a six-membered ring such that all large substituents are equatorial and thus controlled by the stable stereogenic center formed in the initial Michael reaction. The high-energy *cis* diastereomers are not observed in the course of the reaction. In this tandem reaction, the catalyst could play three roles in the reaction: 1) it activates the Michael acceptors by formation of an iminium ion; 2) it generates the active Michael donor by deprotonation of the β-keto ester; and 3) it acts as a base in the intramolecular aldol reaction. However, the possibility that the intramolecular aldol reaction is catalyzed by the imidazolidine compound and proceeds through an enamine mechanism cannot be completely excluded.

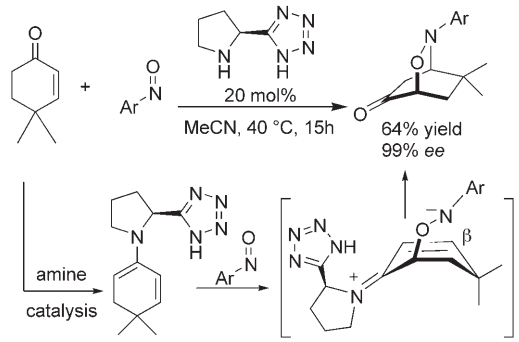
© 2006 Wiley-VCH Verlag GmbH & Co. KGaA, Weinheim

Note that these tandem adducts can also serve as useful starting materials and be transformed into a variety of optically active building blocks with up to five contiguous stereogenic centers in one or two simple high-yielding steps (Scheme 27).[42] The chiral building blocks are amenable to further synthetic elaboration.



Scheme 27. Optically active building blocks derived from chiral cyclohexanones.

Yamamoto et al. recently reported a very interesting enantioselective tandem *O*-nitroso aldol/Michael addition reaction catalyzed by a pyrrolidine-based tetrazole (Scheme 28).[43] They showed that enamine catalysis can be



Scheme 28. Enantioselective tandem *O*-nitroso aldol/Michael addition reaction.

used to promote the *O*-nitroso aldol process and generate the Michael donor (aminooxy anion) in situ for reaction with the β carbon atom of an iminium salt that adopts a boat conformation. As iminium salts are significantly more reactive than the corresponding α,β-unsaturated ketones, cyclization proceeds smoothly to form the bicyclic product. This tandem reaction is applicable to various aromatic nitroso compounds and affords nitroso Diels–Alder adducts in moderate yield with complete regio- and stereocontrol. The enantioselectivity was uniformly high, at above 98% *ee*.

4. Summary and Outlook

Catalytic asymmetric tandem reactions triggered by conjugate additions have been successfully promoted by chiral metal complexes as well as some organocatalysts and have proved to be a powerful tool in the construction of complex molecular structures with multistereocenters in one-pot reactions. Some catalytic systems seem to be impressive and promising. Examples are the copper-catalyzed 1,4-addition of organozinc reagents and electrophilic trappings, the rhodium-catalyzed conjugate addition of arylmetallic reagents and subsequent electrophilic reactions, and several organocatalytic processes. Although these are important achievements, more research is necessary. There is an increasing interest in catalytic asymmetric tandem reactions in both academic research and industrial application because this methodology promises efficiency in the construction of complex molecules as well as economy in terms of the consumption of reagents and purification of products. Consequently it is an exciting area in catalytic asymmetric synthesis, and one can foresee that many more new catalytic asymmetric tandem transformations will be developed in the not-too-distant future.[44]

We gratefully acknowledge Professor Dr. Manfred T. Reetz (Max-Planck-Institut für Kohlenforschung) and Dr. Dominique Cahard (UMR 6014CNRS de l'IRCOF, Université de Rouen) for their helpful discussions and comments. We also thank the referees of this article for their suggestions.

Received: January 18, 2005
Published online: November 15, 2005

[1] a) *Comprehensive Asymmetric Catalysis* (Eds.: E. N. Jacobsen, A. Pfaltz, H. Yamamoto), Springer, Berlin, **1999**; b) *Catalytic Asymmetric Synthesis, 2nd ed.* (Ed.: I. Ojima), Wiley-VCH, New York, **2000**; c) W. S. Knowles, *Angew. Chem.* **2002**, *114*, 2096; *Angew. Chem. Int. Ed.* **2002**, *41*, 1998; d) R. Noyori, *Angew. Chem.* **2002**, *114*, 2108; *Angew. Chem. Int. Ed.* **2002**, *41*, 2008; e) K. B. Sharpless, *Angew. Chem.* **2002**, *114*, 2126; *Angew. Chem. Int. Ed.* **2002**, *41*, 2024.

[2] a) H.-U. Blaser, *Adv. Synth. Catal.* **2002**, *344*, 17; b) H.-U. Blaser, *Chem. Commun.* **2003**, 293–296; c) M. Breuer, K. Ditrich, T. Habicher, B. Hauer, M. Keßeler, R. Stürmer, T. Zelinski, *Angew. Chem.* **2004**, *116*, 806; *Angew. Chem. Int. Ed.* **2004**, *43*, 788.

[3] For a special issue on enantioselective catalysis, see: *Chem. Rev.* **2003**, *103*(8).

[4] P. Perlmutter, *Conjugate Addition Reactions in Organic Synthesis*, Tetrahedron Organic Chemistry, Ser. 9, Pergamon, Oxford, **1992**.

[5] a) B. E. Rossiter, N. M. Swingle, *Chem. Rev.* **1992**, *92*, 771; b) N. Krause, *Angew. Chem.* **1998**, *110*, 295; *Angew. Chem. Int. Ed.* **1998**, *37*, 283; c) S. C. Jha, N. N. Joshi, *ARKIVOC* **2002**, (VII), 167; d) *Applied Homogeneous Catalysis by Organometallic Complexes, 2nd ed.* (Eds.: B. Cornils, W. A. Herrmann), Wiley-VCH, Weinheim, **2002**.

[6] a) T.-L. Ho, *Tandem Organic Reactions*, New York, Wiley, **1992**; b) L. F. Tietze, *Chem. Rev.* **1996**, *96*, 115; c) K. C. Nicolaou, T. Montagnon, S. A. Snyder, *Chem. Commun.* **2003**, 551.

[7] a) E. V. Gorobets, M. S. Mifakhov, F. A. Valeev, *Russ. Chem. Rev.* **2000**, *69*, 1001; b) B. L. Feringa, *Acc. Chem. Res.* **2000**, *33*, 346; c) N. Krause, A. Hoffmann-Röder, *Synthesis* **2001**, 171; d) A. Alexakis, C. Benhaim, *Eur. J. Org. Chem.* **2002**, 3221; e) T. Hayashi, *Synlett* **2001**, 879; f) K. Fagnou, M. Lautens, *Chem. Rev.* **2003**, *103*, 169; g) T. Hayashi, K. Yamasaki, *Chem. Rev.* **2003**, *103*, 2829; h) A. Ajamian, J. L. Gleason, *Angew. Chem.* **2004**, *116*, 3842; *Angew. Chem. Int. Ed.* **2004**, *43*, 3754.

[8] Stoichiometric tandem vicinal difunctionalizations: for β addition to α,β-unsaturated carbonyl substrates followed by α functionalization, see: a) M. J. Chapdelaine, M. Hulce, *Org. React.*

 © 2006 Wiley-VCH Verlag GmbH & Co. KGaA, Weinheim

1990, *38*, 225; for copper-catalyzed diastereoselective additions of diethylzinc to α,β-unsaturated ketones followed by electrophilic trapping, see: b) M. Kitamura, T. Miki, K. Nalano, R. Noyori, *Tetrahedron Lett.* **1996**, *37*, 5141; c) M. Kitamura, T. Miki, K. Nalano, R. Noyori, *Bull. Chem. Soc. Jpn.* **2000**, *73*, 999.

[9] a) A. Alexakis in *Transition Metal Catalysed Reaction*s (Eds.: S.-I. Murahashi, S. G. Davies), IUPAC Blackwell Science, Oxford, **1999**, p. 303; b) T. Ibuka, *Organocopper Reagents in Organic Synthesis*, Rose Press, Osaka, **2000**; c) N. Krause, *Modern Organocopper Chemistry*, Wiley-VCH, Weinheim, **2002**.

[10] a) B. L. Feringa, M. Pineschi, L. A. Arnold, R. Imbos, A. H. M. de Vries, *Angew. Chem.* **1997**, *109*, 2773; *Angew. Chem. Int. Ed. Engl.* **1997**, *36*, 2620; b) E. Keller, J. Maurer, R. Naasz, T. Schrader, A. Meetsma, B. L. Feringa, *Tetrahedron: Asymmetry* **1998**, *9*, 2409; c) L. A. Arnold, R. Naasz, A. J. Minnaard, B. L. Feringa, *J. Am. Chem. Soc.* **2001**, *123*, 5841; d) A. Mandoli, L. A. Arnold, P. Salvadori, B. L. Feringa, *Tetrahedron: Asymmetry* **2001**, *12*, 1929; e) L. A. Arnold, R. Naasz, A. J. Minnaard, B. L. Feringa, *J. Org. Chem.* **2002**, *67*, 7244.

[11] a) R. Naasz, L. A. Arnold, M. Pineschi, E. Keller, B. L. Feringa, *J. Am. Chem. Soc.* **1999**, *121*, 1104; b) M. Pineschi, F. D. Moro, F. Gini, A. J. Minnaard, B. L. Feringa, *Chem. Commun.* **2004**, 1244.

[12] E. W. Dijk, L. Panella, P. Pinho, R. Naasz, A. Meetsma, A. J. Minnaard, B. L. Feringa, *Tetrahedron* **2004**, *60*, 9687.

[13] a) A. Alexakis, G. P. Trevitt, G. Bernardinelli, *J. Am. Chem. Soc.* **2001**, *123*, 4358; b) O. Knopff, A. Alexakis, *Org. Lett.* **2002**, *4*, 3835; c) A. Alexakis, S. March, *J. Org. Chem.* **2002**, *67*, 8753.

[14] a) S. J. Degrado, H. Mizutani, A. H. Hoveyda, *J. Am. Chem. Soc.* **2001**, *123*, 755; b) H. Mizutani, S. J. Degrado, A. H. Hoveyda, *J. Am. Chem. Soc.* **2002**, *124*, 779.

[15] K. Agapiou, D. F. Cauble, M. J. Krische, *J. Am. Chem. Soc.* **2004**, *126*, 4528.

[16] M. Sakai, H. Hayashi, N. Miyaura, *Organometallics* **1997**, *16*, 4229.

[17] S. J. Taylor, M. O. Duffey, J. P. Morken, *J. Am. Chem. Soc.* **2000**, *122*, 4528.

[18] a) Rhodium enolates are known to undergo aldol addition reactions; see: G. A. Slough, R. G. Bergman, C. H. Heathcock, *J. Am. Chem. Soc.* **1989**, *111*, 938; b) T. Hayashi, M. Takahashi, Y. Takaya, M. Ogasawara, *J. Am. Chem. Soc.* **2002**, *124*, 5052.

[19] a) D. F. Cauble, J. D. Gipson, M. J. Krische, *J. Am. Chem. Soc.* **2003**, *125*, 1110; b) B. M. Bocknack, L.-C. Wang, M. J. Krische, *Proc. Natl. Acad. Sci. USA* **2004**, *101*, 5421.

[20] a) K. Yoshida, M. Ogasawara, T. Hayashi, *J. Am. Chem. Soc.* **2002**, *124*, 10984; b) T. Hayashi, N. Tokunaga, K. Yoshida, J. W. Han, *J. Am. Chem. Soc.* **2002**, *124*, 12102; c) K. Yoshida, M. Ogasawara, T. Hayashi, *J. Org. Chem.* **2003**, *68*, 1901.

[21] a) R. Shintani, N. Tokunaga, H. Doi, T. Hayashi, *J. Am. Chem. Soc.* **2004**, *126*, 6240; b) for rhodium-catalyzed asymmetric 1,6-addition and electrophilic trapping, see: T. Hayashi, N. Tokunaga, K. Inoue, *Org. Lett.* **2004**, *6*, 305.

[22] J.-A. Ma, D. Cahard, *Angew. Chem.* **2004**, *116*, 4666; *Angew. Chem. Int. Ed.* **2004**, *43*, 4566.

[23] a) M. Shibasaki, H. Sasai, T. Arai, *Angew. Chem.* **1997**, *109*, 1290; *Angew. Chem. Int. Ed. Engl.* **1997**, *36*, 1236; b) M. Shibasaki, N. Yoshikawa, *Chem. Rev.* **2002**, *102*, 2187; c) M. Shibasaki, M. Kanai, K. Funabashi, *Chem. Commun.* **2002**, 1989.

[24] a) T. Arai, H. Sasai, K. Aoe, K. Okamura, T. Date, M. Shibasaki, *Angew. Chem.* **1996**, *108*, 103; *Angew. Chem. Int. Ed. Engl.* **1996**, *35*, 104; b) K. Yamada, T. Arai, H. Sasai, M. Shibasaki, *J. Org. Chem.* **1998**, *63*, 3666.

[25] C.-X. Zhao, M. O. Duffey, S. J. Taylor, J. P. Morken, *Org. Lett.* **2001**, *3*, 1829.

[26] H. L. van Lingen, W. Zhang, T. Hansen, F. P. J. T. Rutjes, K. A. Jørgensen, *Org. Biomol. Chem.* **2003**, *1*, 1953.

[27] a) T. Ohkuma, M. Koizumi, K. Muñiz, G. Hilt, C. Kabuto, R. Noyori, *J. Am. Chem. Soc.* **2002**, *124*, 6508; b) C. A. Sandoval, T. Ohkuma, K. Muñiz, R. Noyori, *J. Am. Chem. Soc.* **2003**, *125*, 13490.

[28] a) M. Watanabe, K. Murata, T. Ikariya, *J. Am. Chem. Soc.* **2003**, *125*, 7508; b) M. Watanabe, A. Ikagawa, H. Wang, K. Murata, T. Ikariya, *J. Am. Chem. Soc.* **2004**, *126*, 11148; c) R. Guo, R. H. Morris, D. Song, *J. Am. Chem. Soc.* **2005**, *127*, 516.

[29] a) *Stereochemistry of Radical Reactions: Concepts, Guidelines, and Synthetic Applications* (Eds.: D. P. Curran, N. A. Porter, B. Giese), VCH, Weinheim, **1996**; b) M. P. Sibi, N. A. Porter, *Acc. Chem. Res.* **1999**, *32*, 163; c) M. P. Sibi, T. R. Rheault, *Radicals in Organic Synthesis, Vol. 1* (Eds.: P. Renaud, M. P. Sibi), Wiley-VCH, Weinheim, **2001**, p. 461; d) M. P. Sibi, S. Manyem, J. Zimmerman, *Chem. Rev.* **2003**, *103*, 3263, and references therein.

[30] J. H. Wu, R. Radinov, N. A. Porter, *J. Am. Chem. Soc.* **1995**, *117*, 11029.

[31] a) J. H. Wu, G. R. Zhang, N. A. Porter, *Tetrahedron Lett.* **1997**, *38*, 2067; b) N. A. Porter, J. H. Wu, G. R. Zhang, A. D. Reed, *J. Org. Chem.* **1997**, *62*, 6702.

[32] M. P. Sibi, J. Ji, *J. Am. Chem. Soc.* **1996**, *118*, 3063.

[33] Y. Watanabe, N. Mase, R. Furue, T. Toru, *Tetrahedron Lett.* **2001**, *42*, 2981.

[34] O. Corminboeuf, L. Quaranta, P. Renaud, M. Liu, C. P. Jaspere, M. P. Sibi, *Chem. Eur. J.* **2003**, *9*, 28–35.

[35] M. P. Sibi, J. Chen, *J. Am. Chem. Soc.* **2001**, *123*, 9472.

[36] For reviews on organocatalysis, see: a) B. List, *Synlett* **2001**, 1675; b) H. Groger, J. Wilken, *Angew. Chem.* **2001**, *113*, 545; *Angew. Chem. Int. Ed.* **2001**, *40*, 529; c) P. I. Dalko, L. Moisan, *Angew. Chem.* **2001**, *113*, 3840; *Angew. Chem. Int. Ed.* **2001**, *40*, 3726; d) E. R. Jarvo, S. J. Miller, *Tetrahedron* **2002**, *58*, 2481; e) B. List, *Tetrahedron* **2002**, *58*, 5573; f) M. Movassaghi, E. N. Jacobsen, *Science* **2002**, *298*, 1904; g) R. O. Duthaler, *Angew. Chem.* **2003**, *115*, 1005; *Angew. Chem. Int. Ed.* **2003**, *42*, 975; h) P. I. Dalko, L. Moisan, *Angew. Chem.* **2004**, *116*, 5248; *Angew. Chem. Int. Ed.* **2004**, *43*, 5138; i) For a special issue on organocatalysis, see: *Acc. Chem. Res.* **2004**, *37*(8).

[37] a) U. Eder, G. Sauer, R. Wiechert, *Angew. Chem.* **1971**, *83*, 492; *Angew. Chem. Int. Ed. Engl.* **1971**, *10*, 496; b) Z. G. Hajos, D. R. Parrish, *J. Org. Chem.* **1974**, *39*, 1615; c) P. Buchschacher, A. Fürst, *Org. Synth.* **1986**, *63*, 37.

[38] a) G. Zhong, T. Hoffmann, R. A. Lerner, S. Danishefsky, C. F. Barbas III, *J. Am. Chem. Soc.* **1997**, *119*, 8131; b) B. List, R. A. Lerner, C. F. Barbas III, *Org. Lett.* **1999**, *1*,59.

[39] T. Bui, C. F. Barbas III, *Tetrahedron Lett.* **2000**, *41*, 6951.

[40] J. M. Betancort, K. Sakthivel, R. Thayumanavan, C. F. Barbas III, *Tetrahedron Lett.* **2001**, *42*, 4441.

[41] T. Itoh, M. Yokoya, K. Miyauchi, K. Nagata, A. Ohsawa, *Org. Lett.* **2003**, *5*, 4301.

[42] a) N. Halland, P. S. Aburel, K. A. Jørgensen, *Angew. Chem.* **2004**, *116*, 1292; *Angew. Chem. Int. Ed.* **2004**, *43*, 1272; b) J. Pulkkinen, P. S. Aburel, N. Halland, K. A. Jørgensen, *Adv. Synth. Catal.* **2004**, *346*, 1077.

[43] Y. Yamamoto, N. Momiyama, H. Yamamoto, *J. Am. Chem. Soc.* **2004**, *126*, 5962.

[44] Note added in proof: After this manuscript was accepted, four examples on catalytic asymmetric tandem transformations involving conjugate addition appeared; see: a) K. C. Nicolaou, W. Tang, P. Dagneau, R. Faraoni, *Angew. Chem.* **2005**, *117*, 3942; *Angew. Chem. Int. Ed.* **2005**, *44*, 3874; b) M. K. Brown, S. J. Degrado, A. H. Hoveyda, *Angew. Chem.* **2005**, *117*, 5440; *Angew. Chem. Int. Ed.* **2005**, *44*, 5306; c) L. Dong, Y.-J. Xu, L.-F. Cun, X. Cui, A.-Q. Mi, Y.-Z. Jiang, L.-Z. Gong, *Org. Lett.* **2005**, *7*, 4285; d) P. V. Ramachandran, S. Madhi, L. Bland-Berry, M. V. Ram Reddy, M. J. O'Donnell, *J. Am. Chem. Soc.* **2005**, *127*, 13450.

 © 2006 Wiley-VCH Verlag GmbH & Co. KGaA, Weinheim

M. Schädel

DOI: 10.1002/anie.200461072

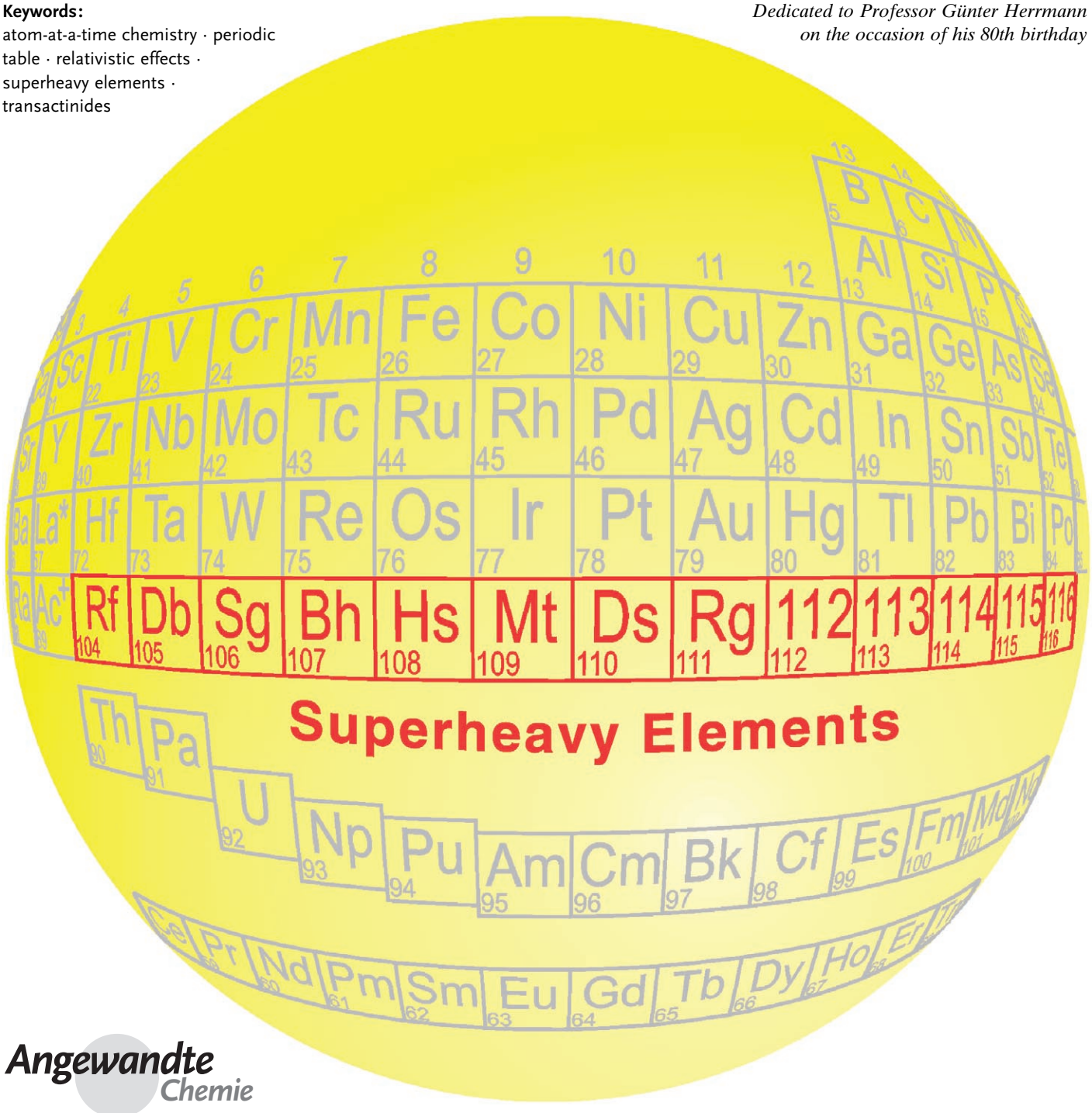
Superheavy Elements

Chemistry of Superheavy Elements

*Matthias Schädel**

Keywords:
atom-at-a-time chemistry · periodic table · relativistic effects · superheavy elements · transactinides

Dedicated to Professor Günter Herrmann on the occasion of his 80th birthday



© 2006 Wiley-VCH Verlag GmbH & Co. KGaA, Weinheim

The number of chemical elements has increased considerably in the last few decades. Most excitingly, these heaviest, man-made elements at the far-end of the Periodic Table are located in the area of the long-awaited superheavy elements. While physical techniques currently play a leading role in these discoveries, the chemistry of superheavy elements is now beginning to be developed. Advanced and very sensitive techniques allow the chemical properties of these elusive elements to be probed. Often, less than ten short-lived atoms, chemically separated one-atom-at-a-time, provide crucial information on basic chemical properties. These results place the architecture of the far-end of the Periodic Table on the test bench and probe the increasingly strong relativistic effects that influence the chemical properties there. This review is focused mainly on the experimental work on superheavy element chemistry. It contains a short contribution on relativistic theory, and some important historical and nuclear aspects.

From the Contents

1. Introduction and Historical Remarks 369
2. Nuclear Aspects 372
3. Atom-at-a-Time Chemistry 374
4. Objectives for Superheavy Element Chemistry 375
5. Experimental Techniques 376
6. Chemical Properties 380
7. Summary and Perspectives 394

1. Introduction and Historical Remarks

How many chemical elements do we know? How many elements are sufficiently chemically characterized to justify their position in the Periodic Table? Simple questions at every chemist should be able to answer. But do you—do we—really know?

The race for new elements beyond uranium started in the mid-1930s involving groups in Rome, Berlin, and Paris. Among the mistakes which led these scientists astray, were presumptions about the structure of the Periodic Table at its far end—the transuranium elements were assumed to belong to Group 7 and the following Groups. The unexpected discovery of nuclear fission[1] marked the first obstacle, and, at the same time, brought new insight and opportunities[2,3]. Soon after, the first transuranium elements, neptunium and plutonium were synthesized. The road to the discovery of heavier elements, successfully applied in the synthesis and separation of americium and curium, was opened when Seaborg introduced the actinide concept.[4] This drastically revised the Periodic Table (see ref. [5,6] for an account of this development, and ref. [7] for a detailed summary of the chemistry of the actinides, thorium through lawrencium—elements with atomic numbers $Z = 90$–103—which follow actinium in the "actinide series", and ref. [8] for a complete coverage of the chemistry of transactinide elements).

The idea of the existence of chemical elements much heavier than uranium emerged very early, at first as illusionary dreams in science-fiction literature. It was not until the mid-1950s—when much was learned about the atomic nucleus from investigations of its decay especially its fission properties—that a scientifically sound discussion of the possible existence of nuclei dubbed "superheavy" began with contributions by John Wheeler[9] and Gertrude Scharff-Goldhaber.[10] After the early success of treating the atomic nucleus as a charged liquid drop (liquid-drop model) in describing the nuclear fission process[11] a new quality appears with the quantized treatment of individual nucleons—protons and neutrons—in nuclear shell models. Similar to electrons in atoms and molecules, and based on the same quantum mechanical law, protons and neutrons form closed shells with "magic numbers", for example, 2, 8, 20, 28, 50, and 82. As with atoms having closed electron shells, nuclei with closed shells exhibit an extra and sometimes very pronounced stability (see ref. [12] and references therein for a concise discussion of the liquid-drop model and the shell contributions).

In the mid-1960s, this nuclear-shell theory received a large boost from computer calculations based upon these new theoretical understandings of the atomic nucleus. Until 1965 it was conceivable that superheavy elements may exist around $Z = 126$ (see Myers and Swiatecki's calculations of nuclear masses and deformations, ref. [13]). However, from then on, new results focused on the $Z = 114$ nucleus with a neutron number of $N = 184$ as the center of an "island of stability". Contributions came from Sobiczewski and co-workers[14] and, during a conference at Lysekil[15] in 1966, from Meldner[16] and others.[15]). First estimates[17–22] yielded relatively long half-lives—as long as a billion years! These times encouraged the search for superheavy elements (SHE) and their investigation with chemical techniques. Among experimentalists, the hunt started with searches for superheavy elements both in nature and at accelerators (see refs. [12,23–28] for reviews of this early phase work).

At about the same time, the first Dirac–Fock and Dirac–Fock–Slater calculations were performed for atoms to determine the electronic structure of superheavy elements.[29–34] These results are summarized in ref. [35] They show that extrapolating chemical properties along groups of elements in

[*] Dr. M. Schädel
KPII–Kernchemie
Gesellschaft für Schwerionenforschung mbH
Planckstrasse 1, 64291 Darmstadt (Germany)
Fax: (+49) 6159-71-2903
E-mail: m.schaedel@gsi.de

© 2006 Wiley-VCH Verlag GmbH & Co. KGaA, Weinheim

the Periodic Table could be a valid approach for estimating the chemical properties of superheavy elements. Simultaneously, the importance of a relativistic treatment of the electronic orbitals was recognized. Several authors discussed relativistic effects which might result in unexpected chemical properties; see ref. [36–39] One of the articles was entitled "*Are elements 112, 114, and 118 relatively inert gases?*".[40] In the last decade a breakthrough towards the theoretical predictions of chemical properties was achieved with the development of relativistic quantum molecular theories applied for heavy and superheavy elements; reviews are given in.[41–44]

Let us come back to the question, how many elements do we know today? To answer this we have to be aware that the "discovery" of an element 1) "is not always a single, simply identifiable event or even culmination of a series of researches … but may rather be the product of several series of investigations … "[45] and 2) that the judgment of what is sufficient evidence to convince the scientific community that the formation of a new element has, indeed, been established, may vary from group to group.[45] Because of conflicting discovery claims and associated disputes over the naming of the elements, a working group was jointly established in 1986 by the International Union of Pure and Applied Physics (IUPAP) and the International Union of Pure and Applied Chemistry (IUPAC). At first, this Transfermium Working Group (TWG) established a set of criteria that must be satisfied before the discovery of a new element is recognized. Secondly, beginning with element 101, it evaluated all discovery claims until the year 1991.[45] This work was continued by the IUPAC/IUPAP Joint Working Party (JWP). Based on their recent report, the last "discovered" chemical element[46] has atomic number 111; synthesized and identified at the Gesellschaft für Schwerionenforschung (GSI) by Hofmann et al.[47] in 1995 and recently substantiated[48] and confirmed.[49,50] Following a proposal by the discoverers, the IUPAC has named element 111 roentgenium with the symbol Rg[51] just one year after element 110 was baptized darmstadtium, Ds;[52] to honor the city of Darmstadt (Germany) where the GSI is located. The official IUPAC Periodic Table presently ends at element 111.

To assure credit for Hofmann et al.,[48,53] for the discovery of element 112—this experiment was again performed at the recoil separator SHIP at GSI's UNILAC accelerator—the JWP[46] has requested a confirmation experiment. The findings by the SHIP group were strongly supported by results from the first chemical separation and investigation of element 108 (this experiment will be discussed in detail in the chemistry Section of this Review).[54] A direct confirmation of the production and the decay of the isotope ^{277}112 was obtained by Morita and co-workers[55] at The Institute of Physical and Chemical Research (RIKEN) in Wako (Japan) with the same technique as used for elements 110 and 111.[49] With high confidence, we can anticipate that the discovery of element 112 will be accepted soon and that the assigned priority for the discovery will go to the SHIP group. Reviews of this group's work, including the discoveries of element 107 (bohrium, Bh), element 108 (hassium, Hs), and element 109 (meitnerium, Mt) can be found in ref. [56–62]

A world-record low cross-section—and therefore extremely difficult to repeat and to confirm—was reached by Morita and co-workers in their recently reported finding of one atom of element 113.[63] All the above mentioned nuclides are the ones in the upper-left part of Figure 1, which shows the uppermost part of the chart of nuclides. From a chemist's point of view, an important characteristic feature of the nuclides produced in nuclear reactions with Pb and Bi targets yields only short-lived products with millisecond half-lives. This life-time prohibits chemical studies with virtually all of the presently available techniques. However, new technological developments will also allow, to some extent, to exploit nuclides produced from some types of nuclear reactions for chemical investigations.

But there are even more chemical elements—and longer lived isotopes of known elements—on the horizon and these are especially exciting for chemists. Oganessian et al. have performed an extended series of experiments irradiating actinide targets with ^{48}Ca at the Flerov Laboratory of Nuclear Reactions (FLNR) in Dubna (Russia) to produce even heavier elements—and more neutron-rich, longer-lived isotopes of known elements (see upper-right part of Figure 1 and Section 2 for more details of the nuclear reactions used and the decays observed). The discoveries of elements 113–116, and the weak evidence for element 118, (see refs. [64–66]) are currently waiting to be confirmed. In producing nuclei close to the former "island of stability" around $Z = 114$ and $N = 184$, these experiments suffer a disadvantage in that their nuclear decay is not "genetically" linked by unequivocal α–α decay sequences to the region of known nuclei—a prerequisite used by the SHIP group for the unique identification.

Chemistry—in addition to unraveling exciting chemical properties of these elements—may become a crucial tool in elemental identification. The first steps towards a chemical separation and identification of element 112 have been made[67–69] and, as this is one of the currently hottest topics in nuclear chemistry, more experiments are under way.[70] The way was paved and the run started with the report[71] of the first observation of the nuclide ^{283}112 at the recoil separator VASSILISSA in Dubna. The nuclide ^{283}112, produced in a reaction with a ^{48}Ca beam and ^{238}U as a target, supposedly has a half-life ($t_{1/2}$) of about a minute—long enough to perform chemical separations with single atoms. More recent reports began to revise the decay properties[66] of this nuclide,



Matthias Schädel earned his PhD (1979) from the Johannes Gutenberg University Mainz. As a postdoc he worked at the Lawrence Livermore and the Lawrence Berkeley National Laboratories with E. K. Hulet and G. T. Seaborg. Since 1985 he has led the nuclear chemistry group at GSI. He organized and chaired the 1st International Conference on the Chemistry and Physics of the Transactinide Elements (1999). He is the editor of the first comprehensive book on the chemistry of superheavy elements. His research interests focus on all nuclear and chemical aspects of transactinides.

 © 2006 Wiley-VCH Verlag GmbH & Co. KGaA, Weinheim

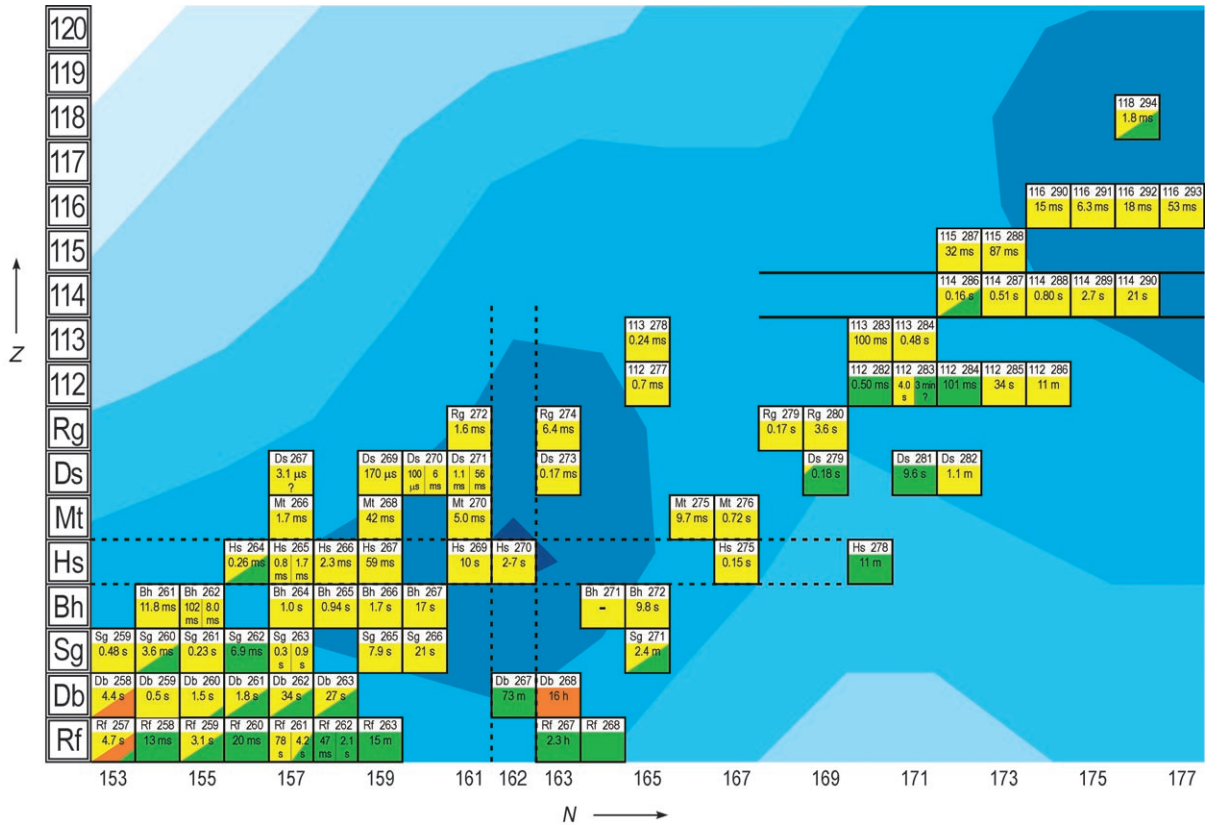


Figure 1. Upper part of the chart of nuclides. Half-lives and color-coded nuclear decay modes (yellow = α-decay, green = spontaneous fission, red = electron capture; see also Section 2) are given together with the mass number for each nuclide. Regions of enhanced nuclear stability around $Z = 108$, $N = 162$ (dashed line) for deformed nuclei and around $Z = 114$ (solid line), $N = 184$ (outside the drawn area) for spherical nuclei are indicated in dark blue. Adapted from ref. [62] with the shell-stability calculations of Sobiczewski and co-workers.

however, it still has a $t_{1/2}$ in an accessible region for chemical studies.

Now, we turn back to chemistry. Element 104, rutherfordium, Rf, marks the beginning of a remarkable series of chemical elements: From a nuclear point of view, they can be called superheavy elements—as they only exist because of their microscopic shell stabilization (see Section 2 for a detailed discussion of this aspect)—and from a chemical point of view they are transactinide elements—because the series of actinides[4] ends with element 103. One of the most important and most interesting questions for a chemist is that of the position of SHE in the Periodic Table of the Elements and their related chemical properties—especially in comparison with the lighter homologues in the respective groups (Figure 2).

From atomic calculations[32,41,43,44], it is expected that the filling of the 6d electron shell coincides with the beginning of the series of transactinide elements. Consequently, chemical behavior similar to that known from the transition metals in the fifth and sixth periods is anticipated. However, it is by no means trivial to assume that rutherfordium in Group 4 of the Periodic Table—and the heavier elements in the following groups—will exhibit chemical properties, which can in detail easily be deduced from their position. To which extent the

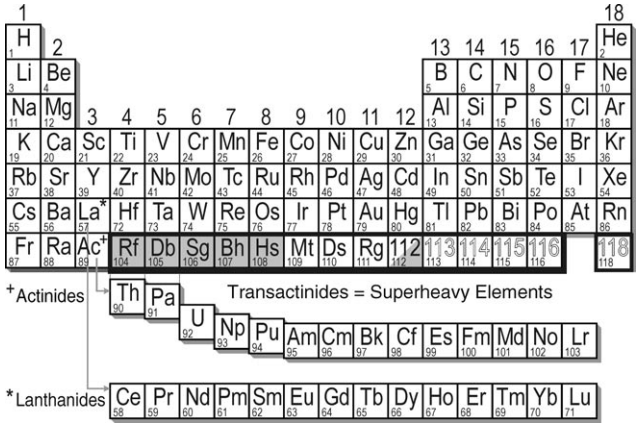


Figure 2. Periodic Table of the Elements. The known transactinide elements 104–112 should take the positions of the seventh-period transition metals below Hf in Group 4 and Hg in Group 12. chemical studies have placed the elements Rf–Hs into Group 4–8. The "chemically unknown" heavier elements (full symbols for known elements and open symbols for as yet unconfirmed reports) still need to be investigated. The arrangement of the actinides reflects that the first actinide elements still resemble, to a decreasing extent, the chemistry of d-block elements: Th below Group 4 elements Zr and Hf, Pa below Nb and Ta, and U below the Group 6 elements Mo and W.

© 2006 Wiley-VCH Verlag GmbH & Co. KGaA, Weinheim

Periodic Table is still a valid ordering scheme regarding chemical properties of the SHE is one of the key questions.

Modern relativistic atomic and molecular calculations[41–44] clearly show the very large influence of direct and indirect relativistic effects on the energetic position and the sequence of electrons in their respective orbitals. These effects are also associated with changes in their radial distributions. All of these relativistic changes are so pronounced compared to the results of non-relativistic calculations, that it would not be surprising if the SHE had significantly different chemical properties to those anticipated. Therefore, it is of great interest to study chemical properties of SHE in detail and to compare these with the properties deduced from extrapolations and from modern relativistic molecular calculations in combination with empirical models. First-generation experiments with rutherfordium[72–74] and element 105,[75,76] dubnium, Db, gave enough justification to place Rf into Group 4 and Db into Group 5 of the Periodic Table. Chemical properties of SHE, or transactinide elements, have been studied up to element 108 (see ref. [8] for a complete compilation) and the first experiments are under way to reach element 112 and beyond.

This Review briefly deals, in its first part, with important nuclear aspects related to the synthesis and nuclear decay of superheavy elements—including a definition of SHE. It will be shown that only single, short-lived atoms are available for these kinds of chemical studies. This section is followed by a short discussion of recent theoretical work including predictions of chemical properties. The main part (Sections 5 and 6) focuses on 1) experimental techniques, 2) some key experiments to unravel detailed chemical properties of elements 104 and 105 in the liquid phase and in the gas phase, 3) first survey experiments of element 106, seaborgium, Sg, and 4) the first, successful experiments on element 107, bohrium, Bh, and on element 108, hassium, Hs, performed in the gas phase. For a complete coverage of this field see ref. [8] Comprehensive reviews can be found in refs. [77–81] To finish this Introduction it may be appropriate to quote Friedlander and Herrmann stating "… *the upward extension of the Periodic Table … has been one of the triumphs of nuclear chemistry in recent decades*".[82]

2. Nuclear Aspects

2.1. The Region of Superheavy Elements

Characteristic electronic and chemical properties allow the beginning of the transactinide elements to be placed at element 104—but where do the SHE begin? Until the early 1980s a straight forward answer would have pointed towards the remote "island of stability" centered at $Z = 114$ and $N = 184$ which was surrounded by a "sea of instability".[12,83] Up to that time, and typical for closed-shell nuclei, SHE were expected to have a spherical shape. However, based upon more recent experimental results[57,59,84] and theoretical concepts, which take into account shell-stabilized deformed nuclei and emphasize the importance of the $N = 162$ neutron shell,[85,86] we know that the sea of instability has drained and that sandbanks and rocky footpaths connect the region of shell-stabilized spherical nuclei to our known world. In addition, recent theoretical results indicate that the atomic numbers 126[87] and, more likely, 120[88]) are also closed shells; with possibly even more pronounced shell stabilization than for element 114.

Perfectly acceptably, some authors are still using the term SHE in connection with spherical nuclei only. However, others have widened this region and have included lighter elements as, for example, already discussed in an article by Sobiczewski, Patyk, and Cwiok entitled "*Do the superheavy nuclei really form an island?*".[89] An argument is developed[90] to show that it may be well justified to begin the superheavy elements with element 104. The result is especially appealing in as much as the beginning of superheavy elements coincides with the beginning of the transactinide elements.

Two definitions or assumptions are used: 1) Superheavy elements is a synonym for elements which only exist due to their nuclear-shell effect. 2) Following arguments given in ref. [45,91] only those composite nuclear systems that live at least 10^{-14} s shall be considered a chemical element. This time is well justified from nuclear aspects, for example, from maximum lifetimes of excited compound nuclei (see Section 2.2), as well as from chemical aspects, for example, from the minimum formation time of a molecule such as hydrogen. We now apply these two assumptions to a comparison of the calculated and the experimentally observed spontaneous fission half-lives—the most drastic, spontaneous disintegration process of a very heavy nucleus. The results are shown in Figure 3 plotted against a frequently used (in nuclear physics)

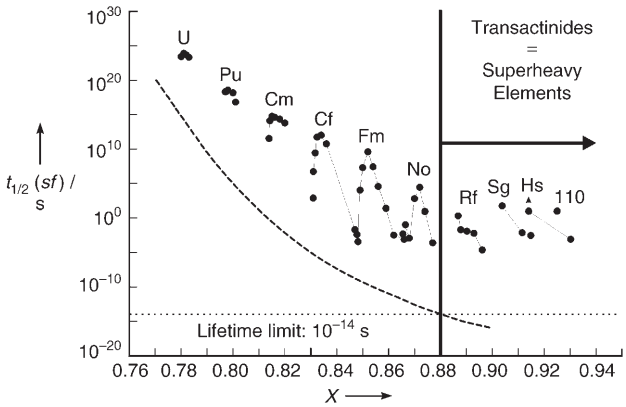


Figure 3. Known spontaneous fission (sf) half-lives ($t_{1/2}$) of nuclides with even numbers of protons and neutrons (dots) and calculated hypothetical half-lives (dashed line) taking into account only the liquid-drop-model contribution plotted versus the fissility parameter *X*. The dotted line shows the lifetime-limit of 10^{-14} s for a chemical element. From ref. [90].

fissility parameter, *X*.[92] This parameter goes with Z^2/A (Z is the atomic number of the nucleus and A is its mass) and it takes into account the proton-to-neutron ratio in a nucleus. This parameter reflects the increasing tendency to spontaneous fission in progressing to heavier nuclei.

 © 2006 Wiley-VCH Verlag GmbH & Co. KGaA, Weinheim

As only the macroscopic liquid-drop part of the nucleus was taken into account in calculating these half-lives (dashed line in Figure 3), the difference between experimentally known half-lives and calculated values reflects the additional shell stabilization of the nuclei[56]. It can be seen from Figure 3 that at a fissility parameter of 0.88—located between nobelium and rutherfordium—the hypothetical "liquid-drop half-lives" drop below the 10^{-14} s margin while the shell contribution allows these nuclides to have lifetimes up to factors of about 10^{15} longer. From this it can be claimed that all elements beginning with element 104—the transactinides—live only because of their microscopic shell stabilization and, therefore, should be called superheavy elements.

2.2. Nuclear Syntheses

While transuranium elements up to and including fermium ($Z = 100$) can be produced by stepwise neutron capture and subsequent β^--decay in a high (neutron) flux nuclear reactor, transfermium elements can only be man-made by nuclear fusion reactions with heavy ions in accelerators.[5,6,60] In the accelerator-based reactions, the Coulomb barrier between the two approaching positively charged, atomic nuclei always has to be overcome. Therefore, the combined, fused system, which is called the compound nucleus, always carries a certain amount of excitation energy. The availability of suitable ion beams and target materials—and the energy balances associated with these combinations—allow a crude distinction between two types of reactions: One frequently termed "cold fusion" and the other one "hot fusion".

Cold-fusion reactions are characterized by relatively low nuclear excitation energies of about 10–15 MeV. They occur when medium-heavy projectiles, for example, ^{58}Fe, ^{62,64}Ni, or ^{68,70}Zn, fuse (at the lowest possible energy) with ^{208}Pb or ^{209}Bi target nuclei. There are many advantages with this reaction which, among others, helped to discover elements 107–112.[57,59,60] However, a severe disadvantage for chemical studies is the very short half-lives of the relatively neutron-deficient nuclei produced. An illustrative view of this reaction mechanism is given, for example, in ref. [12] and in Figure 4. Except for one specific type of experiment[93] cold-fusion reactions are usually not used in chemical studies of the heaviest elements.

Hot-fusion reactions are characterized by excitation energies of about 40–50 MeV when actinide target nuclei, such as ^{238}U, ^{242,244}Pu, ^{243}Am, ^{248}Cm, ^{249}Bk, ^{249}Cf, and ^{254}Es, fuse with light-ion beams, such as ^{18}O, ^{22}Ne, and ^{26}Mg (see Figure 4). Whereas in cold-fusion reactions usually only one neutron is evaporated, four or five neutrons are emitted in hot-fusion reactions before the compound nucleus has cooled. Because of the neutron-richness of the actinides targets, and despite the emission of three or four more neutrons, these reactions are applied to synthesize the most neutron-rich and relatively long-lived isotopes used in chemical investigations of SHE. Half-lives, method of the syntheses, and cross sections are summarized in Table 1 (from ref. [90,94]). More detailed discussions about specific aspects of hot-fusion reactions can be found in ref. [57,60,95,96]

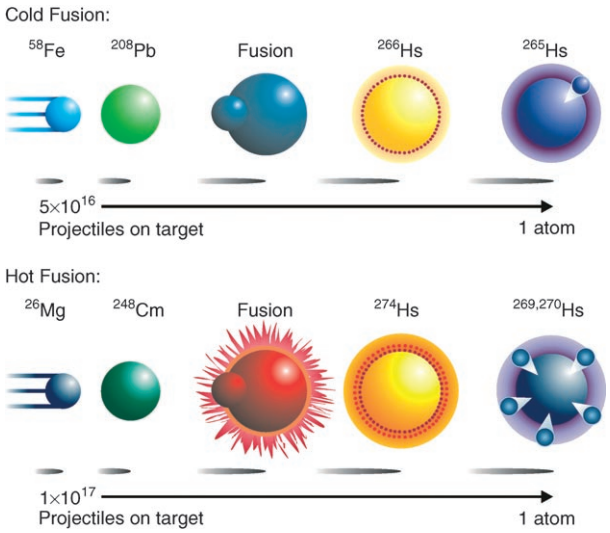


Figure 4. Pictorial view of the ^{208}Pb(^{58}Fe,1n)^{265}Hs reaction as an example for a cold-fusion reaction and ^{248}Cm(^{26}Mg,4–5n)$^{269-270}$Hs for a hot-fusion reaction.

Table 1: Nuclides from hot-fusion reactions (and the cold-fusion reaction Ti + Pb) used in SHE chemistry.[a]

Nuclide	$t_{1/2}$ [s]	Target	Beam	Evap[b]	σ[b]	ν[c]
^{261m}Rf	78	^{248}Cm[d]	^{18}O	5	≈10 nb	3 min^{-1}
		^{244}Pu[e]	^{22}Ne	5	4 nb	1 min^{-1}
^{257}Rf	4	^{208}Pb[e]	^{50}Ti	1	15 nb	5 min^{-1}
^{262}Db	34	^{249}Bk[d]	^{18}O	5	6 nb	2 min^{-1}
		^{248}Cm[d]	^{19}F	5	1 nb	0.3 min^{-1}
^{263}Db	27	^{249}Bk[d]	^{18}O	4	10 nb	3 min^{-1}
^{263}Sg	0.9	^{249}Cf[e]	^{18}O	4	300 pb	6 h^{-1}
^{265}Sg	7.4	^{248}Cm[d]	^{22}Ne	5	≈240 pb	5 h^{-1}
^{266}Sg	21	^{248}Cm[d]	^{22}Ne	4	≈25 pb	0.5 h^{-1}
^{267}Bh	17	^{249}Bk[d]	^{22}Ne	4	≈70 pb	1.5 h^{-1}
^{269}Hs	≈14	^{248}Cm[d]	^{26}Mg	5	≈6 pb	3 d^{-1}
^{270}Hs	2–7	^{248}Cm[d]	^{26}Mg	4	≈4 pb	2 d^{-1}

[a] Data from ref. [90,94]. [b] σ = cross section, Evap = number of emitted neutrons. [c] Production rate assuming typical values of 0.8 mg cm^{-2} for the target thickness and beam intensities of 3×10^{12} particles per second. [d] Reaction commonly used in chemistry experiments. [e] Reaction rarely used or only in very specific experiments, or the nuclide is only observed as a by-product.

For cold-fusion reactions, and hot-fusion reactions, the cross sections—the probability of forming the desired product—constantly decrease with increasing atomic number of the product. In cold-fusion reactions, decreasing cross sections are presumably due to an increasing fusion hindrance of the highly charged nuclei ($Z_{target} \times Z_{proj.}$). In hot-fusion reactions it is predominantly the strong fission competition (fission versus neutron evaporation) in the deexcitation

© 2006 Wiley-VCH Verlag GmbH & Co. KGaA, Weinheim

process of the hot compound nucleus which diminishes the cross section.

Nuclear reaction cross sections (σ) are measured in barn (b); $1\ b = 10^{-24}\ cm^2$. This number is related to simple geometric arguments concerning a projectile hitting a target nucleus. A "typical" nucleus has a radius of about 6×10^{-13} cm (= 6 fm, femtometer); for example, the nuclear radius (r) of Zn is 4.9 fm and of Pb is 7.1 fm.[61] As the geometric cross section of a nucleus is πr^2, a value of about $10^{-24}\ cm^2$ results for a "typical" nucleus. While some nuclear reactions have cross sections between several barn and millibarn, heavy actinides are usually produced with microbarn. Cross sections for the syntheses of *n*-rich, transactinides in hot-fusion reactions vary from about ten nanobarn ($1\ nb = 10^{-33}\ cm^2$) to a few picobarn ($1\ pb = 10^{-36}\ cm^2$). The production rate is the product of three terms: The cross section (in cm^2), the number of target atoms (in cm^{-2}), and the flux of projectiles (usually in s^{-1}).

With typical beam intensities of 3×10^{12} heavy-ions per second and targets of about $0.8\ mg\,cm^{-2}$ thickness (ca. 2×10^{18} atoms cm^{-2}), production yields range from a few atoms per minute for Rf and Db isotopes to five atoms per hour for ^{265}Sg[97]), to some tens of atoms per day for ^{267}Bh[98,99], and a few atoms per day for ^{269}Hs[54,100]. Therefore, all chemical separations are performed with single atoms on an "atom-at-a-time" scale. An additional complication for the experimenter arises from the fact that the time at which the synthesis of an individual atom occurs is unknown, as it is produced in a statistical process.

As briefly sketched in Section 1 (see there for references) experiments with actinide targets and a ^{48}Ca beam give strong evidence for the existence of relatively long-lived nuclides of elements 112–116 and their α-decay daughter products (see upper right part of Figure 1). Somewhat surprisingly, the relatively high cross sections—a few picobarn, that is, production rates of the order of about one atom per day—seem to be almost constant in this region.[60,65,66] One interpretation of this rather pleasant but not fully understood effect sees the origin in the doubly magic character of ^{48}Ca with closed shells at $Z = 20$, $N = 28$. Reactions with ^{48}Ca as a projectile may gain some of advantages of two sides: 1) From the cold-fusion reactions—magic nuclei (target or projectile) allow for a formation of cold compound nuclei with low fission competition—and 2) from the hot-fusion fusion reactions—larger asymmetry in the nuclear charge of the target and projectile eases the fusion process. There is considerable optimism that these reactions could extend chemical studies into the region of element 114.

2.3. Nuclear Decay

Nuclear chemistry techniques are not only highly efficient to collect products from nuclear reactions but are also well adapted to half-lives of a few seconds and longer. Therefore, it is not surprising that many of the longer-lived, neutron-rich isotopes of the heaviest actinides and early transactinides were discovered or were first studied applying these techniques. Alpha decay is the most characteristic decay mode in this region of the chart of nuclides (see Figure 1), and provides a unique nuclide identification of the investigated product. In particular, time-correlated consecutive mother–daughter α–α-decay chains provide unambiguous signals. They are used to identify these nuclides in specific chemical fractions or at characteristic positions after chemical separation. The observation of an α-particle or a fragment from spontaneous fission (sf) is the only means of detecting an individual atom after chemical separation and this can be performed with a very high efficiency. A number of nuclear-decay properties were determined in the course of the chemistry experiments as a "by-product" of these investigations. Specifically designed experiments using chemical separation techniques are given in ref. [90] and references therein. These experiments not only yielded new isotopes or decay modes but were also instrumental in confirming[54] the discovery of element 112.

3. Atom-at-a-Time Chemistry

The one-atom-at-a-time appearance of superheavy elements poses some unique problems for the chemistry at the end of the Periodic Table. As a single atom cannot exist in different chemical forms taking part in the chemical equilibrium at the same time, the classical law of mass action—well established for macroscopic quantities and characterizing a dynamic, reversible process in which reactants and products are continuously transformed into each other—is no longer valid.[101,102] For single atoms, the concept of chemical equilibrium needs to be substituted by an equivalent expression in which concentrations, activities, or partial pressures are replaced by probabilities of finding the atom in one state or the other. An atom can sample these states with frequencies of hundreds (and more) exchange reactions per second if the chemical system is selected such that the free enthalpy of activation between these states is below 17 kcal (≈ 70 kJ).[103]

The time one atom (or molecule) spends in one state or another—the measure of its probability of being in either phase—can be determined in dynamic partition experiments. These experiments are characterized by the flow of a mobile phase relative to a stationary phase while a single atom is frequently changing between the two phases. This situation is realized in many chromatographic separations, for example, in the exchange between a gaseous and a solid phase (wall adsorption) in gas chromatography or between a mobile liquid phase and a stationary ion-exchange resin in liquid chromatography. In these processes, the retention or elution times provide information about the average time an atom has spent in either phase. Such characterizations of the behavior of a single atom yield information which approximates the equilibrium constant that would be obtained from macroscopic amounts of this element. More detailed information on this situation can be found in refs. [79,81,104]

 © 2006 Wiley-VCH Verlag GmbH & Co. KGaA, Weinheim

4. Objectives for Superheavy Element Chemistry

4.1. Architecture of the Periodic Table

The Periodic Table of the Elements (see Figure 2 for one possible version similar to the cover of ref. [105]) is the basic ordering scheme for chemical elements and the most important and useful tool in predicting their chemical behavior. Conceptually, it is, at first, the atomic number and the associated electronic configuration of an element that define its position in the Periodic Table. Secondly, related to this position are chemical properties that arise from the electronic configuration. Trends in the chemical behavior can be linked to trends in the electronic configurations along groups or periods in this scheme. However, as was painfully experienced in the early searches for transuranium elements (see Section 1), simple extrapolations of existing periodic properties must be used cautiously. This is especially true for superheavy elements where relativistic effects on the electronic structure become increasingly strong (see Section 4.2) and will significantly influence the properties of these elements. Deviations from the periodicity of the chemical properties, based on extrapolations from lighter homologues in the Periodic Table, have been predicted for some time (see ref. [29,32,35,40] and references therein). In more general terms, the issue of "Relativity and the Periodic System of Elements" has been in the focus for some time.[38,39,106]

It is one of the highest priorities of the theoretical and the experimental "heavy-element" chemists' work to predict—and to validate or contradict—the chemical behavior of SHE, especially in relation to their position in the Periodic Table. Recently, a new wave of theoretical and experimental investigations has led to a better understanding of the chemistry of superheavy elements. Relativistic quantum-chemical treatments, which reliably calculate the electronic configurations of heavy-element atoms, ions, and molecules—combined with fundamental physicochemical considerations of the interactions of these species with their chemical environment—now allow detailed predictions of the chemical properties of superheavy elements. These properties are often compared with empirical, linear extrapolations of the chemical properties found along groups and periods to disclose the impact of relativistic effects. However, the empirical extrapolations are not purely non-relativistic, as relativistic effects are, to some extent, already present in the lighter elements.

An additional complication for such assessments, is the competition between relativistic and shell-structure effects. This competition obscures a clear-cut correlation between an observed chemical property and one specific effect. It poses an additional challenge for a deeper understanding of the chemistry of elements at the uppermost reaches of the Periodic Table (and for the table's architecture) especially if purely empirical predictions are to be improved upon. However, a number of landmark accomplishments resulted from a number of new and detailed experimental findings and theoretical results over the last decade. For comprehensive summaries and reviews of the theoretical work see refs. [41–44,107,108], for the experimental techniques see refs. [79,81,90,94,109], and ref. [8] for a complete coverage.

4.2. Relativistic Effects

A detailed discussions of relativistic effects in general and specifically for superheavy elements can be found in ref. [38,39,106] and ref. [43,44,108], respectively. The relativistic increase in mass is known given by Equation (1) where

$$m = m_0/[1-(v/c)^2]^{1/2} \quad (1)$$

m_0 is the electron rest mass, v is the velocity of the electron, and c the speed of light. The effective Bohr radius [Eq. (2)] decreases with increasing electron velocity.

$$a_B = \frac{\hbar^2}{m c^2} = a_B^0 \sqrt{1-(v/c)^2} \quad (2)$$

This orbital contraction and stabilization of the spherical s and $p_{1/2}$ electrons—the "direct relativistic effect"—was originally thought to be important only for the "fast", inner K and L shell electrons. However, it has been realized that the direct relativistic effect is still large even for the outermost s and $p_{1/2}$ valence electrons in superheavy elements. Thus, for example, the 7s orbital electrons of element 105 are relativistically contracted by 25% and energetically stabilized.[43] Figure 5

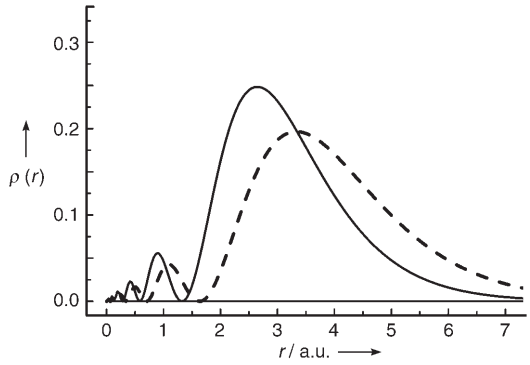


Figure 5. Relativistic (——) and non-relativistic (-----) radial distribution of the 7 s valence electrons in element 105, Db. (1 a.u. = 52.92 pm). Figure adapted from ref. [43].

shows the radial distribution of the "relativistic" 7 s valence electron compared with a hypothetical "non-relativistic" one.

The second relativistic effect—the "indirect relativistic effect"—is the expansion of outer d and f orbitals. The relativistic contraction of the s and $p_{1/2}$ shells results in a more efficient screening of the nuclear charge, so that the outer orbitals, which never come close to the core, become more expanded and energetically destabilized. While the direct relativistic effect originates in the immediate vicinity of the nucleus, the indirect relativistic effect manifests itself in the outer core shells. As an example, for Group 6 elements, Figure 6 shows the stabilization of the ns orbitals, as well as the destabilization of the $(n-1)$d orbitals. The increasingly strong influence of the relativistic effects on the absolute and relative position of the valence orbitals can be seen. This feature is most pronounced for element 106, Sg, where the level sequence of 7s and 6d orbitals is inverted.

© 2006 Wiley-VCH Verlag GmbH & Co. KGaA, Weinheim

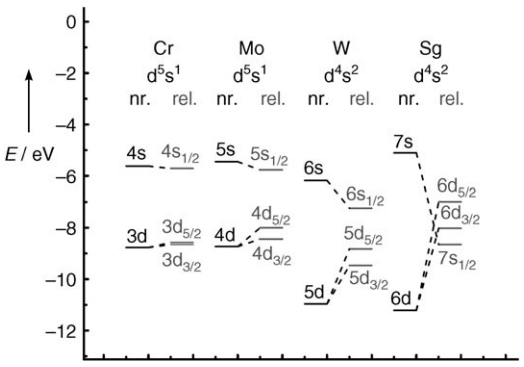


Figure 6. Relativistic (rel.; Dirac–Fock calculation) and non-relativistic (nr.; Hartree–Fock calculation) energy levels of the Group 6 valence *n*s and (*n*−*l*)d electrons. Figure adapted from ref. [108] with data from ref. [33].

A non-relativistic description—calculation or empirical extrapolation within Group 6—would result in a much different and incorrect description of the electronic level configuration for seaborgium. It can be anticipated that these drastic changes may lead to unusual oxidation states, ionic radii that are very different to those predicted from simple extrapolations in a specific group, or significant changes in the ionic and the covalent portions of a chemical bond.

The third relativistic effect is the "spin-orbit (SO) splitting" of levels with $l > 0$ (p, d, f,… electrons) into $j = l \pm {}^1/_2$ states. This effect also originates in the vicinity of the nucleus. For orbitals with the same l value, the SO splitting decreases with increasing number of subshells, that is, it is much stronger for inner shells than outer shells. For orbitals with the same principal quantum number, the SO splitting decreases with increasing l value. In transactinide compounds the SO coupling becomes similar, or even larger, in size than typical bond energies. The SO splitting of the valence 7p electrons in element 118, for example, may be as large as 11.8 eV.[43]

Each of the three effects (direct and indirect relativistic effect and SO splitting) is of the same order of magnitude and grows roughly as Z^2! This is one of the reasons why it is most fascinating to experimentally probe the highest Z elements. Other effects, such as the Breit effect (accounting for magnetostatic interactions) and the QED effect (vacuum polarization and self-energy) are not negligible but of minor importance for chemical properties of SHE.[108]

4.3. Atomic Properties

It is helpful to remember that not only the electronic ground-state configurations (see Table 2) but also other properties, such as ionization potentials, atomic/ionic radii, and polarizabilities, are important parameters which eventually determine the chemical behavior of an element.

A detailed discussion of the theoretical determination of these parameters, and their influence on the chemical behavior of SHE, is given by Pershina in ref. [43,44] and references therein. Knowing the trends in these properties from theoretical calculations helps to assess similarities (or differences) of SHE properties in relation to the properties of their lighter homologues in the Periodic Table. Even if it would be premature (or sometimes even misleading) to judge the chemical properties purely from the electronic ground-state configurations given in Table 2—together with the most stable oxidation states—they can provide some guidance.[43] Earlier predictions of chemical properties are summarized in ref. [35].

Table 2: Ground-state electronic configuration and stable oxidation states for elements 104–118.[a]

Element	Group	Electronic configuration (core: [Rn]5f^{14})	Stable oxidation state[b–d]
104, Rf	4	6d^{2}7s^2	3, ***4***
105, Db	5	6d^{3}7s^2	3, 4, ***5***
106, Sg	6	6d^{4}7s^2	4, ***6***
107, Bh	7	6d^{5}7s^2	3, 4, 5, ***7***
108, Hs	8	6d^{6}7s^2	3, 4, 6, ***8***
109, Mt	9	6d^{7}7s^2	1, 3, 6
110, Ds	10	6d^{8}7s^2	0, 2, 4, 6
111, Rg	11	6d^{9}7s^2	−1, **3**, **5**
112	12	6d^{10}7s^2	**0**, 2, **4**
113	13	6d^{10}7s^2 7p	**1**, 3
114	14	6d^{10}7s^2 7p^2	0, **2**, 4
115	15	6d^{10}7s^2 7p^3	**1**, 3
116	16	6d^{10}7s^2 7p^4	**2**, 4
117	17	6d^{10}7s^2 7p^5	−1, 1, **3**, 5
118	18	6d^{10}7s^2 7p^6	**2**, **4**, 6

[a] Data from ref. [43,44]. [b] Bold = most stable oxidation state in the gas phase. [c] Underlined = most stable in aqueous solution if different from gas phase. [d] Italics = experimentally observed oxidation states.

5. Experimental Techniques

Fast chemical-isolation procedures to study the chemical and physical properties of short-lived radioactive nuclides have a long tradition and have been used since the beginning of radiochemistry. The rapid development of increasingly fast and automated chemical-separation techniques originated from the desire to study short-lived nuclides from nuclear fission (see ref. [110,111] for reviews). Also the discovery of new elements up to Md ($Z = 101$) was accomplished by chemical means.[5] Although from there on, physical techniques prevailed in the discoveries, rapid gas-phase separation chemistry played an important role in the discovery claims of elements 104 and 105.[45] Today, the fastest chemical-separation systems allow the study of the nuclides of transactinide elements with half-lives of less than 10 s. Reviews on these methods and techniques with varying emphasis can be found in ref. [77–79,112–115] and a recent and comprehensive coverage in ref. [116]

Experiments can be grouped into the following steps:

1) Synthesis of the element.
2) Rapid transport of the synthesized nuclide to the chemical apparatus.
3) Formation of a desired chemical species or compound (this can be done before, during, or after the transport).

 © 2006 Wiley-VCH Verlag GmbH & Co. KGaA, Weinheim

4) Fast chemical separation and chemical characterization.
5) Preparation of a sample suitable for nuclear spectroscopy.
6) Detection of the nuclide through its characteristic nuclear-decay properties.

Flow-schemes for such online experiments with transactinides are shown in Figure 7. The atom-at-a-time nature of SHE chemistry requires stringent optimizations of all of these steps. The chemical-separation system has to fulfill several prerequisites simultaneously.[116]

1) Speed becomes increasingly important from the lighter elements, such as Rf ($t_{1/2}(^{261}\mathrm{Rf}) = 78$ s), to the heavier ones, such as Hs ($t_{1/2}(^{269}\mathrm{Hs}) \approx 14$ s).[48]
2) A sufficiently high number of exchange steps are required for an individual atom or compound to ensure that its behavior is characteristic of the element.
3) The system needs to be selective enough, not only to probe a specific chemical property, but also to separate other unwanted nuclear reaction by-products which may obscure a unique identification of the atom under investigation.
4) Since any SHE production is a statistical process—only the average number of produced atoms in a given period is known, not the exact moment in time where a single atom is produced—many repetitions are inevitable for separations which operate discontinuously. This situation has led to the construction of highly automated liquid-chemistry set-ups.
5) Even though in other fields, some techniques have reached the sensitivity required to observe or manipulate single atoms or molecules, the observation of a characteristic nuclear-decay signature is presently the only means of identifying a single atom after chemical separation. Thus at the end, or after a separation process, samples must to be prepared that are suitable for analysis by, for example, high-resolution α-spectroscopy.
6) As the type of chemical species cannot be determined during or after the transactinide separation, the chemical system must be chosen such that a certain chemical state is probable and stabilized by the chemical environment.

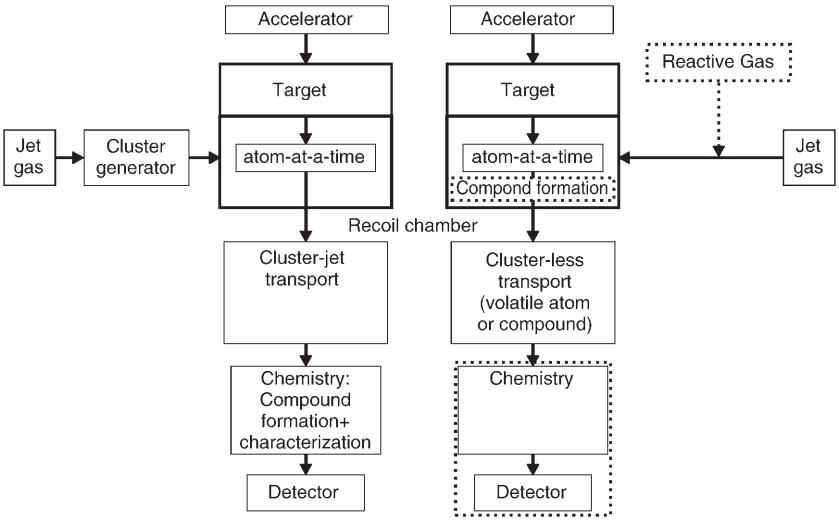


Figure 7. Flow-scheme for two types of online chemistry experiment. Left: Transport of nuclear reaction products with aerosols (cluster) and formation of a chemical compound in the chemistry apparatus; typical for the chemistry of elements Rf to Bh. Right: Transport of volatile species (atoms or compounds formed in the recoil chamber) to the chemistry set up (which is sometimes in one unit together with the detectors); typical, for Hs and element 112 chemistry.

Several approaches have been successful in studying the chemical properties of superheavy elements. One of the main distinctions between the different approaches, is that one type of experiment works in the liquid phase and the other in the gas phase. The same distinctions are made in the following subsections, but first the common initial parts of the experiment are discussed.

5.1. Beams, Targets, Collection, and Transport

Heavy-ion beams, such as ^{18}O, ^{22}Ne, ^{26}Mg, and ^{48}Ca—with velocities of about 10% the speed of light and typical intensities of $3–6 \times 10^{12}$ particles per second—are delivered from an accelerator to the experiment. There, they pass first through a vacuum isolation window and a target-backing before interacting with the actinide target material. The energy loss of the projectiles creates heat which must be removed to prevent damage to the window and the target. For this purpose, wheels with rotating windows and targets as well as stationary arrangements with double-windows and forced gas cooling are used.[116–118]

A stationary apparatus is schematically shown in Figure 8.[118] Cooling gas is forced at high velocity through a narrow gap between the 6 mm diameter vacuum isolation window and the target backing.[117] Typical target thicknesses are about 0.8 mg cm^{-2}. Mainly electrodeposition and molecular plating methods have been used in recent years to deposit the target material onto the backing. The advantages and limitations of these techniques are discussed in ref. [116,117]

To allow increased beam intensities beyond the limit of stationary arrangements "A Rotating Target Wheel for Experiments with Superheavy-Element Isotopes at GSI Using Actinides as Target Material" (ARTESIA) has been developed; see Figure 9. The gain arises from spreading out the beam over a larger target area thus reducing the beam power per surface area unit. Target material is electrodeposited onto three 1.9 cm^2 banana-shaped backing foils.[119]

Common to either arrangement—stationary or rotating set-up—is a recoil chamber behind the target. Nuclear reaction products recoiling out of the target are stopped in helium or another gas. Sufficiently volatile products (atoms or chemical compounds) are transported by the flowing gas

© 2006 Wiley-VCH Verlag GmbH & Co. KGaA, Weinheim

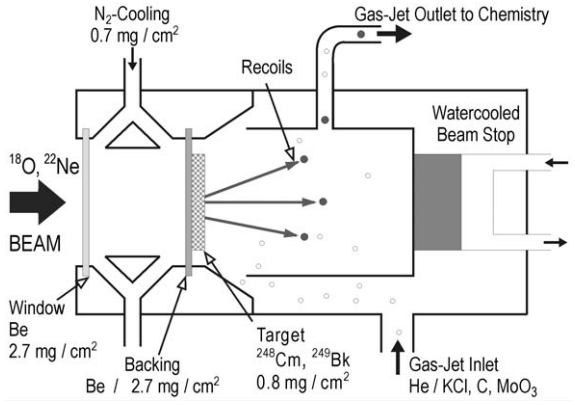


Figure 8. Schematic diagram of a stationary target arrangement together with the recoil chamber.



Figure 9. Photograph of the ARTESIA target wheel with three ^{248}Cm targets. The three long dark streaks indicate the area which was struck by the first fraction of beam particles before the entire target area (white surface) was "baked in" later.

through capillaries to the chemical- or detector-apparatus. For nonvolatile products, usually aerosols (KCl or carbon "clusters") are used as the carrier material in the gas (see ref. [116] for more details). A schematic flow chart of the components used in automated online chemical apparatus is depicted in Figure 10.

5.2. Techniques and Instruments for Liquid-Phase Chemistry

To date, almost all liquid-phase separations of transactinides were performed in discontinuous batch-wise operations with a large numbers of cyclic repetitions.[120] While in several experiments on Rf and Db manual procedures were used (see ref. [116,121] and references therein for summaries of the manual separation techniques) most transactinide separations were carried out with automated instruments.

The implementation of the microcomputer controlled Automated Rapid Chemistry Apparatus (ARCA)[122] yielded the predominant share of today's knowledge about the

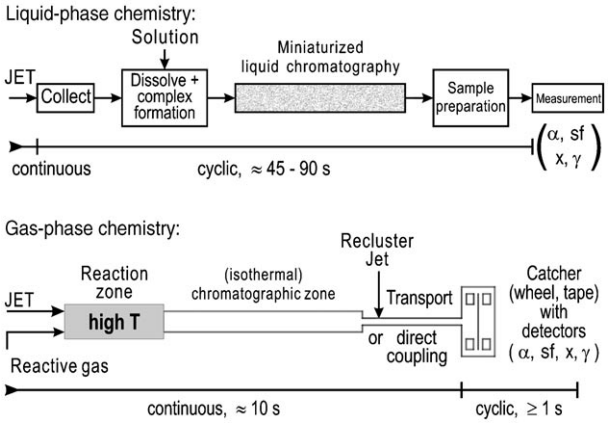


Figure 10. Schematic flow chart of components for automated online chemistry in the liquid phase (top) and in the gas-phase (bottom).

chemical behavior of the elements Rf through Sg in aqueous solution. ARCA II allows fast, repetitive chromatographic separations in miniaturized columns (8 mm long, 1.6 mm internal diameter (i.d.)) with typical cycle times between 45 and 90 s. Depending on the chemistry, columns were filled with cation- or anion-exchange resin or an organic extractant on an inert support material. A photograph of the central parts of the ARCA is shown in Figure 11. Common to all batch-wise separations are time-consuming (ca. 20 s) evaporation steps (for sample preparation) that use IR light and hot He gas. Separation times are typically between 5 s and 10 s.

A breakthrough in the automatization of the sample preparation was achieved with the innovative "Automated Ion exchange separation apparatus coupled with the Detection system for Alpha spectroscopy" (AIDA).[123–125] It has recently been applied to detailed studies of Rf chemistry and the first investigations on Db.[123,125–128]

After batch-wise separations, individual samples are assayed in detection systems for characteristic α-energies and sf fragment energy measurements. To strengthen the nuclide identification each event is logged together with time information. This approach allows energy and time correlations between mother–daughter α–α or α–sf decay sequences to be determined. To date, continuous liquid-phase separation techniques have played a minor role in SHE chemistry (see ref. [81,93,94,114,116] for more details).

5.3. Techniques and Instruments for Gas-Phase Adsorption Chemistry

Despite the fact that the transition metals in Groups 4–11 have very high melting points and that only a few inorganic compounds exist, that are appreciably volatile at temperatures below about 1100 °C, gas-phase separations are important in the chemical investigations of SHE.[116,129] Moreover, as elements in Group 12–18 can presumably be employed directly (in their atomic state) in gas-phase experiments, they will play a major role in the chemistry of element 112 and beyond. Since transactinide nuclei are usually stopped in gas, a fast and efficient link can be established to a gas chromato-

 © 2006 Wiley-VCH Verlag GmbH & Co. KGaA, Weinheim

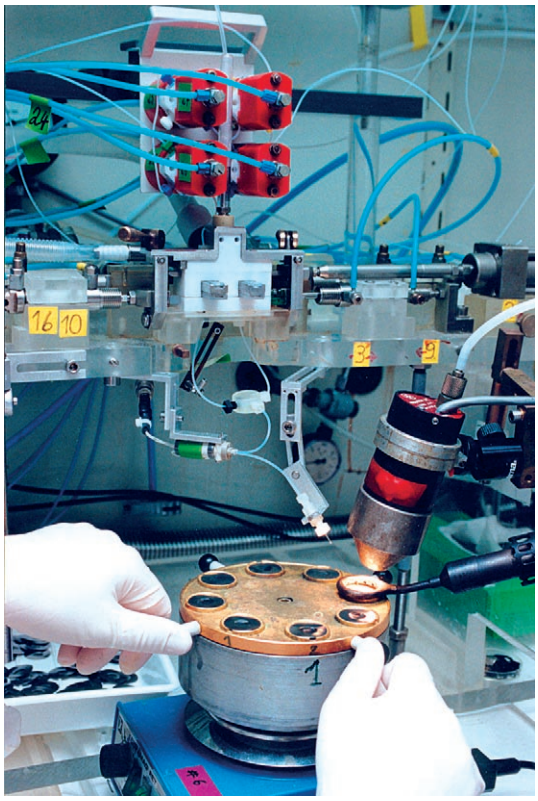


Figure 11. Photograph of the computer-controlled ARCA. The central part is the white block with two protruding magazines each carrying 20 chromatographic columns. The red cylinders are pneumatically operated valves which route the solvent flow. The desired fractions are sprayed from a glass capillary onto round Ta-discs seen on the hotplate in the foreground and are then evaporated to dryness using hot He from a ring-sized nozzle and a power controlled IR-lamp.

graphic system 1) by direct transport of volatile species in the flowing gas, 2) by formation of a volatile compound in or at the recoil chamber, and 3) by a transport with cluster (aerosol) particles. As an additional advantage, gas-phase separations can be operated continuously. Figure 12 shows the basic principle of the isothermal chromatography as compared with thermochromatography.

Early on, separations in the gas-phase played an important role in the investigations of transactinides. The technique was pioneered by Zvara and co-workers at Dubna (see refs. [72,112,130,131] and references therein). In their experiments usually a thermochromatographic column was directly connected to the recoil chamber. For more recent experiments, a coupling of the gas chromatographic columns to a gas-jet transport system was developed.[132] Continuously operating gas-phase separations were extremely instrumental in studying the formation of halide and oxide compounds of the transactinides Rf through Bh and to investigate their characteristic retention time—a measure very often expressed as a "volatility". For reviews see ref. [115,116,133]. Ref. [134] describes the online gas chromatographic apparatus (OLGA) and further setups are explained in ref. [135–137]

The lower part of Figure 10 shows a flow Scheme for a typical isothermal gas-chromatographic separation. Common

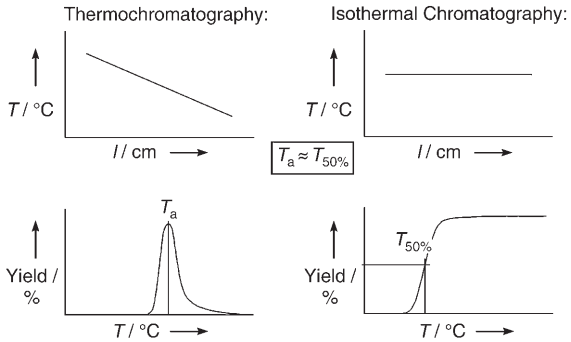


Figure 12. Basic principles of thermochromatography (left) and isothermal gas chromatography (right). The upper panels show temperature profiles (l = column length) and the lower panels the deposition peak in thermochromatography and the integral chromatogram in isothermal chromatography. From ref. [116].

to all of these experiments is the use of the known nuclide half-life to determine a "retention-time-equivalent" to gas chromatographic experiments.[78] On an atom-at-a-time scale, it is the value for 50% yield on a break-through curve measured as a function of various isothermal temperatures. The temperature corresponding to the 50% yield at the exit of the chromatography column is equal to the temperature at which, in classical gas-chromatographic separations, the retention time would be equal to the half-life of the investigated nuclide. Products leaving the chromatography column are usually attached to new aerosols in a so-called "recluster process" and are transported in a gas-jet to a detector system. There samples are assayed for time-correlated, characteristic α-decays and for sf fragments. Instead of reclustering, a direct deposition of products leaving the chromatographic column onto thin metal foils was used in some seaborgium experiments[136,137] and in an early experiment to search for element 107.[138]

A different experimental approach for gas-adsorption studies is provided by thermochromatography.[113,131,139] In this method, a (negative) temperature gradient is imposed on a chromatography column. For the high-temperature version of this method, ranging from about 450 °C to room temperature, tracks from sf fragments are registered along the chromatography column after the end of the experiment.[140] While this method is fast and highly efficient it has the disadvantages that it's temperature range is limited to about 450 °C by the fission-track detectors and, more important, registration of sf fragments alone is not nuclide specific.

Recently, low-temperature versions of thermochromatographic devices were developed and successfully applied in the first chemical separation of hassium.[54] Their temperature gradient ranges from ambient to liquid nitrogen temperature (−196 °C) and they are well adapted to investigate highly volatile or gaseous species. A great advantage of these devices named cryo thermochromatographic separator (CTS)[141]—and its improved version cryo online detector (COLD)[54]—is that the detectors form a chromatographic tube or channel. This arrangement allows the detection of characteristic nuclear decays with a high efficiency and high resolutions in energy and the deposition temperature of an element or compound at low temperatures. Individual cryo-detectors for

© 2006 Wiley-VCH Verlag GmbH & Co. KGaA, Weinheim

condensation of highly volatile products on low-temperature surfaces[142] were used in earlier searches for superheavy elements.[143–145]

With (isothermal) gas-chromatographic experiments, volatile chemical compounds are usually formed by adding a reactive gas in the hot entrance (reaction) zone ahead of the chromatographic column. Compound formation can also be carried out in the recoil chamber. Recent hassium experiments[54,146] are examples for such an in situ volatilization in which a reactive gas is a component in the transport gas. Similarly, even in the very early thermochromatographic experiments, volatile compounds were formed at the exit of the recoil chamber and the appropriate techniques were developed.[112,140,147,148]

5.4. Perspectives of New Technological Developments

All breakthroughs in superheavy element chemistry were linked to—and also in the future will be connected to—new technical developments in experimental techniques and apparatuses. More recently, a completely different kind of coupling of a chemistry apparatus to the SHE production site has attracted much attention and may become an important tool in the future.[116] Coupling a kinematic recoil-separator—the Berkeley gas-filled separator (BGS)—with the automated, fast centrifuge separation system SISAK has been accomplished in a proof-of-principle experiment at the Lawrence Berkeley National Laboratory (LBNL), Berkeley (California). With this system ^{257}Rf ($t_{1/2} = 4$ s) was separated and identified in a continuous online liquid–liquid extraction.[93] Among other advantages, such a system completely removes the primary heavy-ion beam from the reaction products "beam" and it kinematically separates many unwanted nuclides before they even enter the chemical apparatus. The SISAK[93] experiment with its less specific (limited energy resolution) but highly efficient and fast online detection technique using an extractive scintillator,[114,149] greatly profited from the BGS as a preseparator. A miniaturized version dubbed SISAK III[150–152] is very well adapted for studying short-lived nuclides with half-lives of the order of 1 s.

All experiments behind a recoil separator have the advantage that a preseparated "beam" of a desired heavy element becomes available. This approach may open up new frontiers in direct chemical reactions with a large variety of organic compounds,[153] and should allow gas chromatographic studies of superheavy element to be extended to a much larger variety of compounds.

Another promising development is vacuum thermochromatography[154,155] which has been used for lighter elements.[156,157] This technique has the potential for very fast separations in the millisecond region, possibly giving access to short-lived nuclides of elements beyond $Z = 114$.

A not completely new but not fully exploited technique is the so called three-column or multicolumn technique.[158–162] To overcome difficulties with labor- and time-consuming sample-preparation procedures typical for batch-wise experiments, this technique provides a different approach by continuously separating heavy elements in the liquid phase and determining the chemical behavior of a transactinide element from the ratio of long-lived daughter isotopes in one or another fraction. First experiments have been performed with Rf to study the fluoride complexation[158,159,161] and with Db.[163,164] Rf and Db, transported by the He(KCl) jet to the chemistry apparatus, were continuously dissolved, and this solution was passed through three consecutive ion-exchange columns. Primary produced divalent and trivalent actinides were "filtered" out on the first cation-exchange column. In the next anion-exchange column anionic species were retained for some time, while the following cation-exchange column adsorbed cationic species—the long-lived α-decay products of Rf. These were eluted after the end of irradiation and were detected by offline α-spectroscopy.

One of the disadvantages of the multicolumn technique is its limited range of half-lives and distribution coefficients. Its big advantage is its potential to study short-lived isotopes with half-lives of a few seconds. Because of its continuous operation, it may allow these studies to be extended to nuclides with cross sections well below the nanobarn level. Preparations are under way to perform such studies[165] to determine differences in the hydrolysis and complex formation of Mo, W, and Sg and to study the redox potential of Sg^{VI}.

6. Chemical Properties

Experimental results presented in this Section provide important information on the chemical behavior of these elusive elements. Discussing these properties in the context of the properties of other elements, the structure of the Periodic Table, or even the manifestation of relativistic effects is an increasingly challenging task. It must be remembered that with all the constraints in atom-at-a-time chemistry, only a limited number of chemical properties can be studied experimentally.

Formation of (a limited number of) chemical compounds and volatilities of atoms and compounds were investigated with thermochromatography and gas-chromatography experiments by measuring adsorption temperatures and retention times, respectively. The formation of complexes in aqueous solutions, the behavior of these complexes, and their interaction with a second phase (organic complexing solution or ion-exchange resin) is studied in liquid-chromatography and extraction experiments.

Results can only be compared with the behavior of other elements investigated in the same experiment. Moreover, in online gas-phase and thermochromatographic studies a direct comparison is only meaningful if all the investigated nuclides have about the same half-life.[131] This is because most short-lived nuclides decay before they reach, for example, their final deposition temperature in a thermochromatographic experiment; at the end, products migrate very slowly along the temperature gradient. Consequently, a seemingly too high deposition temperature is determined; see Section 6.3.2. for an example.

In the interpretation of experimental results, beyond the pure analogy to the lighter homologues, assumptions are

 © 2006 Wiley-VCH Verlag GmbH & Co. KGaA, Weinheim

made about the oxidation state or the type of compound formed. Many important properties, such as ionic radii and the stability of oxidation states, can only be judged indirectly, for example, by comparison with the known properties of lighter homologues in a group and their chemical behavior. In addition, the chemical composition of SHE compounds is not known and they are not accessible to classical structural investigations. The compositions can only be assumed on the basis of analogy in their experimental behavior. Empirical model assumptions are always needed, for example, to calculate physicochemical quantities such as adsorption enthalpies[166] or sublimation enthalpies.[167] The step towards the interpretation of these results in terms of relativistic effects is an even more sophisticated task.

6.1. Rutherfordium (Rf, Element 104)

The Rf chemistry was pioneered by Zvara and co-workers with experiments in the gas phase[72,130] and by Silva et al. and Hulet et al. in acidic, aqueous solutions.[73,74] These experiments demonstrated that Rf behaves different from trivalent actinides, and—as expected for a member of Group 4 of the Periodic Table—Rf behaves similar to its lighter homologues Zr and Hf. With the advent of a renewed interest in transactinide chemistry in the late 1980s, many techniques have been developed and used to extensively study Rf in comparison with Group 4 elements and, in aqueous solution, in comparison with tetravalent Th and tetravalent Pu ions as Group 4 pseudo-homologues. These experimental results have revealed a number of surprises but were not always free of contradictory results between individual experiments, and some were plagued by adsorption problems. Overviews of Rf chemistry can be found in refs. [77,79,81,90,94,109,121]. Refs. [80,120] concentrate on Rf properties in the aqueous phase and refs. [115,129,130] on the behavior of Rf in the gas phase.

6.1.1. Liquid-Phase Chemistry

Experiments in the aqueous phase concentrated on unraveling the competing strength of hydrolysis and complex formation with halide anions. In parallel, and to compare and understand the measured distribution coefficients (K_d), theoretical model calculations[108,168] were performed to compute hydrolysis constants and complex formation constants and described these processes for Group 4 elements (M = Zr, Hf, Rf). The first hydrolysis step is described in the reaction in Equation (3). At pH > 6 the pH-dependent step-wise hydrolysis (deprotonation) process gives rise to the formation of $M(OH)_5^-$.

$$M(H_2O)_8^{4+} \rightleftharpoons MOH(H_2O)_7^{3+} + H^+ \quad (3)$$

The analogous step-wise complexation with halide anions (X = F, Cl) proceeds for non-hydrolyzed species according to Equation (4).

$$\begin{aligned} &M(H_2O)_8^{4+} + HX \rightleftharpoons MX(H_2O)_7^{3+} + H_2O + H^+ \\ &\ldots \rightleftharpoons \ldots MX_3(H_2O)_5^{+} + HX \ldots \rightleftharpoons \ldots \\ &MX_4(H_2O)_4 + HX \ldots \rightleftharpoons \ldots \\ &MX_5(H_2O)^- + HX \ldots \rightleftharpoons MX_6^{2-} + H_2O + H^+ \end{aligned} \quad (4)$$

For hydrolyzed species it proceeds according to Equation (5).

$$\begin{aligned} &M(OH)_4 + HX \rightleftharpoons M(OH)X + H_2O \\ &\ldots \rightleftharpoons \ldots \\ &M(OH)X_3 + HX \rightleftharpoons MX_4 + H_2O \end{aligned} \quad (5)$$

Which process prevails and which are the most abundant species in solution very much depends—apart from the kind and concentration of the halide anion—on the pH value of the solution. Among all halide complexes the ones with fluoride ions are by far the most stable.

Fully relativistic molecular density-functional theory (DFT) calculations of the electronic structures of hydrated and hydrolyzed species and of fluoride and chloride complexes were used to compute free-energy changes for hydrolysis and complex formation reactions.[168] For M^{4+} species, which undergo extensive hydrolysis at a pH > 0, it was predicted that the hydrolysis decreases in the sequence Zr > Hf > Rf.

Also the fluoride complex formation of non-hydrolyzed species (present in strong acid solutions) decreases in the sequence: Zr > Hf > Rf. However, it was realized that this trend is inverted (Rf ≥ Hf > Zr) at a pH > 0 for the fluorination of hydrolyzed species or fluorocomplexes. Under these less acidic conditions differences between the Group 4 elements are very small. Chloride complexation was calculated to be independent of pH value and always follows the trend: Zr > Hf > Rf.

By combining all the results it was predicted that for a separation—performed on a cation exchange resin in dilute ($< 10^{-2}$ M) HF—the K_d values will have the following trend in Group 4: Zr ≤ Hf < Rf. This reflects the decreasing trend Zr ≥ Hf > Rf in the formation of positively charged complexes.

Experimental results about the Rf behavior in comparison with its lighter homologues (and pseudo-homologues) were obtained from:

1) extracting neutral species into tributylphosphate (TBP) with HCl and HBr solutions,[169–172]
2) extractions of anionic complexes with triisooctyl amine (TiOA) with HF and HCl solutions,[173,174]
3) ion-exchange studies of predominantly cationic species with HF and HNO_3 solutions,[175,176]
4) ion-exchange studies of predominantly anionic species with HF, HCl, and HNO_3 solutions,[123,127,128,175]
5) adsorption experiments on cobalt ferrocyanide.[177]

In all of these experiments Rf nuclear decay was directly observed after the chemical separation procedure. While some were procedures were manually performed batch-extractions with separations of an aqueous and an organic phase, the more recent ones were carried out as column

© 2006 Wiley-VCH Verlag GmbH & Co. KGaA, Weinheim

chromatographic separations with the automated set-ups ARCA II and AIDA (see Section 5.2). Investigations where the behavior of cationic species of Rf (in dilute HF and mixed HF/HNO_3 solutions) were deduced from the observation of long-lived nuclear-decay products have also been performed with the multicolumn techniques (see Section 5.3).[158,159,161,164] These results are in agreement with ARCA and with AIDA data.

The formation and behavior of neutral species were characterized by extracting Zr, Hf, and Rf from 8 M HCl into TBP. Column-chromatographic separations were performed with a (undiluted) TBP coating on an inert support material. The distribution coefficient of Rf was determined as 150(+64/−46) compared to a value of 53(+15/−13) for Hf, obtained in the same experiment.[171,172] This result is in good agreement with previously measured offline data ($K_d(Hf) = 65$, $K_d(Zr) = 1180$) and it gives the extraction sequence $Zr > Rf > Hf$ (Figure 13).

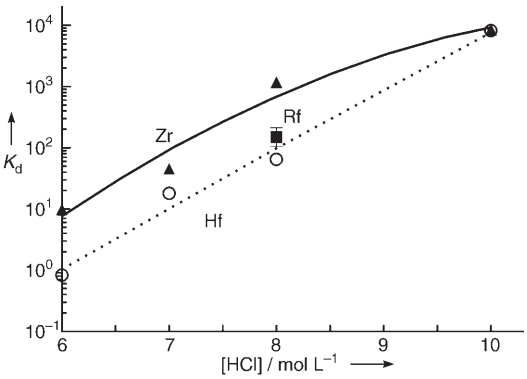


Figure 13. Distribution coefficients (K_d) for the extraction of neutral species of Zr (▲, ——), Hf (○, •••••) and for Rf (■) at 8 M HCl/TBP. Data from refs. [171,172].

While this sequence seems to be somewhat surprising based on empirical extrapolations, this sequence is expected from the above mentioned theoretical considerations on the competition between hydrolysis of the chloride complexes in the aqueous solution and the formation and the extraction of these complexes into the organic phase. The tendency for the hydrolysis of Group 4 chloride complexes (the reverse process of the complex formation) in 8 M HCl is then $Hf > Rf > Zr$. Detailed discussions of earlier and partially conflicting results are given in ref. [79,120]

To investigate cationic species, differences in the Zr, Hf, Th, and Rf behavior in mixed 0.1 M HNO_3/HF solutions were studied in cation-exchange-chromatography experiments with ARCA.[175] Results are shown in Figure 14. For Zr and Hf K_d values drop between 10^{-4} M and 10^{-2} M HF. For Rf this decrease is observed at about one order of magnitude higher HF concentrations, and it appears at even higher concentrations for Th. Therefore, the transition from cationic to neutral and then anionic species requires higher HF concentrations for Rf than for Zr and Hf, but lower than the ones needed for Th. This result establishes the following sequence of F^- complex formation strength at low HF concentrations:

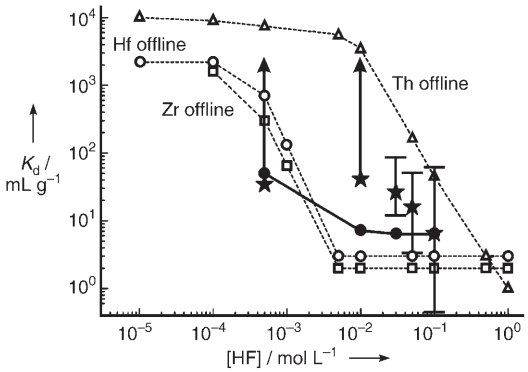


Figure 14. Sorption of Zr, Hf, Th, and Rf on the cation-exchange resin (CIX) Aminex A6 from 0.1 M HNO_3 at various HF concentrations. As indicated some data were obtained in offline (open symbols) and some in online experiments. ⋆ Rf online, ● Hf online. Adapted from ref. [94] with a revised version of data from ref. [175].

$Zr \geq Hf > Rf > Th$.[175] For a similar system confirming data were obtained with AIDA.[176]

These results are on a qualitative basis, that is, the sequence of extraction and complex formation, in agreement with theoretical expectations.[168] However, predicting K_d values quantitatively still remains a challenging task for theory, mainly because of the large variety of positively charged complexes in solution and in extracted form. However, using the ionic radii[43,178] of Zr (0.072 nm), Hf (0.071 nm), Rf (0.078 nm), and Th (0.094 nm) it is appealing to apply the hard soft acid base (HSAB) concept[179] in an empirical approach to find an explanation of the observed extraction sequence. In this concept it is assumed that the hard F^- ion interacts stronger with small (hard) cations. From this, what is expected, in agreement with the observation, is a weaker F^- ion complexation of Rf than with Zr and Hf.

The experimental situation concerning the transition towards anionic species at HF concentrations between 10^{-2} M and 1 M HF remains somewhat ambiguous. In one experimental series performed with an anion-exchange resins,[175] for Zr and Hf the K_d values increase from about 10 to more than 100 between 10^{-3} M and 10^{-1} M HF (measured offline in batch-extraction experiments with long-lived tracers). This result is a continuation of the trend observed on cation-exchange resin. For the Th offline data, and for the Hf and Rf online data, no significant rise of the K_d values was observed on anion-exchange resin for HF concentrations between 10^{-3} M and 1 M HF. While this is expected for Th, which does not form fluoride complexes, it comes as surprise for Hf and Rf. How much this experiment is affected by the 0.1 M HNO_3 in the solution remains unclear. Earlier experimental results suggest that Rf forms anionic F^- complexes in pure 0.2 M HF, in mixed 0.27 M HF/0.1 M HNO_3, and 0.27 M HF/0.2 M HNO_3 solutions.[158,161] However, also these experiments are not free of open questions. More experimental work is needed to confirm or reject these data and to solve this puzzle.

The formation of anionic complexes from more-concentrated acid solutions is much more evident. Recent anion-exchange chromatographic separations with AIDA showed

 © 2006 Wiley-VCH Verlag GmbH & Co. KGaA, Weinheim

that the adsorption of Rf (measured as percent adsorption) increases steeply from 7.0 M to 11.5 M HCl (see Figure 15).[123,125] Typical for a Group 4 element, this behavior

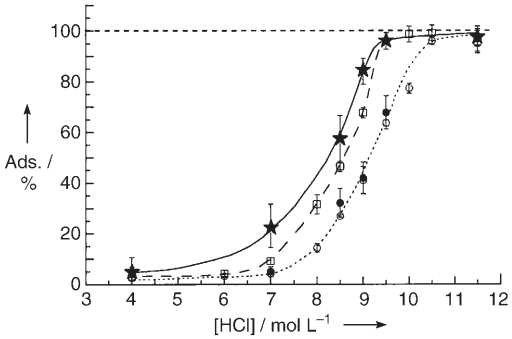


Figure 15. Variation of the percent adsorption of Zr, Hf and Rf on the anion exchange resin CA08Y from HCl at various concentrations. ⋆ Rf (Cm/Gd target), □ Zr (Ge/Gd target), ● Hf (Cm/Gd target), ○ Hf (Ge/Gd target). Adapted from ref. [123].

goes in parallel with that of Zr and Hf, and is distinctively different from that of the pseudo-homologue Th. The adsorption sequence over the entire range is Rf > Zr > Hf. This result can also be interpreted as the sequence in chloride-complexing strength. However, this experimental outcome[123] remains to be understood theoretically as it clearly contradicts earlier predictions.[168] First attempts to shed more light on this question from experimental chemical-structure investigations using EXAFS spectroscopy are under way.[125]

Recent experiments with AIDA provide more exciting and challenging data on the formation of anionic fluoride complexes of Rf in comparison to its Group 4 members Zr and Hf.[127] Measurements were made by anion-exchange chromatography for 1.9 M to 13.9 M HF solutions. In this concentration range it is important to realize that $[HF_2^-]$ increases approximately like the "initial" concentration, $[HF]_0$, while the $[F^-]$ remains almost constant. A decrease of the K_d values of Zr and Hf with increasing [HF] is explained as the displacement of the metal complex from the binding sites of the resin by HF_2^- ions. It is stunning to see that, in contrast to the experimental results obtained in HCl and HNO_3 solutions, Rf behaves distinctly differently from Zr and Hf. As shown in Figure 16, above 2 M HF the percent adsorption for Rf on anion-exchange resin drops much earlier and is significantly less than that of Zr and Hf up to 13.9 M HF.

A plot of K_d values versus the "initial" HF acid concentration, see Figure 17, also reveals a significant difference between Rf and Zr and Hf. A slope of -2.0 ± 0.3 of $\log K_d$ against $\log[HF]$ was determined for Rf while the slope for Zr and Hf is -3.0 ± 0.1, indicating that different anionic fluoride complexes are formed.[127] The slope analysis indicates that Rf is present as the hexafluoride complex $[RfF_6]^{2-}$—similar to the well known $[ZrF_6]^{2-}$ and $[HfF_6]^{2-}$ at lower HF concentration—whereas Zr and Hf are presumably present in the forms of $[ZrF_7]^{3-}$ and $[HfF_7]^{3-}$. The first measurement of a Rf elution curve,[128] performed with 5.4 M HF on anion-exchange columns, is in excellent agreement with previous data.

It was qualitatively discussed and suggested[125,127] that relativistic effects may strongly influence the fluoride-complexing ability of Rf and, therefore, lead to the observed differences. This possibility is deduced from relativistic DFT calculations.[127] In this case, the trend in the orbital overlap population between the valence d orbitals of M^{4+} and the valence orbitals of F^- was found to be Zr ≈ Hf > Rf, suggesting that the Rf complex is less stable than those of Zr and Hf for both the $[MF_6]^{2-}$ and the $[MF_7]^{3-}$ complex structures. This result is different from the theoretically predicted sequence in ref. [168] However, a quantitative theoretical understanding still waits to be established.

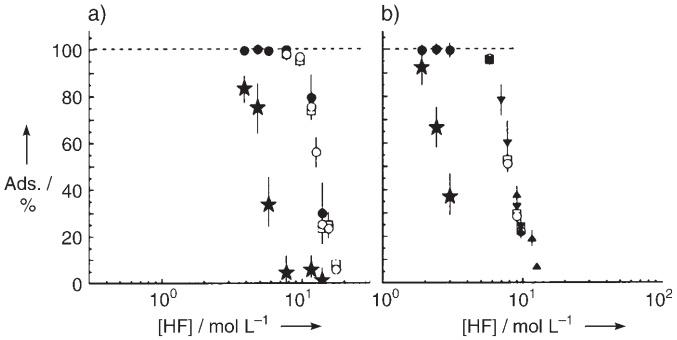


Figure 16. Variation of the percent adsorption of Rf, Hf, and Zr on the anion-exchange resin CA08Y as a function of the initial HF concentration, obtained with the two different size columns: a) 1.6×7 mm and b) 1.0×3.5 mm. ⋆ ^{261}Rf (Cm/Gd), ● ^{169}Hf (Cm/Gd), ○ ^{169}Hf (Ge/Gd), ▼ ^{167}Hf (Eu), □ ^{85}Zr (Ge/Gd), ▲ ^{89m}Zr (Y). Adapted from ref. [127].

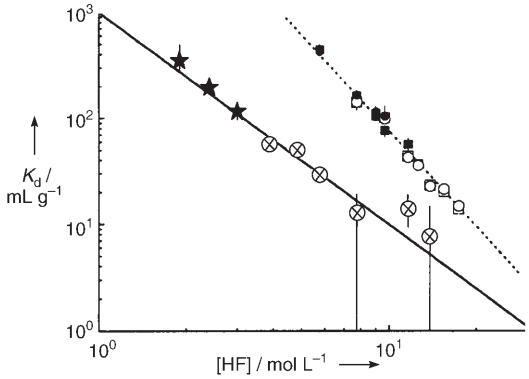


Figure 17. Variation of the distribution coefficient, K_d, of Rf, Zr and Hf (as obtained with two different size chromatographic columns) on an anion-exchange resin as a function of the "initial" HF concentration. ⊗ Rf (a), ⋆ Rf (b), □ Zr (a), ■ Zr (b), ○ Hf (a), ● Hf (b); a) 1.6 i.d. × 7.0 mm, b) 1.0 i.d. × 3.5 mm; i.d. = internal diameter. Adapted from ref. [127].

A hypothetically Th-like or Pu-like behavior of Rf was tested in AIDA with an anion-exchange resin and 8 M HNO_3. While Th and Pu form anionic complexes, and are consequently strongly adsorbed, Rf remains in solution[123] forming cationic or neutral species—as expected for a typical Group 4 element with non-Th-like—and non-Pu-like properties.

6.1.2. *Gas-Phase Adsorption Chemistry*

The first[180] and the subsequent large number of pioneering experiments with Rf in the gas phase (see

 © 2006 Wiley-VCH Verlag GmbH & Co. KGaA, Weinheim

ref. [72,130,181,182] and ref. [183] concerning the element's name) demonstrated that Rf—similar to its Group 4 homologue Hf—forms a chloride that is much more volatile than the actinide chlorides. For some-time thereafter, the question raised interest whether metallic (atomic) Rf behaves chemically like a typical member of Group 4 or whether it could exhibit properties of a p-like element similar to Pb in Group 14. This idea was triggered by a suggestion that relativistically stabilized $7p_{1/2}$ orbitals could result in a $[Rn]5f^{14}7s^27p^2$ ground-state configuration.[184] Support came from (relativistic) multiconfiguration Dirac–Fock calculations which resulted in a Rf ground-state configuration of $6d7s^27p$[185] or a mixing of 80% $6d7s^27p$ and 18% $6d^27s7p$ (among other configurations).[186,187]

Experiments searching for volatile atomic Rf—a typical Pb-like behavior—did not show any p-like properties of Rf and today this discussion is no longer relevant.[187,188] This is not only because of the now trusted $6d^27s^2$ ground state (see Table 2), predicted from a more recent and more accurate coupled-cluster single-double (CCSD) excitations calculation (see Table 2),[189] but also because there is sufficient confidence that a p-like ground state, which is only about 0.24 eV[186] or 0.5 eV[185]) below a d-like state, would not results in typical Pb-like properties. Owing to energetically favored formation of stronger bonds when forming compounds in the d-valence configuration, the low activation energy is easily overcompensated. In addition, ionization potential, atomic, and ionic radii for Rf are very similar to those of Hf.

A new series of online gas-chromatographic studies were performed in the 1990s to compare Rf with its lighter Group 4 homologues by using chlorinating[190] and brominating[191] reagents (see ref. [115,129] for reviews). In the chloride system, theoretical considerations also excluded a Pb-like behavior of Rf.[192] Besides the aim of determining the formation and behavior of Rf compounds, the scope of these experiments was to probe the influence of relativistic effects on chemical properties.[193] This system seems to be especially apt for obtaining a clear answer about the influence of relativistic effects on a chemical property. From relativistic calculations[107,187,194] $RfCl_4$ was predicted to be more volatile than $HfCl_4$, whereas from non-relativistic calculations[107] and from extrapolations of trends[195] within the Periodic Table exactly the opposite behavior is expected. The results of these different volatility predictions are shown in Figure 18 in terms of vapor pressure versus temperature.

Because of the use of nuclides with very different half-lives—a parameter which can strongly influence thermochromatographic results[113,196]—it was almost impossible to precisely determine relative volatilities in the pioneering experiments. More recently, isothermal gas-chromatographic experiments established that Rf chlorides are more volatile than Hf chlorides (see left part of Figure 19).[190,193,197] This feature has been interpreted as being the result of relativistic effects. Unexpectedly, under similar experimental conditions, Zr was observed together with Rf instead of showing a behavior similar to Hf or an even lower volatility. This finding remains puzzling. A study of Rf bromides showed the same sequence in volatility with Rf bromide being more volatile than Hf bromide.[191,197]

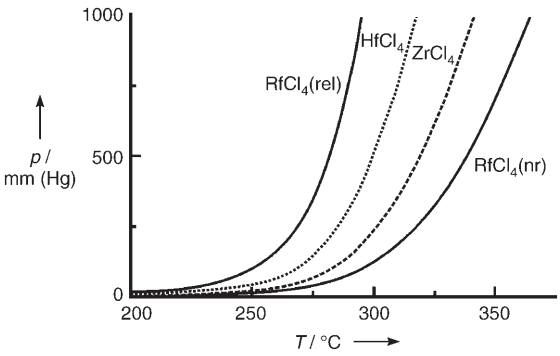


Figure 18. Volatility in terms of vapor pressure as a function of temperature for $ZrCl_4$ and $HfCl_4$ (experimental values) together with theoretical predictions for $RfCl_4$ including relativistic effects (rel) and for a hypothetical non-relativistic (nr) case. Adapted from ref. [107].

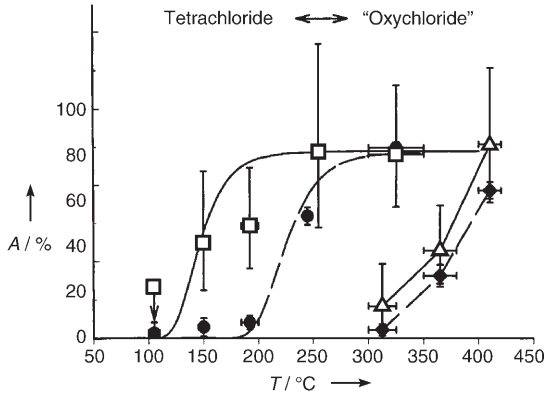


Figure 19. "Break-through" yields for ^{261}Rf (open symbols) and ^{165}Hf (closed symbols) tetrachlorides (left side) obtained from oxygen-free HCl as a reactive gas and for oxide chlorides (right side) formed with $SOCl_2$ vapor and oxygen as reactive gases. ●, ◆ ^{169}Hf ($t_{1/2}$ = 78.6 s); □, △ ^{261}Rf ($t_{1/2}$ = 78(−6/+11 s). Lines in the left part are results from Monte-Carlo simulations. Adapted from ref. [193]. *A* activity, *T* isothermal temperature.

In Monte Carlo simulations of the chromatographic process, the adsorption enthalpies ($\Delta H_a^{0(T)}$) for single molecules on the quartz surface of the column are obtained by finding a best fit to the experimental data by varying ΔH_a as the free parameter.[115,196] Figure 20 shows a compilation[121] of Group 4 element chloride and bromide adsorption enthalpies. The experimental values for Rf show a striking reversal of the (empirically) expected trend, which is however, in agreement with relativistic theoretical model calculations.[107] Therefore, this "reversal" is evidence for relativistic effects.

An estimate of the standard sublimation enthalpy (ΔH_s^0) can be obtained from a well established, empirical linear correlation which exists between $\Delta H_a^{0(T)}$ and ΔH_s^0 for a number of chlorides and other compounds (see ref. [130,195] and references therein). It is noteworthy that by using this procedure a physicochemical quantity for macro-amounts can be deduced from the behavior of a single atom.

 © 2006 Wiley-VCH Verlag GmbH & Co. KGaA, Weinheim

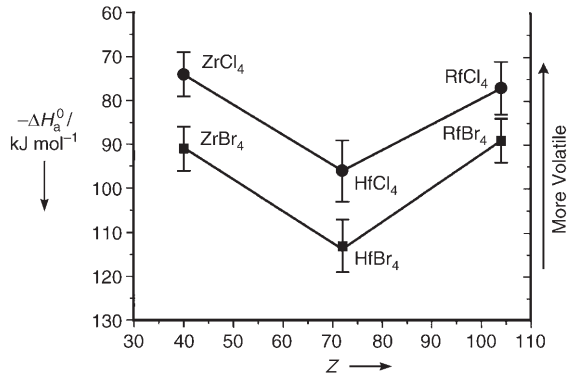


Figure 20. Adsorption enthalpies (ΔH_a^0) of chlorides and bromides of Zr, Hf, and Rf on quartz surfaces. Adapted from ref. [121].

One problem when studying the pure Group 4 halides is the possible formation of Group 4 oxy halide compounds. It was shown in the chloride system that small amounts of oxygen can lead to the formation of a less volatile oxy chloride instead of the pure chloride. If present, the oxy halide compounds may pose problems in the interpretation of experimental results, especially if there are pronounced differences in how easily Zr, Hf, and Rf form an oxy chloride.[193] As seen in Figure 19, oxy halides are less volatile than pure halides. Such a behavior was first observed in a thermochromatographic experiment.[198] It is interesting to note, that the behavior of $RfOCl_2$ and $HfOCl_2$ is much more similar than the behavior of the pure halide compounds is. This observation may be explained by the assumption that oxy chlorides are only present in the adsorbed state and not in the gas phase. The transport mechanism in Equation (6) was proposed.[129]

$$MCl_{4(gas)} + 1/2\,O_2 \rightleftharpoons MOCl_{2(ads)} + Cl_{2(gas)} \quad (6)$$

6.2. Dubnium (Db, Element 105)

A normal continuation in the Periodic Table puts element 105, dubnium, Db, (see ref. [199] for element 105 names) into Group 5, below Nb and Ta. Early thermochromatographic separations of volatile chloride and bromide compounds showed that Db behaves more like a transactinide than an actinide element.[75,112] These experiments also indicated that Db chloride and bromide are less volatile than the Nb halides.[75] In its first aqueous chemistry, Db was adsorbed onto glass surfaces from HCl and HNO_3 solutions, a behavior very characteristic of Group 5 elements.[76] However, an attempt to extract Db fluoride complexes failed under conditions in which extracts Ta complexes but not Nb complexes. This observation provided evidence of unexpected Db properties,[76] and it triggered a number of follow-up investigations in aqueous solutions with ARCA which revealed several, at-first-glance, unanticipated Db properties. In the following Sections, illustrative examples of the Db chemistry will be discussed. Overviews can be found in the same references listed in Section 6.1 for Rf.

6.2.1. Liquid-Phase Chemistry

The first detailed comparison between Db, its lighter homologues Nb and Ta, and the pseudo-homologue Pa was carried out with solutions at different HCl concentrations to which small amounts of HF were added. Four series of liquid–liquid extraction chromatography experiments were performed in ARCA II[122] with TiOA as a stationary phase on an inert support.[200]

The first and second experiments with a total of 340 individual separations tested a typical behavior of the pentavalent ions, namely the complete extraction of Nb, Ta, Pa, and Db into TiOA from 12 M HCl/0.02 M HF and from 10 M HCl. As expected, Db was found to be extracted together with Nb, Ta, and Pa.

In the next series of 721 collection and separation cycles, after the first extraction step, a Nb–Pa fraction was eluted with 4 M HCl/0.02 M HF then a Ta fraction with 6 M HNO_3/0.0015 M HF. It came as a big surprise, that 88 % of the Db was detected in the Nb–Pa fraction and only 12 % tailed into the Ta fraction. This behavior is identical with that of Nb and Pa, and distinctively different from that of Ta—a striking non-Ta-like behavior (under the given conditions).

To distinguish between a Nb-like and a Pa-like behavior, in 536 experiments with 10 M HCl/0.025 M HF Pa was eluted first, then came a Nb fraction with 6 M HNO_3/0.0015 M HF. Db showed an intermediate behavior (25 α events in the Pa fraction and 27 α events in the Nb fraction) indicating that the halide complexing strength of Db is in between that for Nb and Pa. In a follow-up experiment using 0.5 M HCl/0.01 M HF to separate Pa and Nb, Db even showed more Pa-like properties.[201] A summary of these results is shown in Figure 21. These stunning results[200,201] provided strong motivation to continue more detailed investigations of transactinides and laid the basis for a large experimental program.

The interpretation of these results was severely hampered by the use of the mixed HCl/HF solution that did not allow the complex formed to be clearly distinguished. In contrast to the experimentally observed extraction sequence from HCl solutions with small amounts of HF added, the inverse order $Pa \gg Nb \geq Db > Ta$ was theoretically predicted[202] for the extraction from pure HCl solutions. This work considered the competition between hydrolysis[203] and chloride-complex formation. Recent experimental studies performed in the pure F^-, Cl^-, and Br^- system[204] are in excellent agreement with the theoretical predictions which include relativistic effects.[202,205] The fluoride complexation of Db in 0.2 M HF was recently confirmed in an experiment which used three consecutive ion-exchange columns—a cation exchange (filter) column, an anion exchange (chromatography) column, and another (filter) cation exchange column.[163] It was shown that Db forms an anionic fluoride complex which is strongly retained on the anion-exchange resin.

For the system Aliquat 336(Cl^-)—a quaternary ammonium salt which acts like a liquid anion-exchanger—and (pure) 6 M HCl, an extraction sequence of $Pa > Nb \geq Db > Ta$ was determined (see Figure 22). This, in agreement with theoretical predictions,[202,205] is the inverse to that in HCl solution containing some HF. In series of offline and online experi-

© 2006 Wiley-VCH Verlag GmbH & Co. KGaA, Weinheim

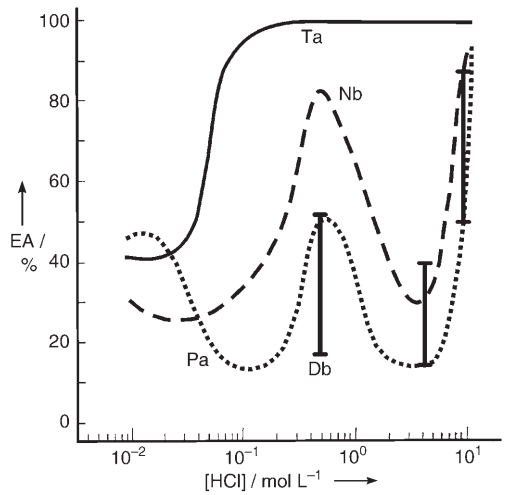


Figure 21. Fractional extracted activity of Ta (——), Nb (-----), and Pa (•••••) tracers as a function of HCl concentration in the system TiOA-HCl/0.03 M HF. The bold bars encompass the upper and lower limits deduced for the Db extraction from the elution position in chromatography experiments at 10 M HCl/0.025 M HF, 4 M HCl/0.02 M HF, 0.5 M HCl/0.01 M HF. The bar for the complete extraction of Db from 12 M HCl/0.02 M HF is not included in the Figure for clarity. Data from refs. [200, 201]. EA = extracted activity.

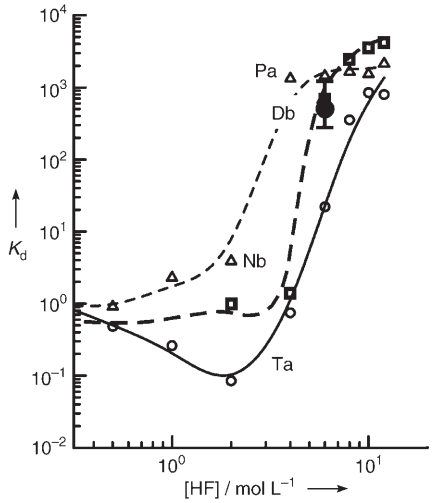


Figure 22. Distribution coefficients for the extraction of Ta (○, ——), Nb (□, – – –), and Pa (△, -----) tracers from pure HCl at various concentrations into Aliquat 336(Cl^-). The K_d of Db at 6 M HCl (●) is plotted with error bars encompassing 68% confidence limits. Data from ref. [204].

ments, K_d values of 1440, 683, 438 (+532/−166), and 22 were measured for the Pa, Nb, Db and Ta, respectively.

In pure HCl solutions, at concentrations above 2–4 M HCl, all the elements Nb, Ta, Pa, and presumably Db, form the same type of complexes, $[M(OH)_2Cl_4]^{2-}$, $[MOCl_4]^-$, $[MOCl_5]^-$, and $[MCl_6]^-$ (M = Nb, Ta, Db, Pa) with increasing HCl concentrations. From the theoretically and experimentally determined strength of chloride-complex formation it is observed that Pa forms a specific complex in a more dilute solution (starting with $[Pa(OH)_2Cl_4]^-$ at 2–4 M HCl) followed by the other elements at higher concentrations. The complexes of Nb start to form next ($[Nb(OH)_2Cl_4]^-$ above 4–5 M HCl), while the $[Ta(OH)_2Cl_4]^-$ complex is formed at or above 6 M HCl. This suggests that at 6 M HCl the complex $[Db(OH)_2Cl_4]^-$ is predominant. Additional experiments[204] confirmed the theoretically expected sequence of complexing strength among the halide anions: fluoride ≫ chloride > bromide. More information on other, previously performed experiments is given in refs. [77, 79–81, 109, 120, 121]

Once well-developed and "tested", fast chemical-separation procedures for Db were at hand—which used the detection of nuclear decay properties of ^{262}Db to characterize the Db chemistry. These techniques were applied to obtain important information on the nuclear properties.[206] With 100 μL of 0.05 M α-hydroxyisobutyric acid, Db fractions were eluted within 6.5 s from a cation exchange resin in ARCA and were prepared for α-spectroscopy. The chemically separated samples had a purity that allowed the successful search for, and discovery of, the new isotope ^{263}Db ($t_{1/2} = 27$ s) and its decay properties to be determined.[206, 207]

6.2.2. *Gas-Phase Adsorption Chemistry*

All detailed investigations to determine the volatility of Db and Group 5 element compounds in the gas-phase have been performed with pentahalides (chlorides and bromides) and with the significantly less-volatile oxy halides. Owing to the high tendency of Group 5 elements to react with trace amounts of oxygen or water vapor to form oxy halides,[131, 208, 209] investigations of pure halides require an intensive purification of all gases and a very careful preconditioning of the quartz chromatography columns with the halogenating reactive carrier gas prior to each experiment. Under certain conditions it was even necessary to add an additional reactive component, for example, BBr_3 was added to the Br_2, to prevent the formation of an oxy bromide.[131, 148] Some of the literature data may have suffered from—and their interpretation may have been obscured by—the unintentional formation of oxy halide compounds. When searching for differences in volatilities of the pure halides of Nb, Ta, and Db, differences in the formation probability of oxy halides along the Group 5 elements may add an additional complication, especially in experiments at the limits of feasibility. For the lighter Db homologues in group 5 the following trends have been observed:

1) The volatility of MX_5 decreases in the sequence F > Cl > Br > I, which can be compared with Cl > Br > I > F in Group 4.
2) All oxy halides are less volatile than the corresponding halides, which is also true in Group 4.
3) Group 5 halides are less volatile than the corresponding ones in Group 4.

A discussion of these properties from a theoretical point of view can be found in refs. [43, 44, 107].

The early thermochromatographic experiments in chlorinating and brominating atmospheres had already qualitatively shown that the Db chlorides and bromides are less

 © 2006 Wiley-VCH Verlag GmbH & Co. KGaA, Weinheim

volatile than the Nb compounds.[75] However, half-life corrections had to be applied which made a quantitative comparison questionable. More recently, the lower volatility (compared to the lighter homologues Nb and Ta) of a Db bromide compound was confirmed in a gas-chromatographic experiment with OLGA.[210] Interestingly, the volatile Ta bromide was only formed when BBr_3 was added to the HBr. A volatility trend of $Nb \approx Ta > Db$ was observed. This sequence is very surprising since theoretical calculations, which included relativistic effects, predict a higher volatility for the $DbBr_5$ that is presumably formed than for $NbBr_5$ and $TaBr_5$;[107,211] similarly to the observed sequence in Group 4. It was speculated,[115] that instead of the pentabromide the $DbOBr_3$ may have been formed and investigated in these experiments. However, this implies that under identical conditions Nb and Ta form pentabromides while Db forms an oxy bromide. This situation would be in agreement with theoretical calculations[212] showing a stronger tendency for Db to form oxy halides than Nb and Ta and could be viewed as an influence of relativistic effects in Db. A different theoretical approach showed a monotonic trend in the stability of monooxides for the series Nb, Ta, and Db.[213]

Several attempts to form the pure Db pentachloride failed. The results of the last series of experiments with OLGA, which used elaborated purification techniques, are shown in Figure 23.[115] Conditions were used which allowed a

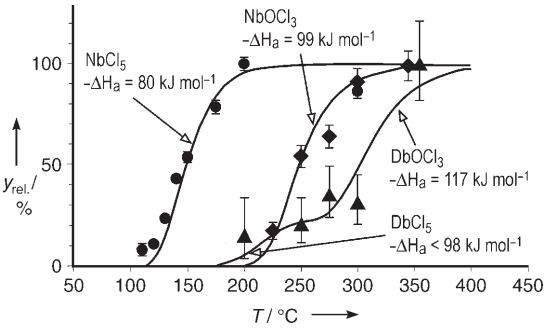


Figure 23. Relative yield (y_{rel}) of Db (▲) measured in online gas-chromatographic experiments with purified HCl. The Nb results were obtained under oxygen-free conditions (●, $pO_2 = 1$ ppm) and with oxygen present (◆, $pO_2 \approx 100$ ppm). Curves are best fit Monte Carlo simulations with the adsorption enthalpies (ΔH_a) as a fit parameter. Adapted from ref. [115].

well established break-through curve for $NbCl_5$ to be measured in preparatory experiments. However, Db showed a behavior, which was interpreted as the result of the presence of two species, namely $DbCl_5$ and $DbOCl_3$. Compared to $NbOCl_3$, $DbOCl_3$ became "volatile" at an approximately 50 °C higher temperature—indicating a lower volatility for $DbOCl_3$ than for $NbOCl_3$. For what was interpreted as a $DbCl_5$ component, only a volatility limit was established. The final comparison on the halide volatility of Group 5 elements including Db remains to be performed.

6.3. Seaborgium (Sg, Element 106)

In 1974, A. Ghiorso, J. M. Nitschke and co-workers discovered element 106 in the reaction $^{249}Cf(^{18}O,4n)^{263}Sg$.[214] For 20 years, ^{263}Sg ($t_{1/2} = 0.9$ s), which is produced at a rate of about six atoms per hour, was the longest-lived known isotope. Its short half-life and a low production rate prohibited chemical investigations for a long time. While the α-decay properties of ^{263}Sg, which were observed in the discovery experiment, were confirmed in investigations of ^{271}Ds (its α-decay chain passes through ^{263}Sg),[49,57] none of these experiments supported evidence for the previously reported sf decay in ^{263}Sg.[215]

With the large number of detailed chemical investigations of Rf and Db came the development of more sensitive, new and improved experimental techniques. Together with the firm belief—based upon nuclear-reaction systematics and calculations—that it would be possible the produce a longer-lived, hitherto unknown isotope of Sg in the $^{22}Ne + ^{248}Cm$ reaction, preparations started in the first half of the 1990s to perform chemical investigations of Sg in the aqueous phase and in the gas phase. A large international collaboration finally involving 16 institutes from nine countries crystallized around nuclear-chemistry groups at the GSI, Darmstadt, the University of Mainz, and the University Bern–PSI, Villigen. Shortly before the first Sg experiment was performed at GSI, a Dubna/Livermore collaboration reported the discovery of $^{265,266}Sg$ with half-lives in the ten-second range in the envisioned reaction.[216,217] The door to detailed chemical investigations of Sg was pushed open.

Seaborgium is expected to behave chemically like a member of Group 6 with Cr, Mo and W as its lighter homologues. Oxides, oxy halides, and hydroxy halides are important and characteristic compounds of these elements. The formation and the properties of such Sg compounds in comparison with lighter homologues have been investigated in the aqueous phase and in the gas phase.

6.3.1. Liquid-Phase Chemistry

The first chemical separation and characterization of Sg in aqueous solution[218,219] was conducted using $^{265,266}Sg$ produced by irradiation of a ^{248}Cm target with ^{22}Ne projectiles from the GSI UNILAC. The nuclear reaction products were transported to ARCA II,[122] dissolved in 0.1 M HNO_3/5×10^{-4} M HF, and were separated on a cation-exchange resin. To probe the Sg behavior in comparison with its lighter Group 6 homologues Mo and W, and to distinguish it from a U-like behavior, 3900 identical separations were performed with a cycle/repetition time of 45 s. The "Sg-fraction" was always the first 10 s of elution. A typical chromatogram obtained with W tracer is shown in Figure 24.

Three correlated α–α decays of ^{261}Rf and ^{257}No—daughter products of ^{265}Sg—were detected. From these three observed atoms it was concluded[218,219] 1) that Sg elutes together with Mo and W, 2) that it behaves like a typical Group 6 element and forms hexavalent ions, 3) that, like its homologues Mo and W, Sg forms neutral or anionic oxide or oxy halide compounds, and 4) that it does not form seaborgyl ions

© 2006 Wiley-VCH Verlag GmbH & Co. KGaA, Weinheim

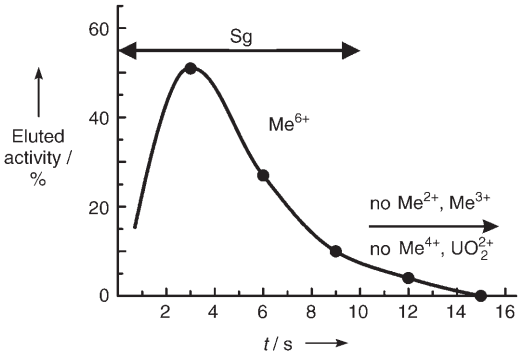


Figure 24. Elution curve for W-tracer (Me^{6+}), modeling the Sg separation on ARCA in 0.1 M HNO_3/5x10^{-4} M HF, together with "lower limit" (lower right arrow) for the elution of di- , tri-, tetravalent ions, and UO_2^{2+}. Elutions were performed at room temperature with a flow rate of 1 mL min^{-1} from 1.6×8 mm columns filled with the 17.5 ± 2 μm particle size cation-exchange resin Aminex A6. Adapted from ref. [219].

($[SgO_2]^{2+}$) making it different from its pseudo-homologue U which remains as $[UO_2]^{2+}$ on the cation exchange column. By analogy with its Mo and W homologues, it can be assumed that under the given conditions Sg forms a (hydrated) anionic complex such as $[SgO_3F]^-$ or more likely $[SgO_2F_3]^-$ or the neutral species SgO_2F_2. The result of the first experiment was that Sg exhibits properties very characteristic of Group 6 elements, and does not show U-like properties.

Owing to the low fluoride concentration in the first experiment, the seaborgate ion ($[SgO_4]^{2-}$) could not entirely be excluded. To check this option and the influence of the fluoride ion, a second series of experiments was performed with pure 0.1 M HNO_3 as a mobile phase.[220] Contrary to the lighter homologues Mo and W, Sg was not eluted from the cation-exchange resin in the absence of HF. From this it is concluded that F^- ions significantly contributed to the complex formation in the first experiment. This observation rules out that Sg was eluted as $[SgO_4]^{2-}$ in the first experiment. The non-tungsten-like behavior of Sg in pure HNO_3 may be attributed to the weaker tendency of Sg^{6+} to hydrolyze.[220,221] While Mo and W can reach the neutral species $MO_2(OH)_2$ (M = Mo, W) for Sg hydrolysis presumably stops at $[Sg(OH)_5(H_2O)]^+$ (sometimes characterized as $[SgO(OH)_3]^+$) or even at $[Sg(OH)_4(H_2O)_2]^{2+}$; these are species which presumably remain adsorbed on the cation exchange resin. This trend in the hydrolysis of metal cations is not only theoretically predicted for Group 6 (Mo > W > Sg) but also for Group 5 (Nb > Ta > Db); see refs. [43,44] for a compilation of theoretically predicted and experimentally observed hydrolysis sequences.

6.3.2. *Gas-Phase Adsorption Chemistry*

As a member of Group 6, Sg is expected—in analogy to its lighter homologues Cr, Mo and W—to be very refractory (that is, high melting) in the elemental state but to form volatile halide, oxy halide, oxy hydroxide and carbonyl compounds.[222] Although only a very limited number of relatively unstable hexahalides exist for Group 6 elements, a much larger variety of more or less stable oxy halides of the types MOX_4 and MO_2X_2 (M = Mo, W; X = F, Cl) are known. They are volatile enough for gas-phase separations between 400 °C and 150 °C. Based on these properties several experiments were performed to probe the Sg behavior in comparison with its lighter homologues. A slightly different kind of experiment was used to investigate the moderately volatile (at temperatures at and above 1000 °C) oxides (MO_3) and slightly more volatile oxy hydroxides ($MO_2(OH)_2$). A discussion of relative stabilities and volatilities of these Group 6 compounds can be found in refs. [129,195,223] from an experimental and empirical point of view and in refs. [43,194,224,225] based upon relativistic theory—including aspects of the stability of the predominant hexavalent oxidation state in Sg.

At the time when the Sg experiments at GSI were under preparation, the nuclear-chemistry group at Dubna did first experiments with what was assumed to be the sf isotope ^{263}Sg ($t_{1/2}$ = 0.9 s) produced in a $^{249}Cf(^{18}O,4n)$ reaction.[140,226,227] As a chemically reactive component, 20 % air saturated with $SOCl_2$ vapor was added to the Ar carrier gas to form volatile chlorides or oxy chlorides. A thermochromatographic technique with fission track detectors was applied (see Section 5.3 for advantages and disadvantages of this technique). Although in two experiments with a quartz wool filter in the start section of the chromatography column no events were observed, in four subsequent experiments without any filter a total of 41 sf tracks were registered along the column.[140] These events peaked at a temperature of approximately 270 °C (and tailed below 100 °C) while the ^{176}W tracer ($t_{1/2}$ = 2.5 h) peaked at a much lower temperature of around 80 °C. The following arguments were given as evidence that the observed tracks are from the decay of ^{263}Sg and are not any "background" from nuclides with $Z < 106$ (Db, Rf, actinides), sputtered target material, or U impurities in the column:[140] 1) A distinct chromatographic peak was observed which could be described by a theoretical curve, 2) a background run with the column at ambient temperature and no reactive gas added gave only 18 sf tracks located directly at the column entrance, and 3) further nuclear decay and cross section arguments supported the ^{263}Sg decay.

Based on these results, the following compounds and scenarios were postulated to describe the observed distributions: Volatile WO_2Cl_2 is formed quickly and deposits in its proper (high) temperature range; the compound then reacts in a few dozens of seconds to yield the more volatile $WOCl_4$ which is found in the lower temperature part of the column. This interpretation was supported by the experimental observation[227] that short-lived Mo and W isotopes are found at higher temperatures compared to the lower temperature deposition region for longer-lived ^{176}W. By analogy, it was proposed that SgO_2Cl_2 was formed and deposited at about 270 °C where it decayed before the more volatile $SgOCl_4$ could be formed and transported. Therefore, no information on similarities or differences in the Sg behavior compared with its lighter homologues can be deduced from the experimental observation. Additional criticism against this experiment mainly came from the open question whether the observed sf tracks really originated from the decay of ^{263}Sg.[81,109]

 © 2006 Wiley-VCH Verlag GmbH & Co. KGaA, Weinheim

In 1995, a large international collaboration started with online isothermal gas-adsorption chromatography experiments at the GSI.[218] In this work, the longer-lived isotopes ^{265}Sg ($t_{1/2} = 7.4$ s) and ^{265}Sg ($t_{1/2} = 21$ s; for nuclear properties see ref. [97])—produced in the reaction of ^{22}Ne with ^{248}Cm—were used to study the formation and volatility of oxy chlorides with the OLGA set-up.[134] The reaction zone was kept at 1000 °C and it was connected to a chromatography column made of fused silica. Reactive gases—Cl_2 saturated with $SOCl_2$ and traces of O_2—were introduced to form oxy chlorides. Break-through curves were measured for Mo, W, and Sg compounds[218,228] in the temperature range between about 150 °C and 400 °C by varying the temperature of the isothermal chromatography column from experiment to experiment. All the products leaving the column were transported to a detector set-up for an unambiguous identification of Sg by its characteristic α-decay chains.[97] Results of the break-through measurements which reflect the volatility are shown in Figure 25. Under these conditions, the formation

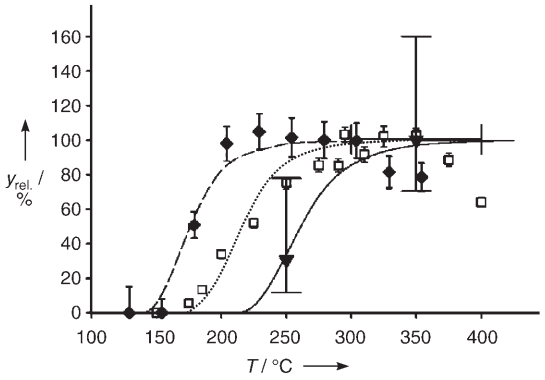


Figure 25. Relative yield (y_{rel}) of MO_2Cl_2 (M = Mo, W, and Sg) breaking through the column as a function of the isothermal temperature in the column. ◆ $^{85}MoO_2Cl_2$ ($t_{1/2} = 58.8$ s), ----- $-\Delta H_a = 90 \pm 3$ kJ mol^{-1}, □ $^{168}WO_2Cl_2$ ($t_{1/2} = 51$ s), ••••• $-\Delta H_a = 96 \pm 1$ kJ mol^{-1}, ▼ $^{265}SgO_2Cl_2$ ($t_{1/2} = 7.4$ s), —— $-\Delta H_a = 98-5/+2$ kJ mol^{-1}. Error bars are given with a 68% confidence limit. They are asymmetric for errors on small numbers.[229] Adapted from ref. [228].

of MO_2Cl_2 compounds (M = Mo, W, Sg) is most likely. The sequence in volatility of $MoO_2Cl_2 > WO_2Cl_2 \approx SgO_2Cl_2$ was established. Monte Carlo simulations of these experimental results gave adsorption enthalpies of $-\Delta H_a(MoO_2Cl_2) = 90 \pm 3$ kJ mol^{-1}, $-\Delta H_a(WO_2Cl_2) = 96 \pm 1$ kJ mol^{-1}, $-\Delta H_a(SgO_2Cl_2) = 98\ (+2/-5)$ kJ mol^{-1}—the first thermochemical properties of Sg to be determined.[228] Thus, it was shown that Sg forms oxy chlorides analogous to those of Mo and W, while U forms the different type of molecule, UCl_6, which has a much higher volatility. This Sg behavior is in line with extrapolations in Group 6 and with relativistic theory calculations.[225] A detailed discussion of the thermochemical characterization of Sg is given in ref. [223].

The adsorption enthalpies were measured with trace amounts (for W) or one-atom-at-a-time (for Sg) at zero surface coverage. Well established, empirical linear correlations[195,223] between adsorption enthalpies (obtained at zero coverage)—measured for a large number of chlorides and oxy chlorides on quartz glass—and sublimation enthalpies allow a macroscopic quantity for Sg to be derived from only a few investigated atoms: $\Delta H_s^0(SgO_2Cl_2) = 127(+10/-21)$ kJ mol^{-1}.[228] Based on this quantity it is expected that the Sg metal has an equally high or even higher sublimation enthalpy than W and, therefore, Sg is one of the least volatile elements or even the least volatile element in the Periodic Table.[129,228]

Owing to the strong tendency of Group 6 elements to form oxides, and to the experimental difficulties to avoid even traces of oxygen, to date, no experimental attempts have been made to study pure halides. However, studies of the formation and of the volatility of oxy hydroxide compounds of Sg were developed[136,230] and were performed in gas-adsorption chromatographic experiments.[137] To cope with the lower volatility of the oxides and oxy hydroxides these studies were carried out in a high-temperature gas-chromatography apparatus.[136] The reaction zone—a quartz wool plug in the entrance section of the quartz column—was kept at about 1050 °C. Here, O_2 gas, saturated with H_2O at 50 °C, was added as a reactive gas. The subsequent main part of the quartz chromatography column (about 40 cm) was held at an isothermal temperature of around 1000 °C. Products leaving the column were collected on 25 μm thin, cooled aluminum foils which were rotated in front of detectors to assay these samples for characteristic decays of Sg and W. While these temperatures are challenging for gas-chromatographic studies, the oxy hydroxide system profits from highly efficient separations not only of actinides but also Rf and Db because the oxide compounds of these elements have very low volatilities.

From the results of preparatory experiments[230] with Mo and W it was expected that for Sg the transport mechanism of the oxy hydroxide compounds would also not be a simple reversible adsorption–desorption but would rather occur through the dissociative adsorption and associative desorption process in Equation (7), sometimes also called "reaction gas-chromatography":[230]

$$MO_2(OH)_{2(gas)} \rightleftharpoons MO_{3(ads)} + H_2O_{(gas)} \quad (7)$$

Even at high temperatures, retention times of these processes are generally longer than simple adsorption–desorption processes. From the behavior of short-lived ^{166,168}W tracer a typical retention time of 8 s was calculated. Therefore, the longer-lived isotope ^{266}Sg ($t_{1/2} = 21$ s) was used in the experiment to investigate oxy hydroxide properties, despite it having a lower cross section than the usually used ^{265}Sg ($t_{1/2} = 7.4$ s). From the observation of only two Sg atoms (two ^{266}Sg α-decays shortly followed by the sf of the ^{262}Rf daughter) passing through the column, it was shown that Sg forms a volatile oxy hydroxide $SgO_2(OH)_2$, a property typical for Group 6 elements.[137]

6.4. Bohrium (Bh, Element 107)

The fourth transactinide element Bohrium is a member of Group 7 and, therefore, is expected to exhibit properties similar to its lighter homologues Mn, Tc, and Re. The same

© 2006 Wiley-VCH Verlag GmbH & Co. KGaA, Weinheim

result is obtained from fully relativistic DFT calculations of the electronic structure of the Group 7 oxy chlorides MO_3Cl (M = Tc, Re, Bh).[231] Of these compounds, BhO_3Cl is the most covalent and relatively stable. Increasing values of dipole moments and of electric-dipole polarizabilities within Group 7 are reasons for the following theoretically expected sequence of volatilities: $TcO_3Cl > ReO_3Cl > BhO_3Cl$.[231] The same order results from classical extrapolations of thermochemical properties down Group 7 which also predict BhO_3Cl to be more stable and volatile than TcO_3Cl and ReO_3Cl.[232] If only trace amounts or single atoms are present it can safely be assumed that the species MO_3Cl is formed with oxidizing chlorinating gases. The oxy halide compounds of Group 7 elements reflect their intermediate position between the lighter transactinides, which form volatile halides, and the highly volatile Group 8 tetroxides.

In addition to the oxy chlorides, also oxides and oxy hydroxides of Group 7 elements are relatively stable and volatile compounds. Early attempts to chemically investigate $BhO_3(OH)$ were based on these properties.[138,233] These experiments, performed with ^{249}Bk and the even more precious ^{254}Es as target material, were not successful because of an insufficient detection sensitivity. However, test experiments with Re have shown that the oxy hydroxide system has some potential for future studies of Bh, especially if volatile Po, Pb, and Bi contaminations, which mask the α-spectra and limit the sensitivity, can be avoided by using a physical preseparator.[234–236]

To date, the only information on chemical properties of Bh was obtained in gas chromatographic experiments[99] on the oxy chlorides which were performed by Eichler and coworkers at the PSI Philips cyclotron in Villigen. Extensive tests with Tc and Re tracer activities had been performed previously.[232] The experimental set-up for the Bh experiment was similar to the one used in the previous Sg experiments (see Figure 26).

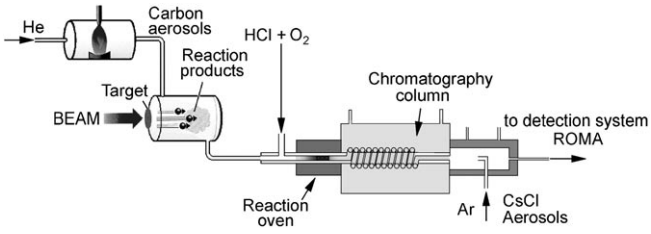


Figure 26. Schematic view of the Bh gas-chromatography experiment. Adapted from ref. [99] original drawing courtesy of R. Eichler.

The isotope ^{267}Bh ($t_{1/2} = 17$ s), which had just been discovered in an experiment at the 88-inch cyclotron at LBNL,[98] was produced in the ^{249}Bk(^{22}Ne,4n) reaction. All reaction products were carried with C-aerosols as a cluster material from the recoil chamber to the OLGA. The reactive gases HCl and O_2 were added in front of the high-temperature zone of the reaction oven which was kept at 1000 °C. In the oven, C-aerosols were burned and the oxy chloride compounds were formed. Relative yields of the compounds were measured as a function of the isothermal temperature in the quartz chromatography column. With the aid of CsCl as a recluster material the compounds which left the chromatography column were transported to the detection system.

A total of six genetically linked ^{267}Bh decay chains were observed;[99] four at an isothermal temperature of 180 °C, two at 150 °C, and none at 75 °C. The results are shown in Figure 27 as relative yields (the four events at 180 °C were

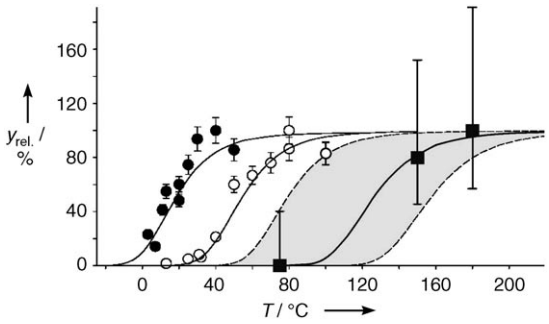


Figure 27. Relative yields (y_{rel}) of the compounds $^{108}TcO_3Cl$ (●), $^{169}ReO_3Cl$ (○) and (most likely) $^{267}BhO_3Cl$ (■) as a function of the isothermal temperature (*T*). The error bars indicate a 68% confidence interval. Solid lines are from Monte Carlo simulations with the standard adsorption enthalpies of −51 kJ mol^{-1} for TcO_3Cl, −61 kJ mol^{-1} for ReO_3Cl, and −75 kJ mol^{-1} for BhO_3Cl. The dashed lines are calculated relative yields based on the 68% confidence interval of the standard adsorption enthalpies of BhO_3Cl from −66 to −81 kJ mol^{-1}. Adapted from ref. [99].

normalized to the required ^{22}Ne-beam intensity and were taken as the 100% value) together with results from tracer experiments and with Monte Carlo simulations using a microscopic model[196] to determine standard adsorption enthalpies. The characteristic 50% yield of the BhO_3Cl curve is located at a higher temperature than the one for TcO_3Cl and ReO_3Cl.

Qualitatively, this result shows that Bh behaves like a member of Group 7 and forms a volatile oxy chloride—presumably BhO_3Cl—which is less volatile than the chloride compounds of the lighter homologues.[99] The sequence of volatility is: $TcO_3Cl > ReO_3Cl > BhO_3Cl$. More quantitatively, the deduced BhO_3Cl adsorption enthalpy of $-\Delta H^0_a = (75 + 9/-6)$ kJ mol^{-1}[99] is in excellent agreement with a theoretical prediction which includes relativistic effects.[231] This result coincides with the value expected from empirical correlations of thermochemical properties assuming Bh is in Group 7.[232] As with the Sg oxy chloride, an empirical correlation was used for BhO_3Cl to estimate the sublimation enthalpy: $\Delta H^0_s(BhO_3Cl) = 89 + 21/-18$ kJ mol^{-1} in comparison with $\Delta H^0_s(ReO_3Cl) = 66 \pm 12$ kJ mol^{-1} and $\Delta H^0_s(TcO_3Cl) = 49 \pm 12$ kJ mol^{-1}.

6.5. Hassium (Hs, Element 108)

Element 108 was discovered by Münzenberg and coworkers at the GSI in 1984 in the reaction ^{208}Pb(^{58}Fe,1n)^{265}Hs.[237] With a half-life of 1.5 ms for ^{265}Hs no chemical studies of Hs seemed to be possible until the more

 © 2006 Wiley-VCH Verlag GmbH & Co. KGaA, Weinheim

neutron-rich isotope ^{269}Hs ($t_{1/2}\approx$14 s) was observed in 1996 in the discovery of element 112[53] as a member of the ^{277}112 α-decay chain. But the observed rate of about one atom per week, although not unexpected, was discouragingly small. However, it was expected that the direct production of ^{269}Hs in the ^{248}Cm(^{26}Mg,5n) hot-fusion reaction could be accomplished with production rate of about a factor of ten higher.[96] The existence of a $t_{1/2}\approx 14$ s isotope[48] ($t_{1/2}\approx 9$ s was obtained from the first observation[53]) and the prospect for a detection of about one atom per day provided enough faith to prepare the first chemistry experiment. Of course, novel techniques for irradiation, separation, and detection had to be developed and deployed to reach the required sensitivity. The first successful Hs chemistry experiment was conducted again in the framework of a large international collaboration at GSI's UNILAC in 2001.[54] It did not only yield the first chemical information on Hs but also provided new and interesting nuclear results.[100] Among these were evidence for the newly found isotope ^{270}Hs, the first nuclide with the $N=162$ neutron-shell, and a confirmation of the element 112 discovery by measuring concordant decay properties in α-decay chains starting from chemically separated element 108 fractions. A compilation of earlier, interesting but less successful attempts to perform Hs chemistry experiments can be found in ref. [129]

The heavier elements in Group 8, Ru and Os, show a unique property among all transition metals—they exploit the highest possible oxidation state (8+) and form highly volatile tetroxides MO_4 (M = Ru, Os). It was therefore most attractive to investigate HsO_4 as the first chemical compound of Hs. The experimental set-up used in the first Hs chemistry experiment is schematically shown in Figure 28. This experiment was unique, in a number of aspects, and different from recent gas-chromatographic experiments:

1) A rotating target wheel ("ARTESIA" in Figure 28) for the precious and highly radioactive ^{248}Cm targets[119]—in combination with a gas-jet transport system—was applied for the first time in SHE chemistry. This set up enabled higher beam intensities to be accepted and, consequently, provided larger production rates.
2) The chemical reaction with the reactive gas O_2 was performed "in situ" in the recoil chamber named in situ volatilization and online detection (IVO).[54,238] An oven attached to the recoil chamber provided a fast and efficient oxidation of stopped recoils. A similar technique has previously been used for lighter elements in combination with high-temperature thermochromatography.[112,140,147,148] In the Hs experiment this approach allowed highly volatile compounds to be transported without any cluster material in a very dry He/O_2 gas mixture over 10 m in a teflon capillary to the detection system.
3) The cryo online thermochromatography separator and detector (COLD)[54,239] was mainly used and as an alternative its forerunner CTS could also be employed.[141] COLD consists of 36 pairs of silicon PIN-photodiodes (with silicon nitride surfaces) coupled to a support which provides a negative temperature gradient between about −20 °C at the inlet and about −170 °C at the exit.

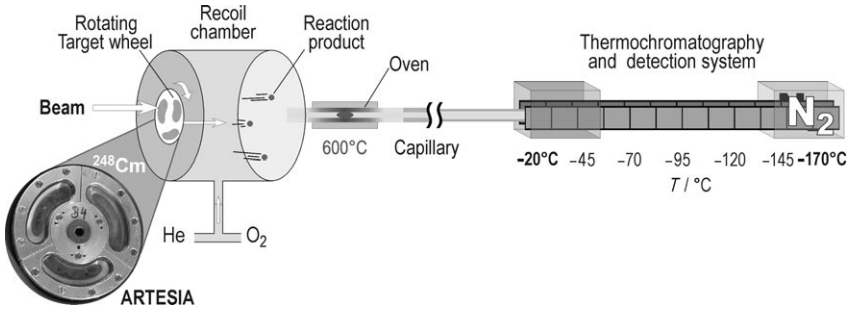


Figure 28. Schematic view of the low-temperature thermochromatography experiment used to investigate HsO_4. Adapted from ref. [54] original drawing courtesy of Ch. Düllmann.

Nuclear decay chains originating from the known isotope ^{269}Hs and from the isotope ^{270}Hs, for which first evidence was obtained in the course of this experiment, were observed[100] in a narrow peak[54,239] along the temperature gradient; see Figure 29 for observed nuclear decay chains and Figure 30 for their distribution along the temperature gradient.

From the observation of seven molecules of HsO_4 and their adsorption position at -44 ± 6 °C (comparison with OsO_4: -82 ± 7 °C), it is concluded that Hs forms a relatively stable, volatile tetroxide—as expected for a typical member of Group 8.[240,241] However, the exact adsorption position is at a surprisingly high temperature,[54] that is, HsO_4 exhibits an unexpected low volatility[242] or, in other terms, has a high, negative adsorption enthalpy. From a best fit of Monte Carlo simulations (solid line in Figure 30) to the experimental data the following adsorption enthalpies on silicon nitride were deduced:[54] $-\Delta H_a^{0(T)}(HsO_4)=46\pm2$ kJ mol^{-1} for HsO_4 and $-\Delta H_a^{0(T)}(OsO_4)=39\pm1$ kJ mol^{-1} for OsO_4.

For the first time, this Hs-chemistry experiment showed that the 1 pb cross-section limit can be reached in SHE chemistry—a crucial prerequisite to explore the chemistry of SHE in the region around element 114.

The second Hs experiment[146] was performed by a collaboration using a set-up dubbed continuously working arrangement for clusterless transport of in situ produced volatile oxides (CALLISTO).[243] Again ^{269,270}Hs were produced in the ^{26}Mg on ^{248}Cm reaction. A small amount of enriched ^{152}Gd was added to one ^{248}Cm target segment to simultaneously produce α-decaying ^{172}Os ($t_{1/2}=19$ s) and ^{173}Os ($t_{1/2}=22$ s). These isotopes were used to monitor the Os behavior under identical conditions. In the CALLISTO experiment, as in the preceding experiment, tetroxides were formed in a recoil chamber and in its hot (600 °C) outlet section. Contrary to the preceding experiment, which had used dry gases, in this experiment water was added (2 g H_2O per kg gas) to the O_2/He mixture. These gases transported volatile products over a distance of about 13 m in polytetrafluroethylene (PTFE) capillaries within 3–4 s to a set of four detector boxes. Each detector box contained a linear array of four detectors

© 2006 Wiley-VCH Verlag GmbH & Co. KGaA, Weinheim

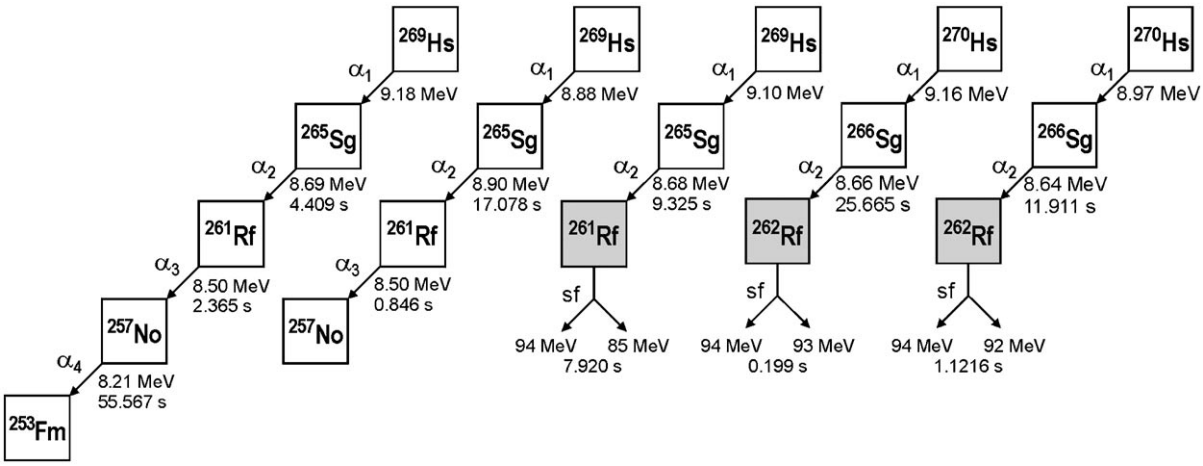


Figure 29. Nuclear decays chains from Hs isotopes observed in the first chemistry experiment of element 108. Indicated are the registered energies for α-particles and sf-fragments and the lifetimes. Adapted from ref. [54, 100].

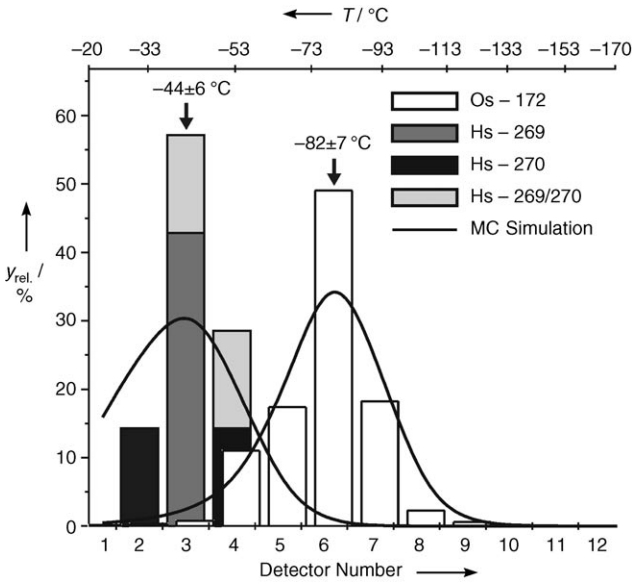


Figure 30. Experimentally observed thermochromatogram of HsO_4 (filled histogram with arrow at detector 3) and of OsO_4 (open histogram with arrow at detecto 6) given in relative yields. Solid lines represent results of a Monte Carlo simulation of the migration process of $^{269}HsO_4$ and $^{172}OsO_4$ along the temperature gradient assuming standard adsorption enthalpies of $-46.0\ kJ\ mol^{-1}$ and $-39.0\ kJ\ mol^{-1}$, respectively. Adapted from ref. [54, 239].

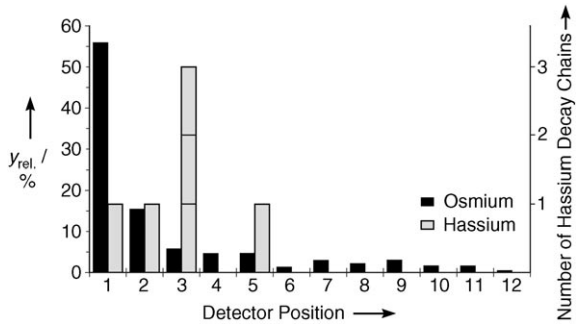


Figure 31. Distribution of the deposited amount of $^{172,173}OsO_4$ and $^{269,270}Hs$ (presumably as HsO_4). For Hs, the positions of the six correlated decay chains are depicted. Data from ref. [146].

(PIN-diodes) facing at a distance of 1 mm a stainless steel plate coated with a thin film of NaOH. Computer controlled, three detector boxes in a row, that is, 12 detectors, were always measuring while the fourth box was refurbished and freshly prepared NaOH was mounted. The water in the transport gas maintained the chemical reactivity of the NaOH layer over the measuring period.

The adsorption of the osmate (VIII) along the chemically reactive NaOH surface is shown in Figure 31 in terms of detector position. More than 50% of the Os is found on detector 1 and the rest of the detectors exhibit a significant tailing. Six decay chains of Hs were detected in the first five detectors (one α–α–α correlation and five α–sf correlations). They were centered at detector 3 (see Figure 31).[146] The low statistics of the six Hs events does not allow any conclusion to be drawn about a possible lower reactivity of the HsO_4 as compared to OsO_4. However, the observation confirms the formation and stability of the volatile HsO_4 compound, and shows the similarity in chemical reactivity between HsO_4 and OsO_4. Presumably, the deposition of Hs is the result of the formation of a hassate(VIII) according to Equation (8).

$$2\,NaOH + HsO_4 \rightarrow Na_2[HsO_4(OH)_2] \quad (8)$$

For the first time, an acid–base reaction was performed with the tetroxide of Hs.[146,243]

6.6. Elements 109–111

To date, no attempts have been made to investigate chemical properties of SHE located in Groups 9–11: meitnerium (Mt, element 109), darmstadtium (Ds, element 110), and roentgenium (Rg, element 111). Low production rates in combination with very short half-lives ($t_{1/2} = 0.1$ s) for isotopes produced in cold-fusion reactions provide an insurmountable hurdle for chemical investigations. However, ^{48}Ca-induced

 © 2006 Wiley-VCH Verlag GmbH & Co. KGaA, Weinheim

nuclear reactions with actinide targets (see Section 6.7) may provide access to longer lived nuclides of these elements which will allow chemical studies. Early on, a large number of preparatory test experiments were performed, mainly as thermochromatographic studies, with lighter homologues radiotracers.[244–247] Based on the work in ref. [248] these tests showed that volatile oxides or hydroxides may be good species for a chemical separation and characterization of Mt and Ds. In Group 11, the presumably rather volatile compound $RgCl_3$ could be compared with $AuCl_3$.[248]

Theoretically, the elements in Group 11 are extremely well studied; see for example, the comprehensive Review by Pyykkö about gold.[249] Highly advanced relativistic coupled-cluster calculations[250] yield for the Rg atom a ground state of $6d^97s^2$, which is in contrast to its lighter homologues. Very large relativistic effects are observed on orbital energies and level sequence for the Rg atom[250] and for the RgH molecule.[251,252] These calculations suggest that the chemistry of Rg will be largely dominated by relativistic effects and, consequently, Rg will behave more like a typical d-block element in contrast to its lighter homologues Ag and Au. The importance of the spin-orbit coupling on the bonding and on molecular properties of Au and Rg hydrides, halides, and oxides was pointed out in ref. [253].

6.7. Element 112

For a large number of reasons, element 112 is one of the most exciting elements for nuclear chemist, from a nuclear and a chemical perspective. While in typical cold-fusion reactions, such as in the discovery of element 112,[53] isotopes with half-lives of milliseconds and microseconds are produced, the hot (or warm) fusion reaction $^{238}U(^{48}Ca,3n)$ seemed to provide access to the isotope $^{283}112$ with a longer half-life. First experiments had observed a sf activity with a half-life of about 5 min produced with a cross section of about 4 pb.[71] New information on the decay properties of $^{283}112$ indicated that this nuclide may preferentially decay by α-emission with a half-life of about 4 s to the $t_{1/2} = 0.2$ s daughter nuclide ^{279}Ds which decays by sf.[66] Either decay mode would allow chemical investigations of element 112. Noted, however, that these findings are yet unconfirmed. Confirmation experiments for $^{283}112$ at the LBNL have remained unsuccessful[254] and a new attempt is being made at the GSI. Also chemistry experiments on element 112 will be able to confirm or disprove these claims.

Even though the first scientific articles are entitled "*Chemical Identification and Properties of Element 112*"[68,69] and "*Chemical and Nuclear Studies of Hassium and Element 112*"[70] the reported results can only be taken as first evidence for a (possible) chemical behavior of element 112. Therefore, an improved experimental program is under way. A large international collaboration has performed two experiments at the GSI—so far with no conclusive results[255]—and is continuing. Nevertheless, the techniques applied and the first results reported in refs. [68–70,255] are so exciting that reporting them herein is justified (though with the appropriate restraint).

Very early on, the question how closely element 112 would resemble the chemistry of Hg—its lighter homologue in Group 12—attracted a lot of attention and was summarized by Fricke.[35] Based on relativistic calculations which show a strong stabilization of the closed $7s^2$ shell, Pitzer[40] indicated the possibility that element 112 is relatively inert—almost like a noble gas—and, in elementary form, would be a gas or a very volatile liquid. Therefore, element 112 should be more volatile than Hg.

A very recent fully relativistic treatment of the interaction of element 112 with metallic surfaces, such as Au and Pd, predicts weaker adsorption of 112 than Hg on these metals.[256] These quantitative, most advanced calculations predict that the adsorption temperature of element 112 on (ideal) Au surfaces will be 93 °C below that for Hg. In addition it is pointed out that element 112 will form a (weak) metal–metal bond (if the Au surface is sufficiently clean) and, therefore, element 112 will adsorb at much higher temperatures than Rn which is adsorbed only by van der Waals forces. Adsorption enthalpies of element 112 on metal surfaces obtained from an empirical model also indicate a weak chemical bond formed on Au surfaces (no bond is formed on an Fe surface) and a "volatile noble metal" character of element 112 was predicted.[167,195,257] The volatility of element 112 was expected to be much higher than that of Hg.

Note, however, that despite its relative inertness, element 112 may have a rich chemistry involving complex formation in (sufficiently oxidizing) aqueous solutions and in the gas phase.[35,252] Theoretically observed[258] dissimilarities between Hg and element 112, for example, different ground-state configurations of the monocations ($d^{10}s^1$ for Hg^+, d^9s^2 for 112^+), large differences in the level sequence of Hg^{2+} and element 112^{2+}, strong level mixing in element 112, can be taken as evidence for interesting differences in the chemical behavior of these two remarkable elements.

The first two experimental attempts to chemically separate and identify the $t_{1/2} = 3$ min sf-isotope $^{283}112$ have been made by Yakushev and co-workers at the FLNR in Dubna.[67–69] Products from the $^{48}Ca + ^{238}U$ reaction—including Hg produced through a small amount of Nd added to the U target—were transported in the elementary state in a He gas flow. In the improved, second experiment the 25 m long capillary with a 2 mm internal diameter was connected to a detector arrangement of eight pairs of gold-coated passivated implanted planar silicon (PIPS) detectors (each with a surface area of 3.25 cm^2 at ambient temperature) for the detection of the mercury-like element 112. After this apparatus came a 5000 cm^3 cylindrical ionization chamber for the detection of a gaseous element 112. This chamber had an aerosol filter at the entrance. In addition, a mixture of Ar and CH_4 was added as a detector gas. The PIPS detectors and the ionization chamber were placed inside a barrel-shaped neutron detector with 126 ^{3}He-counters.[68]

In this experiment, the online produced and measured Hg was found, as expected, on the Au-coated PIPS detectors (95% of the $t_{1/2} = 49$ s ^{185}Hg was adsorbed on the first pair at an He-flow rate of 500 mL min^{-1}, this rose to 99% at 250 mL min^{-1}). At the end of the experiment eight sf-decays had been registered in the ionization chamber and none in the

© 2006 Wiley-VCH Verlag GmbH & Co. KGaA, Weinheim

PIPS detectors. With an expected background of only about one event and based on arguments that exclude any other sf-source originating from the nuclear reaction these sf-events were attributed to the decay of $^{283}112$.[68] It was concluded that element 112 does not form a strong metal–metal bond with Au and that it behaves more like the noble gas Rn rather than Hg. An estimate for the upper limit of the adsorption enthalpy for element 112 (on Au)—based on the non-observation of element 112 on the Au surface—gave $-\Delta H_a(112) \leq 60\ \mathrm{kJ\,mol^{-1}}$.[68] This value can be compared with $-\Delta H_a(\mathrm{Hg}) \approx 100\ \mathrm{kJ\,mol^{-1}}$ and $-\Delta H_a(\mathrm{Rn}) = 29 \pm 3\ \mathrm{kJ\,mol^{-1}}$.[155] However, as excellent as it was, this experiment still leaves some questions open and it does not fully establish the proof that, what was observed, reflects properties of element 112. It should be taken as evidence and it calls for more and more definite, quantitative experiments.

A second series of experiments started in the year 2003 at the GSI in a large international collaboration with ten institutes from five countries.[70] Again, the reaction of ^{48}Ca with ^{238}U was selected to produce $^{283}112$. Simultaneously, ^{220}Rn is also produced as a transfer product from U as well as $^{184-186}$Hg from small amounts of Nd in the target. These experiments are aiming at measuring the adsorption behavior of element 112 on Au in comparison with that of Hg and Rn. Along the Au surface, a temperature gradient from $+35\,^{\circ}\mathrm{C}$ to about $-185\,^{\circ}\mathrm{C}$ is established in a modified version of the COLD detector, which was so successful in the Hs experiment.[54] Test experiments determined the adsorption behavior of Hg and Rn on various transition-metal surfaces (with some interference owing to an ice coverage at the low-temperature end).[259] A schematic view of this set up is shown in Figure 32. In the first GSI experiment on element 112[70] the

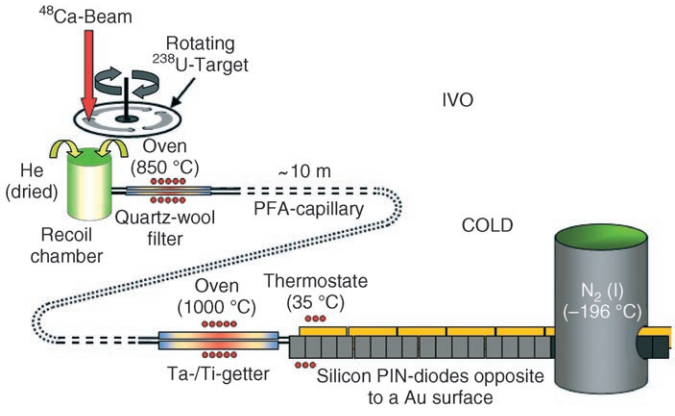


Figure 32. Schematic view of the experimental set up used in the first experiment on element 112 at the GSI.[70] Figure is courtesy of S. Soverna.

Au-catcher was facing an array of 32 silicon PIN-diodes, in the second experiment an improved version was developed and applied which allows measuring much more efficiently in (almost) 4π-geometry.[255] Further improvements made the second experiment also much more sensitive to shorter half-lives in the region of a few seconds.

In the first experiment at the GSI the following was observed:[70]

1) As expected, even at room temperature Hg is mainly adsorbed ($\approx 50\,\%$) on the Au (opposite the first detector) and its exhibits a tail which is in agreement with a Monte Carlo simulation of the adsorption process assuming an adsorption enthalpy of $-\Delta H_a(\mathrm{Hg}) = 101\ \mathrm{kJ\,mol^{-1}}$.
2) From the adsorption behavior of Rn, which begins at detector 29 and peaks around detector 31, and from the measured resolution of the α-spectra, it was concluded that below $-95\,^{\circ}\mathrm{C}$ the Au surface was covered with a thin ice layer.
3) At an expected background of three events, five sf-events were observed which scatter along the entire detector array.
4) A cluster of seven events—very cautiously interpreted as possible candidates for the sf decay of the $t_{1/2} \approx 3$ min $^{283}112$—were observed at detectors 29 to 31.

Again, this result seems to suggest that element 112 behaves like a gaseous metal. However, owing to some small imperfections and open questions, the international collaboration agreed to first repeat this experiment under improved conditions to substantiate the findings of their first experiment. The second experiment—performed at the GSI in the fall of 2004—worked with an improved set up and was sensitive to shorter lived nuclides.[255] However, there was already indication from the first, preliminary data analysis that also this experiment did not yield a final, conclusive result.[255] More experiments are needed to shed light on the chemistry of element 112.

7. Summary and Perspectives

As already observed in the pioneering experiments, more recent results from manifold studies again justify positioning of the transactinides—or superheavy elements (SHE)—, beginning with element 104, into the seventh period of the Periodic Table (see Figure 2). To date chemical studies on their behavior in the aqueous phase have been performed with Rf, Db, and Sg. Studies in the gas phase have been carried out for Rf, Db, Sg, Bh, and Hs, and have now reached element 112.

Up to element 108, all experimental results yield properties which, in general, place these elements into their respective group of the Periodic Table, that is, Rf, Db, Sg, Bh, and Hs into Groups 4, 5, 6, 7, and 8, respectively. This result demonstrates that the Periodic Table still remains an appropriate ordering scheme also regarding the chemical properties of these elements. However, a closer and more subtle look reveals that all the more detailed chemical properties of these elements—in comparison with their lighter homologues—are no longer reliably predictable by simple extrapolations in the Periodic Table. Even if for an element such as Sg for which, from an agreement of the observed chemical properties with empirical observations, an "oddly ordinary"[260] behavior is found, and if it looks as if Sg is "back on track"[261] this cannot be taken as evidence that

 © 2006 Wiley-VCH Verlag GmbH & Co. KGaA, Weinheim

also the heavier elements will behave "as expected". Sometimes relativistic effects and other effects, such as shell effects, may just cancel to "mimic" a normal behavior. However, modern relativistic atomic and molecular calculations, in combination with empirical models, allow for quantitative, or semi-quantitative, comparisons of experimental and theoretical results, and they show excellent agreement in a number of cases. From this situation it can be deduced that relativistic effects strongly influence the chemical properties of the transactinides. This is expected to become even more distinct when proceeding to even heavier elements.

Fascinating and challenging prospects are ahead to embark from the known territories of the element 106 for aqueous chemistry and the element 108 for gas-phase chemistry, to explore the chemical "terra incognita". The region between element 108 and 114 is waiting to be "chemically" discovered. A door to more neutron-rich, longer lived isotopes was opened by the use of the doubly magic nuclei ^{48}Ca as a beam and neutron-rich actinides as target materials (see Section 1 for details and for references). If we assume for the moment that yet unconfirmed results on the existence of relatively longer lived nuclides of spherical SHE around $Z = 114$ can be substantiated, then this opens the possibility for many chemical studies on all the SHE up to at least element 114. For heavier elements, even more challenging experiments are ahead as a result of the decreasing cross sections and shorter half-lives.

Prospects to study chemical properties of SHE beyond element 106 in the aqueous phase mainly depend on the development of methods to cope with production rates of less than one atom per hour and a wide range of half-lives. Existing separation techniques, such as ARCA and AIDA, will remain essential tools to shed more light on the diverse and often unexpected behavior of the lightest SHE. Moreover, this region continues to serve as an excellent test ground for detailed predictions of chemical properties with the most advanced theoretical model calculations.

Well developed gas-phase chemistry techniques are at hand to deepen our insights into many unresolved questions of compound formation, volatility, and adsorption behavior of Group 4–8 halides, oxides, and mixed compounds. With the advent of new techniques, such as the coupling to physical recoil separators, volatile, organometallic compounds may be accessible too. Most challenging and most fascinating will be the upcoming gas-phase studies of metallic transactinides beyond Group 8. Because of their relativistically stabilized inert, closed-shell electrons ($7s^2$ and $7s^27p_{1/2}{}^2$), which put elements 112 and 114 into a unique position among the SHE, chemical studies of these elements have the highest priority for the near future.

Coupling of chemical separation set ups to physical recoil separators will provide a big leap in the quality of separation and detection of SHE. The first successful steps in this direction were made at the BGS in Berkeley. Not only continuously operating liquid–liquid extraction devices, such as the already tested SISAK, but also gas-chromatographic set ups and emerging vacuum-thermochromatography techniques will greatly profit from such a coupled system. In addition to fascinating chemistry aspects, these experiments will certainly provide multifaceted nuclear data and they are vital tools for a clear identification of the atomic number of SHE.

Abbreviations and Acronyms

Acronym	Full name	Section[a]
Aliquat 336	Methyltrioctylammonium chloride	6.2.1
AIDA	**A**utomated **I**on exchange separation apparatus coupled with the **D**etection system for **A**lpha spectroscopy	5.2
ARCA	**A**utomated **R**apid **C**hemistry **A**pparatus	5.2
ARTESIA	**A** **R**otating **T**arget Wheel for **E**xperiments with **S**uperheavy-Element **I**sotopes at GSI Using **A**ctinides as Target Material	5.1
BGS	**B**erkeley **G**as-filled **S**eparator (at the LBNL)	5.4
CALLISTO	**C**ontinuously Working **A**rrangement For C**L**uster**L**ess Transport of **I**n-**S**itu Produced Volatile **O**xides	6.5
COLD	**C**ryo **O**n-**L**ine **D**etector	5.3
CTS	**C**ryo **T**hermochromatographic **S**eparator	5.3
FLNR	**F**lerov **L**aboratory of **N**uclear **R**eactions, Dubna, Russia	1
GSI	**G**esellschaft für **S**chwer**i**onenforschung, Darmstadt, Germany	1
$\Delta H_a^{0(T)}$	Adsorption enthalpy	6.1.2
ΔH_s^0	Standard sublimation enthalpy	6.1.2
IUPAC	**I**nternational **U**nion of **P**ure and **A**pplied **C**hemistry	1
IUPAP	**I**nternational **U**nion of **P**ure and **A**pplied **P**hysics	1
IVO	**I**n situ **V**olatilization and **O**nline **D**etection	6.5
JWP	**J**oint **W**orking **P**arty (of IUPAC and IUPAP)	1
K_d	Distribution coefficient	6.1.1
LBNL	**L**awrence **B**erkeley **N**ational **L**aboratory, Berkeley, California	5.4
OLGA	**Onl**ine **G**as chromatographic **A**pparatus	5.3
RIKEN	The Institute of Physical and Chemical Research, Wako, Japan	1
QED	**Q**uantum **e**lectro**d**ynamics	4.2
sf	**S**pontaneous **f**ission	2.2
SHIP	**S**eparator for **H**eavy **I**on Reaction **P**roducts (at the GSI)	1
SHE	**S**uper**h**eavy **e**lement(s)	1
SISAK	An automated, fast centrifuge separation system for continuous liquid-liquid extraction studies	5.4
SO	**S**pin-**o**rbit	4.2

© 2006 Wiley-VCH Verlag GmbH & Co. KGaA, Weinheim

$t_{1/2}$	Half-life (in nuclear decay)	1
TBP	Tributylphosphate	6.1.1
TiOA	Triisooctyl amine	6.1.1
TWG	**T**ransfermium **W**orking **G**roup (of IUPAC and IUPAP)	1
UNILAC	**Uni**versal **L**inear **Ac**celerator (at the GSI)	1

[a] Section in which the abbreviation or acronym is first mentioned.

I thank my group members at the GSI and my fellow colleagues, especially R. Eichler, H. W. Gäggeler, K. E. Gregorich, J. V. Kratz, Y. Nagame, N. Trautmann, and A. Türler for many years of very fruitful collaborations. V. Pershina is a continuous help to me with her profound theoretical knowledge and S. Hofmann with his expertise about the synthesis and decay of the heaviest elements. S. Soverna and Ch. Düllmann provided me with artistic drawings of experimental set ups. I acknowledge the help of B. Schausten for her work on the graphics, the time W. Brüchle spent reading and correcting my first draft, and, especially, G. Herrmann's and E. K. Hulet's suggestions to improve the manuscript. I thank G. Münzenberg for his continuous support for nuclear chemistry. Last not least, it was G. Herrmann who laid the foundations for the superheavy element chemistry, not only at the GSI.

Received: June 24, 2004
Revised: May 11, 2005
Published online: December 19, 2005

[1] O. Hahn, F. Straßmann, *Naturwissenschaften* **1939**, *27*, 11.
[2] G. Herrmann, *Angew. Chem.* **1990**, *102*, 469; *Angew. Chem. Int. Ed. Engl.* **1990**, *29*, 481.
[3] G. Herrmann, *Radiochim. Acta* **1995**, *70*/71, 51.
[4] G. T. Seaborg, *Chem. Eng. News* **1945**, *23*, 2190.
[5] G. T. Seaborg, W. D. Loveland, *The Elements Beyond Uranium*, Wiley, New York, **1990**.
[6] G. T. Seaborg, *Radiochim. Acta* **1995**, *70*/71, 69.
[7] J. J. Katz, G. T. Seaborg, L. R. Morss, *The Chemistry of the Actinide Elements*, *vol. 1 and 2*, 2. ed., Chapman and Hall, London, **1986**.
[8] *The Chemistry of Superheavy Elements* (Ed.: M. Schädel), Kluwer Academic Publishers, Dordrecht, **2003**.
[9] J. A. Wheeler in *Proceedings of the "International Conference on the Peaceful Uses of Atomic Energy"*, *vol. 2*, Geneva, 8–20 August 1955, New York, UN, **1956**, pp. 155–163 and pp. 220–229.
[10] G. Scharff-Goldhaber, *Nucleonics* **1957**, *15*, 122.
[11] N. Bohr, J. A. Wheeler, *Phys. Rev.* **1939**, *56*, 426.
[12] G. Herrmann, *Angew. Chem.* **1988**, *100*, 1417; *Angew. Chem. Int. Ed. Engl.* **1988**, *27*, 1417.
[13] W. D. Myers, W. J. Swiatecki, *Nucl. Phys.* **1966**, *81*, 1.
[14] A. Sobiczewski, F. A. Gareev, B. N. Kalinkin, *Phys. Lett.* **1966**, *22*, 500.
[15] Proceedings of the International Symposium *Why and how should we investigate NUCLIDES FAR OFF THE STABILITY LINE*, (Eds.: W. Forsling, C. J. Herrlander, H. Ryde), Lysekil, Sweden, August 21–27, **1966**; *Ark. Fys.* **1967**, *36*.
[16] H. Meldner, *Ark. Fys.* **1967**, *36*, 593.
[17] S. G. Nilsson, J. R. Nix, A. Sobiczewski, Z. Szymanski, S. Wycech, C. Gustafson, P. Möller, *Nucl. Phys. A* **1968**, *115*, 545.
[18] U. Mosel, W. Greiner, *Z. Phys.* **1969**, *222*, 261.
[19] J. Grumann, U. Mosel, B. Fink, W. Greiner, *Z. Phys.* **1969**, *228*, 371.
[20] S. G. Nilsson, S. G. Thompson, C. F. Tsang, *Phys. Lett. B* **1969**, *28*, 458.
[21] S. G. Nilsson, C. F. Tsang, A. Sobiczewski, Z. Szymanski, S. Wycech, C. Gustafson, I.-L. Lamm, P. Möller, B. Nilsson, *Nucl. Phys. A* **1969**, *131*, 1.
[22] H. Meldner, G. Herrmann, *Z. Naturforsch. A* **1969**, *24*, 1429.
[23] G. Herrmann in *Int. Rev. of Science, Inorg. Chem. Ser. 2*, *vol. 8* (Ed.: A. G. Maddock), Butterworth, London, **1975**, pp. 221–272.
[24] G. Herrmann, *Nature* **1979**, *280*, 543.
[25] G. T. Seaborg, W. D. Loveland, D.J Morrissey, *Science* **1979**, *203*, 711.
[26] G. N. Flerov, G. M. Ter-Akopian, *Rep. Prog. Phys.* **1983**, *46*, 817.
[27] J. V. Kratz, *Radiochim. Acta* **1983**, *32*, 25.
[28] G. Herrmann in *The Chemistry of Superheavy Elements* (Ed.: M. Schädel), Kluwer Academic Publishers, Dordrecht, **2003**, pp. 291–316.
[29] B. Fricke, W. Greiner, *Phys. Lett. B* **1969**, *30*, 317.
[30] J. B. Mann, *J. Chem. Phys.* **1969**, *51*, 841.
[31] J. B. Mann, J. T. Waber, *J. Chem. Phys.* **1970**, *53*, 2397.
[32] B. Fricke, J. T. Waber, *Actinides Rev.* **1971**, *1*, 433.
[33] J. P. Desclaux, *At. Data Nucl. Data Tables* **1973**, *12*, 311.
[34] J. T. Waber, B. Fricke, *J. Inorg. Nucl. Chem. Suppl.* **1976**, 13.
[35] B. Fricke, *Struct. Bonding* **1975**, *21*, 90.
[36] R. A. Penneman, J. B. Mann, *J. Inorg. Nucl. Chem. Suppl.* **1976**, 257.
[37] O. L. Keller Jr., *J. Inorg. Nucl. Chem. Suppl.* **1976**, 69.
[38] P. Pyykkö, J.-P. Desclaux, *Acc. Chem. Res.* **1979**, *12*, 276.
[39] K. S. Pitzer, *Acc. Chem. Res.* **1979**, *12*, 271.
[40] K. S. Pitzer, *J. Chem. Phys.* **1975**, *63*, 1032.
[41] V. G. Pershina, *Chem. Rev.* **1996**, *96*, 1977.
[42] P. Schwerdtfeger, M. Seth in *Encyclopedia of Computational Chemistry*, *vol. 4* (Eds.: P. von R. Schleyer, P. R. Schreiner, N. L. Allinger, T. Clark, J. Gasteier, P. Kollmann, H. F. Schaefer III), Wiley, New York, **1998**, pp. 2480–2499.
[43] V. Pershina in *The Chemistry of Superheavy Elements* (Ed.: M. Schädel), Kluwer Academic Publishers, Dordrecht, **2003**, pp. 31–94.
[44] V. Pershina in *Relativistic Electronic Structure Theory. Part 2. Applications, Theoretical and Computational Chemistry*, *vol. 14* (Ed.: P. Schwerdtfeger), Elsevier, Amsterdam, **2004**, pp. 1–80.
[45] a) R. C. Barber, N. N. Greenwood, A. Z. Hrynkiewicz, Y. P. Jeannin, M. Lefort, M. Sakai, U. Ulehla, A. H. Wapstra, D. H. Wilkinson, *Prog. Part Nucl. Phys.* **1992**, *29*, 453, b) R. C. Barber, N. N. Greenwood, A. Z. Hrynkiewicz, Y. P. Jeannin, M. Lefort, M. Sakai, U. Ulehla, A. H. Wapstra, D. H. Wilkinson, *Pure Appl. Chem.* **1991**, *63*, 879, c) R. C. Barber, N. N. Greenwood, A. Z. Hrynkiewicz, Y. P. Jeannin, M. Lefort, M. Sakai, U. Ulehla, A. H. Wapstra, D. H. Wilkinson, *Pure Appl. Chem.* **1993**, *65*, 1757.
[46] P. J. Karol, H. Nakahara, B. W. Petley, E. Vogt, *Pure Appl. Chem.* **2003**, *75*, 1601.
[47] S. Hofmann, V. Ninov, F. P. Heßberger, P. Armbruster, H. Folger, G. Münzenberg, H. J. Schött, A. G. Popeko, A. V. Yeremin, A. N. Andreyev, S. Saro, R. Janik, M. Leino, *Z. Phys. A* **1995**, *350*, 281.
[48] S. Hofmann, F. P. Heßberger, D. Ackermann, G. Münzenberg, S. Antalic, P. Cagarda, B. Kindler, J. Kojouharova, M. Leino, B. Lommel, R. Mann, A. G. Popeko, S. Reshitko, S. Saro, J. Uusitalo, A. V. Yeremin, *Eur. Phys. J. A* **2002**, *14*, 147.
[49] K. Morita, K. Morimoto, D. Kaji, H. Haba, E. Ideguchi, J. C. Peter, R. Kanungo, K. Katori, H. Koura, H. Kudo, T. Ohnishi, A. Ozawa, T. Suda, K. Sueki, I. Tanihata, H. Xu, A. V. Yeremin,

 © 2006 Wiley-VCH Verlag GmbH & Co. KGaA, Weinheim

A. Yoneda, A. Yoshida, Y.-L. Zhao, T. Zheng, S. Goto, F. Tokanai, *J. Phys. Soc. Jpn.* **2004**, *73*, 1738.

[50] K. Morita, K. Morimoto, D. Kaji, S. Goto, H. Haba, E. Ideguchi, R. Kanungo, K. Katori, H. Koura, H. Kudo, T. Ohnishi, A. Ozawa, J. C. Peter, T. Suda, K. Sueki, I. Tanihata, F. Tokanai, H. Xu, A. V. Yeremin, A. Yoneda, A. Yoshida, Y.-L. Zhao, T. Zheng, *Nucl. Phys. A* **2004**, *734*, 101.

[51] www.iupac.org/news/archives/2004/naming111.html **2004**.

[52] J. Corish, G. M. Rosenblatt, *Pure Appl. Chem.* **2003**, *75*, 1613.

[53] S. Hofmann, V. Ninov, F. P. Heßberger, P. Armbruster, H. Folger, G. Münzenberg, H. J. Schött, A. G. Popeko, A. V. Yeremin, S. Saro, R. Janik, M. Leino, *Z. Phys. A* **1996**, *354*, 229.

[54] C. Düllmann, W. Brüchle, R. Dressler, K. Eberhardt, B. Eichler, R. Eichler, H. W. Gäggeler, T. N. Ginter, F. Glaus, K. E. Gregorich, D. C. Hofmann, E. Jäger, D. T. Jost, U. W. Kirbach, D. M. Lee, H. Nitsche, J. B. Patin, V. Pershina, D. Piquet, Z. Qin, M. Schädel, B. Schausten, E. Schimpf, H.-J. Schött, S. Soverna, R. Sudowe, P. Thörle, S. N. Timokhin, N. Trautmann, A. Türler, A. Vahle, G. Wirth, A. B. Yakushev, P. Zielinski, *Nature* **2002**, *418*, 859.

[55] K. Morita, **2004**, personal communication, and *J. Phys. Soc. Jpn.* **2004**, submitted.

[56] G. Münzenberg, *Rep. Prog. Phys.* **1988**, *51*, 57.

[57] S. Hofmann, *Rep. Prog. Phys.* **1998**, *61*, 639.

[58] P. Armbruster, *Annu. Rev. Nucl. Part. Sci.* **2000**, *50*, 411.

[59] S. Hofmann, G. Münzenberg, *Rev. Mod. Phys.* **2000**, *72*, 733.

[60] S. Hofmann in *The Chemistry of Superheavy Elements* (Ed.: M. Schädel), Kluwer Academic Publishers, Dordrecht, **2003**, pp.1 – 29.

[61] "On Beyond Uranium—Journey to the end of the Periodic Table": S. Hofmann, *Science Spectra Books Series*, *vol. 2*, Taylor & Francis, London, **2002**.

[62] S. Hofmann, G. Münzenberg, M. Schädel, *Nucl. Phys. News* **2004**, *14*, 5.

[63] K. Morita, K. Morimoto, D. Kaji, T. Akiyama, S. Goto, H. Haba, Ideguchi, R. Kanungo, K. Katori, H. Koura, H. Kudo, T. Ohnishi, A. Ozawa, T. Suda, K. Sueki, H. Xu, T. Yamaguchi, A. Yoneda, A. Yoshida, Y.-L. Zhang, *J. Phys. Soc. Jpn.* **2004**, *73*, 2593.

[64] Yu. Ts. Oganessian, V. K. Utyonkov, Yu. V. Lobanov, F. Sh. Abdullin, A. N. Polyakov, I. V. Shirokovsky, Yu. Ts. Tsyganov, G. G. Gulbekian, S. L. Bogomolov, A. N. Metsentsev, S. Iliev, V. G. Subbotin, A. M. Sukhov, A. A. Voinov, G. V. Buklanov, K. Subotic, V. I. Zagrebaev, M. G. Itkis, J. J. Patin, K. J. Moody, J. F. Wild, M. A. Stoyer, N. J. Stoyer, D. A. Shaughnessy, J. M. Kenneally, R. W. Lougheed, *Phys. Rev. C* **2004**, *69*, 021601.

[65] Yu. Ts. Oganessian, V. K. Utyonkov, Yu. V. Lobanov, F. Sh. Abdullin, A. N. Polyakov, I. V. Shirokovsky, Yu. Ts. Tsyganov, G. G. Gulbekian, S. L. Bogomolov, B. N. Gikal, A. N. Metsentsev, S. Iliev, V. G. Subbotin, A. M. Sukhov, A. A. Voinov, G. V. Buklanov, K. Subotic, V. I. Zagrebaev, M. G. Itkis, J. J. Patin, K. J. Moody, J. F. Wild, M. A. Stoyer, N. J. Stoyer, D. A. Shaughnessy, J. M. Kenneally, R. W. Lougheed, *Nucl. Phys. A* **2004**, *734*, 109.

[66] Yu. Ts. Oganessian, V. K. Utyonkov, Yu. V. Lobanov, F. Sh. Abdullin, A. N. Polyakov, I. V. Shirokovsky, Yu. Ts. Tsyganov, G. G. Gulbekian, S. L. Bogomolov, B. N. Gikal, A. N. Metsentsev, S. Iliev, V. G. Subbotin, A. M. Sukhov, A. A. Voinov, G. V. Buklanov, K. Subotic, V. I. Zagrebaev, M. G. Itkis, J. J. Patin, K. J. Moody, J. F. Wild, M. A. Stoyer, N. J. Stoyer, D. A. Shaughnessy, J. M. Kenneally, P. A. Wilk, R. W. Lougheed, R. I. Il'kaev, S. P. Vesnovskii, *Phys. Rev. C* **2004**, *70*, 064609.

[67] A. B. Yakushev, G. V. Buklanov, M. L. Chelnokov, V. I. Chepigin, S. N. Dmitriev, V. A. Gorshov, S. Hübener, V. Ya. Lebedev, O. N. Malyshev, Yu. Ts. Oganessian, A. G. Popeko, E. A. Sokol, S. N. Timokhin, A. Türler, V. M. Vasko, A. V. Yeremin, I. Zvara, *Radiochim. Acta* **2001**, *89*, 743.

[68] A. B. Yakushev, I. Zvara, Yu. Ts. Oganessian, A. V. Belozerov, S. N. Dmitriev, B. Eichler, S. Hübener, E. A. Sokol, A. Türler, A. V. Yeremin, G. V. Buklanov, M. L. Chelnokov, V. I. Chepigin, V. A. Gorshov, A. V. Gulyaev, V. Ya. Lebedev, O. N. Malyshev, A. G. Popeko, S. Soverna, Z. Szeglowski, S. N. Timokhin, S. P. Tretyakova, V. M. Vasko, M. G. Itkis, *Radiochim. Acta* **2003**, *91*, 433.

[69] A. B. Yakushev, I. Zvara, Yu. Ts. Oganessian, A. V. Belozerov, S. N. Dmitriev, B. Eichler, S. Hübener, E. A. Sokol, A. Türler, A. V. Yeremin, G. V. Buklanov, M. L. Chelnokov, V. I. Chepigin, V. A. Gorshov, A. V. Gulyaev, V. Ya. Lebedev, O. N. Malyshev, A. G. Popeko, S. Soverna, Z. Szeglowski, S. N. Timokhin, S. P. Tretyakova, V. M. Vasko, M. G. Itkis, *Nucl. Phys. A* **2004**, *734*, 204.

[70] H. W. Gäggeler, W. Brüchle, C. E. Düllmann, R. Dressler, K. Eberhardt, B. Eichler, R. Eichler, C. M. Folden, T. N. Ginter, F. Glaus, K. E. Gregorich, F. Haenssler, D. C. Hoffman, E. Jäger, D. T. Jost, U. W. Kirbach, J. V. Kratz, H. Nitsche, J. B. Patin, V. Pershina, D. Piguet, Z. Qin, U. Rieth, M. Schädel, E. Schimpf, B. Schausten, S. Soverna, R. Sudowe, P. Thörle, N. Trautmann, A. Türler, A. Vahle, P. A. Wilk, G. Wirth, A. B. Yakushev, A. von Zweidorf, *Nucl. Phys. A* **2004**, *734*, 433.

[71] Yu. Ts. Oganessian, A. V. Yeremin, G. G. Gulbekian, S. L. Bogomolov, V. I. Chepigin, B. L. Gikal, V. A. Gorshkov, M. G. Itkis, A. P. Kabachenko, V. B. Kutner, A. Yu. Lavrentev, O. N. Malyshev, A. G. Popeko, J. Roháchecka, R. N. Sagaidak, S. Hofmann, G. Münzenberg, M. Veselsky, S. Saro, N. Iwasa, K. Morita, *Eur. Phys. J. A* **1999**, *5*, 63.

[72] I. Zvara, V. Z. Belov, L. P. Chelnokov, V. P. Domanov, M. Hussonnois, Yu. S. Korotkin, V. A. Shegolev, M. R. Shalaevsky, *Inorg. Nucl. Chem. Lett.* **1971**, *7*, 1109.

[73] R. J. Silva, J. Harris, M. Nurmia, K. Eskola, A. Ghiorso, *Inorg. Nucl. Chem. Lett.* **1970**, *6*, 871.

[74] E. K. Hulet, R. W. Lougheed, J. F. Wild, J. H. Landrum, J. M. Nitschke, A. Ghiorso, *J. Inorg. Nucl. Chem.* **1980**, *42*, 79.

[75] I. Zvara, V. Z. Belov, V. P. Domanov, M. R. Shalaevskii, *Sov. Radiochem.* **1976**, *18*, 328.

[76] K. E. Gregorich, R. A. Henderson, D. M. Lee, M. J. Nurmia, R. M. Chasteler, H. L. Hall, D. A. Bennett, C. M. Gannett, R. B. Chadwick, J. D. Leyba, D. C. Hoffman, G. Herrmann, *Radiochim. Acta* **1988**, *43*, 223.

[77] M. Schädel, *Radiochim. Acta* **1995**, *70*/71, 207.

[78] H. W. Gäggeler in *Proc. of The Robert A. Welch Foundation 41st Conference on Chemical Research, The Transactinide Elements*, October 27–28, **1997**, Houston, Texas, pp. 43 – 63.

[79] J. V. Kratz in *Heavy Elements and Related New Phenomena* (Eds.: W. Greiner, R. K. Gupta), World Scientific, Singapur, **1999**, pp. 129 – 193.

[80] M. Schädel, *Radiochim. Acta* **2001**, *89*, 721.

[81] J. V. Kratz, *Pure Appl. Chem.* **2003**, *75*, 103.

[82] G. Friedlander, G. Herrmann in *Handbook of Nuclear Chemistry, vol. 1* (Eds.: A. Vértes, S. Nagy, Z. Klencsár), Kluwer Academic Publishers, Dordrecht, **2003**, pp. 1 – 41.

[83] G. N. Flerov in *Proceedings of the "Nobel Symposium 27. Super-Heavy Elements—Theoretical Predictions and Experimental Generation"*, Ronneby, Sweden, June 11 – 14, **1974**; *Phys. Scr.* **1974**, *10A*, 1.

[84] G. Münzenberg, *Radiochim. Acta* **1996**, *70*/71, 237.

[85] A. Sobiczewski, I. Muntian, Z. Patyk, *Phys. Rev. C* **2001**, *63*, 034306.

[86] I. Muntian, Z. Patyk, A. Sobiczewski, *J. Nucl. Radiochem. Sci.* **2002**, *3*, 169.

[87] M. Bender, K. Rutz, P.-G. Reinhard, J. A. Maruhn, W. Greiner, *Phys. Rev. C* **1999**, *60*, 034304.

[88] a) W. Greiner, *J. Nucl. Radiochem. Sci.* **2002**, *3*, 159; b) K. Rutz, M. Bender, T. Bürvenich, T. Schilling, P.-G. Reinhard, J. A. Maruhn, W. Greiner, *Phys. Rev. C* **1997**, *56*, 238.

 © 2006 Wiley-VCH Verlag GmbH & Co. KGaA, Weinheim

[89] A. Sobiczewski, Z. Patyk, S. Cwiok, *Phys. Lett. B* **1987**, *186*, 6.
[90] M. Schädel, *Acta Phys. Pol. A* **2003**, *34*, 1701.
[91] B. G. Harvey, G. Herrmann, R. W. Hoff, D. C. Hoffman, E. K. Hyde, J. J. Katz, L. Keller, M. Lefort, G. T. Seaborg, *Science* **1976**, *193*, 1271.
[92] G. Münzenberg in *Handbook of Nuclear Chemistry, vol. 2* (Eds.: A. Vértes, S. Nagy, Z. Klencsár), Kluwer Academic Publishers, Dordrecht, **2003**, pp. 283 – 321.
[93] J. P. Omtvedt, J. Alstad, H. Breivik, J. E. Dyne, K. Eberhardt, C. M. Folden III, T. Ginter, K. E. Gregorich, E. A. Hult, M. Johansson, U. W. Kirbach, D. M. Lee, M. Mendel, A. Nähler, V. Ninov, L. A. Omtvedt, J. B. Patin, G. Skarnemark, L. Stavsetra, R. Sudowe, N. Wiehl, B. Wierczinski, P. A. Wilk, P. M. Zielinski, J. V. Kratz, N. Trautmann, H. Nitsche, D. C. Hoffman, *J. Nucl. Radiochem. Sci.* **2002**, *3*, 121.
[94] M. Schädel, *J. Nucl. Radiochem. Sci.* **2002**, *3*, 113.
[95] W. Reisdorf, M. Schädel, *Z. Phys. A* **1992**, *343*, 47.
[96] M. Schädel, S. Hofmann, *J. Radioanal. Nucl. Chem.* **1996**, *203*, 283.
[97] A. Türler, R. Dressler, B. Eichler, H. W. Gäggeler, D. T. Jost, M. Schädel, W. Brüchle, K. E. Gregorich, N. Trautmann, S. Taut, *Phys. Rev. C* **1998**, *57*, 1648.
[98] P. A. Wilk, K. E. Gregorich, A. Türler, C. A. Laue, R. Eichler, V. Ninov, J. L. Adams, U. W. Kirbach, M. R. Lane, D. M. Lee, J. B. Patin, D. A. Shaughnessy, D. A. Strellis, H. Nitsche, D. C. Hoffman, *Phys. Rev. Lett.* **2000**, *85*, 2797.
[99] R. Eichler, W. Brüchle, R. Dressler, C. E. Düllmann, B. Eichler, H. W. Gäggeler, K. E. Gregorich, D. C. Hoffman, S. Hübener, D. T. Jost, U. W. Kirbach, C. A. Laue, V. M. Lavanchy, H. Nitsche, J. B. Patin, D. Piquet, M. Schädel, D. A. Shaughnessy, D. A. Strellis, S. Taut, L. Tobler, Y. S. Tsyganov, A. Türler, A. Vahle, P. A. Wilk, A. B. Yakushev, *Nature* **2000**, *407*, 63.
[100] A. Türler, C. E. Düllmann, H. W. Gäggeler, U. W. Kirbach, A. Yakushev, M. Schädel, W. Brüchle, R. Dressler, K. Eberhardt, B. Eichler, R. Eichler, T. N. Ginter, F. Glaus, K. E. Gregorich, D. C. Hofmann, E. Jäger, D. T. Jost, D. M. Lee, H. Nitsche, J. B. Patin, V. Pershina, D. Piquet, Z. Qin, B. Schausten, E. Schimpf, H.-J. Schött, S. Soverna, R. Sudowe, P. Thörle, S. N. Timokhin, N. Trautmann, A. Vahle, G. Wirth, P. Zielinski, *Eur. Phys. J. A* **2003**, *17*, 505.
[101] R. Guillaumont, J. P. Adloff, A. Peneloux, *Radiochim. Acta* **1989**, *46*, 169.
[102] R. Guillaumont, J. P. Adloff, A. Peneloux, P. Delamoye, *Radiochim. Acta* **1991**, *54*, 1.
[103] R. J. Borg, G. J. Dienes, *J. Inorg. Nucl. Chem.* **1981**, *43*, 1129.
[104] D. Trubert, C. Le Naour in *The Chemistry of Superheavy Elements* (Ed.: M. Schädel), Kluwer Academic Publishers, Dordrecht, **2003**, pp. 95 – 116.
[105] J.-P. Adloff, R. Guillaumont, *Fundamentals of Radiochemistry*, CRC, Boca Raton, **1993**.
[106] P. Pyykkö, *Chem. Rev.* **1988**, *88*, 563.
[107] V. Pershina, B. Fricke in *Heavy Elements and Related New Phenomena* (Eds.: W. Greiner, R. K. Gupta), World Scientific, Singapore, **1999**, pp. 194 – 262.
[108] V. Pershina, D. C. Hoffman in *Theoretical Chemistry and Physics of Heavy and Superheavy Elements* (Eds.: U. Kaldor, S. Wilson), Kluwer Academic Publishers, Dordrecht, **2003**, pp. 55 – 114.
[109] J. V. Kratz: *Chemistry of Transactinides* In: *Handbook of Nuclear Chemistry, vol. 2* (Eds.: A. Vértes, S. Nagy, Z. Klencsár), Kluwer Academic Publishers, Dordrecht, **2003**, pp. 323 – 395.
[110] N. Trautmann, G. Herrmann, *J. Radioanal. Chem.* **1976**, *32*, 533.
[111] G. Herrmann, N. Trautmann, *Annu. Rev. Nucl. Part. Sci.* **1982**, *32*, 117.
[112] I. Zvara, B. Eichler, V. Z. Belov, T. S. Zvarova, Yu. S. Korotkin, M. R. Shalaevskii, V. A. Shegolev, M. Hussonnois, *Sov. Radiochem.* **1974**, *16*, 709.
[113] I. Zvara, *Isotopenpraxis* **1990**, *26*, 251.
[114] N. Trautmann, *Radiochim. Acta* **1995**, *70*/71, 237.
[115] A. Türler, *Radiochim. Acta* **1996**, *72*, 7.
[116] A. Türler, K. E. Gregorich in *The Chemistry of Superheavy Elements* (Ed.: M. Schädel), Kluwer Academic Publishers, Dordrecht, **2003**, pp. 117 – 157.
[117] J. M. Nitschke, *Nucl. Instrum. Methods* **1976**, *138*, 393.
[118] M. Schädel, W. Brüchle, B. Haefner, *Nucl. Instrum. Methods Phys. Res. Sect. A* **1988**, *264*, 308.
[119] K. Eberhardt, M. Schädel, E. Schimpf, P. Thörle, N. Trautmann, *Nucl. Instrum. Methods Phys. Res. Sect. A* **2004**, *521*, 208.
[120] J. V. Kratz in *The Chemistry of Superheavy Elements* (Ed.: M. Schädel), Kluwer Academic Publishers, Dordrecht, **2003**, pp. 159 – 236.
[121] K. E. Gregorich in *Proc. of The Robert A. Welch Foundation 41st Conference on Chemical Research*, The Transactinide Elements, October 27 – 28, **1997**, Houston, Texas, pp. 95–124.
[122] M. Schädel, W. Brüchle, E. Jäger, E. Schimpf, J. V. Kratz, U. W. Scherer, H. P. Zimmermann, *Radiochim. Acta* **1989**, *48*, 171.
[123] H. Haba, K. Tsukada, M. Asai, S. Goto, A. Toyoshima, I. Nishinaka, K. Akiyama, M. Hirata, S. Ichikawa, Y. Nagame, Y. Shoji, M. Shigekawa, T. Koike, M. Iwasaki, A. Shinohara, T. Kaneko, T. Maruyama, S. Ono, H. Kudo, Y. Oura, K. Sueki, H. Nakahara, M. Sakama, A. Yokoyama, J. V. Kratz, M. Schädel, W. Brüchle, *J. Nucl. Radiochem. Sci.* **2002**, *3*, 143.
[124] Y. Nagame, H. Haba, K. Tsukada, M. Asai, K. Akiyama, M. Hirata, I. Nishinaka, S. Ichikawa, H. Nakahara, S. Goto, T. Kaneko, H. Kudo, A. Toyoshima, A. Shinohara, M. Schädel, J. V. Kratz, H. W. Gäggeler, A. Türler, *Czech. J. Phys. Suppl.* **2003**, *53*, A299.
[125] Y. Nagame, H. Haba, K. Tsukada, M. Asai, A. Toyoshima, S. Goto, K. Akiyama, T. Kaneko, M. Sakama, M. Hirata, T. Yaita, I. Nishinaka, S. Ichikawa, H. Nakahara, *Nucl. Phys. A* **2004**, *734*, 124.
[126] Y. Nagame, M. Asai, H. Haba, K. Tsukada, S. Goto, M. Sakama, I. Nishinaka, A. Toyoshima, K. Akiyama, S. Ichikawa, *J. Nucl. Radiochem. Sci.* **2002**, *3*, 129.
[127] H. Haba, K. Tsukada, M. Asai, A. Toyoshima, K. Akiyama, I. Nishinaka, M. Hirata, T. Yaita, S. Ichikawa, Y. Nagame, K. Yasuda, Y. Miamoto, T. Kaneko, S. Goto, S. Ono, T. Hirai, H. Kudo, M. Shigekawa, A. Shinohara, Y. Oura, H. Nakhara, K. Sueki, H. Kikunaga, N. Kinoshita, N. Tsuruga, A. Yokoyama, M. Sakama, S. Enomoto, M. Schädel, W. Brüchle, J. V. Kratz, *J. Am. Chem. Soc.* **2004**, *126*, 5219.
[128] A. Toyoshima, H. Haba, K. Tsukada, M. Asai, K. Akiyama, I. Nishinaka, Y. Nagame, K. Matsuo, W. Sato, A. Shinohara, H. Ishizu, M. Ito, J. Saito, S. Goto, H. Kudo, H. Kikunaga, C. Kato, A. Yokoyama, K. Sueki, *J. Nucl. Radiochem. Sci.* **2004**, *5*, 45.
[129] H. W. Gäggeler, A. Türler in *The Chemistry of Superheavy Elements* (Ed.: M. Schädel), Kluwer Academic Publishers, Dordrecht, **2003**, pp. 237 – 289.
[130] I. Zvara, Yu. T. Chuburkov, V. Z. Belov, G. V. Buklanov, B. B. Zakhvataev, T. S. Zvarova, O. D. Maslov, R. Caletka, M. R. Shalaevsky, *J. Inorg. Nucl. Chem.* **1970**, *32*, 1885.
[131] I. Zvara in *Transplutonium Elements* (Eds.: W. Müller, R. Lindner), North-Holland, Amsterdam, **1976**, pp. 11 – 20.
[132] U. Hickmann, N. Greulich, N. Trautmann, H. Gäggeler, H. Gäggeler-Koch, B. Eichler, G. Herrmann, *Nucl. Instrum. Methods* **1980**, *174*, 507.
[133] H. W. Gäggeler, *J. Radioanal. Nucl. Chem.* **1994**, *183*, 261.
[134] H. W. Gäggeler, D. T. Jost, U. Baltensperger, A. Weber, A. Kovacs, D. Vermeulen, A. Türler, *Nucl. Instrum. Methods Phys. Res. Sect. A* **1991**, *309*, 201.

 © 2006 Wiley-VCH Verlag GmbH & Co. KGaA, Weinheim

[135] B. Kadkhodayan, A. Türler, K. E. Gregorich, M. J. Nurmia, D. M. Lee, D. C. Hoffman, *Nucl. Instrum. Methods Phys. Res. Sect. A* **1992**, *317*, 254.
[136] A. Vahle, S. Hübener, R. Dressler, M. Grantz, *Nucl. Instrum. Methods Phys. Res. Sect. A* **2002**, *481*, 637.
[137] S. Hübener, S. Taut, A. Vahle, R. Dressler, B. Eichler, H. W. Gäggeler, D. T. Jost, D. Piquet, A. Türler, W. Brüchle, E. Jäger, M. Schädel, E. Schimpf, U. Kirbach, N. Trautmann, A. B. Yakushev, *Radiochim. Acta* **2001**, *89*, 737.
[138] M. Schädel, E. Jäger, W. Brüchle, K. Sümmerer, E. K. Hulet, J. F. Wild, R. W. Lougheed, K. J. Moody, *Radiochim. Acta* **1995**, *68*, 7.
[139] I. Zvara, *J. Radioanal. Nucl. Chem.* **1996**, *204*, 123.
[140] I. Zvara, A. B. Yakushev, S. N. Timokhin, Xu Honggui, V. P. Perelygin, Yu. T. Chuburkov, *Radiochim. Acta* **1998**, *81*, 179.
[141] U. W. Kirbach, C. M. Folden III, T. N. Ginter, K. E. Gregorich, D. M. Lee, V. Ninov, J. P. Omtvedt, J. B. Patin, N. K. Seward, D. A. Strellis, R. Sudowe, A. Türler, P. A. Wilk, P. M. Zielinski, D. C. Hofmann, H. Nitsche, *Nucl. Instrum. Methods Phys. Res. Sect. A* **2002**, *484*, 587.
[142] N. Hildenbrand, C. Frink, N. Greulich, U. Hickmann, J. V. Kratz, G. Herrmann, M. Brügger, H. Gäggeler, K. Sümmerer, G. Wirth, *Nucl. Instrum. Methods Phys. Res. Sect. A* **1987**, *260*, 407.
[143] P. Armbruster, Y. K. Agarwal, W. Brüchle, J. P. Dufour, H. Gäggeler, F. P. Heßberger, S. Hofmann, P. Lemmertz, G. Münzenberg, K. Poppensieker, W. Reisdorf, M. Schädel, K.-H. Schmidt, J. H. R. Schneider, W. F. W. Schneider, K. Sümmerer, D. Vermeulen, G. Wirth, A. Ghiorso, K. E. Gregorich, D. Lee, M. Leino, K. J. Moody, G. T. Seaborg, R. B. Welch, P. Wilmarth, Y. Yashita, C. Frink, N. Greulich, G. Herrmann, U. Hickmann, N. Hildenbrand, J. V. Kratz, N. Trautmann, M. M. Fowler, D. C. Hoffman, W. R. Daniels, H. R. von Gunten, H. Dornhöfer, *Phys. Rev. Lett.* **1985**, *54*, 406.
[144] J. V. Kratz, W. Brüchle, H. Folger, H. Gäggeler, M. Schädel, K. Sümmerer, G. Wirth, N. Greulich, G. Herrmann, U. Hickmann, P. Peuser, N. Trautmann, E. K. Hulet, R. W. Lougheed, M. J. Nitschke, R. L. Ferguson, R. L. Hahn, *Phys. Rev. C* **1986**, *33*, 504.
[145] R. J. Dougan, K. J. Moody, E. K. Hulet, G. R. Bethune, *Lawrence Livermore National Laboratory, Nuclear Chemistry Division*, FY 87 Annual Report (UCAR 10062/87), **1987**, pp. 4–17.
[146] A. von Zweidorf, R. Angert, W. Brüchle, S. Bürger, K. Eberhardt, R. Eichler, H. Hummrich, E. Jäger, H.-O. Kling, J. V. Kratz, B. Kuczewski, G. Langrock, M. Mendel, U. Rieth, M. Schädel, B. Schausten, E. Schimpf, P. Thörle, N. Trautmann, K. Tsukada, N. Wiehl, G. Wirth, *Radiochim. Acta* **2004**, *92*, 855.
[147] V. Z. Belov, T. S. Zvarova, M. R. Shalaevsky, *Sov. Radiochem.* **1975**, *17*, 87.
[148] I. Zvara, O. L. Keller Jr., R. J. Silva, J. R. Tarrant, *J. Chromatogr.* **1975**, *103*, 77.
[149] B. Wierczinski, K. Eberhardt, G. Herrmann, J. V. Kratz, M. Mendel, A. Nähler, F. Rocker, U. Tharun, N. Trautmann, K. Weiner, N. Wiehl, J. Alstad, G. Skarnemark, *Nucl. Instrum. Methods Phys. Res. Sect. A* **1996**, *370*, 532.
[150] H. Persson, G. Skarnemark, M. Skålberg, J. Alstad, J. O. Liljenzin, G. Bauer, F. Haberberger, N. Kaffrell, J. Rogowski, N. Trautmann, *Radiochim. Acta* **1989**, *48*, 177.
[151] J. Alstad, G. Skarnemark, F. Haberberger, G. Herrmann, A. Nähler, M. Pense-Maskow, N. Trautmann, *J. Radioanal. Nucl. Chem.* **1995**, *189*, 133.
[152] M. Johansson, J. Alstad, J. P. Omtvedt, G. Skarnemark, *Radiochim. Acta* **2001**, *89*, 619.
[153] C. Düllmann, *Volatile Heavy Element Organometallics*, oral contribution to the 2nd Intenational Conference on the Chemistry and Physics of the Transactinide Elements (TAN 03), Napa, California, November 16–20, **2003**.
[154] H. Gäggeler, B. Eichler, N. Greulich, G. Herrmann, N. Trautmann, *Radiochim. Acta* **1986**, *40*, 137.
[155] R. Eichler, M. Schädel, *J. Phys. Chem. B* **2002**, *106*, 5413.
[156] B. Grapengiesser, G. Rudstam, *Radiochim. Acta* **1973**, *20*, 85.
[157] G. Rudstam, B. Grapengiesser, *Radiochim. Acta* **1973**, *20*, 97.
[158] Z. Szeglowski, H. Bruchertseifer, V. P. Domanov, B. Gleisberg, L. J. Guseva, M. Hussonnois, G. S. Tikhomirova, I. Zvara, Yu. Ts. Oganessian, *Radiochim. Acta* **1990**, *51*, 71.
[159] Z. Szeglowski, H. Bruchertseifer, V. P. Domanov, B. Gleisberg, L. J. Guseva, M. Hussonnois, G. S. Tikhomirova, I. Zvara, Yu. Ts. Oganessian, *Sov. Radiochem.* **1992**, *33*, 663.
[160] G. Pfrepper, R. Pfrepper, A. B. Yakushev, S. N. Timokhin, I. Zvara, *Radiochim. Acta* **1997**, *77*, 201.
[161] G. Pfrepper, R. Pfrepper, R. Kraus, A. B. Yakushev, S. N. Timokhin, I. Zvara, *Radiochim. Acta* **1998**, *80*, 7.
[162] Z. Szeglowski, *Acta Phys. Pol. A* **2003**, *34*, 1671.
[163] D. Trubert, C. Le Naour, F. Monroy Guzman, M. Hussonnois, L. Brillard, J. F. Le Du, O. Constantinescu, J. Gasparro, V. Barci, B. Weiss, G. Ardisson, *Radiochim. Acta* **2002**, *90*, 127.
[164] D. Trubert, M. Hussonnois, L. Brillard, V. Barci, G. Ardisson, Z. Szeglowski, O. Constantinescu, R *adiochim. Acta* **1995**, *69*, 149.
[165] G. Pfrepper, R. Pfrepper, A. Kronenberg, J. V. Kratz, A. Nähler, W. Brüchle, M. Schädel, *Radiochim. Acta* **2000**, *88*, 273.
[166] B. Eichler, I. Zvara, *Radiochim. Acta* **1982**, *30*, 233.
[167] B. Eichler, *Kernenergie* **1976**, *10*, 307.
[168] V. Pershina, D. Trubert, C. Le Naour, J. V. Kratz, *Radiochim. Acta* **2002**, *90*, 869.
[169] K. R. Czerwinski, C. D. Kacher, K. E. Gregorich, T. M. Hamilton, N. J. Hannink, B. Kadkhodayan, S. A. Kreek, D. M. Lee, M. J. Nurmia, A. Türler, G. T. Seaborg, D. C. Hoffman, *Radiochim. Acta* **1994**, *64*, 29.
[170] C. D. Kacher, K. E. Gregorich, D. M. Lee, Y. Watanabe, B. Kadkhodayan, B. Wierczinski, M. R. Lane, E. R. Sylwester, D. A. Keeney, M. Hendricks, N. J. Stoyer, J. Yang, M. Hsu, D. C. Hoffman, A. Bilewicz, *Radiochim. Acta* **1996**, *75*, 127.
[171] R. Günther, W. Paulus, J. V. Kratz, A. Seibert, P. Thörle, S. Zauner, W. Brüchle, E. Jäger, V. Pershina, M. Schädel, B. Schausten, D. Schumann, B. Eichler, H. W. Gäggeler, D. T. Jost, A. Türler, *Radiochim. Acta* **1998**, *80*, 121.
[172] W. Brüchle, E. Jäger, V. Pershina, M. Schädel, B. Schausten, R. Günther, J. V. Kratz, W. Paulus, A. Seibert, P. Thörle, S. Zauner, D. Schumann, B. Eichler, H. Gäggeler, D. Jost, A. Türler, *J. Alloys Compd.* **1998**, *271–273*, 300.
[173] K. R. Czerwinski, K. E. Gregorich, N. J. Hannink, C. D. Kacher, B. Kadkhodayan, S. A. Kreek, D. M. Lee, M. J. Nurmia, A. Türler, G. T. Seaborg, D. C. Hoffman, *Radiochim. Acta* **1994**, *64*, 23.
[174] C. D. Kacher, K. E. Gregorich, D. M. Lee, Y. Watanabe, B. Kadkhodayan, B. Wierczinski, M. R. Lane, E. R. Sylwester, D. A. Keeney, M. Hendricks, D. C. Hoffman, *Radiochim. Acta* **1996**, *75*, 135.
[175] E. Strub, J. V. Kratz, A. Kronenberg, A. Nähler, P. Thörle, S. Zauner, W. Brüchle, E. Jäger, M. Schädel, B. Schausten, E. Schimpf, L. Zongwei, U. Kirbach, D. Schumann, D. T. Jost, A. Türler, M. Asai, Y. Nagame, M. Sakama, K. Tsukada, H. W. Gäggeler, J. P. Glatz, *Radiochim. Acta* **2000**, *88*, 265.
[176] H. Haba, K. Tsukada, M. Asai, I. Nishinaka, M. Sakama, S. Goto, M. Hirata, S. Ichikawa, Y. Nagame, T. Kaneko, H. Kudo, A. Toyoshima, Y. Shoji, A. Yokoyama, A. Shinohara, Y. Oura, K. Sueki, H. Nakahara, M. Schädel, J. V. Kratz, A. Türler, H. W. Gäggeler, *Radiochim. Acta* **2001**, *89*, 733.
[177] A. Bilewicz, S. Siekierski, C. D. Kacher, K. E. Gregorich, D. M. Lee, N. J. Stoyer, B. Kadkhodayan, S. A. Kreek, M. R. Lane, E. R. Sylwester, M. P. Neu, M. F. Mohar, D. C. Hoffman, *Radiochim. Acta* **1996**, *75*, 121.

 © 2006 Wiley-VCH Verlag GmbH & Co. KGaA, Weinheim

[178] R. D. Shannon, *Acta Crystallogr. Sect. A* **1976**, *32*, 751.
[179] R. G. Pearson, *J. Am. Chem. Soc.* **1963**, *85*, 3533.
[180] I. Zvara, Yu. T. Chuburkov, R. Caletka, T. S. Zvarova, M. R. Shalaevsky, B. V. Shilov, *At. Energ.* **1966**, *21*, 8; I. Zvara, Yu. T. Chuburkov, R. Caletka, T. S. Zvarova, M. R. Shalaevsky, B. V. Shilov, *J. Nucl. Energy* **1966**, *21*, 60; I. Zvara, Yu. T. Chuburkov, R. Caletka, T. S. Zvarova, M. R. Shalaevsky, B. V. Shilov, *Sov. J. At. Energy* **1966**, *21*, 709.
[181] I. Zvara, Yu. Ts. Chuburkov, R. Caletka, M. R. Shalaevsky, *Sov. Radiochem.* **1969**, *11*, 161.
[182] Yu. T. Chuburkov, I. Zvara, B. V. Shilov, *Sov. Radiochem.* **1969**, *11*, 171.
[183] Until the name rutherfordium (Rf) was endorsed by the IUPAC (*Pure Appl. Chem.* **1997**, *69*, 2471) for element 104 the Dubna group frequently used the name kurchatovium (Ku).
[184] O. L. Keller, Jr., *Radiochim. Acta* **1984**, *37*, 169.
[185] J. P. Desclaux, B. Fricke, *J. Phys.* **1980**, *41*, 943.
[186] V. A. Glebov, L. Kasztura, V. S. Nefedov, B. L. Zhuikov, *Radiochim. Acta* **1989**, *46*, 117.
[187] B. L. Zhuikov, V. A. Glebov, V. S. Nefedov, I. Zvara, *J. Radioanal. Nucl. Chem.* **1990**, *143*, 103.
[188] B. L. Zhuikov, Yu. T. Chuburkov, S. N. Timokhin, K. U. Jin, I. Zvara, *Radiochim. Acta* **1989**, *46*, 113.
[189] E. Eliav, U. Kaldor, Y. Ishikawa, *Phys. Rev. Lett.* **1995**, *74*, 1079.
[190] B. Kadkhodayan, A. Türler, K. E. Gregorich, P. A. Baisden, K. R. Czerwinski, B. Eichler, H. W. Gäggeler, T. M. Hamilton, D. T. Jost, C. D. Kacher, J. Kovacs, S. A. Kreek, M. R. Lane, M. Mohar, M. P. Neu, N. J. Stoyer, E. R. Sylwester, M. D. Lee, M. J. Nurmia, G. T. Seaborg, D. C. Hoffman, *Radiochim. Acta* **1996**, *72*, 169.
[191] E. R. Sylwester, K. E. Gregorich, M. D. Lee, B. Kadkhodayan, A. Türler, J. L. Adams, C. D. Kacher, M. R. Lane, C. A. Laue, C. A. McGrath, D. A. Shaughnessy, D. A. Strellis, P. A. Wilk, D. C. Hoffman, *Radiochim. Acta* **2000**, *88*, 837.
[192] M. V. Ryzhkov, V. A. Gubanov, I. Zvara, *Radiochim. Acta* **1992**, *57*, 11.
[193] A. Türler, G. V. Buklanov, B. Eichler, H. W. Gäggeler, M. Grantz, S. Hübener, D. T. Jost, V. Ya. Lebedev, D. Piquet, S. N. Timokhin, A. B. Yakushev, I. Zvara, *J. Alloys Compd.* **1998**, *271–273*, 287.
[194] V. Pershina, B. Fricke, *J. Phys. Chem.* **1994**, *98*, 6468.
[195] B. Eichler, R. Eichler in *The Chemistry of Superheavy Elements* (Ed.: M. Schädel), Kluwer Academic Publishers, Dordrecht, **2003**, pp. 205 – 236.
[196] I. Zvara, *Radiochim. Acta* **1985**, *38*, 95.
[197] A. Türler, H. W. Gäggeler, K. E. Gregorich, H. Barth, W. Brüchle, K. R. Czerwinski, M. K. Gober, N. J. Hannink, R. A. Henderson, D. C. Hoffman, D. T. Jost, C. D. Kacher, B. Kadkhodayan, J. Kovacs, J. V. Kratz, S. A. Kreek, D. M. Lee, J. D. Leyba, M. J. Nurmia, M. Schädel, U. W. Scherer, E. Schimpf, D. Vermeulen, A. Weber, H. P. Zimmermann, I. Zvara, *J. Radioanal. Nucl. Chem.* **1992**, *95*, 327.
[198] V. P. Domanov, U. Zin Kim, *Radiokhimiya* **1989**, *31*, 12.
[199] Until the name dubnium (Db) was endorsed by the IUPAC (*Pure Appl. Chem.* **1997**, *69*, 2471) for element 105 the Dubna group used the name nielsbohrium (Ns) in some of their publications while the Berkeley group and a large collaboration working on the chemistry of element 105 frequently used the name hahnium (Ha).
[200] J. V. Kratz, H. P. Zimmermann, U. W. Scherer, M. Schädel, W. Brüchle, K. E. Gregorich, C. M. Gannet, H. L. Hall, R. A. Henderson, D. M. Lee, J. D. Leyba, M. J. Nurmia, D. C. Hoffman, H. Gäggeler, D. Jost, U. Baltensperger, Y. Nai-Qi, A. Türler, C. Lienert, *Radiochim. Acta* **1989**, *48*, 121.
[201] H. P. Zimmermann, M. K. Gober, J. V. Kratz, M. Schädel, W. Brüchle, E. Schimpf, K. E. Gregorich, A. Türler, K. R. Czerwinski, N. J. Hannink, B. Kadkhodayan, D. M. Lee, M. J. Nurmia, D. C. Hoffman, H. Gäggeler, D. Jost, J. Kovacs, U. W. Scherer, A. Weber, *Radiochim. Acta* **1993**, *60*, 11.
[202] V. Pershina, *Radiochim. Acta* **1998**, *80*, 75.
[203] V. Pershina, *Radiochim. Acta* **1998**, *80*, 65.
[204] W. Paulus, J. V. Kratz, E. Strub, S. Zauner, W. Brüchle, V. Pershina, M. Schädel, B. Schausten, J. L. Adams, K. E. Gregorich, D. C. Hoffman, M. R. Lane, C. Laue, D. M. Lee, C. A. McGrath, D. A. Shaughnessy, D. A. Strellis, E. R. Sylwester, *Radiochim. Acta* **1999**, *84*, 69.
[205] V. Pershina, T. Bastug, *Radiochim. Acta* **1999**, *84*, 79.
[206] M. Schädel, W. Brüchle, E. Schimpf, H. P. Zimmermann, M. K. Gober, J. V. Kratz, N. Trautmann, H. Gäggeler, D. Jost, J. Kovacs, U. W. Scherer, A. Weber, K. E. Gregorich, A. Türler, K. R. Czerwinski, N. J. Hannink, B. Kadkhodayan, D. M. Lee, M. J. Nurmia, D. C. Hoffman, *Radiochim. Acta* **1992**, *57*, 85.
[207] J. V. Kratz, M. K. Gober, H. P. Zimmermann, M. Schädel, W. Brüchle, E. Schimpf, K. E. Gregorich, A. Türler, N. J. Hannink, K. R. Czerwinski, B. Kadkhodayan, D. M. Lee, M. J. Nurmia, D. C. Hoffman, H. Gäggeler, D. Jost, J. Kovacs, U. W. Scherer, A. Weber, *Phys. Rev. C* **1992**, *45*, 1064.
[208] H. W. Gäggeler, *J. Radioanal. Nucl. Chem.* **1994**, *183*, 261.
[209] A. Türler, *Radiochim. Acta* **1996**, *72*, 7.
[210] H. W. Gäggeler, D. Jost, J. Kovacs, U. W. Scherer, A. Weber, D. Vermeulen, A. Türler, K. E. Gregorich, R. A. Henderson, K. R. Czerwinski, B. Kadkhodayan, D. M. Lee, M. J. Nurmia, D. C. Hoffman, J. V. Kratz, M. K. Gober, H. P. Zimmermann, M. Schädel, W. Brüchle, E. Schimpf, I. Zvara, *Radiochim. Acta* **1992**, *57*, 93.
[211] V. Pershina, W. D. Sepp, B. Fricke, D. Kolb, M. Schädel, G. V. Ionova, *J. Chem. Phys.* **1992**, *97*, 1116.
[212] V. Pershina, W. D. Sepp, T. Bastug, B. Fricke, G. V. Ionova, *J. Chem. Phys.* **1992**, *97*, 1123.
[213] M. Dolg, H. Stoll, H. Preuss, R. M. Pitzer, *J. Phys. Chem.* **1993**, *97*, 5852.
[214] A. Ghiorso, M. Nitschke, J. R. Alonso, M. Nurmia, G. T. Seaborg, E. K. Hulet, R. W. Lougheed, *Phys. Rev. Lett.* **1974**, *33*, 1490.
[215] V. A. Druin, B. Bochev, Yu. V. Lobanov, R. N. Sagaidak, Yu. P. Kharitonov, S. P. Tretyakova, G. G. Gulbekyan, G. V. Buklanov, E. A. Erin, V. N. Kosyakov, A. G. Rykov, *Sov. J. Nucl. Phys.* **1979**, *29*, 591.
[216] Yu. A. Lazarev, Yu. V. Lobanov, Yu. Ts. Oganessian, V. K. Utyonkov, F. Sh. Abdullin, G. V. Buklanov, B. N. Gikal, S. Iliev, A. N. Mezentsev, A. N. Polyakov, I. M. Sedykh, I. V. Shirikovsky, V. G. Subbotin, A. M. Sukov, Yu. S. Tsyganov, V. E. Zhuchko, R. W. Lougheed, K. J. Moody, J. F. Wild, J. H. McQuaid, *Phys. Rev. Lett.* **1994**, *73*, 624.
[217] R. W. Lougheed, K. J. Moody, J. F. Wild, J. H. McQuaid, Yu. A. Lazarev, Yu. V. Lobanov, Yu. Ts. Oganessian, V. K. Utyonkov, F. Sh. Abdullin, G. V. Buklanov, B. N. Gikal, S. Iliev, A. N. Mezentsev, A. N. Polyakov, I. M. Sedykh, I. V. Shirikovsky, V. G. Subbotin, A. M. Sukov, Yu. S. Tsyganov, V. E. Zhuchko, *J. Alloys Compd.* **1994**, *213*/214, 61.
[218] M. Schädel, W. Brüchle, R. Dressler, B. Eichler, H. W. Gäggeler, R. Günther, K. E. Gregorich, D. C. Hoffman, S. Hübener, D. T. Jost, J. V. Kratz, W. Paulus, D. Schumann, S. Timokhin, N. Trautmann, A. Türler, G. Wirth, A. Yakushev, *Nature* **1997**, *388*, 55.
[219] M. Schädel, W. Brüchle, B. Schausten, E. Schimpf, E. Jäger, G. Wirth, R. Günther, J. V. Kratz, W. Paulus, A. Seibert, P. Thörle, N. Trautmann, S. Zauner, D. Schumann, M. Andrassy, R. Misiak, K. E. Gregorich, D. C. Hoffman, D. M. Lee, E. Sylwester, Y. Nagame, Y. Oura, *Radiochim. Acta* **1997**, *77*, 149.
[220] M. Schädel, W. Brüchle, E. Jäger, B. Schausten, G. Wirth, W. Paulus, R. Günther, K. Eberhardt, J. V. Kratz, A. Seibert, E. Strub, P. Thörle, N. Trautmann, A. Waldeck, S. Zauner, D.

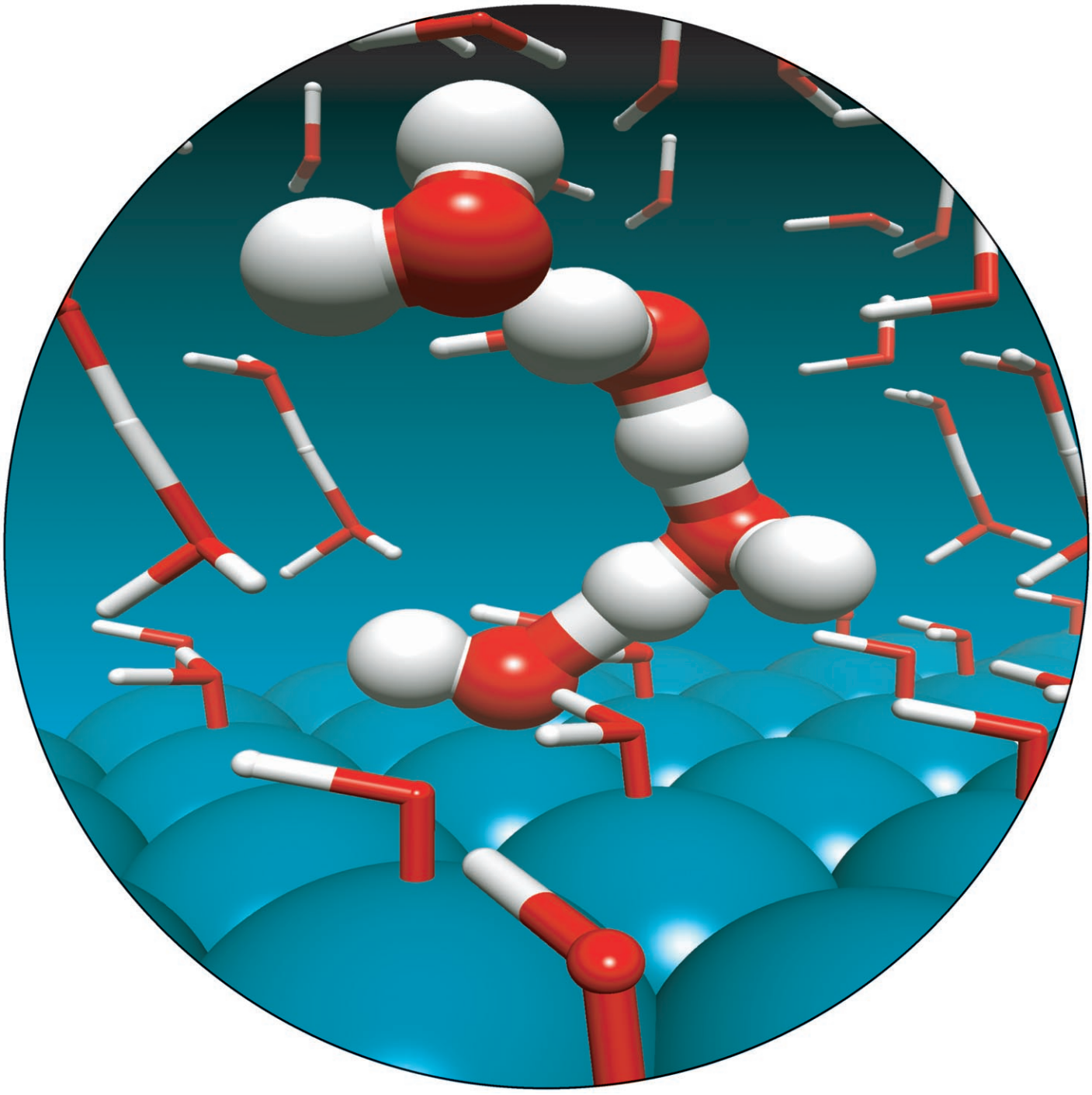
 © 2006 Wiley-VCH Verlag GmbH & Co. KGaA, Weinheim

Schumann, U. Kirbach, B. Kubica, R. Misiak, Y. Nagame, K. E. Gregorich, *Radiochim. Acta* **1998**, *83*, 163.
[221] V. Pershina, J. V. Kratz, *Inorg. Chem.* **2001**, *40*, 776.
[222] C. Nash, B. E. Bursten, *New J. Chem.* **1995**, *19*, 669.
[223] B. Eichler, A. Türler, H. W. Gäggeler, *J. Phys. Chem. A* **1999**, *103*, 9296.
[224] V. Pershina, B. Fricke, *J. Phys. Chem.* **1995**, *99*, 144.
[225] V. Pershina, B. Fricke, *J. Phys. Chem.* **1996**, *100*, 8748.
[226] S. N. Timokhin, A. B. Yakushev, H. Xu, V. P. Perelygin, I. Zvara, *J. Radioanal. Nucl. Chem.* **1996**, *212*, 31.
[227] A. B. Yakushev, S. N. Timokhin, M. V. Vedeneev, H. Xu, I. Zvara, *J. Radioanal. Nucl. Chem.* **1996**, *205*, 63.
[228] A. Türler, W. Brüchle, R. Dressler, B. Eichler, R. Eichler, H. W. Gäggeler, M. Gärtner, K. E. Gregorich, S. Hübener, D. T. Jost, V. Ya. Lebedev, V. Pershina, M. Schädel, S. Taut, S. N. Timokhin, N. Trautmann, A. Vahle, A. Yakushev, *Angew. Chem.* **1999**, *111*, 2349; *Angew. Chem. Int. Ed.* **1999**, *38*, 2212.
[229] W. Brüchle, *Radiochim. Acta* **2003**, *91*, 71.
[230] A. Vahle, S. Hübener, H. Funke, B. Eichler, D. T. Jost, A. Türler, W. Brüchle, E. Jäger, *Radiochim. Acta* **1999**, *84*, 43.
[231] V. Pershina, T. Bastug, *J. Chem. Phys.* **2000**, *113*, 1441.
[232] R. Eichler, B. Eichler, H. W. Gäggeler, D. T. Jost, D. Piguet, A. Türler, *Radiochim. Acta* **2000**, *88*, 87.
[233] I. Zvara, V. P. Domanov, S. Hübener, M. R. Shalaevskii, S. N. Timokhin, B. L. Zhuikov, B. Eichler, G. V. Buklanov, *Sov. Radiochem.* **1984**, *26*, 72.
[234] V. P. Domanov, S. Hübener, M. R. Shalaevskii, S. N. Timokhin, D. V. Petrov, I. Zvara, *Sov. Radiochem.* **1983**, *25*, 23.
[235] M. Schädel, E. Jäger, E. Schimpf, W. Brüchle, *Radiochim. Acta* **1995**, *68*, 1.
[236] R. Eichler, B. Eichler, H. W. Gäggeler, D. T. Jost, R. Dresseler, A. Türler, *Radiochim. Acta* **1999**, *87*, 15.
[237] G. Münzenberg, P. Armbruster, H. Folger, F. P. Heßberger, S. Hofmann, J. Keller, K. Poppensieker, W. Reisdorf, K.-H. Schmidt, H.-J. Schött, M. E. Leino, R. Hingmann, *Z. Phys. A* **1984**, *317*, 235.
[238] C. Düllmann, B. Eichler, R. Eichler, H. W. Gäggeler, D. T. Jost, D. Piquet, A. Türler, *Nucl. Instrum. Methods Phys. Res. Sect. A* **2002**, *479*, 631.
[239] C. Düllmann, R. Dressler, B. Eichler, H. W. Gäggeler, F. Glaus, D. T. Jost, D. Piquet, S. Soverna, A. Türler, W. Brüchle, R. Eichler, E. Jäger, V. Pershina, M. Schädel, B. Schausten, E. Schimpf, H.-J. Schött, G. Wirth, K. Eberhardt, P. Thörle, N. Trautmann, T. N. Ginter, K. E. Gregorich, D. C. Hoffmann, U. W. Kirbach, D. M. Lee, H. Nitsche, J. B. Patin, R. Sudowe, P. Zielinski, S. N. Timokhin, A. B. Yakushev, A. Vahle, Z. Qin, *Czech. J. Phys.* **2003**, *53*, A291.
[240] V. Pershina, *J. Nucl. Radiochem. Sci.* **2002**, *3*, 137.
[241] V. Pershina, T. Bastug, B. Fricke, S. Varga, *J. Chem. Phys.* **2001**, *115*, 792.
[242] V. Pershina, GSI Scientific Report 2003, GSI 2004-1 **2004**, p. 191.
[243] "Gaschemische Untersuchung in situ gebildeter flüchtiger Oxide des Rutheniums, Osmiums und Hassiums": A. von Zweidorf, PhD Thesis, University Mainz, **2003**, and A. von Zweidorf, *Gaschemische Untersuchung in situ gebildeter flüchtiger Oxide des Rutheniums, Osmiums und Hassiums*, Ibidem Verlag, Stuttgart, **2003**.
[244] B. Eichler, V. P. Domanov, *J. Radioanal. Chem.* **1975**, *28*, 143.
[245] V. P. Domanov, B. Eichler, I. Zvara, *Sov. Radiochem.* **1984**, *26*, 63.
[246] V. P. Domanov, I. Zvara, *Sov. Radiochem.* **1984**, *26*, 731.
[247] F. Zude, W. Fan, N. Trautmann, G. Herrmann, B. Eichler, *Radiochim. Acta* **1993**, *62*, 61.
[248] J. Merinis, G. Bouissières *Anal. Chim. Acta* **1961**, *25*, 498.
[249] P. Pyykkö, *Angew. Chem.* **2004**, *116*, 4512; *Angew. Chem. Int. Ed.* **2004**, *43*, 4412.
[250] E. Eliav, U. Kaldor, P. Schwerdtfeger, B. A. Hess, Y. Ishikawa, *Phys. Rev. Lett.* **1994**, *73*, 3203.
[251] M. Seth, P. Schwerdtfeger, M. Dolg, K. Faegri, B. A. Hess, U. Kaldor, *Chem. Phys. Lett.* **1996**, *250*, 461.
[252] M. Seth, P. Schwerdtfeger, M. Dolg, *J. Chem. Phys.* **1997**, *106*, 3623.
[253] W. Liu, C. van Wüllen, *J. Chem. Phys.* **1999**, *110*, 3730.
[254] W. Loveland, K. E. Gregorich, J. B. Patin, D. Peterson, C. Rouki, P. M. Zielinski, K. Aleklett, *Phys. Rev. C* **2002**, *66*, 044617.
[255] R. Eichler, W. Brüchle, R. Buda, S. Bürger, R. Dressler, C. E. Düllmann, J. Dvorak, K. Eberhardt, B. Eichler, C. M. Folden, H. W. Gäggeler, K. E. Gregorich, F. Haenssler, H. Hummrich, E. Jäger, J. V. Kratz, B. Kuczewski, D. Liebe, D. Nayak, H. Nitsche,D. Piquet, Z. Qin, U. Rieth, M. Schädel, B. Schausten, E. Schimpf, A. Semchenkov, S. Soverna, R. Sudowe, N. Trautmann, P. Thörle, A. Türler, B. Wierczinski, N. Wiehl, P. A. Wilk, G. Wirth, A. B. Yakushev, A. von Zweidorf, *Radiochim. Acta* **2005**, in press.
[256] V. Pershina, T. Bastug, C. Sarpe-Tudoran, J. Anton, B. Fricke, *Nucl. Phys. A* **2004**, *734*, 200.
[257] B. Eichler, H. Rossbach, *Radiochim. Acta* **1983**, *33*, 121.
[258] E. Eliav, U. Kaldor, Y. Ishikawa, *Phys. Rev. A* **1995**, *52*, 2765.
[259] S. Soverna, R. Dresseler, C. E. Düllmann, B. Eichler, R. Eichler, H. W. Gäggeler, F. Haenssler, J.-P. Niklaus, D. Piquet, Z. Qin, A. Türler, A. B. Yakushev, *Radiochim. Acta* **2005**, *93*, 1.
[260] R. Lougheed, *Nature* **1997**, *388*, 21.
[261] M. Jacoby, *Chem. Eng. News* **1997**, *75*, 5.

© 2006 Wiley-VCH Verlag GmbH & Co. KGaA, Weinheim

Communications

DOI: 10.1002/anie.200502540



Ab initio predictions have been used to follow the changes in the structure and reactivity of the water/metal interface as a function of applied potential. The results provide an electrochemical phase diagram for water over Pd(111) derived from first principles. For more information see the Communication by M. Neurock and J.-S. Filhol on the following pages.

WILEY InterScience DISCOVER SOMETHING GREAT
© 2006 Wiley-VCH Verlag GmbH & Co. KGaA, Weinheim

Electrocatalysis

DOI: 10.1002/anie.200502540

Elucidation of the Electrochemical Activation of Water over Pd by First Principles**

*Jean-Sébastien Filhol and Matthew Neurock**

The water/metal interface is critical to the performance of a number of chemical, biological, and materials systems, including electrocatalysts for fuel cells, corrosion-resistant surfaces, electrochemically deposited electronic and magnetic films, and inorganic scaffolds for biomolecular adhesion. The reactivity and electrochemical behavior of the metal/solution interface is dictated by the explicit atomic and electronic structure that forms at the interface as a response to environmental conditions, such as an applied potential. Elucidating the structure and chemistry at this interface, however, is a considerable challenge because of the large number of molecular configurations that result from factors such as the various orientations of the water molecules in the hydrogen-bonded network, the presence and formation of different ions at various positions within the interface, and the range of reactions that can occur at different applied surface potentials. Spectroscopic resolution of the molecular-level transformations that occur at this interface as a function of the applied electrochemical conditions is difficult to obtain. Although theory has made important advances in elucidating gas-phase reactions on metal substrates, there have been very few ab initio studies of the metal/solution interface in the presence of an applied potential[1–3] These previous studies were pioneering, as they provided insights into the reactivity of the interface. Their treatment of the metal, the solution phase, and the polarizability of the interface with potential, however, was not quantitative enough to model the detailed surface chemistry accurately. Herein, we report the development and application of an ab initio quantum mechanical approach to simulate the specific changes in the atomic structure of the water/metal interface and its reactivity as a function of applied potential. The approach is used to derive what we believe is the first interfacial electrochemical phase diagram to be developed by ab initio calculations. More specifically, we examine the activation of aqueous water over Pd(111). The results demonstrate that the polarization of the interface is critical in correctly establishing the structure and the reactivity of the interface as a function of potential.

[*] J.-S. Filhol, Prof. M. Neurock
Departments of Chemical Engineering and Chemistry
University of Virginia
Charlottesville, VA 22904-4741 (USA)
Fax: (+1) 434-982-2658
E-mail: neurock@virginia.edu

[**] We gratefully acknowledge support of this work by the US Army Research Office through grant number DAAD19-03-1-0169.

Supporting information for this article is available on the WWW under http://www.angewandte.org or from the author.

Generalized gradient corrected, periodic density functional theoretical calculations were carried out to determine the structures and the corresponding free energies for each of the phases that can form for water on the Pd(111) surface over a potential range of −0.5 to 2.5 V. The details of the calculations as well as the approach are reported in the Supporting Information. To simulate an applied potential, the metal slab is charged by selectively adding (or subtracting) a predetermined number of electrons (n_e) to (or from) the system. A compensating background charge (n_{bg}) was subsequently distributed homogeneously over the unit cell to maintain overall charge neutrality. Explicit water molecules were introduced into the vacuum region between the metal slabs to model the solution/metal interface. The density of water was optimized, which results in a value close to that of bulk water. The charged slab, along with the compensating background charge, polarizes the water region and thus simulates the electrochemical double layer (see Supporting Information for details of the calculations). The charged slab and compensating background charge interact with each other and thus influence the total energy of the system. To calculate an unbiased electronic energy, the DFT-calculated value E_{DFT} is corrected for the interaction between the electrons in the slab and the background charge by using the expression given in Equation (1).

$$E_{\mathrm{DFT}}(n_{\mathrm{e}},n_{\mathrm{bg}}) = E_{\mathrm{slab}}(n_{\mathrm{e}}) + E_{\mathrm{slab\text{-}bg}}(n_{\mathrm{e}},n_{\mathrm{bg}}) + E_{\mathrm{bg}}(n_{\mathrm{bg}}) \quad (1)$$

In Equation (1), E_{slab} is the energy of the slab without the background, E_{bg} is the energy of the background without the slab and $E_{\mathrm{bg\text{-}slab}}$ is the interaction energy between the slab and the background. The correction results in the total electron energy E_{elec} defined in Equation (2).

$$E_{\mathrm{elec}} = E_{\mathrm{DFT}} + \int_0^q \langle \overline{V_{\mathrm{tot}}}(Q)\rangle \mathrm{d}Q \quad (2)$$

$\overline{V_{\mathrm{tot}}}(Q)$ refers to the average electrostatic potential and Q refers to the excess charge of the unit cell. More details of this derivation are given in the Supporting Information. The total free energy of the system E_{free} must also include contributions for the excess electrons q at the Fermi potential φ_{vac}. This inclusion of these contributions results in Equation (3) for the potential-dependent free energy E_{free}.

$$E_{\mathrm{free}} = E_{\mathrm{DFT}} + \int_0^q \langle \overline{V_{\mathrm{tot}}}(Q)\rangle \mathrm{d}Q - q\,\varphi_{\mathrm{vac}} \quad (3)$$

The method described above was used to map out the phase diagram for the electrooxidation and electroreduction of water over Pd. Although a diverse range of structures at the water/metal interface is possible, we follow only the most thermodynamically stable structures. The free energies for the interfacial water, hydride, and hydroxide/metal interfaces and their reactive transitions are simulated as a function of potential to establish the electrochemical phase diagram for water on the Pd(111) substrate.

 © 2006 Wiley-VCH Verlag GmbH & Co. KGaA, Weinheim WILEY InterScience DISCOVER SOMETHING GREAT

Water adsorbs at the potential of zero charge on the Pd(111) surface in a form similar to that of the well-known hexagonal bilayer structure[4] in which water molecules assemble in a hexagonal ring structure on the surface, as seen in Figure 1a (top metal/water interface) and 1b (bottom metal/water interface). The water molecules closest to the surface are bound with the oxygen end oriented toward the surface because of the interaction of the filled $1b_1$ orbital of water and empty d states on the metal. As we sweep to more-negative potential, the water at the surface rotates to orient its positively charged hydrogen atoms toward the more negatively charged metal surface as is seen in the left-hand panel of Figure 1. This potential-dependent change in orientation is known as the water flip–flop mechanism and is well established in electrochemistry. Furthermore, the Pd–H bond distance decreases while the Pd···O distance increases, as shown in Figure 1. The distance between the oxygen atoms and the surface decreases as the potential is made more positive. The changes were found to be continuous over the range of potentials examined, thus reflecting the continuous polarization of the interface.

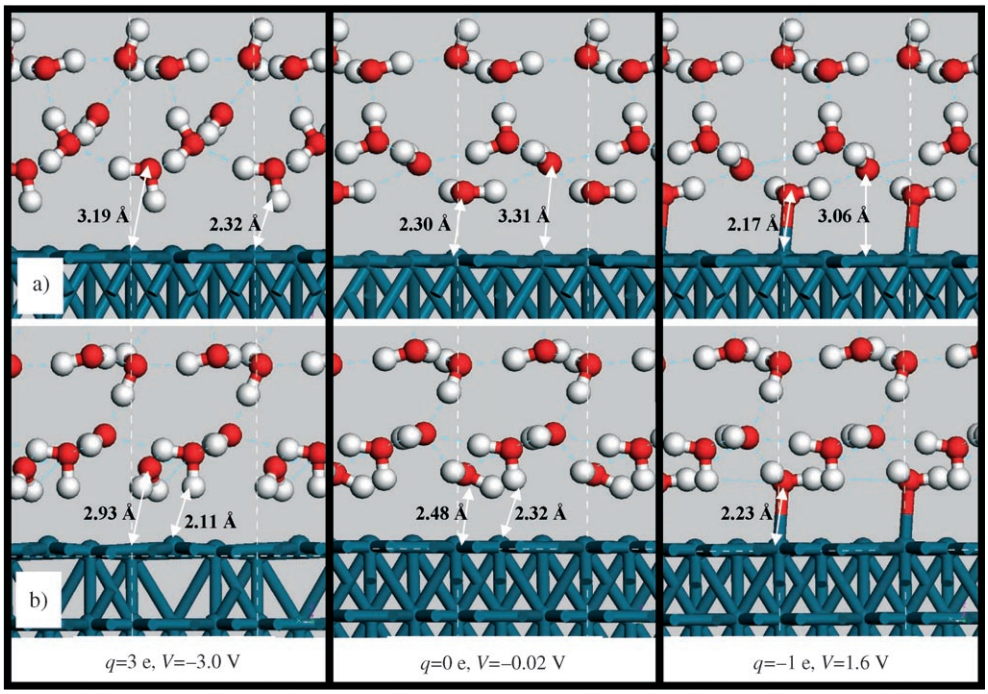


Figure 1. The optimized structure of the water/palladium interface at different applied potentials. The upper set of figures refers to the surface structure that forms at the top of the electrode (a). The lower set of figures refers to the surface structure that forms at the bottom of the electrode (b). The potential (referenced to the NHE) and the corresponding charge are given at the bottom of the Figure below each interface. The unit cell is outlined with white dashed lines. The blue dashed lines refer to the hydrogen bonds.

These changes in the positions of water molecules can be attributed to the presence of the strong electric field that results at the surface from the charging of the metal slab. The large dipole moment of the water molecule (1.85 D) aligns with the local electric field at the interface. This leads to the specific orientation of the water molecules. At more-positive potentials the water molecules are aligned with their oxygen end directed toward the surface, whereas at more-negative potentials the hydrogen atoms point toward the surface. The resulting force on the water molecules at the metal surface is balanced by the direct bonding between the water and the surface, hydrogen bonding between coadsorbed water molecules, and hydrogen bonding with water molecules in the solution layer. The dipole moments tend to migrate toward the zone where the electric field is maximized (namely, close to the surface). This situation helps to explain why the second layer of water tends to move closer to the surface.

Above 1100 mV, the free energy of the hydroxide phase becomes lower than that of the water phase, thus resulting in a phase change. The water molecules bound through their oxygen atoms are initially activated. The reaction involves the formation of a proton along with a surface hydroxyl intermediate, both of which are stabilized by hydrogen bonding with neighboring water molecules in solution and on the surface. The proton that forms rapidly transfers to water molecules in the solution layer above the surface by means of proton shuttling (Figure 2a). Proton transfer is enhanced in this way by the repulsive interaction between the solvated proton and the positively charged surface. Diffusion is thus the result of electromigration.

In addition to the direct water-activation path, the hydroxide ion that forms at the surface can subsequently assist in water activation by abstracting a proton from a water molecule in the second layer. This situation leads to the activation of water molecules in the second solvent layer. The change of structure from the water phase to the hydroxide phase is reversible with potential. Nevertheless, the potential associated with this change is discontinuous between these two routes. This discontinuity is related to the changes in the structure described above that occur between the two routes. Water dissociates to form a surface hydroxide ion and a hydrated proton. The structural reorganization that takes place upon dissociation ultimately leads to the resulting discontinuity. The structure that forms is shown in Figure 2c.

At more negative potentials, the dissociation of water is activated by the interaction between the metal and the hydrogen atoms on water to form a surface hydride and a hydroxide anion that moves into the solution phase. The phase change between the water and the hydride route is calculated to occur at 0.5 V. The atomic hydrogen that forms is situated at the threefold-symmetric face-centered-cubic sites, whereas the hydroxide ion migrates away from the

 © 2006 Wiley-VCH Verlag GmbH & Co. KGaA, Weinheim

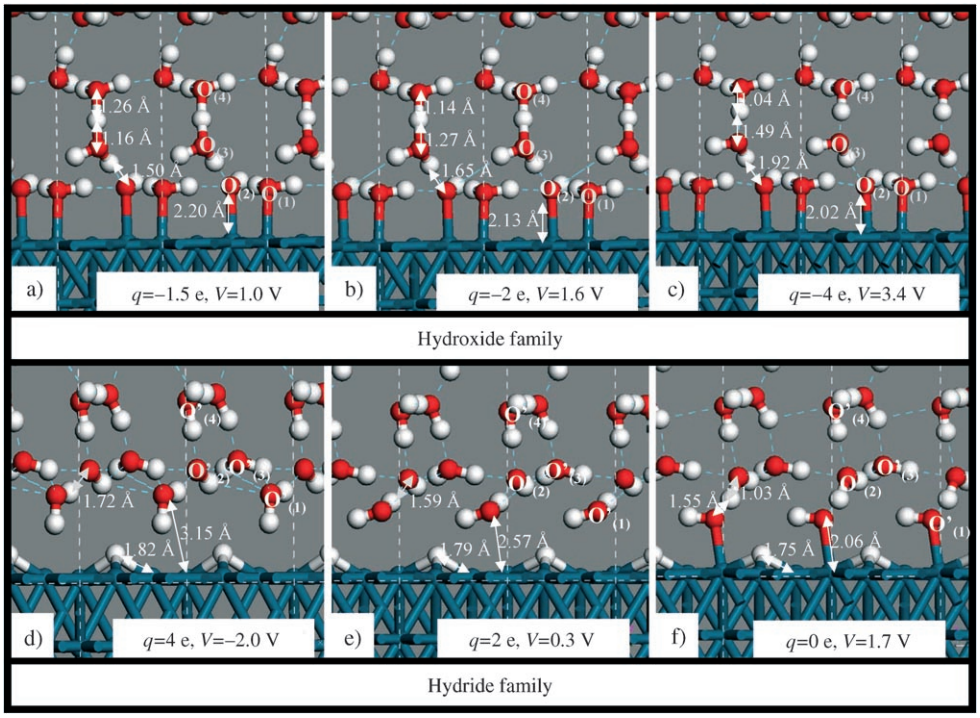


Figure 2. Evolution of the structure of the palladium/hydroxide interface (top of electrode) as a function of applied potential (a–c). The evolution of the palladium-hydride interface (bottom of electrode) as a function of potential (d–f). The associated metal potential (referenced to the NHE) and charge of the slab are presented in each case. The unit cell is outlined with a white dashed line. The blue dashed line shows hydrogen bonds.

surface through a sequence of rapid proton-transfer steps, and subsequently forms three hydrogen bonds with neighboring water molecules. At even lower potentials, the OH^- intermediate diffuses further away from the surface by means of proton shuttling along a chain of water molecules. Figure 2 d–f shows the transfer of the proton from $(O'_{(1)}H)^-\cdots(H_2O'_{(2)})$ to $(O'_{(1)}H\text{-}H\text{-}O'_{(2)}H)^-$ and then onto $(O'_{(1)}H_2)\cdots(O'_{(2)}H)^-$.

The discontinuity of the potential between the water and hydroxide routes at 0.5 V can be attributed to the transfer of an electron from the surface when one of the adsorbed water molecules dissociates to form the charged OH^- species and the surface hydride. This process allows for the reduction of the surface charge and an increase in the potential. When the potential of the cell is decreased further, the strong electrostatic repulsion between the surface and the OH^- ions leads to field-induced diffusion of the OH^- ions, even at 0 K.

The free energies for the water, hydride, and hydroxide phases can be followed as a function of potential and thus used to construct the phase diagram for the electrochemical activation of water shown in Figure 3 a. The most stable surface structure at potentials below 0.5 V is that of the hydride, which is accompanied by the formation of OH^- ions in solution. The most stable surface structure between 0.5 and 1.1 V corresponds to water adsorbed on Pd. The hydroxide surface is the most favorable at potentials greater than 1.1 V; in this case, the protons that form are stabilized as H_3O^+- or $H_5O_2^+$-type intermediates in solution. At any given potential, the energy difference between the water, hydride, and hydroxide curves constitutes the overall free-energy differences for the reactions that connect these phases. An important point to note is that the free-energy differences (reaction energies) change as the potential is changed. This is a result of the polarization of the interface. The lines drawn at 0.5 and 1.1 V in Figure 3 denote the phase transitions, where two different surface phases coexist. The surface phase can be transformed at constant potential by changing the number of electrons passed.

The evolution of the charge with the change in applied potential for the most stable states is presented in Figure 3 b. The variation of the charge with potential is nearly linear and displays capacitor-like behavior in which step changes occur as a result of the phase transitions. The slopes of the three lines are different from each other, which suggests that there are changes in the unit-cell capacitance that are linked to the strong change in the charge repartition. This is the polarization of the interface that leads to changes in the properties of the metal, such as adsorption and surface reactivity, as the potential is changed. Nevertheless, at 0.5 and 1.1 V, there are discontinuities in the charge. These discontinuities arise as a result of the phase transition between the two redox species at constant potential. This first-order phase transition is linked to the coexistence of two different species on the electrode surface that are interconverted on changing the charge [Eq. (4) and Eq. (5)].

$$Pd{-}H_2O + 1\,e^- \rightarrow Pd{-}H + OH^- \quad (\text{at } 0.5\text{ V}) \tag{4}$$

$$Pd{-}OH + H^+ + 1\,e^- \rightarrow Pd{-}H_2O \quad (\text{at } 1.1\text{ V}) \tag{5}$$

The electrochemical activation of water over Pd has been examined experimentally, thus allowing for a comparison with the theoretical results.[5,6] The electroadsorption of hydrogen

 © 2006 Wiley-VCH Verlag GmbH & Co. KGaA, Weinheim

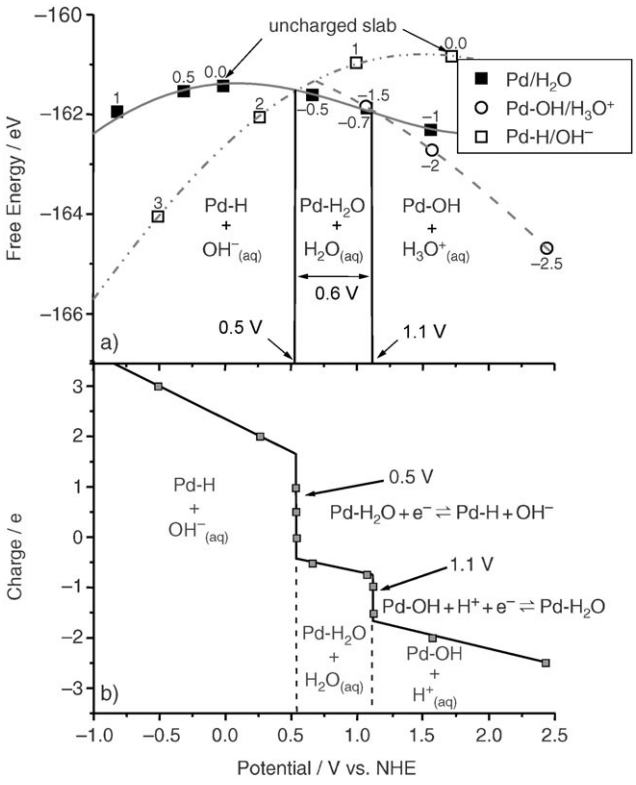


Figure 3. a) The evolution of the palladium/water interfacial free energy as a function of the biased potential referenced to the NHE. The number close to each calculated point is the slab charge. The most stable surface structure is the one that has the lowest free energy. b) The evolution of the slab charge with potential for the corresponding stable structures. The three different stable structures are presented. The associated electrochemical reactions associated with the transition from one stable structure to another one are given.

over Pd(111) takes place through the surface reaction Pd–$H_2O + 1e^- \rightarrow$Pd–H + OH^-, which proceeds experimentally at 0.4 V versus the normal hydrogen electrode (NHE).[6] This reaction was found to be irreversible. This experimental irreversibility is consistent with the large hysteresis found in our simulations in which hydrogen does not electrodesorb from the surface back into H^+ ions, even at much higher potentials (at 0 K). These observations suggest that hydrogen electrodesorption is a slow and activated process. The reversible formation of a hydroxide layer from adsorbed water was found by experiment[5] to occur at a potential of 0.7–0.9 V in acidic solution. The reversibility of this reaction is consistent with our results in which the switch from the water to the hydroxide route occurs directly. The experimental results show that the transitions from the surface-hydride to the surface-water phase and the surface-water to the surface-hydroxide phase occur at 0.4 V and 0.7–0.9 V, respectively. This is in good accordance with our results, which show transitions at 0.5 and 1.1 V, respectively.

The ab initio method developed herein enabled us to simulate the molecular changes in surface structure at the metal/solution interface during the electrocatalytic oxidation and reduction of water on Pd(111). The ability to simulate the polarizability of the water/metal interface was found to be important in predicting the appropriate response of the interface to changes in potential. The electrooxidation of water was predicted to occur at 1.1 V in an acidic solution. The electroreduction of water occurs at 0.5 V in a basic solution. Although the results may be improved by employing larger models of the surface and carrying out finite-temperature calculations, they still show reasonably good agreement with the experimental results. Adsorbed water is activated by the uptake of an electron from the metal to form an adsorbed hydride and an aqueous hydroxide ion. This reaction occurs through a similar proton-transfer path. The synergistic cooperation between the metal and the solution is required to activate water in both electrooxidation and electroreduction processes. The simulations tend to correctly capture other important physicochemical processes, such as the potential-dependent water orientation, the reductive and oxidative activation of water, and the electromigration of ions in solution. The method developed is general and should be applicable for following potential-dependent behavior of the interfacial transformations for many other electrochemical systems.

Received: July 20, 2005
Published online: November 24, 2005

Keywords: ab initio calculations · electrochemistry · phase diagrams · water chemistry

[1] J. W. Halley, A. Mazzolo, Y. Zhou, D. Price, *J. Electroanal. Chem.* **1998**, *450*, 273.
[2] S. P. Mehandru, A. B. Anderson, *J. Phys. Chem.* **1989**, *93*, 2044.
[3] A. B. Anderson, N. M. Neshev, R. A. Sidik, P. Shiller, *Electrochim. Acta* **2002**, *47*, 2999.
[4] M. Henderson, *Surf. Sci. Rep.* **2002**, *46*, 1.
[5] A. E. Bolzan, A. C. Chialvo, A. J. Arvia, *J. Electroanal. Chem.* **1984**, *179*, 71.
[6] N. Tateishi, K. Yahikozawa, K. Nishimura, Y. Takasu, *Electrochim. Acta* **1992**, *37*, 2427.

 © 2006 Wiley-VCH Verlag GmbH & Co. KGaA, Weinheim

Electrocatalyst Design

DOI: 10.1002/anie.200501792

Fine Size Control of Platinum on Carbon Nanotubes: From Single Atoms to Clusters**

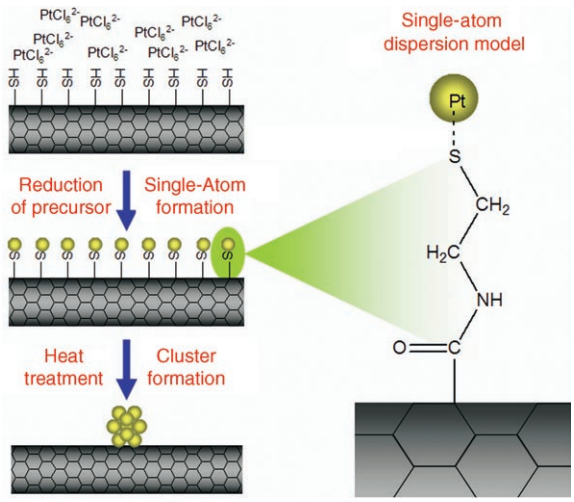
*Yong-Tae Kim, Kazuyoshi Ohshima, Koichi Higashimine, Tomoya Uruga, Masaki Takata, Hiroyoshi Suematsu, and Tadaoki Mitani**

Electrocatalyst design is a key factor for enhancing the performance of a fuel cell. Since dispersity and cluster size mainly affect the properties of the electrocatalyst, it is necessary to devise a proper synthetic route to highly dispersed and size-controlled clusters.[1,2] Many studies on dispersion and size control of Pt clusters on carbon supports for electrocatalysts have been conducted to investigate the effect of size on electrocatalytic activity from a fundamental scientific viewpoint and to enhance the performance of fuel cells with low noble-metal loadings in engineering applications.[3–11]

Two main chemical routes have been suggested for the preparation of highly dispersed and size-controlled Pt clusters on carbon supports: the colloidal method and impregnation.[12] Several outstanding studies[13–16] have shown that the colloidal method is a successful way to control the size and shape of clusters. However, ligands or protectors should be eliminated from the surface of the resulting electrocatalysts, since the ligands act as surface poisons in electrocatalytic reactions; this process is fairly difficult to perform while still retaining the clusters' size and shape.[17] In contrast, the impregnation method, in which deposition of a precursor is followed by gas- or liquid-phase reduction, is simpler and cheaper than the colloidal method. However, with this method it is quite difficult to control the size and dispersity of clusters on carbon supports, especially those having inert surfaces, since the affinity of the carbon surface for the precursor solution exerts the dominant effect on dispersity in the deposition step.[3]

Herein we suggest a new concept based on a fundamental bottom-up approach to synthesize highly dispersed and size-controlled Pt clusters on carbon supports beyond the limitations of the above two main routes. We call this the single-atom-to-cluster (SAC) approach. It is shown schematically in Scheme 1 and is composed of two steps:

1) Reduction of the Pt precursor $H_2[PtCl_6]$ with $NaBH_4$ on thiolated multiwalled carbon nanotubes (S-MWNTs) to form a monolayer of single Pt atoms (Pt-S-MWNT). The characterization of the single-atom dispersion model is summarized in the Supporting Information.
2) Elimination of the thiol groups by heat treatment at various temperatures T_h followed by slow quenching (q) to room temperature to form Pt clusters ($Pt_{h\text{-}q}$/MWNT) from single atoms.



Scheme 1. SAC approach for the formation of size-controlled Pt clusters.

We adopted MWNTs as support for two reasons: First, they have a flat, smooth surface structure without any surface pores that could hinder atoms or clusters from drifting on the surface during the thermal cluster-formation process. Second, MWNTs have superior physicochemical properties as an electrocatalyst support relative to more commonly used carbon black or active carbon.[18–20]

We characterized samples of Pt-S-MWNT, $Pt_{h\text{-}q}$/MWNT (treated at various T_h), and Pt/MWNT prepared by supporting Pt clusters on an untreated MWNT using TEM with an accelerating voltage of 100 kV. The TEM images (Figure 1b–

[*] Y.-T. Kim, K. Ohshima, Prof. T. Mitani
Department of Physical Materials Science
School of Materials Science
Japan Advanced Institute of Science and Technology (JAIST)
1-1 Asahidai, Nomi, Ishikawa 923-1292 (Japan)
Fax: (+81) 761-51-1149
E-mail: mitani@jaist.ac.jp
K. Higashimine
Center for Nano Materials and Technology
Japan Advanced Institute of Science and Technology (JAIST)
1-1 Asahidai, Nomi, Ishikawa 923-1292 (Japan)
Dr. T. Uruga, Dr. M. Takata, Dr. H. Suematsu
Japan Synchrotron Radiation Research Institute (JASRI)/SPring-8
1-1-1 Kouto, Mikazuki, Hyogo 679-5198 (Japan)
Dr. M. Takata
Core Research for Evolutional Science and Technology
Japan Science Technology Cooperation (CREST/JST)
4-1-8 Honcho, Kawaguchi, Saitama 332-0012 (Japan)

[**] This work was partly supported by the Ministry of Education, Science, Sports and Culture of Japan, Grant-in-Aid for Scientific Research (B) No. 17310059 and Nanotechnology Support Project (Proposal No. 2004B0544-ND1b-np-Na/BL02B2, 2005A0701-ND1d-np-Na/BL02B2, 2005A0702-NXa-np/BL01B1) with the approval of Japan Synchrotron Radiation Research Institute (JASRI). We thank Prof. Mikio Miyake for kind help with thermolysis and Dr. Kenichi Kato, Dr. Keiichi Osaka, and Mr. Kazuo Kato for their assistance in measuring XRD and XAFS with synchrotron radiation at SPring-8.

Supporting information for this article is available on the WWW under http://www.angewandte.org or from the author.

© 2006 Wiley-VCH Verlag GmbH & Co. KGaA, Weinheim

f) and size distribution (Figure 1h) of $Pt_{h\text{-}q}$/MWNT at various T_h show that size-controlled clusters are supported on MWNT in $Pt_{h\text{-}q}$/MWNT. However, Pt-S-MWNT has an ambiguous image attributable to dispersed single atoms (Figure 1a). It was possible to observe the disappearance of this ambiguous image and the appearance of clear features with increasing irradiation time by in situ TEM observations with an accelerating voltage of 300 kV (a video clip showing the entire process of cluster formation can be found in the Supporting Information). This phenomenon is due to the formation of clusters through aggregation of single atoms on strong electron-beam irradiation at 300 kV. The clusters in Pt/MWNT (Figure 1g) are considerably larger than in $Pt_{h\text{-}q}$/MWNT and are not uniform, and this reflects the limitations of the impregnation method when using supports with an inert surface.

The structure and electronic state of the size-controlled Pt clusters were characterized by X-ray analysis (Figure 2). The change in crystal structure was confirmed by powder XRD (Figure 2a). Pt-S-MWNT has no peak corresponding to Pt(111) near $2\theta = 27.5°$ ($\lambda = 1.08$ Å), probably because of the dispersed single atoms. However, the sharpening of the XRD patterns of $Pt_{h\text{-}q}$/MWNT with rising T_h can be understood as a narrowing effect due to the increasing cluster size. Moreover, the coexistence of sharp and broad peaks for $Pt_{h\text{-}q}$/MWNT ($T_h = 873$ K) reflects the nonuniform size distribution shown in Figure 1h. Thus, the SAC approach more effectively controls cluster size within a range of a few nanometers.

The electronic state of the size-controlled Pt clusters was investigated X-ray photoelectron spectroscopy (XPS, Figure 2b). The Pt 4f binding energy (BE) in Pt-S-MWNT is significantly shifted (by 2.8 eV) to an energy (BE = 73.0 eV) higher than that of Pt foil (BE = 71.2 eV). This shift is similar to that of Pt 4f from the bulk state to isolated Pt atoms,[21] which was attributable to the final-state effect in the Pt 4f core level.[22] Accordingly, the Pt particles in Pt-S-MWNT can probably be considered to be single Pt atoms. On the other hand, the BE of $Pt_{h\text{-}q}$/MWNT approaches that of the bulk state with rising T_h, which is consistent with growing cluster size.

Since X-ray absorption fine structure (EXAFS) and near edge structure (XANES) measurements are generally quite sensitive to structural changes of materials, as demonstrated by computational modeling,[23] we conducted T_h-dependent XANES and EXAFS measurements on the Pt L_{III} absorption edge. The XANES spectra and the radial distribution function (RDF) of the Fourier-transformed EXAFS spectra are presented in Figure 2c and d, respectively. In accordance with the TEM, XRD, and XPS results, we observed a clear change of structure, from single atom to bulk state, in both measurements with increasing T_h. Especially the clear increase in the peak near 2.8 Å, corresponding to 1NN (first nearest neighbor) Pt–Pt distance, in the RDF of the EXAFS

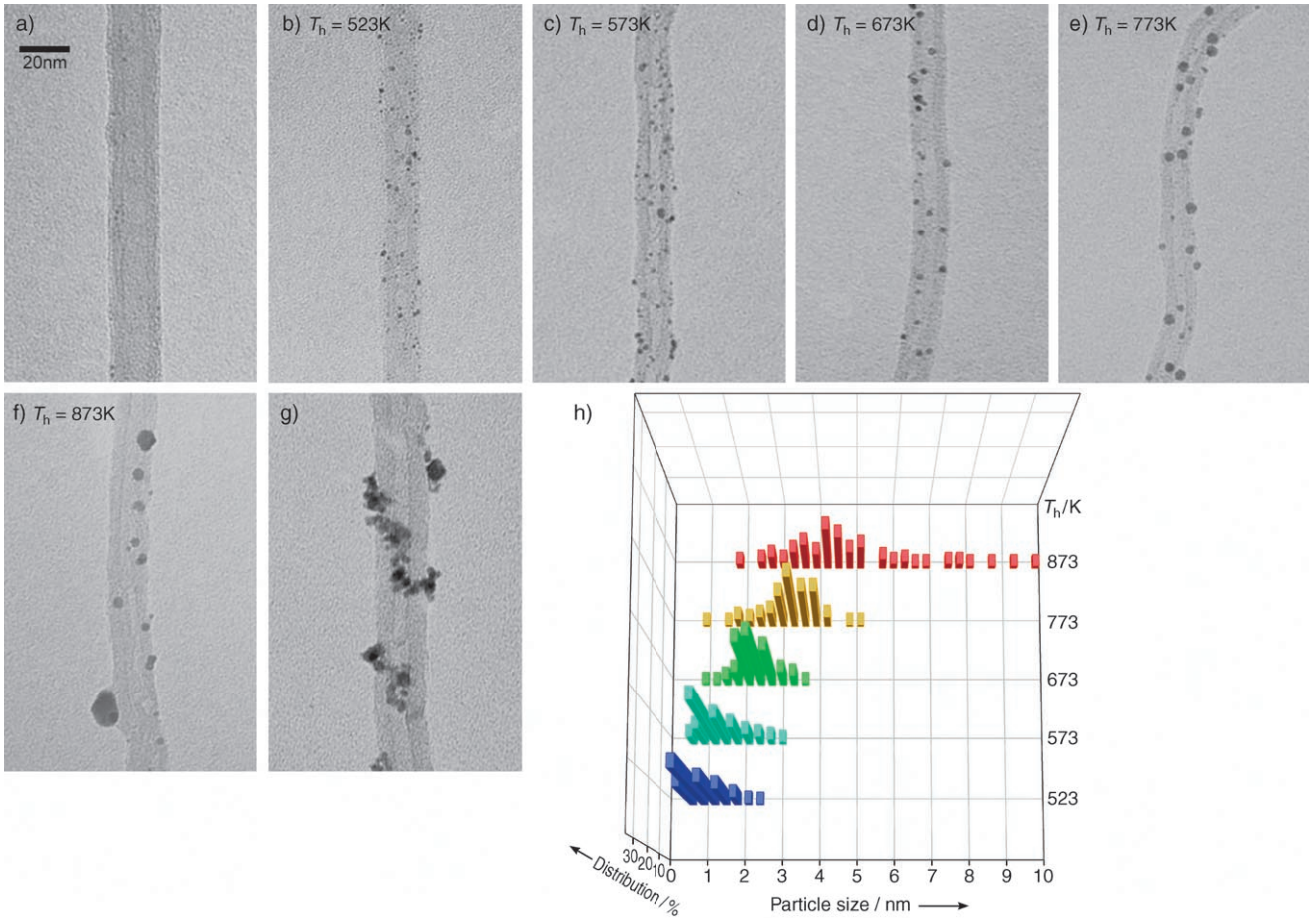


Figure 1. TEM images of a) Pt-S-MWNT, b–f) $Pt_{h\text{-}q}$/MWNT, g) Pt/MWNT; h) size distribution diagram of $Pt_{h\text{-}q}$/MWNT treated at various T_h.

 © 2006 Wiley-VCH Verlag GmbH & Co. KGaA, Weinheim

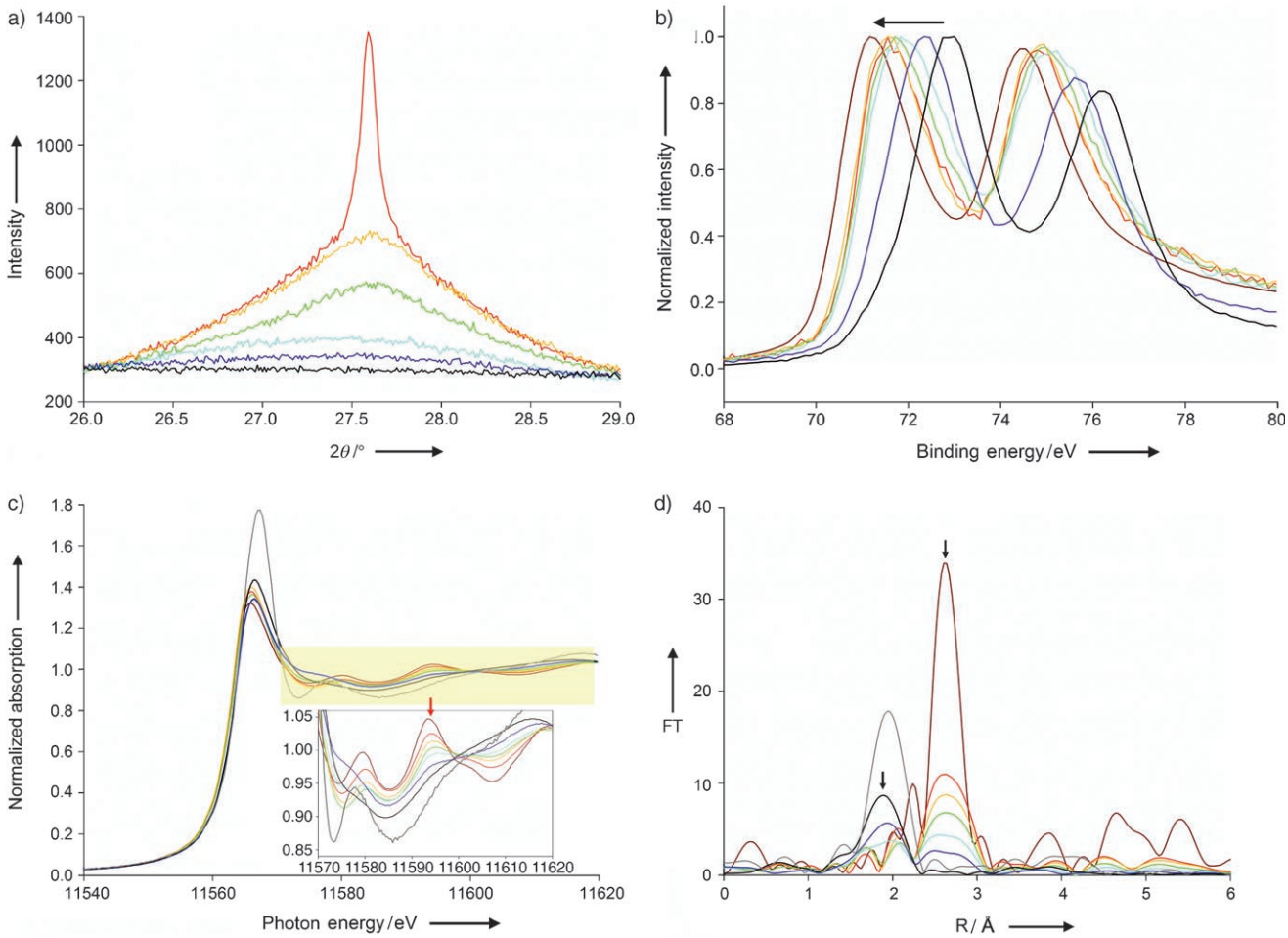


Figure 2. X-ray analyses of Pt-S-MWNT, $Pt_{h\text{-}q}$/MWNT treated at various T_h, and reference materials: $H_2[PtCl_6]$/MWNT as ionic state and Pt foil as bulk state. a) Powder XRD patterns. b) Pt 4f peak shifts of XPS spectra; the arrow indicates the shift of the Pt 4f peak position. c) XANES spectra of Pt L_{III} absorption edge. d) RDF of Fourier-transformed EXAFS spectra; the arrows indicate the peaks corresponding to the Pt–S (around 1.9 Å) and Pt–Pt (around 2.8 Å bonds. —— $H_2[PtCl_6]$/MWNT, —— Pt-S-MWNT, —— $Pt_{h\text{-}q}$/MWNT (T_h = 523 K), —— $Pt_{h\text{-}q}$/MWNT (T_h = 573 K), —— $Pt_{h\text{-}q}$/MWNT (T_h = 673 K), —— $Pt_{h\text{-}q}$/MWNT (T_h = 773 K), —— $Pt_{h\text{-}q}$/MWNT (T_h = 873 K), —— Pt foil.

data (Figure 2d) indicates increasing size with increasing T_h. The EXAFS pattern of Pt-S-MWNT exhibits no peak near 2.8 Å and a strong peak near 1.9 Å for the 1NN Pt–heterogeneous atom distance, that is, only heteroatoms such as the S atom of thiol groups are present around Pt atoms, without any Pt–Pt bonding. Moreover, the valence state of Pt single atoms is considered to be close to that of the bulk state, with a similar height of the white line in the XANES spectra. Accordingly, these results strongly support our single-atom dispersion model.

To investigate the mechanism of the SAC approach to size control we carried out an in situ synchrotron XRD measurement with heat treatment using a large Debye–Scherrer camera which enabled us to observe fine changes of crystal structure with very high speed. Figure 3 shows the in situ XRD patterns and temperature program, respectively. Note that the peak intensity and shape in these in situ measurements do not directly correspond to those of the samples treated at the same T_h in ex situ measurements (Figure 2a), because there are several differences in measurement conditions such as different furnace types, heating rates, atmospheres, and gas flux. As can be seen in Figure 3a, three peaks at each T_h are almost overlapping. This is attributed to the peak-saturation phenomenon after heat treatment for 120 min (raising the temperature for 1 min and waiting for 119 min), which means that the cluster growth stops during or after this waiting process. This phenomenon, which is considered to be a key to understanding the dependence of cluster size on T_h, could be clarified by adopting a well-known concept: the melting point of clusters becomes lower with decreasing size.[24]

According to the Lindemann criterion,[25] the melting point decreases with decreasing cluster size because the larger fraction of surface atoms increases the average atomic displacement. This concept can be described by Equation (1),

$$\frac{T_m(r)}{T_m(\infty)} = \exp\left[-\left(\alpha-1\right)\left(\frac{r}{3h}\right)-1\right]^{-1} \quad (1)$$

derived by Shi,[26] in which r is the cluster radius, α the ratio of mean-square atom displacement on the surface to that inside the cluster, h the height of the atom monolayer in its crystal

 © 2006 Wiley-VCH Verlag GmbH & Co. KGaA, Weinheim

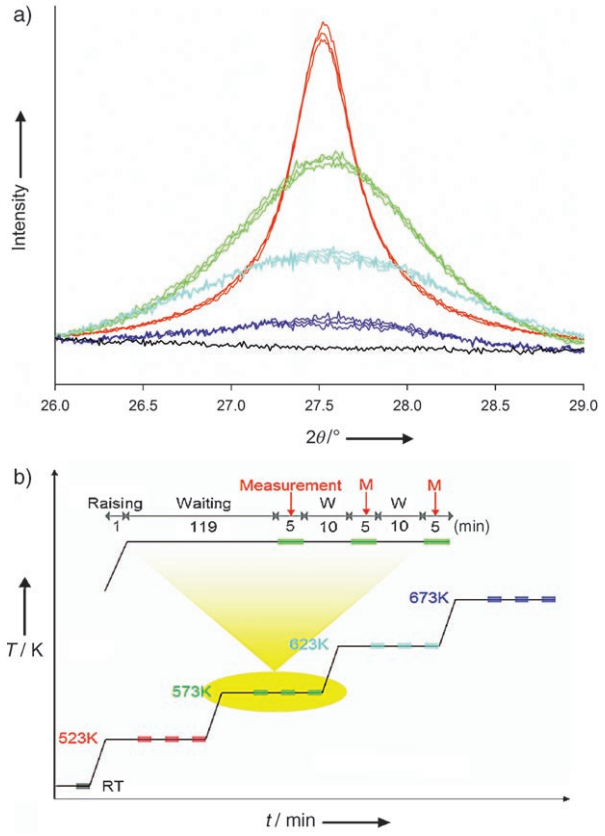


Figure 3. In situ XRD measurements. a) XRD patterns of Pt-S-MWNT as starting material with simultaneous heat treatment. b) Temperature program for in situ XRD measurement. In this program, XRD patterns were recorded three times in a 5-min interval with a 10-min interval in-between at each T_h. Inserting the time interval meant we could more certainly confirm that no more change in the XRD patterns had occurred. —— Pt-S-MWNT, —— $T_h = 523$ K, —— $T_h = 573$ K, —— $T_h = 623$ K, —— $T_h = 673$ K.

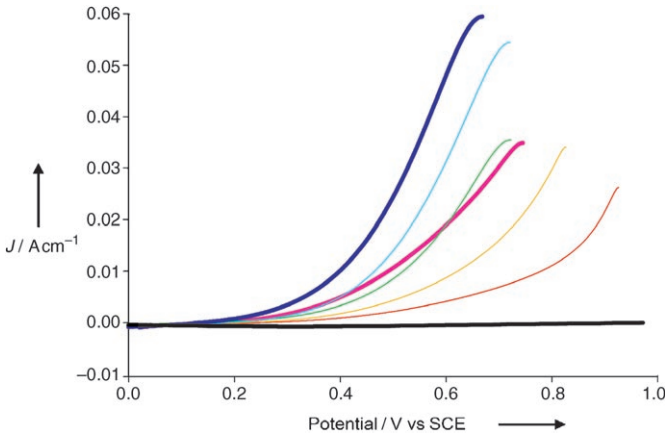


Figure 4. CV patterns for MOR of Pt-S-MWNT and $Pt_{h\text{-}q}$/MWNT treated at various T_h and of Pt/CB. Current densities J are based on the geometric surface area of the working electrode. —— Pt-S-MWNT, —— $Pt_{h\text{-}q}$/MWNT ($T_h = 523$ K), —— $Pt_{h\text{-}q}$/MWNT ($T_h = 573$ K), —— $Pt_{h\text{-}q}$/MWNT ($T_h = 673$ K), —— $Pt_{h\text{-}q}$/MWNT ($T_h = 773$ K), —— $Pt_{h\text{-}q}$/MWNT ($T_h = 873$ K), —— Pt/CB.

structure, and $T_m(r)$ and $T_m(\infty)$ are the melting points in Kelvin of cluster and bulk material, respectively. From Equation (1), it is clear that T_m is dependent on the cluster radius. In other words, when T_m (in this study, T_h) is fixed, the radius (i.e., cluster size) is determined. In our heat treatment, heated clusters (or atoms) drift and meet on a flat MWNT surface that facilitates high drift mobility,[27] and then coincidently melt into larger clusters. After some repetition of this process, growth stops when clusters reach the size having a melting point equivalent to T_h. Hence, this mechanism enables us to control the cluster size by simply setting T_h.

To investigate the electrocatalytic activity of size-controlled clusters in the methanol oxidation reaction (MOR), cyclic voltammetry (CV) was performed with a working electrode coated with prepared samples in 0.5 M H_2SO_4 + 2 M CH_3OH electrolyte with a scan rate of 50 mV s^{-1}. Single Pt atoms of Pt-S-MWNT (black line in Figure 4) have no MOR activity. This result is fairly reasonable, because at least three Pt atoms are required to act as an active site for MOR, according to the model presented in a previous report.[28] Activity appears, however, when Pt clusters are formed by heat treatment. With decreasing cluster size, electrocatalytic activity increases, accompanied by a downward shift in the onset potential, that is, a smaller overpotential for MOR. In comparison to Pt/CB, prepared by supporting Pt clusters on commercial carbon black (Vulcan XC-72), the CV patterns of $Pt_{h\text{-}q}$/MWNT have a sharp threshold, probably due to the superior intrinsic conductivity of MWNTs. We consider that the shift of the onset potential originates from the change of electronic structure, especially the d-band structure of the clusters, induced by increased s–d mixing attributed to the quantum-size effect of the clusters.

In conclusion, we have confirmed the validity and usefulness of the SAC approach to the formation of highly dispersed and size-controlled Pt clusters on MWNTs. The introduction of thiol groups on the MWNT surface resulted in extreme single-atom dispersion, and fine size control of clusters from the dispersed single atoms was achieved by using the concepts of melting-point decrease and high drift mobility on the flat MWNT surface. The introduction of sufficient surface thiol groups is therefore a key factor in the SAC approach. This unique approach is applicable not only to Pt and MWNTs, but also to all kinds of transition metals that form a bond with thiol groups and all kinds of supports or substrates. Furthermore, we believe that this technique can be adapted to all disciplines that require the formation of size-controlled clusters (or of atoms) on supports or substrates, such as catalysts for environmental or fine chemistry, composite electrode materials for lithium secondary batteries and ultracapacitors, as well as electrocatalysts for fuel cells.

Experimental Section

MWNTs prepared by a conventional CVD method were purchased from Helix Material Solutions. Raw soot containing MWNTs was heated for 2 h at 400 °C in static air and subsequently treated with 6 M hydrochloric acid at 70 °C for 12 h. Thiolation of the MWNTs was conducted by a method based on the formation of amide bonds, as

 © 2006 Wiley-VCH Verlag GmbH & Co. KGaA, Weinheim

reported previously.[29] Purified MWNTs were stirred in concentrated H_2SO_4/HNO_3 (3/1, 98 and 70% respectively, Kanto Chemical) for 15 min to prepare carboxylated MWNTs, and then chlorinated by refluxing for 12 h with $SOCl_2$ (Wako) at 70°C. After evaporating any remaining $SOCl_2$, thiolated MWNTs (S-MWNTs) were subsequently obtained by reaction with $NH_2(CH_2)_2SH$ (Wako) in dehydrated toluene (Aldrich) for 24 h at 70°C. A suspension of 20 mg of carbon support (MWNT, S-MWNT, or carbon black (CB, Vulcan XC-72)) and 3.125 mL of 10 mM $H_2[PtCl_6]$ (Aldrich), equivalent to 20% weight ratio of Pt to carbon, was prepared by sonication in 40 mL of deionized water. Subsequently, the Pt precursor was simultaneously reduced and supported on the carbon support by using $NaBH_4$ (Kanto chemical) and then washed with deionized water and ethanol several times. After evaporation and drying, we obtained 20% Pt supported on carbon supports, such as MWNT, S-MWNT, and CB, referred to as Pt/MWNT, Pt-S-MWNT, and Pt/CB, respectively. The 20% Pt precursor supported on MWNT ($H_2[PtCl_6]$/MWNT) was prepared by simple evaporation of solvent from a solution of 20 mg of MWNT and 3.125 mL of 10 mM $H_2[PtCl_6]$. Heat treatment of Pt-S-MWNT was performed for 10 min at 523, 573, and 673 K, and for 60 min at 773 and 873 K, in an H_2 gas flow of 100 sccm (standard cubic centimeter per minute). The samples obtained by heat treatment followed by slow quenching of Pt-S-MWNT are denoted by $Pt_{h\text{-}q}$/MWNT (T_h).

The TEM (H-7100 (100 kV) and H-9000NAR (300 kV), Hitachi) images in Figure 1 and those of the in situ measurements in the video clip were obtained with accelerating voltages of 100 and 300 kV, respectively. X-ray diffraction (XRD) analysis was carried out with synchrotron radiation of BL02B2, SPring-8, equipped with a large Debye–Scherrer camera[30] adjusted to a wavelength of 1.08 Å by an Si(111) plane monochromator. In situ XRD patterns were obtained by raising T_h of the H_2-filled sample capillary with the temperature program shown in Figure 3b. XPS (PHI 5600, ULVAC-PHI) was used to confirm the electronic state of Pt clusters and for elemental analysis. The X-ray source was $Al_{K\alpha}$ with an energy of 1486.6 eV operating at 15 kV and 300 W, and the obtained binding energies were referred to C 1s (284.5 eV) of the carbon supports. XANES and EXAFS data for Pt L_{II} and L_{III} absorption edges were obtained in transmission mode with the synchrotron radiation of BL01B1, SPring-8, at room temperature. X-rays were monochromated with two Si(111) plane gratings and detected by two ion chambers, which were continuously purged with a gas mixture of 15% Ar and 85% N_2 in I_0 and 100% Ar gas in I_1. Data reduction was carried out with the computer software REX2000 (Rigaku). The XANES spectrum was normalized by the Victoreen function and the RDF of EXAFS was obtained by a Fourier transform, in the range from 3 to 14 $Å^{-1}$ in k space, on k^3-weighted EXAFS oscillations. The electrocatalytic activity in the MOR was evaluated by CV (608A, ALS). The voltammograms were recorded at a scan rate of 50 $mV s^{-1}$ from −0.24 to 0.96 V (vs SCE) in a 0.5 M H_2SO_4 + 2 M CH_3OH electrolyte after purging with N_2 gas for 1 min and electrochemical cleaning with a fast scan rate. The working electrode was a glassy carbon electrode, 3 mm in diameter, coated with the electrocatalyst layer. Three milligrams of 20% Pt supported on carbon powder and 6 μL of ethanol containing 5 wt% Nafion solution were placed in 150 μL of isopropyl alcohol and suspended with sonication for 1 h. A 6-μL portion of this slurry was dropped onto a glassy carbon electrode and dried in an oven at 60°C for 1 h. The counter- and reference electrodes were a Pt wire and a saturated calomel electrode (SCE), respectively.

Received: May 24, 2005
Revised: September 28, 2005
Published online: December 9, 2005

[1] A. Wieckowski, E. R. Savinova, C. G. Vayenas, *Catalysis and Electrocatalysis at Nanoparticle Surface*, Marcel Dekker, New York, **2003**.
[2] W. Vielstich, A. Lamm, H. Gasteiger, *Handbook of Fuel Cells: Fundamentals, Technology and Applications*, Wiley, New York, **2003**.
[3] K. Kinoshita, P. Stonehart in *Modern Aspects of Electrochemistry* (Eds.: J. O. M. Bockris, B. E. Conway), Plenum, New York, **1977**, p. 12.
[4] M. Watanabe, M. Uchida, S. Motoo, *J. Electroanal. Chem.* **1987**, *229*, 395.
[5] V. H. Bönnemann, W. Brijoux, R. Brinkmann, E. Dinjus, T. Jousen, B. Korall, *Angew. Chem.* **1991**, *103*, 1344; *Angew. Chem. Int. Ed. Engl.* **1991**, *30*, 1312.
[6] M. Min, J. Cho, K. Cho, H. Kim, *Electrochim. Acta* **2000**, *45*, 4211.
[7] T. Hyeon, S. Han, Y.-E. Sung, K.-W. Park, Y.-W. Kim, *Angew. Chem.* **2003**, *115*, 4488; *Angew. Chem. Int. Ed.* **2003**, *42*, 4352.
[8] F. Maillard, M. Martin, F. Gloaguen, J.-M. Leger, *Electrochim. Acta* **2002**, *47*, 3431.
[9] T. Yoshitake, Y. Shimakawa, S. Kuroshima, H. Kimura, T. Ichihashi, Y. Kubo, D. Kasuya, K. Takahashi, F. Kokai, M. Yudasaka, S. Iijima, *Physica B* **2002**, *323*, 124.
[10] X. Sun, R. Li, D. Villers, J. P. Dodelet, S. Desilets, *Chem. Phys. Lett.* **2003**, *379*, 99.
[11] K. Sasaki, J. X. Wang, M. Balasubramanian, J. McBreen, F. Uribe, R. R. Adzic, *Electrochim. Acta* **2004**, *49*, 3873.
[12] A. S. Arico, S. Srinivasan, V. Antonucci, *Fuel Cells* **2001**, *1*, 133.
[13] G. Schmid, *Nanoparticles: From Theory to Application*. Wiley-VCH, Weinheim, **2003**.
[14] R. Wang, J. Yang, Z. Zheng, M. D. Carducci, J. Jiao, S. Seraphin, *Angew. Chem.* **2001**, *113*, 567; *Angew. Chem. Int. Ed.* **2001**, *40*, 549.
[15] V. F. Puntes, K. M. Krishnan, A. P. Alivisatos, *Science* **2001**, *291*, 2115.
[16] Y. Sun, Y. Xia, *Science* **2002**, *298*, 2176.
[17] T. J. Schmidt, M. Noeske, H. A. Gasteiger, R. J. Behm, P. Britz, W. Brijoux, H. Bonnemann, *Langmuir* **1997**, *13*, 2591.
[18] P. Serp, M. Corrias, P. Kalck, *Appl. Catal. A* **2003**, *253*, 337.
[19] G. Che, B. B. Lakshmi, E. R. Fisher, C. R. Martin, *Nature* **1998**, *393*, 346.
[20] S. H. Joo, S. J. Choi, I. Oh, J. Kwak, Z. Liu, O. Terasak, R. Ryoo, *Nature* **2001**, *412*, 169.
[21] W. Eberhardt, P. Fayet, D. M. Cox, Z. Fu, A. Kaldor, R. Sherwood, D. Sondericker, *Phys. Rev. Lett.* **1990**, *64*, 780.
[22] G. K. Wertheim, S. B. DiCenzo, S. E. Youngquist, *Phys. Rev. Lett.* **1983**, *51*, 2310.
[23] A. I. Frenkel, C. W. Hills, R. G. Nuzzo, *J. Phys. Chem. B* **2001**, *105*, 12689.
[24] M. Takagi, *J. Phys. Soc. Jpn.* **1954**, *9*, 359.
[25] F. A. Lindemann, *Phys. Z.* **1910**, *11*, 609.
[26] F. G. Shi, *J. Mater. Res.* **1994**, *9*, 1307.
[27] B. C. Regan, S. Aloni, R. O. Ritchie, U. Dahmen, A. Zettl, *Nature* **2004**, *428*, 924.
[28] B. D. McNichol, *J. Electroanal. Chem.* **1981**, *118*, 71.
[29] J. Liu, A. G. Rinzler, H. Dai, J. H. Hafner, R. K. Bradley, P. J. Boul, A. Lu, T. Iverson, K. Shelimov, C. B. Huffman, F. Rodriguez-Macias, Y.-S. Shon, T. R. Lee, D. T. Colbert, R. E. Smalley, *Science* **1998**, *280*, 1253.
[30] E. Nishibori, M. Takata, K. Kato, M. Sakata, Y. Kubota, S. Aoyagi, Y. Kuroiwa, M. Yamakata, N. Ikeda, *Nucl. Instrum. Methods Phys. Res. Sect. A* **2001**, *467–468*, 1045.

Keywords: carbon · electrocatalysts · electrochemistry · nanotubes · platinum

 © 2006 Wiley-VCH Verlag GmbH & Co. KGaA, Weinheim

Epoxidation Catalysts

DOI: 10.1002/anie.200502382

Trimethylamine as a Gas-Phase Promoter: Highly Efficient Epoxidation of Propylene over Supported Gold Catalysts**

*Biswajit Chowdhury, Juan. J. Bravo-Suárez, Masakazu Daté, Susumu Tsubota, and Masatake Haruta**

Propylene oxide (PO) is an important bulk chemical for the production of a wide variety of derivatives, among which polyether polyols and propylene glycol are the main end products.[1] The world PO production of about 5 million tons per year comes from two current industrial processes: the chlorohydrin process and the organic hydroperoxide process (Halcon method). These two methods consist of two reaction stages and produce large amounts of by-products and co-products, which makes optimization difficult.[2]

Although bulk gold was for a long time regarded as a poor catalyst, gold nanoparticles (2–5 nm) deposited on a variety of metal oxides are surprisingly active for many reactions.[3] An alternative route for synthesizing PO by reductive activation of O_2 by H_2 over nanoparticulate gold catalysts has been under investigation for the past few years.[4–7] We have estimated that the requirements for a viable industrial process are a propylene conversion of 10%, a PO selectivity of 90%, and a H_2 efficiency of 50% for the H_2O_2 formed in situ for epoxidation purposes. Recently, we reported a trimethylsilylated $Ba(NO_3)_2$-Au/titanosilicate (Ti/Si 3:100) catalyst that thus far exhibits the highest PO yield among the gold catalysts.[8] The main hurdles for the industrial application of this catalyst are its fast deactivation caused by the accumulation of oligomerized and oxidized PO by-products around the gold nanoparticles, the lower activity of the successively regenerated catalyst, and its low H_2 efficiency. Nowadays, the development of catalysts for use on a commercial scale seeks high atom efficiencies of chemical reactions to reduce manufacturing costs and to minimize burdens on the environment. A comparison of different processes shows that the epoxidation with O_2 and H_2 at 90% PO selectivity and 50% H_2 efficiency gives an atom efficiency of 50%, which is close to the 76% PO selectivity for the epoxidation with O_2 alone (Supporting Information). This clearly demonstrates that, at present, a more feasible and rational path towards higher atom efficiency is the direct epoxidation of propylene with O_2 and H_2.

We now report that the presence of trimethylamine (TMA), a strong Lewis base with a pK_a value of 9.9,[9] at extremely low concentrations (10–20 ppm) in the reactant gas mixture can remarkably improve the catalytic performance of gold nanoparticles deposited on titanosilicate in terms of catalyst lifetime, catalyst regeneration, PO selectivity, and H_2 efficiency to a level where commercial requirements are almost fulfilled. We have previously shown that a small amount of H_2O can act as a gaseous promoter by drastically altering the catalytic activity of supported gold nanoparticles for low-temperature CO oxidation.[10] The concept behind this investigation was that gaseous trimethylamine should have a positive effect on the overall PO catalyst efficiency. One of the assumptions is that TMA can poison the Lewis acidic sites of the support, mainly isolated Ti^{4+} centers. By oligomerization,[11] cracking, and isomerization, these sites form PO by-products that cause catalyst deactivation. Another possible benefit of TMA is that its adsorption on the gold surface can suppress H_2 combustion to produce water, which results in an improved hydrogen efficiency.

The catalyst activity data show that deactivation is appreciably depressed for the trimethylsilylated $Ba(NO_3)_2$-promoted Au/titanosilicate catalyst (Figure 1) in the presence of 13–15 ppm TMA as a gaseous promoter, leading to a more stable propylene conversion. Up to 80% of the high initial activity of the catalyst remains after 5 h of operation with almost constant PO selectivity and H_2 efficiency. Surprisingly, the catalyst regenerated in the presence of TMA exhibits an improved performance compared to the fresh catalyst as it presents a slightly better propylene conversion, about 4% higher PO selectivity, and about 15% higher H_2 efficiency. In a series of experiments we found enhancements in H_2 efficiency with reaction time and in PO selectivity as the concentration of TMA in the feed mixture was increased up to 20 ppm (Supporting Information). We also observed that for different reaction conditions the presence of TMA during pre-treatment and during the reaction led to the best catalyst performance. Ethylene oxide is produced industrially at a steady space–time yield of 0.032–0.32 $g\,h^{-1}\,(cm^3\,cat)^{-1}$ at 10–35 atm.[12] The rate of production of PO in this report is 0.064–0.080 $g\,h^{-1}\,(g\,cat)^{-1}$ (1 g cat = 2.5 cm^3 cat) even when operating at atmospheric pressure, which indicates that the present process comes close to commercial levels.

To investigate the reason behind the improved catalyst performance after regeneration with TMA, UV/Vis/NIR

[*] Dr. M. Haruta
Materials Chemistry Course
Faculty of Urban Environmental Sciences
Tokyo Metropolitan University
1-1 Minami-Osawa, Hachioji 192-0397, Tokyo (Japan)
Fax: (+81) 426-77-2821
E-mail: haruta-masatake@center.tmu.ac.jp
Dr. J. J. Bravo-Suárez, Dr. M. Daté, Dr. S. Tsubota
Research Institute for Innovation in Sustainable Chemistry
National Institute of Advanced Industrial Science and Technology (AIST)
Onogawa 16-1, Tsukuba 305–8569 (Japan)
Dr. B. Chowdhury
(on leave) Department of Chemistry
Uluberia College (Calcutta University)
West Bengal-711315 (India)

[**] We thank Dr. J. R. Monnier of Eastman Chemical Company for his valuable suggestion of using trimethylamine as a gas-phase promoter and Prof. S. T. Oyama for his critical comments and valuable discussion. B.C. acknowledges financial assistance from AIST, and the governing body of Uluberia College, West Bengal, India, for granting special study leave to carry out this work.

Supporting information for this article is available on the WWW under http://www.angewandte.org or from the author.

InterScience
© 2006 Wiley-VCH Verlag GmbH & Co. KGaA, Weinheim

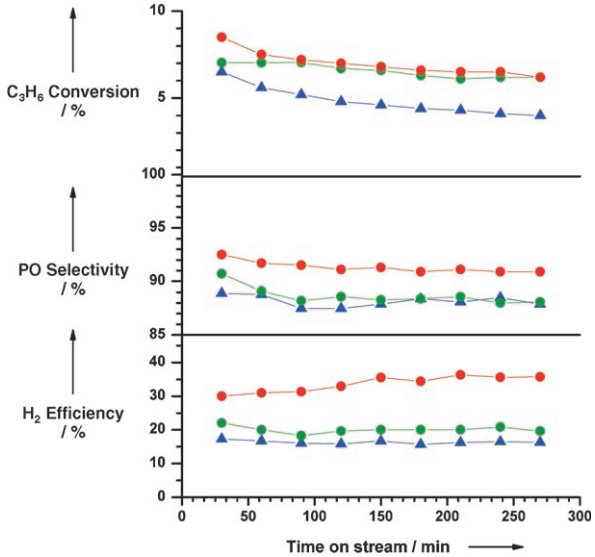


Figure 1. Effect of trimethylamine (13–15 ppm) on the activity of a trimethylsilylated Au-$Ba(NO_3)_2$/titanosilicate (Ti/Si 3:100) catalyst for propylene epoxidation with O_2 and H_2 at 423 K. Reactant gas: $C_3H_6/O_2/H_2/Ar = 1:1:1:7$; space velocity (SV) = 4000 mL h^{-1} (g cat)$^{-1}$ (PO: propylene oxide); blue ▲: fresh catalyst in the absence of TMA; green ●: fresh catalyst in the presence of TMA; red ●: regenerated catalyst in the presence of TMA.

spectral measurements were carried out in situ. The in situ NIR spectra of the trimethylsilylated Au/titanosilicate catalyst show bands in the region of 6000–5500 cm^{-1} (Figure 2) assigned to the overtones and combination bands of CH_3 groups.[13] This pattern changes when the catalyst is heated in an Ar stream containing 10 vol.% H_2 and 10 vol.% O_2 at 523 K. The bands between 5920 and 5738 cm^{-1} decrease significantly in intensity and the intensity of the silanol bands around 7320 cm^{-1} increases for the untreated gold catalyst (Figure 2, spectra a and b), thereby indicating hydrolysis of

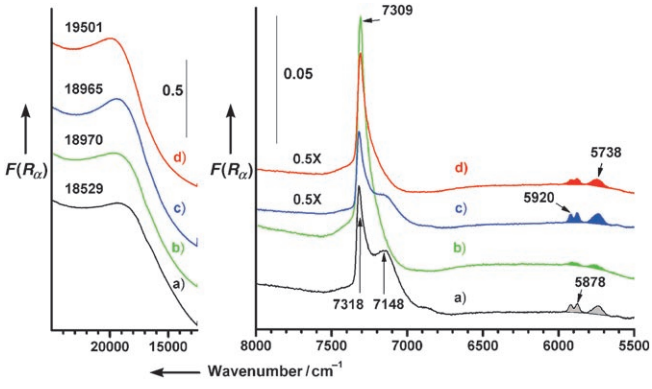


Figure 2. In situ UV/Vis/NIR spectra of trimethylsilylated Au/titanosilicate (Ti/Si 3:100) catalyst: a) in a stream of Ar at 298 K; b) in a stream of O_2, H_2, and Ar at 523 K for 1 h; c) in a stream of Ar at 298 K after treatment in a stream of Ar containing 13–15 ppm TMA at 523 K; d) in a stream of H_2, O_2, and Ar at 523 K for 1 h after treatment in a stream of Ar containing 13–15 ppm TMA at 523 K. Spectra are referenced to $BaSO_4$.

$-O-Si-O-Si(CH_3)_3$ groups. Treatment of the silylated gold catalysts with trimethylamine, however, protects the $Si-CH_3$ bonds in the $-O-Si-O-Si(CH_3)_3$ structure from the destructive effects of moisture, as evidenced by the preservation of the intense bands in the 6000–5500 cm^{-1} range in the NIR spectrum. It is also clear that the intensity increase of the silanol bands is less pronounced for the trimethylamine-treated silylated catalyst than for the catalyst that has only been silylated. These experimental results strongly suggest that the interaction between trimethylamine and the silicon atoms of the silane groups through the nitrogen lone pairs could preserve the $Si-CH_3$ bonds of the $-O-Si-O-Si(CH_3)_3$ structures in the vigorous reaction environment.[14,15]

During in situ UV/Vis/NIR measurements attention was also paid to the position of the gold plasmon resonance (Figure 2), which is shown in the case of untreated and TMA-treated trimethylsilylated Au/titanosilicate catalysts during regeneration with O_2 and H_2. In these spectra a single peak, assigned to the plasmon resonance of metallic gold nanoparticles, is observed around 18500–19500 cm^{-1}. Raising the temperature from 298 to 523 K in the presence of O_2 and H_2 gives rise to a slight blue shift in the plasmon resonance peak. This shift may be due to a change in the dielectric constant around the surface of the gold nanoparticles, as described by a multi-layer core–shell model.[16,17] In Figure 2 we compare the spectra at 298 K in argon of the untreated and TMA-treated samples—a blue shift of 436 cm^{-1} is observed (spectra a and c). Similarly, a higher blue shift of 531 cm^{-1} is also found at 523 K in the presence of a mixture of O_2, H_2, and Ar (spectra b and d). These blue shifts after treatment in a stream containing TMA are in good agreement with the depression of H_2 combustion, that is, an increase in H_2 efficiency, and indicate TMA adsorption on the gold surface.

A mechanism for PO formation on the TMA-treated trimethylsilylated $Ba(NO_3)_2$-Au/titanosilicate has been developed that takes into account the present experimental results as well as literature reports (Figure 3). In this process, hydrogen and oxygen react to form H_2O_2 and H_2O over the Au surfaces, thus the H_2 efficiency is usually below 100%. The potential capacity of Au surfaces to form peroxo species has been predicted and later confirmed experimentally.[18–21] The presence of this oxygen species was proved for propylene epoxidation with H_2O_2 in MeOH solvent over a TS-1 catalyst.[22] Once the H_2O_2 is produced on the gold particles, it can be converted into hydroperoxo species at tetrahedrally coordinated Ti cation sites. These Ti–hydroperoxo species can subsequently react with propylene adsorbed on the SiO_2 surfaces to form PO. In situ UV/Vis measurements of the silylated Au/titanosilicate catalyst during propylene epoxidation (Supporting Information) revealed a broad feature at 29400–23800 cm^{-1} that corresponds to the well-known charge-transfer interaction between a hydroperoxide ligand (OOH^-) and Ti^{4+}.[23] As evidenced by reactivity studies and UV/Vis results, the blue shift in the Au plasmon position suggests that the TMA is partly adsorbed on the Au surfaces and depresses direct H_2O formation. Due to its basic properties, PO should compete strongly with TMA to adsorb on the catalyst surface. Pre-adsorption of TMA on Ti^{4+} can therefore inhibit PO adsorption and its subsequent oligomerization,

 © 2006 Wiley-VCH Verlag GmbH & Co. KGaA, Weinheim

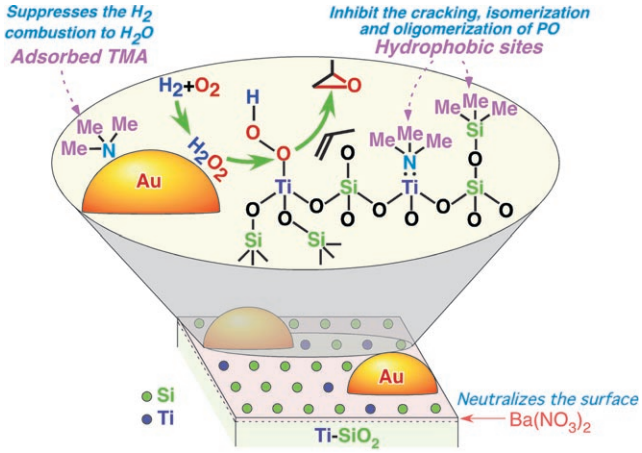


Figure 3. Probable reaction pathways for propylene epoxidation with O_2 and H_2 in the presence of trimethylamine on trimethylsilylated Au-$Ba(NO_3)_2$/titanosilicate catalyst. The accumulation of PO and its derivatives on the catalyst surface can be minimized by changing the surface nature into a hydrophobic one to prevent catalyst deactivation. Hydrogen combustion over Au surfaces can also be suppressed by the adsorption of trimethylamine to improve the atom efficiency of the overall reaction.

which is considered to be one of the main deactivation mechanisms of Au/titanosilicate catalysts.

We therefore conclude that PO can be efficiently produced at around 423 K in the gas phase with propylene, O_2, H_2, and a trace amount (10–20 ppm) of trimethylamine over gold nanoparticles deposited on three-dimensional mesoporous titanosilicates. A steady space–time yield of PO of 1.1–1.4×10^{-3} mol h^{-1} $(g\,cat)^{-1}$ at atmospheric pressure, which is close to that of ethylene oxide in the current industrial process, was achieved for more than 250 min with a propylene conversion up to 8.5% and a PO selectivity of 91% under an hourly space velocity of 4000 mL h^{-1} $(g\,cat)^{-1}$. The efficient regeneration of the Au/titanosilicate catalyst using a trace amount of TMA along with a mixture of hydrogen, oxygen, and argon at 523 K, and the improvement of the hydrogen efficiency to 35%, opens the door to commercialization of this catalytic process. The beneficial role of TMA on the Au/titanosilicate surface was probed by in situ UV/Vis/NIR spectroscopy. This economic synthetic method can be used to produce PO effectively, and is an example of a chemical process that can meet industrial standards while being environmentally benign.

Experimental Section

The titanosilicate support (Ti/Si 3:100) was prepared as reported previously.[8] In a typical preparation of titanosilicate-supported Au catalysts by the DP (deposition–precipitation) method, a solution of $HAuCl_4\cdot4H_2O$ (2 mmol) in water (100 mL) was heated to 343 K, and the pH was adjusted to 7.0 by adding aqueous NaOH solution. The support powder (1.0 g) was dispersed and stirred for 15 min while NaOH solution was added dropwise to maintain the pH at 7.0. Then, $Ba(NO_3)_2$ (0.2 mmol) dissolved in water (5 mL) was added and the mixture was stirred for another 45 min at the same temperature and pH. The solid was collected by filtration, dried under vacuum for 12 h, and then calcined in air at 573 K for 4 h.

The activity of all catalysts was evaluated within 24 h of gold deposition in an effort to minimize any deactivation due to aging. Unless otherwise stated, each fresh catalyst was silylated and then pre-treated with 10 vol.% H_2 in Ar for 30 min followed by 10 vol.% O_2 in Ar for 30 min at 523 K before reaction in a fixed-bed, U-shaped quartz reactor (internal diameter 10 mm). The catalysts were trimethylsilylated at 423 K by passing methoxytrimethylsilane vapor (maintained at 298 K) in an Ar stream over the catalyst for 30 min, followed by flushing with Ar at 473 K (5 h). Then, a feed of propylene, O_2, H_2, and Ar (1:1:1:7 volume ratio) was passed through the catalyst bed at 423 K. Argon containing 5–45 ppm TMA was used as a base gas while studying the effect of TMA on propylene epoxidation. The feed and products were analyzed with on-line GCs equipped with a TCD (Porapak Q column), a FID (HR-20M column), and an auto injector.

In situ UV/Vis/NIR diffuse-reflectance spectra were recorded with a Cary 5000 Varian spectrometer equipped with a Harrick Scientific reaction chamber (Model HVC-DRP) in conjunction with the praying mantis diffuse-reflectance attachment (DRP-XXX). Spectra of catalysts and reference ($BaSO_4$ and titanosilicate support) were recorded under the same reaction and regeneration conditions in the range 200–2500 nm (50000–4000 cm^{-1}). Catalyst samples were pre-treated with TMA in the original reaction line in a similar manner to that of the catalytic activity measurements, then cooled to room temperature, and transferred into the in situ UV/Vis/NIR reaction chamber.

Received: July 8, 2005
Revised: October 12, 2005
Published online: December 9, 2005

Keywords: epoxidation · gold · heterogeneous catalysis · propylene oxide · trimethylamine

[1] J. R. Monnier, *Appl. Catal.* **2001**, *221*, 73–91.
[2] M. McCoy, *Chem. Eng. News* **2001**, *79*, 19–20.
[3] M. Haruta, *Chem. Rec.* **2003**, *3*, 75–87.
[4] T. Hayashi, K. Tanaka, M. Haruta, *J. Catal.* **1998**, *178*, 566–575.
[5] B. S. Uphade, T. Akita, T. Nakamura, M. Haruta, *J. Catal.* **2002**, *209*, 331–340.
[6] N. Yap, R. P. Andress, W. N. Delgass, *J. Catal.* **2004**, *226*, 156–170.
[7] A. Zwijnenburg, M. Makkee, J. A. Moulijn, *Appl. Catal.* **2004**, *270*, 49–56.
[8] A. K. Sinha, S. Seelan, S. Tsubota, M. Haruta, *Angew. Chem.* **2004**, *116*, 1572–1574; *Angew. Chem. Int. Ed.* **2004**, *43*, 1546–1548.
[9] E. F. Silva, F. H. Svendsen, *Ind. Eng. Chem. Res.* **2003**, *42*, 4414–4421.
[10] M. Date, M. Okumura, S. Tsubota, M. Haruta, *Angew. Chem.* **2004**, *116*, 2181–2184; *Angew. Chem. Int. Ed.* **2004**, *43*, 2129–2132.
[11] M. Dusi, T. Mallat, A. Baiker, *J. Catal.* **1999**, *187*, 191–201.
[12] W. E. Evans, P. I. Chipman, US Patent 6,717,001, **2004**.
[13] M. L. Peña, V. Dellarocca, F. Rey, A. Corma, S. Coluccia, L. Marchese, *Microporous Mesoporous Mater.* **2001**, *44*, 345–356.
[14] C. P. Tripp, M. L. Hair, *J. Phys. Chem.* **1993**, *97*, 5693–5698.
[15] X. Cao, R. J. Hamers, *J. Am. Chem. Soc.* **2001**, *123*, 10988–10996.
[16] W. Cai, H. Hofmeister, T. Rainer, *Physica E* **2001**, *11*, 339–344.
[17] W. Cai, H. Hofmeister, T. Rainer, W. Chen, *J. Nanopart. Res.* **2001**, *3*, 443–453.
[18] P. P. Olivera, E. M. Patrito, H. Sellers, *Surf. Sci.* **1994**, *313*, 25–40.
[19] P. Landon, P. J. Collier, A. J. Papworth, C. J. Kiely, G. J. Hutchings, *Chem. Commun.* **2002**, *18*, 2058–2059.

 © 2006 Wiley-VCH Verlag GmbH & Co. KGaA, Weinheim

[20] M. Okumura, Y. Kitagawa, K. Yamaguchi, T. Akita, S. Tsubota, M. Haruta, *Chem. Lett.* **2003**, *32*, 822 – 823.
[21] C. Sivadinarayana, T. V. Choudary, L. L. Dacmen, J. Eckert, D. W. Goodman, *J. Am. Chem. Soc.* **2004**, *126*, 38 – 39.
[22] A. Corma, H. Garcia, *Chem. Rev.* **2002**, *102*, 3837 – 3892.
[23] F. Geobaldo, S. Bordiga, A. Zecchina, E. Giameldo, G. Leofanti, G. Petrini, *Catal. Lett.* **1992**, *16*, 109 – 115.

 © 2006 Wiley-VCH Verlag GmbH & Co. KGaA, Weinheim

Proton Transfer

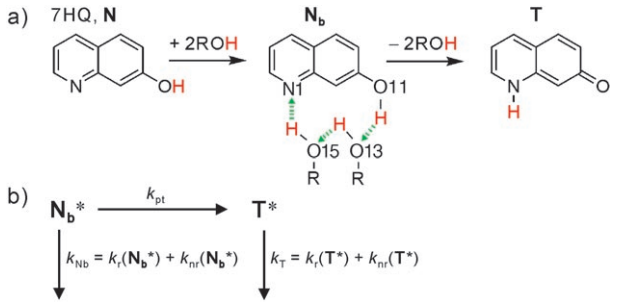
DOI: 10.1002/anie.200503209

Excited-State Triple Proton Transfer of 7-Hydroxyquinoline along a Hydrogen-Bonded Alcohol Chain: Vibrationally Assisted Proton Tunneling**

*Oh-Hoon Kwon, Young-Shin Lee, Byung Kuk Yoo, and Du-Jeon Jang**

Proton transfer plays a key role in a variety of biological and chemical phenomena such as water autoionization, fast proton diffusion, acid–base neutralization, DNA mutagenesis, enzyme catalysis, and proton pumping through membrane protein channels.[1–5] Hydrogen-bonded (H-bonded) chains extending over a long distance have been thought to be particularly effective in mediating the translocation of protons by a Grotthus-type mechanism.[3] However, even in cases of relatively simple and well-characterized systems, the experimental elucidation of the molecular mechanism of proton transfer along H-bonded chains is difficult because the event is intrinsically transient.

Amphoteric aromatic molecules are especially interesting to study excited-state proton transfer (ESPT) because they can be experimental molecular models for biological proton-relay systems.[5–7] In this regard, 7-hydroxyquinoline (7HQ), which has two prototropic groups (photoacidic enol and photobasic imine), has been extensively explored.[1,8–13] Protic solvent molecules are indispensable for the tautomerization of 7HQ, because the two prototropic groups are too far apart to donate/accept a proton directly.[11,12] Leutwyler et al. showed that a Grotthus-type proton-relay process of excited 7HQ takes place along a H-bonded ammonia wire in the gas phase.[1] Varma et al. proposed the biphasic ESPT mechanism of Scheme 1a for the tautomerization of 7HQ in bulk alcohols.[11] The first step is attributed to solvent reorganization for a normal molecule (**N**) to form a cyclically H-bonded complex with two alcohol molecules (ROH), while the subsequent step is intrinsic proton transfer in the complex to produce a tautomeric molecule (**T**). The first, solvent-reorganization step is reported to determine the overall tautomerization dynamics of 7HQ in bulk alcohols.[11] Consequently, it is desirable to explore the proton-relay dynamics of the cyclically H-bonded 7HQ–$(ROH)_2$ complex ($\mathbf{N_b}$) directly without their being veiled by the rate-determining slow step of solvent reorganization to better understand the intrinsic dynamics of the ESPT of 7HQ. In this regard, the ESPT of $\mathbf{N_b}$, prepared by adding a small amount of alcohols in nonpolar solvents, has been investigated,[12] although it is not understood adequately yet. Here we report on an investigation of the intrinsic proton-relay dynamics of $\mathbf{N_b}$ with variation of alcohol, solvent, isotopes, and temperature, and show that triple proton transfer along the cyclically H-bonded chain occurs asymmetrically with tunneling as the rate-determining first step.



Scheme 1.

Figure 1a shows that the lowest absorption of 7HQ shifts to the red and loses the sharp vibronic structure with increasing concentration of ethanol in *n*-heptane. This implies that 7HQ molecules associate with ethanol molecules by H-bonding in *n*-heptane, as reported for *n*-hexane.[12] The addition of ethanol does not result in perceivable absorption around 410 nm, that is, proton-translocated **T** does not form in the ground state. The emission spectra of Figure 1a show that excitation of the complexes at 345 nm gives rise to prominent **T*** fluorescence at 530 nm and normal fluorescence at 360 nm.[11,12] This shows that ESPT of 7HQ is operative in *n*-heptane in the presence of ethanol. The increasing intensity of **T*** fluorescence with increasing $[C_2H_5OH]$ suggests that excitation produces **T*** from the complexes of 7HQ with ethanol.

Figures 1b and 1c indicate that a 7HQ molecule associates with two alcohol molecules in *n*-heptane to form $\mathbf{N_b}$ as shown in Equation (1).[12]

$$7HQ + 2\,ROH \overset{K}{\rightleftarrows} 7HQ{-}(ROH)_2 \qquad (1)$$

[*] Dr. O.-H. Kwon,[+] Y.-S. Lee, B. K. Yoo, Prof. Dr. D.-J. Jang
School of Chemistry
Seoul National University
NS60, Seoul 151-742 (Korea)
Fax: (+82) 2-889-1568
E-mail: djjang@snu.ac.kr

[+] Present address:
Laboratory for Molecular Sciences
Arthur Amos Noyes Laboratory of Chemical Physics
California Institute of Technology
Pasadena, CA 91125 (USA)

[**] The Korea Research Foundation is appreciated for the grant of KRF-2004-015-C00230. Scholarships from the BK 21 Program are also acknowledged.

Supporting information for this article is available on the WWW under http://www.angewandte.org or from the author.

© 2006 Wiley-VCH Verlag GmbH & Co. KGaA, Weinheim

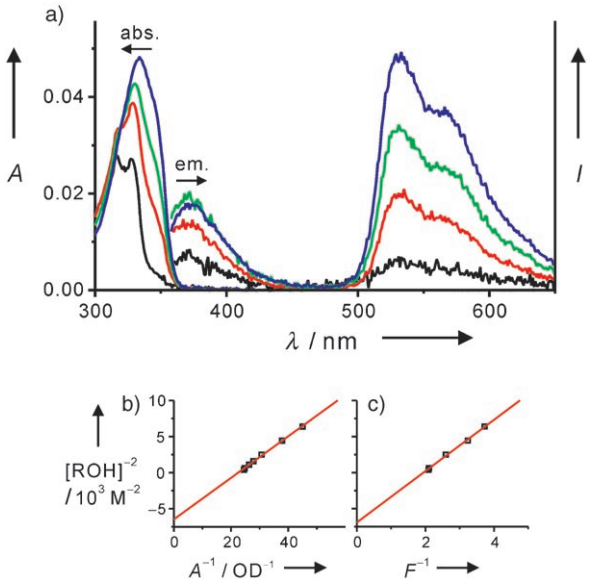


Figure 1. a) Absorption and emission spectra (with excitation at 345 nm) of 7HQ at ethanol concentrations of 5 (black), 10 (red), 15 (green), and 30 mM (blue) in *n*-heptane. b, c) Plots, with best linear fits (lines), of squared reciprocals of molar ethanol concentration [ROH] versus reciprocal absorbance A^{-1} at 345 nm (b) and reciprocal fluorescence intensity F^{-1} at 570 nm (c).

The complex-formation constant K in Equation (1) can be deduced by plotting $[ROH]^{-2} = cX - K$ linearly, where c is a constant and X is (absorbance)$^{-1}$ or (fluorescence)$^{-1}$.[13] The K value of 6500 M^{-2} obtained for absorbance numerically agrees with that of 6900 M^{-2} obtained for fluorescence. The good linearity of Figure 1c reveals that **T*** is formed from 7HQ–$(ROH)_2$ complexes on photoexcitation. We also confirmed, by measuring absorbance changes on gradually adding several other alcohols, that a 7HQ molecule associates with two alcohol molecules to form 7HQ–$(ROH)_2$ in *n*-heptane (see the Supporting Information). Table 1 shows that K decreases with increasing complexity of the alkyl chain and with decreasing Kamlet–Taft acidity α. Thus, the acidity of the alcohol is inferred to play an important role in the formation of H-bonded complexes. The magnitudes of α and Kamlet–Taft basicity β for H-bonding molecules provide explicit measures of the H-bond-donating and the H-bond-accepting abilities of the molecules, respectively.[15] The most stable ground-state structure of 7HQ–$(ROH)_2$ is reported to have the cyclic geometry of $\mathbf{N_b}$.[16] The H-bond involving the imino group is calculated to be 0.2 Å longer than that involving the enol group in the complex $\mathbf{N_b}$.[16] Thus, the H-bond strength of ROH···N is inferred to be relatively low and thus determine the formation of $\mathbf{N_b}$.

On excitation of a sample containing C_2H_5OH at 355 nm, normal fluorescence recorded at 420 nm shows a biphasic decay profile composed of 74 (97%) and 800 ps (3%), while **T*** fluorescence monitored at 550 nm rises in 75 ps and decays in 2.3 ns (Figure 2). On excitation of a sample containing C_2H_5OD, the rise time (710 ps) of **T*** fluorescence correlates

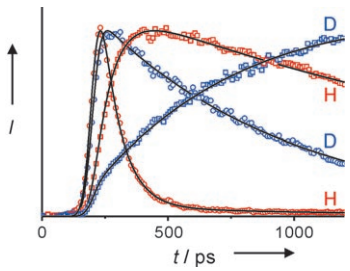


Figure 2. Fluorescence kinetic profiles (excitation at 355 nm and monitoring at 420 (circles) and 550 nm (squares)) of 7HQ in *n*-heptane with C_2H_5OH (H) and C_2H_5OD (D) concentrations of 30 mM. Lines are best-fit curves.

well with the fast decay time (710 ps) of normal fluorescence. The slow decay time of normal fluorescence and the lifetime of **T*** fluorescence are 1.7 and 6.2 ns, respectively. All the time constants mentioned above do not vary with ethanol concentration, although the fractional initial amplitudes of the two decay components do. This indicates that the collision-induced formation of $\mathbf{N_b}$ does not occur to conduct ESPT within the lifetime of **N***. Therefore, the fast-decay component is attributed to the decay of $\mathbf{N_b}$ coupled to ESPT, while the long decay time is assigned to the fluorescence lifetime of noncyclically H-bonded 7HQ complexes with ethanol.

We have analyzed the observed kinetic constants of $\mathbf{N_b}$* and **T*** by employing the irreversible two-state model described in Scheme 1b, where k_r and k_{nr} denote the rate constants of radiative and nonradiative relaxation, respectively. Then we can derive Equations (2) and (3) to show the temporal behaviors of [$\mathbf{N_b}$*] and [**T***], respectively.

$$[\mathbf{N_b}^*] = [\mathbf{N_b}^*]_0 \, e^{-(k_{Nb}+k_{pt})t} \quad (2)$$

$$[\mathbf{T}^*] = \left(\frac{[\mathbf{N_b}^*]_0 \, k_{pt}}{k_{Nb} + k_{pt} - k_T}\right)\left[e^{-k_T t} - e^{-(k_{Nb}+k_{pt})t}\right] \quad (3)$$

The k_{Nb} values of 7HQ–$(C_2H_5OH)_2$ and 7DQ–$(C_2H_5OD)_2$ were assumed to be the same as the reciprocals of the slow decay times of normal fluorescence in samples containing C_2H_5OH and C_2H_5OD, respectively. Thus, k_{pt} values for 7HQ–$(C_2H_5OH)_2$ and 7DQ–$(C_2H_5OD)_2$ complexes were

Table 1: Dependence of K, k_{pt}, and KIE of $\mathbf{N_b}$ on alcohol and solvent.

Solvent[a]	Alcohol[b]	α[c]	β[c]	K [M^{-2}]	k_{pt}^{-1} [ps]	KIE
n-Heptane	2,2,2-trifluoroethanol	1.51	0	10400 ± 400	15 ± 5	3.0 ± 1.0
	methanol	0.93	0.62	9500 ± 400	62 ± 3	15.2 ± 0.9
	ethanol	0.83	0.77	6500 ± 300	82 ± 4	15.0 ± 0.8
	2-propanol	0.76	0.95	6100 ± 300	134 ± 6	12.2 ± 0.6
	2-methyl-2-propanol	0.68	1.01	4200 ± 400	214 ± 10	8.5 ± 0.4
n-Decane	ethanol	0.83	0.77	–[d]	85 ± 4	14.4 ± 0.8
	2-methyl-2-propanol	0.68	1.01	–[d]	212 ± 10	8.5 ± 0.4
n-Dodecane	ethanol	0.83	0.77	–[d]	93 ± 4	13.1 ± 0.7
	2-methyl-2-propanol	0.68	1.01	–[d]	252 ± 10	7.2 ± 0.3

[a] The viscosities of *n*-heptane, *n*-decane, and *n*-dodecane at 25 °C are 0.41, 0.92, and 1.45 cP, respectively.[14] [b] At 30 mM. [c] With bulk alcohols because the values of monomeric alcohols, which have similar trends to those of bulk alcohols, are not available in the literature for some of the employed alcohols.[15] [d] Not measured.

 © 2006 Wiley-VCH Verlag GmbH & Co. KGaA, Weinheim

deduced to be $(82\,\text{ps})^{-1}$ and $(1220\,\text{ps})^{-1}$, respectively. We compared a kinetic isotope effect (KIE) calculated as k_{pt}^{H}/k_{pt}^{D} with an alternative KIE value obtained from the quantum yields and the fluorescence lifetimes to check the validity of our kinetic analysis. The two values obtained with each employed alcohol in *n*-heptane coincide within our experimental errors (see the Supporting Information).

The proton-relay process in $\mathbf{N_b}$ may occur by transfer of three hydrogen atoms concertedly through a single transition state or of three protons stepwise with formation of intermediate complexes.[17] Proton-inventory experiments with variation of the degree of deuteration of protic hydrogen atoms in $\mathbf{N_b}$ for the determination of k_{pt} can give us a clue to this issue.[17–21] In isotopically mixed systems, eight different types of complexes can be present: HHH, HDH, HHD, HDD, DHH, DDH, DHD, and DDD, where the successive three letters denote protic hydrogen atoms attached to O11, O13, and O15 of $\mathbf{N_b}$, respectively. The overall rate constants ($k_{all} = k_{Nb} + k_{pt}$) of $\mathbf{N_b}$ of the above complexes are k_{all}^{HHH}, k_{all}^{HDH}, k_{all}^{HHD}, k_{all}^{HDD}, k_{all}^{DHH}, k_{all}^{DDH}, k_{all}^{DHD}, and k_{all}^{DDD}, respectively. If $X_D = [\text{protic D}]/([\text{protic H}] + [\text{protic D}])$ and $X_H = 1 - X_D$, then we can deduce Equations (4) and (5) for overall rates according to the protic hydrogen isotopes of the enol group of 7HQ.

$$\begin{aligned} d[7HQ]/dt = -\{&X_H^2 k_{all}^{HHH} + X_H X_D (k_{all}^{HDH} + k_{all}^{HHD}) \\ &+ X_D^2 k_{all}^{HDD}\}[7HQ] \end{aligned} \tag{4}$$

$$\begin{aligned} d[7DQ]/dt = -\{&X_H^2 k_{all}^{DHH} + X_H X_D (k_{all}^{DDH} + k_{all}^{DHD}) \\ &+ X_D^2 k_{all}^{DDD}\}[7DQ] \end{aligned} \tag{5}$$

Although isotopic fractionation constants were assumed to be unity, we note that their actual values are slightly different from unity.[21] The isotope distribution should be directly measured by an NMR technique.[21] However, we have roughly calculated the distribution using the OH stretching frequencies of the four involved species[22] because of the very low concentrations of $\mathbf{N_b}$ in our samples. The estimated equilibrium constant of $7HQ + CH_3OD \rightleftharpoons 7DQ + CH_3OH$ at 23 °C is 1.03.

Because the isotopic exchange of a protic hydrogen atom is much slower than ESPT, we expect the fluorescence of $\mathbf{N_b}$ to decay biexponentially according to Equation (6).

$$F(t) = X_H \exp(-k^H t) + X_D \exp(-k^D t) \tag{6}$$

Then, the experimentally observed parameters k^H and k^D in Equation (6) consist of the eight different k_{all} values according to Equations (7) and (8), respectively.

$$\begin{aligned} k^H = &k_{all}^{HHH} + (k_{all}^{HHD} + k_{all}^{HDH} - 2k_{all}^{HHH}) X_D \\ &+ (k_{all}^{HHH} + k_{all}^{HDD} - k_{all}^{HHD} - k_{all}^{HDH}) X_D^2 \end{aligned} \tag{7}$$

$$\begin{aligned} k^D = &k_{all}^{DHH} + (k_{all}^{DDH} + k_{all}^{DHD} - 2k_{all}^{DHH}) X_D \\ &+ (k_{all}^{DHH} + k_{all}^{DDD} - k_{all}^{DDH} - k_{all}^{DHD}) X_D^2 \end{aligned} \tag{8}$$

The quadratic correlations of k^H and k^D with X_D given in Figure 3 yield k_{all}^{HHH}, k_{all}^{HDD}, k_{all}^{DHH}, and k_{all}^{DDD} as $(80\,\text{ps})^{-1}$, $(220\,\text{ps})^{-1}$, $(250\,\text{ps})^{-1}$, and $(720\,\text{ps})^{-1}$, respectively. If ESPT occurs concertedly without tunneling effects then, according to the rule of the geometric mean, $k_{obs}^{HHH}/k_{obs}^{DHH} = k_{obs}^{DHH}/k_{obs}^{HDD} = k_{obs}^{HDD}/k_{obs}^{DDD} = (k_{obs}^{HHH}/k_{obs}^{DDD})^{1/3}$ should hold.[17–21] However, $k_{obs}^{HHH}/k_{obs}^{DHH}$, $k_{obs}^{DHH}/k_{obs}^{HDD}$, $k_{obs}^{HDD}/k_{obs}^{DDD}$, and $(k_{obs}^{HHH}/k_{obs}^{DDD})^{1/3}$ are observed to be 3.1 ± 0.1, 0.86 ± 0.15, 3.3 ± 0.8, and 2.1 ± 0.3, respectively. These values indicate that the rule of the geometric mean is not valid in the ESPT of $\mathbf{N_b}$, which implies that the three protons move asymmetrically or that tunneling is involved in the rate-limiting step.

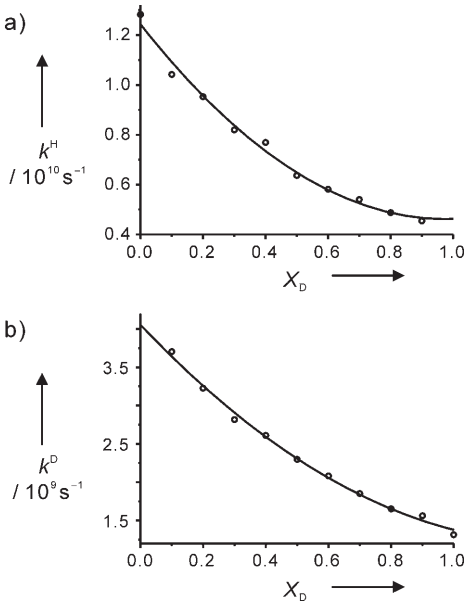
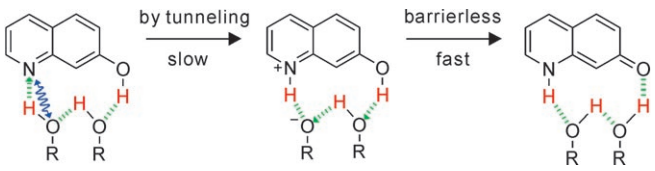


Figure 3. Plots of k^H (a) and k^D (b) with variation of X_D for 7HQ in *n*-heptane with [C_2H_5OH] of 50 mM. Solid lines are best quadratic fittings to obtain k_{all}^{HHH}, k_{all}^{HDD}, k_{all}^{DHH}, and k_{all}^{DDD} as $(80 \pm 1\,\text{ps})^{-1}$, $(220 \pm 37\,\text{ps})^{-1}$, $(250 \pm 4\,\text{ps})^{-1}$, and $(720 \pm 120\,\text{ps})^{-1}$, respectively.

Alcohol-dependent kinetic measurements show that k_{pt} of $\mathbf{N_b}$ tends to increase with increasing α (Table 1). Because $\mathbf{N_b}$ formed with 2,2,2-trifluoroethanol, which has $\beta = 0$ and the highest α value, shows the highest k_{pt} value, β is not considered to affect k_{pt} noticeably. The structure of a cyclically H-bonded 7HQ–$(CH_3OH)_2$ complex at the excited state has been calculated to show that the N···HO H-bond is substantially longer than any of the other two H-bonds in the complex.[16] The dependence of k_{pt} on α indicates that ESPT becomes more exoergic with stronger acidity of the alcohol. This suggests that the H-bond-donating ability of an alcohol in the coordinate of N···HO is crucial for the dynamics of ESPT. Keeping in mind that the decay time of $\mathbf{N_b}^*$ and the rise time of $\mathbf{T}^*$ coincide and that k_{pt} depends on alcohol acidity, we propose that ESPT of $\mathbf{N_b}$ is initiated by the slow deprotonation of the alcohol molecule H-bonded to the nitrogen atom of 7HQ to form a zwitterionic intermediate complex (Scheme 2).[12c] The ESPT is then completed by rapid proton relay



Scheme 2.

© 2006 Wiley-VCH Verlag GmbH & Co. KGaA, Weinheim

from the enol group of the 7HQ cation to the transient alkoxide anion through the neutral alcohol molecule.

The potential-energy surface from ab initio calculations showed that there are no metastable intermediate complexes.[16] The intermediate complex of Scheme 2 is too unstable to be kinetically significant, because both the alkoxide moiety and the 7HQ cation are energetically very unfavorable. Therefore, we infer that the observed rate constant of ESPT is mainly determined by the initial single proton transfer of the N···HO coordinate.

The KIE value of k_{pt} observed in 7HQ–$(C_2H_5OH)_2$ complexes in *n*-heptane at room temperature is 15.0 (Figure 2 and Table 1). Recall that our proton-inventory results deviate from the rule of the geometric mean and that single proton transfer through the H-bond of N···HO determines k_{pt}. The large KIE in the single proton transfer implies that the rate-determining step is mainly a tunneling process. The KIE values with diverse alcohols are also listed in Table 1. The less acidic alcohol makes the ESPT reaction less exothermic and more symmetric energetically to increase the contribution of tunneling and reduce the rate constant.[20,23] Thus, $\mathbf{N_b}$ with methanol ($\alpha = 0.93$) has a KIE five times greater than that of $\mathbf{N_b}$ with 2,2,2-trifluoroethanol ($\alpha = 1.51$). However, KIE tends to decrease with decreasing α if α decreases gradually and the molecular size increases rapidly. We consider that the effect of mobility reduction on KIE prevails over that of decreasing α in the above case. This hints that heavy-atom motions, which are isotopically insensitive, as well as short heavy-atom distances, are essential in tunneling. The intrinsic proton relay governed by tunneling requires optimized bond angles and short H-bond lengths in addition to the cyclic H-bonded structure. The reorganization of the H-bond bridge for $\mathbf{N_b}$ to form such a precursor configuration optimal for tunneling is not sensitive to isotope effects and consists mostly of heavy-atom motions. Configurational optimization and intrinsic tunneling occur in two orthogonal reaction coordinates of the potential hypersurface, and solvent fluctuations are suggested to play a crucial role in optimization. In the regime where hydrogen-atom motions including tunneling limit the rate exclusively, KIE is predicted to be independent of solvent viscosity and much greater than unity. Alternatively, when heavy-atom reorganization assists quantum tunneling, KIE depends on viscosity. The heavy-atom reorganization that is required to reach the optimal configuration for pretunneling becomes slow with increasing viscosity. Thus, the tunneling contribution and KIE tend to be small with increasing viscosity.[24] Table 1 shows that KIE and k_{pt} decrease with the increasing solvent viscosity. The dependence of k_{pt} on viscosity suggests that the rate of the overall proton-transfer reaction at high viscosity is also affected to some extent by the configurational-optimization rate of $\mathbf{N_b}$*, and this supports the above idea that solvent fluctuations enhance tunneling in the ESPT of $\mathbf{N_b}$. The overall proton transfer of 7HQ in neat methanol is reported to occur on a timescale of 200 ps with KIE of 1.4.[12b] The rate is low and the KIE is small because large-amplitude solvent reorganization to form $\mathbf{N_b}$ is known to be the rate-determining step.[11]

The Arrhenius plots of k_{pt} in Figure 4 show that the KIE is independent of temperature within our experimental errors,

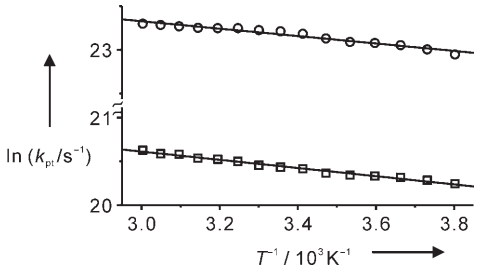


Figure 4. Arrhenius plots of k_{pt} in *n*-heptane with [C_2H_5OH] (circles) and [C_2H_5OD] (squares) of 30 mM. Activation energies (preexponential factors) extracted for C_2H_5OH and C_2H_5OD are 0.84 ± 0.05 kcal mol^{-1} ($(4.8 \pm 0.4) \times 10^{10}$ s^{-1}) and 0.93 ± 0.03 kcal mol^{-1} ($(3.7 \pm 0.2) \times 10^{9}$ s^{-1}), respectively.

although k_{pt} is slightly dependent on temperature. When the tunneling contribution is large, the ratio of preexponential factors $A(H)/A(D)$ is much less than unity in general. However, if tunneling becomes extremely effective for both H and D, then the ratio becomes much greater than unity. The deduced activation energies E_a of 7HQ–$(C_2H_5OH)_2$ and 7DQ–$(C_2H_5OD)_2$ are quite small (0.84 and 0.93 kcal mol^{-1}, respectively). This supports the suggestion that tunneling determines the ESPT rate. The fact that the two E_a values are very close to each other indicates that the KIE of 15.0 ± 0.8 is mostly determined by the $A(H)/A(D)$ ratio of 13.0 ± 1.3. This suggests that the rate-determining process for the ESPT of $\mathbf{N_b}$ takes place with extensive tunneling contribution in the reaction coordinate of N···HO. Temperature independence of the KIE has also been reported in enzymatic proton transfers[25] and solvent-mediated proton transfers.[11,20] Temperature-independent and large KIEs in enzymes have been explained with a model employing vibrationally enhanced proton tunneling.[26–28]

The temperature dependence of the rate constant arises from the temperature dependence of the population of the states that allow the proton to tunnel through the barrier. The observed small values of E_a are inferred to originate from the activation energy required to form a pretunneling configuration with heavy-atom motions. We have observed that the fast-decaying component of normal fluorescence disappears abruptly below the glass temperature of the solvent (Figure 5). This supports the idea that solvent fluctuations assist tunneling in the proton relay of 7HQ along a H-bonded alcohol chain. A similar conclusion was reached for temper-

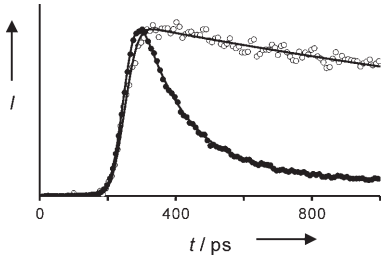


Figure 5. Normal-fluorescence kinetic profiles of 7HQ in *n*-heptane with [C_2H_5OH] of 20 mM measured at 180 (open circles) and 200 K (filled circles). The sample was excited at 355 nm and monitored at 420 nm.

 © 2006 Wiley-VCH Verlag GmbH & Co. KGaA, Weinheim

ature-dependent rate constants and temperature-independent KIE in the ground-state reverse proton transfer of 7HQ in neat alcohols.[11]

The picture of the ESPT mechanism in the cyclically H-bonded complex of 7HQ–$(ROH)_2$ is in line with the novel idea of Leutwyler et al. that photoexcited 7HQ–$(NH_3)_3$ in the gas phase requires the additional excitation of ammonia-wire vibrations to undergo proton transfer, and this reveals the crucial role of the coordinated solvent in proton tunneling.[1] Note that 7HQ–$(CH_3OH)_2$ in the gas phase does not undergo ESPT although 7HQ–$(CH_3OH)_3$ does.[22] The ESPT activity only in the 7HQ–$(CH_3OH)_3$ cluster has been attributed to shortened heavy-atom distances between the prototropic groups of 7HQ and nearby H-bonded methanol molecules. The efficiency of proton tunneling is closely related to the distances of heavy atoms in the reaction coordinates. The slight reorganization of $\mathbf{N_b}$ in condensed phases to form the pretunneling configuration having optimal bond angles and short H-bond lengths can be achieved by the assistance of solvent fluctuations.

In summary, the triple proton transfer of cyclically H-bonded 7HQ–$(ROH)_2$ complexes formed in nonpolar *n*-alkanes occurs asymmetrically on a timescale of 10–200 ps with unusually large, temperature-independent, and viscosity-dependent KIEs near room temperature. The ESPT is triggered by proton transfer from the alcohol molecule to the imino group and completed by rapid proton transfer from the enol group to the transient alkoxide moiety. Thus, intrinsic proton relay is governed by single proton tunneling to the nitrogen atom, although heavy-atom motions, depicted as a wavy arrow in Scheme 2, assist the H-bonded complex of $\mathbf{N_b}$ in reaching the optimal precursor configuration. Tunneling in our system is conceptually identical to vibrationally assisted tunneling observed in enzymatic proton transfer. Solvent fluctuations replace low-frequency protein motions in our system. The detailed dynamics of ESPT in $\mathbf{N_b}$ requires multidimensional reaction coordinates to be described properly and thus poses great theoretical challenges.

Experimental Section

7HQ (99%) from Acros, alcohols, and *n*-alkanes (anhydrous) were used as purchased. The protic hydrogen atoms of 7HQ and ROH were exchanged with ^{1}H (H) and ^{2}H (D) atoms for proton-inventory experiments by dissolving 7HQ in nonpolar solvents containing RO^1H and RO^2H (isotopic purity $\geq$99.5%), respectively. The concentrations of 7HQ were kept at 1×10^{-5} M in our samples. Absorption spectra were obtained with a UV/Vis spectrophotometer (Scinco, S-3100), and emission spectra with a home-built fluorimeter.[20] An actively/passively mode-locked 25 ps Nd:YAG laser (Quantel, YG 701) and a 10 ps streak camera (Hamamatsu, C2830) attached to a CCD detector (Princeton Instruments, RTE128H) were employed to monitor fluorescence kinetics.[20] Samples were excited with third-harmonic pulses (355 nm) of the laser. Unless specified otherwise, static and kinetic measurements were carried out at 23°C.

Received: September 9, 2005
Published online: December 2, 2005

Keywords: hydrogen bonds · isotope effects · N heterocycles · proton transfer · time-resolved spectroscopy

[1] C. Tanner, C. Manca, S. Leutwyler, *Science* **2003**, *302*, 1736–1739.
[2] M. Rini, B.-Z. Magnes, E. Pines, E. T. J. Nibbering, *Science* **2003**, *301*, 349–352.
[3] M. Gutman, E. Nachliel, *Annu. Rev. Phys. Chem.* **1997**, *48*, 329–356.
[4] A. Douhal, S. K. Kim, A. H. Zewail, *Nature* **1995**, *378*, 260–263.
[5] M. A. Lill, V. Helms, *Proc. Natl. Acad. Sci. USA* **2002**, *99*, 2778–2781.
[6] M. Kasha, *J. Chem. Soc. Faraday Trans. 2* **1986**, *82*, 2379–2392.
[7] J. Waluk, *Acc. Chem. Res.* **2003**, *36*, 832–838.
[8] S. F. Mason, J. Philip, B. E. Smith, *J. Chem. Soc. A* **1968**, 3051–3067.
[9] a) P. J. Thistlethwaite, P. J. Corkill, *Chem. Phys. Lett.* **1982**, *85*, 317–321; b) P. J. Thistlethwaite, *Chem. Phys. Lett.* **1983**, *96*, 509–512.
[10] a) E. Bardez, *Isr. J. Chem.* **1999**, *39*, 319–332; b) E. Bardez, I. Devol, B. Larrey, B. Valeur, *J. Phys. Chem. B* **1997**, *101*, 7786–7793.
[11] J. Konijnenberg, G. B. Ekelmans, A. H. Huizer, C. A. G. O. Varma, *J. Chem. Soc. Faraday Trans. 2* **1989**, *85*, 39–51.
[12] a) T. Nakagawa, S. Kohtani, M. Itoh, *J. Am. Chem. Soc.* **1995**, *117*, 7952–7957; b) M. Itoh, T. Adachi, K. Tokumura, *J. Am. Chem. Soc.* **1984**, *106*, 850–855; c) S. Kohtani, A. Tagami, R. Nakagaki, *Chem. Phys. Lett.* **2000**, *316*, 88–93.
[13] Y. Tanimoto, M. Itoh, *Chem. Phys. Lett.* **1978**, *57*, 179–182.
[14] a) *CRC Handbook of Chemistry and Physics*, *78th ed.* (Ed.: D. R. Lide), CRC, Boca Raton, **1999**; b) K.-S. Kim, H. Lee, *J. Chem. Eng. Data* **2002**, *47*, 216–218.
[15] a) M. J. Kamlet, J.-L. M. Abboud, M. H. Abraham, R. W. Taft, *J. Org. Chem.* **1983**, *48*, 2877–2887; b) J.-L. M. Abboud, K. Sraidi, G. Guiheneuf, A. Negro, M. J. Kamlet, R. W. Taft, *J. Org. Chem.* **1985**, *50*, 2870–2873; c) B. Frange, J.-L. M. Abboud, C. Benamou, L. Bellon, *J. Org. Chem.* **1983**, *48*, 4553–4557.
[16] W.-H. Fang, *J. Am. Chem. Soc.* **1998**, *120*, 7568–7576.
[17] R. L. Schowen, *Angew. Chem.* **1997**, *109*, 1502–1506; *Angew. Chem. Int. Ed. Engl.* **1997**, *36*, 1434–1438.
[18] O. Klein, F. Aguilar-Parrilla, J. M. Lopez, N. Jagerovic, J. Elguero, H.-H. Limbach, *J. Am. Chem. Soc.* **2004**, *126*, 11718–11732.
[19] Y. Chen, F. Gai, J. W. Petrich, *J. Am. Chem. Soc.* **1993**, *115*, 10158–10166.
[20] O.-H. Kwon, Y.-S. Lee, H. J. Park, Y. Kim, D.-J. Jang, *Angew. Chem.* **2004**, *116*, 5916–5920; *Angew. Chem. Int. Ed.* **2004**, *43*, 5792–5796.
[21] a) D. Gerritzen, H.-H. Limbach, *J. Am. Chem. Soc.* **1984**, *106*, 869–879; b) P. M. Tolstoy, P. Schah-Mohammedi, S. N. Smirnov, N. S. Golubev, G. S. Denisov, H.-H. Limbach, *J. Am. Chem. Soc.* **2004**, *126*, 5621–5634.
[22] Y. Matsumoto, T. Ebata, N. Mikami, *J. Phys. Chem. A* **2002**, *106*, 5591–5599.
[23] P. M. Kiefer, J. T. Hynes, *J. Phys. Chem. A* **2004**, *108*, 11793–11808.
[24] J. Basran, M. J. Sutcliffe, N. S. Scrutton, *Biochemistry* **1999**, *38*, 3218–3222.
[25] A. Kohen, R. Cannio, S. Bartolucci, J. P. Klinman, *Nature* **1999**, *399*, 96–499.
[26] R. R. Dogonadze, A. M. Kuznetsov, V. G. Levich, *Electrochim. Acta* **1968**, *13*, 1025–1044.
[27] A. M. Kuznetsov, J. Ulstrup, *Can. J. Chem.* **1999**, *77*, 1085–1096.
[28] E. Hatcher, A. V. Soudackov, S. Hammes-Schiffer, *J. Am. Chem. Soc.* **2004**, *126*, 5763–5775.

 © 2006 Wiley-VCH Verlag GmbH & Co. KGaA, Weinheim

Semiconductors

DOI: 10.1002/anie.200503172

Transition-Metal Doped Zinc Oxide Nanowires**

*Benjamin D. Yuhas, David O. Zitoun, Peter J. Pauzauskie, Rongrui He, and Peidong Yang**

The introduction of impurity atoms into semiconducting materials is the primary method for controlling the properties of the semiconductor, such as band gap or electrical conductivity. This practice is routinely performed with bulk semiconductors and, more recently, has been extended to nanoscale semiconductors as well. In particular, II–VI and III–V semiconductors that have been doped with transition metals are currently generating much research interest, principally for their novel magnetic properties. These semiconductors are commonly called dilute magnetic semiconductors and are envisioned to be potential building blocks for spintronic devices.

One such material is transition-metal doped zinc oxide ($Zn_{1-x}M_xO$), which has been theoretically predicted to be ferromagnetic at room temperature.[1,2] Although this system has been under experimental study for some time, the vast majority of research conducted on this material has been done on bulk crystals or thin films.[3–8] There are very few reports on the fabrication of one-dimensional nanostructures of $Zn_{1-x}M_xO$, and high-temperature, vapor-phase methods are employed in the syntheses.[9,10] Although this approach has proven quite effective for the production of a multitude of nanoscale semiconductors, gas-phase syntheses are considerably limited in regards to homogeneous doping and alloying because of high-growth temperatures.

Solution-based synthetic schemes possess inherent advantages in the above areas over vapor-phase routes, in addition to ecological benefits. Whereas there have been several reports on the synthesis of pure ZnO nanowires from the solution phase,[11–13] the only solution-based methods for the production of $Zn_{1-x}M_xO$ yield isotropic quantum dots, such as those reported by Gamelin et al.[14,15] To date, no reports of anisotropic, transition-metal doped ZnO nanowires grown from the solution phase exist. We present herein the synthesis and characterization of cobalt-doped zinc oxide ($Zn_{1-x}Co_xO$) nanowires grown by a solution-phase synthesis. The synthetic process presented herein also allows for the doping of different transition metals (e.g., Mn, Fe, Cu); however, this report is limited to the cobalt-doped system.

The nanowires were synthesized by the thermal decomposition of zinc acetate and cobalt(II) acetate in refluxing trioctylamine (see the Experimental Section). Figure 1 shows scanning electron microscopy (SEM) and transmission electron microscopy (TEM) images of both pure and Co-doped ZnO nanowires. The nanowires grow in bundles that are tethered to a common hexagonal base. The diameter of the nanowires is statistically invariant regardless of the cobalt concentration. The average nanowire diameter is approximately 35 nm; the wires, thus, have aspect ratios that range from 80–160.

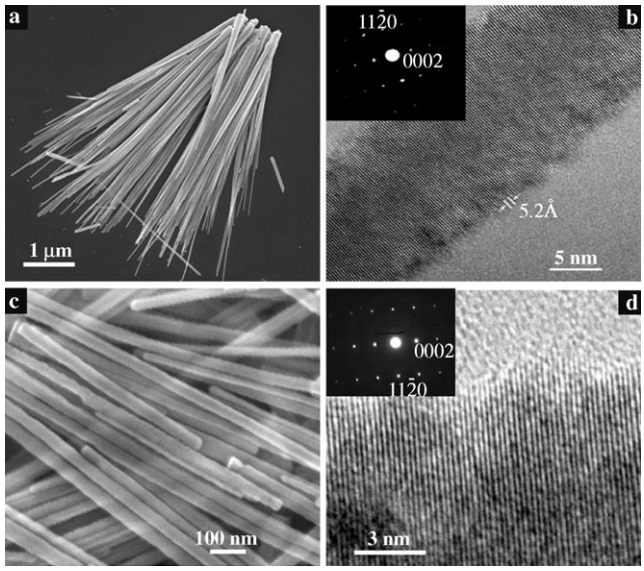


Figure 1. a) SEM image of undoped ZnO nanowires. b) High-resolution TEM image of a single ZnO nanowire, with an accompanying electron-diffraction pattern in the inset; similar images for Co-doped ZnO nanowires are shown in (c and d), in which Co content = 11.34%.

From the TEM images and selected-area electron-diffraction patterns (inset, Figure 1b, d), it is seen that the wires are single-crystalline, with a growth direction along the [0001] axis. This one-dimensional growth of pure ZnO nanowires has been reported previously in aqueous solutions.[11,12] In those examples, the one-dimensional growth was enabled by the presence of an amine moiety; we believe that the trioctylamine solvent plays a similar role in our system. It should also be noted that we observed similar single-crystalline diffraction patterns whether we examined a single wire or its base, thus indicating that the base likely nucleates first, followed by individual nanowire growth in the [0001] direction.

[*] B. D. Yuhas, Dr. D. O. Zitoun,[+] P. J. Pauzauskie, R. He, Prof. P. Yang
Department of Chemistry
Lawrence Berkeley National Laboratory
University of California
Berkeley, CA 94720 (USA)
E-mail: p_yang@berkeley.edu

[+] Current Address: LAMMI bat. 15
Université Montpellier II
Place Eugene Bataillon
34095 Montpellier Cedex 5 (France)

[**] This work was supported by the US Department of Energy. D.O.Z. is a DGA post-doctoral fellow. We thank Tevye Kuykendall and Josh Goldberger for their assistance in transmission electron microscopy (TEM) imaging. We thank Yulia Pushkar and Vittal Yachandra for their experimental assistance with electron paramagnetic resonance (EPR). P.J.P. thanks the NSF for a graduate research fellowship. Work at the Lawrence Berkeley National Laboratory was supported by the Office of Science, Basic Energy Sciences, Division of Materials Science, US Department of Energy. We thank the National Center for Electron Microscopy for the use of their facilities.

InterScience
© 2006 Wiley-VCH Verlag GmbH & Co. KGaA, Weinheim

The cobalt concentration in the nanowires was determined by energy-dispersive X-ray (EDX) spectroscopy. The cobalt concentration (in atom%) can be varied from less than 1% to greater than 15% depending on the amount of cobalt precursor used; the most heavily doped sample in this investigation had a cobalt concentration of 11.34%. The cobalt amounts between different bundles of wires, as well as along individual wires, are very consistent; we saw a homogeneous concentration of cobalt in our samples and no evidence of a lateral or longitudinal concentration gradient in individual wires. Also, no indication of cobalt metal or cobalt oxide impurities in our final product was observed. Powder X-ray diffraction patterns of nanowires with various levels of cobalt doping are presented in Figure 2. In all cases, wurtzite

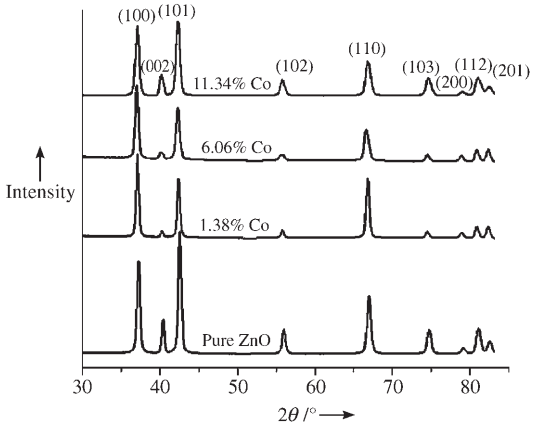
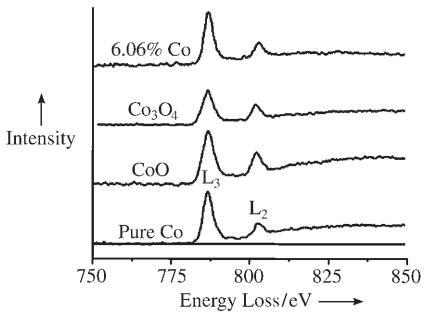


Figure 2. Powder X-ray diffraction patterns of pure and Co-doped ZnO nanowires.

is the only phase in existence, which indicates that doping is uniform throughout the nanowires. No significant shift in the lattice constants of the nanowires was seen either, although the cobalt and zinc ionic radii are so similar ($Zn^{2+} \approx 0.60$ Å, $Co^{2+} \approx 0.56$ Å) that any expected shift in lattice constant would be beyond the resolution of our diffractometer.

Electron energy-loss spectroscopy (EELS) was employed to determine the oxidation state of the cobalt in the wurtzite lattice. Figure 3 shows the EELS spectra obtained from the doped nanowires and three cobalt-containing standards. It is



Sample	L_3/L_2 Area Ratio
6.06% Co	2.93
Pure Co	3.77
CoO	2.90
Co_3O_4	2.43

Figure 3. EELS spectra of 6.06% Co-doped ZnO Nanowires and cobalt-containing standards.

known that the L_3 and L_2 EELS peaks of the first-transition-series elements are sensitive to the oxidation state of the metal.[16,17] By comparing the areas of the L_3 and L_2 peaks in the EELS spectra, the oxidation state of the cobalt in the nanowires can be determined. The table in Figure 3 lists the resulting area ratios, and it can be seen that the nanowires correlate very well with the ratio obtained from CoO, a divalent cobalt compound, thus indicating that cobalt exists in a divalent state (Co^{2+}) in the ZnO host semiconductor.

The nanowires are of excellent optical quality, as shown by a series of photoluminescence (PL) measurements (Figure 4). When excited with ultraviolet light, the pure ZnO nanowires exhibit band-edge luminescence near 380 nm, accompanied by a broad defect band centered at approximately 550 nm. Both of the above peaks diminish in intensity upon cobalt inclusion, and a new peak centered at 680 nm appears. This wavelength corresponds well with the $^4T_1(P) \rightarrow {}^4A_2(F)$ transition that is indicative of a Co^{2+} ion in a tetrahedral crystal field,[18–21] and this transition is visible in all of our doped-nanowire samples.

The single peak at 680 nm splits into several separate components at low temperature, and this splitting is reproducible from sample to sample. It is known from previous electronic absorption studies[18–21] of transition-metal ions in various host semiconductor thin films and from crystal-field theory that the $^4T_1(P)$ energy level splits into four levels because of spin–orbit coupling. However, it is also known that Co^{2+} ions doped into ZnO can exhibit appreciable mixing between the $^4T_1(P)$ level and the higher-energy ^2G orbitals.

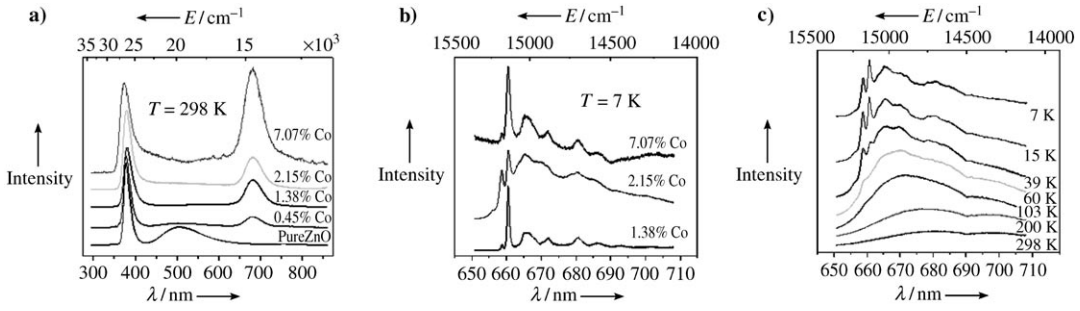


Figure 4. a) Room-temperature PL spectra of doped and undoped ZnO nanowires. The cobalt concentrations, as determined by EDX spectroscopy, are given above each spectrum. b) Low-temperature PL series of doped nanowires, which focus on the Co^{2+} ion transition ($^4T_1(P) \rightarrow {}^4A_2(F)$). c) Variable-temperature series of a sample of 2.15% Co-doped nanowires. All spectra have been vertically offset for clarity.

 © 2006 Wiley-VCH Verlag GmbH & Co. KGaA, Weinheim

This orbital mixing complicates assignment of the PL peaks. In addition, other factors that must be considered are the surrounding Zn^{2+} ions, which can exert an additional anisotropic C_{3v} crystal-field potential on the dopant Co^{2+} ions, as well as the zero-field splitting parameter of the cobalt dopant. We consistently observed at least five peaks below 40 K in our low-temperature PL spectra. Their centers, from highest energy, are located at 15190, 15150, 15015, 14887, and 14700 m^{-1}. The fine structure is lost due to increased thermal energy above this temperature. We can relate these peaks to $^4T_1(P)$, $^2T_1(G)$, $^2E(G)\rightarrow$ground-state $^4A_2(F)$ internal Co^{2+} transitions based on previous reports.[20,21]

Finally, we examined the interaction of the cobalt dopant with the host ZnO semiconductor by electron paramagnetic resonance (EPR) spectroscopy. This technique has been used previously to characterize the environment of paramagnetic species in host lattices, such as $BaTiO_3$,[22,23] TiO_2,[24] and ZnO.[25,26] A series of EPR spectra at various temperatures is plotted in Figure 5a. A large resonance with a peak-to-peak

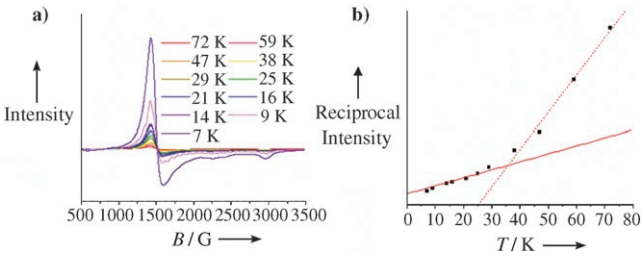


Figure 5. a) Temperature-dependent EPR spectra of $Zn_{1-x}Co_xO$ nanowires (Co = 2.15%). b) Reciprocal intensity versus temperature for the same sample. Intensities were obtained by numerical integration of the as-collected spectra twice. The solid line is a plot of the Curie Law, and the dashed line is fitted to the higher-temperature data points.

bandwidth of nearly 180 Gauss dominates the spectrum, with an additional smaller resonance that appears at higher field. The Landé g factors can be calculated as 4.43 and 2.23, which are assigned to $g_\perp$ and $g_\parallel$, respectively.[26] The reciprocal EPR intensity versus temperature for the sample of 2.15% Co is plotted in Figure 5b. The Curie Law predicts that this would be a straight line for isolated, paramagnetic Co^{2+} ions;[27] however, we observe a deviation from Curie behavior in the temperature region 25–30 K. The behavior is found in other nanowire samples with different cobalt concentrations as well. However, we are limited to measuring lightly doped nanowires by this method; nanowires with a cobalt concentration greater than 3% give very weak signals because of increased dipolar coupling between the cobalt centers.

This apparent deviation from normal paramagnetic behavior is interesting, particularly in light of various reports on the magnetic properties of this system. Indeed, many of those data, including our own and the studies cited herein, show magnetic behavior that cannot be modeled by a simple paramagnetic or ferromagnetic mechanism. It is a rather complex phenomenon, particularly considering the fact that detailed structural characterization indicates that transition-metal doping is homogenous and that there are no secondary phases present.

In summary, we have presented the synthesis of $Zn_{1-x}Co_xO$ nanowires from a solution-based synthetic route. Structural, optical, and spectroscopic characterizations indicate that the cobalt doping is substitutional for zinc cations in the host lattice. Although all signs suggest a completely uniform doping process, we note the existence of complex magnetic behavior that raises the possibility of multiple magnetic phases. Investigations are ongoing by us to elucidate the true nature of the observed magnetic behavior further.

Experimental Section

In a typical synthesis, zinc acetate (2.66 mmol) and cobalt(II) acetate (0.13 mmol, 0.05 equiv; a dopant concentration of 1.38 atom%) were mixed in a round-bottomed flask with trioctylamine (25 mL). The flask was fitted with a condenser and rapidly heated to 310 °C. The solids dissolved as the temperature increased, and the solution changed from clear to royal blue. The solution turned green after approximately 15–20 min, thus indicating the start of nanowire formation. The reaction was continued for 45–180 min depending on the length of wires desired and cooled to room temperature. The green precipitate was washed several times with ethanol to remove any cobalt precursor, as well as any cobalt metal particles. The green suspensions are stored in ethanol, and dilute solutions are stable for months. A typical synthesis yields approximately 60 mg of nanowires. The average cobalt concentration in the nanowires is typically 2–3% less than the amount added at the start of the reaction.

SEM images were taken on a JEOL-6340F field-emission scanning electron microscope operated at 5.0 kV. TEM images and EDX and EELS spectra were acquired on a Phillips CM200-FEG transmission electron microscope operated at 200 kV. Powder X-ray diffraction measurements were taken on a Bruker D-8 general area diffraction detection system. The X-ray source was $Co_{K\alpha}$ ($\lambda = 1.79$ Å).

PL measurements were performed on a single bundle of nanowires at each Co concentration by excitation with a He–Cd continuous wave laser emitted at 325 nm. A liquid-He-cooled cryostat was used for low-temperature PL measurements. EPR spectra were acquired on a Bruker EMX spectrometer operating at X-band (9.25 GHz) microwave frequency. The spectra were taken at a modulation amplitude of 2.5 Gauss and a microwave power of 10 mW. The g values were calculated from the resonance equation $h\nu = g\beta H_r$ (h is the Planck constant, ν is the microwave frequency, β is the Bohr magneton, and H_r is the resonant magnetic field).

Received: September 6, 2005
Published online: December 12, 2005

Keywords: doping · nanostructures · nanowires · semiconductors

[1] T. Dietl, H. Ohno, F. Matsukara, J. Cibert, D. Ferrand, *Science* **2000**, *287*, 1019.
[2] K. Sato, H. Katayama-Yoshida, *Phys. E* **2001**, *10*, 251.
[3] P. Sharma, A. Gupta, K. V. Rao, F. J. Owens, R. Sharma, R. Ahuja, J. M. O. Guillen, B. Johansson, G. A. Gehring, *Nat. Mater.* **2003**, *2*, 673.
[4] K. Ueda, H. Tabata, T. Kawai, *Appl. Phys. Lett.* **2001**, *79*, 988.
[5] D. C. Kundaliya, S. B. Ogale, S. E. Lofland, S. Dhar, C. J. Metting, S. R. Shinde, Z. Ma, B. Varughese, K. V. Ramanujachary, L. Salamanca-Riba, T. Venkatesan, *Nat. Mater.* **2004**, *3*, 709.

 © 2006 Wiley-VCH Verlag GmbH & Co. KGaA, Weinheim

[6] J. H. Kim, H. Kim, D. Kim, Y. Ihm, W. K. Choo, *J. Eur. Ceram. Soc.* **2004**, *24*, 1847.
[7] J. H. Park, M. G. Kim, H. M. Jang, S. Ryu, Y. M. Kim, *Appl. Phys. Lett.* **2004**, *84*, 1338.
[8] S. Ramachandran, A. Tiwari, J. Narayan, *Appl. Phys. Lett.* **2004**, *84*, 5255.
[9] Y. Q. Chang, D. B. Wang, X. H. Luo, X. Y. Yu, X. H. Chen, L. Li, C. P. Chen, R. M. Wang, J. Xu, D. P. Yu, *Appl. Phys. Lett.* **2003**, *83*, 4020.
[10] J.-J. Wu, S.-C. Liu, M.-H. Wang, *Appl. Phys. Lett.* **2004**, *85*, 1027.
[11] L. Greene, M. Law, J. Goldberger, F. Kim, J. Johnson, Y. Zhang, R. Saykally, P. Yang, *Angew. Chem.* **2003**, *115*, 3139; *Angew. Chem. Int. Ed.* **2003**, *42*, 3031.
[12] L. Vayssieres, *Adv. Mater.* **2003**, *15*, 464.
[13] M. Yin, Y. Gu, I. L. Kuskovsky, T. Andelman, Y. Zhu, G. F. Neumark, S. O'Brien, *J. Am. Chem. Soc.* **2004**, *126*, 6206.
[14] D. A. Schwartz, N. S. Norberg, Q. P. Nguyen, J. M. Parker, D. R. Gamelin, *J. Am. Chem. Soc.* **2003**, *125*, 13205.
[15] D. A. Schwarz, K. R. Kittilstved, D. R. Gamelin, *Appl. Phys. Lett.* **2004**, *85*, 1395.
[16] Z. L. Wang, J. S. Yin, Y. D. Jiang, *Micron* **2000**, *31*, 571.
[17] D. H. Pearson, B. Fultz, C. C. Ahn, *Appl. Phys. Lett.* **1988**, *53*, 1405.
[18] H. A. Weakliem, *J. Chem. Phys.* **1962**, *36*, 2117.
[19] J. Ferguson, D. L. Wood, L. G. Van Uitert, *J. Chem. Phys.* **1969**, *51*, 2904.
[20] H.-J. Schulz, M. Thiede, *Phys. Rev. B* **1987**, *35*, 18.
[21] P. Koidl, *Phys. Rev. B* **1977**, *15*, 2493.
[22] E. Possenriede, P. Jacobs, O. F. Schrimer, *J. Phys. Condens. Matter* **1992**, *4*, 4719.
[23] R. N. Schwartz, B. A. Wechsler, *Phys. Rev. B* **1993**, *48*, 7057.
[24] B. Z. Rameev, F. Yildiz, L. R. Tagirov, B. Aktas, W. K. Park, J. S. Moodera, *J. Magn. Magn. Mater.* **2003**, *258*, 361.
[25] N. Jedrecy, H. J. von Bardeleben, Y. Zheng, J.-L. Cantin, *Phys. Rev. B* **2004**, *69*, 041308.
[26] M. Diaconu, H. Schmidt, A. Pöppl, R. Böttcher, J. Hoentsch, A. Klunker, D. Spemann, H. Hochmuth, M. Lorenz, M. Grunmann, *Phys. Rev. B* **2005**, *72*, 085214.
[27] J. E. Wertz, J. R. Bolton, *Electron Spin Resonance*, Chapman and Hall, New York, **1986**, p. 458.

 © 2006 Wiley-VCH Verlag GmbH & Co. KGaA, Weinheim

Total Synthesis

DOI: 10.1002/anie.200501995

Total Synthesis, NMR Solution Structure, and Binding Model of the Potent Histone Deacetylase Inhibitor FR235222**

Manuela Rodriquez, Stefania Terracciano, Elena Cini, Giulia Settembrini, Ines Bruno, Giuseppe Bifulco, Maurizio Taddei, and Luigi Gomez-Paloma**

The organization of DNA into chromatin plays a major role in gene regulation. Changes in chromatin architecture (chromatin remodeling) can be modulated by acetylation, methylation, phosphorylation, and ubiquitination of N-terminal histone tails.[1] Histone acetylation is the best-understood mechanism of chromatin remodeling, and is essentially governed by the antagonistic activity of histone acetyltransferases (HATs) and histone deacetylases (HDACs).[2] As acetylation is a key component of gene expression, HAT and HDAC inhibitors or activators have been studied as potential therapeutic agents.[3] In the frame of the various histone acetylase inhibitors, natural cyclopeptides play an important role as reversible or irreversible zinc chelators with effective anticancer and antiprotozoal activities. The conformational features of selected members of this class of compounds (for example, apicidin and congeners) have been established by X-ray and NMR spectroscopic studies and by comparison of their biological activity with that of simplified synthetic analogues.[4]

Cyclopeptide FR235222 (**1**; see Scheme 2), which was recently isolated from the fermentation broth of *Acremonium* sp.,[5] showed a potent and selective inhibition of T cell

[*] Dr. M. Rodriquez, E. Cini, G. Settembrini, Prof. M. Taddei
Dipartimento Farmaco Chimico Tecnologico
Università di Siena
via A. Moro 2, 53100 Siena (Italy)
Fax: (+39) 0577-234-333
E-mail: taddei.m@unisi.it

Dr. M. Rodriquez, Dr. S. Terracciano, Prof. I. Bruno, Prof. G. Bifulco, Prof. L. Gomez-Paloma
Dipartimento di Scienze Farmaceutiche
Università di Salerno
via Ponte don Melillo, 84084 Fisciano, Salerno (Italy)
Fax: (+39) 089-962-828
E-mail: gomez@unisa.it

[**] Financial support by the University of Salerno, the University of Siena, and MIUR (Rome) is gratefully acknowledged. L.G.P., I.B., and G.B. also wish to acknowledge the use of the instrumental (NMR spectroscopy and mass spectrometry) facilities of the Center of Competence in Diagnostics and Molecular Pharmaceutics supported by Regione Campania (Italy) through POR funds. L.G.P. thanks Professor R. Abagyan for the use of ICM 3.2 (The Scripps Research Institute and Molsoft LLC, La Jolla, USA). We thank undergraduates P. De Nicola, M. De Vito, and F. Cristofano for technical assistance.

Supporting information for this article is available on the WWW under http://www.angewandte.org or from the author.

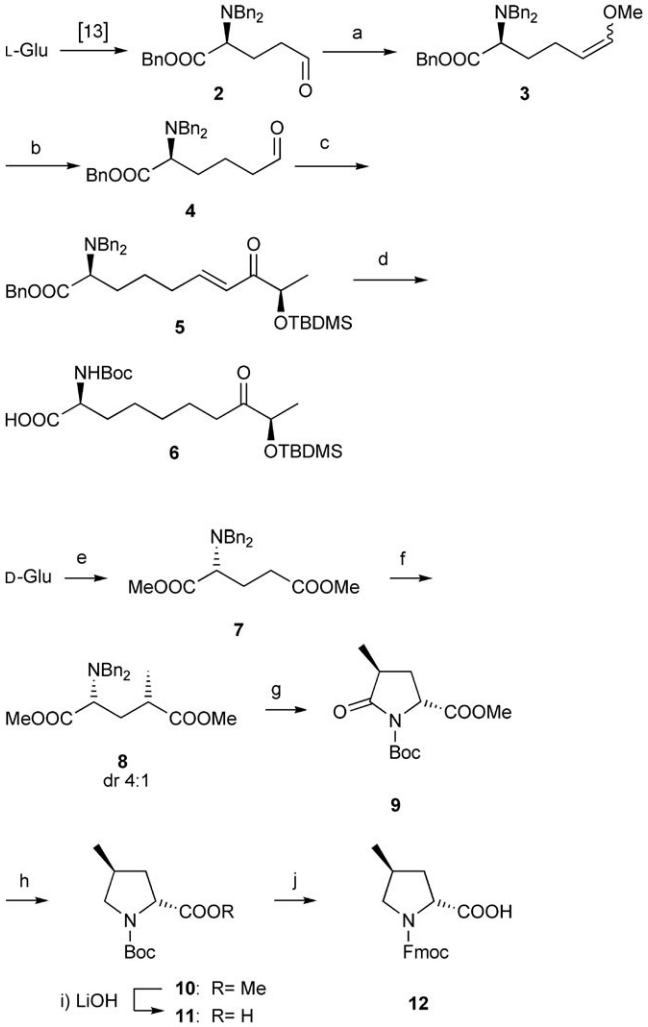
© 2006 Wiley-VCH Verlag GmbH & Co. KGaA, Weinheim

proliferation and lymphokine production, and also exhibited a potent inhibition of HDAC.[6] This immunosuppressant activity highlights **1** as an attractive target for chemical synthesis and, in fact, Ma and co-workers recently reported its total synthesis.[7] The availability of a synthetic sample of **1** was also deemed important to examine its HDAC binding features, taking into account that details of the determinants for the recognition between cyclopeptides and HDAC enzymes are only partly and indirectly known. Finally, besides the inherent interest evoked by its biological properties, we envisaged that a convergent synthetic approach, combined with key information on its bioactive conformation and HDAC binding interaction, would pave the way to the assembly of focused libraries of simplified agents and to the rational design of more powerful and selective analogues.

Hence, in the context of our continuous efforts in synthesizing peptide-related molecules,[8] and animated by the opportunities that would result in terms of chemical biology and medicinal chemistry studies,[9] we looked for an effective and possibly flexible route to **1**. Even at first glance it is apparent that the most difficult task, from a synthetic viewpoint, resides in the stereoselective access to the two key noncoded amino acids present in **1**, namely (2*S*,9*R*)-2-amino-9-hydroxy-8-oxodecanoic acid (Ahoda) and *trans*-4-methyl-D-proline, in the form of suitably protected building blocks for their subsequent incorporation into standard solid-phase peptide chemistry protocols.

Ahoda, the long-chain α-amino acid residue, is a typical structural element of class I and II HDAC peptide inhibitors,[3b] all of which invariably present one of such substrate-analogue moieties,[10] with the function to chelate the Zn^{II} ion in the active site. Although Ahoda is present in many other cyclopeptide HDAC inhibitors,[4b,11] only one synthesis has been reported to date.[7,12] We decided to follow a retrosynthetic approach, in which the configuration at C2 was derived from L-glutamic acid and the configuration at C9 was derived from (*R*)-lactic acid. Thus, compound **2**, prepared as previously reported,[13] was homologated to the six-carbon-chain aldehyde **4** via the enol ether **3** (Scheme 1). Wittig–Horner–Emmons reaction with dimethyl (*R*)-[3-(*tert*-butyldimethylsilyloxy)-2-oxobutyl]phosphonate[14] gave compound **5** in good yield as a single diastereoisomer. Reduction and contemporaneous protecting-group exchange was carried out by catalytic hydrogenation (in a Parr apparatus) to give *N*-Boc-*O*-TBDMS-Ahoda (**6**), ready for use in peptide synthesis. HPLC and 600-MHz ^{1}H NMR analyses of **6** established that racemization did not occur along the full synthetic pathway.

Substituted prolines have been extensively investigated as rigid elements for conformationally restricted peptidomimetics, and many synthetic procedures have been described to implement a wide variety of functional groups on pyrrolidine-2-carboxy derivatives.[15] In particular, 4-methylproline (4-MePro), which is also present in other natural products,[16] has been recently prepared by stereocontrolled hydrogenation of the corresponding methylene derivative obtained from 4-hydroxyproline.[17] Appealing as it is, with its use of a naturally occurring starting material, this method becomes economically demanding when access to 4-MePro of the D series is desired, as in our case. In an attempt to rationalize our needs



Scheme 1. Reagents and conditions: a) $MeOCH_2PPh_3Cl$, KHDMS, THF, 0 °C; 75%; b) HCl/AcOEt; 94%; c) (*R*)-$(MeO)_2P(O)CH_2COCH(O$-TBDMS)CH_3, LiCl, DIEA, MeCN; 87%; d) $Pd(OH)_2$, H_2 (6 atm), Boc_2O, MeOH; 75%; e) BnBr, NaOH, Na_2CO_3, H_2O followed by $SOCl_2$ in MeOH; 76%; f) KHMDS, THF, MeI, −78 °C; 92%; g) $Pd(OH)_2$, H_2 (6 atm), MeOH, then Boc_2O, Et_3N, DMAP, MeCN followed by column chromatography; 60%; h) $BH_3{\cdot}Me_2S$ in THF, 40 °C, 72 h; 60%; i) LiOH, THF, H_2O; j) TFA/CH_2Cl_2, TIS, followed by FmocOSu, Na_2CO_3, H_2O; 77%. KHMDS = potassium 1,1,1,3,3,3-hexamethyldisilazane, TBDMS = *tert*-butyldimethylsilyl, DIEA = ethyldiisopropylamine, Boc = *tert*-butyloxycarbonyl, Bn = benzyl, DMAP = 4-dimethylaminopyridine, TFA = trifluoroacetic acid, TIS = triisopropylsilane, FmocOSu = 9-fluorenylmethyloxycarbonyl-*N*-hydroxysuccinimide.

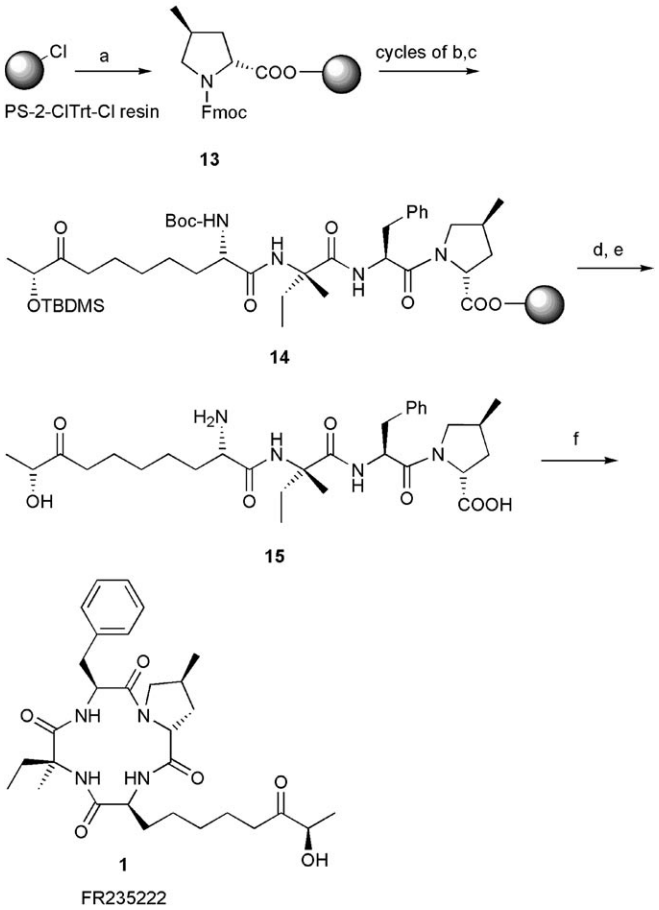
in terms of the chiral pool,[18] we sought an efficient route by starting again from glutamic acid. Clearly, a key step was the stereoselective preparation of (2*R*,4*S*)-4-MeGlu.

Special care was taken in the selection of the protection scheme, as it was known that the NHBoc group strongly favors the attack of MeI on the opposite side of the Glu γ-enolate, as a consequence of a chelat-ion-controlled transition state.[19] Assuming that the formation of another anionic site at the nitrogen atom was therefore detrimental for our purposes, we found that the *N*,*N*-dibenzyl dimethyl ester **7** could be stereoselectively methylated in position 4 to give **8** as a 4:1 mixture of diastereomers.[20] Upon catalytic hydro-

 © 2006 Wiley-VCH Verlag GmbH & Co. KGaA, Weinheim

genation, **8** directly produced the ring-closure lactam, from which, after *N*-Boc protection, the major isomer **9** was isolated by column chromatography (60% yield). The configuration of **9** was determined by comparison with previously reported NMR data.[15,21] Chemoselective reduction of the lactam carbonyl group, followed by ester hydrolysis and Boc/Fmoc protecting-group exchange, finally gave the required Fmoc-amino acid **12** in three steps (46% yield).

With compounds **6** and **12** in hand, the synthesis of **1** was attempted by following a typical solid-phase peptide chemistry protocol (Scheme 2), using a 2-chlorotrityl resin.[22] Fmoc-D-4-MePro was loaded on the resin and followed by HATU/HOBT promoted couplings with L-Phe and L-Iva. Product **6** was introduced as the last amino acid before cleavage from the resin with AcOH/TFE/TIS, which gave the linear precursor (**15**) of FR235222 in 70% yield. After removal of TBDMS and Boc groups from Ahoda by treatment with TFA/H_2O/TIS (95% yield),[23] the unprotected linear tetrapeptide was cyclized by exposure to HATU (2 equiv) and DIEA (2 equiv) in a very dilute solution to avoid side formation of the cyclodimeric sequence of **1** as by-product. The cyclized product was obtained in 68% yield after purification by HPLC. The analytical data ($[\alpha]_D$, electrospray mass spectrometry, ^1H and ^{13}C NMR spectroscopy) measured on the synthetic sample were virtually indistinguishable from those reported for the natural product.[24]



Scheme 2. Final stages of the total synthesis of **1**: a) DIEA, CH_2Cl_2; b) 20% piperidine, DMF; c) Fmoc-AA or Ahoda derivative **6**, HOBT, HBTU, NMM, DMF; d) AcOH/TFE/CH_2Cl_2 (2:2:6); e) TFA/H_2O/TIS (94:4:1); f) HATU, CH_2Cl_2, $c = 7.7 \times 10^{-5}$ M. DIEA = *N*,*N*-diisopropylethylamine, DMF = *N*,*N*-dimethylformamide, AA = amino acid, HOBT = *N*-hydroxybenzotriazole, HBTU = *O*-(benzotriazol-1-yl)-1,1,3,3-tetramethyluronium hexafluorophosphate, NMM = *N*-methylmorpholine, TFE = 2,2,2-trifluoroethanol, PS-2-ClTrt-Cl resin = polystyrene/2-chlorotrityl chloride resin.

Next we determined the solution conformation of **1**, a logical prerequisite for the subsequent analysis of the nature of its binding interactions with HDAC enzymes. Although cyclopeptides represent an important class of HDAC inhibitors with potential activity as antitumor and antiprotozoal compounds, no relevant information on the type and nature of the molecular determinants for their interactions with HDAC isozymes has yet been reported. The crystal structures of HDAC–ligand complexes are, in fact, limited to small-molecule inhibitors, such as trichostatin A (TSA) and suberoylanilide hydroxamic acid (SAHA), with no examples of inhibitors with a large head (cap) group.[25] A conformational analysis of **1** was carried out by restrained molecular mechanics (MM) and dynamics (MD) calculations (1 ns, see Supporting Information).

The solution structure depicted in Figure 1 was obtained by using 21 distance constraints, previously collected in a series of ROESY spectra ($CDCl_3$ and [D_6]DMSO, 600 MHz, $t_{mix} = 50$, 100, and 150 ms). Visual inspection of this conformation shows that the molecule consists of a central core, which comprises the tetrapeptide backbone, the methylproline (MePro) ring, and the whole isovaline moiety, from which phenylalanine and Ahoda side-chain appendages project facing in opposite directions (Figure 1). The MePro residue is characterized by a *trans* geometry of its peptide linkage, as witnessed by an intense ROESY cross-peak between H^{α} of Phe and $H^{\delta}{}_2$ of MePro. The tetrapeptide backbone describes a γ turn and a γ inverse turn, as indicated by the ϕ/ψ torsion angle values (4-MePro: +76/−83; Ahoda: +78/−60; Iva: −89/+93; Phe: −108/+102). Three hydrogen-bonding interactions, all between residues i and $i+2$, stabilize the two γ turns. Thus, the Phe-CO and NH moieties are H-bonded to Ahoda-NH and CO (2.09 and 1.92 Å, respectively), whereas 4-MePro-CO is weakly H-bonded to Iva-NH (2.7 Å).

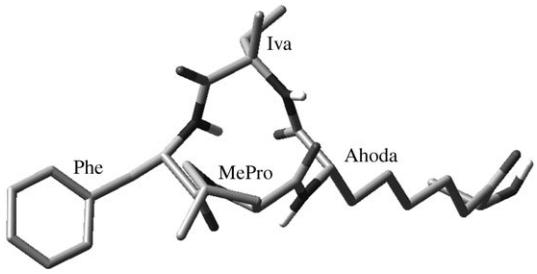


Figure 1. NMR solution conformation of FR235222 (**1**) obtained by restrained MD calculations by using ROESY ($t_{mix} = 100$ ms) data collected at 600 MHz in $CDCl_3$ and [D_6]DMSO.

The next step was a docking study between FR235222 (**1**) and HDAC with the software ICM 3.2 (MolSoft LLC,

 © 2006 Wiley-VCH Verlag GmbH & Co. KGaA, Weinheim

La Jolla, CA), which takes advantage of a particularly efficient proprietary docking algorithm. For ICM docking the receptor is represented by a series of grid potentials, and both ligand and receptor are flexible and explicit molecules. Moves of ligand and receptor (side chain and loops) are computed on the basis of pseudo-Brownian dynamics.[26] The docking procedure was first validated by reproducing TSA positioning in the histone deacetylase-like protein (HDLP) binding pocket, with the TSA–HDLP complex (3D coordinates: PDB archive code 1C3R) as reference.[25,27] As the final root-mean-square deviation (RMSD) computed on TSA heavy atoms (docked versus X-ray) was less than 0.1 Å, we proceeded further on docking FR235222. Figure 2 shows an

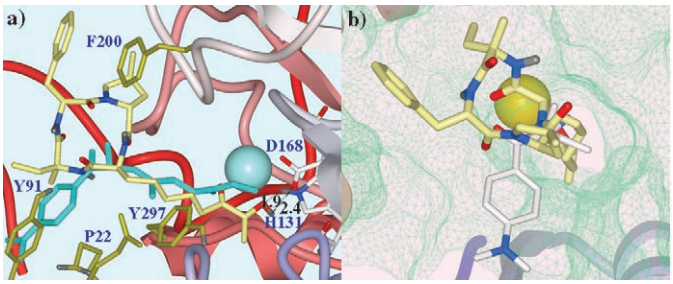


Figure 2. a) 3D model of the interaction between FR235222 (**1**) and HDLP. For a more convenient visual inspection of the positioning of **1** in the active site, TSA is also displayed in cyan. The protein is represented by ribbons (blue to red, N to C terminus) with only a selection of side chains shown. Gold: side chains externally delimiting the binding site; white: those involved in H-bonding interactions (black dashed lines with distances in Å). Only heavy atoms are displayed, except for polar hydrogen atoms (gray). The Zn^{II} ion is represented by a CPK sphere in light blue. b) The different kinds of surface complementarity exhibited by TSA (carbon atoms: white) and FR235222 (carbon atoms: yellow) cap groups toward HDLP are shown. The HDLP molecular surface is depicted as green wire frames (see also text).

expanded view of the model of FR235222 bound to the active site of HDLP. To allow a meaningful comparison, TSA is also displayed in the same original positioning as that found in the crystallographic structure of the TSA–HDLP complex. Notably, this 3D model highlights the fact that, although substantially different in cap groups, both TSA and FR235222 project their zinc-chelating elements in a very similar fashion.

Among the principal polar interactions that stabilize the FR235222 molecule within the HDAC binding pocket, the two oxygen atoms of the α-hydroxyketone terminal function of Ahoda embrace the metal ion, with the hydroxy group also involved in two key ligand–protein hydrogen bonds with H131 and D168, two of the main residues taking an active role in the enzymatic catalysis (see Figure 2a). Van der Waals interactions are also of great importance in the FR235222–HDLP recognition process, especially for the accommodation of the cap group. Indeed, the tetrapeptide cap group of **1** and the outward side of the enzyme exhibit complementary surfaces that correspond with the rim of the tubular pocket that leads to the zinc ion, the latter being filled by the Ahoda long chain.

Also remarkable is the difference of positioning between the TSA and FR235222 head groups (Figure 2b). On the basis of such a model, our hypothesis is that cyclic tetrapeptide inhibitors of this kind are able to bind with high affinity to HDAC because there is a large, shallow cavity that can accommodate the globe-shaped tetrapeptide core, thus allowing the substrate-mimetic chain to extend and reach the zinc ion. In more detail, the phenyl group of TSA is bent toward Y91 (E98 in HDAC1) and P22 (P29), whereas the FR235222 macrolactam domain is projected on the other side, and fills a cavity delimited by F200 and Y91 (Figure 2a). The role of the methyl group of 4-MePro raises the speculation that more bulky groups at this position could potentially allow additional van der Waals and hydrophobic interactions with the protein surface. A final consideration relates to the backbone features of the cyclopeptide core. The consecutive γ turn and γ inverse turn are certainly essential for the correct global shape of the core and for the positioning of the Ahoda side chain. This should be taken into account for the design of simplified active analogues.

On the basis of this model it appears that, besides the macrolactam scaffold, three quite voluminous appendages may be housed within the cavity between F200 and Y91. In other words, there should be quite a wide range of allowed decorations that may conveniently replace the Phe and Iva residues of FR235222, a finding partly confirmed by structure–activity relationship data on cyclopeptide HDAC inhibitors of this type.[28] In a rational design of new peptidomimetic HDAC inhibitors, assuming that the zinc-binding element can be easily implemented by a variety of different solutions,[10] novel scaffolds should be selected from among rigid mono- or bicyclic elements bearing two or three decorating appendages. These should preferably be aromatic side chains to take advantage of the location of F200 and Y91, two sites for favorable π–π stacking interactions.

In conclusion, we have synthesized FR235222 (**1**) by using a convergent approach, classical solid-phase peptide synthesis (SPPS) protocols and macrolactamization in dilute solution. Two non-proteinogenic residues, Ahoda and 4-MePro, were stereoselectively prepared in suitably protected forms for their subsequent employment in SPPS. In addition, we have studied the NMR solution structure of **1** and, more importantly, carried out docking studies with HDAC-like protein. Our integrated study allowed us to derive a 3D model for cyclopeptide interaction with the active site of HDAC, thus highlighting critical differences between the binding modes of small-molecule and cyclopeptide inhibitors.

Received: June 9, 2005
Published online: November 28, 2005

Keywords: inhibitors · natural products · peptides · solid-phase synthesis · total synthesis

[1] a) M. Biel, V. Wascholowski, A. Giannis, *Angew. Chem.* **2005**, *117*, 3248–3280; *Angew. Chem. Int. Ed.* **2005**, *44*, 3186–3216; b) E. J. Richards, S. C. Elgin, *Cell* **2002**, *108*, 489–500; c) B. M. Turner, *Cell* **2002**, *111*, 285–291.

 © 2006 Wiley-VCH Verlag GmbH & Co. KGaA, Weinheim

[2] a) B. D. Strahl, C. D. Allis, *Nature* **2000**. *403*, 41 – 45; b) M. Izuka, M. M. Smith, *Curr. Opin. Genet. Dev.* **2003**, *13*, 154 – 160; c) D. Chung, *Trends Mol. Med.* **2002**, *8*, S10 – S11; d) H. Hess-Stummp, *Eur. J. Cell Biol.* **2005**, *84*, 109 – 121.

[3] For HAT inhibitors, see: a) M. Biel, A. Krestovali, E. Karatzali, J. Papamatheakis, A. Giannis, *Angew. Chem.* **2004**, *116*, 4065 – 4067; *Angew. Chem. Int. Ed.* **2004**, *43*, 3974 – 3976; for HDAC inhibitors, see: b) P. A. Marks, T. Miller, V. M. Richon, *Curr. Opin. Pharmacol.* **2003**, *3*, 344 – 351; c) T. A. Miller, D. J. Witter, S. Belvedere, *J. Med. Chem.* **2003**, *46*, 5097 – 5116.

[4] a) P. T. Meinke, P. Liberator, *Curr. Med. Chem.* **2001**, *8*, 211 – 235; b) S. B. Singh, D. L. Zink, J. M. Liesch, R. T. Mosley, A. W. Dombrowski, G. F. Bills, S. J. Darkin-Rattray, D. M. Schmatz, M. A. Goetz, *J. Org. Chem.* **2002**, *67*, 815 – 825.

[5] H. Mori, Y. Urano, F. Abe, S. Furukawa, S. Furukawa, Y. Tsurumi, K. Sakamoto, M. Hashimoto, S. Takase, M. Hino, T. Fujii, *J. Antibiot.* **2003**, *56*, 76 – 79.

[6] H. Mori, Y. Urano, F. Abe, S. Furukawa, S. Furukawa, F. Sakai, M. Hino, T. Fujii, *J. Antibiot.* **2003**, *56*, 80 – 86.

[7] W. Xie, B. Zou, D. Pei, D. Ma, *Org. Lett.* **2005**, *7*, 2775 – 2777. This publication appeared in print while our article was being reviewed.

[8] L. R. Lampariello, D. Piras, M. Rodriquez, M. Taddei, *J. Org. Chem.* **2003**, *68*, 7893 – 7895, and references therein.

[9] For a review on combinatorial libraries in medicinal chemistry, see: D. L. Boger, J. Desharnais, K. Capps, *Angew. Chem.* **2003**, *115*, 4270 – 4309; *Angew. Chem. Int. Ed.* **2003**, *42*, 4138 – 4176.

[10] The solutions sought by Nature and medicinal chemists to engineer substrate (acetyllysine) analogues for HDAC inhibition encompass various chains of appropriate length, all ending with a functional group with good metal-ion binding properties, such as hydroxamate, hydroxycarbonyl, or diamine groups. Accordingly, a relatively unsubstituted C_6 chain with a suitable end group can be considered the minimal structural requirement for HDAC inhibition, even if, for optimal activity, a so-called cap (head) group is also necessary. The latter is the most variable portion among different HDAC inhibitors, and ranges from a simple phenyl group to large molecular moieties, as in FR235222.

[11] For examples, see: a) Y. Masuoka, K. Shin-Ya, K. Furihata, K. Nagai, Y. Suzuki, H. Seto, *J. Antibiot.* **2001**, *54*, 187 – 190; b) K. Yoskimura, S. Tsuboya, K. Okazaky, *Chem. Abstr.* **1995**, *123*, 548.

[12] For synthesis of the simple 2-amino-8-oxodecanoic acid, see: a) J. A. Bajgrowicz, A. El Hallaoui, R. Jacquier, C. Pigiere, P. Viallefont, *Tetrahedron* **1985**, *41*, 1833 – 1841; b) W. Kuriyama, T. Kitahara, *Heterocycles* **2001**, *55*, 1 – 6; c) L. Mou, L. Singh, *Tetrahedron Lett.* **2001**, *42*, 6603 – 6606; d) S. Kim, E.-Y. Kim, H. Ko, Y. H. Jung, *Synthesis* **2003**, 2194 – 2198; e) T. S. Cooper, P. Laurent, C. J. Moody, A. K. Takle, *Org. Biomol. Chem.* **2004**, *2*, 265 – 276; f) M. Rodriquez, I. Bruno, E. Cini, M. Marchetti, M. Taddei, L. Gomez-Paloma, *J. Org. Chem.* **2005**, in press.

[13] M. Rodriquez, M. Taddei, *Synthesis* **2005**, *3*, 493 – 495.

[14] A. Chen, I. Savage, E. J. Thomas, P. D. Wilson, *Tetrahedron Lett.* **1993**, *34*, 6769 – 6772.

[15] For examples, see: a) A. M. P. Koskinen, H. Rapoport, *J. Org. Chem.* **1989**, *54*, 1859 – 1866; b) Q. Wang, N. A. Sasaki, P. Potier, *Tetrahedron* **1998**, *54*, 15759 – 15780; c) J. Zhang, W. Wang, C. Xiong, V. J. Hruby, *Tetrahedron Lett.* **2003**, *44*, 1413.

[16] T. Golakoti, W. Y. Yoshida, S. Chaganty, R. E. Moore, *Tetrahedron* **2000**, *56*, 9093 – 9102.

[17] J. L. Del Valle, M. Goodman, *J. Org. Chem.* **2003**, *68*, 3923 – 3931.

[18] An alternative route based on stereoselective taken into consideration, see: a) N. K. Yee, Y. Dong, S. R. Kapadia, J. J. Song, *J. Org. Chem.* **2002**, *67*, 8688 – 8691; b) J. K. Thottathil, J. L. Moniot, R. H. Mueller, M. K. Y. Wong, T. P. Kissick, *J. Org. Chem.* **1986**, *51*, 3140 – 3143. However, in our hands this route was less convenient.

[19] S. Hanessian, R. Margarita, *Tetrahedron Lett.* **1998**, *39*, 5887 – 5890.

[20] Unfortunately, the tetrabenzyl Glu derivative, an intermediate also used in Ahoda synthesis, showed too little reactivity under the same conditions, likely as a result of steric hindrance from the benzyl groups.

[21] M. C. Moody, D. W. Young, *J. Chem. Soc. Perkin Trans. 1* **1997**, 3519 – 3530.

[22] a) S. Terracciano, I. Bruno, G. Bifulco, J. E. Copper, C. D. Smith, L. Gomez-Paloma, R. Riccio, *J. Nat. Prod.* **2004**, *67*, 1325 – 1331; b) A. Napolitano, M. Rodriquez, I. Bruno, S. Marzocco, G. Autore, R. Riccio, L. Gomez-Paloma, *Tetrahedron* **2003**, *59*, 10203 – 10211.

[23] The amount of TIS used as carbocation scavenger had to be carefully adjusted, because of its ability to promote a reductive amination (as side reaction) between the free amino terminus and the Ahoda carbonyl group in position 8, which gives rise to an eight-membered ring.

[24] H. Mori, Y. Urano, T. Kinoshita, S. Yoshimura, S. Takase, M. Hino, *J. Antibiot.* **2003**, *56*, 181 – 185.

[25] M. S. Finnin, J. R. Donigian, A. Cohen, V. M. Richon, R. A. Rifkind, P. A. Marks, R. Breslow, N. P. Pavletich, *Nature* **1999**, *401*, 188 – 193.

[26] a) R. A. Abagyan, M. Totrov, D. Kuznetsov, *J. Comput. Chem.* **1994**, *15*, 488 – 506; for more recent applications of ICM docking, see: b) M. Shapira, B. M. Raaka, F. L. Sharmistha, M. Totrov, Z. Zhou, S. R. Wilson, R. A. Abagyan, H. G. Samuels, *Proc. Natl. Acad. Sci. USA* **2003**, *100*, 7354 – 7359; c) M. Shapira, R. A. Abagyan, M. Totrov, *J. Med. Chem.* **2003**, *46*, 3045 – 3059; d) C. N. Cavasotto, R. A. Abagyan, *J. Mol. Biol.* **2004**, *337*, 209 – 225.

[27] D. F. Wang, O. Wiest, P. Helquist, H. Y. Lan-Hargest, N. Wiech, *J. Med. Chem.* **2004**, *47*, 3409 – 3417.

[28] a) S. L. Colletti, R. W. Myers, S. J. Darkin-Rattray, A. M. Gurnett, P. M. Dulski, S. Galuska, J. J. Allocco, M. B. Ayer, C. Li, J. Lim, T. M. Crumley, C. Cannova, D. M. Schmatz, M. J. Wyvratt, M. H. Fisher, P. T. Meinke, *Bioorg. Med. Chem. Lett.* **2001**, *11*, 107 – 111; b) S. L. Colletti, R. W. Myers, S. J. Darkin-Rattray, A. M. Gurnett, P. M. Dulski, S. Galuska, J. J. Allocco, M. B. Ayer, C. Li, J. Lim, T. M. Crumley, C. Cannova, D. M. Schmatz, M. J. Wyvratt, M. H. Fisher, P. T. Meinke, *Bioorg. Med. Chem. Lett.* **2001**, *11*, 113 – 117; c) R. Furumai, Y. Komatsu, N. Nishino, S. Khochbin, M. Yoshida, S. Horinouchi, *Proc. Natl. Acad. Sci. USA* **2001**, *98*, 87 – 92.

 © 2006 Wiley-VCH Verlag GmbH & Co. KGaA, Weinheim

Materials Science

DOI: 10.1002/anie.200502318

"Perovskitization"-Assisted Electrochemical Reduction of Solid TiO_2 in Molten $CaCl_2$**

Kai Jiang, Xiaohong Hu, Meng Ma, Dihua Wang, Guohong Qiu, Xianbo Jin, and George Z. Chen**

The present inability to increase on-board hydrogen storage beyond 6 wt% of the storage materials and/or devices suggests that a longer time is needed before commercially viable hydrogen-powered vehicles join the battle against global warming. This situation would not be quite so constraining, however, if car manufacturers could replace steel components by titanium ones as both are equally strong but titanium is about 40% lighter (and more corrosion resistant). A lighter titanium car would then allow an additional load capacity for the heavy hydrogen-storage system. However, titanium (≈ $8000 per ton of sponge from the Kroll process) is far more expensive than steel (≈ $150 per ton of steel from carbothermic reduction; steel producers consequently emit about 5×10^{11} kg of CO_2 per annum into the atmosphere).

The discovery[1a,b] of direct electrochemical reduction of solid TiO_2 (an insulator) to Ti metal in molten $CaCl_2$ promises an alternative to the Kroll process, which consumes far more energy (45–55 kWh per kg of Ti) than the industrial production of other common metals (for example, 4–6 kWh kg^{-1} for steel and 12–14 kWh kg^{-1} for Al).[1–3] It also suggests innovative approaches to other metallic and semimetallic materials directly from the respective oxide powders by either electrolytic[1,4] or metallothermic means.[3,5] Industrial pilot tests of the electrolytic route have started,[6] but the most urgent need is to increase the electrolysis speed and current efficiency, both of which are currently unsatisfactory, probably owing to the slow process of removing dissolved oxygen from the metal phase.[1–6] However, this should not really be the case because the particles in the produced Ti pellet are usually 10–20 μm in size[1] and it has been demonstrated that the removal of oxygen from a 1–2-mm thick Ti foil takes only a few hours using the same method.[1b,3d]

In all reported studies of electroreduction of solid oxides, such as TiO_2,[1b,d,4a,7,8a] Nb_2O_5,[4b,c] Cr_2O_3,[1e,4d,8b] ZrO_2,[4e,f] NiO,[8b] SiO_2,[4g,h,8c,d] and various mixed oxides,[1c,f,4e] oxygen ionization ($MO_x + 2xe \rightleftarrows M + xO^{2-}$ or $MO_x + xCa^{2+} + 2xe \rightleftarrows M + xCaO$) has been confirmed to be the overall cathodic reaction, although the kinetic steps involved in the process were found to be much more complex. In particular, for TiO_2, Nb_2O_5, ZrO_2, and Cr_2O_3, calcium-enriched oxide or perovskite phases of various compositions are often observed in partially reduced cathodes. However, the mechanism of formation of these intermediate products and their influence on the reduction process are not fully understood.[1c,4a,7] For electroreduction of TiO_2 to Ti metal, there were also arguments for calcium deposition being a necessary step ($Ca^{2+} + 2e \rightleftarrows Ca$; $TiO_2 + 2Ca \rightleftarrows Ti + 2CaO$),[3,5] although such claims disagree with results from in-depth cyclic voltammetric investigations.[1d,7a]

Herein, we demonstrate a novel concept of perovskitization-assisted electroreduction of TiO_2 to Ti metal in molten $CaCl_2$. The result of this process is a significantly increased electrolysis speed and efficiency. In this context, "perovskitization" refers to the interaction or reaction between solid TiO_x ($1 \le x \le 2$) and calcium oxide or cation driven by chemical or electrochemical potentials, leading to structural transformation into perovskite phases that may have a general formula of $Ca_\delta TiO_x$ ($x/\delta \ge 2$).

Due to electric neutrality, the injection of electrons into a solid oxide can lead to either removal of oxygen anions,[1,4,7] which is needed for producing metals, or uptake of metal cations from the electrolyte into the oxide phase.[1a–e,4a,7] The latter occurs in Li-ion batteries and has been used to synthesize $LiTiO_2$ and $LiTi_2O_4$ in molten LiCl;[8a] similar processes are to be expected in molten $CaCl_2$.

Figure 1A presents a cyclic voltammogram (CV) of TiO_2 (curve a) in molten $CaCl_2$. Details of the Mo/oxide-powder working electrode and the Ag/AgCl reference electrode have been described elsewhere.[8] The CV exhibits three main reduction peaks at −0.23 V (c1), −0.41 V (c2), and −1.13 V (c3). Peak c3 possibly includes two unresolved processes, as implied by the inflexion at −1.02 V. In recent studies of thin TiO_2 coatings,[1d,7a] these features were attributed to $TiO_2 \rightarrow Ti_3O_5$ (c1) $\rightarrow Ti_2O_3$ (c2) $\rightarrow$ TiO $\rightarrow$ Ti (c3), respectively.[1d,7a] In particular, potentiostatic electrolysis at potentials around peaks c1 and c2 produced perovskite, which was claimed to result from the chemical reaction (1) where the O^{2-} ion results from partial electroreduction of TiO_2.[7a]

$$TiO_2 + Ca^{2+} + O^{2-}(\text{or } CaO) \rightleftharpoons CaTiO_3 \quad (1)$$

In this work, SEM and EDX analyses of the Mo–TiO_2 electrode after potentiostatic electrolysis also revealed that the product at potentials more-negative than peak c3 was Ti metal. However, at more-positive potentials, particularly around peaks c1 and c2, various titanate/titanite or perovskite phases were observed, but their O/Ti atomic ratio remained close to 2 and the Ca/Ti ratio was ≤ 0.5. We therefore believe

[*] K. Jiang, X. H. Hu, M. Ma, Dr. D. H. Wang, G. H. Qiu, Dr. X. B. Jin, Prof. Dr. G. Z. Chen
College of Chemistry and Molecular Sciences
Wuhan University
Wuhan, 430072 (P.R. China)
Fax: (+86) 27-6875-6319
E-mail: wangdh@whu.edu.cn
mel@whu.edu.cn
Prof. Dr. G. Z. Chen
School of Chemical, Environmental and Mining Engineering
University of Nottingham
Nottingham, NG72RD (UK)
Fax: (+44) 115-951-4115
E-mail: george.chen@nottingham.ac.uk

[**] The authors thank the National Natural Science Foundation of China for financial support (Grant No 20125308).

Supporting information for this article is available on the WWW under http://www.angewandte.org or from the author.

InterScience
© 2006 Wiley-VCH Verlag GmbH & Co. KGaA, Weinheim

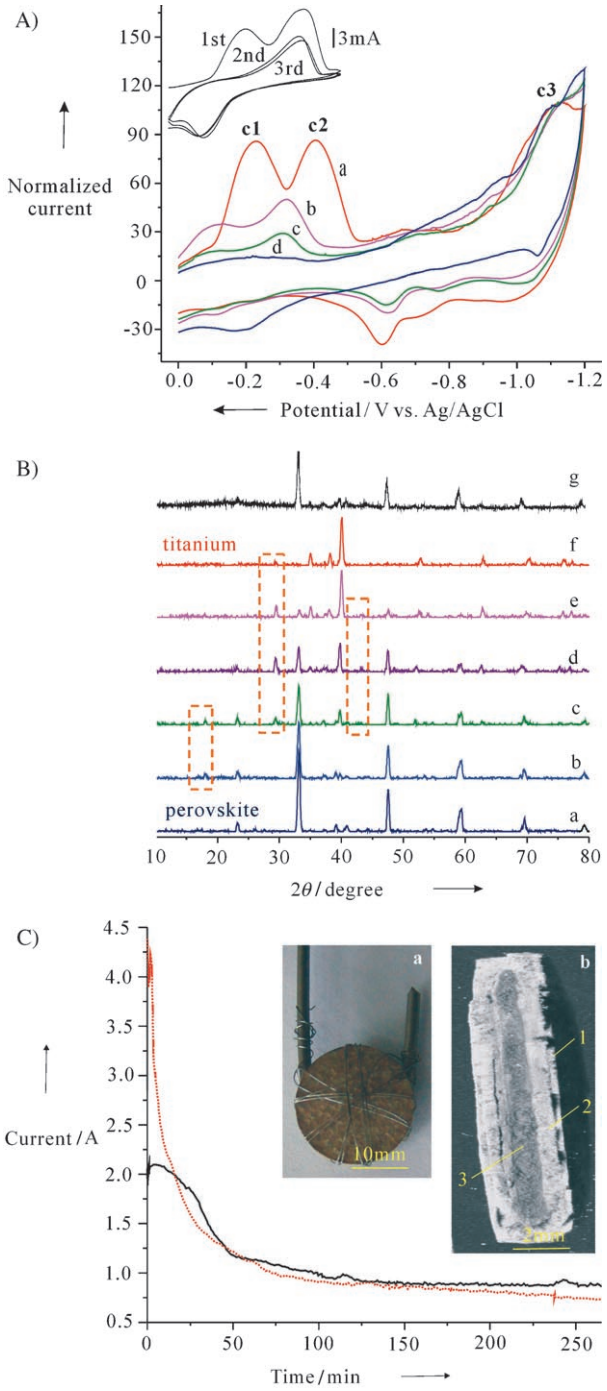


Figure 1. A) CVs of the Mo/perovskite-powder electrode at 850 °C. The powder was ground from perovskitized pellets of mixed TiO_2 and CaO with a Ca/Ti ratio of 0 (a), 0.25 (b), 0.5 (c), and 1.0 (d). Scan rate: 20 mVs^{-1}. The insert shows the consecutive CVs of the Mo–TiO_2 electrode in a narrower potential range. B) XRD spectra of synthetic $CaTiO_3$ before (a) and after electrolysis at 3.2 V and 850 °C for 10 (b), 30 (c), 60 (d), 120 (e), and 240 min (f). Spectrum (g) was measured from a partially reduced TiO_2 pellet. C) Current–time plots of the electrolysis of TiO_2 (dashed line, 1.0 g pellet) and $CaTiO_3$ (solid line, 1.7 g pellet) at 3.2 V and 850 °C. The inserts are (a) the $CaTiO_3$ pellet wrapped by Mo wires as an assembled cathode, and (b) the cross-section of a partially reduced TiO_2 pellet with the layered interior structure of (EDX analyses) 1: Ti metal; 2: perovskite, O/Ti = 1.49; 3: perovskite, O/Ti = 1.89. All results were obtained in molten $CaCl_2$.

electrochemical reactions (2) and (3) also occur.[1b–e,4a,7a]

$$TiO_2 + 2\alpha e \rightarrow TiO_x + \alpha O^{2-} \quad (x = 2-\alpha,\ 0 \le \alpha \le 0.5) \tag{2}$$

$$TiO_x + \delta Ca^{2+} + 2\delta e \rightleftharpoons Ca_\delta TiO_x \quad (0 \le \delta \le 0.5) \tag{3}$$

Continuous cycling of the potential to more-negative regions than peak c3 caused the current to decrease due to oxygen removal being irreversible in pure molten $CaCl_2$ that contains very few oxygen ions.[1d,7a] However, if limited to less-negative potentials, stable CV currents were observed.[1d] In particular, potential cycling around peaks c1 and c2 caused the two to merge, accompanied by the appearance of a reoxidation peak between 0.0 and −0.1 V, (insert, Figure 1 A). This behavior agrees with reactions (2) and (3).[1d,7a]

The SEM and EDX results also showed intermediate phases containing Ti and O (O/Ti ≤ 1), but no Ca, at potentials slightly more positive than peak c3. This can be explained by the perovskite decomposing when the oxygen content is lowered to a certain level, probably O/Ti = 1.[4a] Therefore, the electroreduction of TiO_2 may involve reactions (1)–(3) as well as reactions (4)–(7). Reaction (4) is a

$$TiO_x + CaO \rightarrow CaTiO_y \quad (1 + x = y \le 3) \tag{4}$$

$$CaTiO_y + 2\beta e \rightleftharpoons TiO_z + CaO + \beta O^{2-} \quad (\beta = y - z - 1) \tag{5}$$

$$Ca_\delta TiO_x + 2\gamma e \rightleftharpoons TiO_z + \delta CaO + \gamma O^{2-} \quad (\gamma > \delta,\ z \le 1) \tag{6}$$

$$TiO_z + 2ze \rightarrow Ti + zO^{2-} \tag{7}$$

more general form of reaction (1). Obviously, combinations of reactions (1)–(7) can lead to other reaction types[4a] but these should have the same overall thermodynamic consequences.

When electrolyzing the large TiO_2 porous preforms that are presently used in industrial tests, in situ perovskitization, represented by reactions (1), (3), and (4), causes expansion in the solid phase and slows ion transport in the pores existing between the oxide particles.[1c,d,7] In previous work[1c,7b] and herein, it was observed that, before full reduction, electrolyzed TiO_2 pellets, even at voltages higher than 3.0 V, always have layered structures, as shown in Figure 1 C b. EDX analyses revealed a large amount of Ca in the inner layers whose O/Ti ratios were, however, different (core > intermediate layer). The XRD spectra of these partially reduced TiO_2 pellets indicate the presence of a perovskite phase (see Figure 1 B g and Table 1).

On the basis of these findings and analyses, we can conclude that in situ perovskitization proceeds inevitably by both electrochemical and chemical reactions during the electroreduction of solid TiO_2 in molten $CaCl_2$. The perovskite phases formed can be further reduced to Ti at more-negative potentials, but they also retard the electroreduction kinetically. Therefore, if in situ perovskitization can be avoided, electrolysis of TiO_2 preforms should be faster.

We achieved ex situ partial and full perovskitization by sintering a pressed mixture of TiO_2 and CaO or $Ca(OH)_2$ powders at 1300 °C (see Figure 2 A and Experimental Sec-

 © 2006 Wiley-VCH Verlag GmbH & Co. KGaA, Weinheim

Table 1: XRD phase analyses of different electrolysis products.

TiO_2, 900 °C	3.0 V, 0.5 h	perovskite (81.3 %) + Ti_2O_3 (18.7 %)
	3.0 V, 2 h	perovskite (83.7 %) + Ti_2O_3 (10.6 %) + Ti_3O_5 (5.7 %)
	3.0 V, 4 h	perovskite (89.9 %) + TiO (11.1 %)
TiO_2, 900 °C	2.8 V, 1 h	perovskite (50.7 %; *31.2 %*)[a] + TiO_2 (49.3 %; *68.8 %*)[a]
	2.8 V, 2 h	perovskite (*65.6 %*)[a] + Ti_3O_5 (*18.2 %*)[a] + unknown (*16.2 %*)[a]
$CaTiO_3$, 850 °C	2.8 V, 5 h	Ti (*87.2 %*)[a,b] + unknown (*12.8 %*)[a]
	2.6 V, 5 h	Ti (*51.8 %*)[a,b] + perovskite (*38.8 %*)[a] + unknown (*9.4 %*)[a]
	2.4 V, 11.5 h	Ti (*50.1 %*)[a,b] + perovskite (*37.7 %*)[a] + unknown (*12.2 %*)[a]

[a] The presence of some unknown phases prevented the XRD spectrum quantitative analysis software from determining the proportions of the different phases observed. The numbers in italics were estimated from the area of the strongest XRD peak of each phase and are presented here as approximate references with caution. Use of the total area of three of the strongest peaks of each phase led to similar results. [b] The electrolyzed $CaTiO_3$ samples listed in the table fell apart into a powder after washing in water, and contained up to 7 wt % oxygen as measured by LECO. Their XRD spectra exhibit all the main titanium peaks, although these were shifted to lower diffraction angles close to those of the standard Ti_xO ($x \geq 2$) phases. The negative shifts of the Ti peaks are understandable because of lattice expansion caused by dissolved oxygen. The XRD spectra of typical fully and partially electrolyzed $CaTiO_3$ samples are presented in the Supporting Information.

tion). The CVs of the synthetic powder are also shown in Figure 1 A. The currents on these CVs are normalized against peak c3. It can be seen that peaks c1 and c2, which lead to in situ perovskitization according to the above discussion, have been effectively supressed. Figure 1 C compares the current–time plots recorded during electrolysis of similar $CaTiO_3$ and TiO_2 pellets under identical conditions. Interestingly, the current in TiO_2 is obviously larger than that in $CaTiO_3$ for the first 20 min. This may be due to reactions (2) and (3) occurring with TiO_2 but not with $CaTiO_3$. XRD analyses of the electrolysis products at different times (Figure 1 B) revealed that the metal phase grows at the expense of the perovskite phase, and at least one early and one later intermediate phase appear and vanish with time (see the peaks enclosed in the vertical rectangles in Figure 1 B and also data in Table 1 and Figure S3 in the Supporting Information). These results may indicate that $CaTiO_3$ is reduced to Ti via relatively stable intermediate Ti^{III} and/or Ti^{II} states, thereby supporting reactions (5) and (6).[7a] The oxygen content in the $CaTiO_3$ pellet electrolyzed for 265 min at 3.2 V was lower than the detection limit of EDX over relatively large areas inspected by SEM (Figure 2), and was only 2800 ppm according to fusion elemental analysis. In contrast, an identical TiO_2 pellet electrolyzed for 265 min showed a very thin metallic surface but its interior still contained layered perovskite phases similar to those shown in Figure 1 B g and 1 C b. Complete reduction of the TiO_2 pellet to Ti metal (2100 ppm oxygen) took about 600 min. Clearly, the faster reduction of $CaTiO_3$ occurs because in situ perovskitization is avoided. The removal of CaO [reaction (5)] may also leave a more porous structure and very fine TiO_z particles, both of which help to speed up the electrolysis.

Three more points are worth mentioning. First, the CVs of simply mixed TiO_2 and CaO powders show some, although limited, changes of peaks c1 and c2. Second, in the presence of trace amounts of Mg (< 0.3 wt %), Mg-containing phases (often crystallites) were detected in partially reduced TiO_2 electrodes by SEM and EDX.[8c,d] The highest atomic ratios were Mg/Ti ≈ 0.5 and O/Ti ≈ 1.5, in agreement with a process similar to reaction (3) that deserves more general investigation.[8a] Third, although electrolysis of $CaTiO_3$ was faster, the current efficiency still remained low (28 % for $CaTiO_3$ vs. 15 % for TiO_2). The large background current (Figure 1 C) due to electronic conduction in the melt[9] and cell configuration might be responsible, and these are being addressed separately.[1g]

Finally, the reduction of TiO_2 preforms by Ca vapor was recently reported to be quicker in the presence of CaO or $CaCl_2$.[3b] However, the additives were used as a flux (for by-product) and the trace $CaTiO_3$ phase in the sintered (800 °C) preform was ignored. More recently, the electrochemical reduction of solid Nb_2O_5 in the presence of small amounts of carbon (< 5 wt %), $CaCO_3$, and/or CaO (< 20 wt %) has been reported.[10] Nonetheless, the function of the additives was claimed to be the creation of O^{2-} vacancies in the oxide phase, and only small amounts of the calcium niobate phases were detected by XRD in the sintered oxide pellets. The effect of these calcium niobate phases was regarded to be detrimental to the reduction.[10a]

In summary, we have demonstrated, for the first time, that ex situ perovskitization can significantly increase the speed and efficiency of the electroreduction of solid TiO_2 in molten $CaCl_2$. We anticipate that the fast reduction of $CaTiO_3$ can also be applied to extract Ti metal directly from natural perovskite, and from the by-product of steel making from ilmenite ($FeTiO_3$), which is often enriched in Mg and/or Ca. This process may also, in principle, be applied for the electroreduction of other oxides, such as ZrO_2, Nb_2O_5, and Ta_2O_5.

Experimental Section

Synthesis: The conventional synthesis of $CaTiO_3$ is by a solid-state reaction between TiO_2 and $CaCO_3$ or CaO at temperatures of about 1350 °C. This phase has also been prepared by other techniques, including organometallic, liquid-mix, and mechanochemical methods. In this work, partial and complete chemical perovskitization of TiO_2 was achieved as described below. The TiO_2 powder (AR grade; particle size: 0.1–0.2 μm, Kemi'ou Reagent Plant, Tianjin, China) was thoroughly ball-milled (overnight) with a prescribed amount of CaO or $Ca(OH)_2$ (AR grade, Fengcheng Reagent Plant, Shanghai, China) in the presence of distilled water (enough to turn the mixture into a thin slurry). The mixture was dried in air at 120 °C (overnight), die-pressed into small cylindrical pellets (6 MPa), and then sintered at 1300 °C for 5 h. The color change (white to brown) and SEM and XRD analyses showed that, depending on the Ca/Ti atomic ratio (0 to 1) in the mixture, the sintered pellet (diameter: ≈ 2.0 cm; thickness: 0.2–0.3 cm) had been partially or fully converted into porous $CaTiO_3$ (perovskite), as shown in Figures 1 B a and 2 A. The porosity was estimated to be 40–50 % on the basis of the pellet's mass and volume, and the densities of the oxides ($CaTiO_3$: 4.02 g cm^{-3}; TiO_2: 4.23 g cm^{-3}). Pure TiO_2 pellets were also prepared similarly but were sintered at lower temperatures (900–1000 °C) for shorter times

 © 2006 Wiley-VCH Verlag GmbH & Co. KGaA, Weinheim

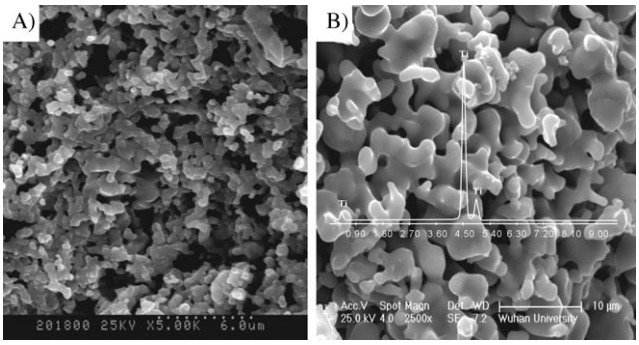


Figure 2. SEM images of the interior of a $CaTiO_3$ pellet before (A) and after (B) electrolysis (3.2 V, 850 °C, 265 min, molten $CaCl_2$). The EDX spectrum measured over the image area of (B) is also shown.

(2 h). The pellets were used directly in the assembled cathode (see Figure 1 C a) for constant-voltage electrolysis in a two-electrode cell.

Constant-voltage electrolysis: Molten dried $CaCl_2$ was used as the electrolyte in the electrolysis experiments and the subsequent cyclic voltammetry and chronoamperometry studies. Two commercial $CaCl_2$ salts were used in this work: the anhydrous salt (AR grade, the content of Mg and alkali metals was about 0.3 % counted by sulfate, Silian Reagent Plant, Shanghai, China) and the dihydrate salt (ACS grade, the content of Mg and alkali metals was less than 0.005 wt. %, Shanghai Bioengineering Co. Ltd,).

The $CaCl_2$ salt in a graphite crucible (inner diameter: 9.0 cm; height: 23.5 cm) was placed in a sealable stainless-steel reactor, which was assembled in a vertical programmable furnace (Wuhan Experimental Furnace Plant). The furnace temperature was first raised to and maintained at 200–300 °C for more than 12 h, then to 450 °C for 2 h under argon, and finally to the working temperature (850–900 °C).

After melting, pre-electrolysis of the freshly prepared molten salt at 2.6–2.8 V was applied to remove some redox-active impurities from it. A graphite rod (diameter: 2.0 cm; length: 20 cm) and a steel wire (diameter: 2.9 mm; length: $\approx$60 cm) were used as the anode and cathode, respectively. Pre-electrolysis lasted until the current reached a low and stable value, that is, the background or residual current, which was found to depend strongly on temperature, cell voltage, and the purity of the $CaCl_2$ salt.

The oxide pellet was either wrapped with molybdenum wires or sandwiched between two molybdenum meshes to form the assembled cathode (Figure 1 C a). After pre-electrolysis, the steel-wire cathode was replaced by the assembled oxide cathode and electrolysis was carried out at 2.4–3.2 V. During all pre-electrolysis and electrolysis processes, the electrolytic cell was sealed in the stainless-steel retort and was continuously purged with an argon flow.

After termination of the constant-voltage electrolysis at a prescribed time, the cathode was removed from the molten salt, cooled in argon, and then washed with water in air to dissolve the solidified salt on the cathode. The electrolyzed pellets were visually inspected for color and dimension changes, and then broken into two halves whose cross-sections were examined under optical and scanning electron microscopes. For powder X-ray diffraction and fusion elemental analyses, the electrolyzed pellets were manually ground into a powder with a mortar and pestle, further washed with water, and dried at about 120 °C in air or vacuum before further analysis.

Cyclic voltammetry and chronoamperometry: The recently reported Mo–oxide powder electrodes[8a,b] and a quartz-sealed Ag/AgCl reference electrode[8c] were used to perform cyclic voltammetry and chronoamperometry (potentiostatic electrolysis) in molten $CaCl_2$. Typically, the Mo-cavity powder electrode[8b] and the oxide-powder-modified Mo electrode[8a] were loaded with 0.1–1.0 mg of oxide powder. The sub-micrometer TiO_2 powder was used either directly or pre-mixed with the CaO powder before loading onto the electrode. The perovskite powders were obtained by finely grinding the respective perovskite pellets that were prepared as described above.

About 45 g of dried $CaCl_2$ was filled into a small graphite crucible (inner diameter: 1.8 cm; height: 25 cm), dehydrated, and pre-electrolyzed as described above. The graphite crucible also functioned as the counter electrode. The three-electrode cell was then sealed in a quartz tube, which was placed in a furnace and heated to the working temperature (850 °C). During the experiments, argon was continuously fluxed through the quartz tube. Cyclic voltammetry was performed with a CHI 605A Electrochemical System (Shanghai Chenhua, China). After chronoamperometric experiments for a prescribed time, the Mo–oxide powder electrodes were washed with distilled water, dried, and examined by SEM and EDX.

Spectroscopic analysis: The XRD patterns were obtained with a D8 Advance X-ray diffractometer (Bruker, Germany) with $Cu_{K\alpha 1}$ radiation ($\lambda = 1.5406$ Å) at 40 kV and 40 mA. The scan rate of 2θ was 4 deg min^{-1}. Micrographic and composition analyses were performed with a FEI Sirion Field Emission Gun SEM system equipped with a CCD camera and an EDAX GENESIS 7000 energy-dispersive X-ray spectrometer (EDX). Products were also sent to the Materials Test and Inspection Research Institute of Wuhan Iron and Steel (Group) for analysis of their oxygen content with an Oxygen Determinator (model RO-416DR, LECO, USA).

Received: July 3, 2005
Published online: December 12, 2005

Keywords: electrochemistry · green chemistry · perovskites · solid-state reactions · titanium

[1] a) D. J. Fray, T. W. Farthing, Z. Chen, PCT Patent, WO9964638, **1998**; b) G. Z. Chen, D. J. Fray, T. W. Farthing, *Nature* **2000**, *407*, 361; c) G. Z. Chen, D. J. Fray, *Light Met.* **2004**, 881; d) G. Z. Chen, D. J. Fray, *J. Electrochem. Soc.* **2002**, *149*, E455; e) G. Z. Chen, E. Gordo, D. J. Fray, *Metall. Mater. Trans. B* **2004**, *35*, 223; f) A. J. Muir Wood, R. C. Copcutt, G. Z. Chen, D. J. Fray, *Adv. Eng. Mater.* **2003**, *5*, 650; g) D. J. Fray, PCT Patent, WO2004018735A1, **2002**.

[2] D. Yan, *Energy Saving of Non-ferrous Metall.* **2004**, *21*, 12 (in Chinese).

[3] a) I. Park, T. Abiko, T. H. Okabe, *J. Phys. Chem. Solids* **2005**, *66*, 410; b) T. H. Okabe, T. Oda, Y. Mitsuda, *J. Alloys Compd.* **2004**, *364*, 156; c) T. H. Okabe, D. R. Sadoway, *J. Mater. Res.* **1998**, *13*, 3372; d) T. H. Okabe, M. Nakamura, T. Oishi, K. Ono, *Metall. Mater. Trans. B* **1993**, *24*, 449.

[4] a) C. Schwandt, D. J. Fray, *Electrochim. Acta* **2005**, *51*, 66; b) X. Y. Yan, D. J. Fray, *Metall. Mater. Trans. B* **2002**, *33*, 685; c) X. Y. Yan, D. J. Fray, *J. Electrochem. Soc.* **2005**, *152*, D12; d) E. Gordo, G. Z. Chen, D. J. Fray, *Electrochim. Acta* **2004**, *49*, 2195; e) G. Z. Chen, D. J. Fray, *Light Met.* **2001**, 1147; f) K. S. Mohandas, D. J. Fray, poster presentation at *EUROMAT 2005*, 5–8 Sept. **2005**, Federation of European Materials Societies, Prague, Czech Republic; g) T. Nohira, K. Yasuda, Y. Ito, *Nat. Mater.* **2003**, *2*, 397; h) K. Yasuda, T. Nohira, K. Amezawa, Y. H. Ogata, Y. Ito, *J. Electrochem. Soc.* **2005**, *152*, D69.

[5] a) K. Ono, R. O. Suzuki, *JOM* **2002**, *54*, 59; b) R. O. Suzuki, K. Teranuma, K. Ono, *Metall. Mater. Trans. B* **2003**, *34*, 287; c) R. O. Suzuki, *J. Phys. Chem. Solids* **2005**, *66*, 461.

[6] a) http://www.darpa.mil/dso/thrust/matdev/titanium.htm; b) S. Ashley, *Sci. Am.* **2003**, *289*, 38.

[7] a) K. Dring, R. Dashwood, D. Inman, *J. Electrochem. Soc.* **2005**, *152*, E104; b) K. Dring, M. Jackson, R. Dashwood, H. Flower, D. Inman in *Cost-Affordable Titanium—A Symposium Dedicated to Professor Harvey Flower* (Eds.: F. H. Froes, M. A. Imam, D.

 © 2006 Wiley-VCH Verlag GmbH & Co. KGaA, Weinheim

Fray), Minerals, Metals & Materials Soc., Warrendale, **2004**, p. 95.
[8] a) K. Jiang, X. H. Hu, H. J. Sun, D. H. Wang, X. B. Jin, Y. Y. Ren, G. Z. Chen, *Chem. Mater.* **2004**, *16*, 4324; b) G. H. Qiu, M. Ma, D. H. Wang, X. B. Jin, X. H. Hu, G. Z. Chen, *J. Electrochem. Soc.* **2005**, *152*, E328; c) P. Gao, X. B. Jin, D. H. Wang, X. H. Hu, G. Z. Chen, *J. Electroanal. Chem.* **2005**, *579*, 321; d) X. B. Jin, P. Gao, D. H. Wang, X. H. Hu, G. Z. Chen, *Angew. Chem.* **2004**, *116*, 751; *Angew. Chem. Int. Ed.* **2004**, *43*, 733.
[9] a) U. Stohr, W. Freyland, *Phys. Chem. Chem. Phys.* **1999**, *1*, 4383; b) G. Z. Chen, D. J. Fray, *J. Appl. Electrochem.* **2001**, *31*, 155.
[10] a) Q. Xu, L. Q. Deng, Y. Wu, T. Ma, *J. Alloys Compd.* **2005**, *396*, 288; b) L. Q. Deng, Q. Xu, T. Ma, B. Li, Y. C. Zhai, *Acta Metall. Sin. (Chin. Ed.)* **2005**, *41*, 551.

 © 2006 Wiley-VCH Verlag GmbH & Co. KGaA, Weinheim

Cluster Compounds

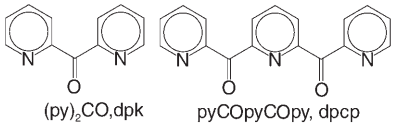
DOI: 10.1002/anie.200502519

Co^{II} Chemistry of 2,6-Bis(2-pyridylcarbonyl)-pyridine: An Icosanuclear Co Cluster Exhibiting Superparamagnetic Relaxation**

Athanassios K. Boudalis, Catherine P. Raptopoulou, Belén Abarca, Rafael Ballesteros, Mimoun Chadlaoui, Jean-Pierre Tuchagues, and Aris Terzis*

High-nuclearity transition-metal complexes (clusters) are of special interest in chemistry and physics because, both in terms of size and physical properties, they bridge the gap between the microscopic and macroscopic world, and between quantum and classical systems. In terms of size, the smallest classical nanoparticles fabricated today are the same size as the largest metal clusters that are synthesized by bottom-up methods.[1] In terms of physical properties, certain transition-metal clusters exhibit single-molecule magnetism[2] at low temperatures, that is, they retain their magnetization in zero field in a manner analogous to that of classical macroscopic magnets, but at the same time they exhibit quantum tunneling of magnetization (QTM),[3] clearly a quantum property. For these reasons transition-metal clusters are of great interest from the viewpoint of fundamental research, and applications have been proposed relating to memory devices[4] and quantum computing.[5] From the structural viewpoint, while the number of polynuclear 3d-metal complexes continues to grow rapidly, some nuclearities remain rare. Icosanuclear complexes are particularly uncommon.

A key factor in synthesizing such compounds is the proper use of ligands that can bind together a large number of metal ions. Di-2-pyridyl ketone ($(py)_2CO$ or dpk, Scheme 1) has afforded a host[6] of polynuclear clusters with a variety of transition-metal ions, including an Fe^{II} enneanuclear single-molecule magnet.[7] A metal-assisted nucleophilic attack by H_2O or ROH on the carbonyl group of this ligand yields its *gem*-diol or hemiacetal form, respectively. Subsequent deprotonation of the hydroxy groups gives the mono- or dianion (in the case of the *gem*-diol form), which can adopt a large number of coordination modes and bridge up to five metal ions.[7–10] We therefore supposed that a similar ligand with a second carbonyl group could be attacked on both carbonyl groups to provide additional donor atoms. The 2,6-bis(2-pyridylcarbonyl)pyridine ligand[11] (pyCOpyCOpy or dpcp, Scheme 1) has two carbonyl groups, each bonded to two 2-pyridyl units in a way similar to that in $(py)_2CO$. We thus thought that dpcp could have similar solvolysis, deprotonation, and coordination properties. Recent reports by Mak and co-workers on a series of Cu^{II},[12] Fe^{III},[13] and Cu^{I} and Ag^{I}[14] complexes verified this hypothesis.



Scheme 1. The $(py)_2CO$ and pyCOpyCOpy ligands.

Reaction of 4 equivalents of $Co(O_2CMe)_2{\cdot}4H_2O$ with 1 equivalent of dpcp in hot DMF and subsequent layering of the resulting solution with Et_2O led to deep purple crystals of $[Co_{20}(\mu_3\text{-}OH)_6(O_2CMe)_4(\mu_2\text{-}O_2CMe)_{12}(\mu_3\text{-}O_2CMe)_6(HL)_4(dmf)_2]{\cdot}2H_2O{\cdot}1.6\,dmf$ (**1**·$2H_2O$·1.6 DMF), where HL^{3-} = $pyC(O^-)(OH)pyC(O^-)_2py$ [Eq. (1)].

$$20\,Co(O_2CMe)_2\cdot 4H_2O + 4\,dpcp + 2\,DMF \xrightarrow{DMF,\ \Delta} [Co_{20}(OH)_6(O_2CMe)_{22}\{pyC(O)(OH)pyCO_2py\}_4(dmf)_2] + 66\,H_2O + 18\,MeCO_2H \quad (1)$$

The molecular structure[15] of **1** is shown in Figure 1. Complex **1** crystallizes in space group $P\bar{1}$. The asymmetric unit consists of a Co^{II}_{10} segment, and the other half of the molecule is generated by symmetry through an inversion

[*] Dr. A. K. Boudalis, Dr. C. P. Raptopoulou, Dr. A. Terzis
Institute of Materials Science, NCSR "Demokritos"
15310 Aghia Paraskevi Attikis (Greece)
Fax: (+30) 210-651-9430
E-mail: tbou@ims.demokritos.gr
Prof. B. Abarca, Prof. R. Ballesteros, Dr. M. Chadlaoui
Departamento de Química Orgánica
Facultad de Farmacia, Universidad de Valencia
Avda. Vicente Andrés Estellés s/n, 46100 Burjassot, Valencia (Spain)
Prof. J.-P. Tuchagues
Laboratoire de Chimie de Coordination du CNRS, UPR 8241
205 route de Narbonne, 31077 Toulouse Cedex 04 (France)

[**] This work was supported by the Greek State Scholarship Foundation (IKY) through a Postdoctoral grant to A.K.B., by the Greek General Secretariat of Research and Technology through a grant within the frame of the Competitiveness EPAN 2000–2006, Centers of Excellence #25, by the Spanish Ministerio de Ciencia y Tecnología, Dirección General de Investigación project BQU2003-09215-CO3-03, and by the Generalitat Valenciana GRUPOS 03/100.

Supporting information for this article is available on the WWW under http://www.angewandte.org or from the author.

InterScience
© 2006 Wiley-VCH Verlag GmbH & Co. KGaA, Weinheim

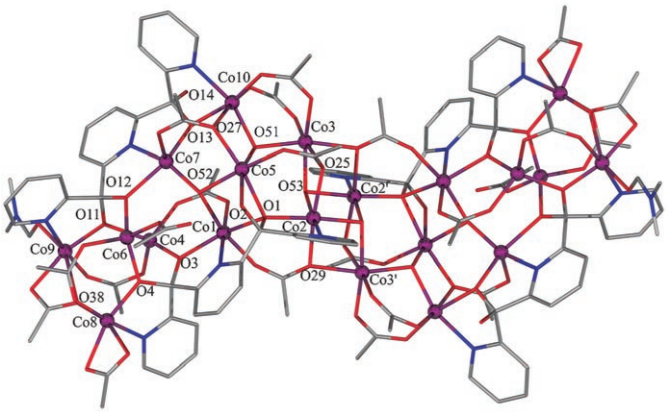
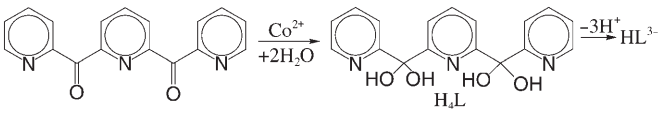


Figure 1. Molecular structure of **1**. For clarity, hydrogen atoms have been omitted and only Co atoms and monoatomic O bridges in one of the asymmetric units have been labeled. Color code: Co purple; O red; N blue. Distances [Å]: Co-$O_{hydroxo}$ 1.986–2.116, Co-N 2.055–2.147, Co-$O_{acetato}$ 1.965–2.593, Co-O_{alkoxo} 1.947–2.227.

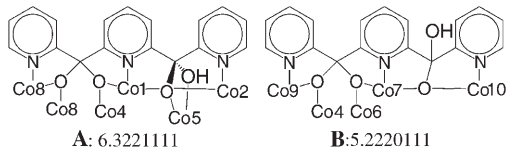
center. The structure of **1** consists of a central double cubane with two missing vertices connected to two warped $\{Co_6O_6\}$ rings through two $\{Co_2O_4\}$ moieties (for a detailed discussion, see below).

The dpcp ligand has undergone hydrolysis of both carbonyl groups (Scheme 2), and both symmetry-independent



Scheme 2. Formation of the bis(*gem*-diol) form (H_4L) of dpcp and its triple deprotonation; note that H_4L and HL^{3-} do not exist as free species; they exist only as ligands in metal complexes.

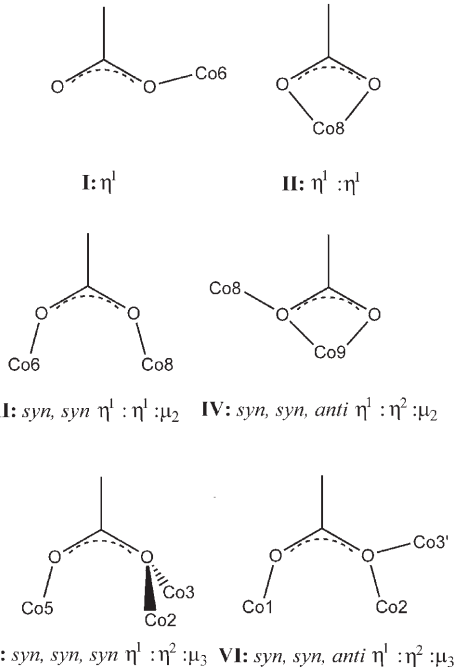
ent ligands are present in their triply deprotonated bis(*gem*-diol) form (HL^{3-}). One of these (**A**) is sextuply bridging (μ_6), with a coordination mode that can be characterized as 6.3221111 in the Harris notation,[16] and the other (**B**) is quintuply bridging (μ_5, 5.2220111; Scheme 3). Both ligation modes are novel.



Scheme 3. Crystallographically established coordination modes of the HL^{3-} ligands in **1** with Harris notations.

Of further interest are the six different coordination modes of the acetate ligands in the cluster (Scheme 4): one terminal monodentate (**I**), one terminal chelating (**II**), two doubly bridging (**III**, **IV**), and two triply bridging (**V**, **VI**).

The central incomplete double cubane comprises Co2, Co2′, Co3, and Co3′ ($'=-x, 2-y, 1-z$), which exhibit



Scheme 4. Crystallographically established coordination modes of the acetate ligands in **1**.

distorted octahedral coordination spheres and are bridged solely by monoatomic bridges, two of which are μ_3-hydroxide ligands (O53 and O53′), and four are acetate oxygen atoms of type **V** (O25, O25′) and type **VI** (O29 and O29′) bridges (Figure 2).

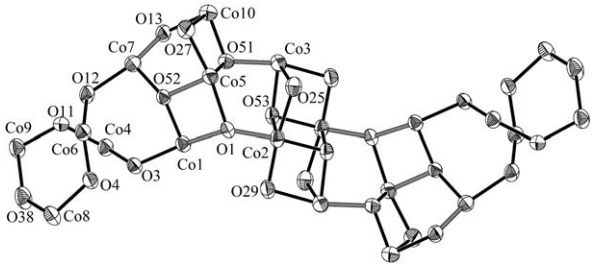


Figure 2. ORTEP plot of the central core of **1**. Only Co^{II} atoms and monoatomic O bridges are shown.

The external hexanuclear ring comprises Co1, Co7, Co6, Co8, Co9, and Co4. Of these, Co7 is pentacoordinate with a square-pyramidal geometry (trigonality index $\tau = 0.083$),[17] Co4 and Co6 are tetracoordinate with tetrahedral geometries, and the other metal ions are hexacoordinate with distorted octahedral geometries. The bridging of the ring is principally accomplished by six monoatomic bridges, that is, one μ_3-hydroxo (O52), four μ_2-alkoxo-type bridges (O3, O4, O11, O12) from the two trianionic ligands, and one oxygen atom (O38) from the μ_2-acetate ligand of type **IV**. Finally, the dinuclear moiety connecting the central incomplete double cubane subcore with the external ring through two alkoxo bridges (O14, O1) consists of atoms Co5 and Co10 bridged by

 © 2006 Wiley-VCH Verlag GmbH & Co. KGaA, Weinheim

one carboxylate and one hydroxide oxygen atom (O27 and O51, respectively).

The molecular structure is further stabilized by a series of intramolecular hydrogen bonds between the μ_3-hydroxide and acetate oxygen atoms (O52–H(O52)···O41, O2–H(O2)···O42, O51–H(O51)···O31) and between a hydroxy group of the ligand and an acetate oxygen atom (O14–H(O14)···O22). Concerning the formal charges of the Co ions, X-ray crystallography revealed the existence of one alcohol [H(O14)] and three hydroxide [H(O51), H(O52), H(O53)] hydrogen atoms per asymmetric unit, which were located from difference Fourier maps. Thus, charge-balance considerations require that all cobalt atoms are formally divalent.

Complex **1** is the first icosanuclear and second largest non-organometallic Co cluster synthesized to date, the largest being $[Co_{24}(\mu_3\text{-}OH)_{14}(\mu\text{-}OH)_4(\mu_3\text{-}OMe)_2(\mu_3\text{-}Cl)_2Cl_4(mhp)_{22}]$ ($mhp^- =$ anion of 6-hydroxy-2-methylpyridine) reported by Winpenny and co-workers.[18] It is also one of the few structurally characterized non-organometallic, icosanuclear 3d-metal clusters with exclusively O and/or N ligation.[19] A handful of icosanuclear 3d-metal clusters involve S^{2-} or Se^{2-} bridges.[20] A space-filling plot of **1** (see Supporting Information) reveals that the molecule is approximately cylindrical in shape, with a length of about 3 nm and a diameter of about 1.5 nm.

Since cobalt(II) clusters are potential single-molecule magnets,[21] variable-temperature (2.0–300 K) magnetic susceptibility data (at 0.1 and 1 T) and a magnetization isotherm at 2 K (0–5.5 T) were recorded for **1** (Figure 3). The $\chi_M T$ product for **1** at 300 K (1-T field) of 51.23 $cm^3 mol^{-1} K$ is significantly higher than the spin-only value expected for 20 noninteracting ions with $S = 3/2$ (37.4 $cm^3 mol^{-1} K$). This is attributed to the orbital contribution of Co^{II}, which is known to be significant in an octahedral field. The continuous decrease in $\chi_M T$ with decreasing temperature is indicative of dominant antiferromagnetic interactions. The decrease is more pronounced below 10 K, and $\chi_M T$ reaches 6.90 $cm^3 mol^{-1} K$ at 2 K, due to the zero-field splitting of the ground state of the cluster, which is typically large for complexes containing high-spin, six-coordinate Co^{II} ions. In a 0.1-T field, however, this decrease is smoother (10.90 $cm^3 mol^{-1} K$ at 2 K) because of the weaker Zeeman splitting of the ground state. However, the nonzero value at 2 K and the continuous increase in χ_M on cooling indicate the existence of a magnetic ground state, or a diamagnetic ground state with low-lying magnetic excited states which are populated even at 2 K. This is also corroborated by the magnetization isotherm at 2 K, which does not show saturation up to a field of 5.5 T, possibly due to simultaneous population of numerous spin states.

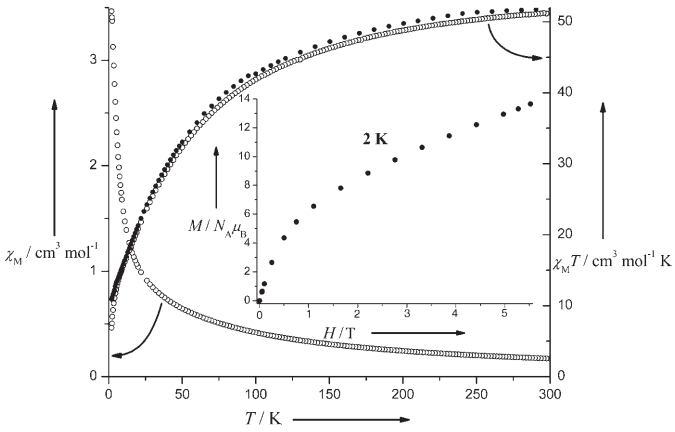


Figure 3. χ_M and $\chi_M T$ versus T plots for **1** in the range 2.0–300 K in fields of 1 T (○) and 0.1 T (●). The magnetization isotherm at 2 K between 0 and 5.5 T is shown in the inset.

To clarify this, and to probe the relaxation properties of **1**, zero-field ac susceptibility measurements between 1.9 and 10 K were carried out at frequencies of 50, 100, 500, 1000, and 1400 Hz (Figure 4). These showed frequency-dependent out-of-phase signals, which may be attributed to superparamagnetic relaxation of the magnetization of **1**. However, since no maxima were observable down to 1.9 K, quantitative estimation of the relaxation kinetics was not possible. The $\chi_M' T$ product extrapolates to about 11 $cm^3 mol^{-1} K$ at 0 K, which suggests an effective $S = 4$ ground state. Due to the size and complexity of the molecule, however, quantitative interpretation is not possible.

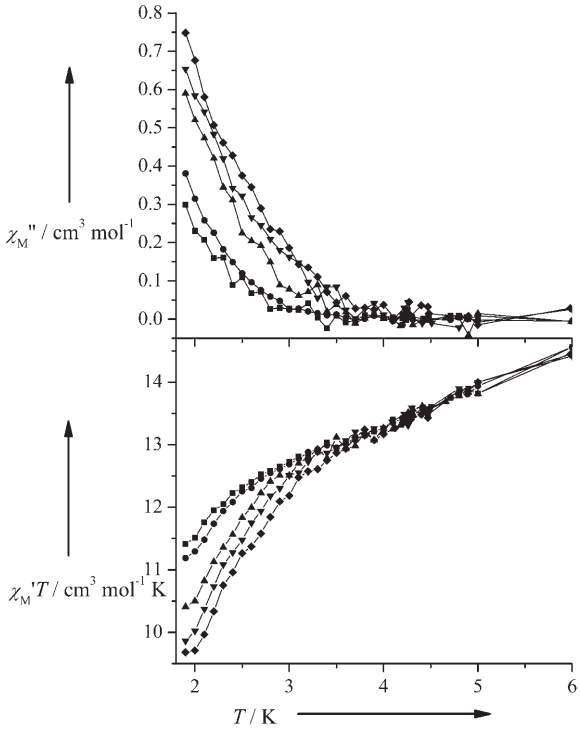


Figure 4. Frequency dependence of the in-phase $\chi_M' T$ product and the out-of-phase χ_M'' magnetic susceptibility versus T for **1** at frequencies of 50 (■), 100 (●), 500 (▲), 1000 (▼), and 1400 Hz (◆).

In summary we have isolated and characterized the first icosanuclear Co^{II} cluster, which is also a rare example of 3d-metal clusters with O and N ligation. Moreover, this work emphasizes the coordinative flexibility and versatility of the dpcp ligand and its synthetic utility in polynuclear metal chemistry.

 © 2006 Wiley-VCH Verlag GmbH & Co. KGaA, Weinheim

Experimental Section

1: Solid dpcp (40.0 mg, 0.138 mmol) was added to a solution of $Co(O_2CMe)_2{\cdot}4H_2O$ (138 mg, 0.553 mmol) in DMF (15 mL). The color of the solution changed immediately from dark purple to deep wine red. The solution was heated for 10 min just below the boiling point of DMF, during which time a color change to very deep purple was observed. The solution was cooled to room temperature and layered with double the volume of Et_2O in a layering tube. Dark purple crystals formed after about one week. These were collected by decantation, repeatedly washed with Et_2O, and dried in vacuo (yield ca. 30%). The dried solid analyzed as **1**·0.2 DMF. Elemental analysis (%) calcd for $C_{118.6}H_{132.14}Co_{20}N_{14.2}O_{68.2}$: C 35.37, H 3.34, N 4.94; found: C 35.32, H 3.38, N 4.89. IR (KBr disk): $\tilde{\nu}$ = 3423 (vs), 1664 (s), 1602 (vs), 1574 (vs), 1559 (vs), 1436 (vs), 1419 (vs), 1063 (m), 1027 (m), 827 (w), 797 (w), 761 (w), 663 (m), 617 cm^{-1} (w).

Received: July 19, 2005
Published online: December 12, 2005

Keywords: cluster compounds · cobalt · magnetic properties · N,O ligands

[1] A. J. Tasiopoulos, A. Vinslava, W. Wernsdorfer, K. A. Abboud, G. Christou, *Angew. Chem.* **2004**, *116*, 2169–2173; *Angew. Chem. Int. Ed.* **2004**, *43*, 2117–2121.
[2] a) G. Christou, D. Gatteschi, D. N. Hendrickson, R. Sessoli, *MRS Bull.* **2000**, *25*, 66–71; b) D. Gatteschi, R. Sessoli, *Angew. Chem.* **2003**, *115*, 278–309; *Angew. Chem. Int. Ed.* **2003**, *42*, 268–297.
[3] a) J. R. Friedman, M. P. Sarachik, J. Tejada, R. Ziolo, *Phys. Rev. Lett.* **1996**, *76*, 3830–3833; b) L. Thomas, F. Lionti, R. Ballou, D. Gatteschi, R. Sessoli, B. Barbara, *Nature* **1996**, *383*, 145–147.
[4] M. Cavallini, J. Gomez-Segura, D. Ruiz-Molina, M. Massi, C. Albonetti, C. Rovira, J. Veciana, F. Biscarini, *Angew. Chem.* **2005**, *117*, 910–914; *Angew. Chem. Int. Ed.* **2005**, *44*, 888–892.
[5] M. N. Leuenberger, D. Loss, *Nature* **2001**, *410*, 789–793.
[6] G. S. Papaefstathiou, S. P. Perlepes, *Comments Inorg. Chem.* **2002**, *23*, 249–274.
[7] A. K. Boudalis, B. Donnadieu, V. Nastopoulos, J. M. Clemente-Juan, A. Mari, Y. Sanakis, J.-P. Tuchagues, S. P. Perlepes, *Angew. Chem.* **2004**, *116*, 2316–2320; *Angew. Chem. Int. Ed.* **2004**, *43*, 2266–2270.
[8] A. Tsohos, S. Dionyssopoulou, C. P. Raptopoulou, A. Terzis, E. G. Bakalbassis, S. P. Perlepes, *Angew. Chem.* **1999**, *111*, 1036–1038; *Angew. Chem. Int. Ed.* **1999**, *38*, 983–985.
[9] G. S. Papaefstathiou, S. P. Perlepes, A. Escuer, R. Vicente, M. Font-Bardia, X. Solans, *Angew. Chem.* **2001**, *113*, 908–910; *Angew. Chem. Int. Ed.* **2001**, *40*, 884–886.
[10] G. S. Papaefstathiou, A. Escuer, R. Vicente, M. Font-Bardia, X. Solans, S. P. Perlepes, *Chem. Commun.* **2001**, 2414–2415.
[11] B. Abarca, R. Ballesteros, M. Elmasnaouy, *Tetrahedron* **1998**, *54*, 15287–15292.
[12] X.-D. Chen, T. C. W. Mak, *Inorg. Chim. Acta* **2005**, *358*, 1107–1112.
[13] X.-D. Chen, M. Du, F. He, X.-M. Chen, T. C. W. Mak, *Polyhedron* **2005**, *24*, 1047–1053.
[14] X.-D. Chen, T. C. W. Mak, *J. Mol. Struct.* **2005**, *748*, 183–188.
[15] Crystal data for **1**·2 H_2O·1.6 DMF ($C_{122.8}H_{149.2}Co_{20}N_{15.6}O_{71.6}$): M_r = 4167.98, triclinic, $P\bar{1}$, a = 16.643(7), b = 17.733(8), c = 21.976(8) Å, α = 105.03(1), β = 111.18(1), γ = 91.56(1)°, V = 5788(4) $Å^3$, Z = 1, T = 298 K, $F(000)$ = 2108, ρ_{calcd} = 1.196 $g\,cm^{-3}$, $\mu(Mo_{K\alpha})$ = 1.457 mm^{-1} (λ = 0.71073 Å), 11130 reflections measured, 10633 unique reflections (R_{int} = 0.0302), 1040 refined parameters, $R_1(F)$ = 0.0798 and $wR_2(F^2)$ = 0.2207 for 7068 reflections with $I > 2\sigma(I)$. CCDC-278700 contains the supplementary crystallographic data for this paper. These data can be obtained free of charge from the Cambridge Crystallographic Data Centre via www.ccdc.cam.ac.uk/data_request/cif.
[16] R. A. Coxall, S. G. Harris, D. K. Henderson, S. Parsons, P. A. Tasker, R. E. P. Winpenny, *J. Chem. Soc. Dalton Trans.* **2000**, 2349–2356.
[17] A. W. Addison, T. N. Rao, J. Reedijk, J. van Rijn, G. C. Verschoor, *J. Chem. Soc. Dalton Trans.* **1984**, 1349–1356.
[18] E. K. Brechin, S. G. Harris, A. Harrison, S. Parsons, A. G. Whittaker, R. E. P. Winpenny, *Chem. Commun.* **1997**, 653–654.
[19] S. Maheswaran, G. Chastanet, S. J. Teat, T. Mallah, R. Sessoli, W. Wernsdorfer, R. E. P. Winpenny, *Angew. Chem.* **2005**, *117*, 5172–5176; *Angew. Chem. Int. Ed.* **2005**, *44*, 5044–5048.
[20] For example: a) S. Dehnen, A. Schäfer, D. Fenske, R. Ahlrichs, *Angew. Chem.* **1994**, *106*, 786–790; *Angew. Chem. Int. Ed. Engl.* **1994**, *33*, 746–749; b) J.-F. You, R. H. Holm, *Inorg. Chem.* **1991**, *30*, 1431–1433; c) H. L. Cuthbert, A. I. Wallbank, N. J. Taylor, J. F. Corrigan, *Z. Anorg. Allg. Chem.* **2002**, *628*, 2483–2488.
[21] a) E. C. Yang, D. N. Hendrickson, W. Wernsdorfer, M. Nakano, L. N. Zakharov, R. D. Sommer, A. L. Rheingold, M. Ledezma-Gairaud, G. Christou, *J. Appl. Phys.* **2002**, *91*, 7382–7384; b) M. Murrie, S. J. Teat, H. Stoeckli-Evans, H. U. Güdel, *Angew. Chem.* **2003**, *115*, 4801–4804; *Angew. Chem. Int. Ed.* **2003**, *42*, 4653–4656.

 © 2006 Wiley-VCH Verlag GmbH & Co. KGaA, Weinheim

Electrostatic Interactions

DOI: 10.1002/anie.200502586

Designing Intermolecular Interactions between Halogenated Peripheries of Inorganic and Organic Molecules: Electrostatically Directed M–X···X′–C Halogen Bonds**

Guillermo Mínguez Espallargas, Lee Brammer, and Paul Sherwood*

Halogen atoms (X) typically form a covalent single bond to only one other atom within a molecule, which places them most frequently at the periphery of that molecule and, thus, at molecular interfaces in condensed phases. Such terminally

[*] G. Mínguez Espallargas, Dr. L. Brammer
Department of Chemistry
University of Sheffield
Sheffield S3 7HF (UK)
Fax: (+44) 114-222-9346
E-mail: lee.brammer@sheffield.ac.uk
Dr. P. Sherwood
Computational Science and Engineering Department
CCLRC Daresbury Laboratory
Daresbury, Warrington WA4 4AD (UK)

[**] This work was supported by the Cambridge Crystallographic Data Centre and the CCLRC Centre for Molecular Structure and Dynamics. We thank Stephen L. Purver and Harry Adams (University of Sheffield) for initial work on compound **1** and its crystal structure.

Supporting information for this article is available on the WWW under http://www.angewandte.org or from the author.

© 2006 Wiley-VCH Verlag GmbH & Co. KGaA, Weinheim
WILEY InterScience DISCOVER SOMETHING GREAT

bonded halogen atoms, while not bordering on ubiquity like hydrogen atoms, are nevertheless abundant and found in a wide range of organic and inorganic molecules.[1] Thus, the development of reliable intermolecular interactions that involve such halogen atoms has the potential for widespread application in supramolecular chemistry and crystal engineering. We have pursued such a design and recently reported the application of directional M–Cl···X–C nucleophile–electrophile interactions in the synthesis of both neutral[2] and ionic molecular crystals.[3]

The basis for the design of these interactions was the known behavior in intermolecular interactions of inorganic halogen species (M–X) as directional Lewis bases and of organic halogen species (C–X) as directional Lewis acids. Specifically metal–halide groups (M–X) have been shown to be potent and directional hydrogen-bond acceptors,[4] with applications in crystal design and synthesis.[5] Organic halogen species (C–X), particularly for X = I, Br, and Cl, form halogen bonds[6] most commonly with organic bases, for example, N/O···X–C,[7] but potentially also with other halogen atoms.[8] Halogen bonds have been applied to various aspects of supramolecular assembly in the solid state.[6,9] However, although the nature of hydrogen bonds that involve inorganic halogen species is quite well established, in line with that of other strong hydrogen bonds, the nature of halogen bonds that involve organic halogen species is not fully established. Indeed, at the weakest end of the scale of interaction energies, interactions between chlorocarbon groups C–Cl···Cl–C, which are directional in the solid state, have been the subject of dispute in regard to whether they are weakly attractive[10] or guided by adopting the least-repulsive interaction geo metry.[11] Halogen bonds are often discussed in terms of a charge transfer between the Lewis base and the C–X σ* orbital,[6] by analogy to halogen bonds that involve dihalogen molecules, for example, N···X–X,[12] or most emphatically I^-···I–I, which gives rise to the symmetrical I_3^- molecular ion and much related polyiodide network chemistry.[13] However, our most recent study of M–Cl···X–C networks in crystals of the compounds *trans*-[MCl_2(3-Xpy)$_2$] (M = Pt, Pd; 3-Xpy = 3-halopyridine; X = I, Br, Cl, F) shows that the absence of M–Cl···F-C interactions, the apparent relative interaction strengths (I > Br > Cl) and the prevalent interaction geometry (approximately linear Cl···X–C and markedly bent M–Cl···X interactions) are all consistent with the relative magnitude and anisotropic nature of the electrostatic potential around the inorganic and organic halogen species.[2] Thus, an electrostatic component to M–X···X′–C interactions may be quite important, although the use of only one type of halide ligand and the adoption of five separate propagated networks with M–Cl···X–C interactions limited the extent to which the importance of the electrostatic contribution could be assessed relative to other contributors, notably charge transfer.

The present study overcomes these difficulties by examining a series of eight isostructural compounds in which both the organic and inorganic halogen species have been varied in a systematic manner: (4-X′pyH)$_2$[CoX_4] (4-X′pyH = 4-halopyridinium; **1**: X′ = Cl, X = Cl; **2**: X′ = Br, X = Cl; **3**: X′ = Cl, [CoX_4] = $CoCl_{1.56}Br_{2.44}$; **4**: X′ = Br, [CoX_4] = $CoCl_{1.62}Br_{2.38}$; **5**: X′ = Cl, X = Br; **6**: X′ = Br, X = Br; **7**: X′ = Cl, X = I; **8**: X′ = Br, X = I). This series of compounds provides a unique opportunity to assess the relative importance of the charge-transfer and electrostatic contributions to the M–X···X′–C halogen bonds through consideration of the structural changes imparted by changing either the organic or the inorganic halogen species. Compounds **3** and **4** further allow interpolation between the discrete steps afforded by changing all the organic or inorganic halogen species. Theoretical calculations have been used to understand the structural changes that arise across the series through examination of the changes in electrostatic potential and to understand the unusually large distortion from the tetrahedral geometry of the anions that has been observed across all of the crystal structures.

The crystal structures of **1**–**8**, determined at 150 K, show that each forms networks propagated by N–H···X_2Co hydrogen bonds and Co–X···X′–C halogen bonds (Figure 1). Pairs

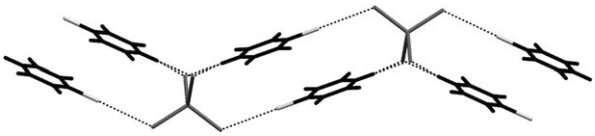


Figure 1. Network formed in crystal structures of **1**–**8**. Cobalt and halide ligands shown in dark gray, organic halogen atoms in light gray, and all other atoms in black (C, H, N).

of cations link each anion to its neighbor in the zigzag chain, with the cations adopting a stacked arrangement with mutually opposed molecular dipoles. The interaction geometries are summarized in Table 1. Notably the anions exhibit a large distortion (approximately C_{2v}) from the idealized tetrahedral geometry wherein the angles between the pairs of halide ligands that participate in hydrogen bonding are markedly decreased in magnitude (average Cl-Co-Cl: 98.0°; Br-Co-Br: 99.6°; I-Co-I: 102.4°) whereas the pairs of halide ligands involved in halogen bonding exhibit slightly enlarged angles (average Cl-Co-Cl: 110.9°; Br-Co-Br: 111.5°; I-Co-I: 112.4°).

The N–H···X_2Co bifurcated hydrogen bonds are asymmetric, as is common for tetrahedral halometallate anions,[5a] and become weaker and more symmetric on going from chloride to iodide ligands. Interestingly the hydrogen bonds are systematically more symmetric for the chloropyridinium cations than for the bromopyridinium cations when pairs of compounds that contain the same anion are compared.

Most interesting, however, are the Co–X···X′–C halogen bonds. All exhibit approximately linear geometries at the organic halogen atom (C–X′···X: 168.6–174.9°), whereas the Co–X···X′ angle is markedly bent (range: 120.3–123.7°), which confirms the nucleophilic–electrophilic nature of these interactions and, thus, the distinct roles of the two halogen atoms. Using the halogen–halogen distance measure $R_{XX'}$, normalized to account for differences in the van der Waals radii of the different halogen atoms,[7,15] it is clear that the halogen bonds are shorter, and by implication stronger, for the heavier organic halogen species (C–X), but weaker for

 © 2006 Wiley-VCH Verlag GmbH & Co. KGaA, Weinheim

Table 1: Selected bond lengths, halogen bonds, and hydrogen-bond geometries for **1**–**8**.

	Co–X [Å]	C–X′ [Å]	X···X′ [Å] [$R_{XX'}$][a]	Co–X···X′ [°]	X···X′–C [°]	H···X[b] [Å] [R_{HX}][a]	N–H···X [°][b]
(4-ClpyH)$_2$[CoCl$_4$] (**1**)	2.2500(5)	1.723(2)	3.3428(6)	123.69(2)	173.75(7)	2.300 [0.78]	141.9
	2.2915(5)		[0.955]			2.825 [0.96]	134.0
(4-BrpyH)$_2$[CoCl$_4$] (**2**)	2.2532(9)	1.882(3)	3.2609(10)	121.61(4)	174.9(1)	2.249 [0.76]	146.0
	2.2842(10)		[0.906]			2.953 [1.00]	131.2
(4-ClpyH)$_2$[CoCl$_{1.56}$Br$_{2.44}$] (**3**)	2.3610(8)[c]	1.715(4)	3.4261(13)[c]	123.31(4)[c]	172.6(1)[c]	2.440[d] [0.81]	137.7[d]
	2.3586(9)[d]		[0.958][g]			2.831[d] [0.95]	136.6[d]
(4-BrpyH)$_2$[CoCl$_{1.62}$Br$_{2.38}$] (**4**)	2.3596(8)[e]	1.884(5)	3.3423(9)[e]	121.44(3)[e]	173.9(2)[e]	2.370[f] [0.79]	142.8[f]
	2.3477(10)[f]		[0.909][g]			2.968[f] [0.99]	133.5[f]
(4-ClpyH)$_2$[CoBr$_4$] (**5**)	2.3855(4)	1.718(3)	3.4898(8)	123.20(2)	171.1(1)	2.543 [0.83]	136.6
	2.4209(5)		[0.967]			2.854 [0.94]	137.1
(4-BrpyH)$_2$[CoBr$_4$] (**6**)	2.3859(9)	1.884(5)	3.3873(11)	121.23(3)	171.9(2)	2.478 [0.81]	140.6
	2.4162(10)		[0.915]			2.957 [0.97]	134.4
(4-ClpyH)$_2$[CoI$_4$] (**7**)	2.5820(7)	1.721(5)	3.7203(13)	121.70(3)	168.6(2)	2.877 [0.91]	132.1
	2.6021(7)		[0.997]			3.016 [0.95]	139.2
(4-BrpyH)$_2$[CoI$_4$] (**8**)	2.5806(7)	1.879(5)	3.6018(7)	120.26(3)	169.0(2)	2.811 [0.89]	135.0
	2.5994(8)		[0.940]			3.072 [0.97]	137.3

[a] $R_{XX'} = d(X\cdots X')/(r_X + r_{X'})$, where r_X and $r_{X'}$ are the van der Waals radii[14] of halogen atoms X and X′, respectively (following the definition of Lommerse et al.[7]); R_{HX} is defined analogously for the H···X separation. [b] Geometries calculated using hydrogen-atom positions normalized to standard nuclear positions, as established by neutron diffraction (N–H: 1.01 Å). [c] X = 78% Br, 22% Cl. [d] X = 44% Br, 56% Cl. [e] X = 76% Br, 24% Cl. [f] X = 43% Br, 57% Cl. [g] Arithmetic average.

the heavier inorganic halogen species (Co–X) (Table 1, Figure 2). The observed trend with respect to halogen bonds involving the Lewis acidic C–X group is consistent with

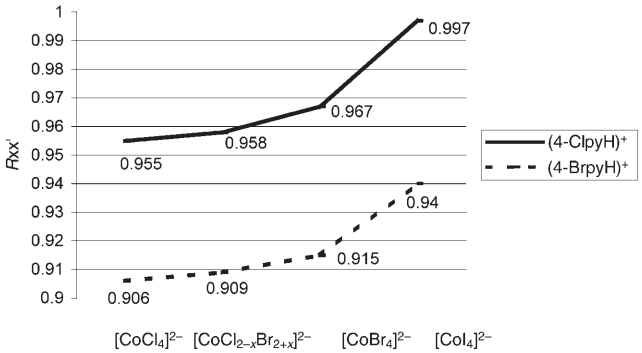


Figure 2. Variation of (Co)X···X′(C) halogen-bond lengths with change of the halogen atom. The distances $R_{XX'}$ are normalized as defined in Table 1 to account for differences in the van der Waals radii of the different halogen atoms.[7,15]

previous reports.[2,3,6–8] However, these results appear to be counter to the conventional wisdom that for halogen bonds involving halide ions (X^-) as the nucleophile, for example, $X^-\cdots$I–I (XI_2) or $X^-\cdots$Br–C, the halogen bonds are stronger or at least more prevalent for $I^- > Br^- > Cl^- > F^-$.[6,16] This prevailing view is based on a description of the halogen bonds as n→σ* charge-transfer interactions between the anion and the dihalogen or C–X group. Such an interaction is well established for trihalide ions and follows the presumed trend as evidenced by the geometries of the isostructural pairs $CsBrI_2/CsI_3$ and (RpyH)[ClI_2]/(RpyH)[BrI_2] (R = *N*-hexadecyl), wherein lengthening of the I–I bond occurs and this change is more pronounced for $I^- > Br^-$ and for $Br^- > Cl^-$, respectively.[17] Such a charge transfer would be less prominent for a C–X group as the σ* orbital will be higher in energy than for the corresponding I_2 molecule. Nevertheless, Resnati and co-workers have proposed that $I^-\cdots$Br–C halogen bonds are stronger than $Br^-\cdots$Br–C halogen bonds,[19] by inference from IR C–H stretching frequencies in *N*-methyl-3,5-dibromopyridinium halides, thus suggesting that n→σ* charge transfer is greater for the I^- ion, a better electron donor than the Br^- ion. One would, therefore, anticipate by analogy that the trend in decreasing $R_{XX'}$ distance, and thus increasing strength, would be X = Cl→Br→I if the n→σ* charge transfer were the dominant contributor to the halogen-bond strength for Co–X···X′–C in **1**–**8**. As the trend is the reverse (Figure 2), an alternative explanation must be sought.

As we have recently established that an electrostatic contribution is likely to be important in M–Cl···X–C halogen bonds,[2] we examined this possibility for M–X···X′–C halogen bonds in **1**–**8** through selected theoretical calculations. The electrostatic potential associated with the two cations and the three anions used has been calculated by using idealized geometries based upon those determined experimentally. All halogen atoms show an anisotropic potential that arises from their anisotropic charge distribution, with the most positive (or least negative) potential associated with the axial region *trans* to the covalent bond (M–X or C–X) and the most negative (or least positive) potential lying in an equatorial belt approximately orthogonal to the covalent bond (Figures 3 and 4). Distortion of the anion also leads to polarization and enhancement of the negative potential associated with the two halide ligands related by the smallest X-Co-X angle (compare the top of Figure 3a–c with the bottom of Figure 3d–f).

Anion–cation interactions involve the association of the most electropositive part of the cation, the N–H group, with the region of the most negative potential on the anion, located between the compressed pair of halide ligands. The Co–X···X′–C halogen bonds then bring together the most positive (axial) region of the organic halogen atoms with the region of greatest negative potential on the remaining inorganic

 © 2006 Wiley-VCH Verlag GmbH & Co. KGaA, Weinheim

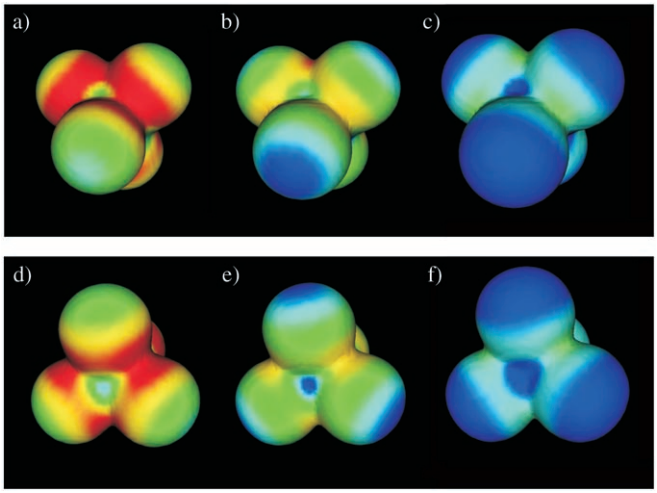


Figure 3. Calculated electrostatic potentials for the anions $[CoCl_4]^{2-}$ (a, d), $[CoBr_4]^{2-}$ (b, e), $[CoI_4]^{2-}$ (c, f); displayed on density isosurfaces of 0.0025 electrons bohr^{-3}, with a color range from red at 200 kcal mol^{-1} to blue at 160 kcal mol^{-1}. The views are approximately orthogonal to the twofold symmetry axes of the anions, with the halide ligands of the compressed CoX_2 moiety involved in hydrogen bonding at the top of the figures and those involved in halogen bonds at the bottom (cf. Scheme 1). The views (d–f) are rotated by 90° about the molecular twofold axes (vertical) relative to views (a–c).

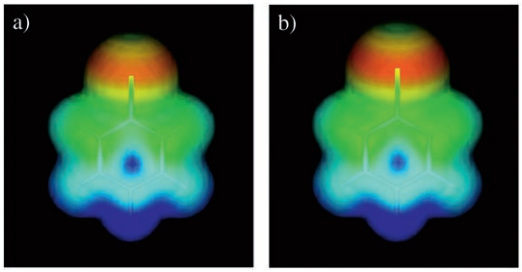
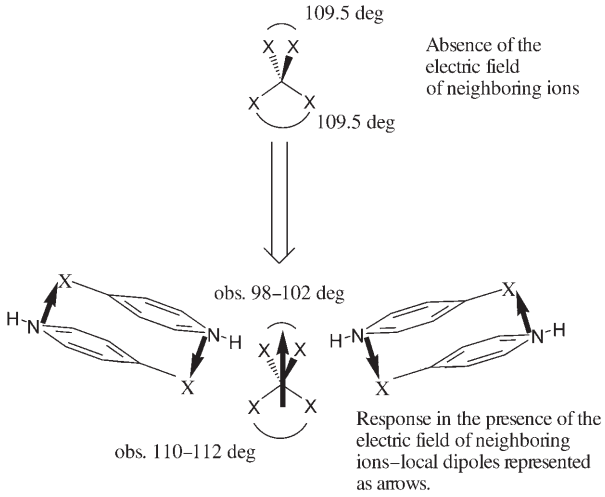


Figure 4. Calculated electrostatic potentials for the cations a) 4-chloropyridinium (4-ClpyH)$^+$ and b) 4-bromopyridinium (4-BrpyH)$^+$, displayed on density isosurfaces of 0.0025 electrons bohr^{-3}, with a color range from red at 70 kcal mol^{-1} to blue at 140 kcal mol^{-1}.

halogen atoms, thus resulting in near-linear X···X′–C angles and Co–X···X′ angles of approximately 120°.

The clear trend in the electrostatic potential across the three anions is a decrease in the magnitude of the negative potential on the corresponding density isosurfaces in the sequence $[CoCl_4]^{2-} > [CoBr_4]^{2-} > [CoI_4]^{2-}$ (Figure 3 a–c or d–f), which correlates with the trend of increasing halogen bonds lengths ($R_{ClX} < R_{BrX} < R_{IX}$; see Table 1). In addition, the positive potential along the C–X axis of the organic halogen species decreases from Br to Cl (Figure 4) in parallel with the trend $R_{XBr} < R_{XCl}$. These correlations taken together with the observed X···X′–C and Co–X···X′ angles are clearly consistent with the Co–X···X′–C halogen bonds being governed by a directional electrostatic interaction. The discrimination between the hydrogen bonding and halogen-bonding sites on the anions is also emphasized by the observation that in the structures of **3** and **4**, the two halide sites with a high chloride content are involved in hydrogen-bond formation whereas the two with a lower chloride content form the halogen bonds.[20]

Finally, we also determined the likely cause of the unusually large distortion from the idealized tetrahedral geometry observed for all of the anions in **1**–**8**. The distortion is consistent with being a response to the local electric field of the surrounding ions, thereby generating a dipole moment along the twofold axis of the anion (Scheme 1). This



Scheme 1. Distortion of anion geometry in response to the electric field generated by neighboring ions. obs. = observed; dipole moments represented as arrows from + to −.

supposition is supported by theoretical calculations in which an optimization of the $[CoCl_4]^{2-}$ geometry was conducted in the presence of a simple model electric field that mimicked the orientation, if not the precise magnitude, of the field experienced by the ion in the crystal. The optimization resulted in compression of the Cl-Co-Cl angle closest to the positive end of the field and an increase in the associated pair of C–Cl bond lengths, with the reverse situation for the halide ligands closest to the negative end of the field.[21] This result is in qualitative agreement with the observed distortion of the $[CoCl_4]^{2-}$ ion in the crystal structures of **1** and **2**.

Comparison of intermolecular interaction geometries in chemically related compounds is often fraught with difficulty because of large differences between the crystal structures of the compounds, which can have a profound effect on the metrics of a given intermolecular interaction. The present study provides a remarkable opportunity to undertake such a comparison across eight isostructural compounds with systematic variation of both inorganic and organic halogen components for the recently identified, but potentially highly efficacious, class of M–X···X′–C halogen bonds. These interactions are highly directional, and X···X′ separations normalized to account for the change in size of the halogen atoms confirm that the interaction is shorter (stronger) for the heavier organic halogen species and demonstrate for the first time that this is also the case for the lighter inorganic halogen species. The trends in electrostatic potential at the halogen atoms, which becomes more positive for (C)Br > (C)Cl and more negative for (M)Cl > (M)Br > (M)I, are consistent with

 © 2006 Wiley-VCH Verlag GmbH & Co. KGaA, Weinheim

these observations, thus clearly indicating that the electrostatic interaction between the halogen atoms is the dominant contribution in both directing and governing the strength of the M−X···X′−C halogen bonds. Given the abundance of the halogen atoms in molecular surfaces of both organic and inorganic systems, a clear understanding of the nature of M−X···X′−C halogen bonds provides an impetus for a wide range of applications to supramolecular construction of organic–inorganic hybrid materials and has the potential to yield applications in the control of conformations in metal complexes, molecular recognition, and substrate binding in catalysis.

Experimental Section

Crystal synthesis: All starting materials were purchased from Aldrich, Lancaster, or Avocado and used as received. Blue crystals of compounds **1**, **2**, **5**, and **6** were obtained in high yields following the evaporation of acidified solutions of $CoCl_2{\cdot}6H_2O$ or $CoBr_2$ combined with the appropriate 4-halopyridinium chloride, which had been previously dissolved in an excess of concentrated aqueous HX to prevent the formation of the mixed halide. Elemental analyses were in accord with expected values. Compounds **7** and **8** were obtained as green crystals by an analogous approach with $CoI_2{\cdot}2H_2O$ and acidification with concentrated aqueous HI, but only as the minor product, the major product being brown crystalline compounds $(4\text{-}XC_5NH_5)_2[CoI_4]{\cdot}I_2$, which will be discussed fully in a later publication. Crystals of mixed halide compounds **3** and **4** were obtained similarly but without acidification of the solutions. Small yields of compounds **3**, **4**, **7**, and **8** prohibited bulk analyses. Full details of the synthetic procedures can be found in the Supporting Information.

X-ray crystallography: X-ray data were collected at 150 K for **1**–**8** on a Bruker SMART 1000 diffractometer using $Mo_{K\alpha}$ X-rays. Data were corrected for absorption using empirical methods (SADABS) based upon symmetry-equivalent reflections combined with measurements at different azimuthal angles.[22] Crystal structures were solved and refined against all F^2 values using the SHELXTL suite of programs.[23] Non-hydrogen atoms were refined anisotropically and hydrogen atoms were placed in calculated positions refined using idealized geometries (riding model) and assigned fixed isotropic displacement parameters. For mixed halide compounds **3** and **4**, the Cl/Br ratio was allowed to refine independently for the two independent sites, thus leading to Cl/Br ratios of 0.562:0.438 and 0.221:0.779 for **3** and 0.570:0.430 and 0.241:0.759 for **4**, with physically reasonable displacement parameters for both sites. A summary of the data collection and structure refinements is provided in the Supporting Information. CCDC 279107–279114 contain the supplementary crystallographic data for this paper. These data can be obtained free of charge from the Cambridge Crystallographic Data Centre via www.ccdc.cam.ac.uk/data_request/cif.

Theoretical calculations: Electrostatic potential calculations for idealized $[CoX_4]^{2-}$ (X = Cl, Br, I) and $(4\text{-}X'pyH)^+$ (X′ = Cl, Br) ion geometries were conducted using the GAMESS-UK[24] package, which employs the B3LYP DFT functional.[25] The basis set used was the all-electron Ahlrichs DZ (double zeta) quality basis[26] on Co and Sadlej pVTZ (polarized valence triple-zeta) basis[27,28] for all other elements. Geometries for $[CoX_4]^{2-}$ ions were idealized using distances (taken from the crystal structure determinations) of 2.25 (Cl), 2.40 (Br), and 2.59 Å (I) and averaged X-Co-X angles from the pairs of crystal structures containing each anion. The halopyridinium ions used geometries constructed by averaging bond lengths and angles over all crystal structures and idealizing to a C_{2v} geometry, with C–X lengths of 1.72 (Cl) and 1.88 Å (Br). The distortion of the $[CoCl_4]^{2-}$ ion was simulated by undertaking a geometry optimization of the $[CoCl_4]^{2-}$ ion (tetrahedral starting geometry) using an Ahlrichs DZ quality basis[26] throughout, with a simple model electrical field generated by placing +1 and −1 charges at distances of 10 Å from the Co center displaced along the molecular twofold axis and by imposing C_{2v} symmetry on the anion.

Received: July 23, 2005
Published online: December 6, 2005

Keywords: crystal engineering · electrostatic interactions · halogen bonds · noncovalent interactions · organic–inorganic hybrid composites

[1] a) For example, of 325 709 crystal structures in version 5.26 of the Cambridge Structural Database[1b] (Nov. 2004), the number containing molecules with C−X bonds are 1595 (C–I), 7294 (C–Br), 27 064 (C–Cl), and 16 555 (C–F). The corresponding figures for compounds containing terminal M−X bonds (M = d- or f-block-metal centers) are 3361 (M–I), 4189 (M–Br), 26 892 (M–Cl), and 747 (M–F); b) F. H. Allen, *Acta Crystallogr. Sect. B* **2002**, *58*, 380.

[2] F. Zordan, L. Brammer, P. Sherwood, *J. Am. Chem. Soc.* **2005**, *127*, 5979.

[3] a) L. Brammer, G. Mínguez Espallargas, H. Adams, *CrystEngComm* **2003**, *5*, 343; b) F. Zordan, L. Brammer, *Acta Crystallogr. Sect. B* **2004**, *60*, 512; c) F. Zordan, S. L. Purver, H. Adams, L. Brammer, *CrystEngComm* **2005**, *7*, 350; d) see, also: R. D. Willett, F. Awwadi, R. Butcher, S. Haddad, B. Twamley, *Cryst. Growth Des.* **2003**, *3*, 301.

[4] a) G. Aullón, D. Bellamy, L. Brammer, E. A. Bruton, A. G. Orpen, *Chem. Commun.* **1998**, 653; b) L. Brammer, E. A. Bruton, P. Sherwood, *Cryst. Growth Des.* **2001**, *1*, 277.

[5] a) L. Brammer, J. K. Swearingen, E. A. Bruton, P. Sherwood, *Proc. Nat. Acad. Sci. USA* **2002**, *99*, 4956; b) J. C. Mareque Rivas, L. Brammer, *Inorg. Chem.* **1998**, *37*, 4756; c) G. R. Lewis, A. G. Orpen, *Chem. Commun.* **1998**, 1873; d) A. L. Gillon, G. R. Lewis, A. G. Orpen, S. Rotter, J. Starbuck, X.-M. Wang, Y. Rodríguez-Martín, C. Ruiz-Pérez, *J. Chem. Soc. Dalton Trans.* **2000**, 3897; e) A. Angeloni, A. G. Orpen, *Chem. Commun.* **2001**, 343; f) B. Dolling, A. L. Gillon, A. G. Orpen, J. Starbuck, X.-M. Wang, *Chem. Commun.* **2001**, 567; g) M. Felloni, P. Hubberstey, C. Wilson, M. Schröder, *CrystEngComm* **2004**, *6*, 87; h) V. Balamurugan, M. S. Hundal, R. Mukherjee, *Chem. Eur. J.* **2004**, *10*, 1683; i) C. J. Adams, P. C. Crawford, A. G. Orpen, T. J. Podesta, B. Salt, *Chem. Commun.* **2005**, 2457.

[6] P. Metrangolo, H. Neukirch, T. Pilati, G. Resnati, *Acc. Chem. Res.* **2005**, *38*, 386.

[7] J. P. M. Lommerse, A. J. Stone, R. Taylor, F. H. Allen, *J. Am. Chem. Soc.* **1996**, *118*, 3108.

[8] V. R. Pedireddi, D. S. Reddy, B. S. Goud, D. C. Craig, A. D. Rae, G. Desiraju, *J. Chem. Soc. Perkin Trans. 2* **1994**, 2353.

[9] a) M. Freytag, P. G. Jones, B. Ahrens, A. K. Fischer, *New J. Chem.* **1999**, *23*, 1137; b) E. Corradi, S. V. Meille, M. T. Messina, P. Metrangolo, G. Resnati, *Angew. Chem.* **2000**, *112*, 1852; *Angew. Chem. Int. Ed.* **2000**, *39*, 1782; c) P. Metrangolo, G. Resnati, *Chem. Eur. J.* **2001**, *7*, 2511; d) R. Bailey Walsh, C. W. Padgett, P. Metrangolo, G. Resnati, T. W. Hanks, W. T. Pennington, *Cryst. Growth Des.* **2001**, *1*, 165; e) P. K. Thallapally, G. R. Desiraju, M. Bagieu-Beucher, R. Masse, C. Bourgogne, J.-F. Nicoud, *Chem. Commun.* **2002**, 1052; f) A. Crihfield, J. Hartwell, D. Phelps, R. Bailey Walsh, W. T. Pennington, T. W. Hanks, *Cryst. Growth Des.* **2003**, *3*, 313; g) P. Metrangolo, T. Pilati, G. Resnati, A. Stevenazzi, *Chem. Commun.* **2004**, 1492; h) T. Caronna, R. Liantonio, T. A. Logothetis, P. Metrangolo, T. Pilati, G. Resnati, *J. Am. Chem. Soc.* **2004**, *126*, 4500.

 © 2006 Wiley-VCH Verlag GmbH & Co. KGaA, Weinheim

[10] G. R. Desiraju, R. Parthasarathy, *J. Am. Chem. Soc.* **1989**, *111*, 8725.
[11] S. L. Price, A. J. Stone, J. Lucas, R. S. Rowland, A. E. Thornley, *J. Am. Chem. Soc.* **1994**, *116*, 4910.
[12] R. D. Bailey, M. R. Grabarczyk, T. W. Hanks, E. M. Newton, W. T. Pennington, *J. Chem. Soc. Perkin Trans. 2* **1997**, 2781.
[13] a) A. J. Blake, F. V. Devillanova, R. O. Gould, W.-S. Li, V. Lippolis, S. Parsons, C. Raddek, M. Schröder, *Chem. Soc. Rev.* **1998**, *27*, 195; b) P. H. Svensson, L. Kloo, *Chem. Rev.* **2003**, *103*, 1649.
[14] A. J. Bondi, *J. Chem. Phys.* **1964**, *68*, 441.
[15] $R_{XX'} = d(X\cdots X')/(r_X + r_{X'})$, where r_X and $r_{X'}$ are, respectively, the van der Waals radii[14] of halogen atoms X and X′ (following the definition of Lommerse et al.[7]); R_{HX} defined analogously for the H···X separation.
[16] It is anticipated that qualitative trend for halide anions should be the same as for an analogous series of perhalometallate ions, such as $[CoX_4]^{2-}$ ions.
[17] a) In $[CsI_3]$,[18a] $d(I{-}I) = 2.84$ Å; b) in $[CsBrI_2]$,[18b] $d(I{-}I) = 2.78$ Å; c) in (*N*-hexadecylpyridinium)$[BrI_2]$,[18c] $d(I{-}I) = 2.78$ Å; d) in (*N*-hexadecylpyridinium)$[ClI_2]$,[18c] $d(I{-}I) = 2.77$ Å.
[18] a) J. Runsink, S. Swen-Walstra, T. Migchelson, *Acta Crystallogr. Sect. B* **1972**, *28*, 1331; b) G. B. Carpenter, *Acta Crystallogr.* **1966**, *20*, 330; c) G. V. Shilov, O. N. Kazheva, O. A. D'yachenko, M. S. Chernov'yants, S. S. Simonyan, V. E. Gol'eva, A. I. Pyshchev, *Zh. Fiz. Khim.* **2002**, *76*, 1436.
[19] T. A. Logothetis, F. Meyer, P. Metrangolo, T. Pilati, G. Resnati, *New J. Chem.* **2004**, *28*, 760.
[20] We have shown recently that N–H···X hydrogen bonds form in preference to C–X′···X halogen bonds at the sites of greatest accumulation of negative charge on the halide when halide ions were compared with halometallate ions; see reference [3c].
[21] Calculated values for the $[CoCl_4]^{2-}$ ion in the model electrical field: Co-Cl(1) 2.421, Co-Cl(2) 2.338 Å; Cl(1)-Co-Cl(1′) 101.5, Cl(2)-Co-Cl(2′) 119.4°; where, Cl(1) and Cl(1′) are closest to the positive end of the field and Cl(2) and Cl(2′) are closest to the negative end. Slightly different values are obtained when using different basis sets, but the qualitative trend always matches the observed experimental distortion.
[22] a) G. M. Sheldrick, *SADABS:* Empirical absorption correction program, University of Göttingen, **1995**, based upon the method of Blessing;[22b] b) R. H. Blessing, *Acta Crystallogr. Sect. A* **1995**, *51*, 33.
[23] *SHELXTL* 5.1, Bruker Analytical X-Ray Instruments, Inc., **1998**.
[24] GAMESS-UK is a package of ab initio programs written by M. F. Guest, J. H. van Lenthe, J. Kendrick, K. Schoffel, P. Sherwood, with contributions from R. D. Amos, R. J. Buenker, H. J. J. van Dam, M. Dupuis, N. C. Handy, I. H. Hillier, P. J. Knowles, V. Bonacic-Koutecky, W. von Niessen, R. J. Harrison, A. P. Rendell, V. R. Saunders, A. J. Stone, A. H. de Vries; the package is derived from the original GAMESS code: M. Dupuis, D. Spangler, J. Wendoloski, NRCC Software Catalog, Vol. 1, Program No. QG01 (GAMESS), **1980**.
[25] a) P. J. Stephens, F. J. Devlin, C. F. Chabalowski, M. J. Frisch, *J. Phys. Chem.* **1994**, *98*, 11623, and references therein; b) *GAMESS-UK* uses the VWN 3 (RPA-type) parameterization; for details, see: R. H. Hertwig, W. Koch, *Chem. Phys. Lett.* **1997**, *268*, 345.
[26] The DZ Basis sets used were those incorporated into GAMESS-UK from A. Schafer, H. Horn, R. Ahlrichs, *J. Chem. Phys.* **1992**, *97*, 2571.
[27] All Basis sets and ECP data were obtained from the Extensible Computational Chemistry Environment Basis Set Database, Version 02/25/04, as developed and distributed by the Molecular Science Computing Facility, Environmental and Molecular Sciences Laboratory, which is part of the Pacific Northwest Laboratory (PO Box 999, Richland, Washington 99352, USA) and funded by the US Department of Energy. The Pacific Northwest Laboratory is a multiprogram laboratory operated by Battelle Memorial Institute for the US Department of Energy under contract DE-AC06-76RLO 1830. Contact David Feller or Karen Schuchardt for further information.
[28] A. J. Sadlej, *Theor. Chim. Acta* **1992**, *81*, 45, and references therein.

 © 2006 Wiley-VCH Verlag GmbH & Co. KGaA, Weinheim

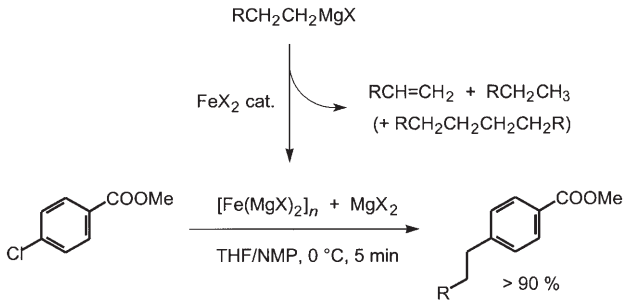
Synthetic Methods

DOI: 10.1002/anie.200502859

Unusual Structure and Reactivity of a Homoleptic "Super-Ate" Complex of Iron: Implications for Grignard Additions, Cross-Coupling Reactions, and the Kharasch Deconjugation**

Alois Fürstner, Helga Krause, and Christian W. Lehmann*

Our recent investigations on iron-catalyzed cross-coupling reactions of organomagnesium reagents with various electrophiles were guided by the perception that bare, low-valent iron clusters formed in situ according to Scheme 1 might



Scheme 1. Proposed formation of low-valent, intermetallic iron clusters serving as the actual catalysts in cross-coupling reactions of aryl chlorides and alkyl Grignard reagents with two or more carbon atoms. NMP = *N*-methylpyrrolidone.

account for the observed turnover.[1–5] Since the analysis of the released gas suggests that this reduction process involves a β-hydride elimination/reductive coupling event,[6] it should proceed only with Grignard reagents containing at least two

[*] Prof. A. Fürstner, H. Krause, Dr. C. W. Lehmann
Max-Planck-Institut für Kohlenforschung
45470 Mülheim/Ruhr (Germany)
Fax: (+49) 208-306-2994
E-mail: fuerstner@mpi-muelheim.mpg.de

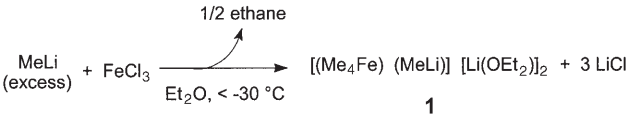
[**] Generous financial support by the MPG and the Fonds der Chemischen Industrie is gratefully acknowledged. We thank Dr. B. Scheiper for performing the reaction of enol triflate **8**.

WILEY InterScience DISCOVER SOMETHING GREAT
© 2006 Wiley-VCH Verlag GmbH & Co. KGaA, Weinheim

carbon atoms. In line with this notion, MeMgBr essentially *fails* to react with methyl 4-chlorobenzoate in the presence of $[Fe(acac)_3]$ (acac = acetylacetone) or $FeCl_n$ ($n = 2$, 3) as precatalysts, whereas all higher alkyl Grignard reagents are cross-coupled with exceptional ease under these conditions (Scheme 1).[1] This strikingly different behavior is general; in fact, methyl groups are transferred only to highly activated substrates such as enol triflates, acid chlorides, and very electron-deficient heteroarenes.[7,8]

To confirm this dichotomy in the proposed mechanism further, we set out to elucidate the structure of the reagent derived from FeX_n and MeMgBr. It was previously proposed that a host of homoleptic non-stabilized alkyl-iron species and/or iron-ate complexes of different composition is formed depending on the chosen stoichiometry, although none of these putative intermediates has ever been confirmed by spectroscopic or structural data.[9,10] Only the rapid reduction of $FeCl_3$ to $FeCl_2$ on treatment with the first equivalent of MeLi or MeMgBr is formally secured.[11]

Reaction of an anhydrous ethereal solution of $FeCl_3$ with MeLi at low temperature (< −30 °C), removal of the precipitated LiCl, and evaporation of the solvent at −78 °C afforded a red solid **1**, which dissolves in THF to give bright yellow colored solutions (Scheme 2). This material was previously



Scheme 2. Formation of the iron "super-ate" complex **1** from $FeCl_3$ and MeLi.

thought to consist of $[Me_4Fe][Li(OEt_2)]_2$.[12] Although the reported protonolysis data roughly matched this composition,[12] all previous attempts to further characterize this compound remained unsuccessful.[13] Gratifyingly, however, we managed to obtain crystalline samples suitable for crystal structure analysis upon slow cooling of saturated solutions of **1** in Et_2O from about −40 °C to −78 °C. Greatest possible care has to be taken due to the *exceptional* sensitivity of this product, which ignites in air and rapidly decomposes both in solution and in solid form at ≥ 0 °C.

The remarkable structure of the resulting complex **1**[14] comprises a homoleptic ferrate moiety in which four methyl groups surround the Fe^{II} atom in an almost ideal tetrahedral arrangement (Figure 1).[15] The molecule possesses crystallographic mirror symmetry with the iron atom, one lithium, and two methyl groups situated in special positions. The average of the four independent C-Fe-C angles is 109(3)°. For three (only two are crystallographically independent) of the four methyl groups the average Fe–C distance is 2.185(4) Å, whereas the distance to the fourth methyl group is shortened to 2.095(4) Å. The three former methyl groups each exhibit two further short distances to three lithium atoms (2.279(4)–2.321(5) Å). These lithium atoms form an equilateral triangle[16] and, together with the iron atom, a tetrahedral metal framework that shows T_d symmetry. Three of the four sides of this cluster are capped in a μ^3-fashion by the already

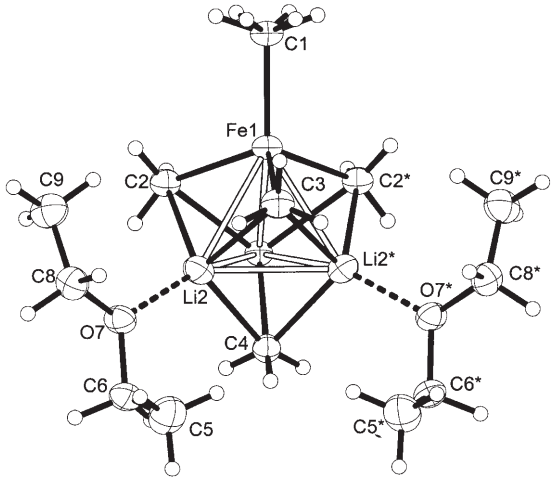


Figure 1. Structure of the iron "super-ate" complex **1** in the solid state. Li1 is the unlabeled ellipsoid in the back of the tetrahedral metallic frame. Selected bond lengths [Å]: Fe1–C1 2.095(4), Fe1–C2 2.188(3), Fe1–C3 2.182(4), Li1–C2 2.279(4), Li1–C4 2.181(7), Li2–C3 2.298(5), Li2–C4 2.190(6). The hydrogen atoms of methyl group C1 are disordered. Anisotropic displacement parameter ellipsoids are drawn at the 50% probability level.

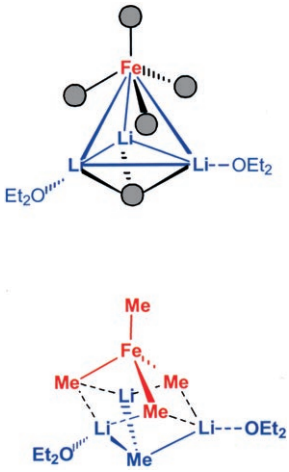
mentioned methyl groups, the fourth face is capped symmetrically by a fourth methyl group (av Li–C distance 2.186(6) Å) *devoid* of any direct contact to the iron center. The coordination sphere of two of the lithium atoms is completed by O-ether contacts (Li2 and Li2*), whereas Li1 forms a close contact of 2.301(6) Å to the carbon atom of the terminal Fe-methyl group of a neighboring molecule.

Overall, the structure of **1** shows a striking similarity to the solid-state structure of the methyllithium tetramer.[17] The structure of $(MeLi)_4$ has crystallographic T_d or $\bar{4}3m$ symmetry, resulting in only one independent Li–Li distance (2.68(5) Å), which is within one standard uncertainty of the average length of the tetrahedral edge in **1**. The comparison between the Li–C distances in $(MeLi)_4$ and **1** underlines this similarity further.[18]

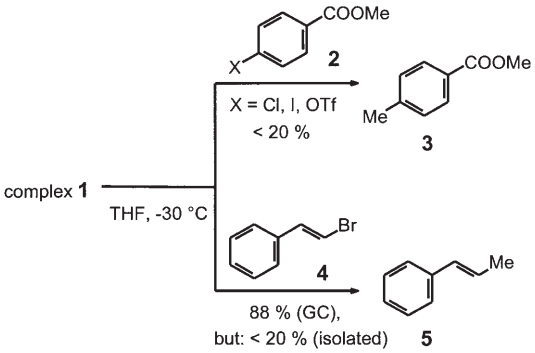
Based only on interatomic distances, it is difficult to deduce a "simple" model for the chemical bonding in **1**. Graphical representations emphasizing either the ferrate substructure with its "intertwined" lithium cap or the tetrahedral metallic frame are depicted in Scheme 3. Overall, the product derived from $FeCl_3$ and excess MeLi analyzes as $[(Me_4Fe)(MeLi)][Li(OEt_2)]_2$ (**1**). As such, **1** represents the first *alkyl*-ate complex of iron devoid of any stabilizing ligands that has been structurally characterized and adds one more example to the very small family of homoleptic iron complexes with η^1-bound carbon entities other than CO.[19,20]

Next, the reactivity of **1** was checked in a set of prototype transformations. As expected, this compound essentially fails to alkylate *p*-XC_6H_4COOMe (**2**; X = Cl, I, OTf; Scheme 4), thus corroborating the notion that ate-complexes play no role in the iron-catalyzed cross-coupling reactions of higher alkyl Grignard reagents mentioned above (cf. Scheme 1).[1] Likewise, alkenyl halides such as **4** were found to be rather poor substrates; this result is in striking contrast to previous reports that an iron-ate complex of the putative composition

 © 2006 Wiley-VCH Verlag GmbH & Co. KGaA, Weinheim



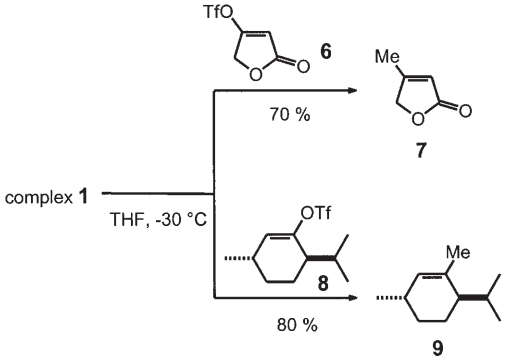
Scheme 3. Two different representations of the structure of the Fe^{II}-ate complex **1**: Top: Graphical illustration of the metal cluster forming the inner core; the methyl units are represented as balls, four of which reside over the faces of this tetrahedron. Bottom: The ferrate unit is color-coded in red; its negative charges are counterbalanced by the intertwined lithium "cap" carrying an extra methyl group.



Scheme 4.

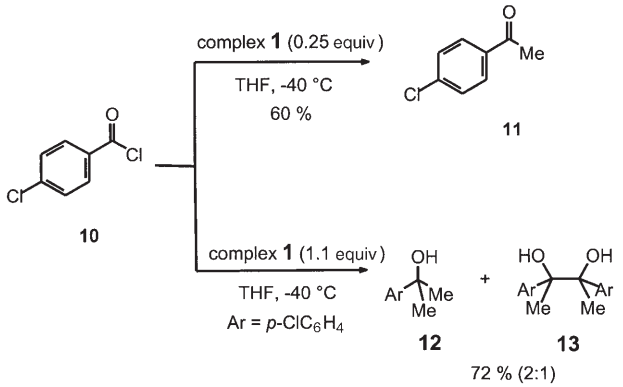
"Me_4FeLi_2" formed in situ methylates bromide **4** in high yield and selectivity.[9,21] Moreover, the claimed stability of the in situ species up to 40 °C[9] is inconsistent with our data.

Complex **1**, however, transfers its methyl groups to more activated electrophiles such as enol triflates, as previously communicated (Scheme 5).[7] Along the same lines, acid



Scheme 5.

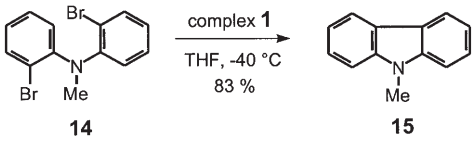
chloride **10** affords the corresponding acetophenone derivative **11**, again without any competing side reaction of the aryl chloride moiety interfering (Scheme 6). When **1** is used in excess, the reaction proceeds further to give the carbonyl



Scheme 6.

addition product **12** and the corresponding pinacol **13**, suggesting that the ate-complex also acts as a single-electron transfer (SET) agent towards the ketone initially formed. This result is highly reminiscent of early work of Ashby et al. who found that the amount of pinacol produced in attempted additions of MeMgBr to aromatic ketones is *directly proportional to the iron impurities of the magnesium metal* used to form the Grignard reagent.[22] Our results, therefore, suggest that the reagent responsible for this striking correlation is an ate-complex of the type described herein.[23] More generally speaking, this finding sheds light into the well established but hardly understood "alchemistic" effects exerted by certain transition-metal residues on the course of Grignard reactions.[24]

The SET potential of complex **1** is also responsible for the conversion of dibromide **14** to carbazole **15** (Scheme 7). This



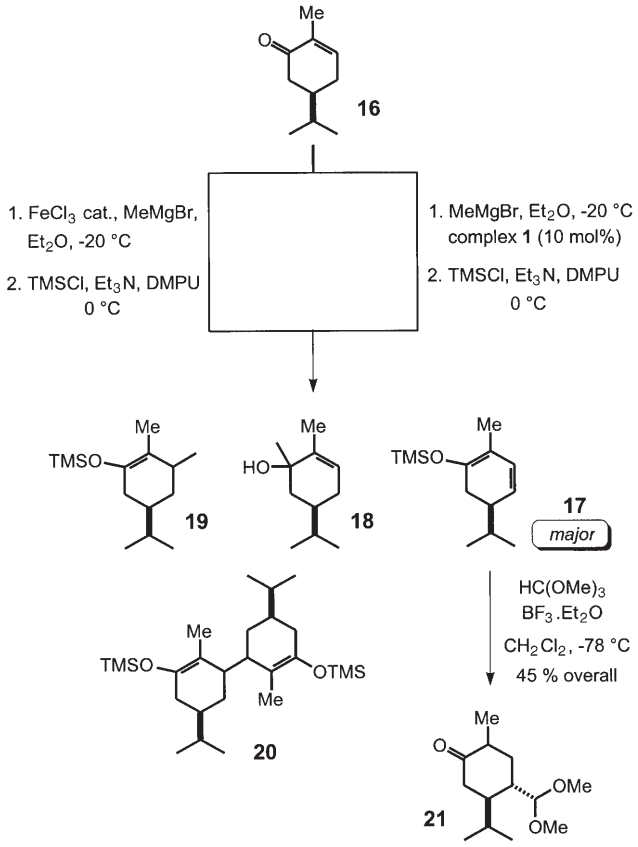
Scheme 7.

Ullmann-type coupling was recently effected with the putative complex "Me_4FeLi_2" formed in situ.[25] Since the defined metalate **1** provides the same result, it seems reasonable to assume that it constitutes the actual intermediate operative under the in situ conditions.

Finally, we propose that ate-complexes similar to **1** also play a vital role in the deconjugation of α,β-unsaturated enones pioneered by Kharasch et al. using catalytic amounts of $FeCl_3$ and excess MeMgBr.[26] A modified version of this process allows the formation of thermodynamic silyl enol ethers that are difficult to obtain otherwise.[27] Although this method has undergone significant empirical optimization,[27,28] the identity of the active species remained obscure,

 © 2006 Wiley-VCH Verlag GmbH & Co. KGaA, Weinheim

except for the vague statement that it might consist of a "mixture of activated zero-valent iron and Grignard reagent".[27] To check whether ate-complexes play any significant role in this transformation, we treated dihydrocarvone **16**[29] according to the original recipe ($FeCl_3$ cat., MeMgX)[30] as well as with complex **1** as the catalyst (Scheme 8). The crude product spectrum obtained after



Scheme 8. Conversion of dihydrocarvone **16** to the silyl enol ether **17**, the corresponding 1,2- and 1,4-addition products **18** and **19**, and the dimer **20**. TMSCl = trimethylsilyl chloride, DMPU = *N*,*N*′-dimethyl-*N*,*N*′-propylene urea.

quenching of the reaction with $TMSCl/Et_3N$ is virtually identical for both cases. The silyl enol ether **17** is the major compound accompanied by the corresponding 1,2- and 1,4-addition products **18** and **19** as well as dimer **20** (diastereomeric mixture) formed again by an SET event. Compound **17** can be further elaborated into product **21**, which served as a key intermediate for the preparation of the cytotoxic diterpenoids of the sarcodictyin family.[30] These comparative experiments strongly suggest that iron "super-ate" complexes constitute the actual "Kharasch reagent", at least in those optimized cases where the reaction is performed at low temperature.

In summary, we disclosed the first structurally characterized ate-complex of Fe^{II} bearing only alkyl substituents without any further stabilizing ligands; the fact that **1** incorporates an additional molecule of methyllithium represents a particularly remarkable structural feature. Since defined homoleptic complexes of iron, in contrast to those of the neighboring elements in the periodic table, are extremely scarce,[20] we hope that our data will help to unravel the as of yet largely unknown chemistry and catalytic potential of such species. Concerning its reactivity profile, compound **1** obviously combines many different facets including nucleophilic behavior, a prominent electron-transfer capacity, as well as a significant basicity. With this in mind, we like to express a "caveat" concerning selectivity claims for reactions invoking putative iron-ate complexes of different "formal" compositions found in the early literature,[9] notably in those cases where the reactions have been performed at higher temperatures.

Received: August 11, 2005
Published online: December 2, 2005

Keywords: ate complexes · cross-coupling · Grignard reaction · iron · single-electron transfer

[1] a) A. Fürstner, A. Leitner, M. Méndez, H. Krause, *J. Am. Chem. Soc.* **2002**, *124*, 13856–13863; b) A. Fürstner, A. Leitner, *Angew. Chem.* **2002**, *114*, 632–635; *Angew. Chem. Int. Ed.* **2002**, *41*, 609–612; c) A. Fürstner, A. Leitner, G. Seidel, *Org. Synth.* **2005**, *81*, 33–42.

[2] a) A. Fürstner, A. Leitner, *Angew. Chem.* **2003**, *115*, 320–323; *Angew. Chem. Int. Ed.* **2003**, *42*, 308–311; b) G. Seidel, D. Laurich, A. Fürstner, *J. Org. Chem.* **2004**, *69*, 3950–3952; c) A. Fürstner, D. De Souza, L. Parra-Rapado, J. T. Jensen, *Angew. Chem.* **2003**, *115*, 5516–5518; *Angew. Chem. Int. Ed.* **2003**, *42*, 5358–5360; d) A. Fürstner, L. Turet, *Angew. Chem.* **2005**, *117*, 3528–3532; *Angew. Chem. Int. Ed.* **2005**, *44*, 3462–3466; e) A. Fürstner, M. Méndez, *Angew. Chem.* **2003**, *115*, 5513–5515; *Angew. Chem. Int. Ed.* **2003**, *42*, 5355–5357; f) B. Scheiper, F. Glorius, A. Leitner, A. Fürstner, *Proc. Natl. Acad. Sci. USA* **2004**, *101*, 11960–11965; g) A. Fürstner, D. Kirk, M. D. B. Fenster, C. Aïssa, D. De Souza, O. Müller, *Proc. Natl. Acad. Sci. USA* **2005**, *102*, 8103–8108; h) O. Lepage, E. Kattnig, A. Fürstner, *J. Am. Chem. Soc.* **2004**, *126*, 15970–15971; i) R. Martin, A. Fürstner, *Angew. Chem.* **2004**, *116*, 4045–4047; *Angew. Chem. Int. Ed.* **2004**, *43*, 3955–3957; j) A. Fürstner, R. Martin, K. Majima, *J. Am. Chem. Soc.* **2005**, *127*, 12236–12237.

[3] Reviews: a) H. Shinokubo, K. Oshima, *Eur. J. Org. Chem.*, **2004**, 2081–2091; b) C. Bolm, J. Legros, J. Le Paih, L. Zani, *Chem. Rev.* **2004**, *104*, 6217–6254; c) A. Fürstner, R. Martin, *Chem. Lett.* **2005**, *34*, 624–629.

[4] Pioneering studies on the use of iron for cross-couplings: a) M. Tamura, J. K. Kochi, *J. Am. Chem. Soc.* **1971**, *93*, 1487–1489; b) J. K. Kochi, *Acc. Chem. Res.* **1974**, *7*, 351–360; c) G. Cahiez, H. Avedissian, *Synthesis* **1998**, 1199–1205; d) G. A. Molander, B. J. Rahn, D. C. Shubert, S. E. Bonde, *Tetrahedron Lett.* **1983**, *24*, 5449–5452; e) C. K. Reddy, P. Knochel, *Angew. Chem.* **1996**, *108*, 1812–1813; *Angew. Chem. Int. Ed. Engl.* **1996**, *35*, 1700–1701; f) A. Fürstner, H. Brunner, *Tetrahedron Lett.* **1996**, *37*, 7009–7012; g) J.-L. Fabre, M. Julia, J.-N. Verpeaux, *Tetrahedron Lett.* **1982**, *23*, 2469–2472; h) A. Yanagisawa, N. Nomura, H. Yamamoto, *Tetrahedron* **1994**, *50*, 6017–6028.

[5] Recent contributions from other groups: a) B. Hölzer, R. W. Hoffmann, *Chem. Commun.* **2003**, 732–733; b) W. Dohle, F. Kopp, G. Cahiez, P. Knochel, *Synlett* **2001**, 1901–1904; c) M. Hojo, Y. Murakami, H. Aihara, R. Sakuragi, Y. Baba, A. Hosomi, *Angew. Chem.* **2001**, *113*, 641–643; *Angew. Chem. Int. Ed.* **2001**, *40*, 621–623; d) M. A. Fakhfakh, X. Franck, R. Hocquemiller, B. Figadère, *J. Organomet. Chem.* **2001**, *624*,

 © 2006 Wiley-VCH Verlag GmbH & Co. KGaA, Weinheim

131 – 135; e) M. Nakamura, K. Matsuo, S. Ito, E. Nakamura, *J. Am. Chem. Soc.* **2004**, *126*, 3686 – 3687; f) T. Nagano, T. Hayashi, *Org. Lett.* **2004**, *6*, 1297 – 1299; g) M. Nakamura, S. Ito, K. Matsuo, E. Nakamura, *Synlett* **2005**, 1794 – 1798; h) K. Itami, S. Higashi, M. Mineno, J. Yoshida, *Org. Lett.* **2005**, *7*, 1219 – 1222; i) I. Sapountzis, W. Lin, C. C. Kofink, C. Despotopoulou, P. Knochel, *Angew. Chem.* **2005**, *117*, 1682 – 1685; *Angew. Chem. Int. Ed.* **2005**, *44*, 1654 – 1658; j) R. B. Bedford, D. W. Bruce, R. M. Frost, J. W. Goodby, M. Hird, *Chem. Commun.* **2004**, 2822 – 2823.

[6] B. Bogdanovic, M. Schwickardi, *Angew. Chem.* **2000**, *112*, 4788 – 4790; *Angew. Chem. Int. Ed.* **2000**, *39*, 4610 – 4612.

[7] a) B. Scheiper, M. Bonnekessel, H. Krause, A. Fürstner, *J. Org. Chem.* **2004**, *69*, 3943 – 3949; b) see also: C. Duplais, F. Bures, I. Sapountzis, T. J. Korn, G. Cahiez, P. Knochel, *Angew. Chem.* **2004**, *116*, 3028 – 3030; *Angew. Chem. Int. Ed.* **2004**, *43*, 2968 – 2970.

[8] Recent applications: a) M. Hocek, H. Dvoráková, *J. Org. Chem.* **2003**, *68*, 5773 – 5776; b) N. Maulide, J.-C. Vanherck, I. E. Markó, *Eur. J. Org. Chem.* **2004**, 3962 – 3967; c) M. Hocek, R. Pohl, I. Cisarová, *Eur. J. Org. Chem.* **2005**, 3026 – 3030.

[9] Review: T. Kauffmann, *Angew. Chem.* **1996**, *108*, 401 – 418; *Angew. Chem. Int. Ed. Engl.* **1996**, *35*, 386 – 403.

[10] Leading references: a) E. J. Corey, G. H. Posner, *Tetrahedron Lett.* **1970**, *11*, 315 – 318; b) E. J. Corey, H. Yamamoto, D. K. Herron, K. Achiwa, *J. Am. Chem. Soc.* **1970**, *92*, 6635 – 6636; c) T. Kauffmann, B. Laarmann, D. Menges, G. Neiteler, *Chem. Ber.* **1992**, *125*, 163 – 169; d) T. Kauffmann, K.-U. Voß, G. Neiteler, *Chem. Ber.* **1993**, *126*, 1453 – 1459.

[11] H. J. Berthold, H. J. Spiegl, *Z. Anorg. Allg. Chem.* **1972**, *391*, 193 – 202.

[12] H. J. Spiegl, G. Groth, H. J. Berthold, *Z. Anorg. Allg. Chem.* **1973**, *398*, 225 – 230.

[13] Attempted crystallizations are reported in ref. [9].

[14] X-ray crystal structure analysis of **1:** $C_{13}H_{35}FeLi_3O_2$, $M_r = 300.08\ g\,mol^{-1}$, yellow-orange plate, crystal size $0.08 \times 0.06 \times 0.05\ mm^3$, orthorhombic, space group *Pnma*, $a = 12.3527(5)$ Å, $b = 15.9319(8)$ Å, $c = 9.9546(5)$ Å, $V = 1959.08(16)$ Å^3, $T = 100$ K, $Z = 4$, $\rho_{calcd} = 1.017\ g\,cm^{-3}$, $\lambda = 0.71073$ Å, $\mu(Mo_{K\alpha}) = 0.762\ mm^{-1}$, Nonius Kappa CCD diffractometer, $3.30 < \theta < 27.08°$, 17506 measured reflections, 2231 independent reflections, 1601 reflections with $I > 2\sigma(I)$, structure solved by direct methods and refined by full matrix least-squares on F_o^2 to $R_1 = 0.050$ [$I > 2\sigma(I)$], $wR_2 = 0.114$, 116 parameters, H atoms mixed, $S = 1.038$, residual electron density $+0.5/-0.3\ e\,Å^{-3}$. CCDC-279956 contains the supplementary crystallographic data for this paper. These data can be obtained free of charge from the Cambridge Crystallographic Data Centre via www.ccdc.cam.ac.uk/data_request/cif.

[15] The four independent C-Fe-C angles are 113.67(15), 109.24(9), 109.28(9), and 105.83(15)°.

[16] The standard uncertainty of the average edge is within three times the average standard uncertainties of each individual edge.

[17] a) E. Weiss, G. Hencken, *J. Organomet. Chem.* **1970**, *21*, 265 – 268; b) for a review on the structure of organolithium compounds, see: W. N. Setzer, P. v. R. Schleyer, *Adv. Organomet. Chem.* **1985**, *24*, 353 – 451; c) A. Streitweiser, S. M. Bachrach, A. Dorigo, P. von R. Schleyer in *Lithium Chemistry* (Eds.: A.-M. Sapse, P. von R. Schleyer), Wiley, New York, **1995**, pp. 1 – 43.

[18] The C–Li distance in Me_4Li_4 is 2.31(5) Å, the average C–Li distance in **1** is 2.25(6) Å.

[19] Reviews: a) R. C. Kerber in *Comprehensive Organometallic Chemistry II, Vol. 7*, 2nd ed. (Eds.: E. W. Abel, F. G. A. Stone, G. Wilkinson), Pergamon, Oxford, **1995**, pp. 101 – 229; b) J. R. Green, W. A. Donaldson in *Encyclopedia of Inorganic Chemistry, Vol. 4* (Ed.: R. B. King), Wiley, Chichester, **1994**, pp. 1735 – 1784; c) A. Segnitz in *Methoden der Organischen Chemie (Houben-Weyl), Vol. 13/9a*, 4th ed. (Ed.: A. Segnitz), Thieme, Stuttgart, **1986**, pp. 175 – 523; d) for a review on iron-alkyl species carrying extra stabilizing ligands, see: A. Yamamoto, *J. Organomet. Chem.* **1986**, *300*, 347 – 367.

[20] a) T. A. Bazhenova, R. M. Lobkovskaya, R. P. Shibaeva, A. K. Shilova, M. Gruselle, G. Leny, E. Deschamps, *J. Organomet. Chem.* **1983**, *244*, 375 – 382; b) T. A. Bazhenova, L. M. Kachapina, A. E. Shilov, M. Y. Antipin, Y. T. Struchkov, *J. Organomet. Chem.* **1992**, *428*, 107 – 123; c) H. Müller, W. Seidel, H. Görls, *J. Organomet. Chem.* **1993**, *445*, 133 – 136; d) H. Müller, W. Seidel, H. Görls, *Z. Anorg. Allg. Chem.* **1996**, *622*, 756 – 758; e) W. Seidel, K.-J. Lattermann, *Z. Anorg. Allg. Chem.* **1982**, *488*, 69 – 74; f) T. A. Bazhenova, R. M. Lobkovskaya, R. P. Shibaeva, A. E. Shilov, A. K. Shilova, M. Gruselle, G. Leny, B. Tchoubar, *J. Organomet. Chem.* **1983**, *244*, 265 – 272; g) A. Klose, E. Solari, C. Floriani, A. Chiesi-Villa, C. Rizzoli, N. Re, *J. Am. Chem. Soc.* **1994**, *116*, 9123 – 9135.

[21] Although GC shows seemingly clean conversions, the isolated yields of **5** remained disappointingly low using either defined **1** or the in situ system, see Scheme 4.

[22] a) E. C. Ashby, T. L. Wiesemann, *J. Am. Chem. Soc.* **1978**, *100*, 189 – 199; b) E. C. Ashby, J. D. Buhler, I. G. Lopp, T. L. Wiesemann, J. S. Bowers, Jr., J. T. Laemmle, *J. Am. Chem. Soc.* **1976**, *98*, 6561 – 6570.

[23] Complex **1**, however, seems to be unable to transfer electrons to dialkyl ketones as evident from the clean addition to 4-*tert*-butylcyclohexanone. This result is again in excellent agreement with the report by Ashby et al. who showed that the iron content in the magnesium has no effect in Grignard additions to aliphatic carbonyl compounds. Moreover, they are in line with the finding that certain iron salts beneficially effect the stereoselective course of addition of cyclic ketones as reported by Reetz et al., see: M. T. Reetz, S. Stanchev, *J. Chem. Soc. Chem. Commun.* **1993**, 328 – 330.

[24] M. S. Kharasch, O. Reinmuth, *Grignard Reactions of Nonmetallic Substances*, Constable, London, **1954**.

[25] a) M. Uchiyama, Y. Matsumoto, S. Nakamura, T. Ohwada, N. Kobayashi, N. Yamashita, A. Matsumiya, T. Sakamoto, *J. Am. Chem. Soc.* **2004**, *126*, 8755 – 8759; b) short review: R. W. Hoffmann, *Angew. Chem.* **2005**, *117*, 6433 – 6435; *Angew. Chem. Int. Ed.* **2005**, *44*, 6277 – 6279.

[26] M. S. Kharasch, P. O. Tawney, *J. Am. Chem. Soc.* **1941**, *63*, 2308 – 2315.

[27] a) M. E. Krafft, R. A. Holton, *J. Am. Chem. Soc.* **1984**, *106*, 7619 – 7621; b) M. E. Krafft, R. A. Holton, *J. Org. Chem.* **1984**, *49*, 3669 – 3670.

[28] a) J. Meinwald, L. Hendry, *J. Org. Chem.* **1971**, *36*, 1446 – 1447; b) N. Ito, T. Etoh, *J. Chem. Soc. Perkin Trans. 1* **1996**, 2397 – 2405.

[29] Dihydrocarvone was prepared as described in ref. [30]. The reported ^{13}C NMR data of this compound, however, are incorrect; compound **16** analyzes as follows: ^{13}C NMR (75 MHz, $CDCl_3$): $\delta = 200.5$, 145.2, 142.0, 141.9, 135.2, 31.9, 29.7, 19.5, 19.4, 15.5 ppm.

[30] S. M. Ceccarelli, U. Piarulli, C. Gennari, *Tetrahedron* **2001**, *57*, 8531 – 8542.

 © 2006 Wiley-VCH Verlag GmbH & Co. KGaA, Weinheim

Oxidation Reactions

DOI: 10.1002/anie.200502897

Redox Behavior of Fe-Mo-O Catalysts Studied by Ultrarapid In Situ Diffraction**

*S. D. M. Jacques, O. Leynaud, D. Strusevich, A. M. Beale, G. Sankar, C. M. Martin, and P. Barnes**

The term "Fe-Mo-O" is used to denote a mixed-phase catalyst system as used, for example, in the production of formaldehyde, which is an important building block for complex chemicals in many consumer products. Almost all formaldehyde is manufactured by either: 1) dehydrogenation of a methanol-rich air mixture over a silver catalyst or 2) direct oxidation of methanol over a Fe-Mo-O-based catalyst.[1,2a] The latter process is advantageous in that the exothermic reaction can be carried out at comparatively lower temperatures, typically 375–350 °C, and the catalyst offers comparatively higher activity and selectivity.[2b] The mechanism is assumed to follow a Mars/van Krevelen like process of oxidative dehydrogenation of hydrocarbons and has been demonstrated for an industrial Fe-Cr-Mo-O preparation.[3] Methanol oxidation proceeds with a partial reduction of the active iron molybdate $Fe_2(MoO_4)_3$ phase [Eq. (1)], followed by catalyst regeneration:[4,5]

$$CH_3OH + Fe_2(MoO_4)_3 \rightarrow 2\,(\beta\text{-}FeMoO_4) + MoO_3 + CH_2O + H_2O \quad (1)$$

There have been several notable studies on Fe-Mo-O catalysts[3,6–14] that covered aspects of catalytic activity, deactivation, and mechanism. In particular, the Mo/Fe ratio is considered to be important; industrial preparations use a Mo/Fe ratio greater than 1.5:1 comprising a mixture of two phases $Fe_2(MoO_4)_3$ and MoO_3. It is thought that the primary function of MoO_3 is to provide a reservoir of molybdenum to balance losses through sublimation at reactor hot spots that would otherwise prevent regeneration of the active phase and lead to the formation of Fe_2O_3, which favors total oxidation.[1,7,15] However, there have not been any previous diffraction studies that focus on the interplay between these phases and their effect on the catalytic reaction and regeneration. Herein, we show the importance of observing these reactions by using rapid time-resolved in situ powder diffraction; in particular, we capture the responses of the Fe-Mo-O catalyst under accelerated aging conditions and show the importance of the multiple-phase form in maintaining catalyst longevity.

A special environmental cell system has been designed to apply redox cycling conditions to catalyst material while collecting (in situ) powder diffraction data on the synchrotron; this cell is illustrated in Figure 1 and described with operational details in the Experimental Section.

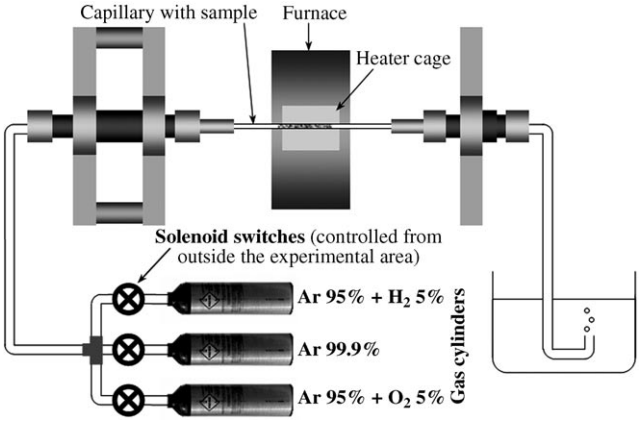


Figure 1. Schematic representation of the redox environmental cell consisting of a capillary furnace and gas-delivery system. The incident and diffracted synchrotron X-ray beams are in a perpendicular plane (to the diagram), with the exit window of the furnace spanning an angular range of 120°.

Diffraction patterns of the catalyst material, both as prepared and after reduction, were analyzed first to confirm the starting materials and basic methodology. The three-component phases expected, $Fe_2(MoO_4)_3$, MoO_3, and β-$FeMoO_4$, account for all the constituent peaks in the diffraction patterns once allowance has been made for differential thermal expansion up to the operating temperature of 472 °C: For $Fe_2(MoO_4)_3$, its two very similar allotropes[19] can be accommodated by using the high-temperature form[20] extrapolated to 472 °C; for MoO_3, in-house high-temperature neutron data[21] were necessary to unravel the mixed (positive/negative) expansion contributions; for β-$FeMoO_4$, reliable data[22] could be found only for ambient conditions, and so the diffraction peaks at 472 °C were identified by indexing the remaining peaks (with the Crysfire

[*] Dr. S. D. M. Jacques, Dr. O. Leynaud, D. Strusevich, Prof. P. Barnes
Industrial Materials Group
Materials Chemistry Centre, Department of Chemistry
University College London
20 Gordon Street, London WC1H 0AJ (UK)
and
Department of Crystallography
Birkbeck College
Malet Street, London WC1E 7HX (UK)
Fax: (+44) 207-631-6803
E-mail: barnes@img.cryst.bbk.ac.uk
Dr. A. M. Beale
Department of Inorganic Chemistry and Catalysis
Sorbonnelaan 16, 3584 CA, Utrecht (The Netherlands)
Prof. G. Sankar
The Royal Institution
21 Albemarle Street, London W1X 4BS (UK)
Dr. C. M. Martin
CLRC Daresbury Laboratory
Daresbury, Warrington WA4 4AD (UK)

[**] The authors acknowledge the EPSRC for financial support, the staff of Daresbury Laboratory, and the engineers Paul Stukas (Birkbeck College) and Mike Sheehy (Royal Institution) for design/construction of the furnace.

Supporting information for this article is available on the WWW under http://www.angewandte.org or from the author.

 © 2006 Wiley-VCH Verlag GmbH & Co. KGaA, Weinheim

program[23]) by using the ambient unit cell as a starting guide. The peak positions of the three phases at 472 °C were then all refined independently against the experimental patterns using the Celref program.[24] This approach provided an essential starting set of parameters (Table 1) for the subsequent multiphase Rietveld refinements of the in situ patterns obtained during the redox cycles; no peaks remained unexplained, though there was a residual intensity mismatch for some MoO_3 peaks during the Rietveld refinement because of the preferred orientation of MoO_3, which is typical of lamellar structures[21] (an example fit is given in the Supporting Information).

Table 1: Space groups, starting unit-cell parameters, and weight fractions for the three-component phases.[a]

Phase	Space group	Unit-cell parameters [Å]	Initial fraction [%]	Reduced fraction [%]
$Fe_2(MoO_4)_3$	*Pbcn*	$a=12.88$; $b=9.206$; $c=9.323$	51	27
β-$FeMoO_4$	*C*12/*m*1	$a=10.36$; $b=9.447$; $c=7.107$ $\beta=106.4°$	<1	19
MoO_3	*Pnma*	$a=14.20$; $b=3.702$; $c=3.989$	49	54

[a] These data were obtained by fitting simulated patterns to the diffraction patterns for the initial catalyst and the same after reduction at 472 °C.

Figure 2a shows the time-resolved in situ patterns obtained during a reduction-oxidation-reduction cycle at 472 °C. The collection time for each pattern was 30 seconds and the sequence covers 60 minutes spanning almost a complete cycle.

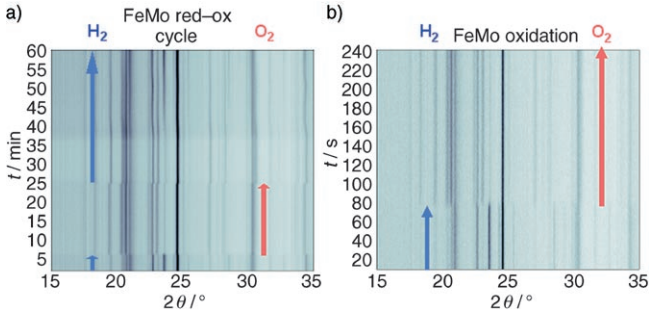


Figure 2. Contour images of in situ powder diffraction from a Fe-Mo-O catalyst at 472 °C under successive reducing (red) and oxidizing (blue) atmospheres: a) 120×30 s patterns that show the end of one reduction cycle, a full oxidation cycle, and part of a second reduction step; b) an ultra-rapid acquisition (patterns every 2 s), thus illustrating the extreme rapidity of the oxidation stage.

The change in diffraction patterns on introduction of the oxidizing gas (at 5 minutes) is dramatic, thus appearing to be discontinuous on the minute timescale. By comparison, the changes during subsequent reduction (25–60 min) are far more gradual. The sequence of changes in the position of peaks is somewhat complicated by a small movement of the sample capillary in the diffractometer as the gas is changed: thus, there are peak shifts at 5 minutes that arise from both structural changes and capillary movement, whereas the immediate shifts at 25 minutes are entirely because of capillary movement. This effect was effectively "subtracted out" in the subsequent data analysis. Multiphase Rietveld structure refinement (cyclic mode of Fullprof[25] using WinPLOTR software[26]) was performed over 120 patterns (Figure 3a), in which the unit cells and scale factors (effectively molecular-weight fractions) were allowed to vary but the fractional atomic coordinates and the profile parameters were kept fixed because of the unavoidable preferred orientation effects mentioned previously. The resulting variations in weight fraction versus time are given in Figure 3a; the general trends are clear over and above the irregularities (e.g., ≈50 min), which arise from inhomogeneities in gas flow/penetration through the large specimen agglomerates required to pack the capillary (see the Experimental Section). The Supporting Information shows that these irregularities can be smoothed out by using larger specimen capillaries (4 mm in diameter), but at the expense of data speed/resolution, which is required for the oxidation stage (see later).

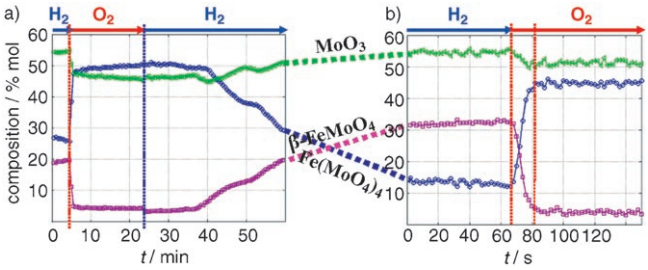


Figure 3. Phase composition (% mol weight fractions) of $Fe_2(MoO_4)_3$, β-$FeMoO_4$, and MoO_3 obtained by multiphase Rietveld fitting to the data shown in Figure 2 (same gas environment notation): a) Variations on the minute timescale that show incomplete reduction, even after 36 min; b) capturing the rapid oxidation stage on a second timescale.

The disproportionate rapidity of the oxidation stage, relative to reduction, required reexamination while pushing the system performance to its limit. The result is shown in Figure 2b, which shows the oxidation stage captured in two-second diffraction intervals. Multiphase Rietveld refinements were performed on the two-second diffraction patterns that span the transition to quantify this further. The resulting scatter is unavoidably increased, nevertheless the time profile obtained (Figure 3b) clearly shows the progression of this transition and that the oxidation reactions are virtually completed within 15 seconds. At present, one can only speculate on why there should be such a huge difference in the reduction and oxidation rates: First, one notes that the standard redox potential of $+0.77$ V for $Fe^{3+}+e^- \rightarrow Fe^{2+}$ rather suggests a favored reduction (forward direction) though one should also consider the observation[14] that this process might occur through two steps at the catalyst surface, first Mo^{6+} to Mo^{5+} before Fe^{3+} to Fe^{2+}. Other explanations that relate to higher anionic mobilities for the β-$FeMoO_4$

 © 2006 Wiley-VCH Verlag GmbH & Co. KGaA, Weinheim

phase, which aid the solid-state transport of oxygen during oxidation, remain questionable in light of the rapid oxidation rates observed. A more intriguing possibility, for which there is some supporting evidence,[27,28] concerns the physicochemical nature of the reduction reaction itself [see Eq. (2)],

$$H_2 + Fe_2(MoO_4)_3 \rightarrow 2\,(\beta\text{-}FeMoO_4) + MoO_3 + H_2O \quad (2)$$

whereby H_2O production will block access of hydrogen to the Fe-Mo-O active sites during reduction; by contrast, known rapid oxygen uptake[29] clearly aids the reoxidation process. Importantly, one also notes that the presence of other crystalline Mo/Fe reduced phases are clearly ruled out by the diffraction data.

In conclusion, this study has demonstrated the power of ultra-rapid in situ powder diffraction for obtaining new insight into the high-temperature solid-state redox processes that occur in a mixed catalyst system. The combination of intense synchrotron wiggler radiation, X-ray optics, and an ultra-rapid/high-resolution detector enables one to follow both slow reactions and those that are too fast for capture by conventional laboratory or synchrotron techniques. It is possible to rationalize the behavior according to a Mars/van Krevlen type process: the $Fe_2(MoO_4)_3$ phase undergoes reduction in an atmosphere of 5% H_2/Ar according to equation (2) and subsequent regeneration in an atmosphere of 5% O_2/Ar according to Equation (3):

$$2(\beta\text{-}FeMoO_4) + MoO_3 + {}^1/_2O_2 \rightarrow Fe_2(MoO_4)_3 \quad (3)$$

The speed of the redox processes at 472 °C has been uniquely determined: Even though these are multiphase solid-state reactions, the oxidation stage is found to be extremely fast; oxidation is effectively completed within 15 seconds at 472 °C, in contrast to the reduction stage, which is incomplete even after 36 minutes. This difference in rate appears to be contrary to the existing viewpoint (e.g, Pernicone[12]) that reduction of $Fe_2(MoO_4)_3$ is easier than oxidation of β-$FeMoO_4$. This difference in reactivity will be critical for maintaining phase stability and catalyst activity. The absence of any additional phases suggests that reaction (3) proceeds so quickly that other solid-state side reactions that lead to deactivation [e.g., Eq. (4)] are avoided:

$$2(\beta\text{-}FeMoO_4) + {}^1/_2O_2 \rightarrow Fe_2O_3 + 2\,MoO_3 \quad (4)$$

Therefore, we have demonstrated that the addition of an excess of MoO_3 in the as-prepared catalyst is beneficial for maintaining the stability of the active phase as well as replenishing any sublimed molybdenum that might occur. Finally, we note that although there have been previous attempts to capture redox processes that occur in single-phase systems this investigation is the first diffraction study, as far as the authors are aware, of such rapid reactions within a mixed-phase solid-state system. Many other catalytic systems can now realistically become candidates for detailed study by this method, including the optimization of catalyst composition and working temperature.

Experimental Section

The industrial-like iron molybdate catalyst was prepared with a Mo/Fe atomic ratio of 3:1 by using a coprecipitation method similar to that by Soares et al.[6] using appropriate amounts of $[Mo_7(NH_4)_6O_{24}]\cdot 4H_2O$ and $[Fe(NO_3)_3]\cdot 9H_2O$. The product was calcined at 375 °C for 2 h and then pelletized, crushed, and coarsely sieved to obtain suitable agglomerates for mounting inside the furnace quartz capillary.

The environmental cell system consists primarily of a capillary furnace and gas-delivery system (Figure 1). The furnace is sufficiently small (100 × 47 mm) to facilitate connection of the capillary to a gas inlet/outlet. A thermocouple adjacent to the sample regulates the temperature, the recorded temperatures corrected by means of prior calibrations with a probable error of ± 10 °C, which is confirmed by the subsequent regression analysis of the high-temperature MoO_3 unit-cell dimensions. Inert (100% Ar), reducing (5% H_2/Ar), and oxidizing (5% O_2/Ar) gases can be passed through the heated sample capillary during data collection, with remote start/stop control. The sample, contained in the 1-mm diameter quartz capillary, is protected from loss into the flowing gas by quartz wool plugs.

All data collection was carried out on station 6.2 of the SRS synchrotron (Daresbury, UK). This station has been recently commissioned[16,17] as a high-flux multipole wiggler beamline facility for materials processing. In powder diffraction mode, the optics system delivers an incident X-ray footprint of 0.5 × 3 mm for capillary operation, with a selected incident wavelength of 1.400 Å. Diffraction data were collected by using the RAPID2 detector,[16] which realizes a medium-high angular resolution (0.06°) at ultra-high count rates (20 MHz global) through its multi-wire/multi-electronic-channel mode of operation, over a nominal 2θ range of 60°. The resulting rapid powder diffraction patterns are of sufficient quality for Rietveld[18] structure refinement.

Received: August 15, 2005
Published online: December 2, 2005

Keywords: iron · oxidation · redox chemistry · synchrotron · X-ray diffraction

[1] B. Stiles, T. A. Koch, *Catalyst Manufacturer*, 2nd ed., Marcel Dekker, New York, **1995**, p. 197.
[2] a) R. Crichton, *Informally Speaking, The Formaldehyde Newsletter from Perstorp Formox*, Claes Lundström, Perstorp Formox AB, SE-284 80 Perstorp, Sweden (or http://www.perstorpformox.com), **2003**, Spring/Summer, pp. 12–13; b) A. Andersson, *Informally Speaking, The Formaldehyde Newsletter from Perstorp Formox*, Claes Lundström, Perstorp Formox AB, SE-284 80 Perstorp, Sweden (or http://www.perstorpformox.com), **2003**, Autumn/Winter, pp. 10–12.
[3] D. S. Lafyatis, G. Creten, G. F. Froment, *Appl. Catal. A* **1994**, *120*, 85 – 103.
[4] A. V. Demidov, I. G. Danilova, G. N. Kustova, L. M. Plyasova, N. G. Skomorokhova, L. L. Sedova, V. B. Nakrokhin, B. I. Popov, *Kinet. Catal.* **1992**, *33*, 910 – 914.
[5] G. Alessanadrini, L. Cairati, P. Forzatti, P. L. Villa, F. Trifirò, *J. Less-Common Met.* **1977**, *54*, 373 – 386.
[6] A. P. V. Soares, M. Farinha Portela, A. Kiennemann, L. Hilaire, J. M. M. Millet, *Appl. Catal. A* **2001**, *206*, 221 – 229.
[7] A. P. V. Soares, M. Farinha Portela, A. Kiennemann, *Catal. Commun.* **2001**, *2*, 159 – 164.
[8] A. P. V. Soares, M. Farinha Portela, A. Kiennemann, L. Hilaire, *Chem. Eng. Sci.* **2003**, *58*, 1315 – 1322.
[9] J.-L. Li, Y.-X. Zhang, C.-W. Liu, Q.-M. Zhu, *Catal. Today* **1999**, *51*, 195 – 199.

 © 2006 Wiley-VCH Verlag GmbH & Co. KGaA, Weinheim

[10] J. H. Wilson III, C. G. Hill, Jr., J. A. Dumesic, *J. Molec. Catal.* **1990**, *61*, 333 – 352.
[11] C. J. Machiels, W. H. Cheng, U. Chowdhry, W. E. Farneth, F. Hong, E. M. McCarron, A. W. Sleight, *Appl. Catal.* **1986**, *25*, 249 – 256.
[12] N. Pernicone, *Catal. Today* **1991**, *11*, 85 – 91.
[13] V. Diakov, D. Lafarga, A. Varma, *Catal. Today* **2001**, *67*, 159 – 167.
[14] H. Zhang, J. Shen, X. Ge, *J. Solid State Chem.* **1995**, *117*, 127 – 135.
[15] M. Bowker, R. Holroyd, A. Elliott, P. Morrall, A. Alouche, C. Entwistle, A. Toerncrona, *Catal. Lett.* **2002**, *83*, 165 – 176.
[16] A. Berry, W. I. Helsby, B. T. Parker, C. J. Hall, P. A. Buksh, A. Hill, N. Clague, M. Hillon, G. Corbett, P. Clifford, A. Tidbury, R. A. Lewis, R. J. Cernik, P. Barnes, G. E. Derbyshire, *Nucl. Instrum. Methods Phys. Res. Sect. A* **2003**, *513*, 260 – 263.
[17] R. J. Cernik, P. Barnes, G. Bushnell-Wye, A. J. Dent, G. P. Diakun, J. V. Flaherty, G. N. Greaves, E. L. Heeley, W. Helsby, S. D. M. Jacques, J. Kay, T. Rayment, A. Ryan, C. C. Tang, N. J. Terrill, *J. Synchrotron Radiat.* **2004**, *11*, 163 – 170.
[18] H. M. Rietveld, *J. Appl. Crystallogr.* **1969**, *2*, 65 – 71.
[19] A. W. Sleight, L. H. Brixner, *J. Solid State Chem.* **1973**, *7*, 172 – 174.
[20] W. T. A. Harrison, *Mater. Res. Bull.* **1995**, *30*, 1325 – 1331.
[21] E. Lalik, PhD thesis, University of London (UK) **2003**.
[22] A. W. Sleight, B. L. Chamberland, J. F. Weiher, *Inorg. Chem.* **1968**, *7*, 1093 – 1098.
[23] R. Shirley, *The CRYSFIRE System for Automatic Powder Indexing: User's Manual*, The Lattice Press, Surrey, **1999**.
[24] J. Laugier, B. Bochu, Celref software, part of the LMGP Suite using the GETSPEC software referred to by: U. D. Altermatt, I. D. Brown, *Acta Crystallogr. Sect. A* **1987**, *43*, 125 – 130.
[25] J. Rodriguez-Carvajal, FULLPROF: A Program for Rietveld Refinement and Pattern Matching Analysis, *Abstr. Satellite Meeting Powder Diffraction, XV Congr. It. Union Cryst.*, **1990**, 127.
[26] "WinPLOTR: a Windows tool for powder diffraction patterns analysis": T. Roisnel, J. Rodríguez-Carvajal, *Mater. Sci. Forum* **2001**, *378*, 118 – 123.
[27] N. Pernicone, F. Lazzerin, G. Lanzvecchia, *J. Catal.* **1968**, 10, 83 – 84.
[28] A. P. V. Soares, M. F. Portela, A. Klennemann, *Catal. Rev.* **2004**, *47*, 125 – 174.
[29] K. Otsuka, Y. Wang, *Appl. Catal.* **2001**, *222*, 145 – 161.

 © 2006 Wiley-VCH Verlag GmbH & Co. KGaA, Weinheim

Phenol Synthesis

DOI: 10.1002/anie.200502940

Direct Phenol Synthesis by Selective Oxidation of Benzene with Molecular Oxygen on an Interstitial-N/Re Cluster/Zeolite Catalyst**

*Rajaram Bal, Mizuki Tada, Takehiko Sasaki, and Yasuhiro Iwasawa**

Phenol is one of the most important chemicals in industry, and the world production exceeds 7.2 megatons per year. Industrially, phenol has been produced from benzene by the three-step cumene process, which is not only energy consuming but also less efficient. The process is known for its very low yields ($\approx 5\,\%$ based on the amount of benzene initially used) and for the large amounts of by-products such as acetone and α-methylstyrene. Direct phenol synthesis from benzene is an alternative way to overcome these problems, and O_2,[1–4] H_2O_2,[5,6] N_2O,[7–14] $H_2 + O_2$,[15,16] air/CO,[17] and O_2/H_2O[18] have been used as oxidants. The liquid-phase oxidation reactions of benzene with molecular oxygen in batch closed reactors have been reported to proceed over an iron–heteropolyacid catalyst in the presence of excess catalyst and over a CuO/Al_2O_3 catalyst with ascorbic acid as a reducing agent; however, the yield of phenol is very low.[1,2] A Cu/ZSM-5 catalyst showed a maximum phenol selectivity of 60 % with a yield of 1.2 % at 673 K.[3] Despite good performances with N_2O and H_2O_2 as oxidants, no economically and environmentally favorable catalytic systems for the selective oxidation of benzene with O_2 to give phenol have been discovered to date because of the difficulties associated with the activation of molecular oxygen. The direct synthesis of phenol with molecular oxygen is thus still regarded as one of the 10 most difficult challenges for catalysis,[19–21] and the development of highly selective catalysts for this reaction is of great interest. Rhenium, which can adopt several oxidation states, provides unique catalytic performances in re-forming of petroleum feedstocks, alkene metathesis, selective oxidation of methanol to formaldehyde, and ammoxidation of

[*] Dr. R. Bal, Dr. M. Tada, Prof. Dr. Y. Iwasawa
Department of Chemistry
Graduate School of Science, The University of Tokyo
Hongo, Bunkyo-Ku, Tokyo 113-0033 (Japan)
Fax: (+81) 3-5800-6892
E-mail: iwasawa@chem.s.u-tokyo.ac.jp
Prof. Dr. T. Sasaki
Department of Complexity Science and Engineering
Graduate School of Frontier Sciences, The University of Tokyo
Kashiwanoha, Kashiwa-shi, Chiba 277-8561 (Japan)

[**] This work was supported by the 21st Century COE Program of the MEXT of Japan. R.B. thanks the Japan Society for the Promotion of Science (JSPS) for a postdoctoral fellowship. XAFS measurements were performed at KEK-IMSS-PF with the approval of the Photon Factory Advisory Committee (PAC) (No. 2003G092).

Supporting information for this article is available on the WWW under http://www.angewandte.org or from the author.

WILEY InterScience DISCOVER SOMETHING GREAT
© 2006 Wiley-VCH Verlag GmbH & Co. KGaA, Weinheim

propene.[22–27] Recently we found that a Re/HZSM-5 catalyst was active in direct phenol synthesis,[4] but the selectivities to date have not exceeded 60%. Herein we report the highly selective oxidation of benzene with O_2 over a new Re cluster/HZSM-5 catalyst in the presence of NH_3. The selectivity for phenol is as high as 88% in the steady-state reaction and 94% in the pulse reaction.

Zeolite-supported Re catalysts were prepared by chemical vapor deposition (CVD) of methyl trioxorhenium (MTO; CH_3ReO_3) and impregnation of ammonium perrhenate (NH_4ReO_4) with several zeolites such as HZSM-5, H-Beta, H-USY, and H-Mordenite. All catalysts were pretreated at 673 K in a He flow before use. Table 1 shows the performances of the Re/zeolite catalysts for the selective oxidation of benzene with O_2. A Re-CVD/HZSM-5 catalyst (SiO_2/Al_2O_3 19:1) preferentially produced phenol with 88% selectivity in the presence of NH_3 (Table 1). No other liquid products were detected and the only by-product was gaseous CO_2. The activity and selectivity of the Re-CVD/HZSM-5 catalyst did not decrease over a period of at least 6 h under steady-state conditions (Supporting Information). Notably, the coexistence of NH_3 is indispensable for the selective oxidation: neither oxidation nor combustion proceed in the absence of NH_3. The addition of H_2O and N_2O gave no positive effects on the catalytic performance. The phenol formation rate and selectivity increased with increasing NH_3 pressure because the coexisting NH_3 produces active Re clusters as described below, and reached maxima at partial pressure of NH_3 of about 35–42 kPa (Figure 1). Excess ammonia leads to lower phenol formation rates and selectivities owing to competitive adsorption (with respect to benzene) and undesirable catalyst poisoning. Pretreatment of the catalyst with NH_3 for longer than 1 h is necessary for selective catalysis, thus indicating the formation of the active structure in situ under the reaction conditions in the presence of NH_3.

Table 1: Catalytic performances for the direct synthesis of phenol on Re/zeolite catalysts at 553 K.[a]

Catalyst	SiO_2/Al_2O_3	Method	Re [wt%]	TOF [10^{-5} s^{-1}][b]	Selectivity [%][c]
HZSM-5	19:1	–	–	trace	0
Re/HZSM-5[d]	19:1	CVD	0.58	trace	0
Re/HZSM-5	19:1	CVD	0.58	66	88
Re/HZSM-5[e]	19:1	CVD	0.58	52	86
Re/HZSM-5[f]	19:1	CVD	2.2	84	82
Re/HZSM-5[g]	19:1	CVD	0.58	75	94
Re/HZM-5[h]	19:1	CVD	0.58	86	91
Re/HZSM-5	19:1	Imp.	0.6	12	28
Re/HZSM-5	19:1	Phys.[i]	0.6	trace	0
Re/HZSM-5[d]	24:1	CVD	0.58	trace	0
Re/HZSM-5	24:1	CVD	0.58	36	68
Re/HZSM-5	24:1	Imp.	1.2	19	15
Re/HZSM-5[d]	39:1	CVD	0.59	trace	0
Re/HZSM-5	39:1	CVD	0.59	31	48
Re/HZSM-5[j]	39:1	CVD	0.40	47	46
Re/HZSM-5	39:1	Imp.	1.2	16	14
Re/H-Beta	37:1	CVD	0.53	19	12
Re/H-USY	29:1	CVD	0.60	trace	0
Re/H-Mordenite	220:1	CVD	0.55	26	23
SiO_2–Al_2O_3	19:1	–	0	0	0
Re/SiO_2–Al_2O_3	19:1	Imp.	1.2	trace	0

[a] Catalyst = 0.20 g; $W/F = 6.7\ g_{cat}\,h\,mol^{-1}$; $He/O_2/NH_3/benzene = 46:12:35:7$ (mol%). The detailed carbon mass balance and material balance were examined in most of the experimental runs and values between 97 and 99% were found. [b] Consumed benzene/Re (s^{-1}). [c] Selectivity for phenol (carbon%). [d] In the absence of NH_3. [e] $W/F = 5.2\ g_{cat}\,h\,mol^{-1}$. [f] $W/F = 10.9\ g_{cat}\,h\,mol^{-1}$; $He/O_2/NH_3/benzene = 46:12:35:7$ (mol%). [g] Pulse reaction on the NH_3-pretreated catalyst (0.1 g); 1 pulse of benzene + O_2 (He/O_2/benzene = 81:12:7 (mol%)). [h] Pulse reaction on the NH_3-pretreated catalyst (1.0 g); 1 pulse of benzene + O_2 (He/O_2/benzene = 81:12:7 (mol%)). [i] Physical mixing of MTO. [j] Reference [4]; $He/O_2/NH_3/benzene = 55:7:31:7$ (mol%). CVD = chemical vapor deposition, Imp. = impregnation, W/F = weight of catalyst/feed rate.

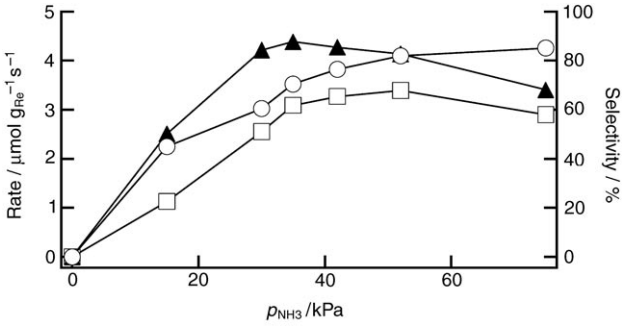


Figure 1. Dependence of the catalytic activity and selectivity on NH_3 pressure in the selective benzene oxidation over the Re/HZSM-5 catalyst (Re: 0.58 wt%, CVD, SiO_2/Al_2O_3 19:1) at 553 K. ○: benzene consumption rate, □: phenol formation rate, ▲: phenol selectivity.

Lower activities and selectivities were attained through impregnation and physical mixing of the catalysts (Table 1, Supporting Information). The CVD catalyst was almost 18 times more active than the impregnation catalyst. Physical mixing and impregnation of results in the transformation of the Re^{7+} catalyst precursors into partly aggregated and ill-defined Re species, unlike the active Re clusters formed in the CVD catalyst (see below). The selectivity for phenol is highly dependent on the structure, acid strength, and SiO_2/Al_2O_3 ratio of the zeolites (Table 1). Lower SiO_2/Al_2O_3 ratios led to large increases in the catalytic activity (TOF: 31.0×10^{-5} s^{-1} to 65.6×10^{-5} s^{-1}) and selectivity (48 to 88%). The rate of phenol formation decreased in the following order: HZSM-5 (SiO_2/Al_2O_3 19:1) > HZSM-5 (SiO_2/Al_2O_3 24:1) > HZSM-5 (SiO_2/Al_2O_3 39:1) ≫ H-Mordenite > H-beta > H-USY. Thus HZSM-5 (SiO_2/Al_2O_3 19:1) is the most favorable support among the employed zeolites for the Re species. The results also suggest that Al-OH in the HZSM-5 framework is a bonding site for active Re species. The selectivity decreased slightly from 88 to 82% by increasing the Re loading (0.58→2.2 wt%) and W/F (6.7→10.9 $g_{cat}\,h\,mol^{-1}$), whereas the conversion increased from 0.8% (TOF: 65.6×10^{-5} s^{-1}) to 6% (TOF: 83.8×10^{-5} s^{-1}) as shown in Table 1.

The Re L_I- and L_{III}-edge EXAFS analysis revealed significant changes in the structure of supported Re species on HZSM-5 (Table 2 and Supporting Information). Table 2 shows the structural parameters of the active Re-CVD/HZSM-5 catalyst determined by curve-fitting of the Re L_{III}-

 © 2006 Wiley-VCH Verlag GmbH & Co. KGaA, Weinheim

Table 2: Curve-fitting results of the Re L_{III}-edge EXAFS data measured at 15 K for the Re/HZSM-5 catalyst.[a]

Sample	Shell	C.N.[b]	Bond length [nm]	σ^2 [10^{-5} nm^2]	ΔE_0
He-treated	Re=O	2.5±0.3	0.173±0.001	1.5±0.6	R_f=2.1%
	Re–O	1.2±0.5	0.206±0.001	2.9±2.8	
	Re–Re	1.2±0.6	0.275±0.001	5.0±1.5	
NH_3-treated	Re=O	0.3±0.2	0.172±0.001	2.3±2.4	R_f=0.5%
	Re–N	2.8±0.3	0.204±0.001	5.8±0.9	
	Re–Re	5.2±0.3	0.276±0.002	5.2±0.2	
After reaction	Re=O	3.7±0.2	0.173±0.001	1.4±0.3	R_f=1.3%
	Re–O	1.3±0.7	0.213±0.003	9.1±7.7	

[a] Catalyst: Re: 0.58 wt%, CVD, SiO_2/Al_2O_3=19:1. Fourier-transform spectra (k=30–160 nm^{-1} and fitted in R space of R=0.10–0.32 nm). [b] C.N. = coordination number. EXAFS = extended X-ray absorption fine-structure.

edge EXAFS data measured at 15 K.[28] After the CVD of MTO to HZSM-5 followed by treatment with He at 673 K, two different Re–O bonds were observed at 0.173±0.001 nm (C.N. (coordination number) = 2.5±0.3) and 0.206± 0.001 nm (C.N. = 1.2±0.5), which are attributed to Re=O and Re–O_{bridge} and/or Re–$O_{lattice}$, respectively. A Re–Re contribution was observed at 0.275±0.001 nm with a C.N. of 1.2±0.6, which indicates that MTO was probably transformed into the Re dimer species in the pore of HZSM-5. The Re dimer is completely inactive in the selective benzene oxidation (Figure 2). The pulses of benzene, a mixture of benzene and O_2, and a mixture of benzene and NH_3 on the Re dimer did not produce phenol at all.

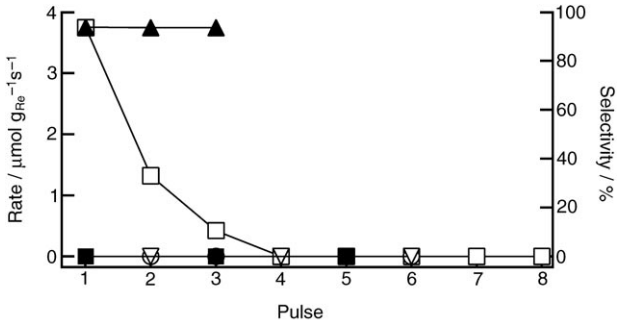
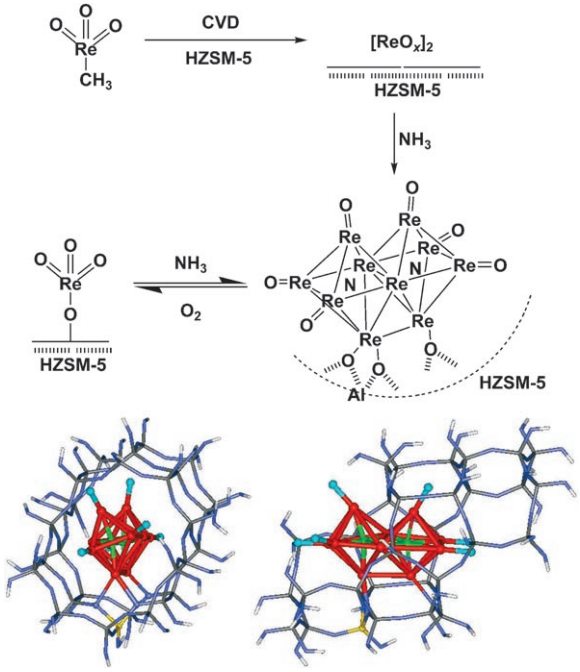


Figure 2. Pulse reactions for selective benzene oxidation at 553 K over the Re/HZSM-5 catalyst (Re: 0.58 wt%, CVD, SiO_2/Al_2O_3 19:1) after pretreatment with NH_3 at 553 K for 2 h. 1 pulse: He/O_2/benzene = 81:12:7; W/F = 6.7 g_{cat} h mol^{-1}; catalyst = 0.10 g. □: phenol formation rate, ▲: phenol selectivity. ■: phenol formation rate in the absence of O_2. ▽ and ○: phenol formation rates on the Re dimer and ReO_4 monomer, respectively, both in the presence and absence of O_2.

Treatment of the inactive Re dimer with ammonia at the reaction temperature brought about catalytic activity for phenol synthesis. The phenol formation rate increased with increasing periods of treatment with NH_3 (75 kPa) at 553 K and reached a saturated value of 3.8 μmol $g_{cat}^{-1}s^{-1}$ after treatment with NH_3 for 2 h, which indicates that the structural transformation to the active Re species is completed after exposure to NH_3 for 2 h.

Indeed, the L_{III}-edge EXAFS data dramatically changed with the NH_3 treatment (Supporting Information). The C.N. of Re–Re bonds (Table 2) increased from 1.2±0.5 with the Re dimer to 5.2±0.3 at 0.276±0.002 nm, demonstrating the formation of Re clusters. If we assume that the Re_6 octahedron is a cluster unit,[27] the C.N. of the Re–Re bonds indicates Re_{10} clusters edge shared with two Re_6 octahedra. Furthermore, it was found that the NH_3-treated Re cluster catalyst released N_2 molecules at 685 K (Temperature programmed desorption (TPD) spectra; Supporting Information). The number of encapsulated nitrogen atoms was 0.12 N_2/Re, which corresponds to one nitrogen atom per Re_6 octahedron. An NH_3-treated HZSM-5 without Re showed no N_2 desorption in TPD. The Re–N(O) bonds in the NH_3-treated Re-CVD/HZSM-5 catalyst were observed at 0.204± 0.001 nm (C.N. = 2.8±0.3) by EXAFS (Table 2). Re=O double bonds at 0.172±0.001 nm (C.N. = 0.3±0.2) were also observed. The XPS Re 4f binding energy was 43.8 eV, which indicates a Re^{3+} state.

We have simulated the structure of the active Re clusters in the pore of HZSM-5 by density functional theory (DFT) calculations (Scheme 1). These revealed that a nitrogen atom is located at the interstitial position of each Re_6 octahedral framework of the Re_{10} clusters and is attached to the wall of a zeolite pore through Re–O bonds.[29] Notably, the interstitial nitrogen atoms are key to the stabilization of the Re_{10} clusters. Neither the hollow-site nitrogen atom (Re_3–N), nor the bridged nitrogen atom (Re–N–Re), nor bridged NH species (Re–NH–Re) stabilize the cluster framework with Re–Re



Scheme 1. Proposed structures of the supported Re clusters on HZSM-5 and the modeling of an active interstitial-N/Re_{10}-cluster inside the pore of HZSM-5 by DFT.

 © 2006 Wiley-VCH Verlag GmbH & Co. KGaA, Weinheim

bonds at 0.276 ± 0.002 nm determined by EXAFS. We have also simulated many Re clusters coordinated with oxygen atoms. However, the clusters were destabilized by oxygen coordination, and more oxygen decomposed the Re_{10} framework. The stable interstitial-N/Re_{10} cluster presented in Scheme 1 was modeled as a unique solution in the DFT calculations.

The Re_{10} clusters with interstitial nitrogen atoms were highly selective in the catalytic phenol synthesis (Table 1 and Figure 2). Benzene was converted into phenol by a pulse of a mixture of benzene and O_2 on 0.1 g of the NH_3-pretreated catalyst (Figure 2). Notably, the selective oxidation with molecular oxygen on the active Re_{10} clusters proceeds without ammonia. Repetition of the pulse caused a large decrease in the catalytic activity, and formation of phenol stopped after the admission of three pulses of the feed (Figure 2). The selectivity was constant (94%) during the reaction of the three pulses. These results demonstrate that the active Re_{10} clusters were converted into inactive Re species without significant formation of unselective Re species on the way. In the absence of O_2, the Re clusters did not produce phenol, suggesting that the oxygen of the active Re cluster framework is not active in the selective oxidation. In the pulse reaction on 1.0 g of the NH_3-pretreated catalyst the conversion of benzene into phenol increased to 10% (TOF (turnover frequency): $86.1 \times 10^{-5}\ s^{-1}$), while keeping a high phenol selectivity of 91% (Table 1).

After the pulse reactions with a mixture of benzene and O_2, the Re species showed no Re–Re bond, whereas Re=O and Re–O bonds were observed at 0.173 ± 0.001 nm (C.N. = 3.7 ± 0.2) and at 0.213 ± 0.003 nm (C.N. = 1.3 ± 0.7) as shown in Table 2 (Supporting Information). The XPS Re 4f peak was observed at 48.5 eV. These results demonstrate that the Re_{10} clusters were oxidized with O_2 and decomposed to inactive ReO_4 monomers with Re^{7+} (Scheme 1).

The Re_{10} clusters are not stable under O_2 in the absence of NH_3. Oxygen not only produces phenol but also converts the active Re_{10} clusters into the inactive ReO_4 monomers competitively. The amount of phenol molecules produced in the pulse reactions was 3.2% of the amount of the Re_{10} clusters. Under the steady-state conditions in the presence of NH_3, the population of the active Re_{10} clusters in the Re species is 3.7%. A mechanism for the oxidation may involve oxygen-free radical formation on the Re_{10} clusters. Alternatively, molecular oxygen associatively adsorbed on the partially reduced Re_{10} clusters may be the active oxygen species. In the latter case, the theoretical maximum phenol selectivity would be 94%.

In conclusion, we have found that the novel HZSM-5-supported interstitial-N/Re-clusters prepared by the CVD of CH_3ReO_3 are active for the selective catalytic oxidation of benzene to phenol with molecular oxygen in the presence of ammonia. The impressive selectivities are as high as 94% at 553 K.

Experimental Section

HZSM-5 (SiO_2/Al_2O_3 19:1) was synthesized by a procedure similar to that described in the literature.[30] Other zeolites were purchased from TOSOH, Japan. The supported Re catalysts were prepared by two methods: 1) conventional impregnation by using NH_4ReO_4 and 2) CVD by using CH_3ReO_3. In the CVD procedure, ZSM-5, Beta, USY, Mordenite were pressed and sieved to 355–710 μm granules and calcined at 873 K for 2 h. The zeolites were then treated further at 673 K for 0.5 h under vacuum. The whole apparatus was heated at 333 K, and the zeolites were exposed to MTO vapor for 14 h. The catalysts were pretreated under a helium flow at 673 K for 1 h and cooled in a He flow. The selective catalytic reactions were conducted in a fixed-bed down-flow reactor by charging 0.2 g of the catalyst. A typical composition of the reaction gases was $He/O_2/NH_3$/benzene = 46:12:35:7 and W/F was typically $6.7\ g_{cat}\ h\ mol^{-1}$. The products were analyzed by two online GCs with an FID detector by using a NEUTRABOND-1 Column for hydrocarbons and with a TCD detector by using a Unibeeds C column for inorganic materials. Pulse experiments were carried out with 0.1 g of catalyst, and the volume of each pulse was 0.42 mL.

Received: August 18, 2005
Published online: December 2, 2005

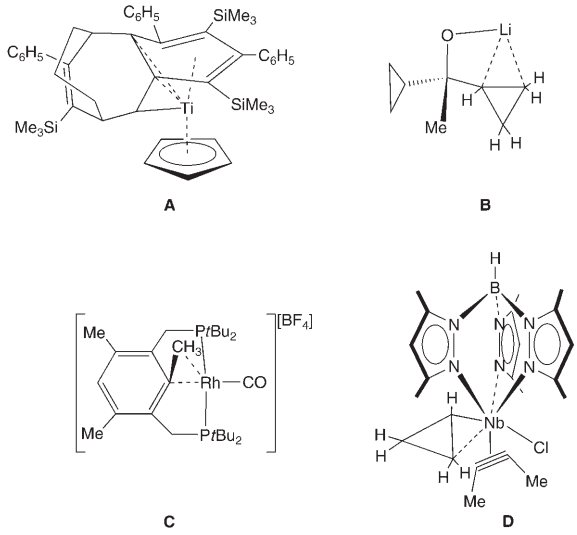
Keywords: chemical vapor deposition · cluster compounds · heterogeneous catalysis · oxidation · zeolites

[1] Y. J. Seo, Y. Mukai, T. Tagawa, S. Goto, *J. Mol. Catal. A* **1997**, *120*, 149.
[2] T. Miyahara, H. Kanazaki, R. Hamada, S. Kuroiwa, S. Nishiyama, S. Tsuruya, *J. Mol. Catal. A* **2001**, *176*, 141.
[3] H. Yamanaka, R. Hamada, H. Nibuta, S. Nishiyama, S. Tsuruya, *J. Mol. Catal. A* **2002**, *178*, 89.
[4] T. Kusakari, T. Sasaki, Y. Iwasawa, *Chem. Commun.* **2004**, 992.
[5] Y. J. Seo, T. Tagawa, S. Goto, *J. Chem. Eng. Jpn.* **1994**, *27*, 307.
[6] D. H. Bremner, A. E. Burgess, F. B. Li, *Appl. Catal. A* **2000**, *203*, 111.
[7] G. I. Panov, G. A. Sheveleva, A. S. Kharitonov, V. N. Romannikov, L. A. Vostrikova, *Appl. Catal. A* **1992**, *82*, 31.
[8] G. I. Panov, *CATTECH* **2000**, *4*, 18.
[9] J. L. Motz, H. Heinichen, W. F. Hölderich, *J. Mol. Catal. A* **1998**, *136*, 175.
[10] W. F. Hölderich, *Catal. Today* **2000**, *62*, 115.
[11] G. Centi, C. Genovese, G. Giordano, A. Katovic, S. Perathoner, *Catal. Today* **2004**, *91*, 17.
[12] E. J. M. Hensen, Q. Zhu, R. A. van Santen, *J. Catal.* **2005**, *233*, 136.
[13] F. Kollmer, H. Harsmann, W. F. Hölderich, *J. Catal.* **2004**, *227*, 398.
[14] E. J. M. Hensen, Q. Zhu, R. A. van Santen, *J. Catal.* **2003**, *220*, 260.
[15] S. Niwa, M. Eswaramoorthy, J. Nair, A. Raj, N. Itoh, H. Shoji, T. Namba, F. Mizukami, *Science* **2002**, *295*, 105.
[16] H. Ehrich, H. Berndt, M. Pohl, K. Jähnisch, M. Baerns, *Appl. Catal. A* **2002**, *230*, 271.
[17] M. Tani, T. Sakamoto, S. Mita, S. Sakaguchi, Y. Ishii, *Angew. Chem.* **2005**, *117*, 2642; *Angew. Chem. Int. Ed.* **2005**, *44*, 2586.
[18] T. Dong, J. Li, F. Huang, L. Wang, J. Tu, Y. Torimoto, M. Sadakata, Q. Li, *Chem. Commun.* **2005**, 2724.
[19] J. Haggin, *Chem. Eng. News* **1993**, *71*, 23.
[20] B. Cornils, W. A. Herrmann, *J. Catal.* **2003**, *216*, 33.
[21] B. Lücke, K. V. Narayana, A. Martin, K. Jähnisch, *Adv. Synth. Catal.* **2004**, *346*, 1407.
[22] J. C. Mol, *J. Mol. Catal. A* **2004**, *213*, 39.
[23] Y. Yuan, T. Shido, Y. Iwasawa, *Chem. Commun.* **2000**, 1421.
[24] Y. Yuan, Y. Iwasawa, *J. Phys. Chem. B* **2002**, *106*, 4441.
[25] H. Liu, H. Imoto, T. Shido, Y. Iwasawa, *J. Catal.* **2001**, *200*, 69.
[26] N. Viswanadham, T. Shido, Y. Iwasawa, *App. Catal. A* **2001**, *219*, 223.

 © 2006 Wiley-VCH Verlag GmbH & Co. KGaA, Weinheim

[27] N. Viswanadham, T. Shido, T. Sasaki, Y. Iwasawa, *J. Phys. Chem. B* **2002**, *106*, 10955.
[28] EXAFS measurements were performed in transmission mode at a BL-12C station of the KEK-IMSS-PF.
[29] All ab initio calculations were performed by using a commercially available density functional code (Material Studio DMol3 ver3.0, Accelrys, USA) in which the exchange–correlation interaction was treated by the Perdew-Wang 91 functional (PW91) within a generalized gradient approximation. Double-numeric basis sets with polarization functions (DNP), the size of which is comparable to 6-31G* was adopted. All electrons are explicitly included, and the relativistic effect was considered for Re core electrons; B. Delley, *J. Chem. Phys.* **1990**, *92*, 508; J. P. Perdew, Y. Wang, *Phys. Rev. B* **1992**, *45*, 13244.
[30] R. J. Argatter, M. Kensington, G. R. Landolt, N. J. Audubon, US 3,702,886, **1972**.

 © 2006 Wiley-VCH Verlag GmbH & Co. KGaA, Weinheim



C–C Activation

DOI: 10.1002/anie.200503036

A Rhodium Complex with One Rh···C–C and One Rh···H–C Agostic Bond**

*Simon K. Brayshaw, Jennifer C. Green, Gabriele Kociok-Köhn, Emma L. Sceats, and Andrew S. Weller**

The metal-mediated activation of carbon–carbon single bonds is the subject of significant contemporary interest,[1] with the putative intermediates in such processes being complexes in which the metal is bound through a C–C σ interaction.[2] Complexes showing such M···CC interactions are extremely rare, and are limited to intramolecular (agostic) interactions that have been reported for complexes **A**–**D**;[3–6] although in one case (**A**) the bonding mode has been queried.[7] The lack of well-characterized examples of such species is in contrast with M···HC agostic complexes that are well established;[2,8–10] and further examples of genuine, fully-characterized examples of M···C–C σ interactions are of clear importance regarding the fundamental study of C–C activation processes. We report here the facile synthesis of a complex that has such a Rh···CC interaction, its full characterization, and some preliminary reactivity studies.

Treatment of [RhCl(nbd)(P*i*Pr$_3$)] with Na[BAr$^F_4$] (nbd = norbornadiene, BAr$^F_4$ = B(C$_6$H$_3$(CF$_3$)$_2$)$_4$) and a tenfold excess of norbornadiene in fluorobenzene at room temperature results in the formation of [Rh(P*i*Pr$_3$)(C$_{14}$H$_{16}$)][BAr$^F_4$] (**1**) as the only organometallic product (Scheme 1). Complex **1** has been characterized by single-crystal X-ray diffraction, NMR spectroscopy, and DFT calculations. Also formed are the organic products of norbornadiene dimerization, which include Binor-S, consistent with the previously reported Rh^I-catalyzed dimerization of norbornadiene.[11]

The solid-state structure of **1** (Figure 1) has a cationic rhodium center coordinated with one P*i*Pr$_3$ ligand, which shows an additional weak γ-agostic C–H interaction from one of the isopropyl groups (Rh–C2 2.901(3), Rh–H2a 2.52(3) Å).[8,12] The other ligand is a saturated hydrocarbon derived from Binor-S (by dimerization of norbornadiene) in which one cyclopropane ring has opened and is now part of a rhodacyclobutane (C11–C15 2.204(4) Å). The Rh–C distances associated with this four-membered ring lie within the range of Rh–C single bonds (Rh–C11 2.032(3), Rh–C15 2.042(3) Å), and are similar to those reported in [Rh(η^5-C$_5$Me$_5$)(PMe$_3$)(CH$_2$)$_3$].[13] The coordination sphere of rhodium is completed by a close approach of the remaining Binor-S cyclopropane ring (C21-C25-C26) (Rh–C21 2.352(3), Rh–C25 2.369(3) Å). These distances are longer than expected for a Rh–C single bond but lie well within the combined van der Waals radii of Rh and C (3.7 Å), suggesting a significant interaction. With an overall cationic charge and metallacyclobutane ring, in the solid-state the rhodium center in **1** is best described as being Rh^{III}.

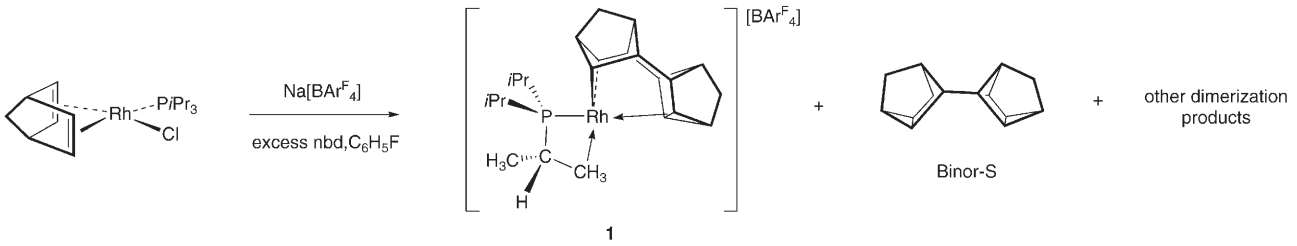
The question that immediately arises is as to the nature of this close contact with the cyclopropane ring: is it two agostic Rh···HC interactions or one Rh···CC interaction? In the solid state, the hydrogen atoms associated with the cyclopropane ring are certainly close enough to the Rh center to potentially engage in an agostic interaction (Rh–H25 2.30(5), Rh–H21 2.32(3) Å).[8] However, within the limits of the X-ray diffraction experiment the C–H bonds are not significantly length-

[*] Dr. S. K. Brayshaw, Dr. G. Kociok-Köhn, Dr. A. S. Weller
Department of Chemistry
University of Bath
Bath, BA2 7AY (UK)
Fax: (+44) 122-538-6231
E-mail: a.s.weller@bath.ac.uk
Prof. J. C. Green, E. L. Sceats
Inorganic Chemistry Laboratory
South Parks Road, Oxford OX1 3QR (UK)

[**] We thank the EPSRC, under grant GR/T10169, and the Royal Society for support.

Supporting information for this article is available on the WWW under http://www.angewandte.org or from the author.

InterScience
© 2006 Wiley-VCH Verlag GmbH & Co. KGaA, Weinheim



Scheme 1.

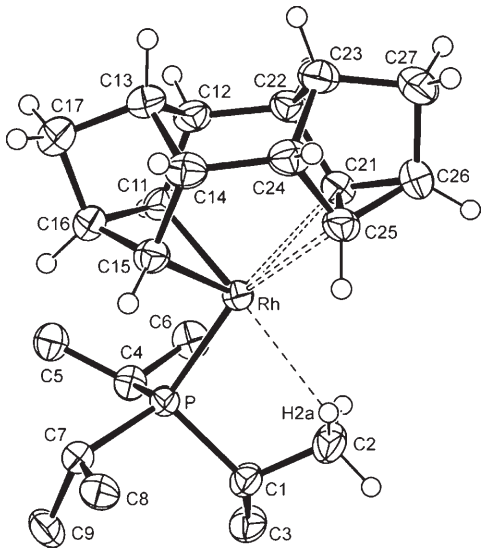
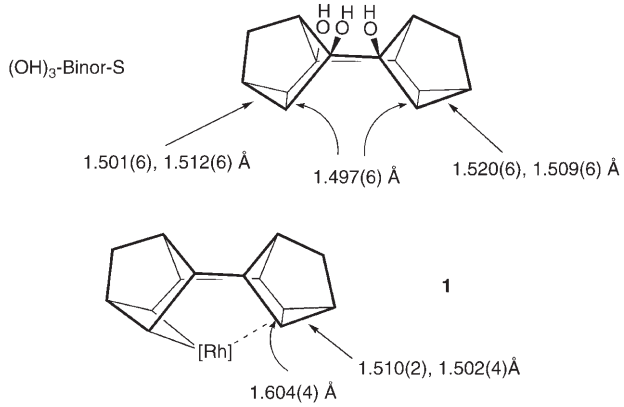


Figure 1. Solid-state structure of the cationic portion of **1**. Thermal ellipsoids are shown at the 50% probability level. Hydrogen atoms on the phosphine ligand, apart from those associated with C2, are omitted for clarity. Selected bond lengths [Å] and angles [°]: Rh–P 2.2693(7), Rh–C11 2.032(3), Rh–C15 2.042(3), Rh–C21 2.352(3), Rh–C25 2.369(3), Rh–C2 2.901(3), Rh–H2a 2.52(3), C21–C25 1.604(4), C21–C26 1.510(4), C25–C26 1.502(4), C11–C15 2.204(4), C21–H21 0.97(3), C25–H25 0.95(3); P-C1-C2 109.7(2), P-C1-C3 117.1(2).



Scheme 2.

ened (C25–H25 0.97(3), C21–H21 0.95(3) Å), contrary to what would be expected for an agostic M···HC interaction. In contrast, compared with free Binor-S (as determined from the structure of the tris-hydroxylated derivative[14]), the C–C bond that is in close proximity with the metal is lengthened by $\approx$0.1 Å, whereas the two other C–C bonds in the cyclopropane unit remain unchanged (Scheme 2). A similar, but slightly smaller, increase in C–C bond length (0.049 Å) has been noted in **D**.[6] The DFT calculated structure of **1** (see below; see Supporting Information for full details) is in close agreement with the experimentally determined structure, showing a lengthening of the C21–C25 bond (1.620 Å), while the calculated C–H bond lengths (1.104/1.105 Å) are not significantly lengthened compared with the other calculated C–H distances (cf. C24–H24 1.104 Å). These observations all point towards a Rh···CC interaction rather than Rh···HC interactions, and are supported by the NMR data and DFT calculations presented below.

In solution at 298 K, the ^{1}H and ^{13}C{^{1}H} NMR spectra of **1** show only five and four[15] resonances, respectively, for the Binor-S ligand, indicating C_s symmetry in solution (in contrast to the solid-state structure), which demonstrates that this ligand undergoes a fluxional process at room temperature. These resonances have been unequivocally assigned by using ^{1}H–^{1}H and ^{13}C–^{1}H correlation experiments. In particular, the signals associated with the four carbon atoms close to rhodium (C11, C15, C21, C25) are all equivalent ($\delta(^{1}H) = 3.23$, $\delta(^{13}C) = 25.5$ ppm) and show coupling to both ^{103}Rh and ^{31}P in the ^{13}C{^{1}H} NMR spectrum, suggesting a significant time-averaged Rh···C interaction in solution. Upon progressive cooling to 200 K the fluxional process is halted ($\Delta G^{\neq} = 48 \pm 2$ kJ mol^{-1}), and 10 signals are observed in both the ^{1}H and ^{13}C{^{1}H} NMR spectra for the Binor-S ligand, which is thus consistent with the solid-state structure. At 200 K the measured ^{1}J(C,H) value for the cyclopropane carbons (C21, C25) in **1** (170 Hz) is similar to that for the equivalent carbons in free Binor-S (174 Hz), suggesting that Rh···HC agostic interactions are not present, as these would be expected to result in a significant decrease in the observed J(C,H) coupling constant.[9] The contact carbons all show coupling to rhodium at low temperature, but consistent with a weaker agostic interaction, ^{1}J(Rh,C) for C21/C25 is smaller than for C11/C15 (9 versus 22 Hz respectively). Coupling to ^{103}Rh or ^{31}P is not observed in the ^{1}H NMR spectrum, although the signals are broadened somewhat (fwhm 13 Hz). Over all temperatures the Rh···H_3C interactions from the P*i*Pr$_3$ ligand (Rh···HC(2)) must be rapidly exchanging and this secondary agostic interaction is not observed in solution. A single doublet ($\delta = 49.2$ ppm, J(Rh,P) = 211 Hz) is observed in the ^{31}P{^{1}H} NMR spectrum at room temperature that is essentially invariant on cooling to 200 K.

Topological analysis of the electron density (ρ) in complex **1** has been performed (see Supporting Information for full

 © 2006 Wiley-VCH Verlag GmbH & Co. KGaA, Weinheim

details), using DFT calculations in conjunction with Bader's "Atoms in Molecules" (AIM) approach,[16] to quantify the nature of the bonding interactions between Rh and the Binor-S fragment. Such calculations have previously been used to analyze the extent of bonding in situations where simple analysis of bond lengths (obtained from crystallographic studies) cannot provide a complete understanding of the interactions present. Indeed recent AIM analysis of the titanium complex **A**,[7] which contains a short Ti···CC contact in the solid state, indicates that there is no agostic interaction between the Ti and the C–C single bond. This result was contrary to that from previous DFT calculations,[5] for which a natural orbital analysis was used as evidence for an agostic interaction, and highlights the power of methods, such as AIM, which use criteria solely based on a topological analysis of the electron distribution to characterize bonding interactions. AIM analysis of **1** (see Figure 2 and Supporting Information) shows the expected (3, −1) bond critical points (BCPs) between C25–C21 (BCP 1), Rh–C15 (BCP 14), Rh–C11 (BCP 15), and furthermore, the manifestation of an agostic Rh···CC interaction is observed through the presence of (3, −1) BCPs between Rh–C25 (BCP 8) and Rh–C21 (BCP 9). Crucially, no BCP was located between Rh–H25 or Rh–H21, and in a self-consistent check a BCP *is* located between Rh and the isopropyl C2–H2a. Figure 3 shows the topology of the charge density in the plane defined by Rh, C25, and C21. The existence of an agostic CC bond is clearly proven by the presence of: a) BCPs 8 and 9, b) bond paths (BPs) between Rh and C25/C21, and c) an interatomic surface, which forms the boundary between two atoms sharing a BP.

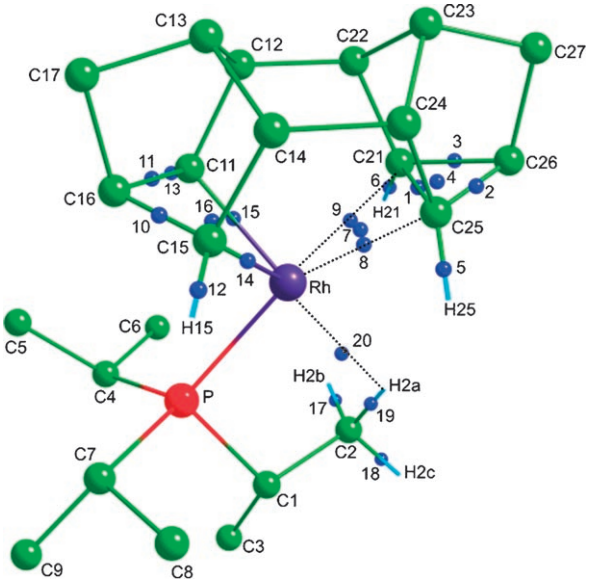


Figure 2. Calculated structure of complex **1** including selected protons (pale blue), BCPs and RCPs (plotted as dark blue spheres). Selected calculated bond lengths [Å]: C25–C21 1.620, Rh–C25 2.273, Rh–C21 2.273, C15–C11 2.185, Rh–C15 2.027, Rh–C11 2.031, C21–H21 1.105, C25–H25 1.104 Å. Broken lines (••••) represent the agostic interactions present in **1**.

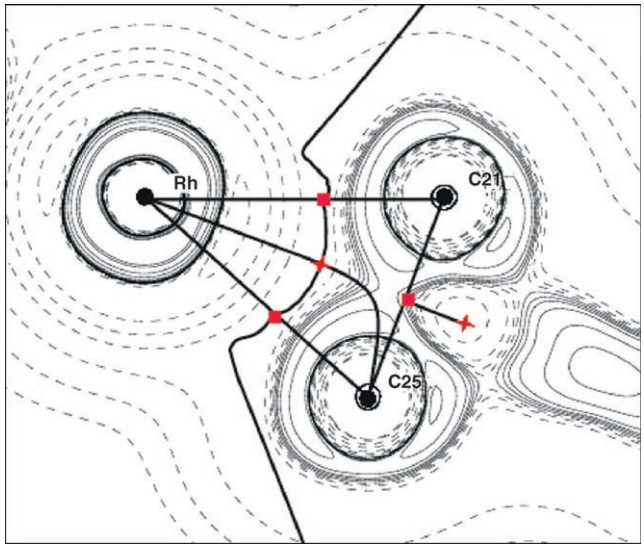
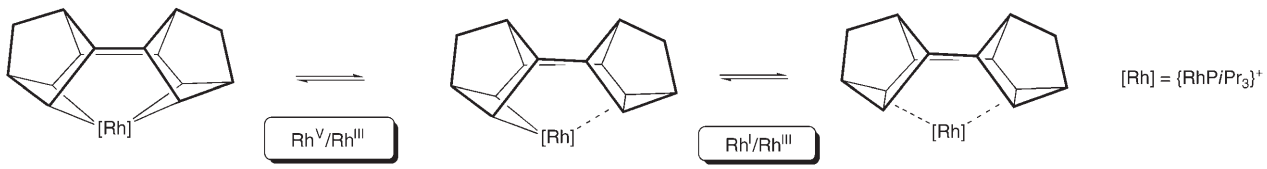


Figure 3. Theoretical bond paths, interatomic surfaces, and $\nabla^2\rho(\boldsymbol{r})$ contour map in the plane defined by Rh, C21, and C25 in complex **1**. Bond critical points are denoted by red squares, and ring critical points are denoted by red crosses.

The fluxional process occurring in **1** in solution at room temperature for the Binor-S fragment is one that equivalences the rhodacyclobutane and cyclopropane fragments observed in the solid state, presumably by concerted or stepwise C–C oxidative addition/reductive elimination. Two possible mechanisms for this invoke a rhodium(v) bis(rhodacyclobutane) intermediate, or a rhodium(i) bis(cyclopropane) (i.e. Binor-S) intermediate (Scheme 3). We favor the latter Rh^{III}/Rh^{I} couple on the basis of the scarcity of Rh^{V} complexes, and reactivity studies (see below) which show that complex **1** reacts more like a latent Rh^{I} rather than a Rh^{III} or Rh^{V} species. DFT calculations are presently being used to elucidate the mechanism and precise geometries of the transition state(s) or intermediates involved in the fluxional process and will be reported upon elsewhere. Further support for the Rh^{III}/Rh^{I} couple comes from cyclopropane activation by Rh^{I} complexes that has been reported previously. For example, experiments



Scheme 3.

 © 2006 Wiley-VCH Verlag GmbH & Co. KGaA, Weinheim

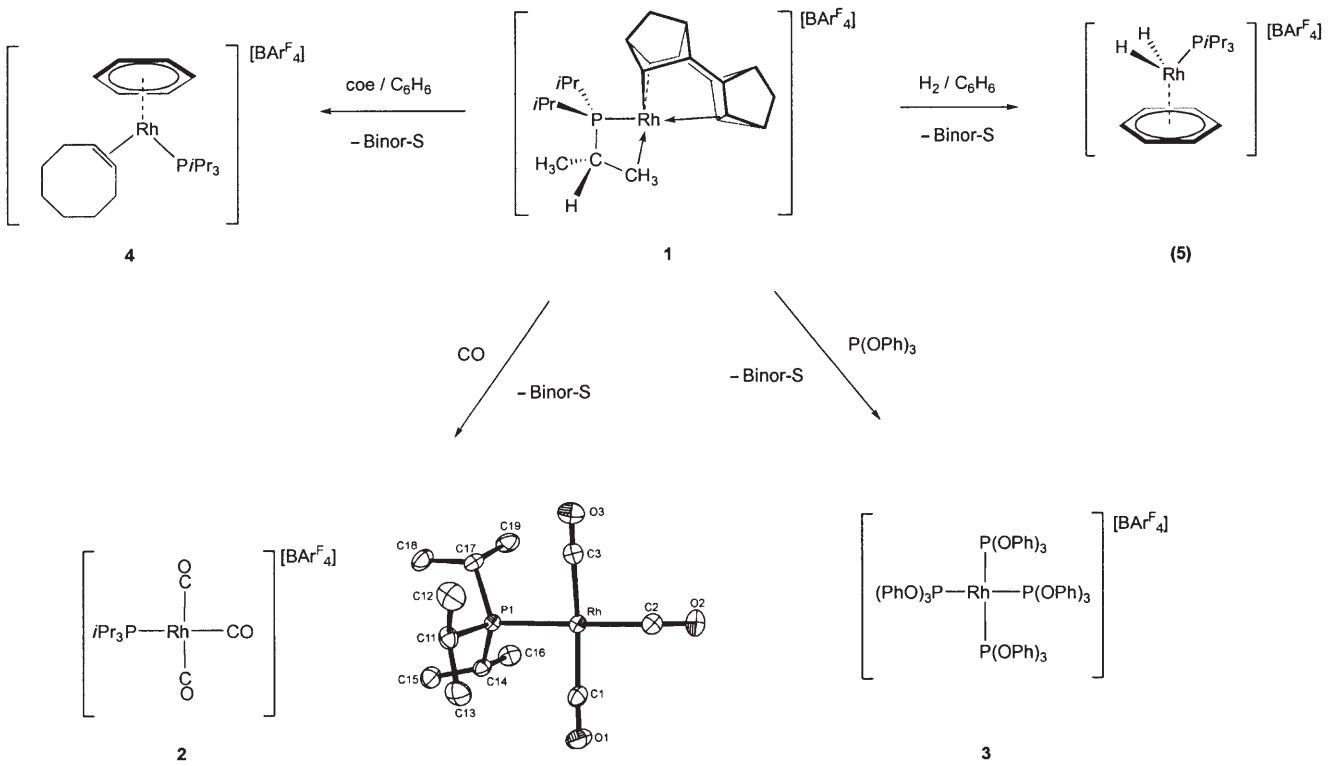
and calculations on the reaction of cyclopropane with a neutral {Cp*Rh(PMe_3)} fragment[13,17] to form a rhodacyclobutane product suggest intermediates with a Rh^I···CC interaction, similar to that experimentally observed for **1**; while complex **1** also has direct relevance to the recently reported catalytic carbon–carbon bond activation of cyclopropanes using [Rh(PPh_3)$_3$Cl],[18] which is suggested to proceed through intermediates with Rh^I···CC interactions.

Complex **1** decomposes in CH_2Cl_2 solution over a period of 24 h, but is relatively stable in fluorobenzene (days, argon atmosphere). In solution, **1** reacts as if it were a source of Rh^I coordinated with Binor-S (Scheme 4), suggesting that the cyclometalated Rh^{III} species observed at low temperature and in the solid state is a resting state for a reactive {Rh(P*i*Pr$_3$)}$^+$ fragment.[19] Thus, reaction with simple Lewis bases such as CO and P(OPh)$_3$ gives free Binor-S and the rhodium(I) complexes [Rh(P*i*Pr$_3$)(CO)$_3$][BAr^F_4] (**2**) or [Rh{P(OPh)$_3$}$_4$][BAr^F_4] (**3**),[20] respectively. The solid-state structure of **2** reveals the expected square-planar Rh^I species. Complex **1** does not react with benzene or exchange with free Binor-S (the latter by EXSY NMR experiments). However, addition of cyclooctene (coe) and benzene to a dichloromethane solution of **1** does result in the facile displacement of Binor-S to form the rhodium(I) complex [Rh(P*i*Pr$_3$)(η^2-C_8H_{14})(η^6-C_6H_6)][BAr^F_4] (**4**).[21] Addition of H_2 and benzene to **1** results in oxidative addition of H_2 and the elimination of Binor-S to afford the rhodium(III) complex [Rh(P*i*Pr$_3$)(H_2)(η^6-C_6H_6)][BAr^F_4] (**5**).[22] Finally, complex **1** is also an isolated resting state of a norbornadiene dimerization catalyst, as addition of excess of diene results in the rapid formation of Binor-S and related dimerization products.

In summary, a rare example of a coordinated C–C single bond with a transition metal has been synthesized and characterized structurally, spectroscopically, and by theoretical calculations. The stability of this complex is no doubt associated with the fact that C–C σ orbitals in the strained cyclopropane ring are sufficiently high in energy to engage in bonding with the metal center,[10] coupled with the chelating nature of the Binor-S derived ligand that brings the cyclopropane fragment into close proximity with the metal center. The facile synthesis of **1** and the rapid equilibrium at room temperature between cyclopropane and metallacyclobutane species suggests that such complexes may prove useful in the further study of C–C activation processes.

Experimental Section

Norbornadiene (100 μL, 930 μmol) was added to a mixture of Na[BAr^F_4] (93 mg, 105 μmol) and [Rh(P*i*Pr$_3$)(nbd)Cl] (40 mg, 102 μmol) in fluorobenzene (3 mL), and the solution was stirred for 2 h. The mixture was filtered, and the filtrate was layered with pentanes and held at 5 °C for 48 h to give **1** as yellow crystals (80 mg, 60 %). ^{1}H (400 MHz, CD_2Cl_2, 298 K): $\delta = 7.71$ (m, 8H; BAr^F_4), 7.55 (m, 4H; BAr^F_4), 3.23 (br, 4H; H11/15/21/25), 2.43 (virtual octet, J(H,H) ≈ J(P,H) = 7 Hz, 3H; PCH), 2.31 (br, 2H; H16/26), 2.13 (br, 2H; H13/23), 1.94 (br, 4H; H12/22/14/24), 1.37 (br, 4H; H17/27), 1.31 ppm (dd, J(P,H) = 14.2, J(H,H) = 7.2 Hz, 18H; CH_3); ^{31}P{^{1}H} (162 MHz): $\delta = 49.24$ ppm (d, J(Rh,P) = 211 Hz); ^{13}C{^{1}H} (101 MHz): $\delta = 162.08$ (q, J(B,C) = 50.0 Hz; B–C), 135.12 (BAr^F CH), 129.21 (m, *C*CF_3), 124.93 (q, J(F,C) = 273 Hz; CF_3), 117.79 (BAr^F CH), 43.63 (s, C12/22/14/24), 34.88 (C13/23), 33.08 (C17/27), 25.53 (dd, J(Rh,C) = 12.4 Hz, J(P,C) = 4.4; C11/15/21/25), 23.69 (dd, J(P,C) = 22.9, J(Rh,C) = 1.3 Hz; PCH), 19.69 ppm (CH_3); elemental analysis calcd (%) for $C_{55}H_{49}BF_{24}PRh$: C 50.40, H 3.76; found: C 50.62, H 3.76.



Scheme 4.

 © 2006 Wiley-VCH Verlag GmbH & Co. KGaA, Weinheim

^{1}H NMR (400 MHz, CD_2Cl_2, 200 K): $\delta = 7.71$ (m, 8H; BAr^F_4), 7.52 (m, 4H; BAr^F_4), 3.41 (m, 2H; H11/15), 2.78 (d, J(H,H) = 6.2 Hz, 2H, H21/25), 2.65 (m, 1H; H16), 2.30 (m, 3H; PCH), 2.23 (d, J(H,H) = 9.4 Hz, 2H; H22/24), 2.02 (m, 1H; H23), 1.94 (m, 1H; H13), 1.64 (t, J(H,H) = 6.6 Hz, 1H; H26), 1.45 (s, 2H; H27), 1.42 (br m, 2H; H12/14), 1.16 (dd, J(P,H) = 14.0, J(H,H) = 7.1 Hz, 18H; CH_3), 1.01 ppm (s, 2H; H17). ^{13}C{^{1}H} NMR (101 MHz; J(C,H) values were determined from a coupled HMQC experiment): $\delta = 161.1$ (q, J(B,C) = 49.6 Hz; BC), 133.9 (s; BAr^F_4 CH), 127.9 (q, J(F,C) = 32.2 Hz; CF_3), 123.8 (q, J(F,C) = 237 Hz; CF_3), 116.9 (s; BArF CH), 58.3 (J(C,H) = 148 Hz; C16), 44.6 (J(C,H) = 135 Hz; C12/14), 40.3 (J(C,H) = 138 Hz; C22/24), 35.13 (J(C,H) = 144 Hz; C13), 33.74 (J(C,H) = 133 Hz; C17), 32.52 (J(C,H) = 152 Hz; C23], 30.73 (J(C,H) = 136 Hz; C27), 25.30 (d, J(Rh,C) = 22, J(CH) = 160 Hz; C11/15), 23.78 (d, J(Rh,C) = 9.2, J(C,H) = 170 Hz; C21/25), 22.29 (d, J(P,C) = 24, J(CH) = 124 Hz; PCH), 21.42 (J(C,H) = 185 Hz; C26), 18.68 ppm (J(C,H) = 126; CH_3); ^{31}P{^{1}H} (162 MHz): $\delta = 47.01$ ppm (d, J(Rh,P) = 209 Hz).

Crystallographic data**:** Crystals of **1** were grown from C_6H_5F/pentane. Intensity data were collected at 150 K on a Nonius Kappa CCD diffractometer, using graphite-monochromated $Mo_{K\alpha}$ radiation ($\lambda = 0.71073$ Å). $C_{55}H_{49}BF_{24}PRh$, $M_r = 1310.63$, $P2_1/n$, $a = 14.8240(2)$, $b = 16.3870(3)$, $c = 22.3530(5)$ Å, $\beta = 99.5330(10)°$ $V = 5355.02(17)$ Å^3, $Z = 4$, $\mu = 0.471$ mm^{-1}, unique reflections = 12123 [R(int) = 0.0647], $R_1 = 0.0458$, $wR_2 = 0.1020$ [$I > 2\sigma(I)$]. The hydrogen atoms H21, H25, and H2A-C were located in the final difference map and freely refined. CCDC-280042 and CCDC-280043 contain the supplementary crystallographic data for this paper. These data can be obtained free of charge from The Cambridge Crystallographic Data Centre via www.ccdc.cam.ac.uk/data_request/cif.

Received: August 25, 2005
Published online: December 2, 2005

Keywords: agostic interactions · C—C activation · fluxionality · rhodium · X-ray diffraction

[1] a) C. H. Jun, *Chem. Soc. Rev.* **2004**, *33*, 610; b) B. Rybtchinski, D. Milstein, *Angew. Chem.* **1999**, *111*, 918; *Angew. Chem. Int. Ed.* **1999**, *38*, 870; c) M. Murakami, Y. Ito *Top. Organomet. Chem.* **1999**, *3*, 97.
[2] G. J. Kubas, *Metal Dihydrogen and σ-Bond Complexes*, Kluwer Academic/Plenum Publishers, New York, **2001**.
[3] B. Goldfuss, P. von R. Schleyer, F. Hampel, J . *Am. Chem. Soc.* **1996**, *118*, 12183.
[4] a) A. Vigalok, B. Rybtchinski, L. J. Shimon, Y. Ben-David, D. Milstein, *Organometallics* **1999**, *18*, 895; b) a related complex with a PCN pincer ligand has been reported: M. Gandelman, L. J. W. Shimon, D. Milstein, *Chem. Eur. J.* **2003**, *9*, 4295.
[5] R. Tomaszewski, I. Hyla-Kryspin, C. L. Mayne, A. M. Arif, R. Gleiter, R. D. Ernst, *J. Am. Chem. Soc.* **1998**, *120*, 2959.
[6] J. Jaffart, M. L. Cole, M. Etienne, M. Reinhold, J. E. McGrady, F. Maseras, *Dalton Trans.* **2003**, 4057.
[7] R. F. W. Bader, C. F. Matta, *Inorg. Chem.* **2001**, *40*, 5603.
[8] W. Baratta, C. Mealli, E. Herdtweck, A. Ienco, S. A. Mason, P. Rigo, *J. Am. Chem. Soc.* **2004**, *126*, 5549.
[9] M. Brookhart, M. L. H. Green, L. L. Wong, *Prog. Inorg. Chem.* **1988**, *36*, 1.
[10] E. Clot, O. Eisenstein, *Principles And Applications Of Density In Inorganic Chemistry, Vol. 113*, Springer-Verlag, Berlin, **2004**, pp. 1.
[11] R. R. Schrock, J. A. Osborn, *J. Am. Chem. Soc.* **1971**, *93*, 3089.
[12] N. M. Scott, R. Dorta, E. D. Stevens, A. Correa, L. Cavallo, S. P. Nolan, *J. Am. Chem. Soc.* **2005**, *127*, 3516.
[13] R. A. Periana, R. G. Bergman, *J. Am. Chem. Soc.* **1986**, *108*, 7346.
[14] L. D'Accolti, C. Fusco, V. Lucchini, G. B. Carpenter, R. Curci, *J. Org. Chem.* **2001**, *66*, 9063.
[15] C16/26 were not observed in the ^{13}C NMR spectrum recorded at 298 K. The calculated coalescence temperature for C16/C26 is 280 K; consequently, a broad, difficult to observe signal would be expected at room temperature.
[16] a) R. F. W. Bader, *Atoms in Molecules: A Quantum Theory*, Clarendon, Oxford, UK, **1990**; b) R. F. W. Bader, *Chem. Rev.* **1991**, *91*, 893.
[17] C. E. Webster, M. B. Hall, *Organometallics* **2001**, *20*, 5606.
[18] S. C. Bart, P. J. Chirik, *J. Am. Chem. Soc.* **2003**, *125*, 886.
[19] Y. C. Tsai, M. J. A. Johnson, D. J. Mindiola, C. C. Cummins, W. T. Klooster, T. F. Koetzle, *J. Am. Chem. Soc.* **1999**, *121*, 10426.
[20] A. M. Trzeciak, Z. Olejnik, J. J. Ziólkowski, T. Lis, *Inorg. Chim. Acta* **2003**, *350*, 339.
[21] H. Werner, G. Canepa, K. Ilg, J. Wolf, *Organometallics* **2000**, *19*, 4756.
[22] G. Canepa, C. D. Brandt, K. Ilg, J. Wolf, H. Werner, *Chem. Eur. J.* **2003**, *9*, 2502.

 © 2006 Wiley-VCH Verlag GmbH & Co. KGaA, Weinheim

Helical Structures

DOI: 10.1002/anie.200503258

Cholesterol-Aided Supramolecular Control over Chromophore Packing: Twisted and Coiled Helices with Distinct Optical, Chiroptical, and Morphological Features**

Ayyappanpillai Ajayaghosh, Chakkooth Vijayakumar, Reji Varghese, and Subi Jacob George*

Dedicated to Professor S. Chandrasekaran on the occasion of his 60th birthday

The controlled ordering and orientation of chromophores at the supramolecular level on the nano- to micrometer scale is important owing to their potential applications in optoelectronic devices.[1] Although long-range supramolecular ordering of chromophoric assemblies has been extensively studied,[2,3] the control of such hierarchical assemblies to give

[*] Dr. A. Ajayaghosh, C. Vijayakumar, R. Varghese, S. J. George
Photosciences and Photonics Unit
Chemical Sciences and Technology Division
Regional Research Laboratory, CSIR
Trivandrum 695019 (India)
Fax: (+91) 471-490-186
E-mail: aajayaghosh@rediffmail.com

[**] This work was supported by the Department of Science and Technology (DST), the Government of India (New Delhi) and the Council of Scientific and Industrial Research (CSIR, Task Force Program CMM 10). C.V., R.V., and S.J.G. are grateful to the CSIR, Government of India, for research fellowships. This work is contribution No. RRLT-PPU-213.

Supporting information for this article is available on the WWW under http://www.angewandte.org or from the author.

WILEY InterScience DISCOVER SOMETHING GREAT
© 2006 Wiley-VCH Verlag GmbH & Co. KGaA, Weinheim

functionally and morphologically different nanoscopic architectures through a preferred packing of the individual chromophores remains elusive. This is particularly true with linear π-conjugated systems, which play crucial roles in organic electronic devices, as the charge-transport properties of conjugated molecules are strongly influenced by the long-range ordering of the chromophores.[4–6] In this context, we have been interested in the self-assembly-induced modulation of optical and morphological properties in oligo(*p*-phenylenevinylene) (OPV) derivatives.[7] However, a precise control over the packing of chromophores into a desired morphology in such a system is still a matter of great importance.

Herein, we show that substitution patterns of cholesterol-appended OPVs allow unprecedented control over the alignment of chromophores and result in distinct optical, chiroptical, and morphological properties. There have been several reports on cholesterol-appended chromophoric systems that self-assemble to form supramolecular architectures and gels.[8,9] Nevertheless, this is the first report on the use of cholesterol moieties as the driving force for biasing the organization of chromophores through different packing modes, leading to control over nanoscopic properties of the resultant hierarchical self-assembly.

The mono- and disubstituted cholesterol-appended OPVs **1** and **2**, respectively, were prepared by treatment of the corresponding bis(hydroxymethyl)-OPVs[7a] with cholesteryl chloroformate and characterized by ^{1}H NMR spectroscopy and MALDI-TOF mass spectrometry.[10] Solutions of the mono- and disubstituted OPVs in chloroform (3×10^{-4} M) showed identical absorption and emission spectra[10] with an absorption maximum at $\lambda = 408$ nm (π–π* transition) and emission maxima at $\lambda = 466$ and 494 nm. The quantum yields of fluorescence (Φ_f) for solutions of **1b** and **2b** in chloroform were measured as $\Phi_f = 0.76$ and 0.82, respectively, using quinine sulfate as standard, and $\Phi_f = 0.32$ and 0.55, respectively, for solutions of **1b** and **2b** in decane at 20 °C using Rhodamine 6G as standard. Similarly, the absorption and emission spectra of solutions of **1b** and **2b** in decane at elevated temperatures showed identical features to those in chloroform. However, the UV/Vis spectrum of **1b** in decane at 20 °C exhibited a broad absorption ($\lambda_{max} = 402$ nm) with a red-shifted shoulder around 470 nm (Figure 1a). This is a general feature of OPV derivatives in nonpolar hydrocarbon solvents.[6a,7a,d] On the contrary, **2b** showed a structured absorption with a blue-shifted maximum ($\Delta\lambda_{max} = 10$ nm) and two new bands at $\lambda = 414$ and 444 nm (Figure 1b). Noticeably, the new band of **2b** at 444 nm is blue-shifted by nearly 26 nm relative to the shoulder band of **1b**. Similar blue-shifted spectra, which are ascribed to the formation of H aggregates, were reported by others for some OPV derivatives.[11]

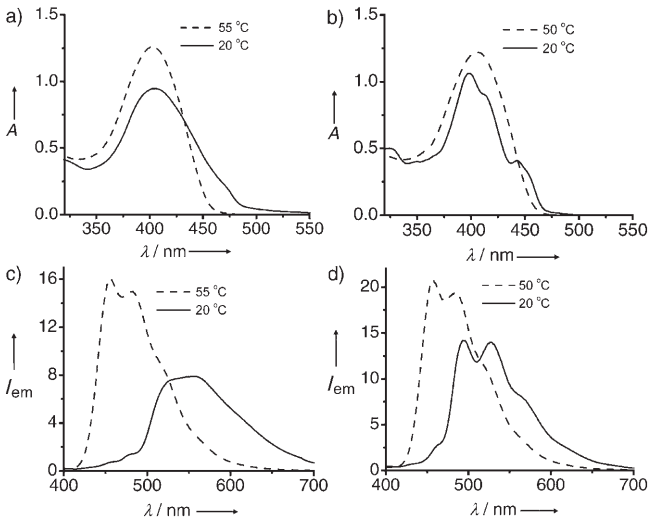
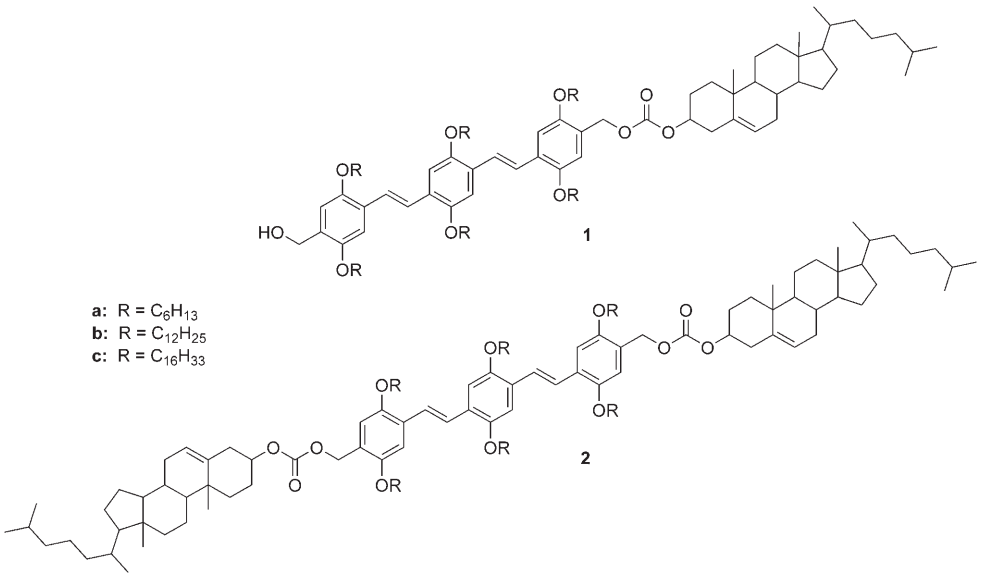


Figure 1. Absorption spectra of a) **1b** and b) **2b**, and emission spectra of c) **1b** and d) **2b** in decane ($c = 3\times10^{-4}$ M, $l = 1$ mm, $\lambda_{ex} = 370$ nm).

The emission spectra of **1b** and **2b** in decane at 50 °C showed identical features with two maxima ($\lambda_{max} = 456$ and 484 nm for **1b**; $\lambda_{max} = 457$ and 485 nm for **2b**). However, in decane at 20 °C, **1b** showed a broad structureless emission between 500–700 nm with a maximum around 560 nm (Figure 1c), whereas **2b** displayed a structured emission with two emission maxima at 494 and 528 nm (Figure 1d). The variation of the absorption and emission spectra with solvents and temperature reveals that in decane at ambient temperatures these molecules form aggregates whose electronic properties are different from each other. Although these observations can be rationalized by invoking H-type[9e,11] and J-type[6a] aggregation in analogy to previous reports,



© 2006 Wiley-VCH Verlag GmbH & Co. KGaA, Weinheim

we find difficulties with such assignments for two reasons: The red and blue shifts of the aggregates of **1b** and **2b** with respect to the corresponding monomers are not very predominant. Furthermore, the emission spectrum of **2b** is more intense than that of **1b**. By normal practice, if the blue-shifted absorption spectrum of **2b** is assigned to the presence of H aggregates, it should be less intense relative to the spectrum of the J aggregates of **1b**. Therefore, we prefer to address these aggregates as "pseudo-H" and "pseudo-J" with twisted and tilted chromophore stacks for **2b** and **1b**, respectively. In such cases, the difference in the excited state dipole moment orientation of the two aggregates results in distinct optical and chiroptical features.

Solutions of **1b** and **2b** in chloroform were circular-dichroism-inactive (Figure 2). However, the CD spectrum of

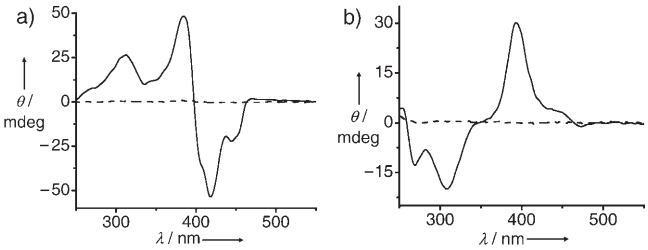


Figure 2. CD spectra of a) **2b** and b) **1b** in chloroform (-----) or decane (——). $c = 3\times10^{-4}$ M, $l = 1$ mm.

2b in decane (3×10^{-4} M) showed an exciton-coupled bisignate signal with negative ($\lambda_{max} = 418$ nm) and positive ($\lambda_{max} = 385$ nm) Cotton effects, which change sign exactly through the π–π* absorption maximum at 398 nm (Figure 2a). This behavior is characteristic of a left-handed helical bias of the supramolecular chirality.[12] In the case of **1b**, the CD spectrum in decane showed a strange behavior with first a positive ($\lambda_{max} = 393$ nm) followed by two negative ($\lambda_{max} = 308$ and 269 nm) Cotton effects. The non-bisignate exciton couplet with opposite signals indicates the possibility of different chiral dispositions. Furthermore, the measure of chirality, g, for **1b** is low ($g_{393nm} = 5.2\times10^{-4}$) relative to that for **2b** ($g_{385nm} = 9.3\times10^{-4}$) which indicates a weak exciton coupling in the former. These differences in the CD spectra reiterate the differences between the aggregates of **1b** and **2b** and agree with the absorption and emission properties.

A striking consequence of the different arrangements of chromophores for **1b** and **2b** is the disparity in the gelation behavior between the two.[10] Although both compounds induce the gelation of a variety of hydrocarbon solvents, gels with **2b** were relatively weaker than those with **1b**. The critical gelator concentration (CGC) of **2b** in decane is 7.0 mM whereas that of **1b** is only 3.4 mM, which is nearly twofold less and points to more efficient gelation of the latter. Plots of the concentration of gelator against the melting temperature of the gel showed enhanced stability for the gel of **1b** (Figure 3a). The gel with **1b** showed a weak yellow emission whereas the gel from **2b** displayed a relatively strong green emission (Figure 3a). Furthermore, the weak yellow emission of the former reveals better electronic conjugation with

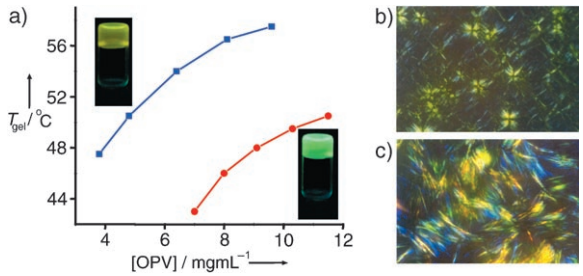


Figure 3. a) Plots of T_{gel} versus the concentration of **1b** (blue) and **2b** (red) in decane. Insets: Photographs of the corresponding gels under illumination; b, c) OPM pictures (400× magnification) of the decane gels of **1b** (3.5×10^{-3} M; b) and **2b** (7.2×10^{-3} M; c).

strong π interaction between the chromophores relative to those of the latter. The optical polarizing microscopy (OPM) textures of **2b** showed streaklike textures[13a] with strong birefringence. On the other hand, **1b** showed four-arm brush textures similar to cholesterol gelators[13b] and chiral OPV

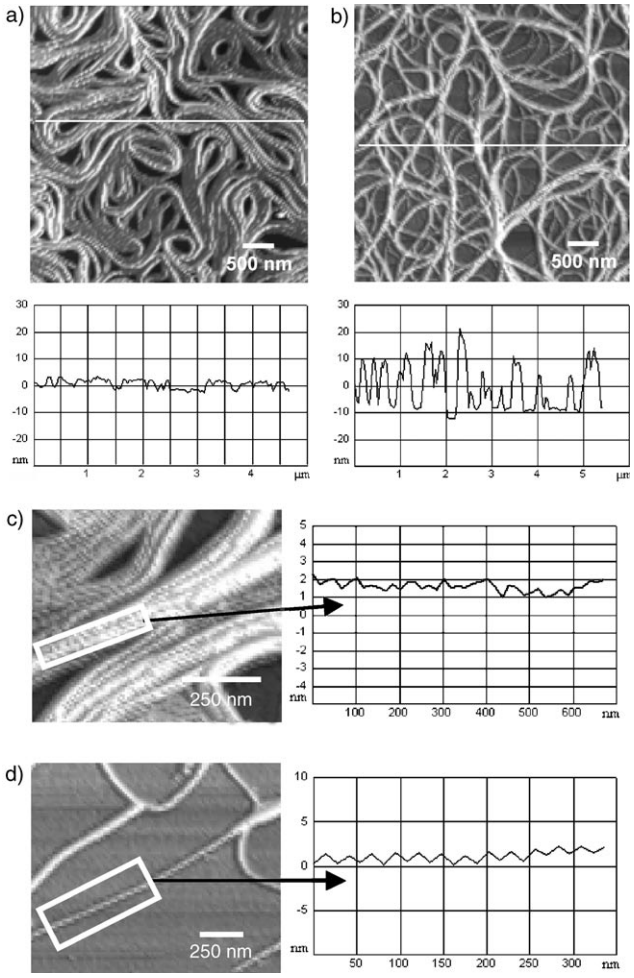


Figure 4. AFM images of a) **1b** and b) **2b** with the corresponding height profiles shown. c) Zoomed region of assembly **1b** and d) isolated fibers of **2b** with the corresponding section analyses. Samples were prepared from solutions in decane ($c = 1\times10^{-5}$ M) and transferred to freshly cleaved mica sheet by drop-casting. See Supporting Information for detailed section analyses.

© 2006 Wiley-VCH Verlag GmbH & Co. KGaA, Weinheim

gelators.[7c] This observation reveals the differences in the supramolecular anisotropy leading to different mesoscopic structures. It is clear that hydrogen bonds in **1b** make significant contributions to the observed differences in the gelation and mesoscopic properties, whereas the orientation of the chromophore plays a crucial role in the optical and chiroptical properties.

The atomic force microscopy (AFM) textures of **1b** and **2b** obtained from solutions in decane showed significant differences, although both assemblies adopt right-handed (*P*) helical structures. The helicity of **1b** is in agreement with the CD spectrum, whereas that of **2b** disagrees with the bisignate CD signal. Such a contradiction of the observed CD and morphological features have previously been reported.[5c,14] In many cases, the initially formed 1D aggregates with a left-handed twist may wind in the opposite direction during the higher-order assembly to result in an ultimate right-handed twist, as can be seen to some extent in some of the large fibers of **2b**. AFM analysis reveals ribbonlike structures of **1b** that are flat and aligned sideways to form coiled superstructures. The width of the individual ribbons varies from 30 to 70 nm, with an average height of 4–8 nm. The height of 8 nm corresponds to two individual tapes lying one over the other. Interestingly, **2b** showed a morphology comprised of entangled helical fibers of different sizes. The width of the smallest fiber is 40 nm, with a height of 4 nm and is several micrometers in length. The height profiles of wide areas of the samples showed a uniform height for **1b**, whereas a height variation of 4–50 nm was observed for **2b**.[10] Furthermore, section analysis along the axis (Figure 4c and d) revealed that assemblies of **1b** have an irregular helical pitch of 40–80 nm whereas those of **2b** are almost uniform with zigzag patterns and have a pitch length of 46 nm. Irregular movements of the AFM tip through the long axis of the assembly with variable pitch length and uniform height profile are characteristic of a flexible and flattened coiled tapelike morphology of **1b**. In contrast, the uniform zigzag patterns along the axis and variable height profiles of **2b** are characteristic of twisted helical fibrillar assemblies of different size that are intertwined.

On the basis of the differences in the optical, chiroptical, gelation, and morphological properties, it is clear that the packing of the chromophores in the assemblies of **1** and **2** are remarkably different. The features of the absorption, emission, and CD spectra strongly support a well-organized twisted helical arrangement of the chromophores in the dicholesterol-substituted molecules **2** whereas a tilted extended packing of the hydrogen-bonded chromophores is favored for the monocholesterol derivatives **1** (Figure 5). The extended supramolecular assembly of the twisted packing (pseudo-H aggregates) leads to twisted helical assemblies, whereas the tilted packing (pseudo-J aggregates) may result in a coiled helical assembly as shown in Figure 5.

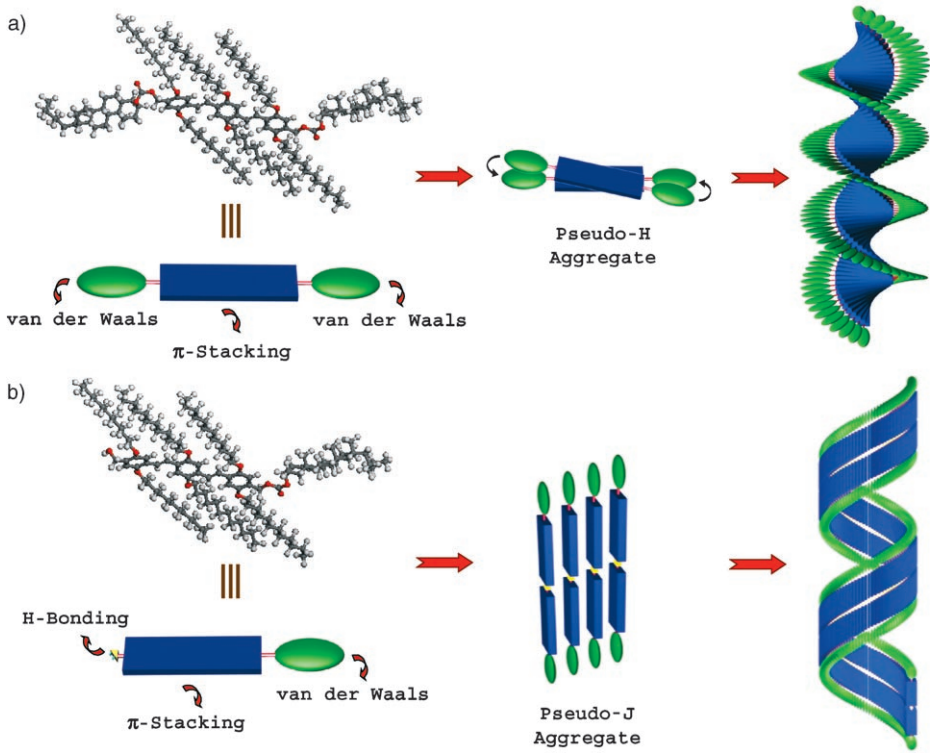


Figure 5. Probable mode of self-assembly of a) **2b** and b) **1b** in decane.

In conclusion, we have shown that symmetrical and unsymmetrical functionalization of OPVs with cholesterol moieties allows a controlled supramolecular organization which results in helical nanoscopic architectures that display remarkable differences in optical, chiroptical, and morphological properties, as illustrated by the two classes of molecules **1** and **2**. The approach described here can be used as a general strategy to control the chromophore ordering which may be useful to the design of nanoscopic functional assemblies for optoelectronic applications.

Received: September 14, 2005
Revised: October 14, 2005
Published online: December 2, 2005

Keywords: cholesterol · gels · helical structures · self-assembly · supramolecular chemistry

[1] a) J.-M. Lehn, *Supramolecular Chemistry, Concepts and Perspectives*, VCH, Weinheim, **1995**; b) S. I. Stupp, V. Le Bonheur, K. Walker, L. S. Li, K. Huggins, M. Keser, A. Amstutz, *Science* **1997**, *276*, 384–389; c) A. E. Rowan, R. J. M. Nolte, *Angew. Chem.* **1998**, *110*, 65–71; *Angew. Chem. Int. Ed.* **1998**, *37*, 63–68; d) J. J. L. M. Cornelissen, A. E. Rowan, R. J. M. Nolte, N. A. J. M. Sommerdijk, *Chem. Rev.* **2001**, *101*, 4039–4070.

[2] For selected chromophore assemblies, see: a) H. Engelkamp, S. Middelbeek, R. J. M. Nolte, *Science* **1999**, *284*, 785–788; b) F. Würthner, C. Thalacker, A. Sautter, W. Schärtl, W. Ibach, O.

 © 2006 Wiley-VCH Verlag GmbH & Co. KGaA, Weinheim

Hollricher, *Chem. Eur. J.* **2000**, *6*, 3871 – 3886; c) T. Yamaguchi, N. Ishii, K. Tashiro, T. Aida, *J. Am. Chem. Soc.* **2003**, *125*, 13934 – 13935; d) F. Würthner, S. Yao, U. Beginn, *Angew. Chem.* **2003**, *115*, 3368 – 3371; *Angew. Chem. Int. Ed.* **2003**, *42*, 3247 – 3250; e) M. Kimura, T. Kuroda, K. Ohta, K. Hanabusa, H. Shirai, N. Kobayashi, *Langmuir* **2003**, *19*, 4825 – 4830; f) A. Ajayaghosh, S. J. George, A. P. H. J. Schenning, *Top. Curr. Chem.* **2005**, *258*, 83 – 118.

[3] a) A. C. Grimsdale, K. Müllen, *Angew. Chem.* **2005**, *117*, 5732 – 5772; *Angew. Chem. Int. Ed.* **2005**, *44*, 5592 – 5629; b) P. Leclère, A. Calderone, D. Marsitzky, V. Francke, Y. Geerts, K. Müllen, J. L. Brédas, R. Lazzaroni, *Adv. Mater.* **2000**, *12*, 1042 – 1046; c) D. Wasserfallen, I. Fischbach, N. Chebotareva, M. Kastler, W. Pisula, F. Jäckel, M. D. Watson, I. Schnell, J. P. Rabe, H. W. Spiess, K. Müllen, *Adv. Funct. Mater.* **2005**, *15*, 1585 – 1594.

[4] For reviews on π-conjugated systems, see: a) F. J. M. Hoeben, P. Jonkheijm, E. W. Meijer, A. P. H. J. Schenning, *Chem. Rev.* **2005**, *105*, 1491 – 1546; b) A. P. H. J. Schenning, E. W. Meijer, *Chem. Commun.* **2005**, 3245 – 3258.

[5] a) F. S. Schoonbeek, J. H. van Esch, B. Wegewijs, D. B. A. Rep, M. P. de Haas, T. M. Klapwijk, R. M. Kellogg, B. L. Feringa, *Angew. Chem.* **1999**, *111*, 1486 – 1490; *Angew. Chem. Int. Ed.* **1999**, *38*, 1393 – 1397; b) B. W. Messmore, J. F. Hulvat, E. D. Sone, S. I. Stupp, *J. Am. Chem. Soc.* **2004**, *126*, 14452 – 14458; c) J. Bae, J.-H. Choi, Y.-S. Yoo, N.-K. Oh, B.-S. Kim, M. Lee, *J. Am. Chem. Soc.* **2005**, *127*, 9668 – 9669.

[6] a) A. P. H. J. Schenning, P. Jonkheijm, E. Peeters, E. W. Meijer, *J. Am. Chem. Soc.* **2001**, *123*, 409 – 416; b) P. Jonkheijm, A. Miura, M. Zdanowska, F. J. M. Hoeben, S. De Feyter, A. P. H. J. Schenning, F. C. De Schryver, E. W. Meijer, *Angew. Chem.* **2004**, *116*, 76 – 80; *Angew. Chem. Int. Ed.* **2004**, *43*, 74 – 78.

[7] a) A. Ajayaghosh, S. J. George, *J. Am. Chem. Soc.* **2001**, *123*, 5148 – 5149; b) A. Ajayaghosh, S. J. George, V. K. Praveen, *Angew. Chem.* **2003**, *115*, 346 – 349; *Angew. Chem. Int. Ed.* **2003**, *42*, 332 – 335; c) S. J. George, A. Ajayaghosh, P. Jonkheijm, A. P. H. J. Schenning, E. W. Meijer, *Angew. Chem.* **2004**, *116*, 3504 – 3507; *Angew. Chem. Int. Ed.* **2004**, *43*, 3422 – 3425; d) S. J. George, A. Ajayaghosh, *Chem. Eur. J.* **2005**, *11*, 3217 – 3227.

[8] a) P. Terech, R. G. Weiss, *Chem. Rev.* **1997**, *97*, 3133 – 3159; b) J. H. van Esch, B. L. Feringa, *Angew. Chem.* **2000**, *112*, 2351 – 2354; *Angew. Chem. Int. Ed.* **2000**, *39*, 2263 – 2266; c) K. J. C. van Bommel, A. Friggeri, S. Shinkai, *Angew. Chem.* **2003**, *115*, 1010 – 1030; *Angew. Chem. Int. Ed.* **2003**, *42*, 980 – 999.

[9] a) K. Murata, M. Aoki, T. Suzuki, T. Harada, H. Kawabata, T. Komori, F. Ohseto, K. Ueda, S. Shinkai, *J. Am. Chem. Soc.* **1994**, *116*, 6664 – 6676; b) R. Wang, C. Geiger, L. Chen, B. Swanson, D. G. Whitten, *J. Am. Chem. Soc.* **2000**, *122*, 2399 – 2400; c) K. Sugiyasu, N. Fujita, S. Shinkai, *Angew. Chem.* **2004**, *116*, 1249 – 1253; *Angew. Chem. Int. Ed.* **2004**, *43*, 1229 – 1233; d) P. Xue, R. Lu, D. Li, M. Jin, C. Tan, C. Bao, Z. Wang, Y. Zao, *Langmuir* **2004**, *20*, 11234 – 11239; e) S.-i. Kawano, N. Fujita, S. Shinkai, *Chem. Eur. J.* **2005**, *11*, 4735 – 4742.

[10] See Supporting Information.

[11] a) P. A. van Hal, M. M. Weink, J. M. Kroon, R. A. J. Janssen, *J. Mater. Chem.* **2003**, *13*, 1054 – 1057; b) T. Mori, T. Watanabe, K. Minagawa, M. Tanaka, *J. Polym. Sci. Part A* **2005**, *43*, 1569 – 1578.

[12] N. Berova, K. Nakanishi in *Circular Dichroism: Principles and Applications* (Eds.: N. Berova, K. Nakanishi, R. W. Woody), *4th ed.*, Wiley-VCH, Weinheim, **2000**, p. 337.

[13] a) L. Lu, R. G. Weiss, *Chem. Commun.* **1996**, 2029 – 2030; b) X. Huang, P. Terech, S. R. Raghavan, R. G. Weiss, *J. Am. Chem. Soc.* **2005**, *127*, 4336 – 4344.

[14] A. Lohr, M. Lysetska, F. Würthner, *Angew. Chem.* **2005**, *117*, 5199 – 5202; *Angew. Chem. Int. Ed.* **2005**, *44*, 5071 – 5074.

 © 2006 Wiley-VCH Verlag GmbH & Co. KGaA, Weinheim

Supramolecular Chemistry

DOI: 10.1002/anie.200501994

"Gating" the Pores of a Metal Oxide Based Capsule: After Initial Cation Uptake Subsequent Cations Are Found Hydrated and Supramolecularly Fixed above the Pores**

Achim Müller, Yunshan Zhou, Hartmut Bögge, Marc Schmidtmann, Tamoghna Mitra, Erhard T. K. Haupt, and Alois Berkle*

Dedicated to Professor Dante Gatteschi on the occasion of his 60th birthday

Biological cell contact with the outer world depends essentially on ion fluxes, the cations involved follow—during passive transport through transmembrane channels—a route in the direction of the electrochemical gradient ("downhill").[1] They travel through the membrane channel and come to a halt when the electrochemical gradient reaches zero. (The electrochemical gradient is based on the combination of the voltage and concentration gradient for the ion under consideration.) The gradients are maintained by active transporters and pumps, which enable/facilitate rapid membrane voltage changes to be produced by the passive transport. The cations can be initially attracted by negatively charged carboxylate functional groups of amino acids pointing towards the entrance of the channel, as in the case of the bacterial K^+ ion channel.[1a] The question arises whether this type of gating mechanism can be modeled with porous capsules/artificial cells, that is, on the basis of rather robust, spherical, highly negatively charged nanosized capsules of the type $[\{(Mo^{VI})Mo^{VI}_5O_{21}(H_2O)_6\}_{12}\{Mo^{V}_2O_4(ligand)\}_{30}]^{x-}$ [2] ($x = 72$ for the SO_4^{2-} ligand, as for the anion **1a** in **1**),[3a] which has 20 pores and a cavity, linked together by 20 channels.[2] The capsules are comparable with biological cells in the sense that they are busy areas showing traffic in both directions through the channels, from the surface to the interior and back. For an

[*] Prof. Dr. A. Müller, Dr. Y. Zhou, Dr. H. Bögge, M. Schmidtmann, T. Mitra, A. Berkle
Fakultät für Chemie
Universität Bielefeld
Postfach 100131, 33501 Bielefeld (Germany)
Fax: (+49) 521-106-6003
E-mail: a.mueller@uni-bielefeld.de
Dr. E. T. K. Haupt
Institut für Anorganische und Angewandte Chemie
Universität Hamburg
20146 Hamburg (Germany)

[**] We thank Prof. D. Rehder (Hamburg) for useful discussions regarding the NMR spectra and Dr. L. Zhang (Bielefeld) for metal analyses. Financial support from the Deutsche Forschungsgemeinschaft, the Fonds der Chemischen Industrie, the Volkswagenstiftung, the European Union, and the German–Israeli Foundation for Scientific Research & Development (GIF) is gratefully acknowledged.

WILEY InterScience DISCOVER SOMETHING GREAT

© 2006 Wiley-VCH Verlag GmbH & Co. KGaA, Weinheim

understanding of the influx it is important to know that the negative charge density increases from the capsule periphery to the 30 sulfate ligands at the internal (tunable) cavity surface where, after entering, the cations are finally positioned.[3,4] This type of cation transport/uptake process based on the capsules can optimally be studied if highly charged cations are chosen, such as the Pr^{3+} ion, which, because of their high charge, have a high affinity to the negatively charged capsule (though a few NH_4^+ ions are also integrated[5]). In addition the Pr^{3+} ions have a moderate dehydration energy (allowing us to detect cation entrance as well as trapping of the hydrate complex), and the favorable crystallographic attribute of a high electron density. In this investigation, evidence is obtained that with sufficient uptake of the highly positively charged Pr^{3+} ions, the pores and channels block further uptake as a result of the lowering of the charge, that is, the (formal) electrochemical gradient approaches zero. (The consideration of the electrochemical gradient is in this case of course formal, because of the small number of ions involved.) As a consequence, further $[Pr(H_2O)_9]^{3+}$ complexes present in solution are trapped above the pores forming a new type of supramolecular species corresponding to a sphere-surface coordination chemistry.

valence sum (BVS) calculations).[7] The release of NH_4^+ ions from **1a**, which occurs during the formation of **2a**, was studied by ^{15}N-HSQC NMR (^{15}N-decoupled) spectroscopy.

The structure analysis shows that **2a** has—as does **1a**[3a] and several other related capsules[2]—the "classical" approximate icosahedral {pentagon}$_{12}${linker}$_{30}$ skeleton. This structure can also be easily demonstrated by Raman spectroscopy as **2a** shows the characteristic "few-line" spectrum in which the highest intensity band at 876 cm^{-1} is assigned to the interesting, totally symmetric A_g breathing vibration of the

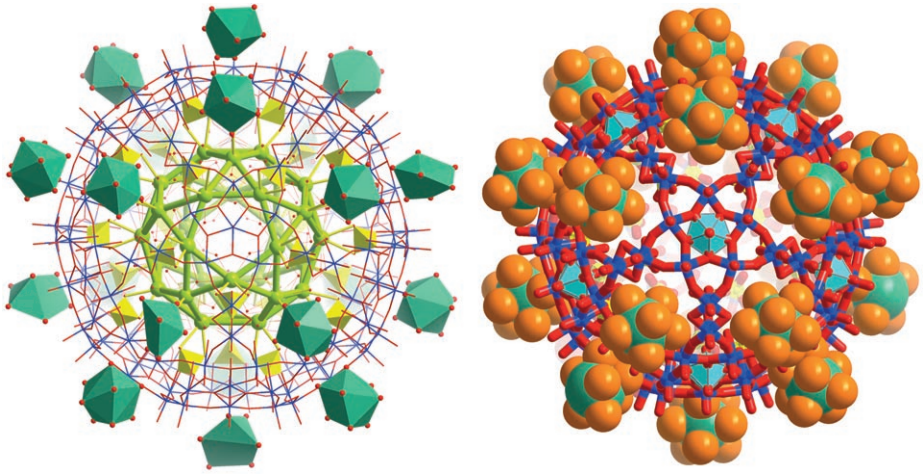


Figure 1. Left: Structure of **2a** emphasizing the outer, hydrated Pr^{3+} ions (dark green polyhedra) as well as the inner Pr^{3+} ions forming an under-occupied icosidodecahedron (light green); additionally shown: the metal oxide skeleton of the capsule (wire-frame model; Mo blue, O red) and the SO_4^{2-} ions (yellow tetrahedra); selected bond lengths in Å. Right: Space-filling representation of the outer, hydrated Pr^{3+} ions with the metal oxide capsule skeleton shown as a wire-frame model (same color code as on the left) with the central pentagonal bipyramids of the pentagonal units in polyhedral representation (light blue; see also text).

$$(NH_4)_{72-n}[\{(H_2O)_{81-n}+(NH_4)_n\}\subset\{(Mo^{VI})Mo^{VI}{}_5O_{21}(H_2O)_6\}_{12}-\{Mo^{V}{}_2O_4(SO_4)\}_{30}]\cdot\approx 200\,H_2O\equiv(NH_4)_{72-n}\,\mathbf{1a}\cdot\approx 200\,H_2O\quad\mathbf{1}$$

Crystals of **2** (space group $R\bar{3}c$)[6,7] can be obtained by interaction of **1a** with Pr^{3+} ions under (deliberately chosen) high-concentration conditions which should guarantee a comparably high uptake of Pr^{3+} ions. In this context it should be realized that in biological situations the ion-concentration differences between the outside of the cell and its interior (as in the case of Na^+ and K^+ ions) is a basic condition for several fundamental life processes, such as signal transduction, also the ion flux into the channel, which is limited by the narrowest part of the channel, increases with high ion concentrations outside the cell.[1a]

$$(NH_4)_{27}[Pr(H_2O)_9]_{10}[(Pr)_5\subset\{(Mo^{VI})Mo^{VI}{}_5O_{21}(H_2O)_6\}_{12}-\{Mo^{V}{}_2O_4(SO_4)\}_{30}]\cdot\approx[185\,H_2O+12\,Cl^-+3\,Pr^{3+}+3\,NH_4{}^+]-$$
$$\equiv(NH_4)_{27}[Pr(H_2O)_9]_{10}\,\mathbf{2a}\cdot[\text{cocrystallized components}]\quad\mathbf{2}$$

Capsule **2** was characterized by elemental analyses, thermogravimetry (to determine the amount of crystal water), and spectroscopic methods (IR, Raman) as well as single-crystal X-ray diffraction analyses (including bond (large number of) 240 bridging oxygen atoms in the capsule. Remarkably, in **2a**, Pr^{3+} centers are found inside as well as in hydrated form outside the capsule (Figure 1). Each of the five encapsulated Pr^{3+} ions, which are disordered over 30 equivalent positions forming an icosidodecahedron, is coordinated to a sulfate group that acts as a bidentate ligand to a {Mo_2} linker. The coordination sphere of the internal Pr^{3+} ions is completed by the oxygen atoms of the encapsulated water molecules. In this sense the water molecules, which are formally organized in shells and linked by strong hydrogen bonds, "behave" as polydentate/macrocyclic ligands;[8a] structurally speaking the encapsulated water molecules in **2a** form a partially occupied $\{H_2O\}_{60+20}$ type shell.[8b] Additionally, in this case the $\{H_2O\}_{60+20}$ shell, together with the Pr positions inside the cavity, form an interesting spherical shell type aggregate; the Pr positions are located a little below/inside the water cage (Figure 2).

The important discovery is that in crystals of **2** ten Pr^{3+} ions are, as a result of a kind of pore closing, found located above the pores, which does not happen with lower Pr^{3+} ion concentrations; in those cases the Pr^{3+} ions are only found encapsulated within the cavity (see details in ref. [9] and the Note added in proof ref. [20]). The non-encapsulated Pr^{3+} ions are found mostly with classical ninefold hydration[10a–d]

 © 2006 Wiley-VCH Verlag GmbH & Co. KGaA, Weinheim

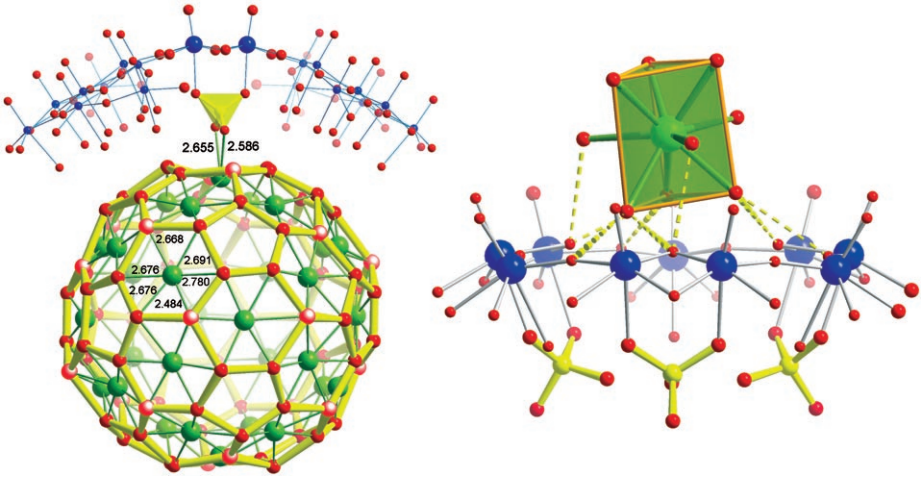


Figure 2. Left: Part of the structure of **2a**: The under-occupied 30 Pr^{3+} ion positions inside the capsule form, together with the $\{H_2O\}_{80}$ cluster shell positions [formally described as $\{H_2O\}_{60}$ (distorted rhombicosidodecahedron in red) + $\{H_2O\}_{20}$ (dodecahedron in pale red)], a new type of spherical cluster shell which is emphasized (Pr green, O red and pale red). The pale red positions are located on the C_3-axis (partly occupied by the $\{H_2O\}_{20}$ water molecules). A fragment of the metal oxide skeleton of the capsule is also shown (ball-and-stick representation; Mo blue, O red) symmetrically coordinated to one sulfate group (yellow tetrahedron). Right: Structure of a $[Pr(H_2O)_9]^{3+}$ complex above a pore (not all are so well-defined as in this case), highlighting the H-bonds (broken yellow lines) between the water ligands and oxygen atoms of the $\{Mo_9O_9\}$ pore (Pr green, Mo blue, S yellow, O red).

while the water ligands are hydrogen bonded to the O atoms of the $\{Mo_9O_9\}$ pores/rings. This can formally be considered as an outer sphere complex situation (see ref. [10e]) with the capsule acting as polydentate ligand. In any case, **2a** can be considered as a new type of supramolecular species with the "guests" located at the sphere surface (see Figure 1 and Figure 2, right; O···O distances: approximately 2.8 to 3.0 Å).[3d] The situation is a consequence of the following process: After initial uptake of the five highly charged Pr^{3+} ions and their positioning at the internal cavity functional groups, the formal electrochemical gradient,[11] which can be generally speaking correlated with the driving force for the uptake of the cation under consideration, decreases owing to the decrease in the overall negative charge of the capsule. The consequence is that finally no more cations can pass through the "closed" pores/channels,[12] which corresponds to a type of modeling of voltage gating.[1]

In this context we considered the presence of the NH_4^+ ions encapsulated in **1a** in more detail. From earlier X-ray crystallography investigations there was only indirect evidence that a few encapsulated NH_4^+ ions are present in **1a**.[3a] But these ions are rather strongly fixed in the capsule cavity and cannot easily be removed; this result follows from combined thermogravimetry, mass spectroscopy, and temperature-dependent elemental analyses studies up to 450 °C. Remarkably, the release of the "last" NH_3 molecules out of the capsules upon heating occurs at comparably high temperature (i.e. 420 °C). This NH_3 release is favored by an interesting cavity internal reaction occurring at 360 °C by which the $\{Mo^V_2\}$ linkers reduce the sulfate ligands while the SO_2 formed is released; [13a] the redox process increases the size of the channels drastically. Information on the basic responsive behavior of the encapsulated NH_4^+ ions upon cation uptake has now been obtained: The ^{15}N-HSQC spectrum[13b] of ^{15}N enriched **1** dissolved in DMSO[13c] (Figure 3) shows the existence of a few internal sites occupied with NH_4^+ ions[13d]—a situation comparable with the observation of different sites occupied with encapsulated Li^+ ions in the corresponding capsule according to information obtained not only from X-ray crystallography but also from ^{7}Li NMR spectra[14])—whereas the related broadened ^{1}H signals are, as expected, all shifted upfield (as are the Li^+ signals in the corresponding system). Of the various ^{15}N signals some are shifted upfield, and some downfield compared to the external ammonium signal. There is a slow proton exchange between the encapsulated NH_4^+ ions at different sites with the external ammonium ions present in solution. To understand the behavior of the encapsulated $^{15}NH_4^+$ ions in **1a** as a response to the entrance of cations in general (**1a** is always used in these type of ion transport studies), Ca^{2+} ions were added which are known to be easily encapsulated and firmly fixed at as many as 20 equivalent positions below the channels.[4] $CaBr_2$ was used instead of the paramagnetic praseodymium salt to enable NMR spectroscopy monitoring of the effect of metal uptake on the mobility of encapsulated NH_4^+ ions. The important result is that with the addition of small amounts of $CaBr_2$, all the signals caused by the presence of the small

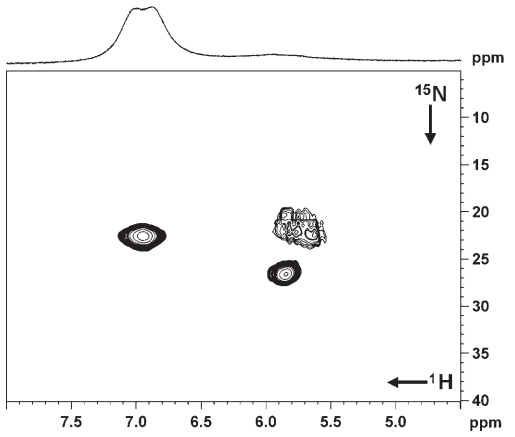


Figure 3. ^{15}N-HSQC NMR (^{15}N-decoupled) spectrum of a solution of ^{15}N-enriched **1** in DMSO showing the presence of the encapsulated NH_4^+ ions. The correlation peak (7/23 ppm) for the intense ^{1}H doublet for the free, solvated ammonium ions is accompanied by additional correlations (which disappear after cation uptake) with exclusively upfield proton (5.5–6 ppm) and up-and downfield nitrogen chemical shifts (21–26 ppm) corresponding to the encapsulated NH_4^+ ions. The shapes of the signals of the 1D-^{1}H NMR spectrum are due to a slow H^+ exchange which is responsible for the broadening of the signal of the "free" and encapsulated ammonium cations. Extended ^{15}N-NMR studies demonstrate that the shape of these signals also depends on the amount of water present.

 © 2006 Wiley-VCH Verlag GmbH & Co. KGaA, Weinheim

number of encapsulated NH_4^+ ions vanish. Clearly, this change is due to breaking of the equilibria and release of the internal ammonium cations. This result can be clearly transferred not only to our Pr^{3+} situation but also to other cation uptakes related to counterion transport in general. The term "gating" is justified as the first cations taken up eject the few NH_4^+ ions from the cavity,[13c] with increasing Pr^{3+} ion concentrations trapping occurs, and furthermore, each ion has its own characteristic chemical potential.[11]

We also examined other exchange processes occurring within the capsule, such as the exchange of acetate by (hydrogen) sulfate in the preparation of **1** (see Experimental Section): Addition of protons to the aqueous solution leads to the formation of acetic acid which is easily released. The consequence is a drastic increase of the channel size allowing the entrance of SO_4^{2-} ions. A formally related situation of interest is another acid–base system inside the capsule, that is, the ammonium/ammonia equilibrium. By increasing the "pH" of a solution of **1**, that is, by avoiding capsule decomposition, some NH_3 can be formed in small amounts which could, in principle, easily pass through the pores. Interestingly, NH_3 gas channels are presently being discussed in biological systems. (We considered this problem because the NH_4^+ ion transport through the pores is involved in the Pr^{3+} uptake.) In this context some general facts should be mentioned: Ammonium is one of the most important nitrogen sources in nature, that is, for bacteria, fungi, and plants whereas it is toxic in high concentrations to animals. Though it has long been known that the ammonium-transport proteins are present in all domains of life, only recent functional studies with members of this family have yielded controversial results with respect to the chemical nature of the transported species (NH_4^+ or NH_3). In a special case, structural data and energetic considerations strongly indicated the presence of hydrophobic functioning ammonia gas channels.[15] In this sense an interesting aspect was pointed out by Heitman and Agre[16] as to whether it is possible that ammonia has other important physiological roles, possibly as a signaling molecule.

The present studies with varying ion concentrations inside and outside the capsule are interesting in relation to the fact that living cells can only function properly if the inner-cell ion concentrations are different from those in the surrounding local environments, that is, under non-equilibrium conditions.[1] Finally, our porous capsules, because of their basic container function (see for example, ref. [17]), can offer the chance to perform a variety of encapsulation chemistry processes,[18] and to carry out coordination chemistry under confined conditions and on nanosized sphere surfaces. Generally speaking, the capsules can be considered as nano test-tubes; in this context recent related discussions on "*record breaking test tubes*" may be referred to.[19]

Experimental Section

1: (same compound as in ref. [3a], but obtained with a simpler synthetic method as heating is avoided): $(NH_4)_2SO_4$ (8.0 g, 60.5 mmol) and subsequently H_2SO_4 (21 mL, 2 M) was added under stirring to a solution of $(NH_4)_{42}[Mo_{132}O_{372}(H_2O)_{72}(CH_3COO)_{30}]\cdot \approx (10\,CH_3COONH_4 + 300\,H_2O)$ (2.0 g, 0.07 mmol)[2e,f] in water (160 mL). The mixture was kept in an open beaker for crystallization. After 2 weeks the precipitated brown crystals were collected by filtration and washed with a small amount of 2-propanol, and then with diethyl ether. Yield: 1.8 g. Characteristic IR bands (KBr disk): $\tilde{\nu} = 1618$ [m, $\delta(H_2O)$], 1400 [s, $\delta_{as}(NH_4)$], 1195 (w), 1136 (m), 1038 (w) [$\nu_{as}(SO_4)$], 970 (s), 935 (w) [ν (Mo=O)], 856 (w), 800 (vs), 727 (s), 631 (w), 571 cm^{-1} (m). Characteristic Raman bands (solid state, KBr dilution, $\lambda_e \approx 1064$ nm): $\tilde{\nu} = 949$ [m, ν (Mo=O)], 876 [s, $\nu(O_{bri}$ breathing/$A_{1g})$] 374 (m), 304 cm^{-1} (w). Elemental analysis (%) calcd: N 3.5, S 3.35; found: N 3.5, S 3.6.

2: H_2SO_4 (1.5 mL, 0.5 M) was added under stirring to a solution of **1** (1.26 g, 0.034 mmol) in water (16 mL), shortly afterwards a solution of $PrCl_3\cdot 6\,H_2O$ (1.85 g, 5.20 mmol) in water (4 mL) was added. (Note the deliberate use of a high concentration in contrast to normal synthetic conditions.) The resulting mixture was stirred for one minute and then immediately filtered into an open beaker for crystallization. After four days the precipitated dark brown crystals were separated out and washed with ice-cold water. Yield: 1.0 g (74% based on **1**). Characteristic IR bands (KBr disk): $\tilde{\nu} = 1622$ [m, $\delta(H_2O)$], 1400 [m, $\delta_{as}(NH_4)$], 1190 (sh), 1138 (m), 1055 (sh), 970 (s), 940 (sh) [ν(Mo=O)], 856 (w), 800 (s), 725 (s), 633 (w), 571 cm^{-1} (m). Characteristic Raman bands (solid state, KBr dilution, $\lambda_e \approx 1064$ nm): $\tilde{\nu} = 951$ [m, ν (Mo=O)], 876 [s, $\nu(O_{bri}$ breathing/$A_{1g})$] 375 (m), 309 cm^{-1} (w). Elemental analysis (%; see ref. [6]) calcd: Pr 8.22, N 1.36, Cl 1.37; found: Pr 8.3, N 1.4, Cl 1.5.

Received: June 9, 2005
Revised: October 30, 2005
Published online: December 9, 2005

Keywords: gated channels · ion transport · molybdenum · polyoxometalates · porous capsules

[1] a) B. Alberts, A. Johnson, J. Lewis, M. Raff, K. Roberts, P. Walter, *Molecular Biology of The Cell*, 4th ed., Garland Science, New York, **2002**; b) R. MacKinnon, *Angew. Chem.* **2004**, *116*, 4363–4376; *Angew. Chem. Int. Ed.* **2004**, *43*, 4265–4277, and references therein; c) G. Adam, P. Läuger, G. Stark, *Physikalische Chemie und Biophysik*, 4th ed., Springer, Berlin, **2003**, p. 202; d) G. Karp, *Cell and Molecular Biology: Concepts and Experiments*, 4th ed., Wiley, New York, **2005**; e) G. Yellen, *Nature* **2002**, *419*, 35–42.

[2] a) L. Cronin in *Comprehensive Coordination Chemistry II: From Biology to Nanotechnology, Vol. 7* (Eds.: J. A. McCleverty, T. J. Meyer), Elsevier, Amsterdam, **2004**, pp. 1–56; b) A. Müller, S. Roy in *The Chemistry of Nanomaterials: Synthesis, Properties and Applications* (Eds.: C. N. R. Rao, A. Müller, A. K. Cheetham), Wiley-VCH, Weinheim, **2004**, pp. 452–475; c) A. Müller, P. Kögerler, C. Kuhlmann, *Chem. Commun.* **1999**, 1347–1358; d) A. Müller, S. Roy, *Coord. Chem. Rev.* **2003**, *245*, 153–166; e) A. Müller, S. K. Das, E. Krickemeyer, C. Kuhlmann, *Inorg. Synth.* **2004**, *34*, 191–200 (Ed.: J. R. Shapley); f) L. Cronin, E. Diemann, A. Müller in *Inorganic Experiments*, 2nd ed. (Ed.: J. D. Woollins), Wiley-VCH, Weinheim, **2003**, pp. 340–346 (see also: A. Müller, E. Krickemeyer, H. Bögge, M. Schmidtmann, F. Peters, *Angew. Chem.* **1998**, *110*, 3567–3571; *Angew. Chem. Int. Ed.* **1998**, *37*, 3359–3363).

[3] a) A. Müller, E. Krickemeyer, H. Bögge, M. Schmidtmann, B. Botar, M. O. Talismanova, *Angew. Chem.* **2003**, *115*, 2131–2136; *Angew. Chem. Int. Ed.* **2003**, *42*, 2085–2090 (to obtain compound **1**, heating is not necessary as acidification of the solution at room temperature leads to an easy release of the acetic acid formed and concomitant introduction of/replacement by SO_4^{2-} ions); b) W. G. Klemperer, G. Westwood, *Nat. Mater.* **2003**, *2*, 780–781 *(News & Views)*; c) A. Müller, S. K. Das, S. Talismanov,

 © 2006 Wiley-VCH Verlag GmbH & Co. KGaA, Weinheim

S. Roy, E. Beckmann, H. Bögge, M. Schmidtmann, A. Merca, A. Berkle, L. Allouche, Y. Zhou, L. Zhang, *Angew. Chem.* **2003**, *115*, 5193 – 5198; *Angew. Chem. Int. Ed.* **2003**, *42*, 5039 – 5044; d) In ref. [3c] the option of trapping on the sphere surface was mentioned, but without referring to a synthesis of a compound and its formula and structure; furthermore, the system mentioned does not allow encapsulation of metal cations, it does not occur because of the low charge of the capsule.

[4] A. Müller, H. Bögge, M. Henry, *C. R. Chim.* **2005**, *8*, 47 – 56.

[5] The charge of 72− given for **1a** does not consider the encapsulated NH_4^+ ions, the number and position of which cannot be determined by single-crystal X-ray studies because the ions occur at the same positions as the encapsulated H_2O molecules. The exchange of NH_4^+ with the added Pr^{3+} ions does not influence the conclusion of "gating" as the influence of increasing Pr^{3+} concentration on the primary uptake and subsequent trapping could be demonstrated unequivocally by different experiments; the general behavior of NH_4^+ ions upon cation uptake is discussed in the text.

[6] The chemical formula of **2** refers to the maximum possible number of water molecules and is calculated from the cell volume and that of all cell components, not considering the crystal water molecules. The given calculated values for Cl, N, Pr are related to a formula with 25 crystal water molecules less than given (note: **2**, as found for all similar compounds, shows slow weathering and loses water of crystallization). Furthermore, the number of encapsulated NH_4^+/H_2O units is not referred to in the formula, as it is not possible to distinguish between these by X-ray crystallography. The presence of the disordered small ion lattice components (see formula of **2**) is typical for these types of spherical clusters containing large voids. They occur especially in the present case as a result of the high concentration condition of the synthesis. In the case of **1** the additional lattice components (the NH_4^+ and CH_3OO^- ions) could be determined in detail with NMR spectroscopy (F. Taulelle, L. Allouche, A. Senouci, M. Henry, A. Müller, unpublished results).

[7] Crystal data for **2**: $H_{814}Cl_{12}Mo_{132}N_{30}O_{839}Pr_{18}S_{30}$, $M_r = 31252.47\ g\,mol^{-1}$, rhombohedral, space group $R\bar{3}c$, $a = 50.3036(11)$, $c = 61.3381(18)$ Å, $V = 134418(6)$ Å^3, $Z = 6$, $\rho = 2.316\ g\,cm^{-3}$, $\mu = 2.958\ mm^{-1}$, $F(000) = 90156$, crystal size $= 0.40 \times 0.30 \times 0.25\ mm^3$. Crystals of **2** were removed from the mother liquor and immediately cooled to 183(2) K on a Bruker AXS SMART diffractometer (three circle goniometer with 1 K CCD detector, $Mo_{K\alpha}$ radiation, graphite monochromator; hemisphere data collection in ω at 0.3° scan width in three runs with 606, 435, and 230 frames ($\varphi = 0$, 88, and 180°) at a detector distance of 5.00 cm). A total of 265004 reflections ($1.62° < \Theta < 26.99°$) were collected of which 32585 reflections were unique ($R_{int} = 0.0416$). An empirical absorption correction using equivalent reflections was performed with the program SADABS. The structure was solved with the program SHELXS-97 and refined using SHELXL-97 to $R = 0.0625$ for 24263 reflections with $I > 2\sigma(I)$, $R = 0.0939$ for all reflections; max./min. residual electron density 2.440 and $-2.380\ e\,Å^{-3}$ (SHELXS/L, SADABS from G. M. Sheldrick, University of Göttingen, **1997**/**2003**; structure graphics with DIAMOND 2.1/3.0 from K. Brandenburg, Crystal Impact GbR, 2001/2004). Further details on the crystal structure investigations may be obtained from the Fachinformationszentrum Karlsruhe, 76344 Eggenstein-Leopoldshafen, Germany (fax: (+49) 7247-808-666; e-mail: crysdata@fiz-karlsruhe.de), on quoting the depository number CSD-415386.

[8] a) F. A. Hart in *Comprehensive Coordination Chemistry, Vol. 3* (Ed.: G. Wilkinson), Pergamon, Oxford, **1987**, pp. 1091 – 1099; b) This is comparable to the situation within the capsule cavity containing $H_2PO_2^-$ ligands;[3a] see also: M. Henry, H. Bögge, E. Diemann, A. Müller, *J. Mol. Liq.* **2005**, *118*, 155 – 162.

[9] Important in the context of pore/channel gating is that under more dilute concentrations **1a** "attracts" only a smaller number of Pr^{3+} ions, which does not lead to the corresponding pore closing discussed herein. One related example refers to the compound with the stoichiometry $(NH_4)_{25}(NH_2CHNH_2)_6Pr_3[\{(NH_2CHNH_2)_{20} + (Pr)_4\} \subset \{(Mo^{VI})Mo^{VI}{}_5O_{21}(H_2O)_6\}_{12}\{Mo^{V}{}_2O_4(SO_4)\}_{30}] \cdot \approx 280\,H_2O$ (**3**). For the capsule anion **3a**, three encapsulated Pr^{3+} ions are found disordered over the same thirty equivalent positions found in **2a**; see: A. Müller, Y. Zhou, L. Zhang, H. Bögge, M. Schmidtmann, M. Dressel, J. van Slageren, *Chem. Commun.* **2004**, 2038 – 2039.

[10] a) D. T. Richens, *The Chemistry of Aqua Ions*, Wiley, Chichester, **1997**; b) F. A. Cotton, G. Wilkinson, C. A. Murillo, M. Bochmann, *Advanced Inorganic Chemistry*, 6th ed., Wiley, New York, **1999**, p. 1111; c) F. A. Hart in *Comprehensive Coordination Chemistry, Vol. 3* (Ed.: G. Wilkinson), Pergamon, Oxford, **1987**, p. 1074; d) H. C. Aspinall, *Chemistry of the f-Block Elements*, Gordon and Breach, Amsterdam, **2001**; e) A. Martell, R. D. Hancock, *Metal Complexes in Aqueous Solutions*, Plenum, New York, **1999**.

[11] The following formulation described in biophysical and biochemical text books (e.g. ref. [1a]) is representative for biological ion membrane processes; we can only give a simplified illustrative view of the present ion transport as it is based on a relatively small inorganic capsule system compared to the biological case: A solute tends to move from a region of high to a region of low concentration which finally results in an equilibrium. Consequently, movement down a concentration gradient is accompanied by a favorable free-energy change ($\Delta G < 0$). The free-energy change per mole of solute moved across a membrane (ΔG_{conc}), is equal to $-RT\ln C_o/C_i$ (C_o and C_i are the outside and inside concentrations of the ion, respectively). If the solute is an ion, moving it into a cell across a membrane whose inside is at a voltage V relative to the outside will cause an additional free-energy change (per mole of solute moved) of $\Delta G_{volt} = zFV$. Just where the concentration and voltage gradients are equal, $\Delta G_{conc} + \Delta G_{volt} = 0$, the ion distribution across the membrane is at equilibrium.[12] (In the present case, this is formally the situation after the five Pr^{3+} have been taken up.) In other words, the equilibrium corresponds to the situation where the electrochemical potential, that is, the chemical potential of the ion in the presence of an electrical potential (corresponding additional term zFV to which all encapsulated ions contribute) inside and outside is equal (see especially: P. Atkins, J. de Paula, *Atkins' Physical Chemistry*, 7th ed., Oxford University Press, Oxford, **2002**, p. 1023). In the present type of experiment the chemical potential of the encapsulated Pr^{3+} ions depends strongly on their interactions with the sulfate receptors.

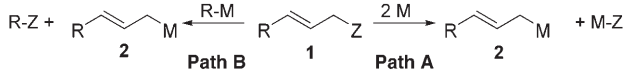
[12] In biological cells a part of the "channel protein" blocks the passive ion channel owing to a minor conformational change as an effect of decreased electrochemical gradient.[1]

[13] a) A. Malecki, A. Bielanski, Cracow, unpublished results; b) The gradient selected ^{15}N-HSQC spectrum was measured with the sensitivity enhanced version of the pulse sequence on a Bruker AVANCE 400 spectrometer, adjusted to a ^1H–^{15}N coupling constant of 75 Hz. The measurement time was 36 min with 8 scans and 128 increments of a saturated solution of the ^{15}N-enriched compound **1** in DMSO (for the method see: L. E. Kay, P. Keifer, T. Saarinen, *J. Am. Chem. Soc.* **1992**, *114*, 10663 – 10665). To study the influence of cation uptake approximately 30 mg $CaBr_2$ were added to 0.7 mL saturated solution of **1**; c) The ^{15}N-NMR spectrum was measured in DMSO and not in water to avoid increased H exchange, which would complicate the results; d) The correct number of encapsulated NH_4^+ ions will be determined with a higher field instrument in the near future.

 © 2006 Wiley-VCH Verlag GmbH & Co. KGaA, Weinheim

[14] a) A. Müller, D. Rehder, E. T. K. Haupt, A. Merca, H. Bögge, M. Schmidtmann, G. Heinze-Brückner, *Angew. Chem.* **2004**, *116*, 4566 – 4570; *Angew. Chem. Int. Ed.* **2004**, *43*, 4466 – 4470; Corrigendum: A. Müller, D. Rehder, E. T. K. Haupt, A. Merca, H. Bögge, M. Schmidtmann, G. Heinze-Brückner, *Angew. Chem.* **2004**, *116*, 5225; *Angew. Chem. Int. Ed.* **2004**, *43*, 5115; b) E. T. K. Haupt, C. Wontorra, D. Rehder, A. Müller, *Chem. Commun.* **2005**, 3912 – 3914.
[15] L. Zheng, D. Kostrewa, S. Bernèche, F. K. Winkler, X.-D. Li, *Proc. Natl. Acad. Sci. USA* **2004**, *101*, 17090 – 17095.
[16] J. Heitman, P. Agre, *Nat. Genet.* **2000**, *26*, 258 – 259.
[17] D. J. Cram, J. M. Cram, *Container Molecules and Their Guests*, Royal Society of Chemistry, Cambridge, **1994**.
[18] M. Gross, "Encapsulating Chemistry", *Chem. Br.* **2003**, *39*(August Issue), 18.
[19] a) J. Rebek, *Chem. World* **2005**, *2*(July Issue), 28; b) A. Khlobystov, D. Britz, *Chem. World* **2005**, *2*(July Issue), 29.
[20] Note added in proof, November 23, 2005: In the case of the interaction of a solution of **1a** with increasing concentrations of Ca^{2+}, practically continuous increasing cation uptake (with subsequent gating) occurs, which is easily demonstrated by the "blue shift" of the lowest wavenumber band of the three $\nu_{as}(SO_4)$ signals measured in the IR spectrum of the resulting precipitate.

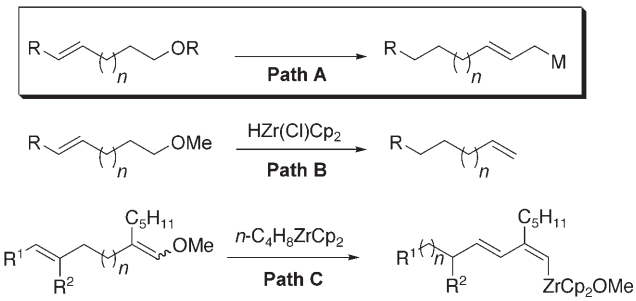
 © 2006 Wiley-VCH Verlag GmbH & Co. KGaA, Weinheim



Scheme 1.

which undergoes an oxidative insertion into the C–Z bond. However, cross-contamination of the product with the Wurtz coupling adduct always occurs (the longer the alkyl chain R in **1**, the more abundant the Wurtz coupling product). Alternatively, the source of the metal can be an organometallic derivative or a metallic salt (Scheme 1, Path B).[5d] However, all of these methods required a presynthesized allyl substrate **1** that has to be prepared independently in as few steps as possible.

Alternatively, allylic organometallic derivatives can also be prepared by carbo- and hydrometallation of allenes and dienes.[6] As one of the major challenges in synthesis nowadays is to assemble target molecules—here, namely, allylic organometallic derivatives—from readily available starting materials in a one-step procedure and in a simple and straightforward manner, we have recently been working on a totally different approach based on a four-component reaction with concomitant creation of chiral quaternary centers.[7] However, the most ideal solution would be to prepare allylic organometallic derivatives of type **2** from unsaturated fatty alcohol derivatives, which are naturally present in large quantities from fatty acids, through a hypothetical successive tandem isomerization–elimination reaction of the internal double bond (Scheme 2, Path A). In this regard, hydrometallation reactions (such as hydroalumination, hydroboration, and hydrozirconation) followed by an isomerization of internal olefins is a known way of rendering unactivated methyl hydrogen atoms accessible to substitution.[8] Moreover, hydrozirconation of internal aliphatic olefins with terminal oxygen-, sulfur-, or nitrogen-containing functionalities has already been investigated and leads to an elimination reaction of the functional group after rearrangement of the zirconium moiety towards the carbon atom that bears the heteroatoms (Scheme 2, Path B).[9] On the other hand, if one equivalent of 1,2-dicarbanionic species[10] would be available and react in this process with the same unsaturated system, the final product should contain an organometallic derivative and therefore Path A would be a realistic route.



Scheme 2.

Organometallic Chemistry

DOI: 10.1002/anie.200501946

Unsaturated Fatty Alcohol Derivatives as a Source of Substituted Allylzirconocene**

*Nicka Chinkov, Anat Levin, and Ilan Marek**

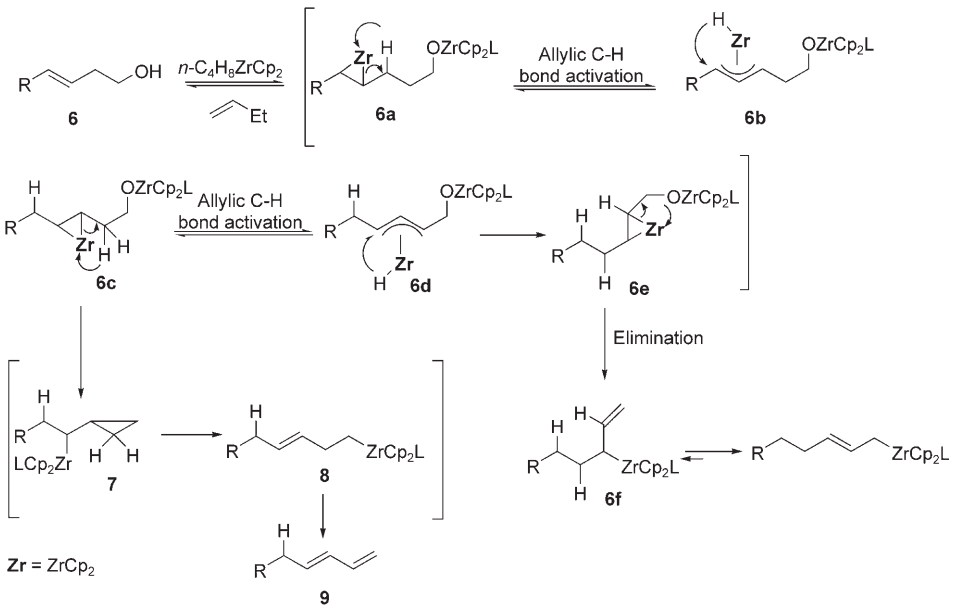
The development and use of allylic organometallic reagents has been an underlying theme of modern organic synthesis.[1] A plethora of methods currently exists for the preparation of diversely substituted allylic organometallic moieties **2** by the displacement of pre-prepared allyl reagents **1** (Scheme 1). The Z group can be a halogen (Cl, Br, I),[1e] chalcogen (O, S, Se, Te),[2] metalloid (Pb, Sn),[3] or hydrogen,[2a,4] but also carbon (in particular tertiary carbinol).[5a–c] The source of the metal can be the element (M) itself (Scheme 1, Path A),

[*] Dr. N. Chinkov, A. Levin, Prof. I. Marek
The Mallat Family Laboratory of Organic Chemistry
Department of Chemistry
Institute of Catalysis Science and Technology
The Lise Meitner-Minerva Center for Computational Quantum Chemistry
Technion-Israel Institute of Technology
Technion City 32000 Haifa (Israel)
Fax: (+972) 4-829-3709
E-mail: chilanm@tx.technion.ac.il

[**] This research was supported by the Israel Science Foundation, administrated by the Israel Academy of Sciences and Humanities (459/04), and by the Fund for the Promotion of Research at the Technion. I.M. is holder of the Sir Michael and Lady Sobell Academic Chair.

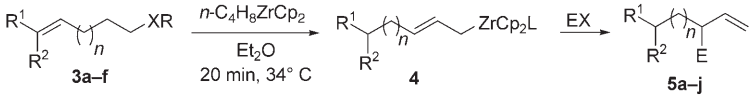
 © 2006 Wiley-VCH Verlag GmbH & Co. KGaA, Weinheim

We previously reported that simple nonconjugated unsaturated enol ethers react smoothly with (1-butene)$ZrCp_2$ (Negishi reagent; Cp = cyclopentadienyl)[10] to lead to polysubstituted dienyl zirconocene derivatives as single geometrical isomers (Scheme 2, Path C).[11] This approach to stereoisomerically pure dienyl metals was based on a tandem allylic C–H bond-activation–elimination sequence, and the mechanism has since been mapped out by deuterium-labeling experiments.[12] Thus, we reasoned that internal aliphatic olefins of type **3**, which bear a leaving group at the terminal position, should undergo a tandem isomerization–elimination reaction with the Negishi reagent in a one-pot operation to give the corresponding substituted allylzirconocene derivatives **4**, which may further react with classical electrophiles (Table 1).



Scheme 3.

Table 1: Preparation of allylzirconocene derivatives from unsaturated fatty alcohol derivatives.



3a–f **4** **5a–j**

Entry	R^1	R^2	*n*	XR	Alkene **3**	EX	Product	Yield [%][a]
1	H	C_5H_{11}	0	OCH_3	**3a**	HCl	**5a**	80
2	H	C_5H_{11}	0	Cl	**3b**	HCl	**5a**	20
3	H	C_5H_{11}	0	OH	**3c**	HCl	**5a**	80
4	C_5H_{11}	H	0	OCH_3	(*E*)-**3a**	HCl	**5a**	60
5	C_5H_{11}	H	0	OCH_3	(*E*)-**3a**	NCS	**5b**	66
6	H	C_5H_{11}	0	OH	**3c**	NCS	**5b**	65
7	H	C_5H_{11}	0	OH	**3c**	PhCHO[b]	**5c**	65
8	H	C_5H_{11}	1	OH	**3d**	NCS	**5d**	65
9	H	C_5H_{11}	1	OH	**3d**	PhCHO[b]	**5e**	73
10	C_4H_9	H	2	OH	**3e**	NCS	**5d**	65
11	C_4H_9	H	2	OH	**3e**	PhCHO[b]	**5e**	73
12	H	C_8H_{17}	6	OH	**3f**	HCl	**5f**	72
13	H	C_8H_{17}	6	OH	**3f**	NCS	**5g**	65
14	H	C_8H_{17}	6	OH	**3f**	PhCHO[b]	**5h**	76

[a] Isolated yield after purification by column chromatography (silica gel) and based on the starting materials **3a–f**. [b] *Anti*/*syn* ratio = 82:18 to 88:12.

We were pleased to observe that this reaction proceeds, but the yield of this transformation was highly dependent on the nature of the leaving group XR. When a good leaving group was used, such as a chlorine atom (Table 1, entry 2), the yield of the terminal alkene **5a**, after hydrolysis, was very low (diene **9** formed as the major product; see Scheme 3). However, alkoxy functions such as the methoxy group (Table 1, entry 1) led to the corresponding allylzirconocene derivatives in good isolated yields after hydrolysis. As alcohol moieties are the logical precursors for the alkoxy groups and as many derivatives of unsaturated fatty acids that contain a terminal hydroxy functionality are commercially available, we decided to concentrate our effort on the most challenging isomerization–elimination reactions of ω-alkenols **3c–f**. In these cases, either two equivalents of the Negishi derivatives were used (the deprotonation of the alcohol precedes the isomerization) or the alkenols were first deprotonated by the addition of one equivalent of *n*BuLi or Et_2Zn. Although the exact nature of the ligand L on the zirconium after the tandem deprotonation–isomerization reaction of the alkenols **3c–f** with (1-butene)$ZrCp_2$ is still unclear, we believe that oligomeric zirconium alcoholates are formed.[13] In all cases the reaction was rapid: only 20 minutes treatment at 34 °C in Et_2O was enough to transform non-allylic alkenol into allylzirconocene derivatives. The stereochemistry of the initial double bond had no effect on the isomerization–elimination processes as *Z*- or *E*-configured double bonds could be used indifferently (compare entries 1 and 5, Table 1). The formation of the new allylic organometallic products **4** was checked by reactions with *N*-chlorosuccinimide or benzaldehyde.[2h] In the latter cases, *anti*-homoallylic alcohols formed predominantly and the diastereoselectivity (*anti*/*syn* = 82:18 to 88:12) closely parallels the isomeric composition of these substituted allylzirconocenes reagents, as determined by low-temperature NMR spectroscopic studies,[14] which suggests that the reaction proceeds through a six-membered chair transition state.

This isomerization–elimination reaction was not limited to (3*Z*)-nonenol (**3c**) with a two-carbon-atom tether. Indeed,

 © 2006 Wiley-VCH Verlag GmbH & Co. KGaA, Weinheim

3d–f (with three-, four-, and eight-carbon-atom tethers, respectively) also underwent this tandem reaction (Table 1, entries 8–14) in 20 minutes at 34 °C. This migration–elimination reaction can be rationalized by the following mechanism on a three-carbon-atom tether (Scheme 3): (1-Butene)$ZrCp_2$ reacts first with the remote double bond of **6** to form a zirconacyclopropane derivative **6a**. Then, through allylic C–H bond activation,[12] the η^3-allyl intermediate **6b** is formed, and after hydrogen migration the zirconacyclopropane **6c** is produced. By repeating the same sequence, the zirconacyclopropane **6e** is finally obtained before its β elimination[15] into the allylzirconocene intermediate **6f**. When a good leaving group is used as in **3b** (Table 1, entry 2), the major side product thus obtained may be rationalized by the zirconium-mediated conversion of homoallylic species into cyclopropane derivatives, as shown by Szymoniak and co-workers,[16] followed by dehydrozirconation into diene **9**.[9] Therefore, when the zirconium alcoholate is used as leaving group, the allylic C–H bond activation of **6c** into **6d** is faster than the 1,3-elimination reaction (**6c** into **7**).

In conclusion, (1-butene)$ZrCp_2$ easily transforms (20 minutes at 34 °C) unsaturated fatty alcohol derivatives into allylzirconocene complexes through a tandem allylic C–H activation–β-elimination reaction. The reaction seems to be independent of the chain length between the unsaturated system and the alcohol moiety. Extension of this new preparative route to more elaborated structures is currently under investigation.

Experimental Section

A solution of *n*-butyllithium in hexanes (4.8 equiv) was added dropwise to a stirred solution of bis(cyclopentadienyl)zirconium dichloride (2.4 equiv) in dry Et_2O (15 mL) at −78 °C under argon atmosphere. The temperature of the solution was allowed to reach −5 °C and was then maintained for 5–6 min. The reaction mixture was then cooled to −50 °C, and the alkenol **3c** (1 equiv) in Et_2O (5 mL) was added dropwise to the solution, keeping the temperature at −50 °C. When the addition was complete, the cooling bath was removed and the reaction mixture was rapidly warmed to room temperature. The solution was then heated and maintained at 34 °C for 20 min to form the allylzirconocene intermediate (monitored by GC of hydrolyzed aliquots), which is ready for further use[17] or, alternatively, can be hydrolyzed with 1N HCl after cooling the solution to room temperature. After hydrolysis, the layers were separated and the aqueous phase was extracted four times with diethyl ether. The combined organic extracts were washed successively with a saturated solution of sodium bicarbonate, brine, and then dried over $MgSO_4$. The obtained residue was finally purified by column chromatography on silica gel to give the functionalized alkenes as reported in Table 1.

Received: June 6, 2005
Revised: August 20, 2005
Published online: December 12, 2005

Keywords: alcohols · allylic compounds · C–H activation · elimination · zirconium

[1] For recent reviews of allylmetal addition, see a) S. R. Chemler, W. R. Roush in *Modern Carbonyl Chemistry* (Ed.: J. Otera), Wiley-VCH, Weinheim, **2000**, chap. 10; b) S. E. Denmark, N. G. Almstead in *Modern Carbonyl Chemistry* (Ed.: J. Otera), Wiley-VCH, Weinheim, **2000**, chap. 11; c) *Stereoselective Synthesis, Methods of Organic Chemistry*, Houben-Weyl, *E21, Vol. 3* (Eds.: G. Helmchen, R. Hoffmann, J. Mulzer, E. Schaumann), Thieme, Stuttgart **1996**; d) W. R. Roush *in Comprehensive Organic Synthesis, Vol. 2* (Eds. B. M. Trost, I. Fleming, C. H. Heathcock), Pergamon, Oxford, **1991**, p. 1; e) Y. Yamamoto, N. Asao, *Chem. Rev.* **1993**, *93*, 2207.

[2] a) M. Schlosser in *Organometallics in Synthesis: A Manual*, 2nd ed., Wiley, Chichester, **2002**, p. 1; b) J. J. Eisch, *Pure Appl. Chem.* **1984**, *56*, 35; c) T. Cohen, M. Bhupathy, *Acc. Chem. Res.* **1980**, *13*, 6900; d) D. Cheng, S. Zhu, X. Liu, S. H. Norton, T. Cohen, *J. Am. Chem. Soc.* **1999**, *121*, 10241; e) K. Deng, J. Chalker, A. Yang, T. Cohen, *Org. Lett.* **2005**, *7*, 3637; f) M. Clarembeau, A. Krief, *Tetrahedron Lett.* **1984**, *25*, 3629; g) A. Osuka, H. Suzuki, *Tetrahedron Lett.* **1983**, *24*, 5109; h) Y. Hanzawa, H. Ito, T. Taguchi *Synlett* **1995**, 299.

[3] a) D. Seyferth, T. F. Jula, *J. Organomet. Chem.* **1974**, *66*, 195; b) D. Seyferth, G. J. Murphy, B. Mauze, *J. Am. Chem. Soc.* **1977**, *99*, 5317; c) O. Desponds, M. Schlosser, *J. Organomet. Chem.* **1991**, *409*, 93.

[4] O. Desponds, L. Franzini, M. Schlosser, *Synthesis* **1997**, 150, and references therein.

[5] a) P. Jones, N. Millot, P. Knochel, *Chem. Commun.* **1998**, 2405; b) P. Jones, P. Knochel, *Chem. Commun.* **1998**, 2407; c) P. Jones, P. Knochel, *J. Org. Chem.* **1999**, *64*, 186; d) K. Fujita, H. Yorimitsu, H. Shinokubo, K. Oshima, *J. Am. Chem. Soc.* **2004**, *126*, 6776, and references therein.

[6] a) S. Yamanoi, T. Imai, T. Matsumoto, K. Suzuki, *Tetrahedron Lett.* **1997**, *38*, 3031; b) "Carbometallation Reactions": I. Marek in *Metal-Catalyzed Cross-Coupling Reactions*, 2nd ed. (Eds.: A. de Meijere, F. Diederich), Wiley-VCH, **2004**, p. 395; c) "Synthesis and Reactivity of Allyltitanium Derivatives": J. Szymoniak, C. Moise in *Titanium and Zirconium in Organic Synthesis* (Ed.: I. Marek), Wiley-VCH, Weinheim, **2002**, p. 451.

[7] a) G. Sklute, D. Amsallem, A. Shibli, J. P. Varghese, I. Marek, *J. Am. Chem. Soc.* **2003**, *125*, 11776; b) I. Marek, *Tetrahedron* **2002**, *58*, 9463; c) S. Achyutha Rao, M. J. Rozema, P. Knochel, *J. Org. Chem.* **1993**, *58*, 2694; d) A. N. Kasatkin, R. J. Whitby, *Tetrahedron Lett.* **2000**, *41*, 6211.

[8] a) J. J. Eisch in *Comprehensive Organic Synthesis* (Eds.: B. M. Trost, I. Fleming), Pergamon, Oxford **1991**, p. 8, 11; b) H. C. Brown, U. S. Racherla, *J. Organomet. Chem.* **1983**, *241*, C37; c) L. O. Bromm, H. Laaziri, F. Lhermitte, K. Harms, P. Knochel, *J. Am. Chem. Soc.* **2000**, *122*, 10218; d) J. Schwartz, J. A. Labinger, *Angew. Chem.* **1976**, *88*, 402; *Angew. Chem. Int. Ed. Engl.* **1976**, *15*, 333.

[9] a) U. Annby, S. Karlsson, S. Gronowitz, A. Hallberg, J. Alvhall, R. Svenson, *Acta Chem. Scand.* **1993**, *47*, 425; b) S. Karlsson, A. Hallberg, S. Gronowitz, *Chem. Scr.* **1988**, *27*, 185. If an excess of the Schwartz reagent is used, the in situ formed terminal alkene undergoes a further hydrozirconation reaction to give the alkylzirconocene derivative.

[10] a) E. Negishi, T. Takahashi, *Bull. Chem. Soc. Jpn.* **1998**, *71*, 755; b) E. Negishi, T. Takahashi, *Acc. Chem. Res.* **1994**, *27*, 124; c) "Synthesis and Reactivity of Zirconocene Derivatives": E. Negishi, S. Huo in *Titanium and Zirconium in Organic Synthesis* (Ed.: I. Marek), Wiley-VCH, Weinheim, **2002**, p. 1.

[11] N. Chinkov, S. Majumdar, I. Marek, *J. Am. Chem. Soc.* **2002**, *124*, 10282.

[12] a) N. Chinkov, S. Majumdar, I. Marek, *J. Am. Chem. Soc.* **2003**, *125*, 13258; b) N. Chinkov, S. Majumdar, I. Marek, *Synthesis* **2004**, 2411; c) "Stereoselective Synthesis of Dienyl Zirconocene Complexes": N. Chinkov, I. Marek in *Topics on Organometallic Chemistry, Vol. 10* (Ed.: I. Marek), Springer, Berlin, **2004**, p. 133;

 © 2006 Wiley-VCH Verlag GmbH & Co. KGaA, Weinheim

d) K. Fujita, H. Yorimitsu, H. Shinokubo, K. Oshima, *J. Am. Chem. Soc.* **2004**, *126*, 6776.
[13] P. Bertus, V. Gandon, J. Szymoniak, *Chem. Commun.* **2000**, 171.
[14] a) Y. Yamamoto, K. Maruyama, *Tetrahedron Lett.* **1981**, *22*, 2895; b) K. Mishima, H. Yasuda, T. Asami, A. Nakamura, *Chem. Lett.* **1983**, 219.
[15] a) C. J. Rousset, D. R. Swanson, F. Lamaty, E. Negishi, *Tetrahedron Lett.* **1989**, *30*, 5105; b) H. Ito, T. Nakamura, T. Taguchi, Y. Hanzawa, *Tetrahedron* **1992**, *48*, 4507.
[16] V. Gandon, C. Laroche, J. Szymoniak, *Tetrahedron Lett.* **2003**, *44*, 4827.
[17] a) H. Ito, T. Taguchi, Y, Hanzawa, *Tetrahedron Lett.* **1992**, *33*, 1295; b) H. Ito, T. Taguchi, Y. Hanzawa, *Tetrahedron Lett.* **1992**, *33*, 7873; c) H. Ito, T. Taguchi, *Tetrahedron Lett.* **1997**, *38*, 5829.

 © 2006 Wiley-VCH Verlag GmbH & Co. KGaA, Weinheim

Synthetic Methods

DOI: 10.1002/anie.200502779

The Chemical Synthesis of Bioactive Glycosylphosphatidylinositols from *Trypanosoma cruzi* Containing an Unsaturated Fatty Acid in the Lipid**

*Dmitry V. Yashunsky, Vladimir S. Borodkin, Michael A. J. Ferguson, and Andrei V. Nikolaev**

Dedicated to Professor Nikolay K. Kochetkov on the occasion of his 90th birthday

Glycosylphosphatidylinositols (GPIs) are a class of natural glycosylphospholipids that anchor proteins and glycoproteins (through their C terminus) as well as phosphoglycans (through the reducing end of the chain) to the membrane of eukaryotic cells. Since the first full assignment of a GPI structure in 1988,[1] a number of GPI anchors have been characterized.[2] The function of the compounds, in addition to the clear one of linking the above biopolymers to membranes, has been extensively discussed.[2,3] There is also evidence that GPIs and/or their metabolites can act as secondary messengers, which modulate biological events including insulin production, insulin-mediated signal transduction, cellular proliferation, and cell–cell recognition. The discovered role as mediators of regulatory processes makes the chemical preparation of the compounds and their analogues of great interest. To date, a number of syntheses of GPIs (yeast,[4] rat brain Thy-1,[5] *Trypanosoma brucei*,[6] *Leishmania*,[7] *T. gondii*,[8] *Plasmodium falciparum*,[9] and *T. cruzi* 1G7 antigen[10]) have been reported.

The protozoan parasite *Trypanosoma cruzi* is a causative agent of Chagas' disease, which affects about 18 million individuals in South and Central America.[11] It is transmitted to mammals in the feces of a biting insect vector (hematophagous triatomine bug) and has four distinct developmental stages. Throughout the life cycle, *T. cruzi* produces both common and stage-specific GPI-anchored cell-surface macromolecules.[12–15] Local release of GPI-anchored mucins by the bloodstream trypomastigote stage of the parasite is believed to be responsible for the development of parasite-elicited inflammation, which causes cardiac and other pathologies associated with the acute and chronic phases of Chagas' disease.[15]

It has recently been discovered[13] that a purified GPI fraction of *T. cruzi* trypomastigote mucins (trypomastigote GPI, or tGPI) revealed extraordinary proinflammatory activities, comparable to those of bacterial lipopolysaccharide. An ability to trigger the induction of tumor necrosis factor-α, interleukin-12, and nitric oxide at the 2–30 pM level (when presented to macrophages) showed that tGPI is one of the most potent microbial proinflammatory agents known. The structure of the cytokine- and NO-inducing tGPI anchor has been defined,[13] and the extreme biological activity was allegedly associated with the presence of unsaturated fatty acids in the *sn*2 position of the alkylacylglycerophosphate moiety[*] (**1** and **2**, Scheme 1) and/or with D-galactose branches along the glycan core (nonstoichiometric, not shown). As the issues regarding the structural features responsible for the activity can only be resolved through synthesis, a multidisciplinary program has been launched in our laboratory aimed at the chemical preparation of various *T. cruzi* trypomastigote mucin GPIs (including those containing D-galactose branches) and the meticulous elucidation of their structure–activity relationships. Herein, we report the first chemical syntheses of tGPIs from *T. cruzi* bearing oleic (compound **1**) and linoleic (compound **2**) acid moieties.

There are two major structural features that make compounds **1** and **2** different from the GPIs synthesized previously:[4–10] 1) the presence of unsaturated fatty acids in the lipid moiety instead of saturated ones; and 2) the presence of 2-aminoethylphosphonate at the O6 position of the D-glucosamine moiety, which is a parasite-specific substituent

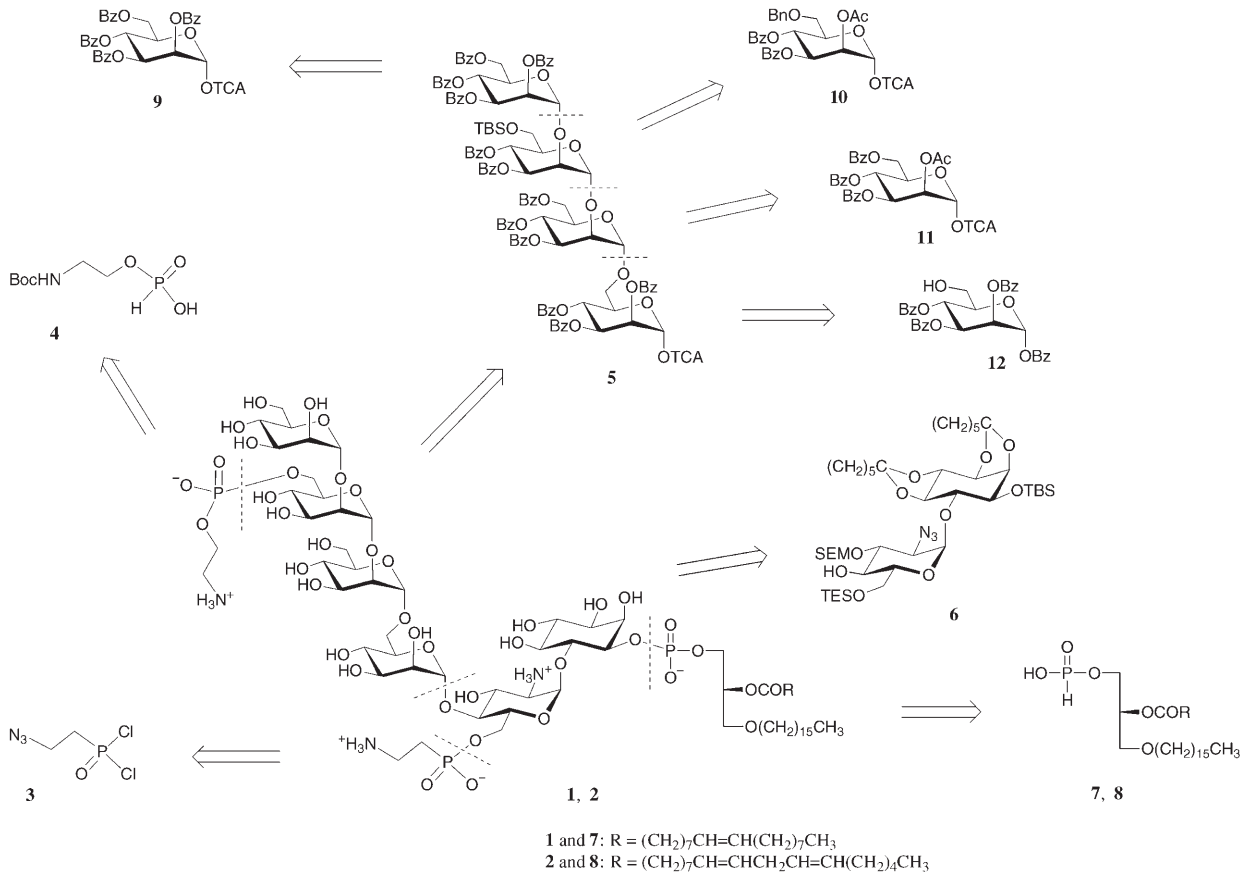
[*] Dr. D. V. Yashunsky, Dr. V. S. Borodkin, Dr. A. V. Nikolaev
Faculty of Life Sciences
Division of Biological Chemistry and Molecular Microbiology
University of Dundee
Carnelley Building, Dundee DD1 4HN (UK)
Fax: (+44) 1382-386373
E-mail: a.v.nikolaev@dundee.ac.uk
Prof. M. A. J. Ferguson
Faculty of Life Sciences
Division of Biological Chemistry and Molecular Microbiology
University of Dundee
Wellcome Trust Building, Dundee DD1 5EH (UK)

[**] This work, D.V.Y., and V.S.B. were supported by a Wellcome Trust Grant 067089/Z/02/Z. Prof. A. S. Shashkov (Moscow, Russia) is greatly acknowledged for NMR spectral characterization of the final compounds. We are grateful to Dr. A. Mehlert (Dundee) and Dr. V. Oleynikov (Moscow, Russia) for mass spectroscopic analyses and to Dr. A. J. Ross (Dundee) for the purification of compounds **1** and **2**.

Supporting information for this article is available on the WWW under http://www.angewandte.org or from the author.

[*] The content of fatty acid components in the biologically active tGPI anchor fraction was: oleic acid, C18:1, 31%; linoleic acid, C18:2, 21%; and palmitic acid, C16:0, 37%.[13]

InterScience
© 2006 Wiley-VCH Verlag GmbH & Co. KGaA, Weinheim



Scheme 1. Retrosynthetic scheme showing key building blocks and D-mannose monosaccharide intermediates. Boc = *tert*-butoxycarbonyl, Bz = benzoyl, SEM = 2-trimethylsilylethoxymethyl, TBS = *tert*-butyldimethylsilyl, TCA = C(NH)CCl_3, trichloroacetimidyl, TES = triethylsilyl.

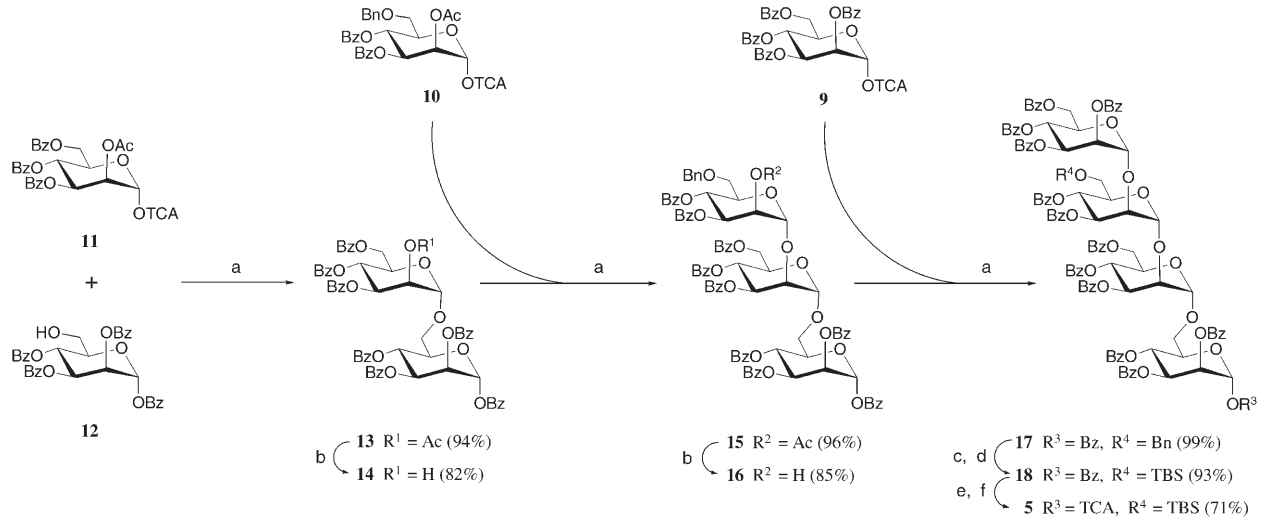
for *T. cruzi* only. As the presence of double bonds was not compatible with the use of benzyl ethers (widely used before[4–10]) as permanent O-protecting groups, a novel strategy was developed which implied exploration of benzoic esters and acid-labile (acetals and *N*-Boc) groups for O,N protection. Various silyl ethers were employed as orthogonal blocking groups for the O6 of D-glucosamine (TES), O6 of D-mannose-3 (primary TBS), and O1 of *myo*-inositol (secondary TBS) to ensure further introduction of the P-containing esters. For the final deprotection, we expected that mild basic treatment in polar solvent would preferentially cleave the benzoates and leave the fatty ester of the lipid mostly intact because of micelle formation.

By following the retrosynthetic disconnection shown in Scheme 1, the GPIs **1** and **2** were assembled from the mannotetraose building block **5**, the azidoglucose–inositol block **6**, and P-containing derivatives phosphonodichloridate **3** and the hydrogenphosphonates **4** and **7** (or **8**), which were used for consecutive introduction of the 2-aminoethylphosphonate, ethanolamine phosphate, and acylalkylglycerophosphate fragments, respectively.

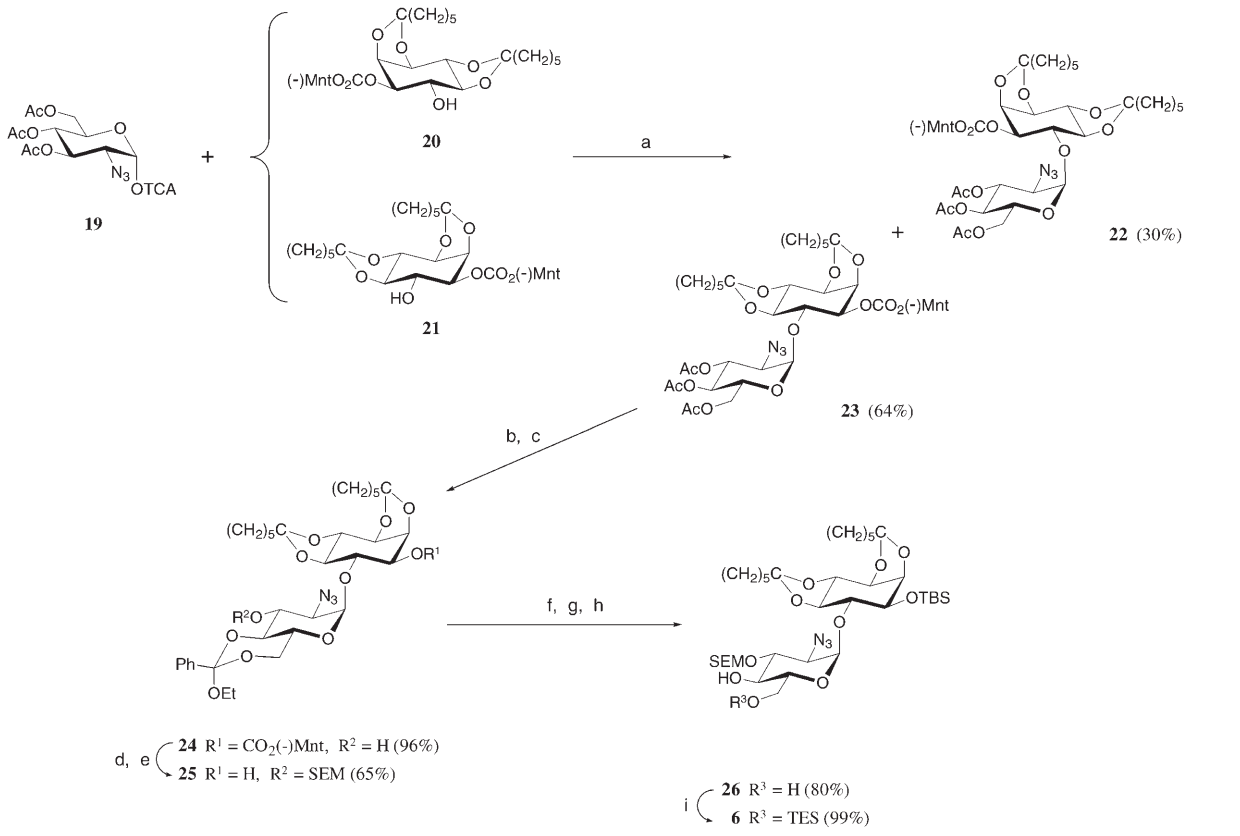
The tetrasaccharide block **5** was prepared from the monosaccharide derivatives **9**–**12**, which were assembled in a step-by-step manner (Scheme 2). Compounds **9** and **12**, in turn, were synthesized from D-mannose as well as the derivatives **10** and **11**, which progressed via the common intermediate 3,4,6-tri-*O*-acetyl-1,2-*O*-(1-methoxyethylidene)-β-D-mannose.[16] The disaccharide **13** (94%) was prepared first by coupling of the glycosyl acceptor **12** and the trichloroacetimidate **11** in the presence of trimethylsilyl triflate (TMSOTf). It was then deacetylated[17] with HCl in MeOH (→**14**) followed by reaction with glycosyl donor **10** and TMSOTf to produce the trisaccharide **15** (96%). Subsequent deacetylation (→**16**) and one more glycosylation with the trichloroacetimidate **9** and TMSOTf provided the tetrasaccharide **17** (99%). The α configuration of the newly created D-mannoside bonds was secured by the structure of mannosyl donors **9**–**11**, which contained participating protecting groups at the O2 position. Compound **17** was then converted to the mannotetraose glycosyl donor **5** (66% yield) by consecutive reprotection at the O6″ position (hydrogenation over Pd catalyst followed by silylation with TBSOTf/Et_3N; →**18**), anomeric debenzoylation with ethylenediamine, and reaction with CCl_3CN in the presence of Cs_2CO_3.

The azidoglucose–inositol block **6** was synthesized (Scheme 3) from the pseudo-disaccharide **23**, which was described by Schmidt and co-workers[4,18] as a glycosylation product of the optically pure D-*myo*-inositol derivative **21**[19] with the azidoglucose trichloroacetimidate **19**. We found that the resolution of diastereomeric (−)-menthyloxycarbonyl-

 © 2006 Wiley-VCH Verlag GmbH & Co. KGaA, Weinheim



Scheme 2. Reagents: a) $TMSOSO_2CF_3$, CH_2Cl_2; b) 2% HCl, $MeOH/CH_2Cl_2$; c) H_2, $Pd(OH)_2/C$, THF; d) $TBSOSO_2CF_3$, Et_3N, CH_2Cl_2; e) $NH_2CH_2CH_2NH_2{\cdot}HOAc$, THF; f) CCl_3CN, Cs_2CO_3, CH_2Cl_2. Bn = benzyl, THF = tetrahydrofuran, TMS = trimethylsilyl.



Scheme 3. Reagents: a) $TMSOSO_2CF_3$, MS4A, Et_2O/CH_2Cl_2; b) 0.02 M NaOMe, $MeOH/CH_2Cl_2$; c) $PhC(OEt)_3$, CSA, CH_2Cl_2; d) SEMCl, iPr_2NEt, CH_2Cl_2; e) 1 M NaOMe, $MeOH/CH_2Cl_2$; f) $TBSOSO_2CF_3$, Et_3N, CH_2Cl_2; g) CH_2Cl_2/CF_3COOH/water (1000:1:0.1); h) 0.1 M NaOMe, $MeOH/CH_2Cl_2$; i) TESCl, pyridine, CH_2Cl_2, −20 °C. CSA = camphor-10-sulfonic acid, Mnt = menthyl, MS4A = 4-Å molecular sieves.

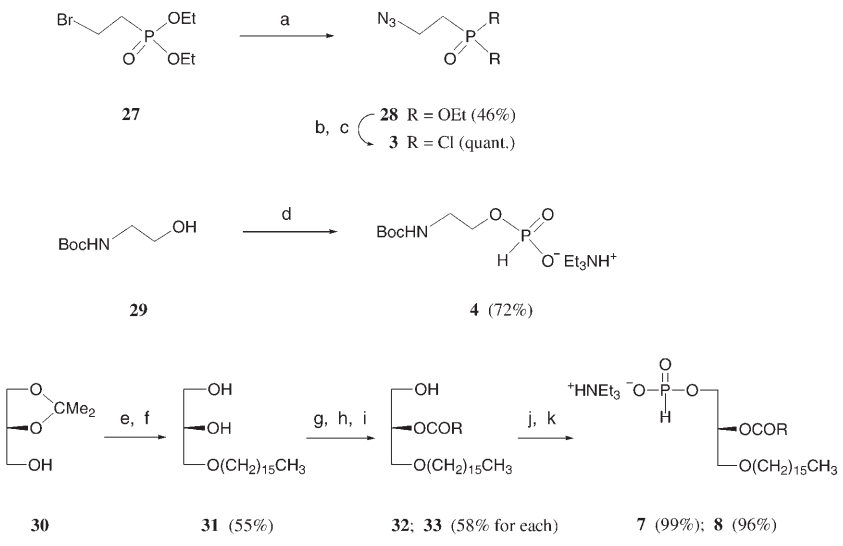
myo-inositols **21** (D product) and **20** (L product) could be avoided, but it was possible to perform glycosylation of the whole mixture and then isolate the required derivative **23** by standard flash column chromatography on SiO_2. Coupling of the mixture **21** + **20** (7:3, according to ^{1}H NMR data; prepared as described in reference [19]) with the glycosyl donor **19**[20] in the presence of TMSOTf and 4-Å molecular sieves proceeded smoothly and gave the easily separable (R_f difference of 0.1) diastereomers **23** and **22**, which were isolated in 64 and 30% yield, respectively (that is, 94% total yield of the glycosylation based on the mixture **21** + **20**). Both compounds had an α configuration of the D-glucoside bond,

 © 2006 Wiley-VCH Verlag GmbH & Co. KGaA, Weinheim

which was confirmed by the characteristic values (3.5 Hz for **23** and 3.6 Hz for **22**) for $J_{1',2'}$ coupling constants. Clearly, the 2-azido-2-glucose-α-D-glucosyl moiety worked as an additional powerful chiral auxiliary and facilitated the separation of D- and L-*myo*-inositol derivatives.

For the transformation **23**→**6**, first, the introduction of the acid-labile 2-trimethylsilylethoxymethyl (SEM) permanent protecting group at the O3′ position was needed. This was performed through the mild basic deacetylation of **23** followed by orthoesterification with $PhC(OEt)_3$ in mild acidic conditions (to form the 4′,6′-orthoester derivative **24**) and reaction with SEM chloride in the presence of *N*,*N*-diisopropylethylamine. Basic cleavage of the (−)-menthylcarbonate gave the 1-hydroxy derivative **25**, which was then successively silylated with TBSOTf/Et_3N, hydrolyzed with 0.1% trifluoroacetic acid (TFA)/water in CH_2Cl_2 (10 min) to open the orthoester (thus forming a mixture of 4′- and 6′-acetates), deacetylated (with MeONa in MeOH; →**26**), and silylated at the O6′ position with Et_3SiCl in pyridine/CH_2Cl_2. Thus, the azidoglucose–inositol block **6** was prepared from compound **23** in seven steps in approximately 50% overall yield.

The 2-azidoethylphosphonodichloridate **3** was prepared (Scheme 4) from diethyl 2-bromoethylphosphonate **27** through the azidation reaction with NaN_3 (→**28**) followed by de-esterification with Me_3SiBr and chlorination with oxalyl chloride in the presence of *N*,*N*-dimethylformamide. The 2-(*N*-Boc)-aminoethyl hydrogenphosphonate **4** was prepared by the reaction of *N*-Boc-ethanolamine **29** with H_3PO_3 in the presence of pivaloyl chloride.[21] The 2-*O*-acyl-1-*O*-hexadecyl-*sn*-glyceryl hydrogenphosphonates **7** and **8** were synthesized starting from commercially available 2,3-*O*-isopropylidene-*sn*-glycerol **30**, which was first alkylated with *n*-hexadecyl iodide in the presence of NaH followed by acid hydrolysis to produce 1-*O*-hexadecyl-*sn*-glycerol **31** (55%). This compound was then successively silylated at the 3-hydroxy group with Et_3SiCl in pyridine, esterified with oleoyl or linoleoyl chloride, and desilylated with 3HF·Et_3N, thus providing the 2-*O*-acylated glycerol derivatives **32** and **33**, respectively. Each of them was converted (almost quantitatively) to the corresponding hydrogenphosphonate derivative (**7** and **8**, respectively) by reaction with triimidazolylphosphine[22] followed by hydrolysis.



7 and **32** R = $(CH_2)_7CH{=}CH(CH_2)_7CH_3$
8 and **33** R = $(CH_2)_7CH{=}CHCH_2CH{=}CH(CH_2)_4CH_3$

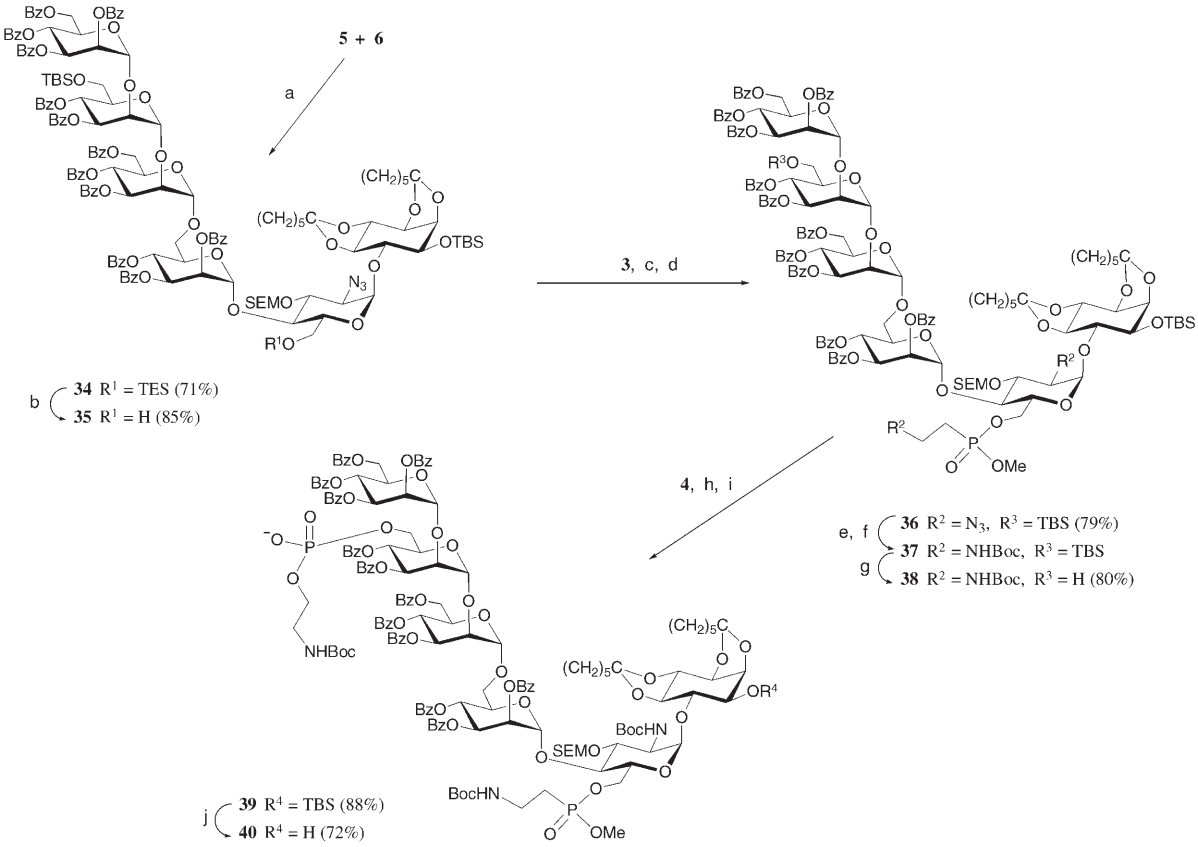
Scheme 4. Reagents: a) NaN_3, nBu_4NHSO_4 cat., toluene; b) TMSBr, MeCN; c) $(COCl)_2$, DMF cat., CH_2Cl_2; d) H_3PO_3, pivaloyl chloride, pyridine; e) $CH_3(CH_2)_{15}I$, NaH, DMF/THF; f) CF_3COOH/water (9:1); g) TESCl, pyridine, CH_2Cl_2; h) oleoyl chloride for **32** (or linoleoyl chloride for **33**), Et_3N, DMAP, pyridine; i) 3HF·Et_3N, MeCN/CH_2Cl_2; j) triimidazolylphosphine, MeCN/CH_2Cl_2; k) Et_3NHHCO_3, water (pH 7). DMAP = 4-dimethylaminopyridine, DMF = *N*,*N*-dimethylformamide.

With all the principal building blocks in hand, we pursued the preparation of the target GPIs **1** and **2**. First, the glycan–inositol backbone **34** was prepared (Scheme 5) by the glycosylation of the glycosyl acceptor **6** with the mannotetraose trichloroacetimidate **5** in the presence of TMSOTf and 4-Å molecular sieves. Subsequent cleavage of the TES group (the "weakest" of the three silyl protecting groups) with acetic acid-buffered tetrabutylammonium fluoride (TBAF) smoothly gave the 6′-hydroxy pseudo-hexasaccharide derivative **35** (60% from **5**), ready to turn to the "P-decoration" procedures. 1*H*-Tetrazole-assisted esterification of **35** with the phosphonodichloridate **3** followed by methanolysis afforded the phosphonic diester **36** (79%) as a diastereomeric mixture[*] ($\delta_P = 28.5, 28.8$). It was then a subject of successive reduction of the azido groups with Ph_3P, N protection with Boc anhydride (→**37**), and selective cleavage of the primary TBS ether with 3HF·Et_3N, thus cleanly producing the 6′′′′-hydroxy glycan–inositol–phosphonate compound **38** (80%). Furthermore, the introduction of the ethanolamine phosphate moiety was performed by the condensation of **38** with the hydrogenphosphonate derivative **4** (activated by pivaloyl chloride)[23] followed by in situ oxidation with iodine in aqueous pyridine. The phosphonate–phosphate block **39** was isolated in 88% yield prior to the final desilylation with TBAF/AcOH (at 55 °C), which gave the 1-hydroxy glycoconjugated derivative **40**.

We reported earlier[24] that the presence of phosphodiester units in a molecule still allows the next O-phosphorylation step to be performed effectively by the hydrogenphosphonate method (that is, P protection for phosphodiesters is not required). Indeed, compound **40** (containing a phosphodiester moiety at the O6′′′′ position) was successfully phospholipi-

[*] The P protection was required at this stage to avoid undesired modifications of the phosphonate moiety during further transformations. Each of the methyl phosphonate derivatives **36**–**42** was formed as a mixture of diastereomers at the phosphorus atom (in a ratio of 1:1), as clearly indicated by the ^{31}P NMR spectra (see Supporting Information).

 © 2006 Wiley-VCH Verlag GmbH & Co. KGaA, Weinheim



Scheme 5. Reagents: a) $TMSOSO_2CF_3$, MS4A, CH_2Cl_2; b) nBu_4NF, AcOH, THF (20 °C, 1.5 h); c) 1*H*-tetrazole, iPr_2NEt, toluene; d) MeOH; e) Ph_3P, water, THF; f) Boc_2O, Et_3N, MeOH; g) 3HF·Et_3N, MeCN/THF; h) pivaloyl chloride, pyridine; i) I_2, pyridine/water; j) nBu_4NF, AcOH, THF (55 °C, 60 h).

dated (Scheme 6) by a pivaloyl chloride assisted reaction with the acylalkylglyceryl hydrogenphosphonate **7**, followed by in situ oxidation with iodine to provide the fully protected oleic ester GPI **41** in 95% yield. Similarly, the protected linoleic ester GPI **42** (85%) was prepared from **40** and the hydrogenphosphonate **8**. Both compounds **41** and **42** were immediately demethylated at the aminoethylphosphonate moiety with $PhSH/Et_3N$[25] to form GPI derivatives **43** and **44**, respectively.

Global deprotection of **43** was performed in two steps. First, controlled O-debenzoylation with 0.05 M methanolic sodium methoxide (3 h) gave the partly protected GPI **45**, which was isolated in 40% yield by flash column chromatography on SiO_2. The presence of the fatty ester in the molecule was clearly indicated by MALDI-TOF mass spectrometry (MS) data.[26] Subsequent cleavage of *O*-acetal and *N*-Boc protecting groups with aqueous 90% TFA followed by purification by reversed-phase chromatography (on a C4 silica column with gradient elution with propan-1-ol/water/TFA, 10:90:0.05→95:5:0.05) provided the targeted oleic ester GPI **1**. The protected derivative **44** was converted to the linoleic ester GPI **2** in a similar manner.

The structures of the glycosylphospholipids **1** and **2** were supported by NMR spectroscopy and MS data. The ^1H, ^{13}C, and ^{31}P NMR spectra for **1** were almost identical to those for **2**. Full structural assignment of **2** was performed by a combination of ^1H and ^{13}C NMR, COSY, ROESY, TOCSY, and heteronuclear single-quantum correlation (HSQC) spectroscopy (see Table 1). The ^{31}P NMR signals were assigned with the $^1H,^{31}P$ heteronuclear multiple-quantum correlation (HMQC) technique. The molecular masses for the GPIs **1** and **2** were confirmed by MALDI-TOF and electrospray (ES) MS.[26]

The synthetic GPIs **1** and **2** revealed biological activity: preliminary experiments using Toll-like receptor (TLR) transfected Chinese hamster ovary (CHO) cell lines showed they stimulated TLR2-transfected cells and not TLR4-transfected cells,[27] like naturally occurring tGPI.[28] A detailed biological evaluation of the compounds is currently in progress and will be published elsewhere in due course.

In summary, a novel approach for the chemical synthesis of glycosylphosphatidylinositols, which exploits the use of non-benzyl-type protecting groups, was designed. The method showed its utility in the first syntheses of *T. cruzi* trypomastigote GPIs containing unsaturated fatty acids in the lipid moiety.

Received: August 5, 2005
Revised: October 3, 2005
Published online: December 8, 2005

 © 2006 Wiley-VCH Verlag GmbH & Co. KGaA, Weinheim

Table 1: Correlation table of **2**: ^{1}H, ^{13}C NMR and ^{31}P chemical shifts at 500, 125, and 202 MHz, respectively. Measurements in $[D_6]$DMSO at 30 °C; δ values [ppm] are given relative to Me_4Si (for ^{1}H and ^{13}C) and external aqueous 85 % H_3PO_4 (for ^{31}P).

Residue[a]	Atom							
	H1	H2	H3	H4	H5	H6		P
	C1	C2	C3	C4	C5	C6		
Ino[b]	4.03	3.81	3.48	3.46	3.16	3.75		−0.6
	75.7	70.45	73.65	72.65	73.1	78.5		
$GlcNH_2$[c]	5.48	2.96	3.82	3.49	4.27	4.07 + 3.94		18.7
	94.3	53.8	70.1	76.25	69.2	63.1		
Man-1	5.11	3.86	3.48	3.60	3.19	3.85 + 3.62		
	101.25	71.8	70.65	66.1	70.8	65.6		
Man-2	4.85	3.78	3.70	3.45	3.62	3.67 + 3.42		
	98.2	77.05	70.1	67.1	72.4	61.2		
Man-3[d]	5.08	3.88	3.61	3.39	3.37	4.10 + 3.75		−1.5
	100.9	77.05	69.9	67.1	70.6	65.4		
Man-4	4.86	3.80	3.75	3.71	3.30	3.68 + 3.49		
	101.85	71.8	69.9	66.6	71.8	60.9		

[a] Important inter-residue correlation peaks in the ROESY spectrum: H1 ($GlcNH_2$)/H6 (Ino); H1 ($GlcNH_2$)/H1,5 (Ino); H1 (Man-1)/H4 ($GlcNH_2$); H1 (Man-2)/H6,6′ (Man-1); H1 (Man-3)/H2 (Man-2); H1 (Man-4)/H2 (Man-3). Important correlation peaks in the $^{1}H,^{31}P$ HMQC spectrum: P^{I} ($\delta_P = 18.7$ ppm) with H6,6′ ($GlcNH_2$) and P-CH_2-CH_2-NH_3^+; P^{II} ($\delta_P = -0.6$ ppm) with H1 (Ino) and H3 (glycerol); P^{III} ($\delta_P = -1.5$ ppm) with H6,6′ (Man-3) and P-O-CH_2-CH_2-NH_3^+. [b] Additional signals of glycerol were present: CH_2-O-P, $\delta_H = 3.80$ ppm, $\delta_C = 63.1$ ppm; CH-O-acyl, $\delta_H = 5.02$ ppm, $\delta_C = 71.0$ ppm; CH_2-O-alkyl, $\delta_H = 3.52$ and 3.47 ppm, $\delta_C = 68.9$ ppm. [c] Additional signals of the aminoethylphosphonate P-CH_2-CH_2-NH_3^+ were present: PCH_2, $\delta_H = 2.01$ ppm, $\delta_C = 26.5$ ppm; NCH_2, $\delta_H = 3.06$ and 3.00 ppm, $\delta_C = 35.0$ ppm. [d] Additional signals of the ethanolamine phosphate P-O-CH_2-CH_2-NH_3^+ were present: $POCH_2$, $\delta_H = 4.05$ and 3.83 ppm, $\delta_C = 65.7$ ppm; NCH_2, $\delta_H = 3.06$ and 3.00 ppm, $\delta_C = 40.0$ ppm.

Keywords: carbohydrates · glycosides · phospholipids · protozoa · synthetic methods

[1] a) M. A. J. Ferguson, S. W. Homans, R. A. Dwek, T. W. Rademacher, *Science* **1988**, *239*, 753; b) S. W. Homans, M. A. J. Ferguson, R. A. Dwek, T. W. Rademacher, R. Anand, A. F. Williams, *Nature* **1988**, *333*, 269.

[2] a) M. J. McConville, M. A. J. Ferguson, *Biochem. J.* **1993**, *294*, 305; b) M. J. McConville, A. K. Menon, *Mol. Membr. Biol.* **2000**, *17*, 1.

[3] a) K. G. Rothberg, J. E. Heuser, W. C. Donzell, Y.-S. Ying, J. R. Glenney, G. W. Anderson, *Cell* **1992**, *68*, 673; b) R. Varma, S. Mayor, *Nature* **1998**, *394*, 798; c) H.-H. Caro, M. Martin-Lomas, M. Bernabe, *Carbohydr. Res.* **1993**, *240*, 119.

[4] a) T. G. Mayer, B. Kratzer, R. R. Schmidt, *Angew. Chem.* **1994**, *33*, 2289; *Angew. Chem. Int. Ed. Engl.* **1994**, *33*, 2177; b) T. G. Mayer, R. R. Schmidt, *Eur. J. Org. Chem.* **1999**, 1153.

[5] a) A. S. Campbell, B. Fraser-Reid, *J. Am. Chem. Soc.* **1995**, *117*, 10387; b) K. Pekari, R. R. Schmidt, *J. Org. Chem.* **2003**, *68*, 1295.

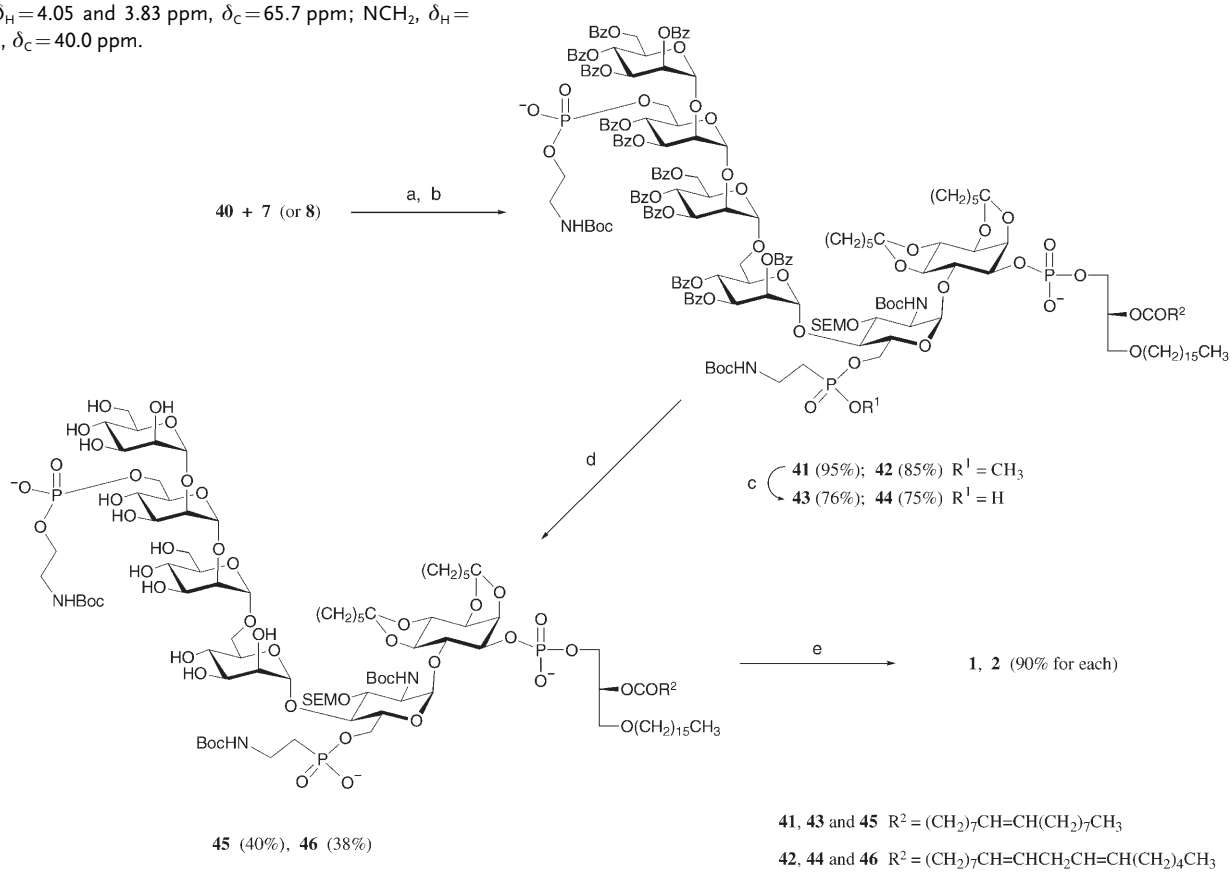
[6] D. K. Baeschlin, A. R. Chaperon, L. G. Green, M. E. Hahn, S. J. Ince, S. V. Ley, *Chem. Eur. J.* **2000**, *6*, 172.

[7] K. Ruda, J. Lindberg, P. J. Garegg, S. Oscarson, P. Konradsson, *J. Am. Chem. Soc.* **2000**, *122*, 11067.

[8] K. Pekari, D. Tailler, R. Weingart, R. R. Schmidt, *J. Org. Chem.* **2001**, *66*, 7432.

[9] J. Lu, K. N. Jayaprakash, U. Schlueter, B. Fraser-Reid, *J. Am. Chem. Soc.* **2004**, *126*, 7540.

[10] A. Ali, D. C. Gowda, R. A. Vishwakarma, *Chem. Commun.* **2005**, 519.



Scheme 6. Reagents: a) pivaloyl chloride, pyridine; b) I_2, pyridine/water; c) PhSH, Et_3N, DMF; d) 0.05 M NaOMe, MeOH; e) CF_3COOH/water (9:1).

 © 2006 Wiley-VCH Verlag GmbH & Co. KGaA, Weinheim

[11] D. H. Molyneux in *Trypanosomiasis and Leishmaniasis* (Ed.: G. Hide et al.), CAB International, Wallingford, UK, **1997**, pp. 39–50.
[12] M. L. S. Güther, M. L. Cardoso de Almeida, N. Yoshida, M. A. J. Ferguson, *J. Biol. Chem.* **1992**, *267*, 6820.
[13] I. C. Almeida, M. M. Camargo, D. O. Procopio, L. S. Silva, A. Mehlert, L. R. Travassos, R. T. Gazzinelli, M. A. J. Ferguson, *EMBO J.* **2000**, *19*, 1476.
[14] V. L. Pereira-Chioccola, A. Acosta-Serrano, I. Correia de Almeida, M. A. J. Ferguson, T. Souto-Padron, M. M. Rodrigues, L. R. Travassos, S. Schenkman, *J. Cell Sci.* **2000**, *113*, 1299.
[15] I. C. Almeida, R. T. Gazzinelli, *J. Leukocyte Biol.* **2001**, *70*, 467.
[16] P. Dais, T. K. M. Shing, A. S. Perlin, *Carbohydr. Res.* **1983**, *122*, 305.
[17] N. E. Byramova, M. V. Ovchinnikov, L. V. Backinowsky, N. K. Kochetkov, *Carbohydr. Res.* **1983**, *124*, c8.
[18] B. Kratzer, T. G. Mayer, R. R. Schmidt, *Eur. J. Org. Chem.* **1998**, 291.
[19] T. G. Mayer, R. R. Schmidt, *Liebigs Ann.* **1997**, 859.
[20] G. Grundler, R. R. Schmidt, *Liebigs Ann. Chem.* **1984**, 1826.
[21] C. Lin, H. Fu, G. Tu, Y. Zhao, *Synthesis* **2004**, 509.
[22] I. Lindh, J. Stawinski, *J. Org. Chem.* **1989**, *54*, 1338.
[23] J. Stawinski, R. Strömberg, *Trends Org. Chem.* **1993**, *4*, 31.
[24] A. V. Nikolaev, T. J. Rutherford, M. A. J. Ferguson, J. S. Brimacombe, *J. Chem. Soc. Perkin Trans. 1* **1996**, 1559.
[25] B. Muller, T. J. Martin, C. Schaub, R. R. Schmidt, *Tetrahedron Lett.* **1998**, *39*, 509.
[26] MS data for **1**, $C_{77}H_{146}N_3O_{41}P_3$ (1861.86): MALDI-TOF MS (negative mode, matrix: 2,5-dihydroxybenzoic acid): *m*/*z* 1861.09 $[M-H]^-$; ES-TOF MS (positive mode): *m*/*z* 931.94 $[M+2H]^{2+}$; ES MS (negative mode): *m*/*z* 930.0 $[M-2H]^{2-}$, 941.0 $[M-3H+Na]^{2-}$, 1861.0 $[M-H]^-$. MS data for **2**, $C_{77}H_{144}N_3O_{41}P_3$ (1859.85): MALDI-TOF MS (positive mode, matrix: 2,5-dihydroxybenzoic acid): *m*/*z* 1923.00 $[M-H+2Na+NH_3]^+$; ES MS (positive mode): *m*/*z* 1240.50 $[2M+3H]^{3+}$, 1791.90 $[M-NH_2C_2H_4PO_2H+H+Na+NH_3]^+$, 1847.70 $[M-NH_2C_2H_4PO_2H+Na+K+2NH_3]^+$. MS data for **45** ($H^+$ form), $C_{110}H_{200}N_3O_{48}P_3Si$ (2452.23): MALDI-TOF MS (negative mode, matrix: 2,5-dihydroxybenzoic acid): *m*/*z* 2451.45 $[M-H]^-$.
[27] I. C. Almeida, unpublished results.
[28] M. A. S. Campos, I. C. Almeida, O. Takeuchi, S. Akira, E. P. Valente, D. O. Procopio, L. R. Travassos, J. A. Smith, D. T. Golenbock, R. T. Gazzinelli, *J. Immunol.* **2001**, *167*, 416.

 © 2006 Wiley-VCH Verlag GmbH & Co. KGaA, Weinheim

Metallabenzenes

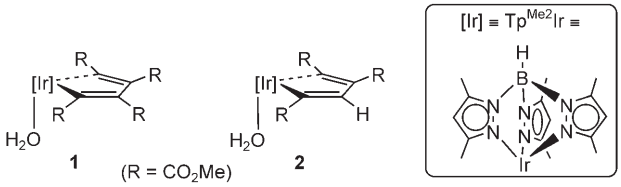
DOI: 10.1002/anie.200502437

Formation of Iridabenzenes by Coupling of Iridacyclopentadienes and Alkenes**

Eleuterio Álvarez, Margarita Paneque, Manuel L. Poveda,* and Nuria Rendón*

Metallabenzenes are interesting structural units that have attracted broad attention.[1] Recently, formation of iridabenzenes by a [2+2+1] cyclotrimerization of alkynes via iridacyclopentadiene intermediates was demonstrated,[2] constituting a valuable addition to previous synthetic methodologies.[1a,3] Herein we describe new iridabenzene structures prepared by a novel synthetic procedure, namely the coupling of an alkene with iridacyclopentadienes.

Two iridacyclopentadiene structures were chosen as probes to test this reactivity: the known[4] compound **1** and the related derivative **2**.



Both **1** and **2** react with C_2H_4 to give the allyl derivatives **4a** and **4b** via intermediate hydride alkenes **3a** and **3b**, respectively (Scheme 1).[5] Compound **4a** was reported previously.[6] Notably, C_2H_4 inserts regioselectively into the Ir–C bond with the H substituent in the β-position.

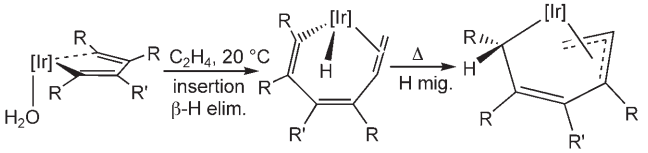
In contrast, complex **1** reacts with propene at 20 °C to form the new derivative **5** as a result of the regioselective insertion of $MeCH{=}CH_2$ into one of the equivalent Ir–C bonds. Interestingly, the insertion of propene is reversible, and upon standing at room temperature for several hours, solutions of **5** in $CDCl_3$ revert to **1** and propene. However, when the reaction of **1** and propene is effected at 60 °C, the

[*] Dr. E. Álvarez, Dr. M. Paneque, Prof. Dr. M. L. Poveda, N. Rendón
Instituto de Investigaciones Químicas
Departamento de Química Inorgánica
Consejo Superior de Investigaciones Científicas (CSIC)
Universidad de Sevilla
Av. Américo Vespucio 49, Isla de la Cartuja, 41092 Sevilla (Spain)
Fax: (+34) 95-446-0565
E-mail: paneque@iiq.csic.es

[**] Financial support from the Spanish Ministerio de Educación y Ciencia (MEC; Projects BQU2001–1995 and CTQ2004-00409/BQU, FEDER support), from the Junta de Andalucía, and from the EU COST Action WG-D17-003 are gratefully acknowledged. N.R. thanks the MEC for a grant.

Supporting information for this article is available on the WWW under http://www.angewandte.org or from the author.

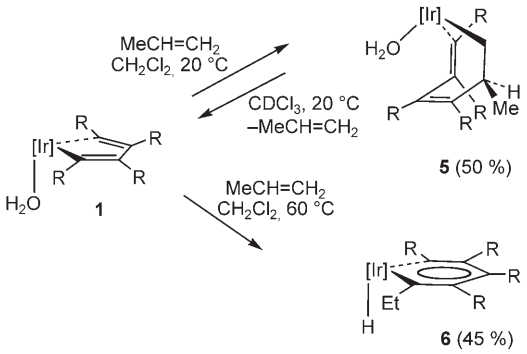
© 2006 Wiley-VCH Verlag GmbH & Co. KGaA, Weinheim



R'= CO_2Me (**1**); H (**2**) R'= CO_2Me (**3a**); H (**3b**) R'= CO_2Me (**4a**); H (**4b**)

Scheme 1. Formation of allylic species by the reaction of **1** and **2** with C_2H_4.

iridabenzene **6** is formed in approximately 45% yield, as determined by ^{1}H NMR spectroscopy (Scheme 2).[7]



Scheme 2. Reaction of compound **1** with propene at different temperatures.

The Ir-bonded ^{13}C nuclei of **6** resonate at $\delta = 274.2$ (Ir-*C*(Et)) and 202.1 (Ir-*C*(CO_2Me)) ppm. Both δ values indicate partial double-bond character of the Ir–C bonds,[8] with a higher stabilization of the alkylidene functionality by the more strongly electron-donating alkyl group. This is also reflected in the solid-state structure, determined by X-ray crystallographic methods (Figure 1). As observed previously for a related $Tp^{Me2}Ir^{III}$ (see **1** and **2** for structure of Tp^{Me2}) metallabenzene, the Ir atom deviates considerably (0.57 Å) out of the plane defined by the five carbon atoms of the ring.[3c]

While a simple olefin insertion can explain the formation of **5** (Scheme 2), generation of iridabenzene **6** requires a more complex reaction pathway proposed to consist of isomerization of the coordinated alkene to a propylidene ligand as in **A**, followed by migratory insertion to give **B**[9] and α-hydride elimination (Scheme 3).

Alkene to alkylidene rearrangement is a rare but known event[10] and, similarly, the migratory insertion[11] and the α-hydride-elimination[12–14] steps find ample literature precedent.

The analogous reaction of propene with iridacycle **2** demonstrates a surprising and unexpected effect of the nature of the iridacycle substituents in the course of the reaction. Thus, treatment of **2** (with H instead of CO_2Me at one of the β-carbon atoms) with propene gives the iridabenzene **7**, which, unlike **6**, is not a hydride but bears, instead, an iridium-bound methyl group (Scheme 4).

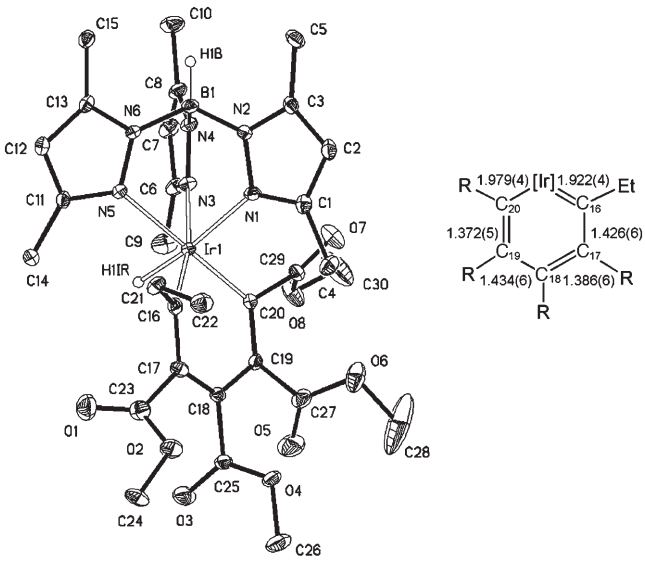
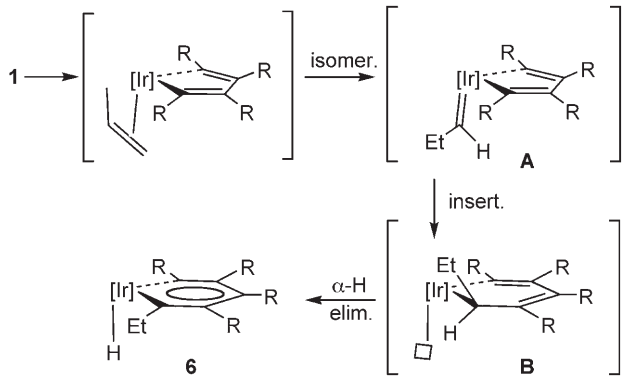
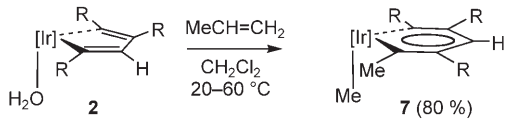


Figure 1. Molecular structure of **6** (30% ellipsoids, H atoms other than the hydride ligand omitted for clarity). Selected bond lengths [Å] and angles [°]: Ir–C(16) 1.922(4), Ir–C(20) 1.979(4); C(16)-Ir-C(20) 90.51(17), C(17)-C(18)-C(19) 125.0(4).



Scheme 3. Proposed mechanism for the formation of **6**.



Scheme 4. Reaction of complex **2** with propene.

In the temperature range from 20 to 60 °C, compound **7** is practically the only reaction product. The NMR spectroscopic and X-ray crystallographic data for **7** confirm this structure. Figure 2 contains an ORTEP representation for this compound, for which the structural features are similar to those of **6** (see above). In this case, the Ir atom deviates by 0.70 Å out of the plane defined by the five carbon atoms of the metallacycle.

The intermediate metal–alkylidene resulting from the isomerization of the propene ligand is also suggested in a possible route to compound **7** (Scheme 5), but for subtle

 © 2006 Wiley-VCH Verlag GmbH & Co. KGaA, Weinheim

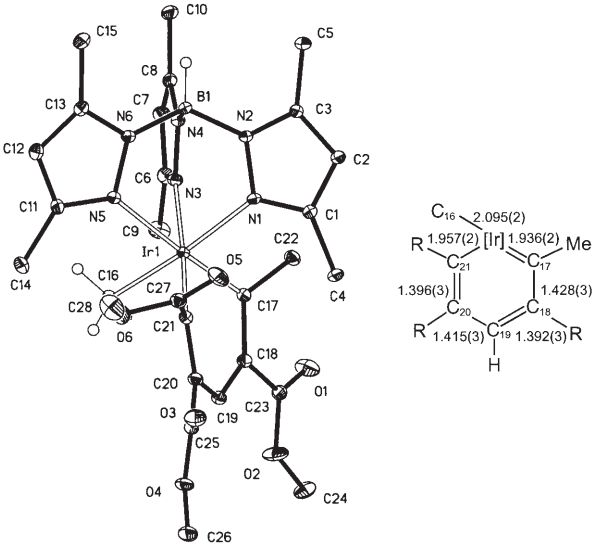
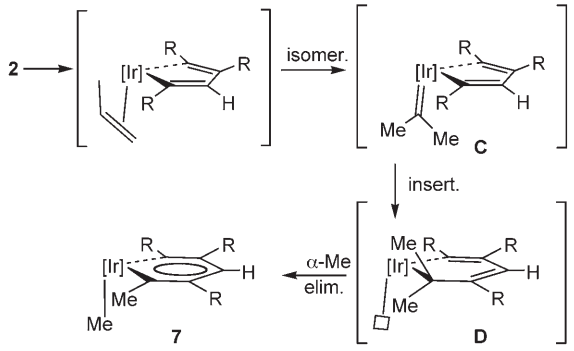


Figure 2. Molecular structure of **7** (30% ellipsoids, H atoms other than those of the methyl ligand omitted for clarity). Selected bond lengths [Å] and angles [°]: Ir–C(16) 2.095(2), Ir–C(17) 1.936(2), Ir–C(21) 1.957(2); C(17)-Ir-C(21) 90.87(9), C(18)-C(19)-C(20) 127.0(2).

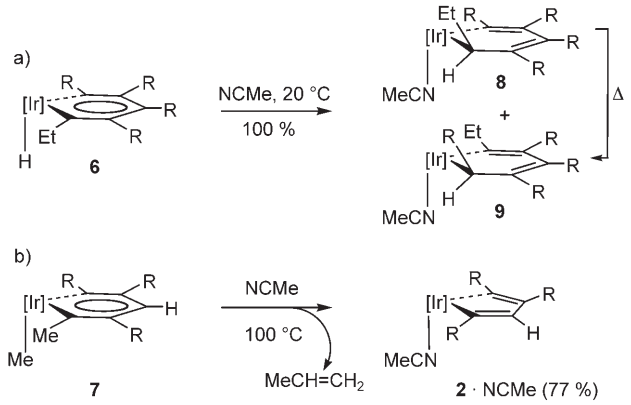


Scheme 5. Proposed mechanism for the formation of **7**.

reasons that are not presently understood, the dimethylcarbene unit, $=CMe_2$ as in **C**, appears to be favored over the linear propylidene, =C(H)Et. This isomerization would be followed by regioselective migration of the alkenyl carbon atom adjacent to the CH group onto the alkylidene carbon atom to give **D**[9] and by an unusual α-Me elimination.[15]

Preliminary studies on the reactivity of iridabenzenes **6** and **7** reveal interesting differences. Thus, the hydride compound **6** reacts with NCMe at 20 °C to give a 6:1 kinetic mixture of **8** and **9**, the products of the migration of the hydride ligand onto the two Ir–C bonds (Scheme 6a).[16] By heating these mixtures, in C_6H_6 or C_6H_{12} at 90 °C with a drop of NCMe, **8** transforms completely into the thermodynamically more favored **9**, possibly via **6**.[17] In contrast, the methyl derivative **7**, does not react with acetonitrile at 20 °C, but at 100 °C it mainly reverts to the iridacycle **2**, isolated in the form of the NCMe adduct **2**·NCMe (Scheme 6b).[18] This clearly demonstrates that the reaction of **2** with propene represented in Scheme 4 is a reversible process.

In conclusion a new route to iridabenzenes involving the coupling of the primary alkene $MeCH{=}CH_2$ with iridacycles **1** and **2** has been demonstrated. Transient iridium alkylidenes, resulting from the isomerization of iridium alkenes, appear to be key intermediates of this rearrangement that involves the formation of new carbon–carbon bonds. In one instance, namely the generation of compound **7** from **2** and $MeCH{=}CH_2$, the C–C bond-forming reaction is reversible.



Scheme 6. Reaction of compounds **6** and **7** with acetonitrile. a) Compound **6** reacts with NCMe at 20 °C to give a mixture of **8** and **9**. b) The methyl derivative **7** does not react with acetonitrile at 20 °C and at 100 °C it mainly reverts to the iridacycle **2.**

Experimental Section

6: Compound **1** (0.5 g, 0.63 mmol) was dissolved in CH_2Cl_2 (12 mL), $MeCH{=}CH_2$ was bubbled through the solution for 7 min, and the resulting solution was stirred under propene in a closed vessel for 12 h at 60 °C. After this period the solvent was removed under reduced pressure, and the formation mainly of a mixture of two isomeric compounds was ascertained by ^{1}H NMR spectroscopy (iridabenzene/isomer ratio: 5:1, ≈65% yield). Compound **6** was separated by column chromatography (silica gel) by using hexane/Et_2O (1:1) as eluant (34% yield). Compound **6** was crystallized from pentane/CH_2Cl_2 (1:1) at −20 °C (23%) as green crystals. The second isolated product was formulated as in reference [7].

7: Compound **2** was dissolved in CH_2Cl_2 (0.32 g, 0.44 mmol; 10 mL), $MeCH{=}CH_2$ was bubbled through the solution for 5 min, and the solution was stirred under propene in a closed vessel for 15 h at room temperature. After this period of time the solution changed from dark yellow to green. The yield of the product **7** was ascertained to be about 80% by ^{1}H NMR spectroscopy. This compound was purified by chromatography on silica gel with hexane/Et_2O (2:1) and isolated in 54% yield. Crystallized from hexane/Et_2O (2:1) at −20 °C gave the product as thin, dark green needles (45%).

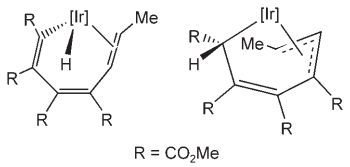
Received: July 12, 2005
Revised: September 23, 2005
Published online: December 2, 2005

Keywords: aromaticity · C–C coupling · iridium · metallabenzenes · metallacycles

[1] a) J. R. Bleeke, *Chem. Rev.* **2001**, *101*, 1205; b) D. L. Thorn, R. Hoffmann, *Nouv. J. Chim.* **1979**, *3*, 39; for recent theoretical work on this type of compound, see: c) M. A. Iron, A. C. B. Lucassen, H. Cohen, M. E. van der Boom, J. M. L. Martin, *J.*

 © 2006 Wiley-VCH Verlag GmbH & Co. KGaA, Weinheim

Am. Chem. Soc. **2004**, *126*, 11699; d) M. A. Iron, J. M. L. Martin, M. E. van der Boom, *J. Am. Chem. Soc.* **2003**, *125*, 13020.
[2] C. S. Chin, H. Lee, *Chem. Eur. J.* **2004**, *10*, 4518.
[3] For recent examples, see: a) H. Xia, G. He, H. Zhang, T. B. Wen, H. H. Y. Sung, I. D. Williams, G. Jia, *J. Am. Chem. Soc.* **2004**, *126*, 6862; b) P. Barrio, M. A. Esteruelas, E. Oñate, *J. Am. Chem. Soc.* **2004**, *126*, 1946; c) M. Paneque, C. M. Posadas, M. L. Poveda, N. Rendón, V. Salazar, E. Oñate, K. Mereiter, *J. Am. Chem. Soc.* **2003**, *125*, 9898; d) V. Jacob, T. J. R. Weakley, M. M. Haley, *Angew. Chem.* **2002**, *114*, 3620; *Angew. Chem. Int. Ed.* **2002**, *41*, 3470.
[4] M. Paneque, M. L. Poveda, N. Rendón, K. Mereiter, *J. Am. Chem. Soc.* **2004**, *126*, 1610.
[5] In the case of **1**, we isolated an intermediate formed by a simple C_2H_4 insertion, as in **5** (unpublished results).
[6] E. Alvarez, M. Gómez, M. Paneque, C. M. Posadas, M. L. Poveda, N. Rendón, L. L. Santos, S. Rojas-Lima, V. Salazar, K. Mereiter, C. Ruiz, *J. Am. Chem. Soc.* **2003**, *125*, 1478.
[7] A hydride–olefin complex related to **3a** was also formed in 10% yield under these conditions. This complex and **6** are formed through separate kinetic pathways: **6** is stable up to 100°C, whereas the hydride–olefin species is converted at 80°C into a hydride–allyl complex related to **4a**. These two species were fully characterized as shown and will be reported in a forthcoming full paper. We anticipate that the Me group from the propene appears in both complexes at the α position of the olefinic or the allyl chain, respectively, indicating that the propene can insert into the Ir–C bond of **1** to give the two possible regioisomers.



[8] We found similar values for the Ir–*C*(CO_2Me) carbon atom of other related iridabenzene derivatives.[3c]
[9] As suggested by a referee, intermediate **B** may be reached by a sequence of olefin insertion and H transposition through the metal center. However, in this case it is difficult to understand why the hydride intermediate involved does not transform into an allyl species as described in Scheme 1 and reference [7]. The same reasoning applies to intermediate **D** in Scheme 5.
[10] a) L. Giannini, G. Guillemot, E. Solari, C. Floriani, N. Re, A. Chiesi-Villa, C. Rizzoli, *J. Am. Chem. Soc.* **1999**, *121*, 2797; b) J. S. Freundlich, R. R. Schrock, W. M. Davis, *J. Am. Chem. Soc.* **1996**, *118*, 3643; c) M. Paneque, M. L. Poveda, L. L. Santos, E. Carmona, A. Lledós, G. Ujaque, K. Mereiter, *Angew. Chem.* **2004**, *116*, 3794; *Angew. Chem. Int. Ed.* **2004**, *43*, 3708; d) G. Parkin, E. Bunel, B. J. Burger, M. S. Trimmer, A. van Asselt, J. E. Bercaw, *J. Mol. Catal.* **1987**, *41*, 29; e) O. V. Ozerov, L. A. Watson, M. Pink, K. G. Caulton, *J. Am. Chem. Soc.* **2003**, *125*, 9604; f) O. V. Ozerov, L. A. Watson, M. Pink, K. G. Caulton, *J. Am. Chem. Soc.* **2004**, *126*, 6363.
[11] a) F. M. Alías, P. J. Daff, M. Paneque, M. L. Poveda, E. Carmona, P. J. Pérez, V. Salazar, Y. Alvarado, R. Atencio, R. Sánchez-Delgado, *Chem. Eur. J.* **2002**, *8*, 5132; b) F. M. Alías, M. L. Poveda, M. Sellin, E. Carmona, *J. Am. Chem. Soc.* **1998**, *120*, 5816.
[12] E. Carmona, M. Paneque, M. L. Poveda, *Dalton Trans.* **2003**, 4022.
[13] D. H. Lee, J. Chen, J. W. Faller, R. H. Crabtree, *Chem. Commun.* **2001**, 213.
[14] R. R. Schrock, S. W. Seidel, N. C. Mösch-Zanetti, K-Y. Shih, M. B. O'Donoghue, W. M. Reiff, *J. Am. Chem. Soc.* **1997**, *119*, 11876.
[15] α-Alkyl or -aryl eliminations, with cleavage of a C–C bond, are rare; see, for example: a) K. Ferré, G. Poignant, L. Toupet, V. Guerchais, *J. Organomet. Chem.* **2001**, *629*, 19; b) M. Albrecht, G. van Koten, *Angew. Chem.* **2001**, *113*, 3866; *Angew. Chem. Int. Ed.* **2001**, *40*, 3750; c) B. Rybtchinski, D. Milstein, *Angew. Chem.* **1999**, *111*, 918; *Angew. Chem. Int. Ed.* **1999**, *38*, 870.
[16] The stereochemistry of the H migration is based only in ample literature precedents of related systems.
[17] Preliminary kinetic studies are in accord with this mechanism: R. P. Hughes, H. A. Trujillo, J. W. Egan, Jr., A. L. Rheingold, *J. Am. Chem. Soc.* **2000**, *122*, 2261.
[18] This compound is also accessible from the reaction of **2** with acetonitrile.

 © 2006 Wiley-VCH Verlag GmbH & Co. KGaA, Weinheim

Peptide Synthesis

DOI: 10.1002/anie.200503298

Efficient Solid-Phase Lipopeptide Synthesis Employing the Ellman Sulfonamide Linker**

*Jose M. Palomo, Maria Lumbierres, and Herbert Waldmann**

Dedicated to Professor H. Kunz on the occasion of his 65th birthday

Lipid-modified proteins are major determinants in the regulation of important biological processes, such as vesicular transport and cell signaling, growth, and differentiation.[1]

Tailor-made lipidated peptides that embody the characteristic lipidated amino acid sequences of their parent proteins have proven to be efficient reagents and chemical tools for chemical-biological, biochemical, biophysical, structural-biological, and cell-biological studies.[2,3]

For the efficient and rapid synthesis of these peptide conjugates, a flexible solid-phase technique is required. Such a technique must feature very mild, preferably neutral, conditions as the characteristic lipidated peptides often

[*] Dr. J. M. Palomo, Dr. M. Lumbierres, Prof. Dr. H. Waldmann
Max-Planck-Institut für Molekulare Physiologie
Abteilung Chemische Biologie
Otto-Hahn-Strasse 11, 44227 Dortmund (Germany)
and
Universität Dortmund
Fachbereich 3, Chemische Biologie
Fax: (+49) 231-133-2499
E-mail: herbert.waldmann@mpi-dortmund.mpg.de

[**] This research was supported by the Max Planck Gesellschaft and the Fonds der Chemischen Industrie. J.M.P. is grateful to EMBO for a long-term fellowship.

Supporting information for this article is available on the WWW under http://www.angewandte.org or from the author.

© 2006 Wiley-VCH Verlag GmbH & Co. KGaA, Weinheim
InterScience

embody acid- and base-labile farnesyl thioethers and palmitic acid thioesters, allow for the introduction of additional reporter groups (e.g., fluorophores, biotin) and tags (e.g., for coupling to expressed proteins), and allow for the release of the peptides from the solid support as carboxylic acids or esters (depending on the precise structure of the natural blueprint, see below), or equipped with a different functional group (e.g., tags for surface immobilization) at the C terminus. Importantly, it must proceed with preparatively viable overall yields, which is particularly true for long multiply lipidated peptides that represent fully lipid-modified parts of lipoproteins. These protein conjugates are often not accessible in their completely lipidated form from gene-technological methods but need to be prepared by semisynthesis from suitably functionalized synthetic lipopeptides and expressed protein parts.[3] A prototypical example for such a lipidated sequence is the N-myristoylated and doubly S-palmitoylated N terminus of endothelial nitric oxide (NO) synthase (eNOS; see below).

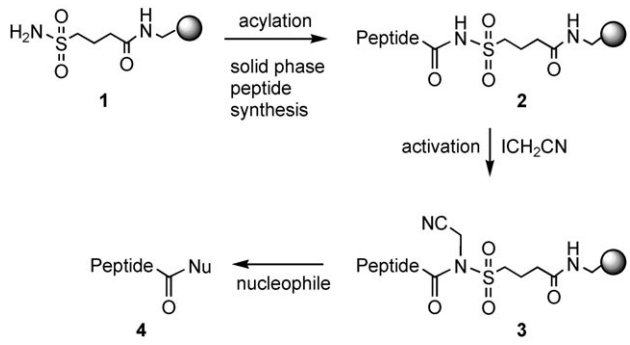
Currently, only the hydrazide linker meets the majority of these criteria.[4,5] However, although it gives access to differently modified lipopeptides, the oxidative cleavage of this anchoring group is accompanied by undesired side reactions,[6] thus resulting in product loss and low overall yields of typically 15–35%. Consequently, lipidated peptides with 10–15 amino acids have become available by means of this technique, but numerous attempts to break this barrier, in particular for multiply lipidated peptides, failed in our hands.

Herein, we describe the successful development of a solid-phase method that meets the demands described above. It employs pre-lipidated amino acid building blocks[4b] together with the Ellman alkyl sulfonamide linker for anchoring to the solid support.

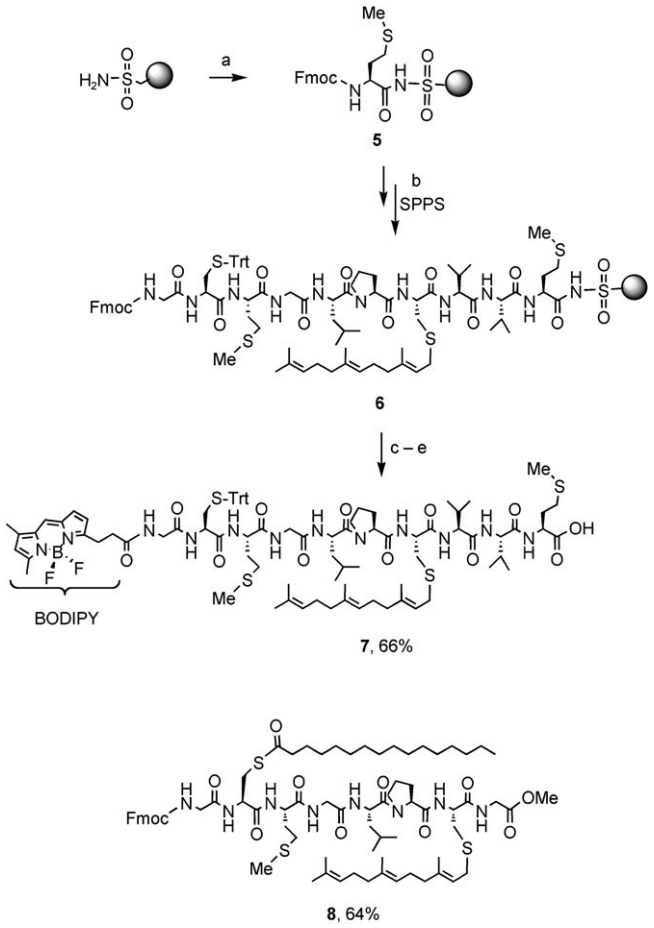
The alkyl sulfonamide linker developed by Ellman et al.[7] is stable to treatment with acid or base. The target compounds are released under very mild conditions by selective N-alkylation of the *N*-acyl sulfonamide and attack of different nucleophiles on the intermediary formed *N*-alkyl acyl sulfonamide (Scheme 1). The linker has been used successfully in the synthesis of different peptide derivatives and other compound classes on solid support.[8]

The lipopeptide solid-phase synthesis method was established by employing the C termini of the Ras proteins as targets. These proteins serve as central molecular switches in biological signaling cascades and are among the most important human oncogenes.[1] They are biosynthesized as precursor proteins with a C-terminal "CAAX-box" sequence (A = amino acid; X = Ser, Met), which is processed to the mature form with an S-farnesylated cysteine methyl ester at the C terminus (H-, K-, and N-Ras) and S-palmitoylated cysteines (H- and N-Ras) upstream.

In an initial sequence, N-Ras-derived CAAX-box peptide **7** was synthesized. To this end, FmocMet (Fmoc = 9-fluorenylmethoxycarbonyl) was coupled to the resin by using PyBOP for activation[7c] (Scheme 2), and after removal of



Scheme 1. Solid-phase peptide synthesis employing the Ellman sulfonamide linker.



Scheme 2. Solid-phase synthesis of N-Ras-derived CAAX box peptide **7** and peptide **8** employing the Ellman sulfonamide linker. a) Fmoc-Met-OH (4 equiv), PyBOP (4 equiv), DIPEA (8 equiv), $CHCl_3$, 8 h, −20 °C; b) 20% piperidine/DMF; standard solid-phase peptide synthesis (SPPS): 1. Fmoc-AA-OH (5 equiv), HBTU/HOBt (5 equiv), DIPEA (10 equiv), DMF, 2 h (for the incorporation of lipidated cysteines: AA (4 equiv), HBTU/HOBt/TMP (4 equiv), CH_2Cl_2/DMF (1:1), 4 h); 2. 20% piperidine/DMF; c) 1. 20% piperidine/DMF; 2. BODIPY-FL (5 equiv), HBTU/HOBt (5 equiv), DIPEA (10 equiv), DMF, 4 h; d) ICH_2CN (25 equiv), DIPEA (10 equiv), NMP, 24 h; e) H_2O (30 equiv), DMAP (0.8 equiv), THF, 24 h. DMF: dimethylformamide, PyBOP: benzotriazole-1-yl-oxytris(pyrrolidino)phosphonium hexafluorophosphate, HOBt: 1-hydroxybenzotriazole, HBTU: *N*-[(1*H*-benzotriazol-1-yl)(dimethylamino)methylene]-*N*-methylmethanaminium hexafluorophosphate *N*-oxide, DIPEA: *N*,*N*-diisopropylethylamine, TMP: trimethylpyridine, NMP: 1-methyl-2-pyrrolidinone, DMAP: dimethylaminopyridine, BODIPY FL: 4,4-difluoro-5,7-dimethyl-4-bora-3a,4a-diaza-(*S*)-indacene-3-propionic acid.

 © 2006 Wiley-VCH Verlag GmbH & Co. KGaA, Weinheim

the Fmoc group the peptide chain was elongated to yield immobilized decapeptide **6**. The farnesylated cysteine building block[4b] was attached to the solid support using HBTU/TMP in CH_2Cl_2/DMF (1:1) to avoid cysteine racemization.[9]

After removal of the N-terminal Fmoc group, the BODIPY FL fluorophore was attached to the lipopeptide. For release from the solid support, the acyl sulfonamide was converted into the cyanomethylsulfonamide by N-alkylation with 25 equivalents of iodoacetonitrile and DIPEA in NMP, followed by treatment with H_2O and DMAP. Thereby, the lipidated CAAX-box peptide was obtained in $>85\%$ purity, and after simple extraction and washing was isolated in 66% yield. To investigate whether the introduction of a base-labile S-palmitoylated cysteine and functionalization at the C terminus are also feasible by means of this technique, doubly lipidated lipopeptide methyl ester **8** was synthesized by analogy and obtained in 64% overall yield. The palmitoylated cysteine building block[4b] was coupled under the conditions described above for the farnesylated cysteine. Selective removal of the Fmoc group and chain elongation without an undesired S→N acyl shift of the palmitic acid in the N-terminally deblocked cysteine peptide were achieved by treatment with 1% DBU in DMF twice for 30 seconds followed by immediate acylation of the liberated amino group with preactivated FmocGly (preactivation carried out with 5 equivalents of HATU and 20 equiv of DIPEA) in CH_2Cl_2/DMF (7:1) as described before.[4]

Notably, in both syntheses competing S-alkylation of methionine or farnesylated cysteine and competing thioester cleavage were not detected.[10]

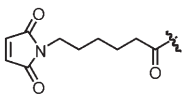
For the synthesis of lipidated Ras peptides terminating in a S-farnesylated cysteine methyl ester, which is characteristic for the fully matured proteins, a viable method for the racemization-free coupling of the bulky FmocCys(Far) building block to the sulfonamide linker had to be developed. While the use of PyBOP and related activation reagents did not yield satisfactory results, in situ formation of the amino acid fluoride by treatment of the carboxylic acid with tetramethylfluoroformamidinium hexafluorophosphate (TFFH) introduced by Carpino et al.[11] provided an advantageous solution to the problem. Preactivation with 3 equivalents of TFFH and 6 equivalents of DIPEA in CH_2Cl_2/DMF (1:1) for 10 min and double or triple coupling for 1.5 h gave high loading levels, which gratifyingly also translated into high overall yields for different Ras peptides (see Table 1). After deprotection of the amino acid side chains,[12] peptides **9**–**13**, which represent the C termini of N-Ras (**9** and **10**), H-Ras (**11** and **12**), K-Ras 4B (**13**), were obtained in 60–75% yield and in multi-milligram amounts.

Considered together, the synthetic Ras peptides shown in Table 1 provide examples that embody both the acid-labile farnesyl thioether and the base-sensitive palmitic acid thioester; different fluorophores (NBD, BODIPY, *N*-methylanthraniloyl (Mant)) attached to the N terminus,[13] to an amino acid side chain, or incorporated into a lipid group; a maleimide suitable for covalent coupling to expressed proteins by means of conjugate addition; and an N-terminally deprotected yet S-disulfide-masked cysteine suitable for coupling to proteins by expressed protein ligation.

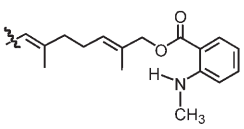
Table 1: Lipidated peptides synthesized on a solid phase employing the Ellman sulfonamide linker as an anchoring group.

Entry	No.	Peptide structure	Parent protein	Yield [%]
1	**9**	NBD-Aca-Gly-Cys(Pal)-Met-Gly-Leu-Pro-Cys(Far)-OMe	N-Ras	65
2	**10**	MIC-Gly-Cys(Pal)-Met-Gly-Leu-Pro-Cys(Far)-OMe	N-Ras	66
3	**11**	Ac-Met-Ser-Cys(Pal)-Lys-Cys(GerMant)-OMe	H-Ras	60
4	**12**	H_2N-Cys(*t*BuSS)-Met-Ser-Cys(*t*BuSS)-Lys-Cys(Far)-OMe	H-Ras	67
5	**13**	NH_2-Lys-Ser-Lys-Thr(O*t*Bu)-Lys-Cys(Far)-OMe	K-Ras 4B	75
6	**14**	Ac-Lys(NBD)-Ser-Gly-Ser-Gly-Gly-Cys(Pal)-Cys(Far)-OMe	Ras 2 from *Saccharomyces cerevis*	44
7	**15**	Biotin-Aca-Leu-Asn-Cys(Pal)-Cys(Pal)-Gly-Gln-Arg-Ala-Cys-Tyr-Arg-Trp-Ser-Lys(NBD)-Arg-Trp-Leu-OH	Phospholipase D	39

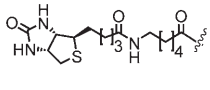
MIC=



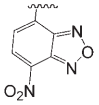
GerMant=



Biotin-aca=



NBD=



© 2006 Wiley-VCH Verlag GmbH & Co. KGaA, Weinheim

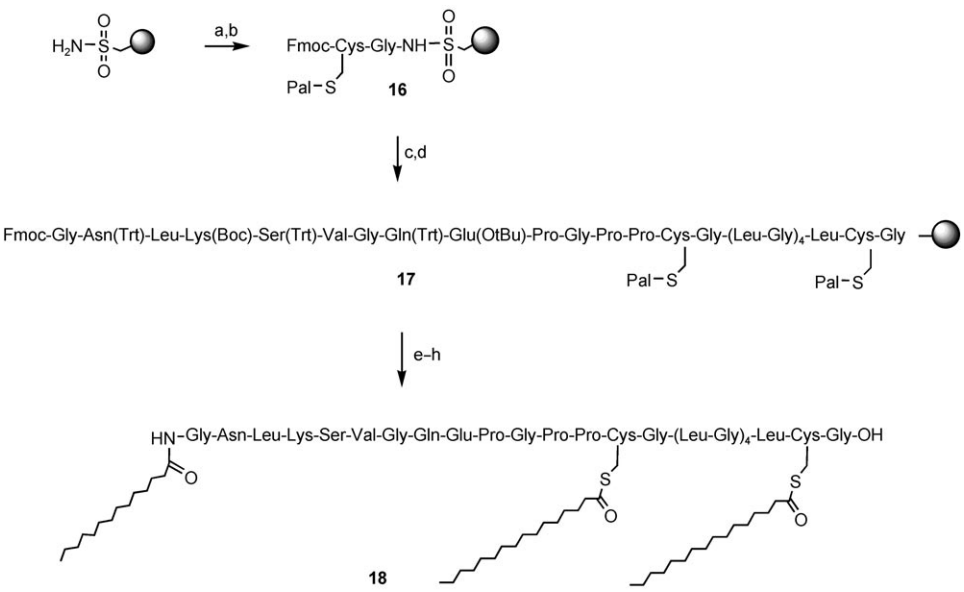
Remarkably, after release from the resin, the purity of these peptides is already fairly high (see also below), so that further purification to homogeneity is achieved readily by straightforward extraction and washing steps and without need for further chromatographic separation.

To determine whether the C-terminal cysteine partially racemizes under the coupling conditions described above, FmocProCys(Far)OMe was synthesized on the solid support and compared with reference compounds incorporating optically pure L and D amino acids synthesized in solution. Examination of the peptides by means of reverse-phase HPLC did not detect any racemization of the cysteine.

To investigate the scope of the method, the synthesis of heptadecapeptide **15**, which represents a characteristic partial structure of phospholipase D,[14] was attempted. This peptide carries two neighboring S-palmitoylated cysteines and embodies a fluorophore as well as a biotin tag. Phospholipase D peptide **15** was obtained in multi-milligram amounts and again in high purity (see Figure 1 and the Supporting Information) after release from the resin and deprotection of the amino acid side chains[14] by treatment with trifluoroacetic acid (TFA)/triethylsilane/H_2O/ethanedithiol (94:1:2.5:2.5) for 2 hours; furthermore, it was isolated in 39% overall yield and characterized with ^{1}H NMR spectroscopic and mass-spectrometric analysis (ESI MS: *m*/*z* calcd for $[M+2Na+H]^{3+}$: 1055.88; found: 1055.67).

Encouraged by this result, the synthesis of the N-terminal triply lipidated hexacosapeptide of eNOS, an enzyme that could not be expressed and isolated in its fully lipidated form, was attempted. This lipopeptide had been prepared by us before by means of an extended and very laborious multistep solution-phase synthesis, which required more than a year of development and execution, was riddled with severe isolation problems, and finally delivered the desired peptide with an overall yield of less than 1%.[15] All attempts to synthesize multiply lipidated peptides of comparable length by means of the hydrazide linker (see above) completely failed in our hands.

Much to our delight, the desired 26-mer peptide could be obtained in 25 mg and 24% yield of isolated product within three weeks by means of the methodology described herein (Scheme 3). This peptide was characterized by ^{1}H NMR spectroscopic and mass-spectrometric analysis (ESI MS: *m*/*z* calcd for $[M+H+K]^{2+}$: 1559.44; found: 1559.50; see also the Supporting Information).



Scheme 3. Solid-phase peptide synthesis of the N-myristoylated and doubly S-palmitoylated N-terminal 26-mer peptide **18** of endothelial NO synthase employing the Ellman sulfonamide linker. a) Fmoc-Gly-OH (8 equiv), DIC (8 equiv), 1-MIM (8 equiv), CH_2Cl_2/DMF (4:1), 24 h, RT; b) 1. 20% piperidine/DMF; 2. Fmoc-Cys(Pal)-OH (4 equiv), HBTU/HOBt/TMP (4 equiv), CH_2Cl_2/DMF (1:1), 4 h; c) 1. 1% DBU in DMF for 2×30 s; 2. DMF (2×15 s); 3. HATU (5 equiv), Fmoc-Leu-OH (5 equiv), DIPEA (20 equiv), CH_2Cl_2/DMF (4:1)—preactivated for 20 min—, 3 h; d) SPPS: 1. 1% DBU in DMF (2×30 s); 2. Fmoc-AA-OH (5 equiv), HATU (5 equiv), DIPEA (10 equiv), DMF, 3 h; repeat (b and c) for Fmoc-Cys(Pal)-OH coupling; e) 1% DBU/DMF (2×30 s); f) DIPEA (8 equiv), $H_3C(CH_2)_{12}COCl$ (4 equiv), NMP; g) 1. ICH_2CN (25 equiv), DIPEA (10 equiv), NMP, 24 h; 2. H_2O (30 equiv), DMAP (0.8 equiv), THF, 24 h; h) CF_3COOH/ethanedithiol/H_2O/TIS (96:2:1:1), 24% yield. DIC: 1,3-diisopropylcarbodiimide, 1-MIM: 1-methylimizadole, DBU: 1,8-diazobicyclo[5.4.0]undec-7-ene, HATU: *N*-[(dimethylamino)-1-*H*-1,2,3-triazolo[4,5-b]pyridin-1-ylmethylene]-*N*-methylmethanaminium; TIS: triisopropylsilane.

In the synthesis of NO-synthase-derived peptide **18**, couplings of the amino acid building blocks and release from the solid support were carried out as described above. The N-terminal glycine was introduced as the Fmoc derivative to give intermediate **17**, and after removal of the Fmoc group the N terminus was acylated with myristoyl chloride. All acid-labile side-chain protecting groups were removed simultaneously after release of the peptide from the resin. The N-myristoylated and doubly S-palmitoylated hexacosa eNOS lipopeptide represents the longest lipidated peptide synthesized on a solid support so far.

The successful and preparatively viable syntheses of this lipopeptide and the peptides shown in Scheme 2 and Table 1 prove that the use of the Ellman sulfonamide linker provides a major advance in terms of efficiency and practicability in methodology development for the synthesis of lipopeptide conjugates and, in extension, to the synthesis of tailor-made semisynthetic lipidated proteins[2,3] for research in chemical biology.

Received: September 16, 2005
Published online: December 6, 2005

 © 2006 Wiley-VCH Verlag GmbH & Co. KGaA, Weinheim

Keywords: lipids · peptides · solid-phase synthesis · sulfonamides

[1] a) J. E. Smotrys, M. E. Linder, *Annu. Rev. Biochem.* **2004**, *73*, 559 – 587; b) A. Wittinghofer, H. Waldmann, *Angew. Chem.* **2000**, *112*, 4360 – 4383; *Angew. Chem. Int. Ed.* **2000**, *39*, 4193 – 4214.

[2] a) K. Kuhn, D. J. Owen, B. Bader, A. Wittinghofer, J. Kuhlmann, H. Waldmann, *J. Am. Chem. Soc.* **2001**, *123*, 1023 – 1035; b) J. Kuhlmann, A. Tebbe, M. Völkert, M. Wagner, K. Uwai, H. Waldmann, *Angew. Chem.* **2002**, *114*, 2655 – 2658; *Angew. Chem. Int. Ed.* **2002**, *41*, 2546 – 2550; c) R. Reents, M. Wagner, J. Kuhlmann, H. Waldmann, *Angew. Chem.* **2004**, *116*, 2765 – 2768; *Angew. Chem. Int. Ed.* **2004**, *43*, 2711 – 2714; d) C. Peters, A. Wolf, M. Wagner, J. Kuhlmann H. Waldmann, *Proc. Natl. Acad. Sci. USA* **2004**, *101*, 8531 – 8536; e) S. Janosch, C. Nicolini, B. Ludolph, C. Peters, M. Völkert, T. L. Hazlett, E. Gratton, H. Waldmann, R. Winter, *J. Am. Chem. Soc.* **2004**, *126*, 7496 – 7503; f) D. Huster, K. Kuhn, D. Kadereit, H. Waldmann, K. Arnold, *Angew. Chem.* **2001**, *113*, 1083 – 1085; *Angew. Chem. Int. Ed.* **2001**, *40*, 1056 – 1058.

[3] For illustrative examples that prove the importance and power of this approach for Ras and Rab proteins, see: a) A. Rak, O. Pylypenko, T. Durek, A. Watzke, S. Kushnir, L. Brunsveld, H. Waldmann, R. S. Goody, K. Alexandrov, *Science* **2003**, *302*, 646 – 650; b) O. Rocks, A. Peyker, M. Kahms, P. J. Verveer, C. Koerner, M. Lumbierres, J. Kuhlmann, H. Waldmann, A. Wittinghofer, P. I. H. Bastiaens, *Science* **2005**, *307*, 1746 – 1752.

[4] a) G. Kragol, M. Lumbierres, J. M. Palomo, H. Waldmann, *Angew. Chem.* **2004**, *116*, 5963 – 5966; *Angew. Chem. Int. Ed.* **2004**, *43*, 5839 – 5842; b) M. Lumbierres, J. M. Palomo, G. Kragol, S. Roehrs, O. Müller, H. Waldmann, *Chem. Eur. J.* **2005**, *11*, 7405 – 7415.

[5] For alternative solid-phase and solution-phase synthesis methods that meet part of the above criteria, see: a) M. Koppitz, T. Spellig, R. Kahmann, H. Kessler, *Int. J. Pept. Protein Res.* **1996**, *48*, 377 – 380; b) P. Mayer-Fligge, J. Volz, U. Krüger, E. Sturm, W. Gernandi, K. P. Schäfer, M. Przybylski, *J. Pept. Sci.* **1998**, *4*, 355 – 363; c) B. Denis, E. Trifilieff, *J. Pept. Sci.* **2000**, *6*, 372 – 377; d) A. Harishchandran, B. Pallavi, R. Nagaraj, *Protein Pept. Lett.* **2002**, *9*, 411 – 417; e) D. P. Galonic, N. D. Ide, W. A. van der Donk, D. Y. Gin, *J. Am. Chem. Soc.* **2005**, *127*, 7359 – 7369; f) D. T. S. Rijkers, J. A. W. Kruijtzer, J. A. Killian, R. M. J. Liskamp, *Tetrahedron Lett.* **2005**, *46*, 3341 – 3345; g) K. Pachamuthu, X. Zhu, R. R. Schmidt, *J. Org. Chem.* **2005**, *70*, 3720 – 3723.

[6] We have repeatedly observed that after oxidative cleavage of the hydrazide linker major fractions of the synthesized lipopeptides remained bound to the solid support by means of an unidentified linkage that could not be cleaved oxidatively or under acidic or basic conditions anymore. The oxidative cleavage of the hydrazide linker most probably proceeds through an intermediate acyl radical (see: M. Völkert, S. Koul, G. H. Müller, M. Lehnig, H. Waldmann, *J. Org. Chem.* **2002**, *67*, 6902 – 6910) that may form a covalent bond with the polymeric support. Numerous attempts to trap such an intermediate under the conditions of release from the solid support were, however, fruitless (for a related observation, see: J. A. Camarero, B. J. Hackel, J. J. de Yorco, A. R. Mitchell, *J. Org. Chem.* **2004**, *69*, 4145 – 4151).

[7] a) B. J. Backes, J. A. Ellmann, *J. Am. Chem. Soc.* **1994**, *116*,11171 – 11172; b) B. J. Backes, A. A. Virgilio, A. A. Ellman, *J. Am. Chem. Soc.* **1996**, *118*, 3055 – 3056; c) B. J. Backes, J. A. Ellman, *J. Org. Chem.* **1999**, *64*, 2322 – 2330.

[8] For a recent review, see: P. Heidler, A. Link, *Bioorg. Med. Chem.* **2005**, *13*, 585 – 599.

[9] Y. M. Angell, J. Alsina, F. Albericio, G. Barany, J. *Pep. Res.* **2002**, *60*, 292 – 299.

[10] The compatibility of methionine and Cys(Trt) with the conditions for the cleavage of the Ellman linker has been described before, see ref. [7c]

[11] L. A. Carpino, D. Ionescu, A. El-Faham, M. Beyermann, P. Henklein, C. Hanay, H. Wenschuh, M. Bienert, *Org. Lett.* **2003**, *5*, 975 – 977.

[12] Serine side chains were protected as trityl ethers, lysine side chains were masked with the methyltrityl (Mtt) group. The side-chain protecting groups were removed from the peptides by treatment with TFA/triethylsilane/dichloromethane (1:2:97) for 2 h after the release of the peptides from the solid support (see D. Kadereit, P. Deck, I. Heinemann, H. Waldmann, *Chem. Eur. J.* **2001**, *7*, 1184 – 1193).

[13] In further experiments, it was shown that a BODIPY fluorophore can also be introduced at the C terminus of lipidated peptides by nucleophilic trapping of the activated sulfonamide with the BODIPY-2-aminoethyl amide (data not shown).

[14] a) F. G. Buchanan, M. McReynolds, A. Couvillon, Y. Kam, V. R. Holla, R. N. DuBois, J. H. Exton, *Proc. Natl. Acad. Sci. USA* **2005**, *102*, 1638 – 1642; b) S. Cockcroft, *Cell. Mol. Life Sci.* **2001**, *58*, 1674 – 1687, and references therein.

[15] a) R. Machauer, H. Waldmann, *Angew. Chem.* **2000**, *112*, 1503 – 1507; *Angew. Chem. Int. Ed.* **2000**, *39*, 1449 – 1453; b) R. Machauer, H. Waldmann, *Chem. Eur. J.* **2001**, *7*, 2940 – 2956.

 © 2006 Wiley-VCH Verlag GmbH & Co. KGaA, Weinheim

Synthetic Methods

DOI: 10.1002/anie.200502886

Convenient and Efficient Pd-Catalyzed Regioselective Oxyfunctionalization of Terminal Olefins by Using Molecular Oxygen as Sole Reoxidant**

*Takato Mitsudome, Takuya Umetani, Naoya Nosaka, Kohsuke Mori, Tomoo Mizugaki, Kohki Ebitani, and Kiyotomi Kaneda**

The evolution of selective oxidation routes that use molecular oxygen (O_2) is one of the ultimate goals of present-day chemical research.[1] In particular, the Pd-catalyzed Wacker oxidation and acetoxylation of terminal olefins have received

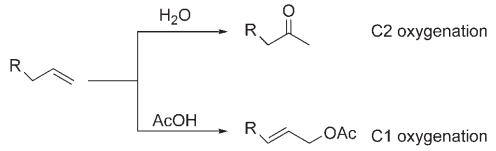
[*] T. Mitsudome, T. Umetani, N. Nosaka, Dr. K. Mori, Dr. T. Mizugaki, K. Ebitani, Prof. K. Kaneda
Graduate School of Engineering Science
Osaka University, 1-3 Machikaneyama
Toyonaka, Osaka 560-8531 (Japan)
Fax: (+81) 6-6850-6260
E-mail: kaneda@cheng.es.osaka-u.ac.jp

[**] This investigation was supported by a Grant-in-Aid for Scientific Research from the Ministry of Education, Culture, Sports, Science, and Technology of Japan (16206078). We thank the center of excellence (21COE; program "Creation of Integrated Ecochemistry", Osaka University) and Dr. Uruga (Spring-8) for X-ray absorption fine-structure (XAFS) measurements.

Supporting information for this article is available on the WWW under http://www.angewandte.org or from the author.

© 2006 Wiley-VCH Verlag GmbH & Co. KGaA, Weinheim
WILEY InterScience DISCOVER SOMETHING GREAT

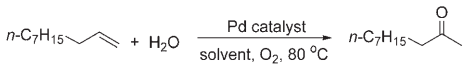
much attention because of useful protocols for direct oxyfunctionalization at the C1 and C2 positions.[2] These processes, however, require cocatalysts, such as copper,[3] heteropolyacids,[4] or benzoquinone,[5] or reducing agents[6] to facilitate the reoxidation of the Pd^0 species by O_2 and prevent its precipitation into inactive metals. Current research has focused on the development of promising methodologies that do not rely on these cocatalysts because of practical and environmental concerns.[7] However, few examples of oxyfunctionalization systems using O_2 as the sole reoxidant have appeared, and these Pd-catalyzed oxidation reactions often suffer from low activities and a limited substrate scope.[8,9] We disclose that $PdCl_2$ in combination with DMA as the solvent is an extremely simple and highly efficient catalytic system for the Wacker oxidation of terminal olefins. This catalytic system allows for an efficient dioxygen-coupled turnover without the need for additional cocatalysts or reducing reagents; it is tolerant toward long-chain and functionalized olefins and is also applicable to Wacker-type intramolecular cyclization. Furthermore, it facilitates acetoxylation of the terminal olefins, thus affording selectively linear allylic acetates. An oxygen atom can be selectively incorporated at the C1 or C2 position of terminal olefins by using an appropriate nucleophile, namely, H_2O or AcOH (Scheme 1). The work-up procedure is also straightforward, and the solution containing the catalyst can be recycled without any loss of activity and selectivity.



Scheme 1. Selectively incorporation of an oxygen atom at the C1 or C2 position of terminal olefins.

The reaction conditions were optimized for the Wacker oxidation of 1-decene (**1a**) using various Pd complexes and solvents under an atmospheric pressure of O_2 (Table 1). The combination of $PdCl_2$ and DMA exhibited the highest catalytic activity, thus affording 2-decanone (**2a**) in 84% yield after 6 h without formation of olefinic isomers (Table 1, entry 1).[10] No Pd precipitation was observed during the above reaction, and the retention of monomeric Pd^{II} species was confirmed after the reaction by Pd K-edge X-ray absorption fine-structure (XAFS) spectroscopic analysis.[11] The use of NMP and DMPA in place of DMA gave moderate yields (Table 1, entries 2 and 3), whereas dimethylformamide (DMF), ethanol, and acetonitrile were significantly less effective (Table 1, entries 4–6). The choice of Pd source was found to influence catalytic efficiency: only $PdCl_2$ could function as a catalyst (Table 1, entry 1 vs. entries 7 and 8). Compound **1a** (20 mmol, 2.8 g) was successfully converted into **2a** (83% yield of isolated product, 2.6 g) with a turnover frequency (TOF) of 17 h^{-1} and a turnover number (TON) of up to 170 (Table 1, entry 9). These values are considerably greater than those reported for other catalytic systems of Pd

Table 1: Wacker oxidation of 1-decene under various conditions,[a] and the peak potentials for reduction (E_{red}) and oxidation (E_{ox}) obtained by cyclic voltammetry.



1a **2a**

Entry	Catalyst	Solvent	Yield [%][b]	E_{red} [V vs. SCE]	E_{ox} [V vs. SCE]
1	$PdCl_2$	DMA	84	−0.70	−0.26
2	$PdCl_2$	NMP	74	−0.69	−0.20
3	$PdCl_2$	DMPA	33	−0.57	−0.13
4	$PdCl_2$	DMF	trace	−0.50	−0.12
5	$PdCl_2$	EtOH	trace	−0.10	0.19
6	$PdCl_2$	MeCN	trace	−0.40	0.10
7	$Pd(OAc)_2$	DMA	trace	–	–
8	$[PdCl_2(NH_3)_4]$	DMA	trace	–	–
9[c]	$PdCl_2$	DMA	85 (83)	–	–

[a] Reaction conditions: 1-decene (0.5 mmol), Pd catalyst (0.005 mmol), solvent (5 mL), H_2O (0.3 mL), 1 atm of O_2, 6 h, 80°C. [b] Values in parenthesis are yields of the isolated product. [c] 1-Decene (20 mmol), $PdCl_2$ (0.1 mmol), DMA (60 mL), H_2O (10 mL), 10 atm of O_2, 10 h. SCE = saturated calomel electrode, NMP = *N*-methylpyrrolidone, DMA = *N*,*N*-diemthylacetamide, DMPA = *N*,*N*-dimethylpropionamide.

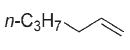
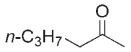
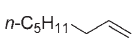
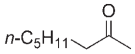
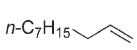
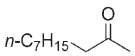
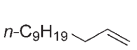
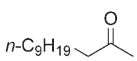
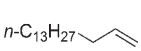
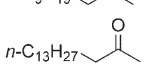
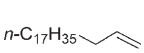
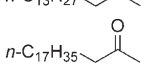
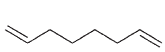
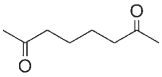
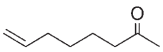
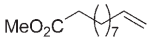
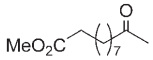
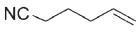
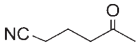
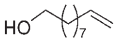
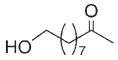
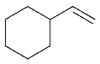
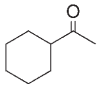
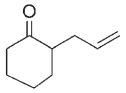
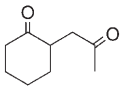
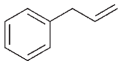
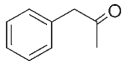
with cocatalysts, such as $PdSO_4$/per(2,6-di-*o*-methyl)-β-cyclodextrin/$H_9PV_6Mo_6O_{40}$/$CuSO_4$ (TOF and TON: 7.7 h^{-1} and 46),[4a] $Pd(OAc)_2$/carbon/molybdovanadophosphate/NH_4Cl/$MeSO_4$ (TOF and TON: 3.3 h^{-1} and 16),[4b] $PdCl_2$/α-cyclodextrin/$CuCl_2$ (1.9 h^{-1} and 19),[3e] and $PdCl_2$/β-cyclodextrin/$CuCl_2$ (0.3 h^{-1} and 15).[3d]

A wide range of terminal olefins were oxidized to form the corresponding methyl ketones in high yields (Table 2).[11] For example, the oxidation of long-chain olefins 1-hexadecene and 1-eicosene occurred efficiently to give the ketones in 85 and 81% yields, respectively (Table 2, entries 5 and 6). In contrast, oxidation of 1-eicosene with $PdCl_2$/$CuCl_2$ in polyethyleneglycol[3c] and $Pd(OAc)_2$/hydroquinone/Fe(phthalocyanine) in DMF[5] resulted in less than 10% yields of 2-eicosenone. In the case of 1,7-octadiene, the use of the $PdCl_2$–DMA catalytic system afforded the corresponding diketone in 81% yield (Table 2, entry 7). The system was also found to be applicable to the oxidation of functionalized terminal olefins possessing cyano and hydroxyl groups. 5-Hexenenitrile and 9-octene-1-ol afforded the corresponding ketones selectively, with suppression of hydration and alcohol oxidation (Table 2, entries 9 and 10).

A further advantage of this catalytic system is the facile separation of the oxidized products from the reaction mixture. Addition of *n*-heptane to the reaction mixture upon completion of the reaction followed by decantation of the *n*-heptane phase containing the oxidized products allows the active Pd species in the residual DMA solution to be recycled. We conducted further oxidations by the addition of successive portions of the olefin to the Pd–DMA phase followed by stirring under identical reaction conditions. The second and third oxidation cycles of **1a** proceeded at rates similar to that of the original reaction, thus affording **2a** in yields of more than 80% with 99% selectivity. The total TON reached 250 after the third recycling process. This separation

 © 2006 Wiley-VCH Verlag GmbH & Co. KGaA, Weinheim

Table 2: Wacker oxidation of various olefins catalyzed by the $PdCl_2$–DMA system.[a]

Entry	Substrate	*t* [h]	Conv. [%]	Product	Yield [%][b]
1		3	85		82 (78)
2		3	82		81 (75)
3		3	86		85 (83)
4[c]		3	88		88 (85)
5[c]		3	88		85 (82)
6[c]		3	82		81 (76)
7[d]		40	100		81 (78)
					19
8[d]		40	97		96 (92)
9[d]		40	84		80 (75)
10[d]		24	89		89 (85)
11[d]		3	86		74 (66)
12[d]		24	96		91 (88)
13[d]		40	94		87 (85)

[a] Reaction conditions: substrate (1 mmol), $PdCl_2$ (0.005 mmol), DMA (3 mL), H_2O (0.5 mL), 6 atm of O_2, 80 °C. [b] Yields were determined by GC analysis; values in parenthesis are the yields of the isolated products. [c] DMA (5 mL). [d] Substrate (0.5 mmol). Conv. = conversion

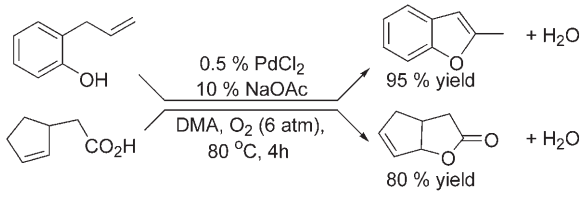
method is strikingly simple in comparison to the previously reported methods using fluoro solvents[12] and ionic liquids.[13]

This catalytic system was also found to be applicable to Wacker-type intramolecular cyclizations, even in the presence of a catalytic amount of sodium acetate.[9] 2-Allylphenol and 2-cyclopentene-1-acetic acid were smoothly converted into 2-methylbenzofuran and 3,3a,4,6a-tetrahydro-2*H*-cyclopenta[b]furan-2-one, respectively, in high yields (Scheme 2).

When AcOH is used as a nucleophile instead of H_2O, regioselective acetoxylation of terminal olefins to the corresponding linear allylic acetates takes place without the use of a cocatalyst (Table 3). For example, **1a** predominantly underwent acetoxylation to provide 2-decenyl ester in 80% yield with 93% selectivity, accompanied by a 6% yield of branched allylic acetate, without the formation of olefinic isomers or Wacker products (Table 3, entry 1). Both the activity and regioselectivity of the acetoxylation are significantly superior to those reported for a $Pd(OAc)_2$–dimethyl sulfoxide (DMSO) system, which required a large amount of benzoquinone as a redox reagent.[14,15] To the best of our knowledge, this is the first demonstration of a cocatalyst-free regioselective acetoxylation of terminal olefins to linear allylic acetates using O_2 as a terminal oxidant.

As well as long-chain aliphatic olefins, acetoxylation proceeded efficiently to give the corresponding linear allylic acetates, even for those olefins with sensitive functional groups, such as ester, nitrile, and acetal groups (Table 3, entries 2–8). This method is a powerful candidate for the α-oxyfunctionalization of versatile terminal olefins, such as hydroboration–oxidation[16] and oxidation using chromyl chloride.[17]

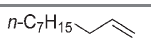
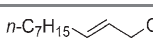
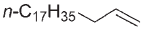
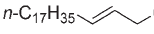
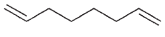
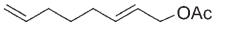
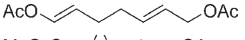
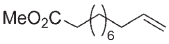
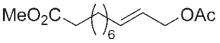
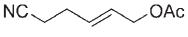
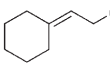
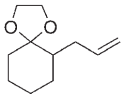
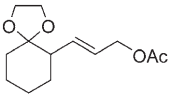
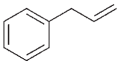
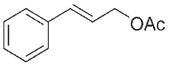
Cyclic-voltammetric analysis of $PdCl_2$ in various solvents was carried out to elucidate the positive effect of DMA on the Wacker oxidation. These spectra showed single irreversible reduction and oxidation peaks: the oxidation peak of the electrogenerated Pd^0 species appeared at a more negative potential value in DMA ($E_{ox} = -0.26$ V) than in other solvents (Table 1, entries 1–6). Interestingly, yields of **2a** increase with increasing negative E_{ox} values of DMA, NMP, and DMPA (Table 1, entries 1–3), which supports the contention that DMA acts as the most efficient solvent for promoting the reoxidation of the Pd^0 species.[11,18] In a separate experiment, XAFS analysis showed that Pd sponge was readily oxidized to a homogeneous Pd^{II} species in a solution of DMA in the presence of two equivalents of HCl under atmospheric O_2 at 80 °C.[11] Wacker oxidation proceeded to afford **2a** in 76% yield in 8 h upon addition of **1a** to this solution of Pd. Kinetic studies revealed that the initial reaction rate of **1a** (R_0) was dependent on O_2 pressure (pO_2) and the concentration of the catalyst ([Pd]) and independent of the concentration of **1a**, H_2O, and H^+. Taking into account the mechanism proposed by Stahl and coworkers for Pd-catalyzed aerobic oxidation, we propose a possible reaction cycle for the present Wacker oxidation in which the rate-determining reoxidation step of Pd^0 k_{cat} competes with its decomposition into inactive Pd^0 metal k_{dec} (Scheme 3).[19] The R_0 value for the Wacker oxidation of **1a**



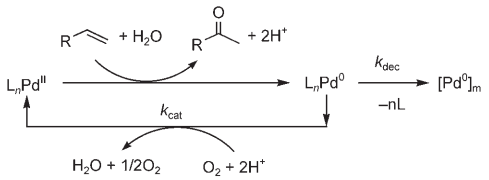
Scheme 2. Intramolecular Wacker-type cyclization by $PdCl_2$ in DMA.

 © 2006 Wiley-VCH Verlag GmbH & Co. KGaA, Weinheim

Table 3: Acetoxylation of various olefins by $PdCl_2$ using molecular oxygen.[a]

Entry	Substrate	Conv. [%]	Major product	Linear/branched[b]	E/Z[c]	Yield [%][d]
1		86		13:1	1:1	86 (85)
2		93		10:1	2:1	90 (82)
3[e]		65		10:1	6:1	43 (40)
				7:1		20 (18)[f]
4[e]		95		8:1	9:1	90 (85)
5[e]		85		10:1	8:1	80 (76)
6[e]		56		45:1	–	56 (50)[g]
7[e]		85		20:1	>99:1	79 (75)
8		85		17:1	>99:1	85 (84)

[a] Reaction conditions: substrate (1 mmol), $PdCl_2$ (0.01 mmol), NaOAc (0.2 mmol), 4-Å molecular sieves (0.2 g), DMA (5 mL), AcOH (0.2 mL), 6 atm of O_2, 40 h, 80 °C. [b] Ratio based on GC analysis of crude product. [c] Ratio based on ^{1}H NMR spectroscopic analysis of the crude product. [d] Yields of linear + branched allylic acetates were determined by GC analysis; values in parenthesis are yields of the isolated products. [e] Substrate (0.5 mmol). [f] $(E,E)/(E,Z)/(Z,Z) = 15:4:1$. [g] Mixture of 1-cyclohexene ethanol acetate/2-cyclohexylidene ethanol acetate (1:1).



Scheme 3. Proposed catalytic cycle. k_{cat} = rate of the reoxidation step, k_{dec} = rate of the decomposition.

can be expressed as follows: $R_0 = k_{cat}\ pO_2[Pd]_t$, $[Pd]_t = [Pd]_0/(1+[Pd]_0 k_{dec} t)$ (the values of k_{cat} and k_{dec} at 80 °C in DMA were determined to be 0.02 and $1.81\,\text{M}^{-1}\text{s}^{-1}$, respectively). The value of k_{cat}/k_{dec} was almost 2.3 times greater than that observed in DMF.[11] These observations clearly show that DMA promotes the reoxidation of the Pd^0 species by O_2 and simultaneously suppresses competing Pd^0 aggregation. It can be said that the use of DMA results in a unique catalytic system capable of performing the Wacker oxidation in the absence of a cocatalyst. With respect to the above acetoxylation, DMA might accelerate the reoxidation of Pd^0 species by O_2.

In conclusion, the combination of $PdCl_2$ and DMA allows highly effective oxygenation of terminal olefins under cocatalyst-free conditions. The use of a different nucleophile (H_2O or AcOH) can lead to a complete switch in regioselectivity between the C1 and C2 positions. The versatility demonstrated by this simple catalytic system holds significant promise for achieving new oxidation system using O_2 as a sole reoxidant.

Received: August 13, 2005
Published online: December 2, 2005

Keywords: acetoxylation · alkenes · oxygen · palladium · Wacker oxidation

[1] a) R. A. Sheldon, J. K. Kochi, *Metal-Catalyzed Oxidations of Organic Compounds*, Academic Press, New York, **1981**; b) M. Hudlucky, *Oxidations in Organic Chemistry*, American Chemical Society, Washington, DC, **1990** (ACS Monograph Series); c) P. T. Anastas, L. B. Bartlett, M. M. Kirchhoff, T. C. Williamson, *Catal. Today* **2000**, *55*, 11; d) *Modern Oxidation Methods* (Ed.: J. E. Bäckvall), Wiley-VCH, Weinheim, **2004**.

[2] a) B. Åkermark, K. Zetterberg, *Handbook of Organopalladium Chemistry for Organic Synthesis, Vol. 2* (Ed.: E. Negishi), Wiley, New York, **2002**, p. 1875; b) P. M. Henry, *Handbook of Organopalladium Chemistry for Organic Synthesis, Vol. 2* (Ed.: E. Negishi), Wiley, New York, **2002**, p. 2119; c) T. Hosokawa, S.-I. Murahashi, *Handbook of Organopalladium Chemistry for Organic Synthesis, Vol. 2* (Ed.: E. Negishi), Wiley, New York, **2002**, p. 2141; d) M. Takacs, X.-T. Jiang, *Current Org. Chem.* **2003**, *7*, 369; e) J. Tsuji, *Palladium Reagents and Catalysts*, Wiley, Chichester, **2004**; f) M. Beller, J. Seayad, A. Tillack, H. Jiao, *Angew. Chem.* **2004**, *116*, 3448; *Angew. Chem. Int. Ed.* **2004**, *43*, 3368.

[3] For example, a) J. Smidt, W. Hafner, R. Jira, J. Sedlmeier, R. Sieber, R. Rüttinger, K. Kojer, *Angew. Chem.* **1959**, *71*, 176; b) J. Smidt, W. Hafner, R. Jira, R. Sieber, J. Sedlmeier, A. Sabel, *Angew. Chem.* **1962**, *74*, 93; *Angew. Chem. Int. Ed.* **1962**, *1*, 80; c) H. Alper, K. Januszkiewicz, D. J. H. Smith, *Tetrahedron Lett.* **1985**, *26*, 2263; d) H. A. Zahalka, K. Januszkiewicz, H. Alper, *J. Mol. Catal.* **1986**, *35*, 249; e) A. Harada, Y. Hu, S. Takahashi, *Chem. Lett.* **1986**, 2083; f) T. Hosokawa, M. Takano, S.-I. Murahashi, *J. Am. Chem. Soc.* **1996**, *118*, 3990; g) K.-M. Choi, T. Mizugaki, K. Ebitani, K. Kaneda, *Chem. Lett.* **2003**, *32*, 180.

[4] a) E. Monflier, S. Tilloy, G. Fremy, Y. Barbaux, A. Mortreux, *Tetrahedron Lett.* **1995**, *36*, 387; b) T. Yokota, A. Sakakura, M. Tani, S. Sakaguchi, Y. Ishii, *Tetrahedron Lett.* **2002**, *43*, 8887.

[5] J. E. Bäckvall, R. B. Hopkins, H. Grennberg, M. M. Mader, A. K. Awasthi, *J. Am. Chem. Soc.* **1990**, *112*, 5160.

[6] The Wacker oxidation using O_2 with propan-2-ol as a reducing reagent: a) T. Nishimura, N. Kakiuchi, T. Onoue, K. Ohe, S. Uemura, *J. Chem. Soc. Perkin Trans. 1* **2000**, *12*, 1915; with THF as a cosolvent; b) C. N. Cornell, M. S. Sigman, *J. Am. Chem. Soc.* **2005**, *127*, 2796.

[7] S. S. Stahl, *Angew. Chem.* **2004**, *116*, 3480; *Angew. Chem. Int. Ed.* **2004**, *43*, 3400.

[8] Examples of Pd-catalyzed Wacker oxidations using O_2 as a sole reoxidant without cocatalyst: a) M. Higuchi, S. Yamaguchi, T. Hirao, *Synlett* **1996**, 1213; b) G.-J. ten Brink, I. W. C. E. Arends, G. Papadogianakis, R. A. Sheldon, *Chem. Commun.* **1998**, 2359.

[9] Examples of Pd-catalyzed Wacker-type intramolecular cyclizations using molecular oxygen as a sole reoxidant without a cocatalyst: a) H. Hiemstra, J. J. Michels, W. N. Speckamp, *J. Chem. Soc. Chem. Commun.* **1994**, 357; b) R. M. Trend, Y. K. Ramtohul, E. M. Ferreira, B. M. Stoltz, *Angew. Chem.* **2003**, *115*, 2998; *Angew. Chem. Int. Ed.* **2003**, *42*, 2892; c) K. Muòiz, *Adv. Synth. Catal.* **2004**, *346*, 1425; d) G. Zeni, R. C. Larock, *Chem. Rev.* **2004**, *104*, 2285.

[10] In our experiment, the $Pd(OAc)_2$–DMSO system, which was effective for an intramolecular Wacker-type cyclization and

 © 2006 Wiley-VCH Verlag GmbH & Co. KGaA, Weinheim

acetoxylation, failed to promote the Wacker oxidation of 1-decene (< 1 % yield in 6 h).
[11] See the Supporting Information for the experimental details.
[12] For example, see: I. Horvath, J. Rabai, *Science* **1994**, *266*, 72.
[13] T. Welton, *Chem. Rev.* **1999**, *99*, 2071.
[14] There has been only one report of the selective synthesis of linear allylic acetates from terminal olefins: M. S. Chen, M. C. White, *J. Am. Chem. Soc.* **2004**, *126*, 1346; however, we confirmed that the acetoxylation of 1-eicosene hardly occurred with the above catalytic system.
[15] Selective synthesis of branched allylic acetates from terminal olefins: M. S. Chen, N. Prabagaran, N. A. Labenz, M. C. White, *J. Am. Chem. Soc.* **2005**, *127*, 6970.
[16] R. C. Larock, *Comprehensive Organic Transformations*, 2nd ed, Wiley, New York, **1999**.
[17] F. Freeman, P. J. Cameron, R. H. Dubois, *J. Org. Chem.* **1968**, *33*, 3970.
[18] J. Pytkowicz, S. Roland, P. Mangeney, G. Meyer, A. Jutand, *J. Organomet. Chem.* **2003**, *678*, 166.
[19] B. A. Steinhoff, S. R. Fix, S. S. Stahl, *J. Am. Chem. Soc.* **2002**, *124*, 766.

 © 2006 Wiley-VCH Verlag GmbH & Co. KGaA, Weinheim

Cleavage Reactions

DOI: 10.1002/anie.200503267

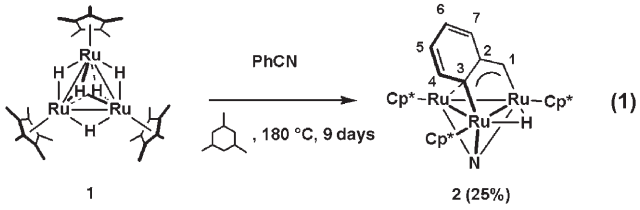
Cleavage of the C≡N Bond on a Triruthenium Cluster: Synthesis and Structure of a Triruthenium Complex Containing a μ_3-Nitrido Ligand**

*Takashi Kawashima, Toshiro Takao, and Hiroharu Suzuki**

Since a nitrile group contains an sp hybridized nitrogen atom as well as dinitrogen, cleavage of the C≡N bond of nitrile is regarded as an analogue of N≡N bond activation of dinitrogen. The nitrogenase enzyme was shown to catalyze reductive cleavage of the C≡N bond of nitrile.[1] Carbon–nitrogen bond cleavage of nitrile by using the dimolybdenum sulfido complex $[(CpMo)_2(S_2CH_2)(\mu\text{-}S)(\mu\text{-}SH)]^+$ ($Cp = \eta^5\text{-}C_5H_5$) under a dihydrogen atmosphere was demonstrated by Rakowski DuBois and co-workers.[2] Heterolytic cleavage of dihydrogen by the sulfido complex was proposed as a prerequisite for further C–N bond cleavage. In general, the electronic property of the hydrido ligand continuously changes from "protonic" to "hydridic" depending upon whether it is combined with a metal center, thus the polyhydrido cluster effectively cleaves the C≡N bond of nitrile. We report herein cleavage of the C≡N bond of nitrile in the reaction of a triruthenium hydrido complex.

Transformation of a nitrile ligand on a triiron framework has been elucidated in the pioneering studies performed by Kaesz and co-workers.[3] They showed step-wise reduction of a μ_3-nitrile ligand to give a μ_3-imido ligand through formation of a μ_3-alkylideneamido complex upon treatment with dihydrogen. In spite of several studies with trimetallic carbonyl clusters of iron,[3,4] ruthenium,[5] and osmium,[6] C≡N bond cleavage has never been observed.

A μ_3-nitrido-μ_3-allyl complex, $[(Cp^*Ru)_3(\mu_3\text{-}N)(\mu_3\text{-}\eta^1{:}\eta^3{:}\eta^1\text{-}CHC_6H_4)(\mu\text{-}H)]$ (**2**; $Cp^* = \eta^5\text{-}C_5Me_5$), was isolated from the reaction of **1** with equimolar benzonitrile at 180 °C in 25 % yield [Eq. (1)].[7] The μ_3-nitrido ligand of **2** was formed



1 2 (25%) (1)

as a result of C≡N bond cleavage of benzonitrile. While there have been numerous examples of the C≡N bond cleavage of nitrile by way of hydration,[8] C≡N bond scission to form a metal nitride is rare.[9] To the best of our knowledge, this is the first example of C≡N bond cleavage performed on a trimetallic complex to form a μ_3-nitrido ligand.

The molecular structure of **2** was determined by an X-ray diffraction study (Figure 1).[10] Although distinction between a μ_3-nitrido and a μ_3-imido ligand only on the basis of the X-ray diffraction study is difficult, the diamagnetic property of **2** rules out the presence of a μ_3-NH group in **2**; an ^{1}H NMR signal of the hydrido ligand was observed at $\delta = -23.02$ ppm.

This is the first example of a μ_3-nitrido cluster complex for late transition metals, while several cubane-type complexes are known.[11] Structural parameters of **2** were quite similiar to those of isoelectronic and isostructural μ_3-methylidyne analogue, $[(Cp^*Ru)_3(\mu_3\text{-}CH)(\mu_3\text{-}\eta^1{:}\eta^3{:}\eta^1\text{-}CHCMeCH)(\mu\text{-}H)]$ (**3**).[12] This implies that the μ_3-nitrido ligand adopts an sp^3 configuration. In the case that the μ_3-N ligand is a three-electron donor, complex **2** becomes diamagnetic and satisfies the 48-electron configuration. The Ru–N bond lengths (Ru(1)–N(1) = 2.037(5) Å, Ru(2)–N(1) = 1.922(6) Å, and Ru(3)–N(1) = 1.942(6) Å) are similar to those found for the μ_3-imido complexes, $[\{Cp^*Ru(\mu\text{-}H)\}_3(\mu_3\text{-}NR)]$ and $[(Cp^*Ru)_3(\mu_3\text{-}NR)(\mu_3\text{-}NR')(\mu\text{-}H)]$.[13]

As we reported recently, the reaction of **1** with benzonitrile at room temperature afforded a perpendicularly coordinated nitrile complex, $[(Cp^*Ru)_3(\mu_3\text{-}\eta^2{:}\eta^2(\perp)\text{-}PhCN)(\mu_3\text{-}H)(\mu\text{-}H)_2]$ (**4**), exclusively [Eq. (2)].[14] Thus, it seems reasonable

[*] T. Kawashima, T. Takao, Prof. H. Suzuki
Department of Applied Chemistry
Graduate School of Science and Engineering
Tokyo Institute of Technology
O-okayama, Meguro-ku, Tokyo 152-8552 (Japan)
Fax: (+81) 3-5734-3913
E-mail: hiroharu@n.cc.titech.ac.jp

[**] This work was partially supported by Grant-in-Aid for Scientific Research on Priority Areas (Grant Nos. 15205009 and 14078101, "Reaction Control of Dynamic Complexes") and the 21st Century COE program from the Ministry of Education, Culture, Sports, Science, and Technology, Japan. We acknowledge Kanto Chemical for generous gifts of pentamethylcyclopentadiene.

Supporting information for this article is available on the WWW under http://www.angewandte.org or from the author.

 © 2006 Wiley-VCH Verlag GmbH & Co. KGaA, Weinheim

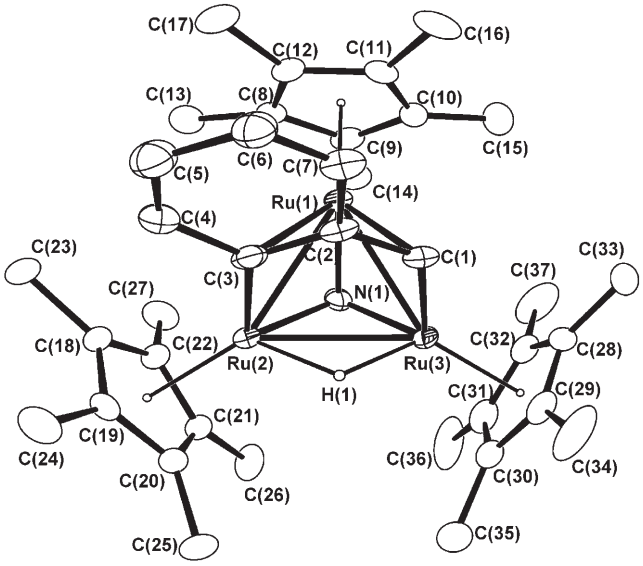
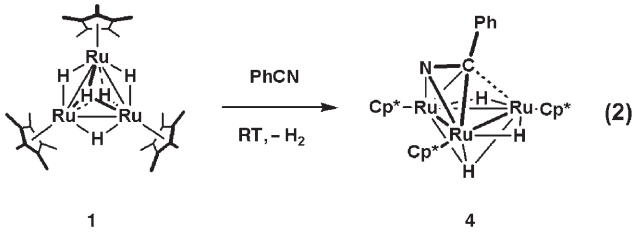


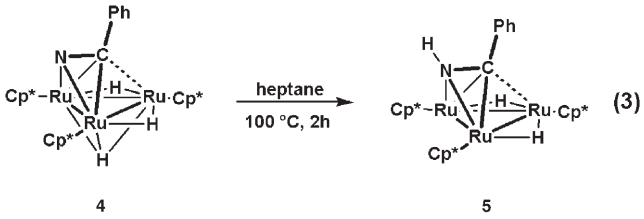
Figure 1. Molecular structure and labeling scheme of **2** with thermal ellipsoids at the 30% level of probability. Selected bond lengths [Å] and angles [°]: Ru(1)–Ru(2) 2.6660(8), Ru(2)–Ru(3) 2.7432(8), Ru(1)–Ru(3) 2.6623(7), Ru(1)–N(1) 2.037(5), Ru(2)–N(1) 1.922(6), Ru(3)–N(1) 1.942(6), Ru(1)–C(1) 2.185(7), Ru(1)–C(2) 2.266(7), Ru(1)–C(3) 2.266(7), Ru(2)–C(3) 2.045(8), Ru(3)–C(1) 1.982(7), C(1)–C(2) 1.402(10), C(2)–C(3) 1.446(11), C(3)–C(4) 1.446(10), C(4)–C(5) 1.365(11), C(5)–C(6) 1.432(12), C(6)–C(7) 1.319(11), C(2)–C(7) 1.475(10); Ru(2)-Ru(1)-Ru(3) 61.97(2), Ru(1)-Ru(2)-Ru(3) 58.95(2), Ru(1)-Ru(3)-Ru(2) 59.08(2), Ru(1)-N(1)-Ru(2) 84.6(2), Ru(2)-N(1)-Ru(3) 90.4(3), Ru(1)-N(1)-Ru(3) 83.9(2), Ru(2)-C(3)-C(2) 123.2(5), Ru(3)-C(1)-C(2) 126.0(6), C(1)-C(2)-C(3) 118.5(6).



(2)

to suppose that the C≡N bond cleavage proceeds through the formation of **4**. In complex **4**, bonding interaction between metal centers and *ortho* protons at the phenyl group was negligible, which clearly indicates that orthometalation is not prerequisite for the C–N bond cleavage. Perpendicular coordination of benzonitrile seems to be rather important as shown below.

Thermolysis of **4** at 180 °C afforded complex **2**. In addition, when the reaction was carried out at a lower temperature, another intermediate for the C≡N bond cleavage was observed. Thermolysis of **4** at 100 °C in heptane resulted in the quantitative formation of a perpendicularly coordinated μ_3-iminoacyl complex, $[(Cp^*Ru)_3(\mu_3\text{-}\eta^2\text{:}\eta^2(\perp)\text{-}PhCNH)(\mu\text{-}H)_2]$ (**5**) [Eq. (3)].[15] The structure of **5** is comparable to that of the cationic μ_3-iminoacyl complex, $[(Cp^*Ru)_3(\mu_3\text{-}\eta^2\text{:}\eta^2(\perp)\text{-}PhCNH)(\mu\text{-}H)_2(\mu_3\text{-}H)][BF_4]$ (**6**), obtained by the protonation of **4**.[14] Complex **5** is soluble in nonpolar solvents, whereas cationic **6** is not.



(3)

The free nitrogen lone-pair in **4** remains uncoordinated and can be readily protonated to give **6**. Thus, the formation of the μ_3-iminoacyl ligand of **5** can be understood in terms of electrophilic migration of a hydrido ligand to the nitrogen atom. The rate of the reaction, however, is comparable to that carried out in THF, which implies that the rate-determining step for the transformation from **4** into **5** is the intramolecular hydrido shift to the nitrogen atom.

A broad signal for the newly formed N–H bond of **5** was observed in the ^{1}H NMR spectrum of the product at $\delta =$ 11.24 ppm. This signal immediately disappeared on addition of CD_3OD, which reveals the protonic character of the hydrogen bound at the iminoacyl group. In the ^{13}C NMR spectrum of **5**, a singlet stemming from the iminoacyl carbon was observed upfield ($\delta = 96.0$ ppm) in comparison to the triply bridging carbon atom of a μ_3-alkylidyne or a μ_3-acetylide ligand, and the chemical shift of $\delta = 96.0$ ppm is comparable to that of the $\mu_3(\perp)$-nitrile carbon of **4** ($\delta =$ 97.8 ppm).[14]

The signal that arises from two hydrido ligands of **5** appears at $\delta = -7.89$ ppm as a singlet in the ^{1}H NMR spectrum. The shape of this signal remains unchanged over the temperature range from −20 to 50 °C. In contrast, signals for the Cp* groups observed at $\delta = 1.77$ and 1.90 ppm at −10 °C coalesce into one signal at 35 °C, which shows that the μ_3-iminoacyl ligand of **5** exhibits dynamic behavior similar to that of the μ_3-nitrile ligand of **4**. This dynamic behavior is rationalized by the switchback motion of the μ_3-iminoacyl ligand, which has been already reported for **4**[14] and the ($\perp$)-alkyne complexes.[16] The activation parameters for this motion are estimated to be $\Delta H^{\ddagger} = 16.4 \pm 0.2$ kcal mol^{-1} and $\Delta S^{\ddagger} = 2.9 \pm 0.7$ cal mol^{-1} K^{-1} on the basis of the variable-temperature NMR studies (see Supporting Information).

The presence of perpendicular coordination of the μ_3-iminoacyl ligand was established by X-ray diffraction studies of **5** on a single red crystal obtained from cold diethyl ether (see Figure 2).[10] The carbon–nitrogen bond was arranged on the crystallographic mirror plane bisecting the Ru_3 triangle, and the nitrogen atom was oriented outside the Ru_3 core. The C(1)–N(1) bond of 1.391(6) Å is longer than in **4** (1.358(6) Å)[14] and represents an intermediate value between that of a carbon–nitrogen single bond (1.45 Å) and carbon–nitrogen double bond (1.28 Å). This value lies in the range of the C–N bond lengths reported for the trimetallic μ_3-iminoacyl complexes that contain an acyclic RNCR′ ligand coordinated parallel to one of the M–M bonds (1.280–1.412 Å).[3c,6b17]

Conversely, the Ru(1)–C(1) bond (2.010(5) Å) is significantly shorter than in **4** (2.124(5) Å).[14] These structural features, namely, the long C–N bond and the short Ru–C

 © 2006 Wiley-VCH Verlag GmbH & Co. KGaA, Weinheim

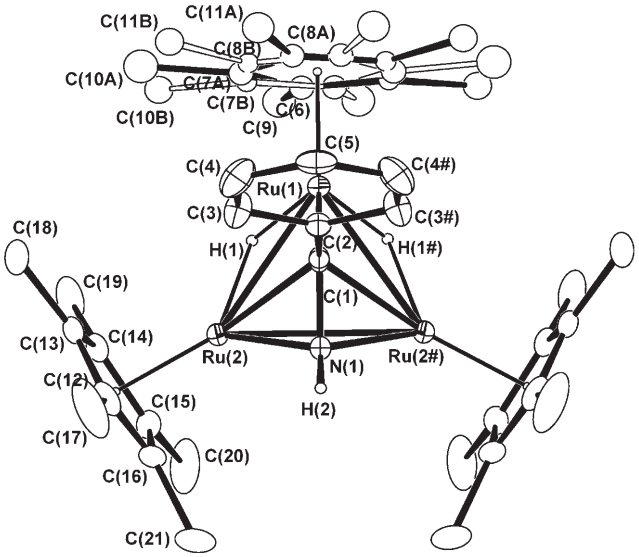
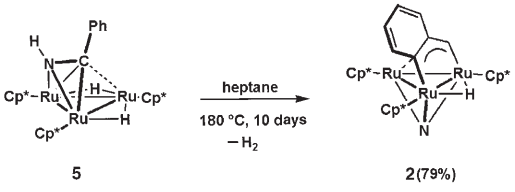


Figure 2. Molecular structure and labeling scheme of **5** with thermal ellipsoids at the 30% level of probability. Selected bond lengths [Å] and angles [°]: Ru(1)–Ru(2) 2.7790(7), Ru(2)–Ru(2#) 3.0826(11), Ru(2)–N(1) 2.017(3), Ru(1)–C(1) 2.010(5), Ru(2)–C(1) 2.369(4), N(1)–C(1) 1.391(6); Ru(2)-Ru(1)-Ru(2#) 67.375(8), Ru(1)-Ru(2)-Ru(2#) 56.314(12), Ru(2)-N(1)-Ru(2#) 99.68(19), Ru(2)-C(1)-Ru(2#) 81.17(15), Ru(1)-C(1)-N(1) 120.5(4), Ru(1)-C(1)-C(2) 124.2(3), N(1)-C(1)-C(2) 115.4(4).

bond, indicate strong back-donation from the ruthenium centers to the π*(CN) orbital, and the C–N bond is liable to be cleaved by thermolysis as a result of the strong back-donation. In contrast, structural parameters of the cationic μ_3-iminoacyl complex **6** were similar to those of **4**,[14] and the C–N bond of the μ_3-iminoacyl ligand of **6** is not cleaved by thermolysis.

Migration of a hydride to the nitrile ligand lowers the bond order of the C–N bond. At the same time, it causes an increase in the electron density at the ruthenium centers. The carbon–nitrogen multiple bond scission on the hydrido cluster arises from such ambivalent roles of the hydrido ligand.

The μ_3-nitrido complex **2** was irreversibly formed in 79% yield by the thermolysis of **5** at 180 °C [Eq. (4)]. One plausible



5 2(79%) (4)

mechanism for the carbon–nitrogen bond cleavage is the "edge" pathway, which was proposed for the carbon–carbon bond scission of a perpendicularly coordinated alkyne ligand.[18] Such perpendicular coordination seems to be effective for back-donation from metal centers to the π*(CN) orbital. In the reaction of the ditungsten complex $[W_2(OCMe_2CF_3)_6]$ with nitrile, an intermediate with a perpendicularly coordinated nitrile ligand to the W–W bond has been proposed for the formation of a nitrido complex by Chisholm and co-workers.[9d] Hidai and co-workers elucidated that strong π donation from a low-valent metal center enhances nucleophilicity of the cyano carbon atom, which causes double protonation at this atom leading to C≡N bond scission.[9e–g]

These sequential transformations from **4** into **2** provide mechanistic insight into the reductive cleavage of a carbon–nitrogen multiple bond on a polyhydrido cluster. The ambivalent nature of the hydrido ligand is essential for the activation of the substrate. The importance of the heterolytic activation of dihydrogen to generate a proton has been also noted by Rakowski DuBois and co-workers in the C≡N bond cleavage by the dimolybdenum sulfido complex.[2]

In summary, μ_3-η^2:η^2(⊥)-iminoacyl complex **5** was formed upon thermolysis of the μ_3-η^2:η^2(⊥)-nitrile complex **4**. Migration of a hydrido ligand to the nitrogen atom causes elongation of the carbon–nitrogen bond as well as shortening of the ruthenium–carbon bond, which facilitates the carbon–nitrogen bond cleavage leading to the formation of **2**. We are currently investigating skeletal rearrangement of the μ_3-(⊥)-nitrile ligand on the Ru_3 plane in the presence of dihydrogen in relation to hydrogenation of the C≡N bond.

Received: September 15, 2005
Published online: December 2, 2005

Keywords: cleavage reactions · cluster compounds · nitrides · ruthenium

[1] B. K. Burgess in *Molybdenum Enzymes* (Ed.: T. G. Spiro), Wiley, New York, **1985**, chap. 4.
[2] a) D. E. Coons, J. C. V. Laurie, R. C. Haltiwanger, M. Rakowski DuBois, *J. Am. Chem. Soc.* **1987**, *109*, 283; b) P. Bernatis, J. C. V. Laurie, M. Rakowski DuBois, *Organometallics* **1990**, *9*, 1607.
[3] a) M. A. Andrews, H. D. Kaesz, *J. Am. Chem. Soc.* **1977**, *99*, 6763; b) M. A. Andrews, H. D. Kaesz, *J. Am. Chem. Soc.* **1979**, *101*, 7238; c) M. A. Andrews, G. Buskirk, C. B. Knobler, H. D. Kaesz, *J. Am. Chem. Soc.* **1979**, *101*, 7245; d) M. A. Andrews, H. D. Kaesz, *J. Am. Chem. Soc.* **1979**, *101*, 7255; e) M. A. Andrews, H. D. Kaesz, *J. Am. Chem. Soc.* **1979**, *101*, 7260.
[4] a) E. Keller, D. Wolters, *Chem. Ber.* **1984**, *117*, 1572; b) P. Suter, H. Vahrenkamp, *Chem. Ber.* **1995**, *128*, 793.
[5] a) W. Bernhardt, H. Vahrenkamp, *Angew. Chem.* **1984**, *96*, 362; *Angew. Chem. Int. Ed. Engl.* **1984**, *23*, 381; b) W. Berhardt, C. Schnering, H. Vahrenkamp, *Angew. Chem.* **1986**, *98*, 285; *Angew. Chem. Int. Ed. Engl.* **1986**, *25*, 279; c) P. M. Lausarot, G. A. Vaglio, M. Valle, A. Tiripicchio, M. T. Camellini, *J. Chem. Soc. Chem. Commun.* **1983**, 1391; d) P. M. Lausarot, M. Turini, G. A. Vaglio, M. Valle, A. Tiripicchio, M. T. Camellini, *J. Organomet. Chem.* **1984**, *273*, 239; e) P. M. Lausarot, L. Operti, G. A. Vaglio, M. Valle, *Inorg. Chim. Acta* **1986**, *122*, 103.
[6] a) R. D. Adams, D. A. Katahira, L. Yang, *J. Organomet. Chem.* **1981**, *219*, 85; b) Z. Dawoodi, M. J. Mays, P. R. Raithby, *J. Organomet. Chem.* **1981**, *219*, 103; c) Z. Dawoodi, M. J. Mays, A. G. Orpen, *J. Organomet. Chem.* **1981**, *219*, 251; d) Z. Dawoodi, M. J. Mays, K. Henrick, *J. Chem. Soc. Dalton Trans.* **1984**, 433; e) J. Banford, M. J. Mays, P. R. Raithby, *J. Chem. Soc. Dalton Trans.* **1985**, 1355; f) P. M. Lausarot, G. A. Vaglio, M.

 © 2006 Wiley-VCH Verlag GmbH & Co. KGaA, Weinheim

Valle, A. Tiripicchio, M. T. Camellini, P. Gariboldi, *J. Organomet. Chem.* **1985**, *291*, 221.

[7] A 50 mL glass autoclave was charged with 1,3,5-trimethylcyclohexane (3 mL), benzonitrile (6.8 μL, 0.067 mmol), and **1** (47.6 mg, 0.068 mmol). The reaction mixture was then stirred at 180 °C for 9 days, during which, the solution changed from brown to brownish-yellow. The solvent was removed under reduced pressure and the residual solid was purified by column chromatography on alumina (Merck, Art. No. 1097) with tetrahydrofuran/methanol 1:1. A third brownish-yellow band which included **2** was collected, and the solvent was removed under reduced pressure. Complex **2** was obtained as an ocher solid (13.3 mg, 25% yield). NMR data for **2**: ^{1}H NMR (400 MHz, [D$_6$]benzene, 23 °C, TMS): $\delta = -23.02$ (s, 1H; Ru-H), 1.33 (s, 15H; Cp*), 1.89 (s, 15H; Cp*), 1.94 (s, 15H; Cp*), 6.82 (dd, ^3J(H,H) = 8.8, 6.0 Hz, 1H; C5-H or C6-H), 7.09 (dd, ^3J(H,H) = 8.0, 6.4 Hz, 1H; C5-H or C6-H), 7.27 (d, ^3J(H,H) = 8.4 Hz, 1H; C4-H or C7-H), 7.59 (d, ^3J(H,H) = 8.4 Hz, 1H; C4-H or C7-H), 9.28 ppm (s, 1H; C1-H). ^{13}C NMR (100 MHz, [D$_6$]benzene, 23 °C): $\delta = 10.2$ (q, ^1J(C,H) = 128.0 Hz; C$_5$*Me*$_5$), 11.5 (q, ^1J(C,H) = 127.1 Hz; C$_5$*Me*$_5$), 11.6 (q, ^1J(C,H) = 127.1 Hz; C$_5$*Me*$_5$), 95.7 (s; *C*$_5$Me$_5$), 99.3 (s; *C*$_5$Me$_5$), 99.5 (s; *C*$_5$Me$_5$), 112.8 (s; C2), 119.4 (d, ^1J(C,H) = 157.6 Hz; C5 or C6), 129.5 (d, ^1J(C,H) = 151.8 Hz; C5 or C6), 131.9 (d, ^1J(C,H) = 160.0 Hz; C4 or C7), 149.1 (d, ^1J(C,H) = 158.8 Hz; C4 or C7), 166.5 (s; C3), 187.4 ppm (d, ^1J(C,H) = 147.7 Hz; C1).

[8] a) S. Murahashi, H. Takaya, *Acc. Chem. Res.* **2000**, *33*, 225; b) V. Yu. Kukushkin, A. J. L. Pombeiro, *Chem. Rev.* **2002**, *102*, 1771.

[9] a) R. R. Schrock, M. L. Listemann, L. G. Sturgeoff, *J. Am. Chem. Soc.* **1982**, *104*, 4291; b) J. H. Freudenberger, R. R. Schrock, *Organometallics* **1986**, *5*, 398; c) M. H. Chisholm, K. Folting-Streib, D. B. Tiedtke, F. Lemoigno, O. Eisenstein, *Angew. Chem.* **1995**, *107*, 61; *Angew. Chem. Int. Ed. Engl.* **1995**, *34*, 110; d) M. H. Chisholm, K. Folting, M. L. Lynn, D. B. Tiedtke, F. Lemoigno, O. Eisenstein, *Chem. Eur. J.* **1999**, *5*, 2318; e) H. Seino, Y. Tanabe, Y. Ishii, M. Hidai, *Inorg. Chim. Acta* **1998**, *280*, 163; f) Y. Tanabe, H. Seino, Y. Ishii, M. Hidai, *J. Am. Chem. Soc.* **2000**, *122*, 1690; g) H. Seino, Y. Mizobe, M. Hidai, *Chem. Rec.* **2001**, *1*, 349.

[10] X-ray Crystallography: All data were collected on a Rigaku R-AXIS RAPID imaging plate diffractometer with graphite-monochromated Mo$_{K\alpha}$ radiation ($\lambda = 0.71069$ Å) at 153 K (for **2**) and 123 K (for **5**). Cell refinement and data reduction were performed by using the Process-Auto program. The structures were solved by the Patterson method (Shelx-97) and refined by least-squares methods based on F^2 (Shelxl-97). Crystal data for **2**·0.5 C$_4$H$_{10}$O: empirical formula $C_{39}H_{56}NO_{0.5}Ru_3$, $M_r = 850.06$, crystal size 0.22 × 0.13 × 0.01 mm, space group $P2_1/c$ (No. 14), $a = 10.8725(13)$, $b = 31.844(4)$, $c = 20.632(3)$ Å, $\beta = 101.705(5)°$, $V = 6994.6(14)$ Å^3, $Z = 8$, $\rho_{calcd} = 1.614$ Mg m^{-3}, $\mu(Mo_{K\alpha}) = 1.308$ mm^{-1}, $2\theta_{max} = 60.0°$. Of the 76184 reflections that were collected, 20658 were unique ($R_{int} = 0.0953$), $R_1 = 0.0715$ [$I > 2\sigma(I)$], $wR_2 = 0.1558$ [$I > 2\sigma(I)$], max./min. residual electron densities 1.994/−3.047 e Å^{-3}. Crystal data for **5**: empirical formula $C_{37}H_{53}NRu_3$, $M_r = 815.04$, crystal size 0.15 × 0.15 × 0.01 mm, space group *C*2/*m* (No. 12), $a = 17.167(5)$, $b = 18.424(6)$, $c = 11.378(4)$ Å, $\beta = 104.813(13)°$, $V = 3479.2(19)$ Å^3, $Z = 4$, $\rho_{calcd} = 1.556$ Mg m^{-3}, $\mu(Mo_{K\alpha}) = 1.310$ mm^{-1}, $2\theta_{max} = 60.0°$. Of the 20761 reflections that were collected, 5197 were unique ($R_{int} = 0.0531$), $R_1 = 0.0437$ [$I > 2\sigma(I)$], $wR_2 = 0.1060$ [$I > 2\sigma(I)$], max./min. residual electron densities 1.210/−1.610 e Å^{-3}. CCDC-278456 (**2**) and CCDC-283543 (**5**) contain the supplementary crystallographic data for this paper. These data can be obtained free of charge from The Cambridge Crystallographic Data Centre via www.ccdc.cam.ac.uk/data_request/cif.

[11] a) H. W. Roesky, Y. Bai, M. Noltemeyer, *Angew. Chem.* **1989**, *101*, 788; *Angew. Chem. Int. Ed. Engl.* **1989**, *28*, 754; b) P. Gómez-Sal, A. Martin, M. Mena, C. Yélamos, *J. Chem. Soc. Chem. Commun.* **1995**, 2185; c) C. D. Abernethy, F. Bottomley, A. Decken, T. S. Cameron, *Organometallics* **1996**, *15*, 1758; d) G. Bai, D. Vidovic, H. W. Roesky, J. Magull, *Polyhedron* **2004**, *23*, 1125.

[12] A. Inagaki, T. Takao, M. Moriya, H. Suzuki, *Organometallics* **2003**, *22*, 2196.

[13] a) Y. Nakajima, H. Suzuki, *Organometallics* **2003**, *22*, 959; b) Y. Nakajima, A. Inagaki, H. Suzuki, *Organometallics* **2004**, *23*, 4040; c) Y. Nakajima, H. Suzuki, *Organometallics* **2005**, *24*, 1860.

[14] T. Takao, T. Kawashima, K. Matsubara, H. Suzuki, *Organometallics* **2005**, *24*, 3371.

[15] A 20 mL glass tube equipped with a greaseless valve was charged with heptane (10 mL) and **4** (57.2 mg, 0.070 mmol). The reaction mixture was stirred at 100 °C for 2 h, during which, the solution turned from brownish-yellow to brown. The solvent was removed under reduced pressure and complex **5** was obtained as a brown solid (52.3 mg, quantitative). NMR data for **5**: ^{1}H NMR (400 MHz, [D$_6$]benzene, 23 °C, TMS): $\delta = -7.89$ (s, 2H; Ru-H), 1.77 (brs, $w_{1/2} = 9.3$ Hz, 30H; Cp*), 1.90 (brs, $w_{1/2} = 21.6$ Hz, 15H; Cp*), 6.39 (d, ^3J(H,H) = 8.4 Hz, 2H; *o*-Ph), 6.63 (t, ^3J(H,H) = 8.0 Hz, 2H; *m*-Ph), 6.79 (t, ^3J(H,H) = 8.0 Hz, 1H; *p*-Ph), 11.24 ppm (brs, $w_{1/2} = 9.5$ Hz, 1H; N-H). ^{13}C NMR (100 MHz, [D$_6$]benzene, 23 °C): $\delta = 12.2$ (brq, $w_{1/2} = 18.4$ Hz; C$_5$*Me*$_5$), 12.6 (brq, $w_{1/2} = 12.7$ Hz; C$_5$*Me*$_5$), 80.0 (brs, $w_{1/2} = 8.6$ Hz; *C*$_5$Me$_5$), 90.6 (brs, $w_{1/2} = 10.0$ Hz; *C*$_5$Me$_5$), 96.0 (s; CN), 125.9 (Ph), 126.7 (Ph), 131.9 (Ph), 151.9 ppm (s; *ipso*-Ph).

[16] T. Takao, Y. Takaya, E. Murotani, R. Tenjimbayashi, H. Suzuki, *Organometallics* **2004**, *23*, 6090.

[17] a) R. D. Adams, N. M. Golembeski, *J. Am. Chem. Soc.* **1979**, *101*, 2579; b) Z. Dawoodi, M. J. Mays, P. R. Raithby, *J. Organomet. Chem.* **1981**, *219*, 103; c) M. I. Bruce, B. K. Nicholson, *J. Organomet. Chem.* **1983**, *250*, 627; d) A. Basu, S. Bhaduri, K. Sharma, P. G. Jones, *J. Chem. Soc. Chem. Commun.* **1987**, 1126; e) S. Aime, R. Gobetto, F. Padovan, M. Botta, E. Rosenberg, R. W. Gellert, *Organometallics* **1987**, *6*, 2074; f) T. Beringhelli, G. D'Alfonso, A. Minoja, G. Ciani, M. Moret, A. Sironi, *Organometallics* **1991**, *10*, 3131; g) M. Day, D. Espitia, K. I. Hardcastle, S. E. Kabir, E. Rosenberg, R. Gobetto, L. Milone, D. Osella, *Organometallics* **1991**, *10*, 3550; h) C. P. Casey, R. A. Widenhoefer, S. L. Hallenbeck, J. A. Gavney, Jr., *J. Chem. Soc. Chem. Commun.* **1993**, 1692; i) C. P. Casey, R. A. Widenhoefer, S. L. Hallenbeck, R. K. Hayashi, J. A. Gavney, Jr., *Organometallics* **1994**, *13*, 4720; j) W. Imhof, *J. Chem. Soc. Dalton Trans.* **1996**, 1429; k) E. Rosenberg, L. Millone, R. Gobetto, D. Osella, K. Hardcastle, S. Hajela, K. Moizeau, M. Day, E. Wolf, D. Espitia, *Organometallics* **1997**, *16*, 2665; l) D.-L. Wang, W.-S. Hwang, L. Lee, M. Y. Chiang, *J. Organomet. Chem.* **1999**, *579*, 211.

[18] A. D. Clauss, J. R. Shapley, C. N. Wilker, R. Hoffmann, *Organometallics* **1984**, *3*, 619.

 © 2006 Wiley-VCH Verlag GmbH & Co. KGaA, Weinheim

Synthesis Design

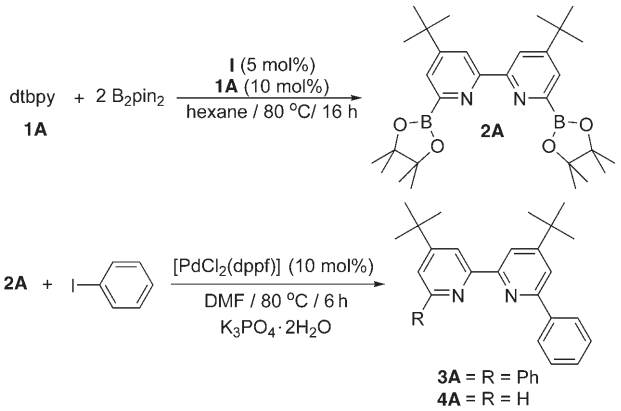
DOI: 10.1002/anie.200503047

Ir-Catalyzed Borylation of C–H Bonds in N-Containing Heterocycles: Regioselectivity in the Synthesis of Heteroaryl Boronate Esters**

*Ibraheem A. I. Mkhalid, David N. Coventry, David Albesa-Jove, Andrei S. Batsanov, Judith A. K. Howard, Robin N. Perutz, and Todd B. Marder**

Aryl and heteroaryl boronates are very important, especially as intermediates for Suzuki–Miyaura cross-coupling reactions;[1] for the Cu-catalyzed C–O and C–N coupling reactions developed by Chan, Lam, and co-workers;[2] and for Rh-catalyzed conjugate additions to carbonyl compounds.[3] The most attractive potential synthesis of these boronate esters would be the direct borylation of C–H bonds in arenes or heteroarenes themselves. A very exciting recent advance has been the development by Ishiyama et al.[4] and Smith and co-workers[5] of in situ prepared, suitably ligated analogues of the iridium tris(boryl) complexes discovered by us,[6] which catalyze the borylation of aromatic C–H bonds under mild conditions. Density functional theory (DFT) calculations by Sakaki and co-workers,[7] in agreement with proposals from the experimental data, suggest that the key catalytic intermediate that leads to C–H activation is the sterically encumbered, five-coordinate $[Ir(Bpin)_3L_2]$ species (Bpin = $B(OCMe_2CMe_2O)$). This intermediate accounts for the selectivity observed, as borylation typically avoids positions *ortho* to either substituents or to ring junctions. We have taken advantage of this selectivity to prepare novel pyrene-2,6-bis(boronate) and perylene-2,5,8,11-tetra(boronate) esters amongst other polycyclic aryl boronates.[8] During the course of our studies on the system developed by Ishiyama et al. (L_2 = 4,4′-*t*Bu_2-2,2′-bipyridine (dtbpy; **1A**)), we were intrigued that GC–MS analysis of the borylation reaction mixtures in situ did not show any borylation of the ligand **1A**, although **1A** could be detected by itself. We envisaged three possible reasons for this: 1) **1A** is firmly attached to the Ir center through the nitrogen atoms at all times; 2) it is simply not a suitable substrate for the catalyst, even if it were to dissociate; or 3) we would be unable to detect borylated **1A** by using our GC–MS method. We noted that pyridine itself is a "poor" substrate for the borylation reaction,[9,10] whereas pyrrole and quinoline are readily borylated;[11] however, 2,6-chloropyridine and 2,6-dimethylpyridine were effectively borylated at the 4-position,[5,12] and 5-bromo-2-cyanopyridine was borylated at the 3- and 4-positions in a 2:1 ratio.[13]

To investigate the question of the borylation of **1A** further, rather than add a stoichiometric amount of **1A** with respect to the Ir center, 20 equivalents of the ligand and 40 equivalents of bis(pinacolato-*O*,*O*′)diboron (B_2pin_2) in hexane (5 mL) were added to $[Ir(cod)(\mu\text{-OMe})]_2$ **I** (cod = cyclooctadiene). GC–MS analysis of the reaction mixture in situ after heating at 80 °C for 16 h showed borylation of **1A** was complete (100 % conversion) and gave rise to a single isomer, which ^1H, ^{13}C, and 2D NMR spectroscopic experiments indicated to be 4,4′-*t*Bu_2-6,6′-$(Bpin)_2$-2,2′-bipyridine (**2A**) with the boryl group on the carbon atom adjacent to the nitrogen atom (Scheme 1). Removal of the solvent in vacuo



Scheme 1. Borylation of **1A**.

followed by addition of 3 equivalents of PhI, 4 equivalents of $K_3PO_4{\cdot}2H_2O$ as the base, 10 mol % of $[PdCl_2(dppf)]$ (dppf = 1,1′-bis(diphenylphosphino)ferrocene) as the catalyst, and dry dimethylformamide (DMF) as the solvent and heating (80 °C, 6 h) gave 4,4′-*t*Bu_2-6,6′-Ph_2-2,2′-bipyridine (**3A**) in 67 % yield of isolated product. The structure of this product was confirmed by single-crystal X-ray diffraction (see the Supporting Information).[14]

Interestingly, the same bis(borylated) dtbpy could be converted cleanly into the monophenyl product **4A** in 31 % yield of isolated product (also structurally characterized by X-ray diffraction;[14] see the Supporting Information) under the same conditions but using only 1.2 equivalents of PhI and 2 equivalents of $K_3PO_4{\cdot}2H_2O$ as the base, thus indicating that 1) cross-coupling took place initially at one ring and 2) when

[*] I. A. I. Mkhalid, Dr. D. N. Coventry, Dr. D. Albesa-Jove, Dr. A. S. Batsanov, Prof. J. A. K. Howard, Prof. T. B. Marder
Department of Chemistry
University of Durham
South Road, Durham, DH1 3LE (England)
Fax: (+44) 191-384-4737
E-mail: todd.marder@durham.ac.uk
Prof. R. N. Perutz
Department of Chemistry
University of York
Heslington, YO10 5DD (England)

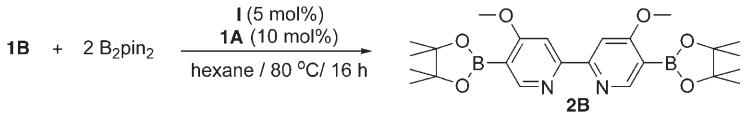
[**] We thank the EPSRC for support (T.B.M. and R.N.P.), the University of Durham for a Sir Derman Christopherson Foundation Fellowship (T.B.M.), One NorthEast (UK) for funding through the Nanotechnology UIC program (T.B.M. and J.A.K.H.), the Saudi Arabia Cultural Attache (London) for a postgraduate scholarship (I.A.I.M.), Mrs. J. Dostal for the elemental analyses, and Frontier Scientific Inc. and NetChem Inc. for generous gifts of bis(pinacolato-*O*,*O*′)diboron (B_2pin_2).

Supporting information for this article is available on the WWW under http://www.angewandte.org or from the author.

 © 2006 Wiley-VCH Verlag GmbH & Co. KGaA, Weinheim

the PhI was depleted, hydrolysis of the remaining C–B bond was relatively facile under the reactions conditions.

In contrast, no borylation of 4-*t*Bu-pyridine was observed even after 2 days at 80 °C in hexane using 5 mol % of catalyst prepared from dimer **I** and 2 equivalents of **1A**; moreover, 10 mol % of the catalyst was required to achieve approximately 6 % conversion into the C–H borylation product. Presumably, 4-*t*Bu-pyridine binds to the Ir center strongly through the N atom, thus blocking the site needed for C–H activation.[10] Interestingly, the ^{2}H NMR spectrum following quenching with $[^2H]_2O$ showed that borylation had taken place *ortho* to the N atom. As we were unable to borylate 4-*t*Bu-pyridine effectively, we examined 4,4′-$(MeO)_2$-2,2′-bipyridine (**1B**) because of its similarity to **1A**. A complete reaction (100 % conversion) of **1B** was achieved after 16 h using 2 equivalents of B_2pin_2 in hexane (5 mL), **I** (5 mol %), and **1A** (10 mol %) at 80 °C, as shown by in situ GC–MS analysis. A single isomer of the bipyridyl bis(boronate) ester (**2B**) was produced in approximately 85 % yield plus approximately 15 % yield of the analogous monoboronate. ^{1}H, ^{13}C, and 2D NMR spectroscopic experiments indicated that borylation took place at the 5-position, *ortho* to the MeO groups, in complete contrast with the borylation of dtbpy (Scheme 2). A single-crystal X-ray diffraction study[14] (Figure 1) confirmed the structure of the product.



Scheme 2. Borylation of **1B**.

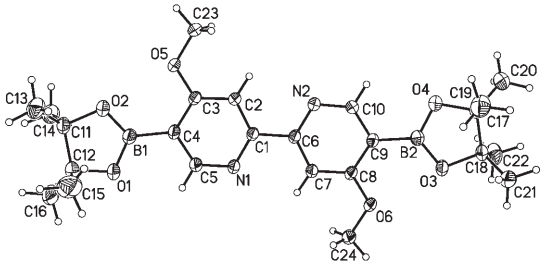
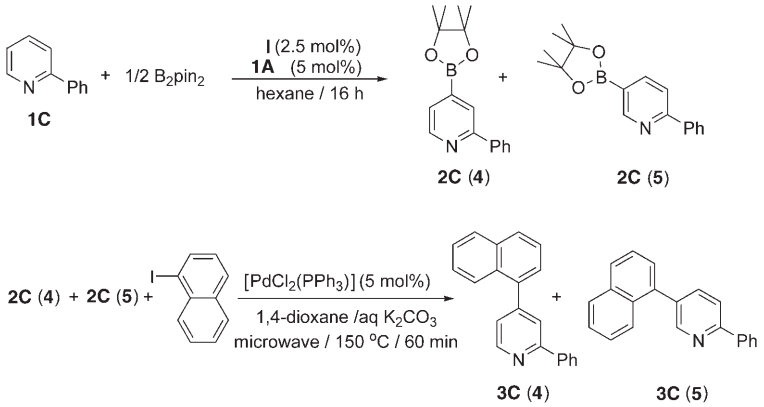


Figure 1. Molecular structure of **2B**.

It would, thus, appear that for electronic reasons the borylation reactions will avoid positions *ortho* to the N atom in a pyridine ring unless extreme steric hindrance makes other positions inaccessible. Preliminary results of DFT calculations (B3LYP, 6-31G*) show that charges on the C atom *ortho* to the N atom and the highest-occupied molecular orbitals (HOMOs) and lowest-unoccupied molecular orbitals (LUMOs) of **1A** and **1B** are very similar. This example is the first wherein purely electronic control leads to exclusive borylation of aromatic compounds *ortho* to a substituent (namely, OMe). A recent discussion of substituent effects in the borylation of cyanoarenes is given in reference [13]. Even though the regioselectivity of the borylation of the two 4,4′-disubstituted bipyridines (bpys) was different, what they have in common is that bpy can be considered to be a 2-pyridyl substituted pyridine, that is, that there is a bulky pyridine-substituent *ortho* to the N atom that blocks N-coordination of either ring because of the steric constraints of the key $[Ir(Bpin)_3(dtbpy)]$ intermediate (see above). It cannot act as a bidentate ligand because the Ir center is already five-coordinate, and it cannot act as a monodentate pyridine (py) ligand because the *ortho* py substitutent is too big to allow coordination at the N atom.

With that model in mind, we decided to examine 2-Ph-pyridine (**1C**) which, along with its derivatives, has received considerable attention as a C,N chelate on Ir centers for electroluminescence in organic light-emitting diode (OLED) devices.[15] We wondered whether a single 2-Ph group would also inhibit N-coordination, thus allowing borylation of the pyridine ring, and whether borylation of the phenyl or pyridine groups would predominate. Indeed, borylation was successful within 16 h at room temperature using 2.5 mol % of **I** and 5 mol % of **1A**, thus giving rise to equal amounts of 2-Ph-4-(Bpin)-pyridine (**2C**(**4**)) and 2-Ph-5-(Bpin)-pyridine (**2C**(**5**)). The solvent was removed from the crude mixture, which was redissolved in 1,4-dioxane to which aqueous K_2CO_3 and $[PdCl_2(PPh_3)_2]$ (5 mol %) were added. This mixture was treated with 1-iodonaphthalene in a 20-mL crimp-top sealed glass vessel and heated to 150 °C for 1 h in a Biotage-Personal Chemistry microwave reactor, thus giving 2-Ph-4-(1-Np)-pyridine (**3C**(**4**)) and 2-Ph-5-(1-Np)-pyridine (**3C**(**5**)) in 61 % yield of the combined isolated products (Scheme 3). Compounds **3C**(**4**) and **3C**(**5**) were separated chromatographically, identified spectroscopically, and their structures confirmed by single-crystal X-ray diffraction[14] (see the Supporting Information).

Finally, to test the generality of the process for the one-pot synthesis of unusual heterocycles, to evaluate whether a single CH_3 group is sufficient to block N-coordination, and to direct borylation *ortho* to the N atom, we carried out the borylation of 2,3-dimethylpyrazine (**1D**) using **I**/**1A** under the same conditions as for **1C**. The product, 2,3-Me_2-5-Bpin-pyrazine (**2D**), was subsequently cross-coupled with 2-bromothiophene to give 2,3-Me_2-5-(2-thienyl)-pyrazine (**3D**),[16] which was isolated in 34 % yield (and also structurally characterized by X-ray diffraction;[14] see the Supporting Information).



Scheme 3. Borylation of **1C**.

 © 2006 Wiley-VCH Verlag GmbH & Co. KGaA, Weinheim

In summary, we have shown that the catalyst will borylate dtbpy unless it is already coordinated to the Ir center. Moreover, we note that a single substituent *ortho* to the N atom is sufficient to inhibit N-coordination to the Ir center, thus "activating" the six-membered heteroarenes to borylation of C–H bonds and providing a design criterion for substrates for selective borylation. Complete regioselectivity has been achieved through either electronic or steric control, which allows, for the first time, borylation of pyridine derivatives *ortho* to the N atom or *ortho* to a MeO substituent (that is, *meta* to the N center). The compound 2-Ph-pyridine, important in the design of triplet-emitting Ir complexes for OLEDs,[15] can be further derivatized at the 4- and 5-positions of the py ring in preference to the Ph ring, thus leading to useful 4-(or 5-)-Ar′-2-Ar-pyridine derivatives. The compound 2,3-dimethylpyrazine was borylated *ortho* to the N atom and cross-coupled with the electron-rich heteroarene 2-bromothiophene. Finally, whilst some of the aryl pyridines, such as **3A** and **4A**, have been reported previously as ligands in Ru and luminescent Ir and Pt complexes,[17] prepared by the addition of PhLi to dtbpy followed by hydrolysis and oxidation, our route is more general and inherently more functional-group tolerant and does not require highly reactive ArLi reagents. We expect this route to be of use in applications that range from pharmaceuticals to new optical and electronic materials.

Received: August 26, 2005
Published online: December 2, 2005

Keywords: boron · boronate esters · boronic acid heterocycles · C–H activation · structure elucidation

[1] a) A. Suzuki, N. Miyaura, *Chem. Rev.* **1995**, *95*, 2451; b) A. Suzuki, *J. Organomet. Chem.* **1999**, *576*, 147; c) P. R. Parry, C. Wang, A. S. Batsanov, M. R. Bryce, B. Tarbit, *J. Org. Chem.* **2002**, *67*, 7541; d) F. Türksoy, G. Hughes, A. S. Batsanov, M. R. Bryce, *J. Mater. Chem.* **2003**, *13*, 1554; e) P. R. Parry, M. R. Bryce, B. Tarbit, *Synthesis* **2003**, 1035; f) N. Saygili, A. S. Batsanov, M. R. Bryce, *Org. Biomol. Chem.* **2004**, *2*, 852; g) A. E. Thompson, G. Hughes, A. S. Batsanov, M. R. Bryce, P. R. Parry, B. Tarbit, *J. Org. Chem.* **2005**, *70*, 388.

[2] D. M. T. Chan, K. L. Monaco, R. Li, D. Bonne, C. G. Clark, P. Y. S. Lam, *Tetrahedron Lett.* **2003**, *44*, 3863.

[3] a) M. P. Sibi, H. Tatamidani, K. Patil, *Org. Lett.* **2005**, *7*, 2571; b) G. Chen, N. Tokunaga, T. Hayashi, *Org. Lett.* **2005**, *7*, 2885.

[4] a) T. Ishiyama, J. Takagi, K. Ishida, N. Miyaura, N. R. Anastasi, J. Hartwig, *J. Am. Chem. Soc.* **2002**, *124*, 390; b) T. Ishiyama, J. Takagi, J. F. Hartwig, N. Miyaura, *Angew. Chem.* **2002**, *114*, 3182; *Angew. Chem. Int. Ed.* **2002**, *41*, 3056.

[5] J.-Y. Cho, M. K. Tse, D. Holmes, R. E. Maleczka, Jr., M. R. Smith III, *Science* **2002**, *295*, 305.

[6] P. Nguyen, H. P. Blom, S. A. Westcott, N. J. Taylor, T. B. Marder, *J. Am. Chem. Soc.* **1993**, *115*, 9329.

[7] H. Tamura, H. Yamazaki, H. Sato, S. Sakaki, *J. Am. Chem. Soc.* **2003**, *125*, 16114.

[8] D. N. Coventry, A. S. Batsanov, A. E. Goeta, J. A. K. Howard, T. B. Marder, R. N. Perutz, *Chemm. Commun.* **2005**, 2172.

[9] J. Takagi, K. Sato, J. F. Hartwig, T. Ishiyama, N. Miyaura, *Tetrahedron Lett.* **2002**, *43*, 5649.

[10] T. Ishiyama, N. Miyaura, *J. Organomet. Chem.* **2003**, *680*, 3.

[11] a) T. Ishiyama, J. Takagi, Y. Yonekawa, J. F. Hartwig, N. Miyaura, *Adv. Synth. Catal.* **2003**, *345*, 1103; b) T. Ishiyama, Y. Nobuta, J. F. Hartwig, N. Miyaura, *Chem. Commun.* **2003**, 2942.

[12] a) J.-Y. Cho, C. N. Iverson, M. R. Smith III, *J. Am. Chem. Soc.* **2000**, *122*, 12868; b) T. Tagata, M. Nishida, *Adv. Synth. Catal.* **2004**, *346*, 1655.

[13] G. A. Chotana, M. A. Rak, M. R. Smith, *III, J. Am. Chem. Soc.* **2005**, *127*, 10539.

[14] For synthetic and crystallization details and the molecular structures, see the Supporting Information. X-ray diffraction experiments were performed with SMART 1 K CCD area-detector diffractometers using $Mo_{K\alpha}$ radiation ($\lambda = 0.71073$ Å) at $T = 120(2)$ K; the structures were solved by direct methods (SHELXTL; Bruker AXS, Inc., Madison, WI, USA). **3A**·2 C_6F_6: $C_{42}H_{32}F_{12}N_2$, $M_r = 792.70$, orthorhombic, space group *Pccn*, $a = 14.021(2)$, $b = 19.509(3)$, $c = 13.2267(19)$ Å, $V = 3618.1(9)$ Å^3, $Z = 4$, $\rho_{calcd} = 1.455$ Mg m^{-3}, $\mu = 0.128$ mm^{-1}, R (F; $F^2 > 2\sigma$) = 0.0550, R_w (F^2, all data) = 0.1583, $S = 1.297$ for 5474 unique data ($\theta < 30.5$) and 317 refined parameters; final difference synthesis within ± 0.54 e Å^{-3}. **4A**·C_6F_6: $C_{30}H_{28}F_6N_2$, $M_r = 530.54$, orthorhombic, space group *Pnma*, $a = 27.2125(17)$, $b = 6.7353(5)$, $c = 14.3175(10)$ Å, $V = 2624.2(3)$ Å^3, $Z = 4$, $\rho_{calcd} = 1.343$ Mg m^{-3}, $\mu = 0.108$ mm^{-1}, R (F; $F^2 > 2\sigma$) = 0.0508, R_w (F^2, all data) = 0.1346, $S = 1.010$ for 4319 unique data ($\theta < 30.51$) and 291 refined parameters; final difference synthesis within ± 0.34 e Å^{-3}. **2B**: $C_{24}H_{34}B_2N_2O_6$, $M_r = 468.15$, monoclinic, space group $P2_1/n$, $a = 9.3567(6)$, $b = 22.0270(13)$, $c = 12.2764(8)$ Å, $\beta = 98.213(3)°$, $V = 2504.2(3)$ Å^3, $Z = 4$, $\rho_{calcd} = 1.242$ Mg m^{-3}, $\mu = 0.087$ mm^{-1}, R (F; $F^2 > 2\sigma$) 0.0717, R_w (F^2, all data) = 0.2121, $S = 1.069$ for 7652 unique data ($\theta < 30.50°$) and 317 refined parameters; final difference synthesis within ± 0.64 e Å^{-3}. **3C(4)**: $C_{21}H_{15}N$, $M_r = 281.34$, monoclinic, space group $P2_1$, $a = 6.7020(8)$, $b = 7.6743(9)$, $c = 14.6965(17)$ Å, $\beta = 97.980(3)°$, $V = 748.57(15)$ Å^3, $Z = 2$, $\rho_{calcd} = 1.248$ g cm^{-3}, $\mu = 0.072$ mm^{-1}, R (F; $F^2 > 2\sigma$) = 0.0426, R_w (F^2, all data) = 0.1261, $S = 0.645$ for 2165 unique data ($\theta < 27.50$) and 260 refined parameters; final difference synthesis within ± 0.33 e Å^{-3}. **3C(5)**: $C_{21}H_{15}N$, $M_r = 281.34$, monoclinic, space group $P2_1$, $a = 7.099(1)$, $b = 12.943(2)$, $c = 7.928(1)$ Å, $\beta = 100.02(1)°$, $V = 717.33(18)$ Å^3, $Z = 2$, $\rho_{calcd} = 1.303$ g cm^{-3}, $\mu = 0.075$ mm^{-1}, R (F; $F^2 > 2\sigma$) = 0.0423, R_w (F^2, all data) = 0.1188, $S = 1.069$ for 2163 unique data ($\theta < 29.98$) and 259 refined parameters; final difference synthesis within ± 0.33 e Å^{-3}. **3D**: $C_{10}H_{10}N_2S$, $M_r = 190.26$, monoclinic, space group $P2_1/n$, $a = 7.1352(19)$, $b = 12.292(3)$, $c = 11.175(3)$ Å, $\beta = 94.168(4)°$, $V = 977.5(4)$ Å^3, $Z = 4$, $\rho_{calcd} = 1.293$ Mg m^{-3}, $\mu = 0.283$ mm^{-1}, R (F; $F^2 > 2\sigma$) = 0.0464, R_w (F^2, all data) = 0.1293, $S = 1.062$ for 2618 unique data ($\theta < 27.50°$) and 142 refined parameters; final difference synthesis within ± 0.25 e Å^{-3}. CCDC 279973–279978 contain the supplementary crystallographic data for this paper. These data can be obtained free of charge from The Cambridge Crystallographic Data Centre via www.ccdc.cam.ac.uk/data_request/cif.

[15] a) M. A. Baldo, S. Lamansky, P. E. Burrows, M. E. Thompson, S. R. Forrest, *Appl. Phys. Lett.* **2005**, *75*, 4; b) S. Lamansky, P. Djurovich, D. Murphy, F. Abdel-Razzag, H. Lee, C. Adachi, P. E. Burrows, S. R. Forrest, M. E. Thompson, *J. Am. Chem. Soc.* **2001**, *123*, 4304; c) C. Adachi, M. A. Baldo, M. E. Thompson, S. R. Forrest, *J. Appl. Phys.* **2001**, *90*, 5048.

[16] The only reference to this compound we have located is in the following patent: Jpn. Kokai Tokkyo Koho, **1980**, 6 pp, CODEN: JKXXAF JP 55120570 19800917 Showa. [Chem. Abstr. **1981**, *94*, 175164].

[17] a) T. B. Hadda, I. Zidane, S. A. Moya, H. Le Bozec, *Polyhedron* **1996**, *15*, 1571; b) M. Lepeltier, T. K.-M. Lee, K. K.-W. Lo, L. Toupet, H. Le Bozec, V. Guerchais, *Eur. J. Inorg. Chem.* **2005**, 110; c) W. Lu, B.-X. Mi, M. C. W. Chan, Z. Hui, C.-M. Che, N. Zhu, S.-T. Lee, *J. Am. Chem. Soc.* **2004**, *126*, 4958.

 © 2006 Wiley-VCH Verlag GmbH & Co. KGaA, Weinheim

Porphyrin Complexes

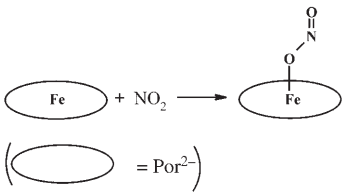
DOI: 10.1002/anie.200502409

Reactions of Nitrogen Oxides with Heme Models: Spectral Characterization of an Elusive Five-Coordinate Fe^{III}(porphyrin) Nitrito Intermediate**

Tigran S. Kurtikyan and Peter C. Ford**

The roles of nitrogen dioxide (NO_2) and of the nitrite ion (NO_2^-) in mammalian biology are drawing increasing attention.[1–4] NO_2 is a strong oxidant and nitrating species that initiates destructive pathways in living systems.[1] Several disease states have been suggested to be connected with exogenously and endogenously formed NO_2.[2,3] Likely endogenous sources of NO_2 are the reactions of nitric oxide (NO) with oxyglobins and with the superoxide ion (O_2^-), which leads to coordinated and free peroxynitrite ($ONOO^-$),[5,6] subsequent decay of which affords both the nitrate ion and NO_2.[7] Furthermore, there is increasing evidence that NO_2 may also be formed through enzymatic pathways with the participation of heme peroxidases.[1a] NO_2 has been shown to be a product of the reaction of NO and nitrate, as mediated by a heme center.[8] With regard to nitrite, the NO_2^- ion is ubiquitous in mammalian tissues and fluids and is the largest reservoir of accessible NO equivalents in the cardiovascular system.[4a,b] Recent studies have suggested that NO_2^- itself is either a vasodilator or forms the known vasodilator NO through reaction with heme centers.[4c] Clearly, there is a continuing incentive to elucidate the interactions of these ligands with heme models to understand the fundamental chemistry relevant to their biological properties.

Reported herein are studies of the reaction of NO_2 with ferroheme models Fe^{II}(por) (por = *meso*-tetraphenylporphyrinato dianion (TPP) or *meso*-tetra-*p*-tolylporphyrinato dianion (TTP)) in porous, sublimed layers. In an earlier study,[9] it was shown that the reaction of Fe(tpp) leads to the formation of the nitrato complex Fe(tpp)(η^2-O_2NO). Herein we demonstrate FTIR and UV/Vis spectroscopic evidence that manifest the formation of the elusive five-coordinate nitrito complex Fe(por)(η^1-ONO) [Eq. (1)] as an intermediate in the



(1)

first stage of this reaction. Notably, the only well-characterized iron porphyrin complexes of NO_2 are those with sterically protecting porphyrins (e.g. "picket fence" porphyrin)[10] and the nitro–nitrosyl complexes Fe(por)(NO_2)(NO) that are stable only under NO.[11] No five-coordinate nitrito complexes of the type Fe^{III}(por)(NO_2) (or Fe^{III}(por)(ONO)) have been characterized previously, even with picket fence porphyrins.

The introduction of small increments of NO_2 gas into a cryostat, at room temperature, that contains sublimed layers of Fe(ttp) (see Experimental Section) leads to the appearance of three new IR spectroscopic bands at $\tilde{\nu} = 1528$, 901, and 751 cm^{-1} that have their isotope counterparts at $\tilde{\nu} = 1495$, 878, and 747 cm^{-1} when $^{15}NO_2$ is used (Figure 1). For the analogous complex with Fe(tpp), only small deviations from these values (1–2 cm^{-1}) are seen (see Table 1), but the last band is masked by an intense TPP band and can be registered only in the difference spectra. The intensity growth of these bands correlates directly with the addition of each portion of NO_2 ($^{15}NO_2$) (Figure 2) and demonstrates the formation of a new species that clearly contains a coordinated NO_2 ligand. This new complex is fairly stable in the solid state at room temperature, but decomposes under vacuum within a few days to give mostly the nitrosyl complex Fe(tpp)(NO) with a strong ν(NO) band at $\tilde{\nu} = 1677$ cm^{-1}.

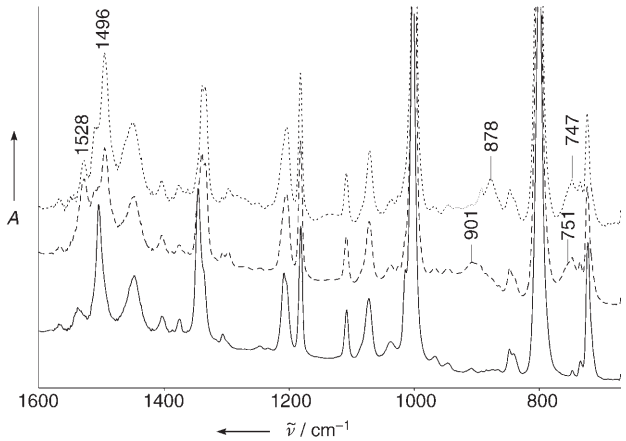


Figure 1. FTIR spectra of Fe(ttp) sublimed layers (solid line) after short (≈30 s) exposure to NO_2 (5×10^{-2} mmHg) followed by evacuation (dashed line)). The same procedure with $^{15}NO_2$ (dotted line).

[*] Prof. Dr. T. S. Kurtikyan
Research Institute of Applied Chemistry (ARIAC)
375005 Yerevan (Armenia)
and
Molecule Structure Research Centre (MSRC) NAS
375014 Yerevan (Armenia)
Fax: (+37) 410-28-2667
E-mail: tkurt@msrc.am
Prof. Dr. P. C. Ford
Department of Chemistry and Biochemistry
University of California
Santa Barbara, CA 93106 (USA)
Fax: (+1) 806-893-4120
E-mail: ford@chem.ucsb.edu

[**] This work was supported by the U.S. Civilian Research and Development Foundation (CRDF Grant No. AC2-2520-TB-03) and by the US Department of Energy (DE-FG02-04ER15506). We thank M. E. Hakobyan for providing us with pure samples of iron(II) porphyrins.

InterScience
© 2006 Wiley-VCH Verlag GmbH & Co. KGaA, Weinheim

Table 1: IR spectroscopic data (cm^{-1}) of nitrito and nitrito–nitrosyl complexes of Fe(por).[a] The data for the complexes with ^{15}N-substituted nitrogen oxides are given in the parenthesis.

Complexes	ν(N=O)	ν(N-O)	δ(O-N=O)	ν(N=O)
Fe(ttp)(ONO)	1528(1496)	901(878)	751(747)	
Fe(ttp)(ONO)(NO)	1507(≈1472)	934(914)	–	1886(1851)
Fe(tpp)(ONO)	1527(1495)	900(877)	–	
Fe(tpp)(ONO)(NO)	1508(≈1474)	936(915)	–	1887(1851)

[a] por = *meso*-tetraphenylporphyrinato dianion (TPP) or *meso*-tetra-*p*-tolylporphyrinato dianion (TTP).

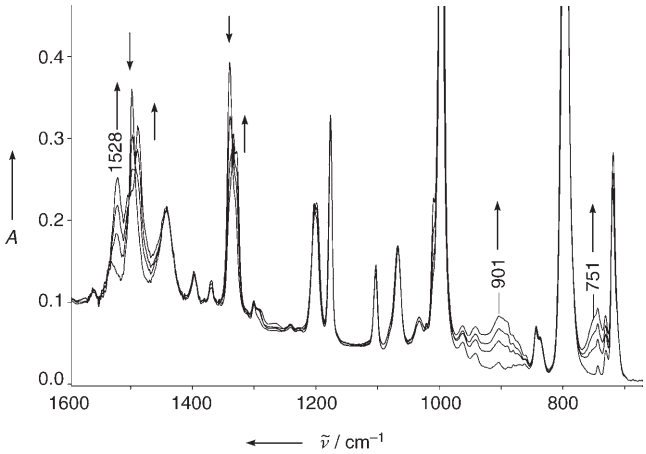
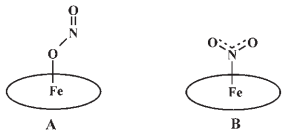


Figure 2. FTIR spectral changes in Fe(ttp) sublimed layer after sequential short time exposures (≈30 s) to NO_2 (4×10^{-2} mmHg) and evacuation after each introduction.

IR spectroscopy provides a diagnostic tool for differentiation between the O-bound nitrito (η^1-ONO) (**A**) and the N-bound nitro (η^1-NO_2) (**B**) coordination modes of the NO_2^- ligand.[12] The high-frequency stretching modes are much



more separated for the O-bound than for the N-bound species. Indeed, for the nitro–nitrosyl complex, Fe(tpp)-(NO_2)(NO), the asymmetric and symmetric ν(NO) modes of coordinated NO_2 are located at 1440 and 1300 cm^{-1}. Other six-coordinate porphyrin nitro complexes also show similar bands. In sublimed films of five-coordinate Co(tpp)(NO_2), these bands are located at 1468 and 1282 cm^{-1}.[13] However, on addition of a sixth ligand (piperidine (Pip) or pyridine (Py)) the bands shift to $\tilde{\nu}=1437$ and 1308 cm^{-1} and to $\tilde{\nu}=$ 1439 and 1310 cm^{-1}, respectively,[14] which are close to the values observed for Fe(tpp)(NO_2)(NO).

On the other hand, the ruthenium complex Ru(tpp)-(ONO)(NO), for which the X-ray crystal structure has revealed nitrito coordination, shows IR spectroscopic bands at $\tilde{\nu}=1522$ and 930 cm^{-1}.[15,11c] Another example is the (thermally unstable) nitrite–nitrosyl manganese analogue Mn(tpp)(ONO)(NO), which was identified[16] in the course of NO disproportionation on the sublimed Mn(tpp) layers. It displays isotope-sensitive IR spectroscopic bands at $\tilde{\nu}=1480$ and 971 cm^{-1}, which were assigned to the coordinated nitrito ligand.[16] A third example is a metastable compound that was recently prepared[17] by photolysis of Fe(tpp)(NO_2)(NO) in a low-temperature KBr pellet. The photoproduct was concluded to be the nitrite–nitrosyl complex Fe(tpp)(ONO)(NO) on the basis of extensive DFT calculations and the observation of N-isotope-sensitive IR spectroscopic bands at $\tilde{\nu}=1507$ and 934 cm^{-1} that were assigned to the ν(N=O) and ν(N-O) stretching modes of the Fe-O-N=O moiety.[17]

The analogy between these spectral data and our observations supports the formation of the nitrito complex Fe-(por)(η^1-ONO) at the initial stage of reaction between NO_2 and Fe(por). However, in the above studies only two bands were reported for coordinated nitrito ligands, although the ONO fragment should display three IR spectroscopic active normal modes. The failure to observe the third mode can now be explained in terms of the intense porphyrin band in the vicinity of $\tilde{\nu}=750$ cm^{-1} in TPP complexes, which masks the low-intensity δ(ONO) deformation expected for the coordinated nitrito ligand. In contrast, Fe(ttp) is relatively free in this spectral range, so an isotope-sensitive band was found for Fe(ttp)(η^1-ONO) in the region where the δ(ONO) was expected.[12]

The IR spectra also rule out an η^2-O_2N chelate structure. In such complexes the $\nu_a(NO_2)$ and $\nu_s(NO_2)$ stretching vibrations are separated only by about 200 cm^{-1} in contrast to the ≈600 cm^{-1} separation of the high-frequency bands observed in the present work.[12]

Additional information regarding the nature of this complex can be drawn from porphyrin vibrational modes that reveal regular changes depending on the spin and oxidation state of axial complexes of Fe(tpp).[18] The band at $\nu\approx1350$ cm^{-1}, which represents a porphyrin core mode ($\nu(C_a$-$C_m)$ mixed with some $\nu(C_m$-phenyl)) and a porphyrin core deformation mode near $\tilde{\nu}=450$ cm^{-1}, is sensitive to the spin state of the metal complexes. For the intermediate-spin state Fe(tpp), these bands lie at $\tilde{\nu}=1346$ and 464 cm^{-1}. Upon coordination with NO_2, they shift to $\tilde{\nu}=1341$ and 434 cm^{-1}, respectively. This is consistent with a change to the high-spin state for the new, five-coordinate Fe(ttp)(ONO) complex. The axial complexes of Fe(ttp) also have such electronic structure-sensitive bands. For this porphyrin ligand, the aforementioned bands are disposed initially at $\tilde{\nu}=1346$ and 455 cm^{-1} and correspondingly shift upon nitrito-complex formation to $\tilde{\nu}=1340$ and 428 cm^{-1}. In the case of Fe(ttp), there is another structure-sensitive band at $\tilde{\nu}=1505$ cm^{-1} that undergoes a shift to $\tilde{\nu}=1495$ cm^{-1} upon the formation of Fe(ttp)(η^1-ONO).

From the highly resolved IR spectral data, one can conclude that the initial products of the reaction of the ferroheme model compounds, Fe(por), with NO_2 are O-coordinated and are five-coordinate Fe(por)(η^1-ONO) complexes rather than bisligated, six-coordinate Fe(por)(η^1-$ONO)_2$ complexes. During the course of adding NO_2 in portions (beginning from very low values), one would expect to observe additional IR spectroscopic bands if both five- and

 © 2006 Wiley-VCH Verlag GmbH & Co. KGaA, Weinheim

six-coordinate structures are formed, but this was not the case. Furthermore, formation of Fe(por)(η^1-ONO)$_2$ would involve oxidation either of the iron to give a Fe^{IV} species or of the porphyrin ring to give the porphyrin radical. For the latter, an intense π cation radical marker band in the vicinity of $\tilde{\nu} = 1300\ cm^{-1}$ [19] should be observed as was seen for the bisnitro complex $Co^{III}(tpp^{\bullet+})(NO_2)_2$,[20] which was obtained in sublimed layers. No such band was seen in the spectra reported herein.

The reaction of Fe(ttp)(ONO) with NO was investigated through preparation of a sample of the layered Fe(ttp)(ONO) material as described above, followed by cooling to 77 K and introducing excess NO. At 77 K there was no apparent reaction, but heating to 150 K led to the appearance of new bands at $\tilde{\nu} = 1886\ cm^{-1}$, 1507, and $934\ cm^{-1}$, whereas the bands at $\tilde{\nu} = 1528$, 901, and $757\ cm^{-1}$, which were assigned to Fe(ttp)(ONO), disappeared (Figure 3, bottom curve). The

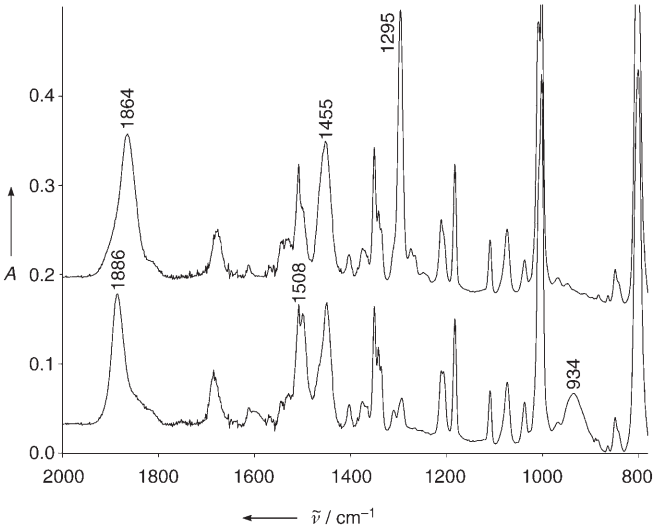
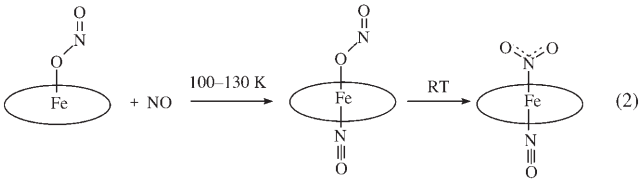


Figure 3. FTIR spectra of sublimed layer containing Fe(ttp)(ONO) after introducing 2 mm NO into cryostat at 77 K, warming to 140 K and recooling (bottom curve); after additional warming to 240 K (upper curve) and recooling.

former bands have their isotope counterparts at $\tilde{\nu} = 1851$, ≈ 1472, and $914\ cm^{-1}$ when ^{15}NO interacts with layers containing Fe(ttp)($O^{15}NO$). Notably, the product spectra are very similar to those reported[17] for metastable species obtained when a low temperature KBr pellet, which contained Fe(tpp)(NO)(NO_2), was photolyzed. The photochemical product displayed IR spectroscopic bands at $\tilde{\nu} = 1507$ and $934\ cm^{-1}$ that were assigned to the ν(N=O) and ν(N-O) nitrito stretching modes of the nitrito–nitrosyl complex Fe(tpp)(ONO)(NO). The ν(N≡O) mode of this transient species was not reported owing to overlap with the nitrosyl band of the starting material, although difference spectra indicate that the photoproduct nitrosyl band shifts to higher frequencies. The coincidence of the spectral data reported herein for the product of the NO reaction with Fe(ttp)(ONO) and the metastable photoproduct implies the formation of an analogous species, namely the η^1-ONO complexes. Thus, we conclude that the low-temperature reaction of NO with Fe(ttp)(ONO) is a simple addition to give Fe(ttp)(η^1-ONO)(NO), which supports the view that Fe(por)(ONO) is a five-coordinate nitrito complex.

Upon warming the initially formed nitrite–nitrosyl complex, isomerization to the more stable nitro–nitrosyl form (Fe(por)(NO_2)(NO))[10,11] as characterized by IR spectroscopic bands at $\tilde{\nu} = 1864$ {ν(N≡O)}, ≈ 1455 {$\nu_a(NO_2)$}, and $1295\ cm^{-1}$ {$\nu_s(NO_2)$} was observed [Figure 3, upper curve, Eq. (2)]. For both the nitrite–nitrosyl complex and its nitro–



(2)

nitrosyl isomer (formed upon warming), the spin-sensitive bands appear at the higher frequencies characteristic of the low-spin iron state.

Formation of the five-coordinate nitrito complex Fe(por)(η^1-ONO) upon initial reaction of NO_2 with Fe(por) is also supported by changes in the UV/Vis spectra (Figure 4). The

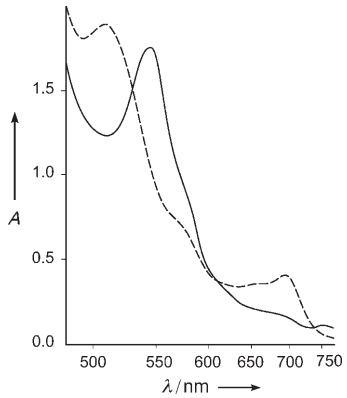


Figure 4. UV/Vis spectrum of Fe(ttp) sublimed layer (solid line) after short time exposure to a NO_2 atmosphere (4×10^{-2} mmHg, dashed line). Spectrum was recorded after FTIR spectroscopic measurement of the same sample evidencing formation of the nitrito complex Fe(ttp)(ONO).

reaction was first monitored by FTIR spectroscopy (by using CaF_2 plates) and then the electronic absorption spectrum of the same sample was recorded. The spectral changes observed are characteristic of conversion from the ferrous into the ferric state, that is, going from Fe(ttp) to Fe(ttp)(ONO). Furthermore, despite the difference in media (solid vs. solution), the electronic spectrum of the latter is quite similar to that obtained by Scheidt and co-workers[21] at the first stage of the reaction between [Fe(tpp)($OClO_3$)] and NO_2^- in CH_2Cl_2. Although the spectrum obtained under these conditions was reasonably assigned as likely being due to an iron(III) nitrite complex, the exact nature of this complex was

 © 2006 Wiley-VCH Verlag GmbH & Co. KGaA, Weinheim

not clear owing to uncertainty regarding stoichiometry (one or two nitrites), mode of ligation (O or N bound), and whether solvent is coordinated. However, the electronic spectral similarities with the thin-film experiments strongly suggest that the unstable species seen in the earlier solution study[21] was indeed the five-coordinate nitrito complex Fe(tpp)(η^1-ONO) characterized here.

Continued addition of NO_2 increments to the layered nitrite complex Fe(por)(η^1-ONO) at room temperature led to the formation of the known nitrato complexes Fe(por)(η^2-O_2NO). This is consistent with a previous study[9] that found that interaction of NO_2 gas with a sublimed layer of Fe(tpp) gave Fe(tpp)(η^2-O_2NO). Notably, the high-frequency ν(N=O) band at $\tilde{\nu} \approx 1530\ cm^{-1}$ for this complex is disposed in the same spectral range as the ν(N=O) of O-coordinated nitrito ligand. This coincidence is likely the reason that the intermediacy of the nitrito complexes in such reactions was not detected in the previous study.

The presence of an intermediate O-coordinated nitrito ligand has been proposed previously [8,22] as a reasonable interpretation of kinetic and spectral data for various transformations that take place in the course of the NO_x interaction with heme models in solids and in solution. The demonstration herein that such five-coordinate iron-porphyrin nitrito complexes are formed from the reaction of Fe(por) and NO_2 at room temperature confirms these suggestions.

In summary, the data reported herein indicate that the first stage of the reaction of NO_2 with the ferrous porphyrins Fe(por) leads to the formation of the previously unknown five-coordinate ferric nitrito complex Fe(por)(η^1-ONO). The mechanism of subsequent transformations upon the addition of new NO_2 increments, which leads to the eventual formation of nitrato complexes, is now under detailed investigation.

Experimental Section

The ferrous porphyrinates Fe(por) are very sensitive to oxygen and are readily oxidized to Fe^{III} derivatives. For this reason the more stable hexacoordinate complexes, Fe(por)$(B)_2$, with nitrogen bases (por = TPP or the *meso*-tetra-*p*-tolylporphyrinato dianion; B is Py or Pip) were used as the precursors. These were synthesized by a known procedure.[23] The low-temperature sublimate was prepared[24] by placing a Fe(por)$(B)_2$ sample in a Knudsen cell and heating to about 470 K under high vacuum ($P = 3 \times 10^{-5}$ Torr). Evacuation for 3 h resulted in the complete elimination of the coordinated axial ligands B, as monitored by measurement of the pressure at the outlet of the cryostat. Liquid nitrogen was then poured into the cryostat, and the Knudsen cell was heated to 520 K, at which temperature sublimation of Fe(por) onto the KBr or CaF_2 substrate occurred. In the latter case, CaF_2 plates were also used as the optical windows of the cryostat. The metal–aryl porphyrins layers obtained in this manner by sublimation onto a low-temperature (77 K) surface are spongelike[25a,b] and have high microporosity.[25c] Potential reactants easily diffuse across these layers, and adducts thus formed can be studied spectroscopically without solvent interference.

Sublimation was typically carried out over periods of 0.3–2.0 h to build up layers of thickness sufficient for UV/Vis and IR spectral studies. The Fe(por) sublimed layer was then heated to room temperature under dynamic vacuum, and small increments of NO_2 gas were introduced for a short-time period followed by a period of pumping out. The FTIR and UV/Vis spectra were measured after each NO_2 introduction.

NO_2 ($^{15}NO_2$), obtained by oxidation of NO (^{15}NO) with excess pure dioxygen, was dried over P_2O_5 and then was purified by fractional distillation until a pure white solid was obtained. ^{15}NO with 98.5% enrichment was purchased from the Institute of Isotopes, Republic of Georgia.

Received: July 11, 2005
Revised: October 7, 2005
Published online: December 2, 2005

Keywords: heme · IR spectroscopy · iron · nitrogen oxides · porphyrinoids

[1] a) M. Kirsch, H.-G. Korth, R. Sustmann, H. de Groot, *Biol. Chem.* **2002**, *383*, 389–399; b) S. Pfeiffer, B. Mayer, B. Hemmens, *Angew. Chem.* **1999**, *111*, 1824–1844; *Angew. Chem. Int. Ed.* **1999**, *38*, 1714–1731.
[2] M. G. Espey, S. Xavier, D. D. Thomas, K. M. Miranda, D. A. Wink, *Proc. Natl. Acad. Sci. USA* **2002**, *99*, 3481–3486.
[3] S. Pfeiffer, A. Lass, K. Schmidt, B. Mayer, *FASEB J.* **2001**, *15*, 2355–2364.
[4] a) N. S. Bryan, T. Rassaf, R. E. Maloney, C. M. Rodriguez, F. Saijo, J. R. Rodriguez, M. Feelisch, *Proc. Natl. Acad. Sci. USA* **2004**, *101*, 4308–4313; b) T. Rassaf, M. Feelisch, M. Kelm, *Free Radical Biol. Med.* **2004**, *36*, 413–422; c) K. Cosby, K. S. Partovi, J. H. Crawford, R. P. Patel, C. D. Reiter, S. Martyr, B. K. Yang, M. A. Waclawiw, G. Zalos, X. Xu, K. T. Huang, H. Shields, D. B. Kim-Shapiro, A. N. Schechter, R. O. Cannon, M. T. Gladwin, *Nat. Med.* **2003**, *9*, 1498–1505.
[5] M. P. Dohle, J. W. Hoekstra, *J. Inorg. Biochem.* **1981**, *14*, 351–358.
[6] a) S. Herold, M. Exner, T. Nauser, *Biochemistry* **2001**, *40*, 3385; b) S. Herold, *FEBS Lett.* **1999**, *443*, 81.
[7] J. L. Bourassa, E. P. Ives, A. L. Marqueling, R. Shimanovich, J. T. Groves, *J. Am. Chem. Soc.* **2001**, *123*, 5142–5143.
[8] T. S. Kurtikyan, G. M. Gulyan, G. G. Martirosyan, M. D. Lim, P. C. Ford, *J. Am. Chem. Soc.* **2005**, *127*, 6216–6224.
[9] T. S. Kurtikyan, T. G. Stepanyan, M. E. Akopyan, *Russ. J. Coord. Chem.* **1999**, *25*, 721–725.
[10] G. R. A. Wyllie, W. R. Scheidt, *Chem. Rev.* **2002**, *102*, 1067–1089.
[11] a) T. Yoshimura, *Inorg. Chim. Acta* **1984**, *83*, 17–21; b) M. K. Ellison, C. E. Schulz, W. R. Scheidt, *Inorg. Chem.* **1999**, *38*, 100–108; c) T. S. Kurtikyan, G. G. Martirosyan, I. M. Lorkovic′, P. C. Ford, *J. Am. Chem. Soc.* **2002**, *124*, 10124–10129.
[12] K. Nakamoto, *Infrared and Raman Spectra of Inorganic and Coordination Compounds*, 3rd ed., Wiley, New York, **1978**, pp. 244–247.
[13] T. S. Kurtikyan, T. G. Stepanyan, A. V. Gasparyan, *Russ. J. Coord. Chem.* **1997**, *23*, 563–567.
[14] T. G. Stepanyan, M. E. Akopyan, T. S. Kurtikyan, *Russ. J. Coord. Chem.* **2000**, *26*, 453–457.
[15] K. M. Miranda, X. Bu, I. M. Lorkovic, P. C. Ford, *Inorg. Chem.* **1997**, *36*, 1992.
[16] G. G. Martirosyan, A. S. Azizyan, T. S. Kurtikyan, P. C. Ford, *Chem. Commun.* **2004**, 1488–1489.
[17] J. Lee, A. Y. Kovalevsky, I. Novozhilova, K. Bagley, P. Coppens, G. B. Richter-Addo, *J. Am. Chem. Soc.* **2004**, *126*, 7180–7181.
[18] H. Oshio, T. Ama, T. Watanabe, J. Kincaid, K. Nakamoto, *Spectrochim. Acta Part A* **1984**, *40*, 863–870.
[19] E. T. Shimomura, M. A. Phillippi, H. M. Goff, W. F. Sholz, C. A. Reed, *J. Am. Chem. Soc.* **1981**, *103*, 6778–6780.
[20] T. S. Kurtikyan, T. H. Stepanyan, *Russ. Chem. Bull.* **1998**, *47*, 695–698.
[21] M. J. Finnegan, A. G. Lappin, W. R. Scheidt, *Inorg. Chem.* **1990**, *29*, 181–185.

 © 2006 Wiley-VCH Verlag GmbH & Co. KGaA, Weinheim

[22] M. D. Lim, I. M. Lorkovic, K. Wedeking, A. W. Zanella, S. M. Massick, P. C. Ford, *J. Am. Chem. Soc.* **2002**, *124*, 9737 – 9743.
[23] L. M. Epstein, D. K. Straub, C. Maricondi, *Inorg. Chem.* **1967**, *6*, 1720 – 1722.
[24] K. Nakamoto, T. Watanabe, T. Ama, M. W. Urban, *J. Am. Chem. Soc.* **1982**, *104*, 3744 – 3745.
[25] a) M. P. Byrn, C. J. Curtis, Y. Hsiou, S. I. Khan, P. A. Sawin, S. K. Tendick, A. Terzis, C. E. Strouse, *J. Am. Chem. Soc.* **1993**, *115*, 9480 – 9497; b) M. P. Byrn, C. J. Curtis, S. I. Khan, P. A. Sawin, R. Tsurumi, C. E. Strouse, *J. Am. Chem. Soc.* **1990**, *112*, 1865 – 1874; c) T. S. Kurtikyan, A. V. Gasparyan, G. G. Martirosyan, G. H. Zhamkochyan, *J. Appl. Spectrosc.* **1995**, *62*, 62 – 66. (Russ.)

 © 2006 Wiley-VCH Verlag GmbH & Co. KGaA, Weinheim

Grignard Reactions

DOI: 10.1002/anie.200502485

Soluble Lanthanide Salts ($LnCl_3 \cdot 2\,LiCl$) for the Improved Addition of Organomagnesium Reagents to Carbonyl Compounds**

*Arkady Krasovskiy, Felix Kopp, and Paul Knochel**

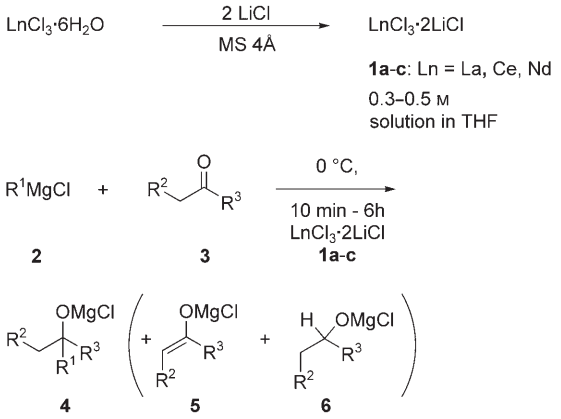
Lanthanide(III) salts have been used extensively to activate carbonyl compounds and imine derivatives for the 1,2-addition of organometallic reagents.[1] Owing to the oxophilic nature of lanthanide salts, the 1,2-addition reaction is favored over competitive reactions such as enolization and reduction (by β-hydride transfer).[2] The activity of the catalyst strongly depends on the drying procedure[3] and especially on its solubility.[4] Only few lanthanide salts are soluble to an appreciable degree in organic solvents.[5] The addition of LiCl has proven to have a beneficial effect and has been used for the synthesis of various organometallic complexes.[6]

Herein, we describe the preparation of THF-soluble lanthanide halides $LnCl_3 \cdot 2\,LiCl$ (Ln = La (**1a**), Ce(**1b**), Nd-(**1c**)), which can be easily prepared as 0.3–0.5 M solutions in THF (Scheme 1). These convenient reagents were found to be superior promoters for the addition of various Grignard reagents to hindered and enolizable ketones. Thus, the treatment of commercially available $LaCl_3 \cdot 6H_2O$, $CeCl_3 \cdot 6H_2O$, or $NdCl_3 \cdot 6H_2O$ with LiCl (2 equiv) in water led to a slurry which was stirred 4 h at 25 °C under high vacuum (0.01 mm Hg). The resulting white powder was stirred with gradual increase of temperature (20 °C/4 h to 160 °C) for 28 h. The solid was dissolved in THF and stirred for one day in the presence of molecular sieves (4 Å). After filtration, transparent, ca. 0.33 M solutions of $LnCl_3 \cdot 2\,LiCl$ (**1a–c**) were obtained, which can be stored indefinitely at 25 °C under argon. The amount of remaining protic impurities was less than 5% as shown by titration.[7] Solutions of $LnCl_3 \cdot 2\,LiCl$ promote the addition of Grignard reagents **2** to various types of hindered and easily enolizable ketones **3** leading to tertiary alcohols of type **4**. The side products usually obtained in these reactions arise from the enolization of the ketone leading to the corresponding magnesium enolate **5** and the β-hydride reduction leading to the alcohol **6**. The addition of lanthanide salts minimizes considerably these side reactions. Thus, the reaction of the secondary alkylmagnesium chloride **2a** with cyclopentanone (**3a**) leads in the absence of lanthanide salts to enolization and formation of aldol products, and only 3–5% of the addition product is obtained (entry 1, Table 1). By adding $CeCl_3$ (1.5 equiv) according to the procedure of Imamoto et al.,[2] we obtained the desired alcohol **4a** in 72% yield, whereas the procedure of Dimitrov et al.[3] ($CeCl_3$, 1 equiv) provided alcohol **4a** in 80% yield. By adding $LnCl_3 \cdot 2\,LiCl$ (Ln = La, Ce, Nd) in THF (1 equiv) to cyclopentanone (**3a**) and stirring the mixture for 1 h and then adding *i*PrMgCl (**2a**) at 0 °C (10 min), we obtained alcohol **4a** in 92–94% yield. The same reactivity trend was observed with cyclohexanone (**3b**). The addition of *i*PrMgCl to this ketone again proceeded quantitatively in the presence of $LnCl_3 \cdot 2\,LiCl$ (Ln = La, Ce) and in better yield than with Imamoto's method (80%)[2] or with Dimitrov's method (93%; entry 2).[3]

α-Tetralone (**3c**) also reacted quantitatively with *i*PrMgCl (**2a**) leading to the alcohol **4c** in 95% yield. In the absence of lanthanide salt, only 30% yield was obtained, whereas Imamoto's method provided product **3c** in 73% yield (entry 3). Readily enolizable ketones such as diphenylacetone (**3d**) reacted with the sterically hindered Grignard reagent *i*PrMgCl (**2a**) only under formation of the corresponding magnesium enolate (only 3% of the addition product was produced), whereas in the presence of $LnCl_3 \cdot 2\,LiCl$ a yield of 95–97% of the tertiary alcohol **4d** was obtained (entry 4).

This behavior was also observed for less reactive Grignard reagents such as functionalized arylmagnesium chlorides **2b–e** prepared by a halogen–magnesium exchange reaction. Due to the low reactivity of these reagents the use of *i*PrMgCl·LiCl for the exchange reaction is essential to convert the arylmagnesium chlorides into reagents of the more reactive type ArMgCl·LiCl.[8] Thus, the reaction of these relatively unreactive magnesium reagents with various ketones proceeded in only moderate yields in the absence of lanthanide salts, whereas excellent yields were obtained in the presence of $LnCl_3 \cdot 2\,LiCl$ (73–95% yield; entries 5–11).

Even Grignard reagent **2e** bearing a sensitive nitro function reacted cleanly with the ketone **3g** in the presence of $LaCl_3 \cdot 2\,LiCl$. In contrast, in the absence of lanthanide salts as well when Imamoto's procedure was employed, no product



Scheme 1. Preparation of soluble lanthanide salts **1** and products of the reaction of organomagnesium reagents **2** with ketones **3**.

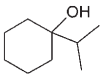
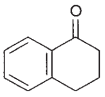
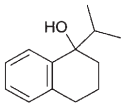
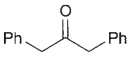
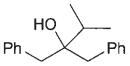
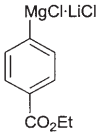
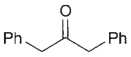
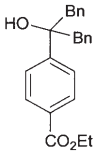
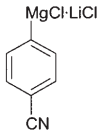
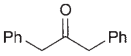
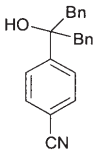
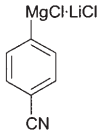
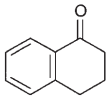
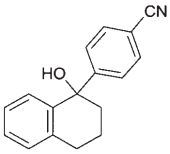
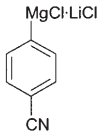
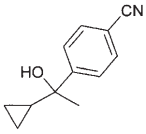
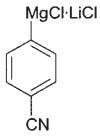
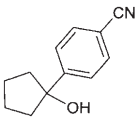
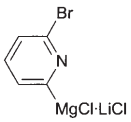
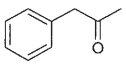
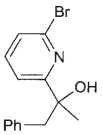
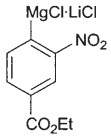
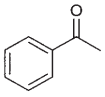
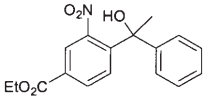
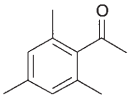
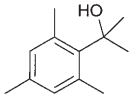
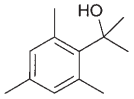
[*] Dr. A. Krasovskiy, Dipl.-Chem. F. Kopp, Prof. Dr. P. Knochel
Ludwig-Maximilians-Universität München
Department Chemie
Butenandtstrasse 5–13, Haus F, 81377 München (Germany)
Fax: (+49) 89-2180-77680
E-mail: paul.knochel@cup.uni-muenchen.de

[**] We thank the Fonds der Chemischen Industrie and Merck Research Laboratories (MSD) for financial support. We also thank Chemetall, BASF, and Bayer Chemicals for generous gifts of chemicals. Ln = La, Ce, Nd.

Supporting information for this article is available on the WWW under http://www.angewandte.org or from the author.

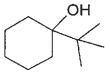
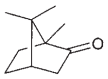
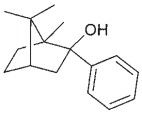
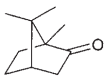
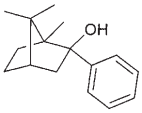
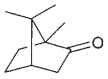
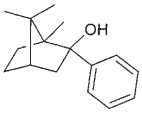
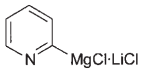
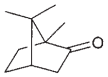
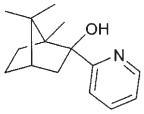
 © 2006 Wiley-VCH Verlag GmbH & Co. KGaA, Weinheim

Table 1: Reactions of ketones **2** with Grignard reagents **1** without additives, and in the presence of $CeCl_3$ or $LnCl_3 \cdot 2\,LiCl$ (Ln = La, Ce, Nd).

Entry	Grignard reagent **2**		Ketone of type **3**		Product of type **4**		Yield [%] without additives[a]	with $CeCl_3$[b]	with $LnCl_3 \cdot 2\,LiCl$
1	*i*PrMgCl	**2a**		**3a**		**4a**	3–5	72 (80)[c]	92[d] 94[e] 92[f]
2	*i*PrMgCl	**2a**		**3b**		**4b**	30	80 (93)[c]	97[d] 98[e]
3	*i*PrMgCl	**2a**		**3c**		**4c**	30	73	95[d] 95[e]
4	*i*PrMgCl	**2a**		**3d**		**4d**	3	–	96[d] 95[e] 97[f]
5		**2b**		**3d**		**4e**	39	11	92[d] 91[e]
6		**2c**		**3d**		**4f**	37	8	86[d] 89[e] 88[f]
7		**2c**		**3c**		**4g**	48	16	87[d]
8		**2c**		**3e**		**4h**	50	–	86[d]
9		**2c**		**3a**		**4i**	27	–	95[d] 94[e]
10		**2d**		**3f**		**4j**	35	–	81[d]
11		**2e**		**3g**		**4k**	0	0	73[d]
12	MeMgCl	**2f**		**3h**		**4l**	1	47	61[d] 65[e]
13		**2g**		**3i**		**4l**	22	57	69[d,g] 71[e,g]

© 2006 Wiley-VCH Verlag GmbH & Co. KGaA, Weinheim

Table 1: (Continued)

Entry	Grignard reagent **2**		Ketone of type **3**		Product of type **4**		Yield [%] without additives[a]	with $CeCl_3$[b]	with $LnCl_3{\cdot}2\,LiCl$
14	*t*BuMgCl·LiCl	**2h**		**3b**		**4m**	4	–	92[d] 93[e]
15	PhMgCl	**2i**		**3j**		**4n**	21	–	93[d]
16	PhMgBr·LiCl	**2j**		**3j**		**4n**	–	–	92[d] (65)[h]
17	PhMgI·LiCl	**2k**		**3j**		**4n**	–	–	89[d]
18		**2l**		**3j**		**4o**	17	53	92[d]

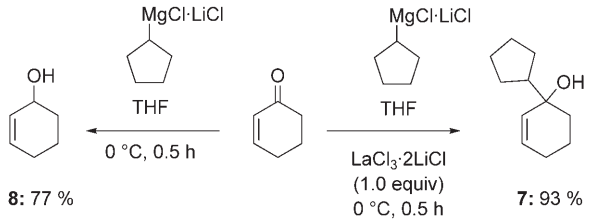
[a] Yield of isolated product obtained by the direct reaction of the ketone with the Grignard reagent. [b] Yield of isolated product obtained in the presence of $CeCl_3$ (1.5 equiv) according to the method of Imamoto. [c] Yield of isolated product obtained in the presence of $CeCl_3$ (1.0 equiv) according to the method of Dimitrov. [d] Reaction performed with $LaCl_3{\cdot}2\,LiCl$ (1.0 equiv). [e] Reaction performed with $CeCl_3{\cdot}2\,LiCl$ (1.0 equiv). [f] Reaction performed with $NdCl_3{\cdot}2\,LiCl$ (1.0 equiv). [g] The Grignard reagent was first transmetalated by addition of $LnCl_3{\cdot}2\,LiCl$ (1.0 equiv) and stirred for 4 h at room temperature before the ketone was added at 0 °C. [h] The reaction was performed in the presence of 10 mol% $LaCl_3{\cdot}2\,LiCl$.

4k could be obtained. The reactions of sterically very hindered ketones such as the mesityl methyl ketone **3h** and hindered Grignard reagents such as mesitylmagnesium bromide **2g** and *tert*-butylmagnesium chloride **2h** gave moderate yields. A significant improvement was achieved when these reactions were performed in the presence of $LaCl_3{\cdot}2\,LiCl$ (entries 12–14).

In a further example, the addition of PhMgCl (**3i**) to camphor (**3j**) was highly diastereoselective and led to the alcohol **4n** in 93% yield (entry 15). The Grignard reagent's halide ion shows only little influence on the addition reaction. Thus, the magnesium reagents obtained by insertion from phenyl bromide and iodide, respectively, also led to the clean formation of the desired product **4n** in good yields (92 and 89%, entries 16 and 17, respectively). Even a catalytic amount of $LaCl_3{\cdot}2\,LiCl$ promoted this addition reaction, and the desired product was still obtained as one diastereoisomer in 65% yield when only 10 mol% $LaCl_3{\cdot}2\,LiCl$ was used (entry 16, value in brackets).

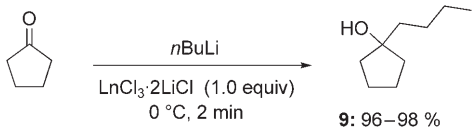
Similarly, the addition of 2-pyridylmagnesium chloride (**2l**) to camphor (**3j**) produced the pyridineisoborneol derivative **4o** as one isomer (92%, entry 18). In the case of α,β-unsaturated ketones such as cyclohex-2-enone, the addition of secondary alkylmagnesium compounds like cyclopentylmagnesium chloride proceeded exclusively in the presence of $LaCl_3{\cdot}2\,LiCl$ leading to the desired tertiary allylic alcohol **7** in 93% yield. In the absence of this salt, the only product observed was the allylic alcohol **8**, which was isolated in 77% yield (Scheme 2).

Lanthanide(III) salts also promote addition of organolithium compounds to ketones. Almost quantitative yields of



Scheme 2. 1,2-Addition of a Grignard reagent to cyclohexenone promoted by $LaCl_3{\cdot}2\,LiCl$.

the desired alcohols were achieved, whereas other methods gave worse results. Thus, the addition of *n*BuLi to cyclopentanone at 0 °C led to the desired alcohol **9** in 96–98% yield, whereas Imamoto's procedure required low temperatures (−78 °C) and longer reaction times (Scheme 3).

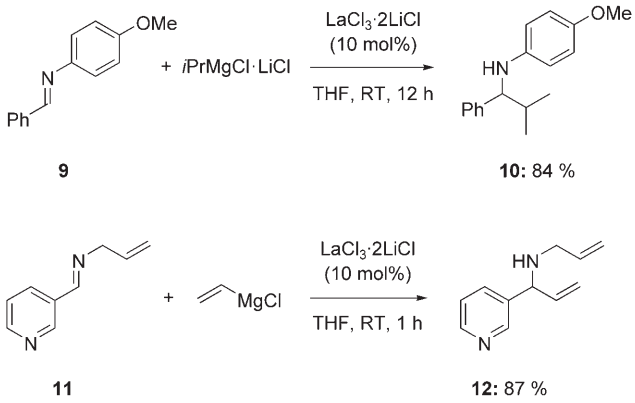


Scheme 3. Addition of *n*BuLi to cyclopentanone promoted by $LnCl_3{\cdot}2\,LiCl$. Imamoto's procedure: −78 °C, 3 h, 77%.

Finally, catalytic amounts of $LnCl_3{\cdot}2\,LiCl$ (10 mol%) were sufficient to promote the addition of Grignard reagents to nonactivated imines such as **9**. In the absence of the catalyst, the amine **10** was isolated in 15% yield, whereas in the presence of $LaCl_3{\cdot}2\,LiCl$ (10 mol%) the addition product **10**

 © 2006 Wiley-VCH Verlag GmbH & Co. KGaA, Weinheim

was obtained in 84% yield. Similarily, the addition of vinylmagnesium chloride to the imine **11** provides the bis-(allyl) amine **12** in 87% yield (Scheme 4).[9]



Scheme 4. $LaCl_3 \cdot 2\,LiCl$-catalyzed addition of Grignard reagents to imines.

In summary, we have shown that $LnCl_3 \cdot 2\,LiCl$ (Ln = La, Ce, Nd)[10] are readily available as THF solutions. They are superior promoters for the addition of various organometallic reagents to ketones. They also catalyze efficiently the addition of organomagnesium compounds to imines. Further applications of these soluble lanthanide salts are currently under investigation in our laboratories.

Experimental Section

Typical procedure (preparation of a solution of $LaCl_3 \cdot 2\,LiCl$ in THF): Commercially available $LaCl_3 \cdot 6H_2O$ (0.10 mol, 35.3 g) was mixed with LiCl (0.20 mol, 8.40 g) in a 500-mL Schlenk flask, and water (100 mL) was slowly added with vigorous stirring. The resulting slurry was stirred under high vacuum (0.01 mm Hg) at room temperature for 4 h. Stirring was continued for 4 h at 40 °C, 4 h at 60 °C, 4 h at 80 °C, 4 h at 100 °C, 4 h at 120 °C, 4 h at 140 °C and finally 4 h at 160 °C. The slow increase of temperature and highly efficient stirring were essential. The resulting solid was cooled to room temperature, and THF was added until a total volume of 300 mL was reached. Then, molecular sieves (50 g; 4 Å) were added, and the resulting mixture was stirred vigorously for 1 d at RT. Finally, the insoluble material (mostly crushed molecular sieves) was removed by filtration through a combined filter system (fresh molecular sieves/filter paper) under an argon atmosphere. By this procedure, a clear and colorless solution of $LaCl_3 \cdot 2\,LiCl$ was obtained which was stored until use at room temperature under argon.

Typical procedure for the $LaCl_3 \cdot 2\,LiCl$-mediated addition of Grignard reagents to ketones and imines (synthesis of **4c**; see Table 1, entry 3): In a flame-dried, argon-flushed 25-mL Schlenk flask equipped with a septum and a magnetic stirring bar was placed $LaCl_3 \cdot 2\,LiCl$ in THF (0.33 M; 6.10 mL, 2.00 mmol, 1.00 equiv). α-Tetralone (292 mg; 2.00 mmol) was added neat, and the resulting mixture was stirred for 1 h at room temperature. The reaction mixture was cooled to 0 °C, *i*PrMgCl (2.10 mL of a 1.00 M solution in THF, 2.10 mmol, 1.05 equiv) was added dropwise, and the reaction mixture was allowed to stir at the same temperature. When the conversion was complete (GC analysis of reaction aliquots), saturated aqueous NH_4Cl (2 mL) and water (2 mL) were added. The aqueous layer was extracted with diethyl ether (4 × 10 mL), and the combined extracts were dried (Na_2SO_4) and concentrated to dryness. The crude residue was purified by flash column chromatography (silica; pentane/Et_2O 10:1) to give **4c** as a colorless, crystalline solid (361 mg, 1.90 mmol, 95%, m.p. 101 °C).

Received: July 16, 2005
Revised: September 29, 2005

Keywords: 1,2-additions · enols · Grignard reaction · imines · lanthanides

[1] a) S. Kobayashi, M. Sugiura, H. W. L. Lam, *Chem. Rev.* **2002**, *102*, 2227; b) S. Kobayashi, K. Manabe, *Acc. Chem. Res.* **2002**, *35*, 209.
[2] a) T. Imamoto, Y. Sugiyura, N. Takiyama, *Tetrahedron Lett.* **1984**, *25*, 4233; b) T. Imamoto, N. Takiyama, K. Nakamura, *Tetrahedron Lett.* **1985**, *26*, 4763; c) T. Imamoto, Y. Sugiyura, N. Takiyama, T. Hatojima, Y. Kamiya, *J. Am. Chem. Soc.* **1989**, *111*, 4392; d) H. Schumann, M. Glanz, J. Gottfriedsen, S. Dechert, D. Wolff, *Pure Appl. Chem.* **2001**, *73*, 279.
[3] V. Dimitrov, K. Koslova, M. Genov, *Tetrahedron Lett.* **1996**, *37*, 6787.
[4] a) U. Groth, M. Jeske, *Angew. Chem.* **2000**, *112*, 586; *Angew. Chem. Int. Ed.* **2000**, *39*, 574; b) U. Groth, M. Jeske, *Synlett* **2001**, 129; c) S. Fischer, U. Groth, M. Jeske, T. Schutz, *Synlett* **2002**, 1922; see also d) W.-D. Z. Li, J.-H. Yang, *Org. Lett.* **2004**, *6*, 1849; e) D. Tsvelikhovsky, D. Gelman, G. A. Molander, J. Blum, *Org. Lett.* **2004**, *6*, 1995; f) M. Shenglof, D. Gelman, G. A. Molander, J. Blum, *Tetrahedron Lett.* **2003**, *44*, 8593; g) P. Eckenberg, U. Groth, T. Köhler, *Liebigs Ann. Chem.* **1994**, 673; h) M. Hatano, T. Matsuma, K. Ishkihara, *Org. Lett.* **2005**, *7*, 573; i) S. Fukuzawa, T. Fujinami, S. Yamauchi, S. Sakai, *J. Chem. Soc. Perkin Trans. 1* **1986**, 1929; j) F. T. Edelmann, D. M. M. Freckmann, H. Schumann, *Chem. Rev.* **2002**, *102*, 1851.
[5] Y. Y. Novikov, P. Sampson, *Org. Lett.* **2003**, *5*, 2263.
[6] a) K. Rossmanith, *Monatsh. Chem.* **1979**, *110*, 109; b) J. Zhongsheng, H. Ninghai, L. Yi, X. Xiaolong, L. Guozhi *Inorg. Chim. Acta* **1988**, *142*, 333; c) Q. Shen, W. Chen, Y. Jin, C. Shan, *Pure Appl. Chem.* **1988**, *60*, 1251; d) C. P. Groen, A. Oskam, A. Kovacs, *Inorg. Chem.* **2000**, *39*, 6001; e) H. J. Heeres, A. Meetsma, J. H. Teuben, R. D. Rogers, *Organometallics* **1989**, *8*, 2637; f) J. Guan, S. Jin, Y. Lin, Q. Shen, *Organometallics* **1992**, *11*, 2483.
[7] The amount of the remaining protic impurities was determined by titration with *n*BuLi using *ortho*-phenanthroline as indicator in analogy to the method for determining the concentration of Li and Mg reagents described by Paquette: H.-S. Lin, L. Paquette, *Synth. Commun.* **1994**, *24*, 2503.
[8] A. Krasovskiy, P. Knochel, *Angew. Chem.* **2004**, *116*, 3396; *Angew. Chem. Int. Ed.* **2004**, *43*, 3333. The reagent *i*PrMgCl·LiCl is commercially available as a solution in THF from Chemetall GmbH (Frankfurt).
[9] Imines of aliphatic aldehydes can also be used, but equimolar amounts of $LnCl_3 \cdot 2\,LiCl$ are required for full conversion. The addition of Grignard reagents to imines of α,β-unsaturated aldehydes required at least 0.3 equiv of $LnCl_3 \cdot 2\,LiCl$.
[10] Additionally, $ErCl_3 \cdot 6H_2O$, $PrCl_3 \cdot 6H_2O$, $YCl_3 \cdot 6H_2O$,and $DyCl_3 \cdot 6H_2O$ were used analogously to prepare solutions of type $LnCl_3 \cdot 2\,LiCl$. Whereas the reactivity of $PrCl_3 \cdot 2\,LiCl$ is similar to that of the La, Ce, and Nd derivatives (**1a–c**), $ErCl_3 \cdot 2\,LiCl$, $YCl_3 \cdot 2\,LiCl$, and $DyCl_3 \cdot 2\,LiCl$ display lower catalytic activities and give mediocre results in the addition reactions.

 © 2006 Wiley-VCH Verlag GmbH & Co. KGaA, Weinheim

Ion Channels

DOI: 10.1002/anie.200502570

Crown Ether–Gramicidin Hybrid Ion Channels: Dehydration-Assisted Ion Selectivity**

*Jochen R. Pfeifer, Philipp Reiß, and Ulrich Koert**

Ion selectivity is a prerequisite for biological ion channels to fulfil their function in cellular regulation and communication.[1] In biological ion channels protein subunits are precisely arranged to assemble ion-selectivity filters.[2] Predictable ion selectivity is a major goal for the use of synthetic channels in biological systems, for example, for the treatment of so-called "channelopathies", diseases triggered by ion-channel defects. Although substantial progress has been made in the field of synthetic ion channels in the past decade,[3] ion-selective channels are still rare.[4,5]

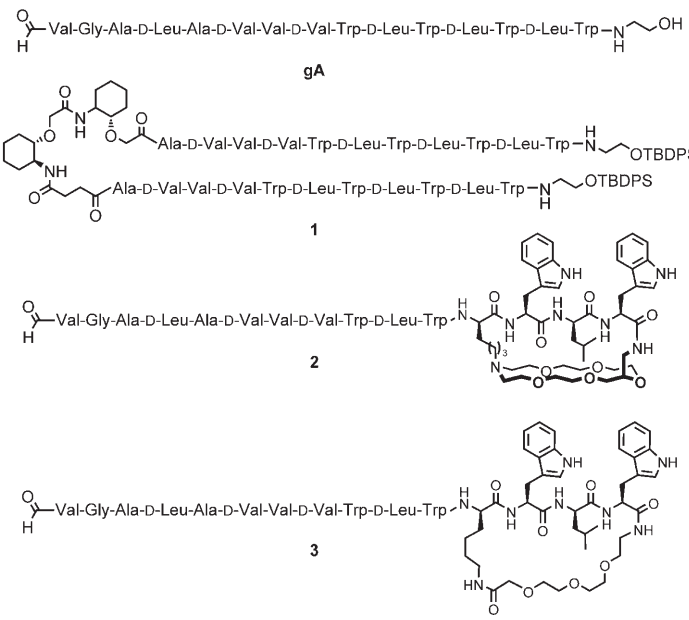
Gramicidin A (**gA**) represents a suitable lead structure for ion-channel engineering.[6] Its channel active structure is a $\beta^{6.3}$ helix with a pore diameter of 4 Å.[7] **gA** transports monovalent cations. Within this group of ions the permeability decreases with increasing dehydration energy (Eisenman I selectivity),[8] as the passage of the cation through the channel requires partial removal of the hydration shell. The necessary dehydration energy at the channel entrance is balanced with the binding energy gained by the interaction of the cation with the carbonyl groups that line the interior of the pore. This classical concept of electrostatic attraction as origin of ion selectivity was confirmed by recent calculations explaining selectivity of protein channels.[9] When comparing K^+ and Cs^+ transport, the higher K^+ dehydration energy leads to a Cs^+/K^+ selectivity of 3:2 (based on conductivity measurements).

The introduction of two cyclohexyl ether δ-amino acids in the central part of a succinyl-linked gramicidin derivative leads to compound **1**, which exhibits a Cs^+/K^+ selectivity of 10:1.[5] The two oxygen atoms of the ether group of **1** (TBDPS = *tert*-butyldiphenylsilyl) act as additional cation-binding sites in the interior of the pore and induce increased Cs^+/K^+ selectivity.

Crown ethers are capable of solvating alkali-metal cations selectively, depending on their size. On the other hand, their complexation/decomplexation ratios are compatible with an ion flux of $10^7\ s^{-1}$ through the channel.[10] Crown ethers are therefore suitable building blocks for synthetic ion channels—however, remarkable effects on ion selectivity have not yet been reported.[11]

Crown ether–**gA** hybrid **2** was designed with the goals of creating additional binding sites at the channel entrance and of tuning the cation desolvation. The D-leucine residue[12] of **gA** was replaced with D-lysine. Both its ε-nitrogen atom and the C-terminal ethanolamine group of **gA** are part of an aza-[18]crown-6 ether (two-point attachment). To function properly, the crown ether moiety must be linked to the channel entrance at least at two positions.[12] The oligoethylene glycol loop–**gA** hybrid **3** was synthesized for comparison.

The synthesis of **2** started with (*S*)-glycidol tosylate,[13] which was converted into the bis(trityl ether) **4** (see Supporting Information). To avoid aqueous workup, the trityl ethers in compound **4** were cleaved by using triethylsilane and a catalytic amount of TES triflate,[14] with subsequent addition of HF (5% in CH_3CN) (Scheme 1). After removal of the solvents, the crude diol was converted into the dibromide **5** via a bismesylate. The template effect of the potassium cation was exploited in the cyclization to the aza crown ether peptide **7** by the slow addition of a solution of dibromide **5** in CH_3CN to a refluxing solution of tetrapeptide **6** and K_2CO_3 in CH_3CN.[15] The presence of additional, soluble KPF_6 was necessary to attain a cyclization yield of 50%. After reduction of the azide and saponification of the methyl ester, peptide cyclization in 10^{-3} M solution gave rise to **8** in a very good yield of 67%. Cleavage of the Boc protecting group followed by peptide coupling with undecamer **9** (peptides were synthesized by a fragment-coupling strategy in solution,[16] see Supporting Information) furnished the target compound **2**. In this last step it was crucial to deactivate the basic tertiary amine nitrogen atom of the aza crown ether in order to suppress epimerization. This was achieved by

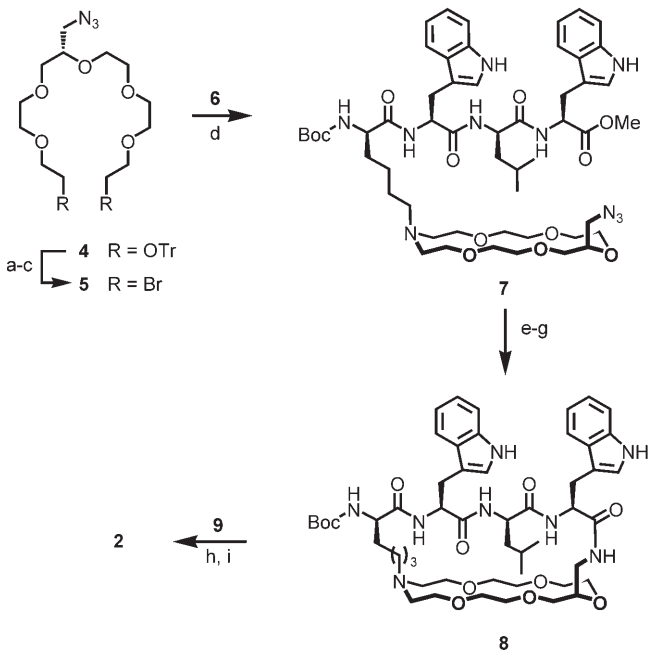


[*] Dipl.-Chem. J. R. Pfeifer, Dr. P. Reiß, Prof. Dr. U. Koert
Fachbereich Chemie
Philipps-Universität Marburg
Hans-Meerwein-Strasse, 35032 Marburg (Germany)
Fax: (+49) 6421-28-25677
E-mail: koert@chemie.uni-marburg.de

[**] Financial support by the Deutsche Forschungsgemeinschaft, the Fonds der Chemischen Industrie, the Volkswagen Foundation, and the Pinguin Foundation is gratefully acknowledged. We thank Dr. U. Linne for ESI TOF mass spectra as well as Nadine Jede and Prof. Diederichsen (Göttingen University) for the use of their CD spectrometer.

Supporting information for this article is available on the WWW under http://www.angewandte.org or from the author.

 © 2006 Wiley-VCH Verlag GmbH & Co. KGaA, Weinheim



6: Boc-D-Lys-Trp-D-Leu-Trp-OMe

9: O(H)-Val-Gly-Ala-D-Leu-Ala-D-Val-Val-D-Val-Trp-D-Leu-Trp-OH

Scheme 1. Synthesis of **2**: a) 1. Et_3SiH, TESOTf (0.01 equiv), CH_2Cl_2, 20 °C, 1 h; 2. HF in CH_3CN (5%), room temperature, 30 min; b) MsCl, NEt_3, CH_2Cl_2, 0 °C; c) LiBr, acetone, 56 °C, 4 h, 79% (three steps); d) **6**, K_2CO_3, KPF_6, CH_3CN, 81 °C, 16 h, 50%; e) H_2, Pd/C, MeOH, 40 °C, 2 h, 82%; f) LiOH, THF/H_2O (4:1), 0 °C, 4 h, 99%; g) HATU, HOAt, $EtNiPr_2$, CH_2Cl_2/DMF (3:1), −18→0 °C, 12 h, 67%; h) TFA in CH_2Cl_2 (50%) EDT, 20 °C, 20 min, 80%, i) **9**, HATU, HOAt, $EtNiPr_2$, KPF_6 (10 equiv), CH_2Cl_2/DMF (3:1), 25 °C, 15 min, 64%. Tr = triphenylmethyl, TES = triethylsilyl, Tf = trifluoromethanesulfonyl, Ms = methanesulfonyl, Boc = *tert*-butoxycarbonyl, HATU = *O*-(7-azabenzotriazol-1-yl)-1,1,3,3-tetramethyluronium hexafluorophosphate, HOAt = 7-aza-1-hydroxy-1*H*-benzotriazole, DMF = *N*,*N*-dimethylformamide, TFA = trifluoroacetic acid, EDT = ethanedithiol.

performing the peptide-coupling reaction in the presence of 10 equivalents of KPF_6.

The ion-channel activity was investigated with the planar lipid bilayer technique.[17] Figure 1 shows representative single-channel current traces for a) **gA**, b) **2**, and c) **3** measured in 1 M CsCl (left column) and 1 M KCl (right column), respectively. The Cs^+ conductivity of **2** is lower than that of **gA**, whereas the K^+ conductivity is higher. Compound **2** represents the first **gA** derivative with an altered conductivity order $K^+ > Cs^+$!

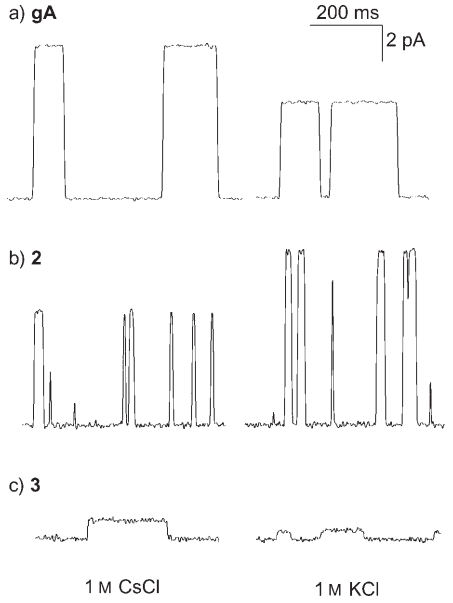


Figure 1. Single-channel current traces for **gA**, aza crown ether–gramicidin **2**, and oligoethylene glycol loop gramicidin **3**. MCl (1 M), 200 mV, DPhPC/DPhPG (4:1).

Upon closer inspection (Table 1), four observations are remarkable:

1) Despite the extensive modifications of the gramicidin structure, conductivities are in the same order of magnitude as for **gA**. Typically the incorporation of artificial building blocks[5,18] or simple amino acid substitutions[19] result in dramatically lower conductivities; see the current trace for oligoethylene glycol loop hybrid channel **3** (Figure 1c).
2) Conductivities for Cs^+ are decreased by 19% in DPhPC/DPhPG (4:1) and even 54% in DOPC relative to the values for **gA**. On the other hand, K^+ conductivity is 36% higher in DPhPC/DPhPG (4:1) and 9% higher in DOPC.
3) Evidently the influence of the crown ether is superposed by the intrinsic ion preference of **gA**. This accounts for the high conductivities for Rb^+. To eliminate the influence of **gA**, relative conductivities were calculated (Figure 2). The diagram reveals that K^+ is the only cation whose transport benefits from the crown ether. K^+ fits best into the aza-[18]crown-6 ether, which results in optimal dehydration assistance and therefore improved ion conductivity.
4) Changes in conductivities depend on the membrane rigidity and charge. Except for Cs^+ in the charged and rigid membrane DPhPC/DPhPG (4:1), conductivities are even higher than those observed for **gA**.

Table 1: Conductivity figures Λ[a] for **2** and **gA** determined for different cations and phospholipids.

	Na^+		K^+		Rb^+		Cs^+	
Membrane	Λ(**2**) pS	Λ(**gA**)	Λ(**2**)	Λ(**gA**)	Λ(**2**)	Λ(**gA**)	Λ(**2**)	Λ(**gA**)
DOPC[b]	11.4	14.6	22.4	20.6	27.0	38.4	16.0	36.7
DPhPC/DPhPG[c]	18.8	14.3	37.7	27.8	55.8	47.2	33.3	40.9

[a] Conductivity [pS], determined from the slope of the current-voltage curve (see Supporting Information). The error margins constitute ±5% as ascertained by at least two independent measurements; [b] DOPC = 1,2-dioleoyl-*sn*-glycero-3-phosphocholine; [c] DPhPC = 1,2-diphytanoyl-*sn*-glycero-3-phosphocholine, DPhPG = 1,2-diphytanoyl-*sn*-glycero-3-[phospho-*rac*-(1-glycerol)], 4:1 mixture

 © 2006 Wiley-VCH Verlag GmbH & Co. KGaA, Weinheim

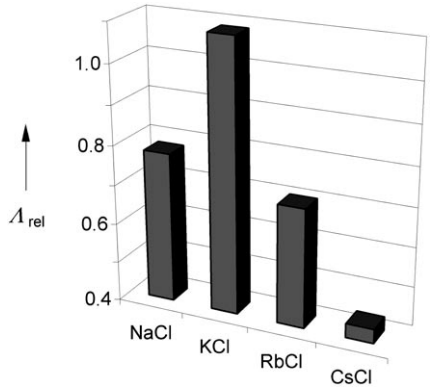


Figure 2. Conductivities for **2** relative to **gA** in DOPC.

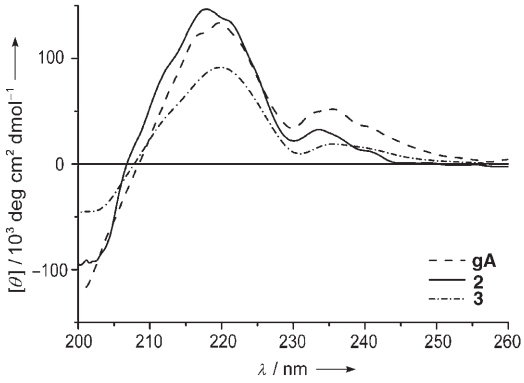


Figure 3. CD spectra in DMPC vesicles for **2**, **3**, and **gA** (22 °C, 10^{-4} M).

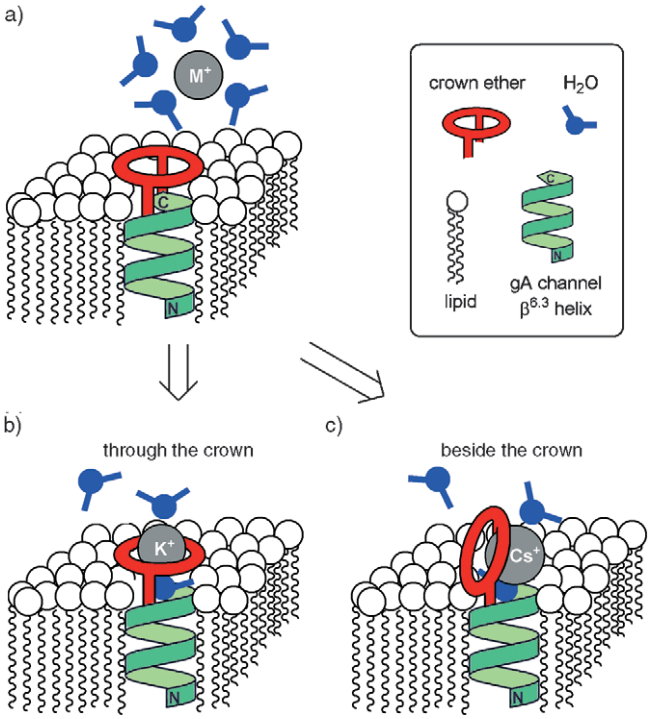


Figure 4. Schematic representation for the entering of a solvated cation into the channel formed by **2**. Approach of the hydrated cation (a). Dehydration assistance occurs by passing through the crown ether (b) or beside the crown ether (c).

CD measurements in a lipid environment (Figure 3) indicate that the formation of the channel active $\beta^{6.3}$ helix is not impeded by the two-point attachment of the crown ether.[20]

The observed single-channel currents can, in principle, arise from passing of the cations through the crown ether (as depicted in Figure 4b for K^+) or from a conformation in which the crown is bent aside (as shown in Figure 4c for Cs^+).

At first glance it might be astonishing that Cs^+ (ionic diameter 326–372 pm) may slip through an [18]crown-6 derivative (internal diameter 260–320 pm).[21] It is known from many X-ray crystal structures of [18]crown-6–alkali-metal complexes that K^+ is located within the macrocycle, whereas the bigger alkali-metal ions prefer a "sunrise" conformation (cation sitting above the plane) or sandwich structures (single cation is held between a pair of crown ether ligands).[22,23] Crystal formation is mostly a thermodynamically controlled process. The conditions applied during single-channel current analysis are far from thermodynamic equilibrium: The high electric field (magnitude of 100 kV mm^{-1}) resting against the membrane exerts a strong force on the migrating ions. It is at least conceivable that the bigger alkali-metal ions are pulled through an [18]crown-6 derivative under these conditions (Figure 4b). One might compare this process with the thermally induced slippage of bulky organic groups through small rings in rotaxane synthesis.[24]

Compound **3**, which lacks the intact crown scaffold but bears a sterically comparable oligoethylene glycol loop at the channel entrance, can assist cation dehydration according to Figure 4c only. The dramatically decreased conductivities for **3** (Figure 1) indicate a different transport mechanism for compound **2** and support the pathway depicted in Figure 4b. Dwell times for transport of Cs^+ (33 ± 4 ms) resemble those observed for K^+ (44 ± 5 ms).

In conclusion, a novel crown ether–**gA** hybrid molecule was synthesized and functionally characterized with respect to ion-selective channel transport. Compound **2** shows a higher preference for K^+ than for Cs^+ and is one of the very rare examples that exhibits higher conductivities than native **gA**.[25] Thus the approach to influence ion selectivity by facilitating desolvation seems to be a very promising concept.

Received: July 22, 2005
Published online: December 8, 2005

Keywords: crown compounds · ion channels · ion selectivity · peptides · synthesis design

[1] E. Neher, B. Sakman, *Nature* **1976**, *260*, 799–802; B. Hille, *Ion Channels of Exitable Membranes*, 3rd ed., Sinauer, Sunderland, **2001**.

[2] a) D. A. Doyle, J. H. Morais-Cabral, R. A. Pfuetzner, A. Kuo, J. M. Gulbis, S. L. Cohen, B. T. Chait, R. MacKinnon, *Science* **1998**, *280*, 69–77; b) J. H. Morais-Cabral, Y. Zhou, R. MacKinnon, *Nature* **2001**, *414*, 37–42; c) Y. Zhou, J. H. Morais-

 © 2006 Wiley-VCH Verlag GmbH & Co. KGaA, Weinheim

Cabral, K. Amelia, R. MacKinnon, *Nature* **2001**, *414*, 43 – 48; d) R. MacKinnon, *Angew. Chem.* **2004**, 116, 4363 – 4376; *Angew. Chem. Int. Ed* **2004**, *43*, 4265 – 4277.
[3] Selected reviews on artificial ion channels: a) G. W. Gokel, O. Murillo, *Acc. Chem. Res.* **1996**, *29*, 425 – 432; b) K. S. Åkerfeldt, J. D. Lear, Z. R. Wasserman, L. A. Chung, W. F. DeGrado, *Acc. Chem. Res.* **1993**, *26*, 191 – 197; c) N. Voyer, *Top. Curr. Chem.* **1996**, *184*, 1 – 37; d) G. W. Gokel, A. Mukhopadhyay, *Chem. Soc. Rev.* **2001**, *30*, 274 – 286; e) U. Koert, L. Al-Momani, J. R. Pfeifer, *Synthesis* **2004**, 1129 – 1146; f) S. Matile, A. Som, N. Sordé, *Tetrahedron* **2004**, *60*, 6405 – 6435.
[4] a) Y. Tanaka, Y. Kobuke, M. Sokabe, *Angew. Chem.* **1995**, *107*, 717 – 719; *Angew. Chem. Int. Ed. Engl.* **1995**, *34*, 693 – 694; b) T. M. Fyles, D. Loock, W. F. van Straaten-Nijenhuis, X. Zhou, *J. Org. Chem.* **1996**, *61*, 8866 – 8874; c) A. J. Wright, S. E. Matthews, W. B. Fischer, P. D. Beer, *Chem. Eur. J.* **2001**, *7*, 3474 – 3481.
[5] H.-D. Arndt, A. Knoll, U. Koert, *Angew. Chem.* **2001**, *113*, 2137 – 2140; *Angew. Chem. Int. Ed.* **2001**, *40*, 2076 – 2078.
[6] *Gramicidin and Related Ion Channel-Forming Peptides*, Wiley, Chichester, **1999**.
[7] R. R. Ketchem, B. Roux, T. A. Cross, *Structure* **1997**, *5*, 1655 – 1669.
[8] G. Eisenman, R. Horn, *J. Membr. Biol.* **1983**, *76*, 197 – 225.
[9] S. Y. Noskov, S. Bernèche, B. Roux, *Nature* **2004**, *431*, 830 – 834.
[10] J. S. Bradshaw, R. M. Izatt, A. V. Bordunov, C. Y. Zhu, Hathaway in *Comprehensive Supramolecular Chemistry Vol. 1* (Eds.: J. L. Atwood, J. E. D. Davies, D. D. Macnicol, F. Vögte, G. W. Gokel), Pergamon, Oxford, **1996**, pp. 35 – 95.
[11] a) M. J. Pregel, L. Jullien, J.-M. Lehn, *Angew. Chem.* **1992**, *104*, 1695 – 1697; *Angew. Chem. Int. Ed. Engl.* **1992**, *31*, 1637 – 1640; b) G. G. Cross, T. M. Fyles, T. D. James, M. Zojaji, *Synlett* **1993**, 449 – 460; c) J.-C. Meillon, N. Voyer, *Angew. Chem.* **1997**, *109*, 1004 – 1006; *Angew. Chem. Int. Ed. Engl.* **1997**, *36*, 967 – 969; d) E. Biron, F. Otis, J.-C. Meillon, M. Robitaille, J. Lamothe, P. Van Hove, M.-E. Cormier, N. Voyer, *Bioorg. Med. Chem.* **2004**, *12*, 1279 – 1290; e) G. W. Gokel, *Chem. Commun.* **2000**, 1 – 9; f) G. W. Gokel, R. Ferdani, J. Liu, R. Pajewski, H. Shabany, P. Uetrecht, *Chem. Eur. J.* **2001**, *7*, 33 – 39; g) J.-Y. Winum, S. Matile, *J. Am. Chem. Soc.* **1999**, *121*, 7961 – 7962; h) A. C. Hall, C. Suarez, A. Hom-Choudhury, A. N. A. Manu, C. D. Hall, G. Kirkovits, I. Ghiriviga, *Org. Biomol. Chem.* **2003**, *1*, 2973 – 2982.
[12] D. C. J. Jaikaran, Z. Zhang, G. A. Woolley, *Biochim. Biophys. Acta* **1995**, *1234*, 133 – 138.
[13] J. M. Klunder, T. Onami, K. B. Sharpless, *J. Org. Chem.* **1989**, *54*, 1295 – 1304.
[14] H. Imagawa, T. Tsuchihashi, R. K. Singh, H. Yamamoto, T. Sugihara, M. Nishizawa, *Org. Lett.* **2003**, *5*, 153 – 155.
[15] K. E. Krakowiak, J. S. Bradshaw, D. J. Zamecka-Krakowiak, *Chem. Rev.* **1989**, *89*, 929 – 972.
[16] H.-D. Arndt, A. Vescovi, A. Schrey, J. R. Pfeifer, U. Koert, *Tetrahedron* **2002**, *58*, 2789 – 2801.
[17] a) P. Mueller, D. O. Rudin, H. T. Tien, W. C. Wescott, *Nature* **1962**, *194*, 979 – 980; b) P. Mueller, D. O. Rudin, *Nature* **1968**, *217*, 713 – 719.
[18] A. Vescovi, A. Knoll, U. Koert, *Org. Biomol. Chem.* **2003**, *1*, 2983 – 2997.
[19] R. E. Koeppe II, J. Hatchett, A. R. Jude, L. L. Providence, O. S. Andersen, D. V. Greathouse, *Biochemistry* **2000**, *39*, 2235 – 2242, and references therein.
[20] B. A. Wallace, *J. Struct. Biol.* **1998**, *121*, 123 – 141.
[21] C. J. Pedersen, *J. Am. Chem. Soc.* **1970**, *92*, 386 – 391.
[22] a) J. W. Steed, *Coord. Chem. Rev.* **2001**, *215*, 171 – 221; b) A. V. Bajaj, N. S. Poonia, *Coord. Chem. Rev.* **1988**, *87*, 55 – 213.
[23] Nevertheless, a (slightly disorderd) structure in which Rb^+ sits perfectly within an [18]crown-6 has been reported: K. V. Domasevitch, V. V. Ponomareva, E. B. Rusanov, T. Gelbrich, J. Sieler, V. V. Skopenko, *Inorg. Chim. Acta* **1998**, *268*, 93 – 101.
[24] P. R. Ashton, M. Bělohradský, D. Philp, J. F. Stoddart, *J. Chem. Soc. Chem. Commun.* **1993**, 1269 – 1274.
[25] a) K. U. Prasad, S. Alonso-Romanowski, C. M. Venkatachalam, T. L. Trapane, D. W. Urry, *Biochemistry* **1986**, *25*, 456 – 463; b) D. A. Busath, C. D. Thulin, R. W. Hendershot, L. R. Phillips, P. Maughan, C. C. Cole, N. C. Bingham, S. Morrison, L. C. Baird, R. J. Hendershot, M. Cotten, T. A. Cross, *Biophys. J.* **1998**, *75*, 2830 – 2844.

 © 2006 Wiley-VCH Verlag GmbH & Co. KGaA, Weinheim

Photocatalysis

DOI: 10.1002/anie.200503084

Nanohybrids Composed of Quantum Dots and Cytochrome P450 as Photocatalysts**

*Binil Itty Ipe and Christof M. Niemeyer**

Semiconductor nanomaterials, such as quantum dots (QDs), quantum rods (QRs), and nanotubes, have potentials in a wide variety of fields ranging from nanoelectronics[1] and nanophotonics to the broad area of nanosensing[2–7] and bioimaging.[8,9] Moreover, the unusual physical and chemical properties of nanomaterials resulting from the spatial confinement of electrons have made them attractive candidates for the fabrication of new devices in energy technology.[10] For example, the absorption of light and the occurrence of electron-transfer reactions at the semiconductor/liquid interface have been investigated in detail for the design of solar cells.[11] In addition, the photocatalytic activity of semiconductor QDs has been a subject of intense research ever since their initial description,[12] and organic reactions carried out with QDs as photosensitizers have also been reported.[13–17]

[*] Dr. B. I. Ipe, Prof. Dr. C. M. Niemeyer
Biologisch-Chemische Mikrostrukturtechnik
Fachbereich Chemie, Universität Dortmund
Otto-Hahn-Strasse 6, 44227 Dortmund (Germany)
and
ISAS – Institute for Analytical Sciences
Bunsen-Kirchhoff-Strasse 11, 44139 Dortmund (Germany)
Fax: (+49) 231-755-7082
E-mail: christof.niemeyer@uni-dortmund.de

[**] This work was supported by the Deutsche Forschungsgemeinschaft and the Alexander von Humboldt Foundation (research fellowship for B.I.I.). We thank Dr. Isamu Matsunaga for the generous donation of the plasmid pQE-30tBSb for overexpression of recombinant P450, Andreas Arndt for help with the overexpression, and Dr. Ljiljana Fruk for help setting up the HPLC assay.

Supporting information for this article is available on the WWW under http://www.angewandte.org or from the author.

WILEY InterScience DISCOVER SOMETHING GREAT
© 2006 Wiley-VCH Verlag GmbH & Co. KGaA, Weinheim

Currently, nanotechnology and biotechnology are being joined to develop novel materials and devices, leading to the establishment of the new field of nanobiotechnology.[18] In this context, we report here on the photoactivated organic transformation catalyzed by hybrid devices composed of semiconductor nanoparticles and the enzyme cytochrome $P450_{BS\beta}$. $P450_{BS\beta}$ belongs to the broad class of monooxygenase enzymes which are well known to catalyze a range of stereospecific and regioselective oxygen-insertion reactions into organic compounds.[19] In particular, $P450_{BS\beta}$ catalyzes the hydroxylation of long-chain fatty acids at the α and β positions using hydrogen peroxide as an oxidant.[20]

The choice of this hybrid system was based, on the one hand, on the knowledge that radical species are involved in the catalytic cycle of P450-mediated oxygenation reactions[21–23] and, on the other hand, on the results of previous studies showing that the irradiation of CdS QDs leads to the formation of excitons (e^- and h^+), which generate superoxide ($O_2^{\bullet-}$) and hydroxyl ($OH^\bullet$) radicals in aqueous solutions.[24–26] We speculated that the superoxide and hydroxyl radicals could activate the enzymes adsorbed at the QD surface, thereby inducing specific monooxygenation of a suitable substrate. Such a photoactivation of enzymes could have significant advantages over conventional activation of $P450_{BS\beta}$ enzymes using H_2O_2, because the light-induced reaction would offer a much higher degree of control for the on/off switching of chemical reactivity than that possible in chemically initiated reactions.

To prepare the QD/$P450_{BS\beta}$ nanohybrids, recombinant $P450_{BS\beta}$ enzyme containing a 6×His tag at its C-terminus,[21] was overexpressed in *E. coli* and purified by nickel nitriloacetate (Ni-NTA) chromatography. CdS nanoparticles approximately 3 nm in diameter capped with a layer of mercaptoacetic acid were prepared in reverse-micellar medium, as previously described.[24] The $P450_{BS\beta}$ enzyme was attached to the CdS QDs by means of the electrostatic interaction between the positively charged hexahistidine tail of the enzyme and the negatively charged mercaptoacetic acid ligand shell of the CdS QDs (Figure 1).

For the preparation of the QD/$P450_{BS\beta}$ hybrid materials, the number of $P450_{BS\beta}$ molecules attached per QD was measured by means of FRET-quenching studies (FRET = fluorescence resonance energy transfer) between CdS (donor) and the heme enzyme (acceptor). Defined volumes of 6×-His-tagged $P450_{BS\beta}$ were titrated against a stock solution of CdS QDs, and the change in fluorescence intensity at 550 nm was monitored. A similar method was recently used to establish the interactions between CdSe QDs and cytochrome c.[27] The concentration of $P450_{BS\beta}$ was determined by means of CO differential absorption studies,[28] whereas the concentration of CdS QDs was calculated from inductively coupled plasma mass spectrometry.[24] Figure 2A shows the fluorescence spectra of QD/$P450_{BS\beta}$ nanohybrids. Each spectrum represents QDs mixed with variable molar equivalents of $P450_{BS\beta}$. The decrease in fluorescence emission of CdS QDs at 550 nm upon titration with $P450_{BS\beta}$ is shown in Figure 2B. It is evident that the continuous quenching of QD fluorescence ceases at approximately six molar equivalents of the $P450_{BS\beta}$ per QD. This surface coverage correlates well with theoretical considerations based on the size of the QDS and the enzyme (see the Supporting Information). The slight decrease in fluorescence observed on further increase of $P450_{BS\beta}$ concentration might be attributed to solution-based quenching effects.[29]

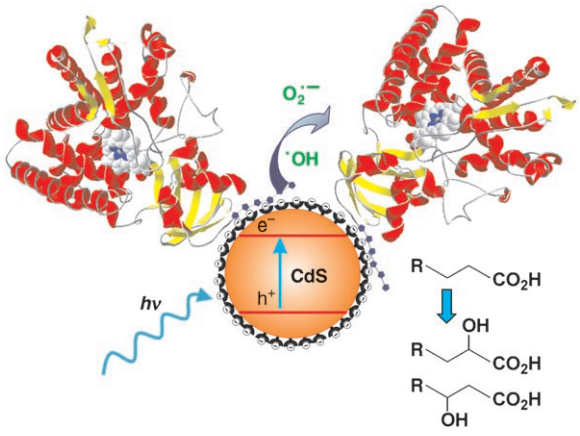


Figure 1. Monooxygenation of myristic acid (R = $(CH_2)_{10}CH_3$) using $P450_{BS\beta}$/QD nanohybrids.

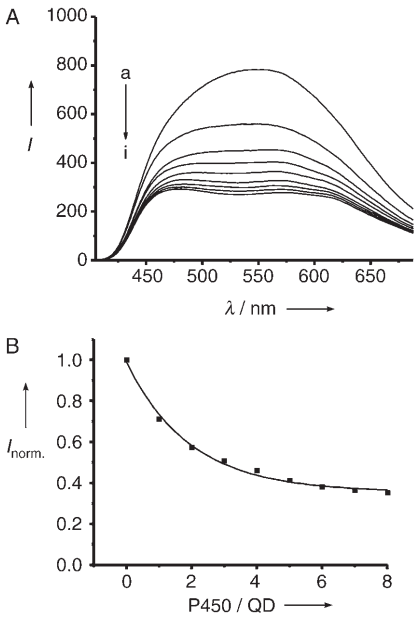


Figure 2. A) Photoluminescence quenching of CdS in the presence of different concentrations of the 6×His-$P450_{BS\beta}$ enzyme. [CdS]/[$P450_{BS\beta}$] ratio: a) 1:0, b) 1:1, c) 1:2, d) 1:3, e) 1:4, f) 1:5, g) 1:6, h) 1:7, i) 1:8. B) Luminescence quenching at 540 nm upon bioconjugate formation at increasing $P450_{BS\beta}$/CdS ratios (data normalized against unconjugated QDs).

In an initial demonstration of the QD/$P450_{BS\beta}$ nanohybrid-mediated photocatalysis we chose the well-established hydroxylation of myristic acid as a model reaction,[21] and we investigated whether hydroxymyristic acid products are formed by using HPLC and ESI-LCMS analysis. To this end, myristic acid (8 mM) in EtOH was added to the $P450_{BS\beta}$/QD hybrid solution (20 μM), and the mixture was irradiated

 © 2006 Wiley-VCH Verlag GmbH & Co. KGaA, Weinheim

for 20 minutes at room temperature. The reaction mixture was extracted with chloroform, and the products were analyzed by LC/ESI-MS. This analysis revealed the characteristic mass peak of hydroxymyristic acid ($[M-H^+]=243.09$, calculated $M=244.37$, see the Supporting Information). In contrast, no product peaks were observed in control experiments with: 1) pure QDs in the absence of $P450_{BS\beta}$; 2) with pure $P450_{BS\beta}$ in the absence of QDs; and 3) without irradiation.

We could also observe subtle changes in the optical absorption of P450 in the presence of the myristic acid substrate. An approximately 5-nm blue shift of the 417-nm absorption of the $P450_{BS\beta}$ attached to the CdS QD was observed (Figure S5B in the Supporting Information), and $P450_{BS\beta}$ alone also showed an $\approx$3-nm blue shift in the presence of myristic acid (Figure S5A). As reported earlier, this blue shift is indicative of the binding of the substrate to the active site of P450.[22,30] Although substrate binding is not a prerequisite for electron transfer,[31] the spectroscopic results together with the nonformation of hydroxymyristic acid products in the absence of $P450_{BS\beta}$ provides evidence that the myristic acid is bound to the active site of the $P450_{BS\beta}$ in the CdS/$P450_{BS\beta}$ nanohybrids.

To further elucidate this system, the product yields of similar reactions were determined systematically using a standardized assay which included esterification of the fatty acids and their subsequent HPLC analysis using hydroxylauric acid as an internal standard for quantification[21] (For a detailed protocol, see the Supporting Information.) Various experiments were carried out under different irradiation times, as well as different surface coverages of the CdS QDs with $P450_{BS\beta}$. The results indicated that both α- and β-hydroxymyristic acid isomers are formed in approximately equal amounts in the $P450_{BS\beta}$/CdS photocatalysis, in analogy to the hydrogen peroxide initiated reaction.[20] As expected, the amount of hydroxylation products increased with increasing amounts of P450 per CdS (Figure 3A) as well as increasing irradiation time (Figure 3B).

To further investigate the P450 enzyme activity, controls were carried out with a binary system composed of CdS QDs and $P450_{BS\beta}$ without the 6×-His tag. Under standardized conditions, the system produced similar amounts of the hydroxylation products, as determined by the HPLC assay (see Figure S7). Hence, it appeared questionable whether the close proximity of the two components in the $P450_{BS\beta}$/CdS nanohybrids is, indeed, beneficial for the enzymatic activity of this system. To estimate proximity effects, we compared the turnover of the $P450_{BS\beta}$/CdS nanohybrids with that of the native enzyme activated with H_2O_2. The turnover of the $P450_{BS\beta}$/CdS system was found to be 61 min^{-1}, while that of P450 with H_2O_2 was 122 min^{-1}. The value is even about six times less than that reported for a similar $P450_{BS\beta}$ catalysis (363 min^{-1}), and therefore our results indicate that the activity of the $P450_{BS\beta}$ in the nanohybrids is significantly less than that of the native enzyme. This might be a consequence of the negative effects of the attached nanoparticles on the enzyme's catalytic performance, such as the deceleration of diffusion processes or the restriction of conformational degrees of freedom. Alternatively, (partial) denaturation of the enzyme molecules might occur during the adsorption and purification steps. Nonetheless, despite this reduction in turnover, the $P450_{BS\beta}$/CdS nanohybrids were capable of producing similar amounts of hydroxylation products as the native enzyme. Therefore, these results suggest that the close proximity between the enzymes and the QDs in the $P450_{BS\beta}$/CdS nanohybrids improves the overall catalytic power over that of the system containing the two components in separated form.

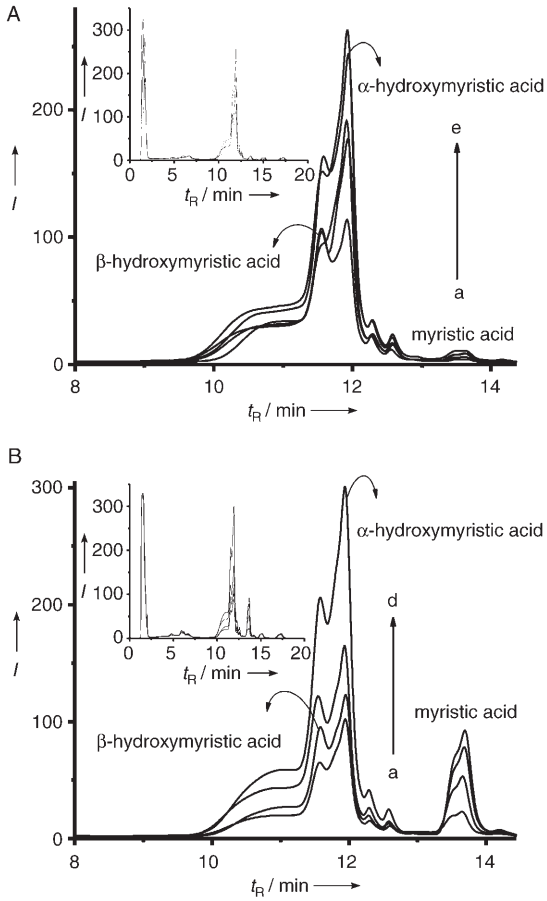


Figure 3. Identification of monooxygenation products by HPLC. Elution profile of myristic acid and its metabolites produced from QD/$P450_{BS\beta}$ hybrids: A) with different CdS/$P450_{BS\beta}$ ratios: a) 1:1, b) 1:2, c) 1:3, d) 1:4. e) 1:5; B) variation of irradiation times: a) 1 min, b) 2 min, c) 5 min, d) 10 min. The insets show complete chromatograms. The left part of the split product peak ($t_R=11.5$ min) corresponds to the β isomer and the right part ($t_R=11.9$ min) to the α isomer of hydroxylmyristic acid. The peak at $t_R=13.6$ min corresponds to myristic acid. The broad shoulder ($t_R=10.8$ min) is an HPLC artifact resulting from large injection volumes (25 μL), see also Figure S6.

To further investigate the $P450_{BS\beta}$/CdS photocatalysis, hydroxylation experiments were carried out in the presence of superoxide dismutase (SOD) enzyme. SOD effectively decomposes superoxide radicals, and we had previously used this activity to prove the identity of $O_2^{\bullet-}$ species produced by CdS QDs.[24] With the $P450_{BS\beta}$/CdS system investigated here, we observed a decrease of the hydroxymyristic acid products formed to approximately 20% chemical yields in the presence of SOD (see Figure S8 in the Supporting Information).

 © 2006 Wiley-VCH Verlag GmbH & Co. KGaA, Weinheim

Similar experiments carried out with the two-component system, that is, the mixture composed of CdS QDs and $P450_{BS\beta}$ without the His tag, revealed a decrease of the hydroxymyristic acid products to approximately 10% chemical yields. These results, again, hint at beneficial proximity effects in the $P450_{BS\beta}$/CdS nanohybrids. Apparently, the close distance between the QD and the P450 reduces the SOD-mediated degradation of superoxide radicals. Nonetheless, the results also suggest that the diffusion of radicals and their decomposition by SOD occurs at faster rates than the uptake and conversion of the radicals by the P450 enzyme.

In conclusion, we here report the design of quantum dot/enzyme nanohybrids that are capable of catalyzing an organic transformation through photoactivation of the QDs. The photogenerated excitons (e^- and h^+) produce $O_2^{\bullet-}$ and/or $OH^\bullet$ radicals, which in turn activate the P450 enzymes to catalyze monooxygenation of fatty acid substrates. In our example myristic acid is hydroxylated to give α- and β-hydroxymyristic acid. Although we could clearly prove the chemical composition and the catalytic activity of the novel $P450_{BS\beta}$/CdS nanohybrids, the characterization of their detailed kinetic properties will require more sophisticated studies. Hence, further work will focus on potential proximity effects that might arise owing to the close distance between the enzyme molecules and the surface of the radical-generating nanoparticle. In general, the light-induced triggering of enzyme activity confers explicit advantages over chemical initiation with respect to the control of enzymatic reactions. Moreover, the $P450_{BS\beta}$/CdS nanohybrids should also enable convenient recycling of the catalyst in organic transformations.[32] In addition to the investigation of other semiconductor QDs for improving the catalytic activity of such nanohybrids, which is currently under way, we are also aiming towards applications as photocatalysts in synthetic organic chemistry and as photosensitizers for intracellular reactions.

Received: August 30, 2005
Revised: October 14, 2005
Published online: December 19, 2005

Keywords: nanostructures · photochemistry · quantum dots · radicals

[1] T. Mokari, E. Rothenberg, I. Popov, R. Costi, U. Banin, *Science* **2004**, *304*, 1787.
[2] C. M. Niemeyer, *Angew. Chem.* **2001**, *113*, 4254; *Angew. Chem. Int. Ed.* **2001**, *40*, 4128.
[3] E. Katz, I. Willner, *Angew. Chem.* **2004**, *116*, 6166; *Angew. Chem. Int. Ed.* **2004**, *43*, 6042.
[4] L. Pavesi, L. D. Negro, C. Mazzoleni, G. Franzco, F. Priolo, *Nature* **2000**, *408*, 440.
[5] A. V. Malko, A. A. Mikhailovsky, M. A. Petrusca, J. A. Hollingsworth, H. Htoon, M. G. Bawendi, V. I. Klimov, *Appl. Phys. Lett.* **2002**, *81*, 1303.
[6] J. M. Bruchez, M. Moronne, P. Gin, S. Weiss, A. P. Alivisatos, *Science* **1998**, *281*, 2013.
[7] I. Willner, F. Patolsky, J. Wasserman, *Angew. Chem.* **2001**, *113*, 1913; *Angew. Chem. Int. Ed.* **2001**, *40*, 1861.
[8] W. C. W. Chan, S. Nie, *Science* **1998**, *281*, 2016.
[9] X. Michalet, F. F. Pinaud, L. A. Bentolila, J. M. Tsay, S. Doose, J. J. Li, G. Sundaresan, A. M. Wu, S. S. Gambhir, S. Weiss, *Science* **2005**, *307*, 538.
[10] F. Raimondi, G. G. Scherer, R. Kotz, A. Wokaun, *Angew. Chem.* **2005**, *117*, 2228; *Angew. Chem. Int. Ed.* **2005**, *44*, 2190.
[11] M. Gratzel, *Energy Resources through Photochemistry and Catalysis*, Academic Press, New York, **1983**.
[12] M. A. Fox, *Acc. Chem. Res.* **1983**, *16*, 314.
[13] S. Marinkovic, N. Hoffmann, *Chem. Commun.* **2001**, 1576.
[14] S. Marinkovic, N. Hoffmann, *Eur. J. Org. Chem.* **2004**, 3102.
[15] M. Warrier, M. K. F. Lo, H. Monbouquette, M. A. Garcia-Garibay, *Photochem. Photobiol. Sci.* **2004**, *3*, 859.
[16] M. L. Curri, A. Agostiano, G. Leo, A. Mallardi, P. Cosma, M. D. Monica, *Mater. Sci. Eng. C* **2002**, *22*, 449.
[17] I. N. Aleksey, I. A. Shumilin, V. V. Nikandrov, *J. Phys. Chem.* **1996**, *100*, 17544.
[18] C. M. Niemeyer, C. A. Mirkin, *Nanobiotechnology: Concepts, Methods and Application*, Wiley-VCH, Weinheim, **2004**.
[19] H. Waldmann, K. Drauz, *Enzymes Catalysis in Organic Synthesis*, Wiley-VCH, **2002**.
[20] I. Matsunaga, A. Ueda, N. Fujiwara, T. Sumimoto, K. Ichihara, *Lipids* **1999**, *34*, 841.
[21] I. Matsunaga, A. Ueda, T. Sumimoto, K. Ichihara, M. Ayata, H. Ogura, *Arch. Biochem. Biophys.* **2001**, *394*, 45.
[22] D.-S. Lee, A. Yamada, H. Sugimoto, I. Matsunaga, H. Ogura, K. Ichihara, S.-i. Adachi, S.-Y. Park, Y. Shiro, *J. Biol. Chem.* **2003**, *278*, 9761.
[23] A detailed description of potential catalytic pathways is included in the Supporting Information.
[24] B. I. Ipe, M. Lehnig, C. M. Niemeyer, *Small* **2005**, *1*, 706.
[25] J. R. Harbour, M. L. Hair, *J. Phys. Chem.* **1977**, *81*, 1791.
[26] A. Henglein, *Ber. Bunsen-Ges.* **1982**, *86*, 301.
[27] I. Geissbuehler, Dissertation, EPFL (Lausanne, Switzerland), **2005**.
[28] T. Omura, R. Sato, *J. Biol. Chem.* **1964**, *239*, 2370.
[29] E. R. Goldman, I. L. Medintz, J. L. Whitley, A. Hayhurst, A. R. Clapp, T. Uyeda, J. R. Deschamps, M. E. Lassman, H. Mattoussi, *J. Am. Chem. Soc.* **2005**, *127*, 6744.
[30] I. Matsunaga, A. Yamada, D.-S. Lee, E. Obayashi, N. Fujiwara, K. Kobayashi, H. Ogura, Y. Shiro, *Biochemistry* **2002**, *41*, 1886.
[31] F. P. Guengerich, W. W. Johnson, *Biochemistry* **1997**, *36*, 14741.
[32] Initial judgements on the stability of the $P450_{BS\beta}$/CdS nanohybrids can be drawn from the observation that continuous irradiation for 20 minutes led to neither precipitation nor to a decrease in enzymatic turnover. However, our efforts of reusing the nanohybrids for an additional round of catalysis have been unsuccessful so far, probably as a result of enzyme denaturation during the workup and extraction procedures.

 © 2006 Wiley-VCH Verlag GmbH & Co. KGaA, Weinheim

Fluorescent Probes

DOI: 10.1002/anie.200500751

A Small-Molecule FRET Probe To Monitor Phospholipase A_2 Activity in Cells and Organisms**

*Oliver Wichmann, Jochen Wittbrodt, and Carsten Schultz**

Biochemical experiments are shifting increasingly from the test tube to living cells. This development is mainly made possible by fluorescent probes[1,2] that, for example, replace radioactivity-based assays. Fluorescent probes usually allow real-time monitoring of events and, when located properly, also give spatial information about the monitored event. Accordingly, the demand for fluorescent probes has vastly increased over the past decade. Although the rapid development of fluorescent proteins from jellyfish and corals fosters the construction of genetically encoded probes,[3] small-molecule probes are mostly provided by chemical methods.[4]

The majority of small-molecule probes are ion sensors. A few substrates that exhibit fluorescence resonance energy transfer (FRET) have been synthesized and used successfully in the past to monitor enzyme activities.[5] One advantage of these probes is their accumulative nature, which, combined with the amplification effect of an enzymatic reaction, gives enormously high sensitivity even if substrate properties are moderate.[5] The disadvantage is that probes are sacrificed in the process, and the lack of reversibility limits the observation of dynamic processes. On the other hand, small, specifically tailored molecules permit the choice of a larger variety of fluorophores with physical properties more diverse than those provided by fluorescent proteins. Furthermore, small-molecule probes should generally give much larger ratio changes owing to the close proximity of the fluorophores. This might be important for applications with limited sensitivity, such as a platereader. Herein we present the synthesis and biological application of a small-molecule FRET probe for phospholipase A_2 (PLA_2). A number of fluorescent assays for monitoring PLA_2 activity have been previously described, albeit without ratio imaging.[6,7] PLA_2s are a group of key enzymes in intracellular signaling and play an important role in inflammation. One of the main functions of PLA_2 is to release arachidonic acid from phospholipids as the key precursor for the synthesis of prostaglandins and leukotrienes.[8,9] Most of the enzymes exhibit activities on membrane surfaces, especially those of the perinuclear region.[10–12]

The design of the probe PENN/SATE (**1**) was based on a phospholipid (Figure 1). As there are many different phospholipases with various substrate specificities, we picked a phosphatidylethanolamine (PE) backbone in which the ester in the *sn*-1 position was altered to a nonhydrolyzable ether, thus eliminating the substrate properties for PLA_1 and unspecific lipases in this position. Another important factor was the selection and attachment of the two fluorescent dyes. In our search for maximal overlap between FRET donor emission and acceptor excitation, we chose the pair 7-nitrobenzo-2-oxa-1,3-diazole amine (NBD) and the 2-hydroxy derivative of 9-diethylamino-5*H*-benzo[*a*]phenoxazin-5-one (Nile red). Their optical properties were almost ideally suited for our purposes (Figure 2). Furthermore, both fluorophores are, under physiological conditions, uncharged and thus lipophilic, which is important for insertion of the dyes into the lipid bilayer of cells.

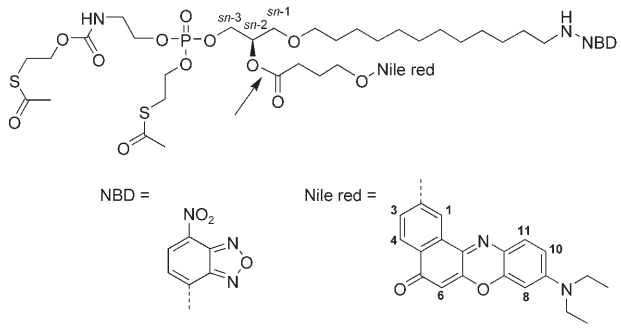


Figure 1. Structure of the PLA_2 reporter **1**. The FRET donor fluorophore NBD is attached to the tip of the *sn*-1 chain, the acceptor Nile red to the butyric acid at *sn*-2. The charged head group moieties are masked by bioactivatable *S*-acetyl-2-thioethyl (SATE) groups. Enzymatic hydrolysis of the thioester and release of thiirane is known to liberate charged groups.[13] The arrow indicates where PLA_2 cleaves the probe.

Nile red was originally used in histology to stain lipid droplets. To make the fluorophore amenable to chemical attachment, functionalized derivatives with hydroxy groups in the 2- or 3-position were previously prepared.[14] We followed a modified procedure to synthesize the 2-hydroxy-Nile red ether attached to butyric acid (NRBA).[14] The latter was introduced in the *sn*-2 position of the probe. We intended to adjust the position of the two fluorophores by differing the length of the fatty acid chain. As a result of this, the double bonds of Nile red were more likely to mimic those of arachidonic acid.[15] Previous probes with identical fatty acid chain lengths, showed good quenching of the donor fluores-

[*] O. Wichmann, Dr. C. Schultz
European Molecular Biology Laboratory
Gene Expression Programme
Meyerhofstrasse 1, 69117 Heidelberg (Germany)
Fax: (+49) 6221-387-206
E-mail: schultz@embl.de
Dr. J. Wittbrodt
European Molecular Biology Laboratory
Developmental Biology Programme
Meyerhofstrasse 1, 69117 Heidelberg (Germany)

[**] The authors thank Heike Stichnoth and Nicole Heath for providing cells and Erika Grzebisz for the supply of Medaka eggs. We gratefully acknowledge Dr. Christina Leslie, University of Colorado, Boulder, for a plasmid of phospholipase A_2 γ, and Dr. Michael Gelb, University of Washington, Seattle, for a plasmid of phospholipase A_2 α, purified cytosolic phospholipase A_2 α enzyme, and helpful discussions.

Supporting information for this article is available on the WWW under http://www.angewandte.org or from the author.

InterScience
© 2006 Wiley-VCH Verlag GmbH & Co. KGaA, Weinheim

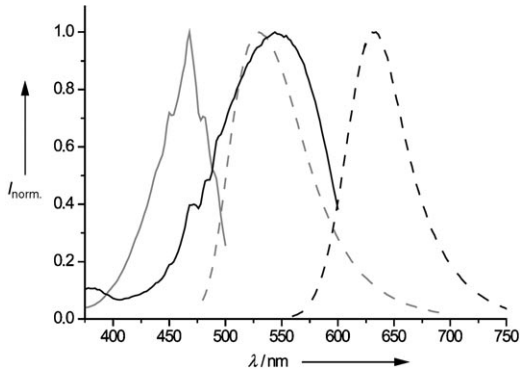
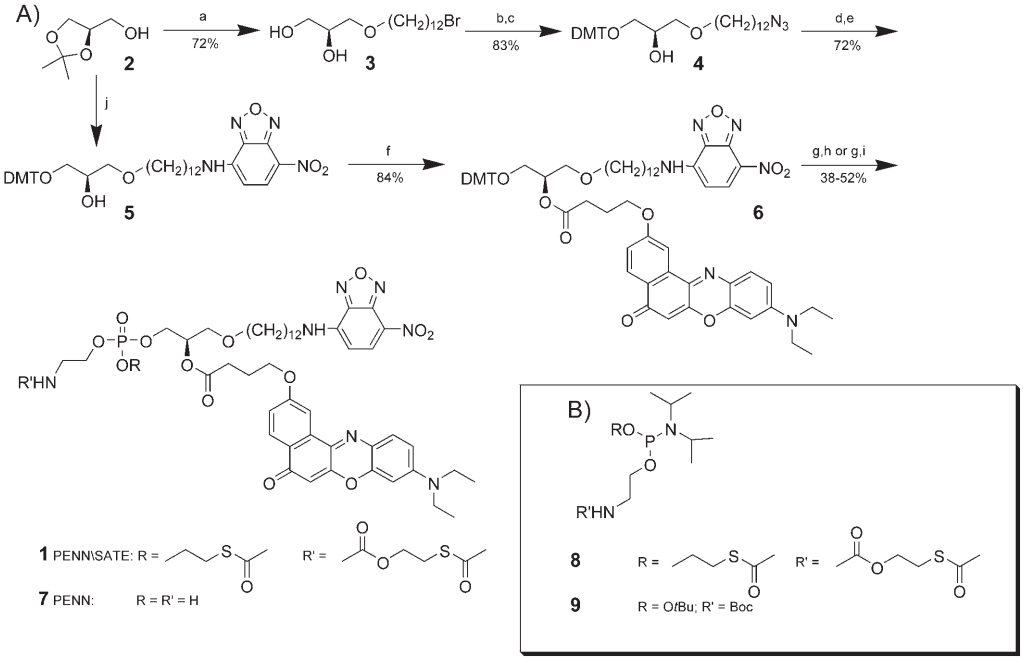


Figure 2. Excitation (——) and emission (-----) spectra of NBD (gray) and Nile red (black) in methanol. Spectra of sonicated Triton X-100 vesicles (3 mM) were almost identical. Overlap of NBD emission and Nile red excitation was perfect to permit FRET. Emission spectra were recorded with excitation at 458 (NBD) and 543 nm (Nile red) and the excitation spectra were recorded with detection at 540 nm and 640 nm, respectively.

cence and a large increase in donor emission after hydrolysis of the ester at the *sn*-2 position.[16] However, changes in the acceptor emission were fairly feeble.

A problem when working with phospholipids in biological experiments is their tendency to form insoluble aggregates. Furthermore, we expected that a charged phospholipid might stick to the outer side of the plasma membrane rather than enter the cell. As cytosolic PLA_2 usually acts at perinuclear membranes inside cells, a membrane-permeant derivative of the probe was necessary. We therefore masked the charged groups of the probe with SATE groups (Figure 1). These groups are well known bioactivatable phosphate-protecting groups that are mostly used to improve the bioavailability of antiviral nucleotides.[13,17] SATE groups can be introduced through the use of premanufactured SATE-protected phosphoamidite reagents, which, after coupling to the alcohol, are readily oxidized to uncharged phosphotriesters.[18] Through this method, all the phospholipid headgroups can be coupled to the glycerol backbone in one step. This methodology appears to be advantageous over other prodrug approaches, such as masking with acetoxymethyl ethers, which not only require less-mild conditions for their introduction[19] but lead to modification of the Nile red dye[29].

The synthesis started from enantiomerically pure 2,3-isopropylidene-*sn*-glycerol (**2**; Scheme 1). The *sn*-1 hydroxy group was alkylated with 1,12-dibromododecane and the ketal was subsequently removed in a one-pot reaction to give compound **3** as was previously described.[16] The remaining bromide was replaced by an azide and the primary alcohol group was protected with 4,4-dimethoxytrityl (DMT) chloride. The resultant compound **4** was reduced with lithium aluminum hydride in THF to form the amino group (92% yield after chromatography) desired for coupling with NBD chloride.



Scheme 1. A) Synthetic pathways to the protected probe PENN/SATE (**1**) and the unprotected probe PENN (**7**). a) 1) 1,12-Dibromododecane (excess), NaH, DMF, room temperature, 16 h, 2) TFA, MeCN, H_2O, room temperature, 2 h; b) NaN_3 (excess), DMSO, 85 °C, 3 h; c) DMT-Cl, Et_3N, DMAP, DMF, room temperature, 16 h; d) LiAlH, THF, 0 °C, 2 h; e) NBD-Cl, DIPEA, methanol, 0 °C→RT, 4 h; f) 4-(Nile red)-oxy-butyric acid, TPSNT, MeIm, CH_2Cl_2, room temperature, 14 h; g) dowex 50 WX-8, CH_2Cl_2, room temperature, 3 h; h) 1) phosphoramidite **8**, 4,5-dicyanoimidazole, DMF 0 °C→RT, 2) *t*BuOOH (excess), 0 °C, 3 h, 38–52% (for g–h); k) 1) phosphoramidite **9**, 4,5-dicyanoimidazole, DMF 0 °C→RT, 2) *t*BuOOH (excess), 0 °C, 30 min, 3) 5% TFA, CH_2Cl_2, room temperature, 1 h, l) 1) 1,12-dibromododecane (excess), NaH, DMF, room temperature, 16 h, 2) NaN_3 (excess), DMSO, 85 °C, 3 h; 3) Ph_3P on resin, THF, 24 h, 4) MeOH/H_2O (9:1), 24 h, 5) TFA, MeCN, H_2O, RT, 3 h, 6) DMT-Cl, Et_3N, DMAP, DMF, room temperature, 14 h. B) Phosphitylation reagents with enzymatically (**8**) and chemically (**9**) cleavable protecting groups. DMF = *N,N*-dimethylformamide, TFA = trifluoroacetic acid, DMSO = dimethyl sulfoxide, DMAP = 4-diaminoamino pyridine, DIPEA = diisopropylethylamine, Boc = *tert*-butyloxycarbonyl.

 © 2006 Wiley-VCH Verlag GmbH & Co. KGaA, Weinheim

In an alternative approach the reduction was performed on a triphenylphosphine-loaded resin. Through the Staudinger reaction, the azide was initially bound to the resin and all side products were removed by thorough washings. The pure amine was eluted with wet methanol. This procedure was advantageous for small amounts, whereas the batch procedure was superior for larger quantities. After successful coupling of NBD, the derivative **5** was esterified with Nile red oxybutyric acid in the presence of 1-(2,4,6-triisopropylbenzenesulfonyl)-3-nitro-1*H*-1,2,4-triazole (TPSNT) and methylimidazole (MeIm) in dichloromethane. This method, with yields up to 87%, was superior to coupling reactions with carbodiimide reagents. The resultant bilabeled compound **6** was then deprotected through the addition of dowex 50 WX-8 to a solution of **6** in dichloromethane. Migration of the *sn*-2 ester to the now deprotected primary alcohol needed to be avoided; we therefore filtered the dichloromethane solution quickly through silica to remove DMT-containing by-products, evaporated the solvent, and immediately started the subsequent phosphitylation reaction in DMF without further purification (a sample of the primary alcohol was purified for analysis). Phosphoramidite **8** and 4,5-dicyanoimidazole were added under argon, and after 16 h the solution was treated with *t*BuOOH for 3 h. Finally, **1** was purified through silica. In a phosphitylation/oxidation/protection reaction with a Boc-protected amino group and a *tert*-butyl group on the phosphoramidite **9**,[16] a variety of probes without bioactivatable protecting groups (PENN, **7**) were prepared after deprotection (Scheme 1). The latter was used for the investigation of the optical properties in an in vitro micelle assay.

Micelles that consist of about 140 molecules were made from Triton X-100 by sonication by following standard procedures.[20] PENN **7** was incorporated in such a way that every tenth micelle received one molecule of the dye. Under these conditions, the fluorescent spectra showed total quenching of green NBD fluorescence and a significant amount of emission with a maximum at 620 nm (typical for Nile red emission), which suggests that the energy transfer was complete (Figure 3 A). Quantum yields for **7** in ethanol were 0.12, whereas NBD-labeled undecanoic acid alone had a quantum yield of 0.36.[21] The value for **7** was identical to that of a previously used FRET probe with the same fluorophores (see Supporting Information). Photostability for **7** was determined in micelles and HeLa cells. Although no photobleaching was observed in vitro, NBD bleached in cells with about 1.5% per exposure (see Supporting Information).

The addition of commercially available PLA_2 from bee venom resulted in an immediate increase in green fluorescence that was accompanied by a substantial decrease in red fluorescence. Ratio changes reached a maximum of 30-fold after 15–30 minutes (Figure 3 A). Reorganization of the micelles by additional sonication showed no further change in the ratio, indicating that the two fluorophores were already spatially separated. Accordingly, the remaining red fluorescence resulted from direct excitation of Nile red. TLC analysis of **7** treated with PLA_2 for 30 min showed cleavage of more than 90% (Figure 3 B). These data suggest that the strong ratio change makes the probe well suitable for applications within living cells.

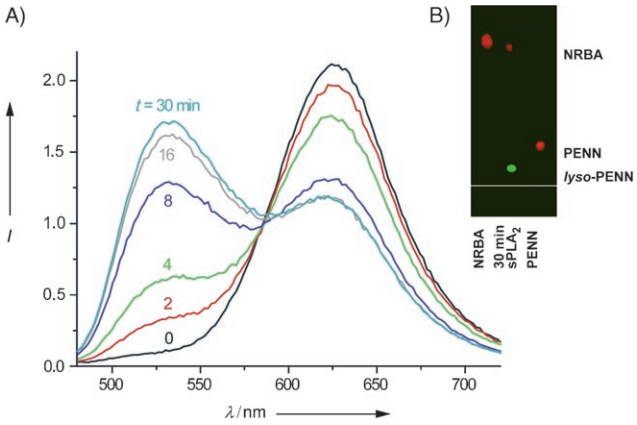


Figure 3. A) Addition of bee venom PLA_2 to a 1 μM solution of **7** in Triton X100 micelles (3 mM) at pH 7.5 led to an increase in NBD fluorescence and a decrease in Nile red fluorescence. Excitation was at 440 nm. The emission ratio change was 30-fold. Sonication after the reaction was complete gave no further ratio change. B) TLC analysis of a parallel reaction and references after 30 min.

Phosphatidylethanolamines are distributed throughout the internal cellular membranes and on the inner side of the plasma membrane. In contrast, cytosolic PLA_2 activity is known to be most pronounced on membranes of the perinuclear region.[11,22,23] Therefore, it was crucial to demonstrate that the probe was able to reach this cell compartment. Incubation of HeLa cells or MDCK II (Maden Darby canine kidney) epithelial cells showed that the probe was predominantly located in the Golgi apparatus, the nuclear envelope, and at higher doses, also in the endoplasmic reticulum (ER) (Figure 4). Owing to an unknown mechanism, the plasma

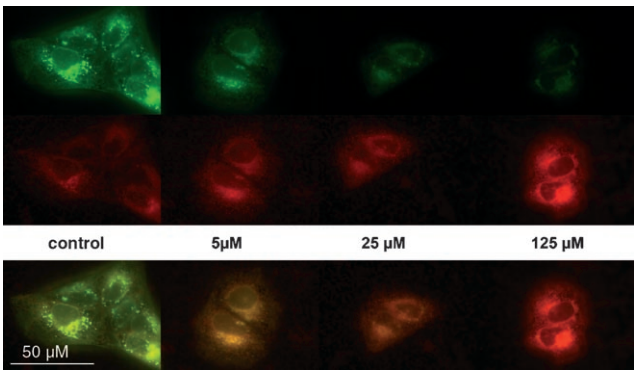


Figure 4. Hydrolysis of **1** by endogenous enzymes in MDCK II cells is inhibited by MAFP in a dose-dependent manner. Upper panel: NBD fluorescence, middle panel: Nile red fluorescence, lower panel: overlay.

membrane stayed free of dye. The locations of dye penetration can most likely be attributed to the Nile red moiety. Experiments with simple Nile red labeled fatty acids showed accumulation in the same regions, whereas unmodified Nile red stained small vesicles or oil droplets (data not shown). Other aromatic dyes such as NBD and lissamine also seem to guide attached compounds into perinuclear membranes.

MDCK II cells loaded with **1** (3 μM) were analyzed with a widefield microscope (Zeiss Axiovert 200M). The endoge-

 © 2006 Wiley-VCH Verlag GmbH & Co. KGaA, Weinheim

nous PLA_2 activity of the cells was stimulated with fetal calf serum (FCS) and cleaved from the probe within 30 to 60 min (Figure 4, control). Fluorescence excitation was at 435–485 nm for NBD fluorescence and 540–580 nm for Nile red. Emission was measured at 515–555 nm (NBD) and 600–660 nm (Nile red). The ratio of the two emission values (donor/acceptor fluorescence) gave a direct readout of the status of the probe: low ratio values reflected an intact probe and high ratio values a cleaved probe. In Figure 4, Nile red fluorescence intensity values are depicted in red and NBD fluorescence is converted to green (false color). An overlay of the two images combined the entire information in one picture and showed the colocalization of the dyes.

Inhibition of PLA_2 by standard inhibitors such as methyl arachidonyl fluorophosphate (MAFP) and bromoenollactone (BEL) was studied next. HeLa cells were plated in square 4-welled coverslips (20×9 mm per chamber), treated with **1** (3 μM) and either an inhibitor or a control substance for 30 min. Ratio pictures (not shown) gave a dose-dependent inhibition of PLA_2 activity with an IC_{50} of approximately 5 μM for the covalent binding inhibitor MAFP and only minimal inhibition by BEL (Figure 5).[24,25]

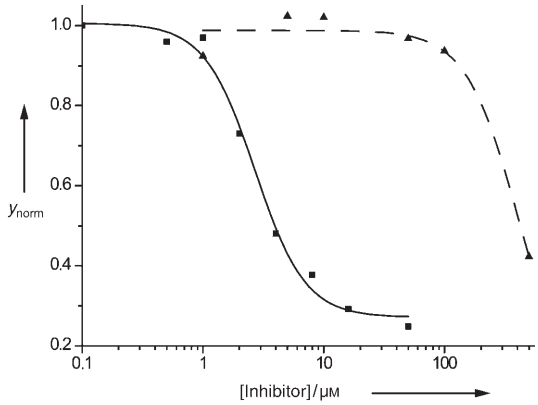


Figure 5. Dose-response curves that result from experiments with HeLa cells, which show diverse sensitivity to different PLA_2 inhibitors y_{norm} = normalized emission ratio (515–555 nm/620+ nm), MAFP ——, BEL -----. This suggests that the probe is sensitive to particular PLA_2 isoforms.

The latter inhibitor is known to be fairly specific towards calcium-independent isoforms of PLA_2 ($iPLA_2$).[25] MAFP sensitivity indicates a serine residue in the catalytic center of the enzyme which hints towards the presence of PLA_2 isoforms such as groups IV and VI to VIII in HeLa cells.[8] Comparison of the MAFP IC_{50} with published data showed similar results for the test tube and in living cells.[26] This demonstrates that **1** is a suitable probe to screen for PLA_2 inhibitors in living cells. This method was, therefore, shown to be applicable for use in plate readers, thereby allowing fairly high-throughput experiments. Initial experiments with a PE EnVision platereader gave promising results. HeLa cells were seeded in a 96-well plate and treated with **1** (5–50 μM) for 30 min before the cells were washed three times with HEPES buffer (pH 7.4). For simplicity, we observed only FRET donor dequenching, which occurred when the FRET acceptor was removed by enzymatic cleavage of the probe. Several grades of cell confluency varying from 30→100% were tested and, as expected, higher cell confluency gave a larger fluorescent readout. Wells with a confluency below 80% were not suitable for detection of enzyme activity. Wells treated with MAFP during the probe incubation showed readouts similar to noise levels, demonstrating that the probe was not cleaved and, therefore, no dequenching of the FRET donor was detectable.

Apart from analysis and screening of PLA_2 inhibitors, we were interested in the demonstration of the onset of PLA_2 activity in living embryos during development. Similar experiments have been previously performed in the gastrointestinal tract of Zebrafish embryos.[27] Such experiments would tell us whether the probe 1) could be used in whole organisms, 2) would be suitable for day-long experiments, and 3) would be toxic to a living organism. We therefore microinjected **1**, which was dissolved in phosphate or balanced salt solution (BSS) buffer (pH 7.4, up to 10% DMSO/Pluronic), underneath a 3-h-old Medaka fish embryo without rupturing the egg-yolk membrane. The embryo was then mounted on a binocular stage that had fluorescence detection. Within 2–7 h the probe had entirely accumulated within the embryo (Figure 6 A), therefore, showing the effectiveness of the

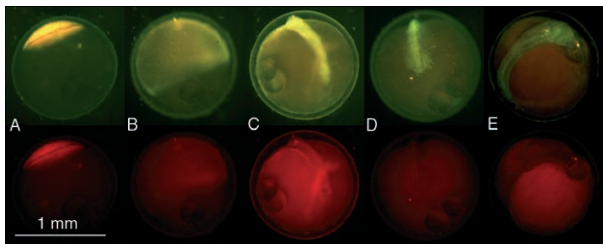


Figure 6. Application of **1** to study PLA_2 expression in Medaka fish embryos. The upper panel shows an overlay of red and green fluorescence, the lower panel shows only the red channel for comparison. A) The embryo (age 3 h) rapidly picked up the probe within 2–7 h. B) At the age of 19 h it showed a partially developed germ ring. C) After 27 h the embryo continued to exhibit substantial FRET, as is depicted by the yellow color. D) and E) After 37 and 48 h, respectively, the embryo showed exclusively green staining by the NBD-labeled lysophosphatidyl ethanolamine, whereas Nile red butyric acid diffused into the fat-rich egg yolk, indicating the onset of PLA_2 activity. The onset of PLA_2 enzyme activity shown here is in good agreement with results published for time courses from Zebrafish embryo extracts.[15] The embryo was observed for 5 days more until the fish hatched. This showed that the probe was not detectably toxic to Medaka fish embryos. Fluorescence persisted within the specimen until the fish hatched.

bioactivatable-protecting-group approach. After 27 h the embryo had grown significantly and exhibited yellow fluorescence (Figure 6 C), which is typical for the overlay of green and red fluorescence in the intact FRET probe. After 37 h, however, the fish embryo had turned green, whereas the egg yolk was bright red (Figure 6 D and E), suggesting that the probe had been cleaved. The green-fluorescent-labeled lipid backbone with the nonhydrolyzable ether bond in the *sn*-1 position stayed in the fish whereas the hydrolyzed Nile red

 © 2006 Wiley-VCH Verlag GmbH & Co. KGaA, Weinheim

butyric acid had apparently diffused into the fat-rich egg yolk, thereby separating the two parts of the probe.

It remains to be established which isoform of PLA_2 is responsible for the cleavage reaction, both in cultured cells and in fish embryos. In vitro experiments with isolated recombinant cPLA$_2$ α showed no cleavage of **7**. Overexpression of cPLA$_2$ α and γ also failed to increase the cleavage of the probe. All experiments performed so far hint towards PAF-AHII as the responsible enzyme for cleavage of **7** in HeLa cells. This result is in accordance with recent data from *C. elegans*, which show that PAF-AHII is essential for epithelial morphogenesis.[28] Only future experiments with purified enzyme can prove hydrolysis of **7** with PAF-AHII.

In conclusion, the PLA_2 probe **1** is highly membrane permeant and accumulates close to the intracellular region of PLA_2 activity. The probe was demonstrated to be useful in monitoring enzyme activities in cultured cells and small organisms and there is much potential for the probe to be used in living-cell high-throughput screening experiments for PLA_2 inhibitors. Small-molecule FRET probes generated by preparative organic chemistry usually exhibit much larger ratio changes than genetically encoded FRET probes. Therefore, this technology should generally be explored more extensively in the future, especially when the probes are membrane permeant and therefore suitable for the treatment of large cell populations.

Experimental Section

1: ^{1}H NMR (400 MHz, $CDCl_3$, 25 °C, TMS): $\delta = 8.48$ (d, $^3J = 8.6$ Hz, 1H; NBD-H), 8.25 (d, $^3J = 8.8$ Hz, 1H; Nile red H^4), 8.06 (d, $^4J = 2.5$ Hz, 1H; Nile red H^1), 7.62 (d, $^3J = 9.1$ Hz, 1H; Nile red H^{11}), 7.19 (dd, $^3J = 8.6$ Hz, $^4J = 2.5$ Hz, 1H; Nile red H^3), 6.70 (dd, $^3J = 9.1$ Hz, $^4J = 2.5$ Hz, 1H; Nile red H^{10}), 6.48 (d, $^4J = 2.5$ Hz, 1H; Nile red H^8), 6.35 (s, 1H; Nile red H^6), 6.16 (d, $^3J = 8.3$ Hz, 1H; NBD-H), 5.53 (t, $^3J = 4.5$ Hz, 0.5H; N*H* carbamate), 5.48 (t, $^3J = 4.5$ Hz, 0.5H; N*H* carbamate), 5.30–5.20 (m, 1H; *sn*-2 C*H*), 4.37–4.10 (m, 12H; Nile red OCH_2, POCH_2 (3×), NHCOOCH_2), 3.61 (d, $^3J = 5.1$ Hz, 1H; *sn*-1 CH_2), 3.56–3.40 (m, 10H; *sn*-1 OCH_2, NBD-NH-CH_2, Nile red NCH_2 (2×), OOCNHCH_2), 3.20 (t, 2.67 , $^3J = 6.3$ Hz, 2H; COSCH_2), 3.15 (t, $^3J = 6.4$ Hz, 2H; COSCH_2), 2.69 (t, $^3J = 7.2$ Hz, 2H OOCCH_2), 2.38 (s, 3H; CH_3COS), 2.37 (s, 3H; CH_3COS), 2.26 (qi, $^3J = 6.7$ Hz, 2H; Nile red O-CH$_2$CH_2), 1.79 (qi, $^3J = 7.2$ Hz, 2H; NBDNH-CH2CH_2), 1.60–1.19 ppm (m, 26H; Nile red NCH$_2$CH_3 (2×), CH_2 chain (10×)); ^{13}C NMR (100 MHz, $CDCl_3$, 25 °C): $\delta = 183.2$, 161.5, 152.1, 150.9, 146.9, 136.5, 134.1, 131.1, 130.9, 128.8, 127.8, 125.7, 124.7, 118.2, 109.7, 106.6, 105.2, 96.3, 71.8, 71.0, 68.3, 67.0, 66.3, 66.2, 63.4, 45.1, 44.1, 41.4, 38.7, 31.9, 30.8, 30.6, 30.4, 29.7, 29.5, 29.4, 29.4, 29.3, 29.2, 29.1, 28.9, 28.5, 28.3, 26.9, 26.0, 12.6 ppm; ^{31}P NMR (162 MHz, $CDCl_3$, 25 °C, H_3PO_4): $\delta = -1.1$ ppm; HR FAB MS (NBA, positive mode): [M+H$^+$] calculated: 1212.4398; [M+H$^+$] found: 1212.4366.

Received: February 28, 2005
Revised: July 9, 2005
Published online: December 2, 2005

Keywords: bioorganic chemistry · fluorescent probes · FRET (fluorescence resonance energy transfer) · phospholipids · signal transduction

[1] J. Zhang, R. E. Campbell, A. Y. Ting, R. Y. Tsien, *Nat. Rev. Mol. Cell Biol.* **2002**, *3*, 906–918.
[2] F. S. Wouters, P. J. Verveer, P. I. H. Bastiaens, *Trends Cell Biol.* **2001**, *11*, 203–211.
[3] A. Miyawaki, A. Sawano, T. Kogure, *Nat. Cell Biol.* **2003**, *5*, S1–S7.
[4] N. Johnsson, K. Johnsson, *ChemBioChem* **2003**, *4*, 803–810.
[5] G. Zlokarnik, P. A. Negulescu, T. E. Knapp, L. Mere, N. Burres, L. X. Feng, M. Whitney, K. Römer, R. Y. Tsien, *Science* **1998**, *279*, 84–88.
[6] H. S. Hendrickson, *Anal. Biochem.* **1994**, *219*, 1–8.
[7] H. S. Hendrickson, E. K. Hendrickson, I. D. Johnson, S. A. Farber, *Anal. Biochem.* **1999**, *276*, 27–35.
[8] I. Kudo, M. Murakami, *Prostaglandins Other Lipid Mediators* **2002**, *68–69*, 383–399.
[9] C. D. Funk, *Science* **2001**, *294*, 1871–1875.
[10] S. Das, W. Cho, *J. Biol. Chem.* **2002**, *277*, 23838–23846.
[11] S. Grewal, S. Ponnambalam, J. H. Walker, *J. Cell Sci.* **2003**, *116*, 2303–2310.
[12] J. H. Evans, D. M. Spencer, A. Zweifach, C. C. Leslie, *J. Biol. Chem.* **2001**, *276*, 30150–30160.
[13] S. Benzaria, H. Pelicano, R. Johnson, G. Maury, J. L. Imbach, A. M. Aubertin, G. Obert, G. Gosselin, *J. Med. Chem.* **1996**, *39*, 4958–4965.
[14] M. S. J. Briggs, I. Bruce, J. N. Miller, C. J. Moody, A. C. Simmonds, E. Swann, *Chem. Soc. Perkin Trans. 1* **1997**, 1051–1058.
[15] S. A. Farber, E. S. Olson, J. D. Clark, M. E. Halpern, *J. Biol. Chem.* **1999**, *274*, 19338.
[16] O. Wichmann, C. Schultz, *Chem. Commun.* **2001**, 2500–2501.
[17] M. Shafiee, S. Deferme, A. L. Villard, D. Egron, G. Gosselin, J. L. Imbach, T. Lioux, A. Pompon, S. Varray, A. M. Aubertin, G. Van den Mooter, R. Kinget, C. Perigaud, P. Augustijns, *J. Pharm. Sci.* **2001**, *90*, 448–463.
[18] C. Dinkel, O. Wichmann, C. Schultz, *Tetrahedron Lett.* **2003**, *44*, 1153–1155.
[19] C. Schultz, *Bioorg. Med. Chem.* **2003**, *11*, 885–898.
[20] Y. A. Hannun, C. R. Loomis, R. M. Bell, *J. Biol. Chem.* **1985**, *260*, 10039–10043.
[21] H. Du, R. C. A. Fuh, J. Z. Li, L. A. Corkan, J. S. Lindsey, *Photochem. Photobiol.* **1998**, *68*, 141–142.
[22] A. Matsuzawa, K. Hattori, J. Aoki, H. Arai, K. Inoue, *J. Biol. Chem.* **1997**, *272*, 32315–32320.
[23] K. Asai, T. Hirabayashi, T. Houjou, N. Uozumi, R. Taguchi, T. Shimizu, *J. Biol. Chem.* **2003**, *278*, 8809–8814.
[24] J. Balsinde, E. A. Dennis, *J. Biol. Chem.* **1996**, *271*, 6758–6765.
[25] J. Balsinde, I. D. Bianco, E. J. Ackermann, K. Condefrieboes, E. A. Dennis, *Proc. Natl. Acad. Sci. USA* **1995**, *92*, 8527–8531.
[26] M. A. Balboa, I. Varela-Nieto, K. K. Lucas, E. A. Dennis, *FEBS Lett.* **2002**, *531*, 12–17.
[27] S. A. Farber, M. Pack, S. Y. Ho, L. D. Johnson, D. S. Wagner, R. Dosch, M. C. Mullins, H. S. Hendrickson, E. K. Hendrickson, M. E. Halpern, *Science* **2001**, *292*, 1385–1388.
[28] T. Inoue, A. Sugimoto, Y. Suzuki, M. Yamamoto, M. Tsujimoto, K. Inoue, J. Aoki, H. Arai, *Proc. Natl. Acad. Sci. USA* **2004**, *101*, 13233–13238.
[29] C. Dinkel, C. Schultz, unpublished results.

 © 2006 Wiley-VCH Verlag GmbH & Co. KGaA, Weinheim